WOODHEAD PUBLISHING IN MATERIALS



Fatigue assessment of welded joints by local approaches

Second edition

D. Radaj, C. M. Sonsino and W. Fricke

CRC

WP

Fatigue assessment of welded joints by local approaches

Related titles:

Cumulative damage of welded joints
(ISBN-13: 978-1-85573-938-3; ISBN-10: 1-85573-938-0)
Written by one of the leading experts in the field, Dr Tim Gurney, this important book examines fatigue in welded joints, both as a result of constant loads and variable amplitude loading.

Fatigue strength of welded structures Third edition
(ISBN-13: 978-1-85573-506-4; ISBN-10: 1-85573-506-7)
Research on the fatigue behaviour of welded structures has improved our understanding of the design methods that can reduce premature or progressive fatigue cracking. The latest edition of this standard text incorporates recent research on understanding and preventing fatigue-related failure through good design.

Fatigue analysis of welded components: designer's guide to the structural hot-spot stress approach
(ISBN-13: 978-184569-124-0; ISBN-10: 1-84569-124-5)
This report from the International Institute of Welding provides practical guidance on the use of the hot-spot stress approach to improve both the fatigue analysis and design of welded structures.

Details of these and other Woodhead Publishing materials books and journals, as well as materials books from Maney Publishing, can be obtained by:

- visiting www.woodheadpublishing.com
- contacting Customer Services (e-mail: sales@woodhead-publishing.com; fax: +44 (0) 1223 893694; tel.: +44 (0) 1223 891358 ext. 30; address: Woodhead Publishing Ltd, Abington Hall, Abington, Cambridge CB1 6AH, England)

Maney currently publishes 16 peer-reviewed materials science and engineering journals. For further information visit www.maney.co.uk/journals.

Fatigue assessment of welded joints by local approaches

Second edition

D Radaj, C M Sonsino and W Fricke

Woodhead Publishing and Maney Publishing
on behalf of
The Institute of Materials, Minerals & Mining

CRC Press
Boca Raton Boston New York Washington, DC

WOODHEAD PUBLISHING LIMITED
Cambridge England

Woodhead Publishing Limited and Maney Publishing Limited on behalf of
The Institute of Materials, Minerals & Mining

Woodhead Publishing Limited, Abington Hall, Abington, Cambridge CB1 6AH, England
www.woodheadpublishing.com

Published in North America by CRC Press LLC, 6000 Broken Sound Parkway, NW, Suite 300, Boca Raton, FL 33487, USA

First published 1998 by Abington Publishing, an imprint of Woodhead Publishing Limited
Second edition 2006, Woodhead Publishing Limited and CRC Press LLC
© Woodhead Publishing Limited, 2006
The authors have asserted their moral rights.

This book contains information obtained from authentic and highly regarded sources. Reprinted material is quoted with permission, and sources are indicated. Reasonable efforts have been made to publish reliable data and information, but the authors and the publishers cannot assume responsibility for the validity of all materials. Neither the authors nor the publishers, nor anyone else associated with this publication, shall be liable for any loss, damage or liability directly or indirectly caused or alleged to be caused by this book.

Neither this book nor any part may be reproduced or transmitted in any form or by any means, electronic or mechanical, including photocopying, microfilming and recording, or by any information storage or retrieval system, without permission in writing from Woodhead Publishing Limited.

The consent of Woodhead Publishing Limited does not extend to copying for general distribution, for promotion, for creating new works, or for resale. Specific permission must be obtained in writing from Woodhead Publishing Limited for such copying.

Trademark notice: Product or corporate names may be trademarks or registered trademarks, and are used only for identification and explanation, without intent to infringe.

British Library Cataloguing in Publication Data
A catalogue record for this book is available from the British Library.

Library of Congress Cataloging in Publication Data
A catalog record for this book is available from the Library of Congress.

Woodhead Publishing ISBN-13: 978-1-85573-948-2 (book)
Woodhead Publishing ISBN-10: 1-85573-948-8 (book)
Woodhead Publishing ISBN-13: 978-1-84569-188-2 (e-book)
Woodhead Publishing ISBN-10: 1-84569-188-1 (e-book)
CRC Press ISBN-13: 978-0-8493-8451-6
CRC Press ISBN-10: 0-8493-8451-6
CRC Press order number: WP8451

The publishers' policy is to use permanent paper from mills that operate a sustainable forestry policy, and which has been manufactured from pulp which is processed using acid-free and elementary chlorine-free practices. Furthermore, the publishers ensure that the text paper and cover board used have met acceptable environmental accreditation standards.

Typeset by SNP Best-set Typesetter Ltd., Hong Kong
Printed by TJ International Limited, Padstow, Cornwall, England

Contents

Foreword *xv*
Preface *xvii*
Author contact details *xix*

1 Introduction 1

1.1 Fatigue strength assessment of welded joints 1
1.1.1 Present state of the art 1
1.1.2 Demands from industrial product development 2
1.2 Basic aspects of assessment procedures 3
1.2.1 Multitude of parameters governing fatigue failure 3
1.2.2 Global and local approaches of fatigue strength assessment 5
1.2.3 Complications of local approaches for welded joints 8
1.2.4 Survey of subject arrangement 10

2 Nominal stress approach for welded joints 13

2.1 Basic procedures 13
2.1.1 Principles of the nominal stress approach 13
2.1.2 Procedures for welded joints 13
2.2 Analysis tools 16
2.2.1 Books, compendia, guidelines and design codes 16
2.2.2 Basic formulae 16
2.2.3 Permissible stresses and design *S*–*N* curves 19
2.2.4 Influence of mean and residual stresses 23
2.2.5 Influence of stress multiaxiality 24
2.2.6 Influence of plate thickness, weld dressing and environment 27

2.2.7 Normalised *S–N* curves 28
2.2.8 Fatigue strength reduction factors 29

3 Structural stress or strain approach for seam-welded joints 33

3.1 Basic procedures 33
3.1.1 Principles of the structural stress or strain approach 33
3.1.2 Structural strain approach as proposed by Haibach 34
3.1.3 Hot spot structural stress approach for tubular joints 37
3.1.4 Hot spot structural stress approach for non-tubular joints 40
3.1.5 Alternative definitions of hot spot structural stress 40
3.1.6 Structural stress approach as proposed by Dong 41
3.1.7 Structural stress approach as proposed by Xiao–Yamada 43
3.1.8 Structural stress approach to weld root fatigue 44
3.2 Analysis tools – structural stress or strain evaluation 45
3.2.1 General survey and relevant guidelines 45
3.2.2 Evaluation of hot spot stresses in tubular joints 46
3.2.3 Evaluation of hot spot stresses in non-tubular joints 48
3.2.4 Specific rules for finite element modelling 51
3.2.5 Further variants of structural stress evaluation 55
3.2.6 Definition of structural stress concentration factors 57
3.2.7 Hot spot stress concentration factors for tubular joints 59
3.2.8 Hot spot stress concentration factors for non-tubular joints 61
3.3 Analysis tools – endurable structural stresses or strains 62
3.3.1 Endurable structural strains in the Haibach approach 62

3.3.2 Endurable hot spot stresses in tubular joints 62
3.3.3 Endurable hot spot stresses in non-tubular joints 65
3.3.4 Endurable structural stresses in the Dong and Xiao–Yamada approaches 68
3.3.5 Endurable multiaxial stresses or strains 70
3.3.6 Structural stress based assessment of weld root fatigue 73
3.4 Demonstration examples 81
3.4.1 Welded tubular and butt joints – structural strain approach 81
3.4.2 Welded tubular joints – various design guidelines 82
3.4.3 Welded bridge girder with cope holes 84
3.4.4 Welded joints in ship structures – weld toe fatigue 84
3.4.5 Welded joints in ship structures – weld root fatigue 89

4 Notch stress approach for seam-welded joints 91

4.1 Basic procedures 91
4.1.1 Principles and variants of the notch stress approach 91
4.1.2 Critical distance approach 94
4.1.3 Fictitious notch rounding approach 96
4.1.4 Modified notch rounding approach 101
4.1.5 Highly stressed volume approach 105
4.2 Analysis tools 105
4.2.1 General survey and assessment procedure 105
4.2.2 Notch stress analysis for welded joints 107
4.2.3 Notch stress concentration factors of welded joints 108
4.2.4 Fatigue notch factors of welded joints 121
4.2.5 Critical distance approach 125
4.2.6 Fictitious notch rounding approach – basic procedures 126
4.2.7 Fictitious notch rounding approach – refined procedures 131
4.2.8 Fictitious notch rounding approach – links to structural stresses 138
4.2.9 Modified notch rounding approach 143
4.2.10 Highly stressed volume approach 145

4.3 Demonstration examples 150
4.3.1 Welded vehicle frame corner 150
4.3.2 Web stiffener of welded I section girder 152
4.3.3 Stress relief groove in welded pressure vessel 155
4.3.4 End-to-shell joint of boiler 157
4.3.5 Stiffener-to-flange joint at ship frame corner 158
4.3.6 Girth butt welds of unusual manufacture 160
4.3.7 Tensile specimen with longitudinal attachment 161
4.3.8 Gusseted shell structure 163
4.3.9 Laser beam welded butt and cruciform joints 165
4.4 Design-related notch stress evaluations 166
4.4.1 Comparison of basic welded joint types 166
4.4.2 Comparison of basic weld loading modes 173
4.4.3 Effect of geometrical weld parameters 180
4.4.4 Typical application in design 186

5 Notch strain approach for seam-welded joints 191

5.1 Basic procedures 191
5.1.1 Principles of the notch strain approach 191
5.1.2 Early application of the approach 195
5.1.3 Comprehensive exposition of the approach 199
5.1.4 Further refinements of the approach 202
5.2 Analysis tools 202
5.2.1 Basic formulae in early applications 202
5.2.2 Basic formulae for wider application 206
5.2.3 Special formulae for multiaxial fatigue 212
5.2.4 Assessment procedure 213
5.3 Demonstration examples 214
5.3.1 Fatigue life of stress-relieved butt-welded joints 214
5.3.2 Fatigue life of butt-welded joints with residual stresses 217
5.3.3 Fatigue life of fillet-welded cruciform joints 221
5.3.4 Fatigue life of welded containment detail 224
5.3.5 Fatigue strength of welded tubular joint 227

6 Crack propagation approach for seam-welded joints 233

6.1 Basic procedures 233
6.1.1 Principles of the crack propagation approach 233
6.1.2 Peculiarities with seam-welded joints 235
6.1.3 Short-crack behaviour 237
6.1.4 Applications of the approach 240

6.2 Analysis tools 242
6.2.1 General survey and relevant references 242
6.2.2 Methods of stress intensity factor determination 243
6.2.3 Crack propagation equations 245
6.2.4 Crack propagation life 247
6.2.5 Stress intensity factors for welded joints 250
6.2.6 Crack shape and crack path 259
6.2.7 Material parameters of crack propagation 263
6.2.8 Initial and final crack size 267
6.2.9 Residual stress effects on crack propagation 268
6.2.10 Particular crack propagation approach 271
6.2.11 Refined crack propagation approach 275
6.3 Demonstration examples 279
6.3.1 Longitudinal and transverse attachment joints 279
6.3.2 Cruciform and T-joints 281
6.3.3 Lap joints and cover plate joints 286
6.3.4 Butt-welded joints 287
6.3.5 Refined analysis of longitudinal attachment joint 292

7 Notch stress intensity approach for seam-welded joints 296

7.1 General considerations 296
7.1.1 Formal aspects of presentation 296
7.1.2 Principles and variants of the approach 296
7.2 Basic procedures and results 297
7.2.1 Notch stress intensity at sharp corner notches 297
7.2.2 Notch stress intensity at blunt corner notches 301
7.2.3 Plastic notch stress intensity at corner notches 304
7.2.4 *J*-integral at corner notches 307
7.2.5 Strain energy density at corner notches 308
7.2.6 Fatigue limit expressed by notch stress intensity factors 310
7.3 Procedures and results for fillet-welded joints 313
7.3.1 Notch stress intensity factors for fillet-welded joints 313
7.3.2 Stress rise in front of fillet welds 317
7.3.3 Endurable notch stress intensity factors of fillet-welded joints 319

7.3.4 Endurable corner notch *J*-integral of fillet-welded joints 321
7.3.5 Endurable corner notch strain energy density of fillet-welded joints 322
7.3.6 Link to the crack propagation approach 323
7.3.7 Link to the hot spot structural stress approach 326
7.4 Weak points and potential of the approach 332

8 Local approaches applied to a seam-welded tubular joint 334

8.1 Subject matter of investigation 334
8.2 Application of the structural stress or strain approach 336
8.2.1 Structural stress analysis and strain measurement 336
8.2.2 Comparison of structural stress concentration factors 340
8.2.3 Fatigue test results in terms of hot spot stress 343
8.3 Application of the elastic notch stress approach 345
8.4 Application of the elastic-plastic notch strain approach 348
8.4.1 Notch stress and strain concentration at weld toe 348
8.4.2 Fatigue strength assessment based on notch strains 351
8.5 Application of the crack propagation approach 355
8.5.1 Basic crack propagation models 355
8.5.2 Crack propagation life according to EU Report 358
8.5.3 Crack propagation life according to British Standard 362
8.6 Method-related conclusions 363

9 Structural stress or strain approach for spot-welded and similar lap joints 366

9.1 Basic procedures 366
9.1.1 Significance of fatigue assessment of spot-welded and similar lap joints 366
9.1.2 Principles of the structural stress approach 367
9.1.3 Weak points of the structural stress approach 371
9.1.4 Application of the structural stress approach 372

9.2 Analysis tools – structural stress or strain evaluation 373
9.2.1 General survey 373
9.2.2 Modelling of weld spot resultant forces 373
9.2.3 Computation and decomposition of weld spot resultant forces 376
9.2.4 General theory of forces and stresses at weld spots 380
9.2.5 Structural stress analysis at weld spots 382
9.2.6 Nominal structural stress in plate at weld spot 383
9.2.7 Nominal structural stress in nugget at weld spot 388
9.2.8 Structural strain measurement at weld spots 389
9.2.9 Weld spot forces by correlation of strain patterns 392
9.3 Analysis tools – non-linear structural behaviour 393
9.3.1 Elastic-plastic deformation at weld spots 393
9.3.2 Large deflections at weld spots subjected to tensile-shear loading 395
9.3.3 Large deflections at weld spots subjected to cross-tension loading 398
9.3.4 Buckling fatigue at spot welds 400
9.4 Analysis tools – endurable structural stresses or strains 405
9.4.1 Endurable structural stresses or strains at weld spots compiled by Radaj 405
9.4.2 Endurable structural stresses at weld spots compiled by Rupp 411
9.4.3 Endurable structural stresses at weld spots compiled by Maddox 417
9.4.4 Endurable structural stresses at laser beam welds in comparison 417
9.4.5 Endurable structural stresses at GMA welds 420
9.4.6 Computer codes for fatigue assessment at weld spots 426
9.4.7 Fatigue life assessment supporting car body design 427
9.5 Demonstration examples 429
9.5.1 Spot-welded axle suspension arm 429
9.5.2 Spot-welded engine support member 430
9.5.3 Laser beam welded pillar-to-rocker connection 432

10 Stress intensity approach for spot-welded and similar lap joints 433

10.1 Basic procedures 433
10.1.1 Principles of the stress intensity approach 433
10.1.2 Weak points of the stress intensity approach 436
10.1.3 Links to other approaches and application relevance 442
10.2 Analysis tools – evaluation of stress intensity factors 443
10.2.1 General survey and basic definitions 443
10.2.2 Stress intensity factors of lap joints based on structural stresses 447
10.2.3 Stress intensity factors of lap joints with unequal plate thickness 453
10.2.4 Stress intensity factors of lap joints in dissimilar materials 457
10.2.5 Stress intensity factors of lap joints under large deflections 459
10.2.6 Early stress intensity factor solutions for lap joints 461
10.2.7 Stress intensity factor formulae based on nominal structural stresses 465
10.2.8 Links to the notch stress approach 467
10.3 Analysis tools – fatigue assessment based on stress intensity factors 471
10.3.1 Endurable stress intensity factors 471
10.3.2 Equivalent stress intensity factors under mixed mode conditions 476
10.3.3 *J*-integral and nugget rotation variants 482
10.4 Comparative evaluation of spot-welded and similar specimens 483
10.4.1 General survey 483
10.4.2 Spot-welded tensile-shear specimens 486
10.4.3 Spot-welded cross-tension and peel-tension specimens 490
10.4.4 Spot-welded hat section specimens 493
10.4.5 Spot-welded H-shaped specimens 501
10.4.6 Spot-welded double-cup specimens 507
10.4.7 Laser beam-welded tensile-shear and peel-tension specimens 510

11 Notch- and crack-based approaches for spot-welded and similar lap joints 513

11.1 Basic procedures 513
11.1.1 Principles of the notch stress, notch strain and crack propagation approaches 513
11.1.2 Weak points and potential of the notch stress approach 517
11.1.3 Weak points and potential of the notch strain approach 518
11.1.4 Weak points and potential of the crack propagation approach 522
11.2 Analysis tools 524
11.2.1 Fatigue assessment through conventional notch stress approach 524
11.2.2 Fatigue assessment through improved notch stress approach 527
11.2.3 Fatigue assessment through notch strain approach 531
11.2.4 Fatigue assessment through simplified small-size notch approach 535
11.2.5 Fatigue assessment through crack propagation approach 538
11.2.6 Residual stress distribution in spot-welded joints 542
11.2.7 Hardness distribution in spot-welded joints 547
11.3 Comprehensive modelling examples 550
11.3.1 General survey 550
11.3.2 Modelling examples presented by Lawrence 551
11.3.3 Modelling examples presented by Sheppard 556
11.3.4 Modelling examples presented by Henrysson 559
11.3.5 Modelling example presented by Nykänen 566

12 Significance, limitations and potential of local approaches 568

12.1 Significance of local approaches 568
12.2 Limitations of local approaches 570
12.3 Potential of local approaches 576

Bibliography *579*
Index *635*

Foreword

Fatigue design of welded components and structures is normally based on *S–N* curves, often contained in official codes or standards. Such *S–N* curves are usually derived from published test data obtained from fatigue tests on representative welded specimens and expressed in terms of nominal stress. However, there are important limitations to this approach that can be addressed using local approaches.

Perhaps the most important limitation arises from the rapidly increasing use, by a wide range of industries, of detailed stress analysis (e.g. finite element analysis) in design. The distinction between nominal and local stresses is not always clear, but an alternative design approach based on structural stress allows better utilisation of modern stress analysis methods. Other limitations prompt the need for ways of modelling the fatigue process, rather than simply relating applied stress and fatigue life as in the *S–N* curve. In particular, there is little scope for allowing for differences (e.g. geometry, welding process, material, defects) between the weld detail under consideration and those tested to generate the *S–N* curve. Furthermore, no information is provided by the *S–N* curve about the progress of fatigue damage, only the total fatigue life is presented. Local approaches based on the notch stress (or local strain) method and/or fracture mechanics attempt to model the whole fatigue process by considering the influence of all significant parameters.

The first edition of this book presented a systematic survey of the various local approaches to the fatigue assessment of weld details, including the basis of each method, background research, development and practical applications. That survey has been updated and built on in this second edition, with particular attention to the important new research done to develop the structural hot spot stress, notch stress and crack propagation approaches. Of special value is the increased coverage of the application of local approaches in the assessment of joints in thin-sheet structural components. The addition of Wolfgang Fricke as author, with his extensive experience of the fatigue design and performance of ships and other large

welded structures, complements the already wide experience Dieter Radaj and Morris Sonsino bring from the automotive, offshore, aircraft and mechanical engineering industries. The resulting authoritative new book provides a valuable aid to designers of fatigue-loaded welded structures from any industry, to broaden their design capabilities beyond the use of basic *S–N* curves, but also to prepare them for the inevitable changes to come in current fatigue design standards. It will also help teachers and those concerned with fatigue R&D who need a broad overview of modern fatigue assessment methods and significant published work.

Stephen Maddox
Chairman, Commission XIII, International Institute of Welding

Preface

In the interval of nearly one decade since publication of the first edition of *Fatigue assessment of welded joints by local approaches* substantial progress has been achieved in methods development and application of local approaches. Structural strength and durability assessment based on these approaches have become a vital part of design verification and optimisation, especially in combination with finite element analysis. Welded joints are of primary concern within these assessments because fatigue failures originate mostly from these areas of geometric and material discontinuity.

The task of the first edition was to review the available knowledge on local approaches to the fatigue assessment of welded joints, to gather the data necessary for their practical application and to demonstrate the power of the local concept by way of demonstration examples from research and industry. It covered the hot spot structural stress approach, the elastic notch stress and elastic-plastic notch strain approaches describing crack initiation, and the fracture mechanics approach covering crack propagation. Seam-welded and spot-welded joints in structural steels and aluminium alloys were mainly considered.

The task of the second edition is to add new developments and applications while tightening up the older material. Progress has been tremendous during the last decade, the number of references considered in the book jumping up to nearly one thousand. These developments were set off by increasing demands in automobile design, ocean engineering and shipbuilding among other fields of application. Major method extensions refer to the hot spot structural stress approach, to the notch stress or strain concept with very small notch radius applicable to thin-sheet structural components and to the crack propagation methods. The notch stress intensity factor approach with application to seam-welded joints is now discussed as a new assessment method. The chapters of the book are rearranged, the first part of the book comprising seam-welded joints, the second part spot-welded and similar lap joints. The second edition is completely reworked.

The cooperation of three authors in doing this guarantees a versatile and balanced presentation.

The book is intended for designers, structural analysts and testing engineers who are responsible for the fatigue-resistant in-service behaviour of welded structures. It should become a reference work for researchers in the field, and it should support activities directed to standardisation of local approaches. Last but not least, it should give guidance to those students and experts who want to know more about the theoretical background and experimental confirmation of these methods. This book on fatigue assessment of welded joints supplements the first author's German work *Ermüdungsfestigkeit* covering the fundamentals of fatigue of non-welded materials and structural components.

The authors wish to express their sincere thanks to Steve Maddox, Chairman of Commission XIII 'Fatigue behaviour of welded components and structures' in the International Institute of Welding (IIW), for his appreciative foreword. They gratefully acknowledge the support given by the following colleagues in the correct presentation of some data in the second edition: Pingsha Dong, Hans-Fredrik Henrysson, Adolf Hobbacher and Paolo Lazzarin. The last-mentioned scientist has comprehensively supported the expositions on the notch stress intensity approach for seam-welded joints.

The many insertions into the manuscript of the second edition were put into a well-executed typescript by Claudia Raschke whose effective service facilitated the authors' tasks substantially. The graphical artwork added to the second edition was prepared with great skill by Herbert Jäger. The authors are greatly indebted to these two persons.

It has been a pleasure working with Woodhead Publishing and the copy-editor, Marilyn Grant, who converted the complex reworked manuscript into a handbook of high quality.

Dieter Radaj, Cetin Morris Sonsino and Wolfgang Fricke

Author contact details

Prof Dr-Ing Dieter Radaj, fax: +49 (0)711 440 3163

Prof Dr-Ing Cetin Morris Sonsino, email: c.m.sonsino@lbf.fraunhofer.de

Prof Dr-Ing Wolfgang Fricke, email: w.fricke@tu-harburg.de

1
Introduction

1.1 Fatigue strength assessment of welded joints

1.1.1 Present state of the art

Fatigue failure of structural members, comprising crack initiation, crack propagation and final fracture is an extremely localised process in respect of its origin. Therefore, the local parameters of geometry, loading and material have a major influence on the fatigue strength and service life of structural members. They must be taken into account as close to reality as possible when performing fatigue strength assessments and especially so when optimising the design in respect of fatigue resistance.

Design rules for fatigue-resistant structures, on the other hand, take local effects only roughly into account. They are based mainly on the nominal stress approach, which is a global concept in principle. The permissible nominal stresses depend on the 'notch class', 'detail class' or 'fatigue class' (FAT) of the welded joint being considered. They are supplemented by general design recommendations.

The code-related state of the art is unsatisfactory in those fields of engineering where structural members are subjected to fatigue-relevant variable load amplitudes with appreciable numbers of cycles or where nominal stresses cannot be meaningfully defined. Local concepts are applied in these areas based on local strain measurements, mainly by strain gauges, and by local stress calculations mainly based on the finite element method. Both the testing engineer and the structural analyst urgently need well-founded methods for evaluating these local stresses and strains in respect of fatigue strength and service life.

These needs can be met only insufficiently if at all. The multitude of proposals on how to assess the fatigue resistance of structural members based on local parameters is difficult to overview and evaluate.[1] Different fields of engineering, 'schools' of researchers and national communities prefer different approaches. All proposals are more or less incomplete in respect of user demands, and the local parameter data, for the most part, lack

statistical proof. As a result, the application of local approaches lags behind the possibilities provided by computerised structural analysis.

1.1.2 Demands from industrial product development

The demands originating from industrial product development concerning local approaches are twofold:

- An overview covering methods and data available for application is needed.
- Standardisation of the procedures and their incorporation into design codes are required.

This book is intended mainly to satisfy the first demand. Industrial users should obtain all the available information so that they can decide on the best way to treat their individual fatigue problems on the basis of local approaches. They must then supplement the information available from the book and the quoted literature by their own empirical and experimental data.

The second demand can only partly be satisfied. There is no generally acknowledged theory of local fatigue strength available on which a uniform analytical scheme could be based. On the one hand there are manifold procedural variants and data sets and on the other hand there are innumerable fatigue problems in industry. Any general standardisation of the local approaches would interfere with the development of further methods, which must always be adapted to the application being considered. Only carefully selected parts of the procedure are suited to standardisation or at least to defining a guideline. Substantial progress with regard to the standardisation of analytical strength assessments based on local stresses (structural or notch stresses) has been achieved by the IIW recommendations[3] and by the FKM guideline.[1]

The subjects in this book are restricted to welded joints, which are of paramount economic relevance. Additionally, welded joints show peculiarities in respect of fatigue behaviour which make a separate treatment of the fatigue assessment methods desirable. Finally, part of the local approaches has been developed for welded joints independently of the methods developed for non-welded members. Restriction to welded joints is therefore well justified.

The following books give additional guidance on fatigue assessment of welded joints by local approaches: Haibach[2] (in-service fatigue strength, highly related to design, emphasis on analysis and statistics) and Radaj[4] (also related to design, covers early stage of development of local approaches). The contribution by Seeger[8] in a more general handbook lays emphasis on assessment methods with inclusion of variable-amplitude and

multiaxial loading conditions. The fundamentals of the analysis of fatigue strength and its application to non-welded members are presented in books by Haibach,[2] Dowling[951] and Radaj.[6] The analysis of welding residual stresses and distortion is found in Radaj's book.[7]

1.2 Basic aspects of assessment procedures

1.2.1 Multitude of parameters governing fatigue failure

The local approaches to fatigue assessment reviewed in this book aim to cover the dominating parameters of extremely complex physical processes in order to make them controllable by the engineer. These processes comprise primarily microstructural phenomena (moving dislocations, micro-crack initiation on slip bands and further crack growth by local slip mechanisms at the crack tip) but can be approximately described by a macroscopic elastic or elastic-plastic stress and strain analysis according to continuum mechanics which refers to the cyclic deformation causing initiation and propagation of the 'technical crack' with inclusion of the final fracture, Fig. 1.1. A technical crack is considered to have been initiated (usually at the surface) if its surface length reaches values which can be detected by common technical means, e.g. 1 mm, and its depth 0.5 mm.

The initiation of the technical crack by cyclic loading under definite local material conditions is primarily governed by the amplitudes of the cyclic stress and strain components at the notch root, with the volume of the highly stressed material, the multiaxiality of the cyclic stress state and its static mean value (possibly fluctuating) also being of importance. The total number of parameters influencing the critical values of the cyclic stress and strain components which describe crack initiation are summarised in Table 1.1 which refers to the local approach insofar as local stresses and strains are introduced to characterise the loading type. The number of influencing parameters is large, but can be handled within the procedure of strength assessment. However, a problem arises from the restricted possibilities of decoupling the effects of these influencing parameters in the case of engineering tasks.

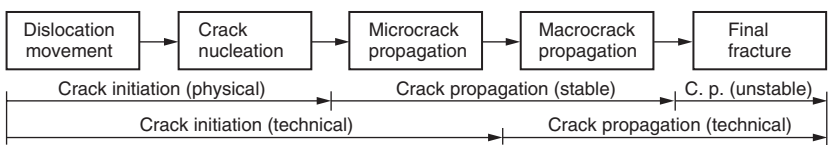


Fig. 1.1. Micro- and macrophenomena of material fatigue.

Table 1.1. Parameters governing fatigue crack initiation; after Radaj[5]

Structural member	Surface	Material
Shape	Roughness	Type
Size	Hardness	Alloy
Dimensions	Residual stress	Microstructure
Loading type	**Loading course**	**Environment**
Stress amplitude	Amplitude spectrum	Temperature
Mean stress including residual stress	Amplitude sequence	Corrosion
Multiaxiality including phase angle	Rest periods	

Crack propagation by cyclic loading is primarily governed by the amplitudes of the cyclic stress intensity factor or of the cyclic *J*-integral at the crack tip. Most of the parameters which determine the critical value of stress, strain or energy at the crack tip causing crack propagation are identical to those which cause crack initiation. Only the influence of the surface diminishes whereas crack shape, crack size and crack path gain in importance.

The multitude of parameter constellations governing fatigue are advantageously structured according to Haibach,[2] based on the main testing and analysis procedures used to obtain the above-mentioned critical values for fatigue strength or service life assessments, Fig. 1.2.

The description of fatigue strength proceeds from the *S*–*N* curve (nominal stress amplitude versus number of cycles) of the unnotched specimen (a). The *S*–*N* curve of the notched specimen (b) is gained therefrom by considering the stress concentration factor and the notch radius. Finally, the *S*–*N* curve of the structural component (c) results from additionally considering size and surface effects (including residual stresses). This path a–b–c or e–f–g is connected with the problem of strength dependent on shape and size (German idiom 'Gestaltfestigkeit'). On the other hand, the fatigue life curve resulting from variable-amplitude loading can be derived from the *S*–*N* curve resulting from constant-amplitude loading by introducing a damage accumulation hypothesis. This is the path a–e, b–f or c–g from conventional fatigue strength to service fatigue strength. The problem of damage accumulation can be partly solved by determining the fatigue life curve of the notched specimen under standard load sequences, path d–f–g instead of c–g.

The structuring of the parameter field and procedures mentioned above does not mean that every fatigue strength assessment starts with the *S*–*N* curve of the unnotched specimen and ends with the life curve of the struc-

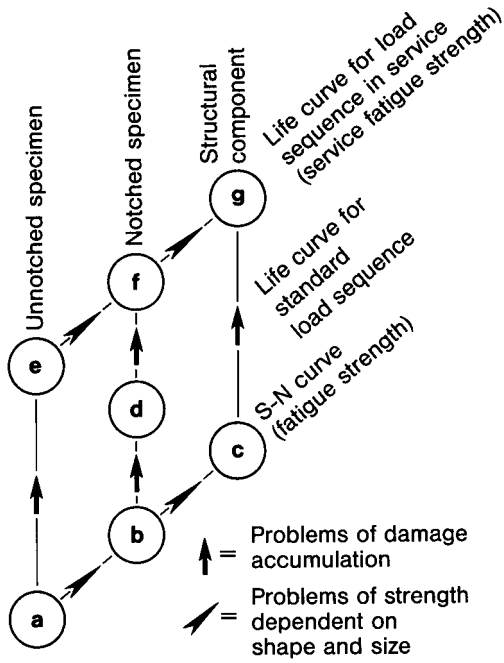


Fig. 1.2. Field of parameter constellations governing fatigue failure, structured on the basis of the main testing and analysis procedures; after Haibach.[2]

tural component. Actually, the *S–N* curve of the component is often gained proceeding from the *S–N* curve of the notched specimen. Also, the life curves of structural components are mostly determined without reference to specimen testing.

1.2.2 Global and local approaches of fatigue strength assessment

Strength assessments comprise the explicit or implicit comparison of loads, stresses or strains with their critical values, which cause a defined damage, a definite deformation, an incipient technical crack or total fracture. The loads comprise forces and moments, the stresses and strains are of the nominal, structural or notch type, and stress intensity factors and the *J*-integral are derived therefrom. The critical values are designated as strength values. The stresses and strains follow from the forces and moments according to continuum theories, that is, mainly according to elasticity and plasticity theory. The strength values are determined from loading tests using simple specimens, component-like specimens or the component itself.

Considering the fatigue strength, the constant-amplitude test, the variable-amplitude test and the corresponding crack propagation test are the most important. The assessment of fatigue strength is also performed in such a manner that the specimen or component life is determined at given load values instead of the strength at preset numbers of cycles. The former procedure is in agreement with the prevailing kind of fatigue test evaluation (number of cycles dependent on load amplitude).

Strength assessments are termed 'global approaches' if they proceed directly from the external forces and moments or from the nominal stresses in the critical cross-section derived therefrom, under the assumption of a constant or linearised stress distribution (therefore 'nominal stress approach'). The global approaches originally use critical values of load or nominal stress which are related to global phenomena, such as fully plastic yielding or total fracture of the specimen.

Strength assessments are termed 'local approaches' if they proceed from local stress or strain parameters. The local processes of damage by material fatigue are considered, that is, cyclic crack initiation, cyclic crack propagation and final fracture. Crack initiation is covered by the 'notch stress approach' or 'notch strain approach' which are based on the stresses or strains at the notch root (or at comparable regions of stress concentration). Crack propagation and final fracture, on the other hand, are described by the 'crack propagation approach' which proceeds from an existing incipient crack. The strength assessment according to the complete local approach therefore consists of the notch stress or notch strain approach, and the crack propagation approach. An approach acting as a link between the global and local concepts is the 'structural stress approach', Fig. 1.3, which reflects the stress concentrations originating from the macrogeometry, while the notch effect of the weld is implicitly taken into account by lowering the S–N curve.

Different variants of the local approach can be distinguished according to the local stress or strain parameters chosen and the type of failure criteria introduced. The most important basic variants of the global and local approach are shown in Fig. 1.4, each variant characterised by the typical load, stress or strain parameter and the corresponding strength diagram. The local parameters result from the global parameters proceeding from the left-hand side to the right-hand side of the graph by increasingly taking local conditions into account. The following strength diagrams are presented: external force F–N curve, nominal stress S–N curves for standard notch or detail classes, structural stress S–N curve, notch stress and notch strain S–N curves, Kitagawa diagram (fatigue-critical stress range plotted versus the depth of short cracks) and crack propagation rate $\mathrm{d}a/\mathrm{d}N$ plotted versus the stress intensity factor range ΔK of longer cracks. The latter diagram may be supplemented by the stress intensity factor K–N curve

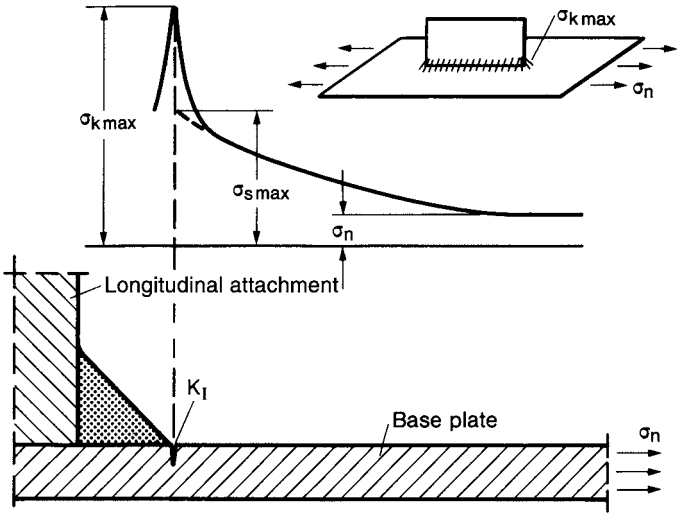


Fig. 1.3. Maximum structural stress $\sigma_{s\,max}$ constituting the link between nominal stress σ_n and maximum notch stress $\sigma_{k\,max}$ illustrated by the example of a single-side fillet-welded longitudinal attachment; stress intensity factor K_I initially dependent on maximum notch stress; superposition principle in the elastic range: $K_I \propto \sigma_{k\,max} \propto \sigma_{s\,max} \propto \sigma_n$.

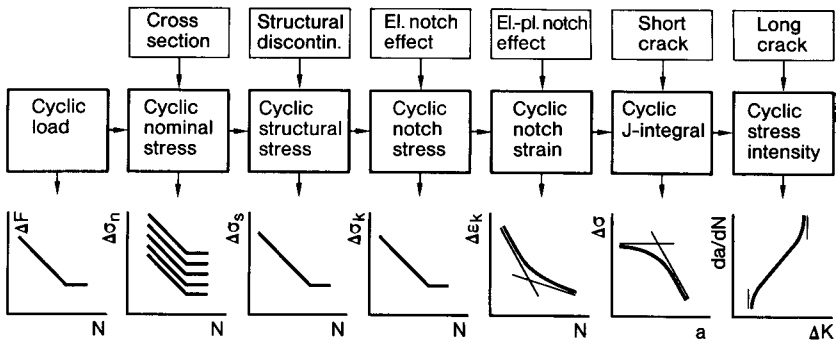


Fig. 1.4. Global and local approaches for describing fatigue strength and fatigue life, cyclic parameters and strength diagrams; el. meaning 'elastic' and el.pl. meaning 'elastic-plastic'; with ΔF cyclic load, $\Delta\sigma_n$ cyclic nominal stress, $\Delta\sigma_s$ cyclic structural stress, $\Delta\sigma_k$ cyclic notch stress, $\Delta\varepsilon_k$ cyclic notch strain, $\Delta\sigma$ cyclic stress at crack tip, da/dN crack propagation rate, N number of cycles to failure, a crack length and ΔK cyclic stress intensity factor; notch stress intensity approach to be supplemented.

which can be derived in special cases. The more recently developed notch stress intensity approach may be seen as being closely related to the notch stress, notch strain and fracture mechanics approaches, despite being a concept in its own right.

As can be seen from the above, the technical term '*S–N* curve' designates the fatigue strength versus number of cycles. The fatigue strength is expressed by nominal stress amplitudes or nominal stress ranges ('cyclic nominal stresses') as usual or by relevant structural stresses, notch stresses or notch strains. Also other load parameters such as forces, moments, (notch) stress intensity factors, *J*-integrals or damage parameters may be introduced resulting in the corresponding curves.

The global approach, which even today is basic in most fatigue-related applications, designates the beginning of research and development aimed at fatigue-resistant designs. The local approaches evolved from the global approach insofar as the local consideration related to the local fatigue phenomena supplements and extends the global approach, at first without claiming independent usage. Considering the history, the local approach received the following essential development impulses:

- evaluation of fracture surfaces (fatigue fracture versus static final fracture): clam shell markings, notch effect (1850);
- measuring techniques for local stresses and strains (photoelasticity since 1930, inductive strain gauge with short measuring length since 1950, small-scale resistance strain gauges since 1965);
- application of the notch stress theory (first edition of Neuber's book in 1937, Neuber's macrostructural support formula published in 1960);
- application of fracture mechanics (Paris equation for crack propagation published in 1963);
- application of the finite element method in structural design based on appropriate computer technology (since 1970);
- application of short crack fracture mechanics (since 1990);
- application of notch stress intensity factors (since 1995).

At first, researchers from the United States were prominent in the application-related development of the local approach (e.g. application of the Neuber formula and of the Paris equation). The starting point was the low-cycle fatigue strength at elevated temperatures. At about the same time, the high-cycle fatigue strength was considered under local aspects (e.g. fatigue notch factors) mainly by researchers in Germany. Later on, efforts to substantiate the local approaches continued in Germany and also in Italy. The structural stress approach was promoted by international efforts. The extensive literature dealing with the local approach in general, confined to non-welded materials and structures, has been compiled by Radaj.[6]

1.2.3 Complications of local approaches for welded joints

Welded joints show several peculiarities that complicate the local approaches which are rather complex even in the case of non-welded

members. This statement holds true at least as far as an attempt is made to take all the details into account which are of relevance in respect of fatigue. The peculiarities can be subdivided into inhomogeneous material, welding defects and imperfections, welding residual stresses and distortions as well as the geometric weld characteristics. They often remain unconsidered in the local approaches. In general, the material characteristic values of the base material are used, the effect of residual stresses is only roughly taken into account and the worst case of the geometric weld parameters is considered. Welding defects and imperfections are individually taken into account within the local approach based on a worst case scenario.

Inhomogeneous material is characteristic of welded joints. The filler material added to the base material is of similar type in general but specifically alloyed in order to achieve a high quality of manufacture, for example, in respect of the transfer of droplets, the weld pool shape and the suppression of hot cracking. The filler material mixes with the parent material in the weld pool while individual alloying elements may be burned or evaporated and other elements may intrude from the ambient atmosphere or materials. Micropores may occur if the evaporation is impeded and microseparations are fostered if the material is susceptible to hot cracking. Microinclusions may vary in respect of type and number. Such irregularities may especially occur in the areas of the weld toe and weld root. The heat-affected zone adjacent to the weld pool shows different microstructures according to the thermal cycles experienced. These are characterised by different grain sizes and hardness values resulting in locally different yield limits, crack initiation strengths and crack propagation resistances. Only part of the above problems is removed in cases of welding without filler material.

Welding defects and imperfections typical of welded joints are, for example, cracks, pores, cavities, undercuts, lack of fusion, overlap, inadequate penetration and burn through holes. They are taken into account within the nominal stress approach by the concept of quality classes. The permissible nominal stress depends on the quality class. The local approaches on the other hand evaluate each defect or imperfection individually, as mentioned above.

Welding residual stress and distortions are another characteristic of welded joints. Welding is generally performed by melting the surfaces of the parts to be joined, together with the filler material, using a concentrated heat source. The subsequent rapid cooling produces residual stresses and distortions via thermal strains and microstructural transformation (Radaj[7]). These welding residual stresses may reach the yield limit in the weld area and decrease sharply in its neighbourhood. They have a generally low level outside the weld area, but produce local stress concentrations at notches. These welding residual stresses are generally reduced by cyclic loading or

changed in a favourable manner if the ductility of the material is adequately high and the cyclic loading sufficiently severe. The high-cycle fatigue strength of welded joints is changed by the effect of residual stresses. This is the case not only in respect of unfavourable tensile residual stresses produced by welding but also in respect of favourable compressive residual stresses produced by postweld treatment. The welding distortions give rise to secondary stresses under external loading of welded joints which may be large especially in thin-walled structural members.

The geometric weld characteristics are partly undefined and often greatly scattering. For example, the radius of curvature at the weld toe or weld root and the slope of the weld contour near the weld toe (alternatively the amount of weld reinforcement) are variable within a large scatter range. The same holds true for the amount of burn-in of seam welds or for the joint face diameter of spot welds. These geometric parameters of welded joints depend on the type and setting of the welding process, on the welded materials, on the plate thickness, and on the margin of tolerance when positioning the structural components to be joined which may produce misalignments and gaps. The geometric weld characteristics can be determined precisely, at least to some extent. The weld toe geometry may be recorded using external casting techniques or profile measurements. The seam weld root or spot weld edge may be made visible after transverse cutting and polishing.

1.2.4 Survey of subject arrangement

The methods of fatigue strength assessment of welded joints based on local parameters are difficult to subdivide and generalise for the purpose of a comprehensive survey. The variety of procedural variants is large. Every author in the field uses his own special combination of methods and procedural steps. The procedural steps change to some extent with progress in the science. The range of applicability is always restricted. There is no general theory of the local approaches available or possible but there have been special procedures developed for definite tasks with limited transferability. Therefore, the subject arrangement in this book closely follows the main contributions in the field without neglecting the task of connecting and harmonising the different approaches.

The book is subdivided into 12 chapters. The local approaches related to seam-welded joints are presented in Chapers 3–8, those related to spot-welded joints in Chapters 9–11. The well-established non-local but basic nominal stress approach is summarised in Chapter 2. The introduction and conclusions make up Chapters 1 and 12.

Chapter 3 describes the (hot spot) structural stress or strain approach applied to seam-welded joints. The fatigue strength is assessed on the basis

of the structural stresses or strains at the 'hot spot' in front of the weld toe. The notch effect of the weld toe is not explicitly considered.

Chapter 4 describes the notch stress approach applied to seam-welded joints. The (technical) fatigue limit is assessed on the basis of fatigue-effective notch stress amplitudes gained from an elastic notch stress analysis. The assessment refers to total fracture of the welded joints.

Chapter 5 describes the notch strain approach applied to seam-welded joints. The fatigue life or strength is assessed on the basis of the notch strain amplitudes gained from an elastic-plastic notch stress and strain analysis. The assessment refers to the initiation of a technical crack (crack depth approximately 0.5 mm). The notch strain approach is supplemented by a crack propagation analysis in the case of finite life considerations. Both approaches together constitute the basis of the total life assessment.

Chapter 6 describes the crack propagation approach applied to seam-welded joints. The fatigue life is assessed on the basis of the simplified macrocrack propagation analysis formally extended into the microcrack range, starting with assumed microcracks and ending with cracks penetrating the wall thickness. The notch stresses initially and the structural stresses further on are the basis for the stress intensity factors needed for the crack propagation analysis.

Chapter 7 describes the more recently developed notch stress intensity approach applied to seam-welded joints. The fatigue strength or life is assessed on the basis of the notch stress intensity factor amplitudes (or of the locally averaged strain energy density amplitudes) at the weld toe, which is considered to be a corner notch. The assessment refers typically to crack initiation, but is extended to total fracture fatigue data. Links to the (hot spot) structural stress approach and to the crack propagation approach are established.

Chapter 8 describes the comparative application of the different approaches (structural stress, notch stress, notch strain and crack propagation approach) to a seam-welded tubular joint, with the inclusion of experimental data.

Chapter 9 describes the structural stress or strain approach applied to spot-welded and similar lap joints. The fatigue strength is assessed on the basis of the (hot spot) structural stresses or strains at the weld spot edge. The notch effect of the weld spot edge is not explicitly considered. The assessment refers to cracks penetrating the plate thickness in general.

Chapter 10 describes the stress intensity approach applied to spot-welded and similar joints. The fatigue strength is assessed on the basis of the stress intensity factor amplitudes at the sharp edge notch of the weld spot, gained from an elastic analysis. The assessment refers mainly to cracks penetrating the plate thickness.

Chapter 11 describes the notch stress or strain and crack propagation approaches applied to spot-welded and similar lap joints. The assessment procedures are only roughly similar to those described with reference to seam-welded joints. The existence of an initial crack-like notch at the weld spot edge, the small plate thickness (thin sheet material) and the three-dimensional shape of the weld spots (contrary to a mainly two-dimensional shape in the case of seam welds) result in substantial differences in procedural details and associated data. The assessment refers mainly to cracks penetrating the plate thickness.

The material within the chapters is assigned to sections according to the following scheme, as far as possible. First, the basic procedures for non-welded members followed by the basic procedures for welded joints are described in a general and introductory manner. The analysis tools for executing the basic procedures (procedural details, formulae, data bases, computational aids) are presented next. Demonstration examples and (in two cases) design evaluations conclude the chapters.

The presentation scheme above could not be strictly implemented in all relevant chapters. Chapter 2, which considers the nominal stress approach, is restricted to basic information without demonstration examples. Chapter 8, which provides a comparison of the approaches, is naturally not subject to the above assignment scheme. Also Chapter 7, describing the notch stress intensity factor approach, does not comply with this scheme. Here, the fundamentals of this recently developed method are explained first, using non-welded members as examples. Then, the application to fillet-welded joints is demonstrated.

Chapters 9, 10 and 11, related to spot-welded joints, do not have an introductory section related to non-welded members since this information is already available in the corresponding chapters dealing with seam-welded joints. In Chapter 11, about the notch stress, notch strain and crack propagation approaches, the demonstration examples are substituted by comprehensive modelling examples with reference to the main contributors in the field.

2

Nominal stress approach for welded joints

2.1 Basic procedures

2.1.1 Principles of the nominal stress approach

The nominal stress approach for assessing the fatigue strength and service life (usually up to final fracture) of non-welded structural members proceeds from the nominal stress amplitudes in the critical cross-section and compares them with the *S*–*N* curve of the endurable nominal stress amplitudes, Fig. 2.1. The slope and scatter range of the *S*–*N* curve can be defined approximately based on the normalised *S*–*N* curve scheme if specific test data are not available. The nominal stress *S*–*N* curve comprises the influence of material, geometry (inclusive of notch and size effect) and surface (inclusive of hardening and residual stresses). The acting forces and moments can also be introduced directly into the diagram instead of the nominal stresses, an obvious choice in cases where nominal stresses cannot be meaningfully defined. The service life results from the nominal stress *S*–*N* curve and the nominal stress spectrum according to a simple hypothesis of damage accumulation, mostly according to a modified and relative form of Miner's rule. The nominal stress amplitude spectrum follows from the load amplitude spectrum taking the critical cross-section and the type of loading into account. The service life calculation is generally performed in respect of final fracture, but it can also be made in respect of crack initiation. The effects of loading sequence and overloading remain for the most part unconsidered if a load amplitude spectrum or a load amplitude matrix is taken as the basis. They can principally be taken into account, if the load–time function is available and the damage contributions are summed up cycle by cycle in the original sequence.

2.1.2 Procedures for welded joints

The nominal stress approach for assessing the fatigue strength and service life (usually up to final fracture) of welded joints proceeds in the same way

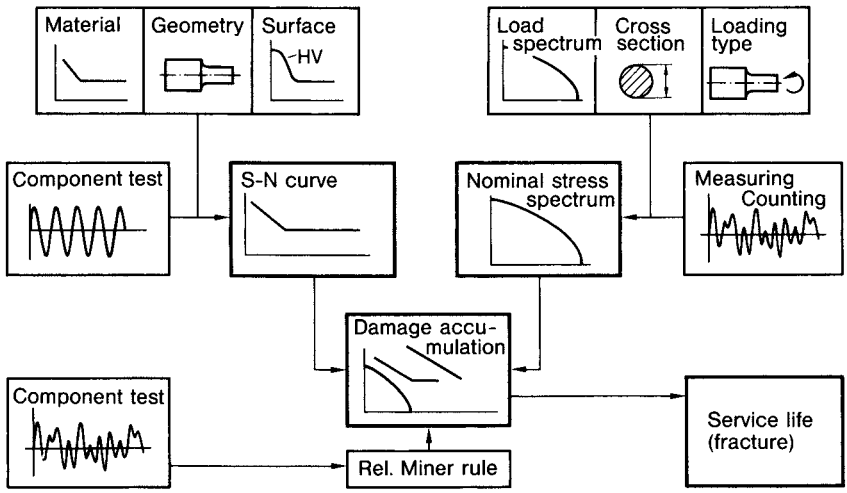


Fig. 2.1. Nominal stress approach for assessing the fatigue strength and service life of non-welded structural components; graph depicting main parameters and main procedural steps; after Kloos *et al.*[38]

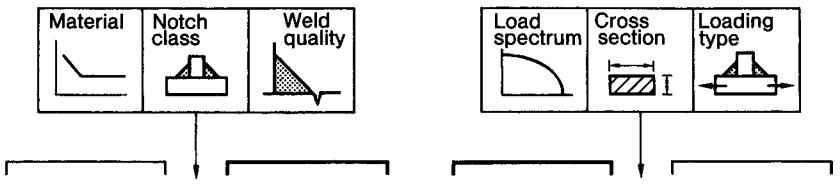


Fig. 2.2. Main parameters controlling the nominal stress approach for welded structures; see Fig. 2.1 for further parts of the graph.

as the approach for non-welded members. Only some of the main parameters that exert influence are introduced differently, Fig. 2.2. The nominal stress *S–N* curve is defined dependent on material, notch or detail class and weld quality class in the case of welded joints compared with the dependency on material, geometry and surface parameters in the case of non-welded members. The nominal stress is defined in the cross-section of the base plate, with one exception: partial penetration welds may be assessed on the basis of the nominal stresses (normal and shear components) in the throat section of the weld (named 'nominal weld stress').

Notch or detail classes on the one hand and weld quality classes on the other hand are assigned to sets of uniform design *S–N* curves which are generally linearised, parallelised and equidistantly positioned in logarithmic scales of the parameters *S* and *N*. The welded joints are graded

according to their shape, type of weld, type of loading and quality of manufacture. They are then allocated to the detail classes representing the design *S–N* curves based on the results of relevant fatigue tests. The German designation 'notch class' is only correct to the extent that the varying fatigue strength is caused by a varying notch effect. The English designation 'detail class' or 'fatigue class' (FAT) is more general.

The endurable or permissible nominal stress amplitudes are substantially reduced by high tensile residual stresses caused by welding. Such high tensile residual stresses may occur in large structural members in contrast to small test specimens. On the other hand, the reduced permissible stress amplitudes can be considered as no more dependent on the stress ratio R (defined without the residual stress). Stress-relieved welded joints or postweld-treated joints with compressive residual stresses in the critical area allow higher permissible stress amplitudes dependent on the stress ratio. Fatigue testing to determine permissible stress amplitudes in welded joints should generally be performed with high R-values ($R \geq 0.5$).

Another efficient means of defining endurable or permissible nominal stress amplitudes for fatigue-loaded welded joints is the normalised *S–N* curve defined with a uniform scatter band which is applicable to some extent independently of notch or detail class, stress ratio and steel or aluminium alloy type. Normalisation is achieved by referring the endurable stress amplitude σ_{nA}, to the technical endurance limit, σ_{nAE} ($P_f = 50\%$, $N = 2 \times 10^6$ cycles) under the condition of identical R-values. Not every *S–N* curve of a welded detail can be normalised in this way. Both the slope of the *S–N* curve and the number of cycles at the transition to the high-cycle fatigue range (knee point) may differ from the usual values. The slope actually depends on notch severity, extent of elastic-plastic support and crack propagation behaviour. Flatter than usual *S–N* curves are determined especially for full-size structural members, post-weld-treated joints and compressive-loaded specimens (Gimperlein[25]). Welded joints with high residual stresses may show a step in the *S–N* curve at the number of cycles where the residual stresses are relieved by increasing stress amplitudes (Radaj,[4] *ibid.* Fig. 42).

The nominal stress approach is the basis of fatigue assessment in many areas of mechanical and structural engineering such as the construction of bridges, cranes, vessels, pipes, rail vehicles and ships among others. The approach is incorporated in the relevant design codes. Only areas of engineering with exceptionally high demands for lightweight design and damage tolerance do completely without this approach, the preference being for local approaches: these areas are primarily automotive and aircraft engineering. The approach is supplemented or even substituted by the structural stress approach in the first-mentioned code-regulated areas especially in unconventional applications.

2.2 Analysis tools

2.2.1 Books, compendia, guidelines and design codes

The analysis tools supporting the nominal stress approach for welded joints are only briefly reviewed below because this book is dedicated to local approaches. Other publications and especially the relevant design codes should be consulted for application of the nominal stress approach.

Many books are available dealing with the fatigue strength of materials and structures (a comprehensive bibliography is presented by Radaj[6]). The topic of fatigue strength assessment is treated in more detail only in some of these publications. The reader is referred to Haibach,[2] Radaj[4,6] and Seeger,[8] as well as to Maddox,[43,45] Gurney,[26] Neumann[48,49] and Neumann and Hobbacher.[50] A concise overview of advanced procedures for vehicle safety components in aluminium alloys is given by Sonsino *et al*.[62] Compendia are available which present the published fatigue strength data for welded joints in structural steels[52] and aluminium alloys[32,33,39] based on a uniform statistical evaluation.

The nominal stress approach is basic to design guidelines and design codes, for example, British standards,[13–17] the ASME boiler and pressure vessel code,[10] IIW recommendations,[3,30,31] European recommendations and codes,[21–24] German standards[9,19,20,72] and one Japanese standard.[34] Guidelines for assessing the acceptability of flaws and imperfections (including fitness for purpose evaluations) are included in the references above.

2.2.2 Basic formulae

The nominal stress approach for welded joints made of steel or aluminium alloy is essentially based on formulae reviewed hereafter. These formulae are more or less identical to those used within the local approaches if the nominal stress or strain parameters are substituted by the corresponding local stress or strain parameters.

The explanations are given with reference to the medium-cycle *S–N* curve linearised in logarithmic scales:

$$\sigma_{nA} = \left(\frac{N_E}{N}\right)^{1/k} \sigma_{nAE} \qquad (N \le N_E) \tag{2.1}$$

where σ_{nA} is the nominal stress amplitude which is endurable at number of cycles N, and σ_{nAE} is the constant-amplitude endurance limit which is related to N_E ($N_E = 10^7$ cycles for normal stresses or $N_E = 10^8$ cycles for shear stresses according to the IIW recommendations[3]). Alternatively, the nominal stress range, $\Delta\sigma_n = 2\sigma_{nA}$ (with nominal stress amplitude σ_{nA}), may be introduced. Any other reference point on the linearly dropping part of

the *S–N* curve may be chosen instead of the endurance limit. A definite failure probability P_f is assigned to the considered *S–N* curve, e.g. $P_f = 50\%$. The gradient of the *S–N* curve is characterised by the inverse slope k (k = 3.0 for normal stresses or k = 5.0 for shear stresses according to the IIW recommendations[3]). The *S–N* curves are staggered according to the detail and quality classes (see Section 2.2.3).

In the low-cycle fatigue range, the static yield limit $\sigma_{Y0,2}$ is generally the limiting parameter for the fatigue strength, and in the high-cycle fatigue range the endurance limit σ_{nAE} has the same function. In both ranges, the limit stresses are independent of the number of cycles.

Some experts (Sonsino *et al.*[68]) point out that the *S–N* curve may take a further drop in the high-cycle fatigue range ($N > 10^7$) even under defined non-corrosive laboratory conditions (proposed inverse slope $k^* = 22$ corresponding to a decrease in fatigue strength of 10% per decade of cycles). The term 'technical endurance limit' as distinguished from the 'true endurance limit' at a higher number of cycles is used in the following in order to imply that a further drop of the *S–N* curve is not excluded. A commentary worth reading on whether the endurance limit 'really exists' can be found in Gurney's book (Gurney,[26] *ibid.* pp. 14–15).

It should be noted that the normal stresses above may be substituted by shear stresses under relevant conditions. The endurable stress amplitudes are correspondingly reduced in the latter case, with the consequence that a lower detail class is prescribed.

A scatter band of endurable values is associated with the *S–N* curve described by eq. (2.1). A Gaussian normal distribution in logarithmic scales is assumed within the scatter band. The characteristic parameters of the scatter band are the standard deviations s_σ and s_N relating to $\Delta\sigma_{nA}$ and N, respectively, and alternatively, the more application-related scatter range indices T_σ and T_N:

$$s_\sigma = \frac{1}{2.56}\log\frac{1}{T_\sigma} \tag{2.2}$$

$$s_N = \frac{1}{2.56}\log\frac{1}{T_N} \tag{2.3}$$

$$T_\sigma = \frac{\sigma_{nA10}}{\sigma_{nA90}} \tag{2.4}$$

$$T_N = \frac{N_{10}}{N_{90}} \tag{2.5}$$

where the endurable nominal stress amplitudes σ_{nA10} and σ_{nA90} and also the endurable number of cycles N_{10} and N_{90} refer to the failure probabilities $P_f = 10\%$ and $P_f = 90\%$, respectively.

The following relationship between the scatter range indices holds, based on eq. (2.1):

$$T_N = (T_\sigma)^k \tag{2.6}$$

The basic steps in proving the fatigue strength or life of welded structural members are the following. The actual nominal stress amplitude σ_{na} should not exceed the permissible nominal stress amplitude $\sigma_{na\ per}$ which is characterised by a definite acceptable failure probability, e.g. $P_f = 2.3\%$. The permissible amplitudes are derived from the endurable amplitudes, the latter referring to $P_f = 50\%$, by introduction of the safety factor j_σ which depends on the considered P_f value and the assumed scatter range index T_σ:

$$\sigma_{na} \le \sigma_{na\ per} \tag{2.7}$$

$$\sigma_{na\,per} = \frac{\sigma_{nA}}{j_\sigma} \tag{2.8}$$

Alternatively, permissible and endurable numbers of cycles, N_{per} and N_A, are related by the safety factor j_N:

$$N \le N_{per} \tag{2.9}$$

$$N_{per} = \frac{N_A}{j_N} \tag{2.10}$$

This is identical to using the endurable stress amplitude σ^*_{nA} at $N^*_A = j_N N_A$ cycles as the permissible stress amplitude at N_A in eq. (2.7).

The following relationship between the safety factors holds, based on eq. (2.1):

$$j_N = (j_\sigma)^k \tag{2.11}$$

The proof of fatigue strength of welded structural members under variable-amplitude loading, as opposed to constant-amplitude loading considered hitherto, proceeds from the service life S–N curve linearised in logarithmic scales. The probability of load amplitude occurrence, assumed to be normally distributed in the logarithmic scale, is additionally taken into account (Haibach,[2] Seeger[8]). The actual nominal stress amplitude $\bar{\sigma}_{na}$, with the occurance probability P_o, defined in the relevant design code (e.g. $P_o = 10\%$) should not exceed the permissible nominal stress amplitude $\bar{\sigma}_{na\ per}$ (with a definite failure probability, e.g. $P_f = 2.3\%$). The permissible amplitudes are derived from the endurable amplitudes by introducing the safety factor $\bar{j}_\sigma$ which is now a superposition of the partial factors j_r relating to fatigue resistance (or strength) and j_l relating to loading (or stress):

$$\bar{\sigma}_{na} \le \bar{\sigma}_{na\ per} \tag{2.12}$$

$$\overline{\sigma}_{\mathrm{na\,per}} = \frac{\overline{\sigma}_{\mathrm{nA}}}{\overline{j_\sigma}} \tag{2.13}$$

$$\overline{j_\sigma} = j_\mathrm{r} j_\mathrm{l} \tag{2.14}$$

In general, the service life curve considered as basic above will not be available from fatigue testing because of excessive costs. The proof of service fatigue strength must then be based on Miner's damage accumulation rule[385] (originally proposed by Palmgren, therefore often quoted as Palmgren–Miner's rule) proceeding from the number of load cycles n_i at level i compared with the number of cycles to failure N_fi on this level. The actual total damage D should not exceed the permissible total damage D_per:

$$D \le D_\mathrm{per} \tag{2.15}$$

$$D = \sum_{i=1}^{m} \frac{n_\mathrm{i}}{N_\mathrm{fi}} \tag{2.16}$$

$$D_\mathrm{per} = 1.0 \text{ or } 0.5 \tag{2.17}$$

The reference S–N curve of the structural detail to be used for evaluating eq. (2.16) includes the following modification. The linearised curve with slope k in the range $N < N_\mathrm{E}$ is elongated with slope $k' = 2k - 1$ (as proposed by Haibach[2]), sometimes up to the cut-off limit of $N = 10^8$ cycles (see Fig. 2.6 and Fig. 2.7 later). This takes into account the damaging effect of nominal stress amplitudes below the nominal stress endurance limit when they are combined with nominal stress amplitudes exceeding the endurance limit. Additionally, in order to remain sufficiently conservative, the permissible damage sum may be reduced from 1.0 in the original version of Miner's rule (Eurocode 3[23]) to 0.5 in the 'relative Miner's rule' (IIW recommendations[3]), eq. (2.17). More detailed reviews on the applicability of Miner's rule on welded joints were compiled by Gurney,[27] Maddox and Razmjoo,[44,46] Niemi[51] and Sonsino *et al.*[65,67] There are further investigations comparing life predictions according to various concepts on the basis of their application to definite welded structural members and loading conditions (Byggnevi,[18] Katajamäki *et al.*,[37] Martinsson and Samuelsson,[47] Petterson[53]).

The software tools available for fatigue life evaluation based on the nominal stress approach have been reviewed and validated by Jung *et al.*[35,36] in comparison to software tools using local approaches.

2.2.3 Permissible stresses and design S–N curves

Permissible stress amplitudes are derived from endurable stress amplitudes on the basis of eq. (2.8), introducing the safety factor j_σ, which depends on the scatter bandwidth and on what failure probability is acceptable. A

graphical survey of the permissible stress amplitudes in various design codes for welded joints made of steel, derived from the technical endurance limit at $N = 2 \times 10^6$ cycles with $P_f = 50\%$ (or 10% in one case) is given in Fig. 2.3. The curve of endurable stress amplitude versus failure probability is based on the scatter range index $T_\sigma = 1:1.5$ typical for seam-welded joints in the endurance limit range. The resulting permissible stresses are associated with failure probabilities $P_f = 0.1$–2.3%. A (two-sided) confidence level of 75–95% can generally be associated with the mean value. Failure probabilities, P_f, as far as they relate to design S–N curves, may be substituted by survival probabilities, P_s, according to the relationship $P_s = (100 - P_f)$ [%]. The following design codes are included in the diagram: IIW recommendations,[3] BS 5400,[13] Eurocode 3,[23] DIN 15018,[19] AD-S2,[9] TRD301,[72] DS 804[20] and ASME pressure vessel code.[10]

The safety factors $\bar{j}_\sigma$, j_r and j_l, eqs. (2.13) and (2.14), depend on the accepted failure probability P_f (transformed and normalised in the safety index β), on the standard deviations of resistance and loading, s_r and s_l, and on the probabilities of occurrence and failure, P_o and P_f, defined in the codes. Accepted computational failure probabilities are in the range $P_f \approx 10^{-3}$–10^{-5} for most applications, corresponding to conventional safety factors of 1.7–2.2 on stress under ordinary circumstances. The accepted failure probability depends on the consequences of failure.

The design S–N curves representing the permissible stresses refer to notch or detail classes. They differ in respect of curve shape, curve position and number of curves depending on the considered design code. They are independent of the static tensile strength of the material. The set of curves

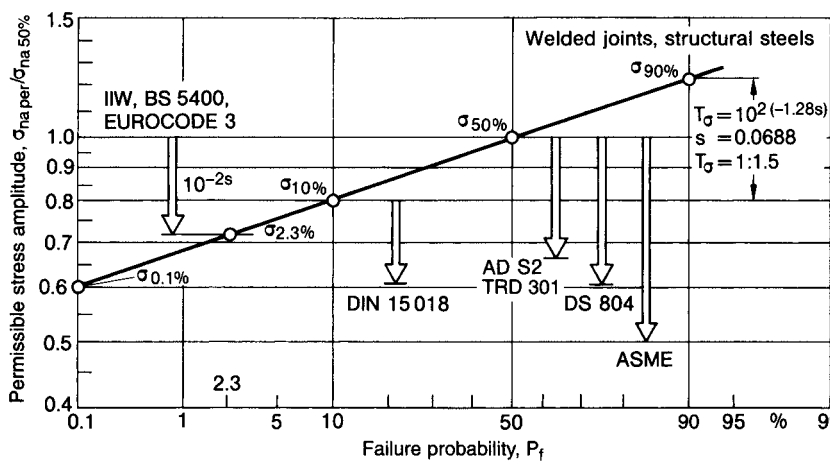


Fig. 2.3. Permissible stress amplitudes derived from endurable stress amplitudes (failure probability curve of the test results at $N = 2 \times 10^6$ cycles) according to various design codes: after Olivier *et al.*[259,260] (with supplements).

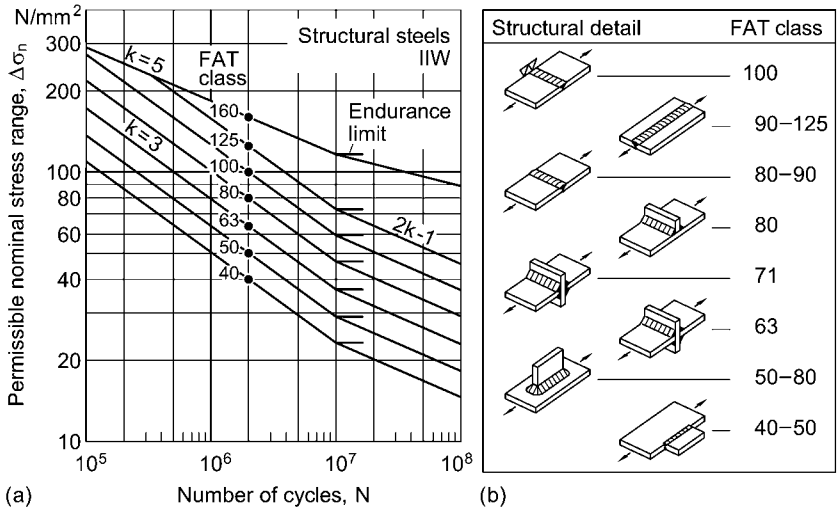


Fig. 2.4. Design *S–N* curves: permissible range of nominal stress in structural steels (P_f = 2.3%) (a), for different notch or detail classes (FAT classes) of welded joints (b); according to IIW fatigue design recommendations.[3]

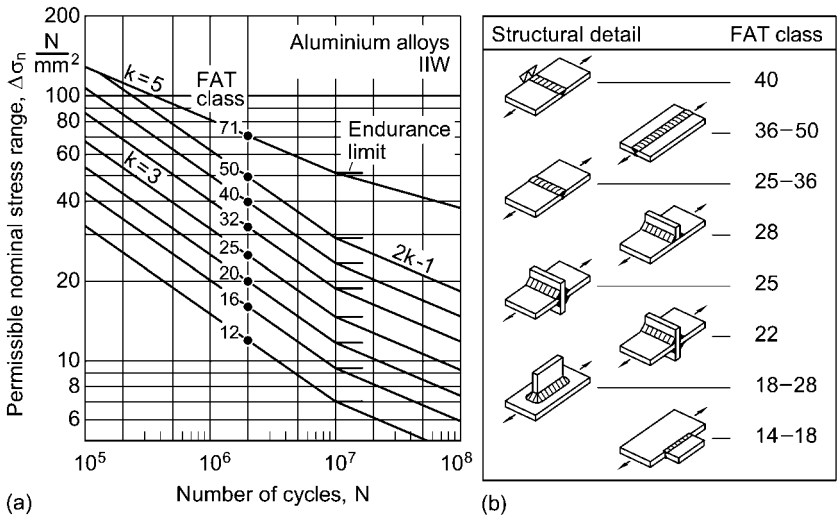


Fig. 2.5. Design *S–N* curves: permissible range of nominal stress in aluminium alloys (P_f = 2.3%) (a), for different notch or detail classes (FAT classes) of welded joints (b); according to IIW fatigue design recommendations.[3]

from the IIW recommendations[3] for seam-welded joints made of structural steels and aluminium alloys are shown in Fig. 2.4 and Fig. 2.5, respectively. Permissible nominal stresses relating to the failure probability $P_f = 2.3\%$ are plotted. The *S–N* curves of the structural details are limited from above by the *S–N* curve of the parent material. The inverse slope k is identical for steels and aluminium alloys. Similar curves (but with fewer classes) are presented by British Standards.[13,15] The detail classifications of some typical welded joints supplement the diagrams above. Comparable *S–N* curves from the ECCS design recommendations which are basic for the Eurocode 3 and Eurocode 9, respectively, are shown in Fig. 2.6 and Fig. 2.7. The technical endurance limit for constant-amplitude loading is assumed at the first knee point ($N = 5 \times 10^6$ cycles), whereas the *S–N* curves for variable-amplitude loading (effective *S–N* curves) used in the calculation of damage accumulation are elongated with further dropping into the high-cycle range (inverse slope $k' \approx 2k - 1$). The *S–N* design curves are more extensively reviewed by Maddox[43] and Gurney.[26]

The quality classes on the other hand may be allotted to neighbouring *S–N* curves starting from the detail or notch class curve being considered. The IIW guideline[31] on assesssment of fitness for purpose of welded structures defines corresponding *S–N* curves with inverse slope $k = 3.0$ referring to 15 quality classes in total. A similar diagram can be found in the relevant British Standard BSPD 6493, meanwhile replaced by BS 7910.[17]

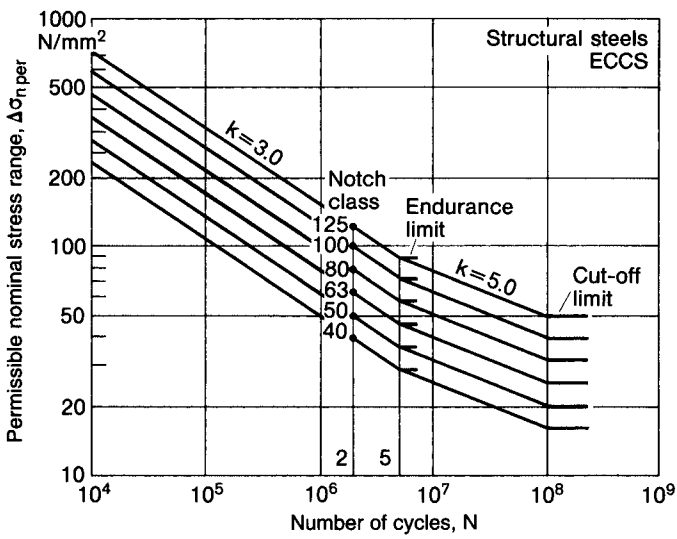


Fig. 2.6. Design *S–N* curves: permissible nominal stress range (P_f = 2.3%) for different notch or detail classes of welded joints made of structural steels; after ECCS fatigue design recommendation[21] (simplified diagram with some curves omitted).

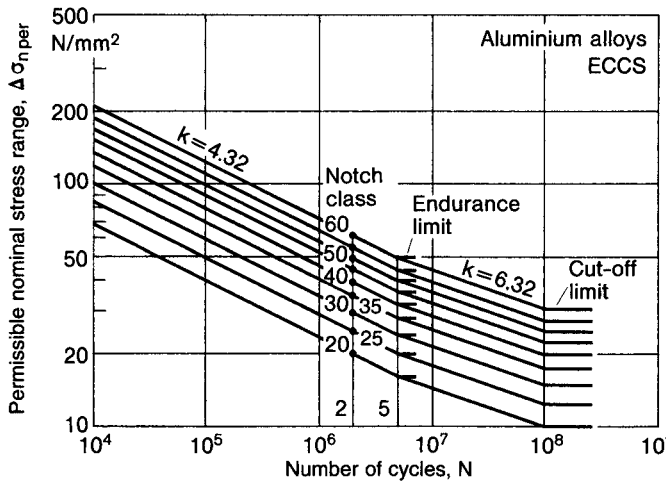


Fig. 2.7. Design *S–N* curves: permissible nominal stress range (P_f = 2.3%) for different notch or detail classes of welded joints made of aluminium alloys; after ECCS fatigue design recommendation[22] (simplified diagram with some curves omitted).

2.2.4 Influence of mean and residual stresses

The permissible design stress ranges (or amplitudes) are presented as independent of the mean stress (expressed by the stress ratio R) in the diagrams of Figs 2.4–2.7. The argument behind this simplification is the assumption that high tensile residual stresses which keep the propagating crack permanently open are acting in welded components in contrast to small test specimens. This is typically the case, for example, for longitudinally welded girders, where the residual stresses in the weld reach the yield limit and the fatigue failures start from imperfections in this area. Stress relieved or postweld-treated welded joints with compressive residual stresses in the critical area allow higher permissible stresses which depend on the stress ratio, R. The principle of this concept together with proposed parameter values is graphically shown by the Haigh diagram in Fig. 2.8. Definite functional relationships are recommended by Eurocode 3,[23] IIW design recommendations,[9] FKM guideline[1] and by Haibach.[2]

The procedure according to the IIW fatigue design recommendations[3] is described in more detail. The influence of the mean nominal stress σ_{nm} on the endurable nominal stress range (or amplitude) is assumed to be independent of σ_{nm} in general, but a fatigue enhancement factor can be introduced in certain cases. Stress-relieved welded components allow a fatigue enhancement factor rising linearly up to 1.6 between $R = 0.5$ and $R = -1$. Small-scale specimens made of thin-sheet material can claim a factor up to

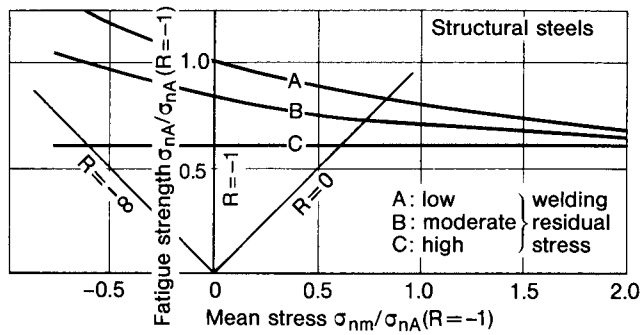


Fig. 2.8. Endurable nominal stress amplitude of welded joints made of structural steels dependent on mean stress (Haigh diagram); after Haibach.[2]

1.3 between $R = -0.25$ and $R = -1$. The FKM guideline[1] proposes a procedure closely related to the Haigh diagram in Fig. 2.8 introducing three different values of the mean stress sensitivity M, defined as the ratio of endurable stress amplitudes at $R = -1$ and $R = 0$ minus one.

The specification of a relatively low R-independent permissible design stress amplitude for as-welded joints was recently shown to be too conservative (Krebs *et al.*[40]). The underlying hypothesis of a constant upper stress at the yield limit is proven to be unrealistic by a re-evaluation of the relevant fatigue test results in the open literature. It is claimed that the R-dependency of the endurance limit and the slope of the S–N curve do not differ fundamentally between as-welded and postweld heat-treated specimens. The technical endurance limit at 2×10^6 cycles is larger by a factor of 1.25 for $R = -1$ in comparison to $R = 0$.

2.2.5 Influence of stress multiaxiality

Fatigue loading of welded joints by multiaxial nominal stresses (in the plate or in the weld) occurs in the form of biaxial nominal stress amplitudes $\sigma_{\perp a}$ interacting with weld-parallel shear stress amplitudes $\tau_{\parallel a}$. The weld-parallel normal stress amplitudes $\sigma_{\parallel a}$ are disregarded. The interacting stress amplitudes $\sigma_{\perp a}$ and $\tau_{\parallel a}$ may be in phase (proportional loading) or out-of-phase (non-proportional loading). A phase shift angle of 90° is considered to be the testing condition for non-proportional loading. The interaction equations recommended by Eurocode 3[23] and IIW recommendations[3] are presented below (Bäckström,[11] Bäckström and Marquis[12]).

There is only one case of multiaxial (instead of biaxial) nominal stresses relevant to the fatigue assessment of load-carrying non-penetrating fillet-welded joints: the nominal weld stress amplitudes $\sigma_{w\perp a}$, $\tau_{w\perp a}$, $\sigma_{w\parallel a}$ and $\tau_{w\parallel a}$ in

the throat section of load-carrying non-penetrating fillet welds. This exceptional case is disregarded below.

In the case of proportional biaxial constant-amplitude loading, the maximum principal stress amplitude is introduced as fatigue relevant:

$$\sigma_{\mathrm{eq\,a}} = \frac{1}{2}\left(\sigma_{\perp \mathrm{a}} + \sqrt{\sigma_{\perp \mathrm{a}}^2 + 4\tau_{\parallel \mathrm{a}}^2}\right) \qquad (\sigma_{\parallel \mathrm{a}} = 0) \tag{2.18}$$

In the case of proportional biaxial variable-amplitude loading, Miner's rule is applied to the first principal stress amplitudes (permissible damage sums according to Eurocode 3[23] or IIW recommendations[3]):

$$D_{\mathrm{per}} = D_1 = 1.0 \text{ or } 0.5 \tag{2.19}$$

In the case of non-proportional biaxial constant-amplitude loading, normal and shear stress amplitudes are assessed separately and then combined by damage summation in accordance with a Miner-analogue rule for the fatigue-relevant equivalent stress amplitude, $\sigma_{\mathrm{eq\,a}}$:

$$\left(\frac{\sigma_{\mathrm{eq\,a}}}{\sigma_{\perp \mathrm{A}}}\right) = \left(\frac{\sigma_{\perp \mathrm{a}}}{\sigma_{\perp \mathrm{A}}}\right)^3 + \left(\frac{\tau_{\parallel \mathrm{a}}}{\tau_{\parallel \mathrm{A}}}\right)^5 \qquad (\sigma_{\perp \mathrm{a}} < \sigma_{\perp \mathrm{A}}, \tau_{\parallel \mathrm{a}} < \tau_{\parallel \mathrm{A}}, \sigma_{\parallel \mathrm{a}} = 0) \tag{2.20}$$

with the permissible stress amplitudes $\sigma_{\perp \mathrm{A}}$ and $\tau_{\parallel \mathrm{A}}$. The equation presumes a definite number of cycles, N, for which it is applied. The exponents 3 and 5 originate from the different inverse slopes of the S–N curves for normal stress and shear stress loading, respectively.

In the case of non-proportional biaxial variable-amplitude loading, Miner's rule is applied seperately to the two stress components followed by a linear total damage superposition (permissible damage sums according to Eurocode 3[23] or IIW recommendations[3]):

$$D_{\mathrm{per}} = D_\sigma + D_\tau = 1.0 \text{ or } 0.5 \tag{2.21}$$

Other conventional multiaxial fatigue damage criteria are based on the distortion strain energy (named after von Mises) or the maximum shear stress (named after Tresca). They are recommended by the ASME code.[10] The von Mises equivalent stress amplitude $\sigma_{\mathrm{eq\,a}}$, which in the case of biaxial loading conditions consists of the stress amplitude $\sigma_{\perp \mathrm{a}}$ normal to the weld and the shear stress amplitude $\tau_{\parallel \mathrm{a}}$ parallel to the weld, reads as follows:

$$\sigma_{\mathrm{eq\,a}} = \sqrt{\sigma_{\perp \mathrm{a}}^2 + 3\tau_{\parallel \mathrm{a}}^2} \tag{2.22}$$

The corresponding Tresca equivalent stress amplitude is:

$$\sigma_{\mathrm{eq\,a}} = \sqrt{\sigma_{\perp \mathrm{a}}^2 + 4\tau_{\parallel \mathrm{a}}^2} \tag{2.23}$$

All the conventional criteria and also the more recently proposed critical plane approach (see Section 3.3.5), as far as these are restricted to proportional (or in-phase) loading conditions, describe the fatigue strength within defined areas of the application sufficiently well, but they fail more or less under non-proportional (or out-of-phase) loading conditions, especially with changing principal stress directions. The investigations by Sonsino and co-authors[41,42,59–61,63,64,66,69] underline the complexity of the problem.

First, the *S–N* curves from fatigue tests on fillet-welded tube-to-plate joints in steel, loaded by combinations of bending and torsional moments, are considered, Fig. 2.9 (upper curves). The endurable nominal bending stress amplitude σ_{ba} without superimposed shear stress amplitudes ($\tau_{na}/\sigma_{ba} = 0$) are lowered by the shear stress amplitudes ($\tau_{na}/\sigma_{ba} = 0.58$). The reduction is greater for out-of-phase conditions ($\delta = 90°$) than for in-phase conditions ($\delta = 0°$). The predictions according to eq. (2.22) correlate approximately with the test results for in-phase loading. The prediction of life is by a factor of four unconservative in the case of out-of-phase loading, when introducing the maximum stress amplitudes in eq. (2.22) independent of their phase positions, or by a factor of twelve when using the maximum of the superimposed momentary stress amplitudes. Similar results are reported by Razmjoo[55,56] who found a factor of ten for life between in-phase and out-of-phase loading when plotting the first principal stress amplitude. Comparable results by Siljander *et al.*[58] were evaluated based on a critical plane damage criterion.

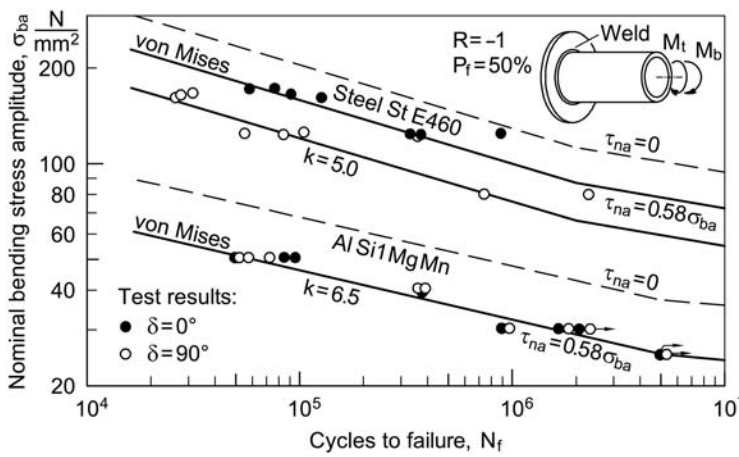


Fig. 2.9. S–N curves from fatigue testing of tube-to-plate welded joints in steel and aluminium alloy; pure bending and in-phase and out-of-phase combined bending and torsional loading in comparison; failure defined as through-thickness fracture; after Sonsino.[59,60]

The corresponding test results and predictions for an aluminium alloy, Fig. 2.9 (lower curves), reveal that both the in-phase and the out-of-phase loading conditions are associated with roughly the same strength reduction. The different fatigue behaviour of the welded joint in steel and aluminium alloy, respectively, when tested under in-phase and out-of-phase loading conditions in comparison, indicates an influence of the material, mainly of its ductility.

Further aspects of fatigue under multiaxial stress conditions at welded joints are discussed with regard to the structural stress approach (Section 3.3.5), the notch stress approach (Section 4.2.10), the notch strain approach (Section 5.2.3) and the crack propagation approach (Section 6.1.1). The state of knowledge on multiaxial fatigue behaviour of welded joints is unsatisfactory (Susmel and Tovo[71]), but permanently enhanced by ongoing research.

2.2.6 Influence of plate thickness, weld dressing and environment

The influence of plate thickness on the endurable stress ranges (or amplitudes) is taken into account where the plate thickness t is larger than t_0 = 16–25 mm depending on code regulations. The strength reduction factor γ_t is defined as follows,

$$\gamma_t = \left(\frac{t_0}{t}\right)^n \qquad (t > t_0) \tag{2.24}$$

where the plate thickness t_0 is assigned to the design S–N curve, the actual plate thickness is t and the exponent n = 0.1–0.3 is dependent on the type of welded detail (IIW recommendations[3]).

Weld toe dressing by grinding, remelting (TIG dressing) or needle peening allows the respective detail class to be upgraded provided certain quality standards of processing are met (Haagensen and Maddox[28]). The increase in fatigue strength is claimed to be more pronounced for high strength materials.

The influence of elevated temperatures, substantially above ambient temperature, is taken into account by a factor reducing the endurable stress ranges (or amplitudes) which depends on the temperature. In steels, no reduction is necessary up to 200°C or in aluminium alloys up to 70°C. In steels the reduction factor drops to 0.4 between 200 and 600°C (IIW recommendations[3]).

A corrosive environment or unprotected exposure to atmospheric conditions may substantially reduce the endurable nominal stress ranges (or amplitudes). A lower fatigue class with additionally reduced endurance

limit will be appropriate. The degree of reduction depends on the spectrum of load amplitudes as well as on the duration of exposure.

2.2.7 Normalised *S–N* curves

Another efficient means of defining permissible stress amplitudes for fatigue-loaded welded joints is the normalised *S–N* curve defined with uniform scatter band which is applicable to some extent to any notch or detail class, stress ratio and steel type provided the yield limit $\sigma_{Y0.2}$ is not exceeded by the nominal stress, Fig. 2.10. Normalisation is achieved by referring the endurable stress amplitude σ_{nA} to the technical endurance limit σ_{nAE} ($P_f = 50\%$, $N = 2 \times 10^6$ cycles, R = const). The normalised *S–N* curve has been adapted to the slope and knee point used in later codes and guidelines, Fig. 2.11. A uniform k value independent of notch or detail class is questionable according to Gimperlein.[25] Another evaluation of fatigue test data of welded joints in structural steel in respect of the normalised *S–N* curve has been presented by Ritter[57] and reviewed by Seeger.[8] A normalised *S–N* curve for aluminium alloys is shown in Fig. 2.12.

The normalised *S–N* curve for seam-welded joints (Haibach's original version) was also successfully applied to spot-welded joints in steel (Rosetto *et al.*[819]). Fatigue test results from various specimens (tensile-shear-loaded, cross-tension-loaded and non-load-carrying weld spots) in terms of endured nominal stress amplitudes (nominal stress in gross cross-section) were

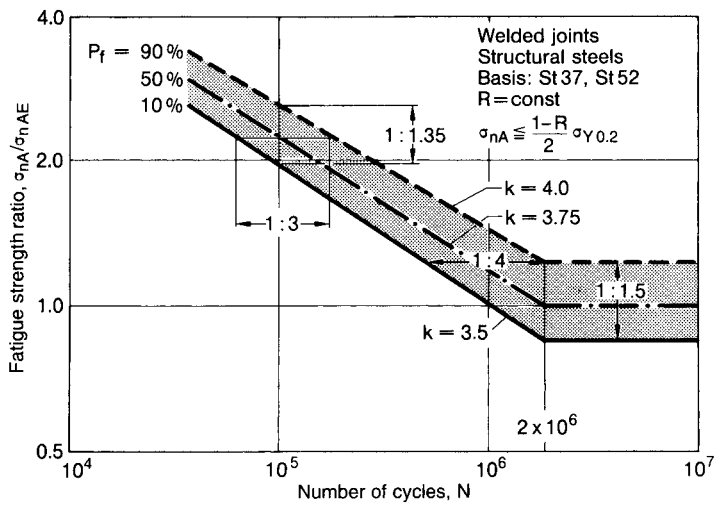


Fig. 2.10. Normalised *S–N* curve for seam-welded joints made of structural steels, any notch or detail class and stress ration *R*; original version proposed by Haibach.[2]

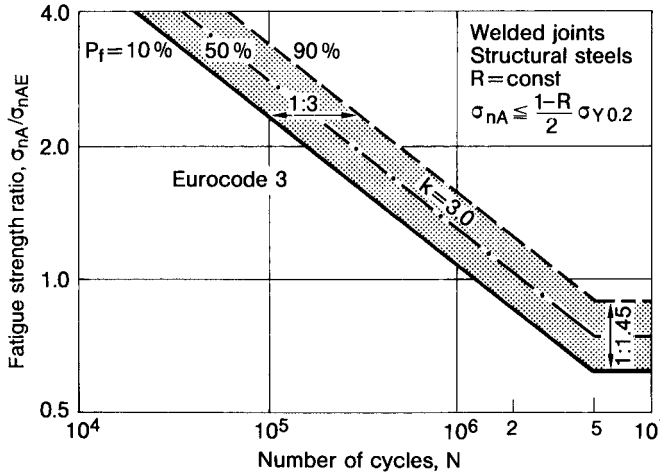


Fig. 2.11. Normalised *S–N* curve for seam-welded joints made of structural steels, any notch or detail class and stress ration *R*; modified version proposed by Haibach.[2]

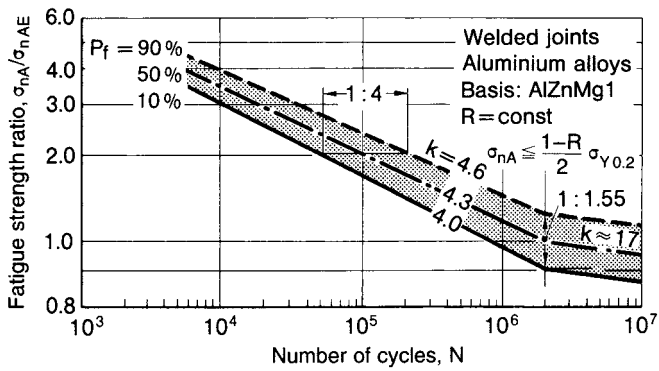


Fig. 2.12. Normalised *S–N* curve for seam-welded joints made of aluminium alloys, any notch or detail class and stress ration *R*; after Haibach and Atzori.[29]

brought together. The chosen reference point at $N = 2 \times 10^6$ cycles is not the knee point of the evaluated *S–N* curves, which may be found closer to $N = 10^7$ cycles. In component-like multi-spot specimens in contrast to the single-spot specimens above, the slope of the *S–N* curve is substantially reduced by various support effects.

2.2.8 Fatigue strength reduction factors

Fatigue strength reduction factors characterise the (technical) endurance limit of typical uniaxially loaded welded joints in relation to the endurance

limit of the non-welded parent material, Fig. 2.13 and Table 2.1. They were widely used before the fatigue-relevant codes and guidelines for welded joints were established. They continue to be a useful means for presenting a well-founded first estimate of endurable stress amplitudes in welded joints, especially in those engineering areas which are not strictly bound to code regulations. They are particularly useful for predicting tendencies and for assessing preliminary designs.

Reduction factors $\gamma_\perp$, $\gamma_\parallel$ and γ_τ are defined for cyclic loading of the weld by nominal stress amplitudes in the parent material directed perpendicular and parallel to the weld (normal and shear stresses $\sigma_{\perp a}$, $\sigma_{\parallel a}$ and $\tau_{\parallel a}$), evaluating their (technical) endurance limits $\sigma_{\perp A}$, $\sigma_{\parallel A}$ and $\tau_{\parallel A}$ in relation to the endurance limit of the non-welded parent material σ_E or τ_E:

$$\gamma_\perp = \frac{\sigma_{\perp A}}{\sigma_E} \qquad (R = -1) \tag{2.25}$$

$$\gamma_\parallel = \frac{\sigma_{\parallel A}}{\sigma_E} \qquad (R = -1) \tag{2.26}$$

$$\gamma_\tau = \frac{\tau_{\parallel A}}{\tau_E} \qquad (R = -1) \tag{2.27}$$

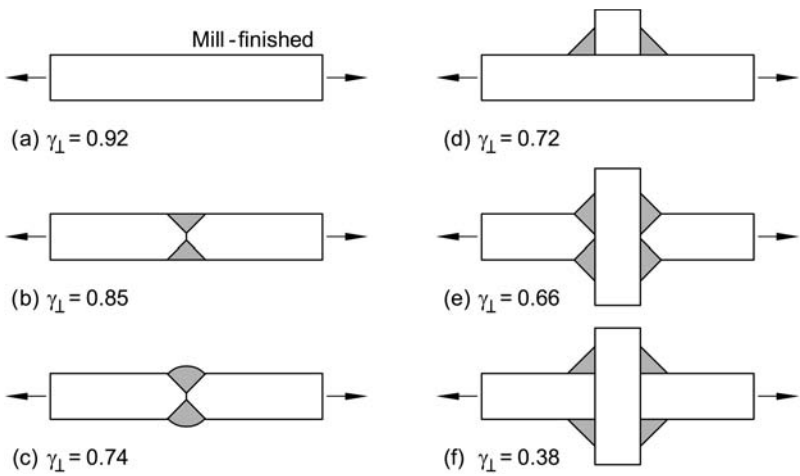


Fig. 2.13. Reduction factor $\gamma_\perp$ of various types of welded joints made of structural steel in the as-welded condition ($\sigma_Y \approx 250\,N/mm^2$, $\sigma_U \approx 400\,N/mm^2$); endurance limit in terms of nominal stress amplitude related to parent material endurance limit ($N_E = 2 \times 10^6$ cycles, $R = -1$); after Stüssi.[70]

Table 2.1. Survey of reduction factors γ of defect-free welded joints made of low-carbon structural steels ($\sigma_Y \approx 250\,N/mm^2$, $\sigma_U \approx 400\,N/mm^2$); $\sigma_E = 240\,N/mm^2$ at $N_E = 2 \times 10^6$ cycles in mill-finished plate, $R = 0$, $P_f = 10\%$; after Radaj[54] (based on data in the open literature)

Weld type	Reduction factor		
	$\overline{\gamma}_\perp$	$\overline{\gamma}_\parallel$	$\overline{\gamma}_\tau$
Load-carrying welds			
Butt weld	0.5–0.9	0.7–0.9	0.6–0.9
Single and double bevel butt weld	0.4–0.7	0.6–0.8	0.5–0.7
Fillet weld	0.3–0.5[a]	0.5–0.7	0.4–0.6
		0.3–0.5[b]	
		0.2–0.4[c]	
Corner weld	0.3–0.5	0.5–0.7	0.4–0.6
Keyhole weld in lap joint	0.2–0.5	0.5–0.7	0.3–0.6
Resistance spot weld	0.1–0.5	0.4–0.5	0.2–0.5
Non-load-carrying welds			
Butt-welded longitudinal gusset plate	0.2–0.3		
Fillet-welded attachments	0.4–0.8[d]	0.4–0.7[e]	0.3–0.6
Bead-on-plate weld	0.6–0.9	0.6–0.9	0.6–0.9

[a] Cruciform or lap joint with transverse fillet weld.
[b] Discontinuous web-to-flange fillet weld.
[c] Lap joint with side fillet welds.
[d] Transverse attachment.
[e] Longitudinal attachment.

The fatigue limit σ_E or τ_E of the parent material is usually determined by testing polished specimens (such reference values are used in Fig. 2.13), but another surface condition may also be chosen, e.g. the mill-finished condition (as in Table 2.1). A dash is positioned on top of the symbol γ in the latter case. Also $R = -1$ may be considered instead of $R = 0$.

Supposing that the fatigue strength of welded joints is independent of the static tensile strength of the material (structural steel or aluminium alloy) – which is a realistic assumption with regard to severely notched welded joints with correspondingly low reduction factors – lower reduction factors are derived for high strength materials. This means that the reduction factors are dependent on the material strength to some extent.

The reduction factors may also be modified by further influence parameters. Approximation formulae for endurable nominal stress amplitudes were derived based on reduction factor considerations which are intended to catch these additional influences (Radaj[54]). The reduction factors presented above are valid in the high-cycle fatigue range. They rise in the medium-cycle fatigue range (or with variable-amplitude loading), especially

so if they are originally low. Note that the fatigue strength of the parent material used for reference also rises. Further important influence parameters are hardening or softening in the critical cross-section, residual stresses produced by welding and multiaxiality of the basic stress state. The stress ratio R of cyclic loading, on the other hand, is considered to be only of minor influence.

3

Structural stress or strain approach for seam-welded joints

3.1 Basic procedures

3.1.1 Principles of the structural stress or strain approach

The structural stress or strain approach for assessing the fatigue strength and service life proceeds from the structural stress or strain amplitudes in the structural member and compares them with a structural stress or strain *S–N* curve. The structural (or 'geometric') stress or strain describes the macrostructural behaviour without consideration of local notch effects. It may be measured by strain gauges or calculated by engineering formulae or finite element analysis. The structural stress *S–N* curve may be set equal to the nominal stress *S–N* curve of the parent material if the area of the structural member considered consists of parent material and is free of notches. The aim should be to shield the notches of a component from crack initiation and thus shift the critical area to the notch-free parent material. This can be achieved, at least to some extent, by appropriate design and manufacturing measures.

The procedure is also applicable to structural members with unshielded notches in the area of crack initiation under consideration, but only in a comparative manner as far as non-welded structures are considered. The structural stress in a newly designed member may be compared with the relevant stress in the older service-proven design, if material, notch effect and service conditions are similar. The structural stress may especially be used to optimise the shape parameters of the structural member. Qualitative assessments, relative considerations and trend statements are the prevailing results of the common finite element analysis which does not take the notch effect into account.

The structural stress approach above extended to welded joints gives an indication of how quantitative statements on fatigue strength or life may be achieved for critical areas without resorting to the notch stress or notch strain approach which requires higher expenditure.

3.1.2 Structural strain approach as proposed by Haibach

Haibach[123,129] showed, in an historically early contribution, that the cyclic strain measured and averaged with a strain gauge of definite length (3 mm) at a definite small distance from the weld toe (2.0–2.5 mm considering the centre of the strain gauge) is well suited for characterisation of the high-cycle fatigue strength of welded joints independent of joint type, weld shape and type of loading transverse to the weld, provided that the fatigue fracture occurs at the weld toe, Fig. 3.1. The vertical broken line in the right-hand part of the figure characterises the transition from the structural strain to the nominal stress approach proposed for an extended analysis.

A similar development of method took place based on proposals of Peterson[176] and Manson[157] in respect of pressure vessel fatigue. A strain gauge of 0.25 in. length (i.e. 6.35 mm) was applied adjacent and perpendicular to the weld toe. The procedure was later transferred to offshore tubular joints and is still the basis of hot spot stress evaluations according to the relevant AWS and API guidelines.[77,82] The original strain gauge length was reduced in order to minimise strain gradient effects.

The distance of the strain gauge from the weld toe is difficult to define in an appropriate manner. The position is appropriate if the measured structural stress can be considered to be equivalent to a local nominal stress and the scatter of the endurable values remains small. This goal should be achieved despite the relatively large scatter of the weld toe radius.

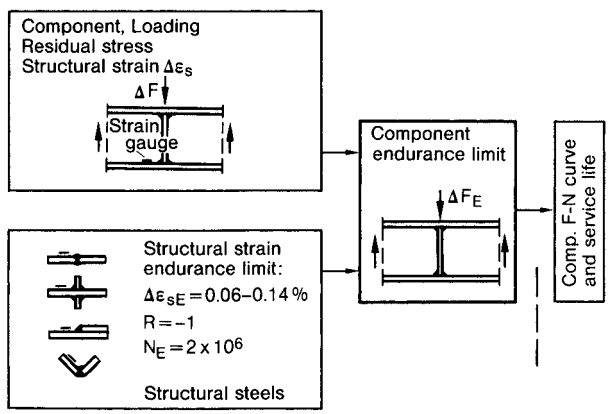


Fig. 3.1. Structural strain approach, version according to Haibach,[123] to assess the fatigue strength of welded structural components; with $\Delta\varepsilon_s$ cyclic structural stain, ΔF cyclic external force, $\Delta\varepsilon_{sE}$ strain endurance limit, ΔF_E endurance limit of external force, N_E number of cycles at endurance limit and R lower to upper force ratio; after Radaj.[5]

A more detailed investigation into this problem has been performed by Atzori *et al.*[78] A cruciform joint under tensile loading is simulated by a finite element model in order to obtain the structural stress or strain which would be measured by a strain gauge of definite length in front of the weld toe. The structural stress at the edge of the model is plotted over the distance x_p from the starting point of the rounded weld toe considering different radii, Fig. 3.2. The higher structural stress is valid for the smaller radius. This is appropriate because the smaller radius means lower fatigue strength in terms of nominal stress. The measured structural stresses converge rapidly to the nominal stress (rapidly in relation to plate thickness). The curves would be shifted to the right as indicated by arrows if the distance x_t from the weld toe centre had been chosen as the reference parameter. The resulting new band of curves would be narrower but the decrease in stress is slower and the sequence of curves reversed.

The conclusion is that the distance of 2.0–2.5 mm (recommended by Haibach) measured from the starting point of the weld toe notch seems to be appropriate to the 3 mm gauge length. This positioning results in a structural stress which is only slightly higher than the nominal stress in the considered cruciform joint (as desired). Of course, the distance could be chosen to be larger in the cruciform joint but not in complex structural components. It should also be considered to be dependent on plate thickness.

In a more recent contribution Atzori and Meneghetti[80] clarified that the strain values at a distance equal to 2–3 mm (or more) from the weld toe lead to incorrect estimates of the notch stress field, especially of the notch stress intensity factor of sharp notches. Whereas secondary bending effects

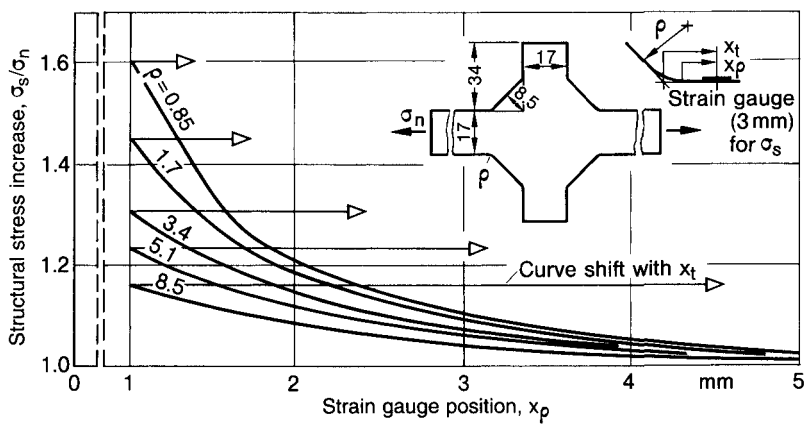


Fig. 3.2. Structural stress increase to be measured by a strain gauge of 3 mm length in front of the weld at a cruciform joint; numerical simulation by finite elements; after Atzori *et al.*[78]

are captured, the effect of plate thickness is not. Local strain values at a distance equal to 0.1 mm (or less) would be necessary to include the thickness effect.

The relationship between the structural strain (or relevant stress) measured according to Haibach and the fatigue-effective maximum notch stress determined according to Radaj or Seeger (weld toe fictitiously rounded, see Sections 4.1.3 and 4.1.4) has been derived by Olivier *et al.*[259] assuming linear-elastic material behaviour. The relation depends on the plate thickness. The endurable strains or stresses given in Section 3.3.1 have been mainly determined for a plate thickness of 10 mm. A higher plate thickness is related to lower endurable strains or stresses. The opposite is true for a lower plate thickness.

The relation between the edge stresses, $\sigma = \varepsilon E$, and the fatigue-effective notch stress $\bar{\sigma}_k$ (with fictitious notch rounding according to Radaj, radius $\rho_f = 1$ mm) plotted for different plate thicknesses, Fig. 3.3, yields the conversion factor for the measured strain ε_m dependent on plate thickness. The

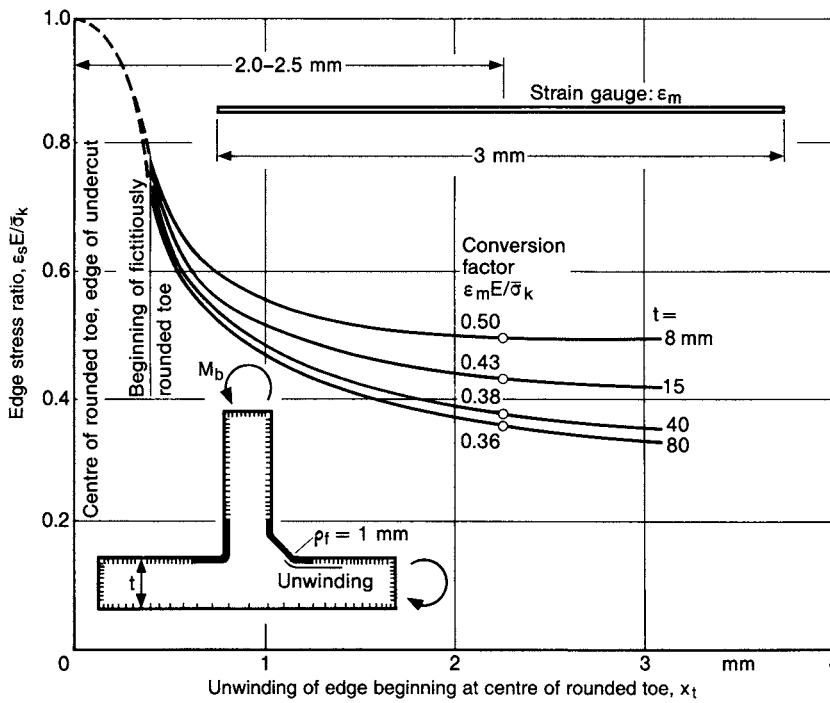


Fig. 3.3. Relation between edge structural stress $\sigma_s = \varepsilon_s E$ (boundary element analysis) and fatigue effective notch stress $\bar{\sigma}_k$ dependent on plate thickness *t*; mean stain ε_m in applied strain gauge; welded T-joint subjected to bending moments; after Olivier *et al.*[259]

endurable structural strain $\Delta\bar{\varepsilon}_s = 0.1\%$ (St52 steel, plate thickness $t = 10\,\text{mm}$, $R = -1$, $P_f = 50\%$) thus results in the endurance limit $\Delta\bar{\sigma}_k = 438\,\text{N/mm}^2$ compared with $\Delta\bar{\sigma}_k = 470\,\text{N/mm}^2$ in Table 4.5.

The structural strain approach, version proposed by Haibach,[123,129] has been applied to vehicle components, boilers, pressure vessels and crane structures. A broader application is impeded by the necessity to manufacture the welded structure under consideration before measurements can start. On the other hand, the procedure can obviously be transferred to a numerical structural analysis, so that designs can be assessed prior to manufacture. As has been mentioned above, the structural strain approach led to the hot spot stress concept and was included in relevant guidelines, e.g. AWS,[82] API,[77] and SAE.[182] Also, the structural strain approach has successfully been applied to describe the effect of joint misalignment, both axial eccentricity and angular distortion, on the fatigue strength of welded joints.

3.1.3 Hot spot structural stress approach for tubular joints

Rather high stresses may occur locally in framework structures consisting of hollow structural sections. They are caused mainly by local bending of the tube walls and by superimposed notch effects. The fatigue strength and life of welded tubular joints of circular or rectangular cross-section can realistically be assessed on the basis of the structural stress concentration. The planar arrangements of tubes most frequently found are shown in Fig. 3.4. They are designated by the capital letters of the alphabet which are similar in shape. The tube ends are subjected primarily to axial forces and secondarily to bending moments.

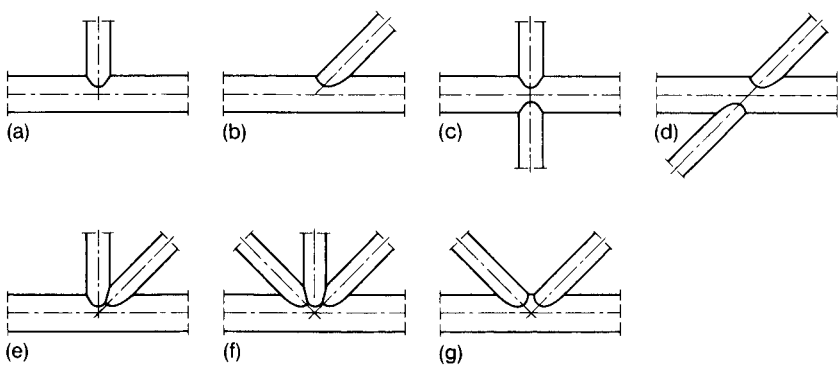


Fig. 3.4. Brace and chord arrangement of tubular joints designated by capital letters of the alphabet: T (a), Y (b), X (c,d), TY (e), KT (f) and K (g) types; after Wardenier.[197]

The hot spot structural stress approach, originally proposed by Dijkstra and de Back[92] (as well as by other researchers) for welded joints made of circular section tubes and later on extended to rectangular section tube joints, aims to determine the structural stress in the tube wall at the crack initiation point of the weld toe (named 'hot spot' because of the local temperature rise produced by cyclic plastic deformation prior to crack initiation) and to compare this stress with the nominal stress in a simple welded joint specimen, for example, the corner joint with a fillet weld, for the purpose of strength assessment, Fig. 3.5. The structural stress at the hot spot is supposed to make strength-characteristic values transferable from the specimen to the tubular joint even in cases of slight differences in local geometry and loading mode. This can be expressed in such a way that the fatigue strength of the welded joint specimen in terms of nominal stress presents the limit value of the structural stress at the hot spot in the tubular joint. Nominal and structural stresses are considered to be equivalent in respect of a definite notch or detail class *S–N* curve. The problem consists in determining the appropriate *S–N* curve and a general solution is not available. There are also close relations to the crack propagation approach insofar as the structural stress is well suited as the reference stress for the stress intensity factor. The varying and scattering notch effect of the weld toe is of secondary influence within the hot spot structural stress approach, but a correction on the *S–N* curve for very thick tube walls turned out to be necessary.

The structural stress at the hot spot is introduced as 'hot spot stress'. It excludes the notch stress by vague definition but it includes the notch effect

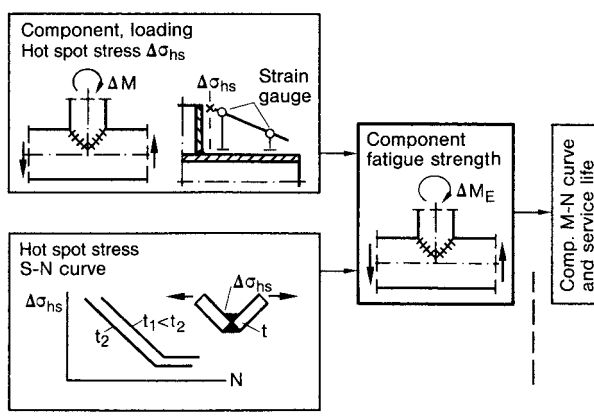


Fig. 3.5. Hot spot structural stress approach, version according to Dijkstra and de Back[92] and other researchers, to assess the fatigue strength of welded tubular joints in offshore applications; with ΔM cyclic external moment, $\Delta\sigma_{hc}$ cyclic hot spot stress, ΔM_E endurance limit of external moment, t_1 and t_2 sheet thickness.

of the crack initiation site in its endurable value. It is not necessarily identical to the maximum structural stress.

The transfer method mentioned above is bound to the several conditions: the point of crack initiation or hot spot must be known in advance. The crack should be initiated at the accessible weld toe, that is, not at the inaccessible weld root. Transverse loading of the weld should prevail. The structural stress (or 'geometric stress') should be separable from the notch stress at the hot spot as unambiguously as possible. The notch effect and the welding quality in the tubular joint and in the comparison specimen should be approximately the same.

The procedure for separating the structural stress from the notch stress at the hot spot is now considered in more detail. Following the proposal of Dijkstra, de Back and others, the axial surface stresses in the tube are measured or calculated at a small and at a larger distance from the weld toe and after that linearly extrapolated to the weld toe, Fig. 3.6. The exact position of the two evaluation points is defined dependent on the diameter and wall thickness of the tube, that is, dependent on the geometrical parameters which determine the stress field in the tubular joint when considered as a cylindrical shell structure. A non-linear instead of the linear extrapolation is occasionally applied.[190,191] Biaxial instead of uniaxial stresses can be evaluated.

The hot spot structural stress approach which is well founded in the medium- and high-cycle fatigue range, i.e. in the range of predominantly elastic behaviour, can be extended to the low-cycle fatigue range, i.e. to the range of elastic-plastic behaviour, by considering strains instead of stresses.

The hot spot structural stress approach is embodied in the design rules for tubular structures such as offshore structures, roof trusses and support towers. It substitutes for the nominal stress approach in this area of application.

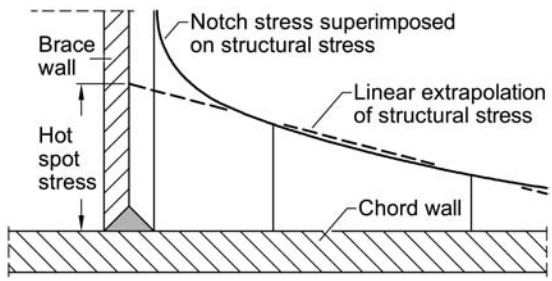


Fig. 3.6. Hot spot stress at weld toe of tubular joint, elimination of non-linear rise in notch stress; after Wardenier.[197]

3.1.4 Hot spot structural stress approach for non-tubular joints

The hot spot structural stress approach has been transferred from tubular to non-tubular joints, the latter mainly in plate-type structures occurring in ship or bridge design (e.g. Sunamoto *et al.*,[187] Fricke and Petershagen,[120] Huther and Lieurade[137]) as well as in commercial vehicles (e.g. Savaidis and Vormwald[183]) or boogies. In certain cases, the structural stress distribution in plate-type structures is similar to that in tubular joints, e.g. at cover plate joints or lap joints, where the loading transverse to the weld creates secondary bending stresses in the plate owing to the structural eccentricity. However, other structural details such as the ends of longitudinal attachments on plates or girder flanges or at plate edges induce a more localised structural stress increase. Parametric studies have shown that the hot spot structural stress approach is also applicable in these cases.

Based on comparative investigations, the evaluation points for stress extrapolation are recommended at distances from the weld toe which are fractions of the plate thickness (Niemi *et al.*[163–165,173]). For weld toes at attachments to plate edges, which have been investigated by Wagner[195,196] and Niemi and Tanskanen,[166] plate thickness is not considered to be a suitable reference parameter. Instead, absolute positions for the stress evaluation points are suggested. On the other hand, the above investigations have shown that the linear extrapolation should be supplemented by a quadratic or even cubic term. This means that the structural stress increase in front of the welded joints being considered occurs with various gradients and non-linearities. Therefore, a uniform schematic approach is difficult to define.

3.1.5 Alternative definitions of hot spot structural stress

The hot spot structural stress approach, if considered as a procedure which transfers the fatigue strength values of welded specimens to the local design detail within a structure, is generally applicable in all cases where the structure can be analysed based on a plate or thin-shell model independent of whether simple engineering formulae or more complex finite element methods are used. The analysis approach suppresses the notch stress by the assumption of a linear stress distribution over the plate or shell thickness. As pointed out by Radaj,[4] this is a consistent way to define structural stresses at the hot spot because a single-valued solution is achieved. The definition is also used in the ASME code[10] for pressure vessels and pipelines, in a proposal referring to automobile structures (see Section 9.4.5) and in the parametric investigations of Fricke *et al.*[119,121] on the fatigue

assessment of welded structural details in ship structures. The hot spot stresses determined accordingly may be somewhat higher than the values gained from linearly extrapolating the measured stress values at the surface. Hot spot stress calculations which use the measurement-related procedure of surface stress extrapolation are nevertheless sometimes chosen in order to apply the hot spot design stresses from relevant codes. The structural stress derived from the structural strain according to Haibach or according to the AWS and API guidelines[77,82] is also somewhat higher than the extrapolated surface stress.

Further suggestions have been made about how to separate the structural stresses from the notch stresses. No mechanical criterion exists for the separation. Whereas the notch stresses are strictly defined based solely on continuum mechanics, this is not possible with the hot spot structural stresses. The latter depend on additional assumptions relating to the stress distribution, as well as on the selected numerical (or experimental) procedures. Modelling and evaluation rules have to be introduced.

Atzori *et al.*[79,81] propose to superimpose the structural stress concentration of a blunt equivalent notch simulating the joint corner with weld (i.e. the global joint geometry) and the notch stress concentration of a sharp equivalent V-notch simulating the weld toe (see Fig. 7.28). Within an alternative procedure, a similar blunt equivalent notch is combined with a sharp equivalent reinforcement notch. Logarithmically scaled stress plots in the same publications show that it is not possible to separate the structural stresses from the notch stresses unambiguously by evaluating and extrapolating the stresses from an intermediate zone at some distance from the weld toe.

Tovo and Lazzarin[725] have shown how to derive the fatigue-relevant notch stress intensity factor from the hot spot structural stress and its gradient on the (upper) plate surface supplemented by the structural stress on the opposite (lower) plate surface (see eq. (7.58)). Further proposals for defining the critical structural stresses by Dong as well as by Xiao and Yamada are reviewed below.

Any more profound discussion and further development of the structural stress and strain approach should refer to the notch stresses and strains because these are the actual parameters controlling crack initiation. This was recognised by Fricke *et al.*[119,121] when deriving structural stress *S*–*N* curves on the basis of the notch stress approach ('generalised structural stress approach').

3.1.6 Structural stress approach as proposed by Dong

The concept of a linearised structural stress distribution over the plate or shell thickness has been modified by Dong *et al.*[94,100] in the form described

below in order better to fit fatigue test results from varying specimen types and sizes into a single hot spot stress parameter *S–N* curve.

The proposed modifications are related to the stresses resulting from coarse-mesh finite element models and supported by crack propagation considerations. Crack propagation starting at the weld toe and traversing the plate thickness is controlled by the total stress normal to the crack path, which can be approximated by the linearised structural stress increased by a notch-related crack-depth-dependent magnification factor.

The linearised stress distribution over plate thickness, Fig. 3.7(a), consisting of membrane and bending stress portions, is used to predict fatigue life up to through-thickness crack formation in the case of monotonic decrease of the original stresses. A stress distribution linearised only over part of the plate thickness or width, Fig. 3.7(b), is recommended particularly in the case of edge attachments, with fatigue life corresponding to a damaging crack depth t_1. Finally, in cases of non-monotonic decrease of the original stresses (e.g. occurring with double-sided attachments), a bilinearised stress distribution, Fig. 3.7(c), is the basis of fatigue life analysis, with the depth t_1 resulting once more from the damaging crack depth or alternatively (Dong's proposal) from the zero line crossing point of the shear stresses (the latter condition cannot be generalised). In cases of symmetric specimens or details, this depth is equal to half the plate thickness, $t_1 = t/2$.

The linearised or bilinearised stress distributions above are derived from coarse-mesh finite element models using special evaluation procedures (Dong *et al.*,[94,100] see Section 3.2.5). Both thin-shell element models and

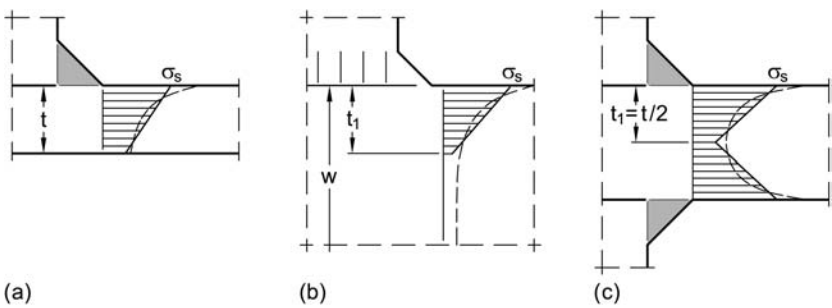


Fig. 3.7. Definition of the structural stress σ_s at the hot spot according to Dong[94] for monotonic decrease of the original stress (dashed curve) (a), for monotonic decrease of original stress in thick or wide plates (e.g. at edge attachments) (b) and for non-monotonic decrease of original stress (e.g. in a thick plate with double-sided attachments) (c); with depth t_1 corresponding to a defined damaging crack depth for edge attachments (b) or to half the plate thickness in symmetrical joints (c).

single-layer solid element models are applicable in the case of through-thickness linearisation. Multi-layer solid element models are necessary in the case of partial thickness linearisation. The selected value of t_1 is of great influence on the structural stress σ_s at the weld toe. Appropriate values of t_1 have to be introduced guided by the knowledge of relevant fatigue test results.

It is impossible to obtain an unambiguous bilinearisation of the structural stresses without defining a uniform base length (or base length ratio) over which partial linearisation takes place. Linearisation over the depth t_1 or over half the plate thickness in double-symmetric constellations provides such a definition. Mesh size insensitivity of the results can additionally be achieved in the latter case. Fatigue relevance is another question. According to the existing state of knowledge, a uniform fatigue-related base length for partial linearisation would be appropriate, but is not confirmed by the actual fatigue test data. This means that bilinearisation is not generally applicable without scaling to fatigue test data in individual cases.

A special structural stress parameter has been derived by Dong *et al.*[101] based on a crack propagation analysis which allows various fatigue test results to be described by a single uniform hot spot stress parameter *S–N* curve with inclusion of the thickness and stress gradient effects (see Section 3.3.4).

3.1.7 Structural stress approach as proposed by Xiao–Yamada

A basically different method for evaluating the structural or geometric stress in welded specimens and welded structural details has recently been proposed by Xiao and Yamada.[199] The method is theoretically founded on a generalised crack propagation analysis for weld toe cracks. It is found that the fatigue life relating to crack propagation (and thus the corresponding fatigue strength) can be expressed by the stress value at a point 1 mm below the surface on the expected crack path (assumed to be normal to the plate surface at the weld toe). This 'one millimetre stress' correlates the crack propagation life or strength of the considered structural detail ('object detail') with the corresponding values of the reference specimen ('reference detail'). The non-load carrying cruciform joint (plate thickness t = 10 mm) is chosen as the reference detail. The one millimetre stress in the reference detail is approximately equal to the nominal stress σ_n, so that the one millimetre stress in an object detail, characterised by the corresponding stress concentration factor $K_{s(1)}$, can be taken directly as the parameter expressing the fatigue life or strength, Fig. 3.8.

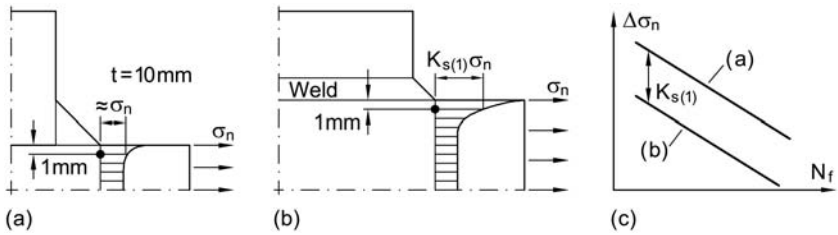


Fig. 3.8. Basic relations in the 'one millimetre stress method' proposed by Xiao and Yamada;[199] reference detail with plate thickness $t = 10$ mm (a), object detail (b) and corresponding S–N curve (c) in logarithmic scales.

The one millimetre stress is computed by finite element models with conventional demands on mesh design. The element size should not exceed 1 mm. No specific meshing rules have to be introduced.

The above method has been proven valid by analysing fatigue test results for several welded joint types reported in the literature (in-plane and out-of-plane two-sided attachments, multi-plate two-sided attachments and a one-sided tubular post structure). When compared to the surface extrapolation technique for hot spot stress determination, the proposed method has the advantage of accounting for the size and thickness effect observed in welded joint fatigue. The applicability of the method to other joint types (e.g. load-carrying cruciform joints or one-sided attachments), loading modes (e.g. plate bending) and crack paths (e.g. weld root fatigue) has not yet been investigated.

3.1.8 Structural stress approach to weld root fatigue

The structural stress approaches described above have been developed for fatigue assessment with regard to crack initiation from the weld toe. In certain cases, especially with non-fused root faces, fatigue cracks may also be initiated at the weld root ('weld root fatigue'). Such cases are covered within the nominal stress approach by relating the 'weld nominal stress' to a design S–N curve of a definite (low) fatigue class. The weld nominal stress is acting in the midsection of common butt welds or in the throat section of fillet welds ('weld thickness').

When the nominal stress approach just mentioned is applied locally at points on the weld line, it turns into a structural stress approach. The weld nominal stresses are thus introduced as being dependent on the weld line coordinate. They can be evaluated from finite element models. Plate nominal and weld nominal stresses can often be directly correlated by the ratio of plate thickness to weld thickness. The maximum weld stresses,

possibly after conversion into an equivalent stress in the case of multiaxial loading, are evaluated in relation to the appropriate design *S–N* curve. In all cases of welded joints with non-fused root faces, the fatigue assessment can alternatively be performed using the crack propagation or the notch stress approach.

The fatigue assessment of welded joints should always include consideration of the risk of weld root fatigue, not only in cases of partial penetration butt welds and load-carrying fillet welds (especially if the weld thickness is small in relation to the plate thickness), but also in cases of better-shaped weld roots.

3.2 Analysis tools – structural stress or strain evaluation

3.2.1 General survey and relevant guidelines

The analysis tools described hereafter in Sections 3.2 and 3.3 comprise the following items: information on design guidelines and analysis tools, hot spot stress evaluations at tubular and non-tubular joints, specific rules for finite element modelling and corresponding stress evaluations, hot spot structural stress concentration factors, endurable hot spot structural stresses or strains in the different versions of the approach, multiaxial stress or strain conditions and the assessment of weld root fatigue.

The major design guidelines relating to fatigue-resistant welded tubular joints (mainly in offshore applications) and comprising the hot spot structural stress approach are the following: ECCS recommendation,[21] Eurocode 3,[23] DEn guideline,[91] AWS design code,[82] and API recommendation.[77] The differences between these guidelines in respect of hot spot stress definition, parametric hot spot stress formulae and permissible hot spot stresses are discussed by van Wingerde *et al.*[190,191] Detailed information on the hot spot structural stress approach can be gained from the books of Wardenier,[197] Marshall,[159] and Packer and Henderson,[168] with reference to the design of welded tubular joints. Non-tubular (i.e. plate-type) welded structures are included in the ECCS recommendations,[21,22] the Eurocode 3,[23] the Eurocode 9,[24] and the IIW recommendations.[3] More detailed guidelines on structural stress analysis are given by Niemi *et al.*[164,165] as well as by several ship classification societies. Marshall and Wardenier[160] review the history and current status of the hot spot structural stress approaches for tubular and non-tubular joints, validating the details of the relevant procedures.

Structural stresses or strains in welded members are mainly determined by simple engineering methods and formulae,[180] finite element analysis[84] or strain gauge measurement.[131,181,198,221] The notch effect of the weld is

excluded as far as possible. Framework structures made from hollow structural sections are first analysed with respect to the axial forces (primary effect) and bending moments (secondary effect) on the basis of special framework programs introducing pinned or rigid member joints.[168]

3.2.2 Evaluation of hot spot stresses in tubular joints

The structural stress component (without notch effect) acting normal to the weld at its toe should be evaluated at the crack initiation point, named the 'hot spot'. This stress is connected with the notch effect which primarily causes fatigue crack initiation. If measurement is the basis, the strain determined normal to the weld is multiplied by the elastic modulus thus yielding a uniaxial stress, which is then extrapolated to the hot spot at the weld toe. The procedure can be refined by biaxial measurements and evaluations resulting in stresses normal to the weld which are generally higher than the uniaxial stress mentioned above. It may also be appropriate to evaluate and extrapolate the first principal stress or a suitable equivalent stress. There are arguments for using strains instead of stresses, especially in the low- to medium-cycle fatigue range where the plastic portion of the strain is predominant. The unrealistically high fictitious hot spot stresses in this range resulting from the purely elastic conversion of plastic strains are thus avoided.

The hot spot stress is determined experimentally and alternatively in relevant finite element calculations proceeding from evaluation points on lines normal to the weld in tubular joints, Fig. 3.9. The crown and saddle points of the brace–chord intersection are preferred with circular hollow sections and the near-corner positions with rectangular hollow sections. The design guidelines prescribe the above positions for the evaluation of the hot spot stresses. The real hot spot may deviate from the above positions to some extent. It is then necessary to evaluate the hot spot stress for further positions of the intersection line of brace and chord tube.

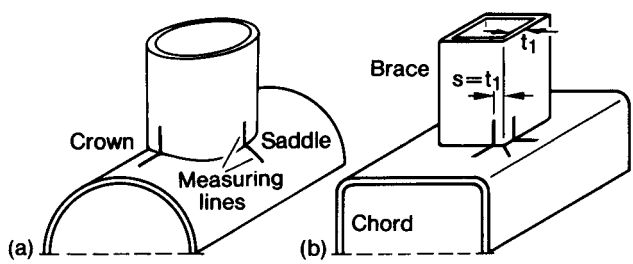


Fig. 3.9. Positioning of strain gauges in lines normal to the weld in tubular joints for hot spot stress evaluation, circular hollow sections (a) and rectangular hollow sections (b); after van Wingerde *et al.*[190,191]

The evaluation points for the linear extrapolation of the structural stress to the weld toe position (see Fig. 3.6) are chosen according to Fig. 3.10 and Table 3.1 in the case of circular hollow sections. Different sources recommend different distances from the weld toe. The terms with the product rt or RT result as basic geometrical parameters in cylindrical shell theory. Their relevance in practical applications has been doubted. The AWS and API guidelines[77,82] do not specify any extrapolation procedure. The inserted value $a = 0.1\sqrt{rt}$ is taken from older proposals. The actual formulation is 'adjacent to the weld toe', thus including part of the notch effect. The DEn,[91] ECSC (European Coal and Steel Community) and CIDECT (Comité International pour le Développement et l'Étude de la Construction

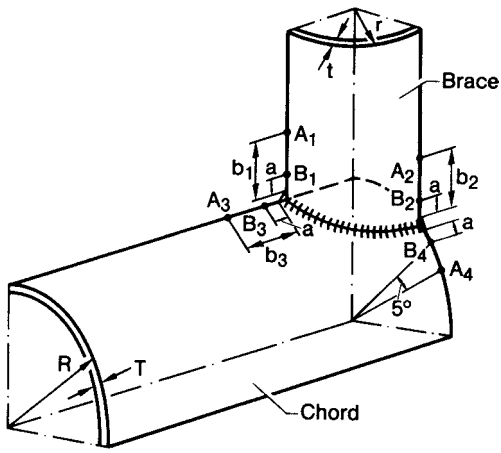


Fig. 3.10. Measuring and evaluation points positioned on circular tube joint for extrapolation of structural stresses on to the hot spot at the weld toe; after Wardenier.[197]

Table 3.1. Position parameters of evaluation points on circular tube joint used as the basis for extrapolation of the structural stress on to the hot spot at the weld toe according to different references, with chord tube radius R, chord tube thickness T, brace tube radius r and brace tube thickness t; compare Fig. 3.10; after Wardenier[197]

Reference	a	b_1, b_2	b_3
Dijkstra, de Back	$0.2\sqrt{rt}$	$0.65\sqrt{rt}$	$0.5\sqrt{RT}$
Gurney, van Delft	$0.4\,t$	$0.65\sqrt{rt}$	$0.4\sqrt[4]{rtRT}$
AWS, API	$0.1\sqrt{rt}$	–	–
DEn, ECSC, CIDECT	$0.4\,t$	$1.0\,t$	$1.0\,T$

Tubulaire) recommendations are preferred today. They can be transferred to rectangular section tubular joints and even to non-tubular members.

A non-linear extrapolation is recommended in those cases where the structural stress increase in the evaluation line is highly non-proportional. Three or more than three evaluation points are then positioned in the line section between $0.4t$ and $1.4t$, and a least square fit on the measured stresses is used to determine the quadratic function that describes the extrapolation to the weld toe.[190,191]

The influence of misalignment on the actual or endurable hot spot stresses in tubular joints is not considered to be a subject of concern. The reason may be that the approach was originally based on measured (and not computed) strains or stresses, so that geometric deviations were automatically covered. Only with increasing use of finite element analysis, performed for the geometrically 'ideal' structure, the question about changes in the hot spot stress caused by misalignment may be posed.

3.2.3 Evaluation of hot spot stresses in non-tubular joints

Hot spots are local areas at risk of fatigue crack initiation. In a welded structure of complex geometry consisting of plate and shell components ('plate-type joints'), it is not at all a trivial problem to identify all the potential hot spots. The hot spot stress procedure must therefore be directed to all these critical areas, not only to the actual crack initiation sites which may be known in advance in certain cases. Further complication arises from the fact that different loading cases have to be considered to act at the same structure with the consequence that different hot spot positions occur.

The hot spot structural stress approach for welded tubular joints has been transferred to welded joints of plate-type structures such as cover plate ends, longitudinal and transverse attachments, gusset plates, overlap joints, circular pads and girders with cope holes. This transfer was mainly promoted by experts at the IIW. Comparable developments in the field of automotive engineering are reviewed in Section 9.4.5. Regarding the fatigue-critical areas or hot spots, three different configurations may occur, which are classified into different types, Fig. 3.11: the weld toes on the plate surface at the ends of attachments (type A), the weld toes on the plate edge at the ends of attachments (type B) and the weld toes on the plate surfaces amid the weld along an attachment (type C, typical also for tubular joints).

Linear or non-linear extrapolation of the strains determined in two or three evaluation points on a line normal to the weld is recommended by Niemi[164] and Niemi and Tanskanen,[166] Fig. 3.12. The distances of the evaluation points from the weld toe depend on the plate thickness Fig. 3.12(a, b). Considering attachments welded to the edge of plate strips (forming in-plane notches, Fig. 3.12(c)), the plate thickness is no longer a

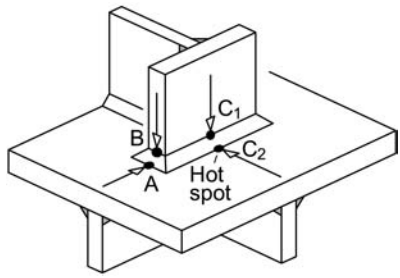


Fig. 3.11. Three types of fatigue-critical weld toes (types A, B, C) in plate-type reference structure proposed by Fricke.[110]

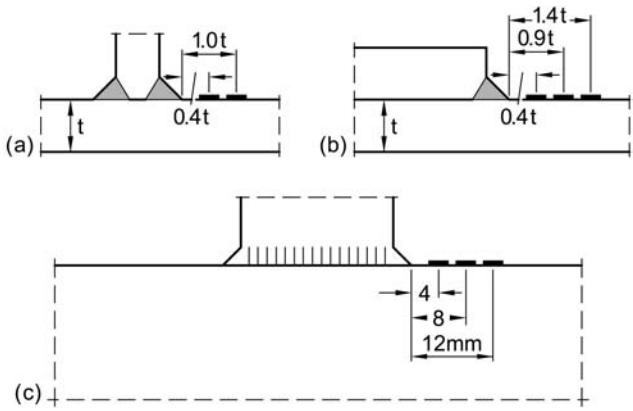


Fig. 3.12. Strain gauge positioning for the hot spot stress determination in plate-type structures: arrangement for linear (a) and non-linear (b) extrapolation of structural stresses on the plate surface of transverse or longitudinal attachments (weld toes of types A and C), and non-linear extrapolation of structural stresses at the plate edge in the case of edge attachments (weld toe of type B) (c); after Niemi and Tanskanen.[164,166]

suitable parameter to position the evaluation points for stress extrapolation. In this case, absolute distances for the evaluation points and quadratic extrapolation for the stresses are proposed. The minor influence of plate width on the extrapolated stresses is neglected.

Further recommendations relating to the hot spot stress extrapolation procedure are given by Alessandri *et al.*,[73] Huther *et al.*,[135–139] Labesse and Recho,[148] Machida *et al.*[155] and Yagi *et al.*[200] A non-linear extrapolation procedure based on the results of a local finite element substructure analysis with extremely fine meshing is proposed by Tveiten and Moan.[188] In numerical analyses, alternative procedures for hot spot stress determination are possible, such as the statically equivalent through-thickness linearisation of the stress distribution over the plate thickness at the weld toe (Radaj,[4] Dong

et al.[100]). A corresponding quasi-static linearisation of the surface stresses in locally refined meshes (element size $t/4 \times t/4$) over a distance t from the weld root (with plate thickness t) is proposed by Longobardi *et al.*[150]

The influence of misalignments on the hot spot stresses in plate-type structures, in contrast to the situation with tubular joints, is of major concern in application. Axial and angular misalignments are observed, which may contribute substantially to the magnitude of the hot spot stress, especially under axial (or membrane) loading, where secondary plate bending effects are induced. Both magnifications and reductions of the hot spot stress are possible. In relatively simple cases, the structural stress change by misalignment can be calculated on the basis of engineering formulae given in various guidelines.[3,17,76,86,151] The effect of misalignment on the hot spot stresses is especially pronounced in thin-walled structures. It is particularly strong for transversely loaded welds. The procedures selected for welding and quality assurance are of paramount influence on the magnitude of the effects.

Various conditions may prevail both for stress analysis or measurement and for endurable stress evaluation. The effect of misalignment on the hot spot stress is covered by stress measurements performed on the actual specimen or structure. It is only exceptionally covered within computational analysis by modelling the actual misalignments. Endurable hot spot stresses on the other hand are gained from test specimens which naturally have some misalignment. The fatigue tests may have been evaluated with or without correction with regard to misalignments. The assessment procedure in the IIW recommendations[133] is specified briefly below.

The stress-raising effects of actual or potential axial or angular misalignments on the hot spot stresses in the structural member to be fatigue-assessed must be taken into account when these are larger than 5%. The magnification of stress can be calculated by the engineering formulae mentioned above or by finite element analysis. If no relevant calculation is available, the magnification factors according to Table 3.2 should be applied to

Table 3.2. Magnification factors on hot spot stresses (membrane portion) for welded joints in those plate-type structures which are sensitive to misalignment effects (condensed information); after IIW recommendations[133]

Type of joint	Magnification factor k_m
Butt joints	1.10–1.25, but not $>(1 + 3e_{per}/t)$[a]
One-sided fillet welds (non-load-carrying)	1.20, but not $>(1 + 0.2\,t_0/t)$[b]
Cruciform joints (load-carrying welds)	1.40, but not $>(1 + 3e_{per}/t)$[a]

[a] e_{per}: permissible axial misalignment, t: plate thickness.
[b] t_0: reference plate thickness ($t_0 = 25$ mm).

the membrane portion of the structural stresses. The joints mentioned there typically show strong misalignment effects. The given factors are derived assuming typical allowable misalignments (e.g. 5–15% of plate thickness for axial misalignment).

3.2.4 Specific rules for finite element modelling

The structural stress analysis for welded tubular or plate-type structural members is mainly performed on the basis of the finite element method. The procedures for determining the hot spot stresses from the structural stress distribution originally developed for strain gauge application can be transferred to the finite element model which simulates the real structural behaviour. This leads to the surface stress evaluation and extrapolation illustrated by Fig. 3.13(a). The alternative procedures of stress linearisation over plate thickness are shown in Fig. 3.13(b, c).

A large number of well-designed textbooks are available covering the fundamentals and application of the finite element method in general. Among these, the treatise of Bathe[84] is rendered prominent here with regard to structural stress analysis. In practice, relatively simple models and coarse meshes are preferred for the hot spot stress analysis in order to limit the computational effort. Basically, two types of finite element models prevail, illustrated in Fig. 3.14 using the plate-type reference structure for fatigue-critical weld toes (Fig. 3.11). Specific modelling rules are reviewed below, which are mainly derived from investigations related to the IIW fatigue design recommendations.[133,165]

In thin-shell element models, the elements are arranged in the middle plane of the individual plates. The weld is frequently not modelled by

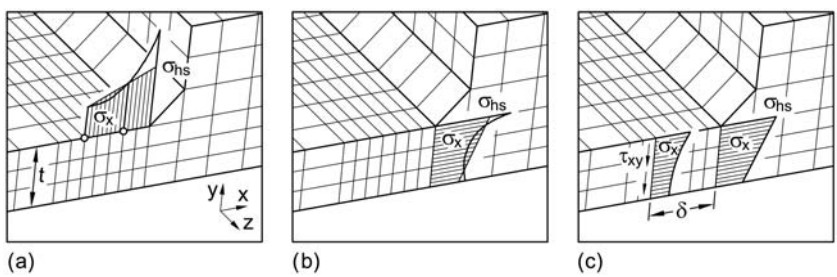


Fig. 3.13. Basic types of hot spot stress evaluation at the weld toe based on coarse finite element modelling (fillet-welded attachment as an example): surface stress linear extrapolation from two evaluation points (a), through-thickness stress linearisation in the weld toe section (b), and linearised equilibrium stresses from normal and shear stresses in some distance from the weld toe (Dong's proposal) (c); after Poutiainen *et al.*[179] (slightly modified).

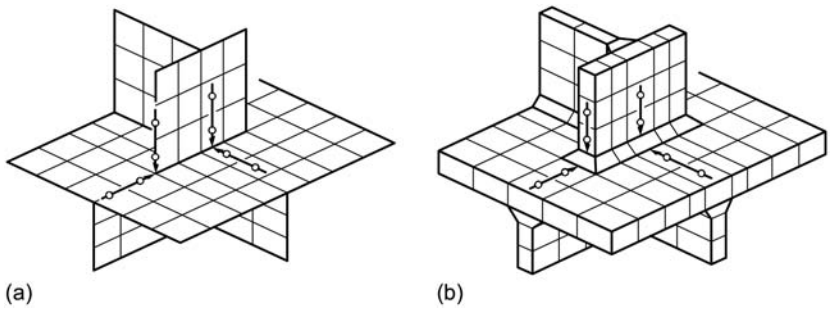


Fig. 3.14. Typical coarse-mesh finite element models for the plate-type reference structure in Fig. 3.11 with hot spot stress evaluation paths designated by arrows: thin-shell element model (a) and single-layer solid element model (b).

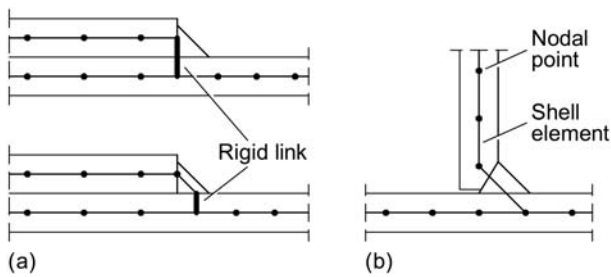


Fig. 3.15. Modelling of eccentric welds in thin-shell element models: cover plate joints (a) and T-joint with single-sided welds (b).

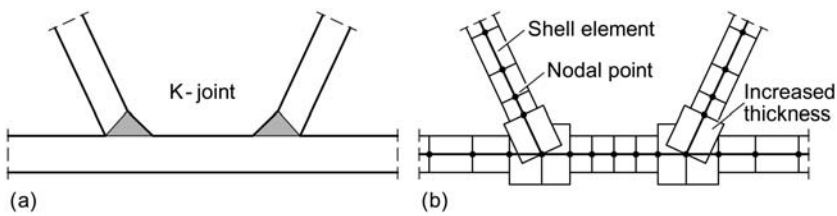


Fig. 3.16. Compensation for weld zone stiffening in thin-shell-element models by increased element thickness; cross-section of welded joint (a) and shell element model (b).

separate elements, except in cases of eccentric weld arrangements, e.g. at cover plate joints and single-side-welded T-joints, Fig. 3.15, or at closely neighbouring welds with corresponding interaction effects, where the weld may be modelled by normal or inclined shell elements, by rigid links or simply by increased element thickness, Fig. 3.16. In these cases, the actual

finite stiffness of the weld in the longitudinal and transverse directions should be taken into account as far as possible. The shell elements in the model should be able to simulate in-plane stress gradients. As mentioned before, thin-shell elements naturally provide a linear stress distribution over the shell thickness, suppressing the notch stresses at weld toes. Alternatively, the structural stresses are frequently extrapolated to the weld toe from the evaluation points recommended in the case of measured surface stresses.

In solid element models, the weld is modelled by prismatic elements. Basically, two plate model types are possible: one type characterised by the arrangement of several element layers and the other by only one element layer over the thickness. The single-layer arrangement is recommended in connection with isoparametric 20-node hexahedronal elements. But the accuracy of the stresses in the critical section is degraded by the non-simulated stress singularity actually occurring at the sharp notch. Therefore, surface stress extrapolation to the hot spot is generally recommended in this case. Improved accuracy can also be achieved by an adjustment of the displacement function to satisfy the free surface condition better at the hot spot by reducing the unbalanced stress components (Soh[185]). The multi-layer arrangement of hexahedronal elements allows linearisation of the stresses over the plate thickness evaluated from the elements butting from the plate side (Poutiainen *et al.*[179]).

The arrows in Fig. 3.14 show typical stress evaluation paths for surface stress extrapolation to the hot spot. In the case of thin-shell models without separate weld elements, it is recommended the stresses be extrapolated to the 'substitute hot spot' at the intersection line of the plates (substituting the weld toe line) in order to compensate for stress reduction caused by the missing weld stiffness in the model (Fricke[110]).

In the following two paragraphs, additional recommendations are given for mesh generation and stress evaluation in connection with surface stress extrapolation to the hot spot at the weld toe (or to the 'substitute hot spot' at the intersection line), which are based on round-robin studies (Fricke[110]) and summarised in IIW recommendations.[133,165]

For plate surface weld toes of types A and C (see Fig. 3.11), the linear stress extrapolation from two evaluation points is widely used. For distances $0.4t$ and $1.0t$ from the weld toe, Fig. 3.17(a), the stresses are typically evaluated at element corner nodes, so that the length of the first element is at least $0.4t$ and of the second $0.6t$. If finer meshes are used, the refinement should be introduced both in the longitudinal and thickness directions (Poutiainen *et al.*[179]). A different stress extrapolation scheme is recommended by some ship classification societies (e.g. Germanischer Lloyd) in connection with coarser meshes and evaluation points at distances of $0.5t$ and $1.5t$ from the weld toe, Fig. 3.17(b). The resulting hot spot stress is approximately the same as the stress resulting from the more common

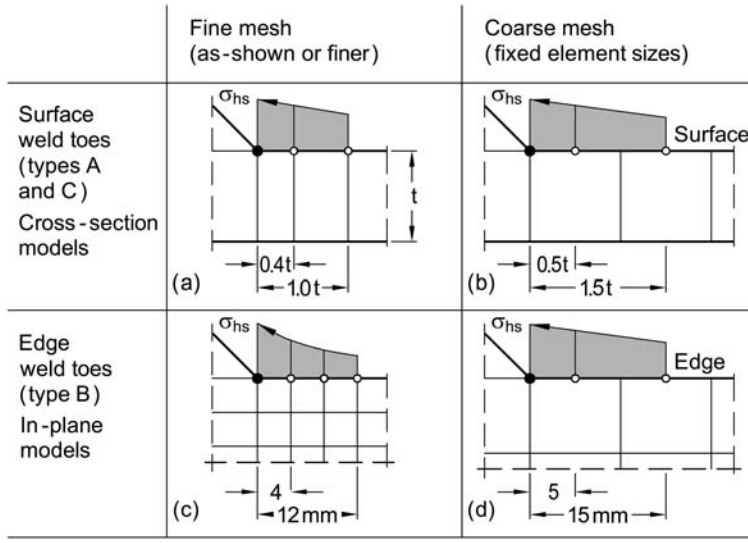


Fig. 3.17. Recommended extrapolation of surface or edge stresses to the hot spot in fine or coarse finite element meshes; after Doerk *et al.*[93]

procedure mentioned above. This is because the computed midside stress at the 0.5*t* location is somewhat larger than the stress, which is obtained from a finer mesh or from strain measurements (Doerk *et al.*[93]). This 'non-converged' midside stress, which is discussed in more detail by Healy,[132] requires a fixed element size equal to plate thickness to obtain consistent results. At plate surface weld toes of type A, the width of the two shell elements or the one solid element in front of the attachment end or weld toe, respectively, should not exceed twice the plate thickness t or once the reinforcement width w_r (i.e. the attachment thickness plus the two weld leg lengths). The influence of element width on the hot spot stress is further discussed by Poutiainen and Niemi[178] and by Doerk *et al.*[93]

For plate edge weld toes of type B (see Fig. 3.11), the situation is different. Following the proposal by Niemi and Tanskanen[166] to use evaluation points at distances of 4, 8 and 12 mm from the weld toe combined with quadratic stress extrapolation, element sizes of 4 mm edge length are required to obtain nodal point stresses which are less affected by the theoretical stress singularity at the sharp weld toe notch, Fig. 3.17(c). An alternative procedure for stress extrapolation in the case of a coarser mesh is proposed by Fricke and Bogdan,[112] using the slightly enlarged midside stresses of larger quadrilateral elements (edge length 10 mm), Fig. 3.17(d).

In the case of multiaxial stress states in the evaluation area, it is recommended that the different stress components be extrapolated individually

to the hot spot. The extrapolated stress components are used to compute the first principal stress which is considered to be fatigue relevant instead of the stress component normal to the weld toe line, provided it remains within an angle of ±60° from the normal.

Software tools supporting the application of the structural stress approach for seam-welded joints are primarily designed as postprocessors of finite element program systems, for example, the program FEMFAT (Finite Element Method FATigue).[107,108] Relevant finite element data processing is demonstrated by Glinsner *et al.*[125,126]

3.2.5 Further variants of structural stress evaluation

The following structural stress evaluations are used within Dong's approach.[94,100] The details depend on the type of finite element model, but the principles are the same. Plane longitudinal sections normal to the weld toe line are considered in the case of the δ-method below. The shear stresses in the sectional planes are neglected. Stresses or line forces may vary over the weld length.

In the case of thin-shell element models, which are widely used for fatigue analyses, the stresses or line forces are evaluated at a small distance δ from the weld toe (next mesh line in general): normal stresses σ_x and shear stresses τ_{xy} or line normal force f_x, line shear force f_y and line bending moment m_z, respectively, in the corresponding section. Statically equivalent linearised structural stresses σ_m (membrane component) and σ_b (bending component) in the weld toe section (besides the shear stresses in this section) are derived by evaluation of equilibrium conditions, demonstrated in Fig. 3.13(c) for a solid element model. These are claimed to be mesh insensitive and more accurate, because the critical stress evaluation in the re-entrant corner point of the weld toe is avoided. As an alternative procedure, the element nodal forces in the weld toe section (i.e. $\delta = 0$) can be evaluated, from which the line forces and moments are calculated on the basis of appropriate shape functions (resulting in the membrane and bending stresses). A linear equation system has to be solved to obtain the line forces and moments for all nodal points connected by the weld toe line (Dong *et al.*[100]). It is recommended that the fillet weld be modelled by inclined shell elements generating a continuous weld line for stress evaluation with inclusion of areas at the ends of attachments. The nodal-force-based method is preferred today to the earlier δ-method. Common stress output from finite element systems may be too inaccurate in the case of coarse meshes.

A postprocessor is offered to handle the element nodal force evaluation in the weld toe line (Kyuba and Dong[147]). The following tasks are accomplished: processing of the shell element nodal forces and moments in the

weld line (output from ABAQUS or NASTRAN), conversion from the global to the local (weld line oriented) coordinate system, line forces and moments with linear distribution between the nodal points derived from the nodal forces and moments (solution of a linear equation system with element length-dependent coefficients) and conversion of the line forces f_x (vector normal to the weld line) and line moments m_z (vector in the weld line) to (membrane and bending) structural stresses introducing the shell thickness t:

$$\sigma_s = \sigma_m + \sigma_b = \frac{f_x}{t} + \frac{6m_z}{t^2} \tag{3.1}$$

In the case of solid element models with two or more layers of elements over plate thickness or plate width (edge attachment), which are used for fatigue analysis in the case of thick or wide sections, the stresses are once more evaluated at a small distance δ from the weld toe (the neighbouring mesh line in general) in combination with an arbitrary depth $t_1 \leq t$. A variable depth is introduced with regard to non-monotonic stress distributions over plate thickness (depth t_1 set equal to $t/2$ in symmetric configurations) as well as with regard to the crack propagation analysis starting with a small initial crack at the weld toe (depth t_1 corresponding to the crack size, which is considered to be the failure criterion). The original distributions of the stress σ_x in the sections A–A and B–B are shown in Fig. 3.18(a) (in section A–A comprising the notch effect). The linearised structural stresses σ_m and σ_b are calculated from the equilibrium conditions applied to the rectangular slab A–A′–B′–B with the boundary stresses in the section lines B–B′ and

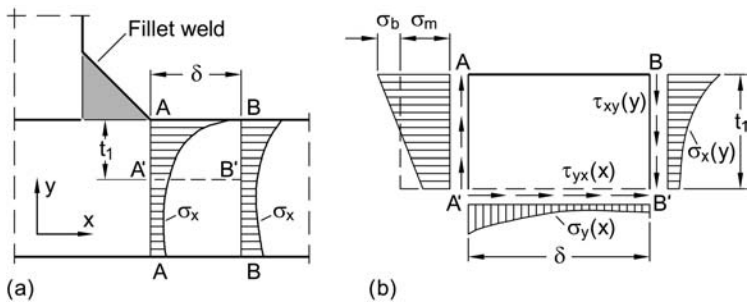


Fig. 3.18. Principle of Dong's equilibrated structural stress evaluation: original distribution of stresses σ_x over plate thickness in weld toe section A–A and in nearby reference section B–B (a), and linearised structural stresses σ_m and σ_b over variable depth t_1 equilibrated by the original stresses at the boundaries B–B′ and A′–B′ of rectangular slab A–A′–B′–B (original stresses gained from a finite element model) (b); after Dong.[94]

A′–B′ gained from the finite element model, Fig. 3.18(b). Once more, it is preferable today to evaluate the element nodal forces in the weld toe section and to apply appropriate shape functions for the stresses (not easily solved in the case of two dimensions) instead of using the δ-method which presumes a reasonably fine mesh to keep δ small. The formulae for the bilinearised stresses are given in Section 6.2.10. Bilinearisation in symmetrical configurations is achieved by simple linearisation over half the plate thickness.

The question of whether Dong's procedures for structural stress evaluation are more robust and mesh-insensitive than those described for tubular or non-tubular joints (see Sections 3.2.2 and 3.2.3) has been addressed by several authors (Doerk *et al.*,[93] Poutiainen *et al.*,[179] Healy[132]). It turns out that the hot spot stresses from surface stress extrapolation may show significant variations in the case of coarse meshes and certain element types. But Dong's procedure also has shortcomings. The required modelling of a continuous weld line in shell element models may create stress variations owing to the influence of the weld stiffness. In the δ-procedure proposed for solid element models, the influence of the shear forces acting in the lateral faces of the elements is neglected, which produces errors depending on the element size (Doerk *et al.*[93]).

The hot spot stresses from surface stress extrapolation, from linearisation over plate thickness and from linearisation over depth $t_1 < t$ (as proposed by Dong) cannot be expected to be identical (see Section 3.1.6 concerning Dong's procedure). Further hot spot stress evaluation procedures based on finite element modelling, which are used in the field of automotive engineering, are reviewed in Section 9.4.5.

3.2.6 Definition of structural stress concentration factors

The structural stress concentration factor K_s is defined by referring the maximum structural stress σ_s to the nominal stress σ_n:

$$K_s = \frac{\sigma_s}{\sigma_n} \tag{3.2}$$

The structural stress σ_s is either the stress component normal to the weld toe line or the first principal stress.

Maximum structural stresses in thin-shell or solid element models of welded structural members generally occur at cross-sectional transitions, at cutouts, at the intersection lines of the jointed parts or at the weld toe or weld root lines. These positions are not necessarily identical to the points of crack initiation, the hot spots. The discrepancy is due to the fact that cracks are initiated mainly at points of excessive notch effect or strength

reduction which may be different from the point of maximum structural stress. Therefore, the structural stress concentration factor of thin-shell or solid element models is useful for direct strength assessments only in those cases where it approximates the hot spot stress concentration.

The application of the structural stress concentration factors for fatigue strength assessment in shipbuilding[142,161,174,175] (reviewed by Radaj[4]) comprises I-section girders and double-bottom structures in a multibox design. Under transverse force bending of these components, the bending stresses in the flange or cover plate are unevenly distributed. The structural stresses in the flange or cover plate are thus increased by a factor α (α = 1.2–1.8 for double-bottom corner joints with flange width to web height ratios, w/h = 0.4–0.6):

$$K_s = \alpha K_{s0} \tag{3.3}$$

where K_s is the structural stress concentration factor, K_{s0} is the structural stress concentration factor with an even flange stress distribution, i.e. in the pure bending mode and α is the factor for the increase of flange stress in the web-flange intersection line above its mean value in the flange.

The hot spot stress concentration factor K_{hs} is defined by referring the structural stress σ_{hs} at the crack initiation point, the hot spot, to the nominal stress σ_n:

$$K_{hs} = \frac{\sigma_{hs}}{\sigma_n} \tag{3.4}$$

The total hot spot stress σ_{hs} may be composed of the hot spot stress components from different loading cases, e.g. axial and bending loads:

$$\sigma_{hs} = \sigma_{na} K_{hs\,a} + \sigma_{nb} K_{hs\,b} \tag{3.5}$$

where σ_{na} and σ_{nb} are the nominal stresses under axial and bending loads, and $K_{hs\,a}$ and $K_{hs\,b}$ are the hot spot stress concentration factors relating to these loads.

The total hot spot stress normal to the weld at definite chord locations in a tubular joint (e.g. crown and saddle point) from different loading cases of different brace tubes is calculated by superimposing the relevant stress components (a repeated subscript indicates summation as the index that is repeated takes the values in parentheses):

$$\sigma_{hs,\,i} = \sigma_{na,\,j} K_{hs\,a,ij} + \sigma_{nb,\,j} K_{hs\,b,ij} \quad (i = 1, 2, \ldots, n;\ j = 1, 2, \ldots, m) \tag{3.6}$$

where $\sigma_{hs,\,i}$ is the total hot spot stress at location i, $\sigma_{na,\,j}$ and $\sigma_{nb,\,j}$ are nominal stresses under axial and bending load of brace j, $K_{hs\,a,ij}$ and $K_{hs\,b,ij}$ are hot spot stress concentration factors at location i under axial and bending load

from brace j (also named 'influencing functions'), n is the number of hot spot locations and m is the number of braces.

3.2.7 Hot spot stress concentration factors for tubular joints

Welded tubular joints consisting of intersecting brace and chord tubes exhibit a pronounced structural stress concentration at the hot spots in the tube intersection area close to the welds. The hot spot stress at the crack initiation point is related to the nominal stress in the brace tube yielding the hot spot stress concentration factor. For symmetrically arranged tubes with circular cross-section, Fig. 3.19, the hot spot stress concentration factor K_{hs} is a function of the independent shape parameters:

$$K_{hs} = f(\lambda,\ \delta,\ \Delta,\ \vartheta,\ \theta,\ \gamma,\ \varepsilon) \tag{3.7}$$

where $\lambda = 2L/D$ is the length-to-diameter ratio of the chord, $\delta = d/D$ is the tube diameter ratio, $\Delta = D/2T$ is the diameter-to-thickness ratio of the chord, $\vartheta = t/T$ is the wall thickness ratio, θ is the brace-versus-chord angle, $\gamma = g/D$ is the gap width ratio, $\varepsilon = e/D$ is the eccentricity ratio, L is the length of the chord between the points of zero moment, D and d are the outside diameters of the chord and the brace, T and t are the wall thicknesses of the chord and the brace, g is the gap width between the brace tubes and e is the eccentricity of the brace node.

The parameter λ comes in only in the case of transverse bending of the chord. The ratios γ and ε are not independent parameters. Therefore, only γ or ε will occur in the stress concentration formula. The diameters D and d refer to tubes with a circular cross-section. They are substituted by the cross-sectional widths in the case of tubes with square cross-section.

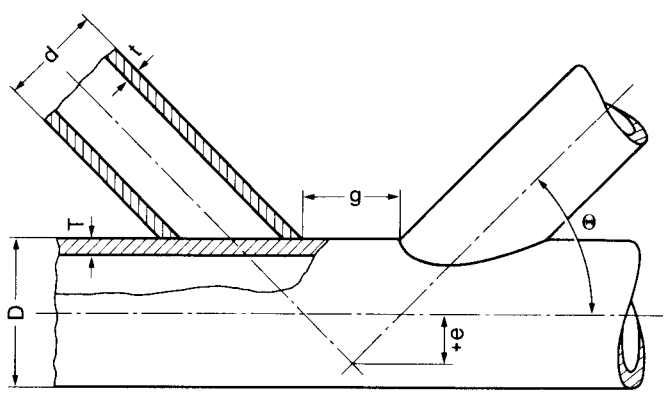


Fig. 3.19. Geometric parameters of symmetric K-type tubular joints.

The Greek letters designating the shape parameters are chosen to correspond to the Roman letters designating the appertaining geometric parameters. They deviate from the convention of the tubular joint experts (the conversion is: $\lambda \to \alpha$, $\delta \to \beta$, $\Delta \to \gamma$, $\vartheta \to \tau$).

A particularly simple form of the function f follows from a least square fit of testing or calculation results in logarithmic scales when evaluating parametric studies (similar to the corresponding notch stress formula, see eq. (4.9)):

$$K_{\mathrm{hs}} = k\lambda^{p_1}\delta^{p_2}\Delta^{p_3}\vartheta^{p_4}(\sin\theta)^{p_5}\gamma^{p_6}\varepsilon^{p_7} \tag{3.8}$$

where k is the coefficient and p_ν are the exponents from the least square fit ($\nu = 1, 2, \ldots 7$).

The parametric formulae for hot spot stress concentration factors of welded tubular joints of different shapes with circular tube cross-section are reviewed by Wardenier[197] (*ibid*. pp. 8-52 to 8-57). A more recent review is given by Efthymiou.[106] Relevant formulae for T-, X- and K-joints with square tube cross-section are published by van Wingerde *et al*.[192] The parametric formulae are mainly derived from finite element results. Strain gauge measurements on acrylic models are sometimes evaluated. A clearly arranged generally applicable procedure for determining the hot spot stress concentration factors of square- and circular-section tubular joints is presented in the fatigue design guidelines by Packer and Henderson[168] (*ibid*. pp. 279–284), van Wingerde *et al.*[191] and Zhao *et al.*[203,204] Further formulae and design charts with hot spot stress concentration factors have been published by van Wingerde *et al.*[193,194] More recent parametric studies are aimed at the structural stress distribution along the intersection line of the tubes (Chang and Dover[88,89]) and on hot spot stress concentration factors for overlapped tubular K joints (Gho *et al.*[124]) and for three-dimensional (multiplanar) tubular joints (Chiew *et al.*[90]). The stress gradient in the wall thickness direction or the degree of local bending is also analysed (Chang and Dover[87]). Some of the formulae mentioned are evaluated in Section 9.2.2.

Note, that the definition of the hot spot stress may be different in the various formulae. The evaluation may be restricted to the crown and saddle points in the case of circular section tubes. The positioning of the evaluation points for linear extrapolation to the weld toe may also be different. A non-linear extrapolation is introduced in some cases. Older publications evaluate the maximum structural stress in the intersection lines of the tubes. Therefore, it is recommended that the original publication be consulted in respect of the stress definition before using a formula. Additionally, accuracy considerations are necessary. In general, the deviation of the formula from the finite element results will be less than ±10%, but much larger deviations have also been recorded (e.g. ±30%, and even more by van Wingerde *et al.*[190,191]).

The structural stress concentrations at the intersection line of thin-shell element models of nozzles in the knuckle region of pressure vessel heads loaded by internal pressure and nozzle-external loads have been computed by Bauer and Saal[85] with systematic variation of the geometrical parameters.

3.2.8 Hot spot stress concentration factors for non-tubular joints

Hot spot stress concentration factors have also been derived for non-tubular (plate-type) members, e.g. I-section girders with cope holes (Miki and Tateishi[162]), flange cover plates, gusset plate weld ends and joints with angled flanges (Fricke *et al.*[113,118,119,122]).

In the first mentioned paper,[162] the hot spot structural stress approach has been applied to assign the appropriate notch or detail class within the nominal stress approach to I-section steel girders with in-plane cope holes used in railway and highway bridges, Fig. 3.20(a). The hot spot stress concentration factor of the cope hole referring to the nominal bending stress in the girder is derived on the basis of elementary engineering considerations, Fig. 3.20(b), finite element analysis and hot spot strain measurements. The hot spot stress concentration factor is presented as a function of the following shape and internal force parameters, $K_{hs} = f(\vartheta, \rho, \Gamma)$, where $\vartheta = t_f/t_w$ is the flange thickness to web thickness ratio, $\rho = R/t_f$ is the hole radius to flange thickness ratio, $\Gamma = Fw/M_b$ is the internal force ratio, t_f and t_w are the thicknesses of flange and web, R is the cope hole radius, F and M_b are the transverse force and the bending moment in the cross-section with the cope hole and w is the width of the flange.

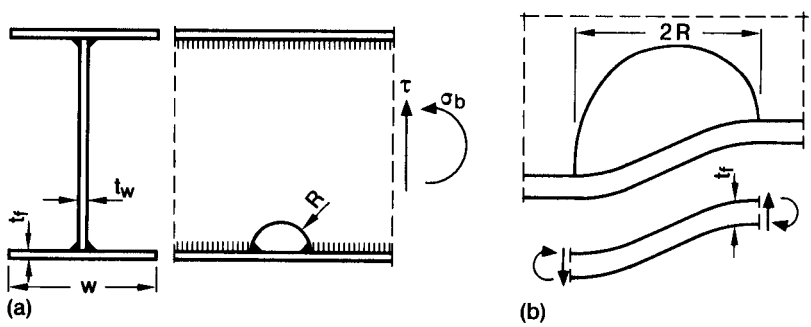


Fig. 3.20. Geometrical and internal force parameters of I-section girder with cope hole (a) and engineering approach to structural stress analysis (b); after Miki and Tateishi.[162]

The equation for K_{hs} is simplified by introducing typical geometric data from Japanese railway and highway bridges including the condition $R/t_f \leq 3.0$:

$$K_{hs} = 1 + 1.6\left(\frac{t_f}{t_w}\right)^{-0.54} + 2.9\left(\frac{t_f}{t_w}\right)^{0.23}\left(\frac{\tau}{\sigma_b}\right) \tag{3.9}$$

where τ is the average shear stress in the web and σ_b is the nominal bending stress in the girder. The hot spot stress concentration factor determined for $t_f/t_w = 1.0$ and $\tau/\sigma_b = 0$–1.0 amounts to $K_{hs} = 2.6$–5.5, i.e. substantially higher values than comparable data published by Fricke and Paetzold.[118] Further application-relevant details are given in Section 3.4.3.

The hot spot structural stress approach has been applied to other welded joint details of bridge girders which were fatigue-tested at full size (Anami and Miki[74]). The effect of cross-sectional transitions on the structural stresses and their endurable values in girders has been investigated by Youn and Kim.[201]

3.3 Analysis tools – endurable structural stresses or strains

3.3.1 Endurable structural strains in the Haibach approach

A strain-gauge-averaged cyclic structural strain of $\Delta\varepsilon_s = 0.063\%$ (associated with failure probability $P_f = 50\%$) is recommended as an endurable strain and a corresponding cyclic structural stress of $\Delta\sigma_s = 80\,N/mm^2$ (associated with $j_\sigma = 1.65$ corresponding to a failure probability $P_f = 0.1\%$) is recommended as a permissible stress for structural steels at $N = 2 \times 10^6$ cycles including high tensile residual stresses produced by welding (Haibach,[2] *ibid.* p. 218), whereas the original endurable cyclic strain for structural steels ($R = -1$, specimens not stress-relieved) comes up to $\Delta\varepsilon_s = 0.06$–$0.14\%$ (larger values for smaller plate thickness).[129] The relevant endurable cyclic strain for the welded aluminium alloy AlZnMg1 amounts to $\Delta\varepsilon_s = 0.26\%$.[130] The endurable strains or stresses for $N = 2 \times 10^6$ cycles are transferable to the medium-cycle fatigue range with $N < 2 \times 10^6$ cycles by applying the inverse slope k according to the normalised S–N curve.

A recommendation for the application of weld toe strain gauges according to Haibach[2,129] is given with Table 3.3. Length and position of the gauge are dependent on plate thickness.

3.3.2 Endurable hot spot stresses in tubular joints

The design S–N curves of permissible hot spot stresses for welded tubular joints given in the technical literature and in the codes limit the scatter band

Table 3.3. Recommendation for the application of weld toe strain gauges; after Haibach[2,129]

Plate thickness [mm]	Gauge length [mm]	Centre distance [mm]
1–5	1.5	>1.0
5–25	3.0	>2.0

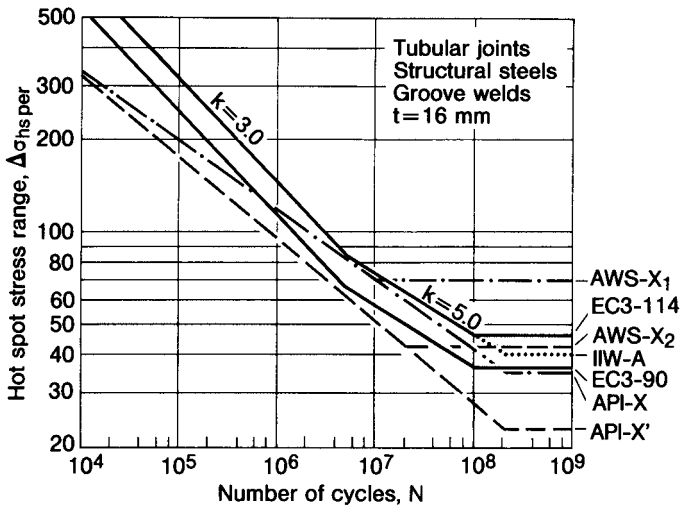


Fig. 3.21. Permissible hot spot stress range for welded tubular joints according to different fatigue guidelines; curve extensions above endurance limit with $k = 5.0$ relating to damage accumulation; after Wingerde *et al.*[190,191]

of test results from below, corresponding to endurable stresses with a failure probability of $P_f = 2.3\%$. It is a characteristic feature of the structural stress approach for welded joints that endurable amplitudes or ranges of cyclic stress are considered, neglecting the influence of static mean stress or stress ratio (high tensile residual stresses being assumed in welded joints).

Basic hot spot stress *S–N* curves for the design of welded tubular joints are plotted for comparison in Fig. 3.21. The term 'basic' means that corrections to these permissible stresses are possible and necessary, for example, a correction for the actual wall thickness or for the actual weld profile (see van Wingerde *et al.*[190,191]). The diagram comprises design curves from the IIW guideline,[30] the HSS recommendation[190,191] based on the Eurocode 3[23] (more or less identical to the DEn guideline,[91] the AWS design code,[82] and

the API recommendation[77]). The variants AWS-X_1 and API-X refer to an improved weld profile, e.g. by grinding or remelting of the weld toe. The curves with the exception of the Eurocode 3 variants have been derived for tubular joints with circular tube cross-sections. Only the HSS recommendation distinguishes between circular section tubes (notch or detail class 114, i.e. 114 N/mm^2 at 2×10^6 cycles) and rectangular section tubes (notch or detail class 90, i.e. 90 N/mm^2 at 2×10^6 cycles). The reference wall thickness is $t = t_0 = 16$ mm. Groove butt welds with complete or partial joint penetration are considered. The design stress curves apply to tubular joints in the as-welded condition. Any load ratio R is allowed.

When using the above design stress curves, one should be aware of the fact that the different curves may have been derived in connection with different hot spot stress or strain definitions (the AWS or API specifications are different from the DEn and Eurocode 3 specifications). Also, different parametric formulae for the hot spot stress concentration are proposed in different guidelines. Therefore, it is important for sufficient reliability of the strength assessment that the appropriate design stress curves, hot spot stress or strain definitions and parametric stress concentration formulae are combined.

The dependency of the endurable hot spot stress on larger than usual wall thickness is expressed by the fatigue strength reduction factor $\gamma = (t_0/t)^n$ (see e.g. (2.24)), where t_0 is the plate thickness assigned to the design S–N curve, t is the actual plate thickness ($t > t_0$) and n is an exponent.

The exponent n for $t > t_0$ is prescribed by DEn[91] to be $n = 0.3$ with $t_0 = 16$ mm or by Eurocode 3[23] to be $n = 0.25$ with $t_0 = 25$ mm as originally proposed by Gurney.[26,127] The thickness correction should be extended down to $t = 4$ mm according to the old IIW recommendations[30] in order to avoid oversizing of tubular joints. The relevant correction found in the ECCS and CIDECT research programs is $n = 0.11 \times \log N$. Design stress curves derived on that basis are shown in Fig. 3.22. There is no gain in strength for thicknesses lower than $t = 4$ mm. A more recent unified diagram is presented by Zhao and Packer.[204]

Considering variable-amplitude loading, Miner's cumulative damage rule can be applied with reference to the hot spot stress S–N curve extended beyond the endurance limit. Each potential point of crack initiation should be treated separately. The permissible damage sum in non-corrosive environment is introduced with $D_{per} = 0.5$–1.0 according to the design guidelines for tubular joints.

For inadequately protected joints in corrosive environments, e.g. offshore structures, the hot spot stress S–N curves in the above figures should be projected linearly onwards for $N > 5 \times 10^6$ cycles on their original slopes, and no endurance limit should be assumed. Furthermore, the

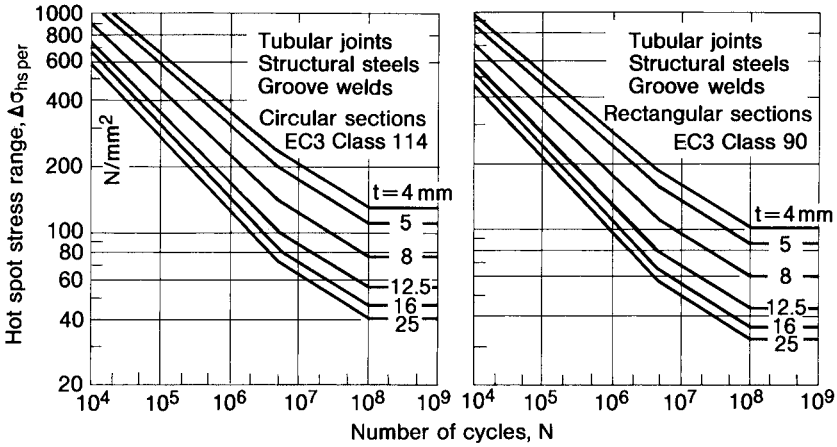


Fig. 3.22. Permissible hot spot stress range for welded tubular joints according to Eurocode 3 (EC3)[23] with wall thickness correction on the basis of design stress curves for $t = t_0 = 16$ mm, circular and rectangular hollow sections; endurance limit at 5×10^6 cycles; after Wingerde *et al.*[190,191]

number of cycles so obtained for a preset stress range should be divided by two to reflect the conditions of corrosion fatigue appropriately (Packer and Henderson[168]).

3.3.3 Endurable hot spot stresses in non-tubular joints

Endurable hot spot stresses in welded joints of plate-type structures have been reviewed and uniformly evaluated by Niemi *et al.*[146,164,170–172] The evaluations include butt-welded and fillet-welded joints, gusset plates, longitudinal attachments, circular pads and cover plates. The materials comprise CMn steels, stainless steels (ferritic and austenitic) and aluminium alloys.

A more recent evaluation of endurable hot spot stresses in plate-type welded joints made of structural steels has been presented by Maddox,[156] who distinguishes between transverse and longitudinal fillet welds. Data from fatigue tests both with small scale and component-like specimens were included. The hot spot stress was measured in accordance with the IIW recommendations,[3,165] thus including the misalignment effect in the hot spot stress.

The evaluation results for transverse fillet welds (corresponding to type C in Fig. 3.11) in structural steels are shown in Fig. 3.23(a). The fatigue test results indicate that the fatigue class FAT 90 (see Fig. 2.4) according to the IIW recommendations[3] transferred from nominal to hot spot stresses

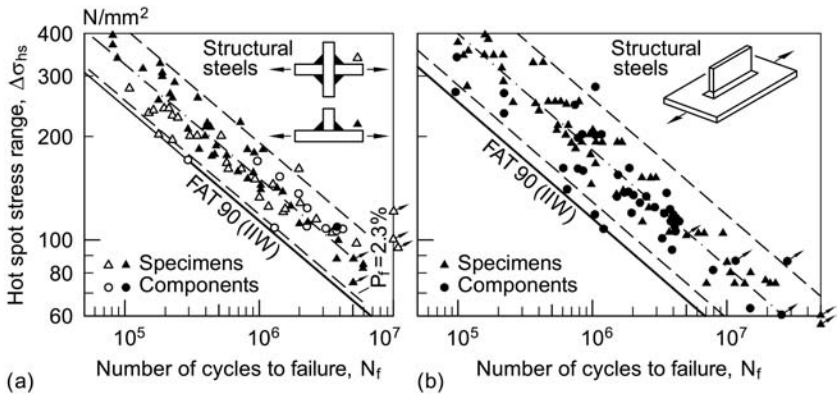


Fig. 3.23. Endurable hot spot stress ranges from fatigue tests and corresponding FAT design curves for load-carrying and non-load-carrying transverse fillet welds and comparable joints (a) and for fillet weld ends at longitudinal attachments (b); after Maddox.[156]

should be appropriate, as was also found for comparable structural details (Lotsberg and Sigurdsson[154]). However, if the results for non-load-carrying and load-carrying fillet welds are evaluated separately, it is obvious that the non-load carrying fillet welds (black symbols) show a higher fatigue strength, which justifies the assignment of fatigue class FAT 100. The different endurable hot spot stresses are attributed to the different weld throat forces and weld toe notch effects in the case of load-carrying and non-load-carrying fillet welds. The difference in notch stress concentration at the weld toe is not attributed to the structural stress at the hot spot, so that this effect has to be taken into account in the endurable hot spot stresses. Poutiainen and Marquis[177] proposed an alternative procedure, namely including this effect in the hot spot stress by superimposing the nominal stress in the weld throat on the structural stress at the weld toe gained from through-thickness stress linearisation in the plate.

The evaluation results for weld toes at the end of longitudinal attachments (corresponding to type A in Fig. 3.11) are shown in Fig. 3.23(b). The evaluation suggests the conservative assignment of fatigue class FAT 90 to the hot spot stresses although FAT 100 would also be appropriate, as indicated by the lower bound of the scatter range ($P_f = 2.5\%$). For weld toes on plate edges (corresponding to type B in Fig. 3.11), fatigue tests (Niemi and Tanskanen[166]) and comparisons between structural stresses and notch stresses (Fricke and Bogdan[112]) at the hot spot have shown that the assignment to the fatigue classes FAT 90 or FAT 100 to the hot spot stresses is appropriate. The lower class should be used with long edge attachments (e.g. $l > 100$ mm).

Several codes and guidelines have defined the hot spot design S–N curve for steel joints according to fatigue class FAT 90, which corresponds to the above findings. The IIW recommendations[3,165] distinguish between the different cases described above by suggesting the fatigue class FAT 100 in general and FAT 90 for cases with load-carrying fillet welds as well as for long edge attachments (length above 100 mm). The endurable hot spot stress ranges above in structural steels have to be substituted by endurable values according to FAT 40 and FAT 36 in aluminium alloys (Partanen and Niemi,[172] Maddox[156]).

The plate thickness effect should be taken into account by eq. (2.24) with the reference thickness $t_0 = 25$ mm and the exponent $n = 0.2$ for butt-welded joints, $n = 0.3$ for fillet-welded joints and $n = 0.1$ for edge attachments (IIW recommendations[3,165]). The effect is considered in more detail below without differentiation between the structural and the nominal stress approach. Gurney[128] proved that eq. (2.24) should be modified in the case of transverse stiffener joints (fillet-welded or with full-penetration double-bevel butt welds) giving increased fatigue strength for sufficiently small attachment lengths (in the loading direction). It is recommended that a reduced 'apparent thickness' $t' \leq t$ be used in eq. (2.24) which depends on the attachment length l (i.e. the stiffener thickness plus the leg lengths of the weld) if this length is sufficiently small (i.e. $l \leq 2t$ in tension loading, $l \leq 0.65t$ in bending loading). Simultaneously, the exponent is slightly reduced.

The large data stock from fatigue tests of welded joints in the 16–200 mm thickness range have been reviewed by Örjasäter[167] in respect of the thickness correction factor. The following conclusions were drawn from the evaluation. The exponential correction is suitable up to 200 mm plate thickness. The major factors with influence on the exponent n are the stress concentration and the statistical size effect. A general thickness correction of $n = 1/3$ (typical for bending loads) is proposed which can be modified according to the structural detail in more accurate calculations. For joints with severe hot spot stress concentrations, such as tubular joints, the exponent is increased to $n = 0.4$. For less severe cases (axial loading, butt welds, ground or remelted weld toes, stress concentration factor $K_t \approx 1.5$) a correction with $n = 0.2$ is appropriate. For smooth structural members (ground flush welds without flaws and parent material) a correction with $n = 0.1$ can be applied. The effects of postweld heat treatment, random loading, stress ratio R and corrosion are also insignificant for the thickness effect.

The potentially higher endurable hot spot stresses in an improved weld profile especially at the weld toe (e.g. by grinding, remelting or peening) are not yet sufficiently accounted for in the hot spot design S–N curves. Considerable gains in fatigue strength may be possible but control of the treatment process and weld profile is necessary in this case (Haagensen and Maddox[28]).

3.3.4 Endurable structural stresses in the Dong and Xiao–Yamada approaches

The fatigue strength in Dong's structural stress approach[94,95,100,101] is characterised by a special structural stress parameter ΔS_s plotted over number of cycles, termed the 'master *S–N* curve', whose parametric form is derived from a two-stage crack propagation analysis:

$$\Delta S_s = \frac{\Delta\sigma_s}{\left[I(\delta_b)^{1/m}\right]}\left(\frac{t}{t_0}\right)^{1/2-1/m} \tag{3.10}$$

$$\delta_b = \frac{|\sigma_b|}{|\sigma_b| + |\sigma_m|} \tag{3.11}$$

with the structural stress range $\Delta\sigma_s$ at the hot spot (in part deviating from the usual hot spot stress definition, see Section 3.1.6), the plate or wall thickness t, the reference thickness t_0, the exponent m from the modified Paris equation describing crack propagation (m = 3.6 used by Dong) and the crack growth integral $I(\delta_b)$ resulting from this equation, which depends on the ratio δ_b of bending stress to total stress (degree of bending) and on the remote boundary conditions during crack propagation (load-controlled, often typical for small test specimens, or displacement-controlled, often prevailing in more complex structures). Additionally, the integral depends on the assumed initial and final crack sizes, a_i and a_f, and (implicitly) on the notch-related magnification factor M_k, Fig. 3.24. The thickness effect is

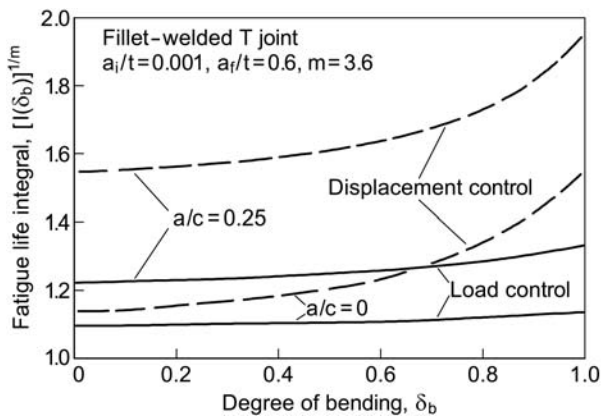


Fig. 3.24. Fatigue life integral as a function of (initial) degree of bending for semi-elliptical surface crack propagation (axis ratio a/c = 0.25) and through-thickness edge crack propagation (a/c = 0) under load-controlled and displacement-controlled loading conditions; fillet-welded T-joint under combined tension and bending loads; with initial (or final) crack length or depth, a_i (or a_f), plate thickness t and crack propagation exponent m; after Dong.[95,96]

included in eq. (3.10) by the thickness exponent $(1/2 - 1/m)$ resulting in 0.22 for $m = 3.6$.

Equation (3.10) above is slightly modified compared with Dong's original formula by introducing the thickness ratio t/t_0 instead of t, with the reference thickness t_0. We think that this is what Dong aimed at when he addressed the unit thickness $t = 1$ (i.e. $t_0 = 1$ mm) in order to present ΔS_s as an equivalent stress with the dimension N/mm^2.

The endurable stress parameter ΔS_s as a function of the number of cycles N has been evaluated by Dong *et al.*[95,103] using fatigue test results both from a proprietary data base (Batelle Institute) and from the open literature (about 50 test series in total), Fig. 3.25. The evaluated test results originate from various types of fillet-welded specimens made of structural steels and subjected to axial and bending loads: transverse and longitudinal attachments, pads and cover plates, cruciform and T-joints as well as edge attachments. Further endurable values of ΔS_s have been published for piping and vessel welds (Dong *et al.*[97,102,104]) as well as for GMA and laser welds in aluminium alloys (Dong *et al.*[105]). Misalignment effects are included in the endurable ΔS_s values to the extent they were present in the underlying tests. Furthermore, a great number of test results refer to symmetric joints, where the bilinear structural stress distribution was applied. Load-controlled testing conditions were assumed for the evaluation.

The fatigue strength in Xiao–Yamada's structural stress approach,[199] which is characterised by the one millimetre stress range (see Section 3.1.7)

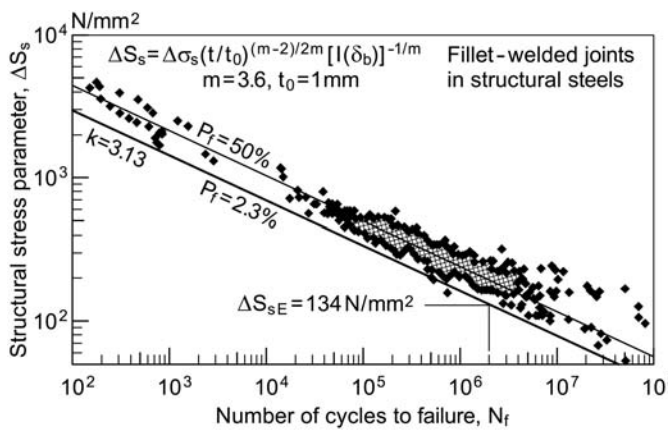


Fig. 3.25. Fatigue test results under load-controlled conditions evaluated based on the structural stress parameter ΔS_s, supplemented by the design *S–N* curve; various joint types, axial and bending loads, plate thickness $t = 8$–105 mm; endurance limit ΔS_{sE} at $N = 2 \times 10^6$ cycles for comparison; correlation coefficient $r = 0.963$; after Dong *et al.*[96]

plotted over number of cycles, has been applied to several welded joint types made of structural steels: in-plane and out-of-plane two-sided attachments, multiplate two-sided attachments and a one-sided tubular post structure. Fatigue test data from the open literature were evaluated. The rather narrow scatter band of the test results is limited from below by the design *S–N* curve D of the JSSC fatigue design recommendations,[34] corresponding to the fatigue class FAT 100 in the IIW recommendations.[3] Wider scatter bands occur in comparison when the hot spot stresses from surface stress extrapolation are used or when Dong's structural stresses at the hot spot are introduced.

3.3.5 Endurable multiaxial stresses or strains

The multiaxial nominal stress criteria described in Section 2.2.5 can be applied locally, thus establishing multiaxial structural stress criteria. Besides the structural stresses normal to the weld toe line, the structural shear stresses parallel to the weld toe line may also contribute to the fatigue damage at the hot spot. As mentioned earlier, this can be taken into account by regarding the first principal stress range as the governing damage parameter. The IIW recommendations[133, 165] consider the first principal stress in a sector of ±60° from the normal to the weld toe line to be fatigue relevant, as long as it is larger than the stress normal to the weld toe line.

Alternative damage parameters are the maximum shear stress range proposed in the ASME code[10] or the equivalent shear stress range based on a critical plane approach modified with regard to welded joints (Bäckström and Marquis;[12,83] Bäckström[11]). The authors just mentioned have reanalysed 233 test results (including 77 with out-of-phase loading) based on the hot spot stresses and the three damage parameters above. They found that the critical plane approach was the most effective one for deriving a uniform hot spot stress *S–N* curve. This curve corresponds to the fatigue class FAT 97 (or FAT 114, provided that only fillet welds are considered), Fig. 3.26. However, the remaining scatter is substantially larger than that observed in uniaxially loaded specimens evaluated on the basis of the hot spot stress approach. The increased scatter is attributed to the differences in specimen geometries, testing methods, plate thicknesses and failure definitions apart from insufficient suitability of the critical plane criterium under non-proportional loading conditions. Both the conventional and the critical plane criteria fail in the case of non-proportional loading with changing principal stress directions, at least in structural steels. The equivalent stresses are lowered compared with proportional loading, with the consequence that the fatigue life is overestimated.

The modified critical plane criterion mentioned above was proposed by Marquis *et al.*[158] based on Findley's original version. Findley[109] observed

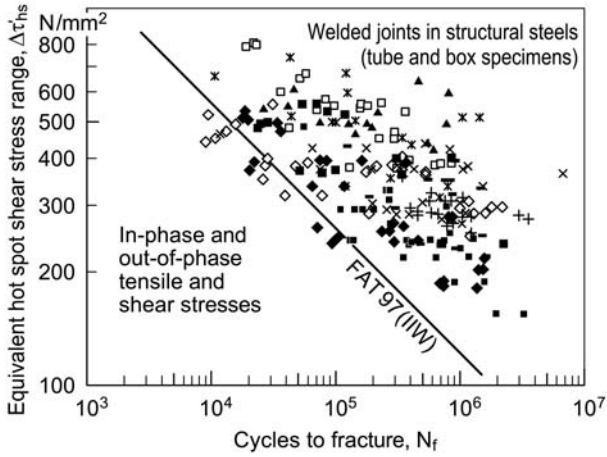


Fig. 3.26. Fatigue test results for welded joints in structural steels (tube and box specimens); in-phase and out-of-phase tensile and shear stresses; modified critical plane criterion; proposed hot spot stress *S–N* curve for design; after Bäckström.[84]

early fatigue damage in shear planes and suggested that the critical shear stress in the shear plane is linearly dependent on the maximum normal stress in the considered plane. The following modifications are introduced in respect of the hot spot structural stress approach applied to welded joints. The critical shear plane of fatigue damage is assumed to be aligned along the weld toe, inclined versus the cross-sectional plane. The maximum normal stresses $\sigma_{hs\,max}$ in the damage plane are computed by assuming the yield stress normal to the weld toe plane in as-welded joints or the maximum hot spot stress in stress-relieved joints. The resulting multiaxial fatigue criterion reads:

$$\Delta\tau_{hs} + 2k\sigma_{hs\,max} \le \Delta\tau'_{hs\,en} \tag{3.12}$$

with Findley's material constant k (k = 0.3 for structural steels) and the endurable equivalent shear stress range $\Delta\tau'_{hs\,en}$ at the hot spot. The maximum value of the left hand side of the equation must be found out of the varied critical plane angles versus the weld toe cross-sectional plane.

A Miner-analogue procedure has been tentatively proposed by Dong and Hong[98] in order to compare in-phase and out-of-phase *S–N* data in bending and torsion loading of fillet-welded tube-to-plate joints (similar to the corresponding procedure in the nominal stress approach, eqs. (2.20) and (2.21), but with a single slope exponent k in tension and shear loading). This feasibility study showed that the procedure has some shortcomings when designated for the inclusion into codes despite sufficiently well collapsing

test data from in-phase and out-of-phase loading conditions. The restriction to pure out-of-phase loading conditions ($\delta = 90°$) is one of these shortcomings.

Therefore, another procedure was proposed by Dong and Hong[99] which complies better with code requirements (with focus on the ASME code[10]). Structural stress evaluations from coarse mesh finite element models are the basis. The transformed von Mises relationship between the ratios of actual and endurable normal and shear stresses, $\Delta\sigma_s/\Delta\sigma_{sE}$ and $\Delta\tau_s/\Delta\tau_{sE}$, respectively, is modified by the dimensionless strength reduction parameter D_E:

$$\left(\frac{\Delta\sigma_s}{\Delta\sigma_{sE}}\right)^2 + \left(\frac{\Delta\tau_s}{\Delta\tau_{sE}}\right)^2 = D_E^2 \tag{3.13}$$

with $(\Delta\sigma_{sE}/\Delta\tau_{sE})^2 = 3$ and D_E depending on phase angle δ and stress ratio $\Delta\tau_s/\Delta\sigma_s$ ($D_E = 1.0$ for in-phase loading conditions). The parameter D_E can be adjusted to the test results (in-phase and out-of-phase loading conditions) which will depend on the material type, but also on the testing and evaluation peculiarities.

It is a straightforward assumption that the von Mises distortional strain energy density criterion remains valid whereas its critical value is adjusted to the test results for $\delta = 0°$ and $\delta = 90°$ using a representative stress ratio, e.g. $\Delta\tau_s/\Delta\sigma_s = 1/\sqrt{3}$. Validity of the von Mises criterion under out-of-phase loading conditions means that the maximum values of the superimposed momentary stress amplitudes are evaluated resulting in the following relationship:

$$D_E^2 = \frac{1}{2}\left\{1 + \sqrt{1 - \mu\frac{12(\Delta\sigma_s)^2(\Delta\tau_s)^2\sin^2\delta}{\left[(\Delta\sigma_s)^2 + 3(\Delta\tau_s)^2\right]^2}}\right\} \tag{3.14}$$

A material-dependent adjustment coefficient μ is inserted into the von-Mises-based relationship taken from Dong and Hong.[99] Referring to Sonsino's[59,60] results in Fig. 2.9, $\mu = 0.955$ for steels and $\mu = 0$ for aluminium alloys (evaluated steel data: $\sigma_{ba} = 87\,\text{N/mm}^2$ for $\delta = 0°$ and $\sigma_{ba} = 66\,\text{N/mm}^2$ for $\delta = 90°$, with $\Delta\tau_s/\Delta\sigma_s = 1/\sqrt{3}$). Inserting $\delta = 90°$, $\Delta\tau_s/\Delta\sigma_s = 1/\sqrt{3}$ and $\mu = 1.0$ into eq. (3.14), the result is $D_E^2 = 0.5$. This is the lowest possible value within the generalised von Mises frame represented by the equation.

The above approach can also be formulated on the basis of the Tresca criterion resulting in a minor change: the factor connected with $(\Delta\tau_s)^2$ in relation to $(\Delta\sigma_s)^2$ in eq. (3.14) is 4 instead of 3.

The structural strain approach can also be used in the low-cycle fatigue range ($N = 10^3$–10^5 cycles) even with biaxial in-phase or out-of-phase loading conditions (restricted to a non-varying principal strain direction in

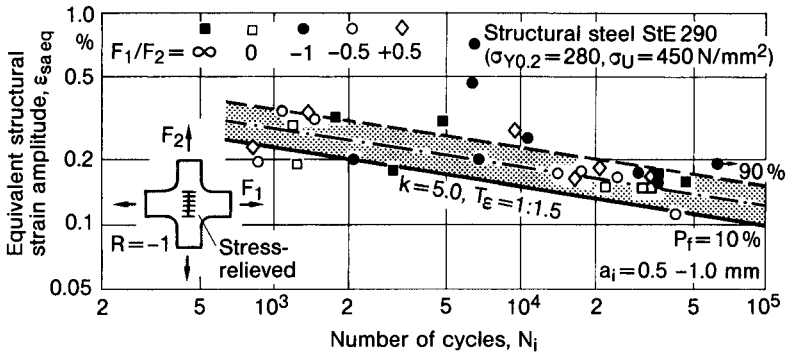


Fig. 3.27. Endurable equivalent structural stain amplitudes in biaxial low-cycle fatigue (crack initiation, in-phase and out-of-phase loading conditions) of GMA welds (non-machined and stress-relieved) in structural steel (GMA: gas metal arc); after Sonsino.[59,60]

the von Mises latter case), Fig. 3.27. The equivalent structural strain amplitude according to the octahedral shear strain energy criterion, eq. (5.48) should be evaluated (Sonsino[59,60]). The strain amplitudes are measured at a distance of 2 mm from the weld toe (double-V-butt weld). Test results for biaxial loading are compared with the scatter band for uniaxial loading. A better correlation is found when evaluating the notch strains (see Section 5.2.3). The position of the diagram points designating uniaxial loading in the direction of the weld (white squares in lower position) and transverse to it (black squares in higher position) indicates the difference in the notch effect of the two loading modes, ripples on the weld surface in the first case and a marked toe notch in the second.

According to the present state of the art, multiaxial fatigue cannot generally be described based solely on structural stresses or strains. As fatigue failures start from notches in general, notch stress or strain concepts must be considered. Also the influence of the material (steels versus aluminium alloys) on the multiaxiality effect must be taken into account (see Table 4.6).

3.3.6 Structural stress based assessment of weld root fatigue

The fatigue strength of welds with well-shaped weld roots occurring with full-penetration one-sided welds, i.e. double or single bevel butt welds, which may be at risk of weld root fatigue, should be assessed based on the (hot spot) structural stress at the weld root evaluated from the relevant finite element model. Hot spot stress concentration factors for groove butt welds in tubular joints are also available (Lee[149]).

The fatigue class of permissible stresses to be introduced depends on the quality condition at the weld root. A reduced fatigue strength on the root side in comparison to the toe side is suggested within the nominal stress approach for specific cases. For example, according to the IIW recommendations,[3] common butt joints through-welded from one side without ceramic backing are classified one or two fatigue classes lower than the corresponding butt joints welded from two sides, provided the root is inspected by non-destructive testing. Without non-destructive testing, the joint is further downgraded as defects are assumed at the root side. These classes have to be applied locally within the structural stress approach.

The fatigue strength of welds with non-fused root faces occurring with non-penetrating welds, which may be at risk of weld root fatigue, should be assessed with the nominal stress in the weld throat section or a similarly defined comparable weld section (weld thickness a). The basic types of such welds are shown in Fig. 3.28. The two-sided welds in the upper part of the figure are sufficiently well designed because weld bending with gap opening enhancing crack formation is largely avoided. The corresponding one-sided welds in the lower part of the figure are only acceptable as far as weld bending is kept under control by other means, e.g. by transverse stiffening plates.

The weld nominal stress σ_w (= $\sigma_{w\perp}$) in two-sided partial penetration butt welds, possibly covered by fillet welds, Figs. 3.28(a, b), is given by:

$$\sigma_w(a) = \frac{F}{2al} = \sigma_n \frac{t}{2a} \tag{3.15}$$

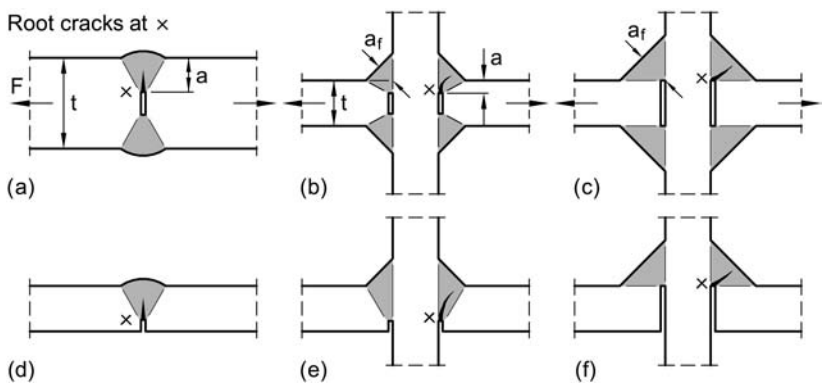


Fig. 3.28. Welded joints with non-fused root faces at risk of weld root fatigue: two-side butt weld with root face (a), double bevel butt weld with root face (b), two side fillet weld (c), one-side butt weld with root face (d), single bevel butt weld with root face (e) and one-side fillet weld (f); with plate thickness t and weld thickness a.

with the axial force F, the nominal stress σ_n in the plate, the butt weld thickness a, the weld length l and the plate thickness t. In cases of multiaxial loading, correspondingly defined shear stresses $\tau_{w\perp}$ and $\tau_{w\parallel}$ in directions transverse and longitudinal to the weld occur simultaneously. The weld nominal stresses can be defined locally, thus resulting in the structural stress approach to weld root fatigue. The appropriate fatigue classes are low: FAT 36 or FAT 40 in steel, FAT 12 or FAT 14 in aluminium alloys (IIW recommendations[3]).

The situation is slightly more complex in the case of two-sided fillet welds, possibly covering butt welds, Fig. 3.28(b, c). The weld nominal stress σ_w is then related to the throat section of the fillet weld (thickness a_f):

$$\sigma_w(a_f) = \frac{F}{2a_f l} = \sigma_n \frac{t}{2a_f} \tag{3.16}$$

But this definition is not in agreement with the stress tensor convention because σ_w is assumed to be inclined by 45° to the throat section instead of perpendicular action. Therefore, the 'stress' $\sigma_w(a_f)$ is better named 'internal force vector' than 'stress tensor'. It provides the nominal stresses $\sigma_{w\perp}$ and $\tau_{w\perp}$ by vector decomposition. It is easy to extend this concept to the additional stress component $\tau_{w\parallel}$ in the throat section: all three components make up the 'vector sum stress' σ_w (not yet a strength parameter in multiaxial loading, but a basis for appropriate formulations, e.g. by Lotsberg[152]):

$$\sigma_w = \sqrt{\sigma_{w\perp}^2 + \tau_{w\perp}^2 + \tau_{w\parallel}^2} \tag{3.17}$$

In the case of butt welds covered by fillet welds, Fig. 3.28(b), the weld nominal stresses, $\sigma_w(a)$ according to eq. (3.15) and $\sigma_w(a_f)$ according to eq. (3.16), are available, raising the question of which one should be used in strength assessments. Obviously, even using the smaller one of the two stresses gives conservative results.

The bending stresses and the singular notch stresses in the throat section are only implicitly covered by using the aforementioned weld nominal stress in two-sided non-penetrating welds together with the relevant low fatigue classes. An approach with explicit consideration of the superimposed weld bending stresses applicable also to one-sided non-penetration welds, is reviewed at the end of this section. Plate bending moments, and also those moments caused by axial misalignment, are supported by opposing joint-axial forces in the two-sided welds, so that their inclusion in the weld nominal stress is easily achievable. Plate bending is less effective with regard to weld root fatigue compared with weld toe fatigue (see Andrews[75] and Fricke *et al.*[115,116] concerning the misalignment effect).

The local application of the weld nominal stress approach to the assessment of weld root fatigue is demonstrated by the example of fillet-welded

attachment ends, Fig. 3.29 (Fricke *et al.*[115,116]). In the front view, Fig. 3.29(a), the fatigue-relevant structural stresses σ_p in the plate acting normal to the weld line are shown, with the local structural stress $\sigma_{p,l}$ at the plate edge averaged over a length equal to half the plate thickness t. In the cross-sectional side view, Fig. 3.29(b), the throat thickness a is shown together with the remote tension load F applied to the attachment. In the top view, Fig. 3.29(c), the weld-throat-related reference area is shown, for which the local weld nominal stress $\sigma_{w,l}$ is determined.

The size and shape of the throat area, which is thought to be turned into the flange surface, are defined on the basis of a stress intensity factor analysis by the boundary element method for the weld root line surrounding the attachment end. These stress intensity factors are considered to be the most important parameters determining the fatigue life in crack propagation starting at the weld root. The comparison of the stress intensity factors at a tension-loaded square crack-like interface (simulating the root face at the attachment end) with those at a tension-loaded strip-shaped crack-like interface (simulating the root face at some distance from the attachment ends) indicates that the local plate stress times the area, $t \times t/2$, at the attachment end can be set into equilibrium with the local weld stress times the reference area:

$$\sigma_{w,l} = \sigma_{p,l} \frac{t^2}{2\left(2at + a^2\right)} \tag{3.18}$$

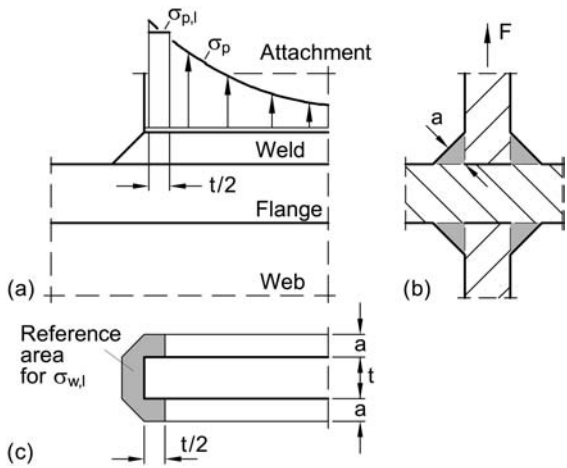


Fig. 3.29. Fillet weld around attachment end on web-supported flange: front view (a) with local structural stress $\sigma_{p,l}$ in plate, cross-sectional side view (b) with tension load F and throat thickness a as well as top view (c) with local weld nominal stress $\sigma_{w,l}$ in reference throat area; after Fricke and Doerk.[115]

The local plate stress $\sigma_{p,l}$ can be evaluated from a thin-shell or solid element model representing the attachment. The evaluation is performed at the intersection line of the shell element model or in the upper weld toe plane of the solid element model. The size of the finite elements should not be larger than the plate thickness t for reasons of accuracy. Also, stress evaluations in the elements representing the weld are possible as an alternative procedure, provided the stresses are related to the reference area. In order to consider eq. (3.18) as an equilibrium condition, $\sigma_{w,l}$ should be defined as an internal force per unit area acting in the throat area turned into the flange surface. Successful application of eq. (3.18) within the assessment of weld root fatigue based on the relevant design *S–N* curves is described in Section 3.4.5.

In the same way as just described with regard to the local weld normal stress $\sigma_{w,l}$, the local weld shear stress $\tau_{w,l}$ in the weld-throat-related reference area can be derived. The shear stress has to be considered in the case of weld-longitudinal loading of the attachment. This stress acts in the weld-transverse direction in front of the attachment end and in the weld-longitudinal direction at the ends of the flank side welds. This analogous procedure is straightforward, provided the stresses are set in relation to the same design *S–N* curve, although there is no foundation from the crack propagation point of view described above for normal stress conditions.

In cases of simultaneous weld loading by $\sigma_{w,l}$ and $\tau_{w,l}$ (biaxial loading) at the attachment end, the resultant local weld stress $\sigma_{w,l\,res}$ relevant for weld root fatigue may be calculated by vector summation (Fricke and Doerk,[115] compare eq. (3.17)):

$$\sigma_{w,l\,res} = \sqrt{\sigma_{w,l}^2 + \tau_{w,l}^2} \tag{3.19}$$

This equation is proposed with well-founded argumentation and verified by fatigue tests.

There are cases of application where the bending stresses in the weld throat section are dominant in relation to the membrane-type weld nominal stresses. One example is provided by the single-sided butt and fillet welds with non-fused root faces under axial or bending loads applied to the joint (Fig. 3.28(d, e, f)). Another example is provided by fillet-welded cover plates subjected to out-of-plane forces causing high plate bending moments at the edge fillet welds. The degree of weld bending, δ_{wb}, may be characterised as follows:

$$\delta_{wb} = \frac{|\sigma_{wb}|}{|\sigma_{wb}| + |\sigma_{wm}|} \tag{3.20}$$

with the weld bending stress σ_{wb} and the weld membrane stress σ_{wm}, summing up to the weld total stress linearised over the throat thickness a.

In load-carrying double-sided fillet welds of cruciform joints, the degree of bending is approximately $\delta_b \approx 0.3$ (Sørensen *et al.*[184]), but in one-sided welds or transversely loaded cover plates, it may reach any value up to $\delta_b = 1.0$. Whereas the weld bending effect in cruciform joints is implicitly covered by the endurable weld nominal stresses, this is not the case with more pronounced weld bending effects. The endurable weld nominal stresses decrease further with increasing bending effects.

The weld bending effect can be taken into account explicitly, provided the finite element analysis is extended to the stress distribution in the throat section. The following specific procedure has been used by Sørensen *et al.*[184] who presented the first (and certainly not last) finite element based solution of the problem. The weld is modelled by isoparametric twenty node hexahedronal elements, so that two elements describe the throat section line, Fig. 3.30(a). The simple eight node hexahedronal elements require finer meshing with 2×2 elements adjacent to the throat section line. The first principal stress σ_1 is evaluated at the nodal points in the throat section line. The resulting non-linear stress distribution is linearised by the stress values in the two element midside nodes at distances of a quarter of the throat thickness from the weld root or weld surface, respectively, Fig. 3.30(b). The stresses at these 'quarter-points' are linearly extrapolated to the weld root, where a stress singularity originally occurred, thus defining the 'hot spot weld stress', $\sigma_{w\,hs}$ (not to be confused with the hot spot structural stress in the plate). Different load cases are superimposed by extrapolating the six superimposed stress components (σ_x, σ_y, σ_z, τ_{xy}, τ_{yz}, τ_{zx}) to the weld root and then forming the first principal stress there. Specific meshing rules have to be observed in the neighbourhood of the weld.

The hot spot weld stress was successfully used to describe a uniform narrow scatterband of (weld root) fatigue test results for fillet-welded cover plate and cruciform specimens made of structural steel, comprising different degrees of weld bending, Fig. 3.31. The 'characteristic *S–N* curve' is defined by the inverse slope $k = 3.93$ and the failure probability $P_f = 5\%$.

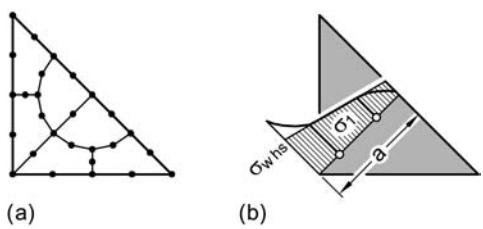


Fig. 3.30. Fillet weld modelling by 20 node hexahedronal elements (a), stress extrapolation from the two 'quarter-points' in the throat section line to the weld root hot spot (b); with throat thickness *a*, first principal stress σ_1 and hot spot weld stress $\sigma_{w\,hs}$; after Sørensen *et al.*[184]

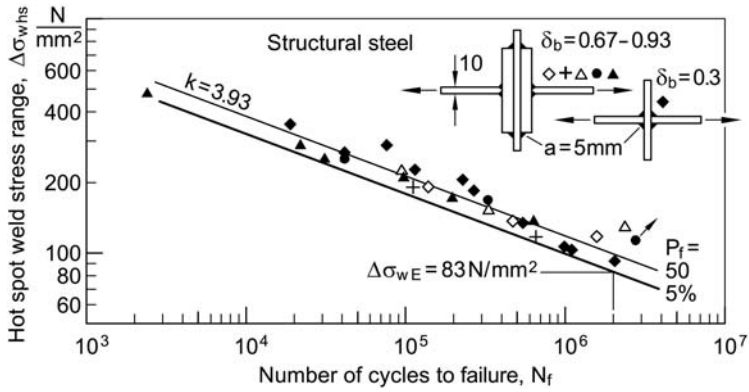


Fig. 3.31. Endurable hot spot weld stress from (weld root) fatigue tests ($R = 0$) performed on fillet-welded cover plate and cruciform joints with different degrees of weld bending, δ_b; characteristic *S–N* curve with $P_f = 5\%$; after Sørensen *et al.*[184]

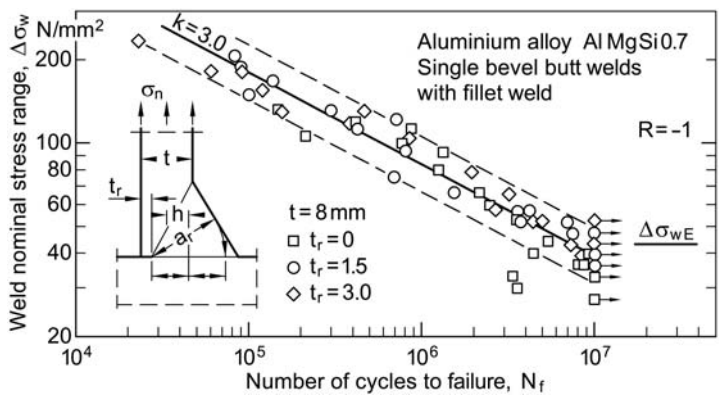


Fig. 3.32. Endurable weld nominal stresses (with inclusion of bending effect) in aluminium alloy from weld root fatigue tests performed on single bevel butt welds with fillet weld, with and without root face; base material AlMgSi0.7 (AA6005-T5) with filler material AlMg4.5MnZr; after Zenner and Grzesiuk.[202]

An evaluation according to IIW conventions with the prescribed inverse slope $k = 3.0$, but with $P_f = 5\%$ results in $\Delta\sigma_{wE} = 61\,\mathrm{N/mm^2}$, which corresponds well to the IIW fatigue class FAT 45 for cruciform joints with double-sided load-carrying fillet welds expressed in weld nominal stresses ($\Delta\sigma_E = 45 \times 1.3 = 58.5\,\mathrm{N/mm^2}$ for $P_f = 2.3\%$).

Another investigation on weld root fatigue based on weld nominal stresses inclusive of bending effects is related to single bevel butt welds with fillet weld, with and without a root face, Fig. 3.32 (Zenner and Grzesiuk[202]).

The cruciform joints are made of an aluminium alloy used in the form of hollow extruded sections for vehicle structures: base material AlMgSi0.7 (AA6005-T5) and filler material AlMg4.5MnZr, with plate thickness $t = 8\,\text{mm}$. The root face depth amounts to 0, 1.5 and 3.0 mm.

The weld nominal stress comprises membrane and bending effects. These are determined by the following procedure. The weld cross-sectional shape is approximated by an equilateral triangle. The throat section is assumed to be a bisector plane and rotated into the weld leg plane, establishing the reference section with 'height' a_r, for which the membrane and bending stresses are calculated. The remote plate nominal stress σ_n is thus associated with the following weld nominal stress σ_w:

$$\sigma_w = \sigma_n \frac{t}{a_r}\left(1 + 6\frac{h}{a_r}\right) \tag{3.21}$$

$$h = t_r + \frac{1}{2}(a_r - t) \tag{3.22}$$

with the plate thickness t, the weld thickness a_r (from root to throat) and the root face depth t_r.

The weld nominal stress S–N curve (failure probability $P_f = 50\%$) was extracted by regression analysis with a preset inverse slope ($k = 3.0$). The endurance limit $\Delta\sigma_{wE}$ assumed at $N = 10^7$ cycles was found by the staircase test method using the priniciple of maximum likelihood. The value $\Delta\sigma_{wE} = 41.5\,\text{N/mm}^2$ from Fig. 3.32 is the arithmetic mean of the results for the three root face variants. Obviously, this value is unconservative because earlier failures occurred at $\Delta\sigma_w \geq 30\,\text{N/mm}^2$. The dashed lines designating the usual scatterrange index $T_\sigma = 1.5$ (corresponding to $P_f = 10\%$ and 90%) reveal that two measuring points are significantly outside of the expected range. The stress ratio $R = -1$ is not typical for structural stress evaluations.

A more recent investigation of weld root fatigue in structural steels based on weld nominal stresses which include bending stresses (Fricke *et al.*[117]) is related to fillet-welded ends of hollow section tubes subjected to tensile load, to fillet-welded cover plates subjected to out-of-plane forces and to cruciform joints with load-carrying fillet welds. The weld nominal stress in the leg plane (leg length equal to $\sqrt{2}$ times the throat thickness) is evaluated from the nodal forces in the leg plane using relatively coarse finite element meshes or even from the cross-sectional forces in the plate. The element stresses, on the other hand, are erroneous at the weld root in coarse rectangular meshes because the stress singularity here is not correctly simulated with its angular distribution. The fatigue test results in terms of weld nominal stress S–N curves (membrane and bending stress) are well above the FAT 80 design curve in the IIW recommendations.[3]

3.4 Demonstration examples

3.4.1 Welded tubular and butt joints – structural strain approach

A convincing application has been reported by Haibach[2] based on the test results of Gibstein (the source is unknown), Fig. 3.33. A T-shaped tubular joint is considered loaded by a cyclic bending moment ($R = -1$). The test results are compared with the scatter band of endurable cyclic strains according to Haibach and with strains derived elastically from endurable structural stresses according to the AWS structural welding code.[82] The measured strains are also shown to be in agreement with strains calculated by finite element analysis (Atzori *et al.*[78])

The structural strain approach is well suited to describe the influence of joint misalignment on the fatigue strength which may be caused by imperfect manufacture. The misalignment may consist of axial eccentricity and angular distortion of the joined plates or shells. They cause superimposed bending stresses under axial loading.

Different strain *S–N* curves result from fatigue testing of specimens with misalignments of different type and size. The different curves can be cast into a single curve if the surface strain in front of the crack-initiating weld toe is evaluated. It may be measured by a strain gauge or calculated either by engineering formulae or finite element analysis.

The most convincing test results have been presented by Iida *et al.*[140,141,143] A strain gauge (length 3 mm) is positioned at a distance of 5 mm from the weld toe. Uniform endurable strain curves for high strength steels are derived. Fig. 3.34 shows the endurable cyclic strain for butt-welded

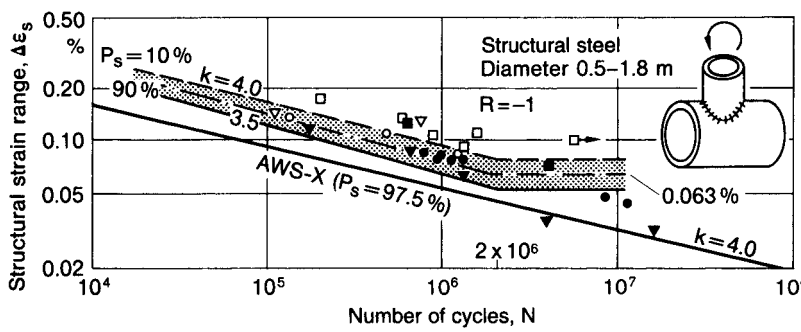


Fig. 3.33. Endurable structural strain range, scatter band from test specimens according to Haibach,[2] test results for tubular joints according to Gibstein (black and white points) and curve from the AWS structural welding code[82] (with survival probability P_s).

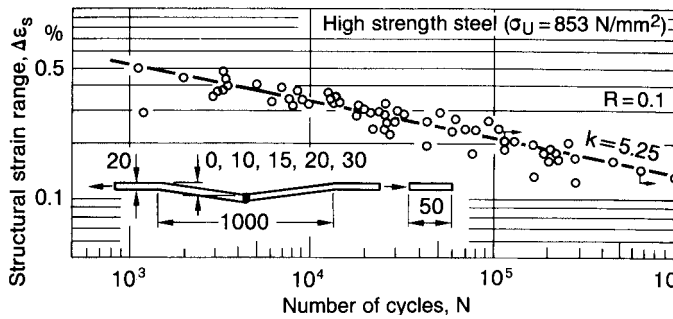


Fig. 3.34. Endurable structural strain range of butt-welded high strength steel (ultimate tensile strength σ_U = 853 N/mm²) with and without joint misalignment; after Iida and Iino.[141]

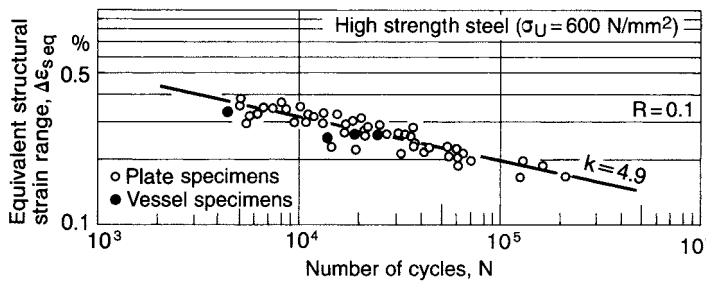


Fig. 3.35. Endurable structural strain range of butt-welded high strength steel (ultimate tensile strength σ_U = 600 N/mm²) with joint misalignment, vessel specimens made of hemispherical shells under internal pressure (black points) and tensile-loaded plate specimens (white points); after Iida *et al.*[143]

specimens with angular distortion (including the non-distorted specimen). Fig. 3.35 gives the same for the misaligned hemispherical shells of a pressure vessel (failure by leaking) in comparison to misaligned tensile-loaded plate specimens. The multiaxiality of the stress state in the shell is taken into account by plotting the equivalent strain according to the octahedral shear strain criterion (decisive for good correlation).

3.4.2 Welded tubular joints – various design guidelines

Three design examples of welded tubular joints have been thoroughly assessed by van Wingerde *et al.*[190,191] in respect of their fatigue strength according to different fatigue design recommendations (AWS D1.1,[82] *ibid.* Chapter 10 and Eurocode 3,[23] *ibid.* Chapter 9) using both the nominal stress and the hot spot structural stress approach. The thickness correction

for $t \leq 16$ mm is introduced for the purpose of comparison resulting in different design stresses in the brace and chord tube. Test results are available in two of the three cases investigated. One T-joint with a groove butt weld and two X-joints with a 90° angle between brace and chord, one with a fillet weld, the other with a groove butt weld, are considered. The square chord width is 200 mm combined with a chord thickness of 12.5, 8.0 and 16.0 mm, respectively. The square brace widths are 140, 80 and 200 mm combined with a brace thickness of 8.0, 4.0 and 8.0 mm, respectively. The problem was formulated to determine the permissible axial force ranges at the brace tube for 2×10^6 cycles of constant-amplitude loading. The result of the investigation is summarised in Table 3.4.

It can be seen from the permissible force ranges in the table that both guidelines, AWS and Eurocode 3 (EC3), are highly inconsistent in respect of applying the nominal stress approach and the hot spot structural stress approach alternatively. In one case only the nominal stress approach according to AWS and EC3 gives similar results. The structural stress approach produces similar results if parametric hot spot stress formulae and hot spot stress *S–N* curves belonging together are combined. On the other hand, the hot spot structural stress approach of AWS and EC3 underestimates the fatigue strength if the wall thickness at the hot spot is lower than the reference value ($t_0 = 16$ mm). The thickness correction of the EC3 design stresses (notch or detail class 90) still guarantees a safety factor of 1.5–2.0 for the design stresses in the two cases considered. A safety factor of 1.0 is allowed by EC3 in general, whereas 1.5 is prescribed in cases of low accessibility and where the consequences of failure are detrimental.

Table 3.4. Permissible force ranges ΔF in brace tube of definite T- and X-joints with square tube section according to various design guidelines and comparison with test results; after van Wingerde *et al.*[190,191]

Joint type	AWS nominal stress[b] ΔF [kN]	AWS hot spot stress ΔF [kN]	EC3[a] nominal stress[c] ΔF [kN]	EC3[a] hot spot stress ΔF [kN]	EC3[a] thickness corrected[d] ΔF [kN]	Test result ΔF [kN]
T-Joint	29	40	28	36	50	99
X-Joint (1)	22	6	2	6	9	15
X-Joint (2)	108	299	212	269	269	—

[a] Eurocode 3.
[b] Nominal punching shear stress range.
[c] Nominal stress range in brace tube.
[d] Thickness correction according to Fig. 3.22.

3.4.3 Welded bridge girder with cope holes

The hot spot structural stress approach has been applied successfully by Miki and Tateishi[162] to assign the appropriate notch or detail class within the nominal stress approach to I-section steel girders with in-plane cope holes, used in railway and highway bridges. The hot spot stress concentration factor is given by eq. (3.9) dependent on shape and internal force parameters. The hot spot stress *S–N* curve limiting the scatter band of test results from below is determined from fatigue tests on girder specimens and characterised by $\Delta\sigma_{hs\ per} = 80\,N/mm^2$ at $N = 2 \times 10^6$ cycles. Permissible nominal stress values were established independently. Proceeding from a well-established nominal stress *S–N* curve for the girder specimen with a cope hole ($\tau/\sigma_b \approx 0.4$) and the relative arrangement according to the formula for the hot spot stress concentration factor, eq. (3.9), design stress curves are derived dependent on the stress ratio τ/σ_b, Table 3.5. The stress ratio in the table is limited to $\tau/\sigma_b \leq 0.7$. It is recommended that the hot spot structural stress approach be applied if the above value is exceeded. Obviously, the permissible values of nominal stress and structural stress are not related by the structural stress concentration factor as should be expected.

3.4.4 Welded joints in ship structures – weld toe fatigue

Early relative design evaluations comprising typical welded structural members in shipbuilding have been performed on the basis of structural stress concentration factors gained from finite element analysis referring to points of crack initiation. One example of the investigations reviewed by Radaj,[4] (*ibid*. pp. 127–135) is shown in Fig. 3.36 with K_{s0} according to eq. (3.3).

More recently, numerous hot spot structural stress analyses have been presented for structural details related to ship design (Fricke *et al.*,[111,113,114,118–122] Huther and Lieurade,[137] Paetzold *et al.*,[169] Storsul *et al.*,[186] Tveiten and Moan,[188] Ulleland *et al.*,[189] Youn and Kim[201]). In order to

Table 3.5. Base values of design stress curves at $N = 2 \times 10^6$ cycles for I-section girders with in-plane cope holes valid for Japanese railway and highway bridges; after Miki and Tateishi[162]

Stress ratio τ/σ_b	Nominal stress range $\Delta\sigma_{n\ per}$ [N/mm^2]	Stress ratio τ/σ_b	Nominal stress range $\Delta\sigma_{n\ per}$ [N/mm^2]
0	71	0.4–0.5	45
>0–0.2	63	0.5–0.6	40
0.2–0.3	56	0.6–0.7	36
0.3–0.4	50		

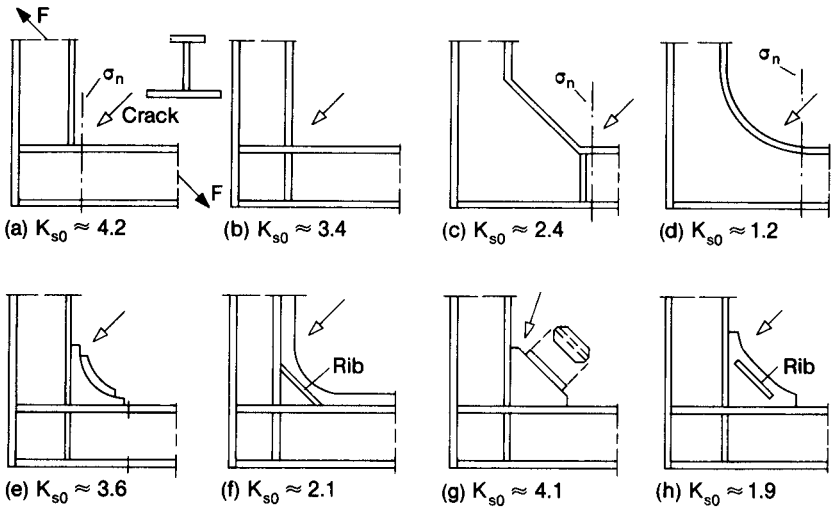


Fig. 3.36. Corner joints of I-section girders subjected to diagonal force, *F*, in the fatigue tests, design variants (a) to (h) with structural stress concentration factors K_{s0}; after Iida and Matoba.[142]

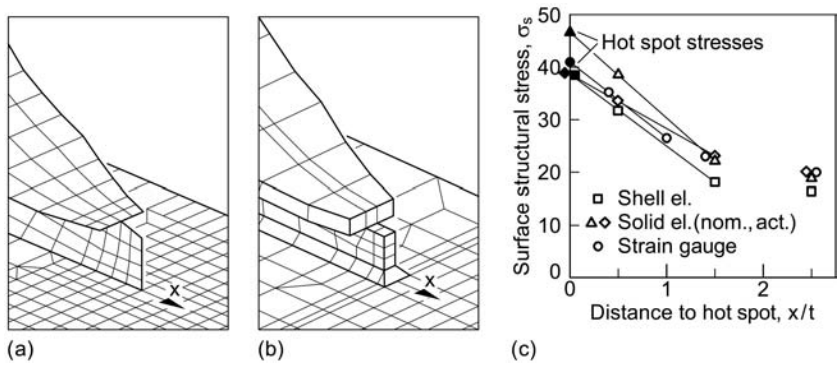


Fig. 3.37. Hot spot stresses gained by linear extrapolation of surface stresses in front of a gusset plate between I-section beams forming a corner joint subjected to bending load; thin-shell element model (a), solid element model (b) and structural stress evaluations compared with strain gauge measurements (c); solid element model with nominal weld size (nom.) and actual weld size (act.); after Paetzold *et al.*[169]

demonstrate the effectiveness of the recommended meshing and evaluation rules for consistent hot spot stress values even in coarse meshes, a relevant example is given by Fig. 3.37. The hot spot in front of a gusset plate between I-section beams forming a corner joint subjected to a bending load is considered. Such corner stiffeners are applied in ship hulls. The reinforcing

plate on top is introduced to reduce the risk of buckling and vibration. The structural stresses from thin-shell and solid element models, respectively, are compared with those from strain gauge measurements. The solid element model is applied both with nominal and actual weld sizes. The hot spot stresses in the finite element models are gained from linear extrapolations using evaluation points at $0.5t$ and $1.5t$ (with flange thickness $t = 20$ mm). The hot spot stress from measurement is based on the $0.4t$ and $1.0t$ evaluation points. The substitute hot spot at the end of the intersection line is referenced in the thin-shell element model. The hot spot stresses from computation and measurement show a high degree of correspondence, with the exception of the data from the model where the nominal leg length (8.5 mm) of the weld deviates from its actual value (11.5 mm).

Round robin studies were performed in order to determine the variations in actually measured and computationally predicted hot spot stresses and in corresponding fatigue lives when different evaluation and assessment procedures are applied by different investigators to identical structural detail specimens. The results for three of these structural detail specimens, Fig. 3.38, are summarised in Tables 3.6 and 3.7. Data from strain measurements and extrapolations as well as from fatigue testing (Fricke,[110] Kim and Lotsberg,[145] Lotsberg and Sigurdsson,[154] Yagi *et al.*[200]) are evaluated. Different procedures to compute the hot spot structural stress and to predict the fatigue life are applied. The relevant computational hot spot structural stress analyses based on finite element models with coarse meshes were published by Fricke,[110] Doerk *et al.*[93] and Hong and Dong.[134] Fine meshes were used based on the recommendations by Xiao and Yamada.[199] The variations in the hot spot stress results are mainly caused by different types of models and elements and also by different ways of weld modelling.

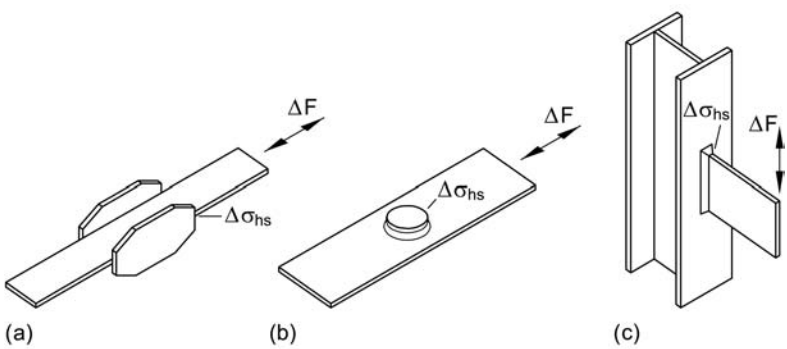


Fig. 3.38. Structural detail specimens in round robin investigation of fatigue assessment based on the hot spot structural stress approach: edge attachment (a), cover plate (b) and load-carrying flange attachment (c).

Table 3.6. Measured and computed structural stresses at the hot spot of three structural details according to Fig. 3.38, investigated in a round robin study; after Fricke–Kahl (*Marine Structures*, 18 (2005), 473–488)

Structural detail Nominal stress σ_n	Hot spot structural stress σ_{hs} [N/mm^2]						
	Measurement	Finite element analyses					
		IIW procedure		Dong's procedure		Xiao–Yam.'s procedure	
		Shell el.	Solid el.	Shell el.	Solid el.	Shell el.	Solid el.
Edge attachment σ_n = 80 N/mm^2	190	151–163	154–166	119–125	—	147	—
Cover plate σ_n = 150 N/mm^2	243	228–249[a]	219–239[a]	231–237[a]	203–239[a]	—	222[a]
Flange attachment σ_n = 150 N/mm^2	278	246–327	266–278	252–255[b]	—	246–293[c]	—

[a] with k_m = 1.2 for angular misalignment.
[b] with t_1 = 20 mm.
[c] with variation of mesh size and element type.

Table 3.7. Measured and predicted fatigue lives for three structural details according to Fig. 3.38, investigated in a round robin study; after Fricke–Kahl (*Marine Structures*, 18 (2005), 473–488)

Structural detail Nominal stress $\Delta\sigma_n$	Fatigue life N_f [cycles] for $P_f = 2.3\%$						
	Fatigue tests	Fatigue assessments					
		IIW procedure		Dong's procedure		Xiao–Yam.'s procedure	
		Shell el.	Solid el.	Shell el.	Solid el.	Shell el.	Solid el.
Edge attachment $\Delta\sigma_n = 80\,N/mm^2$	533,000	337,000–423,000	318,000–399,000	315,000–364,000	—	630,000	—
Cover plate $\Delta\sigma_n = 150\,N/mm^2$	209,000	130,000–169,000	150,000–190,000	97,400–106,000	94,800–158,000	—	183,000
Flange attachment $\Delta\sigma_n = 150\,N/mm^2$	389,000[a]	41,700–97,900	67,900–77,500	44,800–46,400[a]	—	79,500–134,000	—

[a] with crack length $t_c = 20\,mm$.

The deviations both in hot spot structural stresses and in fatigue lives between the different procedures and investigators are unsatisfactory to some extent, but measured and predicted fatigue lives correlate to an acceptable degree (conservative predictions in most cases) with the exception of the flange attachment specimen where compressive residual stresses (verified by measurement, Kim *et al.*[144]) extend the actual fatigue life substantially.

Another round robin study referring to the fatigue life prediction for a T-joint consisting of two rectangular hollow sections ('snake-jaw connection') and subjected to a complex torsional loading mode has been initiated and supervised by the (American) Society of Automotive Engineers (SAE). The best fatigue life prediction was presented by Kyuba and Dong.[147]

3.4.5 Welded joints in ship structures – weld root fatigue

The structural stress-based procedure for the assessment of weld root fatigue at the ends of attachments has been applied to the cruciform joint specimen shown in Fig. 3.39 (Fricke and Doerk[115]). The axially loaded specimen half under consideration has quarter-circle cut-outs on both sides, with the fillet weld executed around them (throat thickness $a = 4$ mm). The structural stress distribution in the plate and in the weld along the weld line is thus changing with stress concentrations at the cut-outs. The axial cyclic load range is $\Delta F = 50$ kN. The corresponding hot spot stress range gained from a finite element model (stress extrapolation along the edge of the cut-out)

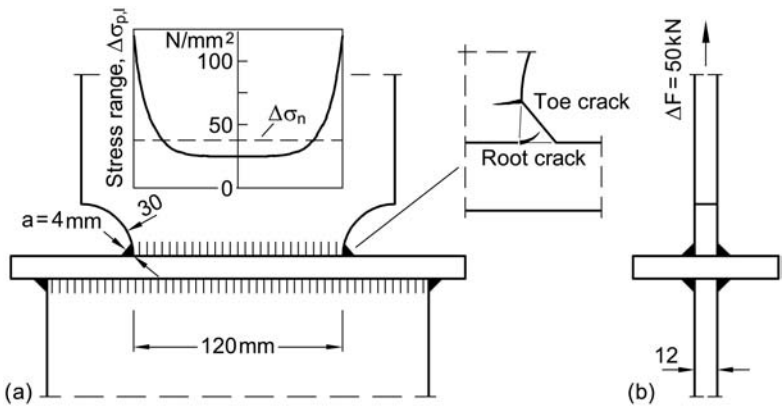


Fig. 3.39. Fillet-welded cruciform joint specimen with double-sided quarter-circle cut-outs subjected to axial cyclic load ΔF, front view (a) and side view (b), the former with computed local stress range $\Delta\sigma_{p,l}$ and nominal stress range $\Delta\sigma_n$ in plate, as well as with enlarged detail showing crack initiation at weld toe and weld root.

is $\Delta\sigma_{hs} = 90\,N/mm^2$, establishing the hot spot stress concentration factor $K_{hs} = 2.6$ (with reference to the nominal stress range $\Delta\sigma_n = 35\,N/mm^2$). The corresponding local weld stress range at the cut-out derived from eq. (3.18) is $\Delta\sigma_{w,l} = 57\,N/mm^2$ resulting in the weld stress concentration factor $K_w = 1.24$ (with reference to the weld nominal stress range $\Delta\sigma_{w,n} = 46\,N/mm^2$). The reduction in the stress concentration factor can be explained from the additional weld throat area around the cut-out.

The two evaluated structural stress ranges, $\Delta\sigma_{hs}$ and $\Delta\sigma_{w,l}$, are compared with the relevant permissible values for a definite fatigue life (e.g. $N = 2 \times 10^6$ cycles) according to the IIW recommendations.[133] The hot spot stress range $\Delta\sigma_{hs} = 90\,N/mm^2$ is set in relation to the permissible value $\Delta\sigma_{hs\,per} = 90\,N/mm^2$ (fatigue class FAT 90 for edge attachments). The local weld stress range $\Delta\sigma_{w,l} = 57\,N/mm^2$ has to be compared with $\Delta\sigma_{w,l\,per} = 40\,N/mm^2$ (fatigue class FAT 40 for weld stresses). Obviously, weld root fatigue at the weld ends is predicted for the selected reference number of cycles, although misalignment effects might displace crack initiation to the weld toe.

The predicted fatigue behaviour could not be verified by fatigue testing. Root cracks did not appear at the weld ends, but in the middle part of the weld line, despite lower structural stresses in this area. The explanation was found in tensile residual stresses ($\approx 180\,N/mm^2$) near the weld toe at the weld line centre compared with compressive residual stresses ($\approx -200\,N/mm^2$) near the weld toe at the weld ends in the as-welded condition (residual stresses measured by the neutron diffraction method). Comparative computations based on a thermomechanical finite element model showed that the details of the welding process are of minor influence on the residual stress distribution. On the other hand, specimens which were post-weld treated by stress relief annealing exhibited a reduced fatigue strength with crack initiation at the weld ends, as predicted.

4

Notch stress approach for seam-welded joints

4.1 Basic procedures

4.1.1 Principles and variants of the notch stress approach

The fatigue strength of a structural component depends heavily on its notch effects. 'Notch effect' means both stress concentration and strength reduction by notches. The fatigue strength of the material in plain specimens is of secondary importance in comparison with the fatigue strength in the notched component which depends on shape and size for a given material (German idiom 'Gestaltfestigkeit'). The most simple assessment procedure based on the notch effect refers to the fatigue strength for infinite life or a defined large number of cycles (e.g. $N > 10^6$) under constant amplitude loading, i.e. to the endurance limit. The requirement for design with reference to the endurance limit is that fatigue failures are to be avoided independent of service life demands. Fatigue crack initiation or at least further propagation must be avoided to this end. The assumption, well founded in this case, is that no appreciable plastic deformation occurs at the notch root, i.e. that the notch effect in terms of stresses can be approximated as purely elastic. The endurance limit of the structural component is reduced according to the elastic stress concentration, but less than proportionally so depending on the cyclic notch sensitivity of the material. The local conditions at the notch root are thus decisive for the fatigue strength of the whole structural component.

The above consideration is a simplified one insofar as cracks may exist or may be initiated but may not propagate ('dormant cracks'). Also, minor cyclic plastic deformation may occur without further effect. Thus the endurance limit may be observed despite microcracks or plastic deformation.

The basic procedure for fatigue strength assessment according to the notch stress approach (or 'locally elastic stress approach'[9] because notch-free parts are included) is shown in Fig. 4.1. Both, geometry and loading of the structural component determine the elastic stress concentration factor,

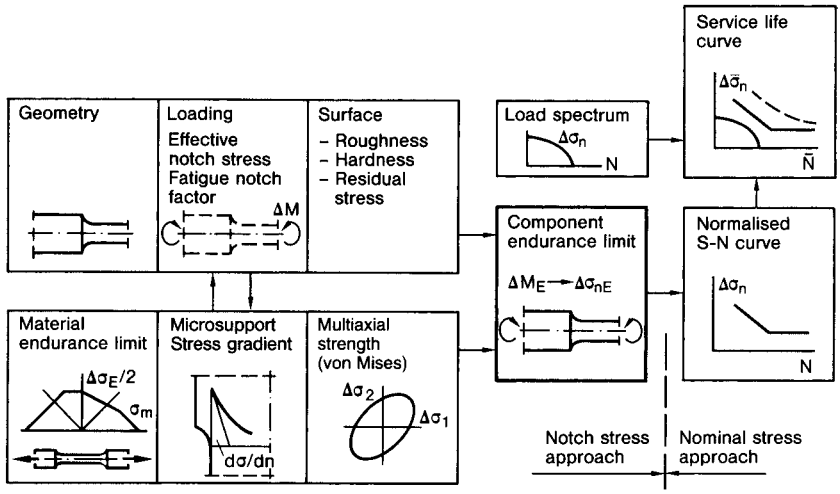


Fig. 4.1. Notch stress approach to assess the endurance limit of non-welded structural components; with ΔM cyclic external moment, $\Delta\sigma_E$ endurance limit of the material, σ_m mean stress, $d\sigma/dn$ notch stress gradient, $\Delta\sigma_1$ and $\Delta\sigma_2$ cyclic principal stresses, ΔM_E endurance limit in terms of external moment, $\Delta\sigma_{nE}$ endurance limit in terms of nominal stress, $\Delta\sigma_n$ cyclic nominal stress, $\Delta\bar{\sigma}_n$ maximum cyclic nominal stress, N and $\bar{N}$ numbers of cycles to failure; after Radaj.[5]

which depends on the dimensional ratios but not on the dimensions themselves or on the elastic modulus. The fatigue notch factor characterising the strength-effective stress concentration is derived therefrom taking a microstructural notch support hypothesis into account in the case of sharp notches. The term 'microstructural notch support' means that the maximum notch stress according to the theory of elasticity is not decisive for crack initiation and propagation but instead some lower local stress gained by averaging the notch stresses over a material-characteristic small length, area or volume at the notch root (explicable from grain structure, microyielding and crack initiation processes). Microstructural support occurs not only with sharp notches but also with mild notches if these are sufficiently small (e.g. microholes). The fatigue notch factor thus depends on the notch radius and a material-characteristic microstructural length in addition to the parameters controlling the stress concentration factor.

Different microstructural notch support hypotheses may be used for fatigue strength assessments:

– the stress gradient approach proposed by Siebel and Stieler[314] (included in Fig. 4.1),
– the stress averaging approach originally proposed by Neuber,[252–254]

– the critical distance approach proposed by Peterson,[266]
– the highly stressed volume approach originally proposed by Kuguel[246]

Only the latter three hypotheses have found wide application to welded joints, the stress averaging approach mainly used in the form of fictitious notch rounding. Further variants of the stress averaging methods applicable to notch tips are related to a distinct area or volume instead of the conventional line section. Reference should also be made to Topper and El Haddad's[334] approach, which is based on short crack behaviour in sharp notches. Against expectation, only minor differences in the calculated fatigue strength values were found when using the above methods in comparison (Taylor *et al.*,[330–332] Bellett *et al.*,[212] Crupi *et al.*[219]). As these notch stress-related methods are also applicable to cracks, relationships can be derived between the material parameters characterising the notch support (averaging or critical distance concepts) and fracture mechanics based material parameters referring to non-propagation of cracks in plain or notched specimens (the threshold stress intensity factor ΔK_{th}, Taylor's definition of notch-equivalent cracks, or the length parameter a^* introduced by Topper and El Haddad[223,334,689] substituting ΔK_{th}).

The endurance limit of the material may be taken from the endurable amplitude versus mean stress diagram (after Haigh) if mean stresses are acting, additionally taking into account roughness, hardness and residual stresses at the notch root. The von Mises distortional strain energy criterion is introduced in the case of multiaxial stresses with non-varying principal stress directions. This presumes ductile materials. The maximum principal normal stress criterion should be applied in the case of brittle materials. More sophisticated criteria are applicable in cases of out-of-phase (i.e. non-proportional) multiaxial notch stresses (Sonsino,[59,60] Dang Van[222,754]).

The notch stress approach referring to the fatigue strength for infinite (or high-cycle) life can be extended into the finite life (or medium-cycle) range on the basis of the notch strain approach. The elastic part of the strain S–N curve (i.e. the elastic strain versus life curve) is used to transfer the fatigue notch factor considered to characterise crack initiation from the endurance limit into the medium-cycle fatigue range ($N > 5 \times 10^4$ cycles). The complete elastic-plastic notch strain approach combined with crack propagation analysis, on the other hand, is indispensable in the medium- to low-cycle fatigue range and for solving problems of service fatigue strength.

A more recent further development of the notch stress approach on the basis of small-size notches (i.e. notch radius $\rho = 0.05$–0.1 mm), applicable to spot-welded and similar lap joints in thin sheet material, is described in Section 11.2.4 (with discussion in Section 11.1.3). A notch stress approach in a wider sense is the notch stress intensity approach described in Chapter 7. Whereas the conventional notch stress approach refers to material para-

meters derived from unnotched specimens, the latter approach has the stress singularity at sharp re-entrant corner notches as its basis.

The notch stress approach in the simple form described above has been successfully applied to non-welded machine parts such as crankshafts, connecting rods, angle levers and gearwheels with an expected infinite life (Peterson,[265] Lang,[247] Sonsino[316]). The approach is presented in the following sections with regard to its application to seam-welded joints.

The notch stress approach for welded joints should be applied in cases where the nominal or structural stress approach is deficient or impossible. It can be used for an absolute assessment of fatigue strength but should then be combined with evidence from test results. The classification of unconventional welded joints into the design *S–N* curve scheme of the codes can be achieved proceeding from a notch stress analysis but considerable care is necessary in doing this sufficiently close to reality. The approach is especially well suited for relative design evaluations based on parametric studies. In the finite life range, the notch stress approach should be combined with the notch strain and crack propagation approaches.

4.1.2 Critical distance approach

Lawrence *et al.*[377,378,384] have developed a calculation method to predict the fatigue strength and life of seam- and spot-welded joints which comprises an elastic notch stress analysis for determining the fatigue notch factor of crack initiation (defined by an initial crack depth of $a_i \approx 0.25\,\text{mm}$), an elastic-plastic notch strain analysis to take cyclic plasticity and relaxation effects into account and a crack propagation analysis up to final fracture. Only the purely elastic part of the method related to stress concentration and fatigue notch factors is described in this chapter whereas the notch strain approach is reviewed in Chapter 5 and the crack propagation analysis in Chapter 6. The crack initiation consideration according to Lawrence is mainly a notch strain approach because the strain *S–N* curve is taken as the basis and cyclic relaxation can be included. This is stressed in respect of the possibly disturbing fact that Lawrence mainly uses the elastic part of the strain *S–N* curve, i.e. the Basquin relationship,[347] in order to simplify the approach.

The elastic notch stress analysis for determining the fatigue notch factor of crack initiation for welded joints was first published by Mattos and Lawrence[384] in 1977, i.e. later than the first publications by Radaj[275,276,280] using Neuber's fictitious notch rounding concept, but earlier than the presentation of the more comprehensive notch stress approach by the same author.[282–285,289] Therefore, the purely elastic part of the Lawrence approach is dealt with first in this chapter.

Lawrence *et al.*[377] stress that the first step in any fatigue analysis is to identify the location(s) where a fatigue crack is most likely to be initiated. A notch stress analysis must be performed to determine the elastic stress concentration factor (necessary for the determination of the crack initiation life) and the variation of stress along the prospective inward path of the fatigue crack (necessary for the determination of the crack propagation life). The notch stress analysis is performed on the cross-sectional model of the welded joint under tension and bending loads using the finite element method (the weld toe of a butt weld being considered). Simple engineering formulae for the stress concentration factors of seam-welded joints are derived from parametric studies with variable geometry. Bending effects resulting from straightening of misaligned or distorted welded joints are included in the analysis.

The fatigue notch factor K_f is derived from the stress concentration factor K_t using the critical distance approach proposed by Peterson.[265–267] The K_f value is lowered in relation to the K_t value especially for sharp notches (microstructural support effect). The decrease depends on the ratio a^*/ρ with the material constant a^* and the notch radius ρ, Fig. 4.2. Low and

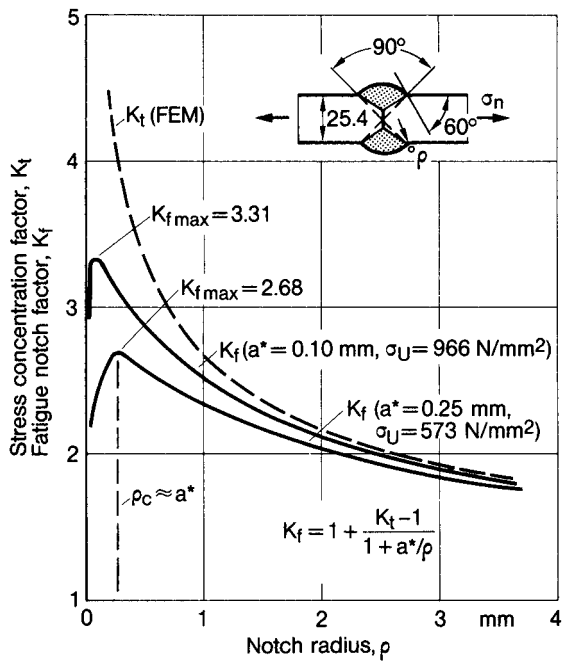


Fig. 4.2. Elastic stress concentration factor (from finite element analysis, FEM) and fatigue notch factor of butt weld dependent on toe notch radius for two structural steels (material parameters a^* and σ_U); after Lawrence *et al.*[377]

high strength steels as well as aluminium alloys are considered by Lawrence.

The problem with welded joints is that the notch radius which is of primary influence on the stress concentration factor is widely scattering. Lawrence *et al.*[378] propose introduction of the maximum value $K_{f\,max}$ into the fatigue analysis which occurs with the critical notch radius, $\rho_c \approx a^*$. This results in a worst case analysis.

The worst case condition $\rho_c \approx a^*$ is derived for the 'deep' elliptical notch in the tension-loaded infinite plate resulting in the stress concentration factor depending on the square root of inverse notch radius. The weld toe or weld root notches may deviate more or less from the above condition. It can be shown on the basis of the elliptical notch that the material constant a^* is linked to the fictitious notch radius of Neuber in the worst case analysis by $\rho_f = 4a^*$ which means that the assumption $\rho_f = 1$ mm in the notch stress approach by Radaj is identical to the assumption $a^* = 0.25$ mm in the relevant approach by Lawrence (low strength steels assumed in both cases).

The fatigue notch factor calculated by Lawrence refers to crack initiation in the medium- to high-cycle fatigue range ($N > 10^5$ cycles). It is considered to be independent of the number of cycles endured. This definition deviates from the conventional one which is related to the endurance limit without crack initiation ($N > 10^6$, Lawrence himself refers to $N = 10^7$ in a later publication). The further procedural steps according to Lawrence are reviewed in connection with the notch strain approach (see Section 5.1.2).

4.1.3 Fictitious notch rounding approach

The notch stress approach, version according to Radaj,[269–303] is restricted to the determination of the endurance limit of the welded joint with possible extensions into the medium-cycle fatigue range, Fig. 4.3. It is applicable both to seam- and spot-welded joints. It has been mainly used for low strength steels. A salient feature of the approach is the assessment of the microsupport effect at the mostly sharp toe and root notches of the welded joints according to the Neuber microstructural support hypothesis. The sharp notches in the cross-sectional model have to be fictitiously rounded in order to obtain the fatigue-effective maximum notch stress resulting in the prospective fatigue notch factor of the welded joint by reference to the nominal stress (first applications in connection with a photoelastic notch stress analysis[276] in 1969 and a finite element notch stress analysis[280] in 1975). The fictitious notch radius is given by $\rho_f = \rho + s\rho^*$ with the real notch radius ρ, a material constant ρ^* and the multiaxiality coefficient s (Neuber[254]). The fatigue-effective maximum notch stress has to be compared with the endurance limit of the parent material, possibly adjusted according to the local hardness, but relative statements based solely on the fatigue notch

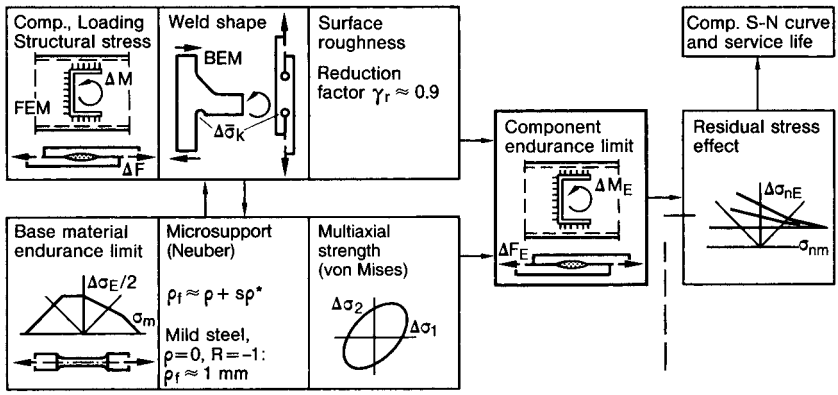


Fig. 4.3. Notch stress approach, version according to Radaj, to assess the endurance limit of welded structural components; with ΔM cyclic external moment, ΔF cyclic external force, $\Delta\bar{\sigma}_k$ cyclic fatigue-effective notch stress, $\Delta\sigma_E$ endurance limit of the material, σ_m mean stress, ρ_f fictitious notch radius, ρ actual notch radius, ρ^* microstructural length, s multiaxiality coefficient, R stress ratio, $\Delta\sigma_1$ and $\Delta\sigma_2$ cyclic principal stresses, ΔF_E endurance limit in terms of external force, ΔM_E endurance limit in terms of external moment, $\Delta\sigma_{nE}$ endurance limit in terms of nominal stress, σ_{nm} mean nominal stress, FEM meaning 'finite element method' and BEM meaning 'boundary element method'; after Radaj.[5]

factor are more important. Despite the fact that the approach was proposed for any radii of notch curvature, it has mainly been applied as a worst case condition in which the real notch radius is introduced as zero. The fictitious notch radius then results in $\rho_f \approx 1$ mm in the case of welded joints of low strength structural steel, but the approach is not restricted to these steels.

The procedure which was originally demonstrated by the example of a welded joint between two channel-section bars subjected to a torsional moment comprises the following steps. At first, the structural stresses or internal forces in the butting plates at the weld toe and root notches are determined without considering the notch effect, Fig. 4.4. This can be achieved by using engineering formulae, the finite element method or strain gauges. Secondly, the structural stresses or internal forces are transferred as external forces to the cross-sectional model of the welded joint with fictitiously rounded notches in order to determine the fatigue notch factors by applying the notch stress theory, the boundary element method or the finite element method, Fig. 4.5.

Two different methods are available for the transfer of the structure-internal forces and the calculation of the notch stresses, the 'principal internal force method' and the 'internal force splitting method' (see Section 4.2.8). Internal displacements can be used instead of internal forces for the

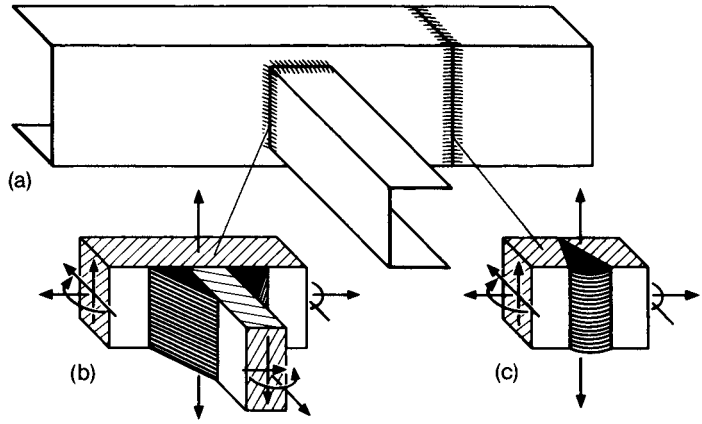


Fig. 4.4. Structural component (a) with the (magnified) welded joints (b, c) loaded by the internal forces of the structure.

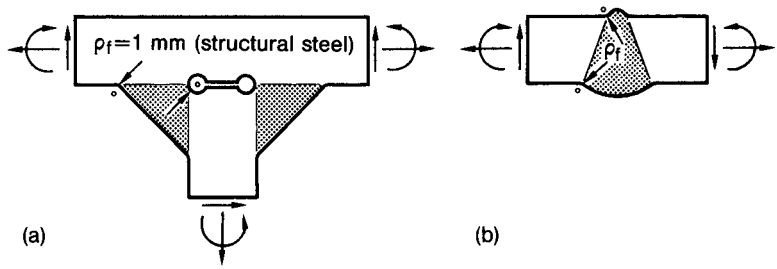


Fig. 4.5. Cross-sectional models of the welded joints in Fig. 4.4(b, c), loaded by the internal forces of the structure and fictitiously notch-rounded.

parameter transfer from the structural component to the cross-sectional model. Special procedures on the basis of the above are necessary at the weld ends where structural stress singularities may occur.

The fatigue strength reduction factor often used with welded joints (see Section 2.2.8 and Radaj[4]) results from the reciprocal value of the fatigue notch factor. However, it has to be taken into account that the fatigue notch factor is defined in relation to a plain polished specimen whereas the strength reduction factor refers to a plain specimen in the mill-finished condition. Therefore, a correction factor has to be introduced when calculating the strength reduction factor from the fatigue notch factor. This factor is approximately 1/0.9 for low strength steels.

The multiaxiality of the stress state at the notch root is taken into account by the von Mises distortional strain energy criterion valid for ductile materials and non-varying principal stress directions. Proceeding in an approxi-

mate manner, the same fictitious radius of curvature is applied in tensile or compressive, transverse and longitudinal shear loading of the notch root. A smaller radius has to be introduced in longitudinal shear loading within a more accurate analysis. Any other strength criterion can principally be introduced when considering multiaxial stress states at the notch root.

A static mean stress can be taken into account on the basis of the relevant Haigh diagram but the Neuber microstructural support hypothesis has not yet been verified for non-zero mean stresses. The material characteristic values of the parent material are used, modified in accordance with the hardness in the area of crack initiation as far as necessary.

The result of the notch stress approach above is the endurance limit of the welded joint being considered in terms of nominal stress range. It is recommended that the result be corrected in respect of residual stresses, to cover the medium-cycle fatigue range using the slope of the normalised *S–N* curve (as far as applicable) and to assess the service life on the basis of a suitable modification of Miner's rule. This means switching from the notch stress approach to the nominal stress approach in the finite life range. Alternatively, the elastic notch stress analysis with fictitiously enlarged notch radii can be used as the basis of the notch strain approach in the finite life range.

Fictitious notch rounding may involve the following complications (see Section 4.2.7 for remedial measures). It may cause undercut with a stress-raising effect which should be corrected especially in thin sheet applications of the approach where the effect is strong. A special correction may be necessary in the case of cover plate joints. Another correction is recommended in the case of short root faces. Fictitious notch rounding is disputable in the case of tensile (or compressive) loading in the direction of the slit or crack. No stress rise occurs under ideal conditions, whereas the keyhole (or U-shaped) notch induces a substantial notch effect (see Fig. 11.6). A semi-elliptical notch may be introduced in order to keep this notch effect sufficiently low.

It has been checked whether the notch stress approach, version according to Radaj, correctly classifies conventional welded joints made of structural steel in respect of the standardised detail class scheme of the nominal stress approach. A comparative investigation was initiated by the International Institute of Welding (IIW) and successfully performed by Petershagen[261] (see Table 4.1). Another comparison with the data from the *S–N* curve catalogue compiled by Olivier and Ritter[52] was convincing in respect of mean values and scatter ranges (see Fig. 4.8).

Various scientific questions remain partly open despite the above comparisons. These questions refer to the size of the fictitious notch radius in plane and anti-plane shear loading, to the limiting values for crack-like notches, to the effect of a static mean stress inclusive of residual stress and to the effect of microimperfections typical for weld notches. The

attractiveness of the approach from the engineering point of view nevertheless remains high. The procedure fits well into the designer's way of descriptive thinking. It can be performed quickly and without major expenditure.

The engineering approach consists of using a uniform material-dependent fictitious radius independent of the notch root loading mode, in neglecting the local material inhomogeneity and in considering the effect of residual stresses roughly on an empirical basis. The procedure generally remains conservative, even if the corrections for fictitious undercut and short slit length are introduced. In anti-plane shear loading, a reduced fictitious notch radius may be necessary according to theory.

The notch stress approach, version according to Radaj, was originally proposed for achieving relative statements on the fatigue strength of welded joints.[272] The calculated fatigue notch factor K_f when converted to the conventional reduction factor γ of welded joints allowed design comparisons based on a uniform but not necessarily well-known local fatigue strength. Only strength reduction factors γ were set against one another.

By introducing the parent material fatigue strength, with an appropriate hardness modification as far as necessary, it was claimed possible in principle also to perform absolute assessments.[283] Petershagen[261] verified this at an early stage of development of the method in respect of the IIW fatigue design recommendations.[3] He based the assessment on the endurable stress range proposed by Radaj[4,284] (based on Neumann[48]) for low strength structural steels: $\Delta\sigma_E = 240\,N/mm^2$ for the mill-finished material and $\Delta\sigma_E \approx 270\,N/mm^2$ for the polished material ($N = 2 \times 10^6$ cycles, $R = 0$, $P_f = 10\%$), so that $\Delta\sigma_{nE} = 240/(0.9K_f)$ or $\Delta\sigma_{nE} \approx 270/K_f$.

The comparison was performed considering four typical welded joints with different notch effects: the transverse butt weld (toe fractures), the transverse fillet weld at an attachment (toe fractures), the double-bevel butt weld with fillet welds at a cruciform joint (toe fractures) and the double fillet weld at a cruciform joint (root fractures). The results of the comparison are shown in Table 4.1. A reduction by 1/1.08 of the endurable stress with $P_f = 10\%$ was made in order to refer to the failure probability $P_f = 2.3\%$ corresponding to two standard deviations from the mean value (with the scatter range index $T_\sigma = 1:1.5$). Further, a downgrading by one or two notch classes was introduced to take the effect of tensile residual stresses into account (factor 1.12 for one notch class).

The endurable stress ranges obtained by the notch stress approach are about 10% higher than those in the IIW fatigue design recommendations, i.e. about one notch class higher. The comparison allows no convincing validation. It refers to only four welded joints without defined dimensional and shape parameters and the evaluation is connected with too much latitude of interpretation. More convincing statements are possible based on the

Table 4.1. Endurable nominal stress ranges: endurance limit $\Delta\sigma_{nE}$ ($N = 2 \times 10^6$, $R = 0$); notch stress approach, version according to Radaj, in comparison with IIW design recommendations for typical welded joints in structural steel; after Petershagen[261]

Welded joint type	K_f[a]	γ[b]	$\Delta\sigma_{nE}$[c] (P_f = 10%) [N/mm^2]	$\Delta\sigma_{nE}$[d] (P_f = 2.3%) [N/mm^2]	$\Delta\sigma_{nE}$[e] (res. str.) [N/mm^2]	$\Delta\sigma_{nE}$[f] (IIW) [N/mm^2]
Butt joint	1.89	0.60	144	133	106	100
Transverse attachment	2.45	0.46	110	102	91	80
Cruciform joint (toe)	2.50	0.45	108	100	80	71
Cruciform joint (root)	4.03	0.28	67	62	49	45

[a] K_f according to Radaj without mean stress effect.
[b] $\gamma = 1/(0.9K_f)$.
[c] $\Delta\sigma_{nE} = 240\gamma$.
[d] $\Delta\sigma_{nE} = 240\gamma/1.08$.
[e] $\Delta\sigma_{nE}$ with residual stress, reduction according to IIW JWG, Doc. XIII/XV-39-79.
[f] Design stress according to IIW fatigue design recommendations[3] (1996 edn).

investigation of Olivier *et al.*[259,260] (see Fig. 4.8). The notch stress approach has finally been included in the IIW fatigue design recommendations.

An uncertainty exists concerning the difference between fully reversed ($R = -1$) and zero-to-tension ($R = 0$) loading. The original approach referred to zero-to-tension loading (as applied by Petershagen[261,262]). Later on, the fact was taken into account that the fatigue notch factors based on Neuber's microstructural support hypothesis are defined for fully reversed loading only. Transfer to zero-to-tension loading was achieved by the relationship $\gamma(R = 0) \approx \gamma(R = -1) + 0.1$ (restricted to $0.2 \leq \gamma(R = 0) \leq 0.8$) derived from design curves of fatigue strength dependent on stress ratio R. On the basis of more recent experiences and considerations (see Section 4.1.4) it seems justifiable to use identical reduction factors in fully reversed and zero-to-tension loading.

4.1.4 Modified notch rounding approach

Seeger *et al.*[8,243,244,259,260,313] have modified the notch stress approach, version according to Radaj, aiming at a better definition of mean values and scatter ranges. They have proven its reliability for type St52-3 structural steel ($\sigma_{Y0.2}$ = 375–486 N/mm^2, σ_U = 521–600 N/mm^2 in the investigation) in a more general way, Fig. 4.6. The reason for the investigation was the uncertainty about how to classify longitudinally welded hollow section girders used in crane construction according to the standard notch or detail classes of the nominal stress approach (a box girder is shown in the figure). A large

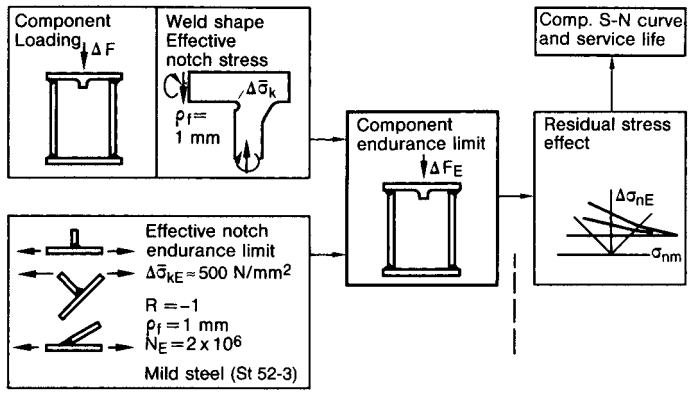


Fig. 4.6. Notch stress approach, version according to Seeger, to assess the endurance limit of welded joints; with ΔF cyclic external force, ρ_f fictitious notch radius, $\Delta\bar{\sigma}_k$ cyclic fatigue-effective notch stress, $\Delta\bar{\sigma}_{kE}$ endurance limit in terms of notch stress, R force ratio, N_E number of cycles at endurance limit, ΔF_E endurance limit in terms of external force, $\Delta\sigma_{nE}$ endurance limit in terms of nominal stress, σ_{nm} mean nominal stress; after Radaj.[5]

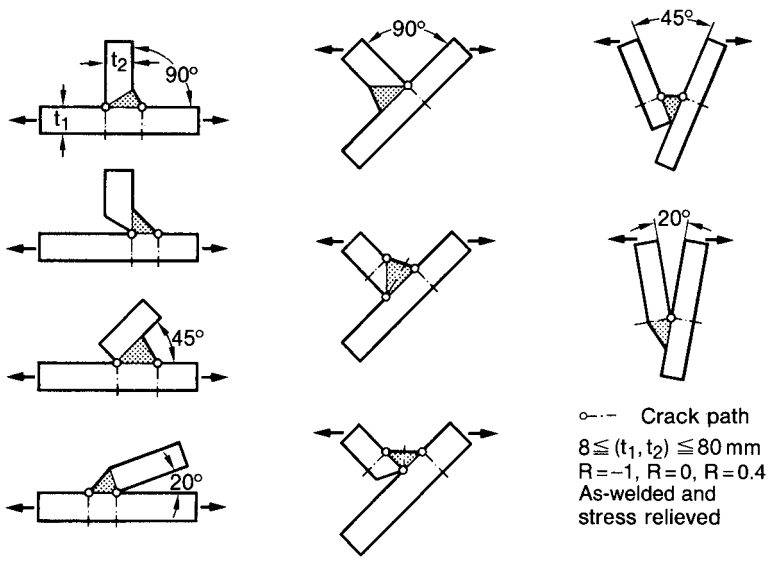


Fig. 4.7. Welded joints used in crane construction, fatigue-tested for determining the endurable notch stresses; after Olivier *et al.*[259,260]

number of welded joints with T- and Y-sections, with fillet welds and single-bevel butt welds and with plate thicknesses $t = 8, 15$ and 40 mm were investigated, Fig. 4.7. Fatigue fractures occurred at the weld toe and/or the weld root. The test results were evaluated on a statistical basis.

The following special features are characteristic of the modified approach. The radius of notch rounding is fixed at 1 mm for structural steel independent of the actual radius which scatters around this value. The following question is put forward: what are the appertaining fatigue-effective elastic cyclic notch stresses? Local endurance limit values (both the technical and the true endurance limit inclusive of scatter ranges) are given in Section 4.2.9 for as-welded and stress-relieved conditions. The endurance limit for $R = -1$ is markedly higher than the endurance limit for $R = 0$, as expected. The effect of welding residual stresses is small, at least in the mean of all test specimens. Considering individual specimen types, deviations of up to 30% occurred. It is proposed that the endurance limit values for $R = 0$ in the stress-relieved condition be used on welded structures with high tensile residual stresses (identical with the recommendation for the nominal stress approach according to Eurocode[23] whereas the IIW recommendations[3] demand $R = 0.5$).

The scatter of the endurance limit values results from the scatter of various influence parameters: toe or root radius, toe or root angle, height of weld reinforcement, depth of penetration, residual stresses, microstructural imperfections and surface roughness.

The endurance limit of the structural component is derived from its notch stresses compared with the notch stress endurance limit of the fatigue-tested welded joints, both stresses determined for a fictitious notch radius of 1 mm. Endurable notch stresses are available both for the as-welded and stress-relieved condition. On the other hand, it is possible to switch to the nominal stress approach at this point, in order to assess the effect of residual stresses and to determine the *S–N* curve and the service life of the structural component. The modified notch stress approach described above is well suited to classify unconventional welded joints according to the standard notch or detail classes of the nominal stress approach. This has been demonstrated not only for the box girder in crane construction but also in analysing the fatigue failure at a wind energy conventer.[245]

A similar procedure of notch stress assessment based on mean values of the real weld toe radii combined with Dang Van's multiaxiality criterion has been proposed and extensively applied by Janosch and Debiez.[232–235]

The local endurance limit values stated in Section 4.2.9 for $R = 0$ and $N = 2 \times 10^6$ cycles have been compared by Olivier *et al.*,[259,260] together with their scatter ranges, with relevant data derived for some basic types of conventional welded joints on the basis of the *S–N* curve catalogue by Olivier and Ritter[52] combined with fatigue notch factors published by Radaj,[4,284,295] Fig. 4.8 (the factor for the butt weld is increased from $K_f = 1.89$ to $K_f = 2.27$ taking a generally larger weld toe angle into account). The mean values ($P_f = 50\%$) of the local endurance limit are nearly identical. The values for $P_f = 10\%$ differ to some extent between the conventional joints ($\Delta\sigma_{kA} \approx$

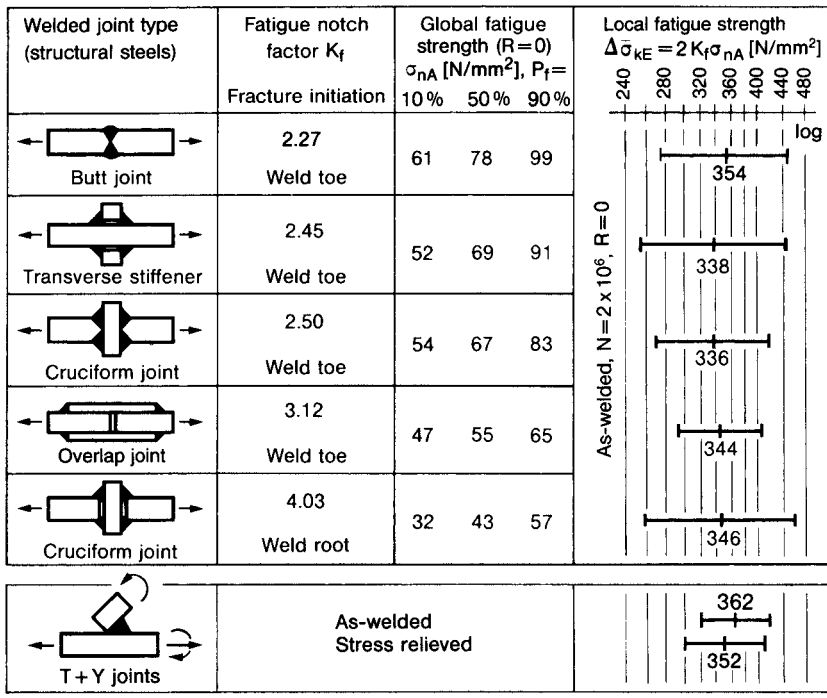


Fig. 4.8. Endurable notch stress ranges $\Delta\sigma_{kE}$ of conventional welded joints fictitiously rounded at weld toe and root ($\rho_f = 1$ mm), with conversion of compiled data for $t \approx 10$ mm, $P_f = 10$, 50 and 90% on the basis of calculated fatigue notch factors, and comparison with the results for T- and Y-joints used in crane construction; after Olivier *et al.*[259,260]

280 N/mm^2) and the T- and Y-joints ($\Delta\sigma_{kA} \approx 320$ N/mm^2), but the difference can be explained by the more uniform testing conditions in the latter case. Similar results are available for $R = -1$.

The evaluation results of Olivier *et al.*[259,260] thus confirm the applicability of the notch stress approach, version according to Radaj, with the calculated fatigue notch factors directly transferred to zero-to-tension loading ($R = 0$), i.e. without the modification $\gamma(R = 0) \approx \gamma(R = -1) + 0.1$. The different joints are correctly classified and uniform local fatigue strength values are given. However, the confirmation is only a rough one despite the seemingly high correspondence of endurable stress values (270 versus 280 N/mm^2). The original version of the approach[283] referred to welded joints in low strength steel of type St37 with fictitious radius $\rho_f = 1$ mm. The high strength steel of type St52-3 offers a higher local fatigue strength, but the latter is associated with higher notch sensitivity and higher welding residual stresses so that the global fatigue strength of the welded joint is not increased in accordance with the local static strength values.

4.1.5 Highly stressed volume approach

Further progress in respect of the notch stress approach for welded joints has been achieved by Sonsino.[316–325] His contributions are directed towards the statistical size effect at the notch root and to the effect of multiaxial local stresses with in-phase and out-of-phase stress amplitudes. His extensions in respect of the notch strain approach are reviewed in Section 5.1.4.

The statistical size effect combined with the microstructural notch support effect is taken into account by assuming that crack initiation (a_i = 0.5–1.0 mm) in the high-cycle fatigue range can be described on the basis of a critical local stress amplitude that depends on the local volume of highly stressed material. Larger volumes are characterised by lower critical stresses. Quantitative data depend on the definition of the highly stressed volume at the notch root. Sonsino uses the depth below the notch root where the maximum notch stress has fallen to 90% (calculated from the normalised stress gradient) and a notch surface area containing the same decrease of stress (mainly dependent on the notch radius). The actual notch radius at the weld toe (or weld root) has to be introduced for that purpose. Relevant diagrams for non-welded materials and welded joints given by Sonsino[59,60,213,316,325] refer to the technical endurance limit.

The approach has been extended to multiaxial fatigue on the basis of an equivalent stress. The von Mises equivalent stress is used in the case of ductile materials and non-varying principal stress directions. A 'criterion of effective equivalent stress' is proposed in the case of varying principal stress directions which occurs, for example, with out-of-phase bending and torsion loading of tube-to-plate joints.[59–61,318] The arithmetical mean of the shear stress amplitudes acting in the notch root surface under different angles is considered to be the parameter which describes crack initiation. The 'hypothesis of highly stressed volume'[316] has to be combined with the averaged shear stress amplitude in order to obtain the 'effective equivalent stress'.

4.2 Analysis tools

4.2.1 General survey and assessment procedure

The analysis tools described hereafter comprise the following items: assessment procedure, notch stress analysis tools, notch stress concentration factors for welded joints, fatigue notch factors and relevant fatigue-effective notch stresses, local hardness factor, tools for the critical distance

approach, the fictitious notch rounding approach (original and modified version) and the highly stressed volume approach.

Fatigue stress assessment based on elastic notch stresses uses the same procedures and relationships as the nominal stress approach (see Chapter 2), with the single difference that it is not the actual, but the fatigue-effective local stresses that are considered in the place of global nominal stresses. This is highlighted by the relevant codes, in particular by the FKM guideline.[1] The difference is an essential one. The theoretical elastic notch stress σ_k must not be used, but instead the fatigue-effective notch stress $\bar{\sigma}_k$, which follows from σ_k by application of a microstructural notch support hypothesis, must be used. This can be expressed by the connection between the fatigue notch factor K_f and the theoretical stress concentration factor K_t, resulting in the relationship between the fatigue-effective notch stress amplitude $\bar{\sigma}_{ka}$ and the corresponding nominal stress amplitude σ_{na}:

$$\bar{\sigma}_{ka} = K_f \sigma_{na} \tag{4.1}$$

The fatigue notch factor K_f will thus be the essential parameter characterising the difference between the various versions of the notch stress approach. This does not necessarily mean that the factor is explicitly determined in the actual procedure. We use it here for a more consistent presentation.

The assessment procedure is based on the comparison of the fatigue-effective notch stress amplitudes $\bar{\sigma}_{ka}$ actually occurring, with the endurable notch stress amplitudes based on probabilities of failure:

$$\bar{\sigma}_{ka} \leq \bar{\sigma}_{ka\,per} \tag{4.2}$$

$$\bar{\sigma}_{ka\,per} = \frac{\bar{\sigma}_{kA}}{j_\sigma} \tag{4.3}$$

where $\bar{\sigma}_{ka\,per}$ is the permissible fatigue-effective notch stress amplitude with acceptable P_f (e.g. $P_f = 2.3\%$), $\bar{\sigma}_{kA}$ is the endurable fatigue-effective notch stress amplitude with defined P_f (e.g. $P_f = 50\%$), j_σ is a safety factor and P_f is the failure probability.

The acting fatigue-effective notch stress amplitude depends on the nominal (equivalent) stress amplitude and the fatigue notch factor. The endurable (equivalent) fatigue-effective notch stress amplitude depends on the material condition, the mean stress (including residual stress), the considered number of cycles to failure and the failure probability. The safety factor depends on technical and economic points of view. The effect of variable-amplitude loading should be determined on the basis of the original or modified version of Miner's rule.

4.2.2 Notch stress analysis for welded joints

The elastic notch stress concentration factor K_t is defined as the ratio of the maximum notch stress σ_k to the nominal stress σ_n, determined under the assumption of linear-elastic material behaviour:

$$K_t = \frac{\sigma_k}{\sigma_n} \tag{4.4}$$

The nominal stress can be related to the gross or net cross-sectional area, i.e. to the cross-section without or with reduction by the notch (in special cases the two may be identical). The nominal stress corresponds to the local structural stress in the case of complex welded structures. The link between notch stress and structural stress concentration under-one-dimensional conditions is considered by Soya[326] and Barro *et al.*[209]

The maximum notch stress is determined on the basis of one of the following methods:

- functional analysis methods based on the theory of elasticity applied to notches (Neuber,[252,253] Muskhelishvili,[251] Savin,[311] Radaj[279,297]),
- numerical methods such as the finite element method[84,344] or boundary element method,[210,214,446]
- measuring methods such as photoelastic, thermoelastic or strain gauge methods.[131,181,198,221,242]

The basis of the notch stress analysis in complex welded structures is the local structural stress (see Section 4.1.3). Post-processors that handle the structural stress results from finite element analysis are useful in respect of subsequent notch stress evaluations (e.g. FEMFAT[107,108]). An advanced CAD basis for finite element or boundary element modelling of actual local weld geometries of joints occuring in pressure vessel technology has been presented by Rudolph *et al.*[309]

The stress concentration factor depends on the (mutually independent) ratios of the geometric (or shape) parameters of the notch, i.e. not on the absolute values of these parameters. It is independent of the elastic modulus and only slightly influenced by Poisson's ratio. The stress concentration factor for a definite geometric configuration depends on the type of loading. It is generally larger in tensile loading than in bending loading, and larger in bending loading than in longitudinal shear loading provided the nominal stress is defined appropriately. The (non-elastic) stress concentration factor after exceeding the yield limit at the notch root depends on the magnitude of the load and the stress–strain behaviour of the material (see Section 5.2.2). Compilations of notch stress concentration factors in general, i.e. not restricted to welded joints, are available, authored by Nishida,[255] Peterson[265] and Radaj and Schilberth.[297]

The geometric data needed for the notch stress analysis of welded joints are partly included in the actual design specification, e.g. base plate thickness, base plate width, fillet throat thickness or fillet leg length, root face length, attachment length, attachment plate thickness. Deviations from the geometric design specification may result from the manufacturing process and should be taken into account when defining the geometric data, e.g. axial and angular misalignment, lack of penetration or reduction of sheet thickness caused by deep-drawing.

However, not all geometric data of welded joints needed for the notch stress analysis are included in the design specifications. Some of these data depend on the welding process and the welding quality achieved such as the notch radius and notch angle at the weld toe, the depth of penetration at the weld root and the width and height of reinforcement of butt welds. Special geometric parameters characterise welding imperfections such as undercut, sagging, burn-through and others. Contrary to design-related parameters, process-related parameters are scattered to a large extent and should be evaluated statistically (e.g. Fig. 4.45). It has been shown by Jakubovskii and Valteris[231] or Hentschel *et al.*[228] that the statistical distribution of fatigue strength can be attributed to the statistical distribution of the geometric parameters. The mean values may be used in the notch stress analysis. It is more common to introduce the worst case assumption in respect of the notch stress concentration factor, i.e. zero toe radius and large toe angles.

Data on toe and root notch radii, toe angles, undercut depths, undercut radii, and reinforcement heights of welds determined by profile measurement can be found in the literature.[187,228,234,264,278,349] The notch radii in the as-welded condition are mainly between 0.1 and 4 mm, the toe angles between 10 and 80°. A mean notch radius of 0.5–1.2 mm can often be assumed at the weld toe and a notch radius of about 0.1 mm at the weld root. Postweld treatments such as grinding, shot-peening or remelting generally produce larger toe notch radii and smaller toe angles.

Any investigation of notch stresses in welded joints has first to find out what the process-related geometric parameters of the considered welds are. Misalignment effects should be included.

4.2.3 Notch stress concentration factors of welded joints

Various joint types (Nishida among others)

Notch stress concentration factors applicable to welded joints were originally determined on the basis of photoelasticity considering cross-sectional models of welded joints. Various publications related to this issue were made available between 1930 and 1970 (Cherry,[216] Coker and Filon,[217]

Coker and Levi,[218] Frocht,[224] Heywood,[229] Nishida,[255] Norris,[257] Peterson,[265] Radaj,[270] Solakian,[315]). The accuracy of these investigations is occasionally poor because of a disturbing photoelastic boundary effect or because of stress relaxation in photoelastic materials. Some of the investigators use a sharp toe notch without defining its radius. The approximation formulae derived by Nishida for shoulder fillets (depicted in Fig. 4.15(b)) seem to be comparable in respect of accuracy with similar formulae derived on the basis of finite element or boundary element results (maximum error 10–20%). The photoelastic method has been superseded by the more powerful computer-based numerical methods (finite element and boundary element) since 1970.

As an example, the stress concentration factors for a butt weld type cross-sectional model (trapezoidal protuberance) are plotted in Fig. 4.9, based on a more general approximation formula given by Nishida[255] which comprises the influence of further geometric parameters such as plate thickness t, reinforcement width b and reinforcement height h. The contour model under consideration is also applicable to friction-welded joints. Appropriate stress concentration factors as a function of forging pressure are given by Thouvenel and Lieurade.[333]

Early theoretical solutions to the parametric weld notch problem have been presented on the basis of Muskhelishvili's complex variable functional analysis method. The protuberance at the edge of a semi-infinite plane, in particular, has been considered with inclusion of Neuber's real variable solution (Karkhin *et al.*[237–240]). Far-reaching solutions based on the same

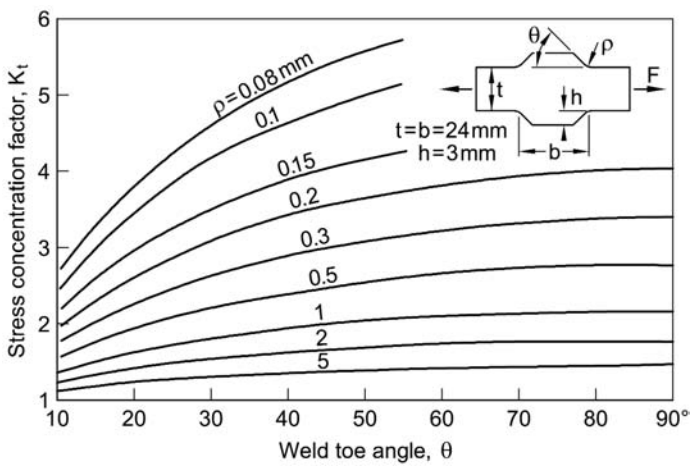


Fig. 4.9. Stress concentration factor at the toe notch of a butt weld type cross-sectional model as function of the weld toe angle for different weld toe radii; after Nishida.[255]

method, initiated by the parametric weld notch problem, have been presented by Radaj.[277,279,297] The method was also used by Wagner[195] dealing with a cruciform joint.

Various joint types (Lawrence)

The stress concentration factors at the toe and root notches of seam-welded joints were determined by Lawrence *et al.*[377] on the basis of the finite element method. The results of the analysis were incorporated in the following approximation formula:

$$K_t = 1 + \alpha\sqrt{\frac{t}{\rho}} \tag{4.5}$$

where K_t is the stress concentration factor at the weld toe or weld root, α is a coefficient depending on weld toe angle and relative root face length, t is the plate thickness and ρ is the toe or root notch radius.

The results of the original investigation[377] which comprised fillet-welded T-joints, cruciform joints and lap joints besides butt welds, Fig. 4.10, are plotted in Fig. 4.11 (finite element results compared with approximation formula). The results have been reviewed by Yung and Lawrence[407] together with data from other publications, Fig. 4.12, comprising also fillet-welded butt joints, surface roughness and undercut. The approximation formulae are condensed to the following generalised form:

$$K_t = \beta\left[1 + \alpha\left(\frac{t}{\rho}\right)^{\lambda}\right] \tag{4.6}$$

where K_t is the stress concentration factor at the weld toe or weld root, α and β are coefficients depending on the shape parameters, t is the plate thickness, ρ is the notch radius at the weld toe or weld root and λ is an exponent depending on the shape parameters.

Some of the reviewed results of Lawrence were published in concise form,[407] Table 4.2. There are no statements available on the accuracy of these formulae.

Various joint types (Rainer)

The investigation of stress concentration factors performed by Rainer[304,305] and summarised by Haibach[2] comprises the cross-sectional models of straight and circumferential seam welds (plane and axisymmetric models) under tension, bending and torsion loading, Fig. 4.13 (survey on available solutions). The stress concentration factors are derived from a finite element analysis with an expectation of high accuracy of the results (fine

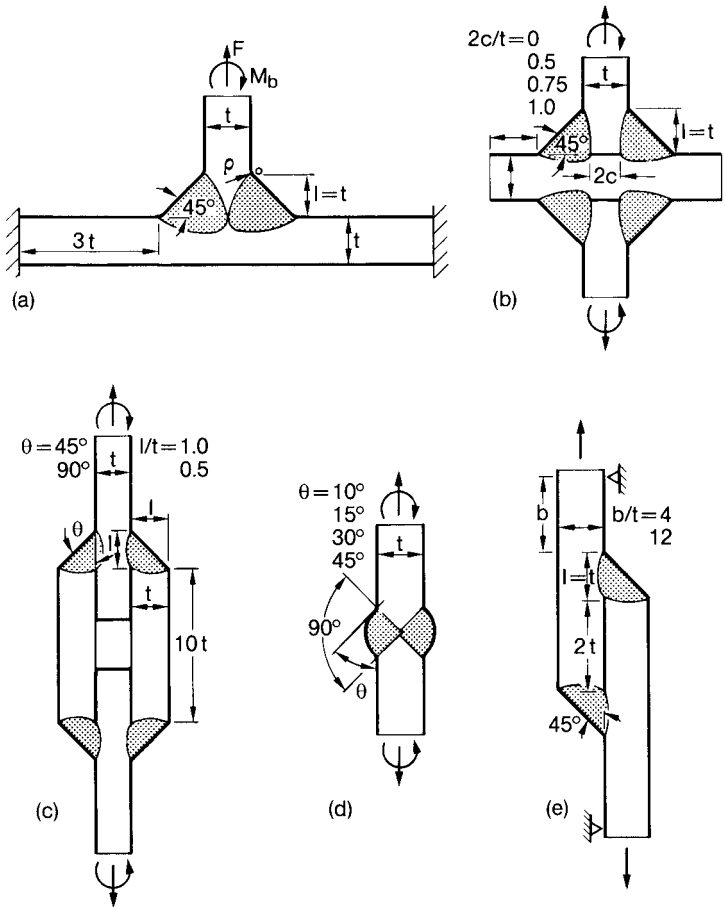


Fig. 4.10. Fillet-welded and butt-welded joints under tensile and bending loads analysed in respect of notch stress concentration by means of the finite element method: T-joint (a), cruciform joint (b), two-sided lap joint (c), butt joint with double-V weld (d), one-sided lap joint (e) after Lawrence *et al.*[377]

meshing and high-order elements, Lagrange and Serendipity type). The finite element results are approximated by rather complex formulae derived for comparable stepped bars with a shoulder fillet, Fig. 4.14. The stress concentration factor K_t of the butt weld toe is presented as a function of the ratios of toe radius to plate thickness, ρ/t, and reinforcement height to plate thickness, h/t (no influence of the tube radius for $r/t > 100$), eq. (4.7). The corresponding weld toe and root factors of the cruciform joint (root face perpendicular to loading direction) or attachment joint (root face in loading direction), constant weld toe angle in both cases ($\theta = \pi/4$), is

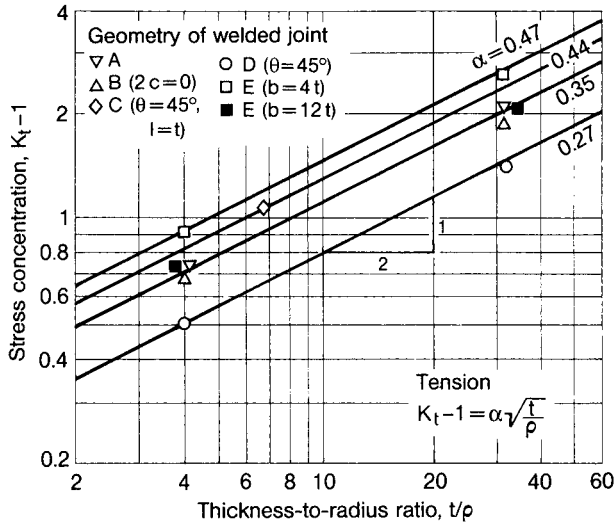


Fig. 4.11. Notch stress concentration factor at weld toe dependent on plate thickness related to notch radius of welded joints under tensile load according to Fig. 4.10 (A–E refers to variants a–e), finite element results (point symbols) versus approximation formulae (solid lines)); after Lawrence.[377]

presented as a function of the toe or root notch radius, ρ, throat thickness, a, root face length, g, and tube radius, r, related to plate or wall thickness, t (influence of tube radius is negligible for $r/t > 100$), eq. (4.8):

$$K_t = 1 + f\left(\frac{\rho}{t}, \frac{h}{t}\right) \tag{4.7}$$

$$K_t = 1 + f\left(\frac{\rho}{t}, \frac{a}{t}, \frac{g}{t}, \frac{r}{t}\right) \tag{4.8}$$

The approximation formulae are also found in Haibach's book.[2] Their accuracy is claimed to be better than 10%.

Various joint types (Radaj)

The stress concentration factors published by Radaj *et al.*[207,293,295] refer to cross-sectional models of a large variety of welded joint types including resistance spot welded and laser beam welded joints. Section 4.4 is completely devoted to a review of these investigations, which are generally based on a worst-case consideration of the fatigue notch factor resulting in a notch radius of 1 mm at the toe or root notch of the weld. Additionally,

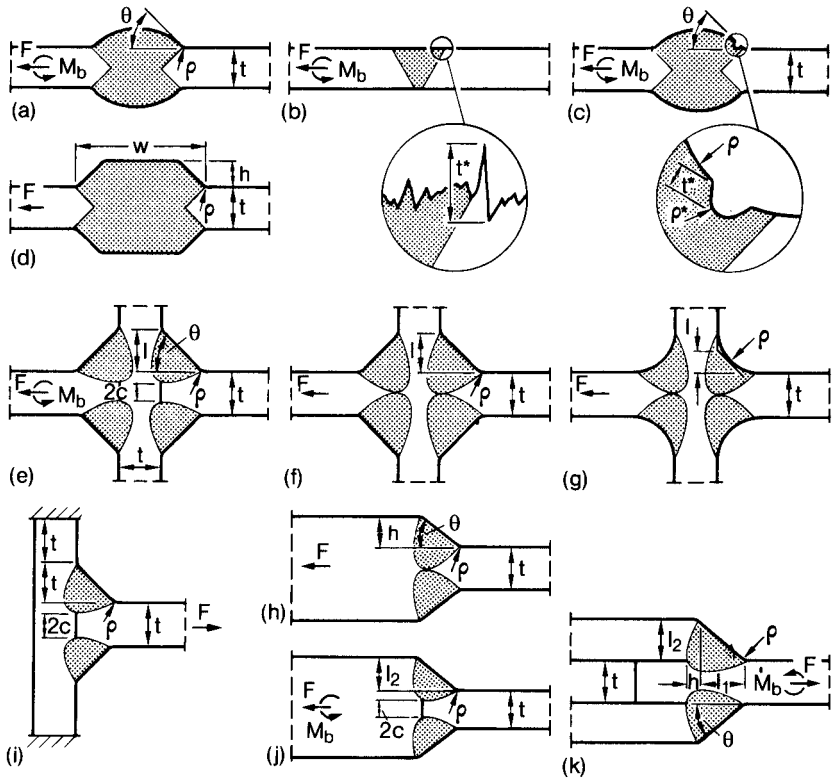


Fig. 4.12. Variants of welded joints under tensile and bending load reviewed by Lawrence *et al.*[377] in respect of notch stress concentration (see Table 4.2): butt joint (a), machined flush butt joint with surface defect (b), butt joint with undercut notch (c), butt joint with wide fillet welds (d), cruciform joint with root face (e), without root face (f) and with concave fillets (g), T-joint with root face (i), fillet-welded stepped bar without root face (h) and with root face (j), lap joint (k).

Table 4.2. Stress concentration factors of welded joints; after Lawrence *et al.*[377]

Welded joint type[a]	Site	Stress concentration factor	Loading
Butt welds (a)	Toe	$1 + 0.27(\tan\theta)^{1/4}(t/\rho)^{1/2}$	Tension
	Toe	$1 + 0.165(\tan\theta)^{1/6}(t/\rho)^{1/2}$	Bending
Cruciform joints (e)	Toe	$1 + 0.35(\tan\theta)^{1/4}[1 + 1.1(c/l)^{5/3}]^{1/2}(t/\rho)^{1/2}$	Tension
	Toe	$1 + 0.21(\tan\theta)^{1/6}(t/\rho)^{1/2}$	Bending
	Root	$1 + 1.15(\tan\theta)^{-1/5}(c/l)^{1/2}(t/\rho)^{1/2}$	Tension
	Root	$1 + 3.22(c/t)^{1/8}(t/\rho)^{1/2}$	Bending
Lap joints (k)	Toe	$1 + 0.6(\tan\theta)^{1/4}(t/l_1)^{1/2}(t/\rho)^{1/2}$	Tension
	Toe	$1 + 0.24(\tan\theta)^{1/6}(t/\rho)^{1/2}$	Bending
	Root	$1 + 0.50(\tan\theta)^{1/8}(t/\rho)^{1/2}$	Tension

[a] Lettering according to Fig. 4.12.

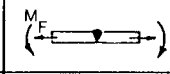
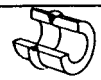
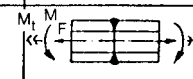
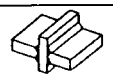
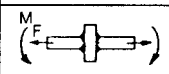
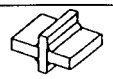
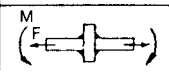
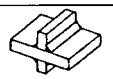
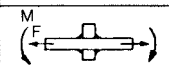
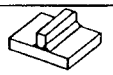
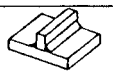
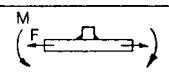
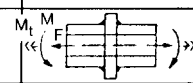
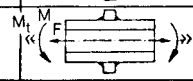
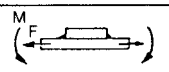
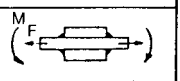
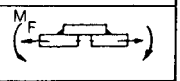
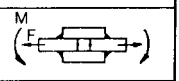
No.	Welded joint	Joint type	Weld type	Loading
1		Butt joint	V butt weld	
2			Double-V butt weld	
3			V butt weld	
4		Cruciform joint	Double-bevel butt weld	
5			Fillet weld	
6		Transverse attachment	Fillet weld	
7		T-joint	Double-bevel butt weld	
8			Fillet weld	
9		Cruciform joint	Fillet weld	
10		Transverse attachment	Fillet weld	
11			Fillet weld	
12		Cover plate joint	Fillet weld	
13			Fillet weld	
14		Lap joint	Fillet weld	
15			Fillet weld	

Fig. 4.13. Welded joints under tensile, bending and torsion loading analysed in respect of notch stress concentration using the finite element method; after Rainer.[304,305]

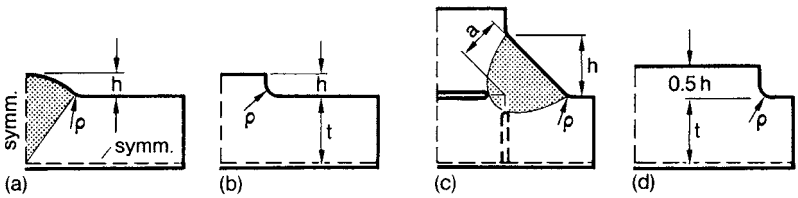


Fig. 4.14. Notch stress concentration at butt welds (a) and transverse attachment or cruciform joints (c) approximated by the notch stress concentration of comparable stepped bars with shoulder fillet (b,d); after Rainer.[304,305]

any stress intensity factor solution for lap joints (see Section 10.4) can be, and to some extent actually has been, evaluated in respect of the stress concentration or fatigue notch factor.

One message coming from the investigations reviewed is that there is no need for approximation formulae if the finite element or boundary element method is readily available for design evaluations. On the other hand approximation formulae derived from the boundary element results of parametric studies present the influence parameters of the investigated problem more clearly. They are thus readily usable for dimensioning and optimisation tasks.

The stress concentration factor K_t is approximated as dependent on the product of the mutually independent shape parameters expressed by the dimension ratios λ_ν, each ratio with individual exponent p_ν ($-1.0 \le p_\nu \le 1.0$, $\nu = 1, 2, \ldots, n$), and the coefficient k:[287,301,302]

$$K_t = k\lambda_1^{p_1}\lambda_2^{p_2}\cdots\lambda_n^{p_n} = k\prod_{\nu=1}^{n}\lambda_\nu^{p_\nu} \tag{4.9}$$

The corresponding K_t–λ_ν curves appear as straight lines in double-logarithmic scales. Note that, in contrast to many other approximation formulae (e.g. eqs. (4.6–4.8), (4.14–4.17) and (4.19–4.21)), the additive term 1 or β is missing.

The approximation formulae for the stress concentration factors at the weld toe K_{t1}, and weld root K_{t2}, of the tensile loaded cruciform joint with flat fillet welds (see Section 4.4.4) read as follows:[301,302]

$$K_{t1} = k_1\left(\frac{a}{t_1}\right)^{p_1}\left(\frac{t_2}{t_1}\right)^{p_2}\left(\frac{g}{t_1}\right)^{p_3}\left(\frac{\rho_1}{t_1}\right)^{p_4} \tag{4.10}$$

$$K_{t2} = k_2\left(\frac{a}{t_1}\right)^{q_1}\left(\frac{t_2}{t_1}\right)^{q_2}\left(\frac{g}{t_1}\right)^{q_3}\left(\frac{\rho_2}{t_1}\right)^{q_4} \tag{4.11}$$

where k_1 and k_2 are coefficients from a least square fit, p_ν and q_ν are exponents from a least square fit ($\nu = 1, 2, 3, 4$), a is the throat thickness of the

fillet weld, t_1 and t_2 are the thicknesses of the loaded and non-loaded plate, respectively, g is the root face length, and ρ_1 and ρ_2 are the notch radii at the weld toe and weld root.

The coefficients k_1 and k_2 and the exponents p_v and q_v were derived on the basis of a notch stress analysis performed with the boundary element method and least-square fitted subsequently, covering a relatively large field of geometrical parameter ratios (approximately factor 10 for each of them):[301,302]

$$K_{t1} = 1.192\left(\frac{a}{t_1}\right)^{-0.311}\left(\frac{t_2}{t_1}\right)^{-0.004}\left(\frac{g}{t_1}\right)^{0.130}\left(\frac{\rho_1}{t_1}\right)^{-0.392} \tag{4.12}$$

$$K_{t2} = 1.155\left(\frac{a}{t_1}\right)^{-0.720}\left(\frac{t_2}{t_1}\right)^{-0.047}\left(\frac{g}{t_1}\right)^{-0.433}\left(\frac{\rho_2}{t_1}\right)^{-0.371} \tag{4.13}$$

The accuracy of these formulae is claimed to be better than 14–21% maximum deviation from the boundary element results, the average error being substantially lower.

Butt weld and cruciform joints (Anthes)

The stress concentration factors according to Anthes *et al.*[205,206] refer to double-V butt welds and cruciform joints with flat fillet welds under tension and bending loading calculated by the boundary element method (see Section 4.4.3, Figs. 4.59–4.61). The stress concentration factor K_t of the butt welds is approximated as a function of weld toe angle θ and plate thickness t, and notch radius ρ:

$$K_t = 1 + \alpha(\sin\theta)^{\lambda_1}\left(\frac{t}{\rho}\right)^{\lambda_2} \tag{4.14}$$

where α is a coefficient equal to 0.728 under tension and 0.527 under bending load, λ_1 is an exponent equal to 0.932 under tension and 0.887 under bending load and λ_2 is another exponent equal to 0.382 under tension and 0.410 under bending load.

The stress concentration factor K_t of the cruciform joint at the weld toe or weld root is approximated as a function of weld toe angle θ and of notch radius ρ, throat thickness a and root face length g related to plate thickness t:

$$K_t = \beta + f\left(\frac{t}{\rho}, \frac{a}{t}, \frac{g}{t}, \theta\right)(\sin\theta)^{\lambda_1}\left(\frac{t}{\rho}\right)^{\lambda_2} \tag{4.15}$$

where β is a constant and λ_1 and λ_2 are exponents dependent on tension or bending loading and on toe or root notch reference.

The accuracy of the above formulae is claimed to be better than 9% in the case of the butt weld joint and better than 10–20% in the case of the cruciform joint (maximum deviations from the boundary element results).

Transverse attachment and cruciform joints (Ushirokawa and Tsuji)

The stress concentration factors K_t at the weld toe presented by Ushirokawa[336,230] refer to fillet welded attachment joints and cruciform joints, as well as to butt weld joints under tension and bending loading, Fig. 4.15. They have been determined by the finite element method and approximated by the following type of formula:

$$K_t = \left\{1 + f_1(\theta)\left[f_2\left(\frac{\rho}{t},\ \frac{h}{t},\ \frac{h^*}{t}\right)\right]\right\} f_3\left(\frac{g}{t},\ \frac{h}{t},\ \frac{h^*}{t}\right) \tag{4.16}$$

where θ is the weld toe angle (defined as notch opening angle), ρ is the notch radius at the weld toe, t is the plate thickness, h and h^* are the leg lengths of the fillet weld or the reinforcement height and width of the butt weld and g is the root face length.

Some results for tension loading from the finite element analysis and from the approximation formula are plotted in Fig. 4.16. It is not clear from the publication[230] what secondary parameters have been specified in the analysis. It seems that $\theta = 3\pi/4$, $h/t = h^*/t = 3/4$, $g/t = 1$ have been chosen in the case of the fillet welds and $h^*/t = 1/2$, $h/t \approx 1/8$ in the case of the butt weld. The reference thickness used in the analysis is $t = 20$ mm. The accuracy of the approximation formula is claimed to be better than +24% or –7%, respectively.

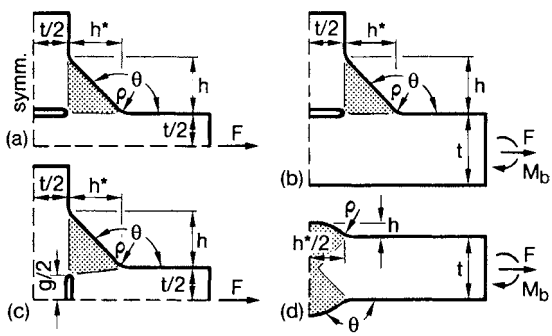


Fig. 4.15. Variants of welded joints under tensile and bending loads analysed in respect of notch stress concentration factor at weld toe by means of the finite element method: double-sided and single-sided transverse attachment joints (a, b), cruciform joint (c) and double-V butt weld (d); after Ushirokawa.[230,336]

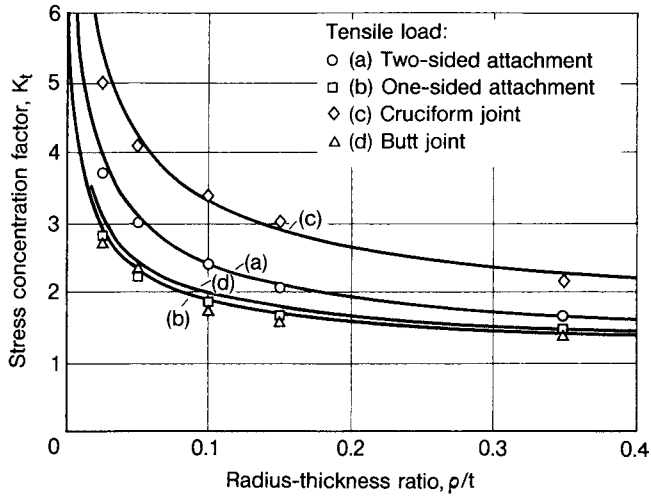


Fig. 4.16. Notch stress concentration factor dependent on notch radius related to plate thickness of welded joints under tensile load according to Fig. 4.15; finite element results compared with approximation formulae; after Ushirokawa.[230,336]

The stress concentration factors K_t at the weld toe of attachment joints under tension and bending loading, Fig. 4.17, determined by Tsuji[335,230] on the basis of the boundary element method, are approximated by the following type of formula:

$$K_t = 1 + f_1\left(\frac{s}{t}\right) f_2\left(\frac{w}{t},\ \frac{h}{\rho}\right) f_3(\theta) \tag{4.17}$$

where θ is the weld toe angle, ρ is the notch radius, t is the plate thickness, h is the leg length of the fillet weld, and s and w are attachment overall length and width parameters (see Fig. 4.17).

The function $f_3(\theta)$ is transferred from Nishida's solution[255] for stepped bars with flat shoulder fillets. The boundary element results refer to $\theta = 45°$ only. The accuracy of the approximation formula is claimed to be better than 'a few per cent'.

Butt weld joints (Lehrke)

The stress concentration factors determined by Lehrke[248] refer to the toe notch of double-V butt welds with full penetration and to the root notch of these welds with partial penetration, both welds under tension loading. The stress concentration factor at the weld toe, K_{t1}, is derived on the basis of the notch stress intensity factors of V-shaped sharp notches supplemented by

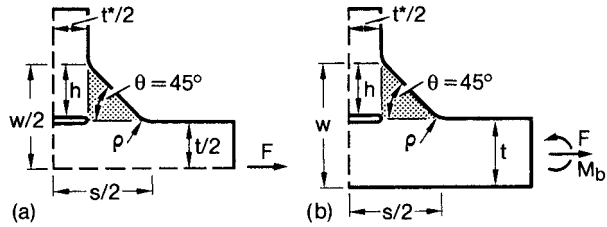


Fig. 4.17. Variants of welded joints under tensile and bending loads analysed in respect of notch stress concentration factors at weld toe using the boundary element method: double-sided and single-sided transverse attachment joint (a, b); after Tsuji.[230,335]

the notch stress solution for hyperbolic notches according to Neuber.[252,253] The stress concentration factor at the weld root, K_{t2}, is derived proceeding from the stress intensity factor of an internal crack in a plate of finite width supplemented by the blunt crack tip extension according to Tada *et al.*:[628]

$$K_{t1} = \frac{4\left(2\tan\frac{\theta}{2}\right)^{1-2m}}{2\theta + \sin(2\theta)}\left(\frac{t}{4\rho}\right)^{m} \qquad (w = t) \tag{4.18}$$

$$K_{t2} = 1 + \frac{2}{\sqrt{\cos\left(\frac{\pi g}{2t}\right)}}\sqrt{\frac{g}{2\rho}} \qquad (g/t < 0.7) \tag{4.19}$$

where θ is the weld toe angle, m is an exponent dependent on θ, ρ is the notch radius, t is the plate thickness, g is the root face length and w is the reinforcement width between the weld toes.

The stress concentration factors according to eqs. (4.18) and (4.19) are compared with boundary element results in Fig. 4.18 and Fig. 4.19. The accuracy of the formulae seems to be better than 5% which is remarkably high compared with the other approximation formulae, most of which have a more complex structure. The stress concentration factors at the weld toe of fully penetrated butt welds calculated according to different authors in two representative parameter combinations have been compared by Lehrke,[248] Fig. 4.20. The degree of correspondence is satisfactory, but larger deviations were found by Petitpas *et al.*[388] in comparison to finite element analysis results.

T butt joints (Brennan)

Approximation formulae for the notch stress concentration factors K_t at the weld toe of T butt joints (same configuration as Fig. 4.17(b), but with

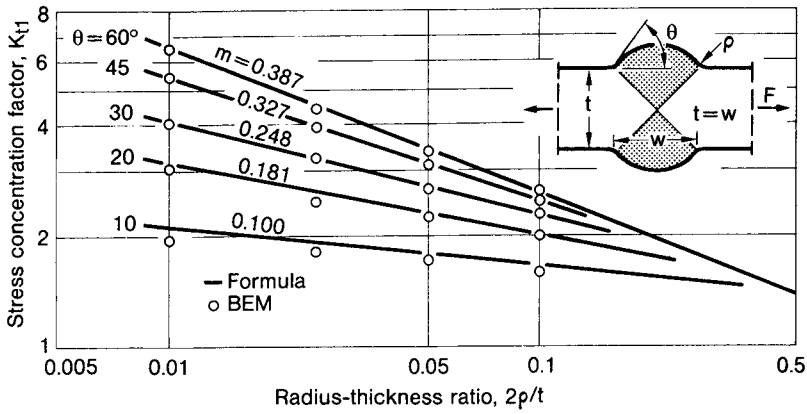


Fig. 4.18. Notch stress concentration factor at weld toe of tensile loaded butt weld dependent on notch radius related to plate thickness for different weld toe angles; after Lehrke.[248]

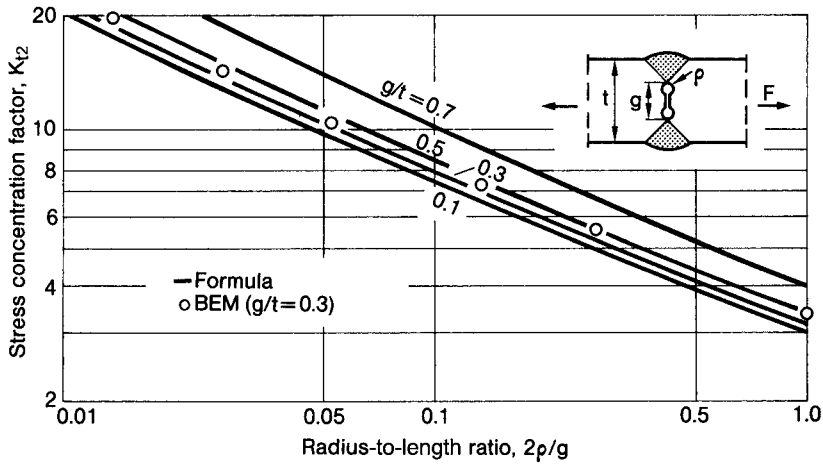


Fig. 4.19. Notch stress concentration factor at weld root of tensile loaded butt weld dependent on notch radius related to plate thickness for different root face length to plate thickness ratios; after Lehrke.[248]

full penetration) have been derived by Brennan *et al.*[215] based on finite element analysis results. The simplified versions of these equations for tension load (index m) and bending load (index b), respectively, read as follows:

$$K_{\mathrm{tm}} = 1.03 + 0.27\theta^{0.22}\left(\frac{\rho}{t}\right)^{-0.47}\left(\frac{s}{t}\right)^{0.18} \tag{4.20}$$

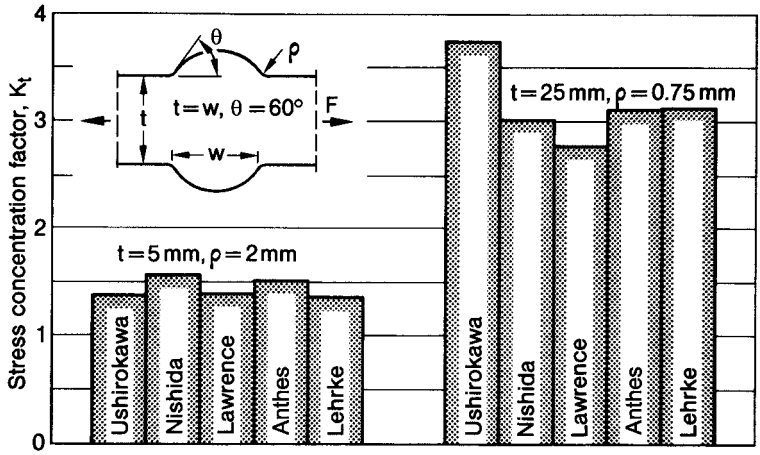


Fig. 4.20. Comparison of notch stress concentration factors at the weld toe of butt welds calculated according to the approximation formulae of various authors; after Lehrke.[248]

$$K_{tb} = 1.01 + 0.34\theta^{0.34}\left(\frac{\rho}{t}\right)^{-0.47}\left(\frac{s}{t}\right)^{0.23} \tag{4.21}$$

with the weld toe angle θ, the weld toe radius ρ, the attachment overall width s and the base plate thickness t. The approximation is restricted to the following parameter ranges:

$$\pi/6 \le \theta \le \pi/3, \qquad 0.3 \le s/t \le 4.0, \qquad 0.01 \le \rho/t \le 0.067$$

The influence of s/t on K_t increases up to $s/t \approx 1.5$, but remains more or less constant thereafter. The eqs. (4.20) and (4.21) substitute older approximations for the s/t-independent case (Niu and Glinka,[552] Monahan[538]). The approximations above were also applied to skewed attachment plates joined to the base plate either by double-sided welds or by a single-sided fillet weld. The weld root is inaccessible in the latter case and must be seperately assessed in respect of fatigue. The application of the simplified equations above to skewed configurations involves deviations from the accurate finite element results remaining below five per cent.

4.2.4 Fatigue notch factors of welded joints

The 'elastic' fatigue notch factor K_f is the essential parameter which defines the fatigue-effective stresses within the notch stress approach (see eq. (4.1)). It was originally defined as the ratio of the endurance limit (at $N_E = 10^6$–10^7 cycles) of the unnotched polished specimen, i.e. the stress amplitude σ_{aE}, to the endurance limit of the notched specimen or structural member,

i.e. the nominal stress amplitude σ_{naE} (with zero mean stress, $\sigma_m = \sigma_{nm} = 0$, i.e. $R = -1$):

$$K_f = \frac{\sigma_{aE}(K_t = 1.0)}{\sigma_{naE}(K_t > 1.0)} \tag{4.22}$$

where K_t is the elastic notch stress concentration factor.

The definition is transferable to the medium-cycle and low-cycle fatigue range and also to non-zero mean stresses but the numerical value of the factor is changed in this case. Only the original restricted definition results in the elastic fatigue notch factor which can be derived on the basis of the elastic notch stresses modified according to an elastic microstructural support hypothesis.

The elastic fatigue notch factor depends on the relative and absolute notch acuity (i.e. on the magnitude of the notch radius relative to the specimen size and on the absolute value of this radius), on the loading type (tension, bending or shear loading) and on the material. It depends additionally on the specimen size and the surface condition.

The elastic fatigue notch factor can be predicted on the basis of the elastic stress concentration factor taking a microstructural support hypothesis into account. Microstructural support means that the fatigue-effective notch stress is substantially lower than the notch stress according to the theory of elasticity in the case of sharp notches. The elastic fatigue notch factor refers either to avoided crack initiation or to the arrest of initiated cracks.

The definition of the fatigue notch factor above becomes less clear when applied to welded joints where the material conditions at the weld notch differ from the parent material characteristics. Additionally, the residual stress condition may not be comparable. The approaches described below take special measures to address this complication. One possible procedure is not to use fatigue notch factors at all, but to consider endurable fatigue-effective notch stresses directly.

The dependency of the fatigue notch factor K_f on the stress concentration factor K_t for welded joints is demonstrated by the diagram in Fig. 4.21 which is based on a material-dependent notch sensitivity:

$$\eta = \frac{K_f - 1}{K_t - 1} \tag{4.23}$$

which is larger for high strength than for low strength steels. The calculation is correlated with experimental results, but the rather large difference in fatigue strength (expressed by K_f) of non-load-carrying (nlc) transverse fillet weld joints and of transverse butt weld joints should not be generalised. What can be learned from the diagram is that, whereas the stress concentration factors may rise to extremely large values with small notch

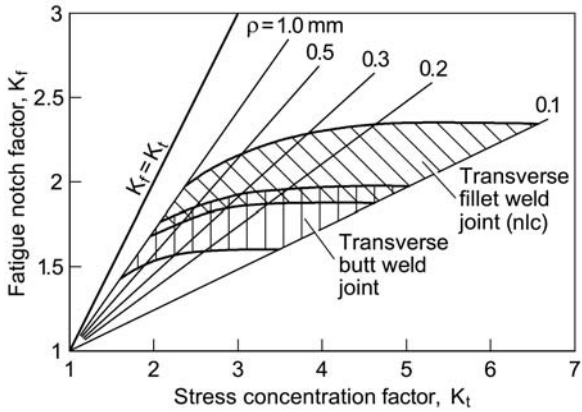


Fig. 4.21. Fatigue notch factor of welded joints (transverse fillet and butt welds; nlc: non-load-carrying) as function of the stress concentration factor under the condition of constant notch sensivity ranges; after Sunamoto *et al.*[187]

radii (actually tending to infinity with $\rho = 0$), the fatigue notch factors are restricted to a comparatively narrow range, $K_f = 1.4–1.9$ for the butt weld joints and $K_f = 1.8–2.3$ for the fillet weld joints (also not to be generalised).

Another important influence parameter on the fatigue notch factor and the locally endurable stresses is hardening or softening of the material at the weld notch. The notch stress approach versions according to Lawrence and Radaj recommend the local hardness changes at the notch root to be taken into account when assessing the endurable notch stresses. The versions according to Seeger and Sonsino, on the other hand, take the hardness changes implicitly into account. Hardness changes relative to the parent material may occur in the heat-affected zone and in the fusion zone both without and with filler material. Hardening or softening is dependent on the material composition and the thermal cycles originating from welding. Typical examples are the hardening of carbon steels and the softening of precipitation hardened aluminium alloys.

The microhardness profile and the microstructural zones of a laser beam butt-weld joint in fine-grained high strength steel are presented in Fig. 4.22. Penetration welding allows for a slim fusion zone with narrow heat-affected zones. The hardness peak occurs with a constant value in the fusion zone. The peak is higher than welding engineers consider acceptable. It should be reduced by appropriate measures, for example preheating or postweld heat treatment. The hardness profile indicates that fatigue crack initiation at the mild toe and root notches is rather improbable. Cracking will more probably be displaced into the parent material.

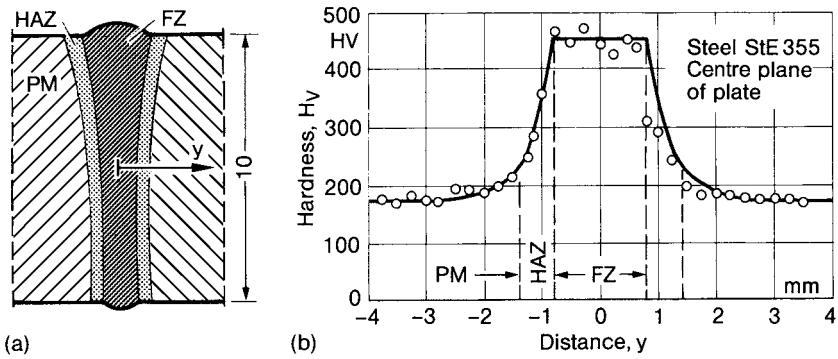


Fig. 4.22. Microstructural zones (a) with parent metal, PM, heat-affected zone, HAZ, and fusion zone, FZ, and hardness profile (b) in centre plane of plate after laser beam welding (square butt weld without filler metal, laser power $P = 8$ kW, welding speed $v = 1.6$ m/min); normalised fine-grained steel of type StE355N ($\sigma_Y \approx 410$ N/mm^2, $\sigma_U \approx 580$ N/mm^2); after Kalla.[236]

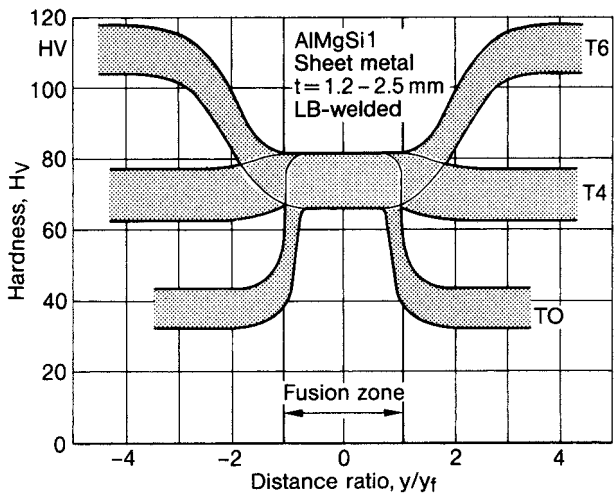


Fig. 4.23. Scatter ranges of measured microhardness profiles of laser beam penetration welded AlMgSi1 aluminium alloys, artificially aged condition T6, naturally aged condition T4 and annealed condition O; distance y from centre plane of weld relative to distance y_f of fusion zone boundary; plate thickness 1.2–2.5 mm and different welding process parameters within well-tried ranges; after Rapp.[306]

The scatter ranges of measured microhardness in laser beam welded AlMgSi1 aluminium alloy sheet metal in different hardening states are shown in Fig. 4.23. Uniform scatter ranges for different plate thicknesses, fusion zone widths and process parameters result from introducing the

fusion zone width as the reference parameter. The artificially aged material (i.e. hardened by heat treatment) undergoes softening in the heat-affected zone. The material in the naturally aged or in the annealed condition remains more or less unaffected in this zone. All three types of material exhibit about the same medium hardness in the fusion zone (produced without filler metal), which is explained by the dendritic structure of the molten metal there.

Various methods have been proposed for transferring the predicted (elastic) fatigue notch factor in the high-cycle fatigue range to the medium-cycle range. One method consists in turning to the nominal stress approach when the normalised *S–N* curve is introduced proceeding from the notch stress based endurance limit of the welded joint. Another method consists in assuming a linear decrease in the fatigue notch factor in double-logarithmic scales between the (elastic) high-cycle value and $K_f = 1.0$ at $N = 1$ cycle and possibly corrected in the low-cycle fatigue range according to the relevant limit load (Prowatke *et al.*[268]) with formulae according to Seeger and Heuler,[392] eqs. (5.35–5.37). Finally, the fatigue notch factor in the medium cycle fatigue range can be predicted on the basis of the notch strain approach (see Chapter 5).

4.2.5 Critical distance approach

The fundamentals of the approach are summarised in Section 4.1.2. The fatigue notch factor of welded joints is derived by Lawrence[378,384] from the stress concentration factor on the basis of the microstructural support hypothesis conceived by Peterson.[266,267] This hypothesis states that the fatigue-effective notch stress should be evaluated at a material-dependent critical depth a^* below the notch root surface, thus deriving the following fatigue notch factor K_f from the notch stress concentration factor K_t:

$$K_f = 1 + \frac{K_t - 1}{1 + \dfrac{a^*}{\rho}} \tag{4.24}$$

where the critical distance a^* is a material constant and ρ is the notch radius.

The material constant a^* depends on the ultimate tensile strength σ_U of the material, Table 4.3. The following approximation for steels is used by Lawrence *et al.*[377,378,384,967]

$$a^* = 0.025\left(\frac{2068}{\sigma_U}\right)^{1.8} \approx \frac{10870}{\sigma_U^2} \tag{4.25}$$

Peterson[267] has used $a^* = 0.254$ mm for soft-annealed steel (≈ 170 HB), $a^* = 0.0635$ mm for quenched and tempered steel (≈ 360 HB), and $a^* = 0.635$ mm for aluminium alloys.

Table 4.3. Material constant a^* from bending-loaded notched bars in steels of different ultimate tensile strength σ_U; after Peterson[265]

σ_U [N/mm^2]	345	518	690	863	1035	1380	1725
a^* [mm]	0.38	0.25	0.18	0.13	0.089	0.051	0.033

The notch radius at the weld toe which is of primary influence on the stress concentration factor is widely scattering. Lawrence *et al.*[378] propose the introduction of the maximum fatigue notch factor $K_{f\,max}$ into the fatigue analysis which occurs at the critical notch radius $\rho_c \approx a^*$ (see Fig. 4.2). Thus, the fatigue notch factor $K_{f\,max}$ of welded joints according to Lawrence results from the stress concentration factor K_t by introducing $\rho = \rho_c = a^*$ in the relevant approximation formula:

$$K_{f\,max} \approx K_t(\rho = a^*) \tag{4.26}$$

Lawrence uses this fatigue notch factor in the high-cycle fatigue range with $N > 10^5$ cycles, that is, not only at the endurance limit. It is then restricted to crack initiation.

The fatigue-effective notch stress corresponding to the fatigue notch factor, $\overline{\sigma}_k = K_f\sigma_n$, is compared with the elastic part of the strain S–N curve (i.e. the Basquin relationship with mean stress correction according to Morrow, eq. (5.3)) in the high-cycle fatigue range ($N > 10^5$ cycles). The relevant local material parameters at the crack initiation site should be derived from hardness measurements. The effect of residual stress can roughly be taken into account by introducing the residual stress as mean stress, $\sigma_m = \sigma_r$, in Basquin's relationship. A more accurate analysis which takes residual stress relaxation by loading into account, is based on the notch strain approach (see Section 5.2.1).

The von Mises distortional strain energy criterion is applied in the case of in-phase biaxial fatigue and the combined shear and normal stress criterion proposed by Findley[109] is used in the case of out-of-phase biaxial fatigue (see eqs. (5.19–5.22)).

4.2.6 Fictitious notch rounding approach – basic procedures

The fundamentals of the approach are summarised in Section 4.1.3. The fatigue notch factor of welded joints is derived by Radaj[4,280,283,284] from the stress concentration factor on the basis of the microstructural support hypothesis conceived by Neuber.[252–254] This hypothesis states that the averaged notch stress in a small material volume at the point of

maximum stress controls crack initiation. The decisive material parameter to describe this effect is the microstructural length over which the stresses are averaged. It is introduced as the substitute microstructural support length, ρ^*. The fatigue notch factor K_f is derived from the stress concentration factor K_t of an elliptical hole according to the following formula (see Radaj[6]):

$$K_f = 1 + \frac{K_t - 1}{\sqrt{1 + \frac{s\rho^*}{\rho}}} \tag{4.27}$$

where s is the multiaxiality factor, ρ^* is the substitute microstructural length and ρ is the notch radius.

The fatigue notch factor K_f of other notches may result directly from the fatigue-effective notch stress $\bar{\sigma}_k$ which is determined by considering the notch with the actual radius ρ enlarged to the fictitious radius ρ_f, that is, the notch stress analysis is performed for a notch with the enlarged radius, thus avoiding the averaging process:

$$K_f = \frac{\bar{\sigma}_k}{\sigma_n} \tag{4.28}$$

$$\rho_f = \rho + s\rho^* \tag{4.29}$$

with the nominal stress σ_n to be appropriately defined.

The material constant ρ^* named 'substitute microstructural length' is considered to be a function of the yield limit $\sigma_{Y0.2}$, Fig. 4.24. The dependency

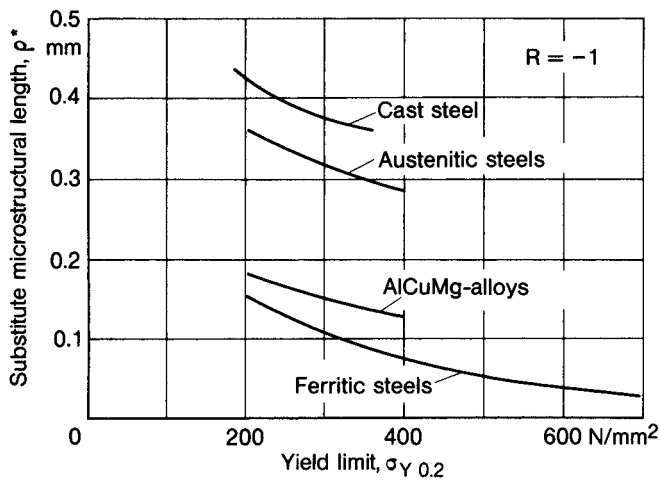


Fig. 4.24. Substitute microstructural length dependent on yield limit for various materials; after Neuber.[254]

on the yield limit $\sigma_{Y0.2}$ instead of the ultimate tensile strength σ_U is disputable. The factor s depends on the multiaxiality of the notch stresses (plane stress, plane strain and in-plane or anti-plane shear loading) and the applied multiaxial strength criterion (Neuber[252–254]). Transverse tension loading of the notch results in $s = 2.0–3.0$, in-plane shear loading in $s = 0.074$, 0.5 or 1.415 (Radaj and Zhang[911,920]) and anti-plane shear loading in $s = 0.5$ or 1.0 (Radaj and Zhang[303]). The superposition of the loading modes is considered in Section 10.2.8, eqs. (10.72–10.76). A uniform value $s = 2.5$ has for the most part been used in applications to welded joints.

Considering seam-welded joints in (low strength) steel, the choice $\rho^* = 0.4\,\text{mm}$ (cast steel in Fig. 4.24) and $s = 2.5$ (plane strain condition at the root of sharp notches combined with the von Mises multiaxial strength criterion for ductile materials) is appropriate. This leads to $\rho_f = 1\,\text{mm}$ in a worst case consideration, resulting in the following maximum fatigue notch factor:

$$K_{f\,max} = K_t(\rho_f = 1\,\text{mm}) \tag{4.30}$$

where $K_t(\rho_f = 1\,\text{mm})$ is the stress concentration factor for the fictitious notch radius $\rho_f = 1\,\text{mm}$.

The fatigue notch factors reviewed in Sections 4.3 and 4.4 are based on this radius. They refer to the technical endurance limit (at $N = 10^6–10^7$ cycles) of the parent metal. Relevant endurable stresses are listed in Table 4.4. A permissible notch stress range of $\Delta\bar{\sigma}_k = 225\,\text{N/mm}^2$ ($N = 2 \times 10^6$, $P_f = 2.3\%$) for $\rho_f = 1\,\text{mm}$ is proposed by the IIW fatigue design recommendations[3] for welded joints in steel in the as-welded condition.

A lower value than above of the constant ρ^* may be appropriate at the nugget edge of spot-welded joints, i.e. $\rho^* = 0.1\,\text{mm}$ for rolled steels resulting in $\rho_f = 0.25\,\text{mm}$, because the cast steel assumption is not valid at the nugget edge. The comparative investigation of spot-welded specimens[816] is based on the lower value (see Figs. 11.7–11.9). A tentative strength assess-

Table 4.4. Fatigue strength of low strength steels (e.g. type St37 $\sigma_U \geq 370\,\text{N/mm}^2$) dependent on stress ratio R and on surface condition ($N = 2 \times 10^6$ cycles, $P_f = 10\%$); after Radaj[4,284]

	Surface condition	
	Non-machined	Polished
Fatigue strength $\Delta\sigma/2 = \sigma_A(R = -1)$	$145\,\text{N/mm}^2$	$163\,\text{N/mm}^2$
Fatigue strength $\Delta\sigma = 2\sigma_A(R = 0)$	$240\,\text{N/mm}^2$	$270\,\text{N/mm}^2$

ment in absolute terms (see Section 11.2.1) did not confirm the rolled steel value but a value between rolled and cast steel.

Considering welded joints in aluminium alloy of type AlMg4.5Mn (AA5083), an investigation related to appropriate ρ^* values has been conducted by Sonsino *et al.*[213,324] Specimens in the parent material and weld deposit with a sharp or mild notch were fatigue tested and evaluated. It was found that ρ^* depends on the stress concentration and the number of cycles endured. Significantly smaller ρ^* values were determined for high stress concentrations compared with low stress concentration. Substantial deviations from the basic data in Fig. 4.24 referring to an alloy of type AlCuMg are observed when considering identical static strength values (Werner *et al.*[341]).

The material constant ρ^* according to eq. (4.27) for welded joints ($t = 5$ and 25 mm) in AlMg4.5Mn aluminium alloy, parent metal ($\sigma_{aE} = 120\,N/mm^2$, $N = 5 \times 10^6$, $P_f = 50\%$) and weld deposit ($\sigma_{aE} = 75\,N/mm^2$, $N = 5 \times 10^6$, $P_f = 50\%$), is plotted in Fig. 4.25. Use of $\rho^* = 0.1$ mm or $\rho_f = 0.25$ mm is recommended for worst case considerations, resulting in the following maximum fatigue notch factor:

$$K_{f\,max} = K_t(\rho_f = 0.25\,mm) \tag{4.31}$$

where $K_t(\rho_f = 0.25\,mm)$ is the stress concentration factor for the fictitious notch radius $\rho_f = 0.25$ mm.

Considering Fig. 4.25, it is obvious that unrealistically large values of ρ^* are determined with the mild notch ($K_t = 1.5$). On the other hand, the rise of the 'material constant' ρ^* in the medium cycle fatigue range may be caused by plastic deformation at the notch root, concealing the microstructural support effect.

The fatigue notch factor above has to be combined with the parent metal endurance limit, $\sigma_{aE} = 120\,N/mm^2$. If the crack starts in the weld deposit, the material parameters of the weld deposit are more appropriate (but usually not available). In the case considered above, $\rho^* = 0.24$ mm or $\rho_f = 0.6$ mm is recommended. The predicted fatigue notch factors refer to welded joints without major residual stresses subjected to fully reversed loading ($R = -1$). The fatigue notch factors in zero-to-tension loading ($R = 0$) are slightly lower. High residual stresses may change the analysis results.

A more recent similar investigation into the local fatigue strength of welded joints ($t = 5$ mm) in the aluminium wrought alloys AlMgSi1 (AA6082-T6: artificially aged) and AlMg4.5Mn (AA5083-T4: naturally aged), differentiating between crack initiation and crack propagation in the parent metal, the heat-affected zone and the weld metal, has been conducted by Morgenstern *et al.*[250] A constant value of the microstructural

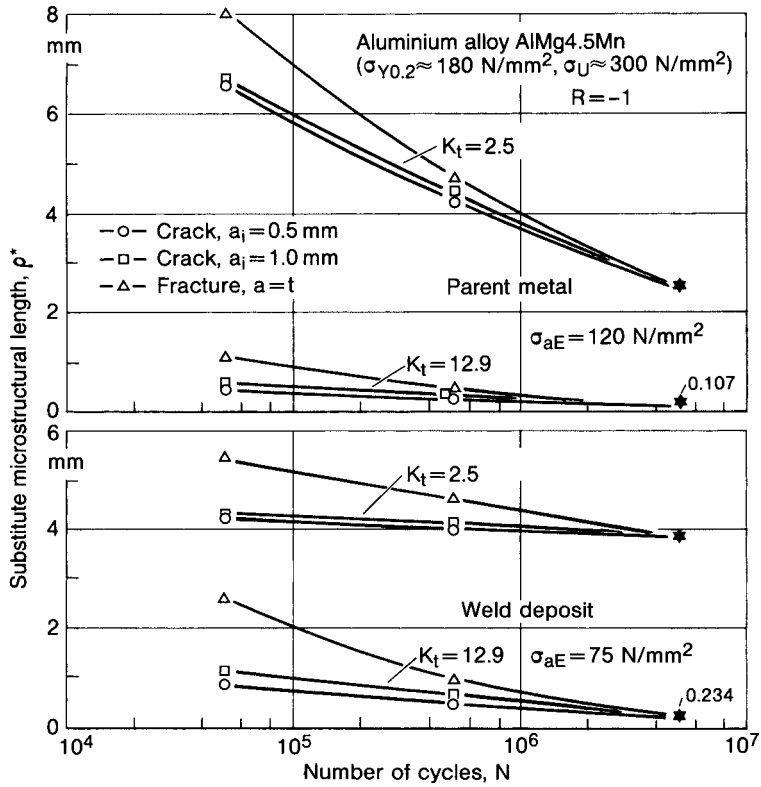


Fig. 4.25. Substitute microstructural length, ρ^*, for type AlMg4.5Mn aluminium alloy, parent metal and weld deposit, with low and high stress concentration factor, K_t, for different failure criteria (crack initiation or fracture), dependent on number of cycles up to failure, N; after Brandt *et al.*[213]

length ρ^* was calculated in the fatigue range between 10^4 and 10^7 cycles based on the fact that the crack initiation S–N curves of the unnotched specimens ($K_t = 1.0$) and the specimens with a crack-like notch ($K_t = 10.2$ and 11.2) showed identical inverse slope exponents ($k = 5.0$–7.0). The substitute microstructural length was $\rho^* = 0.23$–0.54 mm (resulting in $\rho_f = 0.58$–1.35 mm) dependent on the material condition. These data were successfully applied to predict the S–N curves of butt-welded joints without and with an internal root face, representing mild and sharp notch conditions. As the differences in the calculated S–N curves are not great, it seems possible to use a single fictitious notch radius $\rho_f = 1$ mm both for steels and aluminium alloys within worst case engineering approximations (see Section 4.2.6).

4.2.7 Fictitious notch rounding approach – refined procedures

Correction terms to the fatigue notch factor

Fictitious notch rounding may cause severe (fictitious) undercut which results in an unrealistic notch stress increase especially in the case of a low plate thickness. As an example demonstrating the effect of undercut, a T-joint with fillet welds and sharp toe and root notches is considered, Fig. 4.26(a). Fictitious notch rounding without undercut at the weld toe results in essentially unchanged load-carrying cross-sections, Fig. 4.26(b). Rounding with undercut at the weld root or weld toe, on the other hand, weakens the load-carrying cross-sections, Fig. 4.26(c, d). Undercut is no problem in those cases where the undercut covers low stress regions, Fig. 4.26(e).

The weakening of the cross-section can be taken into account in the strength-effective notch stresses or fatigue notch factors by way of a reduction factor which results from the tensile and bending stress increase in the equally weakened unnotched plate.[4,293] The reduction factor depends on the degree of cross-sectional weakening and on the type of loading (tension and bending loads superimposed). Different reduction terms are introduced for the single-sided and double-sided notch, respectively, Fig. 4.27:

$$K_f^* = \frac{\left(1 - \rho_f^*\right)^2}{1 + \rho_f^*\left(1 + \sigma^*\right)} K_f \tag{4.32}$$

$$K_f^* = \frac{2\left(1 - \rho_f^*\right)^2}{2 - \rho_f^*\left(1 + \sigma^*\right)} K_f \tag{4.33}$$

where K_f and K_f^* are the original and reduced fatigue notch factor, respectively, ρ_f^* is the degree of cross-sectional weakening ($\rho_f^* = \rho_f/t$), σ^* is the surface stress ratio ($\sigma^* = \sigma_l/\sigma_u$), ρ_f is the fictitious notch radius, t is the plate thickness and σ_l and σ_u are the remote stresses at the lower and upper plate surfaces.

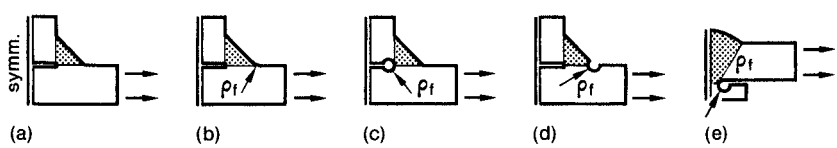


Fig. 4.26. Undercut by fictitious notch rounding: sharp notches without rounding (a), toe notch-rounded without undercut (b), root notch-rounded with undercut (c), toe notch-rounded with undercut (d), root notch-rounded without undercut of the load-carrying cross-section (e).

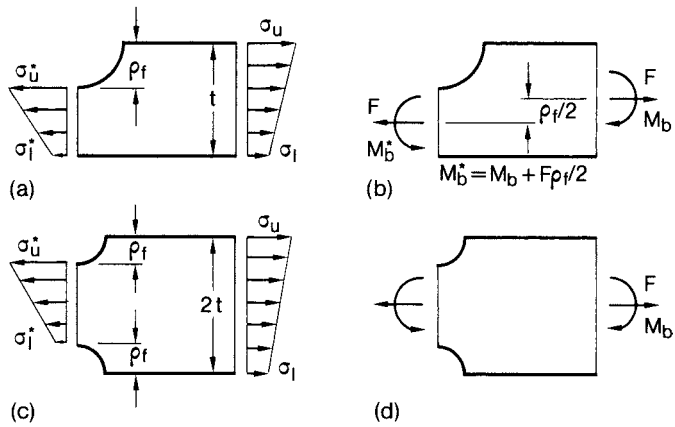


Fig. 4.27. Modification of the superimposed membrane and bending stresses at the upper and lower side of a structural component by fictitious notch rounding with undercut on one side (a, b) or on both sides (c, d) of the cross-sectional model as the basis for the fatigue notch factor correction: force and moment equilibrium (b, d) and associated membrane and bending stresses (a, c).

Another possibility for avoiding the problem of cross-sectional weakening is to perform the notch stress analysis with rather small fictitious notch radii and to use the generalised structure of the stress concentration formulae for welded joints, i.e. $K_t = 1 + \alpha(t/\rho_f)^{1/2}$ or $K_t = \beta(t/\rho_f)^{\lambda}$ (see eqs. (4.5) and (4.6)) to convert the calculated stress concentration factors from the smaller to the larger fictitious notch radius. A first approximation may use the simple square root dependency on the ratio of the ρ_f values.

A special modification of the fatigue notch factor is necessary in the case of two-sided cover plate joints if the cover plates are allowed to bend freely in the model whereas gap closure occurs in reality.[293] The bending effect together with the constriction of the cross-section above the fictitious keyhole lowers the longitudinal stiffness of the cover plate. Therefore, the structural membrane stresses in the centre cross-section of the joint are lowered in the cover plates and increased in the base plate. Without the bending effect and keyhole, the longitudinal stresses in the two plates would be identical at the slit face. A modification is therefore necessary to the fatigue notch factors calculated at the upper and lower half of the keyhole and reduced according to the cross-sectional weakening. Note that the bending moment in the cover plate is assumed to be unchanged within this modification. Different correction terms are introduced for the fatigue notch factors of the upper and lower semi-circle, respectively, of the notch, Fig. 4.28:

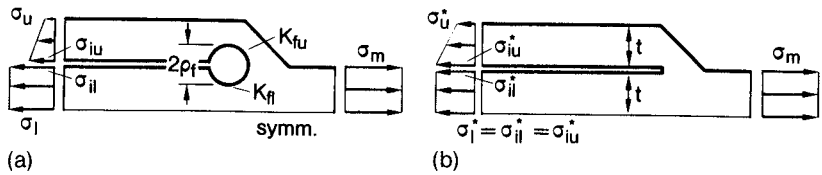


Fig. 4.28. Modification of the membrane plus bending stresses in the middle section of a double-sided cover plate joint (cross-sectional symmetry quarter) by fictitious rounding of the root notch (a) in relation to the ideal gap (b).

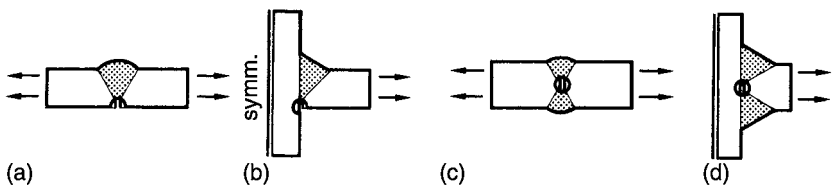


Fig. 4.29. Short slits fictitiously notch-rounded: single-V and double-V butt weld with root face (a, c); single- and double-bevel butt weld with root face (b, d).

$$K_{fu}^{**} = \frac{1}{2}\left(1 + \frac{\sigma_{iu}}{\sigma_{il}}\right)K_{fu}^{*} \tag{4.34}$$

$$K_{fl}^{**} = \frac{1}{2}\left(1 + \frac{\sigma_{il}}{\sigma_{iu}}\right)K_{fl}^{*} \tag{4.35}$$

where K_f^* and K_f^{**} are the original reduced and the modified fatigue notch factors, σ_{iu} is the stress at the inner surface of the upper cover plate and σ_{il} is the stress at the inner surface of the lower base plate.

The fatigue strength is underestimated according to the procedure of fictitious notch rounding in the case of short slits or cracks, the length of which comes near to the notch radius, i.e. near to the dimension of the semi-circular or circular notch, Fig. 4.29. This is shown by theoretical considerations based on the relevant stress intensity factors (Radaj[291]). In order to get a more accurate approximation of the fatigue-relevant notch effect, the fatigue notch factor of the fictitious semi-circular or circular notch has to be slightly reduced.

The correction factor derived by Radaj[897] is based on the idea that the limit value relationship between stress intensity factor and maximum notch stress is applied only to the 'sharp notch component' of the complete notch stress formula which includes the mild notches. Additionally, the increase of crack tip mean stress by the effect of the nearby opposed crack

tip is taken into account. The reduced fatigue notch factor $K_{f\,red}$ is given by eq. (10.77). The reduction for semi-circular or circular notches ($a/\rho_f = 1$) is thus expressed by $K_{f\,red} = 0.745\,K_t$.

The reduction factor was actually derived for the short transverse crack in the tensile-loaded infinite plate. Transfer to the cross-sectional models of welded joints which are characterised by finite dimensions is subject to reservations. The relative assessments in Section 4.4 is presented without this reduction. Therefore, the fatigue notch factors given there for short slits or cracks without a reduction are on the safe side.

Fatigue notch factors in longitudinal shear loading

The stress concentration factor in anti-plane shear loading $K_{t\tau}$ of the cross-sectional model of welded joints, which corresponds to longitudinal shear loading of the weld, can be approximated proceeding from the relevant factor $K_{t\perp}$ in transverse tension loading (shallow notch formula according to Radaj,[281] assuming identical notch radii in shear and tension loading):

$$K_{t\tau} = \frac{1}{2}(K_{t\perp} + 1) \tag{4.36}$$

where $K_{t\tau}$ and $K_{t\perp}$ refer to the nominal structural stresses $\tau_{\parallel}$ and $\sigma_{\perp}$, respectively.

The approximation formula is also valid with the fatigue notch factors if the same fictitious notch radius is assumed in the considered two loading modes:

$$K_{f\tau} = \frac{1}{2}(K_{f\perp} + 1) \tag{4.37}$$

It is independent of the strength criterion if the reference stresses are chosen as stated above. A modified fatigue notch factor $\overline{K}_{f\tau}$ results from referring to the nominal (or structural) equivalent stress σ_{eq} according to the von Mises distortional strain energy criterion:

$$\overline{K}_{f\tau} = \sqrt{3}K_{f\tau} \tag{4.38}$$

On the basis of the notch stress theory[252,253] different fictitious radii are derived[303,911,920] in transverse tension and longitudinal shear loading, $\rho_f = 1\,\text{mm}$ and $\rho_f = 0.2\,\text{mm}$, respectively, in the case of structural steels and a worst case consideration. However, this result has not yet been confirmed experimentally.

The fatigue notch factors in anti-plane shear loading are more accurately determined proceeding from the fictitiously notch-rounded cross-sectional

model applying the potential field option of the boundary element method (see Section 4.4.2).

Fatigue notch factors in biaxial oblique loading

Seam welds are generally loaded by biaxial structural stresses with oblique principal directions. The consideration below is confined to the membrane stress components, Fig. 4.30, but the given formulae can also be used with the corresponding bending stress components in an approximative manner. The referenced model of a straight weld under uniform loading conditions may be locally applied in points of a curved weld line under non-uniform loading conditions. It can also be locally applied in edge points of weld spots where biaxial oblique loading conditions are prevailing.

The principal structural stress components in the loaded plate are σ_1 and $\sigma_2 = \lambda\sigma_1$ with the biaxiality degree λ. Pure shear loading is characterised by $\lambda = -1$, uniaxial tension by $\lambda = 0$ and all-sided tension by $\lambda = +1$. The seam weld is inclined with the oblique angle ψ relative to the direction of the first principal stress. Longitudinal shear loading of the seam weld is characterised by $\lambda = -1$ combined with $\psi = 45°$, and uniaxial transverse tension by $\lambda = 0$ combined with $\psi = 90°$. The principal stresses can be substituted by the stress components $\sigma_\perp$, $\sigma_\parallel$ and $\tau_\parallel$ related to the direction of the seam weld.

The stress concentration factors $K_{t\perp}$ and $K_{t\tau}$ in transverse tension and longitudinal shear loading are assumed to be known from a notch stress analysis (boundary element method or approximation formulae). The stress

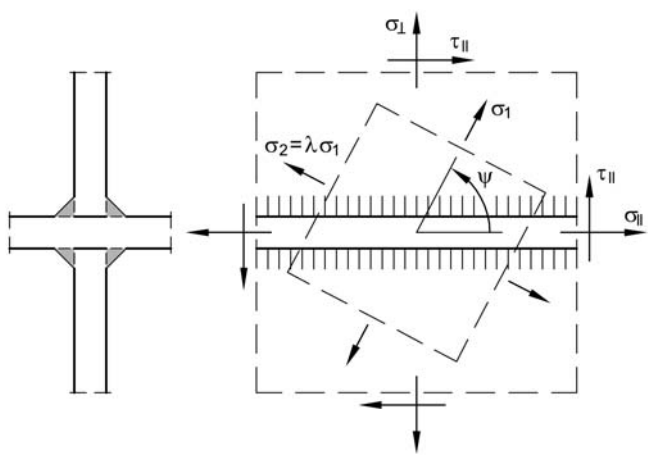


Fig. 4.30. Uniform biaxial oblique loading of a typical straight seam-welded joint (applicable to any other joint or weld type); cross-section and front view; after Radaj.[4,281]

concentration factors $K_{t1} = \sigma_{k1}/\sigma_1$ and $K_{t2} = \sigma_{k2}/\sigma_1$ are introduced relating the maximum principal stresses at the notch root, σ_{k1} and σ_{k2}, to the first principal stress in the plate, σ_1. The von Mises distortional strain energy criterion is applied for the superposition of the maximum notch stresses or relevant stress concentration factors:

$$K_{t\,eq} = \frac{\sigma_{k\,eq}}{\sigma_1} = \sqrt{K_{t1}^2 + K_{t2}^2 - K_{t1}K_{t2}} \tag{4.39}$$

With fictitious notch rounding introduced, the worst case fatigue notch factor $K_{f\,max}$ (with $K_f = \bar{\sigma}_{k\,eq}/\sigma_1$) is determined:

$$K_{f\,max} = K_{t\,eq}(\rho_f = 1\,\text{mm}) \tag{4.40}$$

where $\rho_f = 1$ mm is the fictitious notch radius for steel. This factor characterises the fatigue-effective notch stresses, but does not conform to the original definition of the fatigue notch factor in respect of the reference stress.

The stress concentration factors K_{t1} and K_{t2} in biaxial oblique loading can be calculated from the relevant factors $K_{t\perp}$ and $K_{t\tau}$ in transverse tension and longitudinal shear loading, respectively (Radaj[281]):

$$K_{t1}, K_{t2} = \frac{1}{2}[K_{t\perp}c_\perp + c_\parallel + \nu c_\perp(K_{t\perp} - 1)] \pm \frac{1}{2}\sqrt{[K_{t\perp}c_\perp - c_\parallel - \nu c_\perp(K_{t\perp} - 1)]^2 + (2K_{t\tau}c_\tau)^2} \tag{4.41}$$

$$c_\perp = \frac{1}{2}[\lambda + 1 + (\lambda - 1)\cos 2\psi] \tag{4.42}$$

$$c_\parallel = \frac{1}{2}[\lambda + 1 - (\lambda - 1)\cos 2\psi] \tag{4.43}$$

$$c_\tau = \frac{1}{2}(\lambda - 1)\sin 2\psi \tag{4.44}$$

where K_{t1} and K_{t2} are the stress concentration factors of the first and second principal notch stress, both referring to σ_1, $K_{t\perp}$ and $K_{t\tau}$ are the stress concentration factors in transverse tension and longitudinal shear loading referring to $\sigma_\perp$ and $\tau_\parallel$, $c_\perp$, $c_\parallel$ and c_τ are functions depending on λ and ψ, $\lambda = \sigma_2/\sigma_1$ is the biaxiality degree, ψ is the oblique angle of the notch versus the first principal stress and ν is the Poisson's ratio.

Another approach to the oblique notch problem determines the maximum principal stresses σ_{k1} and σ_{k2} at the notch root approximately from the principal structural stresses σ_1 and σ_2 by considering the oblique notch sections in the principal directions which have enlarged notch radii

and diminished flank angles for geometric reasons. It is then sufficient to know the factor $K_{t\perp}$ as the basis:

$$K_{t1} = 1 + (K_{t\perp} - 1)(\sin\psi + \nu\lambda\cos\psi) \tag{4.45}$$

$$K_{t2} = \lambda + (K_{t\perp} - 1)(\lambda\cos\psi + \nu\sin\psi) \tag{4.46}$$

The principal stress directions in the half-plates of the cruciform joint in Fig. 4.30 may be different. This occurs if the transverse plates are shear-loaded against the base plate. The above formulae remain valid with the instruction to treat the notches on the upper and lower sides separately.

Mean stress, non-proportional loading and residual stress effects

The derivations above of fatigue notch factors in proportional multiaxial loading presuppose zero mean stress when it is recommended to apply the von Mises distortional strain energy criterion to the stress amplitudes. The question remains unanswered what the effect of a static mean stress on the fatigue notch factor is. This effect is taken into account by defining the endurable von Mises equivalent stress amplitude as a function of the von Mises mean stress (see eqs. (5.16, 5.17)) or more realistically as a function of the hydrostatic mean stress, thus differentiating between tensile and compressive mean stresses (e.g. the criterion proposed by Dang Van[222] for non-proportional multiaxial loading with varying mean stress in the high-cycle fatigue range). Janosch *et al.*[235] have applied this type of criterion to weld notches subjected to proportional loading and have taken residual stresses into account. When using the principal shear stress criterion instead of the von Mises distortional strain energy criterion, a similar criterion results which has been proposed by Findley[109] (see eqs. (5.19–5.22)).

The effect of non-proportional multiaxial loading can be assessed by transferring certain hypotheses, criteria and procedures developed for non-welded structures and materials (reviewed by Radaj[6]) to weld notches. This has been done by Sonsino *et al.*[59–61,63,64,69,317,318,321–323] Also, the Dang Van criterion[222] has been applied to this type of loading of welded joints by Janosch *et al.*[235] Wu *et al.*[343] have investigated various criteria using simulated heat-affected zone conditions in type six aluminium alloys with the result that Dang Van's multiaxial strength criterion allows satisfactory life predictions.

The effect of residual stresses on the fatigue strength can principally be described in terms of the mean stress effect. The residual stress state at the weld notch root after the set-up loading cycle has to be determined (see Section 5.3.2). The notch stresses resulting from external loading and the initial notch residual stresses are superimposed within an elastic-plastic notch stress analysis, resulting in the fatigue-relevant persisting residual stresses ('shakedown').

The residual stress state at weld notches is uncertain in general. Residual stress measurements at weld notches are difficult to perform, but the thermal elastic-plastic simulation of the welding process offers a possibility of calculating these stresses (Radaj[7]). An attempt to combine the notch stress approach with the numerical residual stress analysis has been made by Janosch *et al.*[235]

The concurrent effects of notch stress concentration and welding residual stresses on the fatigue strength of welded joints in high strength steels (with yield limit $\sigma_{Y0.2} = 240–700\,N/mm^2$) were investigated by Watanabe *et al.*[337] The result was that the fatigue strength of the joints is mainly controlled by the welding residual stresses when the notch stress concentration is low (toe-ground welds), but that it is mainly controlled by the notch stress concentration when the latter is high (as-welded toe shape). The same has been found by Nitschke-Pagel and Wohlfahrt.[256]

The concurrent effects of notch stress concentration and welding residual stresses on the thickness effect observed in respect to the fatigue strength of welded joints were investigated by Takahashi *et al.*[329] The result was that the contribution of the residual stresses is particularly significant in the high-cycle fatigue range.

4.2.8 Fictitious notch rounding approach – links to structural stresses

The fictitious notch rounding approach for welded joints based on plane cross-sectional models has been linked to the structural stress analysis of the total welded structure which is in general performed on the basis of the finite element method. Three alternatively applicable procedures are available for the purpose of linkage, both for seam-welded and spot-welded joints.[4,284,295] The first one is the 'principal internal force method'. An approximately correct value of the fatigue notch factor of the welded joint under arbitrary oblique biaxial loading is determined proceeding from the complete internal force state in the loaded plate and the fatigue notch factor of the cross-sectional model under the in-plane loading state of the principal structural stress direction. The biaxiality of the loading state can be taken into account by applying the method in both principal directions and superposing the maximum notch stresses according to the selected multiaxial strength criterion.

The calculation of the fatigue-effective notch stresses in the welded component is performed by taking the following steps:

– finite element analysis of the global structure with weld mesh lines or element centre lines coinciding with the weld notch lines, or positioned on both sides of the weld notch lines for subsequent interpolation;

- evaluation of the internal forces in the above-mentioned mesh lines or element centre lines in the form of the absolutely larger principal stresses, σ_1 or σ_2, on the top and bottom surface of the plate, and the transverse shear stress, $\tau_{1\perp}$, acting in the sectional plane of the evaluated principal stresses;
- interpolation of the internal forces with respect to the notch line if the latter is different from the mesh or element centre line;
- transfer of the internal forces to the cross-sectional model with superposition of the counter-acting bending moment caused by shifting the transverse shear force from the notch line in the finite element model to the end section of the cross-sectional model;
- line support of the cross-sectional model in its centre area in order to suppress non-equilibrium effects;
- notch stress analysis of the cross-sectional model with fictitious rounding of the weld notches;
- determination of the fatigue notch factor by referring the maximum notch stress to a characteristic structural stress in the joint, i.e. its nominal structural stress.

The above procedural steps of the principal internal force method are demonstrated in detail by application to a welded frame corner joint (see Section 4.3.1).

The second, more accurate procedure for linkage of the notch rounding approach to the basic structural stress analysis is the 'internal force splitting method' (Radaj[4,284,295]). It keeps track of the complete stress states both in the plate in front of the seam weld and at the notch root. The procedural steps are principally the same as above with the following changes in detail:

- evaluation of the complete set of internal forces, tensile, bending and shear components in planes parallel and perpendicular to the seam weld;
- notch stress analysis of the cross-sectional model with fictitious notch rounding both for the in-plane and out-of-plane loading state; superposition of the notch stress components according to an appropriate multiaxial strength criterion.

The internal force splitting method is applied to biaxial oblique loading of welded joints in Section 4.4.2.

The third procedure for linkage of the notch rounding approach to the basic structural stress analysis is the internal displacement method. Internal displacements (inclusive of rotations) instead of internal forces (inclusive of moments) can easily be transferred from the global structure to the cross-sectional model in the case of predominant loading normal to the weld (method used in Section 8.3). Neither the line support in the centre

area of the cross-sectional model nor equilibrating bending moments for shifted end face shear forces are necessary. The resulting stresses in the cross-sectional model should be compared with the original structural stresses at these positions in order to assess the accuracy of the procedure. A more expensive three-dimensional finite element or boundary element model (inclusive of sub-modeling techniques) of the weld area must be used in the case of oblique loading of the weld.

The procedures described above for determining the fatigue notch factor of continuous seam welds are applied to weld ends with minor modifications. Both the cross-sectional and the longitudinal section models of the weld end, Fig. 4.31, are treated by the principal internal force method on the basis of the principal structural stresses at the weld seam end. An upper limit value of the fatigue notch factor is derived by this procedure.

When determining the internal forces at the end of weld lines in the global structure, a stress singularity may occur in the end point. The singularity is generally blurred by the finite element approximation in an uncontrolled manner. A remedial measure is to evaluate the internal forces in the notch line (see Fig. 4.31), or alternatively, in the weld line at the same distance from the end point as the notch line distance (Radaj[4,282–284,286]).

Butt weld ends in plane components, Fig. 4.32, necessitate a different procedure. Fictitious notch rounding can be applied here within the global structure. The notch stress can be calculated using substructure techniques.

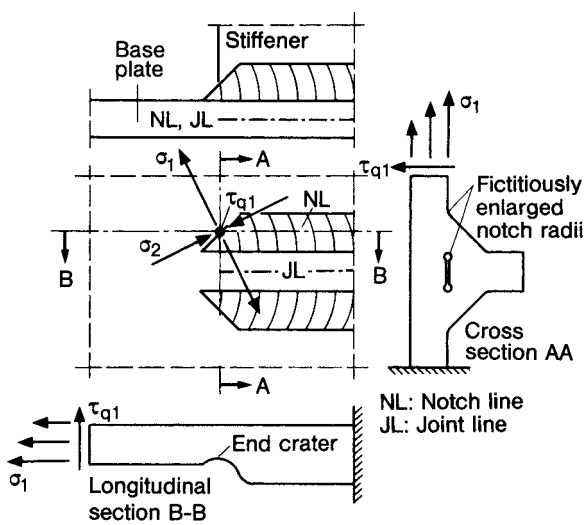


Fig. 4.31. Weld end with cross section and longitudinal section models for determining an upper limit value of the fatigue notch factor; after Radaj.[4,282–284]

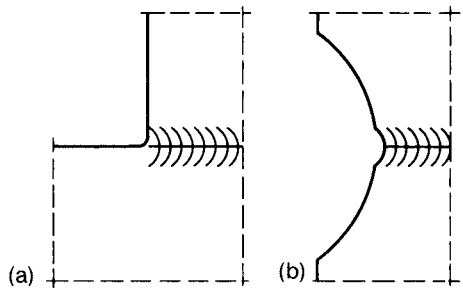


Fig. 4.32. Fictitious notch rounding at butt weld ends at the corner (a) and curved edge (b) of plane structural components; after Radaj.[4,284]

If the fictitiously rounded weld end is part of a larger notch, the total stress concentration can be approximated by multiplying the stress concentration factors of the large and the small notch.

Both the principal internal force method and the internal force splitting method can be formulated in terms of superimposed stress concentration factors. The notch stress concentration factor K_{k1} or K_{k2} (referring to the structural stress σ_{s1} or σ_{s2} at the location of the notch) multiplied by the relevant structural stress concentration factor K_{s1} or K_{s2} (referring to the nominal stress σ_n) results in the total stress concentration factor K_1 or K_2:

$$K_1 = K_{k1}K_{s1} \qquad \left(\frac{\sigma_1}{\sigma_n} = \frac{\sigma_{k1}}{\sigma_{s1}}\frac{\sigma_{s1}}{\sigma_n}\right) \tag{4.47}$$

$$K_2 = K_{k2}K_{s2} \qquad \left(\frac{\sigma_2}{\sigma_n} = \frac{\sigma_{k2}}{\sigma_{s2}}\frac{\sigma_{s2}}{\sigma_n}\right) \tag{4.48}$$

where the indices 1 and 2 refer to the first and second principal stress directions (note that $K_{k1} = K_{t1}$ and $K_{k2} = K_{t2}/\lambda$).

The principal internal force method in terms of stress concentration factors has its origin in the doctoral thesis of Radaj[269] on fillet welded cover plates, published in 1964, i.e. earlier than finite elements were generally available. The cover plate variant with front and flank side fillet welds is suitable for highlighting the principal procedural steps of the method.

A tensile loaded plate specimen with square protuberances simulating the cover plates connected by concave fillet welds (the slit faces between cover plate and base plate are deleted) is considered, Fig. 4.33. The component behaviour in terms of structural stresses is modelled by a tensile loaded plate of finite width with a square elastic core, the relative rigidity of which, E_c/E_p, is adjusted according to the thickness ratio, t_c/t_p:

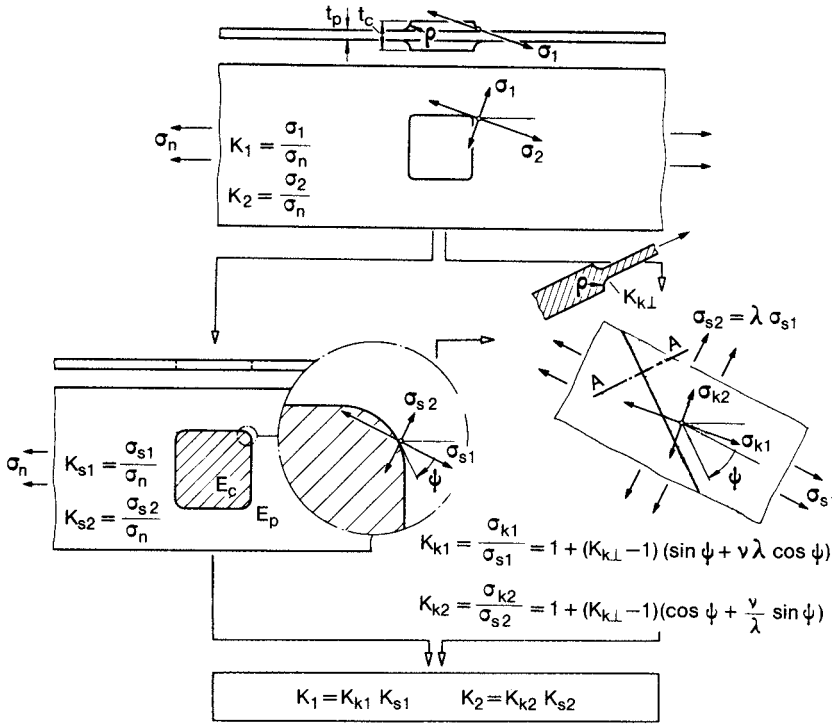


Fig. 4.33. Tensile-loaded plate specimen with square protuberances simulating cover plates connected by concave fillet welds: procedural steps of the principal internal force method in terms of stress concentration factors; after Radaj.[4,272,284]

$$\frac{E_c}{E_p} = \frac{t_c}{t_p} \qquad (\nu_c = \nu_p) \tag{4.49}$$

where E_c and E_p are the elastic moduli of the core and the plate, t_c and t_p are the thicknesses of the cover plate region and the base plate, and ν_c and ν_p are the Poisson's ratios of the core and the plate. Elastic core solutions are available (Argyris and Radaj[208,272,273]).

The maximum structural stresses, σ_{s1} and σ_{s2}, occur close to the starting point of corner rounding. Any other position at the core boundary with non-maximum structural stresses can also be considered. The corner of the core is rounded in order to avoid a stress singularity there. If the core boundary is positioned in the notch root line, a corner radius close to the fillet leg length may be appropriate. The maximum notch stresses, σ_{k1} or σ_{k2}, are determined from the cross-sectional stepped bar model subjected to the structural stresses σ_{s1} or σ_{s2} of the core model. The oblique notch

approximation according to eqs. (4.45) and (4.46) is introduced. The slight difference in principal stress direction between structural and notch stresses is indicated in the figure. Finally, the total stress concentration is found by multiplication of the two relevant stress concentration factors.

4.2.9 Modified notch rounding approach

The fundamentals of the approach are summarised in Section 4.1.4. The fatigue notch factor K_f of welded joints in structural steel according to Seeger *et al.*[8,243,244,259,260,313] can be derived from the stress concentration factor K_t of the weld toe or root notch rounded with radius $\rho = 1\,\text{mm}$ combined with the endurance limit of the unnotched parent material $\Delta\sigma_E$ related to the endurable notch stress range $\Delta\bar{\sigma}_{kE}$ for $\rho = 1\,\text{mm}$:

$$K_f = \frac{\Delta\sigma_E}{\Delta\bar{\sigma}_{kE}} K_t(\rho = 1\,\text{mm}) \tag{4.50}$$

The authors above did not use the fatigue notch factor according to eq. (4.50) but determined endurable stresses for the notches at the weld toe and weld root rounded with radius $\rho = 1\,\text{mm}$ without reference to material data of the unnotched parent material.

The endurable notch stress ranges resulting from a statistical evaluation (fatigue-tested joints according to Fig. 4.7) are plotted in Fig. 4.34 and

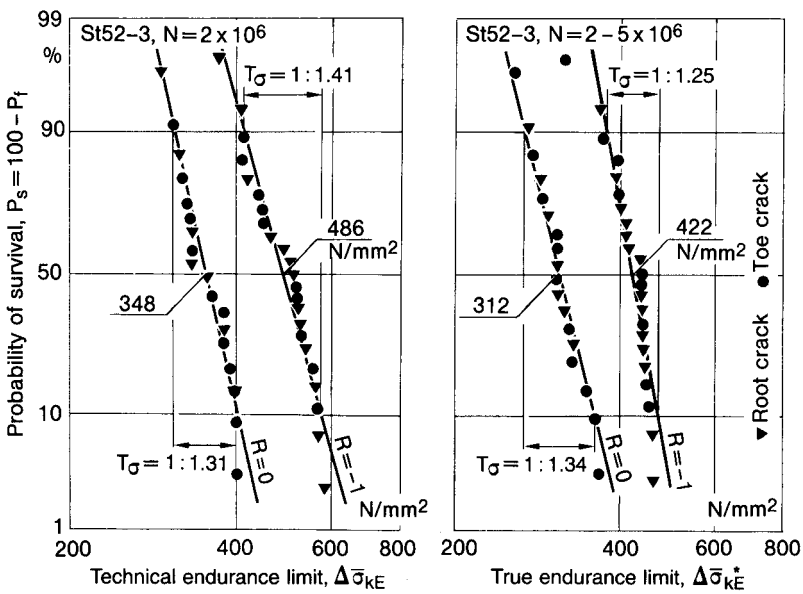


Fig. 4.34. Endurable notch stress range of stress-relieved welded joints, test results by Olivier *et al.*[259,260]

summarised in Table 4.5. The technical endurance limit in longitudinal shear loading is $\Delta\bar{\tau}_{kE} = 320\,N/mm^2$ ($R = -1$, $P_f = 50\%$). The diagrams and data are applicable to welded joints made of low and high strength structural steels.

Seeger and Amstutz[313] propose the following permissible weld notch stress ranges (with failure probability $P_f = 2.3\%$ corresponding to the mean minus two standard deviations) on the basis of the results mentioned above:

$$\Delta\bar{\sigma}_{k\,per}(R=-1) = 360\ N/mm^2, \quad \Delta\bar{\tau}_{k\,per}(R=-1) = 190\ N/mm^2$$
$$\Delta\bar{\sigma}_{k\,per}(R=0) = 260\ N/mm^2$$

The effect of mean stress can be taken into account according to the Haigh diagram in Fig. 4.35, differentiating between three levels of tensile residual

Table 4.5. Endurable notch stress ranges for welded joints in St52–3 structural steel, mean values; after Olivier *et al.*[259,260]

Welded joints in St52–3 structural steel	Technical endurance limit $\Delta\bar{\sigma}_{kE}$ [N/mm²] ($N = 2 \times 10^6$, $P_f = 50\%$)		True endurance limit[a] $\Delta\bar{\sigma}^*_{kE}$ [N/mm²] ($N = 2$–5×10^6, $P_f = 50\%$)	
	$R = -1$	$R = 0$	$R = -1$	$R = 0$
Stress-relieved	494[b]	352[b]	422	312
As-welded	470	362	–	–

[a] Designation 'true' objectionable, see Section 2.2.2.
[b] Minor deviation from Fig. 4.34 because of different evaluations.

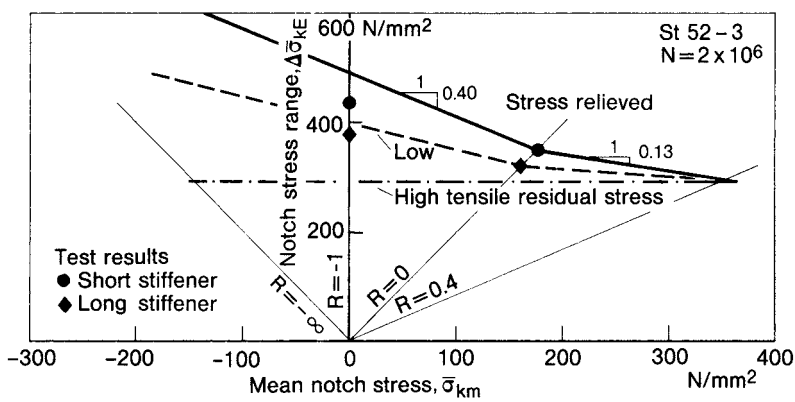


Fig. 4.35. Effect of mean notch stress and welding residual stress on the endurable notch stress range, after Olivier *et al.*[259,260]

stress. Confirming test results are also available for $R = 0.4$ (without test result point in the figure).

The permissible value for welded joints in structural steels according to IIW recommendations[3] is:

$$\Delta\overline{\sigma}_{\mathrm{kE\,per}} = 225\ \mathrm{N/mm^2}$$

The strength reduction by high tensile residual stresses caused by welding is included.

A successful attempt to apply the modified notch rounding approach to welded joints in aluminium alloys using the same fictitious notch radius $\rho_f = 1\,\mathrm{mm}$ as with steel has been made by Morgenstern *et al.*[249,250] The endurable stress range for various joints (as-welded) in aluminium alloys of type AlMg4.5Mn (AA5083-T4) and AlMgSi1 (AA6082-T6) is stated as follows:

$$\Delta\overline{\sigma}_{\mathrm{kE}}(R=0) = 124\ \mathrm{N/mm^2} \quad \left(N_{\mathrm{E}} = 2\times10^6, P_{\mathrm{f}} = 50\%\right)$$

The permissible value for welded joints in aluminium alloys according to IIW recommendations[3] is:

$$\Delta\overline{\sigma}_{\mathrm{kE\,per}} = 70\ \mathrm{N/mm^2}$$

The strength reduction by high tensile residual stresses caused by welding is included.

4.2.10 Highly stressed volume approach

The fundamentals of the approach are summarised in Section 4.1.5. The fatigue notch factor K_f of welded joints (and also of non-welded members) in structural steel according to Sonsino[316] can be derived from the stress concentration factor K_t and the endurable notch stress amplitude σ_{kaE} in relation to the endurance limit of the material σ_{aE}, eq. (4.51). The endurable notch stress amplitude σ_{kaE} is dependent on the highly stressed volume $V_{0.9}$, eq. (4.52) (hypothesis according to Kuguel[246] based on Weibull's statistical theory[338]). The highly stressed volume $V_{0.9}$ is defined as that region where 90% of the maximum notch stress is exceeded. It results from the normalised stress gradient χ perpendicular to the notch surface defining the depth $d_{0.9}$, eq. (4.54), combined with the extension of the above region at the notch surface, approximated for a plane specimen by eq. (4.53):

$$K_{\mathrm{f}} = \frac{\sigma_{\mathrm{aE}}}{\sigma_{\mathrm{kaE}}} K_{\mathrm{t}} \tag{4.51}$$

$$\sigma_{\mathrm{kaE}} = f(V_{0.9}) \tag{4.52}$$

$$V_{0.9} \approx d_{0.9} w \frac{\pi\rho}{8} \tag{4.53}$$

$$d_{0.9} = \frac{0.1}{\chi} \qquad \left(\chi = \frac{1}{\sigma_k}\frac{\mathrm{d}\sigma_k}{\mathrm{d}n}\right) \tag{4.54}$$

The size of the plain tensile specimens providing σ_{aE} must not fall below a minimum size where the highly stressed volume effect starts. The first principal stress is evaluated as maximum notch stress. The notch stress gradient depends on the inverse notch radius, the inverse cross-section dimension and the loading mode. Approximation formulae are given in the literature.[312,314,340] When considering tensile loaded notches, $\chi \approx 2/\rho$ is appropriate.

The prediction of the fatigue notch factor of welded joints according to Sonsino proceeds from the actual notch radius which is introduced at the weld toe as $\rho = 0.45$ mm on the basis of evaluations for welded tube joints (ρ = 0.2–0.8 mm) in structural steel.[59,60] The actual notch radius at the weld toe of a butt-welded aluminium alloy used by Brandt *et al.*[213] was $\rho = 0.14$ mm averaged from measured values $\rho = 0.10$–0.19 mm. The above fatigue notch factor may be stated for different numbers of cycle in the high-cycle fatigue range ($N > 10^5$ cycles).

In the case of multiaxial non-proportional loading, the effective equivalent stress criterion (averaging the shear stresses in all local directions) is applicable (Sonsino[59,60,318,319]).

Sonsino did not use the fatigue notch factor according to eq. (4.51) but determined endurable stresses in welded joints as a function of the highly stressed volume and dependent on the number of cycles endured. This means that the use of material data relating to the notch-free and non-welded condition is avoided.

The approach has been extended by Sonsino[59,60] to multiaxial fatigue on the basis of the von Mises equivalent stress (see eq. (4.46)) covering ductile materials and non-varying principal stress directions. The shear stress term in the equation is modified by a factor derived from the relation of the *S–N* curves in pure torsion loading relative to tension or bending loading, eq. (4.56). Endurable equivalent notch stress amplitudes for welded joints in structural steel are plotted in Fig. 4.36 as a function of the highly stressed volume and in Fig. 4.37 as a function of the number of cycles. Obviously, the elastic approach can be extended into the medium-cycle fatigue range without a plasticity correction on the notch stresses.

Relevant endurable notch stress amplitudes for a GMA-welded aluminium alloy of type AlMg4.5Mn are plotted in Fig. 4.38. They are derived from fatigue-tested notched and unnotched specimens worked from parent metal and weld deposit.[213] A uniform scatter range index T_σ is derived from the fatigue tests according to the concept of normalised *S–N* curves.

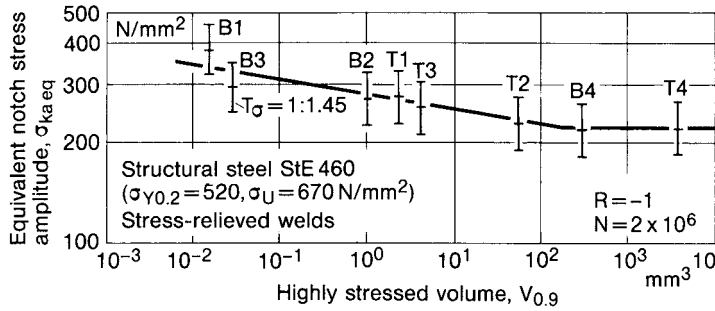


Fig. 4.36. Endurable notch stress amplitude at weld toes in structural steel as a function of the highly stressed volume ($\sigma > 0.9\sigma_k$); tube-to-plate (1, 2) and tube-to-tube (3, 4) joints, non-machined (1, 3) and machined (2, 4) weld toe, bending (B) and torsion (T) loading; after Sonsino.[59,60]

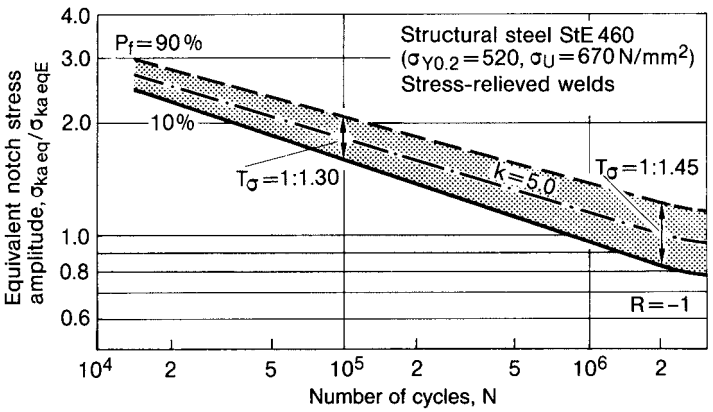


Fig. 4.37. Endurable notch stress amplitude at weld toes in structural steel in the medium-cycle fatigue range related to the endurance limit (large highly stressed volume): scatter band from tests under pure bending load valid for in-phase and out-of-phase superposition of bending and torsion loads; after Sonsino.[59,60]

Multiaxial fatigue considerations referring to the local conditions at the notch root are closely connected with the highly stressed volume approach and also applicable independent from it. The notch stresses and strains result primarily from an elastic analysis, but can also be derived under elastic-plastic conditions (definitely necessary for $N \leq 5 \times 10^4$ cycles). Whereas the von Mises criterion, as well as the Tresca criterion, for ductile materials, and the maximum normal stress criterion for brittle materials can be applied under proportional local loading conditions, the criteria may fail under non-proportional conditions. The appropriate criterion should be selected according to the ductility of the material, Table 4.6.

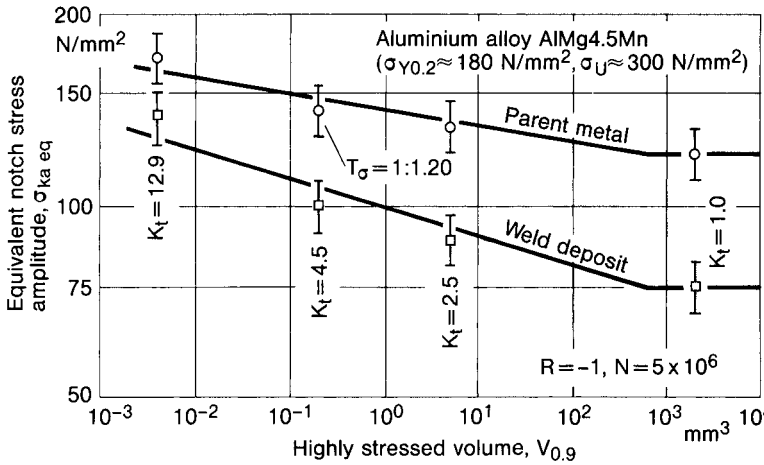


Fig. 4.38. Endurable notch stress amplitude at weld toes in type AlMg4.5Mn aluminium alloy as a function of the highly stressed volume ($\sigma > 0.9\sigma_k$), specimens in parent material and weld deposit; after Brandt *et al.*[213]

Table 4.6. Damage causes and damage criteria for locally non-proportional biaxial loading conditions; after Sonsino[59,60]

Damage cause	Damage criterion
Normal stress $\sigma(\varphi)$[a] in the case of low ductility (aluminium cast alloys, cast iron, sintered steels)	Critical normal stress in plane of maximum normal stress
Combination of normal and shear stresses, $\sigma(\varphi)$ and $\tau(\varphi)$, in the case of medium ductility (aluminium wrought alloys, cast steel)	Critical equivalent stress in plane of maximum value of combined shear and normal stress (plane-related von Mises stress)
Shear stress $\tau(\varphi)$, in the case of high ductility (structural steels)	Critical value of the integral of the shear stresses in all local planes

[a] Stress σ as function of the local plane angle φ.

It is an important point to be kept in mind that multiaxial failure criteria proposed on the basis of unnotched specimen behaviour cannot be expected to work without proper adaptation when applied to specimens with sharp notches such as welded joints. Two effects have to be taken into account. Local elastic-plastic deformation at sharp notches takes place under strain-controlled (instead of stress-controlled) loading conditions and microcrack coalescence follows the sharp notch line.

The criterion of effective equivalent stress $\bar{\sigma}_{eq}$ for out-of-phase (i.e. non-proportional) local loading conditions (biaxial surface stresses σ_x, σ_y and τ_{xy}), applicable to weldments in ductile materials, is specified below (Sonsino[59,66]). The shear stress $\tau(\varphi)$ is calculated in each local plane out of a complete set of planes in different directions φ in the surface, and averaged over all planes to capture the effect of mutual interference of the dislocations and microcracks generated in the different planes. From this evaluation, the damage parameter $F(\delta)$ depending on the phase angle δ is greater for out-of-phase loading, $\delta = 90°$, than for in-phase loading, $\delta = 0°$. This results in a larger equivalent stress and a shorter fatigue life.

Using the ratio of the damage parameters $F(\delta)$, the effective equivalent stress for out-of-phase loading can be determined for different phase angles δ on the basis of the von Mises effective equivalent stress for in-phase loading:

$$\bar{\sigma}_{eq}(\delta) = \bar{\sigma}_{eq}(\delta = 0^\circ)\frac{F(\delta)}{F(\delta = 0^\circ)}\sqrt{S\exp\left[1-\left(\frac{\delta - 90^\circ}{90^\circ}\right)^2\right]} \tag{4.55}$$

$$\bar{\sigma}_{eq}(\delta = 0^\circ) = \sqrt{\sigma_x^2 + \sigma_y^2 - \sigma_x\sigma_y + f_g^2 3\tau_{xy}^2} \tag{4.56}$$

$$S = \frac{1 + K_{t\sigma}}{1 + K_{t\tau}} \tag{4.57}$$

Here, the factor f_g is a size effect factor which reflects the influence of the highly stressed material volume on the endurable stresses. It is determined from the ratio of endurable local equivalent stresses in pure tensile and pure shear loading of the weld, e.g. accomplished by bending and torsional loading of a tube-to-plate welded specimen (Sonsino[59,60]). The factor S is also a size effect factor expressing the influence of stress gradient on the equivalent stress with changing phase angles or principal stress directions. However, the size factor S and consequently the root term in eq. (4.55) is only valid for seam-welded thick plates with low stress concentration factors. In this case, the initial defect population addressed by fluctuating principal stresses is considerably higher than for thin plates with high stress concentration factors. The stress concentration factors $K_{t\sigma}$ and $K_{t\tau}$ refer to tensile and shear loading, respectively.

Fatigue test results for the tube-to-plate welded specimen (in steel) mentioned above, evaluated on the basis of the local effective equivalent stress amplitude $\bar{\sigma}_{eq\,a}$, are plotted in Fig. 4.39. The scatter band refers to the results for pure bending. Obviously, all the other results are sufficiently well related to this scatter band if an enlarged scatter range index is introduced.

It has been reported that the method described above also works well with variable-amplitude loading (Sonsino and Küppers[42,63,64]). Similar

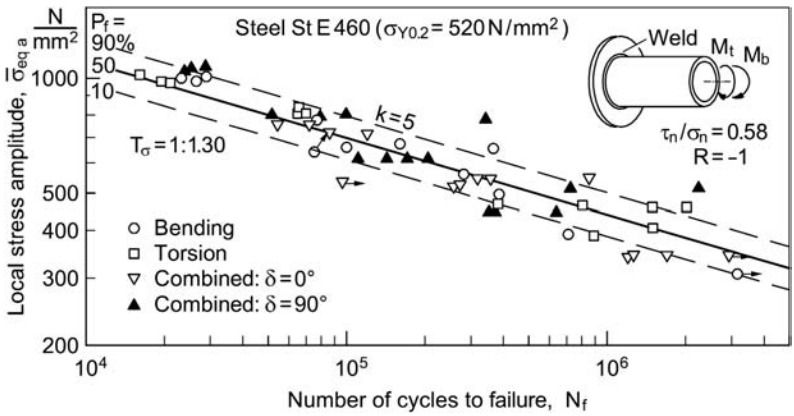


Fig. 4.39. S–N curve of local effective equivalent stress amplitude $\bar{\sigma}_{eq\,a}$ in steel for different pure and combined, in-phase and out-of-phase loading conditions of a tube-to-plate welded specimen; scatter band refers to pure bending loading; local (notch) stresses from an elastic analysis with notch radius ρ = 0.45 mm; after Sonsino.[59,60]

investigations by Witt *et al.*[342] confirmed the applicability of the 'integral damage approach' above in a wider range comprising additional loading variants such as the combination of cyclic and static loading or of loading with different frequencies.

When considering welded joints in less ductile materials (medium ductility according to Table 4.6, e.g. aluminium wrought alloys), another criterion and another set of equations has been derived and successfully applied (Sonsino,[41,42,63,64] compare Wu *et al.*[343]).

4.3 Demonstration examples

4.3.1 Welded vehicle frame corner

This example is taken from the early publications[4,283,284] on the notch stress approach for welded joints where the stress analysis part of the method resulting in the fatigue notch factors has been demonstrated. Only relative statements on fatigue strength are possible on that basis.

The analysed welded vehicle frame corner consists of two channel section bars, the cross-member butting to the side rail web, Fig. 4.40(a). The cross-member is subjected to a torsional moment. Two joint details are considered, a T-joint between cross-member and web and a butt weld between two sections of the side rail, Fig. 4.40(b). The T-joint is alternatively designed applying a double fillet weld on the one hand and a single-bevel butt weld with fillet weld and root face on the other hand.

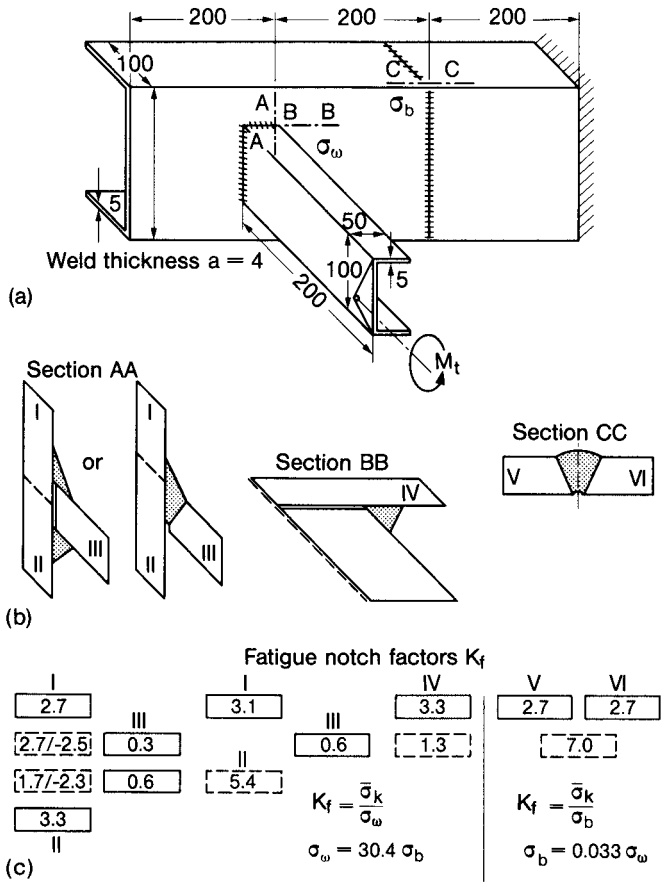


Fig. 4.40. Welded vehicle frame corner (a) with cross-sectional models of welded joints (b) and calculated fatigue notch factors (c), after Radaj.[4,282–284]

The simple T-joint selected should not really be applied in the frame corner because the torsion-bending moment (i.e. the flange bending moment resulting from the torsional moment) in the cross-member causes excessively high torsion-bending stresses in the flange edges at the joint. These structural stresses result in correspondingly increased notch stresses which then initiate fatigue cracks very early. However, the marked increase in structural and notch stress makes this particular design especially suitable for demonstration purposes.

At first, a finite element analysis was performed from which the internal forces at the welded joints were evaluated in terms of the structural stresses. Then, the notch stresses were determined by the cross-sectional models of

sections A–A and C–C, and by the longitudinal-section model of section B–B, applying the internal forces of the finite element solution to these models (principal internal force method).

The calculated fatigue notch factors are summarised in Fig. 4.40(c). The torsion-bending stress, σ_ω, which would arise under warping-rigid support conditions according to the torsion-bending theory, was taken as the reference stress at the T-joint. In contrast, at the butt-welded joint the bending stress σ_b at the outer surface of the flange according to the beam bending theory was chosen as the reference stress. The values of the fatigue notch factors are entered in boxes, the arrangement of which corresponds to the positions of the weld notches in the sections of the welded joints above the boxes.

Fatigue notch factors K_f of a realistic magnitude were determined throughout according to eq. (4.30). The torsion-bending loading of the cross-member increases the risk of failure in the web of the side rail (K_f = 2.7–3.3 or 3.1–5.4), not in the flanges of the cross-member (K_f = 0.3–0.6). The double fillet weld which runs around the end of the flange reveals approximately the same notch effect at this point in the three orthogonal sections (K_f = 2.7, 3.3, 3.3). A particularly severe notch effect occurs at the root face of the single-bevel butt weld (K_f = 5.4). The notch effect of the inner slit of the double fillet weld is smaller than that of the weld toes and equal to it in one case (K_f = 1.3–2.7). The butt weld is not critical despite a severe notch effect at the weld root (K_f = 7.0) because of the low structural stress.

The conclusion from the analysis above is that the fatigue notch factors of welded joints in complex design and loading situations can be determined without major difficulties and used directly for relative statements on fatigue strength.

4.3.2 Web stiffener of welded I-section girder

This example after Radaj[285] has been chosen to demonstrate the use of the notch stress approach to assess the effect of stiffener type and weld type on the fatigue strength of a well-known structural detail in relative terms and to check the applicability of a definite notch or detail class *S–N* curve. Further examples of application to girders and frame members are available (Radaj *et al.*[298–300])

The fictitious notch rounding approach has been applied to a transverse web stiffener welded to a slender I-section girder common in bridge construction, Fig. 4.41. The transverse weld connecting the stiffener to the tensile chord or flange of the girder is at risk of fatigue failure because of the notch stresses at its toe and root. The girder is subjected to pure bending and transverse bending, respectively. The stiffener is used with and without

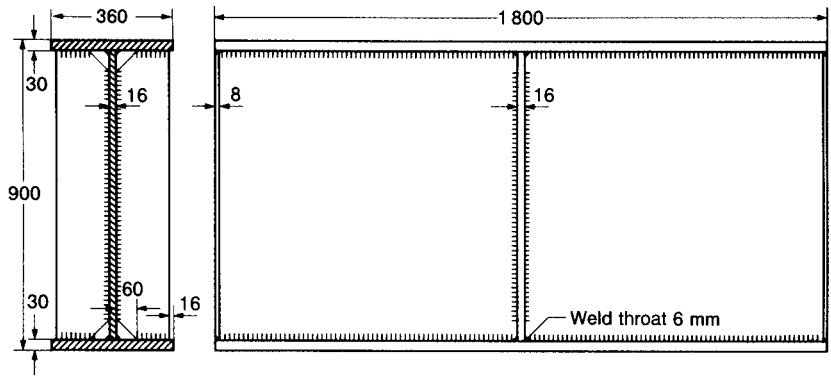


Fig. 4.41. Welded I-section girder with web stiffener; after Radaj.[285]

a cut-out at the inner corner. A double fillet weld is compared with a double-bevel butt weld with fillet weld and root face. A tensile specimen with single-sided attachment has been included in the investigation. The design *S–N* curve of this specimen is generally used to assess the fatigue strength of the stiffener-to-flange joint of the girder.

The result of the structural stress analysis by the finite element method has been the following. The stiffener presses into the tensile flange from above, thereby decreasing the stresses on the inside of the flange and increasing them on the outside. The stress redistribution is advantageous in respect of the notch effect which is restricted to the inside of the flange. Cutting out the inner corner of the stiffener is favourable because the notch effect is completely avoided in an area where the flange stresses are slightly increased under transverse bending of the girder.

The results of the subsequent notch stress analysis by the boundary element method, using fatigue notch factors K_f according to eq. (4.30), have been converted into fatigue strength reduction factors, $\gamma = 1/(0.89K_f) + 0.1$, for zero-to-tension loading ($R = 0$) evaluating the maximum tensile notch stresses at the weld toe (for γ_t) and weld root (for γ_r), and additionally evaluating the structural stress increase on the outside of the flange (for γ_f), Table 4.7. All the reduction factors refer to the maximum nominal bending stress of the girder, i.e. to the bending fatigue strength of the girder without a stiffener.

The following conclusions can be drawn for design and dimensioning from the lowest (tensile) reduction factor in each case in Table 4.7. The transverse stiffener is associated with a reduction factor $\gamma = 0.55–0.73$ for zero-to-tension loading (compared with $\gamma = 0.25–0.75$ for fully reversed loading, Radaj[285]). The high values can only be put into effect in the case of pure bending if measures are taken to improve the weld toe, for example,

Table 4.7. Predicted fatigue strength reduction factors γ (lower limit, evaluation of tensile notch stresses only) for an I-section girder with transverse web stiffener in different design and loading variants; after Radaj[285]

Component	Stiffener type	Weld type	Loading condition	Reduction factors		
				γ_f	γ_t	γ_r
I-section girder	None	None	Pure bending	1.02	—	—
I-section girder	Transverse stiffener without cut-out	Fillet weld	Pure bending	0.95	0.55	0.64
I-section girder	Transverse stiffener without cut-out	Fillet weld	Transverse bending	0.74	0.71	0.57
I-section girder	Transverse stiffener with cut-out	Fillet weld	Transverse bending	0.73	1.08	0.75
I-section girder	Transverse stiffener with cut-out	Double-bevel butt weld	Transverse bending	0.68	0.96	1.21
Tensile specimen	Transverse attachment	Fillet weld	Tension	1.00	0.51	0.71
Tensile specimen	Transverse attachment	Double-bevel butt weld	Tension	1.00	0.52	0.78

by grinding or dressing (in this case even $\gamma > 0.73$ seems to be possible), or in the case of transverse bending if the transverse forces are relatively high (with crack initiation on the outside of the flange). Deep penetration welding or double-bevel butt welds are recommended to prevent crack initiation at the weld root in the case of transverse bending. Cutting out the inner corners of the stiffener improves the notch condition considerably in the case of high transverse forces. This measure is also recommended to avoid weld crossing and because of the limited accessibility at the inner corner. The tensile specimen with transverse attachment can only be correlated with pure bending loading of the girder. The above reduction factors fit sufficiently well into the available code specifications (IIW,[3] Eurocode3,[23] BS 5400,[13] DIN 15018[19]).

The general conclusion from the anlaysis above is that the effect of stiffener type and weld type on the fatigue strength can be determined in detail, thus giving guidance for the choice of a suitable notch or detail class *S–N* curve.

4.3.3 Stress relief groove in welded pressure vessel

This example after Radaj[288] of the notch stress approach has been chosen to assess the effectiveness of a definite design measure on the fatigue strength of a welded joint. Another field of engineering is considered and the analysis is simplified by the omission of the structural stress analysis.

Pressure vessels composed of a cylindrical shell welded to flat ends may have a circular groove at the inner corner intended to facilitate welding and to relieve the notch stresses at the weld root caused by internal pressure loading of the vessel. The questionable relief effect of the groove has been investigated by a notch stress analysis. The weld root with root face is fictitiously rounded. The predominant loading in the transition area between flat end and circular shell is meridional bending so that the comparative investigation could be restricted to this type of loading applied to the cross-sectional model of the grooved joint.

The model is shown in Fig. 4.42(b). The groove dimensions, radius ρ_g and depth d_g, are variable, the radius ρ_f of fictitious rounding of the weld root is constant, $\rho_f = 1$ mm. The fatigue notch factor (according to eq. (4.30)) of the weld root, K_f, refers to the nominal bending stress in the notch-free shell end. The result of the parametric investigation is shown in Fig. 4.42(a). There is only a minor influence of the groove radius (less than 10%) in the case of the semi-circular groove ($d_g = \rho_g$). A slightly larger reduction of the fatigue notch factor is possible by deepening the groove ($d_g = 2\rho_g$). The maximum total improvement compared with the design version without a groove ($K_f = 3.40$) is about 15% in the latter case but the end plate is severely weakened by the deep groove.

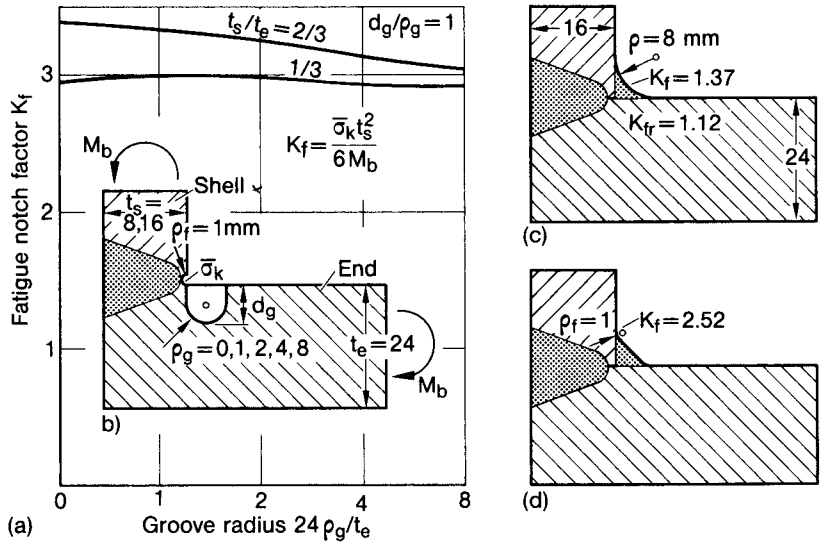


Fig. 4.42. Cross-sectional models of shell-to-end welded joint of a pressure vessel, version with stress relief groove (b), versions with a concave or flat fillet weld at the inner corner (c, d) and calculated fatigue notch factors; the factor at the weld root plotted versus groove radius for two thickness ratios (a); after Radaj.[288]

The conclusion is that the notch stress relief at the weld root achieved by the groove is low and not worth the expenditure in manufacturing. Far better relief is possible with a machined concave fillet weld (with or without a root face) in the inner corner of the vessel, $K_f = 1.37$ (at root $K_{fr} = 1.12$), Fig. 4.42(c) (short crack correction not yet applied). Even for an non-machined flat fillet weld, the stress relief is remarkable, $K_f = 2.52$, Fig. 4.42(d).

The general conclusion from the notch stress analysis above is that the effectiveness of the design measure being considered is well assessed within a simplified procedure.

A notch stress investigation on similar lines as above has been performed by Rodriguez *et al.*[308] considering repair grooves in transverse attachment joints. The well-rounded grooves are machined where flaws or initiated fatigue cracks have to be removed. An equivalent U-shaped notch in the simulation substitutes for various groove shapes occuring in reality. The parametric notch stress analysis (significant parameters are groove depth, groove length, groove root radius and plate thickness, forming the independent dimensional ratios) based on the finite element method referred first to the cross-sectional model and then to a three-dimensional model of the plain plate with a shallow surface notch of limited length (the attachment deleted because of minor influence). A notch stress reduction occurs

in the latter case because of some force flow around the groove. Parametric equations for the stress concentration factors are given which allow the notch stresses to be minimised by appropriately selected groove dimensions.

4.3.4 End-to-shell joint of boiler

This example after Radaj *et al.*[292] has been chosen to demonstrate the assignment of actually produced welded joints to definite notch or detail class *S–N* curves. Additionally, it is shown that experimental and numerical stress analyses can be combined in an advantageous manner.

The notch stress approach for the assessment of the fatigue strength of welded structures has so far been represented as a procedure based solely

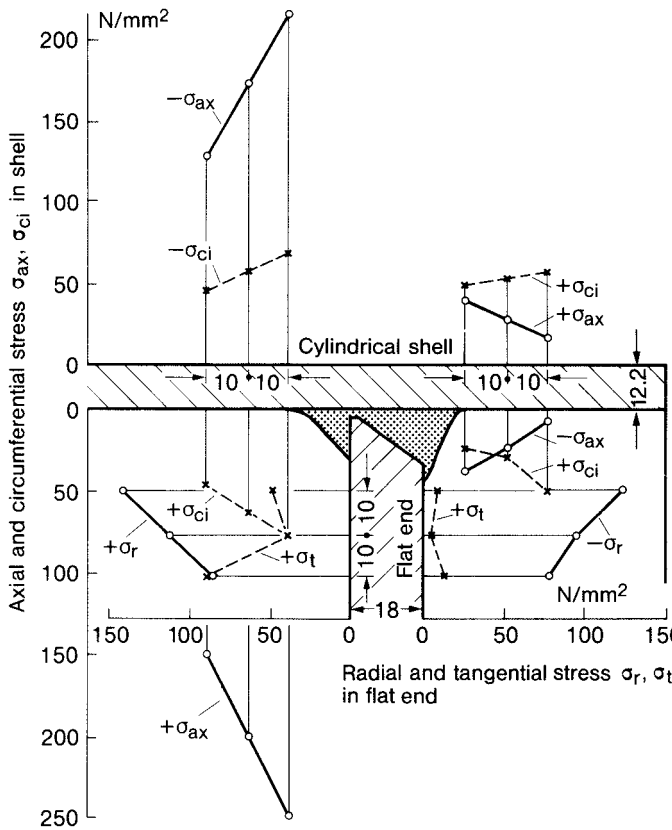


Fig. 4.43. Structural stresses measured at end-to-shell joint between diagonal stays; internal boiler pressure $p = 10.2$ bar; indexing: ci, circumferential; ax, axial; t, tangential; r, radial; after Radaj *et al.*[292]

on numerical analysis. Such a procedure provides a decisive advantage for practical application as the strength of the structure can be assessed at the design stage without prototyping. Sometimes, however, a procedure based on measurements or on a combination of calculation and measurements is appropriate, especially if the approach based on measurements is less expensive, faster and more accurate.

The combination of structural stress measurement, notch stress calculation and fatigue strength assessment based on notch classes was demonstrated for a three-pass boiler end designed for heating water. The welded joint between flat end and cylindrical shell and the welded joint at the diagonal stay in the inside corner area of the boiler which are considered to be at risk of fatigue crack initiation have been analysed for internal pressure loading of the boiler.

By means of strain gauges, the structural stresses are measured at three points in each case in front of the weld seam on the inside and outside of the end and of the shell, Fig. 4.43. Subsequently, the complete internal force state which is required for the notch stress analysis of the cross-sectional model of the welded joint is determined. Tensile force and bending moment result directly from the stresses. The transverse force is calculated from the stress gradient. The fatigue notch factor K_f according to eq. (4.30) is calculated for the fictitiously rounded notches under the internal force state above by using the boundary element method.

Proceeding from the calculated fatigue notch factor, $K_f = 2.3$, of the end-to-shell joint, the appropriate notch class and design S–N curve (notch class K2 associated with the notch factor 2.4) are determined within the framework of a low-cycle fatigue strength assessment according to German code specifications[9,72] for steam boilers. The permissible number of load cycles was indicated on that basis.

The conclusion is that actually produced welded joints can be assigned to definite notch or detail class S–N curves on the basis of the notch stress approach combined with structural stress measurements.

4.3.5 Stiffener-to-flange joint at ship frame corner

This example has been chosen to demonstrate the assessment of the fatigue strength of an actually produced welded joint made of low strength steel on the basis of the endurance limit of the parent material. Once more, experimental and numerical stress analysis are combined.

The stiffener-to-flange joint in the welded frame corner of a ship structure has been investigated by Petershagen[262] and Gimperlein[225] in respect of its fatigue strength on the basis of the notch stress approach using fictitious notch rounding. The frame corner is made of low strength steel plates. It had been prepared for fatigue testing as shown in Fig. 4.44(d).

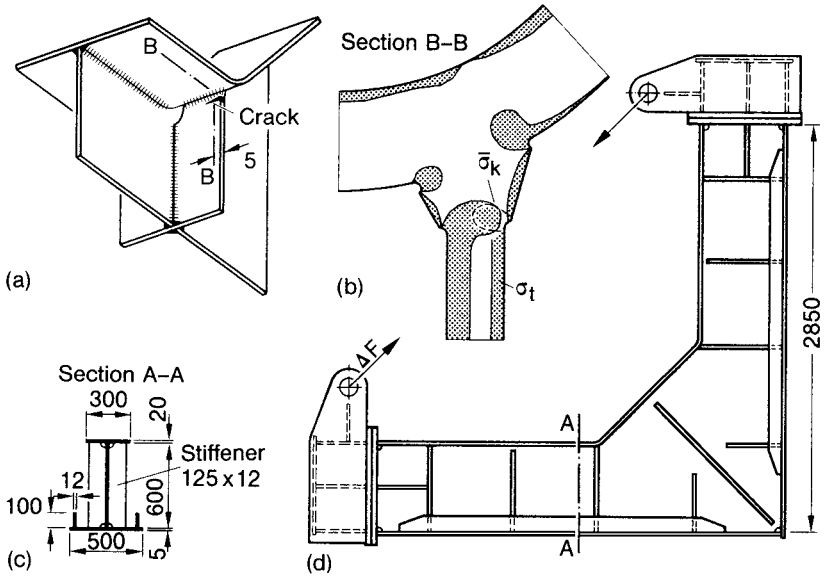


Fig. 4.44. Stiffener-to-flange joint (a) of welded ship frame corner (c,d); calculated contour stresses including the notch stresses in cross-sectional model (b); after Gimperlein[225] and Petershagen.[262]

The zero-to-tension load ΔF acts in the diagonal direction at the corner ends with compressive static preload $F = \Delta F/2$ so that tensile stresses occur in the fatigue-critical area near section A–A, Fig. 4.44(c). The stiffener is T-butting to the flange with a double-bevel butt weld where the flange changes its direction, Fig. 4.44(a). The flange had been bent with limited cold-straining into the minimum radius of curvature allowed in heat-affected areas by the relevant design code.

The fatigue crack is initiated at the upper end of the stiffener plate at the weld toe and propagates along the weld seam. Fatigue testing had been performed up to a crack length of 2–5 mm. The principal direction of the structural stresses in the uncracked stiffener plate coincides with the direction normal to the stiffener edge. Therefore, a cross-sectional model corresponding to section B–B can be used to determine the notch stresses on the basis of the boundary element method, Fig. 4.44(b). The structural stresses or resultant forces at the three ends of the model are derived from strains and strain gradients measured in front of, and linearly extrapolated to, the weld toe. The results are confirmed by finite element analysis.

The weld contour is defined on the basis of measurements on several test specimens. The weld toes are fictitiously rounded with radius $\rho_f = 1$ mm. A weld reinforcement height of 1 mm is introduced in order to cover the worst

case. The scatter of the other dimensions has no significant influence on the notch stresses. The maximum notch stress occurs at the weld toe where the crack is actually initiated.

The values of the resultant forces at the model ends in the numerical analysis are chosen according to the endurance limit load gained from fatigue testing ($N = 2 \times 10^6$ cycles, $P_f = 10\%$). The corresponding endurable notch stress range is $\Delta\bar{\sigma}_{kE} = 223\,N/mm^2$ ($R = 0$). This is 16% less than the value derived for non-welded plain specimens (Table 4.4), $\Delta\bar{\sigma}_E = 240/0.9 = 267\,N/mm^2$ ($R = 0$). The difference may be explained by the effect of tensile residual stresses. Also, welding was performed vertically upwards with geometric irregularities which were not simulated by the model. Finally, deviations may arise from the fact that the local fatigue strength of the molten and solidified weld material (with $\rho_f \approx 1\,mm$) is set equal to the global fatigue strength of the rolled sheet material (with $\rho_f \approx 0.4\,mm$).

The conclusion is that the endurance limit of welded joints in low strength steels can roughly be assessed by comparing the fatigue-relevant notch stress at the weld toe (with $\rho_f = 1\,mm$) with the endurance limit of the parent material.

4.3.6 Girth butt welds of unusual manufacture

This example has been chosen to demonstrate the evaluation of the notch radii of actually produced welds on a statistical basis and to use this information to determine the crack initiation points.

The application of the notch stress approach by Petershagen[264] refers to girth butt welds of pipes which are GMA-welded under increased atmospheric pressure (dry hyperbaric conditions) in order to simulate repairs at sea water depths of 265 to 450 m. The pipe diameter is 0.7 m, the wall thickness 18 mm. The material is type StE445.7TM fine-grained structural steel. Arbitrary welding positions occur because the pipe is not turned during welding. The results of fatigue testing under zero-to-tension load ($R = 0$) correlated with the scatter band of the normalised S–N curve of structural steels. The endurable nominal stress amplitude ($N = 2 \times 10^6$ cycles, $P_f = 50\%$) was $\bar{\sigma}_{nA} = 78\,N/mm^2$.

The actual weld contour was determined by silicone rubber contour moulds which were cut into slices to determine the geometric weld parameters, Fig. 4.45 (a–d). The contour lines of the cross-sectional models were defined on the basis of these measurements with a fictitious enlargement of the actual notch radius by 1 mm (according to eq. (4.29)), i.e. a uniform notch radius was not introduced. Extreme values of the contour parameters were used in the notch stress evaluations of Fig. 4.45(e, f) based on the boundary element method. The crack initiation points were definitely marked by the notch stress maxima $\bar{\sigma}_k$.

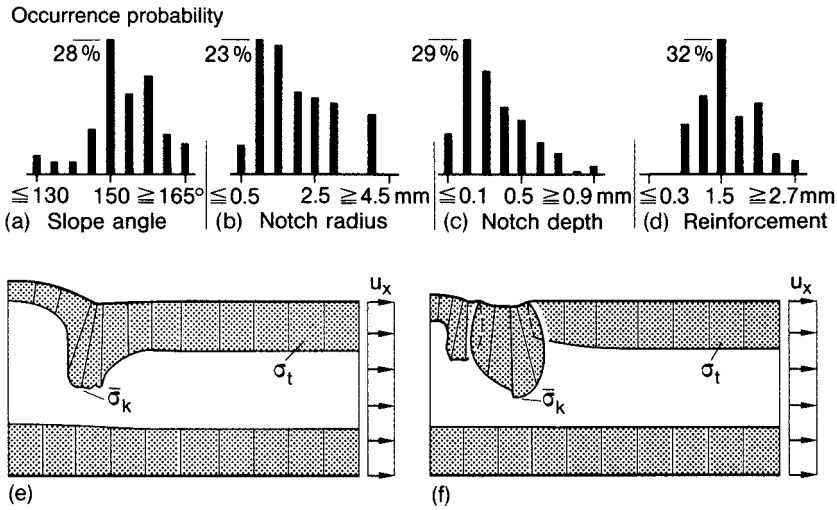


Fig. 4.45. Girth butt welds, GMA-welded under special conditions: geometric weld parameters (a–d), calculated contour stresses comprising the notch stresses (e, f); after Petershagen.[264]

There were no endurable notch stress amplitudes evaluated, only the lifetime cycles in the test were compared with those from the normalised *S–N* curve.

4.3.7 Tensile specimen with longitudinal attachment

This example has been chosen to demonstrate the assessment of the fatigue strength of the longitudinal attachment joint made of high strength steel on the basis of the endurance limit of low strength steels. The use of the boundary element method in three dimensions to determine the stress concentration is also shown.

Petershagen[262] has investigated the tensile specimen with double-sided longitudinal attachments in respect of fatigue strength and notch stresses. The specimens were made of type HF36 high strength shipbuilding steel with a minimum yield limit, $\sigma_{Y0.2} = 355\,N/mm^2$. Constant amplitude tests were performed with these specimens in the as-welded and stress-relieved condition under fully reversed loading ($R = -1$). The tensile residual stress at the crack initiation point of the weld toe in the as-welded condition was in the range of the yield limit as shown by X-ray measurements. The normalised *S–N* curve and its scatter band were confirmed by the test results. The endurable nominal stress range was $\Delta\sigma_{nE} = 107\,N/mm^2$ for the as-welded condition and $\Delta\sigma_{nE} = 132\,N/mm^2$ for the stress-relieved condition ($N = 2 \times 10^6$ cycles, $P_f = 50\%$).

The notch stress concentration at the toe ($\rho_f = 1$ mm) of the flat-fillet weld around the attachment end is evaluated based on the three-dimensional boundary element method. Because of the threefold symmetry of the specimen, only one eighth of it had to be modelled, Fig. 4.46. The geometry is described by surface elements. The structural components 'plate', 'attachment' and 'weld' are defined as substructures. Relevant symmetry conditions and edge displacement u_x simulating the tensile load are introduced.

A fatigue notch factor $K_f = 3.2$ was found (a preliminary factor $K_f = 2.7$ was reported by Petershagen[262] based on the rather coarse mesh shown in Fig. 4.46) Using the endurable fully reversed stress amplitude σ_A = 145 N/mm^2 of the mill-finished low strength structural steel in the non-welded condition ($N = 2 \times 10^6$ cycles, $P_f = 10\%$), see Table 4.4, the endurable nominal stress amplitude for the longitudinal attachment specimen in high strength steel gives $\Delta\sigma_{nE} = 2\sigma_A/(0.9K_f) = 101$ N/mm^2. The comparable value from testing was $\Delta\sigma_{nE}$ = 117 N/mm^2 for the stress-relieved specimen. The endurable stress range for the as-welded condition was lower, $\Delta\sigma_{nE}$ = 96 N/mm^2.

The conclusion is that the fatigue strength of the welded joint made of high strength steel can be assessed based on the endurance limit of low strength steels as far as the as-welded and sharply notched condition is con-

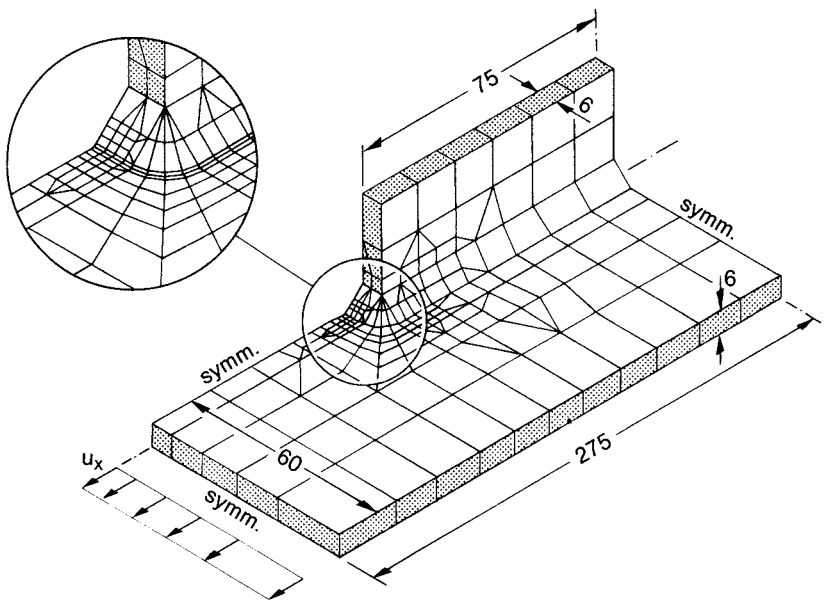


Fig. 4.46. Tensile specimen with double-sided longitudinal attachment, three-dimensional boundary element model, one symmetry eighth of the total structure; after Petershagen.[262]

sidered. The question to what extent the higher strength of the parent metal can be made effective in the welded joint is not discussed here. Reduction of the notch stress concentration is one precondition for making the higher tensile strength fatigue-effective.

A comparable investigation in the fatigue strength of longitudinal attachment joints in steel based on the notch stress approach has been performed by Janosch and Debiez[233] considering different welding procedures (GMA and MMA welding, with and without closing the weld around the attachment ends, as well as with different restart positions), the loading condition being pure bending of the base plate. The mean value of the actual toe notch radius was used ($\rho = 0.7$ mm) and Dang Van's multiaxial strength criterion applied. The endurable notch stresses correlated roughly with those given by Olivier *et al.*[259,260] within the modified notch rounding approach ($\rho_f = 1$ mm).

4.3.8 Gusseted shell structure

This example refers to the notch rounding, approach, modified version according to Seeger. It has been chosen to demonstrate that quantitative statements on a well defined statistical basis are possible. It is not restricted to relative statements as are the aforementioned examples given by Radaj. It avoids the wide margins of adaptation contained in the examples above given by Petershagen.

The modified notch rounding approach has been applied by Köttgen *et al.*[245] to analyse early fatigue failure at the end of a gusset plate in the welded shell structure of a wind energy converter. The structure considered, made of type St52-3 structural steel, is a blade support journal about 6 m long and about 1.8 m in diameter with plate or shell thicknesses between 12 and 45 mm, Fig. 4.47(a). Early crack initiation and propagation at $N = 4 \times 10^5$ cycles occurred at the weld toe of the gusset plate end marked (A).

The rotor blade was mounted into the support journal. The loading was transferred by a fixed bearing at the top and a movable bearing at the bottom of the journal. The predominant loading was the dead weight of the rotating blade (17×10^3 kg), generating a cyclic axial force and a cyclic swivelling moment.

The cyclic nominal stress $\Delta\sigma_n$ at the end of the gusset plate was calculated as membrane stress according to the simple tube bending theory. This stress was permissible according to Eurocode 3,[23] notch or detail class 56 with a safety factor $j_\sigma = 1.37$ against the endurable stress at $N = 2 \times 10^6$ cycles and corresponding to $P_f = 2.3\%$, Table 4.8. The fatigue strength assessment is demonstrated for the finite life of 2×10^6 cycles by way of example. The true endurance limit at $N \geq 10^7$ cycles should be chosen for design purposes. On the other hand, the failure analysis performed by Köttgen *et al.*[245]

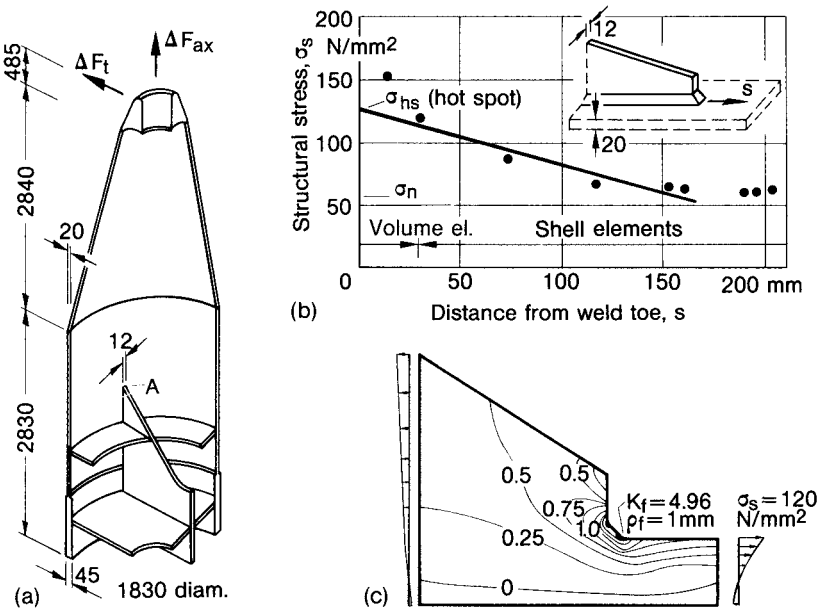


Fig. 4.47. Blade support journal of wind energy converter with fatigue failure at point A (a), structural stresses (b) and notch stresses at gusset plate end (c) inclusive of the fatigue notch factor found by finite element analysis; after Köttgen *et al.*[245]

had to consider the situation at $N = 4 \times 10^5$ cycles on the basis of a normalised S–N curve fixed at $N = 2 \times 10^6$ cycles.

The cyclic structural stress $\Delta\sigma_s$ at the end of the gusset plate was determined based on a finite element analysis of the shell structure. The end of the gusset plate was modelled with solid elements. The linear extrapolation of the surface stresses to the weld toe (i.e. the hot spot) resulted in $\Delta\sigma_{hs} = 128\,\text{N/mm}^2$, but did not correspond to code regulations and included a high degree of arbitrariness in respect of the selected extrapolation points, Fig. 4.47(b). Despite the arbitrariness, it is definitely shown that the structural stress at the gusset plate end is much higher than the nominal stress above mainly because of local shell bending. Using this structural stress as 'modified nominal stress', the permissible stress according to Eurocode 3 is substantially exceeded, Table 4.8.

The British design standard BS7608[15] specifies for the structural detail considered that the design stress has to include the local bending stress adjacent to the weld ends. This stress $\Delta\sigma_n = \Delta\sigma_s = 128\,\text{N/mm}^2$ has to be compared with the permissible stress $\Delta\sigma_{n\,per} = 68\,\text{N/mm}^2$ (standard S–N curve with designation F) which is substantially exceeded.

Table 4.8. Fatigue strength assessment based on different stress types for gusset plate end in welded shell structure of wind energy converter; after Köttgen *et al.*[245]

	Actual stress [N/mm²]	Endurable stress (N = 2 × 10⁶, P_f = 50%) [N/mm²]	Permissible stress (N = 2 × 10⁶, P_f = 2.3%) [N/mm²]	Ratio of actual to permissible stress
Nominal stress $\Delta\sigma_n$	56	77[a]	56[a]	1.0
Structural stress $\Delta\sigma_s$	128	77	56	2.3
Notch stress $\Delta\bar{\sigma}_k$	595	290[b]	212[b]	2.8

[a] Eurocode 3,[23] long attachment, not dependent on R, safety factor j_σ = 1.37 or failure probability P_f = 2.3%.
[b] Haigh diagram according to Olivier *et al.*,[259,260] Fig. 4.35, safety factor j_σ = 1.37 or failure probability P_f = 2.3%.

The cyclic notch stress $\Delta\bar{\sigma}_k$ at the weld toe with fictitious notch radius ρ_f = 1 mm is higher than the structural stress (mainly bending stress) at a distance of 1.5t from the weld toe by the concentration factor K_f = 4.96 resulting in $\Delta\bar{\sigma}_k$ = 595 N/mm², Fig. 4.47(c) (no arbitrariness included). This stress has to be compared with the permissible notch stress based on endurable stresses according to Fig. 4.34, modified for R = 0.4 according to the Haigh diagram in Fig. 4.35 (same value with or without welding residual stresses). Obviously, the permissible stresses are once more substantially exceeded, Table 4.8.

The conclusion from the above analysis is that fatigue cracks will actually occur at $N = 4 \times 10^5$ cycles under the actual structural and notch stresses, and that local shell bending at the gusset plate end is the reason for the fatigue failure.

4.3.9 Laser beam welded butt and cruciform joints

This example has been chosen to demonstrate the application of the notch stress approach within the assessment of fatigue strength of laser beam welded joints in relation to conventional welded joints. The considered plate thickness was t = 8–20 mm.

Laser beam penetration welding (i.e. keyhole welding) generates a slim and deep fusion zone thus altering the cross-sectional shape of these joints in relation to conventional joints. Butt joints are possible by single-side welding even with larger plate thickness generating only slightly tapering weld shapes with only small reinforcement on the top and bottom side, at

least under high-quality production conditions. The notch stress concentration at such welds is rather low. Keyhole-welded cruciform joints, on the other hand, present increased notch stresses at the weld toe while root faces are completely avoided. Welding distortions are relatively small in laser beam welded joints. The maximum hardness in the heat-affected zone of structural steels is increased, but also confined to thinner layers.

Based on the notch stress approach, Weichel and Petershagen[339] found for butt joints and cruciform joints that the endurable nominal stress in laser beam welded joints can be set equal to the corresponding stress of conventional welded joints, i.e. the same notch or detail classes are applicable. The notch stress approach, version according to Seeger, applied to the considered joints gave no contradiction to the endurable stresses according to Table 4.5.

The notch stress approach with extensions into the notch strain and crack propagation approaches was applied to laser beam welded joints in high strength steels by Dahl and Reinhold.[220] A modification of the approach according to Ring[307] on the basis of procedural elements from the versions of Lawrence, Radaj and Seeger was used. The fatigue strength of laser beam welded butt joints and cruciform joints was experimentally found to be up to 50% higher than the corresponding conventional welded joints. But this increase was bound to a plate edge preparation by milling which substantially reduces pore formation and other weld imperfections.

The conclusion from the above analyses related to laser beam welded joints is that the applied local approaches give useful explanations in qualitative terms while quantitative statements are connected with rather large uncertainties.

4.4 Design-related notch stress evaluations

4.4.1 Comparison of basic welded joint types

The notch stress approach, notch rounding version according to Radaj, can be used to assess the fatigue strength of welded joints and structures either in an absolute way based on the local fatigue strength values of the material (as demonstrated in Section 4.3) or in a relative way by comparing different designs of the same material (and comparable residual stresses) without knowledge of the endurable notch stresses, based only on knowledge of the radius of fictitious notch rounding. The latter simplified approach is of considerable value for designers especially when developing new variants from previous well-proven designs. The procedure is easy to use insofar as only a stress analysis of cross-sectional models is necessary. On the other hand, this first rough assessment should be followed by a refined analysis in later design stages taking further influencing parameters

of fatigue strength into account. The results of an extensive design-related notch stress evaluation by Radaj and Helmers[293] are summarised below.

The basic joint types selected for didactic purposes according to their practical relevance are assigned to the following groups: butt joints, cruciform joints, attachment joints, lap joints and corner joints. 'Cruciform joints' are characterised by load-carrying welds whereas the welds in 'attachment joints' are non-load-carrying. Note that the attachment joint may also be of cruciform shape.

Within each group, often used or critically to be discussed variants of plate arrangement, weld positioning and weld shape (including slim shapes from keyhole welding and wide shapes from resistance spot welding) are considered. Small to medium plate thicknesses are evaluated. Some typical imperfections are also referenced.

Only one choice of the dimensions is analysed in each case. It must be kept in mind that the resulting fatigue notch factor depends on the absolute dimensions chosen, for example on the plate thickness.

The welded joints considered are assumed to be made of low strength structural steel. A uniform fictitious notch radius, $\rho_f = 1\,\text{mm}$, is introduced to calculate the fatigue notch factors. This radius corresponds to a worst case consideration. It is also used hereafter in the case of spot welds instead of the lower value, $\rho_f = 0.6\,\text{mm}$, which may be more appropriate (see Section 11.2.1). Note, that the fatigue notch factor also depends on the size of the welded joint (i.e. its absolute dimensions), not only on its shape (i.e. its dimensional ratios), because of the constant fictitious notch radius.

The cross-sectional models are tensile or bending loaded by edge stresses[293] whereas the older investigation[4,284,295] was based on edge displacement loading. The differences in the results of the two loading modes are discussed subsequently.

The fatigue notch factors at the weld toe and weld root were calculated by applying the boundary element method to the cross-sectional models. They were corrected in cases of fictitious undercut or cover plate softening (according to Section 4.2.7). Only one half or one quarter of the model was analysed if symmetry conditions were appropriate. The fatigue notch factors of the weld toe and weld root (in this sequence) are given in the relevant figures under each joint graph. In design applications, additional information on the details of the stress distribution along the contour lines may be helpful. The corresponding plots can be found in the first edition of this book. These plots include the non-corrected stress concentration factors.

Welded butt joints

The conclusions concerning welded butt joints under tensile load, Fig. 4.48, are summarised in the following. First row: an undercut and a root face are

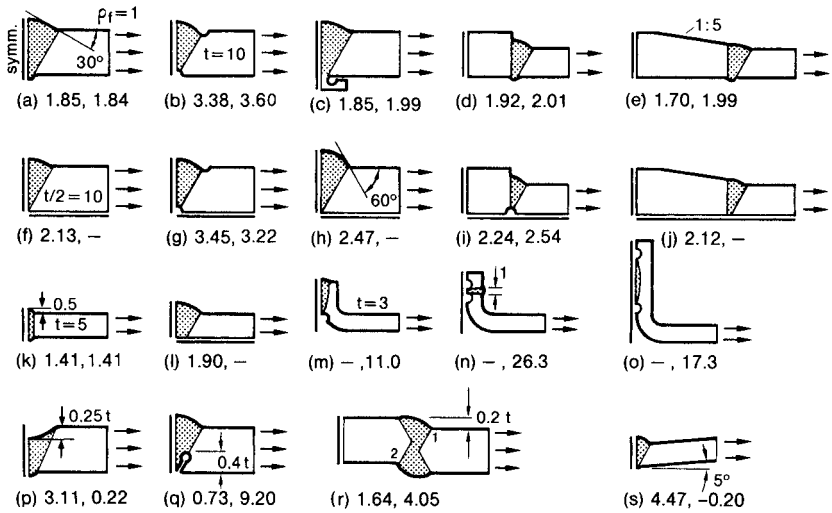


Fig. 4.48. Butt joints, tensile loaded, fatigue notch factors at weld toe, K_{ft} (first number) and weld root, K_{fr} (second number) calculated by Radaj and Helmers[293] using the boundary element method:

First row, single-V butt welds: with root capping pass or ceramic backing strip (a), with toe undercut and root face (b), with backing strip (c), at abrupt change of plate thickness (d), at gradual change of plate thickness (e).

Second row, double-V butt welds: standard type (f), with toe undercut and root face (g), with excessive weld reinforcement (h), at abrupt change of plate thickness (i), at gradual change of plate thickness (j).

Third row, special weld types: keyhole square butt weld (k), double-V butt weld with enlarged groove width (l),flanged edge keyhole slot weld (m),flanged-edge keyhole lap weld (n),flanged-edge resistance spot weld (o).

Fourth row, weld imperfections: sagging (p), lack of fusion at weld root (q), axial misalignment (r), angular misalignment (s).

detrimental, a backing strip is advantageous, tapering is rather ineffective. Second row: the conclusions from the first row are confirmed, the fatigue notch factors are enlarged, a short internal root face is acceptable, an excessive flank angle or a weld reinforcement is detrimental. Third row: the keyhole square butt weld is advantageous, flanged edge welds are detrimental. Fourth row: weld imperfections are detrimental to the extent of eccentricity and cross-sectional weakening. Some of the shape parameters are additionally discussed:

– Unsymmetrical shape relative to the loading direction results in a stress reduction at the toe and a corresponding stress increase at the root (compare (b) with (g)).

- Increased flank angle or weld reinforcement increases the toe stresses as expected (compare (f) with (h)).
- Abrupt change of plate thickness is less detrimental than expected, tapering of the plate edge therefore rather ineffective (compare (d) with (e) or (i) with (j)).
- Keyhole square butt welds with small reinforcement have lower stress concentrations than conventional welds (compare (k) with (a) and (f)).
- Flanged edge welds are detrimental because of the peel bending moment which should be kept as small as possible (compare (m), (n) and (o) with other joints).
- Toe undercut, open root face and other imperfections should be avoided (compare (b) with (a) and see (p), (q), (r) and (s)).

Welded cruciform joints

The conclusions for welded cruciform joints under tensile load, Fig. 4.49, are summarised in the following. First row: generally high fatigue notch factors, they are higher at the weld root than at the weld toe, a reduction of the root face length is advantageous, an undercut is detrimental, a concave fillet is only with sufficiently reduced root face length acceptable, a convex fillet is worse than a flat fillet. Second row: generally low fatigue notch factors, an internal root face is acceptable, an open root face is detrimental, a stress reduction at the toe and a stress increase at the root occur with the single-bevel weld relative to the double-bevel weld. Some of the shape parameters are additionally discussed:

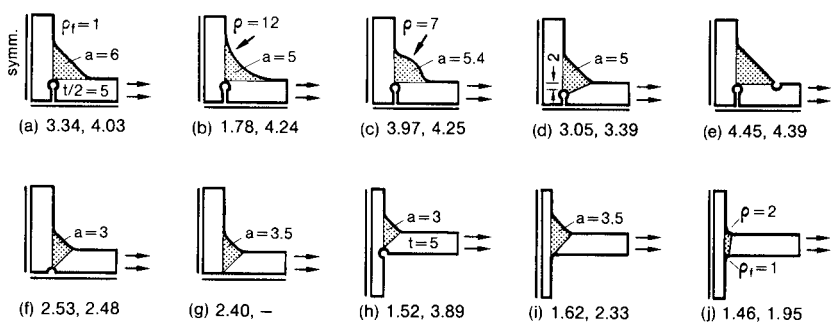


Fig. 4.49. Cruciform joints, tensile loaded, fatigue notch factors at weld toe, K_{ft} (first number) and weld root, K_{fr} (second number) calculated by Radaj and Helmers[293] using the boundary element method: flat fillet weld (a), concave fillet weld (b), convex fillet weld (c), deep penetration fillet weld (d), fillet weld with undercut (e), double-bevel butt weld with root face (f), double-bevel butt weld without root face (g), single-bevel butt weld with root face (h), single-bevel butt weld without root face (i), keyhole butt weld (j).

– Root face length reduction by deep penetration welding or corresponding groove preparation should be combined with the outside weld shape improvement in order to avoid early root failures (compare (d) with (a), (b) and (c)).
– Double-bevel butt welds with or without root face achieve the best results (compare (f) and (g) with (a) to (c)).
– Unsymmetrical shape relative to the loading direction results in a stress reduction at the toe and a corresponding stress increase at the root (compare (h) with (f), or (i) with (g)).
– Toe undercut is detrimental (compare (e) with (a)).
– Keyhole butt welds without imperfections can be superior to single bevel butt welds without root face (compare (j) with (i)).

Welded transverse attachment joints

The conclusions for welded transverse attachment joints, Fig. 4.50, are summarised in the following. First row: generally low fatigue notch factors,

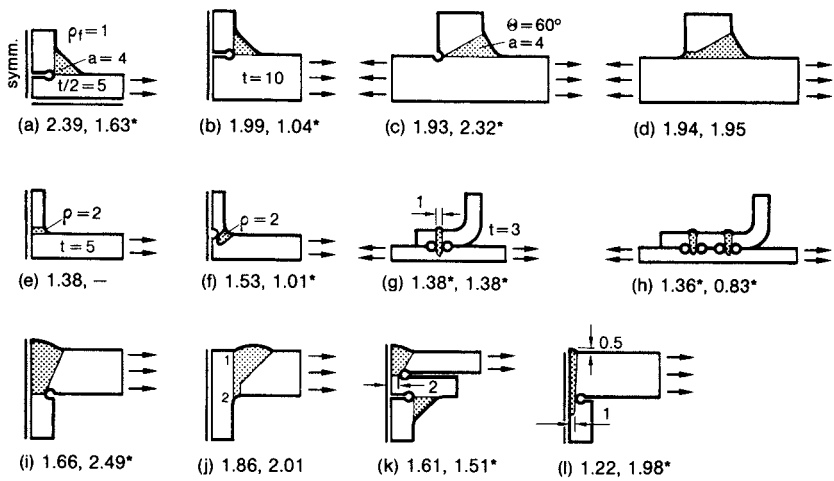


Fig. 4.50. Transverse attachment joints, tensile loaded, fatigue notch factors at weld toe, K_{ft} (first number) and weld root, K_{fr} (second number) calculated by Radaj and Helmers[293] using the boundary element method (the numbers with an asterisk are reduced for fictitious undercut): double-sided attachment with fillet welds (a), single-sided attachment with fillet welds (b), single-sided attachment with single-bevel butt weld and root face (c), single-sided attachment with single-bevel butt weld without root face (d), horizontal keyhole square butt weld (e), diagonal keyhole square butt weld with root face (f), single-keyhole lap weld (g), double-keyhole lap weld (h), V-butt-welded T-joint (i), single-bevel butt-welded T-joint with root capping pass or ceramic backing strip (j), V-butt-welded T-joint with backing strip (k), keyhole-square-butt-welded T-joint (l).

lower values appear at the weld root than at the weld toe in case of internal root faces, the single sided attachment is superior to the double sided attachment, an open root is detrimental. Second row: generally low fatigue notch factors, both the single and double lap welds are acceptable. Third row: low fatigue notch factors, an open root face is detrimental. Some of the shape parameters are additionally discussed:

- Unreduced internal root face length is acceptable in comparison to the toe notch effect (see (a) and (b)).
- Unsymmetrical shape relative to the loading direction results in a stress reduction at the toe (compare (b), (c) and (d) with (a)).
- Open root faces result in high root stresses (see (c) and (i)).
- Keyhole welds show low toe and root stresses (see (e) to (h) and (l)).
- Three-plate T-joints subjected to through-tension loading exhibit no excessive stress concentration (see (i) to (l)).

Welded lap joints

The conclusions for welded lap joints under tensile load, Fig. 4.51, are summarised in the following. First row: high fatigue notch factors, they are lower at the root than at the toe, the single keyhole weld is unacceptable (extreme bending stresses appear in the joint face). Second row: the fatigue notch factors are lowered at the toe and heavily increased at the root, this being detrimental, the single keyhole weld is even more unacceptable. Third row: low fatigue notch factors, all the welds are acceptable. Fourth row: also low fatigue notch factors, they are lowered at the toe in relation to the double side cover plate. Fifth row: low fatigue notch factors appear only with the V-butt weld, high factors appear without this weld. Some of the shape parameters are additionally discussed on the basis of the largest fatigue notch factor of the joints considered:

- Cover plate joints are far superior to lap plate joints (compare third with first row and fourth with second row).
- Unsymmetrical shape relative to the loading direction results in a stress reduction at the toe and a stress increase at the root (compare second with first row and fourth with third row).
- Joggle lap joints with butt weld are far superior to lap plate joints, but not so without this weld (compare fifth with second row).
- Diagonal keyhole welds are superior to conventional fillet welds (compare second with first column without last row).
- Lap plate joints with perpendicular keyhole weld are acceptable only with twin welds (compare (d) with (c) and (i) with (h)).
- Cover plate joints with perpendicular keyhole weld are also acceptable with single welds (compare (m) with (n) and (r) with (s)).

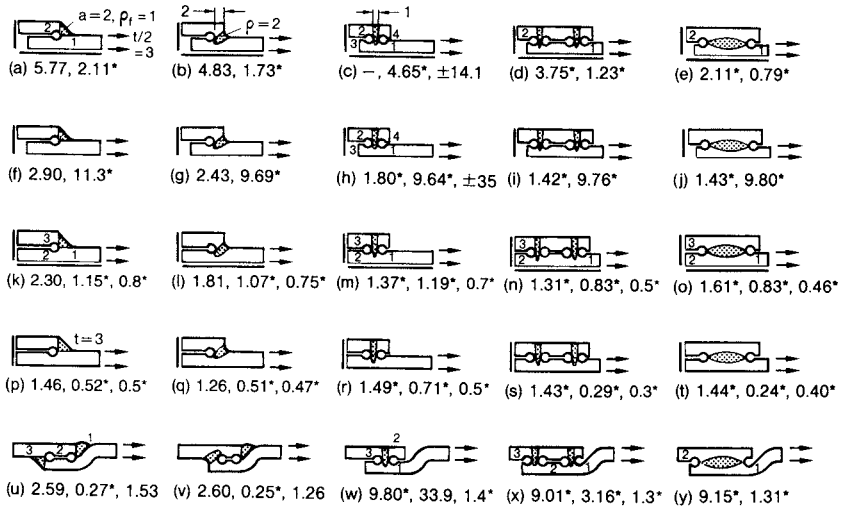


Fig. 4.51. Lap joints, tensile loaded, fatigue notch factors at weld toe, K_{ft} (first number) and weld root, K_{fr} (first to third number, sequence according to the numerals at the notches) calculated by Radaj and Helmers[293] using the boundary element method (the numbers with an asterisk are reduced for fictitious undercut or/and modified in the case of two-sided cover plates):

First row: double-sided lap plate.
Second row: single-sided lap plate.
Third row: double-sided cover plate.
Fourth row: single-sided cover plate.
Fifth row: joggle lap joint.

First column: conventional fillet weld.
Second column: diagonal keyhole weld.
Third column: perpendicular single keyhole weld.
Fourth column: perpendicular twin keyhole welds.
Fifth column: resistance spot weld.

– Resistance spot welds (with small enough pitch resulting in comparable structural stress values) are often equivalent to perpendicular twin or diagonal single keyhole welds in lap joints (compare fifth with fourth or second column without first and last row).
– Resistance spot welds (with small enough pitch resulting in comparable structural stress values) are generally superior to conventional fillet welds in lap joints (compare fifth with first column without last row).

Welded corner joints

The conclusions for welded corner joints under bending load, Fig. 4.52, are summarised in the following. High fatigue notch factors appear for the joint

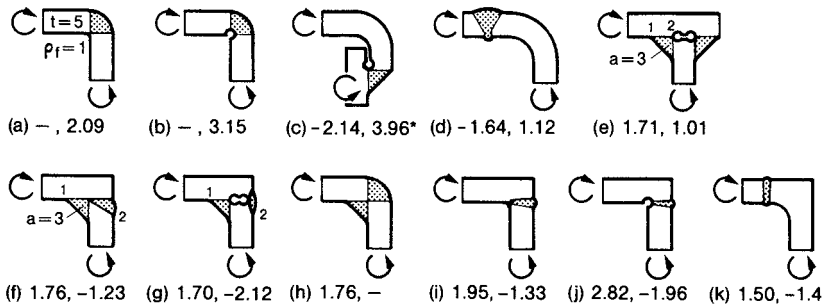


Fig. 4.52. Corner joints loaded by bending moments, fatigue notch factors at weld toe, K_{ft} (first number) and weld root, K_{fr} (second number), or according to the numerals at the notches, calculated by Radaj and Helmers[293] using the boundary element method (the numbers with an asterisk are reduced for fictitious undercut): corner V-weld without root face or root imperfection (a), corner V-weld with root face (b), lap fillet weld (c), curved corner with V-butt weld (d), double-fillet weld (e), single-bevel corner weld with inside fillet weld (f), outside pad weld with inside fillet weld (g), corner V-weld with inside fillet weld (h), keyhole square butt weld without root face (i), keyhole square butt weld with root face (j), rounded corner with keyhole square butt weld (k).

types with an open root face and for the pad weld without deep penetration, low factors appear in the other cases, the lowest factors appear for the preshaped corner plate. Some of the shape parameters are additionally discussed:

- The weld notch at the inside of the corner is the critical one with the exception of the outside pad weld joint (see (a) to (c), (e), (f) and (h) to (j)).
- Undercut or open root face should be avoided at the inside of the corner (see (b), (c) and (j)).
- The conventional flat fillet weld at the inside of the corner supplementing welding from the outside is superior to the keyhole square butt weld (compare (e), (f) and (h) with (i)).
- Joints with preshaped corner region and the weld outside this region are superior to the other joints (compare (d) and (k) with (a) to (c) and (e) to (j)).

4.4.2 Comparison of basic weld loading modes

Stress loading versus displacement loading

The cross-sectional models of welded joints discussed above are loaded by constant tensile stresses (with the exception of the bending-loaded corner

joints). The question arises what changes in the notch stresses occur by prescribing constant edge displacements instead of constant edge stresses, a loading case often met in structural components.

There are two reasons for changes. First, the overall stiffness of the joint controls the basic stress level in the case of displacement loading, i.e. lower stiffness is connected to lower stresses and vice versa. Second, a constant edge displacement causes not only constant tensile stresses but also linearly distributed bending stresses in the loaded edge if the shape of the joint is unsymmetrical transverse to the loading direction, i.e. the stress level is increased on the more rigid side and lowered on the other.

It has been shown by a comparative investigation[4,284,295] into fatigue notch factors that a tensile loaded fillet-welded cruciform joint with a sufficiently large root face length may have a fatigue strength in terms of displacement amplitudes which is not lower than the fatigue strength of the butt-welded joint with a small root face. The difference between the two loading modes is more pronounced if bending effects come in, e.g. for the T-joint under transverse force loading (Radaj,[4] *ibid*. p. 225).

As an example of superimposed bending effects, the calculated fatigue notch factors of two unsymmetrical V-butt weld joints, one with root pass and the other with root face (Radaj,[4] *ibid.* Fig. 167 to be compared with Fig. 4.48 here), are considered under stress and displacement loading, respectively, Table 4.9.

Longitudinal shear loading

Longitudinal shear loading of the weld (corresponding to anti-plane shear loading of the cross-sectional model) is the second basic loading state apart from transverse tension loading which contributes to the total loading state of the weld. Further loading states are longitudinal tension loading, transverse shear loading, longitudinal and transverse bending loading. It is shown by the notch stress theory that the stress concentration factors of simple

Table 4.9. Fatigue notch factors of two V-butt welds in two tensile loading modes; after Radaj[4,284,293,295]

V-butt weld (t = 10 mm)	Stress-loaded joint[293]		Displacement-loaded joint[295]	
	K_{ft}	K_{fr}	K_{ft}	K_{fr}
Weld with root pass	1.85	1.84	1.89	1.69
Weld with root face	1.72	3.63	1.87	3.42

notch cases are uniformly lower in anti-plane shear loading than in tension loading for identical shape parameters of the cross-sectional model (shallow notch formula according to eq. (4.36)).

This fact is confirmed for the more complex notch configurations of welded joints by Radaj and Zhang[303] using the boundary element method (potential field version), Fig. 4.53. These notch stress concentration or fatigue notch factors may be compared with the corresponding factors in tensile displacement loading (see Radaj[4,284,295]) under the condition of identical fictitious notch radii, $\rho_f = 1$ mm, upper row numbers in the figure, and under the condition of a smaller notch radius, $\rho_f = 0.2$ mm, considered valid in antiplane shear loading, lower row numbers in the figure. All the factors are definitely lower in anti-plane shear loading than in tension loading and the ratios of corresponding factors are very similar, provided the secondary bending effects caused by displacement loading of unsymmetrical weld shapes are disregarded. Therefore, the conclusions derived for the tensile loaded welded joints can be transferred to the longitudinal shear loaded welded joints.

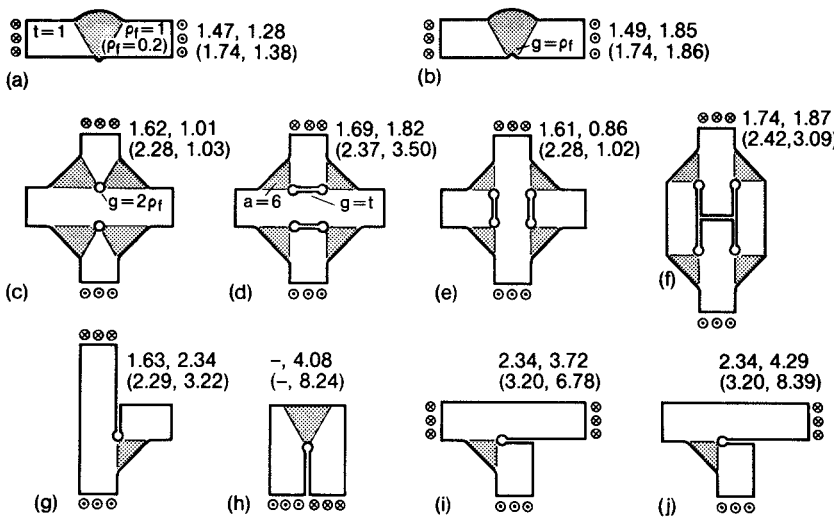


Fig. 4.53. Cross-sectional models of welded joints under anti-plane shear loading, plate thickness $t = 10$ mm and root face length $g = t$, $g = 2\rho_f$ or $g = \rho_f$, fatigue notch factors according to the boundary element method at weld toe (first number) and weld root (second number) for $\rho_f = 1$ mm (upper lines, without parentheses) and $\rho_f = 0.2$ mm (lower lines with parentheses): butt joints (a, b), cruciform joints (c, d), transverse attachment joints (e, g), lap joint (f), edge-welded joint (h), T-joint (i), and corner joint (j); after Radaj and Zhang.[303]

Biaxial oblique loading

Superposition of tension and longitudinal shear loading can be considered to be the most important biaxial oblique loading state of welded joints because it is highly notch stress effective. The third component, longitudinal tension loading is assumed to be free of a notch effect. Bending and transverse shear loading which are also notch-effective are dealt with farther below.

The superposition of tension and longitudinal shear loading can be analysed based on the stress concentration and fatigue notch factors of the underlying 'pure' loading states because the maximum notch stresses occur at approximately the same position at the notch root in the two cases. Thus, the relevant strength hypothesis can be applied directly to the maximum notch stresses.

Results of calculations for the cruciform joint and the transverse attachment joint considered to be typical for welded joints in general are plotted in Fig. 4.54 and 4.55, respectively. The 'internal force splitting method' was applied. The maximum notch stresses calculated according to the boundary element method for the cross-sectional models of the welded joints in tension and longitudinal shear loading, respectively, are superimposed under plane strain conditions for varying oblique angles of the weld notch relative to the principal direction of the basic loading state for three biax-

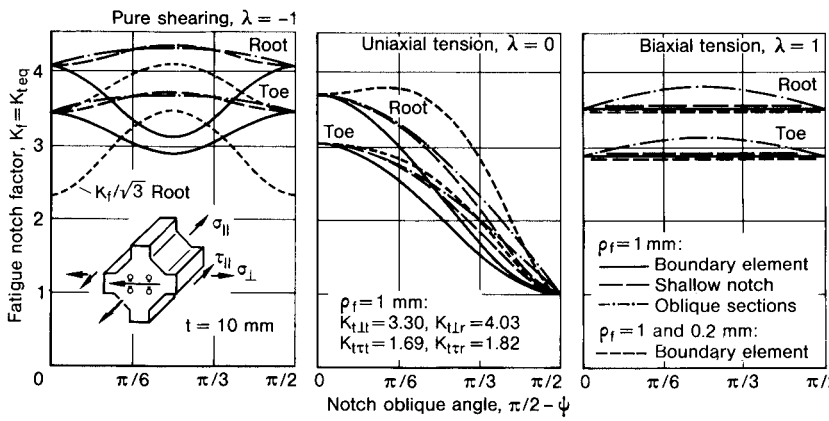


Fig. 4.54. Fatigue notch factor at weld toe and weld root of cruciform joint under biaxial oblique loading; dependence on notch oblique angle for three biaxiality degrees (see Fig. 4.30), fictitious notch radius ρ_f = 1 mm in tension and longitudinal shear loading (boundary element results, shallow notch formula and oblique sections formula), fictitious notch radii ρ_f = 1 mm in tension and ρ_f = 0.2 mm in longitudinal shear loading (boundary element results), reduction $K_f/\sqrt{3}$ (weld root) introduced for graphical reasons; after Radaj and Zhang.[303]

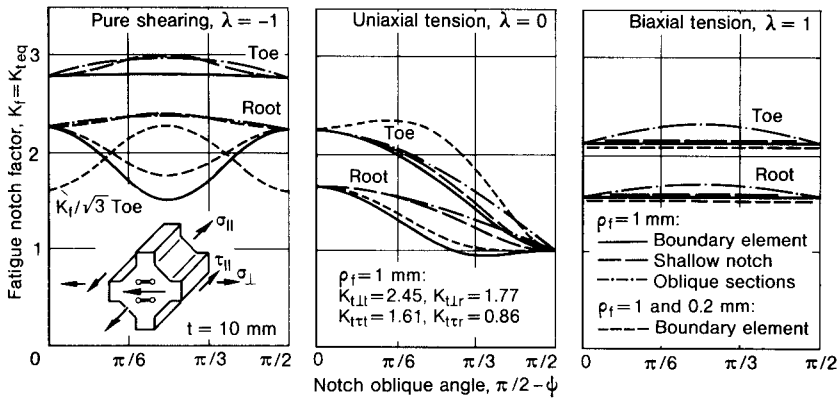


Fig. 4.55. Fatigue notch factor at weld toe and weld root of transverse attachment joint under biaxial oblique loading; dependence on notch oblique angle for three biaxiality degrees (see Fig. 4.30), fictitious notch radius ρ_f = 1 mm in tension and longitudinal shear loading (boundary element results, shallow notch formula and oblique sections formula), fictitious notch radii ρ_f = 1 mm in transverse tension and ρ_f = 0.2 mm in longitudinal shear loading (boundary element results), reduction $K_f/\sqrt{3}$ (weld root) introduced for graphical reasons; after Radaj and Zhang.[303]

iality conditions of this state (see Fig. 4.30 and eqs. (4.39–4.46)). For similar results according to the 'principal internal force method' see Radaj[4] (*ibid.* pp. 179–180).

The calculation was performed for identical notch radii, ρ_f = 1 mm, in tension and shear loading (including the shallow notch solution, eq. (4.37), and the oblique sections approach, eqs. (4.45) and (4.46)), and alternatively for ρ_f = 1 mm in tension loading combined with ρ_f = 0.2 mm in shear loading. The results in both cases are fatigue notch factors, $K_f = K_{t\,eq}$ resulting from the factors $K_{t\perp}$ and $K_{t\tau}$ in tension and shear loading, respectively, for the weld toe (supplementary index t) and weld root (supplementary index r) on the basis of the von Mises distortional strain energy criterion. The combination of ρ_f = 1 mm and ρ_f = 0.2 mm is supported by the notch stress theory but has not yet been confirmed by fatigue testing. A minimum in fatigue strength should occur with pure shear loading of the weld ($\lambda = -1$, $\psi = 45°$) if the above assumption is correct. On the other hand, the solution with identical notch radii is considered to be easier to apply.

The most important conclusion from the diagrams is that the cross-sectional model under uniaxial tension load gives an approximately correct fatigue notch factor (at least under the condition of identical notch radii) in arbitrary biaxial loading states, so that the calculation procedure can be drastically simplified for engineering purposes. The fatigue notch factor of

the weld can be predicted on the basis of the first principal stress in front of the weld applied to the cross-sectional model ('principal internal force method', see Section 4.2.8). The more accurate procedure superimposes the notch effects in tension and bending loading on the one hand and longitudinal shear loading on the other hand as described above ('internal force splitting method', see Section 4.2.8).

Bending loading modes

It is known from the notch stress theory that the stress concentration factors of simple notch configurations are reduced in bending loading relative to tensile loading and that even lower factors occur in anti-plane shear loading. This relation was tested with three typical welded joints, a butt joint, a cruciform joint and a transverse attachment joint, Fig. 4.56. The relation mentioned above is not completely confirmed. The toe factor of the butt joint is lower in tensile than in bending loading which can be explained from the unsymmetrical shape transverse to the loading direction. The effect of unsymmetry on the notch stress is strong in tensile but weak in bending loading. The root factors are extremely low for the cruciform and attachment joint in bending loading, explicable on the basis of the bending stress decrease over the cross-sectional depth so that the factors in anti-

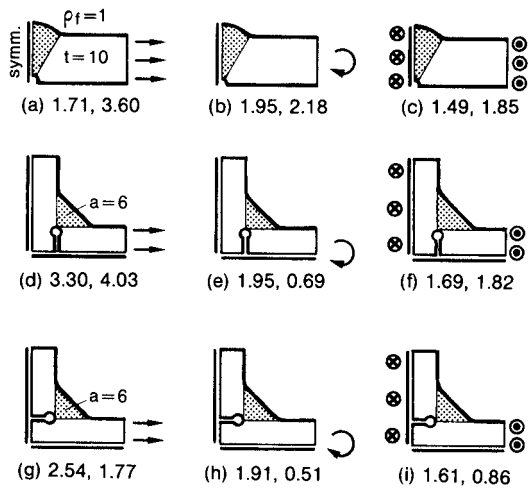


Fig. 4.56. Typical welded joints in tensile (a, d, g), bending (b, e, h) and anti-plane shear (c, f, i) loading; fatigue notch factors at weld toe, K_{ft} (first number), and weld root, K_{fr} (second number), calculated by Radaj and Helmers[293] using the boundary element method: butt joint with root face (a, b, c), cruciform joint (d, e, f), and double-sided transverse attachment joint (g, h, i).

plane shear loading are higher than in bending loading. The reduction in shear loading is not quite realistic because $\rho_f = 1$ mm might be too large in this loading case (see Section 4.2.6).

Superposition of the above loading states results in the addition of the fatigue notch factors of tensile and bending loading and means that the fatigue notch factor of anti-plane shear loading must be taken into account within the valid strength hypothesis. This simple procedure is possible because the stress concentrations of the different loading states occur at nearly the same point of the notch contour.

The loading conditions of welded joints in structural components are often more complex than indicated by the simple cases of tensile, bending and anti-plane shear loading considered above. Especially, in-plane shear loading by transverse forces is an often found loading state. The maximum notch stresses in the different loading states then occur at different positions on the notch contour so that a simple additive superposition of the fatigue notch factors is not possible. It is necessary in these more complex cases to superimpose the local notch stresses (instead of the maximum values) of the loading state components and to determine the maximum thereafter.

A complex loading state of T-joints which can be decomposed into the transverse force F and the bending moment M_b is shown in Fig. 4.57. Force and moment are independently adjustable including the two limit cases where F or M_b are zero. The fatigue notch factor of the lower fillet weld toe is controlled primarily by the transverse force and that of the upper fillet weld toe primarily by the bending moment. The first one should therefore refer to the tensile nominal stress and the second one to the bending nominal stress. The fatigue notch factor of the fillet weld root and the keyhole weld throat on the other hand are controlled by both loading types. None of the two nominal stresses mentioned above is therefore preferable.

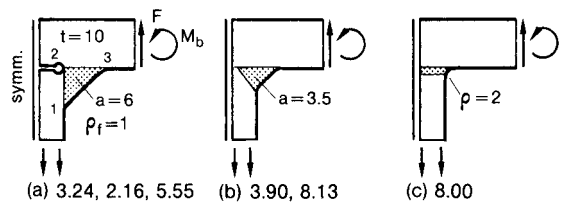


Fig. 4.57. T-joints loaded by transverse shear force F and bending moment M_b; T-joint, fillet-welded with root face (a) and without root face (b), as well as keyhole butt-welded (c); fatigue notch factors at weld toe, K_{ft} (first and second number), and weld root K_{fr} (third number), for pure shear force loading ($M_b = 0$) calculated by Radaj and Helmers[293] using the boundary element method.

In any case, the fatigue notch factors cannot be calculated separately and then superimposed.

The fatigue notch factors in the figure referring to the tensile nominal stress have been calculated for pure transverse force loading, i.e. with the bending moment M_b vanishing. The values of the lower toe notch of the fillet welds are comparable to those of tensile loaded cruciform joints because the bending effect at this notch can be neglected. The values at the corresponding upper notches and at the keyhole weld are much larger, caused by relatively high bending stresses in the relevant cross-section.

4.4.3 Effect of geometrical weld parameters

Effect of plate thickness

The fatigue strength of welded joints in terms of nominal or structural stress depends on the plate thickness. It decreases with increasing thickness. The decrease results to varying degrees from a more severe notch effect, from the statistical size effect, and from lower material and surface quality. The notch stress approach can give an indication of the decrease resulting from the notch effect but it has to be noted that the notch effect depends on further influencing parameters (e.g. attachment length) besides plate thickness and weld toe radius.

Notch stress analyses in respect of the effect of plate thickness on fatigue strength have been performed by Köttgen *et al.*[243] and Olivier *et al.*[259] using the boundary element method on the cross-sectional models of a corner joint and a T-joint, respectively. The models were fictitiously rounded at the weld toe ($\rho_f = 1$ mm) and subjected to bending moments. The exponent of thickness correction in eq. (2.24) resulted as $n \approx 1/3$, Fig. 4.58. This value is identical to the general recommendation from the review of Örjasäter[167] covering a large body of data from fatigue tests on welded joints in the 16–200 mm thickness range.

The thickness effect with postweld-treated joints was investigated by Soya *et al.*[327] on the basis of the notch stress approach. There was no marked influence of TIG dressing or shot-peening on the thickness effect whereas toe-grinding reduced the effect.

Effect of weld toe angle

A further important influencing parameter of the fatigue notch factor of welded joints is the weld toe angle. Its effect has been investigated for the double-V butt weld and the cruciform joint with flat fillet welds in tensile and bending loading by Anthes *et al.*,[205] Fig. 4.59. The toe angle at the butt weld can be substituted by the weld reinforcement height (simple geomet-

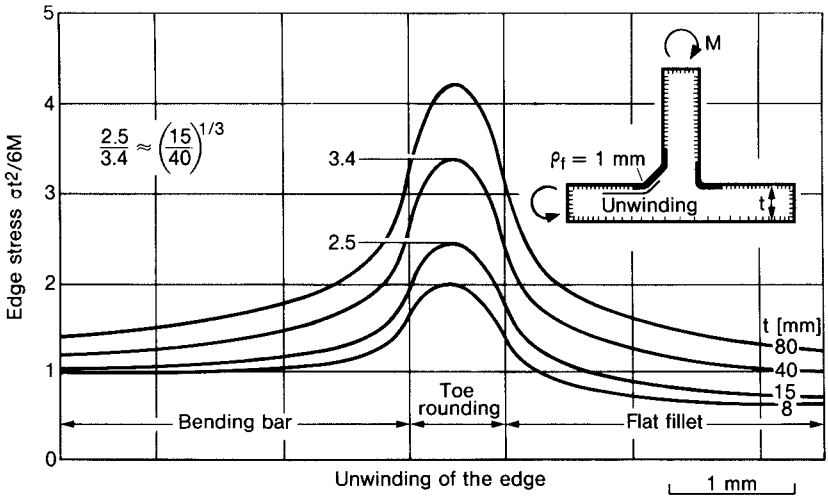


Fig. 4.58. Edge stress curves for different plate thicknesses, calculated by the boundary element method, maximum notch stress increasing with plate thickness according to a cubic root function; after Olivier *et al.*[259]

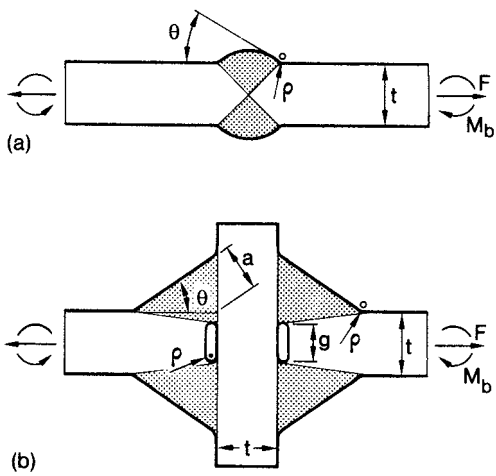


Fig. 4.59. Cross-sectional models of butt joints (a) and cruciform joints (b) for calculating the fatigue notch factors under tensile and bending loading; after Anthes *et al.*[205]

ric relation). The variation of weld toe angle at the cruciform joint was combined with variable root face length and weld throat thickness in the investigation. The ratio of notch radius to plate thickness was varied for both joints. The notch stress concentration factors were calculated using the

boundary element method. Simple engineering formulae are available for these factors as a function of the dimensional ratios.

The results of the above investigation are evaluated as stress concentration factors without introducing a definite fictitious notch radius for determining fatigue notch factors, Fig. 4.60 and Fig. 4.61. The diagrams are given for tensile loading whereas bending loading results in slightly lower stress concentration factors.

The stress concentration factors at the weld toe are rising with the weld toe angle for both joint types especially in the range $\theta \leq 60°$. The stress concentration factors at the weld root are higher than those at the weld toe for the throat to plate thickness ratio being considered, $a/t = 0.7$, especially with low weld toe angles. A higher ratio a/t brings the toe and root factors close together. The stress concentration factors at the weld root which are higher than those at the weld toe, especially in the case of low weld toe angles rise with the root face length ratio g/t. The conclusion for the designer is that weld toe angle and root face length should be reduced as far as possible and that the weld throat thickness should be increased up to the value of plate thickness in critical cases if the root face length cannot be reduced.

The stress concentration factors given above have been used by Anthes *et al.*[206] within the modified notch rounding approach in order to calculate the endurance limit of welded butt joints and transverse attachment joints in structural steel dependent on the weld toe angle for different plate thicknesses. Published fatigue test data correspond to the calculated curves. An

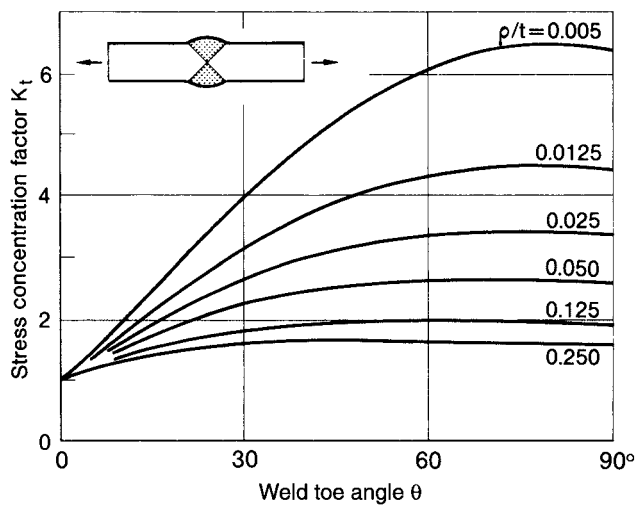


Fig. 4.60. Stress concentration factors of tensile loaded butt joints dependent on weld toe angle calculated by the boundary element method; after Anthes *et al.*[205]

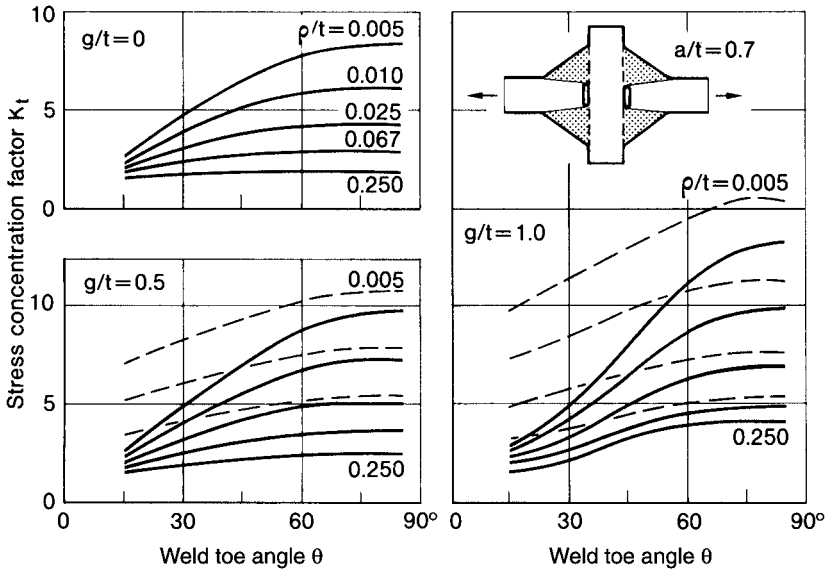


Fig. 4.61. Stress concentration factors at weld toe (solid curves) and weld root (dashed curves) of tensile loaded cruciform joints dependent on the toe angle of the fillet weld, calculated by the boundary element method for different root face lengths; after Anthes *et al.*[205]

application to welded joints in aluminium alloy is reported by Stötzel and Sedlacek,[328] whereas high strength steels are considered by Kaufmann *et al.*[241]

Effect of weld toe undercut

Weld toe undercuts reduce the fatigue strength of butt and fillet welded joints. The IIW guidance[31] on fitness for purpose evaluations defines this reduction in dependency on undercut depth and plate thickness based on the scatter band of available fatigue test results. Gosch and Petershagen[226] substantiated this recommendation by applying the notch rounding approach (fictitious notch radius according to eq. (4.29)) to a typical butt weld contour with undercut, Fig. 4.62, the corresponding cross-sectional model analysed by the boundary element method. The following geometric parameters have an influence on the notch stress concentration: undercut depth a, notch radius ρ, plate thickness t, reinforcement height h, notch opening angle β and reinforcement width w. Only the three first-mentioned parameters are of major influence, the reinforcement height is of minor influence, and the last-mentioned two parameters can be neglected within an undercut-typical parameter choice. The following parameter variations

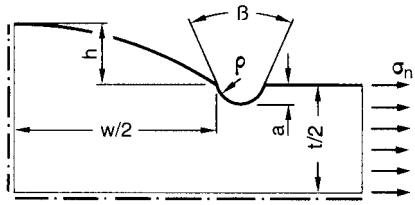


Fig. 4.62. Cross-sectional model of butt-welded joint with undercut (symmetry quarter) used in the notch rounding approach; after Gosch and Petershagen.[226]

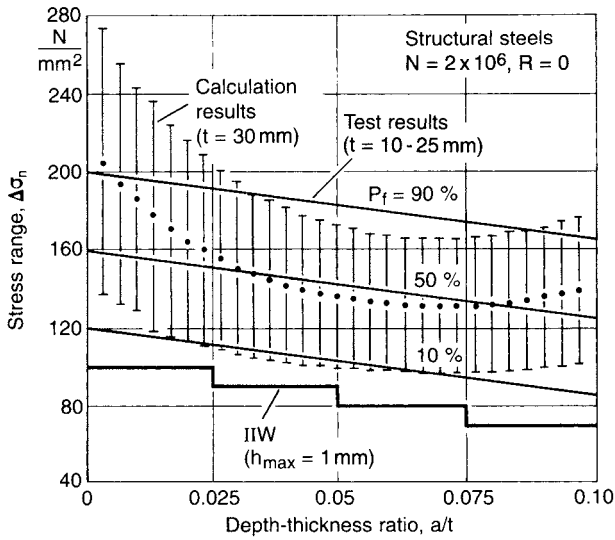


Fig. 4.63. Endurable stress range for welded joints made of structural steel, fitness for purpose assessment according to IIW guidance;[31] scatter range of test results compared with range of calculation results according to the notch rounding approach; after Gosch and Petershagen.[226]

were considered: $0.05 < a < 1.1$ mm, $0.1 < \rho < 5.6$ mm, $10 < t < 40$ mm, $1 < h < 5$ mm.

In order to compare the scatter band of test results with the calculation results, two sets of calculations were performed. In the first set, a given undercut depth a was combined with the smallest notch radius ρ and the largest reinforcement h to obtain the highest stress concentration and therefore the lowest endurable stress range. In the second set, the opposite combination gave the highest endurable stress range. The result of the investigation for $t = 30$ mm is shown in Fig. 4.63. The IIW guidance is sub-

stantiated for $a/t \geq 0.025$. The discrepancy for smaller values of a/t can be explained from too favourable parameter combinations in the calculation for high-quality butt welds. The conclusion is that the quality of welds with undercuts is defined only roughly on the basis of the easy to measure undercut depth as is prescribed by design codes (e.g. depth limit 0.25 mm according to AWS[82]). A more accurate assessment is possible on the basis of the notch stress approach which takes further geometric parameters such as plate thickness, notch radius and reinforcement height into account. The inadequacy of undercut depth alone has also been found by Bell *et al.*[211]

The notch stress approach was also applied by Janosch and Debiez[234] to (fillet-)welded joints in steel with undercuts (GMA and MMA covered electrode welding). Undercut depth and notch radius were measured and statistically evaluated resulting in Gauss-similar distributions of occurrence ($\rho \approx 0.5$–3.0 mm, $a \approx 0$–2.5 mm). It is shown that a uniform endurable notch stress can be derived on the basis of these data ($\Delta\sigma_{kE} = 300$–$380\,N/mm^2$ for zero-to-tension loading, $R = 0.1$). This stress is higher than the relevant stress in the analysis of Gosch and Petershagen[226] because the microsupport effect is included in the latter case. The multiaxiality of the notch stress state including residual stresses was taken into account by the Dang Van criterion.[222]

Shape-optimised weld contour

The fatigue strength of the weld toe is increased by enlarging the radius of notch curvature in the area of crack initiation. The fatigue effective fictitious notch radius is then given by $\rho_f = \rho + s\rho^*$, that is, $\rho_f = (\rho + 1)$ [mm] in the case of low strength structural steels. Additionally a small weld toe angle is advantageous.

A concave instead of a flat fillet is advantageous only as far as toe failures are considered and root failures can be excluded. This means that a concave fillet weld should be combined with a sufficiently reduced root face length. The weld contour at the weld toe can be further improved by noncircular shapes such as ellipses or parabolas which further enlarge the radius of notch curvature in the critical area.

The extended problem of optimising the contour shape to the extent that no stress increase occurs ($K_t \leq 1.0$) has been solved theoretically by considering the plate thickness transition in a stepped bar (solutions reviewed by Radaj[4,6] and Peterson[265]). It can be seen from the results that the thickness should initially increase very moderately, whilst there are various shapes acceptable in the remaining part of the transition.

Based on this knowledge, the tensile loaded cruciform joint with double-bevel butt welds with fillet welds (weld toe angle 30°) was optimised in respect of a minimum fatigue notch factor by iterative boundary element

calculations,[310] Fig. 4.64. The weld toe is ground to relatively large radii. The design version (a) is recommended for manufacturing on the spot, the design version (b) includes pre-manufactured plate ends.

4.4.4 Typical application in design

Design-related notch stress evaluations will be based as far as possible on simple formulae for stress concentration factors or fatigue notch factors. Stress concentration factors for welded joints as a function of shape parameters (i.e. of dimension ratios) have been given by several authors (see Sections 4.2.3 and 4.2.4). The approximative functional relationships are found by systematic trials and combined with a least square error fit in some cases. Systematic trials may be supported by the results of notch stress theory for simpler, mostly single-parameter notch cases. The main problem with these procedures is that the functional dependency to be established is generally a multiparametric one.

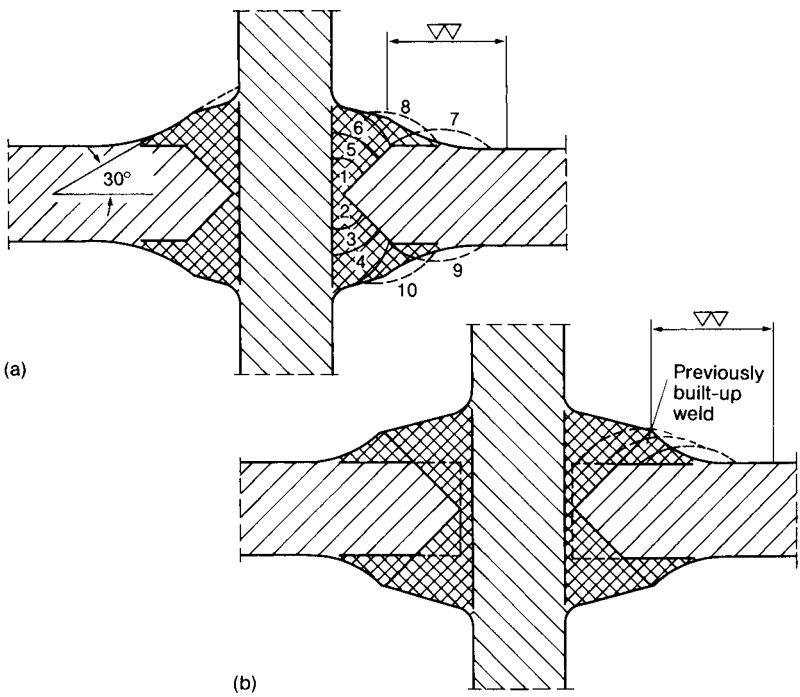


Fig. 4.64. Optimised contour shape at weld toe of tensile loaded cruciform joint; version (a) for manufacturing on the spot, version (b) with premanufactured plate ends; after Ruge and Drescher.[310]

Simple formulae and related graphs are needed to assess design options and to optimise a chosen design. It would be ineffective to solve these tasks solely by sequences of notch stress calculations for definite combinations of shape parameters using the finite element or boundary element method without being guided by approximative functional relations.

A generally applicable method for presenting stress concentration factors (or fatigue notch factors by introducing fictitious notch rounding) as simple functions of the shape parameters of a welded joint within restricted parameter ranges has been proposed by Radaj and Zhang.[301,302] The stress concentration or fatigue notch factor is described by the product of the mutually independent dimension ratios λ_v, each ratio with definite exponents p_v ($-1.0 \le p_v \le 1.0$), and by the coefficient k, eq. (4.9).

The method has been applied to the stress concentration factor of the tensile loaded cruciform joint with load-carrying flat fillet welds, Fig. 4.65. The characteristic dimensions of the cross-sectional model are the plate thicknesses t_1 and t_2, the weld throat thickness a, the root face length g, and the notch radii at weld toe and weld root, ρ_1 and ρ_2 (different fictitious notch radii $\rho_f = \rho + s\rho^*$ can thus be introduced at toe and root). The weld throat thickness a is measured from the ideal weld root point irrespective of the root face length. The selected independent dimension ratios are the plate thickness ratio t_2/t_1, the weld throat to plate thickness ratio a/t_1, the root face length to plate thickness ratio g/t_1 and the notch radius to plate thickness ratios ρ_1/t_1 and ρ_2/t_1. The influence of ρ_2/t_1 is ignored in the stress concentration factor K_{t1} of the weld toe. The same applies to the influence of ρ_1/t_1

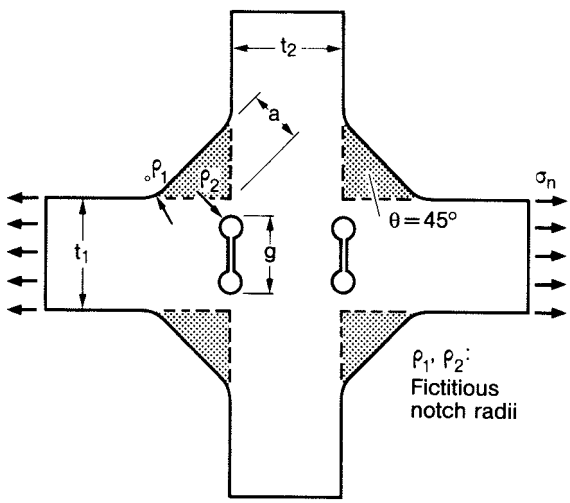


Fig. 4.65. Geometric parameters of the tensile loaded cruciform joint, varied in the notch stress analysis.

on the stress concentration factor K_{t2} of the weld root. The resulting equations for the stress concentration factor, eqs. (4.12) and (4.13), are evaluated in Fig. 4.66 for $g/t_1 = 1.0$ (influence of g/t_1 strong) and $t_2/t_1 = 1.0$ (influence of t_2/t_1 weak).

Simplified formulae for the fatigue notch factors K_{f1} and K_{f2} for structural steel joints are derived by introducing $\rho_1 = \rho_2 = \rho_f = 1\,\text{mm}$ (i.e. a worst case assumption). These formulae are especially well suited for optimisation tasks because the effect of the different geometrical parameters can be extracted at once.

One aim in designing fillet welded joints is to exclude root failures. This means, according to the notch stress approach, that the fatigue notch factor at the weld root, K_{fr}, should be lower than the corresponding factor at the

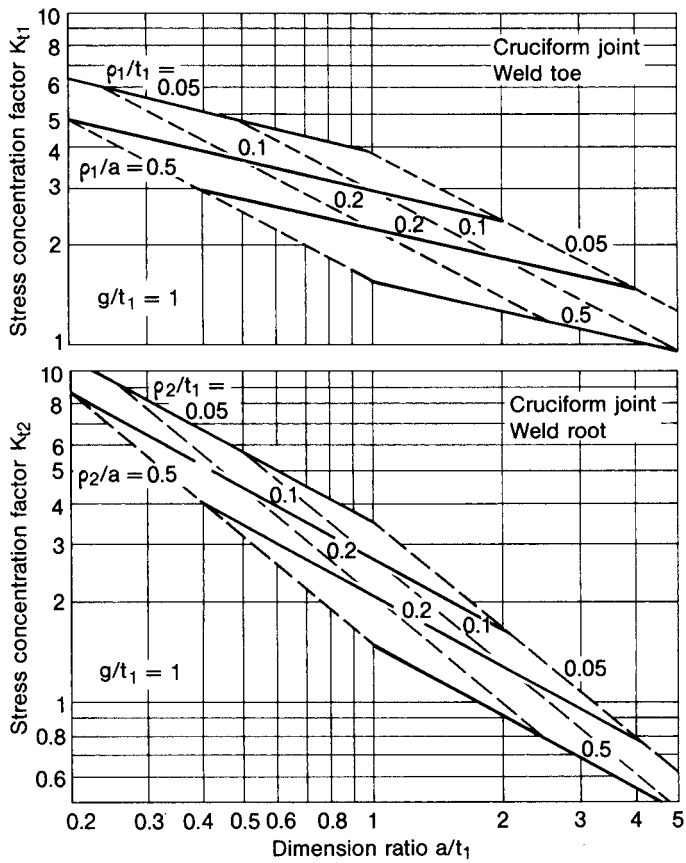


Fig. 4.66. Stress concentration factors at weld toe and weld root of the tensile loaded cruciform joint dependent on dimension ratios; after Radaj and Zhang.[301,302]

weld toe, K_{ft}. It can then be expected that fatigue cracks start at the weld toe first, as is presupposed by the structural stress approach. On the other hand, the strength of the weld toe can be increased by special methods of post-weld surface treatment whereas the strength of the weld root cannot.

A further step has been taken by Petershagen[263] on the basis of the notch stress formulae for welded cruciform joints mentioned above. Considering joints with varying plate thickness, root face length and fillet leg length, the question is put forward what the optimum fillet leg length is for which simultaneous crack initiation at the weld toe and the weld root can be expected. The answer is based on the stress concentration factor formulae (eqs. (4.12) and (4.13)) converted to fatigue notch factor expressions by introducing $\rho_1 = \rho_2 = \rho_f = 1$ mm. Equating the expressions for the weld toe and the weld root, the limit condition $c/2b = 1.15(a/b)^{0.74}$ is derived. The relevant limit curve plotted in Fig. 4.67 separates primary crack initiation at the weld toe, assumed to cause plate fractures, from primary crack initiation at the weld root, assumed to produce weld fractures. The curve is compared with the relevant curves derived on the basis of the crack propagation approach according to Maddox[524] (see Fig. 6.20).

The limit curve above for crack initiation is independent of plate thickness whereas the limit curve for crack propagation depends heavily on it. The corresponding curves and their tendencies are similar. It should be noted that the first mentioned discrepancy is not a refutation and that the

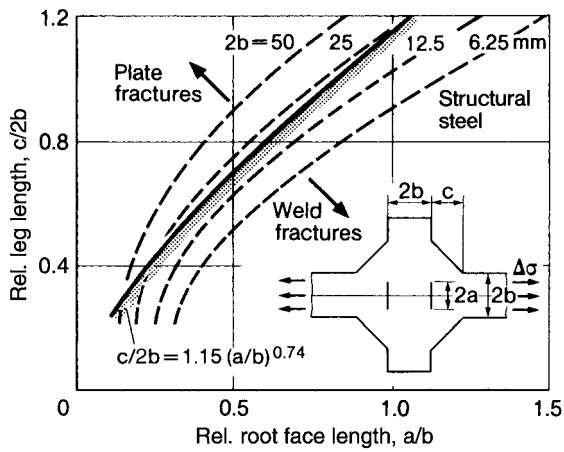


Fig. 4.67. Limit curves separating plate and weld fractures in cruciform joints made of structural steel, dependent on plate thickness, root face length and fillet leg length; notch stress approach describing crack initiation according to Petershagen[263] (solid curve) and crack propagation approach according to Maddox[524] (dashed curves).

last mentioned similarity is not a confirmation because different phenomena are considered: crack initiation versus crack propagation.

The concurrent notch effects of weld toe and weld root have been investigated both experimentally and numerically by Ohta *et al.*[258] considering transverse attachment joints with (non-load-carrying) fillet welds in the as-welded condition and after toe dressing. The fatigue tests were performed with the upper nominal stress set equal to the yield limit of the parent material. Root failures occurred perpendicular to the main loading direction especially with lack of penetration when the stress concentration factor at the weld toe was reduced to $K_t < 1.6$. The stress range with root failures after toe dressing was lower than with toe failures following a root crack without toe dressing. The strength reduction at the weld root is explained by the annealing effect at the weld root by the toe dressing pass.

The effect of lack of penetration on the notch stress profile at the toe of load-carrying fillet welds in cruciform joints has been found to be significant by Barro *et al.*[209] This effect should be identical to the influence of the root face length expressed by the g/t_1 term in eq. (4.12). The influence here is not very strong as can be seen from the relatively small exponent $p_3 = 0.13$. The misalignment effect on the notch stress concentration in cruciform joints has been investigated by Lie and Lan,[517] and by Guan.[227]

5

Notch strain approach for seam-welded joints

5.1 Basic procedures

5.1.1 Principles of the notch strain approach

The notch strain approach for assessing the fatigue strength and service life up to technical crack initiation proceeds from the elastic-plastic strain amplitudes at the notch root and compares them with the strain *S*–*N* curve (i.e. the strain–life curve) of the material in an unnotched comparison specimen (also named 'companion specimen' if directly connected to component testing). The idea behind this approach is that the mechanical behaviour of the material at the notch root in respect of local elastic-plastic deformation, local damage and crack initiation is comparable to the behaviour of a miniaturised, axially loaded, unnotched or mildly notched specimen in respect of overall deformation, overall damage and complete fracture, Fig. 5.1. The comparison specimen is either imagined to be positioned at the notch root or really cut out from this area. It should have the same microstructure, the same surface condition (inclusive of residual stresses) and, if possible, the same volume as the highly stressed material at the notch root. At least, well-founded corrections of the test results with the specimen should be possible for the purpose of comparison. The strength assessment consists in determining the stresses and strains at the notch root in the elastic-plastic condition and comparing them with the strain *S*–*N* curve of the material in the miniaturised specimen up to complete fracture or in a larger specimen up to technical crack initiation (crack depth about 0.5 mm, crack length at the surface about 2 mm), Fig. 5.2. A well-designed introduction to the strain-based approach is given by Dowling.[951]

The stresses and strains at the notch root of the structural member are calculated proceeding from the cyclic stress–strain curve and the macrostructural support formula proposed by Neuber[252–254] (better adapted formulae published by Seeger and Heuler[392] and by Sonsino[400]). Residual notch stresses may be taken into account. Considering the case of a sharp

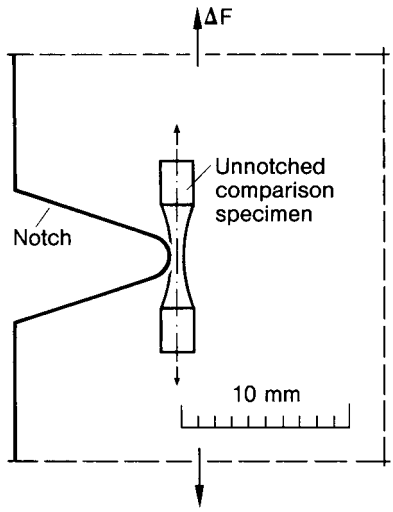


Fig. 5.1. Comparison specimen for simulating the cyclic stress–strain behaviour as well as crack initiation and damage accumulation at the notch root.

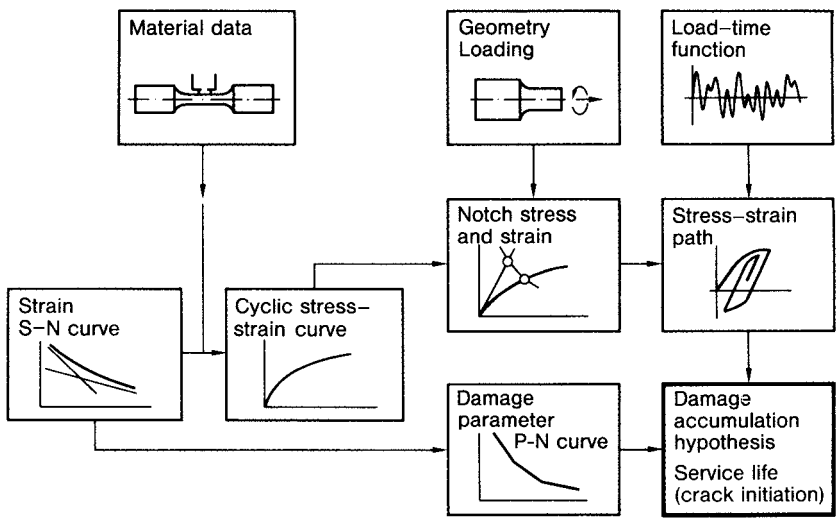


Fig. 5.2. Notch strain approach to assess the fatigue strength and service life of non-welded structural components; graph after Kloos.[374]

notch, the microstructural support effect has additionally to be taken into account according to one of the well-known hypotheses. The amplitudes of the stresses and strains are introduced together with the static mean values. The notch root strain can also be measured instead of being calculated. The comparison specimen is required in this case to determine the stresses which are connected with the elastic-plastic strains. Finally, a sequence of hysteresis loops in the stress–strain diagram (i.e. the stress–strain path) results on the basis of the load–time function.

The strain *S–N* curves of the comparison specimen on the other hand which are dependent on the mean stress can be represented by a single damage parameter *P–N* curve which is supposed to comprise the effect of mean stress. The damage contributions from the stress–strain path are determined cycle by cycle, added up and compared with the damage parameter *P–N* curve. The damage parameter *P–N* curve may also be used with a definite factor for better correspondence with the results from fatigue tests on structural components. The Miner rule in its relative form (damage sum $D \neq 1.0$) may be used proceeding from the strain *S–N* curve if the strain amplitudes have been evaluated as a spectrum or matrix.

Uniaxial loading conditions are the basis of the above considerations in order to simplify the representation. However, biaxial stress conditions corresponding to triaxial strain conditions prevail at the notch root surface of structural components. Additionally, the principal direction of the stresses and strains at the notch root may fluctuate in the case of multiple loading sequences acting simultaneously on the component including mean load variation and mutual phase shift. The numerical procedure becomes extremely complicated in these cases both in respect of theory and application. The yielding behaviour including hardening and softening under multiaxial, proportional or non-proportional stresses and strains (also those resulting from superimposed torsional and axial loading) has to be considered in this case. The appertaining damaging and crack initiation behaviour must be taken into account. Inhomogeneous material properties resulting from welding or surface hardening introduce further complications. Research has clarified only part of the general problem up to now.

The notch strain approach relating to crack initiation, combined with the crack propagation approach, has repeatedly been applied to welded joints, but the degree of correspondence with experimental results was not always satisfactory. Such correspondence cannot be simply achieved, because the notch strain approach was originally designed with regard to medium-cycle fatigue in mild notches in homogeneous material, whereas welded joints are characterised by sharp notches in inhomogeneous material with inclusion of the high-cycle fatigue range. The application to seam-welded joints is described in the subsequent three sections. The following variants of the notch strain approach are possible with regard to the inclusion of the

microstructural notch support effect (see Section 11.1.1, Fig. 11.2). The notch stresses and strains can either be introduced without taking this effect into account (using the notch stress concentration factor K_t) or with its consideration (using the fatigue notch factor K_f). The endurable stresses or strains differ correspondingly, expressed by the notch support factor $n = K_t/K_f$. The result of a combination of the notch strain and crack propagation approaches may be illustrated by the schematic S–N diagram in Fig. 5.3, showing the different curve gradients in the medium- and high-cycle fatigue range (compare Skorupa[396]). Predominantly elastic conditions are assumed in the high-cycle fatigue range under consideration.

A more application-relevant, greatly simplified version of the notch strain approach (designed without supplementary crack propagation analysis) is illustrated by the graph in Fig. 5.4. Remote loading of the welded structure by independently variable forces $F(t)$ causes biaxial non-proportional notch stresses $\sigma_k(t)$ superimposed on the residual (notch) stresses σ_r. The elastic-plastic notch stress analysis allows determination of the notch stresses $\sigma_k(t)$ plotted versus the notch strains $\varepsilon_k(t)$ generating σ_k–ε_k loops. The notch stresses $\sigma_p(t)$ after plastic correction result from it. A multiaxial fatigue criterion of the critical plane type, $\sigma_f(n, \tau_n, \sigma_n)$ is applied with the normal vector n of the considered local plane, as well as with the normal stress σ_n and the shear stress τ_n in this plane (not to be confused with nominal stresses). The cycles $\tau_n(t)$ are extracted by rainflow counting in order to determine the damage $D(n, \sigma_f$–$N)$ depending on plane angle and local fatigue strength in Basquin's representation. Many local planes of different directions have to be analysed (the computational loop) in order to find out which one has

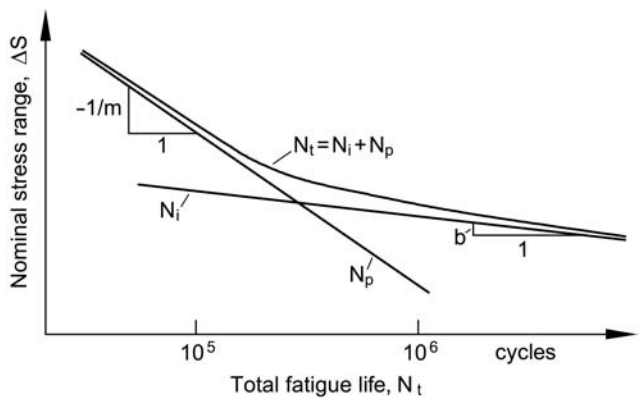


Fig. 5.3. S–N curve of welded joint following from combination of simplified notch strain and crack propagation approaches relating to crack initiation life N_i and crack propagation life N_p, respectively; with exponents m and b in the Paris and Basquin equation, respectively; schematic diagram after Hou and Charng.[367]

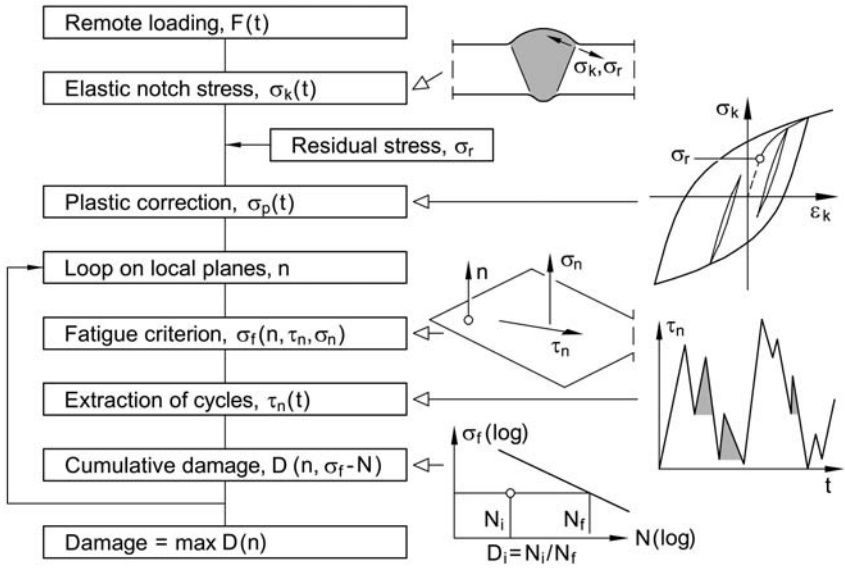


Fig. 5.4. Redesigned graph after Petitpas *et al.*[388] illustrating the main procedural steps of a greatly simplified version of the notch strain approach; explanations given in the text.

the highest damage value $\max D(n)$. The assessment procedure above is based on the notch stresses (contrary to the name 'notch strain approach'), but these stresses are modified or 'corrected' by the plastic notch strains.

5.1.2 Early application of the approach

The earliest application of the notch stress and strain approach to welded joints originates from Lawrence *et al.*,[365,366,375–379,384,394,403,407,967,990] Fig. 5.5. The method which had been originally developed for the low-cycle fatigue range was extended to the medium- and high-cycle fatigue range ($N > 10^4$ cycles). It was realised that the crack initiation process covered by the method was a significant part of the total life of welded joints after several attempts to define the life solely on the basis of crack propagation[433,434,506,507,636]. Two types of welded joints were mainly considered, butt-welded joints with crack initiation at the weld toe and spot-welded joints with crack initiation at the weld spot edge. Low strength and high strength steels as well as aluminium alloys were dealt with.

The basic idea of the notch strain approach, of introducing unnotched comparison specimens at the critical sites of crack initiation, is applied to welded joints according to Fig. 5.6.

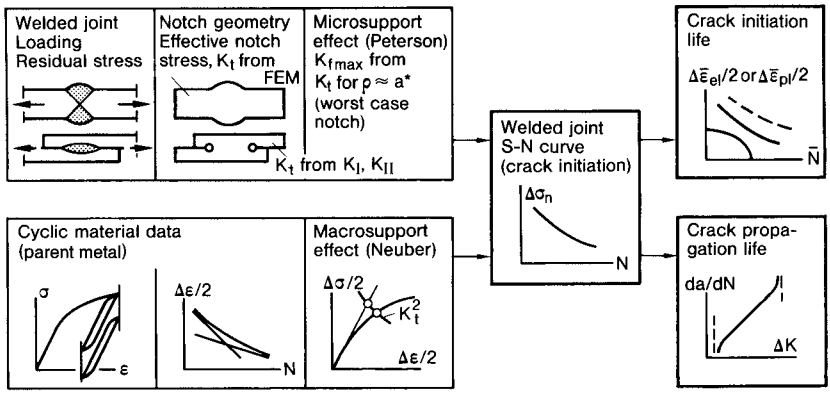


Fig. 5.5. Notch stress and strain approach, version according to Lawrence, to assess the fatigue strength and service life of welded joints; with K_t notch stress concentration factor, K_f fatigue notch factor, ρ notch radius, a^* material constant, K_I and K_{II} stress intensity factors, $\Delta\sigma$ cyclic stress, $\Delta\varepsilon$ total cyclic strain, $\Delta\sigma_n$ cyclic nominal stress, $\Delta\bar{\varepsilon}_{el}$ maximum cyclic elastic strain and $\Delta\bar{\varepsilon}_{pl}$ maximum cyclic plastic strain in variable-amplitude loading, da/dN crack propagation rate, ΔK cyclic stress intensity factor, N number of cycles to crack initiation, and FEM meaning 'finite element method'; after Radaj.[5]

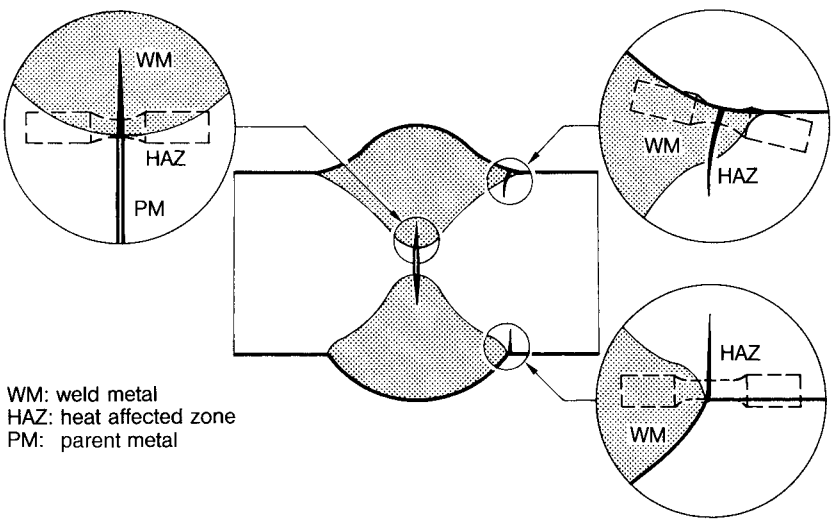


Fig. 5.6. Fatigue crack initiation in a butt weld and corresponding smooth comparison specimens (dashed lines): initiation in weld metal at weld root and in weld metal or heat-affected zone at weld toe; after Lawrence *et al.*[377]

The critical sites are found by an elastic maximum notch stress analysis performed on the cross-sectional model. It can be seen that different material conditions occur at these sites: parent metal, heat-affected zone (possibly hardened or softened) and weld metal (possibly diluted or tempered). Residual notch stresses may be superimposed on the fluctuating notch stresses from remote loading: tensile residual stresses in the as-welded condition or compressive residual stresses generated by mechanical postweld treatment.

The numerical analysis of fatigue life or strength according to Lawrence is characterised by the following procedural steps, some of which may be omitted in the case actually considered in order to simplify the procedure:

- The total life of welded joints consists of the crack initiation life and the crack propagation life.[506,507]
- The crack initiation life is defined by the number of cycles required to produce an initial (technical) crack of depth $a_i = 0.25\,\text{mm}$.
- The crack initiation life is a non-neglectable part of the total life even with crack-like sharp notches especially in the case of high strength steels and aluminium alloys.[506,507]
- The crack initiation life is described by the notch strain approach which is based on the fatigue behaviour of smooth comparison specimens thus circumventing the short crack propagation problem.
- The elastic component of the strain *S*–*N* curve (i.e. Basquin's relationship with mean stress correction according to Morrow) can be used to describe the fatigue strength at the notch root on the basis of the elastic stress concentration factor converted to the worst case fatigue notch factor according to Peterson and inclusive of local residual stresses. This is a simplified procedure in the medium- and high-cycle fatigue range with crack initiation life $N_i \geq 10^5$ cycles.
- Joint straightening causing superimposed bending stresses has to be taken into account in the analysis.
- A more realistic and accurate approach (definitely necessary for $N_i \leq 10^5$ cycles) additionally takes local plasticity and cyclic relaxation at the notch root into account. The Neuber macrostructural support formula is extended by an additive residual stress term for that purpose together with a relationship according to Jhansale and Topper[371] describing the mean stress (including residual stress) relaxation dependent on the strain amplitude.
- The residual stress after the 'set-up loading cycle' is calculated on the basis of the monotonic elastic-plastic notch behaviour.
- The damage per cycle in variable-amplitude loading is assessed on the basis of the local stress–strain cycles and Miner's rule applied to the resulting stress ranges.[384]

- The marked influence of residual stresses on the fatigue strength of welded joints especially in the case of high strength steels can also be demonstrated on the basis of local plasticity and cyclic relaxation.[375]
- Tensile residual stress values at the yield limit of the material are assumed locally in the as-welded condition. A reduction to approximately zero is introduced if postweld stress relief measures have been taken. Compressive residual stress values at the yield limit are taken into account locally in the case of special postweld treatments such as shot-peening.[403]
- Biaxial in-phase notch stress states are dealt with in respect of crack initiation based on the octahedral shear stress or distortional strain energy criterion according to von Mises. Out-of-phase stress states are assessed on the basis of the combined shear and normal stress criterion according to Findley.[109] (Siljander *et al*.[58,394])
- The material parameters of crack initiation are introduced according to the microstructural condition at the crack initiation site derived from microhardness measurements: parent metal, heat-affected zone (possibly hardened or softened) and weld metal (possibly diluted or tempered).
- The crack propagation life is estimated through the observed dependence of the crack growth rate, $\mathrm{d}a/\mathrm{d}N$, on the range of the stress intensity factor, ΔK. The Paris equation is integrated from the initial crack size, a_i, to the final crack size, a_f, see Section 6.2.4.
- Residual stress effects are not taken into account in the crack propagation analysis.

The investigations performed by Lawrence – besides establishing an easy-to-use numerical method of fatigue life assessment – have given valuable insight into the relation between crack initiation and crack propagation life of welded joints. This relation is highly material-dependent besides being dependent on the total number of cycles to fracture. High strength steels compared with low strength steels are characterised by a longer crack initiation period. Another valuable general result refers to the effect of residual stresses on fatigue strength. Residual stresses in welded joints which reach the tensile yield limit locally in the as-welded condition lower the fatigue strength substantially in high strength steels, whereas the benefit from postweld treatments is correspondingly high for these steels.

The notch strain approach, version according to Lawrence, has been further developed in respect of its crack initiation aspects (Lawrence *et al*.[376]). The initial crack depth is reduced from $a_i = 0.25\,\mathrm{mm}$ to $a_i \approx 0.1\,\mathrm{mm}$ and the corresponding crack initiation life is subdivided into a crack nucleation and a short crack propagation period. Notch root crack propagation with crack closure effects resulting from plastic deformation and surface

roughness are simulated numerically.[368] The relevant computer program has been applied to the four main positions of crack initiation in welded joints: toe and root cracking, ripple and weld end cracking. Comparative calculations of the *S–N* curves of a cruciform joint were performed with an advanced model demonstrating the following influencing parameters: weld quality (defined by the initial crack size), residual stress, parent metal strength and plate thickness. An attempt to describe the essential part of the crack initia-tion period by a short crack propagation model taking crack closure into account has also been made by Hou and Charng[367] with satisfactory results.

5.1.3 Comprehensive exposition of the approach

The notch strain approach, version according to Seeger *et al.*,[8] was worked out later than that of Lawrence. It is not specifically directed to welded joints but more generally to steel constructions including welded joints. Its scientific basis is more general and profound, but its relation to application less close. The methods and procedures that it incorporates are more modern, to some extent corresponding to its later date of origin and to its more developed scientific level. This relates especially to the issues of damage parameters, non-proportional biaxial stresses and elastic-plastic limit load behaviour. Additionally, the notch effect of elastic-plastic mismatching at the boundary of the heat-affected zone is addressed.[355,356] Non-uniform material parameters and residual stresses resulting from surface hardening are also considered.[8,345,405] A well-known compilation of material constants ('uniform material law') required by the notch strain approach has been published by Boller and Seeger,[353] and Bäumel and Seeger.[346]

The notch strain approach, version according to Seeger, like any notch strain approach, is directed to crack initiation. The corresponding version of the notch stress approach related to the endurance limit (i.e. to avoiding crack initiation completely) is reviewed in Section 4.1.4. The crack initiation modules based on the notch strain approach are supplemented by a crack propagation module based on the Paris equation but the main concern is on crack initiation.

Referring to the explanation of Fig. 5.2, the following modules are characteristic of the notch strain approach, version according to Seeger, keeping in mind that the procedure is also applicable without a notch while local considerations remain essential (therefore, the designation 'local concept' is preferred by Seeger[8]):

– Cyclic stress–strain curve: The calculation of notch stresses and strains is based on the stabilised cyclic stress–strain curve. The latter is different from the monotonic stress–strain curve. Cyclic stabilisation may be

reached after a period of 10–50% of the crack initiation life. Mean stress relaxation is neglected. The cyclic stress–strain curve is approximated by the relationship named after Ramberg and Osgood.[389] The true stresses and (logarithmic) strains should be inserted. The local material properties at the crack initation site should be introduced.

- Strain S–N curve: The failure condition of technical crack initiation (crack depth $a_i \approx 1$ mm) is described by the strain S–N curve. This curve is approximated by the 'four parameter relationship' proposed by Manson,[380,381] Coffin[357,358] and Morrow[387] which refers to an elastic and a plastic part of the endurable strain amplitude. The plastic part is modified by adding a material-dependent constant strain for $N_i > 10^4$ cycles (Klee[373]). The material properties at the crack initiation site should be introduced.
- Stress–strain path: The cyclic stress–strain path results from the load reversals proceeding from the cyclic stress–strain curve forming hysteresis loops in the stress–strain diagram. The curve sections are approximated by doubling the momentary amplitudes of the primary cyclic stress–strain curve as proposed by Masing[382]. The material exhibits a memory effect when closing the hysteresis loops which are directly related to the amount of damage.
- Notch stress and strain: The notch stresses and strains or, more generally, the local stresses and strains at the crack initiation site are determined based on analytically derived formulae (e.g. the macrostructural support formula derived by Neuber,[252–254] or the amended formulae proposed by Seeger and Heuler[392]), on elastic-plastic finite element analysis or on strain measurements. The term 'yield curve' is used by Seeger[8] for the relationship between applied load and local notch strain.
- Damage parameter P–N curve: The hysteresis loops of the cyclic stress–strain path are generally connected to varying mean stresses and strains. The amount of damage resulting from each hysteresis loop depends on the enclosed area of the loop and its mean stress. The damage parameter is supposed to convert the hysteresis loops with non-zero mean stress to damage-equivalent loops with zero mean stress. The latter can then be related to the strain S–N curve or its equivalent, the damage parameter P–N curve. The damage parameter P_{SWT} proposed by Smith, Watson and Topper[397] is preferred.
- Damage accumulation hypothesis: The damage contributions of all closed hysteresis loops (detectable by rainflow counting inclusive of their sequence) are added up to give the total damage according to Miner's rule. There are different variants in use concerning damage contributions in the high-cycle fatigue range. Crack initiation occurs if the sum of the damage contributions is equal to the value 1.0 or to another value defined on an empirical basis.

– Residual stress effect: Residual stresses at the notch root are taken into account by extending Neuber's macrostructural support formula by an additive residual stress or strain term. The approach is based on the model of thin or thick residual stress layers.[8,345,405]
– Multiple loads and local stress or strain multiaxiality: The modules mentioned above are related to a single load associated with uniaxial local stresses or strains. The combination of multiple loads associated with uniaxial local conditions is easy to cover by simple superposition. The case of a single load producing biaxial stresses or strains at the notch root is dealt with based on the von Mises distortional strain energy criterion presuming ductile materials. Multiple loads acting in a proportional or non-proportional manner combined with biaxial stresses or strains at the notch root are more difficult to treat with.

The notch strain approach, version according to Seeger, has been applied mainly to non-welded structural members. It was applied to a welded structural detail by Heuler and Seeger,[364] i.e. to a single-bevel groove weld with fillet welds between web and inclined flange, Fig. 5.7. The notch stress and strain analysis within the above approach has been further developed by Clormann and Seeger[355,356] in respect of inhomogeneous material (parent metal, heat-affected zone and fusion zone) and sharp notches (fictitiously rounded).

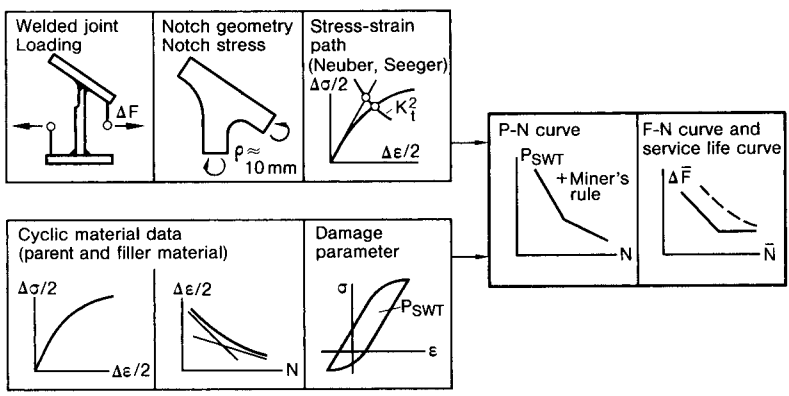


Fig. 5.7. Notch strain approach, version according to Seeger, to assess the fatigue strength and service life of welded joints; with ΔF cyclic remote force, ρ notch radius, $\Delta\sigma$ cyclic stress, $\Delta\varepsilon$ cyclic strain, K_t notch stress concentration factor, N number of cycles to failure, P_{SWT} damage parameter proposed by Smith, Watson and Topper, $\Delta\bar{F}$ maximum cyclic remote force in variable-amplitude loading; after Radaj.[5]

5.1.4 Further refinements of the approach

The notch strain approach for welded joints has been further developed by Sonsino[59–61,318] in respect of multiaxial fatigue (defined by crack initiation with a_i = 0.5–1.0 mm). His contributions comprise a modification of the macrostructural support formula of Neuber in the case of mild notches, the introduction of an equivalent notch strain to describe multiaxial low-cycle fatigue, the corresponding conversion of the 'highly stressed volume criterion' as a strain-related criterion and the formulation of multiaxial fatigue criteria applicable to the notch stresses in the medium- and high-cycle fatigue range.

The macrostructural notch support formula according to Neuber has been derived for sharp notches but is widely applied to mild notches too. The plastic notch strains are overrated in the latter case. Therefore, Sonsino[400] proposes to evaluate only one half of the calculated plastic notch strain. An exact simple formula for the stress–strain behaviour in mild notches is given in the third edition of Neuber's book.[252] It confirms the tendency to reduction in strain.

Biaxial in-phase loading of welded joints in the low- and medium-cycle fatigue range ($N = 10^3$–10^5 cycles) should be described by the equivalent strain at the notch root on the basis of the distortional strain energy criterion when ductile materials are considered.[59,60] The principal strain direction is considered as constant in this case. Out-of-phase loading and multiaxial random loading have been investigated in the medium- and high-cycle fatigue range where the effective equivalent stress criterion (averaging the shear stresses in all local directions) was applicable.[61,318,401]

The 'highly stressed volume criterion' (see Section 4.2.10) expressed in local (total) strains instead of (elastic) stresses has been successfully applied to welded joints in the low-cycle fatigue range.[59,60] The criterion is especially well suited to evaluate the highly stressed or strained volume from a finite element model. The actual notch radii at the weld toe are introduced in this context ($\rho \approx 0.5$ mm for non-machined welds and $\rho = 2.25$ mm for machined welds in the considered investigation[59,60]).

5.2 Analysis tools

5.2.1 Basic formulae in early applications

The fatigue life of welded joints, measured in number of cycles, is composed of the crack initiation and crack propagation portions:

$$N_t = N_i + N_p \tag{5.1}$$

where N_t is the total fatigue life, N_i is the crack initiation life ($a_i = 0.25\,\text{mm}$) and N_p is the crack propagation life.

The crack propagation life of welded joints comprises propagation first through the thickness and then across the width of the specimen or structural member:

$$N_p = N_{pt} + N_{pw} \tag{5.2}$$

where N_p is the crack propagation life, N_{pt} is the crack propagation life through the thickness of the sheet and N_{pw} is the crack propagation life across the width of the specimen or structural member.

The formulae hereafter refer to the crack initiation life. The crack propagation formulae according to fracture mechanics are summarised in Sections 6.2.3 and 6.2.4.

In the high-cycle fatigue range ($N_i > 10^5$ cycles or $N_i > N_t^*$ with transition fatigue life N_t^*), cyclic hardening or softening can usually be ignored, and elastic conditions may generally be assumed. The crack initiation life can then be estimated on the basis of the local stress amplitude using the relationship according to Basquin[347] with mean stress correction according to Morrow[387]

$$\sigma_a = \frac{\Delta\sigma}{2} = (\sigma_f' - \sigma_m)(2N)^b \tag{5.3}$$

where σ_a is the local stress amplitude, $\Delta\sigma$ is the local stress range, σ_f' is the fatigue strength coefficient, σ_m is the local mean stress, b is the fatigue strength exponent and N is the number of cycles to crack initiation.

The following approximation dependent on local hardness is used by Lawrence *et al.*[377,379,407] in the case of steels, Fig. 5.8 ($b \approx -0.1$ for mild steel, further data in Table 5.1):

$$\sigma_f' \approx \sigma_U + 342 \quad [\text{N/mm}^2] \tag{5.4}$$

$$\sigma_U \approx 3.42 H_B \quad [\text{N/mm}^2] \tag{5.5}$$

$$b \approx -\frac{1}{6}\log\frac{2(H_B + 100)}{H_B} \tag{5.6}$$

where σ_f' is the fatigue strength coefficient, σ_U is the ultimate tensile strength ($\sigma_U = R_m$), H_B is the local Brinell hardness at the crack initiation site or (less accurate) of the parent metal and b is the fatigue strength exponent.

The fatigue-effective local stress amplitude at the crack initiation site (e.g. weld toe, weld root, defect edge or weld spot edge) is expressed by the nominal stress range and the fatigue notch factor:

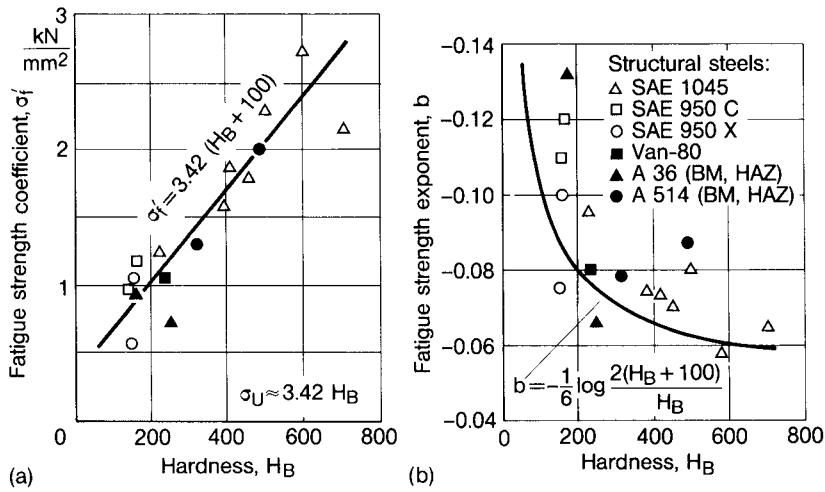


Fig. 5.8. High-cycle fatigue strength parameters, coefficient σ_f' (a) and exponent b (b), for structural steels dependent on Brinell hardness H_B; after Lawrence *et al.*[377]

$$\sigma_a = \frac{\Delta\sigma}{2} = \frac{1}{2}\Delta\sigma_n K_f \tag{5.7}$$

where σ_a is the local stress amplitude, $\Delta\sigma$ is the local stress range, $\Delta\sigma_n$ is the nominal stress range and K_f is the fatigue notch factor.

The fatigue notch factor is derived from the stress concentration factor according to Peterson,[265–267] generally its maximum value determined from a worst case consideration (see Sections 4.1.2 and 4.2.5).

The local mean stress results from remote loading and from initial residual stress (see Fig. 5.13). The local stresses and strains follow the monotonic stress–strain curve (eq. (5.8) according to Ramberg and Osgood[389]) in the set-up loading cycle, proceeding from the initial residual stress σ_r to a stress state on the Neuber hyperbola, eq. (5.9). Further stress–strain loops are described by the hysteresis branches of the cyclic stress-strain curve, eq. (5.10), modified according to Masing,[382] starting at the original Neuber hyperbola and ending at the Neuber hyperbola in a reversed stress–strain diagram, eq. (5.11) (origin in the cusp point), thus generating a new mean stress σ_m:

$$\varepsilon = \frac{\sigma}{E} + \left(\frac{\sigma}{K}\right)^{1/n} \tag{5.8}$$

$$\left(\frac{K_f \Delta\sigma_n}{1-R} + \sigma_r\right)^2 \frac{1}{E} = \Delta\sigma\Delta\varepsilon \tag{5.9}$$

$$\frac{\Delta\varepsilon}{2} = \frac{\Delta\sigma}{2E} + \left(\frac{\Delta\sigma}{2K'}\right)^{1/n'} \tag{5.10}$$

$$(K_f \Delta\sigma_n)^2 \frac{1}{E} = \Delta\sigma\Delta\varepsilon \tag{5.11}$$

where ε is the total local strain, σ is the local stress, E is the elastic modulus, K is the static strength coefficient, n is the static strain-hardening exponent, σ_r is the local residual stress (after the 'set-up loading cycle'), $\Delta\varepsilon$ is the total local strain range, $\Delta\sigma$ is the local stress range, K' is the cyclic strain-hardening coefficient, n' is the cyclic strain-hardening exponent and K_f is the fatigue notch factor.

Mean stress relaxation during cycling (the effect is generally small, see Fig. 5.16) is estimated according to Jhansale and Topper:[371]

$$\frac{\sigma_m}{\sigma_{m0}} = (N-1)^k \tag{5.12}$$

where σ_m is the current value of the local mean stress, σ_{m0} is the local mean stress after the set-up loading cycle, N is the number of elapsed further cycles and k is the relaxation exponent. The relaxation exponent is a function of the strain amplitude (see Lawrence,[377] *ibid*. Fig. 9; e.g. $k = -0.12$ for type A36 mild steel at $\varepsilon_a = 0.2\%$).

Local stress and strain cycles with variable amplitudes are assessed in respect of high-cycle fatigue damage, eq. (5.13), on the basis of Miner's rule,[385] eq. (5.14), applied to the elastic component of the strain *S–N* curve, eq. (5.3) with $\sigma_m = 0$, while taking the mean stress effect into account according to a modified Goodman relationship,[363] eq. (5.15):

$$D_j = \frac{1}{N_j} = \left(\frac{\sigma_{a0}}{\sigma'_f}\right)^{1/b} \tag{5.13}$$

$$D = \sum_{j=1}^{N_i} D_j = 1.0 \tag{5.14}$$

$$\sigma_a = \sigma_{a0}\left(1 - \frac{\sigma_m}{\sigma'_f}\right) \tag{5.15}$$

where D_j is the damage contribution by cycle j, N_j is the crack initiation life with σ_a converted to σ_{a0}, N_i is the crack initiation life with variable-amplitude loading, σ_{a0} is the endurable stress amplitude with $\sigma_m = 0$, σ_m is the mean stress and σ'_f is the fatigue strength coefficient.

The procedure above can also be applied proceeding from the plastic strains and relating these to the plastic component of the strain *S–N* curve (Mattos and Lawrence[384]). Miner's rule based on strains instead of stresses was further used by Iida *et al.*[369]

Biaxial in-phase high-cycle fatigue ($N \geq 10^5$ cycles) with constant principal stress direction at the notch root in ductile materials is predicted on the basis of the von Mises criterion applied independently to the stress amplitudes, eq. (5.16), and to the mean stresses, eq. (5.17), thus transferring eq. (5.3) into eq. (5.18):[58,394]

$$\sigma_{\mathrm{eq\,a}} = \sqrt{\sigma_{\mathrm{xa}}^2 + \sigma_{\mathrm{ya}}^2 - \sigma_{\mathrm{xa}}\sigma_{\mathrm{ya}} + 3\tau_{\mathrm{xya}}^2} \tag{5.16}$$

$$\sigma_{\mathrm{eq\,m}} = \sqrt{\sigma_{\mathrm{xm}}^2 + \sigma_{\mathrm{ym}}^2 - \sigma_{\mathrm{xm}}\sigma_{\mathrm{ym}} + 3\tau_{\mathrm{xym}}^2} \tag{5.17}$$

$$\sigma_{\mathrm{eq\,a}} = (\sigma_{\mathrm{f}}' - \sigma_{\mathrm{eq\,m}})(2N)^b \tag{5.18}$$

where $\sigma_{\mathrm{eq\,a}}$ is the equivalent stress amplitude, $\sigma_{\mathrm{eq\,m}}$ is the equivalent mean stress, σ_{xa}, σ_{ya} and τ_{xya} are the stress component amplitudes, σ_{xm}, σ_{ym} and τ_{xym} are the mean stress components, σ_{f}' is the fatigue strength coefficient, b is the fatigue strength exponent and N is the number of cycles to crack initiation.

Biaxial out-of-phase high-cycle fatigue with fluctuating principal stress directions is treated on the basis of Findley's[109] combined shear and normal stress criterion:[58,394]

$$\tau_{\mathrm{eq\,a}} = \tau_{1\mathrm{a}} + k\sigma_{\perp\max} \tag{5.19}$$

$$\tau_{1\mathrm{a}} = \frac{1}{2}\sqrt{(\sigma_{\mathrm{xa}} - \sigma_{\mathrm{ya}})^2 + 4\tau_{\mathrm{xya}}^2} \tag{5.20}$$

$$\sigma_{\perp\max} = \sigma_{\perp\mathrm{m}} + \sigma_{\perp\mathrm{a}} \tag{5.21}$$

$$\tau_{\mathrm{eq\,a}} = \tau_{\mathrm{f}}'(2N)^b \tag{5.22}$$

where $\tau_{\mathrm{eq\,a}}$ is the equivalent shear stress amplitude, $\tau_{1\mathrm{a}}$ is the principal shear stress amplitude, $\sigma_{\perp\max}$ is the maximum normal stress in the principal shear stress plane, k is a material constant ($k \approx 0.3$), σ_{xa}, σ_{ya} and τ_{xya} are the local stress component amplitudes, $\sigma_{\perp\mathrm{m}}$ is the mean normal stress in the principal shear stress plane, $\sigma_{\perp\mathrm{a}}$ is the normal stress amplitude in the principal shear stress plane, τ_{f}' is the fatigue strength coefficient, b is the fatigue strength exponent and N is the number of cycles to crack initiation.

5.2.2 Basic formulae for wider application

The following equations are arranged according to the sequence of the conceptual description in Section 5.1.2.

The cyclic stress–strain curve according to Ramberg and Osgood is described[389] by:

$$\varepsilon_a = \varepsilon_{a\,el} + \varepsilon_{a\,pl} = \frac{\sigma_a}{E} + \left(\frac{\sigma_a}{K'}\right)^{1/n'} \tag{5.23}$$

where ε_a is the total strain amplitude, $\varepsilon_{a\,el}$ is the elastic strain amplitude, $\varepsilon_{a\,pl}$ is the plastic strain amplitude, σ_a is the stress amplitude, E is the elastic modulus, K' is the cyclic strain-hardening coefficient and n' is the cyclic strain-hardening exponent.

The strain S–N curve according to Manson[380,381] and Coffin[357] inclusive of the mean stress effect according to Morrow[387] describing crack initiation ($a_i \approx 1\,\text{mm}$) is given by:

$$\varepsilon_a = \varepsilon_{a\,el} + \varepsilon_{a\,pl} = \frac{\sigma'_f - \sigma_m}{E}(2N)^b + \varepsilon'_f(2N)^c \qquad (N \le N_E) \tag{5.24}$$

where σ'_f is the fatigue strength coefficient, ε'_f is the fatigue ductility coefficient, b is the fatigue strength exponent, c is the fatigue ductility exponent, σ_m is the mean stress, N is the number of cycles (up to crack initiation, $a_i \approx$ 0.5–1.0 mm) and N_E is the number of cycles at the technical endurance limit.

The cyclic material parameters in eqs. (5.23) and (5.24) are presented by Seeger *et al.*[8,346,353] for non-welded parent metals according to the 'uniform material law', Table 5.1. Accurate data for aluminium alloys are compiled in a report by Sonsino *et al.*[62] Heat-affected zone and weld deposit in butt-welded steel joints were investigated by Tateishi and Hanji.[402]

Table 5.1. Estimates for cyclic material parameters of parent metals according to the 'uniform material law'; after Bäumel and Seeger[8,346]

Material parameter	Steels, unalloyed and low-alloy	Aluminium and titanium alloys	
σ'_f	$1.50\sigma_U$ [a]	$1.67\sigma_U$	
b	–0.087	–0.095	
ε'_f	0.59ψ	0.35	$\psi = 1.0$
c	–0.58	–0.69	for $\frac{\sigma_U}{E} \le 3 \times 10^{-3}$
σ_E [b]	$0.45\sigma_U$	$0.42\sigma_U$	
ε_E [b]	$0.45\frac{\sigma_U}{E} + 1.95 \times 10^{-4}\psi$	$0.42\frac{\sigma_U}{E}$	$\psi = \left(1.375 - 125\frac{\sigma_U}{E}\right) \le 0$
N_E	5×10^5	1×10^6	for $\frac{\sigma_U}{E} > 3 \times 10^{-3}$
K'	$1.65\sigma_U$	$1.61\sigma_U$	
n'	0.15	0.11	

[a] σ_U Ultimate tensile strength, $\sigma_U = R_m$.
[b] σ_E, ε_E Technical endurance limit in terms of stress and strain.

The following relationships enforce compatibility of the strain components in eqs. (5.23) and (5.24):

$$n' = \frac{b}{c} \tag{5.25}$$

$$K' = \frac{\sigma'_f}{(\varepsilon'_f)^{n'}} \tag{5.26}$$

The curve branches of the stress–strain hysteresis loop, rising or dropping from the cusp points with inclusion of the Bauschinger effect,[348] are described after Masing[382] by a double-sized σ–ε curve:

$$\varepsilon = \varepsilon_{cp} + \frac{\sigma - \sigma_{cp}}{E} + 2\left(\frac{\sigma - \sigma_{cp}}{2K'}\right)^{1/n'} \tag{5.27}$$

where σ and ε are the stresses and strains on the hysteresis curve branch, and σ_{cp} and ε_{cp} are the stress and strain at the (lower) cusp point.

The stresses and strains at the notch root in the elastic-plastic state according to Neuber[252–254] for sharp notches, eqs. (5.28) and (5.29), or for mild notches, eqs. (5.30) and (5.31), (Neuber's macrostructural support formulae) are given by:

$$K_{t\sigma} K_{t\varepsilon} = K_t^2 \tag{5.28}$$

$$\sigma_k \varepsilon_k = \sigma_n \varepsilon_n K_t^2 = \frac{(\sigma_n K_t)^2}{E} \tag{5.29}$$

$$K_{t\sigma}(K_{t\varepsilon} - 1) = K_t(K_t - 1) \tag{5.30}$$

$$\sigma_k(\varepsilon_k - \varepsilon_n) = \sigma_n \varepsilon_n K_t(K_t - 1) = \frac{\sigma_n^2 K_t(K_t - 1)}{E} \tag{5.31}$$

where K_t is the elastic stress concentration factor, $K_{t\sigma}$ is the elastic-plastic stress concentration factor, $K_{t\varepsilon}$ is the elastic-plastic strain concentration factor, σ_k is the maximum notch stress in the elastic-plastic state, ε_k is the maximum notch strain in the elastic-plastic state, σ_n is the nominal stress, and ε_n is the nominal strain ($\varepsilon_n = \sigma_n/E$).

The correction of eqs. (5.28) and (5.29) for mild notches according to Sonsino[400] is given by:

$$K^*_{t\varepsilon} = \frac{1}{2}(K_{t\varepsilon} + K_t) \tag{5.32}$$

$$\varepsilon^*_k = \frac{1}{2}(\varepsilon_k + \varepsilon_{kel}) \tag{5.33}$$

where $K^*_{t\varepsilon}$ is the reduced elastic-plastic strain concentration factor referring to ε^*_k, $K_{t\varepsilon}$ is the elastic-plastic strain concentration factor, K_t is the elastic stress concentration factor, ε^*_k is the reduced maximum elastic-plastic notch strain, ε_k is the original maximum elastic-plastic notch strain (eq. (5.29)) and $\varepsilon_{k\,el}$ is the elastic portion of ε_k ($\varepsilon_{k\,el} = \sigma_k/E$).

The notch stresses and strains in the elastic-plastic state are approximated by Glinka[360,361,386] on the basis of the equivalent strain energy criterion applied to localised yielding (stress–strain curve according to eq. (5.23)) at the tip of cracks or sharp notches (assuming plane stress):

$$K_t^2 \frac{\sigma_n^2}{2E} = \frac{\sigma_k^2}{2E} + \frac{\sigma_k}{1+n'}\left(\frac{\sigma_k}{K'}\right)^{1/n'} \tag{5.34}$$

A formally identical relationship is valid in the case of plane strain if the elastic modulus E is correspondingly modified, and K' and n' are derived from a plane strain test.

The increased stresses and strains at the notch root after complete plastification of the net-section are described according to Seeger and Heuler[392] who modified Neuber's sharp notch formula for application in this range:

$$\sigma_k \varepsilon_k = \frac{\sigma_n^2 K_t}{E} \frac{\varepsilon_n^* E}{\sigma_n^*} \qquad (\sigma_n \geq \sigma_{n\,pl}) \tag{5.35}$$

$$\sigma_n^* = \sigma_Y \frac{F}{F_{pl}} = \sigma_n \frac{K_t}{K_{pl}} \qquad (F \geq F_{pl}) \tag{5.36}$$

$$K_{pl} = \frac{\sigma_{n\,pl}}{\sigma_{nY}} \tag{5.37}$$

where σ_n is the nominal stress, σ^*_n is the modified nominal stress, both defined in the net-section, ε^*_n is the modified nominal strain ($\varepsilon^*_n = f(\sigma^*_n)$ according to the stress–strain curve), F is the applied load, F_{pl} is the limit load with elastic-ideal plastic material, K_t is the elastic stress concentration factor, K_{pl} is the limit load factor ($K_{pl} \geq K_t$), $\sigma_{n\,pl}$ is the nominal stress at the limit load with elastic-perfectly-plastic material and vanishing multiaxial stress effects and σ_{nY} is the nominal stress at initial local yielding ($\sigma_{nY} = \sigma_Y/K_t$).

The stress concentration factor K_t has to be substituted by the fatigue notch factor K_f in eqs. (5.28–5.37) in order to assess cyclic loading in respect of fatigue proceeding from the endurance limit of the notched component. But the applied fatigue notch factor should be restricted to the elastic notch support effects.

The damage parameter P–N curves comprise the effect of mean stress σ_m on the S–N curve with respect to crack initiation. The damage parameter P thus allows the conversion of a stress–strain hysteresis

loop with non-zero mean stress into a damage-equivalent loop with zero mean stress. The damage parameter P_{SWT} most often used has been defined for uniaxial loading by Smith, Watson and Topper[397] (multiaxial loading is taken into account by the distortional strain energy criterion or by the principal normal stress criterion):

$$P_{SWT} = \sqrt{(\sigma_a + \sigma_m)\varepsilon_a E} \tag{5.38}$$

where σ_a is the stress amplitude, ε_a the strain amplitude and σ_m the mean stress.

The relevant P–N curve derived by introducing ε_a and $\sigma_a = \varepsilon_{a\,el}E$ from the Manson–Coffin equation (5.24) with $\sigma_m = 0$ or $R = -1$ reads:

$$P_{SWT} = \sqrt{(\sigma'_f)^2(2N)^{2b} + \sigma'_f\varepsilon'_f E(2N)^{b+c}} \tag{5.39}$$

The damage parameter P_{KBM} proposed by Kandil, Brown and Miller[372] and extended in respect of the influence of mean stress by Socie *et al.*[399] assumes crack initiation by the principal shear strain, intensified by the strain normal to the shear crack plane:

$$P_{KBM} = \gamma_{a1} + \varepsilon_{a\perp} + \frac{\sigma_{m\perp}}{E} \tag{5.40}$$

where γ_{a1} is the principal shear strain amplitude, $\varepsilon_{a\perp}$ is the strain amplitude normal to the principal shear plane and $\sigma_{m\perp}$ is the mean stress normal to the principal shear plane.

Inserting the strain quantities from the Manson–Coffin equation (5.24), transformed with the Poisson's ratios $\nu_{el} = 0.3$ and $\nu_{pl} = 0.5$ for the elastic and plastic components, respectively, on the basis of $\sigma_m = 0$ or $R = -1$, the following equation of the P–N curve results:

$$P_{KBM} = 1.65\frac{\sigma'_f}{E}(2N)^b + 1.75\varepsilon'_f(2N)^c \tag{5.41}$$

The damage parameter P_J defined by Vormwald and Seeger[406,655,656] on the basis of the effective cyclic J-integral, ΔJ_{eff}, which takes elastic-plastic crack tip behaviour and crack closure effects into account, should be used instead of P_{SWT} when considering short crack propagation ($a < 1$ mm) resulting in technical crack initiation.

The effect of variable-amplitude loading on fatigue life (Radaj[4]) is determined on the basis of:

- counting the load cycles between the cusp points of the load–time function (e.g. rainflow cycle counting[383]),
- converting the load cycles into local stress–strain hysteresis loops on the basis of the structural yield curve and the cyclic stress–strain curve,

- attributing a P-value to each hysteresis loop based on σ_a, ε_a and σ_m,
- determining the corresponding number of cycles to damage, N_j, for each cycle and therefrom the damage contribution, $D_j = 1/N_j$ (with variants in the high-cycle fatigue range, e.g. different continuations of the S–N curve or a steadily lowered endurance limit).

Adding up the damage contributions of the hysteresis loops with an endurable total damage equal to 1.0 (Miner's rule) or another empirically founded value (relative Miner's rule) results in:

$$D = \sum_{j=1}^{N_i} D_j = \sum_{j=1}^{N_i} \frac{1}{N_j} \tag{5.42}$$

where D is the total damage, D_j is the damage contribution by the load cycle j, N_i is the crack initiation life under variable-amplitude loading and N_j is the crack initiation life under the amplitude of load cycle j. Miner's rule applied on the basis of damage parameters substitutes for the conventional form based on nominal stresses or local stresses or strains (e.g. Iida *et al.*[369]). The damage contribution should be determined immediately after the relevant load cycle in advance of rainflow cycle counting if sequence effects are expected. The rainflow cycle matrix does not retain the information on the sequence of load cycles and the original load–time function cannot be reconstructed from the matrix. The sequence effect is less important in the case of load cycles distributed at random.

The local residual stress has to be taken into account when determining the local stress–strain hysteresis loops. The simplified elastic-plastic analysis can be based on a modification of Neuber's macrostructural support formula. Different such modifications have been proposed by Lawrence *et al.*,[366,375] eq. (5.43) (see eq. (5.9) and Fig. 5.13), Reemsnyder,[390] eq. (5.44), and Seeger *et al.*,[8,345,405] eq. (5.45) (surface layer model):

$$\sigma_k \varepsilon_k = \frac{1}{E}(\sigma_n K_f + \sigma_r)^2 \tag{5.43}$$

$$\sigma_k \varepsilon_k = \frac{1}{E} \frac{(\sigma_n K_f)^2}{\left(1 - \dfrac{\sigma_r}{\sigma_k}\right)^2} \tag{5.44}$$

$$\sigma_k (\varepsilon_k - \varepsilon_r) = \frac{1}{E}(\sigma_n K_f)^2 \tag{5.45}$$

where σ_k is the maximum notch stress in the elastic-plastic state, ε_k is the maximum notch strain in the elastic-plastic state, σ_n is the nominal stress,

K_f is the fatigue notch factor, σ_r is the initial local residual stress and ε_r is the initial local residual strain.

Biaxial high-cycle fatigue ($N \geq 10^5$ cycles, $R = -1$) with a non-varying principal stress direction at the notch root ($\sigma_z = \tau_{xz} = \tau_{yz} = 0$) in ductile materials is predicted on the basis of the octahedral shear stress or distortional strain energy criterion according to von Mises, eq. (5.46), and its simplified version for plane strain conditions ($\varepsilon_y = 0$, $\sigma_y = \nu\sigma_x$, $\tau_{xy} = 0$) at the root of sharp notches ($K_t \geq 2.5$), eq. (5.47), applied on stress amplitudes:

$$\sigma_{eq} = \sqrt{\sigma_x^2 + \sigma_y^2 - \sigma_x\sigma_y + 3\tau_{xy}^2} \tag{5.46}$$

$$\sigma_{eq} = \sigma_x\sqrt{1 - \nu + \nu^2} \qquad (\varepsilon_y = 0, \sigma_y = \nu\sigma_x, \tau_{xy} = 0) \tag{5.47}$$

where σ_{eq} is the equivalent stress (amplitude), σ_x, σ_y and τ_{xy} are surface stress (amplitude) components and ν is the Poisson's ratio.

5.2.3 Special formulae for multiaxial fatigue

The application of the notch stress or strain approach requires the definition or determination of the toe notch radius and further geometric parameters of the weld profile (see Section 4.2.2). Fictitious notch rounding can also be applied (see Section 4.2.6) or small-size notches introduced (see Section 11.2.4). With these data, the notch stress or strain components which provide the basis for the equivalent stresses or strains that characterise biaxial fatigue conditions can be calculated. An excellent survey on the assessment of multiaxial fatigue is given by Socie and Marquis,[398] but application to welded joints is not an issue (see also Socie *et al.*[399]).

Biaxial low-cycle fatigue ($N \leq 10^5$ cycles, $R = -1$) with a non-varying principal strain direction (to some extent also with a varying direction) at the notch root ($\sigma_z = \tau_{xz} = \tau_{yz} = 0$) in ductile materials is predicted by Sonsino[401] on the basis of the octahedral shear strain criterion expressed in total strains, eqs. (5.48) and (5.49), and simplified for plane strain in sharp notches, eq. (5.52), with an approximated Poisson's ratio ν derived either from the fully elastic and fully plastic conditions, $\nu_{el} \approx 0.3$ and $\nu_{pl} = 0.5$, eq. (5.50), or from the cyclic stress–strain curve (Gonyea[362]), eq. (5.51):

$$\varepsilon_{eq} = \frac{1}{\sqrt{2}(1+\nu)}\sqrt{(\varepsilon_x - \varepsilon_y)^2 + (\varepsilon_y - \varepsilon_z)^2 + (\varepsilon_z - \varepsilon_x)^2 + \frac{3}{2}\gamma_{xy}^2} \tag{5.48}$$

$$\varepsilon_z = -\frac{\nu}{1-\nu}(\varepsilon_x + \varepsilon_y) \tag{5.49}$$

$$\nu = \frac{\nu_{el}\varepsilon_{el} + \nu_{pl}\varepsilon_{pl}}{\varepsilon_t} \tag{5.50}$$

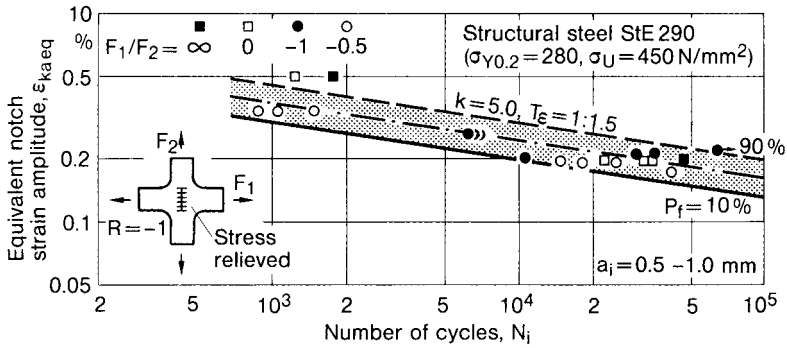


Fig. 5.9. Endurable equivalent notch strain amplitude in biaxial low-cycle fatigue (crack initiation, in-phase and out-of-phase loading conditions) of GMA weldments (non-machined and stress-relieved) in structural steel; after Sonsino.[59,60]

$$\nu = \nu_{pl} - (\nu_{pl} - \nu_{el})\frac{E^*}{E} \tag{5.51}$$

$$\varepsilon_{eq} = \frac{\sqrt{1 - \nu + \nu^2}}{1 - \nu^2}\varepsilon_x \qquad (\varepsilon_y = \gamma_{xy} = 0) \tag{5.52}$$

where ε_{eq} is the equivalent strain (amplitude), ε_x, ε_y, ε_z and γ_{xy} are strain (amplitude) components, ν_{el} is the Poisson's ratio in the fully elastic state, ν_{pl} is the Poisson's ratio in the fully plastic state, ε_{el} is the elastic strain (amplitude), ε_{pl} is the plastic strain (amplitude), ε_t is the total strain (amplitude), and E^* is the secant modulus of the (cyclic) stress–strain curve. Endurable equivalent notch strain amplitudes for welded joints in structural steel (medium-cycle fatigue range) are plotted in Fig. 5.9. Multiaxial notch stress criteria have also been extended into the medium-cycle fatigue range (see Section 4.2.10).

5.2.4 Assessment procedure

The result of the analysis according to the notch strain approach is the fatigue life (in number of cycles), primarily the crack initiation life and secondarily the total life if supplemented by the crack propagation life according to a fracture mechanics analysis (Dowling[950]). The crack initiation life is predicted for a definite load amplitude and mean load or for a definite load sequence. The proof of fatigue life reads:

$$N \le N_{per} \tag{5.53}$$

$$N_{per} = \frac{N_i}{j_N} \tag{5.54}$$

where N is the acting number of cycles, N_{per} is the permissible number of cycles, N_i is the predicted number of cycles up to crack initiation and j_N is the safety factor referring to N_i.

A safety factor $j_N \geq 5.0$ is recommended. Proof of fatigue strength instead of life is not directly possible. An iterative approach based on the prediction of the load F–N curve or load service life curve (at least by sections) is necessary in the latter case.

The notch strain approach should be accompanied by component testing in order to avoid severe assessment errors. Its vigour is the detection of the dominating influence parameters of the design task being considered and an estimate as to what extent design amendments are possible. The distinction between the periods of crack initiation and crack propagation is especially important in this connection. Such an advanced concept of computational fatigue strength assessment has been eleveloped for pressure vessel weldments with emphasis on low-cycle fatigue (Rudolph and Weiß[391]).

5.3 Demonstration examples

5.3.1 Fatigue life of stress-relieved butt-welded joints

The fatigue life of butt-welded joints made of various materials (three structural steels and one aluminium alloy) with identical weld geometry has been predicted on the basis of the notch strain approach for crack initiation combined with the fracture mechanics approach for crack propagation.[384] The cross-sectional geometry is shown within the result plots (Fig. 5.11 and Fig. 5.12), with plate thickness $t = 25.4$ mm, toe angle $\theta = 60°$ and toe notch radius $\rho = 1.3$ mm (i.e. larger than according to the worst case condition). The minor influence of the internal root face is neglected. The static and cyclic properties of the materials considered, A-36 mild steel, HY-80 and HY-130 low-alloy high strength steels and 7075-T6 (AlZnMgCu) aluminium alloy, are listed in Table 5.2 supplemented by the strain S–N curve in Fig. 5.10.

The fatigue notch factor (referring to crack initiation) is calculated for a definite notch radius ($\rho = 1.3$ mm), i.e. not for the worst case radius according to Lawrence. The worst case situation was also analysed but the changes in the results are not very large. The stress concentration factor $K_t = 2.65$ determined by finite element analysis gives the fatigue notch factor $K_f = 2.20$ (or $K_{f\,max} = 2.50$) in the case of A-36 mild steel (with $a^* = 0.025$ mm, see Fig. 4.2). The crack initiation life (for $a_i \approx 0.25$ mm) is calculated on the basis of the elastic component of the strain S–N curve, eq. (5.3), assuming the material properties of the parent metal. Elastic-plastic behaviour, residual stresses and the properties of the heat-affected zone and weld metal have been taken into account in the reanalysis performed slightly later.[378]

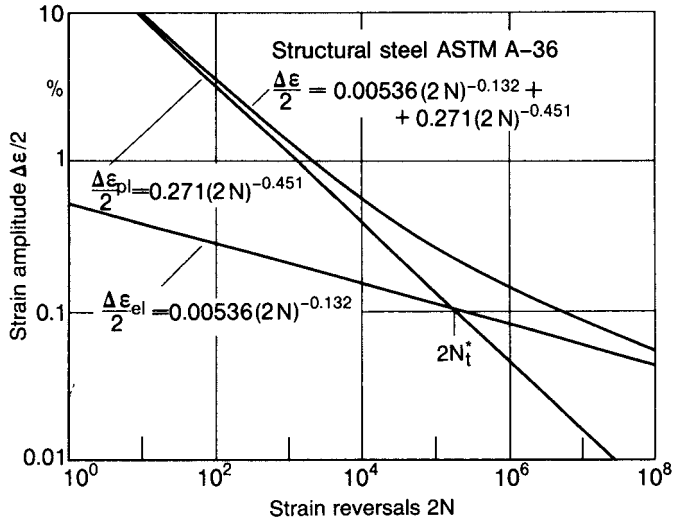


Fig. 5.10. Strain *S–N* curve of ASTM A36 low strength structural steel (σ_Y = 224 N/mm^2, σ_U = 414 N/mm^2) with elastic and plastic components; after Mattos and Lawrence.[384]

Table 5.2. Static and cyclic material parameters in the analysis performed by Mattos and Lawrence[384]

Material	$\sigma_{Y0.2}$[a] [N/mm^2]	σ_U[b] [N/mm^2]	E [N/mm^2]	K' [N/mm^2]	n'
A-36	224	414	1.9×10^5	1097	0.249
HY-80	725	849	1.9×10^5	1311	0.146
HY-130	1015	1105	1.9×10^5	1518	0.100
7075-T6	509	562	0.71×10^5	731	0.049

Material	σ_f' [N/mm^2]	b	ε_f'	c	N_t^*[c] [cycles]	a^* [mm]
A-36	1014	–0.132	0.27	–0.45	110000	0.254
HY-80	1352	–0.096	0.89	–0.62	5200	0.127
HY-130	1490	–0.060	0.90	–0.64	1800	0.077
7075-T6	1849	–0.172	1.65	–1.29	20	0.635

[a] 0.2% offset yield limit, $\sigma_{Y0.2} = R_{p0.2}$.
[b] Ultimate tensile strength, $\sigma_U = R_m$.
[c] Transition fatigue life, N_t^* ($\Delta\varepsilon_p = \Delta\varepsilon_e$).

The crack propagation life on the basis of the Paris equation (6.1) integrated between a_i and a_c (with a_c derived from K_c) is also supplemented.

The predicted *S–N* curves for crack initiation of the stress-relieved and toe-rounded welds made of different materials with identical geometric

parameters are plotted in Fig. 5.11. They are confirmed by test results available for A-36 mild steel and A-514 high strength steel.[378] The crack initiation portion of the total fatigue life of the welded joints is supplemented by Fig. 5.12. The endurance limit referring to crack initiation at $N_i \approx 5 \times 10^6$ cycles is markedly dependent on the static strength of the steels considered, but the relevant total life curves (not shown here) are rather close together.

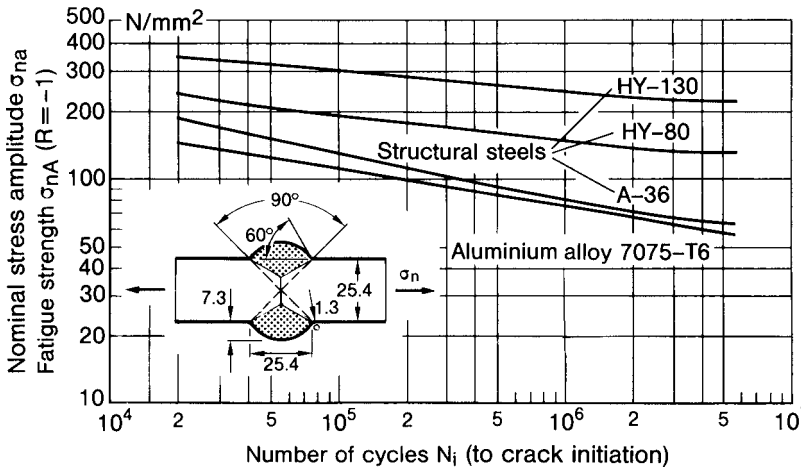


Fig. 5.11. Predicted *S–N* curves for crack initiation of butt welds with identical geometric parameters made of different materials, three structural steels and one aluminium alloy, material properties according to Table 5.2; after Mattos and Lawrence.[384]

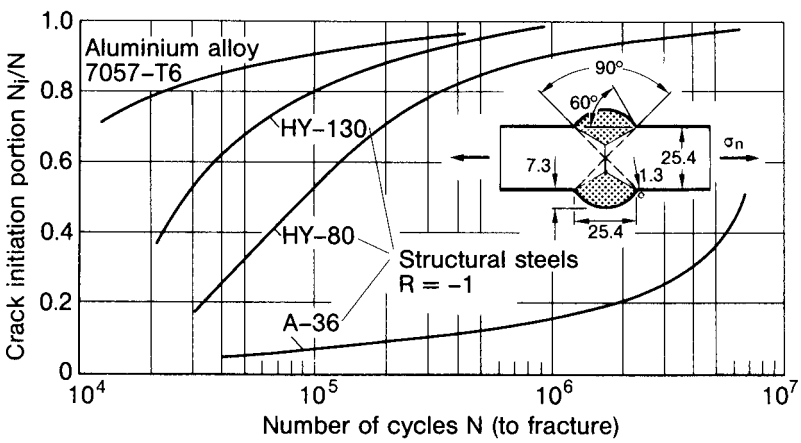


Fig. 5.12. Predicted crack initiation portion ($a_i = 0.25$ mm) of the total fatigue life of the butt welds in Fig. 5.11; after Mattos and Lawrence.[384]

The total lives of welded joints in high strength steel and in mild steel are about the same as often observed in fatigue testing of weldments, but the reason for the unexpected coalescence is different according to Lawrence. Welded joints in mild steel have a short crack initiation life and a long crack propagation life whereas welded joints in high strength steel show the opposite relation.

The crack initiation portion of fatigue life must obviously be larger near the endurance limit where crack initiation should be avoided or where initiated cracks should be restrained from propagation. The crack initiation portion has been found to correlate with the transition fatigue life N_t^*. A large value of N_t^* as is the case with A-36 steel (see Fig. 5.10) results in a low crack initiation or large crack propagation portion. Large values of N_t^* occur with ductile materials.

The notch strain approach combined with the subsequent crack propagation analysis, as demonstrated above, states that a substantial portion of the total life is devoted to crack initiation in the higher-cycle regime. This is not always found in experimental investigations. It has been shown by Hou and Charng[367] that simulation of short crack propagation between $a_0 = 0.1\,\text{mm}$ and $a_i = 0.5\,\text{mm}$ (initiation of a technical crack) results in constant or even falling portions above 10^6 cycles with better correspondence to experimental results. The crack nucleation life below $a_0 = 0.1\,\text{mm}$ was neglected. The modified Paris equation was integrated, using ΔK_{eff} with crack closure according to the modified Dugdale–Newman strip yield model. The life portion related to crack initiation in high strength steels ($a_i = 0.5\,\text{mm}$) at $N \geq 10^6$ cycles is in the range $N_i/N \leq 0.5$, i.e. substantially lower than in Fig. 5.12 referring to $a_i = 0.25\,\text{mm}$.

The fatigue strength of butt-welded joints (plate thickness $t = 5$ and 25 mm) in aluminium alloy AlMg4.5Mn (AA5083) in the stress-relieved condition has been investigated by Brandt *et al.*[213,324,354] using the combination above of crack initiation and propagation approaches in comparison with experimental results. The fatigue life of partial-penetration weldments was found to be substantially less than that of full-penetration weldments as a consequence of greater stress concentration and therefore absence of a substantial crack initiation period in the latter case. Tensile mean stresses ($R = 0$ versus $R = -1$) markedly reduced the fatigue life by diminishing the crack growth period. The extra material provided by the weld reinforcement noticeably increased the fatigue life of the partial penetration weldments.

5.3.2 Fatigue life of butt-welded joints with residual stresses

Whereas the elastic-plastic notch stress and strain analysis can be confined to the elastic portion in the high-cycle fatigue range when considering

welded joints without residual stresses in fully reversed loading ($R = -1$), the elastic-plastic notch behaviour must be taken into account in the case of residual stresses, low-cycle fatigue or zero-to-tension loading ($R \approx 0$).

The notch mean stress σ_{km} (without relaxation) results from the initial notch residual stress σ_{kr} and the effect of the first remote loading cycle, Fig. 5.13. The initial notch residual stress is assumed to be as high as the tensile yield limit, $\sigma_{kr} = \sigma_{Y0.2}$, and remote zero-to-tension loading $\Delta\sigma_n$ is applied, characterised by $R = 0$. The Neuber hyperbolae describing the upper cusp points of the stress–strain cycles at the weld toe are chosen to be identical for the three materials by adjusting $\Delta\sigma_n$ to $\sigma_{Y0.2}$ and E (elastic modulus). The Neuber counterhyperbolae are not identical under the condition above. As can be seen from the figure, the established notch mean stress σ_{km} varies greatly in dependence of the material. The high strength steel (especially in the heat-affected zone) exhibits very low notch root plasticity so that σ_{km} is larger than σ_{kr}, $\sigma_{km} > \sigma_{Y0.2}$. The mild steel with relatively high notch root plasticity stabilises σ_{km} at values near the yield limit,

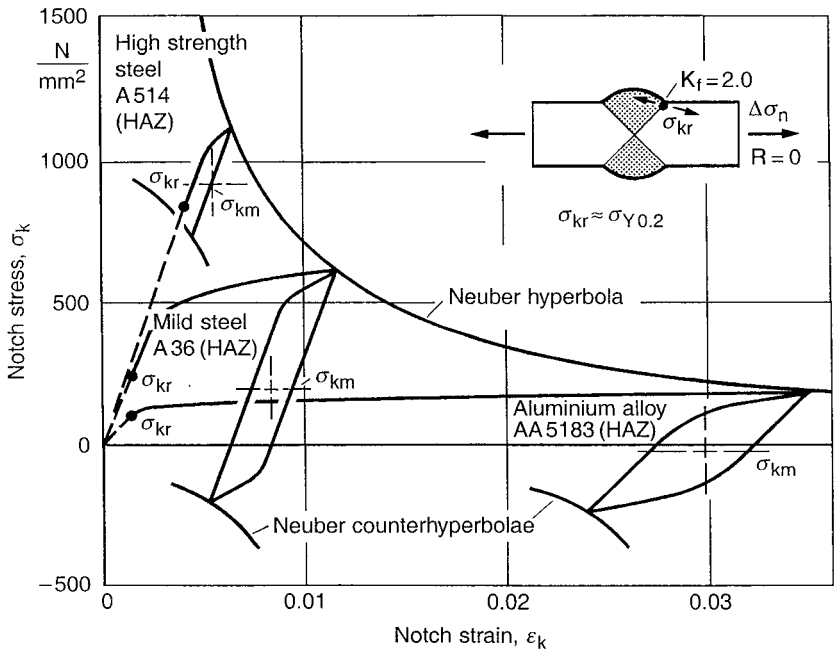


Fig. 5.13. Notch stress–strain cycles with notch mean stress σ_{km} under cyclic nominal stress $\Delta\sigma_n$ (zero-to-tension loading, $R = 0$) and initial notch residual stress $\sigma_{kr} \approx \sigma_{Y0.2}$ (yield limit); $\Delta\sigma_n$ is selected dependent on $\sigma_{Y0.2}$ and E (elastic modulus) so that the Neuber hyperbolae are identical, whereas the Neuber counterhyperbolae are different; butt-welded joints in three materials with identical shape and fatigue notch factor K_f; after Lawrence *et al.*[377]

$\sigma_{km} \approx \sigma_{Y0.2}$. The ductile aluminium alloy (especially in the non-hardened condition of the weld metal) provides very high notch root plasticity so that $\sigma_{km} \approx 0$ (despite $R = 0$). Mean stress relaxation may be superimposed in those cases where both the mean stress and the notch root plasticity are sufficiently high.

Predicted *S–N* curves for A-514 quenched and tempered steel, Fig. 5.14, indicate that high strength steel can sustain high residual stresses which do not relax under cyclic loading. The total fatigue life of such a material is highly dependent on σ_{kr} and R. Stress relief measures or mechanical postweld treatment introducing compressive stresses in the notch root (e.g. shot-peening or static overloading) are very effective in this case. The influence of σ_{kr} and R on the crack initiation life is not great for low strength steels because notch root plasticity and relaxation occur even in the high-cycle fatigue range (transition fatigue life $N_t^* > 10^5$ cycles). However, differentiation with respect to σ_{kr} and R results from the crack propagation analysis. The influence of σ_{kr} and R also vanishes for the aluminium alloy being considered because the high notch root plasticity reduces σ_{km} almost to zero after the set-up loading cycle. The calculated results above have been checked by fatigue testing to some extent.[375]

The calculated fatigue strength ($R = -1$, $N_i = 10^6$ cycles, crack initiation) of a butt-welded joint in steel in dependence of ultimate tensile strength, initial notch residual stress and weld toe angle is shown in Fig. 5.15 (cyclic properties correlated with hardness and hardness with ultimate tensile strength).[377] Stress-relieved weldments ($\sigma_{kr} = 0$) are compared with weldments in the as-welded condition ($\sigma_{kr} = \sigma_{Y0.2}$) and with postweld treated joints ($\sigma_{kr} = -\sigma_{Y0.2}$). The analysis is performed on the basis of the elastic component of the strain *S–N* curve. Plasticity and relaxation effects are neglected. The assumption $\sigma_{km} = \sigma_r$ is introduced as a first approximation (see Fig. 5.13). It can be concluded from the diagram that the residual stress

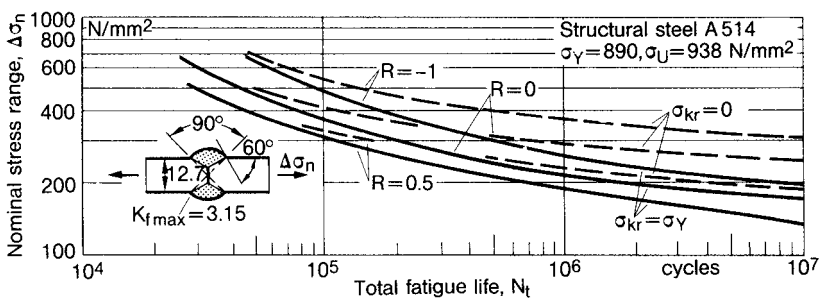


Fig. 5.14. Predicted fatigue life of butt welded joints in ASTM A514/E110 steel: effect of stress ratio R and weld toe initial residual stress σ_{kr}; after Lawrence *et al.*[377]

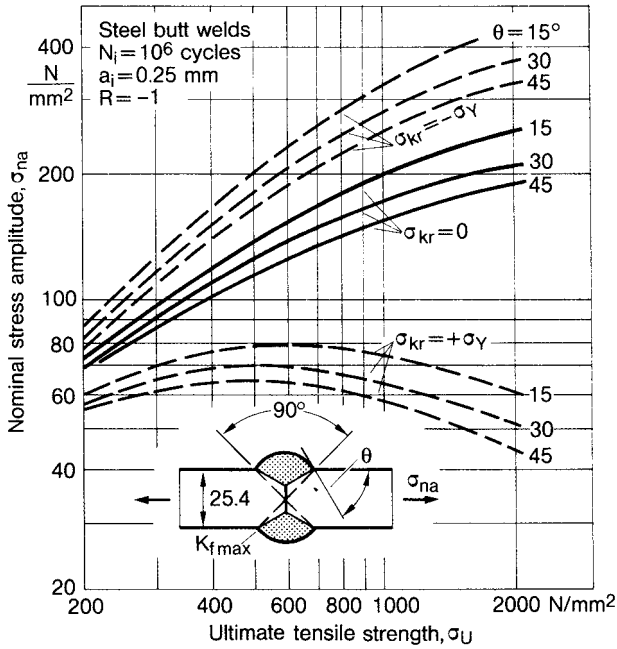


Fig. 5.15. Calculated fatigue strength of butt-welded joints in steel dependent on ultimate tensile strength: effect of weld toe initial residual stress σ_{kr} in relation to yield limit σ_Y for different weld toe angles; after Lawrence *et al.*[377]

effect is extremely strong for high strength steels but not so for low strength steels. Residual stresses close to the tensile yield limit cause the fatigue strength to decrease with increasing ultimate tensile strength. On the other hand, the benefit from mechanical postweld treatment is especially large for high strength steels.

The result of another similar analysis[379] taking notch root plasticity and mean stress relaxation into account is shown in Fig. 5.16 (with stress amplitudes substituted by stress ranges). The tendencies discussed above are confirmed but the calculated fatigue strength is changed to some extent. Mean stress relaxation has a minor influence especially in the case of high strength steels.

Testin *et al.*[403] have also successfully predicted the fatigue strength of groove-welded cruciform joints in steel after shot-peening according to the notch stress and strain approach. Bertini *et al.*[349] have similarly considered butt welds in aluminium alloy of type AA6063 in the as-welded, stress-relief annealed and shot peened condition. They found stabilisation of the notch stresses and strains after the set-up loading cycle (shake-down to elastic conditions after changing the residual stresses).

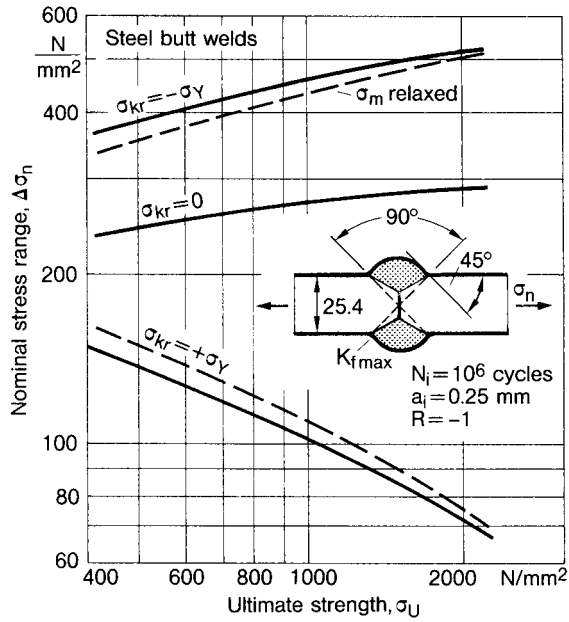


Fig. 5.16. Calculated fatigue strength of butt-welded joints in steel dependent on ultimate tensile strength: effect of weld toe initial residual stress σ_{kr} in relation to yield limit σ_Y and effect of mean stress relaxation; after Lawrence and Mazumdar.[379]

5.3.3 Fatigue life of fillet-welded cruciform and T-joints

The notch strain approach, version according to Lawrence, in combination with a crack propagation analysis has successfully been applied by Jakubczak and Glinka[370] to predict the fatigue life of misaligned cruciform joints with fillet welds comprising internal root faces (see also Lie and Lan[517] as well as Singh *et al.*[395]). Fully reversed axial loading ($R = -1$) was applied. The material under consideration was 15G2ANb low-alloy steel (C 0.18, Mn 1.6, Si 0.4), with static and cyclic material properties according to Table 5.3. The cross-sectional dimensions, Fig. 5.17(a), are the following: plate thickness $t = 8$ mm, plate width $w = 40$ mm, root face length $g = 7.9$ mm, weld leg length $c = 7.8$ mm, plate eccentricity $e = 0.8$ mm, weld toe radius $\rho_A = 0.8$ mm (peak value of a Weibull distribution) and weld root radius $\rho_B = 0.1$ mm. The specimens are tensile-loaded with the ends rigidly clamped, i.e. a secondary bending moment and a secondary shear force are produced in the grips.

The crack initiation analysis (up to $a_i = 0.25$ mm) is performed on the basis of eqs. (5.24), (5.29) and (5.34), and the crack propagation analysis on

Table 5.3. Static and cyclic material parameters of low-alloy steel in the analysis performed by Jakubczak and Glinka[370]

Material	$\sigma_{Y0.2}$[a] [N/mm^2]	σ_U[b] [N/mm^2]	E [N/mm^2]	K' [N/mm^2]	n'
15G2ANb	370	570	2.14×10^5	843	0.14

Material	σ'_f [N/mm^2]	b	ε'_f	c	m	C [N, mm]
15G2ANb	707	–0.076	0.23	–0.5	3.4	1.246×10^{-13}

[a] 0.2% offset yield limit, $\sigma_{Y0.2} = R_{p0.2}$.
[b] Ultimate tensile strength, $\sigma_U = R_m$.

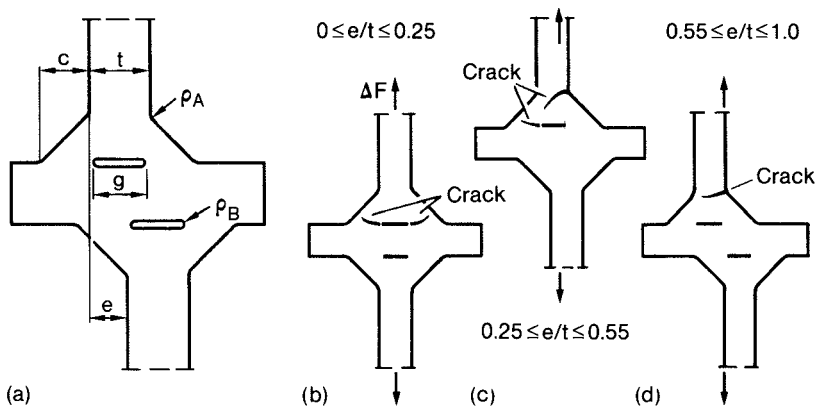


Fig. 5.17. Misaligned cruciform joints with fillet welds; geometric parameters of the cross sectional model (a) and most probable fracture sites depending on degree of misalignment (b, c, d); after Jakubczak and Glinka.[370]

the basis of the Paris equation. The elastic stress concentration factors at the weld toe (with $e = 0$) determined by the finite element method are $K_t = 2.34$ and 1.64 in tensile and bending loading, respectively. The stress concentration factors at the weld root, referring to nominal stresses in the weld leg plane are substantially higher. Conversion to the nominal stresses at the weld toe (as K_t above) results in $K_t = 3.44$ and 1.72, respectively (which seems to be too low for a notch radius of 0.1 mm). The geometry factor Y in the stress intensity factor of the crack propagation analysis is determined proceeding from the stress distribution in the uncracked specimen, i.e. the stresses normal to the anticipated crack path, evaluating weight function

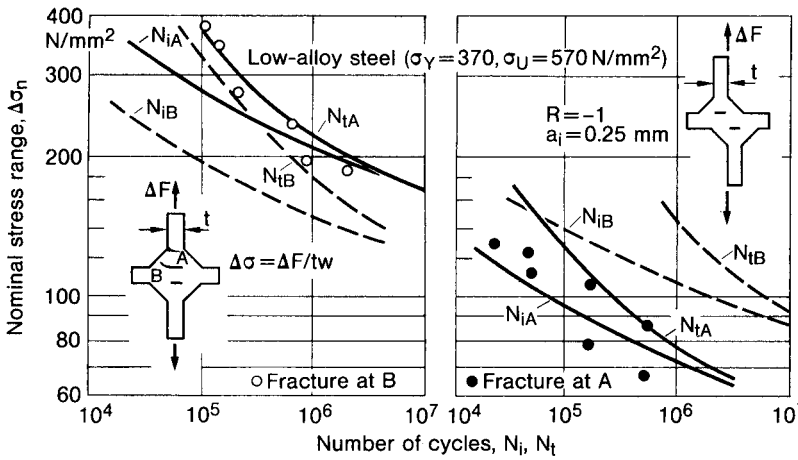


Fig. 5.18. Predicted *S–N* curve for fillet-welded cruciform joint without misalignment ($e/t = 0$) and with misalignment ($e/t = 1$): crack initiation life N_i and total life N_t (the difference being the crack propagation life N_p), crack initiation at weld toe (A) or weld root (B), compared with experimental results; after Jakubczak and Glinka.[370]

integrals according to Emery[456] and Albrecht and Yamada,[409] and superimposing the results for tensile and bending loading.

A typical result of the fatigue life calculation is plotted in Fig. 5.18 and compared with experimental results. The limit cases of zero misalignment ($e/t = 0$) and extremely large misalignment ($e/t = 1$) are considered. The fatigue fractures originate at the weld root (designated by B) in the case of zero misalignment and at the weld toe (designated by A) in the case of large misalignment. Strength and life values are heavily reduced in the latter case. The crack initiation analysis definitely locates the most probable site of fracture (root or toe fracture) which depends strongly on the degree of misalignment. The ranges of misalignment e/t where root fractures, mixed mode fractures and toe fractures occur are included in Fig. 5.17(b, c, d). Note that secondary forces are generated apart from the tensile load ΔF by bending-rigid clamping at the specimen ends (free clamping length $l = 300$ mm).

It is concluded from Fig. 5.18 that both the crack initiation and crack propagation periods are essential for the total life. The crack initiation portion dominates in the high-cycle fatigue range ($N \geq 5 \times 10^6$ cycles) whereas crack propagation is essential in the medium- and low-cycle ranges.

The fatigue strength and life of a fillet-welded cruciform joint in StE355 fine-grained steel ($\sigma_{Y0.2} = 381\,\text{N/mm}^2$, $\sigma_U = 561\,\text{N/mm}^2$) is predicted by Prowatke *et al.*[268] on the basis of the elastic fatigue notch factor according

to Lawrence and Peterson, combined with a stress concentration factor formula published by Rainer.[304,305] Only crack initiation at the weld root is considered. The decisive geometric parameters are the plate thickness t = 12 mm, the leg length c = 7.5 mm and the root face length g = 12 mm. The elastic fatigue notch factor is transferred into the medium-cycle fatigue range assuming a linear decrease down to $K_f = 1.0$ at $N = 1$ cycle. The linear decrease is modified in the low-cycle fatigue range by taking the limit load into account, as predicted according to Seeger and Heuler.[392] Note that the notch strain approach is applied only in respect of this correction. The cyclic material parameters are defined according to Lawrence[377] on the basis of hardness measurements. The predicted S–N curves for the weld metal (H_V = 180 HV) and the heat-affected zone (H_V = 270 HV) run close together.

The fatigue strength of fillet-welded T-joints in high strength structural steel (four point bending specimens) has been determined on the basis of the notch strain approach by Tricoteaux *et al.*[404]

5.3.4 Fatigue life of a welded containment detail

The notch strain approach, version according to Seeger, has been applied to the structural detail of the containment shell of a nuclear reactor.[364] The detail considered, Fig. 5.19(a), is a single-bevel butt weld with fillet welds between inclined flange and web ending in a cope hole. The materials are fine-grained steels, type BHW25 (in the flange) and type TTStE32 (in the web), connected by multilayer welding. The fillets of the weld are machined to large notch radii by grinding. The welded joint is loaded by bending moments, Fig. 5.19(c). The load sequence consists of stepwise variable stress amplitudes and mean stresses, Fig. 5.22(b). The maximum notch stress is compressive in the fillet with the smaller notch radius. Residual stresses are not taken into account.

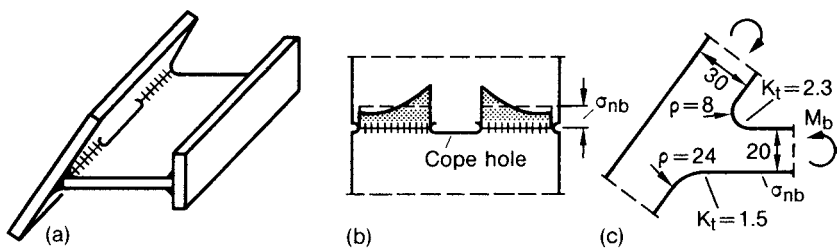


Fig. 5.19. Structural detail (a) of a nuclear reactor containment, definition of nominal bending stress (b) and notch stress concentration factors K_t (c) at the notch root near the cope hole; after Heuler and Seeger.[364]

The first step of the analysis is the determination of the notch stress concentration at the notch root of the fillet weld near the cope hole. Fictitious notch rounding or any other microstructural support hypothesis is not necessary because the notch radii are rather large. The nominal stress in the stress concentration factor is defined as mean bending stress across the weld length, Fig. 5.19(b). It averages the bending stress which is unevenly distributed with a rise at the cope hole where the maximum notch stress is determined by strain gauge measurement. The resulting stress concentration factors are $K_t = 2.3$ and $K_t = 1.5$, Fig. 5.19(c).

The fatigue life up to crack initiation is predicted for the two parent materials and for the weld metal, the latter simulated by a comparison specimen. The comparison specimen is machined out of the actual weld. Crack initiation occurs at the transition from the weld metal to the heat-affected zone, Fig. 5.20(b). The dimensions of the comparison specimen are similar to those of the weld so that size effects are negligible.

The static and cyclic material properties used in the calculations are listed in Table 5.4. The monotonic and cyclic stress–strain curves are plotted in Fig. 5.20(a). Both Neuber's macrostructural notch support formula, eq. (5.29), and a more sophisticated formula according to Seeger, eq. (5.35), are used to determine the elastic-plastic stresses and strains at the notch root. The strain S–N curves with initiated surface crack length, $2c_i = 0.5$ mm, Fig. 5.21(a), are converted to damage parameter P–N curves with P_{SWT} according to eq. (5.39), Fig. 5.21(b). The fatigue life is predicted for the two notches under the load sequence of Fig. 5.22(b) using Miner's rule with $D = 1.0$. The resulting service life curves are plotted in Fig. 5.22(a) and compared with the test result at the notch with the higher K_t-value (crack depth $a_i = 0.5$ mm).

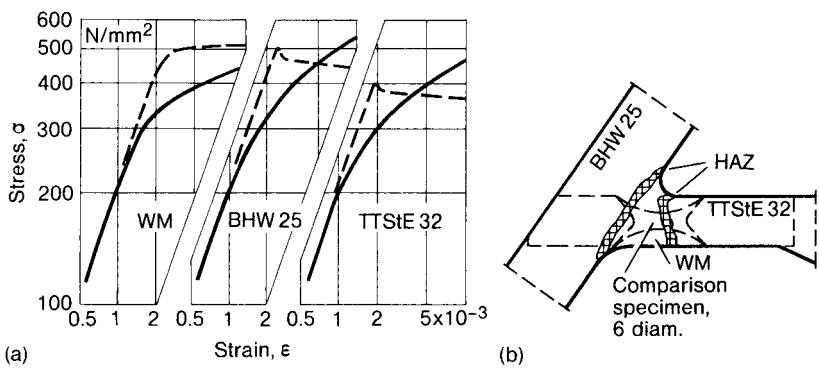


Fig. 5.20. Monotonic (dashed) and cyclic (solid) stress-strain curves (a) of weld metal (WM, as-welded) and of fine-grained steel, types BHW25 and TTStE32, and structural detail (b) with enclosed comparison specimen (dashed lines); after Heuler and Seeger.[364]

Table 5.4. Static and cyclic material parameters in the analysis performed by Heuler and Seeger[364]

Material	$\sigma_{Y0.2}$[a] [N/mm²]	σ_U[b] [N/mm²]	E [N/mm²]	K' [N/mm²]	n'
Weld metal	500	626	2.09×10^5	702	0.095
TTStE32	375	558	2.09×10^5	1033	0.166
BHW25	460	614	2.09×10^5	1220	0.170
Material	σ'_f [N/mm²]	b	ε'_f	c	
Weld metal	679	–0.0575	0.707	–0.607	
TTStE32	813	–0.0775	0.237	–0.466	
BHW25	966	–0.0825	0.253	–0.484	

[a] 0.2% offset yield limit, $\sigma_{Y0.2} = R_{p0.2}$.
[b] Ultimate tensile strength, $\sigma_U = R_m$.

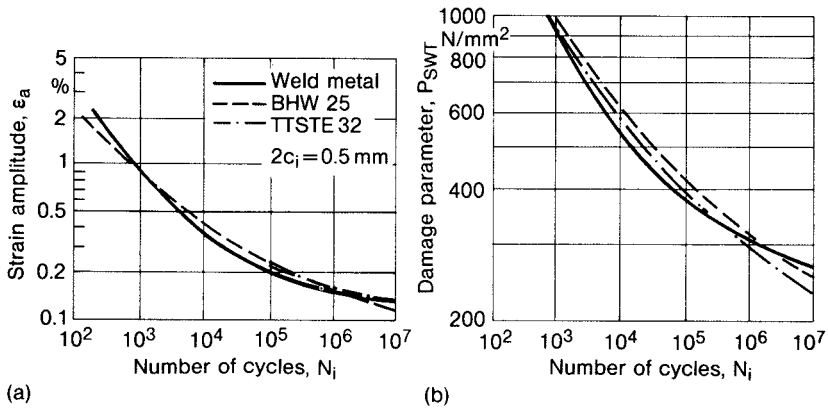


Fig. 5.21. Strain *S–N* curves (a) of weld metal (comparison specimen, as-welded) and parent metals, and damage parameter *P–N* curve (b) of the same materials, crack initiation with surface crack length, $2c_i = 0.5$ mm; after Heuler and Seeger.[364]

The conclusion from the results is that the fatigue life is predicted with acceptable accuracy on the basis of the notch strain approach. The differences between the materials are negligible because weld metal and parent materials have comparable hardness values (H_V = 180–200 HV) whereas the hardness peak in the heat-affected zone ($H_{V\,max}$ = 280 HV) is restricted to a relatively small volume. The validity claimed for Miner's rule (as far as validity can be derived from only one test result) must not be generalised.

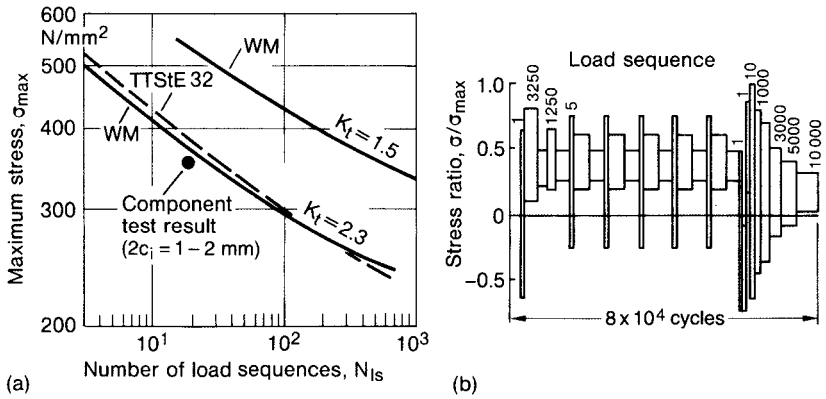


Fig. 5.22. Predicted service life curves (crack length $2c_i = 0.5$ mm) and the component test result (crack length $2c_i = 1$–2 mm) (a) with applied load sequence (b); after Heuler and Seeger.[364]

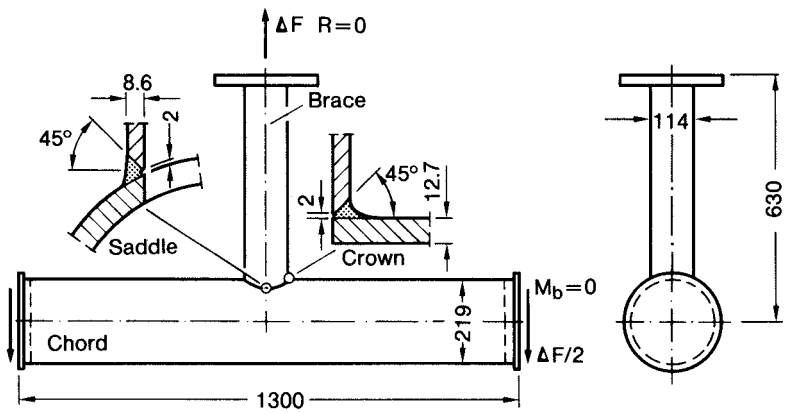


Fig. 5.23. T-shaped welded tubular joint investigated according to the notch strain approach; after Bohlmann.[351,352]

The notch strain approach has also been used to predict the fatigue strength of coped girders (Seeger and Zacher[393]) and of ship structural details (Fricke and Paetzold[359]).

5.3.5 Fatigue strength of welded tubular joint

The notch strain approach has been applied by Bohlmann[351,352] to determine the fatigue strength of a T-shaped welded tubular joint, Fig. 5.23. This structural component consisting of a chord and brace tube is better designated a 'pipe branch' because the chord member's wall inside the brace member

is removed. The brace tube is loaded by a zero-to-tension ($R = 0$) axial force ΔF resulting in transverse force bending of the chord tube (with zero bending moment at the chord ends). The tube joint is fabricated of normalised CMn steel, type StE290.7 ($\sigma_{Y0.01} = 338\,N/mm^2$, $\sigma_U = 469\,N/mm^2$), and manually multipass-welded with electrodes consisting of filler metal, type E5132.

The *S–N* curve in terms of endurable force ranges was first experimentally determined by fatigue tests with force range levels, $\Delta F = 90$, 125 and 210 kN, resulting in endured numbers of cycles between $N = 5 \times 10^4$ and 2×10^6 cycles. Typical fatigue cracks parallel to the weld were detected. They were located in the chord tube at the undercut notch of the weld toe in the heat-affected zone. Their mean position was 35° from the saddle point with a standard deviation of 20°. A crack length $2c_i \approx 2$ mm at the tube surface was defined to be the failure criterion evaluated in the *S–N* diagram. A crack propagation analysis was used to reckon back the number of cycles connected with this crack length from the larger values actually determined. The theoretical analysis was adjusted to the experimentally detected striation markings on the fracture surface. The inverse slope of the mean *S–N* curve, $k = 3.97$, was close to the expected value, $k = 3.75$, of the normalised *S–N* curve of welded joints. A uniform scatterband according to Olivier and Ritter[52] was associated with this *S–N* curve (see Fig. 5.28).

The cyclic material properties are considered to be dependent on the microstructural state at the crack initiation site (mainly heat-affected zone). The cyclic stress–strain curves for parent material, heat-affected zone and weld metal are plotted in Fig. 5.24. The relevant strain *S–N* curves for

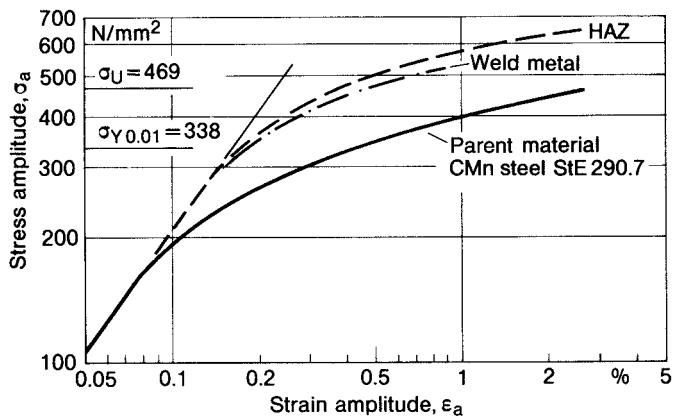


Fig. 5.24. Cyclic stress–strain curves of parent material (type StE290.7 CMn steel), heat-affected zone (HAZ) and weld metal; after Bohlmann.[351,352]

initiation of a technical crack are shown in Fig. 5.25 (without the weld metal which is considered to have a negligibly low crack initiation life because of embedded imperfections). Contrary to expectation, there is only a minor effect of hardness on the fatigue strength in the high-cycle range. The markedly lower endurable plastic strains of the heat-effected zone in the low- and medium-cycle range are compensated to some extent in terms of stresses by the higher-running cyclic stress–strain curve. Relevant damage parameter *P–N* curves, for example, according to Smith, Watson and Topper,[397] Fig. 5.26, differentiate between small-scale and full-scale behaviour of the heat-affected material. Small-scale specimens were used to simulate the thermal cycles of the heat-affected zone experimentally whereas full-scale specimens are dimensioned close to reality (the cooling rate is

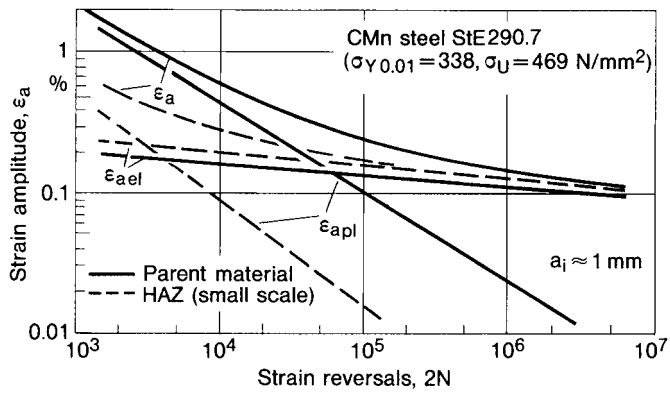


Fig. 5.25. Strain *S–N* curve of type StE290.7 CMn steel, parent material and heat-affected zone (HAZ); after Bohlmann.[351,352]

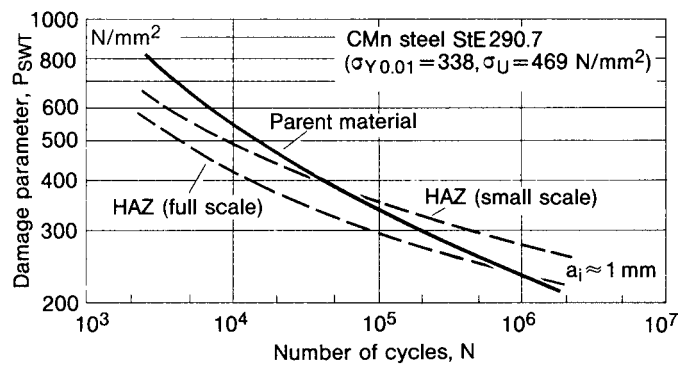


Fig. 5.26. Damage parameter *P–N* curve of type StE290.7 CMn steel, parent material and heat-affected zone (HAZ); after Bohlmann.[351,352]

reduced in the full-scale specimens resulting in a correction of the small-scale data according to Bäumel and Seeger[346]). There are also P–N curves in terms of the damage parameter P_{KBM} derived according to Kandil, Brown and Miller.[372] The cyclic material parameters are summarised in Table 5.5.

The load–strain relationship or 'yield curve' at the crack initiation site is determined using the finite element method. Solid elements are applied in the weld region. The plate thickness here consists of four layers of elements, whereas the weld throat thickness consists of three layers. The notch stresses and strains at the weld toe are not sufficiently well simulated, i.e. they probably remain behind the actual values. The cyclic stress–strain curves are introduced according to parent material, heat-affected zone and weld metal. The location of crack initiation resulting from the maximum damage parameter P_{SWT} is predicted at 26° from the saddle point which meets the real condition (35° ± 20°) sufficiently well. The corresponding local first principal strain and equivalent strain (according to the distortional strain energy criterion) is shown in Fig. 5.27. The maximum structural

Table 5.5. Cyclic material parameters in the analysis of Bohlmann[351,352]

CMn steel StE290.7	K' [N/mm^2]	n'	σ'_f [N/mm^2]	b	ε'_f	c
Parent material	776	0.144	853	–0.095	1.926	–0.660
Heat-affected zone	1089	0.126	1117	–0.098	1.224	–0.781
Weld metal	924	0.119	—	—	—	—

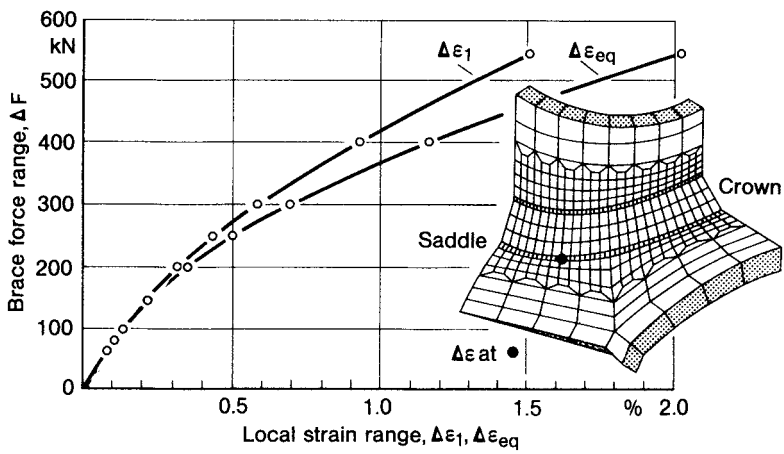


Fig. 5.27. Load–strain curves at point of crack initiation at weld toe of tubular joint determined by the finite element method, first principal strain, $\Delta\varepsilon_1$, and distortional strain energy equivalent, $\Delta\varepsilon_{eq}$, dependent on brace force, ΔF; after Bohlmann.[351,352]

stress at the inner surface of the intersecting tubes was found to be as high as the structural stress at the hot spot on the outside surface, but it is not superimposed by an additional notch effect and thus does not present a major risk of crack initiation.

The fatigue life in terms of number of cycles N (to crack initiation) of the tubular joint for definite load ranges ΔF was calculated based on the damage parameter P–N curves derived by experiment and the load–strain relationship derived by the finite element analysis. A local tensile residual stress equal to the cyclic elastic limit, $\sigma'_{Y0.01} = 234\,N/mm^2$, is taken into account in the damage parameter equation. Typical calculation results for the tubular joint are compared with the experimental findings in Fig. 5.28. The deviation in absolute values and inverse slope of the two curves (P_f = 50%) is unsatisfactory but the calculation results remain on the safe side for $N < 10^6$ cycles. Further variants comprise different damage parameters (P_{SWT} and P_{KBM}, eqs. (5.38–5.41)) and equivalent stresses (von Mises and principal normal stress), the calculation without and with residual stresses, the latter without and with mean stress relaxation (according to eq. (5.12)). The residual stress has a major (reducing) influence on the fatigue life in the high-cycle fatigue range. The mean stress relaxation increases the fatigue strength at lower cycle numbers. The influence of the type of damage parameter and equivalent stress, respectively, are negligible because the relevant shear stresses are low in the case considered.

The material-dependent slope exponent k of the S–N curve of welded structural details in general has been derived by Gimperlein[25] on the basis of Manson–Coffin's strain S–N curve, Ramberg–Osgood's stress–strain curve, Neuber's notch macrosupport formula and Seeger's 'uniform material law' (Table 5.1). It ranges between $k = 1/(-b) = 11.5$ of the elastic strain

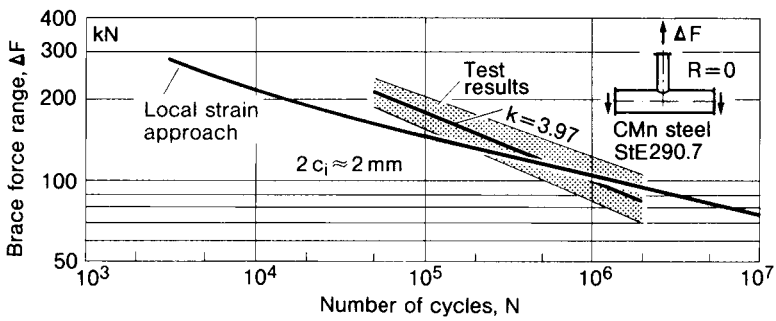


Fig. 5.28. Crack initiation fatigue strength and life (F–N curve, $a_i \approx 1$ mm, $2c_i \approx 2$ mm, damage parameter P_{SWT}, von Mises equivalent stress, residual stress $\sigma_{rs} = \sigma'_{Y0.01}$, without mean stress relaxation) of welded tubular joint according to the notch strain approach compared with test results; after Bohlmann.[351,352]

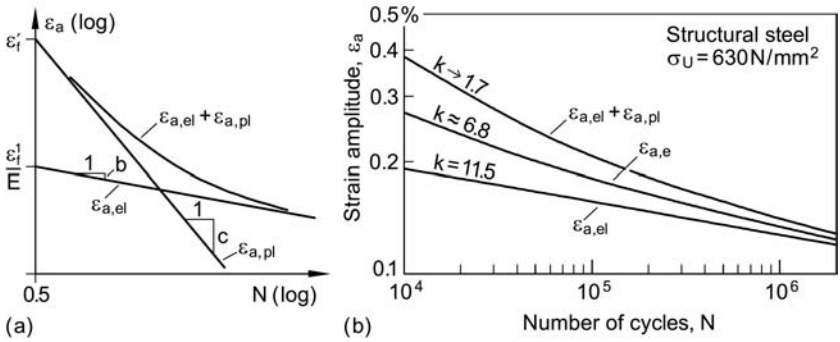


Fig. 5.29. Strain *S–N* curve of plain specimens defined after Manson and Coffin with basic material parameters (a), and the same with the theoretical linear-elastic notch strain amplitude $\varepsilon_{a,e}$ of a structural component in high strength steel (b); after Gimperlein.[25]

component and $k = 1/(-c) = 1.7$ of the plastic strain component, Fig. 5.29(a). To calculate the exponent of structural details referring to the nominal stress *S–N* curve, the theoretical linear-elastic notch strain $\varepsilon_e = K_t\varepsilon_n$ is introduced into Neuber's formula. The result for high strength steel (σ_U = 630 N/mm^2) is the averaged value $k \approx 6.8$, Fig. 5.29(b). The corresponding value for low strength steel (σ_U = 400 N/mm^2) is $k \approx 6.0$. Obviously, differences in the notch support behaviour are not detected by Neuber's formula, but Bohlmann's[351, 352] averaged slope exponent between $N = 10^4$ and $N = 10^7$, $k \approx 6.5$, is confirmed. The argument of Gimperlein[25] is noteworthy in that the value of k depends on the degree of elastic notch support during plastic deformation. The strain or displacement controlled total strain *S–N* curve represents maximum elastic support, the stress or load controlled elastic strain *S–N* curve stands for low elastic support.

6

Crack propagation approach for seam-welded joints

6.1 Basic procedures

6.1.1 Principles of the crack propagation approach

The assessment of fatigue strength according to the notch stress or notch strain approach is related to the initiation of a 'technical' crack (usually at the surface, crack length about 1 mm, crack depth about 0.5 mm). The incipient technical crack can be tolerated in many cases because further cyclic loading is possible with stable crack propagation, first through the wall thickness of the structural member and then over further areas, possibly ending in brittle fracture or ductile tearing of the remaining cross-section. The strength or life assessment based on crack propagation may therefore supplement the aforementioned assessments of crack initiation. On the other hand, there are many cases of application in which the strength or life assessment should be based on an existing crack or crack-like defect. Furthermore, there may be crack-like slits within a structural member, e.g. weld root faces.

The fatigue strength and service life of structural members with an existing crack or crack-like defect, gap or slit can be determined according to the crack propagation approach, Fig. 6.1. The crack propagation rate of a technical crack, subject to medium- or high-cycle fatigue conditions, can be analysed based on the cyclic stress intensity factor ΔK_I (mode I) or its equivalent value on the basis of a simple empirical relationship proposed by Paris and Erdogan.[580] Cyclic crack propagation occurs as soon as the threshold value of the stress intensity factor is exceeded and ends as soon as the critical stress intensity or the load-carrying capacity of the remaining cross-section is reached with larger crack length. The crack path follows the pure mode I condition in general. The cyclic J-integral may be used to describe crack propagation in the case of higher stresses and strains with accompanying larger elastic-plastic deformation at the crack tip. Crack closure has to be taken into account especially in the compressive stress

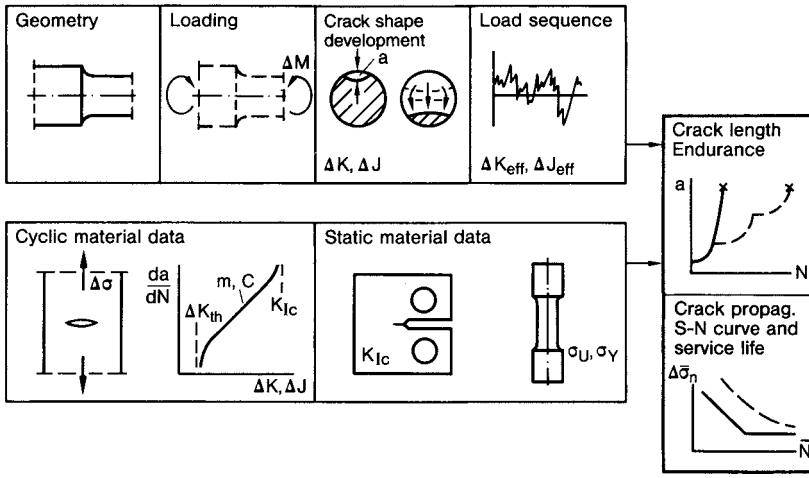


Fig. 6.1. Crack propagation approach to assess the fatigue strength and service life of non-welded structural components; with ΔM cyclic external moment, a crack depth or length, ΔK cyclic (effective) stress intensity factor, ΔJ cyclic J-integral, $\Delta\sigma$ cyclic stress, ΔK_{th} threshold stress intensity factor, K_{Ic} critical stress intensity factor, m and C material constants in the Paris equation, σ_U ultimate tensile strength, σ_Y yield limit, $\Delta\bar{\sigma}_n$ maximum cyclic nominal stress in variable-amplitude loading, N number of cycles and $\bar{N}$ number of cycles to failure; after Radaj.[5]

range. This can be achieved in a simplified manner by neglecting the compressive part of the stress range. The crack length versus number of cycles follows from integrating the crack propagation equation cycle by cycle up to the condition of final fracture. Nominal stress S–N curves and service life curves for structural members containing a crack, crack-like defect or slit may be determined in this way by calculation. The crack initiation life according to the notch stress or notch strain approach and the crack propagation life according to the crack propagation approach may be added up to give the total life.

The conventional approach considers crack propagation exclusively under mode I crack tip loading conditions. There is cyclic crack propagation also possible under mixed mode loading states with the tendency of crack branching thus re-establishing mode I conditions (Pook,[586–589] Quian and Fatemi[590]). Non-branching (i.e. coplanar) mixed mode crack propagation may be observed under mode I and III conditions (Kim[503]). Continuous co-planar crack propagation with an increased rate has been observed with high strength aluminium alloys under pure mode II loading (Otsuka *et al.*[576,577]). In more advanced approaches, the Paris equation may be substituted by crack path-related damage accumulation concepts, among

them the J-integral related damage parameter P_J proposed by Vormwald and Seeger[654–656] which puts emphasis on the short-crack closure effects.

6.1.2 Pecularities with seam-welded joints

Within the crack propagation approach applied to seam-welded joints, it is considered a feature of these joints that flaws, slag intrusions or microcracks resulting from manufacturing measures and subjected to high tensile residual stresses are typical of the notches at the weld toe and weld root, especially when these are combined with undercut or lack of penetration. Additionally it is assumed that crack propagation actually starts with the first load cycle so that the crack initiation phase can be completely neglected. Applying this approach as proposed by Maddox,[521–531] Lawrence,[433,434,506,507,636] Harrison,[476–478] Hobbacher[486,487] and others, Fig. 6.2, the fatigue life of the structural member is predicted. By integration of the Paris equation resulting in the proportional relation $N \propto 1/(K\Delta\sigma_n)^m$, with K being the stress concentration factor, with $m \approx 3$ characterising the exponent in the Paris equation and with $\Delta\sigma_n$ being the nominal stress range. The stress concentration factor K can be related to notch stresses ($K = K_t$) or to structural stresses ($K = K_s$). The procedural variant with K_s neglects the notch effect on the stress intensity. This is acceptable from an engineering point of view

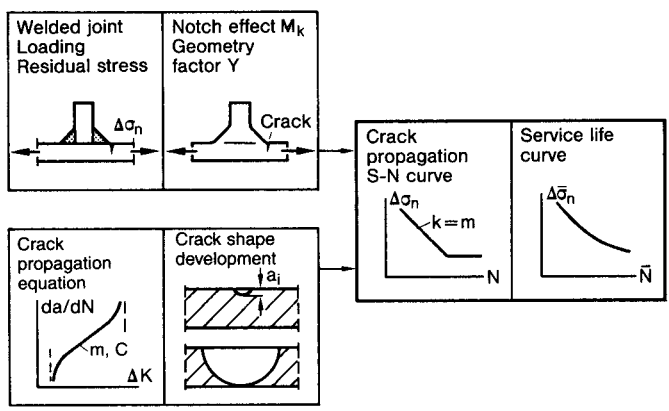


Fig. 6.2. Crack propagation approach as proposed by Maddox, Lawrence and Hobbacher, to assess the fatigue strength and service life of welded joints; with $\Delta\sigma_n$ cyclic nominal stress, M_k magnification factor, Y geometry factor, da/dN crack propagation rate, ΔK cyclic stress intensity factor, m and C material constants, k inverse slope of S–N curve, $\Delta\bar{\sigma}_n$ maximum cyclic nominal stress in variable-amplitude loadings, N and $\bar{N}$ numbers of cycles to failure; after Radaj.[5]

when combined with an appropriate initial crack size and applied to sharply notched welds (Hirt and Kummer[485]). The procedural variant with K_t presumes that the decrease of the notch stress related magnification factor M_k with increasing crack length is taken into account using available approximation formulae. The decrease is extremely steep at the notch root. Therefore, mainly short crack propagation is influenced by the notch stress concentration, but the short crack propagation range is an essential part of the total life.

The crack propagation analysis starting with a small semi-elliptical surface crack and ending with the enlarged crack penetrating the plate thickness (the axis ratio is often assumed to be constant for simplification) results in the *S–N* curve of the welded joint under constant-amplitude loading (inverse slope *k* of the *S–N* curve equals exponent *m* in the Paris equation) or the service life curve under variable-amplitude loading (result identical to Miner's rule).

A more detailed analysis should take the inhomogeneity of material into account which is caused in the weld area by the filler material and the thermal cycles of the welding process (actually a 'layered material problem'[591]). Also, advanced concepts based on crack path-related damage accumulation may be applicable (Karzov *et al.*[502]).

The crack propagation approach which is indispensable for the assessment of sufficiently large crack-like imperfections (e.g. with the aim of proving fitness for purpose[17,488]) or of design-inherent slit faces in welded joints (e.g. in fillet-welded cruciform or lap joints) should be confronted with serious objections if used to predict the fatigue strength and service life of unconventional welded joints or to classify them in respect of standard notch or detail classes. This is usually done proceeding from very small (≤ 0.1 mm), more or less fictitious microcracks at the weld toe, thus neglecting the short-crack initiation phase and calculating crack propagation on the basis of the elastic stress intensity factor of short cracks.

The first objection is that microcracks at the weld toe in high-quality welded joints which additionally propagate with the first loading cycles cannot be proven to exist generally in reality (in contrast to weld root defects). Merely non-metallic inclusions and slag intrusions have been detected in carefully performed metallographic investigations on gas metal arc and manual metal arc welded high strength steels and proposed as initial cracks for the crack propagation analysis.[471,478,481,608,664] But slag intrusions are not readily observed with other materials and welding processes and a noticeable crack initiation phase can be expected in the case of the inclusions and intrusions mentioned above. Another investigation detected facet-like initial fracture surfaces with a depth of 0.01–0.07 mm in fillet-welded structural steel specimens (Miki *et al.*[535,536]). Initial crack depths in welded high strength steels have been measured by Smith[615,616] ($a_i \approx$

0.05 mm), Signes *et al.*[608] (a_i = 0.02–0.15 mm) and Watkinson *et al.*[664] (a_i = 0.01–0.4 mm). In considering the weld toe in aluminium alloys, 'loose grains' have been detected as crack initiator[485] but not generally confirmed. The presumed high tensile residual stresses at the weld notches, on the other hand, occur only with special types of welded joints, welding conditions and material parameters. An additional objection to the fictitious microcrack considered above is that the choice of the dimensions of the microcrack is arbitrary unless based on statistically evaluated experimental findings.

The second objection is that, considering those rare cases in which the microcrack is detectable and immediate crack propagation can be assumed, the elastic stress intensity factor is less suited to describe crack propagation. The result of the analysis, if performed, may be highly unsafe (factor 10 on life and more). It is recommended that short-crack propagation in the plastically deformed notch area (inclusive of crack closure effects if appropriate) be described based on the cyclic *J*-integral (Vormwald and Seeger[654–656]) or based on the notch stress intensity factor (Verremann *et al.*[651–653]).

The third objection is that crack propagation does not take place according to the simplifying assumption that the aspect ratio of the semi-elliptical surface crack remains constant. In general, microcracks are initiated at several positions simultaneously and coalescence to a single crack takes place at a later stage. Additionally, the single crack may propagate more in surface length than in depth. These processes can only partly be simulated numerically and complicate the analysis substantially.

6.1.3 Short-crack behaviour

Short-crack behaviour under non-welded material conditions has been extensively investigated since 1980 (Radaj[6]). Similar investigations in welded joints are rare.

The basic facts of short-crack behaviour are summarised first. Short cracks comprise both the very small microcracks (smaller than microstructural obstacles, e.g. grain boundaries or inclusions) and the larger short cracks in the sense of continuum mechanics, covering several obstacle distances.

First fact: The initiation phase of a technical surface crack (surface length 1 mm, depth 0.5 mm) consists of microcrack propagation. The initiation size of a microcrack is far smaller than the grain size. Microcrack initiation often occurs on the surface of slip bands within individual grains. A shear crack in mode II without any crack closure is observed. Another possible initiation mechanism is the cleavage of microinclusions.

Second fact: The mode II shear crack without slip bands at the crack tip turns into a mode I crack with such bands after traversing several grains.

Short-crack growth may stop or accelerate at this stage. Several short cracks may coalesce, thus forming the initiated technical crack.

Third fact: The presumption of conventional fracture mechanics, that the plastic zone at the crack tip and the associated crack tip rounding are small relative to the crack length, is not applicable to short cracks.

Fourth fact: Short cracks propagate below the threshold conditions of long cracks. The short crack propagation rate may be substantially larger (factor 10 and more) than the neighbouring long crack propagation rates ('anomalous crack growth'). The high stresses and plastic strains at sharp notches promote this behaviour.

Fifth fact: The driving force behind short crack growth in sharp notches is initially generated by the notch root plastic zone and only with larger crack size by the crack tip plastic zone.

A contribution by Buirette *et al.*[432] can be evaluated in respect of the short-crack behaviour in the bainitic heat-affected zone (with compressive residual stresses acting in the surface) of a structural high strength steel (the French CMn steel, type S550MC, yield limit $\sigma_Y = 604\,N/mm^2$, ultimate tensile strength $\sigma_U = 686\,N/mm^2$). Three crack development regimes are identified:[432]

- The microstructural fracture mechanics regime for surface crack length $2c < 50\,\mu m$ or crack depth $a < 90\,\mu m$. Short crack initiation (nearly semi-circular crack shape): in-depth crack growth is much faster than on-surface crack length growth, multiple crack initiation is common, no early crack coalescence occurs. Cracks are stopped at distances of 12–25 μm, which corresponds to the bainitic lath packet boundaries. The microstructural threshold corresponds to half of the prior austenitic grain size (50 μm at the surface).
- The elastic-plastic fracture mechanics regime for a surface crack length $50 < 2c < (450–750)\ \mu m$ or crack depth $90 < a < 150\,\mu m$ depending on the loading level. Short-crack growth (semi-elliptical crack shape): surface crack growth is predominant, coalescence occurs rapidly.
- The linear-elastic fracture mechanics regime for surface crack length $2c > (450–750)\ \mu m$ or crack depth $a > 150\,\mu m$. Long-crack propagation (from semi-elliptical to semi-circular crack shape): a single long crack propagates both in depth and on surface.

Short-crack propagation at manual fillet weld toes has been investigated and described in fracture mechanics terms by Verremann *et al.*[654–656] A technique employing miniature strain gauges installed close to the weld toe (see also Otegui *et al.*[575]) was developed for continuous monitoring of the depth and opening level of cracks starting from a crack depth of 10 μm. For example, under fully reversed loading, the cracks in as-welded specimens were open over nearly the full stress range which results in high crack prop-

agation rates. It is shown that the notch stress intensity factor of the corner notch defining the weld toe transition (opening angle 135°, notch radius approaching zero) can be used to describe the short-crack propagation lives (i.e. the long-crack initiation lives) for various geometry and loading configurations. In particular, the notch stress intensity factor takes into account the size effect on fatigue life observed experimentally (see Section 7.3.1).

It has been shown by Lehrke *et al.*[513] that a sharp corner notch can be substituted by a fictitious initial crack at a notch-free surface for the purpose of a realistic crack propagation analysis. The weld toe is considered to be a corner notch whose opening angle corresponds to the weld toe angle. A stress singularity occurs at the corner notch tip in the case of zero notch radius. The singularity is characterised by the inverse notch radius approaching zero with an exponent which depends on the opening angle of the notch (see Section 7.2.1). The exponent has the value 0.5 in the case of zero opening angle, characterising the square root on inverse radius dependency attributed to crack tip stresses. It decreases with increasing opening angle. The exponent has the value 0.326 for an opening angle 135° representative of fillet welded joints. In all cases, the intensity of the singularity at the sharp notch is described by a notch stress intensity factor, the dimension of which depends on the notch opening angle.

The stress intensity factor of notches with non-zero opening angle cannot be directly used in a crack propagation analysis based on the Paris equation. Particularly incipient crack propagation cannot be assessed on the basis of the threshold stress intensity factor. Therefore, the stress singularity of the corner notch is substituted by an equivalent stress singularity of a fictitious initial crack at the notch-free surface (stress intensity factor K_{eq}), Fig. 6.3. Stress singularities are considered to be equivalent if they

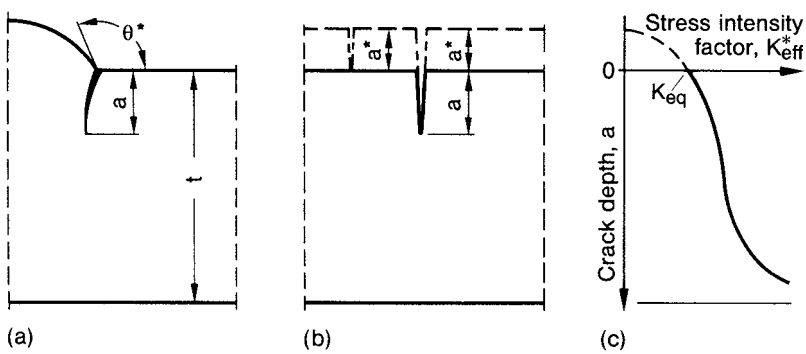


Fig. 6.3. Stress singularity at sharp notch of butt weld toe (a) substituted by equivalent singularity of fictitious initial crack (b) on the basis of identical line-averaged stresses; resulting effective stress intensity factor K^*_{eff} plotted over crack depth (c); after Lehrke.[513]

generate similar crack initiation and propagation behaviour. Similarity in crack initiation can be expected according to the Neuber microstructural support hypothesis if the fatigue-relevant equivalent stress averaged over the substitute microstructural length in the supposed crack growth direction is the same. The resulting depth a^* of the fictitious initial crack depends on the notch opening angle θ^*, the plate thickness t, the substitute microstructural length ρ^* and the stress concentration factor K_t in the case of a small notch radius. The fatigue-effective stress intensity factor K^*_{eff} results from the real crack length a (zero or non-zero) enlarged by the fictitious initial crack length a^*. The fictitious crack will propagate if the effective stress intensity factor is larger than the threshold stress intensity factor, $\Delta K^*_{eff} > K_{th}$, and it will then propagate according to the Paris equation with ΔK^*_{eff} as the controlling stress intensity factor range.

This concept of an equivalent crack length substituting the corner notch at the weld toe removes the uncertainty about the initial crack size at the weld toe and allows a uniform crack propagation analysis for the weld root and the weld toe to the extent the Neuber hypothesis is valid. A demonstration example covering butt joints in aluminium alloy is given in Section 6.3.4.

The unconventional crack propagation procedures used by Dong *et al.*[101] to describe short-crack propagation at weld toes (see Section 6.2.10) are based on an empirical finding that various 'anomalous crack growth' data from the literature relating to notch-induced short cracks can be made to collapse in a single curve of crack propagation rate versus stress intensity factor range if the notch-related magnification factor is introduced with the exponent $m = 2$ (instead of $m = 3$–4). The structural stresses in the ligament of the non-welded specimens considered had to be linearised for the purpose of the above evaluation.

Advanced crack propagation procedures for welded joints based on reversed plastic zone sizes at the crack tip have been proposed by Karzov *et al.*[502] and by Toyosada *et al.*[637–641] (see Section 6.2.11). The first-mentioned approach uses the damage accumulation concept; the second one focuses on short-crack behaviour described by the cyclically recurring plastic zone sizes determined according to a modified Dugdale–Newman model and inserted in a correspondingly modified Paris equation. Toyosada's approach is not convincing in the range of short cracks where the notch effect on the plastic zone is dominant.

6.1.4 Applications of the approach

The crack propagation approach is only rarely suitable for determining absolute values of fatigue strength or service life because many uncertain

assumptions must be introduced into the analysis regarding, for example, the initial crack size, the crack shape and the material parameters in the Paris equation. Also, the short-crack initiation phase is completely neglected in the total life assessment. Therefore, the approach cannot substitute the nominal or structural stress approach of the codes.

However, there are exceptions: it is claimed by British experts (contrary to the objections in Section 6.1.2) and has actually been incorporated in British and European design recommendations[15,21] that the classification of unconventional welded joints into the standard *S–N* curve scheme of the codes can be achieved based on the conventional crack propagation analysis if combined with a calibration. Calibration means that the procedure is first adjusted to the well-established *S–N* curve of a comparable conventional welded joint. Crack propagation analysis may also be used to explain part of the difference in fatigue strength between scaled-down specimens and full-size structural members with inclusion of the thickness effect.

On the other hand, the following cases can only be dealt with by the crack propagation approach (BS7608[15]):

- definition of tolerable flaw sizes or other crack-like imperfections;[17,488,584]
- fitness for purpose assessment for structural members with crack-like flaws whose size, shape and distribution are outside normally acceptable limits;[31]
- definition of intervals for in-service inspections;[419,445,480,584,594,599,600,667]
- assessment of residual fatigue life of a structure in which definite fatigue cracks of readily detectable size already exist (crack propagation life);[460,466,484,501,533,535]
- back-tracing of failures.[441,460,501,535]

Some details of the above applications have been reviewed by Radaj,[4] *ibid.* pp. 295–298.

The crack propagation approach is also well suited to parametric studies as far as the crack initiation phase can be neglected (i.e. mainly residual fatigue life investigations):

- comparison of the fatigue performance of welded joints in different materials and environments;
- comparison of the fatigue strength or life of welded joints with different geometries (shape and size) and loading conditions.

Finally, it should be emphasised that only the combination of crack initiation and crack propagation approaches can establish a more generally applicable method for total fatigue life assessments.

6.2 Analysis tools

6.2.1 General survey and relevant references

The analysis tools described hereafter comprise the following items: books and articles reviewing fatigue fracture mechanics with emphasis on welded joints, methods of stress intensity factor determination, crack propagation equations, crack propagation life, stress intensity factors for welded joints, crack shape and crack path considerations, material parameters of crack propagation, initial and limiting crack sizes, as well as residual stress effects.

The following references are recommended in respect of the application of fatigue fracture mechanics to seam-welded joints:

- books reviewing the fundamentals of fracture mechanics in respect of fatigue;[411,429,436,455,473,475,534,648]
- fundamental articles on the application of fatigue fracture mechanics to welded joints;[450,476,477,483,486,487,519,521,526]
- conference proceedings with articles on the application of fatigue fracture mechanics to welded joints;[454,500,520,538,620]
- compendia reviewing stress intensity factors of cracks dependent on geometric and loading state parameters;[543,601,609,628]
- stress intensity factor solutions for surface cracks in plates;[546,547,595]
- articles on stress intensity factors of cracks or root faces in welded joints: see Section 6.2.5;
- articles on crack path determination and crack shape development: see Section 6.2.6;
- articles with data on material parameters for fatigue crack propagation in welded joints inclusive of the parent material: see Section 6.2.7;
- articles on the effect of residual stresses on crack propagation in welded joints: see Section 6.2.9;
- articles on the effect of variable-amplitude loading on crack propagation in welded joints: see Section 6.2.4;
- articles on short-crack behaviour in welded joints: see Section 6.1.3;
- guidance on assessment of fatigue in welded structures on the basis of crack propagation concepts (e.g. BS7608,[15] BS7910,[17] IIW guidance,[31] Terai *et al.*[633]);
- surveys or articles on back-tracing of failures in welded structures on the basis of fatigue crack propagation analysis (bridge girders, shiphulls, offshore drilling rigs, pipelines): see Section 6.1.4;
- articles on crack propagation related in-service inspection: see Section 6.1.4;
- computer programs supporting the application of the crack propagation approach.[447,497]

6.2.2 Methods of stress intensity factor determination

Stress intensity factors for toe cracks or root faces in welded joints are only rarely available from the compendia[543,601,609,628] even when using appropriate assumptions on negligible geometric parameters or loading state components. The following methods are available for determining unknown stress intensity factors in welded joints.

In the first place, the analytical methods which were the basis for the development of fracture mechanics, but which are confined to cracks in infinite regions (plates or solids) must be mentioned. On the one hand, there are the complex stress function methods, without conformal mapping according to Westergaard, and with conformal mapping according to Muskhelishvili. On the other hand, there are the integral equation methods, one type derived from a dislocation array substituting the crack, the other based on Green's functions (or influende functions) multiplied by the stress in the crack plane before the crack occurred.

One relevant method for welded joints closely related to the analytical methods is the weight function method. As shown by Bueckner[430] and others based on Maxwell–Betti's reciprocal theorem, the weight function for a crack in a particular geometry can be determined on the basis of the known stress intensity factor of a reference loading state, together with its crack face displacement function – the first quantity readily available, the latter less abundant in the literature. The unknown stress intensity factor is computed by an integral over the structural stresses in the provisional crack face before the crack occurred (Emery,[456] Albrecht and Yamada[409]) multiplied by the derivative (with regard to the crack length) of the crack face displacement in the reference loading state and divided by the reference stress intensity factor. This means that the crack face stresses (traction for mode I, in-plane shear for mode II, out-of-plane shear for mode III) are 'weighted' by the reference quantities before being integrated. The weight function method originating in different versions from Bueckner,[431] Rice,[597] Paris *et al.*[581] and Petroski and Achenbach[585] and further developed by Niu and Glinka[554] and Sumi[622] has found wide application on through-thickness cracks and semi-elliptical surface cracks in plain plates and shells by Shen and Glinka,[606] Zheng and Glinka,[673] and Wang and Lambert,[658–660] as well as at weld toes (T butt joint) by Niu and Glinka,[552,553,555] Forbes *et al.*,[463] Brennan *et al.*,[428] and Wang and Lambert.[661,662] Cruciform joints were considered by Lie *et al.*[518] Application to (ship) structural details has been demonstrated by Sumi.[622] The weight function method possesses the significant advantage that only a simple integration scheme is required to find the unknown stress intensity factors. It is not restricted to the plane stress fields above. Rice[597] extended the theory to three dimensions.

In the second place, the numerical methods (finite element[84,344] and boundary element[210,214,446,861]) which are most important in application today have to be mentioned. In order to simulate the stress singularity at the crack or slit tip accurately enough, special elements are defined with a stress singularity at the node connected to the crack tip. The singularity is achieved by shifting midside nodes to the quarter point position, both in the finite element and boundary element models. Whereas in the case of boundary elements, the angular distribution of the singularity is naturally correct, special modelling measures are required in the case of finite elements. In a three-dimensional fan-shaped arrangement, prismatic 15-node elements (i.e. degenerated 20-node hexahedronal elements) are introduced at the crack or slit tip, the relevant midside nodes being shifted as described (see last paragraph of Section 10.2.2 for further details). When using non-degenerated (i.e. rectangular) elements at the crack tip within coarse meshes in two-dimensional models, the angular behaviour of the singularity is not correctly captured, and the error in the resulting stress intensity factors may be correspondingly large. The stress intensity factors are determined by limit value formulae based on the stresses or displacements at the crack faces close to the crack tip, mostly by extrapolation to the crack tip. Alternative methods are the evaluation of the path-independent J-integral around the crack tip or the computation of the change in strain energy with crack enlargement (the 'strain energy release rate') in a reference region around the crack tip when virtual crack extension is assumed. These options are available in several finite element computer programs.

In the third place, stress intensity factors may be estimated on the basis of available solutions combined with approximations in an engineering sense. The problem to be solved may be separated into geometric configurations and loading state components which are superimposed by addition. Procedures for alternating (or independent) introduction of multiple boundary conditions may be appropriate, leading to a superposition by multiplication (BS7910,[17] Radaj and Schilberth,[297] Xu and Bea[670]). The constant nominal stress in the gross section may be substituted by the structural stress linearised in the net section, thus providing the reference stress for the stress intensity factor, which is close to reality (Radaj and Heib[904]). Simple formulae for the stress intensity factors in seam-welded or spot-welded lap joints derived on the basis of beam theory and J-integral are given in Section 10.2.2. Approximate stress intensity factors for slit-type plate bending configurations have been obtained by Pook[888] based on engineering formulae from beam theory combined with the energy release rate concept.

In the fourth place, experimental methods are available for the determination of stress intensity factors, primarily strain gauge and photoelastic

methods, but also indirect methods which evaluate the crack propagation rate. They may be used for experimental verification of theoretical results, but they are not recommended as a substitute for the computational methods which are more efficient and accurate.

6.2.3 Crack propagation equations

The crack propagation approach for assessing the fatigue strength and service life of welded joints mainly uses the crack propagation equation originally proposed by Paris and Erdogan[580] for constant-amplitude loading which approximates the cyclic crack propagation rate primarily under plane strain conditions at the crack tip, Fig. 6.4:

$$\frac{da}{dN} = C(\Delta K)^m \qquad (\Delta K_{th} \ll \Delta K \ll K_{Ic}, R = 0) \tag{6.1}$$

$$\Delta K = M_k Y \Delta\sigma\sqrt{\pi a} \tag{6.2}$$

where a is the crack length or depth, N is the number of cycles, ΔK is the stress intensity factor range (mode I), ΔK_{th} is the threshold stress intensity factor, K_{Ic} is the critical stress intensity factor (brittle final fracture), R is the stress ratio ($R = \sigma_{min}/\sigma_{max}$), C and m are material constants, $\Delta\sigma$ is the range of structural stress normal to the crack (in Fig. 6.4 the gross-section

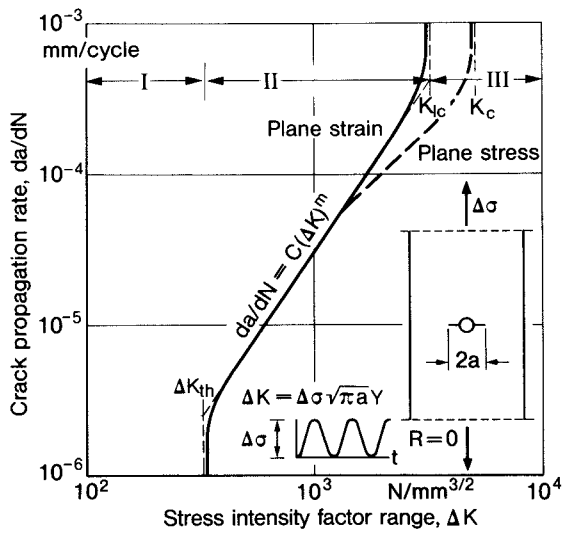


Fig. 6.4. Crack propagation rate under cyclic loading; numerical data typical of structural steels; schematic presentation (not to be used in calculations).

nominal stress), M_k is the magnification factor related to a notch stress concentration and Y is the geometry factor related to crack shape and nearby edges. The plane strain condition may be relaxed in consequence of substituting K_{Ic} by K_c. Crack propagation initially under mixed mode loading conditions will re-establish mode I conditions either by crack branching or by continuously adapting the crack path direction. One exception is the mixed mode I and mode III condition where coplanar crack propagation may be observed (Kim[503]). The stress intensity factor range $\Delta K = \Delta K_I$ in the Paris equation is then substituted by $\Delta K = \Delta K_{eq}$ according to Irwin's strain energy release rate criterion (with Poisson's ratio ν):

$$\Delta K_{eq} = \sqrt{(\Delta K_I)^2 + \frac{1}{1-\nu}(\Delta K_{III})^2} \tag{6.3}$$

Another important exception is slant crack propagation in thin sheets, but without complications when treated as pseudomode I crack propagation.

The following modifications of eq. (6.1) are applied in the high-cycle fatigue range with the material constants C and m newly defined, i.e. they may have different values in eqs. (6.1), (6.4) and (6.5):

$$\frac{da}{dN} = C(\Delta K - \Delta K_{th})^m \tag{6.4}$$

$$\frac{da}{dN} = C\left[(\Delta K)^m - (\Delta K_{th})^m\right] \tag{6.5}$$

Stress ratios $R > 0$ are taken into account by the crack propagation equation (6.6) proposed by Forman *et al.*[464] or its simplified form (6.7):

$$\frac{da}{dN} = \frac{C(\Delta K)^m}{(1-R)K_c - \Delta K} \qquad (R \geq 0) \tag{6.6}$$

$$\frac{da}{dN} = \frac{C(\Delta K)^m}{1-R} \qquad (\Delta K \ll (1-R)K_c,\ R > 0) \tag{6.7}$$

where K_c is the critical stress intensity factor and R is the applied stress ratio ($R = \sigma_{min}/\sigma_{max}$).

Stress ratios $R < 0$ are taken into account by inserting $\Delta K = \Delta K_{eff}$ with ΔK_{eff} being the portion of the stress intensity factor range in which the crack is not closed (approximated by the tensile part of the stress intensity factor range provided that residual stresses are absent but not so with high tensile residual stresses which keep the crack open even under compressive loading):

$$\frac{da}{dN} = C(\Delta K_{eff})^m \qquad (R < 0) \tag{6.8}$$

6.2.4 Crack propagation life

Crack propagation proceeding from the weld toe is considered first. Integration of the crack propagation equation (6.7) – with the parameters $\Delta\sigma$, M_k and Y in eq. (6.2) assumed as constant – from the initial to the critical crack length results in the crack propagation life N_p of the structural member (complete version and version simplified for $a_i \ll a_f$, excluding $m = 2.0$ as an exceptional case):

$$N_p = \frac{2(1-R)}{(m-2)C\left(M_k Y \Delta\sigma\sqrt{\pi}\right)^m}\left[\left(\frac{1}{\sqrt{a_i}}\right)^{m-2} - \left(\frac{1}{\sqrt{a_f}}\right)^{m-2}\right] \tag{6.9}$$

$$N_p = \frac{2(1-R)}{(m-2)C\left(M_k Y \Delta\sigma\sqrt{\pi}\right)^m \left(\sqrt{a_i}\right)^{m-2}} \qquad (a_i \ll a_f) \tag{6.10}$$

where N_p is the number of cycles in crack propagation, a_i is the initial crack length or depth and a_f is the final crack length or depth. The following more convenient form of eq. (6.10) is often used:

$$\frac{N(\Delta\sigma)^m}{1-R} = \frac{I}{C} \tag{6.11}$$

with the crack propagation integral I derived from eq. (6.10) (in contrast to Dong's definition of I according to eq. (6.29), the plate thickness t is not seperated). The introduction of $(1 - R)$ into the forumlae above is not justified if the R effects are taken into account in the value of the parameter C (e.g. the C value in the IIW recommendations[3] or C values derived from fatigue tests on welded joints in the as-welded condition).

The eqs. (6.9) and (6.10) define the $\Delta\sigma$–N_p curve for specimens with an initial crack in the form $(\Delta\sigma)^k N_p = \text{const}$ which was originally proposed by Basquin.[347] The inverse slope k of this curve is equal to the exponent m in the Paris equation. For geometrically similar welded joints (weld and initial crack enlarged with plate thickness), the crack propagation analysis indicates that the fatigue strength varies with the exponent $n = (m - 2)/2m$ of the inverse plate thickness t (eq. (6.10) solved for $\Delta\sigma$ with $a_i \propto t$). Inserting $m = 2.5$–4.0, the result is $n = 0.1$–0.25 (compare exponent n in eq. (2.24)). Larger plate thickness means lower fatigue strength. Similar data are derived with the assumption of identical initial crack sizes and weld toe radii, which can be explained by a more severe notch effect in the thicker plate, accelerating crack propagation in the range of small crack size.

The coefficients M_k and Y are not constant for propagating cracks even if $\Delta\sigma$ is constant because the crack shape and the distance of the crack tip from the plate surfaces or the notch root are varying while the crack is propagating. Only averaged values of M_k and Y can be assumed to be constant.

Numerical integration is appropriate in the case of strongly varying values of M_k and Y. The crack path length ($a_c - a_i$) is subdivided for this purpose into portions Δa_j with mean values a_j within which a constant crack propagation rate $(da/dN)_j$ can be assumed. The numbers of cycles appertaining are summed up:

$$N_p = \sum_{j=1}^{n} N_j = \sum_{j=1}^{n} \frac{\Delta a_j}{(da/dN)_j} \tag{6.12}$$

where N_p is the crack propagation life measured in cycles, N_j is the number of cycles within Δa_j, Δa_j is the crack length portion, $(da/dN)_j$ is the crack propagation rate in this portion and n is the number of crack length portions.

Service life values from eqs. (6.9–6.11) are related to a failure probability $P_f = 50\%$ or $P_f = 2.3\%$ (two standard deviations from the mean in logarithmic scale) depending on the statistical indices of the material constants C and m. The number of cycles for crack initiation has to be added to the crack propagation life in order to obtain the total life.

Crack propagation proceeding from the weld root is another type of problem characterised by crack-like root faces originating from non-penetrating welds (inclusive of the slit faces of lap joints). An initial stress intensity factor K_i is available in these cases. It is shown in the following that the crack propagation life can be expressed by this quantity, thus establishing the theoretical basis of the stress intensity approach.

Two basic models are considered for this purpose: the infinite plate with double-sided external slit faces and the infinite solid with circumferential external slit faces, both models subjected to remote tensile loading, Fig. 6.5.

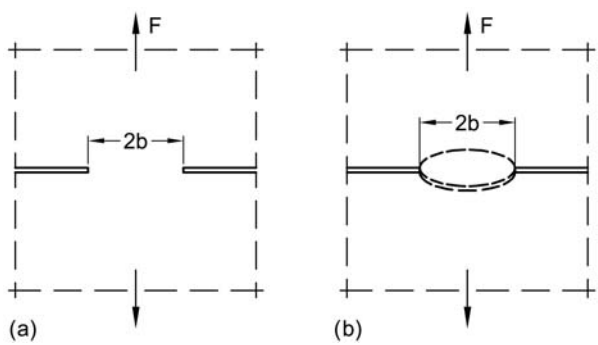


Fig. 6.5. Infinite plate with double-sided external slit faces (a) and infinite solid with circumferential external slit faces (b), subjected to remote tensile loading.

Coplanar crack propagation starting at the slit tips is equivalent to a cross-sectional (or ligament) reduction. The positive crack propagation rate, i.e. plus da/dN, in eq. (6.1) is substituted by the negative ligament reduction rate, i.e. minus db/dN (Partanen *et al.*[884]). The stress intensity factor ranges ΔK (mode I) of the plate and solid model, respectively, have been compiled by Radaj,[6] pp. 285–287:

$$\Delta K = \frac{\Delta F}{\sqrt{\pi b}} \tag{6.13}$$

$$\Delta K = \frac{\Delta F}{2\sqrt{\pi b^3}} \tag{6.14}$$

where ΔF is the tensile load range and $2b$ is the cross-sectional (or ligament) width.

Integration of eq. (6.1) with plus da/dN substituted by minus db/dN is performed between plus b and zero with ΔK from eq. (6.13) and (6.14), respectively, to get the crack propagation life N_p:

$$N_\mathrm{p} = \frac{2b}{(m+2)C(\Delta K_\mathrm{i})^m} \tag{6.15}$$

$$N_\mathrm{p} = \frac{2b}{(3m+2)C(\Delta K_\mathrm{i})^m} \tag{6.16}$$

where ΔK_i is the initial stress intensity factor range, $2b$ is the cross-sectional (or ligament) width and C and m are the material constants in the Paris equation ($m \approx 3$). The factor $2/(m+2)$ or $2/(3m+2)$, respectively, characterises the life reduction in comparison with a constant-rate behaviour (i.e. 2/5 or 2/11 for $m = 3$). The relationships above express K–N curves which are, as before, compatible with Basquin's form of the S–N curve.

The models above cannot be applied to practical problems without severe modification. But they convey the message that the initial stress intensity factor range together with the cross-sectional or ligament width can principally be used to characterise the fatigue strength or life.

The crack propagation equations given above refer to constant-amplitude loading with a constant stress ratio. Stress amplitude and stress ratio may vary in the structure being assessed in respect of fatigue: single overloads or underloads in constant-amplitude loading, variable-amplitude loading in programmed fatigue testing, constant-amplitude loading combined with a variable mean load, and random-amplitude loading.

It can be shown that numerical integration of the Paris equation according to eq. (6.12) applied to variable-amplitude loading, gives results which are compatible with those of the original version of Miner's rule. But major crack growth retardation or acceleration effects may occur at the crack tip

under such loading sequences. A too short or too long service life is predicted in this case. There are programs available in aircraft engineering for crack propagation with retardation (or interaction) effects which support the fatigue assessment of damage-tolerant designs (Radaj,[6] *ibid.* pp. 354–369). The definition of an equivalent constant-amplitude stress range from variable-amplitude loading is sometimes used in other fields of engineering, especially in the case of random-amplitude loading.

Fatigue crack growth in steel butt and fillet welds, respectively, under spectrum loading was investigated by Bayley *et al.*[412] and Blom[420] starting with the initial defect distribution. The crack growth retardation effect in fillet-welded steel joints subjected to periodic overloads has been investigated by Garwood and Maddox.[469] Fatigue tests showed the retardation effect for tensile overloads but not so for compressive overloads. The effect in the welded joints was weaker than in the non-welded material. This was attributed to the presence of tensile residual stresses in the welded joints. Referring to a finite element analysis by Li *et al.*[515] into the crack closure behaviour of a longitudinal crack in a hard layer, an increased fatigue life can be expected for decreasing layer thickness.

The fatigue life of submerged arc welded butt joints in steel under variable-amplitude loading (offshore storm sequences) has been predicted based on the crack propagation approach (Bayley *et al.*[412]). Fatigue at fillet-welded transverse attachments (non-load-carrying) in CMn steel (boogie arm of subway carriage) has similarly been investigated (Blom[420]).

6.2.5 Stress intensity factors for welded joints

The primary concern of the crack propagation approach applied to welded joints is directed towards surface cracks at areas of notch stress concentration such as weld toes. These cracks are assumed to be oblong and mostly continuous in the case of transverse welds or to be semi-elliptical in the case of the weld ends of longitudinal stiffeners (BS7608:[15] $a/2c = 0$ or $a/2c = 0.1$, with crack depth a and crack surface length $2c$). The semi-ellipse is defined as circumscribing the more complex actual shape of several simultaneously initiated but coalescing cracks or of other planar defects.

The maximum stress intensity factor range ΔK at the deepest point of a semi-elliptical surface crack in a plate with superimposed notch effect (e.g. at weld toes) is evaluated from the following engineering formula (BS7910,[17] BS7608[15]) which was originally proposed by Maddox:[524]

$$\Delta K = (M_{km} Y_m \Delta\sigma_m + M_{kb} Y_b \Delta\sigma_b) \frac{\sqrt{\pi a}}{\phi} \tag{6.17}$$

where $\Delta\sigma_m$ and $\Delta\sigma_b$ are the membrane and bending structural stress ranges normal to the crack (determined at the surface without the crack and

notch), Y_m and Y_b are geometry factors on the membrane and bending stresses due to the free surfaces on the front and rear sides of the plate (dependent on a/t and $a/2c$), M_{km} and M_{kb} are magnification factors on membrane and bending stress due to the notch stress concentration (dependent on the geometrical notch parameters and a/t), ϕ is the complete elliptical integral of the second kind characterising the basic influence of the crack front shape (dependent on $a/2c$), a is the crack depth, $2c$ is the crack length on the surface, and t is the plate thickness.

A corresponding equation with the crack depth a substituted by half the surface crack length and with modified factors Y_m and Y_b is valid for the stress intensity factors at the surface points of the semi-elliptical crack front.

The semi-elliptical crack shape is an approximation for the purpose of simplifying the calculation. Actually, the crack front intersects the surface with an angle which deviates from 90 degrees (Pook[586–588]).

The terms in the equation above may be extended by an additional factor representing the influence of the finite plate width. If the equation above is formulated on the basis of stress intensity factor solutions for cracks in plane cross-sectional models (i.e. without the integral ϕ), a corresponding factor representing the influence of the crack front shape must be introduced.

Through-thickness cracks in curved shell structures subjected to internal pressure are associated with an additional increase of the stress intensity factor.[17,297,462] The corresponding additional magnification factor which depends on crack length, shell thickness and shell diameter is applied to surface cracks in a conservative manner.

The elliptical integral ϕ characterises the decrease in the stress intensity factor of an internal elliptical crack relative to the through-thickness crack with a straight crack front. It depends on the aspect ratio of the ellipse, Table 6.1.

The geometry factor Y characterises the influence of the front and rear surface of the plate on the stress intensity factor of the semi-elliptical surface crack. It depends on the ratios a/t and $a/2c$ according to different functions for loading by membrane and bending stresses, Fig. 6.6. It may comprise further geometrical influence parameters.

The magnification factor M_k characterises the effect of notch stress concentration relative to the same crack in a plain plate without a notch effect

Table 6.1. Complete elliptical integral of the second kind, ϕ, dependent on the aspect ratio, a/c, of the elliptical crack; after Maddox[525]

Aspect ratio a/c	0	0.2	0.4	0.6	0.8	1.0
Integral ϕ	1.0	1.051	1.151	1.277	1.418	1.571

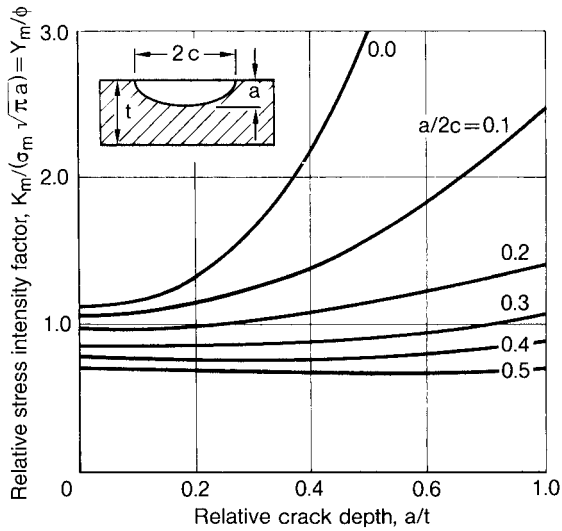


Fig. 6.6. Geometry factor Y_m/ϕ for the stress intensity at the deepest point of a semi-elliptical surface crack in a plain plate of thickness t subjected to membrane stress loading; after Maddox.[525]

(definition according to BS7608[15] and BS7910[17]). It depends mainly on the depth ratio a/t and the weld toe angle θ, and to a minor degree on the ratio $a/2c$ and the loading type, Fig. 6.7 (evaluate the relevant solid-line and dashed-line curves). It drops rapidly to $M_k \approx 1.0$ within $a/t = 0.1$–0.2. The plotted data are based on finite element analysis.

The T butt joint (cross-sectional model of major width) is considered to be representative of tubular welded joints in a local sense, i.e. analysed in respect of structural (membrane and bending) stresses. The results of a more recent, extensive and accurate investigation by Bowness and Lee[422,424] (three-dimensional solid element models, J-integral evaluation, approximative parametric equations for M_k derived therefrom) into the stress intensity factor of weld toe cracks in T butt joints subjected to membrane and bending loads (deepest point) are plotted in Fig. 6.8. Plain plate values by Newman and Raju[546,547,595] are given in comparison. The relative stress intensity factor is defined without inclusion of the ϕ-integral. The relative crack depth extends up to $a/t = 1.0$ (through cracking). Once more, the magnification factors result from relating the solid curves to the dashed curves. The M_k values of shallow cracks ($a/t \leq 0.1$–0.2) are sharply raised as a result of the weld toe notch stresses. For intermediate crack depths ($0.2 \leq a/t \leq 0.9$) the M_k-value drops slightly below 1.0 before increasing once more when the crack approaches the rear surface. In the case of bending loads, the assumption $M_k = 1.0$ is considered to be conservative for $a/t \geq 0.5$. The

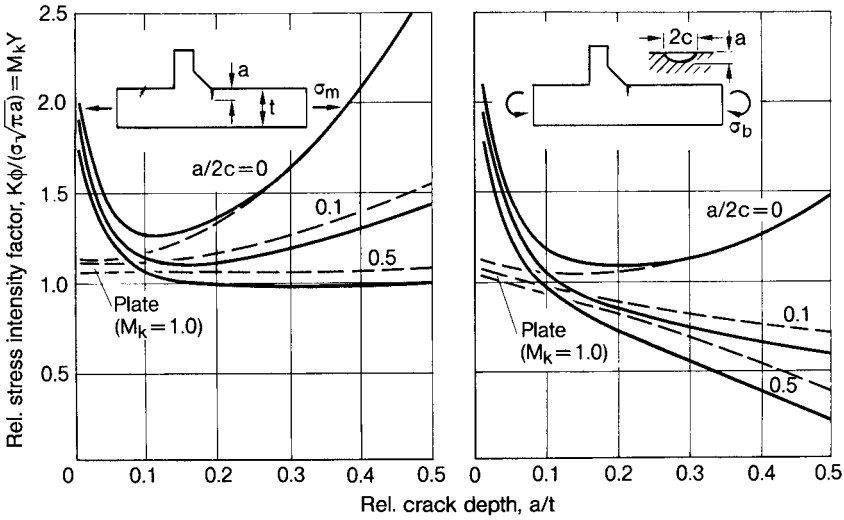


Fig. 6.7. Relative stress intensity factor for semi-elliptical surface crack at fillet weld toe of one-sided transverse attachment joint ('T butt joint') dependent on relative crack depth (solid lines), comparison with values in plain plate (dashed lines); after Fu *et al.*[467]

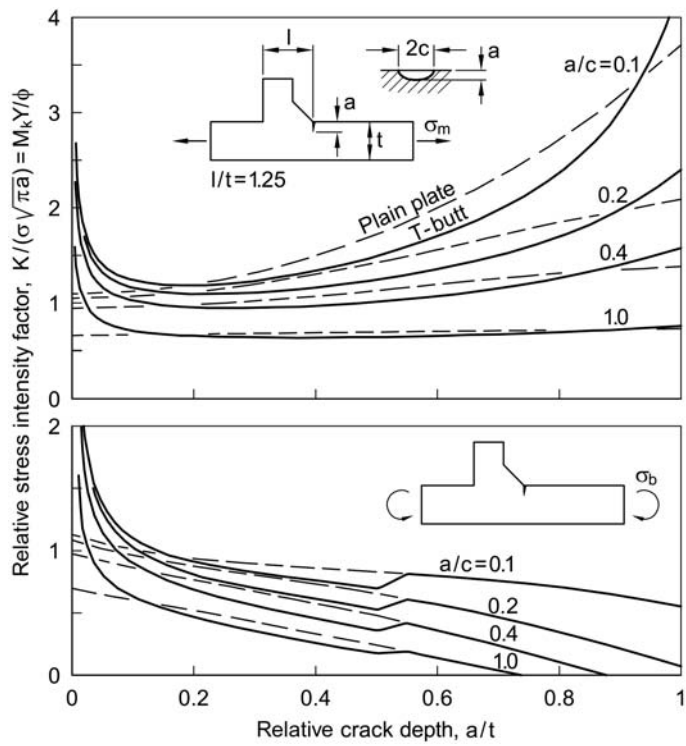


Fig. 6.8. Details as Fig. 6.7; after Bowness and Lee.[422,424]

stress intensity factors in the surface points of the crack front are also available from the above investigation. They are always higher in the T butt joint than in the plain plate, as is expected from the notch stress effect. A comprehensive comparison of the results with those given by Newman and Raju,[546,547,595] Rhee *et al.*,[596] Bell[414] and BSPD6493[17] is published separately (Bowness and Lee[425]).

A similarly extensive parametric investigation of T butt joints with toe cracks has been conducted by Brennan *et al.*[428] It comprises different weld toe angles, weld toe radii, crack depths, crack aspect ratios and attachment widths. The Niu–Glinka weight function method was applied combining the finite element solution for the plane cross-sectional model of the edge-cracked joint with the Newman–Raju equation for the surface crack in a plain plate. Weight functions derived from reference stress intensity factor solutions by the three-dimensional finite element method were used by Wang and Lambert[661,662] to determine the stress intensity factors in the deepest and surface points of semi-elliptical weld toe cracks in T butt joints with the weld toe angle, the relative crack depth and the crack aspect ratio being varied in definite ranges.

An approximation formula for the stress intensity factor of semi-elliptical surface cracks in welded T-joints (used to fasten hydraulic turbine blades) has been derived by Carpinteri *et al.*[437] with reference to a power series expansion of the considered initial stress distribution in the weld toe section. Another, even simpler approximation formula has been proposed by Lee and Bowness[509,510] based on the stress concentration factor and the degree of bending in the crack-free T butt joint (structural detail of a tubular joint).

The influence of the weld toe radius is restricted to a crack depth considerably smaller than the aforementioned ratio a/t (Niu and Glinka[555]). The finite element analysis for determining the magnification factor is generally performed with a sharp notch, that is, with zero notch radius in the finite element model (producing a theoretically infinitely high stress concentration). Therefore, the relevant curves start with a small, finite relative crack depth in this case. The magnification factor is equal to the stress concentration factor, $M_k = K_t$, for $a = 0$. It drops rapidly with $a > 0$ and is approaching $M_k = 1.0$ for $a/2c = 0$. It assumes values $M_k < 1.0$ in the case of a curved crack front, i.e. $a/2c > 0$. The weld toe angle has major influence on the magnification factor up to $a/t = 0.1$–0.2, just as the relative attachment width l/t (attachment plate thickness inclusive of weld leg length related to main plate thickness) has.

The widely used approximation formulae[17,530] for the magnification factor separate the crack depth ratio a/t from the other geometric parameters:

$$M_k = A\left(\frac{a}{t}\right)^j \tag{6.18}$$

where the coefficient A and the exponent j depend on the parameters which characterise the geometric detail of the welded joint being considered: weld toe radius, weld toe angle, attachment width or length and others. The typical values recommended in BS7910[17] are $A = 0.4–0.8$ and $j = –0.2$ to $–0.3$ for $a/t \ll 1.0$, and $M_k = 1.0$ for larger values of $a/t < 1.0$.

Easy-to-use formulae for the factors Y and M_k for cracks at the weld toe of butt welds,[551,553] butt and fillet welds in (non-load carrying) attachment joints and (load-carrying) fillet welds in cruciform joints are available from BS7608[15] and BS7910[17] based on investigations by Smith and Hurworth[612,614] and Maddox *et al.*[529,530] Another set of approximation formulae for welded joints according to Fig. 6.9 has been published by Hobbacher.[489,490] The factor M_k is mainly dependent on the following parameters in a normalised form: weld toe angle for all types of joint, throat thickness for cruciform and lap joints with fillet welds, in the latter case plate thicknesses and overlap length as well (suppressing the bending deformation), plate thicknesses, attachment length and base plate width for the longitudinal attachment joint, and height and length of the attachment relative to the width of the base plate for the edge attachment joint. The attachment length is the most important influencing parameter apart from the weld toe angle and weld toe radius for all types of joint (Maddox,[43] *ibid.* p. 189). Dijkstra *et al.*[448,449,650,666] have given approximation formulae for M_k consisting of three coefficients related to attachment length, weld toe angle and weld toe radius, respectively. Castiglioni and Gianola[438] have derived a formula for M_k in longitudinal attachments which gives prominence to the attachment length, the base plate thickness and the weld toe angle as parameters of influence. Magnification factors M_k for weld toe cracks at non-load-carrying fillet welds in cruciform joints were re-analysed by Lie *et al.*[518]

The stress intensity factors for the longitudinal attachment joints included in the publications above (and in that by Smith and Gurney[613]) refer to the nominal stress at the remote end of the specimen. A more clearly arranged method proceeds from the structural stress concentration at the attachment ends, the hot spot stress, and then analyses the semi-elliptical surface crack under the action of these membrane and bending stresses based on the solution of Newman and Raju.[546,547,595]

The stress intensity factors of surface cracks at the weld toe of tubular joints were extracted from measured crack propagation data in variable-amplitude loading combined with the actual hot spot structural stress ranges in order to prove that the theoretical results gained from appropriate crack propagation modelling ($M_k Y/\phi$ decreasing with a/t) are conservative (Etube *et al.*[457,458]).

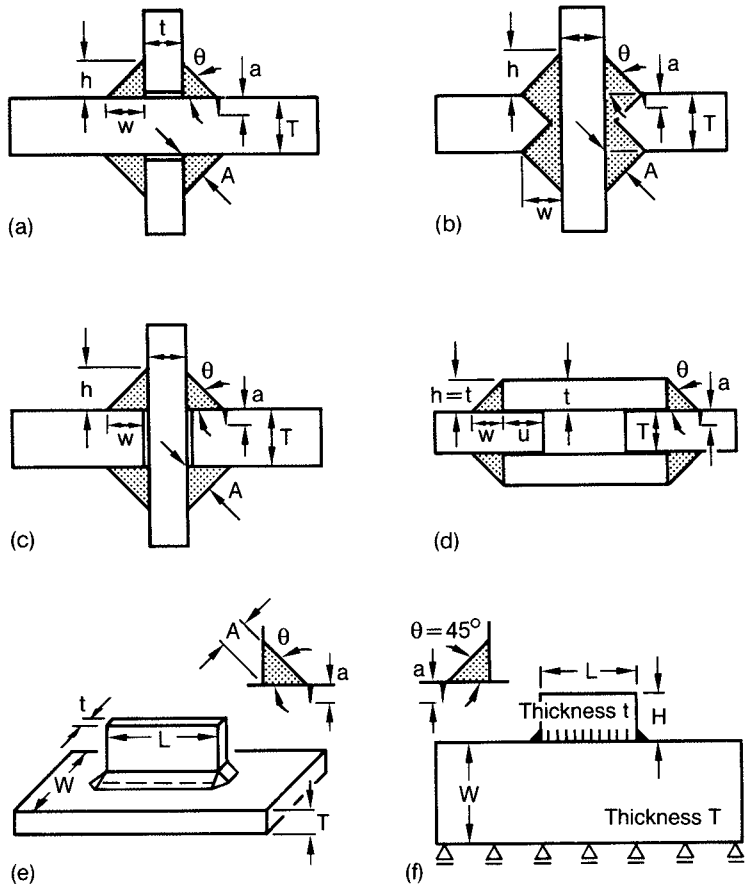


Fig. 6.9. Welded joints with crack initiation at weld toe, with stress intensity factors being available dependent on geometric parameters: transverse attachment (a), cruciform joint with double-bevel butt welds and fillet welds (b), cruciform joint with fillet welds (c), lap joint with fillet welds (d), one-sided longitudinal attachment (e) and two-sided edge attachment (f); after Hobbacher.[489,490]

Just as the weld toe cracks considered hitherto, crack-like weld root faces can be characterised by stress intensity factors in order to determine the fatigue life by crack propagation analysis. Stress intensity factors for crack-like root faces in (load-carrying) cruciform joints with double-bevel butt welds or/and two-sided fillet welds are given by several authors.[465,474,649] Some results are plotted in Fig. 6.10 and Fig. 6.11. Further data are compiled in the stress intensity factor handbook edited by Murakami[543] (*ibid.* pp. 1206–1207). Superimposed root defects were investigated by Noblett and Andrews.[556] The cruciform and T-joints, with varying root face lengths

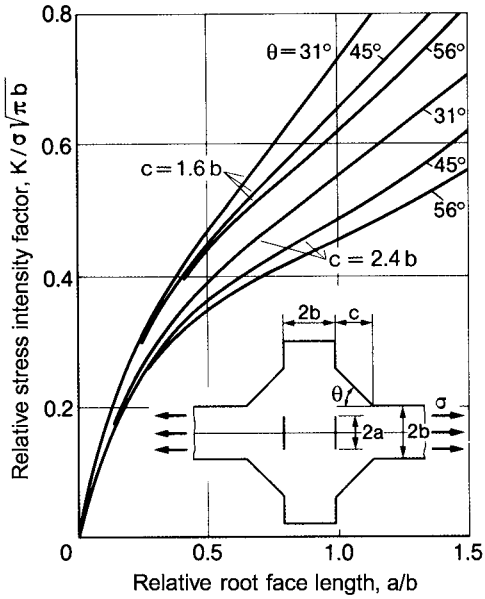


Fig. 6.10. Relative stress intensity factor at root face end in cruciform joint, dependent on root face length, weld leg length and weld toe angle; after Gurney.[474]

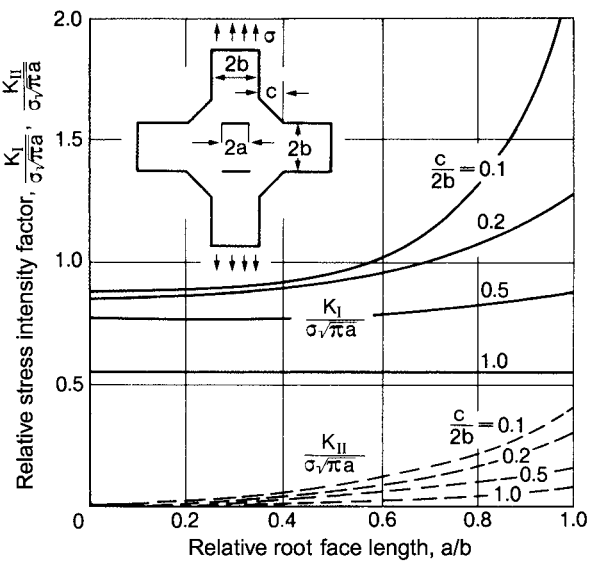


Fig. 6.11. Relative stress intensity factors (mode I and II) at root face end in cruciform joint, dependent on root face length and weld leg length; after Usami and Kusumoto.[649]

and three-point bending loaded with different span widths, were analysed in comparison by Motarjemi *et al.*[541,542] Note that varying root face lengths mean varying degrees of weld penetration. T-shaped weldments were considered by Zwerneman and Frank.[675]

The following further stress intensity factors are available for crack-like root faces in welded joints: root face in transverse attachment joint,[409,467,530,552,553,578,671] slit face in lap joint[557] (see also data by Murakami,[543] *ibid*. pp. 1208–1209), slit face in cover plate joint,[258,409] root face in butt joint,[507,513] and root face in T-joint.[619] The mode III stress intensity factor of the girth butt weld with root face in a straight pipe under torsional loading has been determined by Wais *et al.*[657]

The stress intensity factors referenced above presume force-controlled loading conditions, i.e. the basic structural stresses at the crack site remain unchanged while the crack propagates with increasing stress intensity factor. As far as crack growth in structural components is considered, deformation-controlled loading conditions are often more appropriate. The dependency of the stress intensity factor on crack depth or crack length is then fundamentally changed. The M_k and Y values are comparatively reduced with increasing crack size. The stress intensity factor is thus decreasing.

This effect of stress redistribution on the stress intensity factor is termed 'load shedding'. Force or deformation control refers to the boundary conditions in the model providing the stress intensity factor. The load shedding effect depends on where these boundary conditions are defined, close to the crack or at larger distance, and on the structural behaviour within the boundaries. The load shedding effect also occurs with the shake-down of residual stresses caused by the propagating crack. A comprehensive survey on load shedding in ship structures has been given by Xu and Bea.[670]

A specific modification has been proposed for the assessment of weld toe cracks in tubular joints. Few solutions for stress intensity factors of toe cracks in these joints are available but some success has been achieved in adapting cracked plate or T butt joint solutions. One factor which is considered to be significant in tubular joints is the load shedding due to crack growth mentioned above. Surface-crack growth has the effect of reducing the bending moment in the crack propagation plane relative to the uncracked situation ('moment release', 'hinge effect'). Controversial views exist on the amount of reduction of the bending stresses but the linear moment release assumption yielded some correspondence to experimental results (Aaghaakouchak *et al.*[408] and Tubby[647]):

$$\sigma_{sb} = \sigma_{sb\,0}\left(1 - \frac{a}{t}\right) \tag{6.19}$$

where σ_{sb} is the structural bending stress in the joint with crack, $\sigma_{sb\,0}$ is the structural bending stress in the joint without crack, a is the crack depth and t is the wall thickness.

The load shedding effect in welded tube-to-tube or tube-to-plate joints has been numerically simulated by a rigidly clamped T butt joint with surface-crack growth starting at the weld toe and traversing the plate thickness under arbitrary mode I loads (Wang and Lambert[662]).

Maddox[528] has shown for T-shaped tubular joints under in-plane bending loads that a reliable prediction of crack propagation through the tube wall is gained by combining the three-dimensional surface-cracked plate solutions of Newman and Raju[546,547,595] with the non-reduced structural stresses in the in-plane loaded tubular joint. This procedure was also successfully applied to the in-plane loaded tubular joint investigated by Umbach *et al.*[740] (see Section 8.5.2).

The 'softening effect' in the cracked area of the finite element model of the tubular joint consisting of thin-shell elements can be taken into account by the 'elastic line-spring technique' proposed by Rice and Levy[598] and applied to a T-shaped tubular joint by Huang and Hanock.[492] Spring elements acting in translation and rotation are added to the finite element model in the crack line. The stiffness coefficients of the springs depend on the local crack depth. They are derived from an edge-cracked plain plate specimen subjected to tension forces and bending moments, respectively.

6.2.6 Crack shape and crack path

The knowledge of crack shape and crack path is a constitutive element of a realistic crack propagation analysis. Both phenomena are closely related, but treated independently in the following.

The development of crack shape for surface cracks is extensively dealt with in the literature (Murakami,[543] pp. 692–709). Crack shape development in welded joints is considered by Smith and Smith,[615,616] Otegui *et al.*,[573,574] Chapetti and Otegui,[439] Bell and Vosikovsky,[415] Pang and Gray,[579] Janosch *et al.*,[498] Wang *et al.*,[663] and Toyosada *et al.*[638] A probabilistic analysis is presented by Zhang and Wang.[672] There are two methods available for dealing with the development of crack shape during crack propagation. One method applies the crack extension rules separately to the depth and length directions of the crack assuming a semi-elliptical shape between these principal directions. The other method uses a 'forcing function' to determine the crack length on the basis of the crack depth actually analysed.

It was found by Bell *et al.*[415,416] that, under the assumption of coalescing very small initial cracks of semi-circular shape, the crack shape development as a function of crack depth can be described by the following exponential relationship:

$$\frac{a}{c} = \exp(-ka) \tag{6.20}$$

The factor k depends on plate thickness and stress range, a typical value being $k \approx 0.2\,\text{mm}^{-1}$. But crack shape development is a process which is also dependent on the weld quality (Wernicke[665]).

Coalescence of coplanar surface cracks is a process that occurs frequently especially in the early stage of technical fatigue crack propagation (see Section 6.1.3 concerning the preceding short crack behaviour). The surface crack at the weld toe under steep notch stress gradients has a tendency to propagate more rapidly in the toe line direction than in the depth direction. Coalescence can be described within the crack propagation approach by redefining a single circumscribing semi-elliptical crack shape as soon as two separate cracks meet (Pang and Gray[579]). This results in a realistic reduction of the crack propagation life with the number of initiated coplanar cracks. Coalescing cracks are the basis for recommending oblong surface cracks with $a/2c \leq 0.1$ for the simplified analysis of weld toe fractures in butt joints, cruciform joints and transverse attachment joints among others, instead of simulating the coalescence process.

More detailed experimental investigations into the aspect ratios of surface cracks at the toe of transverse welds revealed the following behaviour (Otegui *et al.*[573–575]). Microcracks exist or are generated by fatigue along the weld toe line at microgeometric discontinuities and inclusions. Some of these microcracks coalesce to form small semi-elliptical cracks with low aspect ratios ($0.1 \leq a/c \leq 0.3$). As these cracks grow, their aspect ratio increases (occasionally up to $a/c = 0.3$ at $a \approx 0.1$–$0.3\,\text{mm}$) and subsequently tends to decrease because of further coalescence. A similar behaviour was detected at the end of longitudinal attachment welds: rapid decrease of the aspect ratio at small crack depths followed by a gradual increase at larger crack depths (Toyosada *et al.*,[638] see Fig. 6.33).

The fatigue life of a T butt weld specimen has been simulated by a probalistic model of crack initiation, propagation and coalescence using the Monte Carlo technique (Lecsek *et al.*[508]). The initiation model considers the variability of fatigue life due to the local weld toe angle and radius, and due to the strain–life behaviour of the material. These data are gained from measurements. A local strain model is used to predict the initiation life and the distribution of multiple cracks along the weld toe line (initial crack size $a = 0.5\,\text{mm}$, aspect ratio $a/c = 1.0$). The information on positions and timing of the initiation event is used as input to the propagation model (based on the Paris equation) which leads to variability of coalescence. In this model (according to To *et al.*[635]), multiple surface cracks grow independently along the weld toe line and coalesce when their tips contact. The surface length of the resulting single crack is equal to the combined surface length of the

coalescing cracks whereas the depth is equal to the depth of the deeper crack. The process is continued to the end of fatigue life, defined as the point at which the maximum crack depth reaches one half of the plate thickness. The calculation is repeated many times in order to obtain an estimate of the statistical life distribution. The fatigue life prediction for the T butt weld specimen above (structural steel, base plate thickness $T = 102$ mm), subjected to a bending load, was slightly underpredicted compared with experimental results. The crack initiation life characterised by the appearance of the first 0.5 mm crack represented 12–22% of the total life on average, the value depending on the stress level.

The assumptions behind the simplified procedure of semi-elliptical crack propagation are coplanar conditions which are enforced to some extent at the weld toe by the dominance of the notch effect in mode I loading. A more complex situation occurs under mixed mode loading conditions. This situation was investigated for the crack-like weld root face in a two-sided butt weld with lack of penetration (Kim[503]). The weld was inclined in a uniaxial tension specimen so that mode I and mode III conditions were superimposed at the weld root. Branch or coplanar crack propagation were observed, depending on the initial mode I stress intensity factor range. Coplanar crack propagation predominated when this range was large. The propagation mode affected the fatigue life: it was larger for branch crack propagation than for coplanar crack propagation, but it was independent of the inclination angle. Evaluation of the initial equivalent stress intensity factor according the strain energy release rate criterion resulted in a uniform *S–N* curve.

A first attempt to describe coplanar crack propagation at the weld toe of a tube-to-plate joint under bending and torsion loads (resulting in mixed mode loading conditions of a semi-circular initial crack parallel to the weld toe line) was made by Amstutz *et al.*[410]

Fatigue cracks occurring in welded (offshore) tubular joints may be characterised by a twofold curving: along the brace-to-chord intersection line and in the chord wall thickness direction. Based on the principal stress criterion, an approximate method for predicting such crack curvatures has been proposed by Bowness and Lee.[421,423]

A special aspect of non-planar crack formation has been highlighted by Chapetti and Otegui.[439,440] By introducing a controlled degree of waviness of the weld toe line (by arc rotation in GMA welding), crack propagation is enforced in a curved plane with crack coalescence restricted to the end points of each wave. The fatigue life of the welded joint can be increased by a factor of two in combination with the reduced notch effect at the apex point of the waved toe line.

The final stage of surface crack growth is the formation of a through-thickness crack. Further propagation of this crack may be of relevance for

estimates of the remaining life of large-size welded structures such as ships or bridges. In a first step, the curved crack path has to be determined. The factors controlling the path are not completely understood. Pook[586–588] has defined the problem in depth and has summarised the state of relevant knowledge.

It is an empirical fact that fatigue cracks (just as brittle fractures) show a trend to mode I growth which may be expressed by various theoretical criteria, e.g. by the criterion of local symmetry. But fatigue cracks may be directionally unstable even under completely symmetrical initial configurations. The directional stability is governed by the T-stress, i.e. the non-singular stress in the direction of the crack (Cotterell[444]). Stability exists for compressive T-stresses, but not so for tensile T-stresses. A curved path is taken in the latter case with a directional trend to free bounderies. Directional stability may be characterised by the ratio of T-stress to stress intensity factor. Further constraints on mode I crack growth have to be considered in the case of three-dimensional configurations (e.g. 'twist cracks').

In welded structures, the path taken by a fatigue crack is particularly complicated by the influence of residual stress fields, stress biaxiality, three-dimensional geometry, structural redundancy and crack curving (Sumi *et al.*[621–625]). As a typical crack path problem, a ship structural detail is presented in Fig. 6.12. The fatigue crack initiated at the weld toe of the

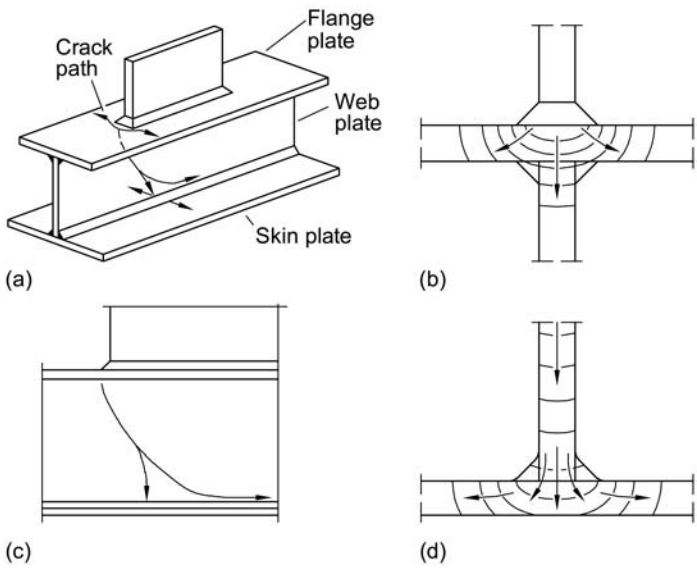


Fig. 6.12. Fatigue crack propagation in a ship structural welded detail; general view (a), initial stage in flange and web plate (b), subsequent stage in web plate (c), and final stage in skin plate (d); after Sumi.[621]

longitudinal attachment end propagates into the flange and web plate of the internal ship hull. Further propagation takes place either into the external skin plate or along its longitudinal weld.

Usually, the maximum mode I stress intensity factor $K_{\mathrm{I\,max}}$ (connected with $K_{\mathrm{II}} = 0$) defines the direction of crack propagation in the subsequent load cycle. The Paris equation inclusive of threshold and crack closure conditions is applied to determine the amount of crack propagation. The analysis of the stress intensity factor along the crack path has to take into account the load and stress redistribution caused by the growing crack in redundant structural compounds. Superelement techniques are applied on the finite element model to achieve this. The analysis presented by Sumi[622] demonstrates some of the above characteristics.

6.2.7 Material parameters of crack propagation

The material parameters m and C in the crack propagation equation (6.1) or (6.7) depend on the following influencing parameters:

- the material, its composition and microstructure;
- the mean stress or stress ratio, with the inclusion of residual stresses (effect on growth mechanism and crack closure);
- the environmental conditions, temperature and degree of corrosiveness;
- the frequency and waveform of the cyclic load at higher temperatures or in corrosive environments.

Data relevant to the specific material, loading and environmental conditions under consideration should be used as far as these are available. The mean plus two standard deviations of $\log(\mathrm{d}a/\mathrm{d}N)$ should be evaluated. An additional safety factor may be introduced. The values of the material constants m and C may be introduced based on published generalised data[494,495,545,604,629,630] if specific test results are not available.

The following recommendation is given by the fatigue assessment code BS7608[15] for structural steels tested in air at $R = 0$ (to be used with safety factor $j = 2$ on mean value C to allow for scatter):

$$m = 2.4\text{–}3.6, \quad C = \frac{1.315 \times 10^{-4}}{895.4^{m}} \quad [\mathrm{N,mm}] \tag{6.21}$$

More specific upper-bound values (resulting in highest-possible propagation rates) are given in the code BS7608[15] for ferritic structural steels (parent metal, weld deposit and heat-affected zone) at $R = 0$, first for high-cycle crack propagation (striation mechanism, $\Delta K \ll K_{\mathrm{c}}$), then for low-cycle crack propagation (cleavage mechanism or microvoid coalescence, $\Delta K \approx K_{\mathrm{c}}$) and finally for corrosive marine environments:

$$m = 3, \quad C = 3 \times 10^{-13}\ [\mathrm{N,mm}] \qquad (\Delta K \ll K_c)$$
$$m = 3, \quad C = 6 \times 10^{-13}\ [\mathrm{N,mm}] \qquad (\Delta K \approx K_c)$$
$$m = 3, \quad C = 2.3 \times 10^{-12}\ [\mathrm{N,mm}] \qquad \text{(marine environments)}$$

The flaw assessment guideline BS7910[17] recommends the following design values as an upper bound (mean plus two standard deviations):

$$m = 3, \quad C = 5.21 \times 10^{-13}\ [\mathrm{N,mm}] \qquad \text{(in air)}$$
$$m = 3, \quad C = 2.3 \times 10^{-12}\ [\mathrm{N,mm}] \qquad \text{(marine environments)}$$

Two-stage crack propagation laws which follow the measured data more closely are considered in the current editions of the guideline (King *et al.*[504]). Both the mean curves and the design curves are given for ferritic and austenitic steels in air and in sea water, with free corrosion and with cathodic protection in the latter case (bilinear da/dN versus ΔK curves in logarithmic scales with inclusion of threshold values). Supplementary data are published by Woollin.[668]

The revised IIW recommendations[133] state the following upper-bound values (mean plus two standard deviations) for structural steels:

$$m = 3, \quad C = 5.0 \times 10^{-13}\ [\mathrm{N,mm}]$$

Other upper-bound values for non-welded structural steels at $R = 0$ have been evaluated from test results (Clark[443]):

$$m = 2.25, \quad C = 5.79 \times 10^{-11}\ [\mathrm{N,mm}]$$

The same author gives relevant data for aluminium alloys at $R = 0$:

$$m = 3, \quad C = 9.82 \times 10^{-12}\ [\mathrm{N,mm}]$$

The revised IIW recommendations[133] state the following upper-bound values (mean plus two standard deviations) for aluminum alloys:

$$m = 3, \quad C = 4.0 \times 10^{-11}\ [\mathrm{N,mm}]$$

Further data for aluminum alloys can be found in the database compiled by Jaccard and Ogle.[494,495] The authors recommend to subdivide the crack propagation rate curve into several linearised sections for the purpose of numerical integration according to eq. (6.12). Data for aluminium alloys (dependent on R) can also be found in Eurocode 9.[24]

The fatigue crack propagation properties under random loading (avoiding crack closure) are considered by Suzuki *et al.*[626]

The threshold stress intensity factor ΔK_{th} in the crack propagation equations (6.4) or (6.5) depends on the following parameters:

– the material, its composition and microstructure;
– the mean stress or stress ratio (effect of crack closure);
– the environmental conditions temperature and degree of corrosiveness.

Data relevant to the specific material, loading and environmental conditions under consideration should be used as far as these are available.[494,495,545,604,629,630]

The following generalised data are evaluated from the literature for non-welded structural steels at the stress ratio $R = 0$ (Radaj,[8] *ibid.* p. 307[6]):

$$\Delta K_{th} = 180\ \mathrm{N/mm^{3/2}} \qquad \text{(lower-bound value)}$$
$$\Delta K_{th} \approx 24\ \mathrm{N/mm^{3/2}} \qquad \text{(mean value)}$$

The following relationship with the endurance limit $\Delta\sigma_E$ is also used:

$$\Delta K_{th} = \frac{3.48 \times 10^3}{\sqrt{\Delta\sigma_E}} \quad [\mathrm{N,mm}] \tag{6.22}$$

Several approximations have been proposed in respect of the influence of the stress ratio (inclusive of welding residual stresses) on the threshold stress intensity factor (Radaj,[6] *ibid.* p. 327). One is the following:

$$\Delta K_{thR} = \Delta K_{th}(1 - R) \qquad (R > 0) \tag{6.23}$$

where ΔK_{th} is the threshold stress intensity factor for $R = 0$, ΔK_{thR} is the threshold stress intensity factor for $R > 0$ and R is the stress intensity factor ratio ($R = K_{min}/K_{max}$).

Further threshold values for ferritic steels are recorded in the flaw assessment guideline BS7910.[17] The recommendation for as-welded structures in ferritic steels with tensile residual stresses assumed at the yield limit ($R \geq 0.5$) is the following:

$$\Delta K_{th} = 63\ \mathrm{N/mm^{3/2}}$$

The IIW recommendations[3] state lower bounds for structural steels:

$$\Delta K_{th} = 190\ \mathrm{N/mm^{3/2}} \qquad (R = 0)$$
$$\Delta K_{thR} = (190 - 144R)\ \mathrm{N/mm^{3/2}} \qquad (R > 0)$$

but not lower than $62\ \mathrm{N/mm^{3/2}}$ in the latter case.

They state for aluminium alloys:

$$\Delta K_{th} = 63\ \mathrm{N/mm^{3/2}} \qquad (R = 0)$$
$$\Delta K_{thR} = (63 - 48R)\ \mathrm{N/mm^{3/2}} \qquad (R > 0)$$

but not lower than $21\ \mathrm{N/mm^{3/2}}$ in the latter case.

The threshold stress intensity factor of ferritic steels is reduced to about half its value in seawater compared with dry air, but can be retained by cathodic protection (Hartt[482]).

Well-established material parameters for crack propagation in welded joints (weld metal and heat-affected zone) have been published by Ohta *et al.*[564–572] They are found to be independent of stress ratio, type of steel and welding conditions. This is explained by the fact that the crack remains completely open during the whole range of cyclic loading because of the tensile residual stresses at the crack tip in the as-welded condition. Deviations from the non-welded parent metal parameters occur mainly at lower propagation rates (increasing the propagation rate and reducing the threshold value).

A safe design curve based on the 99% confidence interval of the test results is defined by the following parameters referring to eq. (6.5):

$$m = 2.75, \quad C = 1.95 \times 10^{-12}\ [\mathrm{N,mm}], \quad \Delta K_{\mathrm{th}} = 63.2\ \mathrm{N/mm^{3/2}}$$

The mean curve applicable to fitness for purpose assessments which introduce an extra safety factor is characterised by:

$$m = 2.75, \quad C = 1.09 \times 10^{-12}\ [\mathrm{N,mm}], \quad \Delta K_{\mathrm{th}} = 77.5\ \mathrm{N/mm^{3/2}}$$

Further data are presented in graphs covering increased temperature, seawater corrosion and compressive loading.[564–572]

Welded joints consist of three zones with different microstructures and mechanical properties: parent metal, heat-affected zone (HAZ) and weld metal. Several papers however indicate that no significant variations exist in the crack growth properties of the three zones (Itoh *et al.*,[493] James,[496] Lee *et al.*,[512] Maddox,[522,523] Masuda *et al.*,[532] Parry *et al.*,[583] Socie and Antolovich[617]). Some others state that these three zones show differences in crack propagation behaviour in the range of low cyclic stress intensity factors approaching the threshold regime (Rading,[593] Spies *et al.*[618]). Lower crack propagation rates in the HAZ and the weld metal in comparison to the parent metal have been found by Tsay *et al.*[645,646] in laser beam-welded high strength steel and titanium alloy used for aircrafts and rocket cases. The crack propagation modes in welded (duplex) stainless steels have been studied by Beretta and Boniardi.[417] Not all of the investigations mentioned above, related to the weld zone effect, properly distinguish between the influence of microstructure and residual stresses, the latter representing a mean stress effect.

The critical stress intensity factor K_c depends on the following parameters:

– the material, its composition and microstructure,
– the plate thickness at the crack tip (with through-thickness cracks) or the degree of stress multiaxiality at the crack tip (with surface cracks or embedded cracks).

The introduction of the limit value K_{Ic} determined under plane strain conditions which is a material constant (fracture toughness) valid for large plate thickness or high degrees of (tensile) stress multiaxiality at the crack tip is recommended. This parameter should be determined by testing under the specific material condition being considered. The values of K_{Ic} for non-welded structural steels and aluminium alloys are in the range:

$$K_{Ic} = 600 - 3000\ \mathrm{N/mm^{3/2}}.$$

Substantial reductions of fracture toughness by coarse grain may be observed in the heat-affected zone of steels. These are avoided by proper heat treatment.

6.2.8 Initial and final crack size

The crack propagation life to be calculated at weld toes is highly dependent on the introduced initial crack size. Therefore, the initial crack size should not be underestimated. On the other hand, it should be larger than a 'short crack' (in the sense of fracture mechanics, see Section 6.1.3), i.e. $a_i \geq 0.1$ mm.

The initial crack size, $a_i \geq 0.1$ mm, may be derived from one of the following sources:

– result of non-destructive flaw or crack inspection, e.g. $a_i = 0.35$–1.9 mm in cast aluminium alloys according to Maddox;[527]
– minimum crack size which can definitely be excluded as remaining undetected in the structural member;
– limiting crack size used in crack initiation fatigue testing or in relevant calculations according to the notch stress or notch strain approach;
– size recommendation from codes, e.g. BS7608[15] or BS7910:[17] $a_i = 0.1$–0.25 mm at the weld toe of flaw-free welded joints (confirmed by Dijkstra *et al.*[449]);
– size deduced from adjusted calculations based on the crack propagation approach for comparable welded joints with well-known fatigue life (calibration), e.g. Labesse *et al.*;[505]
– size derived from the endurance limit and the threshold stress intensity factor on the basis of fracture mechanics (maximum size of a non-propagating crack).

The initial crack size is no problem in cases of weld root fatigue where the root face length substitutes the initial crack length.

The final crack size a_f up to which a crack may be allowed to propagate should be defined with regard to one of the following failure modes (compare BS7608[15]):

- unstable final fracture occurring at K_c or K_{Ic};
- stress corrosion cracking occurring at K_{Iscc};
- leakage resulting from through-thickness crack (in pressure vessels);
- unrestricted yielding in the remaining cross-section;
- unrestricted creep in the remaining cross-section;
- geometric instability of the structural member (buckling).

In many cases of application, a surface crack depth equal to one half or two thirds of the wall thickness can be introduced as the limiting crack size. Further crack propagation up to a through-thickness crack takes only a minor proportion of the total number of loading cycles.

6.2.9 Residual stress effects on crack propagation

The fatigue crack propagation behaviour in welded joints may be substantially changed by the effect of residual stresses, in particular by stresses induced by the welding process and by postweld treatment. The crack initiation site may thus vary. The fatigue life may be reduced or increased by these stresses. Residual stress analysis is therefore mandatory for reliable life estimates. This is not an easy task because the relevant measuring and computational methods are not readily available and may be expensive. Nevertheless, major progress in methods development and application has been achieved continuously. The basis is non-linear thermo-elastic-plastic finite element analysis, using not only the large expensive models, but also appropriately simplified ones (Radaj[592]). Also, the residual stress measuring methods have been developed to a high standard. Integrated finite element analysis of welding residual stress and distortion can thus be a key for success in industrial design development and production planning.

Welding residual stresses, locally redistributed by the growing crack, have an influence on the crack shape development and the crack path (see Section 6.2.6). The crack propagation rate is changed primarily by altered crack opening levels. Tensile residual stresses normal to the crack face cause the crack to remain open when subjected to cyclic loading whereas compressive residual stresses induce early crack closure. The fatigue life is lowered in the former and increased in the latter case. The residual stress effect is greater with lower and smaller with higher applied loads. Residual stress relaxation takes place in the latter case.

The change in crack propagation rate is expressed by the effective value of the stress intensity factor range, ΔK_{eff}, where the crack is open, by its often neglectable threshold value $\Delta K_{\text{th eff}}$, and by the effective stress intensity factor ratio $R_{\text{eff}} = K_{\min}/K_{\max}$ which includes the superimposed residual stress. The material constants C, m and ΔK_{th} remain unchanged. Assuming residual stresses at the tensile yield limit σ_{Y}, the stress cycles from remote loading (their mean stress assumed as zero) will fluctuate downwards from the yield limit, thus resulting in:

$$R_{\text{eff}} = \frac{\sigma_{\text{Y}} - \Delta\sigma}{\sigma_{\text{Y}}} \tag{6.24}$$

Introducing $\Delta\sigma \leq \sigma_{\text{Y}}$ for welded joints according to common practice, the result is $R_{\text{eff}} \geq 0$ (i.e. crack closure is more or less avoided). As small-scale welded specimens do not provide sufficiently high welding residual stresses, these specimens are advantageously fatigue tested with the upper stress held at the yield limit in order to make the test results transferable to full-size structural members with high tensile residual stresses.

Crack propagation analyses with inclusion of welding residual stresses were performed repeatedly (Beghini and Bertini,[413] Bussu and Irving,[435] Cheng *et al.*,[442] Galatolo and Lanciotti,[468] Glinka,[470] Greasley and Naylor,[472] Harrison,[479] Hou and Lawrence,[491] Itoh *et al.*,[493] Lee *et al.*,[511] Mutoh and Sahamoto,[544] Parker,[582] Schiebel,[603] Shi *et al.*,[607] Smith,[611] Tada and Paris,[627] Terada,[631] Terada and Nakajima,[632] Trufiakov *et al.*,[642] Tsai *et al.*,[644] Wu and Carlsson[669]). The investigations by Toyosada *et al.*[638] and Mori *et al.*[539,540] are reviewed to some extent in Sections 6.2.11 and 6.3.5. The more application-related approach by Dong is presented in Section 6.2.10. The growth behaviour of a surface or through-thickness crack transverse to a single-layer weld exhibiting the typical longitudinal residual stress distribution has found special attention owing to its practical relevance. Early initiation of crack growth caused by tensile residual stresses is combined with potential crack arrest in a later stage because of compressive residual stresses. The stress intensity factors are plotted versus crack length in Fig. 6.13.

Quite another situation occurs in thick plates joined by multi-layer welding. As a result of tensile residual stresses at the surface and compressive residual stresses in the interior, embedded cracks propagate mainly from the interior to the surface and surface cracks are slowed down in the interior, thus propagating primarily in surface direction. A crack propagation analysis related to this configuration has been performed by Mochizuki *et al.*[537] A longitudinal surface crack in a multi-layer butt weld in a double-V groove was investigated under transverse zero-to-tension loading. The measured welding residual stresses were converted to inherent strains for the residual stress redistribution analysis. The compressive range of ΔK is

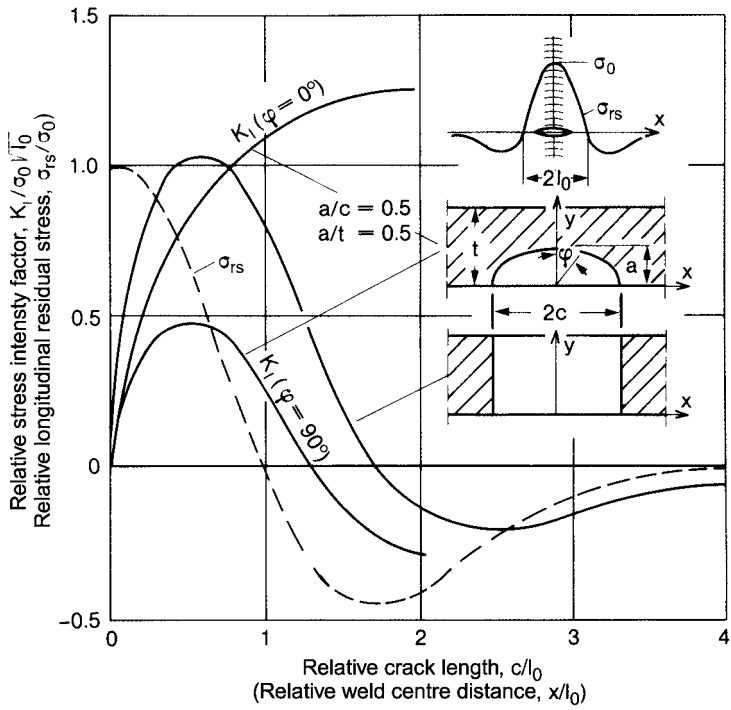


Fig. 6.13. Relative stress intensity factors of weld-transverse cracks subjected to weld-longitudinal residual stresses dependent on relative crack length (solid lines); residual stress distribution without crack (dashed line); after Terada,[631] and Wu and Carlsson.[669]

suppressed when applying the Paris equation. The crack size development (with fixed aspect ratios a/c = 0.25 and 1.0) is analysed with and without residual stresses in comparison.

The following further publications highlight the difference in crack propagation rate observed in welded structures in the as-welded, stress-relieved and postweld treated condition. The crack propagation rate in plasma-welded aluminium alloys is large perpendicular to the weld in the full-size centre-cracked tension specimen (high tensile residual stresses), but reduced in the small-size compact tension specimen (relieved residual stresses), whereas identical rates occur for crack propagation parallel to the weld (Galatolo and Lanciotti[468]). The crack growth rate in the heat-affected zone of friction stir welded high-strength aluminium alloys may be either faster or slower than in the parent material depending on the welding residual stresses (Bussu and Irving[435]). A large effect on the near-threshold crack growth parallel to the weld in the heat-affected zone has been found for friction stir welded aluminium and titanium alloys (John *et al.*[499]).

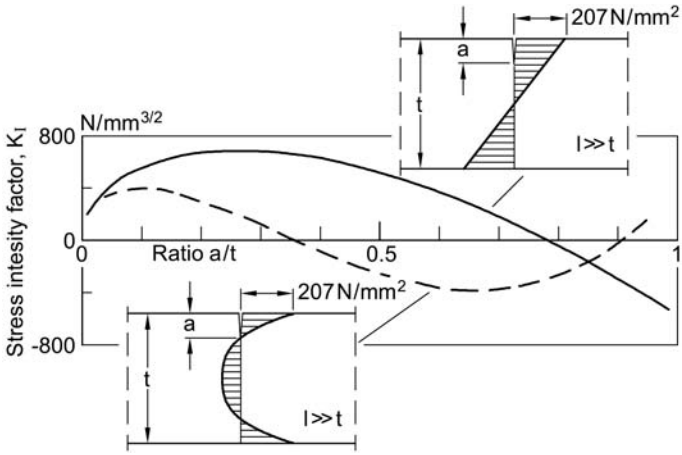


Fig. 6.14. Stress intensity factor dependent on relative crack depth in two welding residual stress states typical for pipe girth welds; weight function solution for displacement-controlled boundary conditions; after Dong and Hong.[452]

The basic behaviour of the stress intensity factor of a (through-thickness) edge crack traversing the wall thickness (dependent on crack depth a relative to wall thickness t) with residual stresses of the bending and self-equilibrating type superimposed, which are characteristic for pipe girth welds, can be studied in Fig. 6.14. Displacement-controlled conditions are considered, resulting in residual stress relaxation by the growing crack. The crack should be arrested in both cases by the compressive stress intensity factors, and this should occur at a smaller crack depth with the self-equilibrating stresses than with the bending stresses.

6.2.10 Particular crack propagation approach

A procedure constituting the crack propagation approach which deviates significantly from the generally preferred mainstream of development has been proposed by Dong *et al.*[100,101,453] It is intended to support Dong's structural stress approach based on finite element models with rather coarse meshes (thin-shell and solid element models). The procedure takes up the concept of a bilinear stress distribution over the plate thickness at the weld toe.

In a first step (originating from the ASME code), the total stresses σ_{tot} in the cross section with the notch (primarily a weld toe) are decomposed into the linearised structural stresses σ_s (with membrane and bending component, $\sigma_m + \sigma_b$) and 'self-equilibrating' notch stresses σ_{se}, Fig. 6.15. The self-equilibrating stresses (solid line) are substituted by two linear

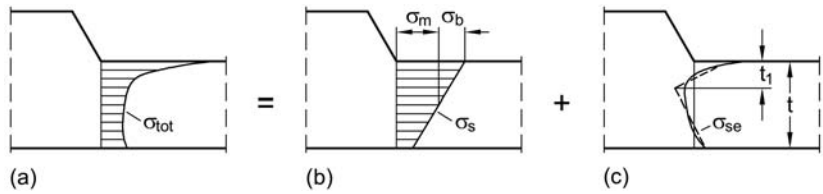


Fig. 6.15. Decomposition of the total (normal) stress σ_{tot} in the cross section at a notch into the linearised structural stresses σ_s and the self-equilibrating notch stresses σ_{se} (solid lines: original stress distribution; dashed line: bilinear stress distribution).

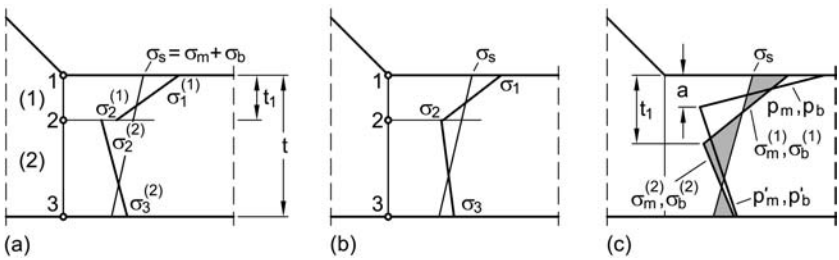


Fig. 6.16. Non-intersecting linearised structural stresses in segments (1) and (2) of the cross-section at a notch (a), with enforced intersection point at depth t_1 (b), and with further varying reference depths corresponding to crack depth a (c); after Dong *et al.*[453]

distributions (dashed lines) intersecting at the reference depth t_1 (empirically supported choice at weld toes: $t_1/t = 0.1$) which are also self-equilibrating, i.e. the resultant force and the resultant moment are zero. The two linear curves may result from finite element analysis, with a single upper layer of elements over the depth t_1 and several layers over the remaining thickness, the related linear curve found from the resultant force and resultant moment in the lower multi-layer part.

The two linearised curves do not intersect in a single point at the depth t_1 in general, Fig. 6.16(a), but it is possible to enforce the intersection point there under the condition of an unchanged resultant force and moment in the total cross-section, Fig. 6.16(b). The relationship between the correspondingly adapted stresses σ_1, σ_2, σ_3 and the original stresses $\sigma_1^{(1)}$, $\sigma_2^{(1)}$, $\sigma_2^{(2)}$, $\sigma_3^{(2)}$ is derived from the above conditions using simple algebra (nodal forces F_1, F_2, F_3 remaining unchanged, Dong *et al.*[100,101,453]):

$$\sigma_1 = \sigma_1^{(1)} + \frac{t - t_1}{2t}\left(\sigma_2^{(1)} - \sigma_2^{(2)}\right) \tag{6.25}$$

$$\sigma_2 = \sigma_2^{(2)} + \frac{t_1}{t}\left(\sigma_2^{(1)} - \sigma_2^{(2)}\right) \tag{6.26}$$

$$\sigma_3 = \sigma_3^{(2)} - \frac{t_1}{2t}\left(\sigma_2^{(1)} - \sigma_2^{(2)}\right) \tag{6.27}$$

Obviously, only global equilibrium is maintained, whereas the local equilibrium conditions at the segments (1) and (2), if considered seperately, are violated (the slight change in stress gradients indicating a change in bending moments is easily recognisable in the figure). This fact is important with regard to bilinear structural stress evaluations which are thus rendered objectionable. The condition enforcing the intersection point at depth t_1 (or at any other depth deviating from the original depth of the intersection point) appears to be misleading.

The concept just described has been further extended with regard to the crack propagation analysis at notches (mostly weld toes) with the aim to determine the magnification factor M_k inclusive of the notch effect (Dong *et al.*[100,101,453]). The bilinear notch stress approximation described above is used as the basis for estimating further self-equilibrating notch stress distributions with varying reference depths corresponding to the respective crack length a, Fig. 6.16(c). The membrane and bending stresses, $\sigma_m^{(1)}$, $\sigma_b^{(1)}$ and $\sigma_m^{(2)}$, $\sigma_b^{(2)}$, for the depth ratio t_1/t corresponding to the damaging crack length (usually $t_1/t = 0.1$) are defined by the aforementioned stresses σ_1, σ_2, σ_3. The condition of self-equilibrium of the bilinear notch stresses is indicated by the shadowed areas against the linear structural stress σ_s. Further bilinear curves intersecting at variable depths a (corresponding to variable crack depths, the related stresses considered as crack face pressures, p_m, p_b, p'_m, p'_b) are generated based on the following conditions: unchanged resultant force and moment, intersection point at depth a and a further optional condition (the four crack face pressures demand four conditions). Originally, the condition of an unchanged total shadowed area was introduced, and later on the simplified condition $(p'_m - p'_b) = (\sigma_m^{(2)} - \sigma_b^{(2)})$ was introduced without major deviations in the results. Obviously, the minimum stress σ_2 at the intersection point remains approximately the same under these conditions, whereas the stress σ_1 at the notch root rises with decreasing crack depth a.

The stresses or crack face pressures above are used to determine the stress intensity factor of cracks originating from the notch root, expressed by the magnification factor M_k. Solutions for linearised crack face pressures are readily available from the literature or can be derived by the weight function method. It was found by Dong that the stress intensity factors from the described procedure correspond roughly with those attained by Glinka *et al.*[552,553] and Forbes *et al.*[463] for comparable notch configurations, also based on the weight function method. The question remains unanswered why the progressively changing bilinear stress distributions, with the property of self-equilibration in combination with a theoretically unfounded additional condition (e.g. constant shadowed area), provide stress intensity

factors which are applicable within Dong's range of validation. It should be noted that notch stresses are recovered which are not available from the original coarse-mesh results. Obviously, crack face pressures are generated which have a distant resemblance to the actual notch stress distribution, inclusive of singular notch stresses for $a = 0$ at sharp notches.

The magnification factor M_{kn} presented by Dong,[100,101,453] contrary to his own statement, seems to have the same definition as the conventional factor M_k: the ratio of the stress intensity factors of the crack with and without the notch effect. Therefore, the magnification factors can be compared directly, independent of the introduced reference stresses (nominal or structural).

A further pecularity of Dong's crack propagation approach is his two-stage crack growth model. The first stage is dominated by the notch-induced self-equilibrating part of the stress state, whereas the second stage is dominated by the linear (or bilinear) structural stress state which can be computed effectively using coarse meshes. The Paris equation for crack propagation is modified to the following unconventional form:

$$\frac{\mathrm{d}a}{\mathrm{d}N} = CM_k^n (\Delta K)^m \tag{6.28}$$

with the stress intensity factor range ΔK derived for the linearised structural stress state, the notch-related magnification factor M_k computed as shown above, the exponent n approximated by $n = 2$, the exponent $m = 3.4–4.0$ introduced as material-independent (for steels) and the coefficient C depending on the material. The magnification factor M_k is applied only in the first short-crack propagation stage where $M_k > 1.0$. The parameter m is derived from a re-evaluation of experimental data gained from short-crack and long-crack behaviour in non-welded specimens. The values of C and m are altered to some extent by applying eq. (6.28) with the re-defined ΔK values. This equation is a useful rough approximation on an empirical basis representing a limited number of experimental results.

The integration of eq. (6.28) from a small initial crack depth ($a_i \approx 0$, e.g. $a_i/t = 0.001$) to the final crack depth equal to plate thickness, $a_f = t$, results in the following crack propagation life N (considered as total life):

$$N = \frac{I(\delta_b)}{C(\Delta\sigma_s)^m t^{m/2-1}} \tag{6.29}$$

with the crack growth integral $I(\delta_b)$ depending on the degree of bending $\delta_b = \sigma_b/(\sigma_m + \sigma_b)$ (see Fig. 3.24) and the structural stress range $\Delta\sigma_s = \Delta\sigma_m + \Delta\sigma_b$. The structural stress parameter ΔS_s according to eq. (3.10), providing the basis of Dong's 'master S–N curve', is derived on the basis of eq. (6.29).

The mean stress effect is taken into account by multiplication of the right-side term in eq. (6.29) by $(1 - R)$ with the load ratio $R = F_{min}/F_{max}$ (compare eqs. (6.9) and (6.10)). The residual stress effect is taken into account by Dong[451] introducing the stress intensity factor ratio $R = K_{min}/K_{max}$ which depends on the ratio a/t of crack depth to wall thickness, on the initial residual stress distribution and on the remote loading condition. The short-crack stage is covered by eq. (6.28) with the right-side term divided by $(1 - R)^{n/2}$.

This procedure has primarily been applied to the axial residual stresses in pipe girth welds (Dong and Hong[452]). Typically, these stresses can be decomposed into membrane stresses (usually negligibly small), bending stresses and self-equilibrating stresses. Bending stresses are dominant in single-sided girth welds (single- and multi-pass), self-equilibrating stresses prevail in double-sided welds (two-pass or multi-pass). The related stress intensity factor should be determined under displacement-controlled loading conditions in order to capture the residual stress redistribution which is caused by the growing crack. Conventional methods, the weight function method among them, can be applied for this purpose. A special finite element based alternating method can also be used (Dong and Hong[452]). A given residual stress distribution is first mapped on the finite element model of the structural detail, followed by equilibrium iterations under the relevant boundary conditions. The K value can then be calculated by iterations between the finite element model (without the crack) and the solution for the infinite body with the crack (see Fig. 6.14).

6.2.11 Refined crack propagation approach

The conventional crack propagation approach is based on crack growth equations of the original Paris type, i.e. on empirically derived simple relationships based on ΔK which allow estimates of fatigue life. Several shortcomings are connected with the conventional approach. The crack initiation period is completely neglected and short-crack behaviour is inadequately simulated. Crack path and crack shape development are presumed and not the result of analysis. Crack closure is only roughly taken into account and residual stress effects are not quantified. Variable-amplitude loading with interaction effects is not realistically described.

There have been two major attempts to overcome these shortcomings with regard to welded joints, an early one by Karzov *et al.*,[502] based on a damage accumulation concept, and a later one by Toyosada *et al.*[637–641] with emphasis on short crack growth. Both concepts refer to the reverse plastic zone at the crack tip as the basic crack growth parameter. The promising approach by Vormwald and Seeger[654–656] based on the effective J-integral for short cracks is still untried with regard to welded joints.

The early refined model of fatigue crack propagation described by Karzov *et al.*[502] is based on solving the elastic-plastic problem of the stress and strain state at the crack tip, on Manson–Coffin's low-cycle fatigue law (applied to the reverse plastic strains at the crack tip) and on the hypothesis of linear damage accumulation. The superimposed monotonic and cyclic deformations at the crack tip and the accumulated damage portions resulting from it are depicted in Fig. 6.17. The plastic zones resulting from monotonic and reverse cyclic deformation are also plotted. Discrete crack length extensions, Δa, are presumed which are portions of the reverse plastic zone size limited by the strain value corresponding to the threshold stress intensity factor K_{th}. The reverse plastic strains in this zone follow from the stress intensity factor K_I along the crack path. The crack path and the related static and cyclic stress intensity factors are determined from the energy release rate in a fine regular mesh of triangular finite elements which are 'softened' where the crack occurs (outdated procedure). The welding residual stress field is described by the corresponding inherent strain distribution, thus allowing for a simplified analysis of stress redistribution. The crack paths in the cross-sectional models of butt and cruciform joints, the latter both with load-carrying and non-load-carrying fillet welds, were determined by the procedure above (Brejew and Karkhin[427]).

Another refined model of fatigue crack propagation has been presented by Toyosada *et al.*[637–641] It is characterised by the following pecularities:

– In the Paris equation, the stress intensity factor range is substituted by the size of the reverse plastic zone at the crack tip positioned within a larger plastic zone from previous loading in the opposed direction, thus defining the RPG load ('Re-tensile Plastic zone's Generated load').

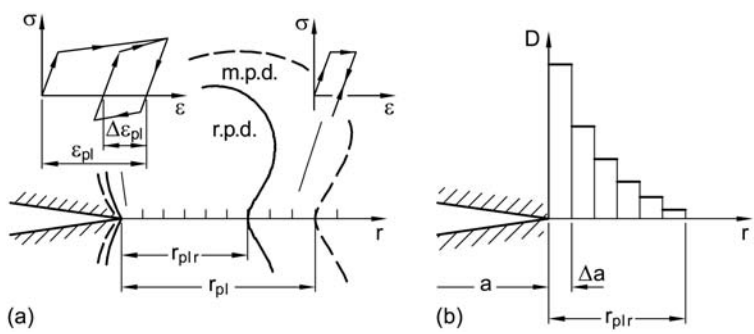


Fig. 6.17. Plastic deformation behaviour (a) and damage distribution (b) at the crack tip subjected to cyclic loading; σ–ε curves in zones of monotonic plastic deformation (mpd) and of reverse plastic deformation (rpd); accumulated damage D in front of the crack tip; with plastic strain ε_{pl}, plastic zone size r_{pl}, reverse plastic zone size r_{plr} and crack length a; after Karzov *et al.*[502]

– Short-crack propagation is included in this modified equation which (remarkably enough) postulates no threshold value.
– The RPG load with inclusion of crack closure is determined by the modified Dugdale–Newman strip yield model describing the plasticity-enlarged 'thickness' of the semi-elliptical crack surfaces on the basis of an equivalent plane straight-fronted crack model. The modified Dugdale–Newman strip yield model has also been used by Hou and Lawrence[491] to demonstrate different crack propagation rates in the as-welded and stress-relieved condition of welded joints. The RPG load can alternatively be determined by compliance measurements (local strain versus remote load).
– Crack initiation is described by shear-mode microcrack propagation within the first (surface) grain, followed by opening-mode propagation in the following grains. Multiple surface cracks coalesce in a single larger surface crack propagating through the plate thickness and continuing propagation as a straight-fronted through-crack.

A computational procedure following this approach is depicted as a flow chart in Fig. 6.18. The basis is a finite element model of the structural detail

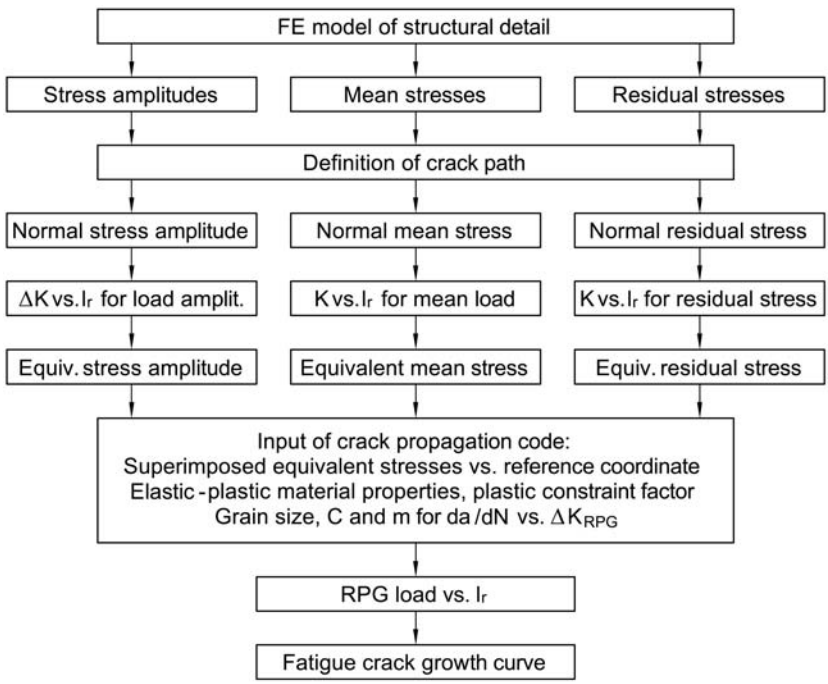


Fig. 6.18. Flow chart of an advanced fatigue crack initiation and propagation code for life assessment of welded structural details; 'normal' referring to crack path; reference crack length l_r defined in Fig. 6.33; 'equivalent' referring to plane model with identical K value; after Toyosada *et al.*[638]

to be investigated, from which stress amplitudes, mean stresses and residual stresses are extracted. After definition of the prospective crack path, the crack-opening stresses normal to the crack path are determined, from which the stress intensity factors versus the reference crack length (defined in Fig. 6.33) result. These stress intensity factors define the equivalent distributed stresses which are the basis of the elastic-plastic (modified) Dugdale–Newman crack propagation model (with crack length equal to surface crack depth) installed to calculate the RPG load versus the reference crack length and therefrom the crack propagation curve. A special cohesive-force-based model is conceived for the simulation of the closed-crack propagation in the first grain.

Within the proposed approach, the governing parameter for fatigue crack propagation is ΔK_{RPG} throughout the fatigue life, from short crack initiation to failure, without a threshold value being observed:

$$\frac{\mathrm{d}a}{\mathrm{d}N} = C_1 (\Delta K_{\mathrm{RPG}})^m \tag{6.30}$$

The original version of this equation introduces the size $\tilde{\omega}$ of the crack tip reverse plastic zone (extension in ligament direction) as the basic parameter:

$$\frac{\mathrm{d}a}{\mathrm{d}N} = C_2 \tilde{\omega}^{m'} \tag{6.31}$$

More precisely, $\tilde{\omega}$ is the size of the overlapping region of the tensile plastic zone at the maximum load $F_{\max}$ and the compressive plastic zone at the minimum load $F_{\min}$ in a given loading cycle. The relationship between $\tilde{\omega}$ and ΔK_{RPG} is formulated as follows, based on results of numerical analysis:

$$\tilde{\omega} = \eta \frac{\pi}{8} \left(\frac{\Delta K_{\mathrm{RPG}}}{2\lambda \sigma_{\mathrm{Y}}} \right)^2 \qquad (\eta = 1.55) \tag{6.32}$$

with the plastic constraint factor λ ($\lambda = 1.04$ in the case of mild steel) and the yield limit σ_{Y}.

The stress intensity factor range ΔK_{RPG} results from the difference between the RPG and maximum stress intensity factors or loads, respectively:

$$\Delta K_{\mathrm{RPG}} = K_{\max} - K_{\mathrm{RPG}} = (F_{\max} - F_{\mathrm{RPG}}) \sqrt{\pi a} \frac{M_{\mathrm{k}}}{tw} \tag{6.33}$$

with the base plate thickness t, the base plate width w and the notch-related magnification factor M_{k}.

The following relationship exists between RPG load F_{RPG}, crack closure load F_{cl} and crack opening load F_{op}:

$$F_{RPG} > F_{cl} > F_{op} \tag{6.34}$$

Before the crack reaches the first grain boundary, a cyclic (notch) strain, which is almost totally plastic, is generated in every loading cycle within the plastic zone. This zone does not change under constant-amplitude loading, since the initiated shear crack remains closed. Its size is controlled by the cyclic yield limit. During the transition stage from a shear crack to an opening and closing crack, the yield strength would increase, approaching the static yield limit as the crack propagates. Then it is expected that the propagation rate will decrease when the crack penetrates the first few grains. A specimen with a sharp notch which has experienced a large number of cycles at the fatigue limit, can thus have non-propagating cracks (formulations close to Toyosada *et al.*[638]).

It is not clear from Toyosada's publications, how the shear crack in the first grain is actually initiated. Obviously, the crack propagation equation is extended without a threshold condition into the short-crack range by considering local plastic zone sizes instead of elastic stress intensity factors. Thus, any cyclic plastic zone may initiate and propagate a crack. In the initially uncracked (but sharply notched) specimen, only the plastic zone of the notch is acting, subsequently superimposed and progressively substituted by the plastic zone of the crack. Using the Dugdale–Newman model is only possible with the plastic zone of the crack, but not with the initial plastic zone of the notch without a crack. This part of Toyosada's model remains unclear.

6.3 Demonstration examples

6.3.1 Longitudinal and transverse attachment joints

The fatigue life of a longitudinal attachment joint under zero-to-tension cyclic loading ($R = 0$) has been analysed on the basis of the crack propagation approach and fatigue-tested in parallel by Maddox.[521,523–525] The dimensions of the specimens are shown in Fig. 6.19(a). The fillet welds (GMA- and MMA-welded) are carried on around the ends of the attachments so that four critical regions of a weld toe transverse to the direction of stressing were provided. The material is CMn steel with yield limit σ_Y = 375 N/mm^2 and ultimate tensile strength σ_U = 527 N/mm^2. The material parameters for the crack propagation analysis, assumed to be identical for parent metal and heat-affected zone, are the following (lower and upper bound): $m = 3$, $C = 0.09 \times 10^{-13}$ and 3.0×10^{-13} [N,mm] (parameters referring to eq. (6.1)).

The stress intensity factor for the semi-elliptical surface crack assumed at the weld toe was determined dependent on the depth-to-thickness

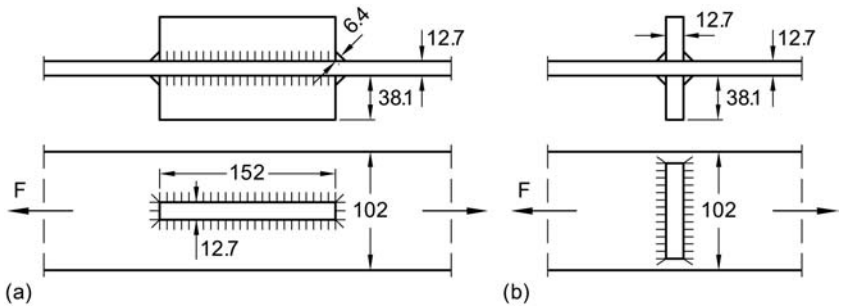


Fig. 6.19. Longitudinal and transverse attachment joints analysed by Maddox.[521,523–525]

ratio a/t for actual weld toe angles ($\theta = 30$–$60°$) and actual averaged crack shape parameters ($2c = 6.71 + 2.58a$ [mm], i.e. $a/2c \leq 0.32$ for $a \leq t$ with plate thickness $t = 12.7$ mm). Initial crack depths $a_i = 0.1$–4.8 mm were produced by precracking under fatigue loading. The initiated cracks propagated across the plate thickness.

The crack propagation life in terms of lower- and upper-bound values was predicted dependent on the generalised stress range $\Delta\sigma^*$, which includes the influence of initial crack size, final crack size ($a_f = t$), crack aspect ratio and weld toe angle. All the actual crack propagation life values found in the fatigue tests were within the predicted scatter band. Adjusted calculation of the total life of the specimens (including the precracking period) gave suitable initial crack depths near $a_i = 0.1$ mm. This size has actually been determined for sharply notched slag intrusions in low and high strength steel specimens after GMA and MMA welding.[608] The analysis was also performed for transverse attachment joints (non-load-carrying fillet welds) according to Fig. 6.19(b).

The investigation of the longitudinal attachment joint in steel was extended to specimens in type AlZnMg aluminium alloy ($\sigma_{Y0.2} = 355$ N/mm^2, $\sigma_U = 411$ N/mm^2) under zero-to-tension and fully reversed loading ($R = 0$ and $R = -1$).[531] Crack closure was taken into account in the latter case by using $\Delta K_{eff} = \Delta K/2$ in the crack propagation equation with the material parameters $m = 3$, $C = 6.9 \times 10^{-12}$ and 1.7×10^{-11} [N, mm], respectively. The specimens were tested without precracking. Adjusted calculation of the total life gave initial crack sizes $a_i \leq 0.01$ mm. Defects of that small size are not detectable by experimental means. Actual fatigue test results were well within the scatter band calculated with $a_i = 0.01$ mm.

The longitudinal attachment specimen in steel was further analysed by Rörup[602] in respect of fatigue crack initiation and propagation under zero-to-compression loading of the specimen. The focus was on the residual stresses and their redistribution during crack propagation affecting

the crack closure behaviour. The effective or crack opening range of the stress intensity factor described the crack propagation behaviour very well.

An extensive crack propagation analysis of fillet-welded transverse attachment joints in steel was performed by Gurney[128] in respect of the thickness effect on fatigue strength (reviewed in Sections 3.3.2 and 3.3.3). The analysis is based on material parameters according to eq. (6.21) with $m = 3.0$ and $m = 4.0$ introduced comparatively, and on the assumption of a semi-circular or straight-fronted initial crack of depth $a_i = 0.15$ mm. The theoretical analysis is used to define the fatigue testing program. It is expressly considered to be unsuitable for calculating absolute strength or life values.

A comparative crack propagation analysis by Branco *et al.*[426,459] confirmed that the differences in fatigue life of GTA, GMA and plasma arc welded thin sheet joints ($t \leq 10$ mm) in CMn steel can be traced to differences in weld toe geometry. The weld toe radius appeared to be more significant than the weld toe angle.

6.3.2 Cruciform and T-joints

The fatigue life of cruciform joints (load-carrying fillet welds) in CMn steel under zero-to-tension cyclic loading ($R = 0$) has also been analysed by Maddox[524] according to the crack propagation approach and compared with testing results. The following mean values of material parameters were used: $m = 3$ and $C = 1.64 \times 10^{-13}$ [N, mm] (parameters referring to eq. (6.1)). Plate fractures and weld fractures are considered.

Plate fractures result from crack initiation at the fillet weld toe. An initial crack depth $a_i = 0.15$ mm was assumed based on an investigation into slag intrusions by Signes *et al.*[608] The crack shape parameter was $a/2c = 0$ or 0.1 (with crack depth a and surface crack length $2c$), the weld toe angle was $\theta = 45°$ and the fillet leg length and the plate thickness were variable quantities. The basic stress intensity factor for $a/2c = 0$ was calculated by finite element analysis.

Weld fractures start at the root line of the weld and propagate in continuation of the root face direction, i.e. close to the fillet leg, the length of which is therefore used for the crack propagation analysis. The initial root face length $2a_i$ is equal to the plate thickness $2b$. The stress intensity factor was taken from a finite element analysis performed by Frank and Fisher.[465]

The crack propagation life was predicted dependent on the stress range based on the analysis for both types of fracture. Actual fatigue test data were well within the predicted scatter range.[524]

The question was put forward what the critical fillet weld leg length is for which fatigue fractures will presumably occur simultaneously at the weld toe (plate fracture) and the weld root (weld fracture). The question was

answered on the basis of the $\Delta\sigma$–N relationships (failure probability P_f = 5%) gained from the crack propagation analysis, Fig. 6.20.

The critical ratio of leg length c to plate thickness $2b$ (for $2b$ = 6.25–25.0 mm and $2a = 2b$) is $c/2b$ = 0.9–1.2. Similar curves have been derived for the AlZnMg alloy specimen.[531] They run higher than the curves for steel, i.e. the critical leg length is larger for the aluminium alloy.

The numerical and experimental crack propagation analysis by Otsuka *et al.*[576,577] of transverse shear loaded cruciform joints with fillet welds and root face (directed parallel to the shear force) in high strength aluminium alloy is remarkable because of its meticulous registration and differentiation of the phenomena. The joint made of 7N01-T4 aluminium alloy (approximately equivalent to AA7004-T4 or AA7005-T4) tends to crack propagation in root face direction under mode II conditions concurrent with the crack propagation direction under mode I conditions.

Both well-aligned and misaligned cruciform joints with load-carrying fillet welds (leg length equal plate thickness) and varying degrees of penetration have been analysed according to the crack propagation approach in respect of fatigue failures originating from the weld toe and weld root (Lie *et al.*[516,517]). The misalignment effect on fatigue is large under axial loading (not so under bending loads) provided the rotations of the (relatively short) plate ends are suppressed. The stress intensity factors of the straight through-thickness crack front at the weld toe (a_i = 0.15 mm) and the weld root were calculated by the boundary element method (quarter point tech-

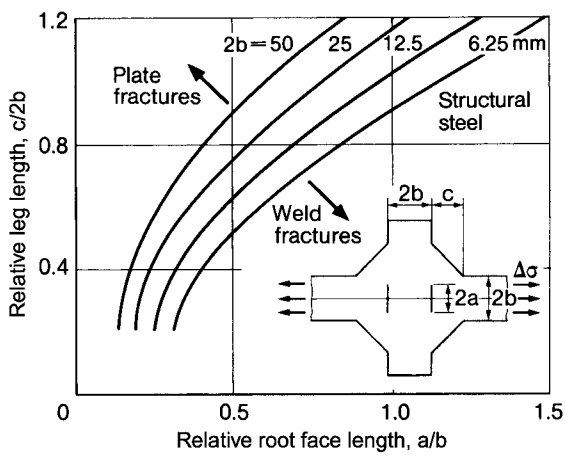


Fig. 6.20. Limit curves separating plate fractures from weld fractures in cruciform joints made of structural steel, dependent on plate thickness $2b$, root face length $2a$ and weld leg length c; after Maddox.[524]

nique) for varying crack lengths. S–N curves were derived based on the Paris equation for different axial eccentricities $e/t \leq 1.0$ and compared with Andrew's[76] experimental results. The failures originated from the weld toe with the exception of joints without misalignment and low penetration. Reference is also made to the fatigue life predictions for cruciform joints presented by Skorupa.[610]

In a way similar to that above, the effect of undercut, misalignment and residual stresses on the fatigue behaviour of butt-welded joints has been analysed (Nguyen and Wahab[548–551]). The reduction of fatigue strength of welded joints with a weld toe undercut is at least twice that of joints without an undercut in comparison with the flush-ground welded plate. A misalignment of 5% of plate thickness and an undercut of 2% of plate thickness are fairly representative for the lower bound of S–N curves of butt-welded joints.

The fatigue strength of cruciform joints with load-carrying fillet welds of various shapes (applied in highway bridges) has been analysed by Mori and Kainuma[539] according to the crack propagation approach and by fatigue testing in comparison. Weld root fatigue is evaluated and a design formula for the weld throat thickness derived. The influence of the welding residual stresses on fatigue failures at weld root and weld toe in comparison is considered in more detail (Mori *et al.*[540]). The fatigue strength limited by weld root failure changes greatly with the testing conditions: the fatigue life is lowered in tests with the upper stress at the yield limit than in tests with the lower stress set to zero (at least in the high-cycle fatigue range). The main reason for this behaviour are the compressive residual stresses at the weld root. A simplified thermo-elastic-plastic finite element analysis of the weld cooling process (the cross-sectional model under plane-strain conditions) resulted in residual stresses perpendicular to the weld root face which are plotted in Fig. 6.21 over the root face and leg length for a closed root face (gap width $g = 0$ mm) and an open root face ($g = 0.1$ mm). The calculated residual stress intensity factors for a crack propagating along the weld leg are compressive in both cases. The residual stresses at the weld toe are tensile in contrast. The effective stress intensity factor ranges ΔK_{eff} under remote loading (to be inserted in the Paris equation) are substantially reduced at the weld root by the compressive residual stresses acting there. The fatigue life is accordingly enlarged. The critical leg length where root failures change into toe failures is determined at $1.2t$ (with base plate thickness t).

Extensive parametric studies of the crack propagation life of cruciform joints with load-carrying fillet welds with varying degrees of penetration (or root face length) have been conducted by Nykänen[559,560] using the finite element crack growth simulation programme FRANC2D/L.[497] This programme allows the crack path to be traced and the crack length to be

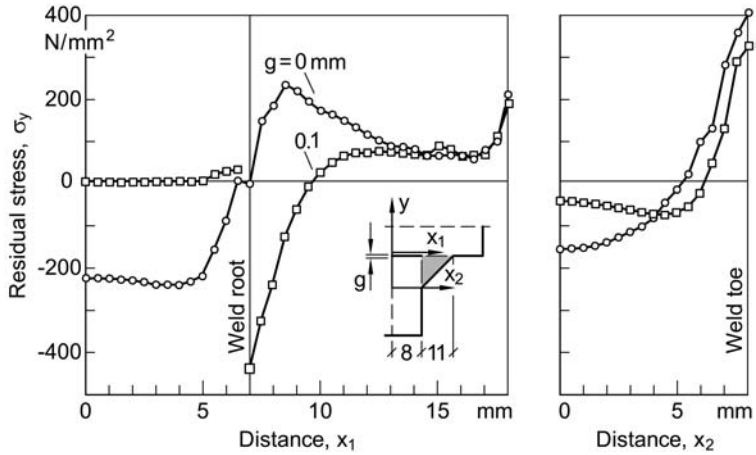


Fig. 6.21. Calculated welding residual stresses perpendicular to the weld root face in cruciform joint, plotted over root face and leg length for closed (g = 0 mm) and open (g = 0.1 mm) root faces; after Mori *et al.*[540]

determined dependent on the number of loading cycles in two-dimensional configurations comprising straight crack fronts. Simultaneous crack growth at the weld root and weld toe (a_i = 0.2 mm) under (initially) mixed mode I and II loading conditions is simulated. The stress intensity factors are evaluated from the J-integral in combination with the maximum tangential stress criterion enforcing the crack path perpendicular to the maximum principal stress. The effect of weld leg length (h/t = 0.0–1.1), root face length (w/t = 0.1–1.0) and weld toe angle (θ = 15, 30, 45°) on the fatigue strength is studied (with base plate thickness t = 50 mm and transverse plate thickness T = 80 mm). Pure tension loading and pure bending loading are considered besides a combined loading case. The theoretical fatigue strength in terms of the nominal stress range is plotted in Fig. 6.22 (pure tension and pure bending), and compared with the IIW recommendations[3] ($\Delta\sigma_{nE}$ = 63 or 45 N/mm^2 for toe or root failures modified by $(C_{mean}/C_{char})^{1/3}$ and $(t/t_0)^n$ with n = 1/5 or 1/3, respectively). Toe failures occur at $\Delta\sigma_n$ = 65–68 N/mm^2 (tension) or $\Delta\sigma_n$ = 86–88 N/mm^2 (bending). Root failures are observed below these values for small ratios h/t and/or large ratios w/t. The effect of plate thickness is also considered in the investigation.

Parametric investigations of cruciform joints with partial penetration single-bevel butt welds (covered by fillet welds) and similar fillet-welded T-joints have been performed in the same way as above by Nykänen *et al.*,[561,562] Fig. 6.23. Fillet-welded corner joints were similarly investigated.[563] Separate crack growth at the weld toe and weld root is assumed in the T-joint and corner joint investigations (obviously, it is an open question what

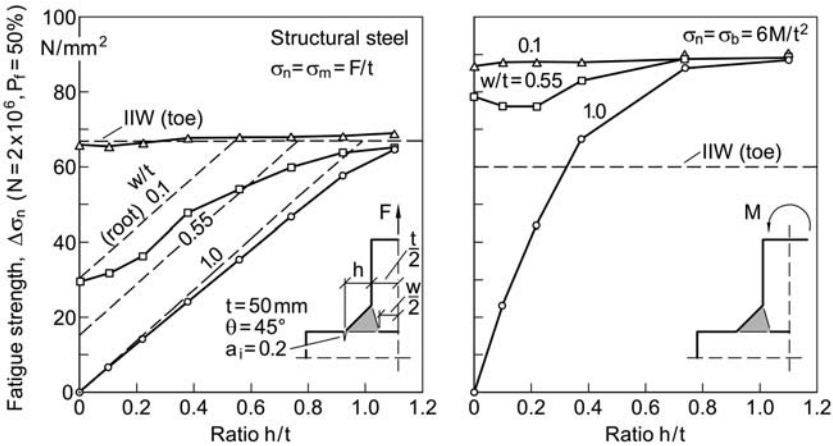


Fig. 6.22. Fatigue strength of cruciform joints (load-carrying fillet welds, varying degrees of penetration) in structural steel limited by toe or root failures dependent on throat thickness and degree of penetration; pure tension and pure bending loads; results of crack propagation analysis for $w/t = 0.1$, 0.55 and 1.0 (solid lines) compared with IIW recommendations[3] (dashed lines); after Nykänen.[559,560]

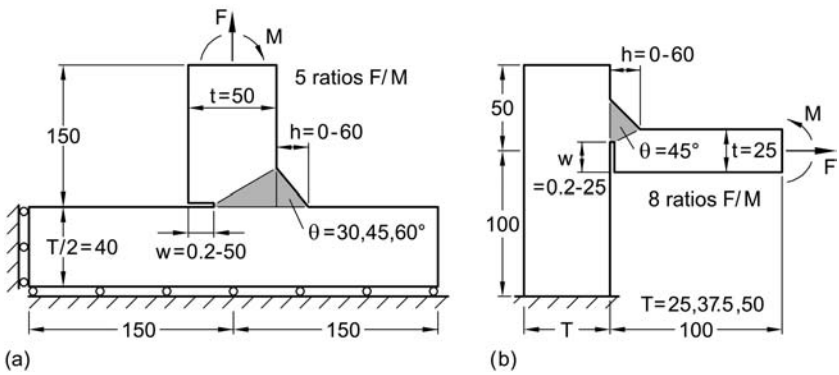


Fig. 6.23. Cruciform joint with partial penetration single bevel butt welds (covered by fillet welds) and similar T-joint under tension and bending loads; geometric parameter ranges covered by the crack propagation analysis of toe and root failures; after Nykänen *et al.*[561,562]

is more realistic: simultaneous or separate crack growth). The geometric parameter ranges are indicated in the figure together with the number of investigated force-to-moment ratios F/M. These ratios correspond to 'degrees of bending' (see eq. (3.11)), with pure tension and pure bending loading as special cases. Major differences in fatigue strength occur between the different combinations, not only between tension and bending loading,

but also depending on to what extent the root face remains closed during the loading cycles. Crack propagation in fillet-welded T-joints was also investigated by Tsai and Kim.[643]

6.3.3 Lap joints and cover plate joints

Two-sided lap joints with transverse fillet welds in steel have been assessed in respect of the design stresses on the basis of initial crack intensity factor ranges by Partanen *et al*.[884] Crack propagation starting at the weld root in zero-to-compression loading and at the weld toe in zero-to-tension loading are compared. The appropriate detail class design stresses are determined on the basis of the equivalent initial stress intensity factors (according to the maximum tangential stress criterion[866]). The initial stress intensity factors are derived by finite element analysis. The detail class according to the IIW recommendations,[3] $\Delta\sigma_{nE} = 63\,N/mm^2$ in the plate section or $\Delta\sigma_{wE} = 45\,N/mm^2$ in the throat section at $N = 2 \times 10^6$ cycles, is shown to be conservative in tensile loading but not so in compressive loading.

The root failures in the lap joints above have been further analysed according to the crack propagation approach by Nykänen.[557] Equivalent stress intensity factor parametric equations referring to the nominal stress in the main plate are derived for zero-to-tension and zero-to-compression loading. The varied parameters are the crack depth a, the weld leg length c and the cover plate length $2l$ which are expressed by the ratios a/c, c/t and l/t, where t is the base plate thickness set equal to the cover plate thickness. The predicted crack paths are different in the two loading cases, Fig. 6.24. The crack path is found in the molten zone close to the cover plate end under zero-to-tension loading and in the base plate underneath the molten zone under zero-to-compression loading. The influence of the dimensional ratios mentioned above on the crack path, and crack depth is distinct only in the zero-to-compression loading case.

The fatigue properties of arc-welded lap joints with weld start and end points were investigated through experiments with 2.3 and 3.2 mm thick mild steel sheets (Seto *et al.*[605]). The macroscopic fatigue crack initiation sites depended on the length of the weld bead relative to the specimen width. In joints with shorter weld beads, cracks mainly initiated at the toe of the weld start points, while joints with longer beads had initial cracks at the toe of the bead centre although the stresses from remote loading remain highest at the start points. Crack propagation analyses, which took the stress distribution around the weld toe and the residual stresses into account, suggested that residual stresses cause the change in position of the crack initiation site.

The fatigue strength of the one-sided cover plate with transverse fillet welds with inclusion of support conditions simulating cover plates on

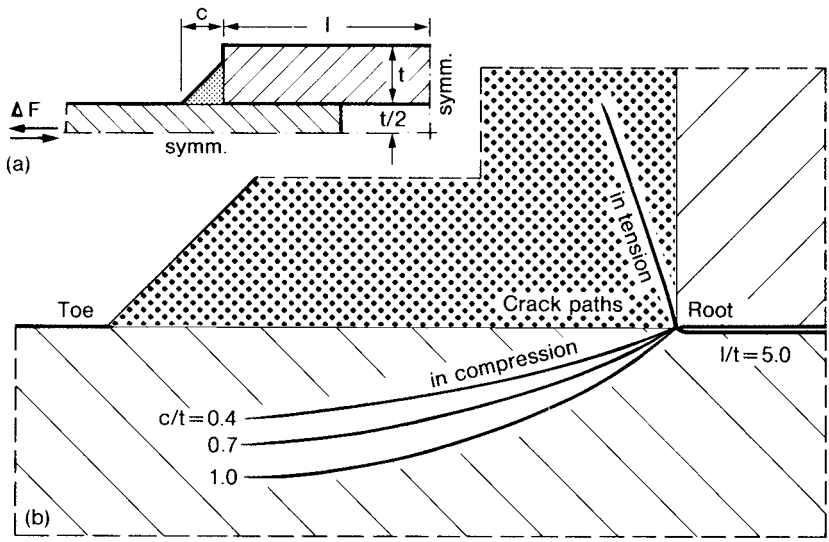


Fig. 6.24. Two-sided lap joint with transverse fillet welds (symmetry quarter) subjected to zero-to-tension or zero-to-compression loading (a) and crack paths starting at the weld root predicted by finite element analysis (b); after Nykänen.[557]

I-section girders has been investigated by Li *et al.*[514] Configurations with various leg lengths, toe angles and degrees of penetration were analysed under cyclic tension and bending loading.

6.3.4 Butt-welded joints

The crack propagation life of butt-welded joints made of steel has been extensively analysed by Lawrence *et al.*[433,434,506,507,636] The crack propagation life of welded joints is understood to be part of the total life (see Sections 5.1.2 and 5.2.1), not to be the total life itself. The limit between the initiation and propagation phase is defined by a crack depth of $a_i = 0.25\,\text{mm}$ (straight crack front). The crack initiation phase cannot be neglected even when considering the crack-like root faces.[507] The following demonstration examples cover only the propagation phase.

The toe crack propagation analysis refers to double-V butt welds without and with root face (lack of penetration) and with characteristic geometric parameters according to Fig. 6.25. The weld toe angle θ and the groove angle ϕ (without root face) are introduced as primary parameters, whereas height h and width w of the weld reinforcement are dependent on the primary parameters according to simple geometric relationships.

The parent material data refer to low strength ferrite-pearlite CMn steels (e.g. ASTM A36, $\sigma_Y = 284\,\text{N/mm}^2$, $\sigma_U = 488\,\text{N/mm}^2$) and high strength

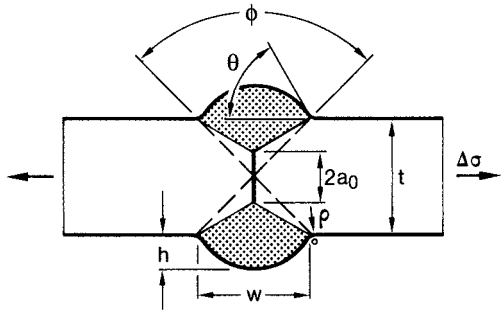


Fig. 6.25. Double-V butt weld joint with root face due to lack of penetration subjected to cyclic tensile loading, characteristic geometric parameters; after Mattos and Lawrence.[384]

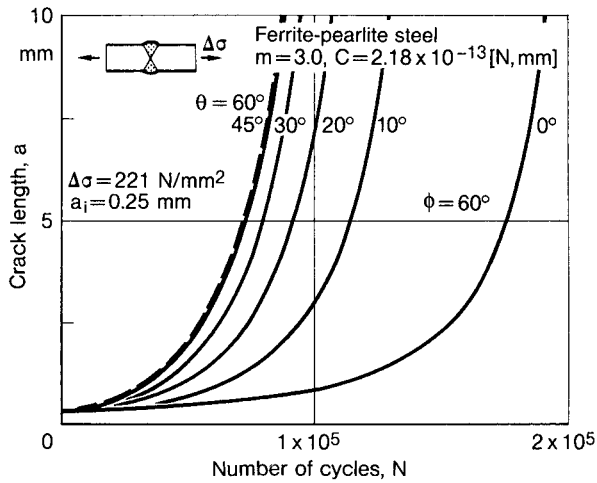


Fig. 6.26. Fatigue crack growth in double-V butt weld joints in structural steel, with plate thickness $t = 25.4$ mm, for different weld toe angles θ; after Lawrence.[506]

low-alloy martensitic steels (e.g. ASTM A514, σ_Y = 746 N/mm^2, σ_U = 844 N/mm^2). The material parameters for the crack propagation analysis are assumed to be identical for parent material, heat-affected zone and weld metal (mean values): $m = 3.0$, $C = 2.18 \times 10^{-13}$ [N, mm] for ferrite-pearlite steels and $m = 2.25$, $C = 2.18 \times 10^{-9}$ [N, mm] for martensitic steels (parameters referring to eq. (6.1)).

Toe crack growth curves for different weld toe angles are plotted in Fig. 6.26. Angles smaller than 45° are advantageous whereas angles larger than 45° have only a minor additional effect on the crack propagation life. The same can be concluded from Fig. 6.27(a) which presents the super-

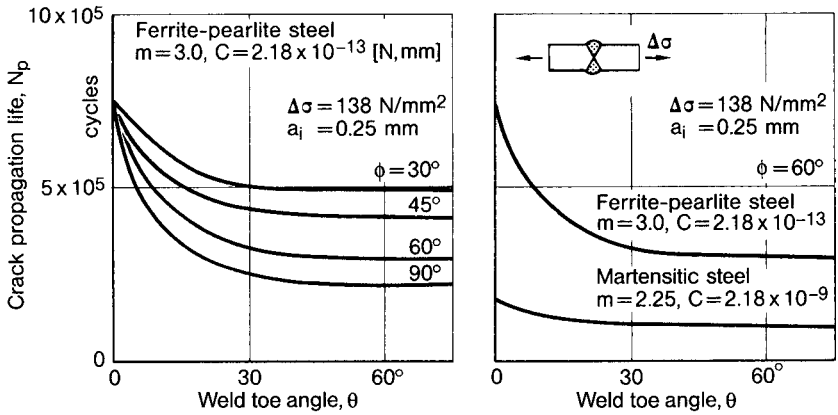


Fig. 6.27. Crack propagation life of double-V butt weld joints in structural steel (t = 25.4 mm), dependent on weld toe angle θ, for different groove angles ϕ and two types of steel; after Lawrence.[506]

imposed effect of the groove angle. A small groove angle means a small height and width of the weld reinforcement, thus reducing the notch stress concentration. The latter is only implicitly included in the finite element analysis from which the stress intensity factor is determined. The crack propagation life is lower for the high strength steel, Fig. 6.27(b).

About two-thirds of the total life are spent for toe crack initiation (a_i = 0.25 mm) in high strength steels. Calculation of the total life on the basis of crack propagation alone reduces the computational initial crack depth to $a_i \approx 0.025$ mm. This fictitious value is unrealistic for the joints under consideration. Crack propagation is found to be more dominant in low strength steels. The bending stresses due to misalignment of the butt-welded joints and their straightening under load has been taken into account in the calculation of the crack propagation life by Burk and Lawrence.[433] The combined effect of weld toe undercut and welding residual stresses on the fatigue strength of misaligned butt-welded joints has also been investigated by Nguyen and Wahab[551] on the basis of the crack propagation approach. Crack propagation in butt welds with a permanent backing bar has been analysed by Nykänen.[558] Butt welds containing a crack-like welding defect were investigated by Zheng and Tienxi.[674]

The effect of initial root face length (or inadequate penetration) on the total life of double-V butt weld joints in high strength structural steel (crack propagation starting at the weld root) according to Tobe and Lawrence[636] is shown in Fig. 6.28. Calculated life curves for two different stress ranges are compared with results from testing. A crack initiation analysis according to Lawrence (see Sections 5.1.2 and 5.2.1) is included in

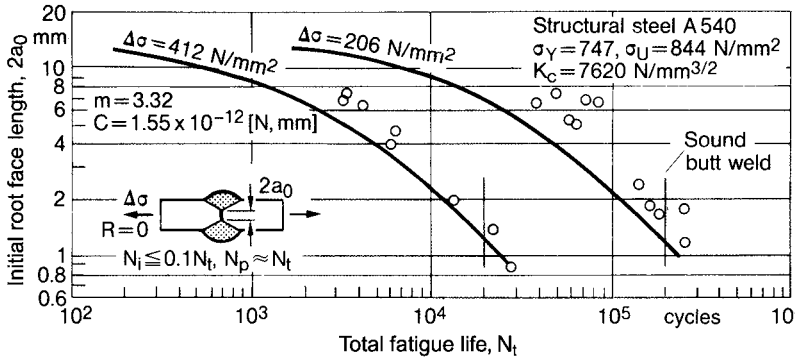


Fig. 6.28. Total life of double-V butt weld joints in high strength steel (plate thickness $t = 25.4$ mm) dependent on initial root face length for two stress ranges; calculated curves compared with experimental results and with data for sound butt welds without root face (lower confidence limit); after Tobe and Lawrence.[636]

the calculation. The crack initiation life comprises less than 10% of the total life, i.e. the total life and the crack propagation life can be set approximately equal. The lower life limit of sound butt welds intersects with the above life curve at the root face length $2a_0 \approx 1$ mm, i.e. any root face length smaller than this is acceptable.

Lawrence and Munse[507] found in an investigation focusing on low strength steel (ASTM A36) that approximately one half of the total fatigue life was spent in crack initiation. The effect was partly attributed to the high compressive residual stresses caused by welding which close the root faces initially. The crack initiation phase was also appreciable for welds in aluminium alloy with lack of penetration.[434]

The fatigue life of GMA butt-welded joints in AlMg4.5Mn aluminium alloy has been investigated by Brandt *et al.*[354] and Lehrke *et al.*[513] applying the newly developed concept of a fictitious initial crack for sharp corner notches (see Section 6.1.3).

The material parameters m and C (mean values) of the Paris equation were experimentally determined resulting in $m = 3.98$ and $C = 1.82 \times 10^{-14}$ [N, mm] for $R = 0$ and $m = 4.27$ and $C = 2.85 \times 10^{-16}$ [N, mm] for $R = -1$ (condensed values for parent metal and weld deposit). Threshold values of the stress intensity range are introduced according to the IIW recommendations,[3] $\Delta K_{th} = 63\,\mathrm{N/mm^{3/2}}$ for $R = 0$ and $\Delta K_{th} = 111\,\mathrm{N/mm^{3/2}}$ for $R = -1$. The hardness in the joint rises up to 80–85 HV. The specimens were stress-relieved (200°C/1 h). Therefore the residual stresses are neglected in the analysis.

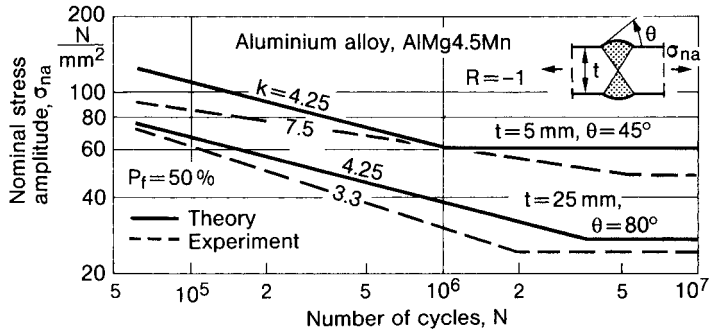


Fig. 6.29. Endurable nominal stress amplitudes (toe failure) dependent on number of cycles for double-V butt weld without root face in aluminium alloy, according to crack propagation analysis (solid lines) and compared with experimental results (dashed lines) for two plate thicknesses and weld toe angles; after Lehrke *et al.*[513]

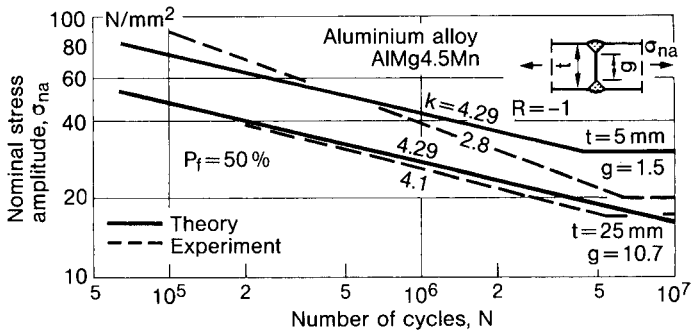


Fig. 6.30. Endurable nominal stress amplitudes (root failure) dependent on number of cycles for double-V butt weld with root face in aluminium alloy, according to crack propagation analysis (solid lines) and compared with experimental results (dashed lines) for two plate thicknesses and root face lengths; after Lehrke *et al.*[513]

The double-V butt weld without root face with crack propagation starting at the weld toe was investigated in respect of the endurable nominal stresses both theoretically and experimentally, Fig. 6.29. The length of the fictitious initial crack substituting the corner notch at the weld toe (see Fig. 6.3) resulted as $a^* = 0.20\,\text{mm}$ for $t = 5\,\text{mm}$, $\theta = 45°$ and as $a^* = 0.96\,\text{mm}$ for $t = 25\,\text{mm}$, $\theta = 80°$. Taking into account that the crack initiation phase has been neglected in the theoretical analysis, the analytical results are not on the safe side.

The double-V butt weld with root face and crack propagation starting at the weld root was also analysed by theory in comparison to experimental data with similar findings as above, Fig. 6.30. Additionally, a parametric

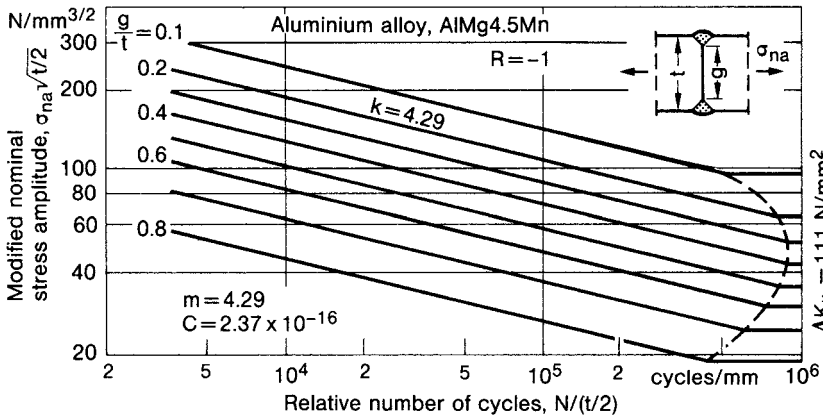


Fig. 6.31. Modified endurable nominal stress amplitudes (root failure) dependent on relative number of cycles for different root face lengths; double-V butt weld joint in aluminium alloy; geometrically similar specimens; fatigue strength based on crack propagation analysis; after Lehrke *et al.*[513]

investigation was performed which reveals the effect of root face length on crack propagation life, Fig. 6.31. The plotted modified nominal stress amplitudes (actually stress intensity factors) which are dependent on the relative number of cycles to final fracture comprise geometrically similar joints independent of their actual plate thickness. The size effect on fatigue strength is not obvious from the diagram, but can be extracted from it by introducing the actual thickness values.

6.3.5 Refined analysis of longitudinal attachment joint

The refined crack propagation approach by Toyosada *et al.*[637–641] has been exemplified by application to a longitudinal attachment welded on a base plate subjected to tensile loading. The fatigue crack is initiated at and propagates from the weld toe at the attachment end, at first through the plate thickness and then across the plate width. The finite element mesh for the local stress analysis at the weld toe, together with the computed elastic stress distribution over the plate thickness is shown in Fig. 6.32.

The fatigue crack is initiated at the weld toe as a shear crack in a first grain. Its opening and closing behaviour after passing the grain boundary is simulated by a representative surface crack before and after coalescence with neighbouring cracks. Prominent surface crack tip positions up to the formation of a through-thickness crack are marked by A, B, C and D supplemented by a diagram showing the experimentally determined change of aspect ratio of the representative surface crack, Fig. 6.33. At point A, the

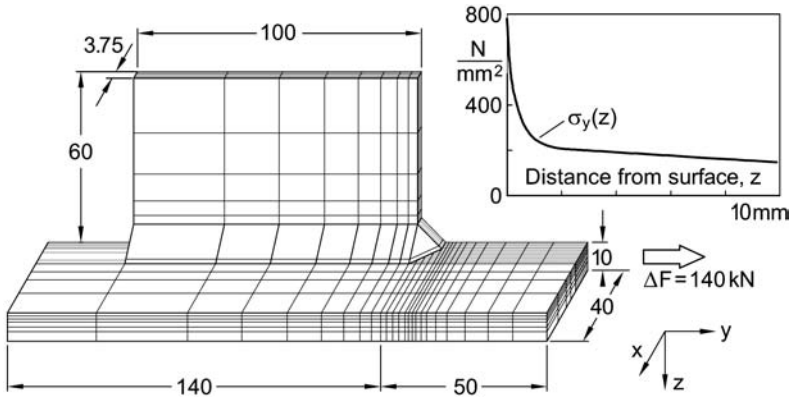


Fig. 6.32. Longitudinal attachment welded on base plate (symmetry half: attachment thickness 7.5 mm, weld thickness 6 mm) subjected to tensile loading; finite element mesh for local stress analysis at weld toe in front of attachment end; elastic through-thickness stress distribution below the weld toe; after Toyosada *et al.*[638]

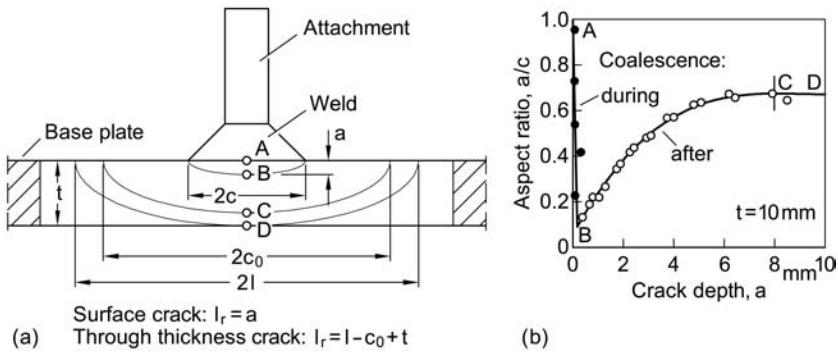


Fig. 6.33. Definition of reference crack length l_r unifying surface and through-thickness crack propagation plots (a) and change of aspect ratio a/c of a representative surface crack during and after coalescence (experimental results) (b); crack tip positions A, B, C and D; after Toyosada *et al.*[638]

shear crack is initiated. At point B, multi-crack coalescence is completed, generating a low aspect ratio (oblong surface crack). Further propagation up to points C (at $0.8t$) and D (through-thickness crack) re-establishes a larger aspect ratio.

The change in the stress intensity factor range related to the nominal stress range, $\Delta K/\Delta\sigma_n$, and in the stress intensity factor due to welding residual stresses, K_w, on the crack path A–B–C–D, plotted versus the reference crack length l_r (defined in Fig. 6.33(a)) is shown in Fig. 6.34. The first steep

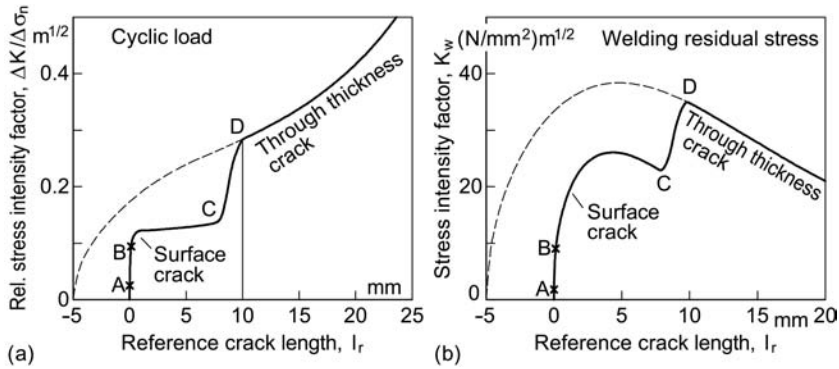


Fig. 6.34. Change in stress intensity factor range ΔK related to nominal (membrane) stress range $\Delta\sigma_n$ (a) and change in stress intensity factor K_w due to welding residual stresses (b) at the weld toe in front of the attachment end; reference crack length l_r and crack path A–B–C–D according to Fig. 6.33(a); after Toyosada *et al.*[638]

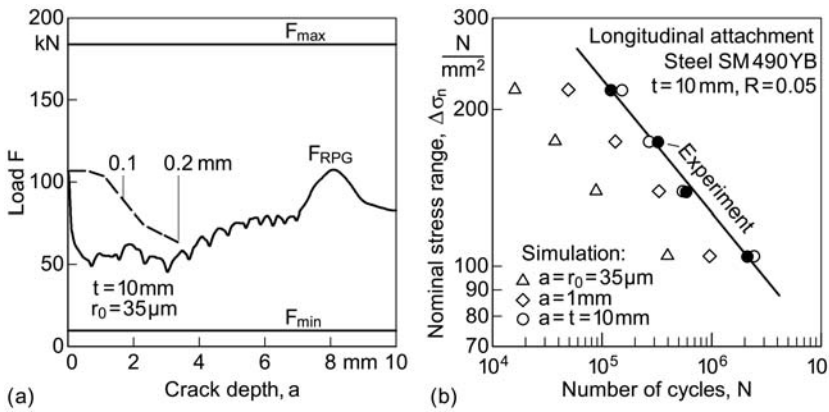


Fig. 6.35. Simulation result for RPG load F_{RPG} ($F_{min} < F_{RPG} < F_{max}$) up to crack penetration (plate thickness $t = 10$ mm) at the weld toe in front of the attachment end (dashed line: RPG load up to a crack depth of 0.2 mm) (a) and predicted *S–N* curves (crack depths equal to grain size, to 1 mm and to plate thickness) in comparison with experimental results (black points and solid line); after Toyosada *et al.*[638]

increase is caused by microcrack coalescence, the second originates from the nearby penetration of the plate thickness. The decreasing curve sections in the residual stress diagram correspond to stress relaxation by the growing crack.

Finally, the RPG load is determined over the crack depth (or reference crack length) and introduced into a crack propagation code for simulating the fatigue life, Fig. 6.35. The RPG load is derived from the cyclic plastic

zone sizes with inclusion of the crack opening and crack closure effects (see Section 6.2.11). The parameter controlling crack propagation is the range between RPG load and maximum load. The oscillation of the RPG load curve results from a rather coarse discretisation of the yield strip into tension-compression elements when applying the Newman–Dugdale model for crack closure simulation (performed on an equivalent two-dimensional crack model). Crack initiation up to a shear crack with crack depth equal to grain size takes less than 10% of the total life. The main portion of fatigue life corresponds to crack propagation up to 1 mm crack depth and from there to a through-thickness crack in approximately equal parts. The *S–N* curves relating to the total fatigue life show a high degree of correspondence between simulation and measurement, but no statistical evaluation is presented. The fatigue strengths in the diagram predicted for the shorter crack depths are not at all compared with experimental data. The results above refer to constant-amplitude loading, but the approach is also capable of simulating the effects of variable-amplitude loading, of regular step-down or step-up load amplitudes or of individual overloads (Toyosada *et al.*[637]).

7

Notch stress intensity approach for seam-welded joints

7.1 General considerations

7.1.1 Formal aspects of presentation

The structuring of contents in this chapter deviates from the common subdivision into 'Basic procedures', 'Analysis tools' and 'Demonstration examples' aimed at in this book. The reason for the deviation is that the notch stress intensity approach, which is well developed in respect of theoretical basis, numerical approximations and experimental verification, is not yet appropriately recognised by the experts in the related fields, i.e. relevant assessment procedures have not yet been agreed on. A further argument in favour of deviating structuring is that the notch stress intensity approach for seam-welded joints has been developed by a single group of researchers, inspired by Atzori and Lazzarin[676–683,691–693,702–715,725] after the preceding relevant publications by Bourkharouba *et al*.[684] and Verreman and Nie.[652,653] Therefore, the task of this chapter is to make the method better known and to give a survey of the related scientific achievements and the proposed practical applications.

After some general considerations, the basic procedures and results are presented (non-welded members) and then applied to fillet-welded joints. Links to the crack propagation approach and to the (hot spot) structural stress approach are established. The complications and the potential of the new approach are finally pointed out.

7.1.2 Principles and variants of the approach

The toe notch of fillet welds or butt welds is a critical region with regard to fatigue crack initiation and propagation. The toe may be a sharp notch (zero notch radius) or a blunt notch (finite notch radius). High notch stresses, actually a stress singularity in the case of sharp notches, occur in this region. These stresses may be described by elastically determined notch stress intensity factors or, in the case of higher loads, by elastic-plastically

determined notch stress or notch strain intensity factors. The notch stress intensity factors may be used to define *J*-integrals, an averaged strain energy density or effective stresses at the corner notch, in order to derive special failure criteria.

The notch stress intensity approach takes account of the notch opening angle (or weld toe angle) and of the notch tip radius (or weld toe radius), proceeding from the nominal or structural stresses in the notched structural member (tensile, bending and shear stresses superimposed). It also comprises the (cyclic) strain-hardening property of the material in the case of elastic-plastic behaviour and a notch support factor when combined with failure criteria.

In its basic version, the approach refers to the elastically determined notch stress intensity factor with minor extensions in the case of a small notch tip radius or minor modifications in the case of small-scale yielding at the notch tip (*J*-integral or averaged strain energy density at the notch tip).

There is no generally adopted fatigue assessment procedure for welded joints based on notch stress intensity factors available up to now, partly because the method is rather new and partly because only fillet welds have been considered up until recently. Relevant investigations in butt welds have meanwhile been performed with satisfactory results.

7.2 Basic procedures and results

7.2.1 Notch stress intensity at sharp corner notches

The well-known concept of stress intensity factors describing the stress singularity at crack tips or slit tips under elastic material conditions (see Chapters 6 and 10) can be transferred to sharp re-entrant corner notches (e.g. V-notches, stepped bars, weld toe notches). Whereas the asymptotic stress drop from the singularity at the crack tip is described by the inverse square root of the radial distance r from the crack tip (the exponent is minus 0.5), a smaller notch-angle-dependent exponent occurs in the case of corner notches, i.e. the order of singularity is reduced. The stress field close to corner notches (just as the stress field close to crack tips) can be described by stress intensity factors (Gross and Mendelson[695]). These are named 'notch stress intensity factors' as distinguished from the conventional stress intensity factors of crack tips.

The singular 'plane' and 'antiplane' stress fields at sharp corner notches can be specified by three notch loading modes (in analogy to the crack opening modes) related to the bisector plane of the notch: symmetric in-plane stresses (mode I), antisymmetric in-plane stresses (mode II) and out-of-plane shear stresses (mode III). The corresponding notch loading modes

are tension loading, transverse shear loading and longitudinal shear loading. The stress field equations were derived by Williams,[726] Hasebe *et al.*,[697] Lazzarin and Tovo[709] and others (one-term asymptotic solutions):

$$\sigma_{ij}^{(1)}(r,\varphi) = K_1 f_{ij}^{(1)}(\varphi) r^{\lambda_1 - 1} \qquad \text{(mode I, ij = φφ, rr, φr)} \tag{7.1}$$

$$\sigma_{ij}^{(2)}(r,\varphi) = K_2 f_{ij}^{(2)}(\varphi) r^{\lambda_2 - 1} \qquad \text{(mode II, ij = φφ, rr, φr)} \tag{7.2}$$

$$\sigma_{ij}^{(3)}(r,\varphi) = K_3 f_{ij}^{(3)}(\varphi) r^{\lambda_3 - 1} \qquad \text{(mode III, ij = rz, φz)} \tag{7.3}$$

where σ_{ij} are the tensors of the in-plane and out-of-plane stresses, K_1, K_2, K_3 are the notch stress intensity factors f_{ij} are the angular functions, λ_1, λ_2, λ_3 are the eigenvalues and r, φ, z are the cylindrical coordinates.

We restrict the presentation of the equations to the characteristic stress components in the bisector plane ($\varphi = 0$), keeping in mind that further stress components occur in other planes, the equations of which show the same principal dependency:

$$\sigma_{\varphi}(r,0) = \frac{1}{\sqrt{2\pi}} K_1 r^{\lambda_1 - 1} \qquad \text{(mode I)} \tag{7.4}$$

$$\tau_{\varphi r}(r,0) = \frac{1}{\sqrt{2\pi}} K_2 r^{\lambda_2 - 1} \qquad \text{(mode II)} \tag{7.5}$$

$$\tau_{\varphi z}(r,0) = \frac{1}{\sqrt{2\pi}} K_3 r^{\lambda_3 - 1} \qquad \text{(mode III)} \tag{7.6}$$

A cylindrical coordinate system is used, Fig. 7.1(a), with the z axis normal to the r-φ plane. The notch stress intensity factors K_1, K_2 and K_3 referring to the loading modes I, II and III are introduced. They depend on the geometrical parameters (i.e. notch depth or bisector length) and the remote loading conditions (i.e. tension or bending load) of the corner notch problem being considered, but not on the coordinates r, φ and z. The factor $1/\sqrt{2\pi}$ can be substituted by $(2\pi)^{\lambda_1 - 1}$, $(2\pi)^{\lambda_2 - 1}$ and $(2\pi)^{\lambda_3 - 1}$, respectively, resulting in notch stress intensity factors $K_1^* = K_1(2\pi)^{0.5-\lambda_1}$, $K_2^* = K_2(2\pi)^{0.5-\lambda_2}$ and $K_3^* = K_3(2\pi)^{0.5-\lambda_3}$.

The parameters λ_1, λ_2 and λ_3 in the exponent designate the first eigenvalue of the corresponding mathematically defined elastic corner stress problems (actually for the infinite region, but transferrable to finite regions under certain conditions). These eigenvalues depend solely on the notch opening angle (Williams,[726] Carpenter[685]), Fig. 7.2: $0.5 \le (\lambda_1, \lambda_2, \lambda_3) \le 1.0$. The eigenvalue 0.5 is related to crack tips, $2\alpha = 0$, and the eigenvalue 1.0 to straight edges, $2\alpha = \pi$ (no singularity). The eigenvalues for mode I loading are slightly smaller than those for mode III loading. They are substantially smaller in relation to mode II loading, thus designating a stronger stress

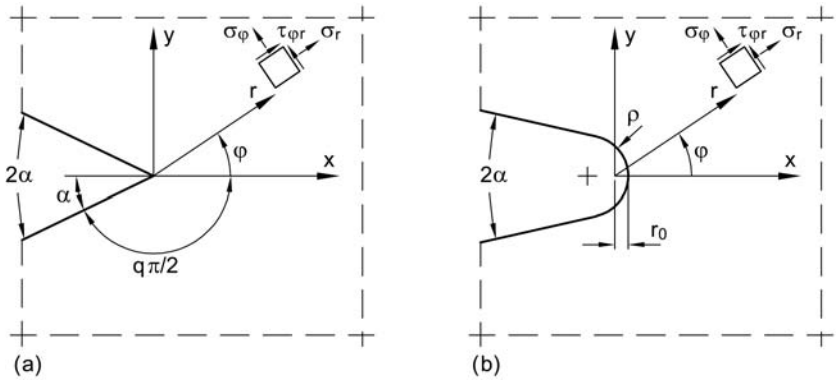


Fig. 7.1. Coordinate systems, symbols and notch stress components at sharp V-notch (a) and at the corresponding blunt notch (b); after Lazzarin and Tovo.[710]

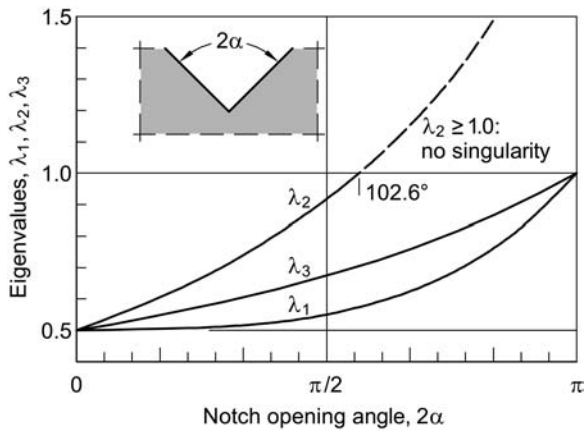


Fig. 7.2. Eigenvalues λ_1, λ_2, λ_3 defining the order of stress singularity at sharp V-notches in the case of mode I, II, III loading conditions; dependence on notch opening angle 2α; after Lazzarin *et al.*[708]

singularity. The stress singularity in mode II loading is weaker and vanishes completely for $2\alpha \geq 102.6°$.

The notch stress intensity factors K_1, K_2 and K_3 can be defined on the basis of the stress distribution according to eqs. (7.4) to (7.6), (Gross and Mendelson[695]):

$$K_1 = \sqrt{2\pi}\lim_{r\to 0}\left(\sigma_\varphi(r,0)r^{1-\lambda_1}\right) \qquad \text{(mode I)} \tag{7.7}$$

$$K_2 = \sqrt{2\pi}\lim_{r\to 0}\left(\tau_{\varphi r}(r,0)r^{1-\lambda_2}\right) \qquad \text{(mode II)} \tag{7.8}$$

$$K_3 = \sqrt{2\pi}\lim_{r\to 0}\left(\tau_{\varphi z}(r,0)r^{1-\lambda_3}\right) \qquad \text{(mode III)} \tag{7.9}$$

The dimensions of K_1, K_2 and K_3 are N/mm$^{1+\lambda_1}$, N/mm$^{1+\lambda_2}$ and N/mm$^{1+\lambda_3}$, respectively. The numerical values of K_1, K_2 and K_3 can be set into comparison, e.g. as failure criteria, provided their dimension is identical, i.e. only under the condition of an identical notch angle beside an identical loading mode (for example, the stress intensity factors of crack tips are used in this way). In mode I loading, the stress intensity factors of cracks are directly comparable with those of sharp notches provided the opening angle is less than 60° (see Fig. 7.2). Higher order failure criteria have to be applied in all other cases (e.g. averaged strain energy density, see Section 7.3.5, or fatigue-effective stresses, see Section 7.3.6).

Considering a cross-section of finite width (net section width t) ahead of the notch (instead of the infinite region) – this width may be set identical to the plate thickness in welded joints – the notch stress intensity factors can be expressed in the following form (Lazzarin and Tovo[709]):

$$K_1 = k_1\sigma_{\mathrm{n}}t^{1-\lambda_1} \qquad \text{(mode I)} \tag{7.10}$$

$$K_2 = k_2\tau_{\perp\mathrm{n}}t^{1-\lambda_2} \qquad \text{(mode II)} \tag{7.11}$$

$$K_3 = k_3\tau_{\parallel\mathrm{n}}t^{1-\lambda_3} \qquad \text{(mode III)} \tag{7.12}$$

The non-dimensional geometry coefficients k_1, k_2 and k_3 depend on the shape and the dimension ratios of the considered corner notch problem (similar to the stress concentration factors of blunt notches) and may be determined by finite element analysis. The nominal stresses in the cross-section considered are introduced as tensile stress σ_{n}, transverse shear stress $\tau_{\perp\mathrm{n}}$ and longitudinal shear stress $\tau_{\parallel\mathrm{n}}$.

The above eqs. (7.10) to (7.12) are well suited to catch the size effect on the static or fatigue strength of corner-notched members (e.g. fillet-welded joints), provided the strength can be characterised by the notch stress intensity factor (identical notch opening angles are a precondition). The following relation is derived from eq. (7.10) for the ratio of endurable nominal stresses σ_{n1} and σ_{n2} for plate thicknesses t_1 and t_2, respectively, provided the notch stress intensity factor K_1 is considered to be relevant to strength:

$$\frac{\sigma_{\mathrm{n2}}}{\sigma_{\mathrm{n1}}} = \left(\frac{t_1}{t_2}\right)^{1-\lambda_1} \tag{7.13}$$

The notch opening angle $2\alpha = 135°$ of fillet-welded joints results in $(1 - \lambda_1) = 0.326$.

In cases of a large net section width between the notch tips, the notch depth a is the essential parameter, leading to the following relationships:

$$K_1 = Y\sigma_n a^{1-\lambda_1} \tag{7.14}$$

$$\frac{\sigma_{n2}}{\sigma_{n1}} = \left(\frac{a_1}{a_2}\right)^{1-\lambda_1} \tag{7.15}$$

with $Y = Y(2\alpha)$, a solution by Dunn *et al.*[688] The notch stress intensity factors for the V-notched strip subjected to tension or in-plane bending load were also determined by Chen.[686]

7.2.2 Notch stress intensity at blunt corner notches

The notch stress intensity factors of sharp corner notches can be used to describe the stress field at blunt corner notches. Vice versa, the stresses at blunt corner notches allow notch stress intensity factors to be approximated. The notch stress field remains more or less the same, provided the reference coordinate system is shifted from the corner point of the sharp notch to a definite point near the notch tip on the bisector line of the blunt notch, see distance r_0 in Fig. 7.1(b).

An analytical general solution for the stress field at blunt corner notches based on notch stress intensity factors has been given by Lazzarin and Tovo[709] for mode I and mode II loading conditions by the method of complex analytical stress functions developed by Kolosoff and Muskhelishvili. The following more restricted solutions are included: the simpler expressions for blunt crack stress fields derived by Creager and Paris[860] and further discussed by Glinka and Newport,[694] as well as the bisector stress solution by Neuber[252] (2nd edn, 1958, *ibid.* p. 172, eq. (38)) for the blunt V-notch of finite depth. The simpler relationships for sharp notches are also included.

In order to demonstrate the basic structure of the stress field equations in mode I and mode II loading respectively, the notch stresses in the bisector plane are presented hereafter (Lazzarin and Tovo[709]):

$$\sigma_\varphi(r,0) = \frac{1}{\sqrt{2\pi}} K_1 r^{\lambda_1 - 1}\left[1 + \frac{(3-\lambda_1) - \chi(1-\lambda_1)}{1+\lambda_1+\chi_1(1-\lambda_1)}\left(\frac{r}{r_0}\right)^{\mu_1-\lambda_1}\right] \tag{7.16}$$

$$\tau_{\varphi r}(r,0) = \frac{1}{\sqrt{2\pi}} K_2 r^{\lambda_2 - 1}\left[1 - \left(\frac{r}{r_0}\right)^{\mu_2-\lambda_2}\right] \tag{7.17}$$

The ranges of λ_1 and λ_2 are given in Section 7.2.1, to be supplemented by $-0.5 \le \mu_1 \le 0$ and $-0.5 \le \mu_2 \le \approx 0.5$ depending on the notch opening angle 2α. The further parameters are:

$$\chi_1 = -\frac{\sin[(1-\lambda_1)q\pi/2]}{\sin[(1+\lambda_1)q\pi/2]} \tag{7.18}$$

$$q = 2\left(1-\frac{\alpha}{\pi}\right) \tag{7.19}$$

$$r_0 = \rho\left(1-\frac{1}{q}\right) \tag{7.20}$$

Creager's solution[860] for blunt cracks results as a special case for $2\alpha = 0$, $q = 2$, $r_0 = \rho/2$, $\lambda_1 = \lambda_2 = 0.5$, $\mu_1 = \mu_2 = -0.5$, $\chi_1 = 1.0$. Glinka's closed-form expressions[694] to Creager's equations are included.

The notch stresses in the bisector plane ahead of the notch tip normalised by their maximum value coincide for different notch radii, when plotted over the notch tip distance $(r - r_0)$ normalised by the notch tip radius ρ. The solution by Lazzarin and Tovo[709] for the blunt V-notch in the infinite region is compared with finite element results for the blunt double-V-notch of a tension-loaded bar, Fig. 7.3. The analytical solution can be used on the bisector line up to the point where the notch stress curve drops below the nominal stress in the net cross-sectional area. The correspondence of the results is very satisfactory, but deteriorates for large crack opening angles (e.g. $2\alpha = 135°$). With additional analytical effort, the stresses in the nominal stress zone can also be approximated (Lazzarin *et al.*[711]).

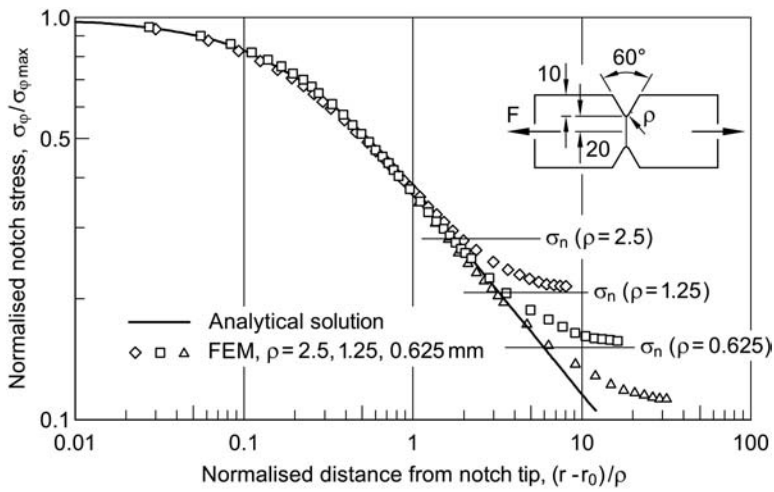


Fig 7.3. Notch stress σ_φ in the bisector plane over distance from notch tip $(r - r_0)$ for blunt V-notches with different notch tip radii ρ; analytical solution for the infinite region in comparison with results from the finite element method (FEM); double-V-notched bar subjected to tension force F; $2\alpha = \pi/3$, $q = 5/3$, $r_0 = \rho/2.5$; after Lazzarin and Tovo.[709]

The details of the notch stress field were further investigated by Atzori *et al.*,[677–681] Dini and Hills,[687] Filippi *et al.*,[692,693] Nui *et al.*[720] and Xu *et al.*[727] It is demonstrated that the stress field in the close neighbourhood to the notch tip, $(r - r_0) \leq \approx 0.2\rho$, depends predominantly on the notch tip radius, and only slightly on the notch opening angle, whereas outside this region the influence of the notch opening angle can be approximated increasingly by the sharp notch solution. These statements are confirmed by Fig. 7.4 in which the notch stresses in the bisector line close to the blunt notch tip are plotted for various notch tip radii with a fixed notch opening angle. The nominal stress used as reference consists of superimposed tensile and bending stresses in the net cross-sectional area. The results in the diagram are gained from a complex analytical stress function solution combined with conformal mapping. The solution refers to a specimen type used for testing brittle materials. It is also shown more generally and in quantitative terms that the singular field does characterise the behaviour of the finite radiused sharp notch in an intermediate area between notch root and remote boundaries (Dini and Hills[687]).

Simple limit value relationships exist between the stress intensity factors of sharp crack tips and the maximum notch stresses of the corresponding blunt crack tips (Radaj and Zhang,[911] see Section 10.2.8). The relationship for mode I loading can be applied to corner notches as an approximation as long as the notch opening angle is sufficiently small, i.e. the exponent $(\lambda_1 - 1)$ should remain near minus 0.5.

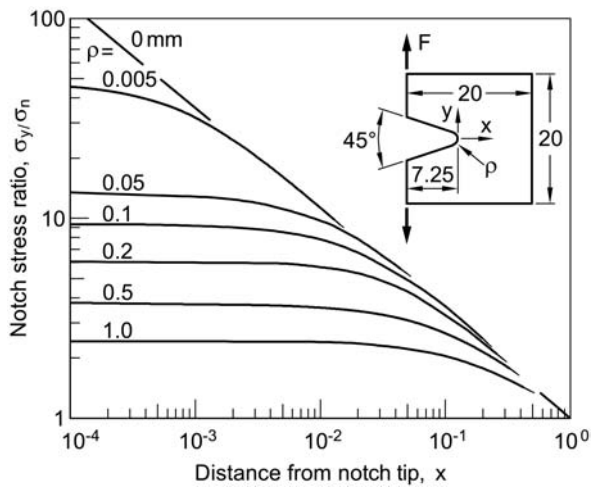


Fig. 7.4. Notch stress σ_y in the bisector plane normalised by nominal stress σ_n for a single-sided blunt V-notch in a square plate; various notch radii ρ, notch opening angle $2\alpha = \pi/4$; analysis results by Nui *et al.*[720]

A more general relationship, not restricted to sufficiently small crack opening angles, was derived by Hasebe *et al.*[697] and Nui *et al.*[720] for mode I loading conditions:

$$K_1 = \frac{\sqrt{\pi}}{2} \lim_{\rho \to 0} \left(\sigma_{\varphi\,\max} \rho^{1-\lambda_1} \right) \qquad \text{(mode I)} \tag{7.21}$$

In analogy to the corresponding crack-related formulae (eqs. (10.66) and (10.65)), the following relationships may be proposed (but are not yet derived and verified) for mode II and mode III loading:

$$K_2 = \frac{3\sqrt{3\pi}}{2} \lim_{\rho \to 0} \left(\tau_{\varphi r\,\max} \rho^{1-\lambda_2} \right) \qquad \text{(mode II)} \tag{7.22}$$

$$K_3 = \sqrt{\pi} \lim_{\rho \to 0} \left(\tau_{\varphi z\,\max} \rho^{1-\lambda_3} \right) \qquad \text{(mode III)} \tag{7.23}$$

The accuracy of the first-mentioned relationship, eq. (7.21), when used with a finite notch radius without extrapolation to the limit value ($\rho \to 0$), was investigated by Atzori *et al.*[678] with the result that K_1 determined for the blunt notch ($\rho > 0$) as described is greater than K_1 determined for the sharp notch ($\rho = 0$) based on the asymptotic stress drop, eq. (7.4), and that the difference increases as the applied notch tip radius increases.

The solution for blunt corner notches was substantially improved by adding a further term to the polynomial arrangement of analytic stress functions (Filippi *et al.*[693]), resulting in satisfactory correspondence with finite element results even with large notch opening angles. Explicit formulae are given describing the notch stress distribution in the bisector line ahead of the notch tip for various notch opening angles (see Atzori *et al.*[680] with regard to bending loads). Additionally, the stress distribution along the free edges of the blunt V-notch subjected to symmetrical (mode I) and anti-symmetrical (mode II) loading was numerically evaluated and compared with finite element results. Here major discrepancies may occur in cases where the maximum notch stress evolves outside the bisector line and the notch shape deviates from the ideal conditions (i.e. from straight lines combined with circle sectors).

7.2.3 Plastic notch stress intensity at corner notches

The previous explanations refer to the stress intensity at sharp corner notches under the condition of linear-elastic material behaviour. They are now extended to non-linear elastic-plastic behaviour. The stress singularity at sharp notches continues to exist provided strain hardening is taken into account. Plastic notch stress intensity factors are defined as distinguished from the conventional elastic notch stress intensity factors.

Theoretical solutions of the elastic-plastic corner notch problem are based on the power law of strain hardening, but with a modification to the well-known relationship given by Ramberg and Osgood (eq. (5.8)). Following Hutchinson,[698] the hardening exponent $1/n$ is substituted by its inverse value n, so that $(1 \le n \le \infty)$ instead of $(0 \le n \le 1)$. This inversely defined hardening exponent is typically in the range of 2–20 for metals. Additionally, the approximation that the elastic strains are negligible compared with the plastic strains can be introduced at and close to the sharp notch tip. The von Mises yield criterion is introduced to catch the multiaxiality effect in ductile materials. Therefore, the solutions for plane stress and plane strain conditions are slightly different.

Early relevant solutions refer to sharp crack tips (Hutchinson,[698] Rice and Rosengren[722]). More recently, Lazzarin *et al.*[715] have solved the problem in the more general case of sharp V-notches (inclusive of cracks) under mixed mode (I and II) loading conditions. The further presentation is restricted to the mode I loading condition which is especially important for strength assessments. The formal aspects can be transferred to the mode II and mode III loading cases. But it has to be noted that the solution for mixed mode loading cannot be expressed as a linear combination of the mode I and mode II solutions. The superposition principle does not apply under nonlinear conditions.

The stress distribution at and close to the notch tip is described by the following relationships:

$$\sigma_{ij}^{(1)}(r,\varphi) = K_{1p} f_{ij}^{(1)}(\varphi) r^{-s} \qquad \text{(mode I,} \quad \text{ij = rr, } \varphi\varphi, \varphi r) \tag{7.24}$$

$$s = \frac{2(1-\lambda_1)}{1+n} \tag{7.25}$$

$$K_{1p} = A K_1^{2/(1+n)} \tag{7.26}$$

Equation (7.24) is a simplified relationship for local yielding without stress redistribution and should be substituted by a more complex relationship in the case of global yielding. The plastic notch stress intensity factor K_{1p} results from the elastic notch stress intensity factor K_1 via a factor A which depends on the notch opening angle and on the material law parameters, but not on the applied load. The order of the stress singularity is reduced by $2/(1 + n)$. The angular function f_{ij} is modified by the hardening exponent n (Filippi *et al.*[691]). The elastic conditions are recovered by introducing $n = 1$.

Typical numerical results gained on the basis of the theory of plastic notch stress intensity factors are presented for illustration referring to AISI 1008 structural steel and a notch opening angle $2\alpha = 60°$. The following material parameters are introduced: elastic modulus $E = 2.06 \times 10^5\,\text{N/mm}^2$,

hardening coefficient $H = 600\,\mathrm{N/mm^2}$, hardening exponent $n = 4.0$, 0.2% offset yield stress $\sigma_{Y0.2} = 125\,\mathrm{N/mm^2}$ (actually the plastic strain at this stress was 0.1884%), Poisson's ratio $\nu = 0.3$. The nominal stress σ_n refers to the net cross-section. The accuracy of the results is checked by comparison with a finite element analysis for a double-V-notched bar subjected to tension load. In Fig. 7.5, the notch stresses in the bisector plane are plotted over the distance from the notch tip for various nominal stresses. Deviations from the theoretical curves (linear in logarithmic scales) occur for larger distances. In Fig. 7.6, the plastic notch stress intensity factor is plotted over the nominal stress in the gross cross-sectional area. The simplified formula, eq. (7.27), deviates substantially from the exact relationship in the range of global yielding.

The relationship corresponding to eq. (7.26) characterising the influence of a finite gross cross-sectional width or gross plate thickness t (compare eq. (7.10)) reads as follows:

$$K_{1p} = k_{1p}\sigma_n t^s \tag{7.27}$$

The size effect on the strength of corner-notched members is thus reduced by $2/(1 + n)$ in the exponent of the plate thickness ratio (the limit value of gain in strength appears in the fully plastic condition of thin plates), Fig. 7.7. Corresponding relationships are derived when using the notch depth instead of the net section width (transfer eqs. (7.14) and (7.15)).

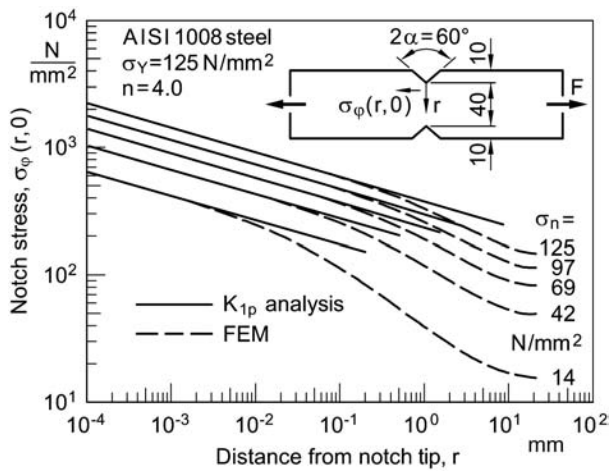


Fig. 7.5. Elastic-plastic notch stresses $\sigma_\varphi(r, 0)$ in the bisector plane over distance r from the notch tip for various nominal stresses σ_n in the gross cross-sectional area; notch opening angle enlarged in the graph; results of theoretical analysis based on plastic notch stress intensity factors K_{1p} in comparison with results by the finite element method (FEM); after Lazzarin and Zambardi.[714]

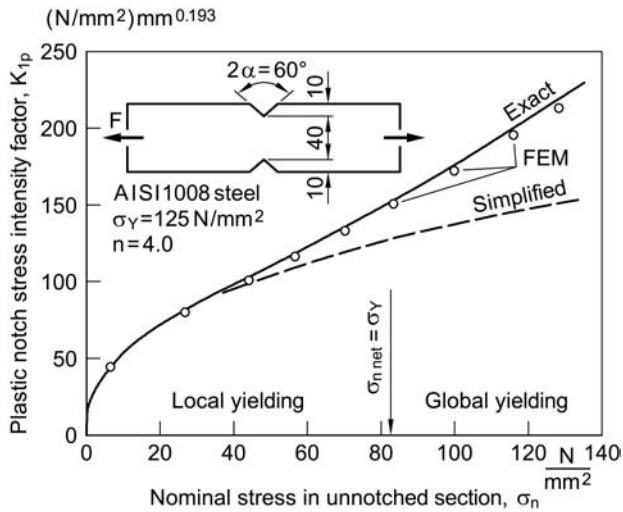


Fig. 7.6. Plastic notch stress intensity factor K_{1p} over nominal stress σ_n in the gross cross-sectional area; notch opening angle enlarged in the graph; exact and simplified theoretical solutions in comparison with results by the finite element method (FEM); ranges of local and global yielding; after Lazzarin and Zambardi.[714]

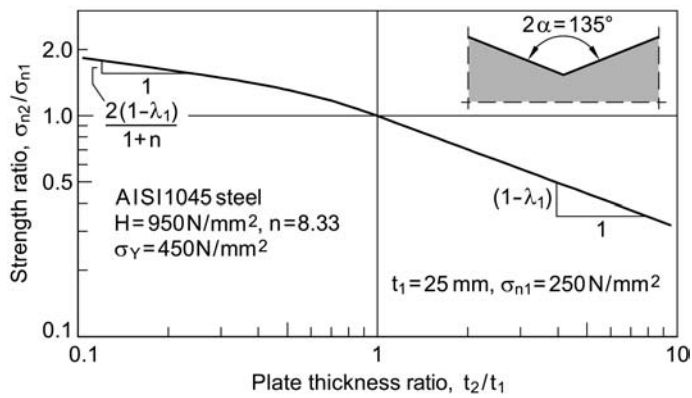


Fig. 7.7. Strength ratio σ_{n2}/σ_{n1} over gross plate thickness ratio t_2/t_1 for tension-loaded edge-notched members ($2\alpha = 135°$) in high strength structural steel; the fully plastic condition on the left-hand side in contrast to the purely elastic condition on the right-hand side; after Lazzarin and Zambardi.[714]

7.2.4 *J*-integral at corner notches

The path-independent line integral proposed by Rice,[921] usually named '*J*-integral', is a powerful tool for analysing the stress or strain concentration at crack tips. It was originally derived for linear-elastic material behaviour,

but later on extended to non-linear elastic or elastic-plastic material behaviour, provided the loading curve is monotonic in the latter case. The intensity of fully plastic stress fields at crack tips subjected to mode I loading could thus be quantified (Hutchinson,[699] Rice and Rosengren[722]).

The *J*-integral concept was extended by Lazzarin *et al*.,[707] among others, to sharp V-notches, at first under linear-elastic and then under elastic-plastic conditions. The integral is dependent on the path for corner notches subjected to mode I or mode II loading.

The J_V-integral for V-notches in linear-elastic materials can be derived in the following form:

$$J_V = 2\left(A_{11}K_1^2 + A_{22}K_2^2\right) \tag{7.28}$$

where A_{11} and A_{22} depend on the notch opening angle 2α and the radius R of the circular path around the notch tip. The dimension of J_V is $(N/mm^2)mm$ according to the derivations. The above integral can be made independent of the path under the restriction of pure mode I (or mode II) loading conditions:

$$J_L = \frac{J_V}{R^{2\lambda_1 - 1}} \tag{7.29}$$

but remains dependent on the notch opening angle 2α.

The integrals above can be extended from linear-elastic to elastic-plastic (power-law) material behaviour (restricted to mode I) resulting in J_{Vp} and J_{Lp} which depend on K_{1p} and s (according to eqs. (7.25) and (7.26)) instead of K_1 and $(1 - \lambda_1)$, see Lazzarin *et al*.[707]

Using the (elastic) J_V or J_L integral approach, the contributions due to mode I and mode II loading can be superimposed, i.e. a well-founded strength criterium for mixed-mode loading can be established (see Section 7.3.4).

Elastic *J*-integrals at corner notches subjected to mode III loading were derived by Quian and Hasebe.[721] The *J*-integral evolves as path independent if the notch flanks are free of loads.

7.2.5 Strain energy density at corner notches

There is a demand for failure criteria (relating to static and fatigue strength) which are generally applicable, in the elastic range as well as in the locally elastic-plastic range, and on sharp and blunt notches independent of the notch opening angle with the inclusion of cracks. There should be no differences in dimensions prohibiting direct comparisons (the notch stress intensity factors for different loading modes and/or different notch opening angles have different dimensions). Such a general criterium may be

formulated on the basis of the strain energy density averaged over a definite region around the notch tip.

In brittle materials, the total strain energy density is relevant (Beltrami's criterion), whereas in ductile materials, the deviatoric strain energy density is more appropriate (von Mises' criterion). According to the biparametric strain energy density criterion proposed by Lazzarin and Zambardi[713] (not to be confused with Sih's equally-named criterium at crack tips), fatigue failure occurs when the mean value of the total or deviatoric strain energy density reaches a critical value in a cylindrical sector volume around the notch tip with a material-characteristic radius R_0 which is assumed to be independent of the loading mode (note that this volume depends on the notch opening angle, i.e. this is not a critical volume approach).

A simpler theoretical derivation is possible for local yielding at the notch tip. The realistic assumption is introduced that the strain energy density can be calculated in a purely elastic manner because the underproportional rise of the notch stresses and the overproportional rise of the notch strains result in a further (approximately) proportional increase of the strain energy density as long as stress redistribution is avoided. The general solution for global yielding is more complex (Lazzarin and Zambardi[714]).

The components of the deviatoric strain energy density $\overline{W}_{\mathrm{d}}$ in a loading cycle with load ratio $R = 0$, averaged over the cylindrical sector with radius R_0, read as follows (Lazzarin *et al.*[708]):

$$\overline{W}_{\mathrm{d}1} = \frac{e_{\mathrm{d}1}}{E} K_1^2 R_0^{2(\lambda_1 - 1)} \qquad \text{(mode I)} \tag{7.30}$$

$$\overline{W}_{\mathrm{d}2} = \frac{e_{\mathrm{d}2}}{E} K_2^2 R_0^{2(\lambda_2 - 1)} \qquad \text{(mode II)} \tag{7.31}$$

$$\overline{W}_{\mathrm{d}3} = \frac{e_{\mathrm{d}3}}{E} K_3^2 R_0^{2(\lambda_3 - 1)} \qquad \text{(mode III)} \tag{7.32}$$

where the angular function integrals $e_{\mathrm{d}1}, e_{\mathrm{d}2}, e_{\mathrm{d}3}$ depend on the notch opening angle and on Poisson's ratio, Fig. 7.8. Similar expressions are related to the total strain energy (Lazzarin and Zambardi[714]). An R-dependent factor has to be introduced into the above equations to take the effect of load ratios $R \neq 0$ into account (the strain energy density in a loading cycle depends on the load ratio R).

It is assumed within a simplified approach that the contributions of the averaged strain energy densities in the modes I, II and III can simply be added in order to establish the total averaged strain energy density whose critical value will initiate failure. This is an acceptable approximation with local yielding. In cases of global yielding, the superposition principle cannot be applied.

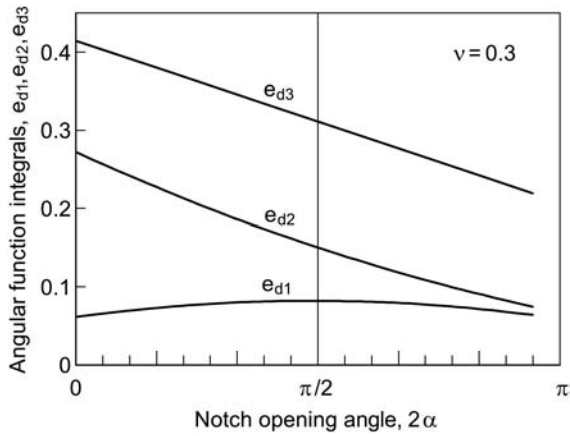


Fig. 7.8. Angular function integrals e_{d1}, e_{d2}, e_{d3} (relating to modes I, II, III; modes I and II with plane strain) over notch opening angle 2α; with Poisson's ratio ν; after Lazzarin *et al.*[708]

7.2.6 Fatigue limit expressed by notch stress intensity factors

The notch stress intensity approach can be used to assess the fatigue crack initiation life of notched members inclusive of seam-welded joints (Bourkharouba *et al.*,[684] Verreman and Nie[652,653]). The fatigue assessment of notched members comprises first the determination of the high-cycle fatigue limit (i.e. the technical endurance limit), second the extension of this limit to the medium-cycle and low-cycle fatigue range (i.e. the notch stress or strain *S–N* curve) and third the formulation of multiaxiality criteria (e.g. the von Mises equivalent stress or strain in ductile materials). The fatigue process is understood as crack nucleation, short-crack growth and long-crack propagation. Crack nucleation is induced by repeated plastic notch tip deformation. Short cracks initiated at sharp notches may be arrested, provided the notch stress gradient is sufficiently steep and the basic stress level sufficiently low (non-propagating short cracks). The high-cycle fatigue limit may be described on the basis of elastic material behaviour.

The high-cycle fatigue limit for notched members was hitherto mainly considered in relation to the fatigue limit of the unnotched material. This is expressed by the fatigue notch factor K_f which turns out to be substantially smaller than the elastic notch stress concentration factor K_t. The relation between the fatigue strengths of blunt and sharp notches (inclusive of cracks) was only exceptionally investigated. Stress intensity factors are basic for such investigations. They allow an assessment without a detailed short-crack propagation analysis, which may be too complicated for engineering

purposes. Instead, the stress field in the damaging zone of the notch, characterised by notch stress intensity factors, is evaluated. It produces the driving force for crack initiation and propagation. Widely used are mean stress criteria (notch stresses averaged over a material-characteristic microstructural length, area or volume at the notch tip) or, alternatively, critical distance criteria (notch stress at a material-characteristic microstructural distance from the notch tip).

The basic idea behind the approach presented hereafter is the consideration of two different fatigue limits in the case of sharp notches (the notch tip radius is zero or very small, the notch stress concentration factor is correspondingly high). One fatigue limit is related to the nucleation of cracks that do not propagate, governed by the stress concentration factor K_t. The other fatigue limit is related to cracks that nucleate and then propagate, the threshold stress intensity factor ΔK_{th} applied to the crack length plus the notch depth being relevant.

It is straightforward with regard to the crack propagation fatigue limit of notches to introduce a crack-propagation-relevant microstructural length derived from the threshold stress intensity factor ΔK_{th} of long cracks and from the relevant crack propagation fatigue limit $\Delta\sigma_{th}$. Such a length parameter a_0 has been defined by El Haddad *et al.*:[689]

$$a_0 = \frac{1}{\pi}\left(\frac{\Delta K_{th}}{\Delta\sigma_{th}}\right)^2 \tag{7.33}$$

It has been shown by Lazzarin *et al.*[712] that the proper integration length for fatigue-effective stresses at crack and notch tips is $2a_0$, independent of the notch tip radius and the notch opening angle.

The following relationships for mode I loading conditions were derived by Atzori *et al.*[678,682] based on the concept just mentioned:

$$K_f = \frac{K_t}{\sqrt{1+\dfrac{4a_0}{\rho}}} = \frac{2\Delta K_1}{\Delta\sigma_n}\frac{1}{\sqrt{\pi(\rho+4a_0)}} \tag{7.34}$$

$$\Delta K_{1cr}(\rho>0) = \Delta K_{1cr}(\rho=0)\sqrt{1+\frac{\rho}{4a_0}} \tag{7.35}$$

with the gross area nominal stress range $\Delta\sigma_n$ and the critical notch stress intensity factor range ΔK_{1cr} beyond which initiated cracks will propagate. The derivation above uses the approximation $(1-\lambda_1)\approx 0.5$ which is justified for $2\alpha \le 60°$. Note that the expression on the right-hand side of eq. (7.34) is thus only approximately dimensionless. More general relationships seem to be possible by substituting 0.5 by $(1-\lambda_1)$ in the exponents. The prediction of fatigue strength according to eq. (7.35) for different notch radii and materials is plotted in Fig. 7.9 and compared with various

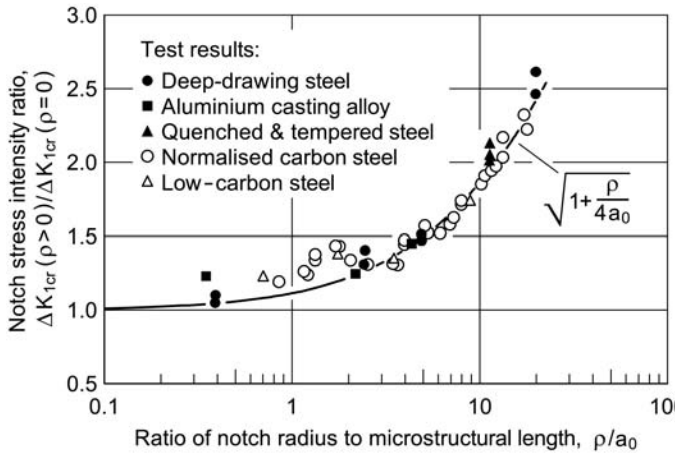


Fig. 7.9. Ratio of critical notch stress intensity factor ranges of blunt and sharp V-notches in different materials dependent on ratio of notch tip radius to microstructural length; analytical curve in comparison with test results presented by Lazzarin *et al.*,[712] Noda *et al.*[719] and Yao *et al.*;[728] after Atzori *et al.*[682]

experimental results taken from the literature.[712,719,728] The degree of correspondence seems to be satisfactory.

Other contributions by Atzori *et al.*[677,679] show that (crack-like) defect sensivity (correlated to a_0) and (blunt) notch sensitivity (correlated to $a^* = K_t^2 a_0$) can be seen as 'two sides of the same medal'. As a consequence, the critical notch depth $a_{n\,cr}$ (at the endurance limit) is introduced dependent on the critical defect size $a_{d\,cr}$ (also at the endurance limit) according to $a_{n\,cr} = K_t^2 a_{d\,cr}$.

The notch stress intensity factors may not directly characterise the fatigue limit as above, but can also be indirectly fatigue relevant as can be seen from the *J*-integral criterion (Section 7.2.4) or from the strain energy density criterion (Section 7.2.5).

Proceeding from the high-cycle fatigue limit, especially at the branching point between the crack nucleation and crack propagation curves in Frost's diagram, $\sigma_{nE} = f(K_t)$, the medium-cycle *S–N* curve can be empirically approximated using a slope exponent *k* which depends on the amount of elastic-plastic notch support during crack initiation and subsequent crack propagation. A more rational approach consists in using crack initiation criteria based on elastic or elastic-plastic notch stress intensity factors in the medium-cycle and low-cycle fatigue range, respectively, allowing extensions into the crack propagation range. Such methods are still in a rudimentary stage of development.

Multiaxiality effects, i.e. the simultaneous action of different loading modes at the sharp or blunt notch, are taken into account by introducing multiaxiality criteria. These can be based on superposition of the effects of the individual loading modes as far as elastic notch stress intensity factors are applicable, i.e. inclusive of the range of local yielding. An elliptic curve expression based on the elastic notch stress intensity factors is proposed by Lazzarin *et al.*[708] for fillet-weld-like notches with a large notch opening angle ($2\alpha = 135°$). Here, the mode II loading condition produces no stress singularity so that the relationship for the limiting state can be restricted to the loading modes I and III:

$$\left(\frac{\Delta K_1}{\Delta K_{1E}}\right)^2 + \left(\frac{\Delta K_3}{\Delta K_{3E}}\right)^2 = 1 \tag{7.36}$$

with the endurance limits K_{1E} and K_{3E} in the pure mode I and mode III loading states.

Equivalent notch stress intensity factors can be defined using the dimension of the mode I or mode III factor, respectively:

$$\Delta K_{1eq} = \sqrt{(\Delta K_1)^2 + h^2(\Delta K_3)^2} \tag{7.37}$$

$$\Delta K_{3eq} = \sqrt{(\Delta K_3)^2 + \frac{1}{h^2}(\Delta K_1)^2} \tag{7.38}$$

$$h^2 = \left(\frac{\Delta K_{1E}}{\Delta K_{3E}}\right)^2 \tag{7.39}$$

where h is a dimensional parameter which depends, in general, on the notch opening angle. Applying the strain energy density failure criterion (see Section 7.2.5), the parameter h can be linked to the radius R_0 which is considered to be a material constant (Lazzarin *et al.*[708]):

$$h^2 = \frac{e_{d3}}{e_{d1}} R_0^{2(\lambda_3 - \lambda_1)} \tag{7.40}$$

7.3 Procedures and results for fillet-welded joints

7.3.1 Notch stress intensity factors for fillet-welded joints

The notch stress intensity factors are well suited to describe the local stress field, strain field and strain energy density field at the toe of fillet welds and to evaluate fatigue test data on this basis. Fatigue-relevant features of these fields are expressed by the notch stress intensity factors independent of whether the real weld notch is sharp or blunt. Only excessively large notch tip radii must be excluded. The available data are mainly related to fillet

weld shapes. A fillet weld has typically a notch opening angle of 135° resulting in a bisector plane inclination of 112.5° against the plate surface. Plane fields which are symmetrical or antisymmetrical relative to the bisector plane are described by K_1 and K_2. An antiplane field (with out-of-plane shear stresses) is defined by K_3. The contribution of K_2 can often be neglected in the fatigue analysis because non-singular stresses are associated with the K_2 loading mode in the case of large notch opening angles.

The notch stress intensity factors for fillet-welded joints (notch opening angle $2\alpha = 135°$) are expressed by eqs. (7.10) to (7.12), which use the plate thickness as characteristic size parameter:

$$K_1 = k_1 \sigma_n t^{0.326} \tag{7.41}$$

$$K_2 = k_2 \tau_{\perp n} t^{-0.302} \tag{7.42}$$

$$K_3 = k_3 \tau_{\parallel n} t^{0.200} \tag{7.43}$$

The dimensionless geometry coefficients k_1, k_2, k_3 are derived from extremely accurate finite element analyses of the cross-sectional joint models evaluating the stresses in the bisector plane where they are decoupled for the three loading modes. Any stress value along the bisector plane, but sufficiently close to the notch tip, can be used to determine the notch stress intensity factor (by applying eq. (7.7), eq. (7.8) or eq. (7.9)) and therefrom the geometry coefficient (by evaluating eq. (7.10), eq. (7.11) or eq. (7.12)). Systematic numerical investigations related to fillet-welded joints were conducted by Lazzarin and Tovo.[710,711]

A first investigation[710] was related to plane models of weld-like outer geometries without the inner slits, Fig. 7.10. The geometry coefficients k_1 and k_2 dependent on the geometrical parameters (dimension ratios) are shown in Fig. 7.11. The numerical results are approximated by polynomials applying the least square method. The coefficient k_1 rises with L/t and $2h/t$, the coefficient k_2 does the opposite. Plastic notch stress intensity factors with corresponding stress distributions were also determined for the above joint-similar models (Lazzarin *et al.*[715]).

A second investigation[710] was related to more realistic cross-sectional models of fillet-welded joints (welded-through cruciform joint, cover plate joint, top-cut cruciform joint) subjected to a tension load, Fig. 7.12. Parametrical variations were considered for the cruciform joint with non-load-carrying fillet welds resulting in the k_1 and k_2 values plotted in Fig. 7.13. The curve courses are similar to those referring to the weld-like plane models (Fig. 7.11). This means that the non-bevelled height of the transverse stiffener plates is of secondary influence.

The plots in Fig. 7.13 refer to cruciform joints under a tension load. Different diagrams are reported for cruciform joints subjected to a bending

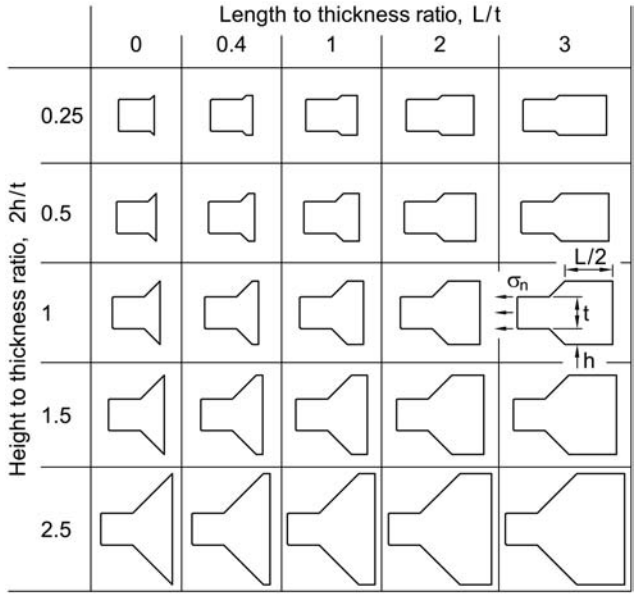


Fig. 7.10. Plane models with weld-like outer geometries (i.e. without the inner slits), investigated numerically using the finite element method; after Lazzarin and Tovo.[710]

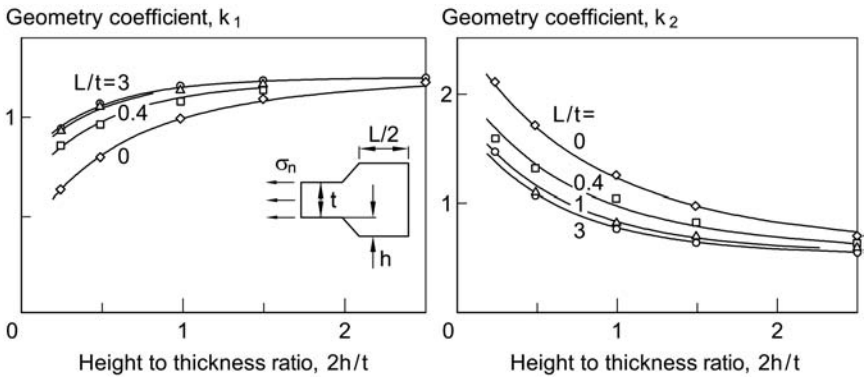


Fig. 7.11. Geometry coefficients k_1 and k_2 dependent on geometrical parameters for plane models with weld-like geometry; finite element results after Lazzarin and Tovo.[710]

load (Atzori *et al.*[680]). In the latter case, the values of k_1 and k_2 are lower, in general, explaining the higher fatigue strength of these joints under bending loading in comparison to tensile loading.

A third investigation[725] with comparisons to the hot spot structural stress approach was related to typical cruciform and lap joints subjected to

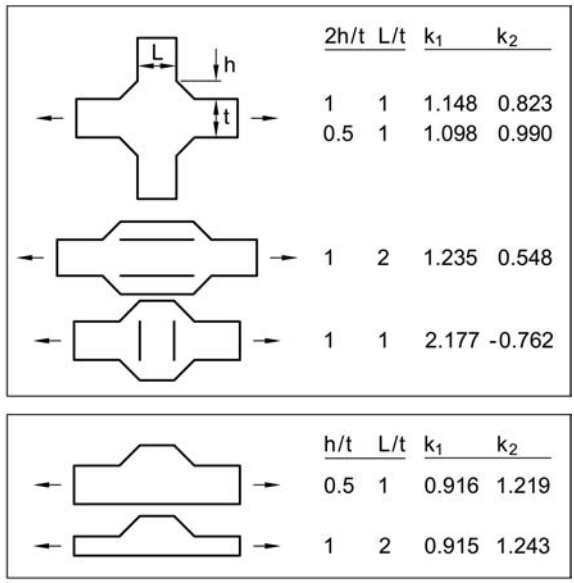


Fig. 7.12. Geometry coefficients k_1 and k_2 relating to cross-sectional models of various fillet-welded joints subjected to tension load; finite element results after Lazzarin and Tovo.[710]

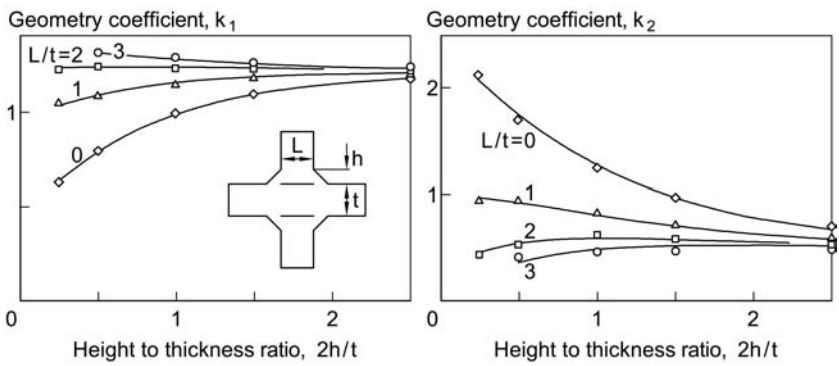
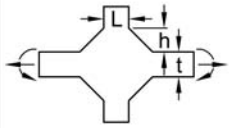


Fig. 7.13. Geometry coefficients k_1 and k_2 dependent on geometrical parameters for cruciform joint with non-load-carrying fillet welds (transverse attachment joint) subjected to tension load; finite element results after Lazzarin and Tovo.[710]

tension force or bending moment, respectively, Fig. 7.14. The k_1 values are always higher for tensile than for bending loading. The opposite holds for the k_2 values, which are less influential on fatigue. Note the substantial rise in the k_1 values for the cruciform and lap joints with load-carrying fillet welds.



Ratios 2h/t	L/t	Geometry coefficients k_{1t}	k_{2t}	k_{1b}	k_{2b}
		Tension load		Bending load	
2	1	1.173	0.662	0.897	0.824
2	0.1	1.165	0.720	0.899	0.821
2	1	1.199	0.625	0.900	0.819
2	3	1.250	0.251	0.900	0.818
2	1	1.432	0.018	0.904	0.790
2	5	1.543	0.465	0.907	0.769

Fig. 7.14. Geometry coefficients k_{1t}, k_{2t} and k_{1b}, k_{2b} relating to typical cruciform and lap joints subjected to tension force or bending moment, respectively; finite element results after Tovo and Lazzarin.[725]

The coefficients k_1, k_2 and k_3 were determined by Susmel and Tovo[723] for a fillet-welded circular tube penetrating a tension-loaded plate strip and for comparable cylindrical attachements. Curve plots over peripheral angle indicate different crack initiation points.

There is an open demand for the notch stress intensity factors of butt-welded joints with different degrees of reinforcement height and width, comprising laser beam welds and GMA welds and referring to the top and root sides of the welds. The notch opening angles may vary between 90° and 180° in these cases. An investigation of such joints was recently presented by Lazzarin *et al.*[703]

7.3.2 Stress rise in front of fillet welds

The stress rise in front of fillet welds was determined based on the notch stress intensity factors in order to validate this approach in general by comparison with accurate finite element results (Lazzarin and Tovo[710]). The radial stress along the free edge of the cross-sectional model, which corresponds to the surface stress in the base plate normal to the fillet weld, was calculated by introducing the notch opening angle $2\alpha = 135°$ and the bisector plane angle $\varphi = 112.5°$ into the general equations of stress, eqs. (7.1) and (7.2), thus yielding:

$$\sigma_r = 0.423 K_1 r^{-0.326} - 0.553 K_2 r^{0.302} \tag{7.44}$$

with the distance r from the sharp notch tip. In this equation, the sign of K_2, positive or negative, is chosen according to William's analytical frame. In the case shown below, K_2 is negative, so that the contribution due to mode II increases the contribution due to mode I.

The stress rise close to the sharp notch tip according to eq. (7.44) for a weld-like plane model subjected to tension load in comparison to accurate finite element results are plotted in Fig. 7.15. The logarithmic scale on the r/t axis is a means to elucidate the details of stress superposition (stress related to K_1 and K_2) and to avoid plotting the stress singularity at $r = 0$. The stress values gained from the two methods are more or less identical up to the second crossing of the nominal stress level.

A second validation of the notch stress intensity factor approach was conducted for the same weld-like model as before, but with a blunt notch instead of the sharp notch. The sharp notch stress equations extended by the notch radius term (eqs. (7.16) to (7.20) reveal the basic structure) are used, Fig. 7.16. Once more, satisfactory agreement with the results of finite element analysis is achieved.

Strain gauges applied to determine a fatigue-relevant local parameter at welds are generally placed on the free surface of the joint at a convenient distance from the notch tip of the weld toe. At this position, the effect of

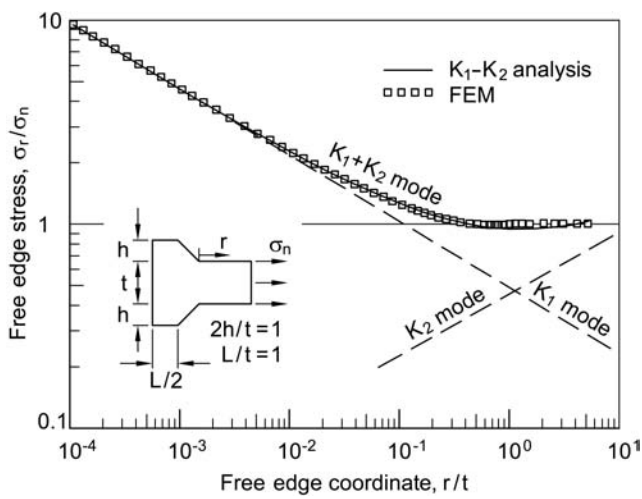


Fig. 7.15. Stress rise close to the sharp notch tip for weld-like model subjected to tension load; contributions of mode I and mode II loading to the free edge stress; K_1-K_2 analysis compared with finite element method (FEM); after Lazzarin and Tovo.[710]

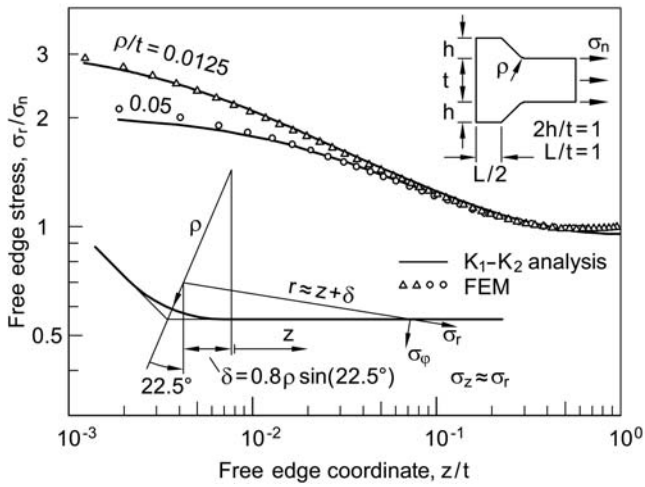


Fig. 7.16. Stress rise close to the rounded notch tip for weld-like model subjected to tension load; 'radial' stress along the straight free edge; K_1-K_2 analysis compared with finite element method (FEM); after Lazzarin and Tovo.[710]

mode II loading is always present. Then, if the fatigue strength is thought of as mainly controlled by the mode I stress distribution, the contribution of mode II loading to the measured strains should be disregarded. This is possible only if one knows both notch stress intensity factors, K_1 and K_2, for a given geometry and remote loading condition. Note that the greater is the distance x from the notch tip, the greater is the perturbing effect due to mode II.

7.3.3 Endurable notch stress intensity factors of fillet-welded joints

The fatigue strength of fillet-welded joints in the medium- to high-cycle fatigue range ($N \geq 10^4$) can advantageously be described by endurable (elastic) notch stress intensity factors (Bourkharouba *et al.*,[684] Verreman and Nie[652,653]). In contrast to the endurable nominal stresses, these are independent of the plate thickness, i.e. the size effect is included. Fatigue test data from the literature (Maddox,[717,718] Gurney[696]) referring to non-load-carrying fillet welds at tensile-loaded transverse attachment joints (mainly cruciform joints) in the as-welded condition were used to demonstrate this, Fig. 7.17 (Lazzarin and Tovo[710]). Large variations in the geometrical data were covered by the experimental investigations: plate thickness t = 13–100 mm, fillet weld leg length h = 5–16 mm, attachment length L = 3–220 mm. Only

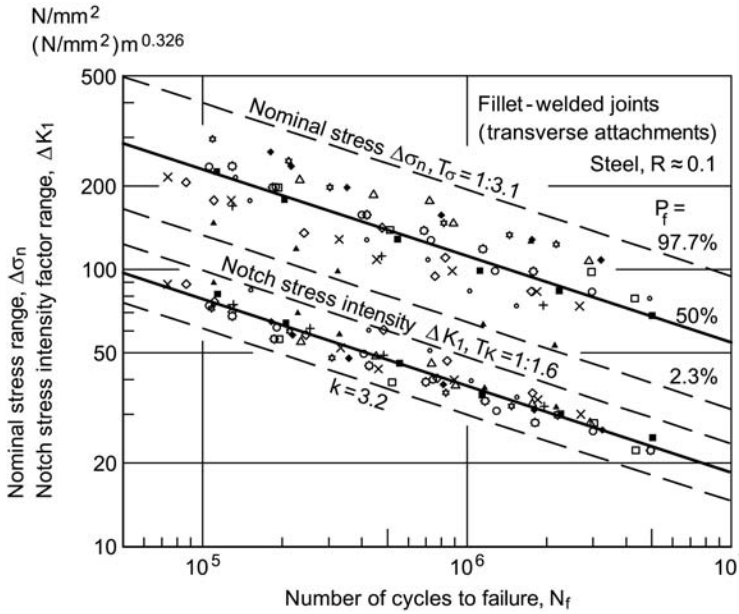


Fig. 7.17. Fatigue test data (toe failures) for fillet-welded transverse attachment joints in steel under tension load; *S–N* curves contrasted with K_1–*N* curves; T_σ and T_K refer to P_f = 2.3% and 97.7%; after Lazzarin and Tovo.[710]

the notch stress intensity factor K_1 was used to summarise fatigue data, whereas the effect of the factor K_2 was considered negligible in this type of joint ($2\alpha = 135°$) because no stress singularity occurs in the latter case. The large scatter of the original nominal stress *S–N* curve was substantially reduced to conventional values experienced with geometrically uniform specimens. An explanation for the fact that not only the crack initiation life but actually the total life is correctly described by endurable ΔK_1 values is given in Section 7.3.6.

The evaluation above based on ΔK_1 was extended to tensile and bending loaded fillet-welded joints in further steels (low and high strength) as well as in aluminium alloys (thickness t = 3–24 mm), Fig. 7.18 (Lazzarin and Livieri[706]). Different relationships were used to correlate ΔK_1 and $\Delta\sigma_n$ in the tension and bending load cases. In the high-cycle range, the fatigue strength of the steel joints is about twice the fatigue strength of the aluminium alloy joints. The size effect on the endurable nominal stresses is characterised by eq. (7.13), leading to an exponent $(1 - \lambda_1) = 0.326$ to the thickness ratio (the value 0.25 is recommended in the Eurocodes, values 0.1–0.3 dependent on joint type are recommended by the IIW).

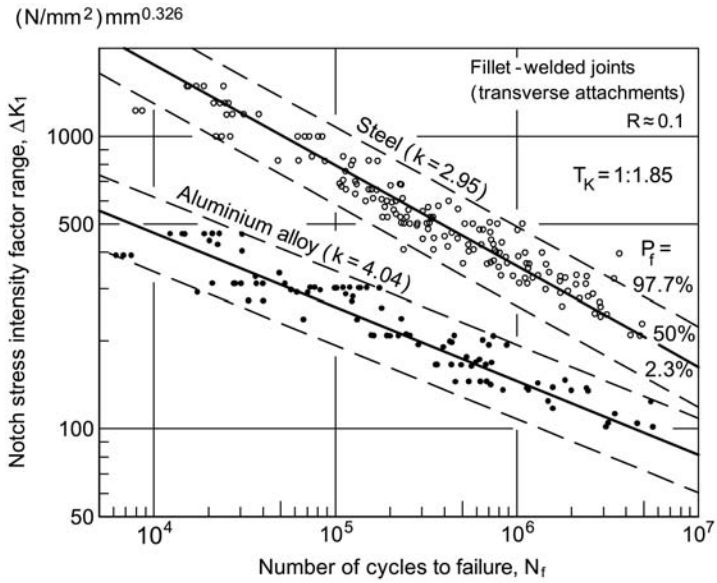


Fig. 7.18. Fatigue test data (toe failures) for fillet-welded transverse attachment joints in steel and aluminium alloy under tension and bending loads in terms of K_1–N curves; T_K refers to P_f = 2.3% and 97.7%; after Lazzarin and Livieri.[706]

Lazzarin and Livieri,[705] Koibuchi *et al.*[700] and Tanaka *et al.*[724] also proposed the use of the cyclic plastic zone size radius R_p at the notch root, approximated by the elastic notch stress intensity factor, for assessing the fatigue strength of fillet-welded joints. The S–N curves for different types of fillet-welded specimens are replaced by a unique R_p–N or R_p/t–N curve.

7.3.4 Endurable corner notch *J*-integral of fillet-welded joints

The J-integral defined for corner notches (Section 7.2.4) can be used as a fatigue-relevant parameter applicable under mixed mode loading conditions, to varying notch opening angles (defined by the toe angle of the butt- or fillet-welded joints) and under conditions of local yielding at the notch tip. Evaluating the published fatigue test results for non-load-carrying transverse stiffener joints (see Section 7.3.3) using a path radius of 1 mm resulted in the J_V–N curves or J_L–N curves, respectively, plotted in Fig. 7.19 for fillet-welded-joints in steels and aluminium alloys. The contribution of ΔK_2 is neglected with reference to the missing stress singularity in the case of large notch opening angles. When comparing the scatter range

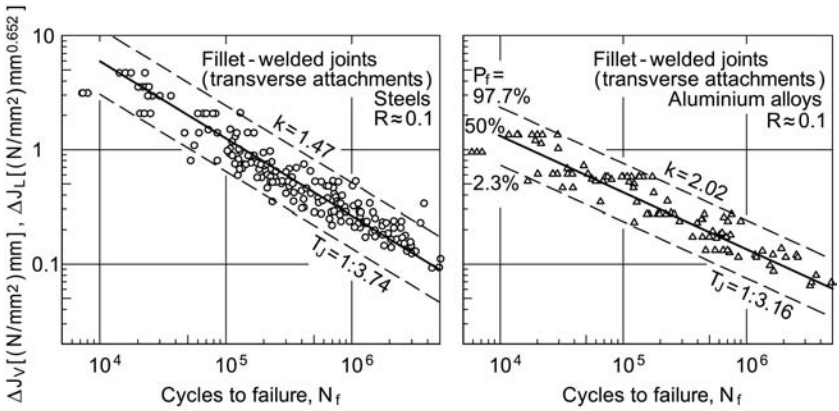


Fig. 7.19. Fatigue test data (toe failures) for fillet-welded transverse attachment joints in steels and aluminium alloys under tension and bending loads in terms of *J–N* curves; scatter band characterises mean values plus and minus two standard deviations; T_J refers to P_f = 2.3% and 97.7%; after Lazzarin *et al.*[707]

indices T_J and T_K, it is to be noted that a quadratic increase occurs solely by substituting a stress parameter by an energy parameter. The presented curves do not yet prove the applicability of the ΔJ-concept with regard to varying notch opening angles and marked mixed mode conditions.

7.3.5 Endurable corner notch strain energy density of fillet-welded joints

The strain energy density averaged in a small volume around the notch tip (or fillet weld toe) with a material-dependent radius R_0 (proposed by Lazzarin, see Section 7.2.5) can be used as a fatigue-relevant parameter applicable under mixed-mode loading conditions, with varying notch opening angles (or fillet weld toe angles), under conditions of local yielding at the notch tip and with varying R ratios. Either the total strain energy or its deviatoric proportion may be evaluated depending on brittle or ductile material behaviour, respectively (Lazzarin *et al.*[708]).

Based on the published fatigue test data for non-load-carrying transverse attachment joints (see Section 7.3.3) enlarged by data presented by Lassen[690,701] (toe angle 30–70°, plate thickness 3–100 mm), the $\overline{W}_1$–N_f curve shown in Fig. 7.20 was derived (with averaged total strain energy density $\overline{W}_1$ in mode I loading). The characteristic radius R_0 = 0.3 mm was chosen based on various considerations of threshold conditions both for the fillet-welded cruciform joints and, in comparison, for butt-welded joints machined flush after welding, thus separating the effect of stress

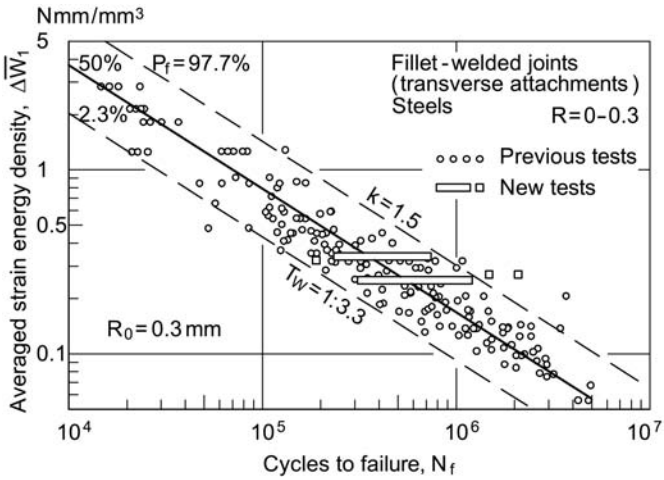


Fig. 7.20. Fatigue test data (toe failures) for fillet-welded transverse attachment joints in steel (as-welded and stress-relieved) subjected to tension and bending loads; $\overline{W}_1$–N_f curves relate to averaged total strain energy density in mode I loading; scatter band characterises mean values plus and minus two standard deviations; T_W refers to P_f = 2.3% and 97.7%; after Lazzarin *et al.*[704]

concentration. Once more, the increase in the scatter range index is caused by the evaluation of energy instead of stress.

The most important feature of the strain energy density $\Delta\overline{W}_1$ criterion is the uniform description of the fatigue strength resulting from toe and root failures. In order to demonstrate this capability, the results of the 'new' test series evaluation comprising both failure types (Livieri and Lazzarin[716]) are plotted into the scatter band of Fig. 7.20 thus creating Fig. 7.21. It is evident that the new data inclusive of the root failures ($2\alpha = 0°$) fit well into the scatter band, the only exceptions being data for austenitic steels in the medium-cycle fatigue range. Recently, also butt-welded joints were included (Lazzarin *et al.*[703]).

7.3.6 Link to the crack propagation approach

According to the crack propagation approach, the fatigue life of welded joints is conceived as the propagation phase of cracks occuring at the toe (or root) of the weld seam. The cracks originate from detected crack-like defects or from assumed initial defects (worst case assumption). The approach is usually based on nominal stresses, provided that structural stress raisers are absent, or on (hot spot) structural stresses in the case of such raisers being present (e.g. longitudinal attachment joint). The notch effect at the location of the initial crack may additionally be taken into account.

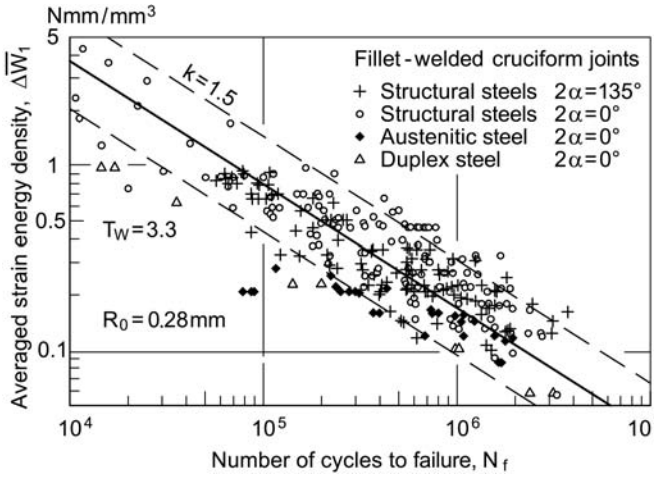


Fig. 7.21. Fatigue test data for cruciform joints in steel ('new' test series evaluation, toe and root failures) superimposed on the scatter band from Fig. 7.20 referring to transverse attachment joints (toe failures); load-carrying and non-load-carrying welds, tension and bending loads; after Livieri and Lazzarin.[716]

The fatigue life prediction can be made more reliable by differentiating between the crack initiation phase and the crack propagation phase. Crack initiation up to an initial macrocrack (crack depth 0.1–0.5 mm) may be treated by microcrack nucleation and propagation concepts, whereas macrocrack propagation can be described by conventional engineering fracture mechanics. Both processes are controlled by the stress intensity at the sharp or blunt weld toe notch as far as medium- to high-cycle fatigue is concerned. Therefore, the notch stress intensity factors are the appropriate means to quantify the total life, provided the analysis directs its focus on regions sufficiently close to the notch tip. The following exposition is based on a detailed investigation by Atzori *et al.*[681] on the link between the notch stress intensity factors and the crack propagation approach in the case of fillet-welded joints.

To perform the crack propagation analysis based on the Paris equation, the stress intensity factor K_I of the initiated or propagating crack in the non-uniform stress field at the notch tip is needed. This stress intensity factor can be determined dependent on the crack length, proceeding from the stress field before the crack occurred (procedure according to Albrecht and Yamada[409] using Bueckner's[430] derivations). The stresses normal to the expected crack path are evaluated. The crack path normal to the base plate surface is the usual choice in the case of fillet-welded joints. The result for crack initiation and propagation in the bisector plane is slightly different.

The formulae below are given for the bisector plane because they have a simpler form. The fatigue strength evaluations by Atzori *et al.*[681] refer mainly to the plane normal to the base plate surface ($\varphi = 22.5°$).

The stresses σ_φ in the bisector plane ($\varphi = 0°$) of tension-loaded fillet-welded joints ($2\alpha = 135°$) with a sharp toe notch ($\rho = 0$) are distributed as follows:

$$\sigma_\varphi = 0.399 K_1 r^{-0.326} \tag{7.45}$$

In the case of a blunt toe notch ($\rho > 0$), the stresses in the bisector plane dependent on the distance ζ from the notch root are given by:

$$\sigma_\varphi = (\zeta + 0.2\rho)^{-0.326}\left[0.399 + 0.034\left(\frac{\zeta}{\rho} + 0.2\right)^{-0.824}\right]K_1 \tag{7.46}$$

The stress intensity factor K_I of a crack of length a along the bisector plane follows by applying Bueckner's weight function method:

$$K_I = 1.122\sqrt{\pi a}\left(0.53 a^{-0.326} K_1\right) \qquad (a \le 0.3t) \tag{7.47}$$

The terms in parenthesis constitute an explicit expression for the notch-related magnification factor M_k multiplied by the nominal stress (see eq. (6.17)). The values of M_k from a similar equation for crack propagation normal to the base plate surface ($\varphi = 22.5°$) are compared in Fig. 7.22 with an approximation by Hobbacher.[490] Note the above restriction on crack length relative to plate thickness, which may also be relevant for residual life calculations when assuming the main portion of propagation life in this region.

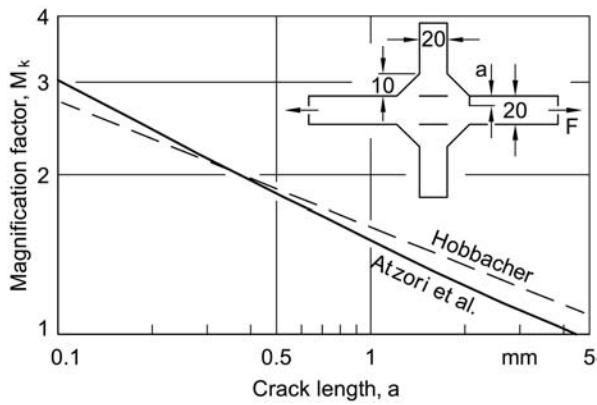


Fig. 7.22. Notch-related magnification factor (or 'shape factor') M_k dependent on crack length a in tension-loaded transverse attachment joint with sharp toe notch; solution by Atzori *et al.*[681] compared with Hobbacher's[490] approximation; after Atzori *et al.*[681]

Equation (7.47) can be rewritten with the basic stress σ_n:

$$K_I = 1.122\sqrt{\pi a}\left[0.53k_1\left(\frac{t}{a}\right)^{0.326}\right]\sigma_n \tag{7.48}$$

The following fatigue-equivalent basic stress range $\Delta\bar{\sigma}_n$ comprising the notch effect of the sharp weld toe can be extracted from eq. (7.48):

$$\Delta\bar{\sigma}_n = \left[0.53k_1\left(\frac{t}{a}\right)^{0.326}\right]\Delta\sigma_n \tag{7.49}$$

By introducing the high-cycle fatigue strength $\Delta\sigma_{nE}$ (technical endurance limit at $N = 5 \times 10^6$ cycles) together with a realistic choice of the initial crack length a_i (a_i = 0.2–0.3 mm for GMA-welded joints in structural steel), the effective fatigue strength $\Delta\bar{\sigma}_{nE}$ will result which is independent of the plate thickness and the other geometrical parameters that have an influence on $\Delta\sigma_{nE}$. The high-cycle fatigue strength is assumed to be the non-propagation condition of the initiated crack at the sharp notch tip. Similar relationships comprising the influence of the notch radius may be derived for blunt toe notches. The endurable values of ΔK_I and $\Delta\sigma_n$ decrease with increasing notch radius. Obviously, another set of equations will result for bending loads.

Atzori *et al.*[681] proved that the fatigue test results mentioned earlier referring to non-load-carrying fillet welds at transverse attachment joints can be described in a uniform manner with a small scatter range by subdividing the total life in the crack initiation and crack propagation portions, each controlled by the relevant stress intensity factor. Crack initiation life is related to the initial crack length a_i = 0.3 mm.

7.3.7 Link to the hot spot structural stress approach

The fatigue strength of fillet-welded details in complex structures may be assessed on the basis of the hot spot structural stress (see Chapter 3). In many cases, it is assumed in the calculation-based variant that the structural stresses are derived from the thin-shell theory approximated by finite elements. A linear distribution over the plate thickness is introduced for the normal stresses and a parabolic distribution for the (in-plane) shear stresses. These simplified distributions can be considered valid up to a distance from the weld toe equal to the plate thickness. The problem to be solved is the relationship between the notch stresses at the weld toe, governed by the notch stress intensity factors and the structural stresses or internal forces (tension force, bending moment, shear force) in the plates meeting at the joint. The solution given below has been developed by Tovo and Lazzarin.[725]

Two types of joints were investigated: single-sided (asymmetrical) welds and double-sided (symmetrical) welds. Because of limited space, only the latter type is referred to in the following. The symmetrical joint types depicted in Fig. 7.23(a) are analysed using a plane sector model according to Fig. 7.23(b) subjected to the internal forces extracted from the thin-shell element model, Fig. 7.23(c). The loading condition at each boundary section of the plane sector model is described by the two stress values at the upper and lower surface of each plate, supplemented by one value of the averaged shear stress. Note that a general three-dimensional stress problem is substituted by a plane model normal to the weld line. The influence of variations of the stress components along the weld line is considered to be secondary.

Any general loading condition of the joint or its sector model can be expressed by a linear superposition of reference loading states. The general state can be decomposed into the reference states. For the double-sided symmetrical joint considered, nine independent equilibrated loading states exist supplemented by three dependent non-equilibrated loading states, Fig. 7.24. They correspond to the same number of four times three characteristic stresses (or internal forces) in the four boundary sections of the sector model. Following Tovo and Lazzarin,[725] these are given by:

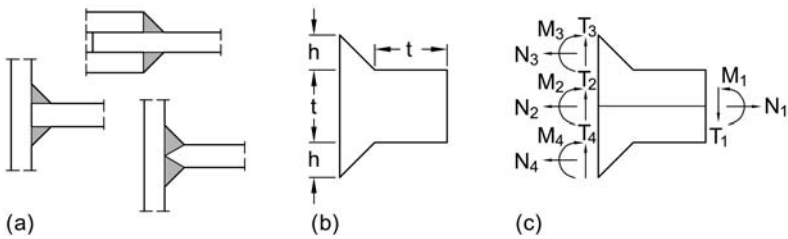


Fig. 7.23. Double-sided (symmetrical) fillet-welded joints (a), plane sector model (b) and internal forces extracted from thin-shell element model (c); after Tovo and Lazzarin.[725]

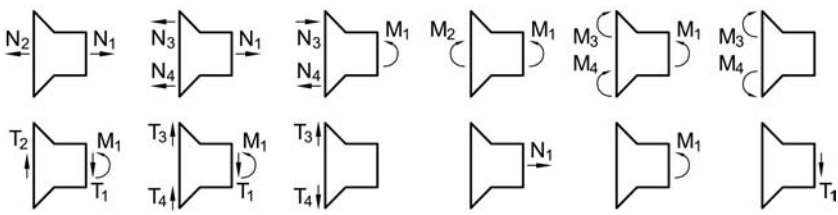


Fig. 7.24. Reference loading states for double-sided symmetrical fillet-welded joints; nine equilibrated states and three non-equilibrated states acting on the sector model; with normal forces *N*, bending moments *M* and transverse forces *T*; after Tovo and Lazzarin.[725]

$$\{\sigma\} = [C]\{a\} \tag{7.50}$$

$$\{\sigma\} = \{\sigma_{1,u}\ \sigma_{1,l}\ \tau_{1,\perp}\ \sigma_{2,u}\ \sigma_{2,l}\ \tau_{2,\perp}\ \sigma_{3,u}\ \sigma_{3,l}\ \tau_{3,\perp}\ \sigma_{4,u}\ \sigma_{4,l}\ \tau_{4,\perp}\}^T \tag{7.51}$$

The matrix $[C]$ comprises the 12 vectors of characteristic stresses in the 12 reference loading states. The weight vector $\{a\}$ designates the proportions of the reference loading cases in the actual loading condition. The stress vector $\{\sigma\}$ designates the actual loading state of the sector model, extracted from the finite element model of the welded structure (indices u and l referring to the upper and lower plate surface, indices 1–4 referring to the boundary sections 1–4 of the sector model).

Based on eqs. (7.41), (7.42) and (7.50), the following relationship is derived for the notch stress intensity factors K_1 and K_2 of the general loading state expressed by the conditions in the reference loading states ($2\alpha = 135°$):

$$\{K\} = \begin{bmatrix} t^{0.326} & 0 \\ 0 & t^{-0.302} \end{bmatrix} [B][C]^{-1}\{\sigma\} \tag{7.52}$$

The vector $\{K\}$ consists of K_1 and K_2. The matrix $[B]$ comprises the values k_1 and k_2 determined by finite element analysis for the 12 reference loading states (with $h/t = 1$ and $j = 1, 2, \ldots, 12$):

$$[B] = \left[\begin{Bmatrix} k_1 \\ k_2 \end{Bmatrix}_j\right] = \begin{bmatrix} 0.943 & 1.941 & 0.912 & 0.864 & 0.940 & & \\ 1.387 & -1.595 & 0.744 & 1.001 & -0.566 & & \\ 0.434 & 0.382 & 0.391 & -1.047 & 0 & 0 & 0 \\ -1.473 & 0.727 & 0.682 & 2.626 & 0 & 0 & 0 \end{bmatrix} \tag{7.53}$$

The numerical values introduced in $[C]$ and $[B]$ refer to $2\alpha = 135°$ and $h/t = 1$. Other choices of 2α and h/t are possible, but need separate evaluation.

The thin-shell element model proposed by Tovo and Lazzarin[725] in the region of the joint (providing the meshing rules) is shown in Fig. 7.25. It is empirically developed and capable of simulating the stiffnesses with sufficient accuracy. The comparison of the geometry coefficients k_1 and k_2 for the cruciform and lap joints in Fig. 7.14, gained from finite element analysis and based on the thin-shell element model, respectively, resulted in satisfactory correspondence.

Substantially simplified relationships are derived with the assumption of an extremely stiff support of the welds connecting the base plate to the cross member (appropriate in the case of cruciform joints, but not in the case of lap joints). As a consequence, the load distribution in the joint is completely

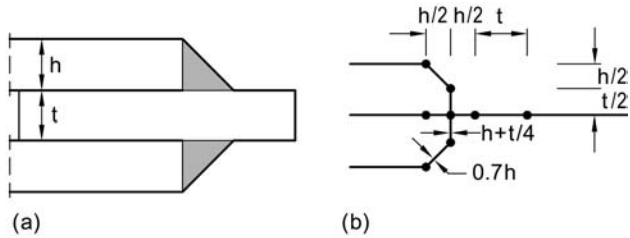


Fig. 7.25. Meshing rules for thin-shell element models (b) of fillet-welded lap joints, cover plate joints or cruciform joints (a); after Tovo and Lazzarin.[725]

defined by the weld configuration at the base plate. The notch stress intensity factors can be expressed in this case solely by the stresses at the end of the base plate in the sector model:

$$K_1 = D_{1,\mathrm{u}}\sigma_\mathrm{u} + D_{1,\mathrm{l}}\sigma_1 + D_{1,\perp}\tau_\perp \tag{7.54}$$

$$K_2 = D_{2,\mathrm{u}}\sigma_\mathrm{u} + D_{2,\mathrm{l}}\sigma_1 + D_{2,\perp}\tau_\perp \tag{7.55}$$

with the stresses σ_u and σ_l in the upper and lower surface of the plate, and with the averaged transverse shear stress $\tau_\perp$ not further indexed. The coefficients $D_{1,\mathrm{u}}$, $D_{1,\mathrm{l}}$, $D_{1,\perp}$ and $D_{2,\mathrm{u}}$, $D_{2,\mathrm{l}}$, $D_{2,\perp}$ recorded by Tovo and Lazzarin[725] depend on the geometry of the considered cruciform joint (fillet-welded single-sided or double-sided welds without or with full penetration).

In thin-shell theory, the (averaged) transverse shear stress is related to the gradient of the bending moment expressed by the gradient of the upper or lower surface stresses:

$$\tau_\perp = -\frac{\mathrm{d}\sigma_\mathrm{u}}{\mathrm{d}x}\frac{t}{6} = \frac{\mathrm{d}\sigma_1}{\mathrm{d}x}\frac{t}{6} \tag{7.56}$$

The numerical result for the double-bevel butt weld with fillet welds (i.e. the full penetration weld) is the following relationship ($2\alpha = 135°$, $h/t = 1$):

$$K_1 = 1.026\sigma_\mathrm{u} + 0.132\sigma_1 - 1.025\frac{\mathrm{d}\sigma_\mathrm{u}}{\mathrm{d}x} \qquad (x = t, \quad t = 1) \tag{7.57}$$

This relationship expresses the fact that the K_1 value (and similarly the K_2 value) depends mainly on the structural stress in the upper surface of the base plate and its gradient, but also (to a minor extent) on the structural stress in the lower surface. The stresses in eq. (7.57) refer to the cross-section of the base plate at $x = t$.

Introducing the hot spot stress $\sigma_{\mathrm{u\,hs}}$ together with $\sigma_{\mathrm{l\,hs}}$ at $x = 0$ results in:

$$K_1 = 1.026\sigma_{\mathrm{u\,hs}} + 0.132\sigma_{\mathrm{l\,hs}} - 1.131\frac{\mathrm{d}\sigma_\mathrm{u}}{\mathrm{d}x} \qquad (x = 0, \quad t = 1) \tag{7.58}$$

The following conclusions are drawn in summary by Tovo and Lazzarin[725] presuming that the notch stress intensity factors can be used to indicate the fatigue strength:

- The fatigue strength is mainly dependent on the structural stress and its gradient on the upper plate surface.
- The stress on the lower plate surface characterising the stress gradient over the plate thickness exerts an additional influence.
- The structural stress approach does not quantify the size effect (i.e. the endurable stresses are dependent on plate thickness), whereas the notch stress intensity approach does.
- Different welded joints showing the same hot spot structural stress may be different in fatigue strength because of different notch stress intensity factors.

Two application examples are given by Tovo and Lazzarin[725] which demonstrate deficiencies in the structural stress approach and draw attention to the advantages of combining the notch stress intensity factor approach with the structural stress approach.

The first example refers to the different K_1 and K_2 values of the cruciform joint with full penetration welds on the one side and with fillet welds without penetration (joint with internal slits) on the other, Fig. 7.26. The structural stresses are identical ($\sigma_x/\sigma_n = 1$), but the notch stress intensity factors, expressed by the gradients of the stress rise to the corner notch, are not. The K_1 factor ratio 1.432/1.173 = 1.221 is not too far from the IIW design recommendation:[3] 71/63 = 1.127. Another conclusion from the stress plot is

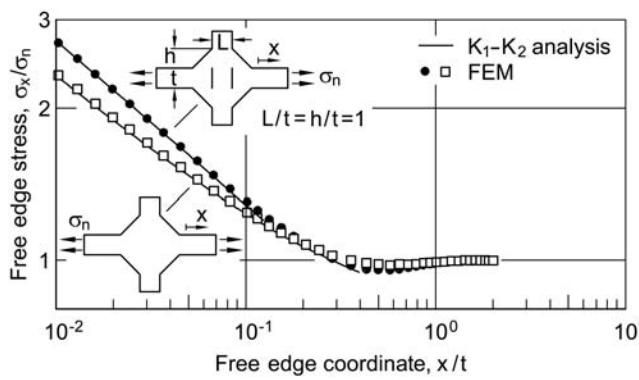


Fig. 7.26. Local stress rise above the structural stress level ($\sigma_s = \sigma_n$) plotted over distance from the sharp notch tip for a sector model of cruciform joints subjected to tension load; joint with slits in comparison to joint without slits; K_1-K_2 analysis compared with finite element method (FEM); after Tovo and Lazzarin.[725]

that direct measurement or calculation of the asymptotic stress rise to the corner notch tip (for determining the fatigue-relevant notch stress intensity factor) must be performed close to the notch tip ($x/t \leq \approx 0.1$), Atzori and Meneghetti.[80]

The second example of a longitudinal attachment joint refers to the fact that the structural stress extrapolation to the hot spot may be misleading when using the results from a thin-shell element model, Fig. 7.27. The stress rise to the weld toe in front of the attachment is well described by the notch stress intensity factors determined on the basis of the relevant structural stresses in the thin-shell element model (at distance $x = t$), as can be seen from comparsion with the results of a fine-meshed three-dimensional solid element model. The structural stresses in the thin-shell element model in the region in front of the weld toe, where the extrapolation to the hot spot is performed ($0.4 \leq x/t \leq 1.0$), are not sufficiently accurate, at least not for the element mesh chosen.

A different methodical proposal (which was originally published by Haibach[123,129]), for how to separate the overall structural stress effect (termed 'geometrical') from the local notch effect of the sharp weld toe has been specified by Atzori *et al.*[79,81] The geometric stress concentration of a blunt notch touching the fillet weld surface provides the basis for the superimposed notch stress concentration by the V-notch at the weld toe, Fig. 7.28. The fatigue strength of fillet-welded joints can thus be estimated in terms of the structural stress at a given number of cycles as a function of the

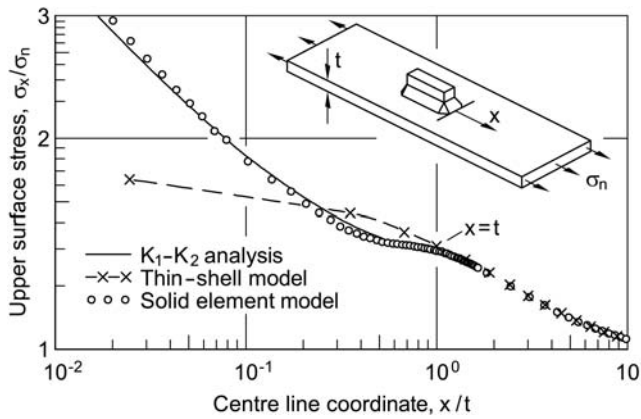


Fig. 7.27. Local stress rise plotted over distance from the weld toe for single-sided longitudinal attachment joint subjected to tension load; K_1-K_2 analysis based on structural stresses σ_u, σ_l and $d\sigma_u/dx$ in thin-shell element model (coarse mesh) at distance $x = t$ from the weld toe compared with results from solid element model (fine mesh); after Tovo and Lazzarin.[725]

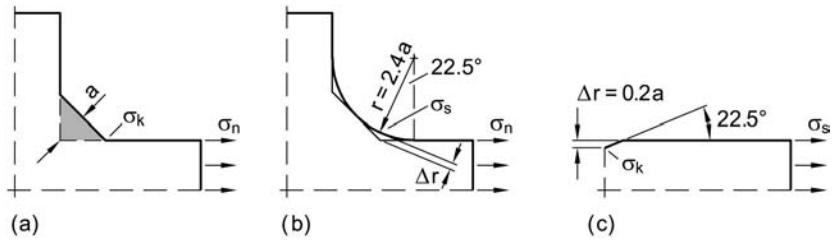


Fig. 7.28. Notch stress σ_k at sharp weld toe (a), represented by structural stress σ_s at blunt equivalent notch with radius r (b) superimposed by notch effect of equivalent V-notch with depth Δr (c); after Atzori *et al.*[81]

equivalent V-notch depth. The size effect and the effectiveness of smoothing the weld toe are also included.

7.4 Weak points and potential of the approach

There are some possible weak points associated with the notch stress intensity approach applied to seam-welded joints in general. The most important one has been addressed by Atzori *et al.*:[681] the notch stress intensity factor and similar corner-notch related parameters may characterise the condition of crack initiation or of non-propagation of initiated cracks, but further crack propagation is governed by crack-related parameters to an increasing extent. Atzori's assumption that the total fatigue life consists predominantly of crack propagation in the notch-related stress field is not generally applicable. The notch stress intensity approach is primarily a crack initiation (or non-propagation) concept and should therefore be combined with a crack propagation analysis describing the residual life. The latter analysis has to take into account the crack path and the crack closure effects. This would correctly indicate the different residual lives under tension and bending loads, respectively, supplementing the different crack initiation lives caused by different K_1 values in the two load cases.

Another possible handicap of the approach is its rather recent development. This development has a sound theoretical basis and the application to the available fatigue test data was performed with the utmost care (considering mainly fillet-welded joints), but not all aspects have yet been sufficiently investigated, among them the following topics: influence of non-singular stress components (K_2-related or parallel to the notch), multiaxiality criteria, crack closure effects, residual stress conditions, variable-amplitude loading, application to laser-beam-welded joints and comparisons with other approaches.

The potential of the notch stress intensity approach seems to be exceptionally great. Notch stress intensity factors describe the stress field at sharp or blunt notches with different notch opening angles in a uniform and theoretically sound manner. Local failure criteria (averaged stress, strain or strain energy density, critical distance, energy release rate and others) can be formulated on this basis. Extensions to non-linear elastic-plastic material behaviour (plastic notch stress intensity factors, *J*-integral and others) have been presented. The failure condition at weld toes and weld roots can be described in a uniform manner. Some problems with the concurrent notch stress approach based on fictitious notch rounding (e.g. the problem of cross-sectional weakening) are avoided. The notch stress intensity approach has not yet been introduced as a tool supporting fatigue-resistant designs, but it has certainly the potential to be accepted as such as soon as codification based on further design-relevant investigations has taken place. There is no other local approach, notch-stress or notch-strain based, that presents a comparably comprehensive data set of endurable values.

8

Local approaches applied to a seam-welded tubular joint

8.1 Subject matter of investigation

The local approaches described in the previous chapters are applied comparatively to a seam-welded tubular joint subjected to cyclic loading in seawater in order to demonstrate some of the characteristic features, benefits and shortcomings of these approaches, i.e. of the structural stress or strain approach, the notch stress and strain approaches and the crack propagation approach. It is shown how a practical problem can be treated within a limited schedule of time and expenditure by applying estimates and modelling based on engineering expertise. The close connection of fatigue testing with numerical analysis makes accuracy statements possible. The reviewed results are taken from an EU Report,[740] relevant publications[730,738,739] and supplementary investigations.[736] The supplementary investigations comprise a redesigned finite element model for the structural stress evaluation, the application of the elastic notch stress and elastic-plastic notch strain approaches and a crack propagation assessment according to British Standard. The investigations have been concluded ten years ago, but the basic situation in respect of procedures, tools and arguments has not substantially changed.

The dimensions and shape of the tubular joint which was fatigue-tested under constant-amplitude (3 specimens) and variable-amplitude (5 specimens) loading in artificial seawater (1 specimen in air) and then numerically analysed are shown in Fig. 8.1. The K-shaped tubular joint consists of two diagonal braces butting on the chord with a slight eccentricity. A gap is formed between the braces on the chord surface ($g = 56\,\text{mm}$). The dimensions of the joint are similar to those in certain smaller offshore rigs.

The parent material of the tubular joint being considered is type StE355 fine-grained structural steel in the normalised condition ($\sigma_{Y0.2} \geq 355\,\text{N/mm}^2$, $\sigma_U \geq 470\,\text{N/mm}^2$, according to Euronorm EN10225). The V-groove between the brace tube ends and the chord tube surface is filled by conventional multi-layer welding.

The brace tubes of the joint are subjected to counteracting fully reversed axial loading thus producing single-sided axial tensile-compressive loading ($R = -1$) in the chord tube (see Fig. 8.1). A minor bending moment is superimposed in the chord tube caused by the slight eccentricity of the brace tube intersection point relative to the chord centre line ($e = 28$ mm). Both constant- and variable-amplitude loading are applied. The spectrum of relative load or stress amplitudes is derived from wave height measurements in the North Sea. Seven different sea states were evaluated resulting in seven spectra with a Gauss normal distribution and an irregularity factor close to 1.0. The superposition of the spectra gives a spectrum according to Fig. 8.2 (prolonged

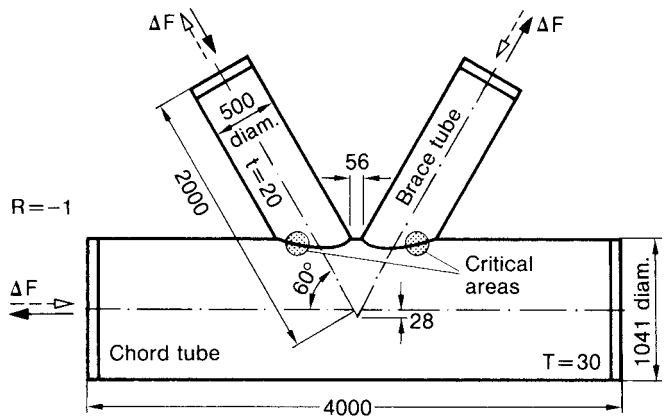


Fig. 8.1. Welded tubular joint, fatigue-tested and analysed according to local approaches, with critical areas of crack initiation and propagation; after EU Report.[740]

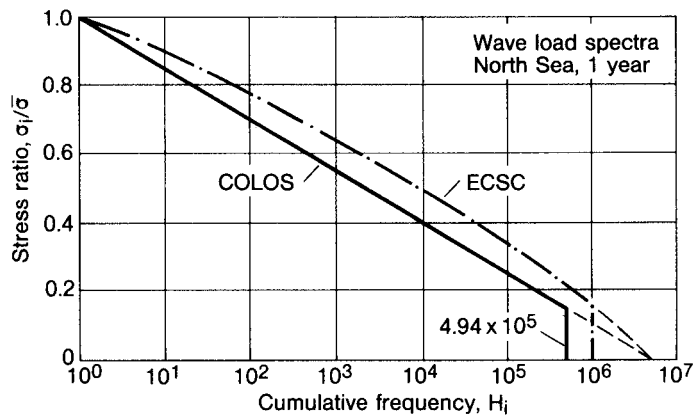


Fig. 8.2. Wave load standard spectra of the North Sea, operation time 1 year, according to COLOS (Common Load Sequence) and according to ECSC (European Coal and Steel Commission); after EU Report.[740]

solid line curve) with a maximum cumulative frequency of 5×10^6 cycles corresponding to a one-year operation.

In order to obtain reasonable testing periods, all amplitudes below 15% of the maximum amplitude are omitted. This results in a spectrum with a maximum cumulative frequency (sequence length) of 4.94×10^5 cycles. It is assumed that the fatigue damage is mainly induced by higher amplitudes and that the small amplitudes will not contribute significantly to the damaging process. This wave load standard spectrum is named COLOS (Common Load Sequence[729]).

A similar spectrum with a sequence length of 1×10^6 cycles, again corresponding to a one-year operation, is applied to the angular joint specimens which are tested by comparison. It is named ECSC spectrum (European Community for Steel and Coal) after the sponsor of the relevant research program.

The random sequence of 4.94×10^5 cycles corresponding to one year of service loading is repeated until fatigue cracks are initiated at the weld toe in the critical areas of the intersection line near to the saddle points (see Fig. 8.1: angular position 0–30° from the saddle point in the outside direction) and then propagated through the wall of the chord tube. The potential-drop technique is used to evaluate the fatigue life up to initiation of a technical crack of 1 mm depth. The total fatigue life is defined to be limited by the through-thickness crack.

The fatigue tests are carried out in artificial seawater at a temperature of 15°C and a pH-value of 8.1. The seawater is continuously aerated and circulated around the critical areas of the joint. No corrosion protection was applied.

8.2 Application of the structural stress or strain approach

8.2.1 Structural stress analysis and strain measurement

The structural stresses are calculated on the basis of a relatively simple finite element model (without weld modelling) with the critical area shown in Fig. 8.3. The program MARC is applied in combination with curved four-node thick-shell elements.[736]

The von Mises structural stress in the outer surface of the critical area is contour plotted in Fig. 8.4. The maximum structural stress on the surface of the chord tube occurs in the intersection line at the peripheral angle $\psi = 120°$ (measured from the inner crown point of the joint), $\sigma_{eq\,max} = 198\,N/mm^2$. The adjacent maximum structural stress in the brace is significantly smaller, $\sigma'_{eq\,max} = 150\,N/mm^2$.

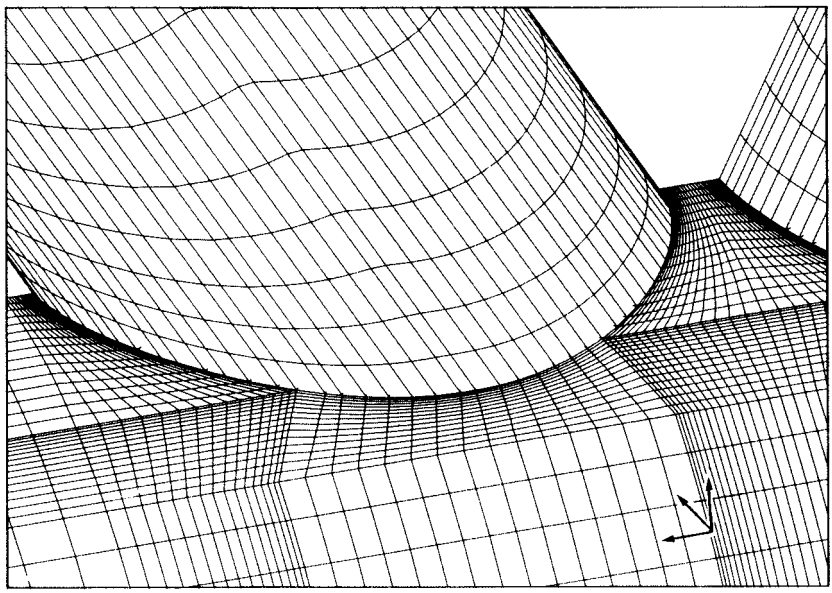


Fig. 8.3. Finite element model of the intersection area of the tubular joint (symmetry half, midplane plot), consisting of curved thick-shell elements; after Radaj *et al.*[736]

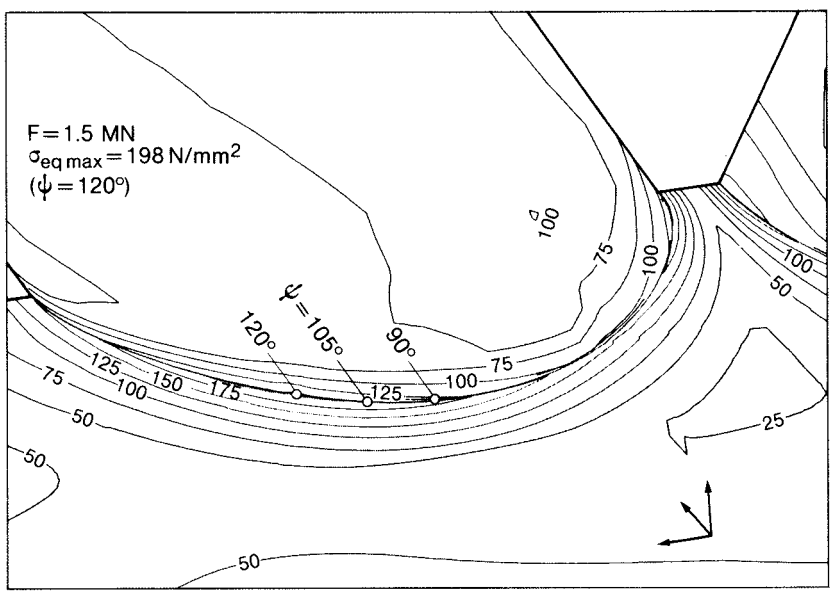


Fig. 8.4. Lines of constant structural stresses (von Mises equivalent stress, midplane plot) at the outer surface of the tubular joint, brace force $F = 1.5\,\text{MN}$; after Radaj *et al.*[736]

A comparison of measured and calculated structural stresses in front of the toe notch along the groove butt weld between brace and chord is given in Fig. 8.5 (see Fig. 8.6 for the position of the strain gauges). The calculated maximum stress adjacent to the weld toe notch ($s = 2$ mm), corresponding

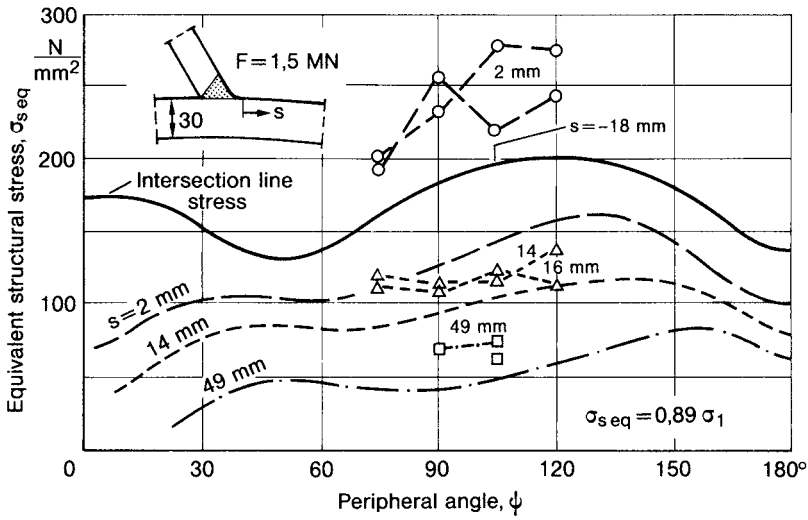


Fig. 8.5. Structural stresses (von Mises equivalent stress) at the outer chord surface at three distances from the weld toe groove; strain gauge measurement compared with finite element analysis results; after Radaj *et al.*[736]

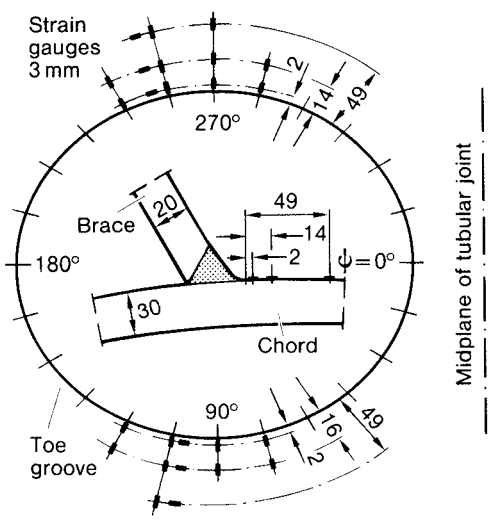


Fig. 8.6. Strain gauge arrangement in the hot spot area of the chord tube in lines normal to the weld and radial to the brace tube (schematically: the elliptical intersection line is really an ovaloid with the vertex shifted to $\psi \approx 82.5°$); after EU Report.[740]

to Haibach's structural strain, occurs at $\psi = 130°$, $\sigma_{eq\,max} = 162\,N/mm^2$. But the evaluation in respect of the notch stresses is performed at $\psi = 105°$ resulting in $\sigma_{eqmax} = 138\,N/mm^2$. The reason for this is that crack initiation was observed here in the tests. There are differences between the calculated and measured stresses in respect of magnitude and curve shape resulting mainly from imperfections in fabrication which are not considered in the finite element model. This model, on the other hand, does not correctly simulate the three-dimensional behaviour of the structure in the weld area, especially not its stiffening effect on chord wall bending. The remedial measure of increasing the shell thickness locally or of using a three-dimensional model in the intersection area was not applied. The measured stresses are generally somewhat higher than the calculated stresses. Additionally, the measured stresses at $s = 2\,mm$ comprise part of the notch effect of the weld toe (see Section 3.1.2).

The position of the hot spot should primarily be determined on the basis of observed crack initiation and only secondarily be confirmed by strain measurements and stress calculations. In the case considered of the as-welded tubular joint, crack initiation was observed in the chord at the weld toe notch at peripheral angles of 90–120° and 240–270° at both braces (see Fig. 8.6 for the designation of angular position). The crack initiation and propagation processes take place unsymmetrically with a high degree of scatter caused by imperfections in geometry, load position and material states. The measured strains indicate the 105 or 255° position for the hot spot. The calculated maximum structural stresses refer to the 130 or 230° position at the left-hand brace (note that the chord is unsymmetrically supported). The localisation of the hot spot on the basis of the measured or calculated structural stresses presumes the notch effect to be position-independent. This assumption is uncertain but can be checked by a comparative notch stress analysis. The peripheral position $\psi = 105°$ has been taken to be the hot spot in the following based on a decision taken in the EU Report.[740]

The hot spot strain ε_{hs}, i.e. the maximum structural strain gained by linear extrapolation of measured strains in front of the weld in the critical areas of the tubular joint, is evaluated based on a strain gauge arrangement according to Fig. 8.6, resulting in a hot spot strain according to Fig. 8.7 (with additional strain gauges supplementing the main positions).[740] Hot spot stress concentration factors are derived from measurements at nine specimens of the tubular joint, $K_{hs} = 2.58–3.56$, defined as the ratio of the hot spot stress on the chord surface to the nominal (axial) stress in the brace ($\sigma_n = 49.75\,N/mm^2$ for $F = 1.5\,MN$). A supplementary measurement with a single joint performed at another laboratory gave $K_{hs} = 4.0$. The hot spot stresses are calculated from $\sigma_{hs} = E\varepsilon_{hs}$ with elastic modulus $E = 2.06 \times 10^5\,N/mm^2$. The scatter range of K_{hs} originates from the imperfections in fabrication already mentioned.

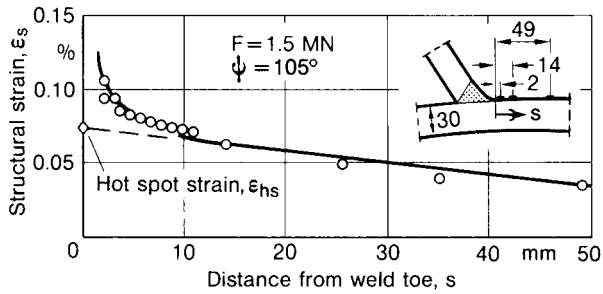


Fig. 8.7. Structural strains measured normal to the weld (mainly from shell bending) and linearly extrapolated to the hot spot at the weld toe, peripheral angle $\psi = 105°$; after EU Report.[740]

Table 8.1. Structural stress concentration factors K_{si}, K_{sc} and K_{hs} of welded tubular joint according to different authors and methods; after Radaj *et al.*[736]

Author	EU Report[740]	Flade	Potvin *et al.*[735]	Words worth[742]	Efthy-miou[106]	Morgan Lee[731–733]	IIW Rec.[204]
Method	Strain gauge	Finite element	Formula FE[a]	Formula AM[b]	Formula FE[a]	Formula FE[a]	Formula FE[a]
K_{si} (K_{sc})	—	4.75	4.44	(4.59)	—	5.13	—
K_{hs}	3.0–3.9	3.53	≈4.0	≈4.26	4.48	—	5.35

[a] FE Finite-element-based.
[b] AM Acrylic-model-based.

8.2.2 Comparison of structural stress concentration factors

The measured and calculated structural stress concentration factors are compared with those of other authors and methods in Table 8.1. The maximum structural stress (first principal stress) is referred to the nominal stress in the brace resulting in structural stress concentration factors. The maximum stresses in the midplane intersection line, index si, in the surface intersection line or 'corner point line', index sc, and in the weld toe notch line or 'hot spot line', index hs, yield the concentration factors K_{si}, K_{sc} and K_{hs}, respectively. The comparison solutions refer to 'balanced axial loading', i.e. the chord tube is supported at both ends.

The strain gauge measurements are taken from the EU Report[740] and are based on the strain gauge arrangement mentioned above, but with non-linear extrapolation of the measured strains to the hot spot (at $\psi = 105°$ from the inner crown point) instead of the linear extrapolation in the report. Additionally, contrary to the EU Report, plane strain conditions are

assumed resulting in 8.5% higher hot spot stresses ($\sigma_1 = E\varepsilon_1/(1 - \nu^2)$ with elastic modulus $E = 2.06 \times 10^5 \text{N/mm}^2$ and Poisson's ratio $\nu = 0.28$). Thus, the stress concentration factors are increased by about 15% resulting in K_{hs} = 3.0–3.9 instead of 2.58–3.56 (the supplementary measurement result, K_{hs} = 4.0, is neglected because it does not fit into the scatter range of the original measurements). A non-linear (e.g. quadratic) extrapolation is recommended (van Wingerde[790,791]) in cases of a non-linear distribution of the measuring results. A non-linear distribution is obvious from Fig. 8.7.

The calculation results of Flade (Radaj *et al.*[736]) are directly evaluated from the finite element model described above, i.e. without any extrapolation procedure. The maximum structural stress in the midplane intersection line occurs at $\psi = 120°$ from the inner crown point, $K_{si} = 4.75$. The maximum structural stress in the weld toe line at $\psi = 130°$ results in $K_{hs} = 3.53$. Direct evaluation is well suited for comparisons of structural stresses but not necessarily so for strength predictions based on endurable hot spot stresses, which are derived from the standard extrapolation scheme.

The structural stress concentration factor at the midplane intersection line of welded tubular joints subjected to balanced axial loading was determined by finite element analysis as early as 1977 by Potvin *et al.*[735] Parametric formulae were derived on the basis of the finite element results. The following formula is valid for the structural stress concentration factor K_s of K-shaped tubular joints:

$$K_s = 1.506\,\delta^{-0.059}\Delta^{0.666}\vartheta^{1.104}\gamma^{0.067}(\sin\theta)^{1.521} \tag{8.1}$$

where δ is the tube diameter ratio, d/D, Δ is the diameter to thickness ratio of the chord, $D/2T$, ϑ is the wall thickness ratio, t/T, γ is the gap width to tube diameter ratio, g/D, θ is the brace versus chord angle, D is the outside diameter of the chord, d is the outside diameter of the brace, T is the wall thickness of the chord, t is the wall thickness of the brace and g is the gap width between the brace tubes on the chord tube surface (see Fig. 3.19). The eccentricity e of the brace intersection point relative to the chord centre line is taken into account in the gap width. The geometric parameters of the tubular joint being considered are D = 1041 mm, d = 500 mm, T = 30 mm, t = 20 mm, $\theta = 60°$, e = 28 mm and g = 56 mm. They are within the range of validity of eq. (8.1). The result is $K_s = 4.44$.

Potvin showed that the experimentally determined hot spot stress concentration factors given by several researchers for the weld toe are about 10% lower on average than the values calculated on the basis of the parametric formulae. This gives $K_{hs} \approx 4.0$ for the tubular joint considered.

Another investigation into the structural stress concentration factors of welded tubular joints subjected to balanced axial loading applicable to the above K-shaped joint was performed by Wordsworth.[742] Acrylic models

were used combined with strain gauge measurements at the hot spot which was detected by brittle lacquer techniques. The tube walls intersect with sharp corners, i.e. without the weld profile. The measured strains are non-linearly extrapolated into the corner point at the intersection of the tube surfaces. The following formulae are derived for the structural stress concentration factors K_{sc} and K_{hs} of K-shaped tubular joints:

$$K_{sc} = \left[\Delta\vartheta\delta(6.78 - 6.42\sqrt{\delta})(\sin\theta)^{1.7+0.7\delta^3}\right] \times \left[1 - (0.012\,\Delta)^{2\gamma/3+0.4}\right]\left[1 - 0.1^{1.3(1+2\gamma)}\right] \tag{8.2}$$

$$K_{hs} \approx \frac{K_{sc}}{\left(1 + \frac{c}{T}\right)^{1/3}} \tag{8.3}$$

where c is the leg length of the weld on the chord surface, and the other parameters are defined after eq. (8.1). The result for the geometric parameters of the tubular joint being considered (including $c = 12.5$ mm) is $K_{sc} = 4.59$ and $K_{hs} \approx 4.26$.

A further evaluation by Efthymiou[106] of hot spot stresses gained by finite element analysis for K-shaped tubular joints subjected to balanced axial loading yielded the following formula for the hot spot stress concentration factor K_{hs}:

$$K_{hs} = \vartheta^{0.9}\Delta^{0.5}(0.67 - \delta^2 + 1.16\delta)\sin\theta\left[1.64 + 0.29\delta^{-0.38}\arctan(8\gamma)\right] \tag{8.4}$$

with the parameters being defined below eq. (8.1). The result for the geometric parameters of the considered tubular joint is $K_{hs} = 4.48$.

A comprehensive finite element analysis performed by Morgan and Lee[731–733] for K-shaped tubular joints subjected to balanced axial loading (and out-of-plane moment loading[733]) resulted in the following parametric formula for the structural stress concentration factor K_s:

$$K_s = \Delta^{0.91}(0.22 - \delta^2 + 1.92\delta)(\sin\theta)^{2.51} \times (-0.81\delta^{-2} + 5.67\delta^{-1} - 4.01)\vartheta^{1.26}(0.13 + 0.12\delta^{-0.41}) \times \arctan\gamma + 0.1\delta^{0.27}\Delta^{0.32}(12.42\vartheta - 0.02)(2\theta)^{0.59\delta} \tag{8.5}$$

with the parameters again being defined following eq. (8.1). The result for the geometric parameters of the considered tubular joint is $K_s = 5.13$.

Finally, the hot spot stress concentration factor was determined according to the IIW fatigue design recommendations[204] for welded hollow section joints resulting in $K_{hs} = 5.35$.

The structural stress concentration factors in Table 8.1 show rather large deviations, especially at the hot spot, but these can be explained to some extent. The difference in stress concentration factors between single- and double-sided supports can be neglected. The factor K_{si} of Potvin is expected to be lower because of a minor element quality. The factor K_{sc} of Wordsworth must be lower because of the stress decrease between mid-plane intersection line and surface corner line. The value $K_{hs} = 3.53$ of Flade is confirmed by the results of measurement in the EU Report, $K_{hs} = 3.0$–3.9, if a 15% increase resulting from non-linear extrapolation is taken into account. The slightly larger values of Potvin and Wordsworth can be explained well by the rough approximations introduced in deriving K_{hs} from K_{si}. Note that deviations of ±10% (if not ±30%) from the result of the parametric formulae have to be expected according to van Wingerde.[190,191] The factor K_{hs} according to the IIW recommendations,[204] $K_{hs} = 5.35$, is conservative because a simpler formulation is used which neglects some of the geometric influence parameters.

8.2.3 Fatigue test results in terms of hot spot stress

The structural stress approach claims (see Section 3.1.3) that the fatigue strength or life up to crack initiation ($a_i \approx 1$ mm) of the welded tubular joint can be derived from fatigue tests with simpler welded specimens if the hot spot stress is chosen as the basis of transfer from the specimen to the tubular joint. The hot spot stresses are taken from the results of measurement linearly extrapolated and evaluated by $\sigma_{hs} = E\varepsilon_{hs}$ without consideration of the plane strain condition, i.e. $K_{hs} = 2.58$–3.56.

The nominal stress S–N curve and service life curve with scatter ranges of a welded angular joint specimen which is used to simulate the fatigue behaviour of a T-shaped tubular joint, Fig. 8.8, are evaluated for that purpose. The applied load spectrum is slightly 'harder' than that of the K-shaped tubular joint (see Fig. 8.2). A correction is therefore applied to the test results based on Miner's rule. The number of cycles up to crack initiation is estimated proceeding from the number of cycles up to through-thickness fracture based on experimental evidence, $N_i \approx 0.4N_t$. The test results for the tubular joint are compared with those for the angular specimen (with N_t corrected and converted to N_i) in Fig. 8.9. The conclusion is that the strength data from the specimens in terms of nominal stress can be used locally as endurable values of the structural stress to assess the fatigue strength of the tubular joint. Note that $K_{hs} = 3.0$ is chosen according to the results of measurement using the linear extrapolation scheme (i.e. deviating from Table 8.1) because the endurable hot spot stresses are thus defined. The relation between S–N curve and service life curve is approximated by Miner's rule modified to the permissible damage sum, $D = 0.5$.

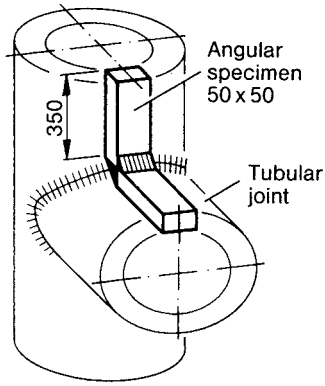


Fig. 8.8. Angular specimen substituting a T-shaped tubular joint in respect of fatigue testing based on structural stresses; after Lachmann *et al.*[730]

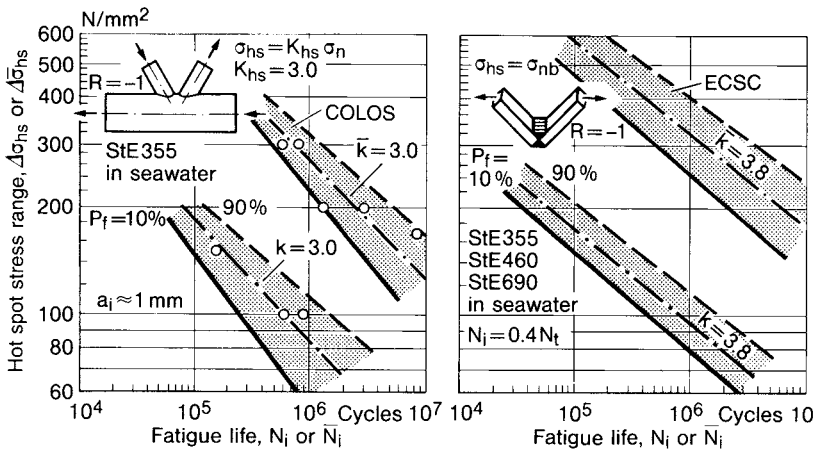


Fig. 8.9. Endurable hot spot stresses in tubular joint (converted nominal stress data[738,739]) compared with endurable nominal stresses in angular specimens (reduced total life data[730,738]), constant- and variable-amplitude loading in seawater; fatigue life up to crack initiation.

The design *S–N* curves and service life curves of hot spot stress applicable to the considered welded tubular joint are taken from the British Department of Energy (DEn) Guidance,[91] Fig. 8.10. These solid line curves designate the failure probability $P_f = 2.3\%$ corresponding to two standard deviations from the medium strength. Failure is defined as a through-thickness crack. The diagram additionally contains the corresponding curves from the fatigue tests with the angular specimen, both crack initiation

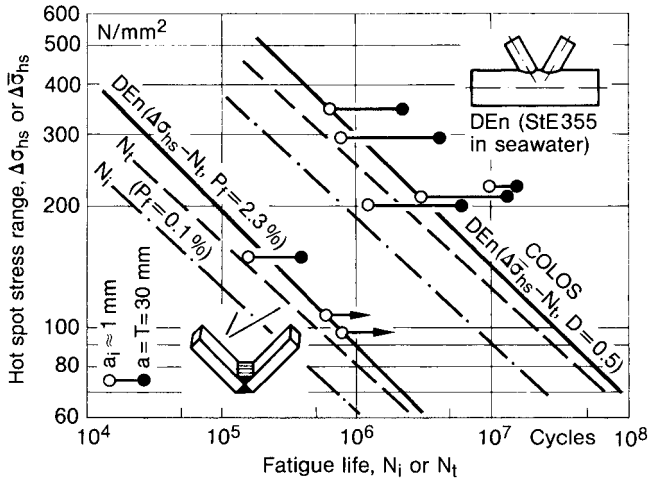


Fig. 8.10. Fatigue test results of welded tubular joints in seawater compared with design curves based on hot spot stress, constant- and variable-amplitude loading in seawater, fatigue life up to crack initiation and up to a through-thickness crack; after Sonsino *et al.*[738,739]

and total fracture curves with the failure probability $P_f = 0.1\%$. The latter value can be recommended for defining permissible stresses. The fatigue test results with the considered welded tubular joint are drawn as point-limited lines across these curves, both for crack initiation and through-thickness crack formation.

The hot spot stress curves according to DEn guideline[91] are well suited for assessing the fatigue strength or service life of welded tubular joints. The test results from the considered tubular joint are found to be well on the safe side of the relevant curves. The hot spot stress design curves for tubular joints in other codes and also in the revised DEn guideline run higher so that the safety margins are reduced.

8.3 Application of the elastic notch stress approach

The (non-extrapolated) structural stress at the hot spot defined as the observed crack initiation point (in the case considered at $\psi = 105°$ from the inner crown point) is needed as the basic stress in the subsequent notch stress and strain analysis. It is taken from the finite element analysis of Flade,[736] $\sigma_{hs} = 163.5\,\text{N/mm}^2$ for $F = 1.5\,\text{MN}$. The maximum structural stress at the toe notch line of the finite element model occurs at $\psi \approx 130°$ and is about 17% larger. It is superimposed by the notch effect which depends heavily on the fabrication-dependent local toe radius. If the toe radius is

locally increased, the point of maximum notch stress may be shifted to $\psi = 105°$. The difference in notch stresses is smaller in the elastic-plastic range and probably superimposed by scattering hardness values.

The elastic notch stress concentration factor of the weld toe at the hot spot ($\psi = 105°$) is determined by a plane cross-sectional model (in finite elements) subjected to prescribed end displacements (including end rotations) taken from the three-dimensional tubular joint model, Fig. 8.11. The

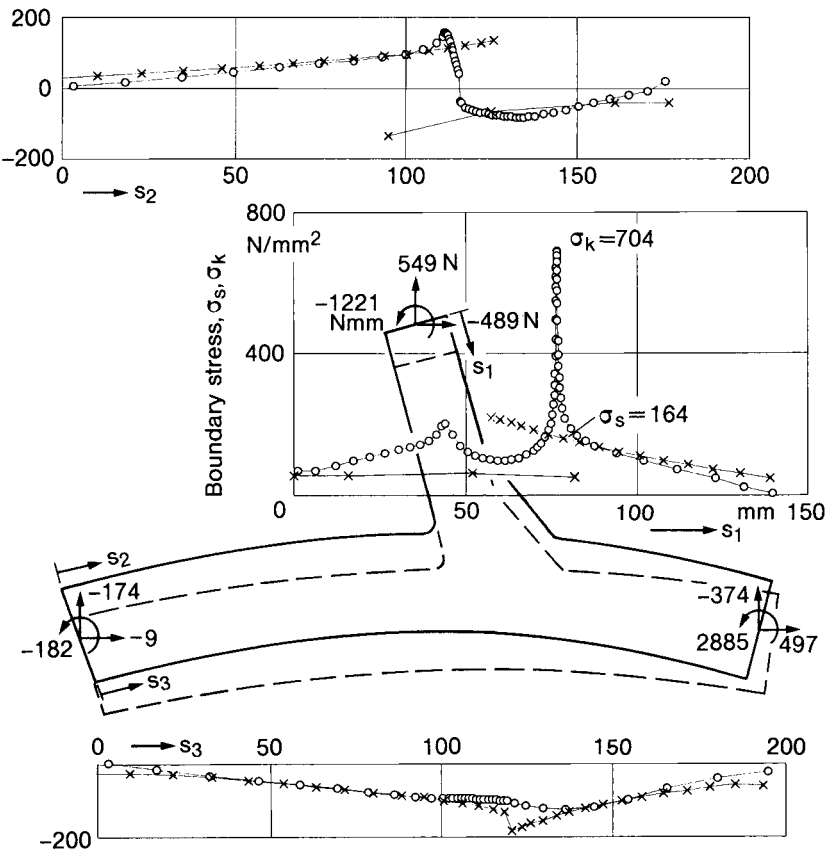


Fig. 8.11. Plane cross-sectional notch stress model of weld area at hot spot (notch radius $\rho = 0.5$ mm) subjected to prescribed end displacements and rotations (25 times enlarged in the plot) derived from three-dimensional tubular joint model (brace force $F = 1.5$ MN); resultant reaction forces at ends, boundary stresses plotted over contour lines (circle points) compared with structural stresses from tubular joint model (cross points); after Radaj *et al.*[736]

principal stress directions in the three-dimensional model approximately coincide with the orthogonal directions of the weld seam (at the hot spot) so that the plane model is positioned according to the principal directions (but this is not a necessary condition). The transfer of the end displacements is an alternative to the hitherto well-proven procedure which transfers the end forces (see Section 4.2.8). The support needed for the non-equilibrated forces is advantageously avoided, but the displacements must be transferred with high accuracy.

The shape parameters of the weld correspond to worst case values measured in the hot spot area of the weld: toe radius ρ = 0.5 mm and toe angle $\theta = 45°$. The undeformed and deformed contours of the cross-sectional model are shown in Fig. 8.11 together with the resultant reaction forces at the ends of the model. The edge stress curves inclusive of the notch stress peaks are arranged above and below the model. They are plotted over coordinates along the edge lines. The structural stresses of the three-dimensional model are included for comparison. The correspondence of the stresses in front of the weld according to the notch stress and structural stress model (circle points and cross points) is unsatisfactory at a larger distance from the weld toe but rather good adjacent to it. The notch stress concentration factor results as K_t = 4.30 (referring to the hot spot stress σ_{hs} = 163.5 N/mm^2). Major deviations between the stresses occur in those areas where the three-dimensional model has a too coarse mesh and (necessarily) where this model fails to simulate the actual cross-sectional shape.

The finite element analysis of the plane cross-sectional model is performed under plane strain conditions because this is the prevailing local condition in the three-dimensional model. The stress concentration factors of the first principal stress and the von Mises equivalent stress are identical under this condition, but the referenced stresses are not. A factor of $(1 - \nu + \nu^2)^{1/2}$ (i.e. 0.894 for Poisson's ratio $\nu = 0.28$) has to be applied to the first principal stress to obtain the equivalent stress.

The elastic notch stress analysis above is repeated with the toe notch radius ρ = 1 mm in order to apply the notch rounding approach (version according to Seeger) in the endurance limit range. The maximum fatigue-effective notch stress relating to F = 1.5 MN is calculated as $\bar{\sigma}_k$ = 575 N/mm^2 or $\bar{\sigma}_{k\,eq}$ = 514 N/mm^2, giving $K_f = \bar{\sigma}_k/\sigma_{hs}$ = 3.51.

The endurance limit of the welded tubular joint without seawater corrosion in terms of the brace force range is assessed on the basis of the endurable notch stress data (for ρ = 1 mm) determined for welded joints in the comparable structural steel of type St52-3 by Olivier *et al.*,[259,260] see Table 4.5. The result is shown in Table 8.2. The predicted force ranges for $R = -1$ are slightly higher than the few test results.

Table 8.2. Endurable brace force ranges without seawater corrosion, predicted on the basis of endurable notch stress data for welded joints in type St52-3 structural steel from Table 4.5 combined with $\bar{\sigma}_k = 575\,N/mm^2$ for $\rho_f = 1\,mm$

Welded tubular joint in structural steel	Technical endurance limit ΔF_E [MN] ($N = 2 \times 10^6$, $P_f = 50\%$)		True endurance limit[a] ΔF_E^* [MN] ($N = 2–5 \times 10^6$, $P_f = 50\%$)	
	$R = -1$	$R = 0$	$R = -1$	$R = 0$
Stress-relieved	1.29	0.92	1.10	0.81
As-welded	1.23	0.94	—	—

[a] Designation 'true' is objectionable, see Section 2.2.2.

8.4 Application of the elastic-plastic notch strain approach

8.4.1 Notch stress and strain concentration at weld toe

The elastic-plastic notch stresses and strains are determined for the cross-sectional model under plane strain conditions assuming that the plastification is locally concentrated and elastically supported so that the elastic conditions in the three-dimensional structure are not changed. The calculation is based on the cyclic stress–strain curve described by the Ramberg–Osgood relationship, eq. (5.23).

Different stress–strain curves are valid for parent material, heat-affected zone and weld metal, Fig. 8.12. The cyclic stress–strain curve of the heat-affected zone runs markedly higher than the other two curves. The reason for this hardening effect is the different microstructure due to the thermal cycles introduced by the (multi-layer) welding process. Crack initiation was originally allocated to this zone. Therefore, its material constants are used in the assessment of strength and life up to crack initiation. The relevant curve is derived from small-scale specimens which had been subjected to the thermal cycles of the heat-affected zone (after Prowatke *et al.*,[268] for the heat-affected zone with static material parameters $\sigma_{Y0.2} = 616\,N/mm^2$ and $\sigma_U = 875\,N/mm^2$). Hardness measurements at the crack initiation site, Fig. 8.13, confirmed the relatively high hardness values at 2 mm below the surface, with a further increase to a maximum value of 362 HV1 at 0.3 mm below the surface, which are points in the heat-affected zone in both cases. These are acceptable maximum values in welded joints. However, the very first microcrack was initiated in a thin surface layer (about 0.2 mm thick) which belongs to the fusion zone. A hardness peak of nearly two times the

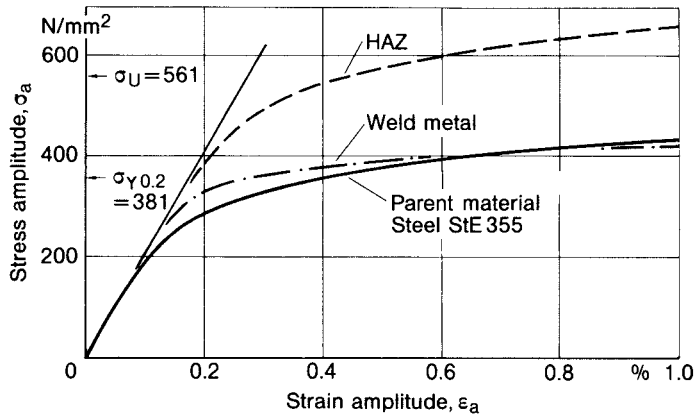


Fig. 8.12. Cyclic stress–strain curves of type StE355 structural steel, parent material in the normalised condition, heat-affected zone (HAZ) and weld metal; after Prowatke *et al.*[268]

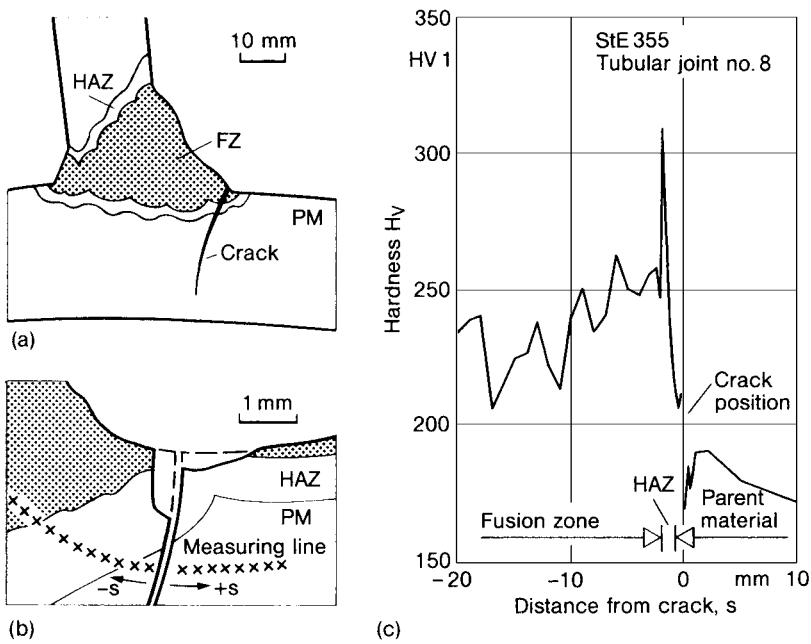


Fig. 8.13. Macrograph of the welded tubular joint in the hot spot area with crack initiation at the toe notch (a), micrograph of the crack initiation site at a peripheral distance of 20 mm from the macrograph and with hardness measuring line at a distance of 2 mm below the surface (b), as well as measured hardness curve (c); (FZ: fusion zone, HAZ: heat-affected zone, PM: parent material); after Radaj *et al.*[736]

parent material value occurs close to the crack initiation point in the heat-affected zone.

The procedures available for calculating the elastic-plastic notch stresses and strains in the cross-sectional model under plane strain conditions are compared considering the case where $F = 1.5\,\text{MN}$ and $\sigma_{k\,eq} = 0.89 \times 704 = 627\,\text{N/mm}^2$ ($K_t = 4.30$, $\rho = 0.5\,\text{mm}$) together with the parent material parameters (after Prowatke *et al.*,[268] for the parent material with static material parameters $\sigma_{Y0.2} = 381\,\text{N/mm}^2$ and $\sigma_U = 561\,\text{N/mm}^2$), Fig. 8.14. These are the Neuber hyperbolae for sharp and mild notches, respectively, starting at the elastic stress concentration, eqs. (5.28) to (5.31), Sonsino's empirical correction of Neuber's sharp notch formula in respect of mild notches, eqs. (5.32) and (5.33), and the finite element solution based on the program MARC. The finite element solution is the most reliable one because it takes the actual shape and loading conditions into account. Neuber's and Sonsino's solutions on the other hand have the advantage of a simple functional representation with Neuber's mild notch formula being the more general one. The latter formula is chosen for the further calculations.

The von Mises yield criterion is combined with the usual isotropic yield and strain hardening laws in the finite element solution. The cyclic curve of the von Mises stress as a function of the equivalent total strain according to the octahedral shear strain criterion is used in the approximative solutions with the Poisson's ratio determined according to Gonyea[362] from the cyclic stress–strain curve, eq. (5.51).

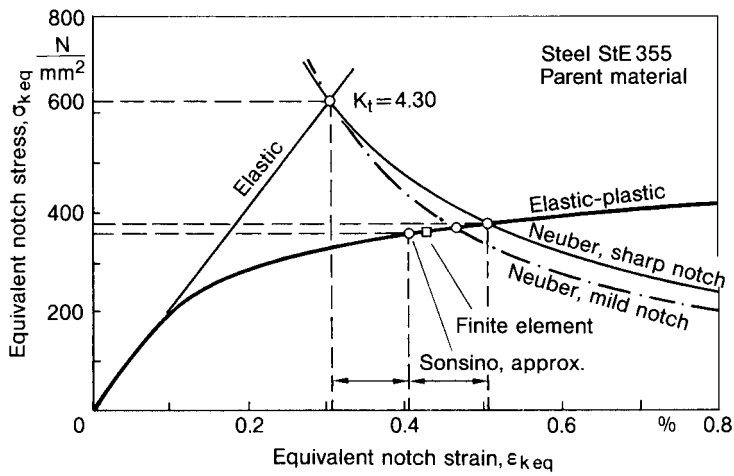


Fig. 8.14. Notch stresses and strains at hot spot of tubular joint, calculation results for the cross-sectional model using parent material parameters; procedures according to Neuber and Sonsino compared with finite element analysis; after Radaj *et al.*[736]

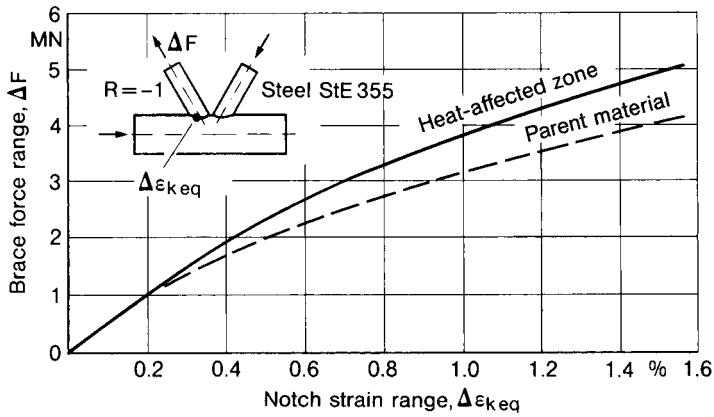


Fig. 8.15. Load–strain curves for point of crack initiation (hot spot) at weld toe (notch radius $\rho = 0.5$ mm) of tubular joint, calculation results from elastic three-dimensional finite element model of the tubular joint combined with elastic-plastic cross-sectional two-dimensional model; equivalent notch strain range as a function of brace force range; after Radaj *et al.*[736]

The load–strain relationship (or yield curve) at the notch root in the hot spot area is determined on the basis of the cyclic stress–strain curves for the heat-affected zone and the parent material in comparison, Fig. 8.15. The equivalent strain according to the distortional strain energy criterion, eqs. (5.48) to (5.52), is evaluated under the plane strain conditions of the model.

8.4.2 Fatigue strength assessment based on notch strains

The fatigue strength and life assessment is performed on the basis of the yield curve determined above in connection with the strain *S–N* curve of the heat-affected zone. The latter curve is plotted in Fig. 8.16 together with the relevant curves for parent material and weld metal. The curves are derived from fatigue tests with small-scale specimens after simulation of the relevant thermal cycles and then expressed by the four-parameter relationship according to Manson and Coffin, eq. (5.24), without the mean stress term. The endurance limit values of the heat-affected zone are markedly higher than the parent metal values because of the hardening effect, at least in unnotched specimens. The two curves merge into one another in the low-cycle fatigue range but the appertaining stresses remain markedly higher in the heat-affected zone (see Fig. 8.12).

The numerical combination of the yield curve of the weld toe notch at the hot spot of the tubular joint with the strain *S–N* curve, both for the heat-affected zone, gives the endurable force range of the tubular joint as

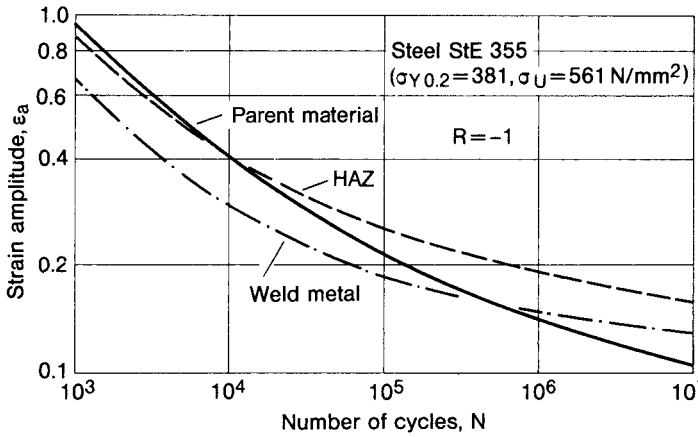


Fig. 8.16. Strain *S–N* curves of StE355 structural steel, parent material in the normalised condition, heat-affected zone (HAZ) and weld metal; after Prowatke *et al.*[268]

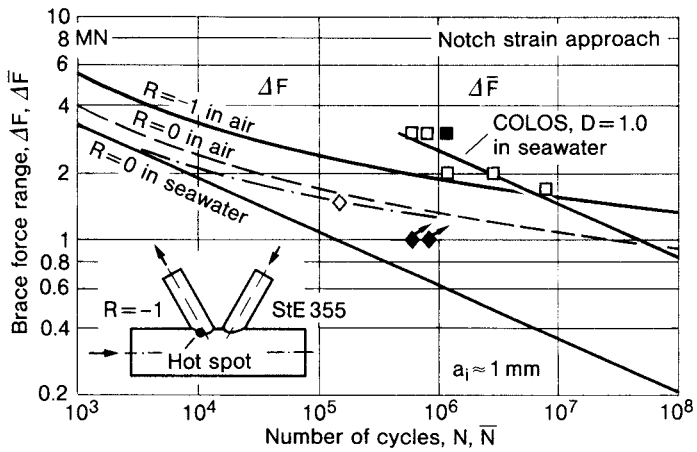


Fig. 8.17. Predicted crack initiation fatigue strength and life (combined *F–N* and $\bar{F}$–$\bar{N}$ curve diagram covering constant- and variable-amplitude loading) of welded tubular joint according to notch strain approach (for notch radius ρ = 0.5 mm using heat-affected zone material parameters) compared with test results; black points designate tests in air, white points tests in seawater, lower three points tests with constant-amplitude loading, upper six points tests with variable-amplitude loading; after Radaj *et al.*[736]

function of the number of cycles to crack initiation (a_i = 0.5–1.0 mm), the *F–N* curve according to Fig. 8.17 (R = –1, without residual stresses and without seawater corrosion). The curve runs flatter than the design stress curves in the codes (k = 3.0 or 3.5). The steeper slope in the codes is related

to full-size welded structures showing higher elastic notch support in the critical area (Gimperlein,[25] see Fig. 5.29).

The notch strain approach is principally applicable to obtain the *F–N* curve under the influence of residual stresses and also the reduction by the effect of seawater corrosion. But the information on the residual stresses caused by welding is missing in the case under consideration and material data covering local corrosion fatigue under seawater are not available (whereas a local approach to corrosion fatigue would be available[743]). Therefore approximative global approaches are applied to assess the effects mentioned above.

Introducing the assumption that high tensile residual stresses reaching the yield limit occur at the weld toe notch of the tubular joint, it is an often applied procedure to consider the *F–N* curve for $R = 0$ without residual stresses as applicable to the condition $R = -1$ with residual stresses. The reduction of the *F–N* curve for $R = -1$ by the factor 0.71 in the life range considered is based on the well-established local endurance limit values of Olivier *et al.*[259,260] for welded joints in high strength steel, see Table 4.5 (352/494 = 0.71, corresponding to the mean stress sensitivity, $M = 0.4$, resulting from 494/352 – 1, an acceptable value for hardened steels which are comparable to the heat-affected zone conditions here considered).

On the other hand, Olivier *et al.*[259,260] present local endurance limit values for $R = -1$ in the stress-relieved and as-welded condition which give the factor 0.95 (see Table 4.5). The conclusion is that the specimens in the investigation used for reference did not contain major tensile residual stresses in the as-welded condition. What the residual stress state in the tubular joint considered really was remains unanswered.

Corrosion fatigue in seawater works in the direction of shorter lives. A procedure accepted by many experts and some design codes is to introduce the factor 0.5 for the lives in the medium-cycle fatigue range and to prolong the inclined *F–N* curve without a change in slope into the high-cycle fatigue range. Such a fictitious *F–N* curve starting with the slope of the calculated *F–N* curve at $N = 10^3$ cycles ($k = 4.23$) is used to establish a safe service life curve for the tubular joint under the wave load standard spectrum of the North Sea (Common Load Sequence COLOS[729]) according to Miner's rule with the permissible damage sum, $D = 1.0$ (unmodified value because of the extremely conservative assumptions under which the *F–N* curve was lowered). The combined *F–N* and $\bar{F}$–$\bar{N}$ diagram in Fig. 8.17 additionally contains the available test results (for $a_i \approx 1$ mm, mainly in seawater). They are in agreement with the predicted curves.

The assessment scheme above includes considerable uncertainties despite the high degree of correspondence with the test results: the calculated hot spot stress value at $\psi = 105°$ used as the basis (this stress is 17% larger at $\psi \approx 130°$), the *F–N* curve in air on the basis of the notch strain

approach, the effect of corrosion by seawater on fatigue and the appropriate hypothesis of damage accumulation under variable-amplitude loading. The unexpectedly large uncertainty in the *F–N* curve in air is now considered in more detail.

Three variants of the underlying assumptions are equally acceptable in the present unsatisfactory state of development of the notch strain approach for welded joints:

- Variant I: Prediction of the *F–N* curve on the basis of the heat-affected zone material parameters for $R = -1$ with the residual stresses being neglected.
- Variant II: Prediction of the *F–N* curve on the basis of the heat-affected zone material parameters for $R = -1$ with assumed high tensile residual stress taken indirectly into account by using the *F–N* curve for $R = 0$, the latter derived on the basis of the mean stress sensivity $M = 0.4$ (as shown above).
- Variant III: Prediction of the *F–N* curve on the basis of the parent material parameters (also as an approximation for the material parameters of the weld metal) for $R = -1$ with assumed high tensile residual stresses reaching the cyclic yield limit, $\sigma_m = \sigma_{rs} = \sigma'_{Y0.2}$, using the strain *S–N* curve equation inclusive of the mean stress effect according to Manson, Coffin and Morrow, eq. (5.24).

The result of the comparative calculations according to the three variants is plotted in Fig. 8.18 together with two available test results (tests trun-

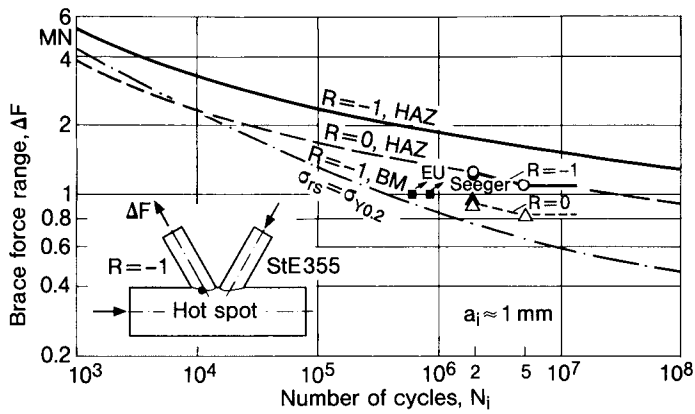


Fig. 8.18. Predicted crack initiation fatigue strength and life of welded tubular joint, three variants of plausible engineering assumptions applied (see text), test results (EU) by comparison and endurance limit values according to notch stress approach (Seeger); after Radaj *et al.*[736]

cated without crack initiation) and with the endurance limit values which resulted from the notch stress approach, using the version according to Seeger, Table 8.2. The latter results are statistically founded.

The difference between the strength values, determined under similarly acceptable assumptions, is unexpectedly large, at least in the medium- and high-cycle fatigue range. The conclusion is that the notch strain approach, including its assumptions is not yet sufficiently well defined in respect of welded joints. The following effects should be further investigated in order to stabilise the procedure.

The first such effect described by Seyffarth[737] is the difference between the heat-affected zone parameters of small-scale specimens subjected to simulated thermal cycles and of specimens cut from the heat-affected zone. It is maintained that small-scale specimens present too high cooling rates. Bohlmann[351,352] has therefore modified the heat-affected zone parameters gained from small-scale specimens in a comparable case (see Section 5.3.5) resulting in a markedly lower F–N curve.

A second such effect is the inhomogeneity of material and hardness at the weld toe which may cause excessive plastic strains adjacent to the hardness peak (Clormann[355,356]). It could be seen from the macrograph and micrograph of Fig. 8.13 that the microcrack started in the fusion zone so that the parent material parameters which are similar to the weld metal parameters are closer to reality than the heat-affected zone parameters. But the strain-controlled fatigue behaviour of the inhomogeneous material at the notch root is not sufficiently understood.

A third such effect is the possible deviation of the plastic strain S–N curve from the linear behaviour in double logarithmic scales in the high-cycle fatigue range (see Klee[373]).

A further effect is relevant in the special case being considered without being method-typical. The predicted F–N curves would run at least 10% lower if the higher structural stress at $\psi \approx 130°$ had been taken as the basis of the notch strain approach.

8.5 Application of the crack propagation approach

8.5.1 Basic crack propagation models

The crack propagation analysis[740,741] starts with an initiated crack of depth a_i = 1 mm. Two different models are used. The first one is a three-dimensional model including the notch effect of the weld toe, Fig. 8.19(a). It consists of a base plate with thickness T = 30 mm (equal to the thickness of the chord wall) and width W = 1000 mm (equal to one half of the length of the intersection line between brace tube and chord tube). A transverse attachment is fastened to one side by means of a groove and fillet weld

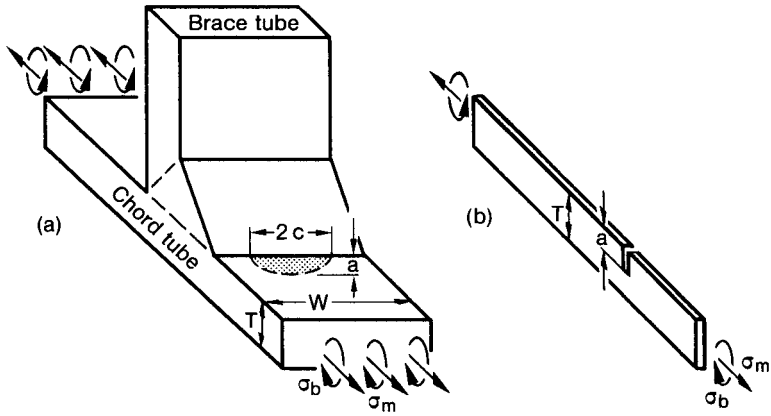


Fig. 8.19. Models simulating crack propagation in welded tubular joint; three-dimensional model including the notch effect (a) and two-dimensional model without notch effect (b); after EU Report.[740]

(T butt joint). A semi-elliptical surface crack is assumed at the weld toe perpendicular to the plate surface. The membrane and bending stresses acting in the base plate correspond to the structural stresses perpendicular to the weld seam measured or calculated at the weld toe of the tubular joint. The other structural stress components at the weld seam, i.e. transverse and longitudinal shear stresses, are neglected so that the crack is subjected mainly to mode I loading.

The stress intensity factor range, ΔK, at the deepest point of the crack is calculated using the superposition according to eq. (6.17). The geometry factors at the deepest point of the semi-elliptical crack, Y_m and Y_b, are determined according to Newman and Raju.[546, 547, 595] The magnification factors, M_{km} and M_{kb}, are derived based on a solution presented by Neuber[252,253] considering a crack at the root of a semi-elliptical notch. The stress concentration factor K_t at the weld toe is approximated by a formula proposed by Köttgen *et al.*[243] for angular welded joints:

$$K_t = 1.12\left(\frac{T}{\rho}\right)^{1/3.1} \tag{8.6}$$

where T is the base plate thickness and ρ is the weld toe radius.

The magnification factor $M_k = M_{km} \approx M_{kb}$ is evaluated from Neuber's solution (introducing the relevant values for a, ρ and K_t) for $T = 30\,\text{mm}$, $\rho = 0.3$, 1.0, 5.0 mm and varying crack depth a, Fig. 8.20. Obviously, this factor can be considered to be approximately independent of the assumed notch radius or stress concentration factor for crack depths $a \geq 0.5\,\text{mm}$. The crack

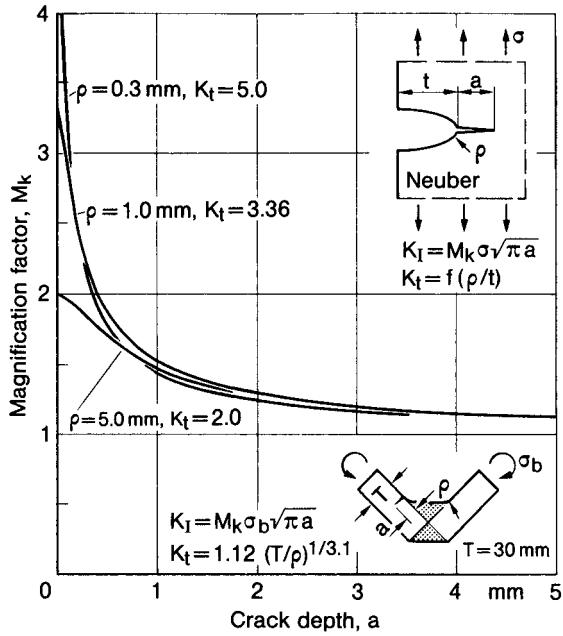


Fig. 8.20. Magnification factor M_k on stress intensity due to notch stress concentration dependent on crack depth for different notch radii; solution by Neuber for semi-elliptical notch transferred to welded angular joint; after Vormwald,[741] in EU Report.[740]

propagation analysis starts with the initial crack size, $a_i = 1\,\text{mm}$, resulting in $M_k = 1.5$.

A second simplified model used in the crack propagation approach[740] is gained by neglecting the three-dimensional character of the crack and also the notch effect. The resulting two-dimensional model is the straight-fronted crack at the edge of an oblong plate subjected to tensile and bending loading, Fig. 8.19(b), well known as the SEN-specimen (single-edge notch). The corresponding stress intensity factor as a function of crack length can be found in various compendia.[543,601,609,628] Crack propagation is once more analysed between the initial crack depth, $a_i = 1\,\text{mm}$, and the final crack depth equal to the plate thickness, $a_f = T = 30\,\text{mm}$.

The material constants m and C defining the crack propagation rate in the structural steel of type StE355 under consideration (parent metal and heat-affected zone), Fig. 8.21, are the following:

$$m = 2.86, \quad C = 5.3 \times 10^{-13}\ [\text{N, mm}]$$
$$(R = 0, P_f = 50\%, \text{in air})$$
$$m = 3.28, \quad C = 7.5 \times 10^{-14}\ [\text{N, mm}]$$
$$(R = 0, P_f = 50\%, \text{in artificial seawater}, f = 1\,\text{Hz})$$

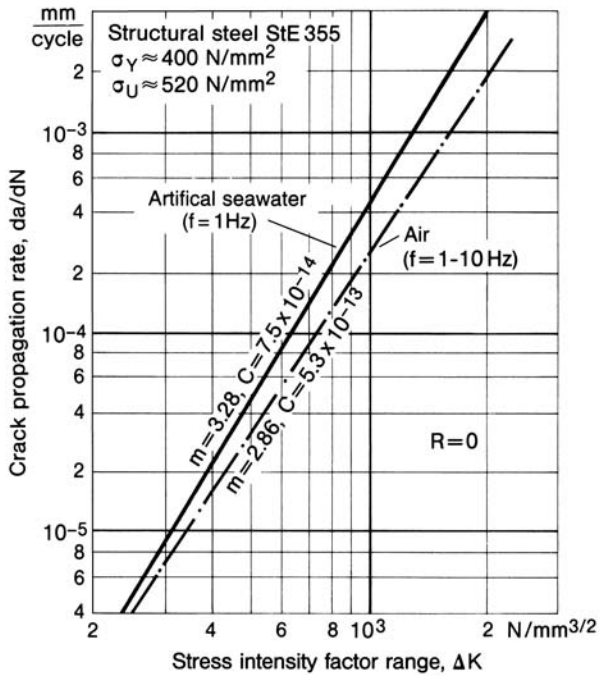


Fig. 8.21. Crack propagation rate dependent on stress intensity factor range for type StE355 structural steel in artificial seawater and in dry air (mean values); after EU Report.[740]

The corresponding constants m and C for $R = -1$ are approximated based on the above values. The constant m remains the same. The constant C is introduced twice as large in combination with the effective stress intensity factor range, $\Delta K_{\text{eff}} = \Delta K/2$, so that the crack propagation rate is slowed down. The calculations are performed with the constants for $R = 0$ combined with unreduced values of ΔK in order to take high tensile residual stresses into account.

8.5.2 Crack propagation life according to EU Report

The crack propagation calculation using the Paris equation was first performed based on the two-dimensional model without notch stress concentration. The following conditions were introduced:

- initial crack size, $a_i = 1\,\text{mm}$;
- final crack size, $a_f = T = 30\,\text{mm}$;
- variable-amplitude loading according to the wave load standard spectrum COLOS for the North Sea and occasionally constant-amplitude loading for comparison;

- axial load range in the chord, $\Delta\overline{F} = 3\,\text{MN}$, corresponding to the total structural stress range, $\Delta\overline{\sigma}_S = \Delta\overline{\sigma}_m + \Delta\overline{\sigma}_b = 294\,\text{N/mm}^2$ (maximum value of the spectrum at the hot spot according to measurement evaluated from the linear extrapolation scheme);
- ratio of bending to membrane structural stress, $\Delta\overline{\sigma}_b/\Delta\overline{\sigma}_m = 3.0$ (strain measurements at the joint actually gave $\Delta\overline{\sigma}_b/\Delta\overline{\sigma}_m = 10.3$);
- material constants m and C together with ΔK for $R = 0$ (despite remote loading with $R = -1$, effect of tensile residual stress) introduced first over the whole plate thickness and then only for $a \leq T/5 = 6\,\text{mm}$, supplemented by $\Delta K_{\text{eff}} = \Delta K/2$ and $R = -1$ in the remaining portion;
- artificial seawater as ambient medium (no cathodic protection) and occasionally air for comparison.

The crack propagation calculation[740] was then performed based on the three-dimensional model with notch stress concentration. The following additional condition was introduced:

- constant aspect ratio, $a/c = 0.4$, based on trial calculations starting with various smaller cracks, and alternatively, $a/c = 0.067$, based on the experimental findings at the tubular joint, taking multiple crack formation and coalescence of microcracks into account.

Interaction effects in variable-amplitude loading were considered to be negligible because the calculations for constant- and variable-amplitude loading resulted in similar life ratios in comparison to the experimental results.

High tensile residual stresses in the neighbourhood of the weld seam which reach the yield limit must generally be assumed for welded joints in the as-welded condition if residual stress measurements are not available. The calculation of crack propagation with m, C and ΔK for $R = 0$ is generally a conservative approximation. The assumption of high tensile residual stresses only for $a \leq T/5 = 6\,\text{mm}$ is based on measurement results at a T-shaped tubular joint by Payne and Porter-Gof[734] (claimed to be the sole residual stress measurement performed on welded tubular joints up to 1990 according to the EU Report[740]).

The results of the crack propagation calculation with the two models subjected to variable-amplitude loading according to the (truncated) standard spectrum COLOS (reduced to $\Delta\overline{\sigma}_s = 200\,\text{N/mm}^2$ or $\Delta\overline{F} = 2.04\,\text{MN}$) introducing m, C and ΔK for $R = 0$ are listed in Table 8.3 and compared with the results of fatigue testing. The crack propagation life, $N_p = 5 \times 10^6$ cycles, corresponds to about 10 years of service in the North Sea.

The crack depth dependent on number of cycles according to the two models (two-dimensional and three-dimensional) with residual stresses for $a \leq T/5 = 6\,\text{mm}$ are compared with the experimental findings in Fig. 8.22 for

Table 8.3. Calculated crack propagation life compared with results of variable-amplitude fatigue tests ($\Delta\bar{\sigma}_s = 200\,N/mm^2$ or $\Delta\bar{F} = 2.04\,MN$); after EU Report,[740] *ibid.* Figs. 130 and 141

Crack propagation life $a = 1 \rightarrow 30\,mm$	Calculation ($P_f = 50\%$)		Fatigue tests (5 joints)	
	2d model	3d model	min	max
N_p [cycles]	6.1×10^6	7.7×10^6	5.7×10^6	11.4×10^6

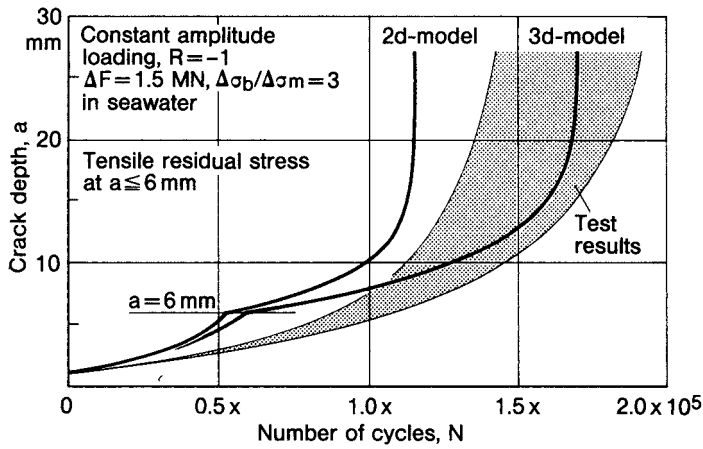


Fig. 8.22. Fatigue crack propagation in welded tubular joint under constant-amplitude loading in artificial seawater; calculation compared with scatter band of test results; after EU Report.[740]

constant-amplitude loading and in Fig. 8.23 for variable-amplitude loading of the tubular joint according to the standard spectrum COLOS ($\Delta\bar{\sigma}_s = 294\,N/mm^2$ or $\Delta\bar{F} = 3\,MN$). The change in the residual stress condition at $a = 6\,mm$ is well visible in the first case but not so well in the second case where the irregularities caused by the subdivision of the load spectrum are superimposed.

The conclusion is that the crack propagation life of the considered tubular joints can be determined according to the crack propagation approach using the simple two-dimensional model, the material constants for $R = 0$ together with an unreduced ΔK value and the structural stress range at the weld toe in the critical area (hot spot).

The neglect of the notch stress concentration seems to be compensated by the neglect of the support effect at the semi-elliptical crack front when considering the stress intensity factor at its deepest point (load shedding).

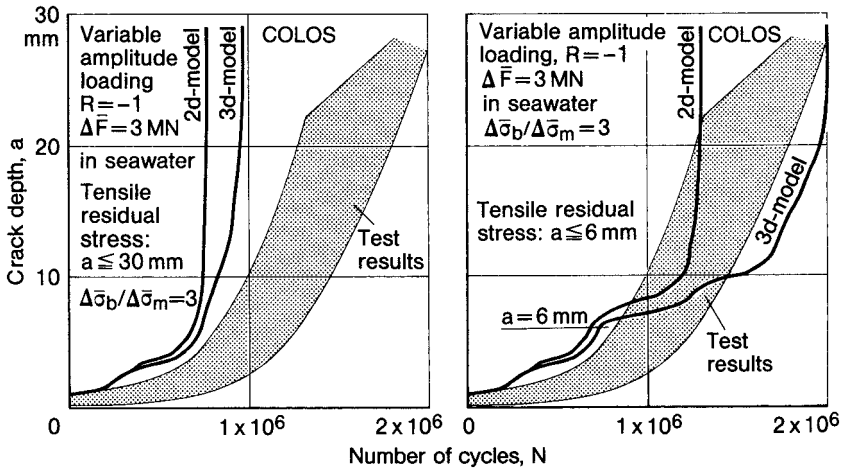


Fig. 8.23. Fatigue crack propagation in welded tubular joint under variable-amplitude loading (Common Load Sequence COLOS); calculation based on two different assumptions on residual stress distribution compared with scatter band of test results; after EU Report.[740]

The assumption of high tensile residual stresses is essential for conservative calculation results.

The calculation results presented above refer to the failure probability $P_f = 50\%$, i.e. mean propagation rates and mean service lives are determined. Both the actual scatter of the input values and further uncertainties in the applied models have to be taken into account when defining the design life of crack propagation, N_p. The (computational) failure probability $P_f = 10^{-3}$ may be appropriate for structural members which are subjected to regular inspections, whereas $P_f = 10^{-6}$ may be prescribed for structural members which cannot be inspected and are not redundant.

The scatter range of the crack propagation life of five tubular joints was $T_N = N_{10}/N_{90} = 1/2.07$, i.e. much smaller than the corresponding scatter range of crack initiation at the same joints ($T_N = 1/3.55$). The safety factor j_{Np} is defined based on the above scatter range and another factor j^*_{Np} is introduced for the uncertainties of the model, thus resulting in the permissible crack propagation life, $N_{p\,per}$:

$$N_{p\,per} = \frac{N_p(P_f = 50\%)}{j_{Np} j^*_{Np}} \tag{8.7}$$

Definite values of the safety factors on the fatigue strength of welded tubular joints are not proposed in the EU Report[740] because the number of fatigue tests was still too small for that purpose.

8.5.3 Crack propagation life according to British Standard

An assessment of crack propagation life was also performed for the three-dimensional model on the basis of the British fatigue design standard BS7608[15] when updating the results of the EU Report[740] for this book. The conditions introduced in the calculation are the same as those stated above on the basis of the EU Report with the following modifications:

- ratio of bending to membrane structural stress $\overline{\sigma}_b/\overline{\sigma}_m = 10.3$ as suggested by strain measurements;
- aspect ratio of the semi-elliptical crack not constant but increasing from $a/c = 0.067$ to $a/c \approx 0.14$ during crack propagation (calculation result with the stress intensity factor at the deepest points of the semi-elliptical crack);
- material parameters m and C (upper bound values) for $R = 0$ together with ΔK for $R = -1$ over the total plate thickness.

The calculation of the stress intensity factor range, ΔK, according to BS7608[15] (*ibid*. Section D.7.2) is performed with the data and results listed in Table 8.4. The parameters and functions in the table are assigned both according to BS7608 and according to eq. (6.17). The crack size and the crack shape functions in BS7608 are based on the solution of Newman and Raju,[546,547,595] i.e. on the same solution which is used in the three-dimensional model of the EU Report. This solution refers to the semi-elliptical crack in a plane plate of finite thickness, i.e. without the weld notch.

Prediction of the crack propagation life has been performed for variable-amplitude loading of the tubular joint based on the standard spectrum

Table 8.4. Input parameters for calculation of stress intensity factor ranges at the end points of semi-axes a and c of a semi-elliptical initial crack in welded tubular joint ($\Delta\overline{F}$ = 3 MN), see eq. (6.17) for parameter definition

BS7608, D.7.2	a	c	B	W	$\Delta\sigma_a$	$\Delta\sigma_b$	$\Delta K_{(Q)}$	$\Delta K_{(S)}$
Equation (6.17)[a]	a	c	T	W	$\Delta\sigma_m$	$\Delta\sigma_b$	$\Delta K_{(a)}$	$\Delta K_{(c)}$
	1 mm	15 mm	30 mm	1000 mm	26 N/mm^2	268 N/mm^2	737.0 N/mm$^{3/2}$	831.2 N/mm$^{3/2}$
BS7608, D.7.2	M_{ka}	M_{kb}	$F_{a(Q)}$	$F_{b(Q)}$	$F_{a(S)}$	$F_{b(S)}$	ϕ	
Equation (6.17)[a]	M_{km}	M_{kb}	$Y_{m(a)}$	$Y_{b(a)}$	$Y_{m(c)}$	$Y_{b(c)}$	ϕ	
	1.464	1.298	1.127	1.082	0.320	0.316	1.0084	

[a] Separate equations for semi-axes a and c.

Table 8.5. Predicted crack propagation life of tubular joint subjected to the wave load standard spectrum of the North Sea; load sequence COLOS, $\Delta\bar{F} = 3\,\text{MN}$, $R = -1$, with material parameters m and C for $R = 0$

	BS7608, D.7.2 3d model	EU Report 2d model	EU Report 3d model
Crack propagation life, N_p	3.6×10^6 cycles	1.73×10^6 cycles	1.21×10^6 cycles

COLOS. The maximum values of this spectrum are identical with the stress ranges calculated using the input parameters of Table 8.4. The results of the life calculation according to BS7608 in comparison to those according the models in the EU Report are presented in Table 8.5. The latter models show slightly higher life values in relation to the left-hand diagram in Fig. 8.23 as a result of the higher bending stress portion in the revised calculation.

8.6 Method-related conclusions

The review above on the application of the local approaches to a welded tubular joint was intended to demonstrate some shortcomings and benefits of the local approaches, together with the necessary expenditure and expertise. The aim was to learn by actual application and comparison with experimental results. Therefore, the conclusions do not primarily refer to the in-service behaviour of the considered tubular joint but to the features of application of the local approaches.

An obvious handicap of the local approaches applied to the welded tubular joint is the uncertainty in respect of decisive local parameters. The notch geometry at the weld toe is largely scattering. Notch radii $\rho = 0.5$–$10\,\text{mm}$ and toe angles $\theta = 25$–$45°$ have been measured according to the EU Report.[740] Performing the analysis with $\rho = 0.5\,\text{mm}$ and $\theta = 45°$ means a worst case consideration which may be too conservative. It is probable that the point of crack initiation (the hot spot) will depend more on the accidental values of the geometric notch parameters than on the measured or calculated structural stress distribution.

Another local parameter which may have influence on the fatigue strength is the residual stress state, especially in the hot spot area. The residual stress state can be traced by local approaches if the initial state is defined. This initial residual stress state is unknown in the case considered. The assumption of high tensile residual stresses is once more a worst case assumption which may be unrealistic. The martensitic hardening in the heat-affected zone may reduce the tensile residual stresses by transformation strains. Additionally, the initial residual stress state depends in a

complicated manner on the layer sequence in the multilayer weld. It is changed in the set-up loading cycle and during variable-amplitude loading.

A third local parameter with major influence on the results is the material condition at the crack initiation point. A hardness peak of nearly two times the parent material value occurs at the crack initiation point in the heat-affected zone which results in additional plastic strains in front of the peak, as mentioned above. The hardness peak is included in the material parameters of the heat-affected zone but the increased plastic strains adjacent to the peak are neglected.

An indication of the amount of resulting uncertainty in the critical areas of the tubular joint is the fact that crack initiation and crack propagation were observed to be non-reproducible in the details. Considering the nine welded joints tested, crack initiation occurred at different peripheral angles including the crown point with only a slight preference for the angle chosen as hot spot position in further investigations. The cracks may initiate at several locations and may propagate in a manifold and mutually interactive manner.

Better control of the manufacturing conditions may render the problem of uncertain local parameters less severe but it will remain a problem typical of welded joints.

Another problem is the scatter of test results. The fatigue tests comprised nine full-size welded tubular joints. This is a large number considering the fact that the test pieces are expensive to manufacture and to test. On the other hand, using only nine test specimens does not allow the desired statistical evaluation of test results. The scatter ranges of manufacture are certainly larger than those of the usual small-scale welding specimens. Empirical knowledge in the scatter of test results related to welded joints in general was introduced to draw the experimentally determined *S–N* curves. Also the damaging process in the test specimens could not be observed with the desired uniformity and reproducibility. This means that the calculation results could only be compared with single results. It seems unrealistic to discuss details such as the inverse slope of the *F–N* curve of the tubular joint on this unsatisfactory basis.

The uncertainties in the local parameters and in the test results mentioned above together with the diversity of possible local approach versions and variants in detail makes it possible to produce any desired result on this basis. The procedures are adjusted in respect of input parameters, modelling assumptions, strength hypotheses and damage criteria among others. Of course, the adjustment (calibration) is performed on the basis of the available (uncertain) knowledge from testing, but the remaining latitude for possible argumentation remains large. The results of the strength and life assessment therefore rest on the adjustment of the calculations to the experimental results gained from the tubular joint being considered. Any

procedure taking place without incorporating knowledge from the component tests would have failed to predict the component life in the North Sea with sufficient certainty.

Adjustment of the calculation procedures to the results of the component tests is a necessary means of keeping the assessment close to reality. The term 'calibration' is used if the adjustment is performed with sufficient expertise. Re-calibration is necessary and usual with growing theoretical and empirical knowledge or with an extended number of component variants.

The following design situations can be handled with benefit on the basis of calibrated calculation procedures, whereas component testing is often too expensive for this purpose:

- Further design and loading variants have to be assessed relative to the tubular joint being considered.
- The effectiveness of definite design or manufacturing measures has to be assessed.
- Optimisation of the design and its manufacture in respect of fatigue strength and service life is demanded.

The application of the local approaches to the tubular joint demonstrated in this chapter did not extend to these options.

9

Structural stress or strain approach for spot-welded and similar lap joints

9.1 Basic procedures

9.1.1 Significance of fatigue assessment of spot-welded and similar lap joints

Spot-welded and similar lap-joints (the latter gas metal arc or laser beam welded) in thin-sheet materials are constitutive in the construction of automobiles. They are the prevailing joining method in structural components of automobiles: car body, chassis components, truck cab, van box. A conventional car body contains several thousands of spot welds. Today they are substituted to some extent by GMA or laser beam seam welds, and also by non-thermal joining methods such as riveting, bolting, clinching and bonding. The space frame concept for car bodies including hydroformed tube-like components without flanges is a forward-looking design variant needing seam welds for joining. Despite the above-mentioned competitive joining methods, spot welding will remain important at least for thin-sheet structures in mild or low-alloy steels (in contrast to aluminium alloys) because it is a cheap and robust joining method. Spot-welded and similar lap joints are also of some importance in the construction of passenger train carriages, but the demands on fatigue strength and relevant design optimisation are less severe in comparison with automobile construction.

The significance of fatigue assessment related to the considered automobile components on the basis of calculation methods (mainly finite element based) is accurately described by Fermér and Svensson[768] as follows: 'The use of calculations and simulations is a key feature of the modern design process. Several properties such as strength, stiffness, durability, handling, ride comfort and crash resistance can today be numerically analysed with varying levels of accuracy. Development time can be shortened by ensuring that some, or rather all, of these properties fulfil established requirements even before the first prototype is being built. Calculations based on fatigue life and accurate loading histories permit

structures and components to be optimised for durability without the need for expensive and time-consuming testing of series of prototypes. Thus designs can be obtained that are less conservative (i.e. better optimised) than those based on traditional criteria, such as maximum load or stress for a series of standard load cases'.

The number of finite-element-based calculations related to fatigue assessments is large for all manufacturers of automobiles. Fatigue failures often originate from spot-welded and similar lap joints (about 90% of all cracks occurring in car bodies in service). This explains the large interest in relevant calculation methods. Method development projects were repeatedly initiated by industrial users and carried out by university institutes and research laboratories in cooperation with software suppliers with the objective of making fatigue life predictions for spot-welded and similar lap joints more accurate and reliable.

9.1.2 Principles of the structural stress approach

The fatigue assessement procedure for spot-welded and similar lap joints in automobiles can be subdivided into the following three steps needed for the fatigue life prediction (Fermér and Svensson[768]).

A good knowledge of the 'load–time histories' and their statistical distribution is of fundamental importance for acceptable predictions. In a first step, these load data are either measured in comparable designs or prototypes, or they are generated through numerical simulations (multi-body vibration systems consisting of rigid frames, point masses, spring and damper elements, see Radaj,[4] today incorporated in 'multi-body-system' codes. This non-local first procedural step is not considered further in the following.

In a second step, some kind of local stress or strain at the weld spot, characteristic of fatigue failure, is established in order to predict the fatigue life in the final step described below. The radial structural stress at the 'hot spots' where failure may occur is well suited for this purpose, at least for relative assessments. It may be used directly or modified by additional influence parameters related to the not explicitly considered notch effect (the structural stress is defined as being linearised over the plate thickness, see Fig. 10.7(b)), or related to the different effects of membrane and bending stresses. A theory is needed (and available) which allows calculation of the structural stresses at the weld spot edge from the weld spot forces. The direct calculation on the basis of a fine-meshed finite element model of the weld spot is too expensive in general for industrial use.

The final step is the fatigue life prediction. The fatigue life of spot-welded and similar lap joints is most frequently based on experimantally determined *S–N* curves, where a suitable structural stress σ_s (or structural strain,

or notch stress, or notch strain, or stress intensity factor, etc.) is related to the number of cycles to failure, N. Failure is mostly defined as a crack penetrating the plate thickness. Single-spot tensile-shear and peel-tension specimens are fatigue-tested besides structure-like multi-spot specimens such as hat section and H-shaped specimens. Rainflow cycle counting together with Miner's accumulated damage rule (with various modifications) is applied to assess the effect of variable-amplitude loading. Linear elastic fracture mechanics following the crack path may be used to achieve a higher degree of accuracy.

The use of local stresses or strains in connection with suitable S–N curves for the fatigue assessment of spot-welded joints is a straightforward procedure of general applicability, but an effort was also made in one case to get along with endurable joint face forces without any further stress analysis (Di Fant-Jaeckels *et al.*[759]).

The second and final steps of the fatigue assessment procedure are first described in more detail referring to the approach proposed by Rupp and Grubisic,[821–828] with basic contributions by Radaj,[803–808] Fig. 9.1. The

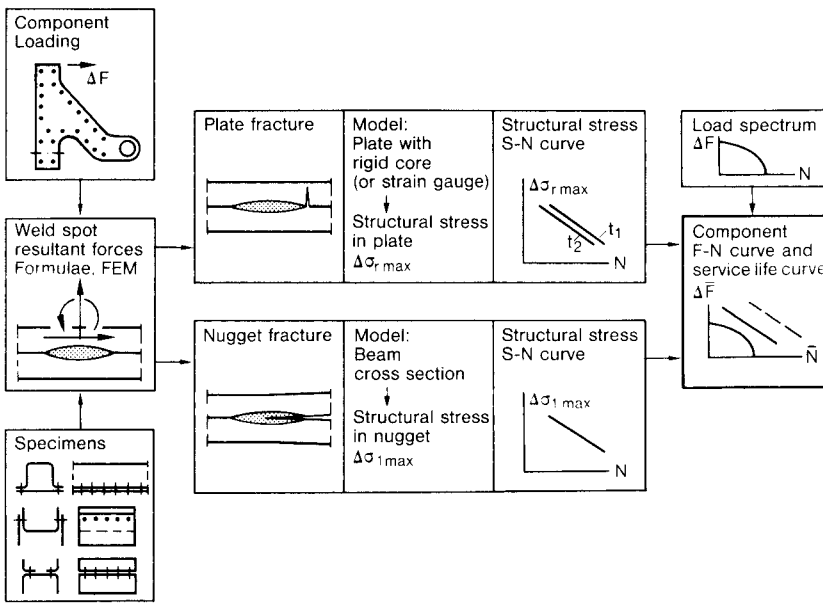


Fig. 9.1. Structural stress approach, version according to Rupp and Grubisic,[821–828] to assess the fatigue strength and service life of spot-welded structural components; with $\Delta\sigma_{r\,max}$ maximum radial stress range approximately equal to maximum von Mises equivalent stress range $\Delta\sigma_{s\,eq\,max}$; with $\Delta\sigma_{1\,max}$ maximum principal stress range according to maximum normal stress criterion; with ΔF cyclic external force, $\Delta\bar{F}$ maximum cyclic external force, N and $\bar{N}$ numbers of cycles to failure, $t_1 < t_2$ sheet thickness, and FEM meaning 'finite element method'; after Radaj.[5]

maximum structural stresses at the weld spots of the structural component (an axle suspension arm is shown in the figure) are set in relation to endurable values derived from fatigue tests with component-like specimens (the hat section and H-shaped specimens are shown in the figure). Structural stresses are chosen as fatigue-relevant quantities which are determined from the resultant internal forces and moments in the joint face of the weld spot (shear forces, cross-tension force and bending moments, the torsional moment being neglected) both in the structural component and in the specimen. The eigenforces, defined in Section 9.2.3, are neglected, too. Two types of potential fatigue fracture are considered in the assessment of fatigue strength under constant-amplitude loading and service life under variable-amplitude loading, the plate fracture occurring at weld spots with a sufficiently large diameter (initiated at the weld spot edge in the high-cycle range or outside the heat-affected zone in the low-cycle range) and the nugget fracture in the joint face prevailing at weld spots with a diameter chosen non-conservatively.

In the case of plate fractures, the maximum radial structural stress on the inner plate surface at, or adjacent to, the weld spot edge is considered to initiate the fractures. This stress is approximately equal to the maximum equivalent stress after von Mises, which is considered to be decisive for fracture initiation in ductile materials. The maximum stress is calculated from engineering formulae which are derived from a rigid core model of the weld spot. It can also be estimated on the basis of strains measured on the outer plate surface at, or adjacent to, the weld spot edge, thereby gaining information on the resultant weld spot forces and moments. The static and cyclic radial stresses from calculation or measurement are transformed to equivalent cyclic radial stresses with a zero stress ratio based on the Haigh diagram. The transformed stresses from the different resultant weld spot forces and moments are superimposed. The maximum transformed stress is determined. Structural stress S–N curves are derived from the fatigue test results related to plate fractures. These curves differ with plate thickness to some extent, thus substantiating a thickness-dependent factor in the assessment procedure. The criterion for stopping the fatigue test is a definite loss of global stiffness of the specimen caused by cracks at the weld spot edge penetrating the plate thickness. Finally, the maximum radial structural stresses in the structural component are set in relation to the endurable stress in the specimen.

In the case of nugget fractures, a specially defined maximum structural stress at the nugget edge is considered to initiate the fractures. This stress is calculated from the resultant weld spot forces on the basis of the beam bending theory. The weld nugget is considered to be axially extended to a compact circular cylinder, the end faces of which are loaded by the weld spot resultant forces and moments acting in the middle plane of the plates.

The maximum equivalent stress is determined from the bending normal stress and the transverse shear stress according to the maximum normal stress criterion which is considered to be decisive for fracture in brittle materials. This is performed separately for the static (or mean) and cyclic (or amplitude) components of the normal and shear stresses. The cyclic stress with a non-zero static component is transformed to an equivalent cyclic stress with a zero static component on the basis of the Haigh diagram. The maximum cyclic equivalent stress at the weld spot edge is extracted. This maximum structural stress is limited by an *S–N* curve gained from the fatigue test results related to nugget fractures.

It is a feature of the considered approach that the calculation of linear damage accumulation according to a modified Miner's rule after rainflow cycle counting and mean stress correction is also performed on the level of the structural stresses. This calculation is carried out both in respect of plate fractures and nugget fractures at intervals on the weld spot edge, evaluating the fatigue-relevant stresses in different planes in each point. That combination of edge point and sectional plane that gives the highest damage sum is considered to be critical. The large amount of calculation involved with this 'local critical plane criterion' is necessary only in such cases where different, more or less arbitrary, load–time functions are superimposed within the structural component.

The fatigue assessment procedure for spot-welded joints based on structural stresses as described above (approach after Rupp and Grubisic) is well established for industrial use. But it fails to take the eigenforces in the lap joint into account, which may have a major influence on the service life to be predicted. The importance of the eigenforces was independently recognised by Sheppard[982,983,985] and Radaj.[807,808] The contributions by Sheppard are predominantly related to the design of a simplified weld spot model compatible with coarse meshes (see Section 9.2.2) and to the derivation of the failure-relevant structural stresses from this model (continued by Pan[972]). The adequacy of the structural stress as a fatigue parameter is proven on the basis of a simplified crack propagation approach. The contributions by Radaj, on the other hand, provide the relationships between the weld spot resultant forces and the structural stresses at the weld spot edge within a general theory (see Section 9.2.4). Henrysson[960] has proposed an approximation resembling Sheppard's approach to include the eigenforces (see Section 11.3.4).

The structural-stress-based fatigue assessment procedure for seam-welded joints (fillet welds) in thin-sheet materials is characterised, similar to the spot weld procedure, by coarse meshes of thin-shell elements describing the structure, by rigid or stiff elements representing the seam weld and special structural stress *S–N* curves. The focus of modelling is directed to

the weld toe where fatigue fractures may be initiated. Definite modelling rules must be followed to guarantee comparable results. The details of the procedure are presented in Section 9.4.5. This procedure deviates substantially from the hot spot structural stress definition used for seam-welded 'thick-shell' or 'thick-plate' structures (see Chapter 3).

9.1.3 Weak points of the structural stress approach

The application of the structural stress approach may involve various weak points. Some of them may be overcome by more adequate finite element modelling and evaluation or by procedural modifications with regard to the endurable stresses. Others are more profound and can only be removed by applying the crack initiation and crack propagation approaches which provide a higher resolution of local phenomena. The robustness of the structural stress approach is lost thereby.

A weak point of the Rupp–Grubisic version of the approach (besides the missing torsional moment in the joint face forces) is the fact that only those structural stresses are introduced as relevant to fatigue which can be attributed to the weld spot resultant forces in the joint face. But there are also structural stresses generated by self-equilibrating forces in each of the two overlapping plates which are termed 'eigenforces'. Actually, it is not a problem to evaluate the eigenforces together with the joint face forces in coarse finite element meshes as shown by Sheppard[982,983] or Henrysson,[960] and the structural stresses from eigenforces are automatically included in the case of a fine mesh at the weld spot. In coarse meshes, modelling rules must be obeyed with regard to the weld spots in the structure in order to obtain the weld spot forces correctly.

Other complications of the approach may arise from large deflections and/or from contacts between the overlapping sheets. The support and equilibrium conditions in the structure are thus changed. It is not a problem to take these effects into account by adequate finite element procedures. The same is true for local plastic deformations occurring at higher load levels with the implication that it is better to use structural strains instead of structural stresses when defining endurable quanities.

A more severe problem with the structural stress approach is the fact that the notch effect of the weld spot edge is completely neglected (it varies with the local loading condition) and that the varying crack initation and propagation processes (inclusive of crack closure) are not explicitly taken into account. These limitations are revealed to some extent by the necessity to use structure-related instead of material-related *S–N* curves. The *S–N* curves in tensile-shear loading (bending and membrane stresses superimposed) and peel tension loading (pure bending stress state) differ to some

extent (the peel-tension curve runs above the tensile-shear curve and has a greater gradient). Combined with the above, a pronounced effect of plate thickness is observed (higher endurable stresses in the thinner sheet material). The problem is solved within the structural stress approach by taking correcting measures in the basic procedure. The two *S–N* curves mentioned above collapse by introducing a suitable factor on the bending or membrane stresses (Rupp *et al.*,[821,824,827,828] Henrysson[960]). The effect of plate thickness is taken into account by a thickness-dependent factor on the stresses (Rupp *et al.*[821,824,827,828] and Zhang *et al.*[846,847]) or by modifying the endured load cycles by a thickness parameter (Henrysson[960]). The original structural stresses are thus converted to more and more fictitous quantities with a limited range of applicability.

Any more accurate or more general method must describe the notch effect and the processes of crack initiation and propagation in more detail, whereby the robustness of the method is lost. The structural stresses remain the basis of these more sophisticated approaches which are described in Chapters 10 and 11.

The weak points considered above with regard to spot-welded lap joints occur also with seam-welded lap joints in thin-sheet material and are overcome here in a similar way.

9.1.4 Application of the structural stress approach

The structural stress approach for spot-welded structural components was developed by Rupp and Grubisic mainly on behalf of the German automobile industry, but is now used in other companies too. It is well established for industrial use and supported by a software tool supplementing the finite element code MSC-Nastran with regard to fatigue life analysis (Heyes and Fermér[776]). Other automobile manufacturers in Europe, in the USA and in Japan prefer the stress intensity approach (see Chapter 10). Advanced versions of the approach may be based on structural stresses and through-thickness crack propagation (Fermér and Svensson[768]). A substantially different form of the structural stress approach was developed and successfully applied by Mayer *et al.*[794–796] (see Section 9.4.7).

The structural stress approach for seam-welded thin-sheet structures proposed by Fayard *et al.*[763–765] and Fermér *et al.*[766,768] has a great potential for general recognition by industrial users, but notch stress and strain approaches supplemented by crack propagation analysis are serious competitors. The successful application of the structural stress approach to spot-welded and seam-welded car bodies tested systematically under constant- and variable-amplitude loading was demonstrated by Fermér *et al.*[767] based on accurate statistical evaluations.

9.2 Analysis tools – structural stress or strain evaluation

9.2.1 General survey

The analysis tools described hereafter in Sections 9.2–9.4 comprise the following items: computational and measurement procedures to obtain the weld spot resultant forces (joint face forces and eigenforces) and therefrom the maximum structural stresses at the weld spot, the analysis of gross elastic-plastic material behaviour and large deflections including buckling fatigue, the presentation of endurable structural stresses from fatigue tests mainly with component-like specimens, comparison of these data with relevant values from the literature, formulae for considering the influence of mean stress, the calculation of damage accumulation, the description of computerised procedures of fatigue strength or life evaluation for spot-welded structures and also the similar situation with seam-welded lap joints.

It should be noted that the bibliography is restricted to references dealing with structural stress assessment. The large body of literature based solely on weld spot forces (Radaj[4]) is not included. Contributions referring to fatigue strength evaluations for spot welds on the basis of notch stresses or strains, crack propagation or stress intensity factors are reviewed in the relevant chapters following hereafter.

9.2.2 Modelling of weld spot resultant forces

The large finite element models of car bodies and similar structural components, characterised by hundreds of thousands of elements and millions of unknowns, include the weld spots positioned at overlapping flanges. The flanges are represented by two rows of rectangular thin-shell elements in general, with the weld spot nodal points on the middle line between the rows ('coarse' weld spot model). A comparable mesh design on the basis of triangular elements is shown in Fig. 9.2. The mesh patterns of the overlapping flanges are congruent. The two weld spot nodal points are connected by a single rigid bar or stiff beam, thus taking the eccentricity of the two nodal points into account. The reduction of the weld spot nugget to a line element between the flange midplanes changes the deformation characteristics of the flange plates substantially (increased flexibility). Therefore, it is usual to prescribe as a modelling rule that the length and width of the shell elements should be approximately twice as large as the weld spot diameter.

Further compensation is possible by increasing the shell thickness towards the weld spot nodal point (Rui *et al.*,[820] 'selective thickening' after Sheppard and Strange[985]). Additional beam elements between the shell elements on

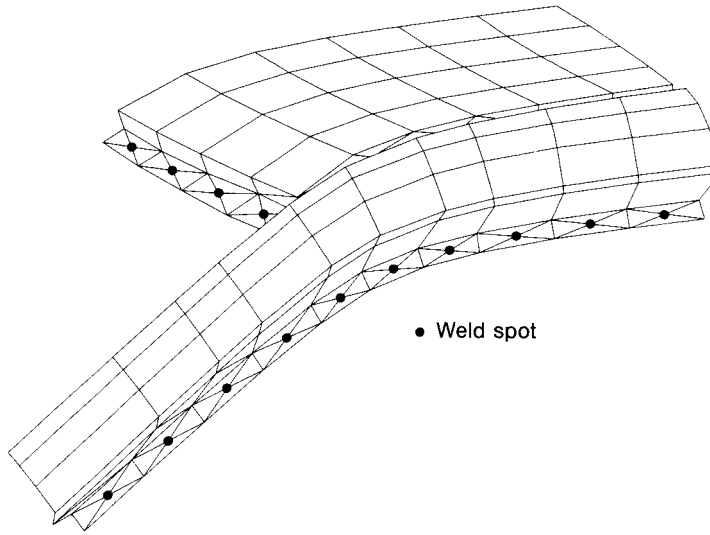


Fig. 9.2. Thin-shell element model (coarse mesh) of the roof pillar of a passenger car with the weld spots marked, applied for the determination of structural stiffness and weld spot forces; after Radaj.[4]

the meshlines intersecting at the weld spot nodal point, necessary for the transfer of torsional moments (shell elements have no in-plane torsional stiffness in their nodal points), may also be used as bending stiffeners instead of selective thickening (Hahn *et al.*[774]). In the fatigue assessment code FEMFAT, the area inside the weld spot periphery is (automatically) modelled by quadrilateral shell elements with an increased elastic modulus, four centre elements surrounded by a ring of eight outer elements where the structural stresses are directly evaluated without reference to the weld spot resultant forces (Brenner *et al.*[750]). Salvini *et al.*[831] proposed the combination of the single beam representing the weld spot with radial beams representing the connection to the surrounding shell elements (coarse mesh), the latter beams being introduced as rigid near the weld spot centre and as elastic near the shell elements (complicated analysis for determining the equivalent elastic beam properties, effect of eigenforces not included). The measures summarised above are necessary to model the spot-welded overlap joint simultaneously in respect of deformation and internal forces. Correct weld spot resultant forces are only gained with correct modelling of deformations because the global structure is statically indeterminate. The local structural stresses at the weld spot cannot directly be evaluated from this coarse weld spot model (with the exception of the refined weld spot model in the code FEMFAT) but only indirectly from the

weld spot resultant forces or from the deformations at some distance around the weld spot. Dong *et al.*[760] show that the mesh insensitivity of the structural stress results is enhanced by equlibrating the stresses with the element nodal point forces in the weld spot periphery instead of evaluating element or nodal point stresses.

Historically, it has been a long development process from the first car body model based on framework elements without simulation of the flanges as early as 1970 to the 'classical' single bar model described above, in 1990. There are simpler variants of the model in use, the most important one being the merging of the two weld spot nodal points into one nodal point. It has also been proposed that the weld spot be simulated by a single quadrilateral shell element with four collapsing nodal points (Vopel and Glas,[841] Vopel and Hillmann[842]). Further proposals include multi-bar instead of single-bar models, with finer meshing of the weld spot area being an often prohibitive precondition: two spoke rims connected by a single bar in their centre points (rim diameter equal to spot diameter) or several connecting bars at the periphery of the weld spot instead of a single one in its centre (Sheppard and Strange[985]). The weld spot is also successfully modelled as a rigid cylindrical core (Radaj,[803,806,814] Henrysson[960]) or by a coarse-meshed elastic cylindrical core (Zhang and Richter[846]). The driving force behind these developments was the fact that continously connected flange roots without flange simulation produce a torsional stiffness of the car body which is up to 30% too high. Also, the local deformations are poorly represented.

Further development of modelling procedures in recent years has made arbitrary meshes on each of the overlapping flanges and arbitrary weld spot positions within these meshes possible. This allows large substructure models to be prepared in parallel by independent teams. This reduces the total modelling time substantially. Also, the weld spots can easily be rearranged without any change in the finite element mesh, which is important in the phase of structural optimisation that aims at highest possible structural stiffness. These newly developed procedures use the displacement functions (or 'shape functions') of the relevant shell element(s) to define the deformation condition at the two ends of the connecting element(s) between the two flanges (advantageously, by formulating multipoint constraint equations). The two-times-four apex points of the weld spot edge (apex points referring to an orthogonal mesh) are usually chosen as connection points in order to take the size of the weld spot into account. The apex points are directly connected by four out-of-plane beam elements (Dunst[761]) or, alternatively, by a single hexahedronal element (Heiserer *et al.*[775]). They can also be connected first to the weld spot centre points by four in-plane beam elements in each flange, which are then connected by a single out-of-plane beam (Jonscher *et al.*[778]). Obviously, only the last-

mentioned method of connection provides the possibility of evaluating the weld spot resultant forces as in the 'classical' method (at least 'in principle').

9.2.3 Computation and decomposition of weld spot resultant forces

The weld spot resultant forces are determined from the single-bar model described above by evaluating the forces (inclusive of the moments) in the two nodal points of the bar or beam element and in the corresponding nodal points of the shell elements connected to them, Fig. 9.3. Only one of two orthogonal sectional planes is shown in the graph. There is no axial force assigned to the beam element in the original graph presented by Sheppard and Strange.[985] Note that the total axial force is equilibrated within both orthogonal sectional planes.

The joint face forces which common fatigue assessments exclusively use are derived from the forces in the upper or lower beam nodal point by applying the equilibrium condition: identical axial and transverse (i.e. shear) forces, but the bending moment modified by the offset transverse force times half the plate thickness. It is a widespread error to assume that the loading state of a weld spot is unambiguously described by the joint face (resultant) forces. A definite joint face force can be associated with quite different support conditions, Fig. 9.4, or, alternatively, with quite different remote loading conditions, Fig. 9.5. Not only the joint face forces are relevant to fatigue but also those forces (inclusive of moments) which are

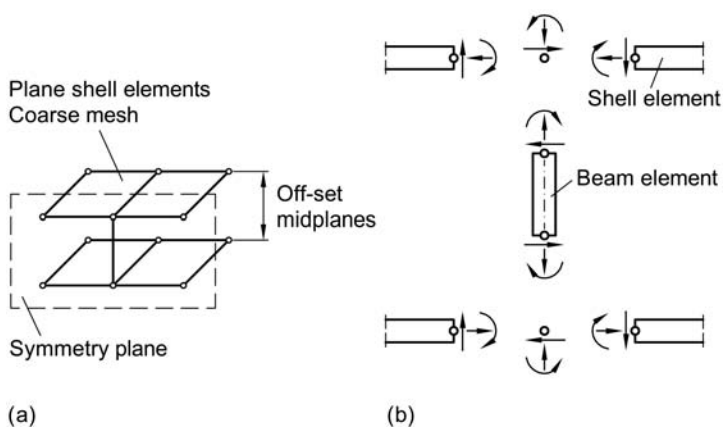


Fig. 9.3. Determination of the weld spot resultant forces (inclusive of the moments) from the element nodal point forces (b) in the beam-to-shell element model (a) of the weld spot subjected to tensile-shear and cross-tension loading; after Sheppard and Strange[985] (modified).

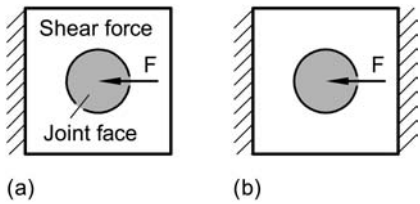


Fig. 9.4. Same joint face force in the weld spot combined with single-sided (a) and double-sided (b) support of the plate; after Radaj.[898]

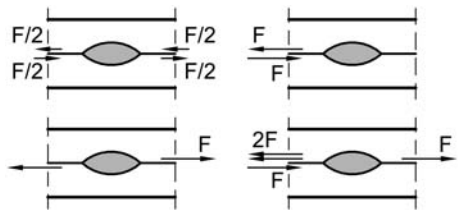


Fig. 9.5. Same joint face force in the weld spot combined with different remote loading conditions of the joint; after Radaj.[898]

equilibrated within the plates without producing a joint face force. These self-equilibrating forces are termed 'eigenforces'. The significance of the eigenforces was independently realised by Radaj and Sheppard. In addition to the above, constraint stresses may be generated in the joint face without resultant joint face forces. They may be treated as minor secondary effects (Radaj[807,808]).

Joint face forces and eigenforces are defined as equilibrium systems acting on the upper and lower plate, respectively. The systems in the two plates are different in general; only the forces in the common joint face are identical with opposite signs. The systems are considered in two orthogonal sectional planes. Any general load system in one plate and one sectional plane may be decomposed into symmetric and antisymmetric parts which constitute the components of the joint face force and eigenforce systems. It is not possible to assign symmetry and antisymmetry exclusively to one of the two systems because symmetry and antisymmetry definitions depend on arbitrary sign conventions for the tensor components.

Two examples are given. The general shear loading state of one half of the weld spot is decomposed into the systems of antisymmetric joint face forces and symmetric eigenforces, Fig. 9.6. The peel-tension loading state, on the other hand, may be decomposed into the systems of symmetric and antisymmetric joint face forces represented by cross-tension force and bending moment, Fig. 9.7.

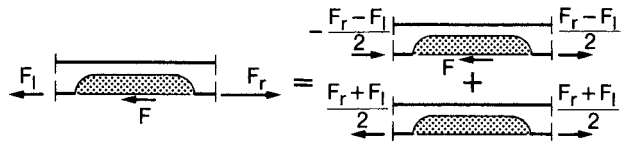


Fig. 9.6. Decomposition of general shear loading of the weld spot into the systems of anti-symmetrical joint face forces and symmetrical eigenforces (indices: l left-hand side, r right-hand side).

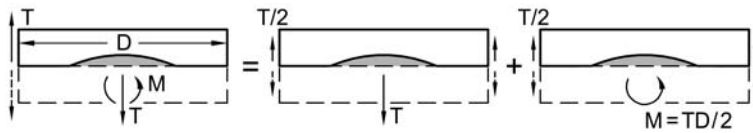


Fig. 9.7. Decomposition of peel-tension loading of a spot-welded joint into cross-tension and bending moment loading in the joint face; after Radaj.[898]

The infinite variety of possible loading states at weld spots are reduced by decomposition to a finite number of basic loading cases, which are superimposed (Radaj[807,808,813,814]). The separation into joint face force and eigenforce systems takes the place of the older proposal[4,803] which defined the basic loading modes of the weld spot proceeding from the stress-singularity-related slit opening modes.

Only the joint face force systems are taken into account as relevant to fatigue in the structural stress approach version proposed by Rupp and Grubisic. Therefore, this approach is restricted to loading cases where the cyclic stresses due to the eigenforces are low in relation to those due to the joint face forces. The approach can be extended to the eigenforce component without major difficulties.

Concluding this Section 9.2.3 on weld spot resultant forces, the force system at the weld spot in the tensile-shear specimen is considered (after Radaj[4]). The mechanical conditions in this specimen, which is widely used for fatigue testing, are often misunderstood with the consequence of inadquate interpretation of the results.

The mechanical peculiarity of this specimen is the transversely offset position of the plates (the midplanes are one half of the added-up plate thicknesses apart), which produces bending moments in the plates when the specimen is subjected to remote tensile loading. These bending moments do not necessarily imply a bending moment in the joint face. The plate bending moments cause considerable bending stresses to be superimposed on the membrane stresses, resulting in deflections, which may be large relative to the plate thickness, or which may lead to contact between the two plates. Both secondary effects of large deformations are ignored below.

The coupling of the membrane and bending effects in a specimen with equal plate lengths and plate thicknesses is discussed using a plane longi-

tudinal-section model, in which the overlap lengths are deleted and the weld spot is contracted to a single point (beam model), Fig. 9.8. The symmetry relative to this point 0 excludes a bending moment being transferred. It is therefore possible to conceive this point as a hinge point. The resulting bending deformation is shown greatly enlarged. Three typical loading cases are considered: remote tensile forces located in the midplane (or joint face) of the weld spot (to be achieved by packing plates in the grip jaws), remote tensile forces located in the two midplanes of the plates with transverse forces equilibrating the bending moment of the two forces, and finally these tensile forces combined with bending-rigid clamping producing a bending moment beside the (increased) transverse force.

The first loading case is characterised by a pure shear force in the joint face and a constant bending moment over the beam length. In the second loading case, a secondary cross-tension force is added to the joint face shear force and the beam bending moment decreases to zero at the loaded beam ends. In the third loading case, the cross-tension force is further increased and the bending moment decreases more rapidly with zero crossing along the beam length.

The joint face forces are further changed and supplemented by a bending moment if unequal plate thicknesses or/and plate lengths are introduced in combination with a finite weld spot diameter and overlapping plate ends.

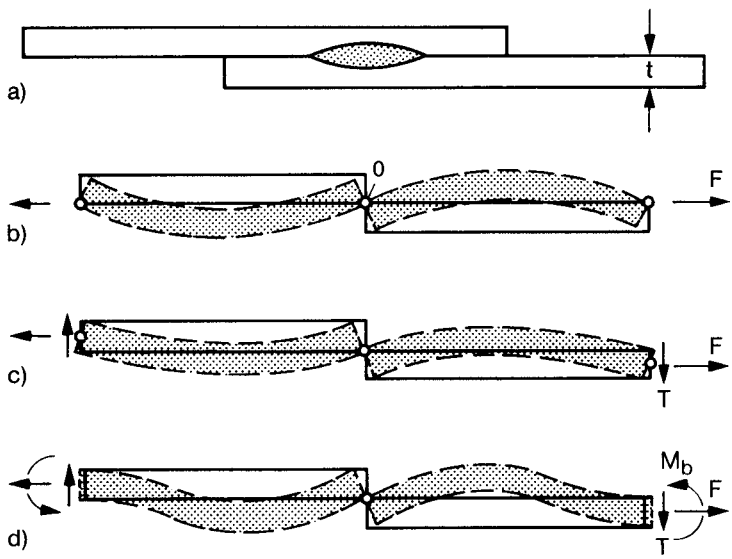


Fig. 9.8. Plane longitudinal-section model (b, c, d) of the tensile-shear specimen (a) with equal plate lengths and plate thicknesses, but without overlap lengths; remote tensile forces located in the midplane of the weld spot (b), in the midplanes of the plate (c) and combined with rigid clamping (d); after Radaj.[4]

The latter make eigenforces possible, but not so in the beam model because no forces can occur in the overlapping beam ends.

Obviously the joint face forces and eigenforces at the weld spot of the tensile-shear specimen depend on the deformation behaviour of the complete specimen inclusive of all geometric parameters and remote loading conditions. Finite element analysis is necessary to determine these forces in actual cases. Simple relationships can be derived based on the beam model, but this model neglects certain, not unimportant, aspects of the plate system representing the specimen. The beam model with hinge supports is statically determinate with rotational equilibrium according to $T = Ft/2l$. The beam model with bending-rigid supports is statically indeterminate so that the deformation must additionally be considered resulting in $T = 3Ft/4l$ and $M_b = Ft/2$ (the opposed deflections of a beam of length l clamped at one end and loaded by T and M_b at the other end are set equal).

9.2.4 General theory of forces and stresses at weld spots

The general complete loading state at spot-welded lap joints is characterised by 40 resultant weld spot forces (inclusive of moments) related to 40 vertex point structural stresses, Fig. 9.9. The relationship between resultant forces and structural stresses is described by a linear equation system, which is derived on the basis of the peripheral stress distributions merged into equilibrium conditions. The complete set of weld spot forces can thus be determined from the vertex point stresses at the weld spot edge. Inversely, the stress distribution around the weld spot can be calculated from the weld spot forces by simple formulae. In practical application, the number of characteristic forces or stresses can be substantially reduced.

The essential components of the general theory developed by Radaj[807,808] are: an orthogonal reference system at the weld spot positioned, if possible, corresponding to the principal loading directions, the decomposition of the weld spot forces into joint face forces and eigenforces, the weld spot modelled as a rigid core for evaluating the stresses connected with the joint face forces, and a homogeneous distribution of the stresses resulting from the eigenforces. The assumptions and possible complications of the method with respect to the engineering aspects and the details of the rigid core model are described in separate publications by Radaj and Zhang.[813,814] The question, how accurately the weld spot resultant forces are evaluated in the case of geometrically imperfect manufacture characterised by dents close to the weld spot is also answered by Radaj and Zhang:[815] The error is about 1% for realistic geometric work tolerances.

A special procedure for determining the arbitrarily defined weld spot resultant forces proceeding from measured surface stresses adjacent to the

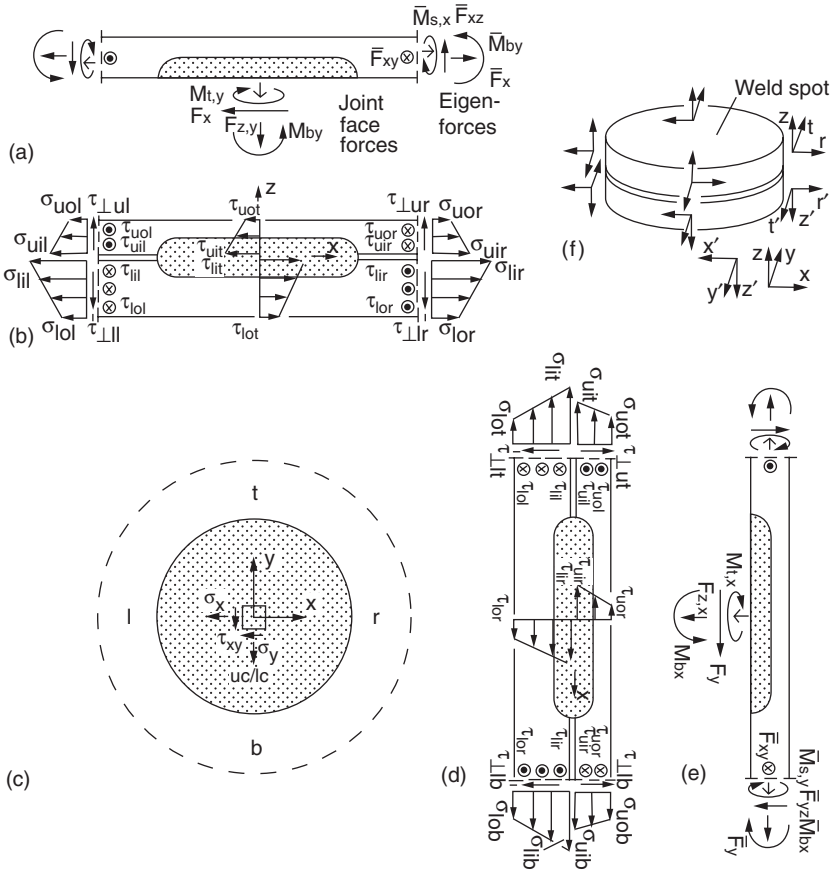


Fig. 9.9. General complete loading state at spot-welded lap joint characterised by 40 resultant weld spot forces (inclusive of moments) related to 40 vertex point structural stresses; top view of weld spot with global coordinate system, centre point stresses (upper and lower surface: indices uc, lc) and vertex point indices t, b, l, r (c), local and global coordinate systems in vertex points (f), joint face forces and eigenforces in upper plate (a, e), vertex point stresses (b, d); after Radaj.[808]

weld spot has been developed by Radaj, Stoppler and de Boer[810,839] with reference to the general theory (see Section 9.2.9).

The further presentations below do not refer to the general theory. Only some elements of the theory are used. But any new methods and software development for the assessment of fatigue strength or life of spot welds in structural components should refer to the general theory when discussing the simplifications.

9.2.5 Structural stress analysis at weld spots

The structural stresses at the weld spot are most efficiently determined based on the weld spot resultant forces. For that purpose simple engineering formulae are available, which are derived using simplifying assumptions with respect to the elastic weld spot behaviour. The maximum structural stresses at the weld spot edge are determined either in the plates or in the nugget depending from where the fatigue cracks propagate. They are termed 'nominal structural stresses'.

A finite element model of the weld spot with fine meshing, the model consisting of solid elements within the weld spot and plane shell elements in the surrounding area, connected by ball-jointed rigid bar elements enforcing plane cross-sections, Fig. 9.10 (see Chen and Deng[751,758] and Radaj[803] concerning the performance of shell elements) can be used in cases where an extremely high accuracy of the stresses is needed. Pure solid element models may also be used.[784,867,871,959,965,972–974] But these costly procedures are bound to the condition that the total finite element model does not become too large. Mainly single-spot joints can be simulated in this way. Fine-mesh simulations have been performed for a variety of spot-weld specimens in connection with the stress intensity approach, Fig. 9.11 (see Section 10.4). More complex components with a large number of weld spots can be analysed with fine meshing at the weld spot proceeding from the nodal point displacements of the coarse mesh and substituting the weld spot area by a fine-meshed submodel (Rui *et al.*[820] Mayer *et al.*[794–796]). The weld spot resultant forces are not determined in this procedure. The result of the finite element calculation will be more accurate than the nominal structural stress approach in cases where the structural stress field is significantly influenced by shape and loading irregularities close to the weld spot. Another procedure without the basis of weld spot resultant forces is the use of a multi-beam connection at each weld spot combined with an axisymmetric arrangement of plane shell elements within and around the weld spot (Vopel and Glas[841]). These configurations are well suited to the structural-stress-based evaluation of damage parameters under complex histories of variable-amplitude loading.

The above models are based on a linear behaviour of the structure (inclusive of the notch stress concentration or stress singularity at the nugget

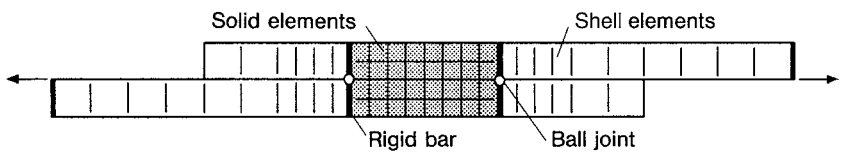


Fig. 9.10. Finite element model of the tensile-shear specimen, cross-sectional view; after Radaj.[4,803]

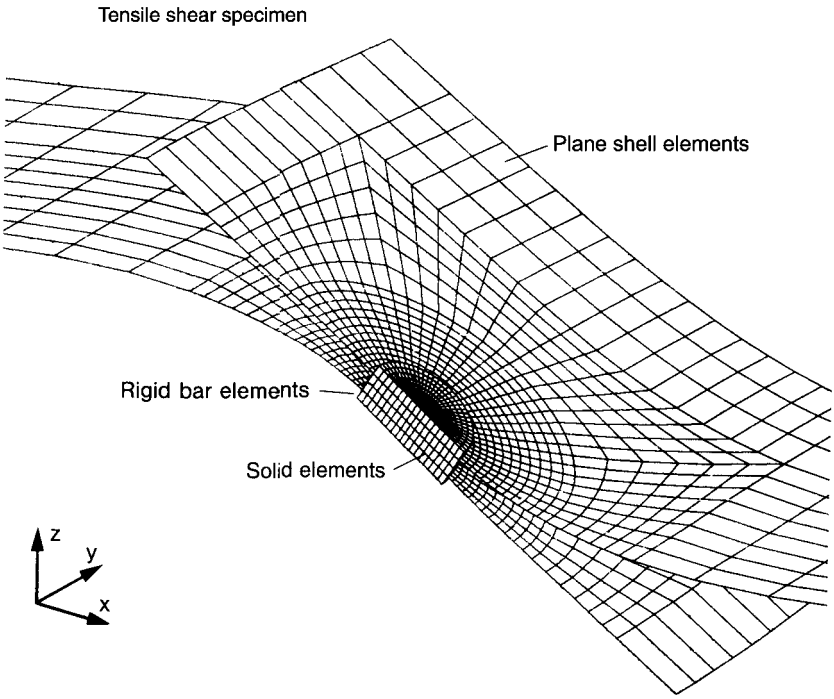


Fig. 9.11. Thin-shell element model (fine mesh) of the tensile-shear specimen, symmetry half, deformed state under tensile-shear loading, rotation of the weld spot and deformations greatly magnified; after Radaj.[4]

edge). Non-linear elastic-plastic material behaviour can be introduced into the finite element model if appropriate (e.g. in the low-cycle fatigue range).[834,836] Large displacements are of minor influence if the geometric structural instability can be excluded.[812] Contacting of the overlapping plates may have an appreciable influence on the structural stress distribution in special cases and should be incorporated in the linear model.[900]

9.2.6 Nominal structural stress in plate at weld spot

The nominal structural stress in the overlapping plates at the nugget edge where the plate fractures originate is defined as the maximum structural stress calculated by engineering formulae in the basic loading cases of the weld spot. The structural stresses in the four vertex points in each of the two overlapping plates have to be considered in order to determine their maximum value. The complex force system at the weld spot is decomposed for that purpose into joint face forces and eigenforces as described in Section 9.2.3. Only the joint face forces are considered in the following.

The weld spot diameter and the plate thickness have to be introduced with their nominal or actual values, respectively.

The joint face forces and the structural stresses in the plates associated with them can be modelled by a rigid cylindrical core substituting the weld spot, Fig. 9.12(a, c). The rigid core simulates the elastic weld spot rather well with respect to the joint face forces (but not the eigenforces). The reason for the good correlation is the fact that the load transfer is locally concentrated at the nugget edge, whereas the interior of the weld spot remains more or less stress-free and accordingly deformation-free. The stress distribution in the infinite or circular plate at the rigid core edge under forces (inclusive of moments) in the core is available from the literature.[180,251,297] The following nominal structural stresses are derived therefrom following Radaj[803,806,814] (with core or weld spot diameter d and plate thickness t).

The nominal structural stress σ_{sn} in the plate from loading the core or weld spot by the force F_x in the plate plane is the maximum radial membrane stress $\sigma_{mr\,max}$ in the plate at the core edge:

$$\sigma_{sn} = \sigma_{mr\,max} = \frac{F_x}{\pi dt} \tag{9.1}$$

The nominal structural stress σ_{sn} from loading the core or weld spot by the bending moment M_{by} in the plate plane is the maximum radial bending stress $\sigma_{br\,max}$ in the plate at the core edge:

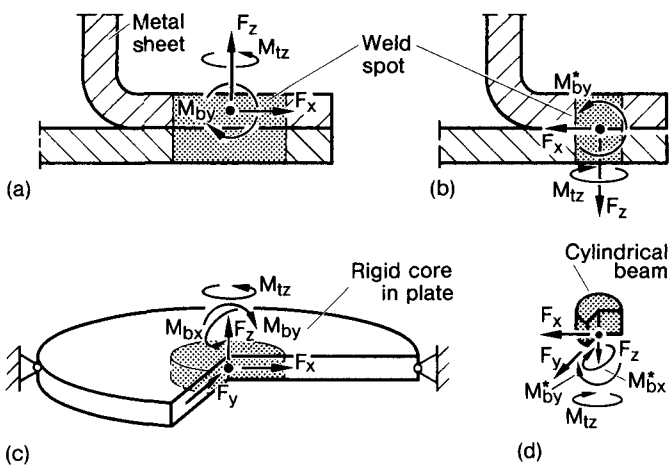


Fig. 9.12. Rigid core model for plate structural stresses with forces referred to middle plane of plate (a, c) and stiff beam model for nugget structural stresses with forces referred to joint face (b, d), original component (a, b) and simplified models (c, d).

$$\sigma_{sn} = \sigma_{brmax} = \frac{6M_{by}}{\pi dt^2} \tag{9.2}$$

The nominal structural stress σ_{sn} from tensile-shear loading by the force F_x in the inner surface of the plate resulting in shear loading of the joint face and producing the bending moment $M_{by} = F_x\, t/2$ in the plate is the superimposed radial membrane and bending stress $\sigma_{mbr\,max}$ in the plate at the core edge:

$$\sigma_{sn} = \sigma_{mbrmax} = \frac{4F_x}{\pi\, dt} \tag{9.3}$$

The nominal structural stress σ_{sn} from loading the core or weld spot by the force F_z normal to the plate plane (cross-tension force) is the maximum radial bending stress $\sigma_{br\,max}$ in the plate at the core edge (circular plate, outer diameter D chosen according to the bending support characteristics of the welded joint under consideration, bending-free support at the outside plate edge):

$$\sigma_{sn} = \sigma_{brmax} = \frac{3F_z}{\pi t^2}\left[\frac{1-(1+\nu)\ln(d/D)}{1+\nu+(1-\nu)(d/D)^2} - \frac{1}{2}\right] \tag{9.4}$$

where ν is the Poisson's ratio.

An approximation according to Radaj[806] for $1 \le D/d \le 16$ with $\nu = 0.3$ has the following form:

$$\sigma_{sn} \approx 1.03\frac{F_z}{t^2}\ln\frac{D}{d} \tag{9.5}$$

The corresponding complete formula for bending-rigid support at the outside plate edge is:

$$\sigma_{sn} = \sigma_{brmax} = \frac{3F_z}{\pi t^2}\left[\frac{\ln(D/d)}{1-(d/D)^2} - \frac{1}{2}\right] \tag{9.6}$$

An approximation according to Radaj[806] for $1 \le D/d \le 16$ with $\nu = 0.3$ is:

$$\sigma_{sn} \approx 0.69\frac{F_z}{t^2}\ln\frac{D}{d} \tag{9.7}$$

Rupp *et al.*[828] use eq. (9.6) with the condition $D/d = 10$ in their version of the approach:

$$\sigma_{sn} = 1.744\frac{F_z}{t^2} \tag{9.8}$$

The nominal structural stresses from cross-tension and bending moment loading have to be superimposed in the case of single-sided peel-tension loading.

The nominal structural shear stress τ_{sn} from loading the core or weld spot by a torsional moment M_{tz} normal to the plate plane is the maximum tangential membrane shear stress $\tau_{mt\,max}$ in the plate at the core edge:

$$\tau_{sn} = \tau_{mt\,max} = \frac{2M_{tz}}{\pi d^2 t} \tag{9.9}$$

The nominal structural stress in each of the two overlapping plates from loading by eigenforces (membrane and bending stresses in an orthogonal reference system, σ_x, σ_y and τ_{xy}, and out-of-plane shear stresses in the same system, $\tau_{\perp x}$ and $\tau_{\perp y}$), is identical to the relevant stress component times a factor $\kappa = 1.0$–1.5 resulting from mutual constraint of the two plates.[813] The factor κ can be chosen individually for each of the stress components just mentioned.

The nominal structural stresses defined for each loading case have to be superimposed if several loading cases contribute to the loading state at the weld spot. A prerequisite of simple addition is that the underlying maximum stress is of the same type and occurs at the same peripheral position. The von Mises distortional strain energy criterion is considered to be valid for crack formation in the case of superimposed stress components (under the assumption of ductile material behaviour). The nominal structural stress σ_{sn} is assumed to be associated with the transverse stress component $\nu\sigma_{sn}$ (with Poisson's ratio ν). The equivalent nominal structural stress $\sigma_{sn\,eq}$ in the plate reads:

$$\sigma_{sn\,eq} = \sqrt{(1 - \nu + \nu^2)\sigma_{sn}^2 + 3\tau_{sn}^2} \tag{9.10}$$

More complex cases of superposition can be solved by considering the complete peripheral stress distribution of each loading case, i.e., constant, sine or cosine distributions (see Radaj[807,808]). Introduction of the superimposed force or moment vector into the calculation is another possibility. The effect of plate edges in finite distances is not taken into account by the above formulae which refer to the infinite plate, but the introduced cosine distributions characterised by their vertex point values remain approximately valid even with nearby straight plate edges (Radaj and Zhang[814]).

A comprehensive numerical and experimental analysis on the superposition of the joint face loading cases based on the above nominal structural stresses with noteworthy extensions has been presented by Nakahara *et al.*[799] The double-cup single-spot specimen (see Section 10.4.6) under mixed-mode loading conditions was used for verification and comparison purposes.

Rupp *et al.*[821,827,828] use a nominal structural stress formula for plate fractures in steel under tensile-shear loading which is derived from earlier pro-

posals of Radaj[803] and adjusted to fatigue test results by a factor κ on the bending stress portion:

$$\sigma_{sn} = \frac{F_x}{\pi dt} + 1.872\kappa\frac{M_{by}}{dt^2} + 1.744\kappa\frac{F_z}{t^2} \qquad (\kappa = 0.6\sqrt{t}) \qquad (9.11)$$

where σ_{sn} is the nominal structural stress in the plate, F_x is the weld spot force in the plate plane, M_{by} is the weld spot bending moment in the plate plane, F_z is the cross-tension force in the weld spot, d is the weld spot diameter, t is the plate thickness and κ is the correction factor on the bending stress portion which depends on the plate thickness and the material.

Maddox[792,793] defines a nominal structural stress σ_{sn} under the assumptions that the weld spot force in the plate plane acts uniformly over half of the weld spot circumference and that the bending moment acts uniformly over the specimen width w ($M_{by} = F_x t/2$ and $F_z \approx 0$ in the case of tensile-shear loading) substituting the weld spot pitch:

$$\sigma_{sn} = \frac{2F_x}{\pi dt} + \frac{6M_{by}}{t^2 w} \qquad \left(M_{by} = \frac{F_x t}{2}\right) \qquad (9.12)$$

When comparing eq. (9.12) with eqs. (9.1) and (9.2), it is evident that the membrane stress is enlarged by a factor of two (in reality a factor between one and two is appropriate in the case of the tensile-shear specimen, i.e. the stress remains on the safe side of strength assessment) and that the bending stress portion is identical for $w = \pi d$ (this is near to the minimum value necessary for safe fabrication, i.e. the stress remains on the unsafe side of strength assessment for larger widths).

Sheppard and Strange[985] define the nominal structural stress σ_{sn} in the plate with reference to the beam-to-shell element model of the weld spot in a coarse finite element mesh (mesh size equal to approximately twice the weld spot diameter, maximum force value out of the four corresponding to the vertex points in each of the two overlapping plates):

$$\sigma_{sn} = \frac{F_x^*}{d^* t} + \frac{6M_{by}^*}{wt^2} + \frac{F_z}{t^2} \qquad (9.13)$$

where F_x^* is the membrane force from the shell elements at the weld spot front side, which is distributed over the effective weld spot diameter, $d^* = \pi d/3 \approx d$, M_{by}^* is basically the bending moment from the shell elements at the weld spot front side which is distributed over the component width w (or a relevant saturation value) and F_z is the cross-tension force acting on the weld spot. Actually, M_{by}^* is given in further detail dependent on the characteristics of the weld spot loading state.

9.2.7 Nominal structural stress in nugget at weld spot

The nominal structural stress in the nugget near its edge where the nugget fractures originate is defined with reference to Rupp[821,827] as the maximum surface stress in a short beam with the circular cross-section of the weld spot under the action of the joint face forces and analysed according to simple beam theory, Fig. 9.12(b, d). The beam stresses in the four vertex points have to be considered in order to determine their maximum value. The weld spot diameter is introduced with its nominal or actual value, respectively.

The nominal structural stress σ_{sn} in the beam from a weld spot cross-tension force F_z normal to the joint face is the axial stress σ_z in the beam:

$$\sigma_{sn} = \sigma_z = \frac{4F_z}{\pi d^2} \tag{9.14}$$

The nominal structural stress σ_{sn} from a weld spot bending moment M^*_{by} (or M^*_{bx}) in the joint face is the maximum bending stress $\sigma_{b\,max}$ in the beam:

$$\sigma_{sn} = \sigma_{b\,max} = \frac{32M^*_{by}}{\pi d^3} \tag{9.15}$$

The nominal structural shear stress τ_{sn} (in the flank side vertex points of the beam) from a weld spot force F_x (or F_y) in the joint face is the maximum accompanying tangential shear stress $\tau_{t\,max}$ in the beam:

$$\tau_{sn} = \tau_{tmax} = \frac{16F_x}{3\pi d^2} \tag{9.16}$$

The nominal structural shear stress τ_{sn} from a weld spot torsional moment M_{tz} in the joint face is the accompanying tangential shear stress τ_t in the beam:

$$\tau_{sn} = \tau_t = \frac{16M_{tz}}{\pi d^3} \tag{9.17}$$

Considering the maximum normal stress criterion to be valid for crack formation (under the assumption of brittle material behaviour), the following superposition has to be performed in the vertex points related to the two orthogonal loading directions:

$$\sigma_{sn\,eq} = \frac{1}{2}\sigma_{sn} + \frac{1}{2}\sqrt{\sigma^2_{sn} + 4\tau^2_{sn}} \tag{9.18}$$

where $\sigma_{sn\,eq}$ is the equivalent nominal structural stress in the beam.

The peripheral distribution of the stress components should be taken into account when superimposing stresses in more complex loading cases. Intro-

duction of the superimposed force or moment vector in the calculation is once more the other possibility.

9.2.8 Structural strain measurement at weld spots

Widely used in practice is the determination of local strain at the weld spot edge on the outside or inside of the overlapping plates based on measurement,[131,181,198,221] Fig. 9.13. On the outside of the plate, the strain gauges are attached close to the edge of the electrode indentation area and aligned radially. On the inside of the plate, they are positioned as close to the weld spot edge as possible after bending up the non-loaded overlapping plate (this slightly alters the structural behaviour) or by means of holes drilled in the mating plate.

The inside measurement is close to the crack initiation site and can thus be better correlated with the fatigue strength of the weld spot than other measurement positions. In the case of outside measurement, the inside strain has to be estimated on the basis of the outside strain. For single-face tensile-shear the ratio is $\sigma_i/\sigma_o \approx -2.0$, for cross-tension $\sigma_i/\sigma_o \approx -1.0$, for double-face tensile-shear and for through-tension $\sigma_i/\sigma_o \approx 1.0$ assuming equal plate thickness and identical plate material in the joint. It is therefore necessary to know which mode of loading prevails at the considered weld spot.

The prevailing mode of loading can be determined, for example, from the ratio of radial strain at the front side to tangential strain at the flank side

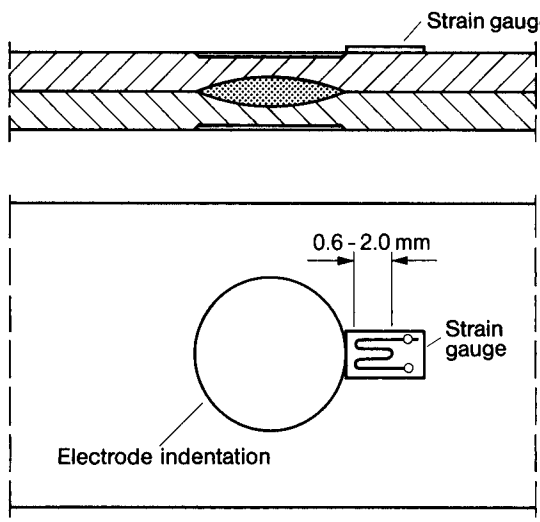


Fig. 9.13. Strain gauge on outer surface of overlapping plate at the edge of electrode indentation.

of the weld spot, provided it is only necessary to distinguish between tensile-shear and cross-tension loading in a single-face joint.[797] Another proposal is based on distinguishing between tensile-shear and cross-tension loading by means of the photoelastic surface coating method.[809] This method is advantageously substituted today by holographic methods based on the Speckle interferometry.[839]

In the case of single strain gauge measurements on the outside or inside of the plate, it is necessary to know the principal loading direction of the weld spot in advance in order to be able to record the maximum strain value. Otherwise, several radially aligned strain gauges should be distributed over the circumference of the weld spot in order to detect the maximum value (Rupp[821]).

As the strain gauges are not small compared with the plate thickness and weld spot diameter (usually applied strain gauge lengths 0.6–2.0 mm), the result of the strain measurement is an averaging over strain distributions which possibly have steep gradients. Therefore, the measured strain depends on the size of the strain gauge and on how far away it is positioned from the electrode indentation or joint face edge. It is, in any case, less than the theoretical maximum value of the corresponding structural stress at the weld spot edge. There is nearly no deviation of the real structural behaviour from plate theory (inclusive of membrane stresses) up to the joint face edge (Zhang and Radaj,[848] *ibid.* Fig. 3), but the diameter of the indentation edge at the outer plate surface is not necessarily identical to the diameter of the joint face edge. The joint face edge, on the other hand, is not necessarily identical to the nugget edge because of the solid-state-welded bonding ring surrounding it under certain conditions. The complications just mentioned, together with the fact that crack initiation at the inner plate surface has a major effect on the structural strain or stress at the indentation edge on the outer surface make it advisable (Salvini *et al.*[829,830]) to position the strain gauge radially at a definite distance from the weld spot edge and to extrapolate the measured strain to the edge ($\Delta r/R$ = 0.3–0.5, with radial distance Δr and weld spot radius R).

Strain gauges bonded to the electrode indentation area of weld spots are also successfully applied to assess the prospective fatigue life, to detect crack initiation and even to measure crack propagation (Satoh *et al.*[744,745,832,833]). This application is described in more detail below.

A small-size rosette of sector strain gauges (gauge length 0.5 mm), Fig. 9.14(a, b), bonded to the electrode indentation surface (diameter 5 mm) is used to measure the radial strains in eight directions, among them the maximum strain indicating the main loading direction in which further evaluation takes place. The strain output obtained is seperated into the strain range $\Delta\varepsilon$ (corresponding to elastic deformation behaviour) and the offset strain $\bar{\varepsilon}$ (corresponding to plastic deformation behaviour), Fig. 9.14(c). The

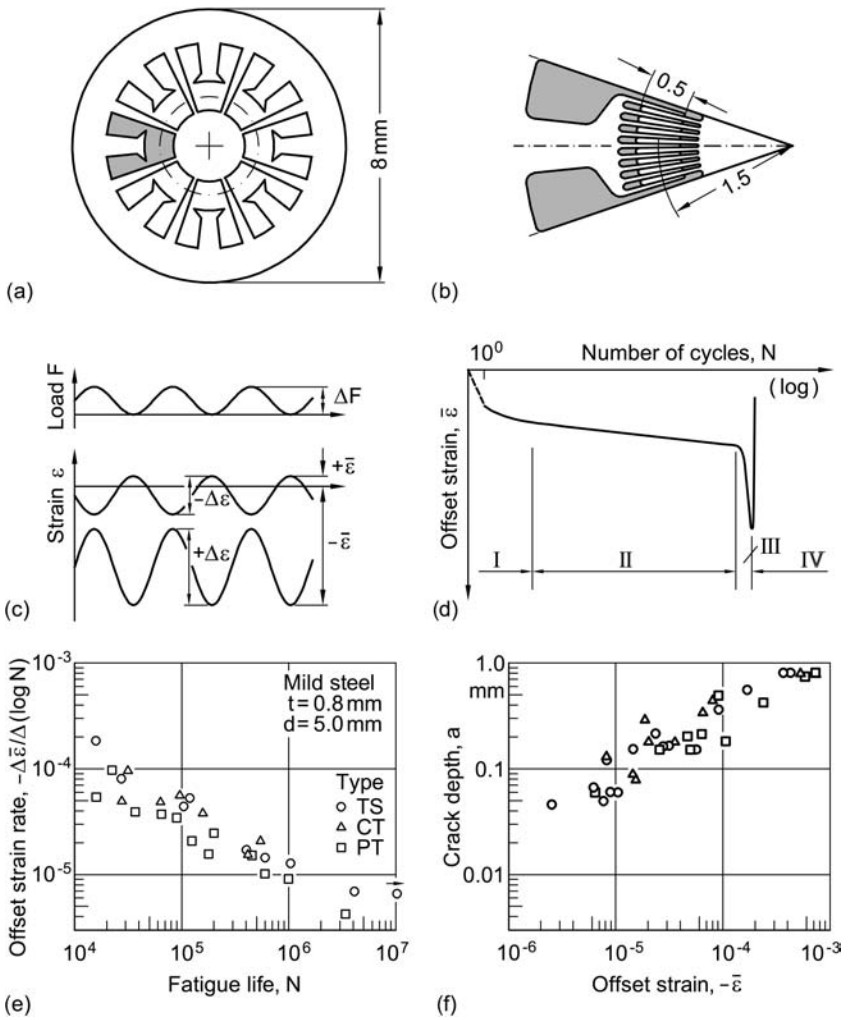


Fig. 9.14. Strain gauge method for predicting the fatigue life of spot-welded joints: small-size rosette (a) of sector strain gauges (b), strain output (in phase and in antiphase, respectively) under cyclic loading (c), schematic representation of offset strain dependent on number of cycles (d), offset strain rate characterising the fatigue life (e) and crack depth dependent on offset strain (f), measurement results refer to mild steel; with TS tensile-shear, CT cross-tension and PT peel-tension; after Abe and Satoh.[745]

offset strain occurs when the cyclic load adopts its zero value. The relationship between the offset strain and the number of cycles is schematically drawn in Fig. 9.14(d): several cycles are needed to stabilise the process (stage I); thereupon a constant rate of accumulation of (compressive)

plastic strains (at the weld spot edge) takes place (stage II); crack initiation and through thickness crack propagation (at the weld spot edge) cause a steep rise in the (compressive) surface strains (stage III); further crack propagation across the sheet width is associated with a steep drop in the (compressive) surface strains (stage IV). A uniform relationship could be established between the offset strain rate in stage II and the fatigue life of various single-spot specimens (tensile-shear, cross-tension and peel-tension), Fig. 9.14(e). Finally, the crack depth was correlated with the offset strain within a uniform scatter band, Fig. 9.14(f). The uniformity of the results is all the more remarkable as the three types of spot-weld loading are applied with rather different load ranges.

9.2.9 Weld spot forces by correlation of strain patterns

The loading state in spot-welded (and similar) lap joints can be determined by evaluating measured surface strains in the vicinity of the weld spot. The pattern of measured strains is decomposed into proportions of reference patterns representing simple basic loading states. Correlation analysis on the basis of Markov chains is used to achieve this (Radaj and Stoppler,[810] Stoppler and de Boer[839]).

The basic loading states used for reference can be defined rather freely. They should describe dominant proportions of the total loading state and they should not be linearly independent of one another. They can be identical with the decomposed loading states of the general theory by Radaj,[808] but they can also be defined independently.

An example is given in Fig. 9.15. The loading state at the middle weld spot in the upper flange of the torsion-loaded single-hat section specimen is considered. This specimen represents a structural component with

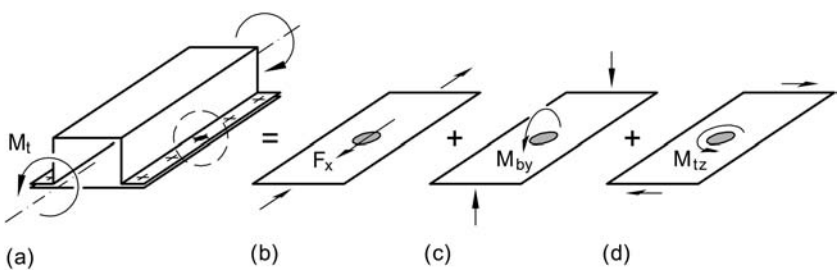


Fig. 9.15. Total loading state at the weld spot in the upper flange of a torsion-loaded single-hat section specimen (a) composed of three basic loading states in a (possibly excentric) core-in-plate model: shear force F_x in joint face plane (b), bending moment M_{by} (c) and torsional moment M_{tz} (d); proposed by Radaj (unpublished).

unknown weld spot forces. The total weld spot loading state is assumed to be composed of the following basic states (which are known from theoretical investigations in the considered case) in a plane core-in-plate model: shear force F_x (acting in the joint face plane), bending moment M_{by} and torsional moment M_{tz}. Actually, these loading states may be altered and further states introduced which may be relevant because of geometrical deviations caused by the fabrication process, e.g. welding distortions. It is assumed that the nearby flange edges and the neighbouring weld spots exert only a minor influence on the strain distribution around the spot. As this is certainly not the case with regard to the nearby flange edges, the corresponding conditions in the reference model should be chosen similarly (e.g. one longitudinal free edge nearby, the other edge further away).

The original strain pattern in the vicinity of the weld spot on the surface of the overlapping plate in the structural component is defined by the strains measured by resistance strain gauges arranged around the weld spot. The strain gauges can be arbitrarily arranged with regard to position and direction, but arrangements are preferred by which the underlying basic strain patterns can be well distinguished. These reference strain patterns are evaluated from strain gauges in identical arrangements around the weld spot in the reference and original configurations. Greater accuracy is achieved by substituting the measured values in the reference configurations by the results of a finite element analysis.

By interpreting the measured or calculated strain values around the weld spot as discrete signal values of a Markov chain, correlation factors are derived by numerical integration procedures which characterise the degree of similarity between the strain pattern measured in the structural component and the strain patterns in the selected basic loading states (inclusive of specimen type). Proportion factors are derived therefrom which characterise the contents in basic loading states (inclusive of their force values). The correlative evaluation of the strain patterns is more robust than corresponding deterministic approaches based on the solution of linear equation systems.

9.3 Analysis tools – non-linear structural behaviour

9.3.1 Elastic-plastic deformation at weld spots

Elastic-plastic cyclic deformations are a precondition of fatigue crack initiation. They are therefore constitutive in fatigue failure and are taken into account within the notch strain approach (see Chapter 11). A special effect resulting from elastic-plastic deformation is the change in slit opening behaviour and residual stresses by the set-up load and by further loading cycles (see Section 11.2.6). Another striking effect of elastic-plastic

deformation is the shift of fatigue cracking from the nugget edge to the outer boundary of the heat-affected zone in the low-cycle fatigue range in the case of steels (see Section 11.2.7).

In the following, another effect of elastic-plastic deformations (associated with large deflections) with some relevance to fatigue assessments is considered: the rotation angle of the weld spot in tensile-shear loading. This angle is negligibly small when loading the weld spot elastically in the high-cycle fatigue range ($\theta \approx 0.5°$ for $F = 1\,\text{kN}$ with $t = 1\,\text{mm}$). The angle is several times larger in the medium- and low-cycle fatigue range, where plastic deformations are additionally effective. A cross-tension force $F_\perp$ is produced besides the shear tension force $F_\parallel$ because of the rotation angle, Fig. 9.16, thereby reducing the fatigue strength of the joint:

$$F_\parallel = F \cos\theta \tag{9.19}$$

$$F_\perp = F \sin\theta \tag{9.20}$$

where F is the external force, $F_\parallel$ and $F_\perp$ are the force components parallel and normal to the joint face and θ is the rotation angle.

A geometrically conditioned maximum angle θ_{max} is achieved in the static tensile-shear test if the initially offset plates are finally in alignment as a result of weld spot rotation with plastic hinges formed at the front and rear side of the weld spot, Fig. 9.17. The formula was derived first by Koenigsberger:[783]

$$\tan\theta_{max} = \frac{t}{\sqrt{d^2 - t^2}} \tag{9.21}$$

where θ_{max} is the maximum rotation angle, d is the nugget diameter and t is the plate thickness.

The approximation $d = 4t$ results in $\theta_{max} = 14.5°$. This limit value is slightly exceeded if the weld spot fails by buttoning under static load, but it can be considered applicable in the low-cycle fatigue range. In the case of weld

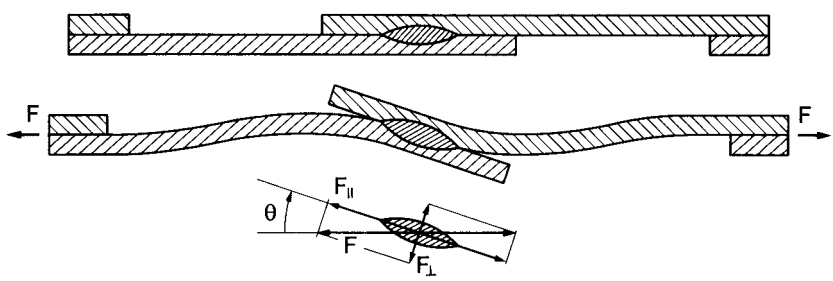


Fig. 9.16. Rotation of weld spot subjected to tensile-shear loading and superimposed cross-tension by the rotation.

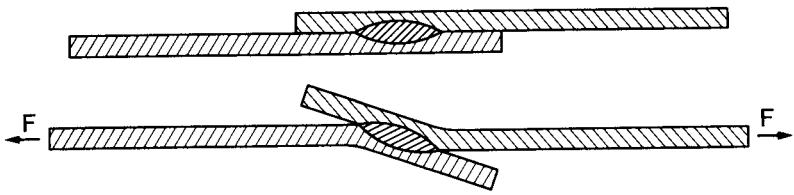


Fig. 9.17. Limit state of aligned tension plates after formation of plastic hinges at the weld spot edge.

spots with hardened heat-affected zone, the diameter of this zone should be used in eq. (9.21) instead of the nugget diameter if the fatigue cracks are shifted to the outside as the result of hardening.

9.3.2 Large deflections at weld spots subjected to tensile-shear loading

The numerical stress analysis of fatigue-loaded welded joints is generally performed taking the assumptions of the linear theory of elasticity for granted. One of these assumptions restricts the deformations (displacements, deflections and rotations) to values that are small in relation to the dimensional parameters of the structural components. The equilibrium conditions are applied to the undeformed structure. Slit or gap closure and associated contact pressure are neglected. The behaviour of the structural components is termed 'geometrically linear'.

There is some indication from experimental results that the geometrically non-linear behaviour is not completely negligible. For example, the tensile-shear specimen with a single weld spot is considered to be more critical under cyclic load than the multi-spot hollow-section specimen because of its reduced weld spot rotation under external loading.

A finite element large-displacement elastic analysis has therefore been applied to the spot-welded tensile-shear specimen subjected to tensile or compressive loading (Radaj and Zhang[812]). Simplified analytical solutions have been presented by Goland and Reissner,[869] Chang and Muki,[857] Lai *et al*.,[876] Pook[886] and Makhnenko *et al*.[879](see Section 10.2.6).

The basic behaviour of the tensile-shear specimen is investigated by modelling the longitudinal section of the specimen as a plate strip model (constant plate width normal to this section). This longitudinal section model simulates the membrane and bending effects which dominate in the middle section of the specimen without taking the inhomogeneous in-plane distribution of the stresses into account. The longitudinal section of the specimen with dimensions conforming to standards is shown in Fig. 9.18. The ends of the specimen are rigidly clamped, generating the support forces

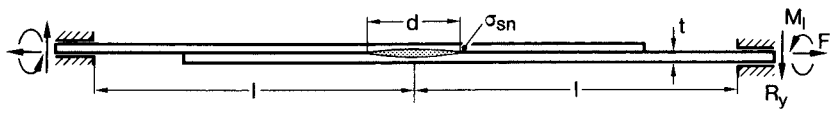
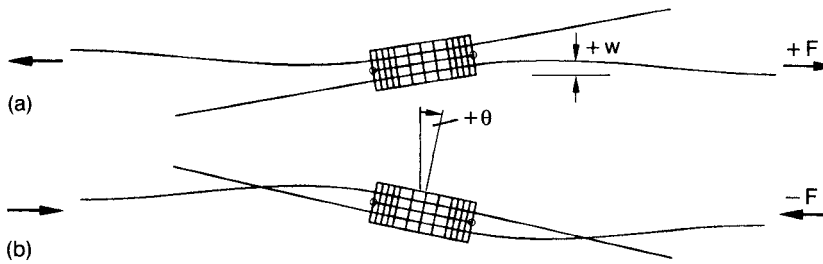


Fig. 9.18. Longitudinal section of tensile-shear specimen, with prescribed longitudinal displacement loading with rotation-rigid support; after Radaj and Zhang.[812]



(c) $l = 17.5$ mm; $t = 1$ mm; $d = 5$ mm; $E = 2.1 \times 10^5$ N/mm^2; $\nu = 0.3$; $E' = E/(1-\nu^2)$; $\sigma_{sn} = 4F = \sigma_Y^* = \pm 500$ N/mm^2; $w_{max} = +0.033$ and -0.041 mm; $\theta = -0.47°$ and $+0.57°$

Fig. 9.19. Deformation plot of plate strip model of tensile-shear specimen: tensile loading (a), compressive loading (b), and introduced parameter values (c); after Radaj and Zhang.[812]

R_y and M_l under the tensile force F. The plate thickness t may be between 0.65 and 2.5 mm in automotive engineering, $t = 1$ mm being the representative value used in the considered investigation. The weld spot diameter d is chosen conservatively as $d = 5\sqrt{t} = 5$ mm. Another less conservative choice would be $d = 3.5t$. The strip length is chosen to be l =17.5 mm. The relevant finite element model consists of plate elements outside the weld spot and of solid elements within. The two element types are connected by pin-jointed rigid bars. Plate and solid elements are in the plane strain condition.

The (enlarged) deformation of the plate strip model under tensile or compressive loading is plotted in Fig. 9.19. The width of the strip is introduced as one unit (i.e. 1 mm) resulting in the nominal structural stress $\sigma_{sn} = 4F/(1 \times 1)$ which is set equal to a nominal yield limit of $\sigma_Y^* = 500$ N/mm^2 (typical for high strength steels). The latter may include a support factor of about 1.5 taking full plastification of the cross-sectional area in bending into account. This is necessary if the purely elastic behaviour considered in the high-cycle fatigue range is transferred to the elastic-plastic behaviour in the low-cycle fatigue range. The plate strip is deflecting and the weld spot rotating in opposite directions in the two loading cases. The slit or gap opens in

tensile loading and closes in compressive loading. The gap closure effect is neglected, i.e. the plate strips penetrate one another after having bridged the gap width which is introduced here as zero.

The deformation under compressive loading was further investigated up to the buckling load (first mode at $\sigma_{nc} = 722\,N/mm^2$, second mode at $\sigma_{nc} = 1177\,N/mm^2$; $\sigma_n = F/t$).

The plate strip model shows a higher stiffness in compressive loading if gap closure is taken into account. The critical stress of the first buckling mode is increased by more than one half. The neighbouring strips come into contact only at the unloaded strip ends. The rotation angle θ and the stress modification factor K (modification by large displacements) are plotted dependent on the relative nominal stress σ_n/E, Fig. 9.20 (note that $\sigma_{sn} = \sigma_Y^* = 500\,N/mm^2$ corresponds to $10^3 \times \sigma_n/E = 0.6$). The continuous curves without gap closure are changed into curves with gap closure which exhibit a discontinuity at zero load. Stresses are greatly reduced by gap closure and show almost no nonlinear effect up to the increased buckling load.

The plate strip model of the tensile-shear specimen has been analysed by Reemsnyder[818] on the basis of the second order beam theory which includes large deflections with the restriction of shallow curvature. The solution is based on functional analysis and reflects the influence of essential parameters in a closed form. The essential parameters are the relative

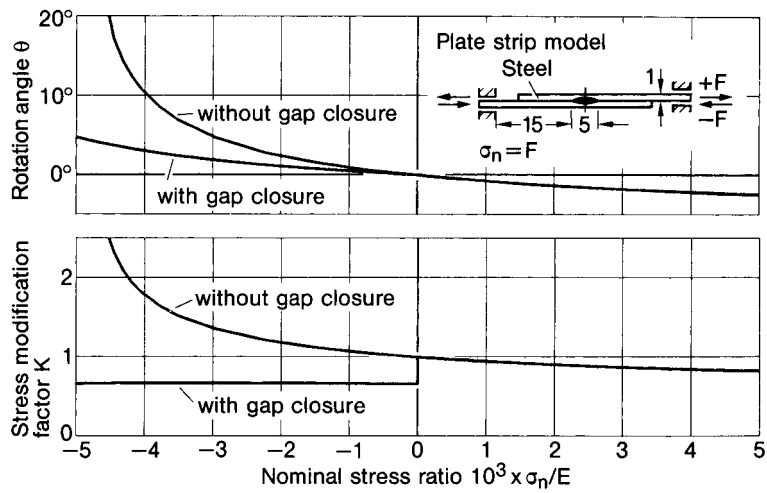


Fig. 9.20. Stress modification factor (referring to the structural stress at the nugget edge) and rotation angle of plate strip model of tensile-shear specimen subjected to tensile and compressive loading, dependent on nominal stress to elastic modulus ratio; results from finite element large displacement analysis; after Radaj and Zhang.[812]

nominal stress σ_n/E (beam in plane-stress condition) or $\sigma_n(1 - \nu^2)/E$ (strip in plane-strain condition) and the length-to-thickness ratio l/t if the diameter-to-thickness ratio d/t is fixed (e.g. $d/t = 3.5$). Test calculations with the derived formulae confirm the results gained by finite element analysis.

Finally, the tensile-shear specimen was analysed by the finite element method, assuming small and large displacements, respectively. For a tensile force value chosen in the medium-cycle fatigue range of the tensile-shear specimen in high strength steel ($t = 1$ mm, $\Delta F = 4$ kN, the structural stress at the weld spot edge is reduced by less than 2% by the effect of large displacements whereas the reduction in rotation angle is 23%. The changes in stress and deformation under comparable compressive loads are larger.

The following conclusions are drawn from the investigation: the effect of large displacements on the structural stress at the weld spot edge is rather small for specimens made of 1 mm thick sheet steel when subjected to tensile-shear loading in the medium- and high-cycle fatigue range. Therefore, a different fatigue strength behaviour of differently shaped specimens under tensile loading cannot be explained on the basis of this effect. The effect is more marked in tensile-loaded specimens made of sheet steel less than 1 mm thick, or in materials with higher strength relative to the elastic modulus. The effect is also more marked for higher loads in the low-cycle fatigue range and for static loading up to fracture. Elastic modelling is not adequate in these cases.

There is a noticeable effect of large displacements in compressive loading not only in the low- and medium-cycle, but also in the high-cycle fatigue range. Compressive shear loading increases the relative value of the structural stresses. The increase is compensated to a high degree by the contact pressure between the gap-free overlapping sheets as long as the deflections are not too large.

9.3.3 Large deflections at weld spots subjected to cross-tension loading

The investigation into large displacement effects has been extended from tensile and compressive shear loading to cross-tension loading of the weld spot (Radaj and Zhang[811]). Design measures are primarily aimed at producing shear loading of the weld spot, because of a relatively high fatigue strength in this loading case, whereas cross-tension or peel-tension loading should be avoided as far as possible. Cross-tension specimens are available for testing the fatigue strength in this unconventional loading state.

The longitudinal section of the specimen with dimensions conforming to standards is shown in Fig. 9.21. The (enlarged) deformation of the relevant plate strip model is plotted in Fig. 9.22. The nominal structural stress at the

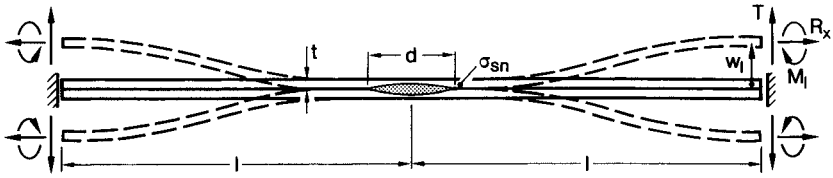
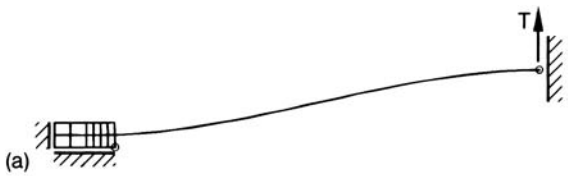


Fig. 9.21. Longitudinal section of cross-tension specimen, with prescribed transverse displacement loading with bending-rigid support; after Radaj and Zhang.[811]



(b) $l = 20$ mm $E = 2.1 \times 10^5$ N/mm^2 $\sigma_{sn} = \sigma_Y^*$
$t = 1$ mm $\nu = 0.3$ $= 500$ N/mm^2
$d = 5$ mm $E' = E/(1-\nu^2)$ $w_l = 0.132$ mm

Fig. 9.22. Deformation plot of plate strip model of cross-tension specimen (a) and introduced parameter values (b); after Radaj and Zhang.[811]

weld spot edge, $\sigma_{sn} = 3T(l - d/2)/t^2$, is set equal to the nominal yield limit $\sigma_Y^* = 500\,\mathrm{N/mm^2}$ (typical for high strength steels). Only tensile loading is investigated whereas compressive loading will generate hardly any stresses at the weld spot edge after gap closure has taken place.

The plate strip model of the cross-tension specimen has been investigated both with finite elements and with the second-order beam theory. One typical result is plotted in Fig. 9.23. The maximum structural stress is modified by the effect of large displacements, factor K (note that $\sigma_{sn} = \sigma_Y^* = 500\,\mathrm{N/mm^2}$ corresponds to $\tau_n^*/E' = 0.04 \times 10^{-3}$ or $\tau_n^* = T/t = 9.52\,\mathrm{N/mm^2}$ in the case considered). The dashed lines designate the unsuccessful attempt to correct the deflections of the small displacement analysis by a factor κ which obviously depends on the load level. An acceptable approximation was found by fitting the deflection w_l from the finite element solution in terms of the parameter τ_n^*/E'.

Finally, the cross-tension specimen was analysed by the finite element method assuming small and large displacements, respectively. For a cross-tension force value chosen in the medium-cycle fatigue range of the cross-tension specimen in high strength steel ($t = 1\,\mathrm{mm}, \Delta T = 2\,\mathrm{kN}$) the structural stress at the weld spot edge is reduced by about 15% by the effect of large displacements.

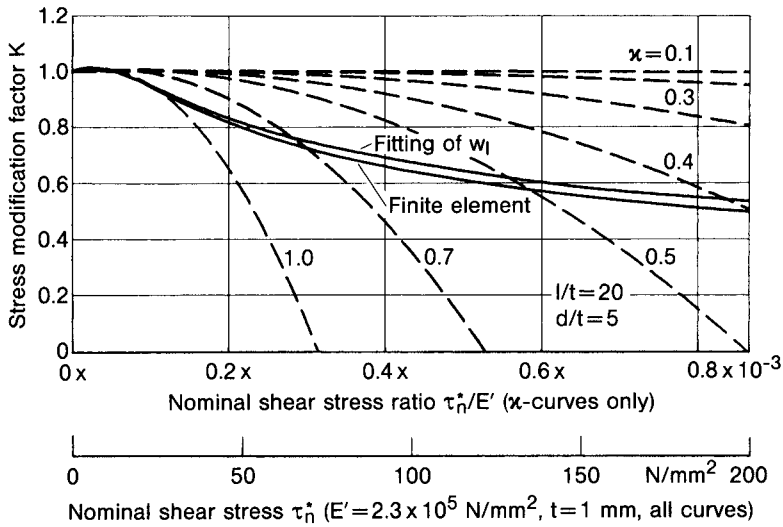


Fig. 9.23. Stress modification factor (referring to the structural stress at the nugget edge) of continuous beam model (with $E' = E/(1 - \nu^2)$) of cross-tension specimen, dependent on nominal shear stress to elastic modulus ratio for different values of the correction factor κ (dashed lines); results from finite element large displacement analysis and from approximation formula based on the load-deflection curve (solid lines); after Radaj and Zhang.[811]

The following conclusions are drawn from the investigation. The effect of large displacements in cross-tension loading on the structural stress at the weld spot edge is larger than in the case of tensile-shear loading but not large enough as to modify the conclusions given there. In cross-compressive loading, the structural behaviour is completely changed by the gap closure effect. The gap closure effect is also appreciable in peel-tension and peel-compression loading (see Section 10.4.5).

9.3.4 Buckling fatigue at spot welds

An important case of a large deflection effect in automotive engineering is flange buckling at spot-welded hollow section members under compressive flange forces. An example is the box section member manufactured from a hat section and a cover plate and subjected to a bending moment, Fig. 9.24. The compressive force in the flange does not result in any stress increase in the flange or at the weld spots as far as the small displacement theory is applied. In reality though, large deflections (relative to flange thickness) do occur with flange bending stresses at the weld spots and in the middle section between two weld spots. A gap is formed between the flanges result-

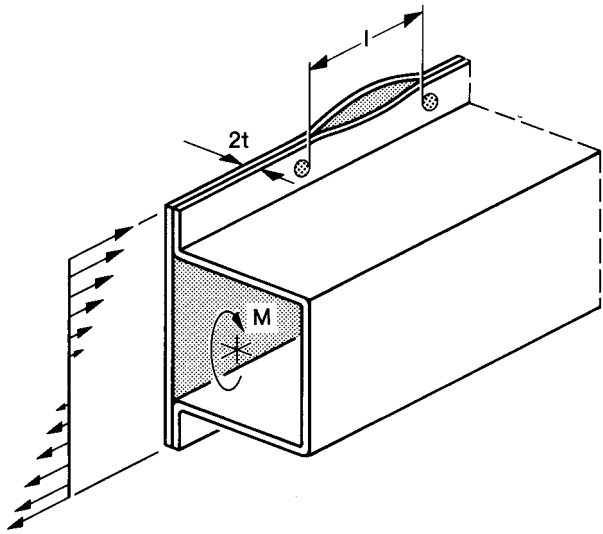


Fig. 9.24. Flange gap formation by flange buckling resulting from compressive flange stresses; after Oshima and Kitagawa.[802]

ing in flange buckling. The fatigue strength of the member in terms of flange nominal stress may be reduced by a factor of three in comparison with the non-welded parent metal.

In the case considered, the cover plate is primarily at risk of buckling. It deflects approximately in the shape of a cosine function between the two weld spots even when subjected to relatively low longitudinal compressive stress because of manufacture-related initial deflections. Cracks are initiated at the weld spot edges and in the middle section between two weld spots at the outer edge of the flange. Secondly, the opposite flange which is restrained by the web deflects in a multi-wave pattern when subjected to relatively higher compressive stress. Cracks occur over the entire length of the flange and at the weld spot edges.

A buckling analysis in respect of fatigue fractures was performed by Oshima and Kitagawa[802] considering the aforementioned box section member. The buckling nominal stress in the flange is determined from the buckling load of a comparable beam clamped rigidly at both ends:

$$\sigma_c = \frac{F_c}{tw_f} = \frac{\pi^2 Et^2}{3l^2} \tag{9.22}$$

where σ_c is the critical nominal stress in the flange at the first buckling mode, F_c is the critical force in the flange at the first buckling mode, t is the flange thickness, w_f is the flange width, E is the elastic modulus and l is the beam length equal to the distance between the weld spots (the pitch).

This critical stress is modified by the elastic support exerted on the flange by the adjacent cover plate or section web, respectively:

$$\sigma_c^* = \sigma_c\left(m^2 + \frac{3l^4}{m^2\pi^2 w_f l_f^3}\right) \tag{9.23}$$

where σ_c^* is the buckling nominal stress modified by an elastic flange support (cover plate or section web), σ_c is the original critical nominal stress at the first buckling mode, m is the buckling mode number, l is the distance between the weld spots (the pitch), w_f is the flange width and l_f is the free clamping length (l_{f1} or l_{f2}).

The support effect depends on the free clamping length of the relevant plate strip, Fig. 9.25:

$$w_1 = \frac{F_1}{EI}\frac{l_{f1}^3}{3} = F_1\frac{4l_{f1}^3}{Et^3} \tag{9.24}$$

$$w_2 = \frac{F_2}{EI}\frac{l_{f2}^3}{3} = F_2\frac{4l_{f2}^3}{Et^3} \tag{9.25}$$

where w_1 and w_2 are the deflections of the cover plate and flange plate strip, F_1 and F_2 are elastic (reactive) support forces at the cover plate and flange plate strip (per unit of strip length), l_{f1} and l_{f2} are the free clamping lengths of the cover plate and flange plate strip, E is the elastic modulus, I is the

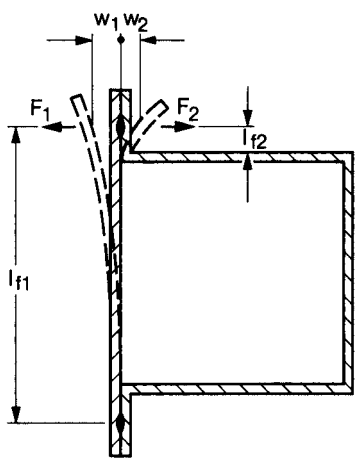


Fig. 9.25. Transverse elastic support of compressive stress loaded flanges forming a gap; free clamping lengths l_{f1} and l_{f2}; after Oshima and Kitagawa.[802]

moment of inertia of the cover plate and flange plate strip (per unit of strip length) and t is the cover plate and flange plate thickness.

Equation (9.23) is derived considering buckling of a beam with continuous elastic transverse support. Whereas the critical stress σ_c of free buckling decreases with the buckling length l, an opposite effect occurs due to the elastic support. The influence of the elastic support increases with the buckling length.

The mode number m should be selected such that the minimum value of the critical stress σ_c^* appears. Considering a cross-section $50 \times 50 \times 0.8$ mm combined with $l = 55$ mm and $w_f = 14$ mm, cover plate buckling is connected with $m = 1$ and $l_{f1} = 63$ mm resulting in $\sigma_c^* = 1.68\sigma_c$ (with $\sigma_c = 142.69\,\mathrm{N/mm^2}$ using $E = 2.05 \times 10^5\,\mathrm{N/mm^2}$). The hat section flange, on the other hand, buckles with $m = 5$ and $l_{f2} = 5.5$ mm resulting in $\sigma_c^* = 40.92\sigma_c$. This means that the cover plate buckles significantly more easily than the hat section flange. Nevertheless, it is prevented from free shortening and deflecting when connected to the hat section with the result that the stresses in the hat section flange increase initially until buckling also occurs. The different buckling behaviour of cover plate flange and hat section flange, respectively, may cause different locations of crack initiation.

On the basis of the buckling stresses and deformations, it is now possible to determine the flange structural stresses at the inner and outer surfaces of the flanges including the weld spot edge, as shown below for the single-wave buckling of the cover plate flange. A manufacture-related initial deflection of the flange is taken into account. The flange structural stresses at the weld spot (neglecting the increase by the weld spot) and in the middle between the weld spots are derived on the basis of the large deflection solution of beam buckling:

$$\frac{\sigma_{ei}}{\sigma_c^*} = \frac{\sigma_{mo}}{\sigma_c^*} = f\left(1 - \frac{3\delta}{1-f}\right) \tag{9.26}$$

$$\frac{\sigma_{eo}}{\sigma_c^*} = \frac{\sigma_{mi}}{\sigma_c^*} = f\left(1 + \frac{3\delta}{1-f}\right) \tag{9.27}$$

where σ_{ei} and σ_{eo} are the flange structural stresses at the inner and outer flange surface at the weld spot, σ_{mi} and σ_{mo} are the flange structural stresses at the inner and outer flange surface at the middle section between the weld spots, σ_c^* is the buckling stress in the flange, f is the flange force ratio, $f = F/F_c^* = \sigma/\sigma_c^*$, δ is the relative flange deflection, $\delta = w_0/t$, F and F_c^* are the flange force and its critical value at buckling, σ is the flange nominal stress, w_0 is the initial deflection at the middle section between the weld spots and t is the flange thickness.

The result of the calculation according to eqs. (9.22), (9.23), (9.26) and

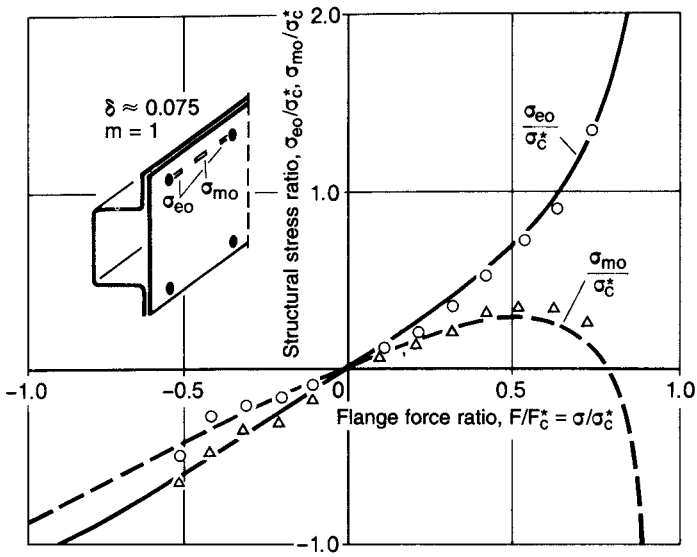


Fig. 9.26. Stresses at outer surface of cover plate flange as a function of flange compressive force: calculation results (solid and dashed lines) compared with measurement results (circular and triangular points); after Oshima and Kitagawa.[802]

(9.27) for the cover plate of the box section member is presented in Fig. 9.26, compressive forces and stresses appearing as positive dimensionless variables. Obviously, $\delta = 0.075$ was selected. The results of strain gauge measurements confirm the results from the numerical analysis which are independent of the geometrical parameters of the box section member with the exception of the initial deflection ratio.

The bending portion of the flange structural stress at the weld spot still has to be multiplied by the structural stress concentration factor of the weld spot in self-equilibrated plate bending:

$$\frac{\sigma_{ci}^*}{\sigma_c^*} = f\left(1 - \frac{3K_{sb}\delta}{1-f}\right) \tag{9.28}$$

where σ_{ci}^* is the total structural stress at the inner flange surface at the weld spot edge, σ_c^* is the buckling stress in the flange, f is the flange force ratio, δ is the relative flange deflection and K_{sb} is the structural stress concentration factor of weld spot ($K_{sb} = 1.0$–1.5).

On the basis of the above derivations, fatigue strength assessments are possible. Especially too, the location of primary crack initiation can be determined.

9.4 Analysis tools – endurable structural stresses or strains

9.4.1 Endurable structural stresses or strains at weld spots compiled by Radaj

Endurable structural stresses or strains in spot-welded joints were for the first time reviewed from the literature by Radaj.[894] The basis of the early investigations into local stresses or strains are mainly measurements by strain gauges which are to a minor part supplemented by stress calculations. Endurable values are primarily given in terms of structural strains measured at the weld spot edge in radial direction. These strain values must be used with care because the strain changes rapidly near weld spots and exact positioning, as well as the size of the strain gauges used, are critical and need standardisation.

The endurable strain range, $\Delta\varepsilon_{r\,en}$ (measured radially) at the weld spot edge on the inside of the plate is usually stated without reference to multiaxiality. It is an obvious step to take the multiaxiality influence into account by using an appropriate criterion, for example, the von Mises distortional strain energy criterion. The maximum normal stress criterion has also been proposed for application. Kurath[785] used the modified maximum shear stress criterion proposed by Findley[109] for multiaxial stress states when evaluating endurable structural stresses at spot welds in the high-cycle fatigue range. The local strain state at the weld spot edge can be approximated as being plane, i.e. the strain in the circumferential direction is completely suppressed.

Endurable values, $\Delta\varepsilon_{r\,en}$, are available mainly for zero-to-tension loading ($R = 0$). The conversion to radial and circumferential structural stresses can be achieved purely elastically, $\Delta\sigma_r = E\Delta\varepsilon_r/(1 - \nu^2)$ and $\Delta\sigma_t = \nu\Delta\sigma_r$, with respect to the high-cycle fatigue strength (but not with respect to the medium- and low-cycle fatigue strength). Hence, the von Mises equivalent stress is $\Delta\sigma_{eq} = E\Delta\varepsilon_r(1 - \nu - \nu^2)^{1/2}/(1 - \nu^2)$, or $\Delta\sigma_{eq} \approx E\Delta\varepsilon_r$ with $\nu = 0.3$. Therefore, $\Delta\varepsilon_{r\,en}$, converted uniaxially and elastically to a stress, results in the endurable equivalent structural stress, $\sigma_{eq\,en}$, with the restriction, however, that $\Delta\varepsilon_r$, as an averaged value at a certain distance from the weld spot edge, is smaller than the actual maximum value, in other words, $\Delta\sigma_{eq\,en}$ cannot be directly related to the numerically determined maximum structural stress values. In addition, as the measured $\Delta\varepsilon_r$ also varies depending on the strain gauge size and on the distance of the strain gauge from the weld spot edge, differing literature data with respect of the value $\Delta\varepsilon_{r\,en}$ are explicable by this fact alone.

The evaluation of the data[756,757,782,791,797,798,825,827] on endurable strain and stress ranges at the weld spot does not result in a uniform picture, for the

reasons mentioned, and in view of the need to reckon back from the strain or stress measured on the outside of the plate to the strain or stress on the inside of the plate. Some of the endurable values hardly differ at all from the values of the unnotched parent material. The investigation by Mori *et al.*[798] denies the possibility of strength assessment on the basis of local strain measurements independent of the structural details. The data presented below are therefore restricted to specific investigations which are substantiated by many test data and seem to be more generally applicable.

The investigation conducted by Kitagawa *et al.*[782] is the source of endurable radial strains, determined in tensile-shear and cross-tension specimens subjected to zero-to-tension loading, the strains being measured with 1 mm strain gauges on the outside of the plate adjacent to the edge of the electrode indentation. Conversion to the values for the inside of the plate as stated in Table 9.1 was based on the factor –2.0 in the case of tensile-shear, and on the factor –1.0 in the case of cross-tension. The values $\Delta\varepsilon_{r\,en}$ for $N = 10^7$ characterise the endurance limit of the joint. They correspond to the stresses $\Delta\sigma_{eq\,en}$ = 168–336 N/mm^2 for unalloyed steel and $\Delta\sigma_{eq\,en}$ = 105–210 N/mm^2 for high strength steel, which thus comes off worse. The elastic conversion of the strain values in the medium-cycle fatigue range results in unrealistically high stress values because of the plastic strain proportions being elastically converted.

The endurable strain amplitudes measured by Mizui *et al.*[797] on the inner surface of the plate at the weld spot edge of various specimens made of low-carbon steel are plotted in Fig. 9.27. The scatter range is rather large, but can be reduced by using stress intensity factors instead of strains (see Section 10.3.1). The mean values of the endurable strain amplitudes ($P_f = 50\%$) are more or less identical to the strain *S–N* curve of the parent material.

The investigation of Rupp *et al.*[827] refer to hat section specimens of unalloyed steel subjected to zero-to-tension torsional moments and internal pressure, i.e. to shear loading and peel-tension loading of the weld spots.

Table 9.1. Endurable strain range, $\Delta\varepsilon_{r\,en}$, at weld spot edge (inner surface of plate) dependent on number of cycles, *N*; mean values from tensile-shear and cross-tension specimens made of steel; after Kitagawa *et al.*[782]

Steel	Yield limit σ_Y [N/mm^2]	Thickness *t* [mm]	Strain range $\Delta\varepsilon_{r\,en} \times 10^4$ for		
			$N = 10^5$	$N = 10^6$	$N = 10^7$
Unalloyed	170–195	0.8–1.6	20–34	12–21	8–16
Low-alloy	225–255	0.8–1.6	16–29	10–17	5–10

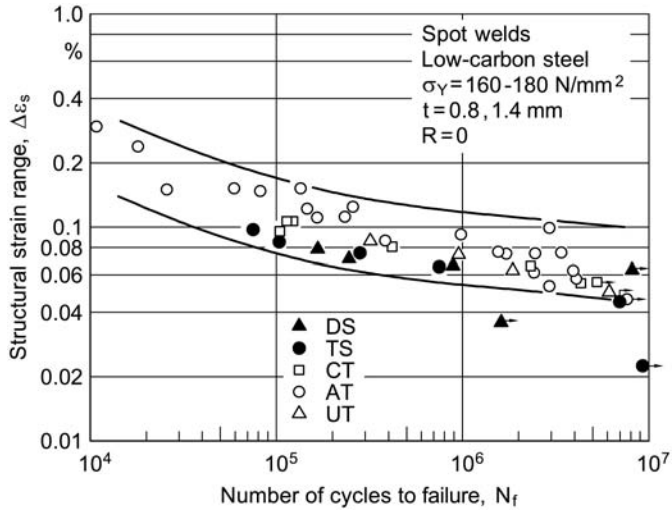


Fig. 9.27. Endurable structural strain range on the inner surface of the plate at the weld spot edge of various specimens made of low-carbon steel (double shear DS, tensile shear TS, cross tension CT, angular tension AT and U-shape tension UT); strain gauge length 2 mm; after Mizui *et al.*[797]

Table 9.2. Endurable structural stress range, $\Delta\sigma_{en} = 2\sigma_{a\,en}$, at weld spot edge (inner plate surface) dependent on number of cycles, *N*; scatter band from hat section specimens subjected to torsional moment and internal pressure, after Rupp *et al.*[827] (the values for $N = 10^7$ are extrapolations)

Steel	Yield limit σ_Y [N/mm²]	Thickness *t* [mm]	Stress range $\Delta\sigma_{en}$ [N/mm²] for		
			$N = 10^5$	$N = 10^6$	$N = 10^7$
Unalloyed	150–175	0.8–2.5	230–490	180–340	130–190

The radial strain measured on the outside surface with a 0.6 mm strain gauge located at a distance of 1 mm (considering the centre of the strain gauge) from the edge of the electrode indentation was converted, based on a finite element solution, to the strain on the inside of the plate and resulted in the endurable stresses $\Delta\sigma_{en} = E\Delta\varepsilon_{r\,en}$ summarised in Table 9.2 (ignoring individual shear fractures at lower endurable stress in the thick-walled hat section specimens under torsional moment). The higher values apply to the lower plate thickness and the lower values to the higher plate thickness. A thickness factor $\kappa = 0.6\sqrt{t}$ is introduced by Rupp *et al.*[821,824,827,828] on the bending portion of the structural stress amplitudes, see eq. (9.11). The

thickness-related fatigue parameter $p_a = \sigma_{sr\,a}\sqrt{t}$ is proposed by Zhang and Richter[846] (with nominal radial structural stress amplitude $\sigma_{sr\,a}$) in order to characterise the fatigue strength and to produce a uniform p_a–N curve for different sheet thicknesses. The last-mentioned authors admit a close correspondence with the stress intensity approach.

Further endurable structural stresses based on sufficiently large data bases (number of specimens, types of loading) were published by Sheppard[983] and Pan[972] using the structural stress according to eq. (9.13), Fig. 9.28. Once more, the high strength steels come off worse in the spot-welded condition in Sheppard's evaluation, but not in Pan's. It was found by Sperle[838] that non-load-carrying spot welds in contrast to load-carrying spot welds exhibit a rise in fatigue strength with an increasing yield limit of the parent material, Fig. 9.29.

The question of the performance of spot-welded joints in advanced high strength steels in comparison to conventional sheet steels, Table 9.3, has been answered on the basis of fatigue tests by Rathbun *et al.*[817] without specification of structural stresses (the introduced stress intensity factor formulae based on structural stresses are partially incorrect). The endurable load ranges in tensile-shear and cross-tension loading of the weld spot are plotted versus number of cycles to failure, Fig. 9.30 (specimens with the edges stiffened by flanges to reduce nugget rotation). The static strength

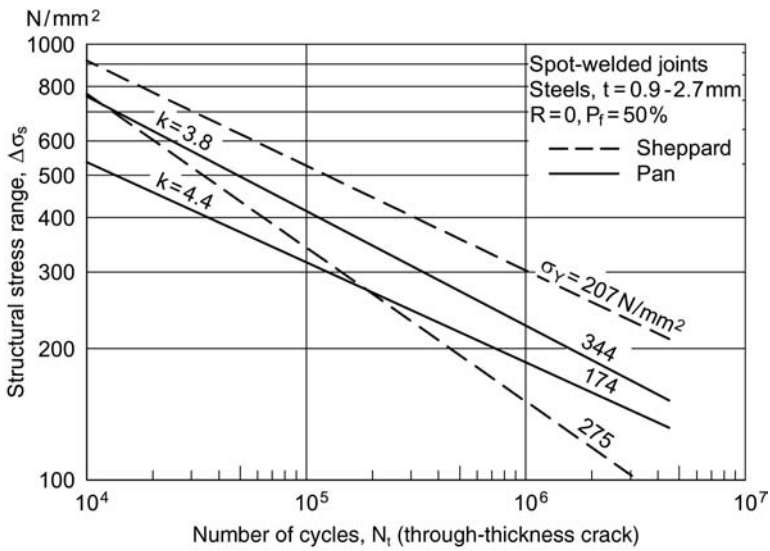


Fig. 9.28. Endurable structural stress range in spot-welded low and high strength steels; various specimens and loading modes; cycles up to a through-thickness crack (failure probability $P_f = 50\%$, load ratios $-1 \le R \le 0.5$); after Sheppard[983] and Pan *et al.*[972,975]

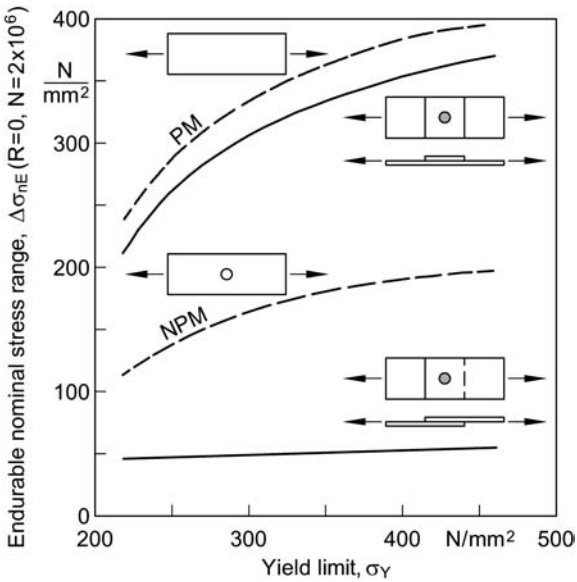


Fig. 9.29. Fatigue strength (endurable nominal stress range, $\Delta\sigma_{nE}$ for $R = 0$ at $N = 2 \times 10^6$ cycles) dependent on yield limit (low and high strength steels); non-load-carrying and load-carrying spot welds in comparison to parent material (PM) and notched parent material (NPM), the notch represented by a hole; after Sperle.[838]

Table 9.3. Material properties and dimensional parameters of spot welds in the investigation by Rathbun *et al.*[817]

Steel	Yield limit σ_Y [N/mm^2]	Tensile strength σ_U [N/mm^2]	Hardness in nugget H_V[HVN]	Sheet thickness t [mm]	Spot diameter d_{av} [mm]
DQSK[a]	200	340	225	1.5	7.6
HSLA50[b]	350–400	420–450	320	1.5	7.9
DP590[c]	350–360	620–630	320	1.4	8.0
TRIP590[d]	430	610	400	1.4	8.4

[a] Drawing quality special killed.
[b] High-strength low-alloy.
[c] Dual phase.
[d] Transformation-induced plasticity.

values of the weld spot entered at $N_f = 10^0$ are connected by dashed lines with the experimentally determined *F–N* or *T–N* curves, respectively, drawn as solid lines. The result for tensile-shear loading is clear: the low-cycle fatigue strength is correlated with the tensile strength of the parent mate-

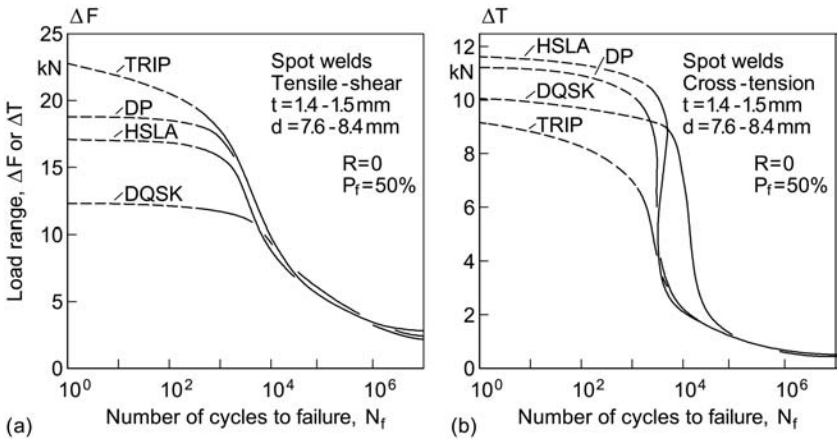


Fig. 9.30. Endurable load ranges of spot welds in tensile-shear loading (a) and cross-tension loading (b); conventional and high strength steels (DQSK: Drawing quality special killed, HSLA50: High-strength low-alloy, DP590: Dual phase, TRIP590: Transformation-induced plasticity); with sheet thickness t and averaged weld spot diameter d; after Rathbun *et al.*[817]

rial, but there is practically no difference in strength in the high-cycle fatigue range. The situation in cross-tension loading is much more complicated. The endurable static loads are not arranged according to the tensile strength of the parent material and extreme curve gradients occur in the medium-cycle fatigue range inclusive of a negative slope in one case expressing longer life for higher stress. The diagrams indicate that weld spots subjected to combined loading will exhibit a much more complicated strength behaviour than is generally assumed.

Spot-welded joints in high strength steel may be superior to those in mild steel in the case of variable-amplitude loading (Abe *et al.*[746]). This is also shown by Satoh *et al.*[835] for two-level cyclic loading. It was also found in these investigations that Miner's damage accumulation rule fails with spot-welded joints in those cases where crack closure plays a dominant role.

The corrosion fatigue strength of spot-welded stainless sheet steels (austenitic or duplex) exposed to 3% NaCl solution was found to be reduced by 30–40% at $N = 10^7$ cycles compared to the fatigue strength in air (Linder and Melander[789]).

Combined shear- and cross-tension loading of the weld spot has been investigated by Kang *et al.*[780] comparing fatigue test results in terms of endurable structural stress ranges with fatigue predictions according to Swellam's model (see Section 10.3.1), Sheppard's model (see Section 11.3.3) and Rupp's model.

The strain-based fatigue life prediction was applied to spot-welded joints by Lee *et al.*,[787,788] and by Ni and Mahadevan.[800] The structural strain is typically evaluated from hexahedronal solid elements with an edge length of 0.35 mm forming four layers over the plate thickness,[800] so that part of the notch effect of the weld spot edge is included in the structural strains. The results thus depend on the applied element size. The local strain approach is further elaborated in Chapter 11.

9.4.2 Endurable structural stresses at weld spots compiled by Rupp

At a later date, Rupp *et al.*[828] have reviewed their own and other results of fatigue testing of component-like spot-welded specimens,[821,824,827] Fig. 9.31. The maximum radial structural stress amplitude is evaluated dependent on the number of cycles which causes a 'technical crack', that is, a crack penetrating the plate thickness or running through the joint face thus reducing the stiffness of the specimen by about 10%. Supplementary results were presented by Wallmichrath and Eibl.[843]

The specimens comprise the single-hat and double-hat section specimens under torsional moments and internal pressure, the H-shaped specimen in tensile-shear and peel-tension loading, a T-shaped connection of single-hat

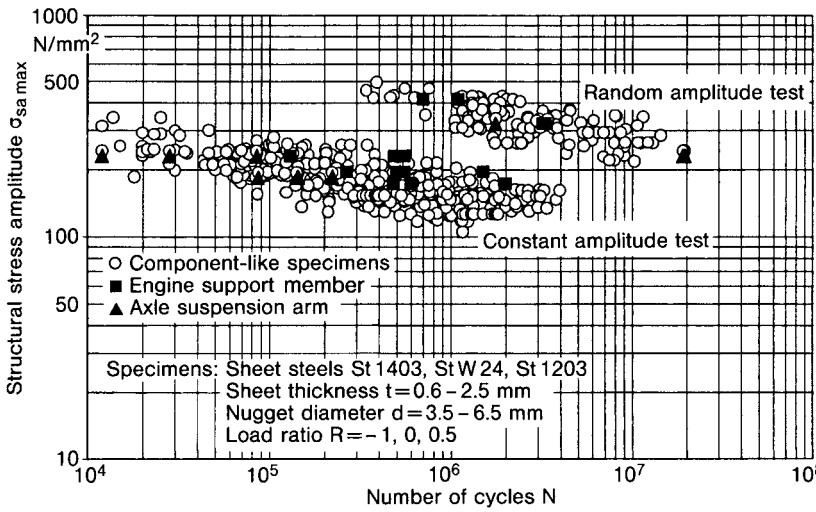


Fig. 9.31. Endurable structural stress amplitudes transformed to $R = 0$ with bending components modified by factor $0.6\sqrt{t}$ in spot-welded component-like specimens and structural components; evaluation of the authors' own and other test results; after Rupp and Grubisic.[824]

section boxes butting via tensile-shear and peel-tension loaded joints, a structural member consisting of two double-hat section boxes telescoped into one another, jointed by spot-welding and subjected to bending moments, and finally single-spot and double-spot reinforced tensile-shear specimens. The investigated steels, sheet thicknesses, nugget diameters and load ratios are given in Fig. 9.31. Fatigue testing was done both with constant and variable load amplitudes. The Gaussian cumulative frequency distribution of amplitudes was used in the random load test which was performed with a spectrum size of $H_0 = 5 \times 10^5$ (irregularity factor $I = 0.99$). The plotted test results for the axle suspension arm and the engine support member are further discussed in Sections 9.5.1 and 9.5.2.

The test results in the original publications[821,824,827] are given in terms of endurable load versus number of cycles. The loads comprise forces, moments and internal pressure. They are converted into (nominal) structural stresses by application of the approximative formulae given in Sections 9.2.6 and 9.2.7.

The following data characterise the fatigue strength under constant-amplitude loading with $R = 0$ of spot-welded, component-like specimens made of sheet steel of type St1403 with plate thickness $t = 0.66$–2.5 mm and nugget diameter $d = 3.5$–6.5 mm according to Rupp *et al.*:[828]

- the local fatigue strength of the sheet metal against plate fracture at $R = 0$ and $N = 10^6$ cycles: endurable structural stress amplitude $\sigma_{sA} = 145\,\mathrm{N/mm^2}$,
- the local fatigue strength of the nugget metal against nugget fracture at $R = 0$ and $N = 10^6$ cycles: endurable structural stress amplitude $\sigma_{sA} = 105\,\mathrm{N/mm^2}$,
- the inverse slope of the S–N curve at $N \le 10^6$ cycles: $k = 6$ (different from single-spot specimens: $k = 3.5$–4.0).

The above values are given for the load ratio $R = 0$ and the failure probability $P_f = 50\%$. The width of the scatter range of number of cycles N is characterised by $T_N = 1/7.2$. This value is relatively large because the test results of different authors and investigations are combined. Slightly lower endurable stresses were determined for spot-welded high strength sheet steel (ZStE380). The endurable stresses of spot-welded austenitic stainless sheet steel were up to 30% lower.[823] The conditions for higher fatigue strength with spot-welded high strength sheet steels were investigated by Grubisic.[772] The above data are summarised in Table 9.4.

The endurable stress in respect of plate fracture given above includes a thickness correction. The bending component of the structural stress is modified by the factor $0.6\sqrt{t}$, i.e., the endurable stresses in the specimens with sheet thickness $t \approx 1$ mm are substantially reduced before being incorporated in Fig. 9.31. On the other hand, the endurable stresses from the

Table 9.4. Endurable structural stress parameters of spot-welds in mild steel (St 1404), high-strength low-alloy steel (ZStE 380), ferritic and austenitic stainless steels (1.4003, 1.4301) and aluminium alloy (AlMg5Mn); after Rupp[823] (slightly modified)

Material	St 1404	ZStE 380	1.4003	1.4301	AlMg5Mn
Sheet thickness t [mm]	0.66–2.5	0.8	1.5–3.0	1.5–3.0	1.2–2.0
Weld spot diameter d [mm]	3.5–6.5	4.4	6.1–8.7	6.1–8.7	5.5–9.9
Hardness in nugget [HV]	200–300	400			100
Fatigue strength σ_{sA} [N/mm^2] ($R = 0$, $P_f = 50\%$)	130	125	120	90	49
Referred number of cycles, N_E	2×10^6	2×10^6	2×10^6	2×10^6	2×10^7
Inverse slope, k	6.0	5.5	4.0	4.0	5.0
Mean stress sensitivity, M	0	0.1	0.1	0.1	0.2

figure must be applied on nominal structural stresses including the thickness correction (see eq. (9.11)). Rupp *et al.*[827] claim that they have experimental and numerical evidence for an actual stress reduction but they also concede that the endurable stresses might be higher in thinner sheet metal.

The argument given above is not convincing. The nominal structural stress formulae derived from the rigid core model are valid independent of sheet thickness as far as pure joint face loading (i.e. loading without eigenforces) is considered. Accordingly, the thickness effect must be exclusively interpreted in terms of varying endurable structural stresses. The latter are higher for thinner sheet metal and lower for thicker sheet metal. This view is supported by the stress intensity approach which considers the stress intensity factor at the weld spot edge to be relevant to fatigue. The stress intensity factor results from the structural stress times the square root on sheet thickness, eqs. (10.2–10.4), i.e. the factor $0.6\sqrt{t}$ can be explained on that basis but not its restriction to bending loads. However, since the correction for sheet thickness is applied in the stress calculation both of the component (operational stress) and of the specimen (endurable stress), the procedure for the strength and life evaluation according to the structural stress approach is not restricted to a special sheet thickness.

Introducing the fatigue strength data given above into the structural stress formulae related to plate fractures (inclusive of the thickness correction[821,827,828]) and nugget fractures in definite loading cases, gives a limit curve separating the two fracture types in a diagram of weld spot diameter over plate thickness, Fig. 9.32. Obviously, the minimum weld spot diameter for avoiding nugget fractures is about 30% larger in peel loading than in shear loading if the plate thickness is small, but the difference is reversed with higher plate thickness. The two curves confirm the generally accepted

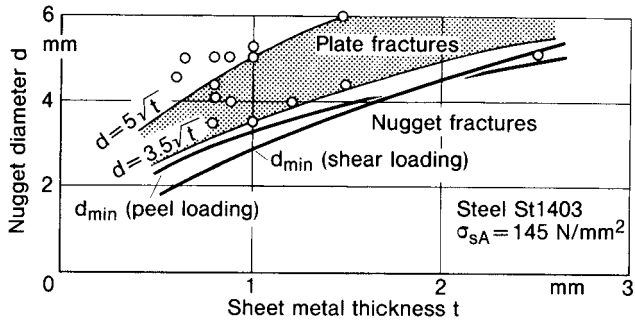


Fig. 9.32. Prediction of plate fractures versus nugget fractures dependent on sheet metal thickness and nugget diameter; range of design formulae (shaded area), observed diameter–thickness combinations with plate fractures (point symbols); after Rupp and Grubisic.[824,828]

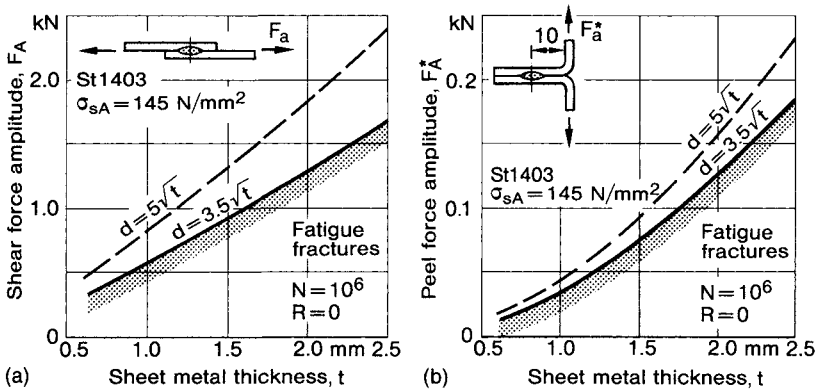


Fig. 9.33. Endurable shear force amplitude (a) and peel force amplitude (b) dependent on sheet metal thickness; diameter to thickness ratios according to design rules; strength assessment according to Rupp and Grubisic;[824] fatigue fractures in shaded area.

design rule $5\sqrt{t} \geq d \geq 3.5\sqrt{t}$. The diagram additionally includes the diameter–thickness combinations in the research projects evaluated,[821,824,827] where mainly plate fractures were observed.

Using the above design rule, the structural stress formulae for plate fractures, the thickness correction and the endurable stress amplitude σ_{sA} = 145 N/mm^2, endurable force amplitudes F_A and F_A^* can be derived for tensile-shear loading and peel-tension loading, respectively, Fig. 9.33. Attention must be paid to the fact that the endurable peel force depends heavily on the bending moment of this force. This moment rises with the distance between weld spot edge and folded web.

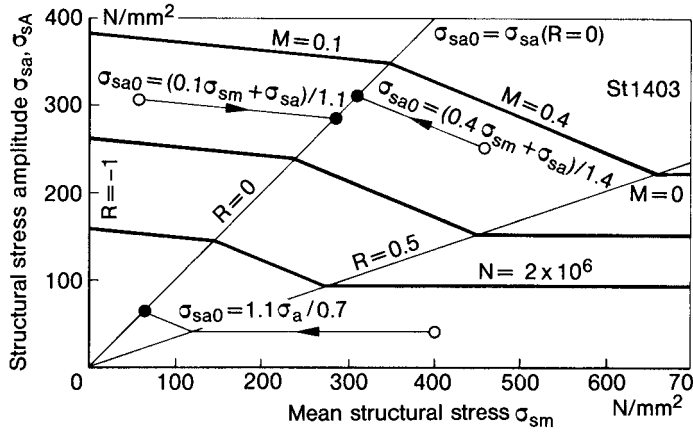


Fig. 9.34. Simplified Haigh diagram with endurable structural stress amplitudes at weld spots (bending stress amplitudes modified by factor $0.6\sqrt{t}$); transformation of stress amplitudes with $R \neq 0$ into equivalent amplitudes with $R = 0$; after Rupp *et al.*[821,827]

The endurable stresses given above are related to the stress ratio $R = 0$, i.e. to zero-to-tension loading. The dependency of the endurable stress amplitude σ_{sA} on mean stress σ_{sm} and varying R values has only been investigated in a selective manner. Rupp *et al.*[827] propose a simplified Haigh diagram based on the available test results for St1403 sheet steel, Fig. 9.34. Different mean stress sensitivities M are used in the sections between $R = -1$, $R = 0$, $R = 0.5$ and for $R > 0.5$: $M = 0.1$, $M = 0.4$ and $M = 0$. The lower curve corresponds to the technical endurance limit (bending stress amplitudes modified by the factor $0.6\sqrt{t}$), the upper curves are related to the finite life range (without giving definite cycle numbers). The diagram is also used to determine transformed stress amplitudes with $R = 0$ from stress amplitudes with $R \neq 0$ to perform the cumulative damage calculation. Relevant formulae are given in the diagram for this purpose.

The maximum stress values plotted in the diagram exceed the ultimate tensile strength of the material despite the reduction by $0.6\sqrt{t}$ (St1403 steel: $\sigma_U \approx 320\,N/mm^2$). In fact, Rupp *et al.*[827] measured local stresses up to $900\,N/mm^2$. The following explanation is given for the discrepancy. The elastic-plastic strains are linear-elastically converted into stresses. Thus, the stresses may be unrealistically increased depending on the extent of plastic deformation. Additionally, the true fracture strength is substantially higher than the ultimate tensile strength. Finally, the limit stresses may be increased by hardening, residual stresses and elastic-plastic support effects.

The results from the random variable-amplitude tests show that the linear cumulative damage calculation should be performed with a critical

damage sum D = 0.5–2.0 based on Miner's rule modified according to Haibach, with the inverse slope k of the S–N curve for $N \leq 2 \times 10^6$ and $k' = 2k - 1$ for $N \geq 2 \times 10^6$. A damage sum $D = 0.5$ is considered to be permissible.

Endurable structural stresses in spot-welded aluminium alloys have been determined by Rupp:[822] component-like specimens, aluminium alloys AlMg5Mn (AA5182) in the annealed condition and AlMg0.4Si1.2 (AA6016) in the age-hardened condition, sheet thickness t = 1.2–2.0 mm, weld spot diameter d = 4.4–9.9 mm, and testing conditions as with steel specimens.[827] Only the test results for AlMg5Mn, constant- and variable-amplitude structural stress S–N curves, are well established, Fig. 9.35. The result of the investigation is summarised in Table 9.5 in comparison with mild steel. As with steel, a sheet-thickness-dependent factor on the endurable stresses has to be introduced in order to get a uniform S–N curve.

The critical damage sum relating to Miner's rule modified for $N \geq 10^7$ cycles amounts to D = 0.5–2.0. A value D = 0.5 is considered to be permissible.

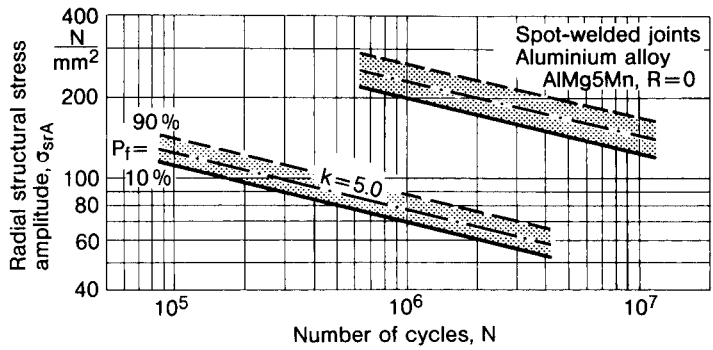


Fig. 9.35. Structural stress S–N curves (constant-amplitude and random variable-amplitude) of spot-welded AlMg5Mn aluminium alloy; radial stress approximately equal to von Mises equivalent stress; after Rupp.[822]

Table 9.5. Endurable structural stress parmeters of spot-welds in AlMg5Mn aluminium alloy in comparison with spot-welds in St1404 mild steel (plate fractures); after Rupp[822]

Material	AlMg5Mn	St1404
Fatigue strength, σ_{sA} ($N = 10^6$, $R = 0$, P_f = 50%)	78 N/mm²	145 N/mm²
Inverse slope, k (of S–N curve)	5	6
Mean stress sensitivity, M ($-1 \leq R \leq 0$)	0.2	0.1
Critical damage sum, D_c	0.5–2.0	0.5–2.0

9.4.3 Endurable structural stresses at weld spots compiled by Maddox

Endurable structural stresses in spot-welded steels from a wide variety of joint types were also evaluated by Maddox[792,793] and supplemented by the results of Lindgren *et al.*,[790] Fig. 9.36. The diagram is to a high degree self-explanatory. The structural stress comprises the local membrane and out-of-plane-bending stresses determined according to eq. (9.12). The bending stresses were neglected when evaluating the LCB and SST specimens because gap closure prevents major bending loading in these cases. The data presented justify the use of the design curve IIW Class 125 with inverse slope $k = 3.0$ as the structural stress limit (compare Fig. 2.4 with the endurance limit according to the new edition[3,133]).

Lindgren *et al.*[790] reported on fatigue tests on load-carrying and non-load-carrying spot-welded hat-section box beams in mild and high strength carbon steels as well as in type 18Cr9Ni stainless steel.

9.4.4 Endurable structural stresses at laser beam welds in comparison

Penetration-welded lap joints (e.g. laser beam welded) show a structural stress and deformation behaviour which is similar to that of resistance

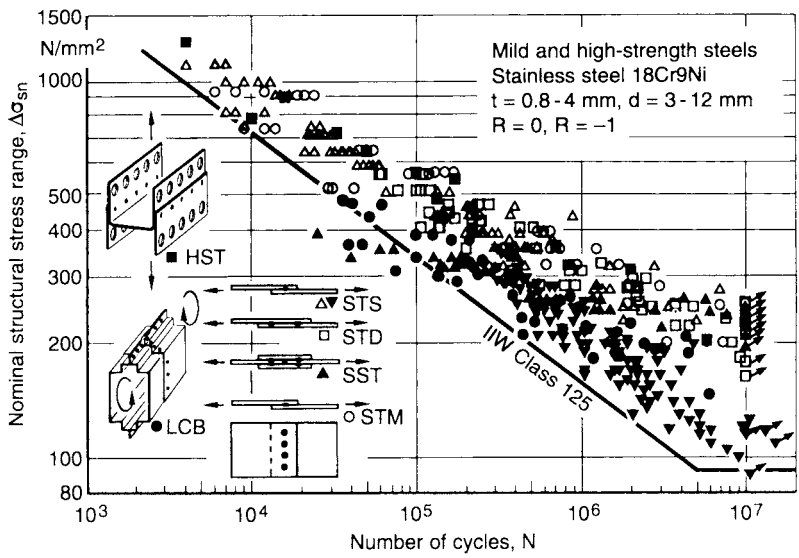


Fig. 9.36. Recommended nominal structural stress *S–N* curve for spot-welded joints in steel according to Maddox,[792,793] with inclusion of test results by Lindgren *et al.*[790]

spot-welded joints. Some geometric aspects are identical: the eccentricity of the overlapping plates and the slit tip at the joint face edge. The structural stress state is less complex in the penetration-welded than in the spot-welded joint insofar as the cross-sectional model represents the complete stress and strain state in the former case. Structural stress calculation is thus greatly simplified and structural strain measurements to determine the weld seam forces can be reduced to simple strain gauge positioning schemes (Zhang and Radaj[848]).

The main difference between penetration seam-welded and resistance spot-welded joints is found in the ratio of joint face width to plate thickness. This ratio is small in the former and large in the latter case. Also, the microstructural and residual stress state cannot be set equal in the two cases.

Unifying aspects in endurable stress analysis of resistance-spot-welded and laser-beam-welded lap joints were introduced early by Atzori *et al.*[748] and by Dattoma and Lazzarin.[755] It was verified by fatigue tests with tensile-shear specimens that the normalised *S–N* curve with unified scatterband in the form originally proposed by Haibach[2] for conventional seam-welded joints, Fig. 2.10 (with inverse slope $k = 3.5$–4.0), is also applicable to spot-welded joints. This transference is independent of how the nominal stress is defined (referring to spot diameter or plate width, with or without bending stresses superimposed). Further normalised *S–N* curves related to spot-welded tensile-shear specimens in various steels (low-carbon, high-strength low-alloy and austenitic) were presented by Aristotile[747] (inverse slope $k = 4.1$) and by Blarasin *et al.*[749] (inverse slope $k = 3.75$).

When comparing seam-welded and spot-welded tensile-shear specimens of identical global geometry, varying the width-to-diameter ratio w/d of the spot-welded joints, the endurable nominal stress amplitude σ_{nA} (membrane portion) found for the seam-welded joints remains applicable to spot-welded joints up to a width-to-diameter ratio $w/d \leq 3.5$, Fig. 9.37. The endurable stress amplitude then falls linearly with further rising ratio w/d in the bilogarithmic diagram expressing an approximately constant value of the nominal structural stress amplitude at the weld spot, $\sigma^*_{sn} = F/td = (w/d)\sigma_n$. Note that $\sigma_{sn} = (4/\pi)\sigma^*_{sn}$ according to eq. (9.3) which results in $\sigma_{sn\,A} = (4/\pi)(w/d)\sigma_{nA} \approx 250\,\mathrm{N/mm^2}$ for spot-welded joints ($N = 10^5$ cycles, $R = 0$, $P_f = 50\%$), to be compared with $\sigma_{sn\,A} = 4\sigma_{nA} \approx 220\,\mathrm{N/mm^2}$ for seam-welded joints.

Blarasin *et al.*[749] showed that the endurable stresses in laser-beam-welded lap joints depend on the ratio of seam width w_s to plate thickness t, Fig. 9.38. Transferring the findings from the theoretical investigation by Nykänen[971] (see Fig. 11.40), the maximum strength occurs with the ratio $w_s/t \approx 1.0$. The lower endurable stress amplitudes of resistance-seam-welded lap joints (with larger ratios w_s/t) mentioned by Blarasin are thus explained.

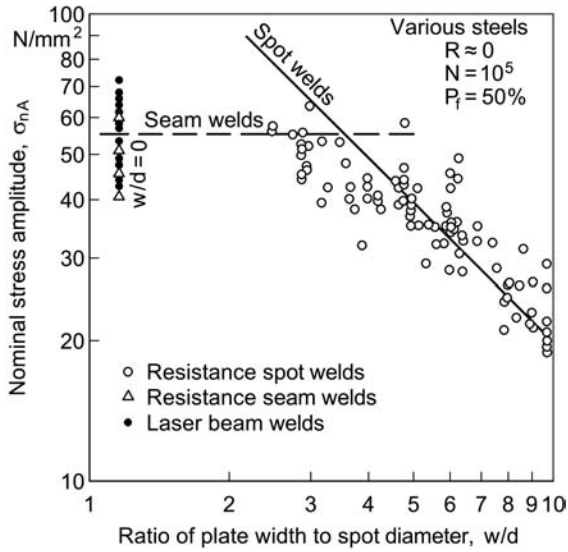


Fig. 9.37. Endurable nominal stress amplitude (membrane portion), σ_{nA}, in plate of resistance-spot-welded tensile-shear specimen dependent on ratio of plate width to spot diameter, w/d, in comparsion to corresponding seam welds (relvant: $w/d = 0$); after Blarasin *et al.*[749]

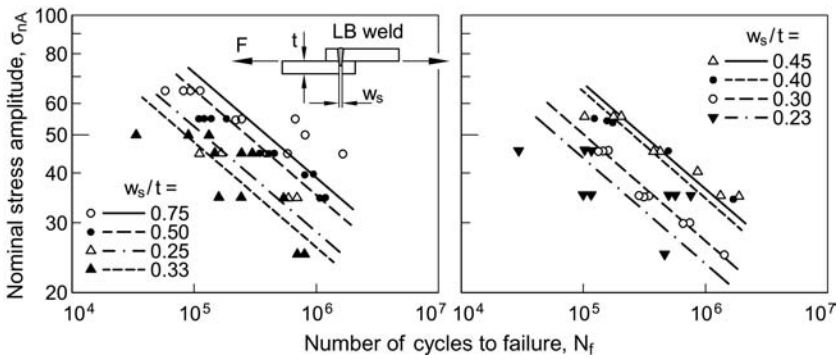


Fig. 9.38. Endurable nominal stress amplitude (membrane portion), σ_{nA}, in plate of laser-beam (LB) seam-welded tensile-shear specimen dependent on number of load cycles to fracture (*S–N* curves) for different ratios of seam width to plate thickness, w_s/t; after Blarasin *et al.*[749]

The endurable structural stress amplitude for laser beam welded lap joints in St1403 sheet steel (thickness t = 0.9–2.0 mm) was found to be σ_{sA} = 140–240 N/mm^2 at $N = 2 \times 10^6$ cycles and $R = 0$ according to tentative fatigue test results by Sonsino *et al.*[837] (the plate fractures re-evaluated on

the basis of the structural stress on the inside surface of the plate by Radaj *et al.*,[907] compare Section 10.4.7).

In another investigation by Hsu and Albright,[777] the shear- and peel-tension stresses at the joint face edge gained from a functional analysis solution (by Goland and Reissner[869]) were combined to an equivalent structural stress according to the von Mises distortional strain energy criterion. The endurable equivalent structural stress range at $N = 10^6$ cycles was found to be $\Delta\sigma_{s\ eq\ en} = 300\,N/mm^2$, i.e. about 75% of the parent material fatigue strength.

The application-relevant question whether laser-beam-welded or resistance-spot-welded lap joints yield higher fatigue life was addressed by Blarasin *et al.*,[749] and by Flavenot *et al.*[770] (tentative investigation) as well as by Wang and Ewing[844] (investigations closely related to actual designs, see Sections 9.5.3 and 10.4.7) with the result that laser-beam-welded joints may be superior, but only under optimised design conditions. Obviously, the question cannot generally be answered because the performance of welds depends substantially on design and process parameters.

9.4.5 Endurable structural stresses at GMA welds

The fatigue assessment above of resistance-spot-welded lap joints and of the corresponding laser-beam-welded joints has to be supplemented by the consideration of GMA fillet-welded joints, as far as thin-sheet structural components mainly in automobile design are concerned (e.g. hydroformed tubes, engine subframes, bus chassis). The hot spot structural stress approach for seam-welded joints (see Chapter 3) has to be applied in the latter case, adapted to the peculiarities of thin-sheet designs, Fig. 9.39.

Fayard *et al.*[762–764] propose a numerical calculation method for the fatigue life prediction for fillet-welded sheet-steel structures and its application in automobile design. The method uses a uniform hot spot structural stress *S–N* curve independent of the geometry of the structural member and the applied loading. The design stress, which is calculated by a specific thin-shell finite element analysis, is defined as the maximum principal structural stress amplitude at the hot spot. The method seems to be transferable to other materials (e.g. aluminium alloys) and other industrial products (e.g. rail vehicles).

The following meshing rules are defined in order to overcome the difficulties occurring with too fine meshes (high expenditure and computer time, stress singularity in intersection line, three-dimensional behaviour in weld zone):

– Rigid elements are used to link the different sheet structures in order to ensure, on the one hand, the displacement compatibility in the joint

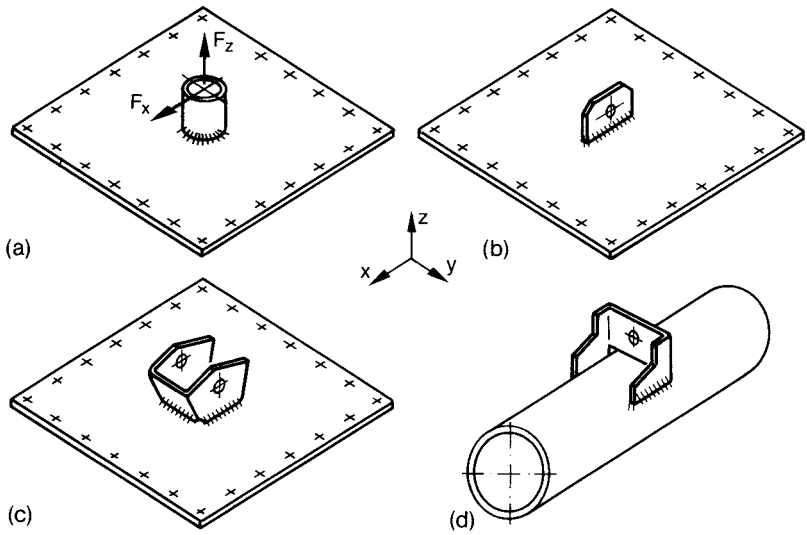


Fig. 9.39. GMA fillet-welded joints in thin-sheet structural components from automobile design; design samples used in fatigue tests for determining the structural stress *S–N* curve; after Fayard *et al.*[763,764]

zone and, on the other hand, to reproduce the local rigidity induced by the weld and also to simulate the force flow from one sheet to the offset other sheet through the weld.

– The size of the shell elements in the joint zone is defined such that the centres of gravity or Gauss points where the stresses are evaluated are located at the weld toe in order to avoid interpolations or extrapolations to the hot spot.
– The size and positioning of the shell elements have to take into account the weld leg length and the sheet thicknesses. Typically, the element size roughly equals the weld leg length.

These meshing rules are described more precisely in Fig. 9.40 for two fillet-welded joints commonly encountered in automobile design. The stresses are evaluated at the centre of gravity of each element.

The design stress is defined as the first principal stress amplitude at the hot spot where crack initiation is expected or observed. Crack propagation is considered to be the dominant mechanism of fatigue damage. A crack depth which equals half the sheet thickness is used as the failure criterion in fatigue testing. With the GMA-welded design samples shown in Fig. 9.39, a uniform scatter range of fatigue test results was found for different loading states, sheet thicknesses and material strengths, Fig. 9.41 (note the semi-logarithmic scale). The test results for differently designed

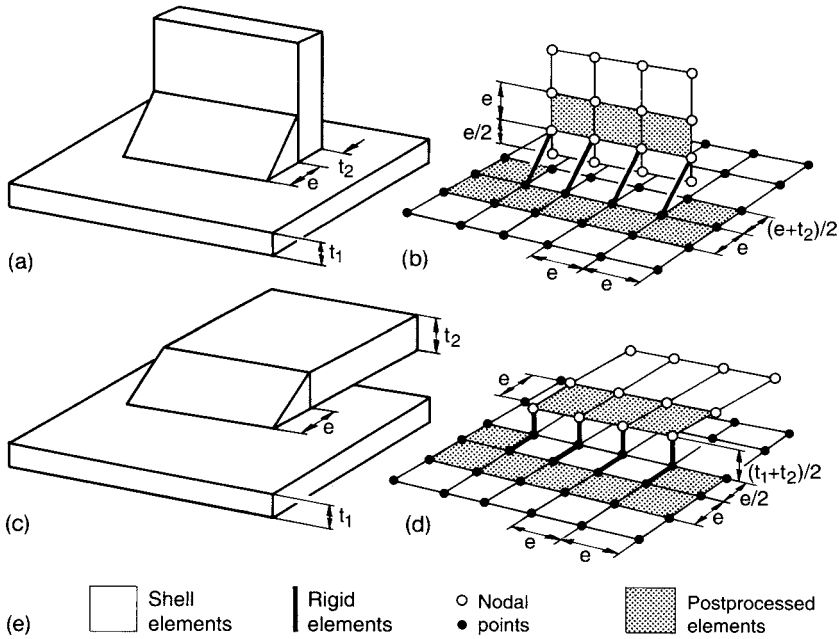


Fig. 9.40. Meshing rules for determining the hot spot structural stress in thin-sheet structural components from automobile design; typical joint geometries (a, c) and related mesh designs (b, d); after Fayard *et al.*[763,764]

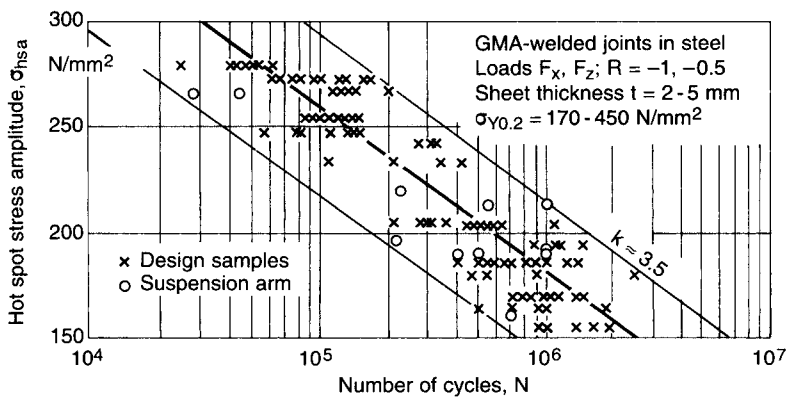


Fig. 9.41. Structural stress *S–N* curve for design based on hot spot structural stress evaluation related to GMA fillet-welded thin-sheet structural components from automobile design; design samples according to Fig. 9.39 and suspension arm variants; failure criterion: crack depth equal to one half of the sheet thickness; meshing rules according to Fig. 9.40.; after Fayard *et al.*[763,764]

suspension arms (evaluation of first visible cracks) analysed according to the above procedure fit well into the scatter range of the design stress curve.

The above approach was further elaborated by Dang Van *et al.*[754] with regard to biaxial local stress conditions. In cases of superimposed (longitudinal) shear loading of the weld toe (possibly in a non-proportional manner), Dang Van's criterion of the principal shear stress amplitude, assumed to be dependent on the hydrostatic mean stress, is applied instead of the criterion of the first principal stress amplitude. The residual stresses are considered to be of minor importance in thin-sheet structures and are therefore neglected in the mean stress. Endurable values of the hot spot stress amplitudes (first principal stress) are differentiated with regard to low strength and high strength steels, Fig. 9.42.

A similar procedural development was presented by Fermér *et al.*[766] The thin-sheet structure with a GMA weld is modelled by coarse-meshed plane shell elements as illustrated by Fig. 9.43. The weld is simulated by shell elements connecting to nodal points in the middle plane of the two joint plates straight below the weld toe line. The highest element stress perpendicular to the weld (not the averaged nodal point stress) consisting of superimposed bending and membrane stresses is evaluated from the nodal point forces (the ends of the seam weld or their corner point are critical in general). The element size is approximately $10\times10\,\text{mm}^2$ (for plate

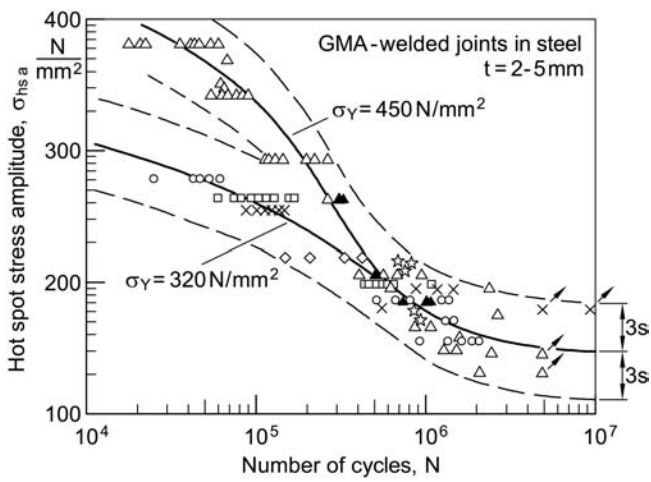


Fig. 9.42. Hot spot stress *S–N* curves for GMA-welded thin-sheet steel joints of automobile structures; first principal stress amplitude evaluated; high strength steels compared with low strength steels (yield limit σ_Y); scatter range with three standard deviations from the mean; after Dang Van *et al.*[754]

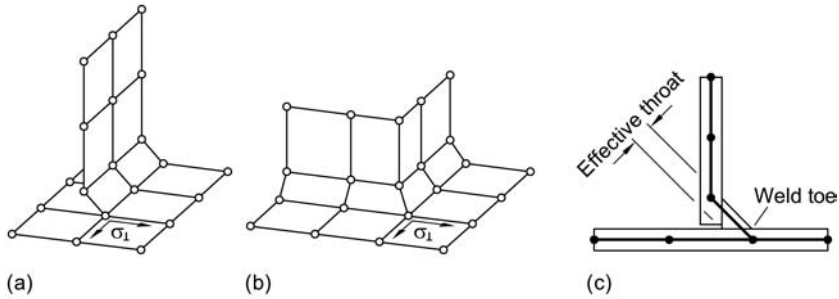


Fig. 9.43. Finite element meshing for hot spot structural stress evaluation at weld seam ends (a) or weld seam corners (b); the fillet weld simulated by shell elements (c); element stresses $\sigma_\perp$ perpendicular to weld (bending and membrane stresses superimposed) at critical nodal points; after Fermér *et al.*[766]

thicknesses t = 1–3 mm). The thickness of the shell elements representing the fillet weld is set equal to its effective throat thickness.

The meshing rules were revised in a subsequent publication (Fermér *et al.*[768]): element size reduced to approximately $5 \times 5\,\text{mm}^2$; thickness of the weld elements defined as twice the thickness of the thinnest sheet being joined; weld ends and weld corners modelled following a smooth notch root curve (i.e. sharp ends or corners are avoided). The nodal point stresses are now calculated using the strain rosette analogy in MSC-NASTRAN.

The maximum structural stresses are compared with endurable values gained from fatigue testing of various relevant specimens and components in thin-sheet steel and aluminium alloy, respectively. A visible crack was the failure criterion. The test results related to load ratios R different from minus one are converted to the condition $R = -1$ using the mean stress sensitivities $M = 0.25$ for $-1 < R < 0$ and $M = 0.097$ for $0 < R \leq 0.5$ found from the tests. Two different S–N curves are established for each material: a higher positioned curve for predominant bending stresses ('flexible' joints, $\sigma_{sb}/(\sigma_{sb} + \sigma_{sm}) \geq 0.5$) and a lower positioned curve for predominant membrane stresses ('stiff' joints, $\sigma_{sb}/(\sigma_{sb} + \sigma_{sm}) \leq 0.5$), Fig. 9.44. Substantially increased endurable stresses are found with the modified meshing rules (finer mesh) and the changed stress evaluation method. Rainflow cycle counting is proposed in combination with Miner's damage accumulation rule, in order to assess the fatigue life under variable-amplitude loading conditions.

A working group in the Japan Society of Automotive Engineers (JSAE) proposes evaluation of the (at weld ends radially aligned) structural strain at a distance of $0.3t$ from the weld toe (with plate thickness t) in critical spots, mainly at weld ends (Kasahara *et al.*[781]). A thickness-dependent structural strain S–N curve is used for assessment of the crack initiation life.

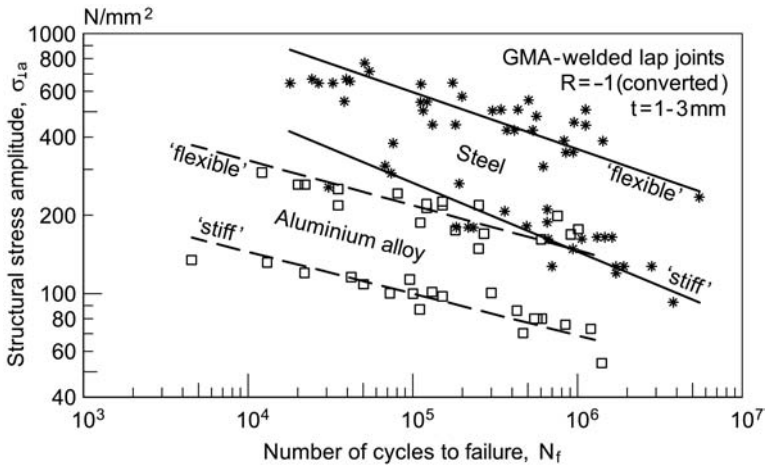


Fig. 9.44. Design stress *S–N* curves based on the hot spot structural stress evaluation for seam-welded thin-sheet components in automobile contruction; revised finite element meshing rules; after Fermér and Svensson.[768]

The endurable structural stresses in GMA-welded aluminium alloy thin-sheet material used for fatigue-loaded suspension components of automobiles (mainly AlMg4.5Mn, sheet thickness t=1–4 mm) were determined from fatigue tests with component-like specimens by Fischer and Grubisic.[769] H-shaped specimens were used with interrupted welds subjected to tensile or tensile-shear loading, and closed channel section specimens with continuous longitudinal welds subjected to longitudinal shear loading by torsional moments at the specimen ends. Constant-amplitude and variable-amplitude loading conditions were applied. Structural stress *S–N* curves with scatter ranges were evaluated and compared. A weight reduction of approximately 25% is predicted for suspension members in aluminium alloy compared with steel.

A round robin study on the fatigue life prediction for a T-joint in steel consisting of rectangular hollow sections (t = 7.9 mm) and subjected to a complex torsional loading mode has been conducted with supervision by the Society of Automotive Engineers (Kyuba and Dong[147]). Reference should also be made to the fatigue assessment program FEMFAT which supports the structural stress analysis based on thin-shell elements in combination with the relevant fatigue notch factors of the considered seam welds (Eichelseder and Unger,[107,108] Brenner *et al.*[750]).

Another investigation of Gurney[773] on behalf of British car manufacturers directed at the fatigue strength of welded thin-sheet steels (2 and 6 mm plate thickness) covered 'simple' welded joints on the one hand and more

complex joints on the other hand. The 'simple' joints comprised non-load-carrying fillet welds with transverse and longitudinal attachments and load-carrying fillet welds in cruciform joints under axial loading. The more complex joints were T-joints of tubes with rectangular cross-sections under in-plane and out-of-plane bending loads.

A question arose whether the thickness effect observed with thicker plates can be extrapolated to the lower thicknesses considered. The test results did not provide a uniform positive answer. Another question was whether the hot spot structural stress approach is applicable and once more the answer was not uniformly positive. Finally, the applicability of Miner's rule under vehicle-typical standard load sequences (Car Loading Standard: CARLOS) was considered with acceptable agreement in the case of the 'simple' joints (damage sum $D = 0.66–1.68$) but with a lower damage sum in the case of the tubular T-joints ($D = 0.35–0.56$). Despite the partly contradictory answers, the author[773] seems to consider the hot spot structural stress approach to be appropriate for thin-sheet structural components of automobiles.

The status of the structural strain approach in the US automotive industry covering damage parameters derived from strain $S–N$ curves, multiaxial loading effects and rainflow counting was reviewed by Conle and Chu.[752,753]

9.4.6 Computer codes for fatigue assessment at weld spots

A computer code has been developed by Störzel and Rupp[840] for applying the structural stress approach (version according to Rupp and Grubisic, Fig. 9.1) to spot-welded joints in cases of real designs from automotive engineering with large numbers of weld spots subjected to complex loading. The tool provides the design engineer with the possibility of fatigue life assessments on a routine basis. The code is named FESPOW from 'fatigue evaluation for spot welds'. The calculation procedure is based on the forces and moments transmitted by the weld spot, i.e. on the joint face forces disregarding the eigenforces. The joint face forces are determined by finite element analysis in general. Therefore, the program is designed as a finite element postprocessor. For the time being, it was restricted to processing the output of the finite element program NASTRAN (FE-Fatigue, distributed by ncode). Similar tools within MSC-FATIGUE are presented by Heyes and Fermér.[776]

The input data of FESPOW consist of output data from NASTRAN and additional user input. The output data from NASTRAN comprise the element forces (inclusive of moments) at the two nodes of the rigid or stiff bar element representing the connection of the overlapping plates by the weld spot (another modelling of the weld spot is not allowed by the

program) and the thicknesses of the joined plates (only plane plate or shell elements are allowed by the program). The input by the user consists of the weld spot diameters, the definition of the load cases to be evaluated inclusive of the load spectra (the output of NASTRAN refers to different unit load cases which must be scaled and superimposed, maximum and minimum loads being primarily important) and the material data in terms of endurable structural stresses such as *S–N* curve, Haigh diagram and critical damage sum.

The output data of FESPOW consist of the maximum damage sum, its peripheral position and the associated maximum structural stress amplitude at each weld spot and for each of the two fracture modes.

Another fatigue-relevant code which is based on the structural stresses around the weld spot, determined directly by finite element analysis (i.e. without referring to weld spot resultant forces), is available within the fatigue assessment program FEMFAT (Brenner *et al.*,[750] see Section 9.4.5).

9.4.7 Fatigue life assessment supporting car body design

A substantially different form of the structural stress-based fatigue assessment for spot welds was developed and successfully applied by Mayer *et al.*[794–796] (with FEMSITE as an auxiliary code). The method is related to the optimisation of car bodies not only with regard to operational life, but also in respect of static and dynamic stiffness. As the car body is a statically indeterminate structure, correct structural stresses can only be gained by realistically simulating the stiffness. This refers especially to the joints. The review below can only point out the basic components of the method. The reader is requested to read the relevant publications to obtain the details.

The structural stress analysis for the car body without glass and hang-on parts ('body in white') in defined static and dynamic load cases is performed using the finite element method as usual. Despite using models with several hundred thousands of elements, the weld spots can only roughly be simulated by the simple beam-to-shell model. Additional auxiliary beam elements are introduced on the grid lines between the 2×4 shell elements meeting at the weld spot in order to stiffen these regions sufficiently. When using arbitrary (non-congruent) meshes on the spot-welded flanges (see Section 9.2.2), the conditions at the connecting points outside the grid points are defined by multipoint constraints on the basis of the element shape functions. The auxiliary beam elements are arranged across (instead of between) the elements concerned. The one connecting beam in the centre is substituted by four beams in the apex points of the weld spot, whose cross-sectional area and geometrical moments of inertia are adapted to the real deformation patterns in typical load cases (tensile-shear,

cross-tension, torsion). All these local modifications of the finite element model of the car body are generated automatically.

The structural stress distribution at the weld spot is calculated using a fine-meshed solid element model of the weld spot and its close neighbourhood. A rectangular double-slab connected by the circular joint face substitutes the 2×4 shell elements at the weld spot or a virtual region around the weld spot in the case of the grid-point-eccentric connection. The slab model is analysed with edge forces or edge displacements derived from the apex point forces of the weld spot. Each edge may be subjected to five forces (inclusive of moments) resulting in a total of 40 single-force load cases. Any unit force from these constitutes a basic load case. The structural stresses associated with the unit load cases (the weld spot centre region being clamped) are stored in a database for the weld spot diameters (d = 4–8 mm) and sheet thickness (t = 0.6–3.0 mm) that are usually applied. The stress distribution in the actual combined loading state is found by superposition of the 40 basic states with the relevant proportion factors. The structural stresses thus determined include part of the notch effect at the weld spot edge (two layers of solid elements are used in each plate independent of plate thickness so that the notch stress proportion is varying). A similar model is used by Ni and Mahadevan.[800]

The endurable structural stresses or strains (including part of the notch effect) are set equal to the parent material characteristic values which are well documented in general. The strain S–N curve provides the endurable strains in constant-amplitude loading. The damage parameter P_{SWT} according to Smith, Watson and Topper[397] together with the relevant P–N curve is used in variable-amplitude loading (see eqs. (5.38) and (5.39)). Non-zero mean stresses are also included in this parameter. The stresses result from a linear-elastic model. The locally elastic-plastic strains are determined from these stresses and the relevant stress–strain relationship without considering compatibility conditions.

The 'statistical' size effect on the endurable values is taken into account by the concept proposed by Kogaev, referring to the length of the crack initiation line (see FKM guideline[1] and Radaj[6]) and modified to a highly stressed volume concept by Mayer *et al.*[795] The crack initiation line is substantially shorter in tensile-shear or peel-tension specimens than in cross-tension specimens. The endurable stresses are correspondingly higher in the latter case.

The complex histories of the local stress components, originating from various remote loads acting on the structure, are handled in time steps by a 'critical plane method', i.e. the fatigue-relevant stress combinations are determined in a great number of sectional planes with different angular orientation within each element. Rainflow counting is performed for all elements and sectional planes. The rainflow matrices are evaluated with regard to the selected damage criterion and damage accumulation hypothesis.

The large number of calculation steps associated with this method can be handled on modern workstations without major problems. Appealing features of the method are its use of modern fatigue assessment methods without restriction to special loading modes or specimen types as well as its reference to the parent material data which are readily available. Special local conditions such as hardening or softening, residual stress or slit closure can principially be taken into account. Weak points are the uncertainty about the crack propagation range in operational life and the missing comparisons with fatigue test data from the literature. The usefulness of the assessment method was proven by the prototypes of several optimised car bodies which showed hardly any cracks after fatigue testing with rough road load histories that simulate the complete operational life.

9.5 Demonstration examples

9.5.1 Spot-welded axle suspension arm

The structural stress approach for the fatigue assessment of spot-welded joints, version according to Rupp *et al.*,[826] was applied to structural components from automobile design in order to demonstrate its general applicability. An axle suspension arm and an engine support member (the latter reviewed in Section 9.5.2) were selected for that purpose. The weld spot forces were determined by the single-beam model between coarse-meshed shell elements. The structural stresses resulted from these forces on the basis of the simple formulae presented in Section 9.2.6. Fatigue testing was performed both with constant- and variable-amplitude loading. Predicted and actual fatigue strengths in terms of endurable structural stress amplitudes were set into comparison. Another more recent validation of the Rupp–Grubisic method was presented by Gao *et al.*[771]

The axle suspension arm consists of two halves of deep-drawn sheet metal joined by weld spots, Fig. 9.45(a). A force amplitude F_a is applied to the outer end of the component whereas the two inner cylindrical bearings are supported by Teflon bushings. The strength situation was investigated experimentally and by calculation for the weld spots with numbers 1–4. Additional seam welds had been omitted in order to create fatigue cracks in this area. On the other hand, the outer end of the suspension arm had to be reinforced by lateral strips in order to avoid crack initiation there.

It turned out that the support conditions in the bearing near the considered weld spots were asymmetrical in respect of the two component halves in the fatigue test. The reason was that the two halves were slightly asymmetrically fabricated and joined. Thus, the eye enclosing the bushing was not exactly round and therefore the path of load transmission was uncertain.

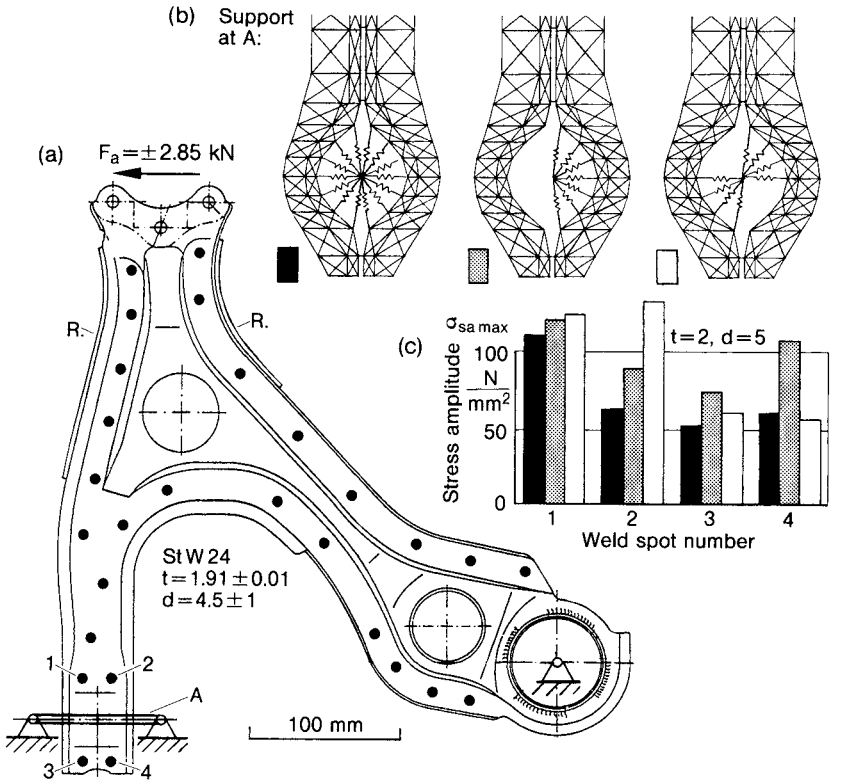


Fig. 9.45. Fatigue strength assessment based on structural stresses for axle suspension arm (a) with different support conditions at the bearing A (b) and structural stress amplitudes resulting from calculation (c); three support conditions in comparison; after Rupp and Grubisic[824] with finite element results provided by Graffe and Graf.

The loading of the considered weld spots and the structural stresses near the weld spots depend substantially on the support conditions in the bearing. Three types of support were investigated in comparison by calculation, Fig. 9.45(b): the symmetrical support, the support by one half of the bearing only and the support in diagonally opposed quarters of the bearing simulated by elastic springs. The calculated maximum radial stress near the weld spots under the three support conditions is plotted in Fig. 9.45(c). The results of fatigue testing and related stress measurements correspond to the last-mentioned support condition.

9.5.2 Spot-welded engine support member

The engine support member consists of an upper and lower half made from deep-drawn sheet steel and joined by spot welding resulting in a box

section, Fig. 9.46(a, b). The upper half is reinforced by a sheet section inserted in the region of the engine mount and fastened by seven weld spots. The upper half of the member is curved to the downside which cannot be seen in the figure. The lower half is more or less a plane plate. A force amplitude F_a is applied to the mount perpendicular to the inclined surface in this area. Conforming with reality, the transverse support member is connected to the longitudinal side members in the finite element model, Fig. 9.46(b), in order to simulate the support flexibility correctly.

The black-dotted weld spot pattern near the mount was investigated both in fatigue testing and by calculation. The grey-dotted weld spot pattern was only numerically analysed. Actually, the first pattern was achieved in fabrication whereas the second pattern was originally prescribed by the designer. The calculated maximum radial structural stresses near the weld spots for the two weld spot patterns are plotted in Fig. 9.46(c). The highest maximum stress is reduced in the actual pattern, i.e. the fatigue strength of the member is thus increased. The weld spots with the numbers 4 and 5 have a low stress level so that they might be combined into a single-spot.

The fatigue testing and the fatigue strength calculation for the axle suspension arm and the engine support member were performed to demonstrate the application of the structural stress approach to spot-welded structures in automobile design. The endurable structural stresses from fatigue testing with component-like specimens had to be compared for this purpose with the endurable stresses observed in the two investigated structural components, see Fig. 9.31.

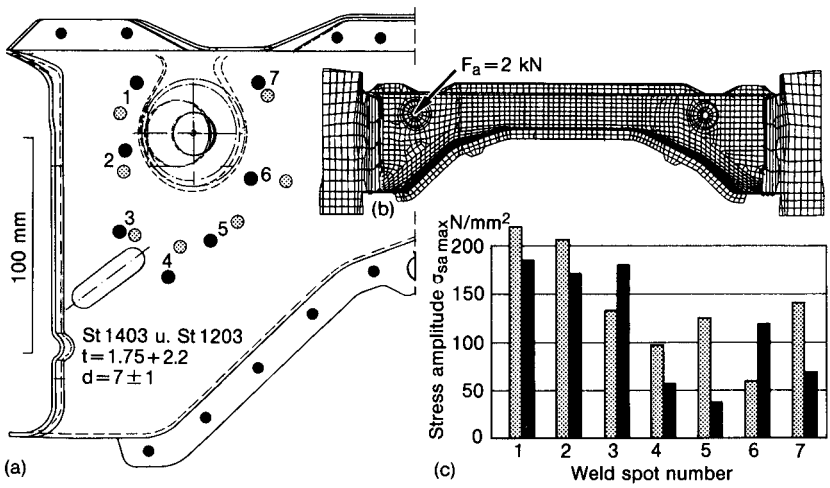


Fig. 9.46. Fatigue strength assessment based on structural stresses for engine support member (a) with finite element model (b) and stress amplitudes resulting from calculation (c); two weld spot patterns in comparison; after Rupp and Grubisic[824] with finite element results provided by Dittmann.

The black-dotted results from the tests with the structural members are positioned well within the field of white-dotted results from the specimen tests despite the fact that the scattering in terms of number of cycles is rather large. Thus, the results from the specimens can be transferred to the structural members based on the structural stress analysis at the weld spots. The fatigue strength or life of the structural members is realistically assessed, the weld spot with the highest loading is identified, and position and type of fracture (plate or nugget fracture) are predicted correctly.

9.5.3 Laser beam welded pillar-to-rocker connection

Tubular T-joints forming a flanged laser-beam-welded connection (pillar-to-rocker connection) were investigated by Wang and Ewing[845] with regard to their prospective fatigue strength, Fig. 9.47. Various positions and shapes of the weld path were considered and compared with the originally spot-welded design. The basis of the relative evaluation was the maximum equivalent structural stress according to the von Mises criterion gained from finite element analysis at the weld seam edges. Laser-beam-welded joints were found to be superior to spot-welded joints, provided the laser weld pattern was optimised.

In the case considered, the basic design of the joint selected for spot-welding was not changed when applying laser beam welding. Spot welding needs overlapping flanges, but laser beam welding can avoid the flanges by the application of deep-penetration square butt welds. More efficient designs with regard to weight, stiffness and fatigue behaviour are thus possible.

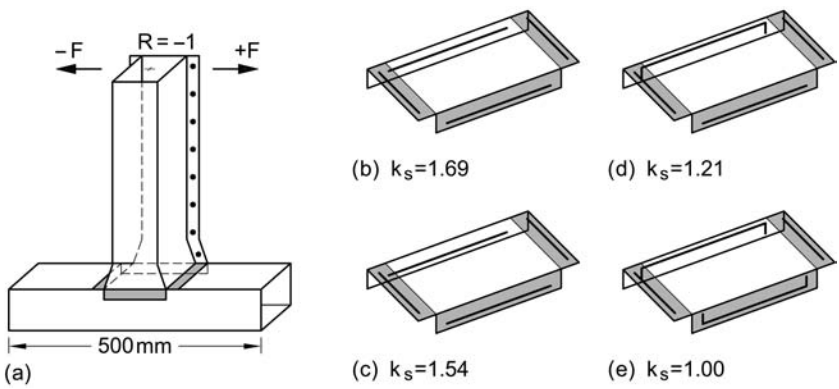


Fig. 9.47. Tubular T-joint (a) (pillar-to-rocker connection in car body) with originally spot-welded and now laser-beam-welded flange connection (b–e); cyclic in-plane bending by reversed force F with rocker ends rigidly clamped; optimisation of weld seam pattern (position and path shape) on the basis of structural stress index k_s relative to best design (e); after Wang and Ewing.[845]

10

Stress intensity approach for spot-welded and similar lap joints

10.1 Basic procedures

10.1.1 Principles of the stress intensity approach

The stress intensity approach uses the stress intensity factor at the slit tip of spot-welded or of similar seam-welded lap joints directly to describe the fatigue strength and service life. It does not include a crack propagation analysis. It has been proposed for spot-welded joints by Pook,[886,887] Yuuki *et al.*,[934–937] Cooper and Smith,[859,927] and Radaj.[893–896] It has also been applied to fillet-welded lap joints by Partanen *et al.*[884] and by Beretta and Sala.[856]

The maximum value of the cyclic equivalent stress intensity factor at the weld spot edge or weld seam root, i.e. at the slit front, is considered to be the decisive parameter characterising the fatigue strength and service life of specimens and structural members. The equivalent stress intensity factor is determined from the stress intensity factors of the crack opening modes I, II and III according to a relevant strength criterion. The latter can be chosen according to proposals by Irwin,[874] Erdogan and Sih,[866] or Sih.[923] These result mainly in the simple form of a square root over the sum of the squared mode-related stress intensity factors. A threshold value of the cyclic equivalent stress intensity factor is used to determine the endurance limit of the welded joint. Crack propagation takes place if the threshold value is exceeded. The medium- and high-cycle fatigue strength or the life up to fatigue failure is expressed by the initial stress intensity factor at the weld spot edge or weld seam root to the extent that the number of cycles between crack initiation and through-thickness penetration remains unambiguously dependent on the initial stress intensity factor. This condition has been proven by Cooper and Smith[859,927] to prevail in the case of tensile-shear loading of weld spots.

The stress intensity approach presumes that the notch at the weld spot edge or weld seam root is crack-like in respect of geometry and that crack

initiation is controlled by the stress intensity factor, which means that superimposed non-singular stress components have no influence. This assumption is not generally supported in reality and can only be used to a certain extent. Additionally, experimental verification that the fatigue crack actually starts at the slit tip considered and not outside of it (as described by Satoh *et al.*[834] or Radaj and Zhang[918]) is necessary.

The endurable stress intensity factors for welded joints are determined experimentally using welded-joint specimens. The threshold stress intensity factor of the parent material can only be considered as a rough guiding value for the technical endurance limit in the welded joint. The approach presupposes that the stress intensity factors are calculated with sufficient accuracy both for the specimen and the structural component.

The stress intensity approach is a structure-based concept because the endurable stress intensity factors and the life up to failure are derived from fatigue tests with welded joints or welded structural members. The crack propagation and notch strain approach on the other hand (see Section 11.1.1) are material-based concepts because material characteristic values are used in the strength and life analysis.

The essential steps of the stress intensity approach when applied to spot-welded joints are shown in Fig. 10.1. At first, the resultant forces at the weld spot, especially the shear forces, the normal force, the bending moments and the torsional moment in the joint face, are determined both for the welded joint in the structural component (the front pillar and a quarter of

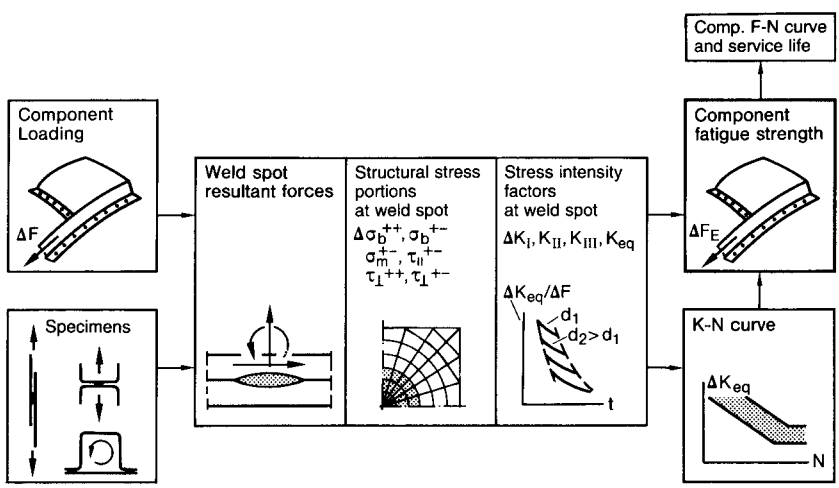


Fig. 10.1. Stress intensity approach according to Radaj, Yuuki and Cooper–Smith for assessing the fatigue strength of spot-welded structural components; after Radaj.[5]

the roof of a car body are shown) and in the specimen. This is achieved by engineering formulae in simple cases and by the finite element method in more complex situations (a coarse mesh being sufficient). Cyclic and static resultant force components have to be separated. The structural stresses at the weld spot edge are derived from the resultant forces or from finite element analysis directly (membrane and bending stresses, longitudinal and transverse shear stresses, these stresses acting in pairs in the same or opposite direction in the two plates). The stress intensity factors of mode I, II and III are determined based on the symmetrical and anti-symmetrical stress portions in the overlapping plates applying simple formulae[892,893,909] or more laborious finite element and boundary element modelling.[934–937] The equivalent stress intensity factor and the most probable direction of crack propagation at the weld spot edge or seam weld root follow from the above stress intensity factors. The maximum equivalent stress intensity factor (normalised by a characteristic force value) depends on the type of loading of the weld spot or seam weld and on the geometric parameters of the welded joint, i.e. on plate thickness and weld spot diameter among others. The ratio of the plate thicknesses has additionally to be taken into account in cases of unequal plate thickness and also the ratio of the elastic moduli in cases of dissimilar materials. Finally, a scatter band of the endurable maximum stress intensity factor plotted against number of cycles can be derived from the results of fatigue tests with spot-welded specimens. This diagram is then used to assess the fatigue strength of spot-welded structural components. Alternatively, the normalised *S*–*N* curve may be applied on the basis of the reference endurance limit of the component, as far as this curve is available for spot-welded joints. The service life curve can be approximated according to the (possibly modified) Miner rule in a final step.

When analysing resistance spot welds, the question has to be answered as to what weld spot diameter should be used in the calculations. It is set equal to the nugget diameter in lower-quality weldments where the slit face ends at the nugget edge. It will extend to the outer rim of the solid phase pressure-welded zone surrounding the nugget in higher-quality welds (see Fig. 11.25).

The cyclic *J*-integral, ΔJ, can be used instead of the cyclic stress intensity factor, ΔK, under certain conditions. It may also substitute for the strength criterion in the case of mixed-mode crack tip loading. But information is also lost with this less differentiating parameter.

Another alternative is to use the cyclic crack opening displacement, $\Delta\delta$, instead of the cyclic mode I stress intensity factor, ΔK_I, in the case of tensile shear loaded spot welds (Davidson and Imhof[862,863]). The cyclic crack (or slit) opening displacement, $\Delta\delta$, is proportional to the cyclic slit opening angle, $\Delta\theta$, between the overlapping plates (see Fig. 10.23). Therefore, $\Delta\theta$ can be used instead of ΔK_I (stiffness approach). This may be an advantage for

testing procedures but neglects the influence of ΔK_{II} and (possibly) ΔK_{III} on the fatigue strength of tensile-shear loaded weld spots (further discussion by Radaj,[4] *ibid*. pp. 340–341, and by Lindgren *et al.*[790]).

10.1.2 Weak points of the stress intensity approach

The basis of the stress intensity approach is now discussed in more detail especially since the approach has not been generally accepted yet. The use of the threshold stress intensity factor which is a material constant of the parent material for determining the technical endurance limit of welded joints exhibits three weak points:

- The threshold stress intensity factor of the parent material is certainly altered to some extent owing to microstructural changes at the weld spot edge or seam weld root which are introduced by the welding heat cycles. Additionally, residual stresses act with the effect of changing the crack opening behaviour.
- Crack initiation and propagation must start from scratch, i.e. this is not the usual propagation problem referring to an existing crack. On the other band, flaws at the weld spot edge or seam weld root may exist from the beginning.
- The propagation direction of the initiated crack will generally deviate from the direction of the slit plane, i.e. the branching crack problem is addressed. The initial stress intensity factor of the original crack is generally not identical to the stress intensity factor of the propagating branched crack.

The first and second weak point can be dealt with to some extent by using structure-based threshold stress intensity factors gained from fatigue tests with spot-welded or seam-welded lap joints. Handling the third complication is primarily a matter of the strength criterion in mixed-mode loading of crack tips resulting in crack branching. There are the equivalent stress intensity factors in terms of K_I, K_{II} and K_{III} available for dealing with the problem, but the effect of non-singular stresses remains unconsidered. On the other hand, conversion into a notch stress problem is possibly opening up the potential of the notch stress approach.

Whereas the application of the stress intensity approach to determine the endurance limit of welded lap joints as described above is straightforward, a more difficult situation occurs with finite life evaluations. Fatigue life here consists of crack initiation and subsequent crack propagation. The initial stress intensity factor is not a sufficiently well-founded reference parameter for the total fatigue life.

The following typical crack initiation and propagation process has been detected by Overbeeke and Draisma[881,882] at weld spots subjected to

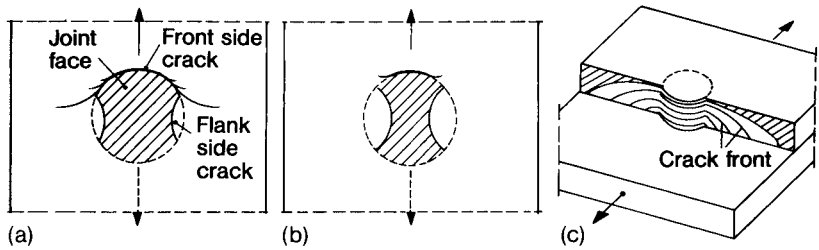


Fig. 10.2. Crack initiation and propagation in spot-welded joints subjected to tensile-shear loading: plate fracture (a), joint-face fracture (b) and crack fronts of plate fracture (c); experimental findings according to Overbeeke and Draisma.[881,882]

tensile-shear loading in the high-cycle fatigue range, Fig. 10.2. Two basically different fracture phenomena are observed, the plate fracture and the joint face fracture. In the case of plate fracture, which occurs with larger spot diameters, small cracks are initiated transverse to the local structural stress (range) at several points of the front-side edge of the weld spot. Whilst they coalesce and propagate over the plate thickness, shear cracks initiate at the flank-side edge of the weld spot, accelerated by the diversion of force flow caused by the front-side crack. In the case of joint face fracture, which occurs with smaller spot diameters, shear cracks are first initiated at the flank-sides of the weld spot, which propagate into the joint face, whilst at the same time transverse cracks appear at the front-side of the weld spot. As a result of the severe notch effect at the weld spot edge, the crack initiation phase is often assumed to be small relative to the crack propagation phase (compare with Gruhle *et al.*[958]).

A more detailed classification of spot-weld fatigue failures observed in tensile-shear and cross-tension specimens has been presented by Pollard,[885] Fig. 10.3. Joint face (or interface) fractures (a) occur with high stress ranges (i.e. low-cycle fatigue) at $R = -1$ and low ratios of weld spot diameter to plate thickness. Plate fractures in the parent material outside the heat-affected zone prevail in low-cycle fatigue with larger diameter to thickness ratio. Plate fractures in the heat-affected zone (b, d) are favoured by lower stress ranges (i.e. medium-cycle fatigue), positive R values and larger diameter to thickness ratios. Plate-traversing fractures occur only with low stress ranges (i.e. high-cycle fatigue). The buttoning-along-nugget (or plug-type) fracture (c, d) may be observed only in cross-tension loading, and the buttoning plate fracture (b, e) only in tensile-shear loading, both fracture types in the medium- to high-cycle fatigue range.

The fatigue failures in well-dimensioned spot welds (tensile-shear or cross-tension loaded) are classified by Rathbun *et al.*[817] into plug-type fractures with or without major plastic deformation in the low-cycle and medium-cycle fatigue range, respectively, whereas plate width fractures

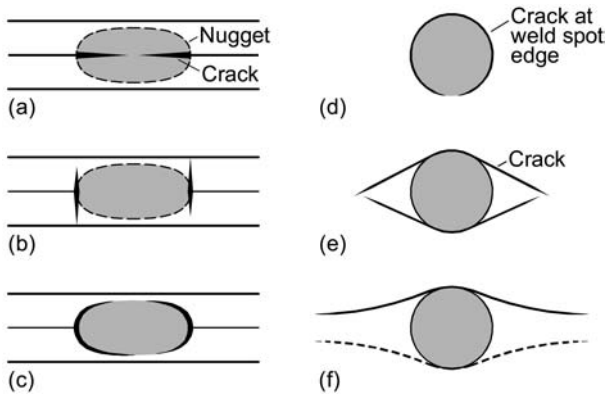


Fig. 10.3. Types of fatigue failure at tensile-shear ($-1 \leq R \leq 0.8$) or cross-tension ($0 \leq R \leq 0.8$) loaded weld spots (longitudinal sections (a, b, c) and top views (d, e, f): joint face (or interface) fracture (a), buttoning (or plug-type) plate fractures (b, c, d) and plate-transverse fracture (f); buttoning-along-nugget fractures (c, d) only with cross-tension, buttoning plate fractures (b, e) only with tensile-shear; after Pollard[885] (modified).

(illustrated by Fig. 10.2(c)) occur in the high-cycle fatigue range. An initially interfacial crack path is observed in the case of expulsions. The fatigue failure modes of single-spot welded joints subjected to multiaxial fatigue loading were considered by Barkey *et al.*[851]

A description of the topology of fatigue fractures at weld spots in peel-tension specimens is given by Radaj *et al.*[906] At first, the annular zone surrounding the weld spot nugget fractures in a static mode as far as its pressure-welded condition is poor. The fatigue crack then propagates at first radially into the joint face and then abruptly turns into the axial direction, reaches the surface of the weld spot, propagates further to its rear side and finally completes the buttoning of the weld spot by a static final fracture. The radial joint face portion of the fatigue fracture increases with lower loads up to approximately the centre of the weld spot. This is the typical process in the medium- to high-cycle fatigue range. With higher loads in the low-cycle fatigue range, static fracture is initiated after only a short crack in radial and axial direction.

Cooper and Smith[859,927] have reduced the complicated fracturing process to a simpler model by considering only plate fractures in tensile-shear loading. They have proven by means of crack propagation measurements using the electric potential method that the crack initiation period in terms of load cycles is extremely small and that the crack propagation rate, $\mathrm{d}a/\mathrm{d}N$, at the deepest point of the crack, remains approximately constant from the onset of crack propagation at the front-side edge of the weld spot until the

crack has reached major parts of the plate thickness. Therefore, the initial stress intensity factor of the uncracked geometry will control the through-thickness propagation period. The constant propagation rate is explained by the fact that the ratio of crack depth to crack width is increasing during crack propagation. On the other hand, it has been shown theoretically by Partanen *et al.*[884] that ligament fractures are controlled by the initial stress intensity factor even with a non-constant propagation rate. The initial stress intensity factor has to be combined with the ligament width (see eqs. (6.15) and (6.16)), multiplied by a reduction coefficient which takes the actually increasing crack propagation rate into account.

The following conclusion can be drawn from the above. The number of cycles, N_{tt}, up to a through-thickness (or through-ligament) crack is proportional to the plate thickness t (or ligament width b), and inversely proportional to the crack propagation rate, da/dN, i.e. $N_{tt} = t/(da/dN)$. The crack propagation rate is defined by the initial stress intensity factor, ΔK_i, so that $N_{tt} = t/[C(\Delta K_i)^m]$.

It follows from the above that $N_{tt} \propto t$ for prescribed stress intensity factor levels, ΔK_i, i.e. longer life for thicker plates. On the other hand, it is found with $(\Delta K_i)^m \approx (\Delta K_i)^3$ and $\Delta K_i \approx \Delta\sigma_s\sqrt{t}$ (very roughly because $\Delta\sigma_s$ is an abbreviation for a more complex structural stress term) that $N_{tt} \propto 1/\sqrt{t}$ for prescribed structural stress levels, $\Delta\sigma_s$, i.e. longer life for thinner plates.

These conclusions are confirmed by a more recent crack propagation analysis based on the Paris equation performed by Zhang and Taylor.[992] Two stages of crack propagation over plate thickness at the front side of the weld spot in tensile-shear loading are considered. In stage one, the small crack is controlled by the initial crack intensity factor at the slit tip, whereas in stage two, the larger semi-elliptical crack is subjected to the (radial) structural stresses in the plate (bending and tension loading). A fixed value of a/t (with crack depth a and plate thickness t) is used as the demarcation between the two stages. The total fatigue life in the two stages is predicted as inversely proportional to $\Delta\sigma_s t^s$ with $s = (1/2 - 1/m)$, i.e. close to $\Delta\sigma_s t^{1/2}$ for larger values of the exponent m (e.g. for the structure-based value $m = 6$).

In the analysis above the crack initiation phase is neglected, i.e. crack propagation is assumed to start with the first loading cycle. Furthermore, fatigue life refers to the through-thickness crack. This makes sense for single spot specimens where crack propagation over the plate width has no major effect on life. The situation is completely changed as soon as multi-spot specimens or structures are considered, where crack propagation across the plate width and/or unloading effects connected with crack formation may contribute substantially to the total fatigue life.

The parent material constants C and m can be used according to Fig. 10.4 in connection with the stress intensity factor ΔK_i determined by Cooper and Smith[859,927] for actual life predictions (crack propagation approach).

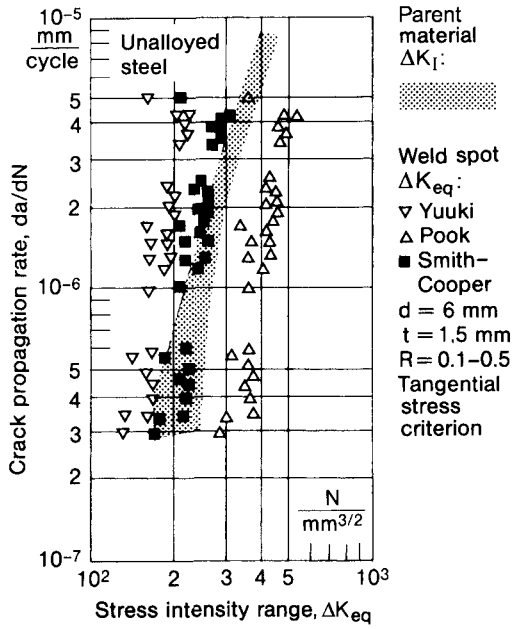


Fig. 10.4. Crack propagation rate dependent on cyclic stress intensity factor for plate fracture in spot-welded unalloyed steel (stress intensity factors according to Yuuki *et al.*,[937] Pook,[886,887] and Smith and Cooper[859,927]) compared with parent material data (screened scatter band; slope exponent $m \approx 4.5$); after Smith and Cooper.[859, 927]

Sufficiently accurate stress intensity factors are a prerequisite for obtaining acceptable results. It can be seen from Table 10.1 that the older stress intensity factors derived by Pook[886,887] and Yuuki *et al.*[937] are certainly not sufficiently accurate. Based on model validations, it is claimed that the analysis results by Radaj are the most accurate ones. It can be concluded from the rather large deviations in the stress intensity factors published by different authors that determining the stress intensity factors at spot welds is not at all a simple task if high accuracy of results is demanded.

The finite element analysis by Swellam *et al.*[928] includes two variants: one with mesh refinement and quarter-point elements at the weld spot edge, the other without these measures, using the stress intensity factor formulae derived by Radaj. Table 10.1 contains the results by the first-mentioned variant modified with regard to uniform parameters d, t and F (an approximation). The original results from the two variants are compared in Table 10.2. Whereas excellent correspondence is achieved in the values of K_{II}, the values of K_I deviate to a larger extent. The explanation for this behaviour is that Swellam used two layers of solid elements in each plate thus

Table 10.1. Comparison of stress intensity factors at the front side (K_I, K_{II}) and the flank side (K_{III}) of the weld spot in the tensile-shear specimen ($F = 1$ kN, $t = 1$ mm, $d = 5$ mm; width and length differ slightly); after Radaj[4,893]

Author	Method	Stress intensity factors [N/mm$^{3/2}$]		
		K_I	K_{II}	K_{III}
Radaj[4,893]	Finite element[a]	60.0 (54.0)[b]	147.8 (137.5)[b]	65.4 (64.3)[b]
Cooper[859,927]	Finite element	63.2	132.4	99.0
Swellam[928]	Finite element[c]	65.6	134.7	—
Pan[972,974]	Finite element[d]	73.8	120.5	—
Yuuki[937]	Finite element	48.6	106.8	—
Pook[886,887]	Functional analysis[e]	163.6	199.8	199.8

[a] Combined with simple stress intensity factor formulae, eqs. (10.13–10.15).
[b] Values with parabolic extrapolation of structural stresses to the weld spot edge; values with structural stresses in the element centre in parenthesis.
[c] Values for $w = 50$ modified by $d'\sqrt{t}/F = 0.72$ with $d' = 6.1/5$, $t = 1.4$, $F = 2$.
[d] Values for $w = 34.9$ modified by $d'\sqrt{t} = 1.21$ or 1.56 with $d' = 6.35/5$ for $t = 0.91$ or 1.5.
[e] Half-space solution modified by $f(d/t)$ according to Chang and Muki.[857]

Table 10.2. Stress intensity factors for the tensile-shear specimen ($t = 1.4$ mm, $d = 6.1$ mm, $l = 140$ mm, $F = 2$ kN); published by Swellam *et al.*[928]

Specimen width w [mm]	Stress intensity factors [N/mm$^{3/2}$]					
	Swellam[a]		Swellam–Radaj[b]		Pook[c]	
	K_I	K_{II}	K_I	K_{II}	K_I	K_{II}
22	170.1	202.7	132.4	202.6	—	—
38	105.1	188.5	83.9	188.4	—	—
50	90.9	186.6	73.1	186.5	—	—
100	54.3	183.1	44.8	183.1	229.7	278.8

[a] Variant with mesh refinement and quarter-point elements.
[b] Variant with stress intensity factor formulae by Radaj.
[c] Solution for infinite width.

establishing a bilinear structural stress distribution over the plate thickness at the weld spot edge instead of a purely linear one. Thus, the surface stresses deviate from those demanded by the stress intensity factor formulae. The error is annulled in the K_{II} formulae (anti-symmetric conditions) whereas an adding up occurs in the K_I formulae (symmetric conditions).

Proceeding from the consideration above of proportional or inverse-proportional relations, K–N curves (with $\Delta K = \Delta K_i$) for different plate

thicknesses should be possible describing the fatigue strength and life of welded lap joints. They should be cut on the lower side by the threshold stress intensity factor, ΔK_{th}, which is not dependent on plate thickness by definition. This expectation is confirmed by fatigue test evaluations in respect of complete fracture comprising a multitude of spot-welded specimens (see Fig. 10.18). The dependency on plate thickness is blurred in the diagram owing to the wide scatter range of the test results. Presumably, this method of presentation of fatigue results in the finite life range will also work with joint face fractures if the plate thickness is substituted by the cross-sectional or ligament width in the corresponding relationships.

10.1.3 Links to other approaches and application relevance

The stress intensity approach is based on structural stress analysis from which the stress intensity factor at the weld spot edge or weld seam root can be derived using simple formulae. The main difference between the stress intensity approach and the structural stress approach is the following. Endurable stress intensity factors are considered in the former approach and endurable structural stresses in the latter. The stress intensity factor results from the structural stresses multiplied by the square root of plate thickness whereas the stress intensity factor representing the endurance limit is independent of plate thickness. The structural stress on the other hand does not contain a thickness term so that the endurance limit stress is dependent on plate thickness. Another difference between the two approaches is that the structural stress at the weld spot edge or seam weld root comprises both the joint face forces and eigenforces, whereas the stress intensity factor reflects mainly the effect of the joint face forces (the non-singular stress terms are missing). Loading modes with a large eigenforce portion are not sufficiently well described by the stress intensity approach.

There is a close link between the stress intensity approach and the notch stress approach. The stress intensity factor controls the notch stresses of blunt cracks or slits provided the non-singular structural stress effects are negligible. Procedures based on stress intensity factors are partly derived from notch stress considerations.

The close link between the stress intensity approach and the crack propagation approach has been demonstrated above in respect of the applicability of the initial stress intensity factor (see Section 10.1.2). The stress intensity approach gets along without explicit crack propagation analysis whilst a constant crack propagation rate may be assumed over the plate thickness. A more detailed analysis in the finite life range should be based on the crack propagation approach supplementing a crack initiation analysis (see Chapter 11).

The stress intensity approach is the preferred method of numerical fatigue strength assessment for spot-welded joints in the Japanese and US automotive industry, whereas the preference in the German automotive industry is for the structural stress approach. A handicap with the application of the stress intensity approach is the limited availability of endurable stress intensity factors, their large scatter range and their dependency on plate thickness in the finite life range. But relative evaluations are possible even with stress intensity factors alone where endurable values are missing. They provide an answer to questions regarding the design of specimens and components. The different spot-welded specimens, for example, have been compared in respect of their endurance limit based on the stress intensity approach alongside of other local approaches.[816] The H-shaped specimen was validated in this way on request of the International Institute of Welding (IIW).[900,902] The conventional double-hat section specimen[917] and a novel double-cup specimen[901,902] were also analysed.

10.2 Analysis tools – evaluation of stress intensity factors

10.2.1 General survey and basic definitions

The analysis tools described hereafter in Sections 10.2 and 10.3 comprise the following items: stress intensity factors of lap joints with equal plate thickness and material derived on the basis of the structural stresses, stress intensity factors for unequal plate thicknesses and dissimilar materials, stress intensity factors of lap joints subjected to large deflections, historically early solutions for stress intensity factors of lap joints, stress intensity factors based on nominal structural stresses, the link to the notch stress approach, endurable stress intensity factors, equivalent stress intensity factors under mixed mode loading and the *J*-integral and nugget rotation variants of the approach.

The reader is referred to the literature concerning supplementary analysis tools such as the finite element method,[84,344] the boundary element method[210,214,446,861] or stress measurement methods.[131,181,198,221,242] Stress intensity factor solutions used in the crack propagation approach are reviewed in Section 6.2.2. The reader should be roughly acquainted with the theory of weld spot resultant forces and nominal structural stresses derived therefrom (see Section 9.2).

Considering the weld spot edge or weld seam root (or slit edge) under geometrically ideal conditions (zero notch radius, gap-free slit faces) in homogeneous elastic materials, the stress state near the slit tip from remote loading will result as partly singular, analogous to the situation with crack

tips. The stress state at the slit tip is described within r–φ polar coordinates in the cross-sectional plane at different peripheral or longitudinal positions, Fig. 10.5 (a curved weld root line is also possible). The stress state may depend on the peripheral angle ψ or the weld length coordinate z or may be independent of these parameters in special loading cases. The singular part of the stress state at the slit tip in the r–φ plane is described by singular terms characterised by the stress intensity factors K_I (normal tension), K_{II} (in-plane shearing) and K_{III} (out-of-plane shearing) superimposed by a non-singular term:

$$\sigma_{ij} = \frac{1}{\sqrt{2\pi r}}[K_I f'_{ij}(\varphi) + K_{II} f''_{ij}(\varphi) + K_{III} f'''_{ij}(\varphi)] + \sigma_{0kl} \qquad (10.1)$$

where σ_{ij} is the stress tensor (convention: ij = rr, rφ, φφ), r and φ are polar coordinates at the slit tip, K_I, K_{II} and K_{III} are the stress intensity factors of mode I, II and III, $f_{ij}(\varphi)$ are cyclic functions and σ_{0kl} is the non-singular stress tensor (locally equal membrane stresses in the two plates, e.g. σ_{0xx}, σ_{0zz} and τ_{0xz} with the coordinate x in the plane of the joint face). The analogies between the stress states at crack or slit tips and at rigid layer tips in the infinite plate or solid were investigated by Radaj and Zhang.[912,913]

In the following Sections 10.2.2–10.2.4, derivations and formulae are recorded which are not always completely consistent with regard to the non-singular stress terms, whereas the stress singularities result independently from these. The reason for the occasional inconsistency is that the theory was developed step by step without there being an awareness of relevance of the non-singular stress terms for certain strength considerations from the very beginning. Theoretical consistency was of minor importance at first and a rigorous definition of the non-singular state was not yet available. The inconsistency could have been removed in the representation of this book, but then comparability with the original publications with regard to formulae, symbols and graphical representations would have been lost to some extent. Instead, the basic contents of the consistent formulation are brought to the reader's attention in advance. It is expected that the

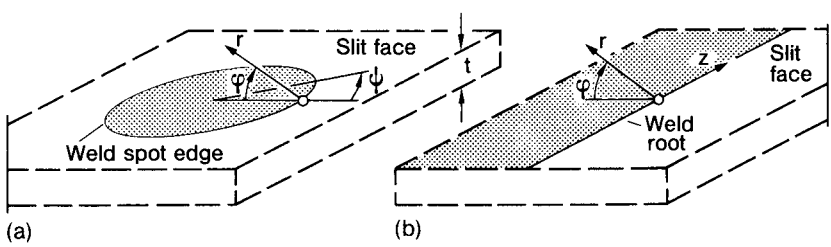


Fig. 10.5. Polar coordinate systems at weld spot edge (a) or weld seam root (b) of lap joints.

reader can then better handle the inconsistencies as far as these are relevant for him.

First, the pure modus I, II and III loading states will be defined, so that the non-singular stress terms follow from the total stresses after deduction of the stresses with a singular effect. The loading state connected with the non-singular stresses is termed 'modus 0'. As stated above, there are three membrane stress states of modus 0. These are supplemented by bending stress states of modus 0.

We define as pure modus I, II and III states the self-equilibrating loading states with the external forces acting in the same line in the opposite direction along the two sides of the slit face, Fig. 10.6. These loading states are characterised by the fact that the external forces are equilibrated completely by themselves, i.e. without an external support. The forces 'flow' completely around the slit tip line (the slit front) producing the stress singularity there. Non-self-equilibrating forces would produce reaction forces at the external supports which are attributable to the non-singular state under certain conditions, but may also have an effect on the stress singularity. This would mean that the considered loading states of pure modus I, II and III are not uniquely defined in respect of the stress singularity. The reader may be familiar with the questionable definition of the modus II and modus III loading states on the basis of counteracting membrane stresses in the two loaded specimen ends combined with a rigid support on the opposite side of the specimen. A bending moment is produced on the support in the modus II loading state and a torsional moment in the modus III loading state.

The pure modus I, II and III loading states according to the above unique definition are not convenient for engineering purposes. In structural

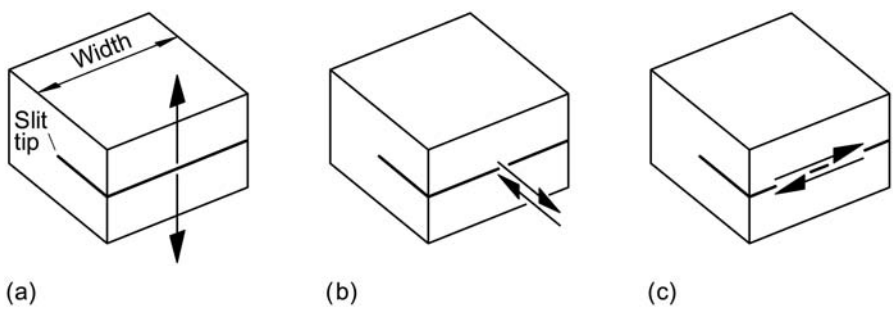


Fig. 10.6. Self-equilibrating loading states generating stress singularities at the slit tip line; pure modus I (a), pure modus II (b) and pure modus III (c); the pairs of forces are assumed to act on the slit faces in opposite directions in the same line each; they are evenly distributed over the specimen width; Radaj's definition.

analysis, membrane and bending stresses are separated. These may be used to determine the stress intensity factors, but it must be kept in mind that the remaining non-singular stress state is then incomplete.

The pure modus I, II and III loading states are now investigated with regard to the structural stress distribution at the slit front in the plane normal to the slit face. At first, equal plate thickness is considered. The external forces and the structural stresses produced by these forces in the specimen are assumed to be evenly distributed over the specimen width (resulting in plane or anti-plane stress states). In pure modus I loading, linearised bending stresses are combined with constant transverse shear stresses. In pure modus II loading, bending and membrane (normal) stresses occur in the ratio three to one. In pure modus III loading, bending and membrane shear stresses are produced, but the condition of an anti-plane stress state can only be fulfilled by the membrane shear stresses, whereas the bending shear stresses are unevenly distributed over the specimen width. Bending shear stresses can only occur within an inhomogeneous stress field. They actually occur at the weld spot edge, as can be seen from the results of structural analysis using the finite element method. They can approximately be taken into account by treating them locally as if they were membrane stresses (see Section 10.2.2).

It follows from the above that the non-singular state consists not only of (structural) membrane stresses as indicated by eq. (10.1) but also of (structural) bending stresses including normal and shear components in both cases. The separation of the complete non-singular state is termed ‘consistent’.

The following notes refer to occasional inconsistencies with regard to the non-singular terms in the following sections. The singular terms may then be inconsistently defined too, but the stress intensity factors are correct. The decomposition of the structural stress state in the case of equal plate thickness depicted by Fig. 10.8 in Section 10.2.2 does not take the condition of self-equilibrating singular loading states into account in all subcases. The decomposition is based on the concept of symmetrical and anti-symmetrical structural stresses, which is identical here with the concept of symmetrical and anti-symmetrical resultant forces. Reference is made to Fig. 10.11 with regard to the consistent decomposition resulting in eqs. (10.16) and (10.17). The corresponding formulae related to bending and membrane shear stresses are not specified. The decomposition of the structural stress state in the case of unequal plate thickness, depicted by Fig. 10.10 in Section 10.2.3, is inconsistent in so far as the non-singular bending stress at the supported specimen end resulting from equidirected bending moments is not separated. The decomposition is based on the concept of symmetrical and anti-symmetrical resultant forces combined with the separated constant membrane stresses. The consistent reformulation of the theory performed

by Radaj and Zhang[909] results in other coefficients $\{k_{\mu u}\}$ whose number is reduced by one. The decomposition of the structural stress state in the case of dissimilar materials, specified in Section 10.2.4 and depicted by Fig. 10.11, is consistent and needs no reformulation of the theory.

It has been shown by Seeger *et al.*[981] that the formulae describing the decomposed structural stresses and the stress intensity factors are substantially simplified by an inconsistent decomposition characterised by non-equilibrating membrane and bending stresses of equal size in the upper and lower specimen ends. But the separated non-singular bending stresses are incomplete in this case.

10.2.2 Stress intensity factors of lap joints based on structural stresses

The stress intensity factors of lap joints can be determined without major expenditure on the basis of the structural stresses at the weld spot edge or weld seam root. The linearisation of the structural stresses over the plate thickness is the first step which is automatically put into effect when using simple plate or shell elements. To make this graphically clear, Fig. 10.7 shows the original stress distribution with singularity (a), the linearised structural stress distribution (b), a parabolic stress distribution resulting from higher order elements (c) and the bilinear stress distribution connected with lower order elements in two layers (d). A bending moment is assumed to be acting over the plate thickness. Only the linearised structural stresses (b) are the correct basis of the formulae below.

Within a second step, the decomposition of the linearised structural stresses into symmetrical and anti-symmetrical portions is performed (Radaj[892]), Fig. 10.8. The basic formulae are derived for equal thickness and similar material of the overlapping plates on the assumption of a relatively large (compared with plate thickness) weld spot diameter or weld seam width (in order to exclude mutual influence of opposed slit tips):

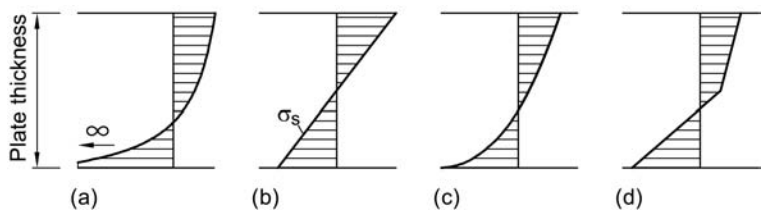


Fig. 10.7. Stress distribution over plate thickness at the weld spot edge, the plate subjected to a bending moment: original stress distribution (a), linearised structural stress distribution (b), parabolic and bilinear stress distributions (c, d).

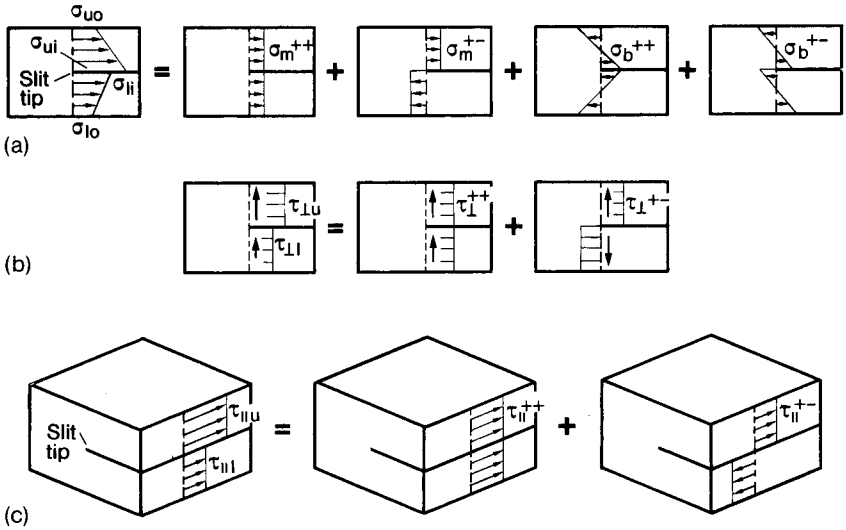


Fig. 10.8. Decomposition of the total structural stress state at the slit tip into symmetrical and antisymmetrical stress portions; membrane and bending stresses (a), transverse shear stresses (b) and longitudinal shear stresses (c); after Radaj and Zhang.[892,908]

$$K_{\mathrm{I}} = \left(\frac{1}{\sqrt{3}} \sigma_{\mathrm{b}}^{++} + 2.23 \tau_{\perp}^{+-} \right) \sqrt{t} \tag{10.2}$$

$$K_{\mathrm{II}} = \left(\frac{1}{2} \sigma_{\mathrm{m}}^{+-} + \frac{1}{2} \sigma_{\mathrm{b}}^{+-} + 0.55 \tau_{\perp}^{++} \right) \sqrt{t} \tag{10.3}$$

$$K_{\mathrm{III}} = \sqrt{2} \tau_{\parallel}^{+-} \sqrt{t} \tag{10.4}$$

where K_{I}, K_{II} and K_{III} are the stress intensity factors of mode I, II and III, σ_{m}^{+-} is the anti-symmetrical membrane stress portion (σ_{m}^{++} is a part of $\sigma_{0\mathrm{kl}}$), σ_{b}^{++} and σ_{b}^{+-} are the symmetrical and anti-symmetrical bending stress portions, $\tau_{\perp}^{++}$ and $\tau_{\perp}^{+-}$ are the symmetrical and anti-symmetrical transverse shear stress portions, $\tau_{\parallel}^{+-}$ is the anti-symmetrical longitudinal shear stress portion ($\tau_{\parallel}^{++}$ is a part of $\sigma_{0\mathrm{kl}}$) and t is the plate thickness.

Stress portions are termed 'symmetrical' if they have the same value and sign at corresponding points above and below the slit face. They are called 'anti-symmetrical' if the value is the same and the sign is reversed. Note that 'same sign' means 'same direction of the stress vector'.

The symmetrical and anti-symmetrical structural stress portions are derived from the total structural stress state by the decomposition procedure mentioned above which separates the non-singular membrane stress portions first (see Fig. 10.8; actually, non-singular bending stress portions should also be considered within a more consistent approach):

$$\sigma_{\mathrm{m}}^{++} = \frac{1}{4}(\sigma_{\mathrm{ui}} + \sigma_{\mathrm{uo}} + \sigma_{\mathrm{li}} + \sigma_{\mathrm{lo}}) \tag{10.5}$$

$$\sigma_{\mathrm{m}}^{+-} = \frac{1}{4}(\sigma_{\mathrm{ui}} + \sigma_{\mathrm{uo}} - \sigma_{\mathrm{li}} - \sigma_{\mathrm{lo}}) \tag{10.6}$$

$$\sigma_{\mathrm{b}}^{++} = \frac{1}{4}(\sigma_{\mathrm{ui}} - \sigma_{\mathrm{uo}} + \sigma_{\mathrm{li}} - \sigma_{\mathrm{lo}}) \tag{10.7}$$

$$\sigma_{\mathrm{b}}^{+-} = \frac{1}{4}(\sigma_{\mathrm{ui}} - \sigma_{\mathrm{uo}} - \sigma_{\mathrm{li}} + \sigma_{\mathrm{lo}}) \tag{10.8}$$

$$\tau_{\perp}^{++} = \frac{1}{2}(\tau_{\perp\mathrm{u}} + \tau_{\perp\mathrm{l}}) \tag{10.9}$$

$$\tau_{\perp}^{+-} = \frac{1}{2}(\tau_{\perp\mathrm{u}} - \tau_{\perp\mathrm{l}}) \tag{10.10}$$

$$\tau_{\parallel}^{++} = \frac{1}{2}(\tau_{\parallel\mathrm{u}} + \tau_{\parallel\mathrm{l}}) = \frac{1}{2}(\tau_{\parallel\mathrm{ui}} + \tau_{\parallel\mathrm{li}}) \tag{10.11}$$

$$\tau_{\parallel}^{+-} = \frac{1}{2}(\tau_{\parallel\mathrm{u}} - \tau_{\parallel\mathrm{l}}) = \frac{1}{2}(\tau_{\parallel\mathrm{ui}} - \tau_{\parallel\mathrm{li}}) \tag{10.12}$$

where σ_{m}^{++} and σ_{m}^{+-} are the symmetrical and anti-symmetrical membrane stress portions, σ_{b}^{++} and σ_{b}^{+-} are the symmetrical and anti-symmetrical bending stress portions, $\tau_{\perp}^{++}$ and $\tau_{\perp}^{+-}$ are the symmetrical and anti-symmetrical transverse shear stress portions, $\tau_{\parallel}^{++}$ and $\tau_{\parallel}^{+-}$ are the symmetrical and anti-symmetrical longitudinal (membrane) shear stress portions, $\tau_{\parallel\mathrm{ui}}^{++}$ and $\tau_{\parallel\mathrm{li}}^{+-}$ are the symmetrical and anti-symmetrical longitudinal shear stress portions in the upper and lower plate at the inner surface (membrane shear stresses superimposed by bending shear stresses), σ_{uo}, σ_{ui}, σ_{lo}, σ_{li} are the structural normal stresses in the upper and lower plate at the outer and inner surface, $\tau_{\perp\mathrm{u}}$ and $\tau_{\perp\mathrm{l}}$ are the structural transverse shear stresses in the upper and lower plate, $\tau_{\parallel\mathrm{u}}$ and $\tau_{\parallel\mathrm{l}}$ are the structural longitudinal membrane shear stresses in the upper and lower plate and $\tau_{\parallel\mathrm{ui}}$ and $\tau_{\parallel\mathrm{li}}$ are the structural longitudinal shear stresses in the upper and lower plate at the inner surface. The structural stress portions σ_{m}^{+-}, σ_{b}^{++}, σ_{b}^{+-}, $\tau_{\perp}^{++}$, $\tau_{\perp}^{+-}$ and $\tau_{\parallel}^{+-}$ produce singular slit tip stresses. The portions σ_{m}^{++} and $\tau_{\parallel}^{++}$ constitute non-singular terms.

The case of longitudinal shear loading requires a special explanation. In the slitted brick model considered in Fig. 10.8(c) (representing an infinite slitted plate strip) only membrane shear stresses are compatible and therefore possible. Superimposed bending shear stresses, i.e. longitudinal shear stresses linearly distributed over plate thickness, are only locally compatible and possible in more inhomogeneous stress fields, e.g. at the edge of

weld spots. These bending shear stresses might be decomposed into symmetrical and anti-symmetrical portions in analogy to the normal bending stresses resulting in four equations analogous to eqs. (10.5–10.8) with σ substituted by $\tau_{\parallel}$. But such a decomposition is of no value for determining the stress intensity factor K_{III} under non-local conditions because of the incompatibility mentioned above.

A simple but accurate engineering hypothesis is introduced for dealing with the local situation. It is assumed that the stress intensity factor K_{III} is controlled solely by the structural shear stresses $\tau_{\parallel ui}$ and $\tau_{\parallel li}$ at the inner surface of the plates independent of the stress situation at some distance from the slit tip, i.e. $\tau_{\parallel u} = \tau_{\parallel ui}$ and $\tau_{\parallel l} = \tau_{\parallel li}$ in eqs. (10.11) and (10.12). The assumption is in agreement with the superposition principle of notch stress theory and is supported by analogy to the first term in eq. (10.14) describing mode II loading. The assumption will be conservative in general.

The formula for the stress intensity factor K_{III} according to eq. (10.4) is based on the analytical solution by Sih[924,925] for the external slit loaded by a pair of concentrated forces acting in opposite directions and on the J^*-integral solution by Radaj and Zhang[908] for the slitted plate strip with constant shear stress loading in opposite directions which was additionally confirmed by boundary element results.

If numerical solutions (e.g. finite element results) are used for the structural stress problem, the stresses on the right-hand sides of eqs. (10.5–10.12) are completely known. If a procedure based on measurement is employed, eight independent stress or strain measurements adjacent to the weld spot edge or seam weld root are generally required to determine the eight unknown stress portions: four measuring points in front of the weld spot edge or seam weld root on the inside and outside of the overlapping plates to distinguish tensile from bending stresses and four additional measuring points at a slightly greater distance to determine the transverse shear stress from the gradient of the bending stresses. With negligible transverse shear, the number of necessary independent measurements is reduced. Procedures are also available which avoid strain measurements at the inside surfaces of the plate (see Section 9.2.8). The non-singular stress portions can be determined by evaluating the surface stresses in the centre line of the weld spot or in the corresponding centre plane of the seam weld using calculation or measuring methods.

Introducing the decomposed stress states from eqs. (10.5–10.12) into eqs. (10.2–10.4), the result is:

$$K_I = [0.144(\sigma_{ui} - \sigma_{uo} + \sigma_{li} - \sigma_{lo}) + 1.115(\tau_{\perp u} - \tau_{\perp l})]\sqrt{t} \quad (10.13)$$

$$K_{II} = [0.25(\sigma_{ui} - \sigma_{li}) + 0.275(\tau_{\perp u} + \tau_{\perp l})]\sqrt{t} \quad (10.14)$$

$$K_{III} = 0.707(\tau_{\parallel ui} - \tau_{\parallel li})\sqrt{t} \quad (10.15)$$

where K_I, K_{II} and K_{III} are the stress intensity factors of mode I, II and III, σ_{uo}, σ_{ui}, σ_{lo} and σ_{li} are the structural normal stresses in the upper and lower plate at the outer and inner surface, $\tau_{\perp u}$ and $\tau_{\perp l}$, are the structural transverse shear stresses in the upper and lower plate, $\tau_{\parallel ui}$ and $\tau_{\parallel li}$ are the structural longitudinal shear stresses in the upper and lower plate at the inner surface and t is the plate thickness.

It has been shown by Radaj and Zhang[909] that decomposition of the original stress state which separates the complete non-singular normal stress portion first, gives the singular stress portions of counterbending (symmetrical portion) and pure tension-bending (anti-symmetrical portion), see Fig. 10.11. This further simplifies eqs. (10.13) and (10.14) by introducing the following stress portions (but the relevant formulae in the paper[908] on unequal thickness joints are not yet sufficiently simplified):

$$\sigma_{cb} = \frac{1}{4}(\sigma_{ui} - \sigma_{uo} + \sigma_{li} - \sigma_{lo}) \tag{10.16}$$

$$\sigma_{tb} = \frac{1}{2}(\sigma_{ui} - \sigma_{li}) \tag{10.17}$$

where σ_{cb} and σ_{tb} are the counterbending and tension-bending structural stress portions and σ_{ui}, σ_{uo}, σ_{li} and σ_{lo} are the structural stresses in the upper and lower plate at the outer and inner surface.

Referring to eq. (10.3) in connection with the last-mentioned decomposition which separates the pure tension-bending stress portion, it becomes clear that the term $0.5\sigma_m^{+-}$ may be substituted (as performed later in the case of unequal thickness or dissimilar materials) by $2.0\sigma_m^{+-}$ remaining with the additive term σ_b^{+-} diminished by the bending stress portion belonging to the membrane stress in pure tension-bending. Thus, eq. (10.8) for σ_b^{+-} has to be correspondingly modified in the latter case.

The remarkable aspects of the above derivations are the following. The stress intensity factors are equal to linearised structural stress terms multiplied by the square root of plate thickness. The latter substitutes the crack length or crack depth in comparable crack problems. The stress intensity factors K_I and K_{II} are not only dependent on the bending and membrane stress portions at the plate surfaces but additionally on the shear stress portions transverse to the surfaces. Also, part of the membrane and bending structural stresses may be non-singular in their effect.

The procedure described for determining the stress intensity factors in lap joints on the basis of the structural stresses in the overlapping plates is bound to the condition that the extension of the notch stress peak at the slit tip is small in relation to the extension of the underlying structural stresses. This condition is met to a large extent because the notch stress singularity occurs at a point and has no extension. Comparative investigations

show the high accuracy not only of the stress intensity factors[812,892,981] but also to a larger extent than expected of the plate deflections.

The procedure described presupposes that the weld spot diameter or weld seam width is large in relation to the plate thickness or at least larger than the plate thickness. The stress singularities at opposite slit tips are mutually influenced if the slit tips come closer together. In this case, the diameter-to-thickness or width-to-thickness ratio (in the case of spot and seam welds, respectively) will have an influence on the stress intensity factors calculated based on the structural stresses in the plate. Investigations of this influence which may be of relevance for penetration-welded joints are not yet available. It can be predicted that the singularity will be unaffected by the plate thickness for a small diameter or width relative to plate thickness, i.e. near the limiting case of vanishing diameter or width. Instead, the averaged structural stresses in the jointing face have to be combined with the square root of diameter or width in the relevant stress intensity factor formulae. On the other hand, the relation between stress intensity factor and averaged slit tip stresses has to be modified if the diameter or width is very small.

The stress intensity factors of spot-welded or seam-welded lap joints determined by a three-dimensional finite element or boundary element analysis require much greater effort and expenditure to attain comparable accuracy of results. One option is the use of elements with stress singularity at the slit or crack tip (Swellam *et al.*[928]). The singularity is modelled by a fan-shaped arrangement of hexahedronal 20-node elements degenerated to prismatic 15-node elements with quarter-point nodes as proposed by Henshell and Shaw,[872] Barsoum[853,854] and Banks-Sills *et al.*,[849,850] Fig. 10.9. The prismatic elements are created by collapsing the nodes on one of the faces of the hexahedronal elements to the crack or slit front. Subsequently, the midside nodes are moved to the quarter-point positions. Each cluster of

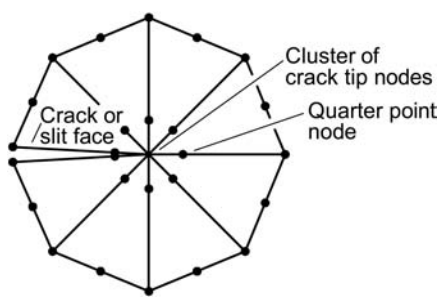


Fig. 10.9. Fan-shaped arrangement of degenerated hexahedronal 20-node elements with quarter-point nodes representing a crack or slit tip; after Swellam *et al.*[928]

nodes at the crack front can either be tied together or left free. The stress singularity is found to be insensitive to the choice of these two kinematic conditions. It is recommended that the size of the crack tip element is less than 5% of the crack or ligament length (Shih *et al.*[922]). A radial size of the crack tip elements of approx. 0.1 mm was found to be adequate for spot-welded joints (Swellam *et al.*[928]). The quarter-point-node elements must have straight edges in the fan plane, otherwise the induced singularity is destroyed (Pu *et al.*[891]).

10.2.3 Stress intensity factors of lap joints with unequal plate thickness

The stress intensity factor formulae in the case of unequal thickness of the overlapping plates are similar but more complicated in structure (Radaj and Zhang[908]). They depend on the mode of decomposition into symmetrical and anti-symmetrical stress or resultant force states which is not as trivial as in the case of equal plate thickness. The decomposition of stresses no longer corresponds to identical decomposition of resultant forces (including moments) which should establish self-equilibrating loading states to the largest extent possible. The decomposition below is inconsistent in so far as the non-singular bending stress portion was not separated first. The numerical values of the stress intensity factors are, of course, independent of the mode of decomposition and the structure of the formulae.

The stress intensity factors K_I, K_II and $K_\mathrm{eq} = \sqrt{K_\mathrm{I}^2 + K_\mathrm{II}^2}$ (corresponding to the Irwin's mixed-mode fracture criterion), derived on the basis of decomposition of the structural stress state according to Fig. 10.10 and eqs. (10.23–10.30), depend on the structural stress portions, on the thickness of the upper (or alternatively lower) plate and, through coefficients, on the plate thickness ratio:

$$K_\mu = \{k_{\mu u}\}^\mathrm{T} \{\sigma_u\} \sqrt{t_u} \qquad (\mu = \mathrm{I},\ \mathrm{II},\ \mathrm{eq}) \tag{10.18}$$

$$\{k_{\mu u}\}^\mathrm{T} = \left[k_{\mu mu}^{+-} k_{\mu bu}^{++} k_{\mu bu}^{+-} k_{\mu \perp u}^{++} k_{\mu \perp u}^{+-}\right] = f(\delta) \tag{10.19}$$

$$\{\sigma_u\} = \begin{Bmatrix} \sigma_{mu}^{+-} \\ \sigma_{bu}^{++} \\ \sigma_{bu}^{+-} \\ \tau_{\perp u}^{++} \\ \tau_{\perp u}^{+-} \end{Bmatrix} \tag{10.20}$$

$$\delta = \frac{t_u}{t_1} \tag{10.21}$$

where K_μ are the stress intensity factors in mode I and II loading and the equivalent stress intensity factor, $\{k_{\mu u}\}^T$ is the transposed vector of the coefficients referred to the upper plate, $\{\sigma_u\}$ is the vector of the decomposed structural stress portions referred to the upper plate, t_u and t_l are the thicknesses of the upper and lower plate and $f(\delta)$ is a function of the plate thickness ratio δ.

Only one (anti-symmetrical) stress term is required for determining K_{III}:

$$K_{III} = k^{+-}_{III\,u}\tau^{+-}_{\parallel u}\sqrt{t_u} \tag{10.22}$$

where K_{III} is the stress intensity factor in mode III loading and $k^{+-}_{IIIu} = f(\delta)$ is the coefficient referring to $\tau^{+-}_{\parallel u}$, the anti-symmetrical longitudinal shear stress portion in the upper plate.

The coefficients k_μ (μ = I, II, III, res) are simple functions of the plate thickness ratio $\delta = t_u/t_l$ introduced as $\delta \le 1.0$ (i.e. the upper plate is assumed to have the smaller thickness). Closed solutions have been derived for $k_{eq\,u} = \sqrt{k^2_{Iu} + k^2_{IIu}}$ and for k^{+-}_{IIIu} on the basis of the J- and J^*-integral, respectively. These have been used to approximate k_{Iu} and k_{IIu} on the basis of the results of boundary element analyses for δ = 1.0, 0.5, 0.25 and 0.125. The aforementioned coefficients as functions of the thickness ratio have been listed and plotted.[908] Note the possible simplification by a consistent decomposition[909] and the proposed amendment of the transverse shear formulae (see Radaj and Zhang,[910] *ibid*. appendix II). The coefficients according to the boundary element analysis are given in Table 10.3. Note that k^{+-}_{IIImu} = 2.0 for δ = 1.0 instead of k^{+-}_{IIImu} = 0.5 for the chosen mode of decomposition according to the reasoning in the paragraph following eq. (10.17).

The structural stress portions σ^{+-}_{mu}, σ^{++}_{bui}, and σ^{+-}_{bui} follow from the decomposition depicted by Fig. 10.10 (with σ^{+-}, σ^{++}_b, σ^{+-}_b, representing σ^{+-}_{mu}, σ^{++}_{bui}, σ^{+-}_{bui}) in which the non-singular constant stress portion σ^{++}_{mu} is separated first, and anti-symmetrical and symmetrical resultant force portions are introduced thereafter. Note that σ^{+-}_{bui} in eq. (10.26) and $\sigma^{+-}_{bb} = \sigma^{+-}_{bui}$ in eq. (10.8) are defined differently. A decomposition into symmetrical and anti-symmetrical resultant forces is applied in respect of the shear stress portions $\tau^{++}_{\perp u}$ and $\tau^{+-}_{\perp u}$, and into symmetrical and anti-symmetrical shear stresses in respect of the shear stress portions $\tau^{++}_{\parallel u}$ and $\tau^{+-}_{\parallel u}$ which are set equal to the inside surface values. The following equations are derived:

$$\sigma^{++}_{mu} = \frac{1}{2}\frac{(\sigma_{ui} + \sigma_{uo})t_u + (\sigma_{li} + \sigma_{lo})t_l}{t_u + t_l} \tag{10.23}$$

$$\sigma^{+-}_{mu} = \frac{1}{2}(\sigma_{ui} + \sigma_{uo}) - \sigma^{++}_{mu} \tag{10.24}$$

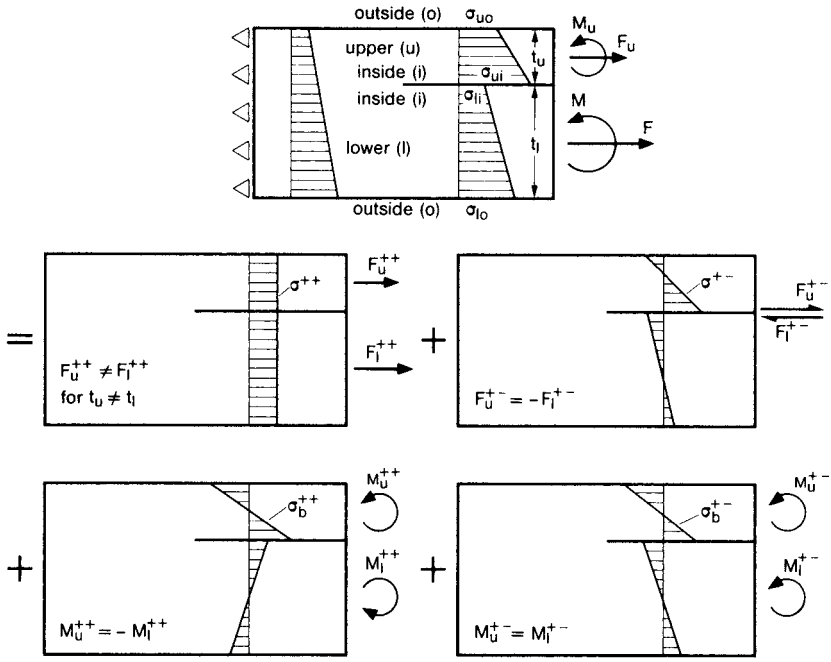


Fig. 10.10. Decomposition of the in-plane structural normal stress state at the slit tip of a lap joint with unequal plate thicknesses into anti-symmetrical and symmetrical resultant force portions after separation of the non-singular constant stress portion; after Radaj and Zhang.[908]

Table 10.3. Coefficients $\{k_{\mu u}\}$ with μ = I, II, III dependent on plate thickness ratio $\delta = t_u/t_l$ for decomposed structural stress states; results from boundary element analysis; after Radaj and Zhang[908]

δ	k_{Imu}^{+-}	k_{Ibu}^{++}	k_{Ibu}^{+-}	$k_{I\perp u}^{++}$	$k_{I\perp u}^{+-}$	
1.0	0	0.576	0	0	2.236	
0.5	0.206	0.399	0.224	0.964	1.997	
0.25	0.306	0.343	0.295	1.441	1.875	
0.125	0.482	0.326	0.134	1.645	1.826	
δ	k_{IImu}^{+-}	k_{IIbu}^{++}	k_{IIbu}^{+-}	$k_{II\perp u}^{++}$	$k_{II\perp u}^{+-}$	k_{IIIu}^{+-}
1.0	2.001	0	0.501	0.550	0	1.42
0.5	1.744	0.169	0.336	0.407	0	1.23
0.25	1.542	0.225	0.276	0.229	0	1.11
0.125	1.393	0.244	0.258	0.113	0	1.02

$$\sigma_{\mathrm{bui}}^{++} = -\frac{1}{2t_{\mathrm{u}}^2}\left[(\sigma_{\mathrm{ui}} + 2\sigma_{\mathrm{uo}} - 3\sigma_{\mathrm{mu}}^{++})t_{\mathrm{u}}^2 + (\sigma_{\mathrm{li}} + 2\sigma_{\mathrm{lo}} - 3\sigma_{\mathrm{mu}}^{++})t_{\mathrm{l}}^2\right] \tag{10.25}$$

$$\sigma_{\mathrm{bui}}^{+-} = -\frac{1}{2t_{\mathrm{u}}^2}\left[(\sigma_{\mathrm{ui}} + 2\sigma_{\mathrm{uo}} - 3\sigma_{\mathrm{mu}}^{++})t_{\mathrm{u}}^2 - (\sigma_{\mathrm{li}} + 2\sigma_{\mathrm{lo}} - 3\sigma_{\mathrm{mu}}^{++})t_{\mathrm{l}}^2\right] \tag{10.26}$$

$$\tau_{\perp\mathrm{u}}^{++} = \frac{1}{2t_{\mathrm{u}}}(\tau_{\perp\mathrm{u}}t_{\mathrm{u}} + \tau_{\perp\mathrm{l}}t_{\mathrm{l}}) \tag{10.27}$$

$$\tau_{\perp\mathrm{u}}^{+-} = \frac{1}{2t_{\mathrm{u}}}(\tau_{\perp\mathrm{u}}t_{\mathrm{u}} - \tau_{\perp\mathrm{l}}t_{\mathrm{l}}) \tag{10.28}$$

$$\tau_{\parallel\mathrm{u}}^{++} = \frac{1}{2}(\tau_{\parallel\mathrm{u}} + \tau_{\parallel\mathrm{l}}) = \frac{1}{2}(\tau_{\parallel\mathrm{ui}} + \tau_{\parallel\mathrm{li}}) \tag{10.29}$$

$$\tau_{\parallel\mathrm{u}}^{+-} = \frac{1}{2}(\tau_{\parallel\mathrm{u}} - \tau_{\parallel\mathrm{l}}) = \frac{1}{2}(\tau_{\parallel\mathrm{ui}} - \tau_{\parallel\mathrm{li}}) \tag{10.30}$$

where $\sigma_{\mathrm{mu}}^{++}$ and $\sigma_{\mathrm{mu}}^{+-}$ are the symmetrical and anti-symmetrical membrane stress portions, $\sigma_{\mathrm{bui}}^{++}$ and $\sigma_{\mathrm{bui}}^{+-}$ are the symmetrical and anti-symmetrical bending stress portions at the upper plate inside surface, $\tau_{\perp\mathrm{u}}^{++}$, $\tau_{\perp\mathrm{u}}^{+-}$, $\tau_{\parallel\mathrm{u}}^{++}$ and $\tau_{\parallel\mathrm{u}}^{+-}$ are the symmetrical and anti-symmetrical, transverse and longitudinal shear stress portions, σ_{uo}, σ_{ui}, σ_{lo} and σ_{li} are the structural stresses in the upper and lower plate at the outer and inner surface, $\tau_{\perp\mathrm{u}}$ and $\tau_{\perp\mathrm{l}}$ are the structural transverse shear stresses in the upper and lower plate, $\tau_{\parallel\mathrm{u}}$ and $\tau_{\parallel\mathrm{l}}$ are the structural longitudinal membrane shear stresses in the upper and lower plate, $\tau_{\parallel\mathrm{ui}}$ and $\tau_{\parallel\mathrm{li}}$ are the structural longitudinal shear stresses in the upper and lower plate at the inner surface and t_{u} and t_{l} are again the thicknesses of the upper and lower plate.

A further simplification of the formulae leading to the stress intensity factors K_{I} and K_{II} is possible, as mentioned above, by a consistent decomposition which separates the complete non-singular membrane and bending stress portion first.[909] The vectors $\{k_{\mu\mathrm{u}}\}$ and $\{\sigma_{\mathrm{u}}\}$ are then reduced by one term. It is not an easy task to derive the new coefficient vector $\{k_{\mu\mathrm{u}}\}$ from the old one.

A remarkable feature of the stress intensity factors evaluated dependent on thickness ratio[908] is the fact that the single-mode crack tip loading conditions for $\delta = 1.0$ change into mixed-mode conditions for $\delta < 1.0$. The (normalised) equivalent stress intensity factors decrease with decreasing δ in tension-bending, counterbending, equidirected bending, countertransverse shear and longitudinal shear loading. The curves of K_{I} and K_{II} dependent on thickness ratio have opposite gradients in all cases.

10.2.4 Stress intensity factors of lap joints in dissimilar materials

A unexpected phenomenon is connected with the stress singularity at the tip of slits or cracks in the interface between dissimilar materials inclusive of elastic-rigid material combinations. The cross-sectional stresses oscillate between the positive and negative values of the conventional inverse square root over distance increase. This takes place in an extremely small zone near the slit tip. The wavelength of the oscillation becomes steadily smaller and converges to zero when approaching the slit tip. A similar (non-singular) oscillation modifies the conventional slit opening displacements near the slit tip (wrinkling of the two slit surfaces).

The oscillatory stress singularity can theoretically be described by a complex stress intensity factor, but this description is unsuitable for practical application to strength problems. An applicable concept has been developed by Radaj and Zhang[910] on the basis of non-oscillatory stress singularities. This concept neglects the oscillation within the small slit tip zone using the same reasoning by which small-scale yielding at the slit tip is usually neglected. The conventional stress intensity factors K_{I} and K_{II} are thus preserved but they are only approximations.

The stress intensity factors $K_{\mathrm{I}}, K_{\mathrm{II}}$ and $K_{\mathrm{eq}} = \sqrt{K_{\mathrm{I}}^2 + K_{\mathrm{II}}^2}$ are presented in a form similar to eqs. (10.18–10.20) with two modifications: the consistent stress portion vector is introduced and the coefficient vector depends on the elasticity ratios apart from the thickness ratio. In order to simplify the equations, the thickness ratio is introduced as $\delta = 1.0$, i.e. only the effect of the elasticity ratios is considered (Radaj and Zhang[910] include the thickness ratio). Only two elasticity constants in each of the two materials being considered are independent of each other. It is assumed that the upper plate material has the smaller elasticity modulus and that plane strain conditions prevail:

$$K_{\mu} = \{k_{\mu}\}^{\mathrm{T}} \{\sigma\} \sqrt{t} \qquad (\mu = \mathrm{I},\ \mathrm{II},\ \mathrm{eq}) \tag{10.31}$$

$$\{k_{\mu}\}^{\mathrm{T}} = \left[\mathrm{k}_{\mu\mathrm{cb}} \mathrm{k}_{\mu\mathrm{tb}} \mathrm{k}_{\mu\perp}^{++} \mathrm{k}_{\mu\perp}^{+-}\right] = f(\alpha,\ \beta,\ \nu_{\mathrm{u}},\ \nu_{\mathrm{l}}) \tag{10.32}$$

$$\{\sigma\} = \begin{Bmatrix} \sigma_{\mathrm{cb}} \\ \sigma_{\mathrm{tb}} \\ \tau_{\perp}^{++} \\ \tau_{\perp}^{+-} \end{Bmatrix} \tag{10.33}$$

$$\alpha = \frac{E'_{\mathrm{u}}}{E'_{\mathrm{l}}} \qquad \left(E'_{\mathrm{u}} = \frac{E_{\mathrm{u}}}{1 - \nu_{\mathrm{u}}^2},\quad E'_{\mathrm{l}} = \frac{E_{\mathrm{l}}}{1 - \nu_{\mathrm{l}}^2}\right) \tag{10.34}$$

$$\beta = \frac{G_{\mathrm{u}}}{G_{\mathrm{l}}} = \frac{1 - \nu_{\mathrm{u}}}{1 - \nu_{\mathrm{l}}} \alpha \tag{10.35}$$

where K_μ are the stress intensity factors in mode I and II loading and the equivalent stress intensity factor, $\{k_\mu\}^T$ is the transposed vector of coefficients, $\{\sigma\}$ is the vector of the structural stress portions, t is the plate thickness, $f(\alpha, \beta, \nu_u, \nu_l)$ is a function of α, β, ν_u and ν_l, σ_{cb} and σ_{tb} are the counterbending and tension-bending structural stress portions, $\tau_\perp^{++}$ and $\tau_\perp^{+-}$ are the symmetrical and anti-symmetrical transverse shear stress portions, α is the ratio of the elastic moduli modified according to plane strain, E_u and E_l are the elastic moduli in the upper and lower plate, ν_u and ν_l are the Poisson's ratios in the upper and lower plate, β is the ratio of the shear moduli, and G_u and G_l are the shear moduli in the upper and lower plate. Considering longitudinal shear loading, the eqs. (10.4) and (10.15) remain valid for $\delta = 1.0$.

The coefficients k_μ (μ = I, II, III, eq) are simple functions of the elasticity ratios. Closed solutions have been derived for k_{eq} and k_{III} on the basis of the J- and J^*-integral, respectively. The solution for k_{eq} has been used to approximate k_I and k_{II} on the basis of $k_{eq} = \sqrt{k_I^2 + k_{II}^2}$ and the results of boundary element analyses for $\alpha = 0.0, 0.125, 0.25, 0.5$ and 1.0 referring to k_I and k_{II}. The aforementioned coefficients as functions of the elasticity ratios (combined with the thickness ratio to some extent) have been listed and plotted.[910,915]

The consistent decomposition of the structural stress state is performed according to the equations derived by Radaj and Zhang.[910] They are restricted here to $\delta = 1.0$, i.e. equal thicknesses of the upper and lower plate. The decomposition of the membrane and bending stress state after separating the complete non-singular stress portion first results in the tension-bending and counterbending portions presented in Fig. 10.11:

$$\sigma_{cb} = \sigma_{cbu} = -2\sigma_{uo} - \sigma_{ui} + 2\sigma_{uo}^* + \sigma_{ui}^* \tag{10.36}$$

$$\sigma_{tb} = \sigma_{tbu} = \frac{1}{2}\left(\sigma_{uo} + \sigma_{ui} - \sigma_{uo}^* - \sigma_{ui}^*\right) \tag{10.37}$$

$$\tau_\perp^{++} = \tau_{\perp u}^{++} = \frac{1}{2}(\tau_{\perp u} + \tau_{\perp l}) \tag{10.38}$$

$$\tau_\perp^{+-} = \tau_{\perp u}^{+-} = \frac{1}{2}(\tau_{\perp u} - \tau_{\perp l}) \tag{10.39}$$

$$\sigma_{uo}^* = \frac{\alpha(11 + \alpha)\sigma_{uo} + 8\alpha\sigma_{ui} + 2\alpha(1 - \alpha)\sigma_{li} - \alpha(1 + 3\alpha)\sigma_{lo}}{1 + 14\alpha + \alpha^2} \tag{10.40}$$

$$\sigma_{ui}^* = \frac{4\alpha\sigma_{uo} + \alpha(3 + \alpha)\sigma_{ui} + \alpha(1 + 3\alpha)\sigma_{li} + 4\alpha^2\sigma_{lo}}{1 + 14\alpha + \alpha^2} \tag{10.41}$$

where σ_{cb} and σ_{tb} are the counterbending and tension-bending structural stress portions ($\sigma_{cbu} = \sigma_{cbl}$, $\sigma_{tbu} = -\sigma_{tbl}$), $\tau_\perp^{++}$ and $\tau_\perp^{+-}$ are the symmetrical and

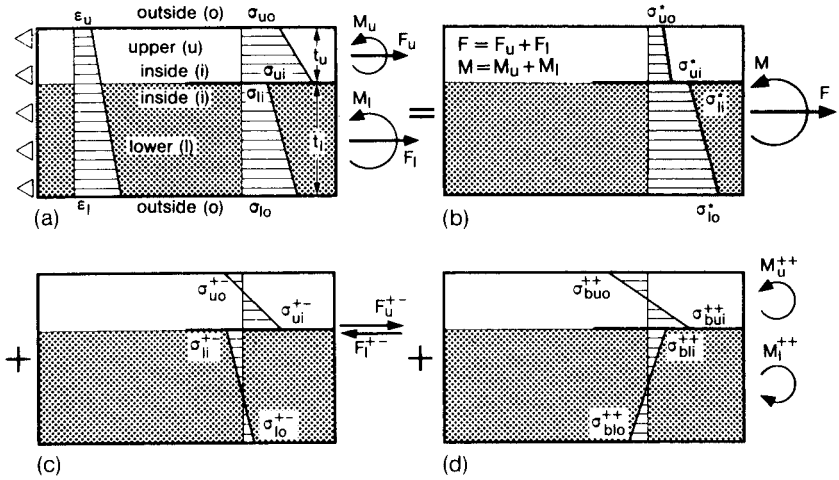


Fig. 10.11. Consistent decomposition of the membrane and bending structural stress state at the slit tip of a bimaterial lap joint (a), into stress portions without singularity effect (b), and into tension-bending and counterbending portions, respectively, with singularity effect (c, d); after Radaj and Zhang.[910]

anti-symmetrical transverse shear stress portions, σ_{uo}, σ_{ui}, σ_{lo} and σ_{li} are the structural stresses in the upper and lower plate at the outer and inner surface, σ^*_{uo} and σ^*_{ui} are the non-singular stresses in the upper plate at the outer and inner surface, $\tau_{\perp u}$ and $\tau_{\perp l}$ are the transverse shear stresses in the upper and lower plate and α is the ratio of the elastic moduli modified according to plane strain.

A remarkable feature of the stress intensity factors evaluated dependent on the elasticity ratio $\alpha = \beta$ (for $\nu_u = \nu_l$) in tension-bending, counterbending, equitransverse shear and countertransverse shear (the basic stress states after decomposition) is an approximately constant (relative) value of K_{eq} in each case with variable contents of K_I and K_{II} (Radaj and Zhang[910]).

The method above has also been applied to the thermal stress singularity at bimaterial crack tips.[915,916]

10.2.5 Stress intensity factors in lap joints under large deflections

The effect of large deflections, including buckling, on the stress intensity factors of lap joints is an effect on the structural stresses which define the stress intensity factors, for example according to eqs. (10.13–10.15) in the case of equal plate thickness and material. Only the structural stresses

are directly influenced by the non-linear effect whereas the stress intensity factors remain linearly dependent on the structural stresses.

By way of example, the cross-sectional models of spot-welded tensile shear and cross-tension specimens are dealt with according to Radaj and Zhang.[811,812] The calculation results for tensile-shear loading based on the finite element method (large displacement option) are plotted in Fig. 10.12 and Fig. 10.13. The material considered is steel. The plate thickness is 1 mm. The load level is expressed by the nominal structural stress without a large displacement effect. The nominal yield limit σ_Y^* is typical for high strength steels, including the elastic-plastic support effect. Higher loading is connected to plastic hinge formation so that the plotted purely elastic curves cannot really occur above σ_Y^* with the plate thickness under consideration. However they indicate the principal behaviour and may well occur with lower plate thickness or larger clamping distance.

There is hardly any effect of large deflections on the stress intensity factors in tensile loading, but there is a strong effect in compressive loading near the buckling load. Both frontal edge points of the joint face are initially subjected to compressive stresses, but one of them is 'snapping' to tensile stresses near the buckling load. Different equivalent stress intensity factor curves are thus related to the two frontal edge points. The behaviour changes fundamentally if gap closure is taken into account. Structural stiffening occurs and mode I slit deformation is suppressed (see Fig. 9.20).

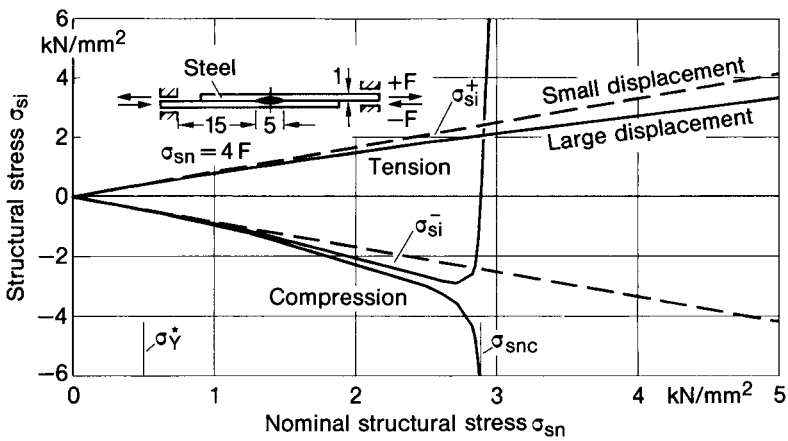


Fig. 10.12. Structural stress at inner plate surface at joint-face edge dependent on load level expressed by the nominal structural stress; cross-sectional model of spot-welded tensile-shear specimen; large displacement analysis including the buckling effect, twofold compression curves corresponding to the two frontal edge points of the joint face; after Radaj and Zhang.[812]

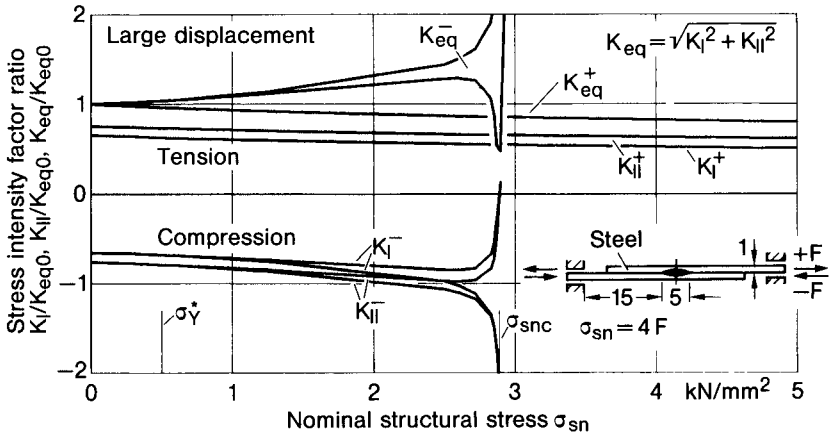


Fig. 10.13. Stress intensity factor ratios at joint-face edge dependent on load level expressed by the nominal structural stress; cross-sectional model of spot-welded tensile-shear specimen; large displacement analysis including the buckling effect, twofold compression curves corresponding to the two frontal edge points of the joint face; after Radaj and Zhang.[812]

10.2.6 Early stress intensity factor solutions for lap joints

Remarkable solutions for the stress intensity factors in tensile-shear loaded seam and spot-welded lap joints were published as early as 1974/75 (Chang and Muki,[857] Pook[886,887]). These solutions have repeatedly been used without being aware of the accuracy problem, at least with the spot weld solutions (see Table 10.1). They are reviewed in the following.

A solution for the straight (e.g. seam-welded) connection between overlapping plates was developed by Chang und Muki.[857] It proceeds from the stress field in an infinite plate strip subjected to the tension and shear forces in the joint face (or joint line) positioned at the corresponding section of the plate strip's longitudinal edge. This ends up with a pair of Fredholm integral equations. The angle of rotation of the joint face (or joint line) is determined from plane strain beam bending theory (applicable to cylindrically bent plates) taking large deflections into account (Goland and Reissner,[869] confirmed by Cooper and Sawyer[858]). The numerical evaluation is restricted to infinitely long plates, i.e. there is no bending moment and no transverse shear force introduced at the infinitely remote loaded ends (clamping device) despite the tensile forces or membrane stresses being offset by the plate thickness. The resulting stress intensity factors depend on the ratio of joint face width to plate thickness and on the load level (relative to the elastic modulus). They increase underproportionally with rising

load. The results given in graphical form were approximated in equation form by Pook[886] (see also Murakami,[543] *ibid.* p. 1199). The Goland–Reissner solution has been extended to more realistic clamping conditions by Lai *et al.*[876] considering the cracked lap-shear specimen used for fatigue testing of adhesive joints.

The approximated small-deflection plate strip solution[886] mentioned above has the following form:

$$K_{\mathrm{I}} = \tau\sqrt{\pi\frac{w_s}{2}}\left[0.770\left(\frac{w_{\mathrm{s}}}{t}\right)^{0.397}\right] \qquad \left(4.0 \le \frac{w_{\mathrm{s}}}{t} \le 10.0\right) \tag{10.42}$$

$$K_{\mathrm{II}} = \tau\sqrt{\pi\frac{w_s}{2}}\left[\frac{2}{\pi} + 0.365\left(\frac{w_{\mathrm{s}}}{t}\right)^{0.710}\right] \qquad \left(4.0 \le \frac{w_{\mathrm{s}}}{t} \le 10.0\right) \tag{10.43}$$

with the nominal shear stress τ in the joint face, the joint face width w_{s} and the plate thickness t.

The above equations include the half-space solution for $w_{\mathrm{s}}/t = 0$ (i.e. $t \to \infty$). The effect of finite thickness is to increase K_{II} to above the half-space values and to generate K_{I} values in the same order as the K_{II} values. Introducing the membrane stress in the plate, $\sigma_{\mathrm{m}} = \tau\, w_{\mathrm{s}}/t$, together with the more adequate square-root on plate thickness parameter, these equations read:

$$K_{\mathrm{I}} = \sigma_{\mathrm{m}}\sqrt{t}\left[0.965\left(\frac{t}{w_{\mathrm{s}}}\right)^{0.103}\right] \qquad \left(0.1 \le \frac{t}{w_{\mathrm{s}}} \le 0.25\right) \tag{10.44}$$

$$K_{\mathrm{II}} = \sigma_{\mathrm{m}}\sqrt{t}\left[0.798\left(\frac{t}{w_{\mathrm{s}}}\right)^{0.5} + 0.457\left(\frac{t}{w_{\mathrm{s}}}\right)^{-0.210}\right] \qquad \left(0.1 \le \frac{t}{w_{\mathrm{s}}} \le 0.25\right) \tag{10.45}$$

The accuracy of these relationships is determined by comparison with the decomposition method (eqs. (10.2), (10.3), (10.6–10.8)) applied to the tensile-shear-loaded straight connection, Table 10.4. The relevant equations are evaluated in the t/w_{s} range where high accuracy of the results can be expected. The results based on the decomposition method are considered to be highly accurate. As can be concluded from the data in the table, Pook's approximation formulae provide an acceptable accuracy as far as straight connections are considered.

The solution given by Pook[886] for the tensile-shear loaded spot-welded lap joints is derived by modifying the solution for the circular connection between half-spaces on the basis of the solution for the straight connection between overlapping plates just presented. The stress intensity factor solution given by Kassir and Sih[875] for the circular patch connection (diameter d) between half-spaces subjected to cross-tension (nominal stress σ) or

Table 10.4. Comparison of normalised stress intensity factors at the tensile-shear loaded straight connection between overlapping plates; with membrane stress σ_m, plate thickness t and joint face width w_s; after Radaj (unpublished)

Author	Method	Ratio t/w_s	Stress intensity factors	
			$K_I/(\sigma_m\sqrt{t})$	$K_{II}/(\sigma_m\sqrt{t})$
Pook[886]	Chang–Muki[857]	0.1	0.762	0.994
		0.25	0.838	1.010
Radaj	Decomposition	0.2	0.866	1.000

shear-loading (nominal stress τ) results in the following maximum stress intensity factors (K_I and K_{II} at the front side, K_{III} at the flank side):

$$K_I = \frac{\sigma}{2}\sqrt{\pi\frac{d}{2}} \tag{10.46}$$

$$K_{II} = \frac{\tau}{2}\sqrt{\pi\frac{d}{2}} \tag{10.47}$$

$$K_{III} = \frac{\tau}{2}\sqrt{\pi\frac{d}{2}} \tag{10.48}$$

For the sake of completeness, the solution for a bending moment load (nominal bending stress $\sigma_b = 32M_b/\pi d^3$) is supplemented:

$$K_I = \frac{3}{8}\sigma_b\sqrt{\pi\frac{d}{2}} \tag{10.49}$$

The stress intensity factor solutions given by Paris and Sih[883] and Benthem and Koiter[855] for the straight strip connection (joint face width w_s) subjected to cross-tension (nominal stress σ), transverse shear loading (nominal stress τ) or longitudinal shear loading (nominal stress τ_{II}) result in the following stress intensity factors:

$$K_I = \frac{2\sigma}{\pi}\sqrt{\pi\frac{w_s}{2}} \tag{10.50}$$

$$K_{II} = \frac{2\tau}{\pi}\sqrt{\pi\frac{w_s}{2}} \tag{10.51}$$

$$K_{III} = \frac{2\tau_{||}}{\pi}\sqrt{\pi\frac{w_s}{2}} \tag{10.52}$$

For the sake of completeness, the solution for a bending moment load (nominal bending stress $\sigma_b = 6M_b/w_s^2$) is supplemented:

$$K_{\mathrm{I}} = \frac{4}{3\pi}\sigma_{\mathrm{b}}\sqrt{\pi\frac{w_{\mathrm{s}}}{2}} \tag{10.53}$$

The first three stress intensity factors are by a factor of $4/\pi = 1.273$ greater than those for the corresponding circular connection. For bending moment loads, the factor is only slightly smaller, $32/9\pi = 1.132$.

Following Pook's idea, the stress intensity factor solution given by Chang and Muki[857] for the straight connection between overlapping plates in tensile-shear loading, eqs. (10.42) and (10.43), is reduced by $\pi/4 = 0.785$ in order to approximate the stress intensity factors at the circular connection between overlapping plates in tensile-shear loading:

$$K_{\mathrm{I}} = \tau\sqrt{\pi\frac{d}{2}}\left[0.605\left(\frac{d}{t}\right)^{0.397}\right] \tag{10.54}$$

$$K_{\mathrm{II}} = \tau\sqrt{\pi\frac{d}{2}}\left[0.5 + 0.287\left(\frac{d}{t}\right)^{0.710}\right] \tag{10.55}$$

$$K_{\mathrm{III}} = K_{\mathrm{II}} \tag{10.56}$$

Once more, the effect of finite plate thickness is to increase K_{II} (and K_{III}) to above the half-space values and to introduce K_{I} values of the same order as the K_{II} values.

Comparing the low accuracy of Pook's results for the circular connection (Table 10.1) with the high accuracy of results for the straight connection (Table 10.4), it is obvious that the deterioration of accuracy must have its origin in two effects: first in the two-dimensional plate bending effects in the former case as opposed to the one-dimensional effects in the latter case (concerns mainly K_{I}) and second in the two-sided shear loading of the connection in the former case in comparison with the one-sided condition in the latter case (concerns mainly K_{II} and K_{III}).

A further attempt to derive the stress intensity factor solution for tensile-shear, cross-tension and peel-tension loaded spot welds in lap joints by modifying the simple solutions for corresponding half-space configurations was made by Swellam *et al.*[929] His derivations include a bending moment load at the weld spot. The empirical modification, eq. (10.95), was found by evaluating the results of fatigue tests with varying geometrical parameters (plate thickness, plate width and spot diameter) and varying loading conditions of the specimens. Further approximation formulae for stress intensity factors which are of relevance for seam- or spot-welded lap joints have been derived by Pook[888] on the basis of the elementary beam and plate bending theories. Stress intensity factors in tensile-shear loaded spot welds have also been derived analytically by Makhnenko *et al.*[879]

10.2.7 Stress intensity factor formulae based on nominal structural stresses

The spot-welded specimen mostly used in connection with design evaluations is the hat section specimen subjected to torsional loading with the effect of prevailing shear forces in the weld spots. These shear forces can be calculated on the basis of the first Bredt formula which correlates the shear flux in the cross-sectional contour of thin-walled hollow-section bars to the torsional moment, eq. (10.57), simplified by a constant wall thickness t, with the assumption of excluded end support effects. The shear flux in the cross-sectional contour is set equal to the shear flux in the longitudinal sections. The latter is discontinuously distributed onto the weld spots, eq. (10.58). The second Bredt formula correlates the angle of twist to the torsional moment in the case of continuous non-welded or seam-welded hollow-section bars, eq. (10.59) which is again simplified by a constant wall thickness t:

$$\tau t = \frac{M_t}{2A^*} \tag{10.57}$$

$$F = \frac{M_t l^*}{2A^*} \tag{10.58}$$

$$\frac{\vartheta}{l} = \frac{M_t s^*}{4GA^{*2}t} \tag{10.59}$$

where τ is the shear stress in the cross-sectional contour, t is the thickness of the cross-sectional contour, M_t is the torsional moment, A^* is the area enclosed by the cross-sectional contour, F is the shear force in the joint face of the weld spot, l^* is the distance between the weld spot centre points (the pitch), ϑ is the angle of twist, l is the specimen length, s^* is the length of the cross-sectional contour and G is the shear modulus.

The weld spot force is approximated by the first Bredt formula with high accuracy because only equilibrium conditions are involved. This is not the case with the angle of twist according to the second Bredt formula which is strictly valid only for continuous bars. The discontinuity introduced by spot-welding causes a reduction of torsional rigidity which is dependent on the pitch.

Nominal stress intensity factors of weld spots in general can be determined as an approximation on the basis of the nominal structural stresses according to eqs. (9.1–9.8) condensed into stress portions according to eqs. (10.16) and (10.17) neglecting the influence of transverse shear stresses and with focus on the vertex points of the weld spot:

$$K_{\mathrm{In}} = \frac{1}{\sqrt{3}}\sigma_{\mathrm{cbn}}\sqrt{t} \tag{10.60}$$

$$K_{\mathrm{IIn}} = \frac{1}{2}\sigma_{\mathrm{tbn}}\sqrt{t} \tag{10.61}$$

where K_{In} and K_{IIn} are the nominal stress intensity factors of mode I and II, σ_{cbn} is the counterbending portion of the nominal structural stress, σ_{tbn} is the tensile-shear portion of the nominal structural stress and t is the plate thickness.

The nominal structural stress σ_{sn} according to eq. (9.3) in tensile-shear loaded weld spots with finite gap width g and plate thickness t is modified as follows:

$$\sigma^{*}_{\mathrm{sn}} = \sigma_{\mathrm{sn}}\left(1 + \frac{3}{4}\frac{g}{t}\right) \tag{10.62}$$

An attempt has been made by Zhang[938–942] to present the maximum stress intensity factors at weld spots in terms of the joint face forces (i.e. neglecting the eigenforces) based on nominal structural stress formulae. But the formula for K_{I} contains a misleading first term, applicable only to the tensile shear specimen under special geometric conditions. Also, the other two terms expressing the effects of bending moments and cross-tension force are not generally valid.

The decomposition of the loading state in the case of laser-beam-welded lap joints (also applicable to spot-welded joints) subjected to tensile-shear and peel-tension loading, respectively, has been specified by Radaj *et al.*,[907] Fig. 10.14, and can be used for force-based stress intensity factor formulae.

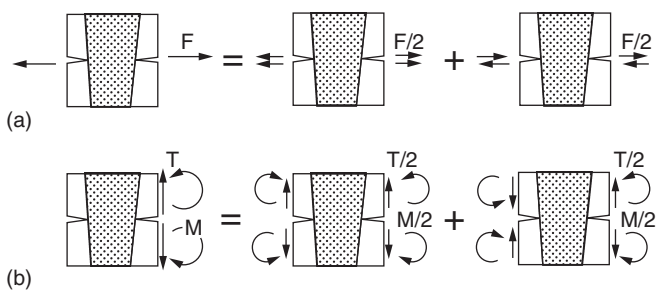


Fig. 10.14. Decomposition of seam weld loading in the tensile-shear specimen (purely tensile-loaded) (a) and in the peel-tension specimen (b), eigenforce groups and joint face force groups; after Radaj *et al.*[907]

10.2.8 Links to the notch stress approach

Considering actually or fictitiously rounded slit tips in welded joints, the relationship between stress intensity factors and maximum notch stresses is of interest. The stress intensity factors can be exactly derived from the maximum notch stresses of the corresponding elliptical hole configuration by a limit value process or approximated by using a single small but finite notch radius:[911]

$$K_{\mathrm{I}} = \lim_{\rho \to 0} \frac{1}{2} \sigma_{\mathrm{k}} \sqrt{\pi \rho} \qquad (K_{\mathrm{II}} = K_{\mathrm{III}} = 0, \quad \sigma_{0\mathrm{kl}} = 0) \tag{10.63}$$

$$K_{\mathrm{II}} = \lim_{\rho \to 0} \sigma'_{\mathrm{k}} \sqrt{\pi \rho} \qquad (K_{\mathrm{I}} = K_{\mathrm{III}} = 0, \quad \sigma_{0\mathrm{kl}} = 0) \tag{10.64}$$

$$K_{\mathrm{III}} = \lim_{\rho \to 0} \tau^{*}_{\mathrm{k}} \sqrt{\pi \rho} \qquad (K_{\mathrm{I}} = K_{\mathrm{II}} = 0, \quad \sigma_{0\mathrm{kl}} = 0) \tag{10.65}$$

where K_{I}, K_{II} and K_{III} are stress intensity factors of mode I, II and III, ρ is the notch radius at the vertex point of the elliptical hole, σ_{k} and τ^{*}_{k} are the maximum notch stresses at the vertex point of the elliptical hole subjected to in-plane normal stress and anti-plane shear stress loading, σ'_{k} is the maximum notch stress close to the vertex point of the elliptical hole subjected to in-plane shear loading and $\sigma_{0\mathrm{kl}}$ is the non-singular stress tensor.

The following equation was added by Radaj and Zhang[911] correlating the shear stress intensity factor K_{II} with the maximum shear stress τ_{k} occurring slightly below the vertex point of the elliptical hole:

$$K_{\mathrm{II}} = \lim_{\rho \to 0} \frac{3\sqrt{3}}{2} \tau_{\mathrm{k}} \sqrt{\pi \rho} \tag{10.66}$$

Additionally, eq. (10.64) was modified for application to notches with circular or semi-circular instead of elliptical shapes correlating the local maximum notch stress σ'_{k} with the radius ρ' of local notch curvature:[911,920]

$$K_{\mathrm{II}} = \lim_{\rho \to 0} \frac{1}{1.682} \sigma'_{\mathrm{k}} \sqrt{\pi \rho'} \tag{10.67}$$

The convergence behaviour of the limit value formulae above should be known in cases of practical application. On the other hand, in practical applications, the elliptical notch is often replaced by a U-shaped or keyhole notch, which provides an exact circle at the notch root independent of slit length. Such notches, actually or fictitiously rounded, are considered within the notch stress approach.

The convergence behaviour of the normalised stress intensity factors $k_{\mathrm{I}} = K_{\mathrm{I}} / \sigma \sqrt{\pi a}$, $k_{\mathrm{II}} = K_{\mathrm{II}} / \tau \sqrt{\pi a}$ and $k_{\mathrm{III}} = K_{\mathrm{III}} / \tau^{*} \sqrt{\pi a}$ (with σ, τ, τ^{*} uniform stresses at the remote plate edge) for a rectangular plate with an elliptical

hole of half-length a is shown in Fig. 10.15. The convergence of k_{II} is poor in relation to k_I or k_{III}. The poor convergence of k_{II} is further analysed dependent on notch shape in Fig. 10.16. Only the notch stresses of the elliptical hole converge to the correct value, whereas those of the U-shaped hole and keyhole are larger by a factor 1.44–1.74. The dependency on notch shape is negligibly small in the case of k_I or k_{III}.

Longitudinal tensile loading of U-shaped and keyhole-shaped slits generates a transverse compressive stress in the vertex points, whereas no transverse stress occurs with ideal slits (non-singular loading mode). This may introduce an error when evaluating K_I from the maximum notch stress in simultaneous transverse loading of the slit but the error can be assessed and corrected.[911]

The stress state in the neighbourhood of sharp notches can be described on the basis of the corresponding stress intensity factors even if the notch radius is not exactly zero but has a small finite value. This 'blunt crack problem' has been approximated by Creager and Paris[860] for $r \ll a$ (crack length a) using a slim parabolic notch shape (these authors consider elliptical and hyperbolical notches but the derived stress equations apply to parabolic notches). The complete equations are confined here to the ligament stresses ($\varphi = 0$) with the notch root located at $r = \rho/2$:

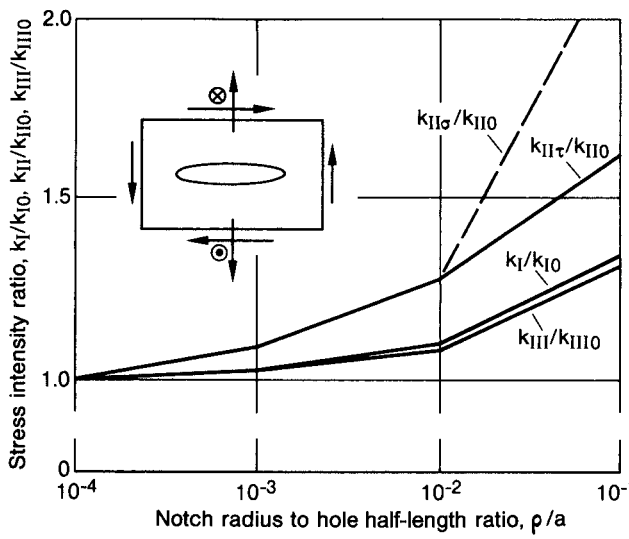


Fig. 10.15. Relative normalised stress intensity factors of mode I, II and III derived from elliptical hole in rectangular plate, subjected to tensile loading, in-plane and anti-plane shear loading; convergence behaviour of limit value formulae; index 0 refers to the stress intensity factor of the sharp slit tip ($\rho/a = 0$) and subscripts σ and τ refer to eq. (10.64) and eq. (10.66), respectively; ratio of plate length to plate width to hole length is 1.0/0.5/0.5; after Radaj and Zhang.[911]

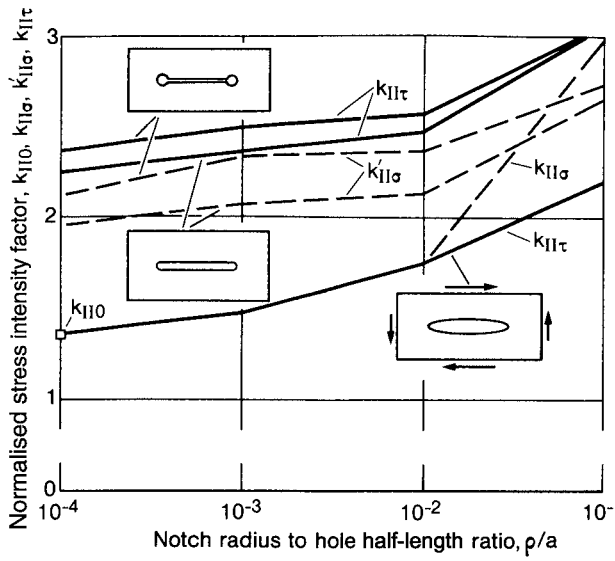


Fig. 10.16. Normalised stress intensity factors (mode II) derived on the basis of an elliptical hole, U-shaped hole and keyhole in a rectangular plate under in-plane shear loading; convergence behaviour of limit value formulae; index 0 refers to the stress intensity factor of the sharp slit tip ($\rho/a = 0$) and subscripts σ and τ refer to eq. (10.64) or (10.67) and eq. (10.66), respectively; ratio of plate length to plate width to hole length is 1.0/0.5/0.5; after Radaj and Zhang.[911]

$$\sigma_\varphi = \frac{K_\mathrm{I}}{\sqrt{2\pi r}}\left(1 + \frac{\rho}{2r}\right) \tag{10.68}$$

$$\sigma_\mathrm{r} = \frac{K_\mathrm{I}}{\sqrt{2\pi r}}\left(1 - \frac{\rho}{2r}\right) \tag{10.69}$$

$$\tau_{\mathrm{r}\varphi} = \frac{K_\mathrm{II}}{\sqrt{2\pi r}}\left(1 - \frac{\rho}{2r}\right) \tag{10.70}$$

$$\tau_{\varphi\psi} = \frac{K_\mathrm{III}}{\sqrt{2\pi r}} \tag{10.71}$$

where σ_φ, σ_r and $\tau_{\mathrm{r}\varphi}$ are the in-plane stress components, $\tau_{\varphi\psi}$ is the antiplane shear stress, r, φ and ψ are polar coordinates (see Fig. 10.5) and ρ is the notch radius. These equations can be used inversely to determine the stress intensity factors from the ligament stresses at the blunt crack tip.

The stress intensity approach has been used to derive the fatigue-effective notch stresses in two special cases (weld root notch of transverse attachment and of cruciform joint) within the notch stress approach, version with fictitions notch rounding.

One practical problem with this version is the difference in the multiaxiality coefficient s for crack tips in tensile loading, in-plane shear loading and out-of-plane shear loading which necessitates different fictitious notch radii. This problem has been solved in part by Radaj and Zhang.[911] Assuming coplanar crack propagation (which is only occasionally the case), the relevant von Mises equivalent stress can be approximated with only one value of s, e.g. $s = 2.0$ for tensile loading, which means only one U-shaped hole or keyhole model with the fictitious notch radius $\rho_f = 2\rho^*$:

$$\bar{\sigma}_{k\,eq} = \sqrt{\bar{\sigma}^2_{k2.0} + 4.7\bar{\sigma}'^2_{k2.0} + 12\bar{\tau}^{*2}_{k2.0}} \tag{10.72}$$

where $\bar{\sigma}_{k\,eq}$ is the maximum fatigue-effective equivalent notch stress, $\bar{\sigma}_{k2.0}$ is the maximum fatigue-effective notch stress with tensile loading ($s = 2.0$), $\bar{\sigma}'_{k2.0}$ is the maximum fatigue-effective notch stress with in-plane shear loading ($s = 2.0$) and $\bar{\tau}^*_{k2.0}$ is the maximum fatigue-effective shear notch stress with out-of-plane shear loading ($s = 2.0$).

Special formulae based on stress intensity factors have been derived for the fatigue-effective notch stress expressed by the fatigue notch factor K_f. These were applied to the weld root of transverse attachment joints with fillet welds (eq. (10.73) based directly on ρ^* from Neuber's averaged stress hypothesis or eqs. (10.74) and (10.75) based on ρ_f in combination with Creager's blunt crack solution) and of cruciform joints with double-bevel butt welds and remaining root face (eq. (10.76)), both joints being subjected to tensile loading:

$$K_f = \sqrt{k_I^2 + 31.64k_{II}^2}\sqrt{\frac{2a}{\rho^*}}$$

$$\left(K_f = \frac{\bar{\sigma}_{k\,eq}}{\sigma_n},\quad k_I = \frac{K_I}{\sigma_n\sqrt{\pi a}},\quad k_{II} = \frac{K_{II}}{\sigma_n\sqrt{\pi a}}\right) \tag{10.73}$$

$$K_f = 2\sqrt{k_I^2 + 1.172k_{II}^2}\sqrt{\frac{a}{\rho_f}} \tag{10.74}$$

$$\rho_f = 2\frac{1 + 1.172\lambda^2}{1 + 31.64\lambda^2}\rho^* \qquad \left(\lambda = \frac{K_{II}}{K_I}\right) \tag{10.75}$$

$$K_f = k_I\sqrt{\frac{2a}{\rho^*}} \qquad (k_{II} \approx 0) \tag{10.76}$$

where $2a$ is the weld root face length, $\rho_f = 2\rho^*$ is the fictitious notch radius and ρ^* is the substitute microstructural support length.

Another problem with the notch stress approach which has been treated on the basis of the singular stress state at slit or crack tips is the application of the notch stress approach to short slits or cracks.[291] The weld root face just mentioned may be short. The fatigue notch factor derived from

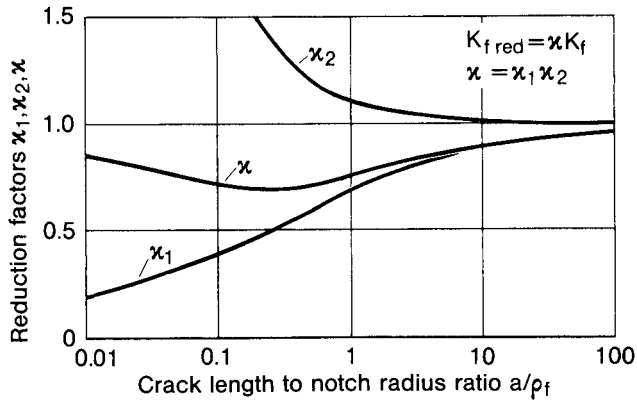


Fig. 10.17. Reduction of the fatigue notch factor of short cracks by the combined effects of a mild instead of a sharp notch (κ_1) and of closely opposed crack tips (κ_2); results with $s = 2.0$; after Radaj.[291]

the averaged crack tip stresses using the concept of fictitious notch rounding is reduced by the combined effects of a mild instead of a sharp notch (reducing K_f) and closely opposed crack tips (increasing K_f). The formula has been derived using the multiaxiality coefficient $s = 2$ applicable to tensile-loaded short cracks, Fig. 10.17:

$$K_{f\,red} = \frac{\sqrt{1 + \dfrac{4a}{\rho_f}}}{1 + 2\sqrt{\dfrac{a}{\rho_f}}} K_f \tag{10.77}$$

where K_f and $K_{f\,red}$ are the unreduced and reduced fatigue notch factors, a is the crack or slit length and ρ_f is the fictitious notch radius. The reduction expressed by eq. (10.77) is only slightly changed when using another multiaxiality coefficient, e.g. $s = 1.0$ for shear loading.

The increasing effect on K_f of the closely opposed crack tips corresponds to the lowered endurable uncorrected stress intensity factor of short cracks.

10.3 Analysis tools – fatigue assessment based on stress intensity factors

10.3.1 Endurable stress intensity factors

The endurable stress intensity factors (endurable in respect of through-thickness cracks) at weld spots in steel specimens subjected to tensile-shear and cross-tension or peel-tension cyclic loading ($R \approx 0$) dependent on number of cycles are summarised in Table 10.5 based on published data.

Table 10.5. Endurable stress intensity factor ranges ΔK_{en} ($P_f = 50\%$) at weld spot edge dependent on number of cycles N; mean values determined from tensile-shear and cross-tension or peel-tension specimens ($R \approx 0$) made of steel; diagram values from the literature converted according to $1\,\text{ksiin}^{1/2} = 34.8\,\text{N/mm}^{3/2}$, $1\,\text{MPa}\,\text{m}^{1/2} = 31.6\,\text{N/mm}^{3/2}$, $1\,\text{kJ} = 1\,\text{kN}\,\text{m}$, $\Delta K_J^2 = E\Delta J/(1-\nu^2)$; after Radaj[4]

Authors	Steel	Yield limit σ_Y [N/mm^2]	Thickness t [mm]	Type of ΔK	Endurable stress intensity, ΔK_{en} [N/mm$^{3/2}$]			
					$N = 10^4$	$N = 10^5$	$N = 10^6$	$N = 10^7$
Wang–Ewing[932,933]	Low-alloy (TS)[a]	157–357	0.8–3.2	ΔK_J	533	342	219	141
	Low-alloy (PS)[b]	252–400	1.3–1.5	ΔK_J	1944	1143	673	396
Pollard[885]	Low-alloy (TS)[a]	217–1085	0.9–2.6	$\Delta K_{I/II}$[d]	837	480	275	158
Mizui *et al.*[797]	Unalloyed	160–180	0.8–1.4	ΔK_{eq}	—	340	225	150
Yuuki *et al.*[934–937]	Unalloyed	170–180	0.8–1.2	ΔK_{eq}	699	427	259	158
Swellam *et al.*[929]	Low-carbon	150–180	0.9–1.4	ΔK_i	199	135	91	62
	HSLA[c]	250–450	1.3–2.0	ΔK_i	265	156	92	54
Pook[887]	Low-alloy (TS)[a]	260–475	7.5	ΔK_I	—	700	340	200

[a] TS: Tensile-shear specimen.
[b] PS: Peel-tension specimen.
[c] HSLA: High-strength low-alloy.
[d] K_I related to plate fractures, $K_{II} = K_{III}$ related to joint face fractures (Pook's formulae).

The endurable values of ΔK_J by Wang and Ewing[932,933] are substantially higher for peel-tension ('coach peel') specimens than for tensile-shear specimens, which may be explained by different initial crack paths (Henrysson[959]). The endurable values ΔK_i by Swellam *et al.*,[929] eq. (10.93) with $R = 0$, evaluated from fatigue tests with tensile-shear, peel-tension and double-face shear specimens deviate in the opposite direction (too small values). The reason is that the underlying stress intensity factors are by a factor 2–5 too small (see comments on eq. (10.96)). The early evaluation by Pook[887] of tensile-shear fatigue tests results by Overbeeke and Draisma[881,882] uses ΔK_I as a reference value ($\Delta K_I \approx \Delta K_{II}$, both being too large, see Table 10.1, thus approximating ΔK_{eq} incorrectly). Pollard[885] distinguishes between ΔK_I related to plate fractures and ΔK_{II} related to joint face fractures. The excessive variations in the endurable stress intensity factors listed in Table 10.5 is an indication that the stress intensity approach is still insufficiently founded with regard to quantitative life or strength assessments.

In addition to the data in the table, the scatter band of the evaluation of Yuuki *et al.*[934–937] referring to the equivalent stress intensity factor range ΔK_{eq} according to the maximum tangential stress criterion is presented in Fig. 10.18. The ΔK_{eq}-related approximation for the number of cycles N up to failure is:

$$N = A_k(\Delta K_{eq})^{-k} \tag{10.78}$$

with the inverse slope k and the coefficient A_k assumed to be material parameters.

A similar diagram established with similar specimens and loading cases is available from Mizui *et al.*[797] based on Yuuki's stress intensity factor formulae. Note that Yuuki's stress intensity factors are too low by a factor of 0.7–0.8 (see Table 10.1). The endurable stress intensity factors for $N = 5 \times 10^6$ cycles roughly agree with the generally accepted threshold stress intensity factor for non-welded structural steels, $K_{th0} = 180\,N/mm^{3/2}$ (for loading mode I and $R = 0$). Comparable results from H-shaped multi-spot specimens under shear and peel-tension loading were published by Zhang *et al.*[943] A similar K–N curve based on theoretical stress intensity factors without a plate thickness adaptation was presented by Lee and Kim[877] (endurable values not directly comparable). The scatter of the fatigue strength or life is relatively large in the cases considered (but smaller than with the corresponding structural stresses or strains) because additional influencing variables such as non-singular stresses originating from eigenforces as well as varying fabrication and material conditions are acting. The influence of plate thickness is not considered (compare Fig. 11.38). Also, the total life of the specimens has been evaluated instead of a defined-crack initiation life. An explanation for the possibility of correlating

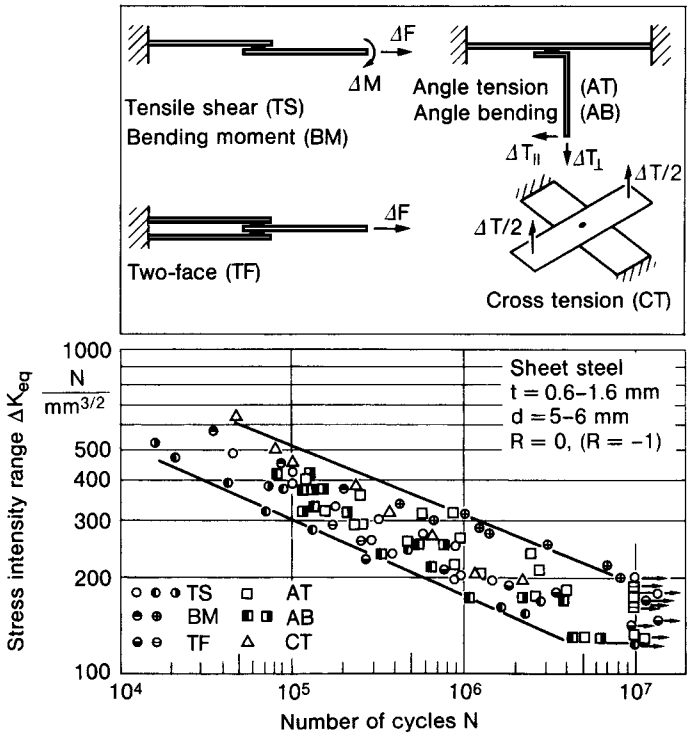


Fig. 10.18. Endurable stress intensity factor range at the weld spot of various specimens and loading modes, according to maximum tangential stress criterion; inverse slope $k = 4.5$; after Yuuki *et al.*[934–937]

through-thickness fractures with crack initiation data has been given by Cooper and Smith[859,927] (see Section 10.1.2). The non-correlating aspects are discussed by Henrysson[963] (see Section 11.3.4).

Endurable stress intensity factors for spot welds in austenitic stainless steel (AISI304, $\sigma_Y = 496\,N/mm^2$) and in duplex stainless steel (SAE2304 with 50% austenite and 50% ferrite, $\sigma_Y = 545\,N/mm^2$) were determined by Linder *et al.*[878] with application to passenger train carriages. Tensile-shear specimens (three variants) and a cross-tension specimen with sheet thickness $t = 1.5$–4.0 mm and weld spot diameter $d = 6$–9 mm were fatigue-tested with the load ratio $R = 0.05$. Specimen failure was defined by a 25% (tensile-shear) or 30% (cross-tension) stiffness drop, respectively, caused by crack growth. The stress intensity factors K_I, K_{II}, K_{III} at the weld spot edge were determined by finite element analysis, resulting in an equivalent stress intensity factor K_{eq} according to eq. (10.90). The scatter band of the K–N curve is positioned similarly to that in Fig. 10.18. The (linear) mean value is described by $\Delta K_{eq} = 9960\,N^{-0.268}$ [$N/mm^{3/2}$]. The slope of this curve is $k =$

3.73. The lower-bound curve (95% confidence corresponding to plus and minus two standard deviations) is by the factor 0.55 below the mean value curve. The threshold stress intensity factor varied depending on specimen type, $\Delta K_{th} = 98–212\,\mathrm{N/mm^{3/2}}$.

On the basis of the maximum tangential stress criterion, the crack paths in different spot-welded specimens dependent on the load level were explained in terms of tendencies, Fig. 10.19. The crack propagation directions calculated according to the stated criterion are compared with the crack paths actually observed at the front face of the weld spot. The cracks are shifted to the outside of the heat-affected zone in the medium- and low-cycle fatigue range ($N \leq 10^5$ cycles) related to higher load range levels (see also Radaj and Zhang[918]).

The endurable stress intensity factors of spot welds given in Fig. 10.18 are mainly related to the load ratio $R \approx 0$. Several authors have addressed the question of the R dependency of endurable loads, stresses or stress intensity factors in spot welds (interchangeable parameters as far as linear-elastic conditions are considered). The factor f_R is introduced to characterise the change in fatigue strength at $R \neq 0$ in relation to its value at $R = 0$:

$$f_R = \frac{\Delta K_{enR}}{\Delta K_{en0}} \tag{10.79}$$

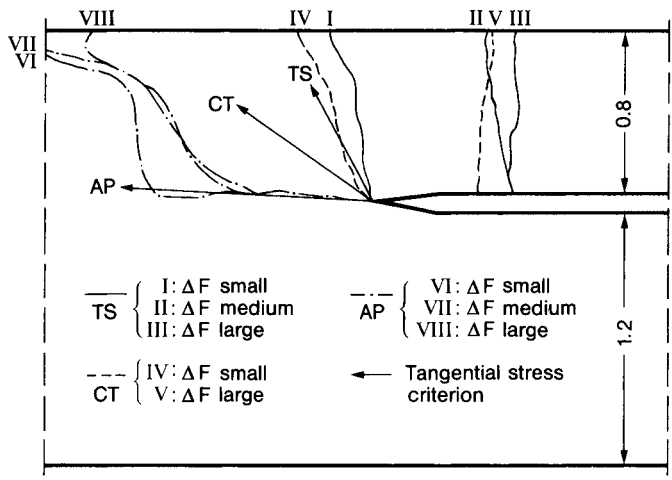


Fig. 10.19. Crack paths in different spot-welded specimens dependent on the load level ΔF determined from fatigue tests; comparison with crack propagation directions according to maximum tangential stress criterion; TS tensile-shear, CT cross-tension, AP angle-to-plate; after Yuuki *et al.*[934–937]

Pollard[885] proposes for tensile-shear (TS) and cross-tension (CT) specimens, respectively:

$$f_R = (1 - 0.4R) \qquad (-1 \le R \le 0.8) \quad \text{(TS)} \tag{10.80}$$

$$f_R = \frac{1}{1 + 0.5R^2} \qquad (0 \le R \le 0.8) \quad \text{(CT)} \tag{10.81}$$

Newman and Dowling[970] use the R correction (with $\gamma = 0.75$ for steel) proposed by Walker[989] for aluminium alloys:

$$f_R = (1 - R)^{1-\gamma} \qquad (0.1 \le R \le 0.75) \quad \text{(TS)} \tag{10.82}$$

Swellam *et al.*[929] assume in contrast with the above:

$$f_R = (1 - R)^{0.85} \qquad (-0.2 \le R \le 0.5) \quad \text{(TS)} \tag{10.83}$$

A straight line in the Haigh diagram corresponds to:

$$f_R = \frac{(1 - R)(1 + M)}{1 - R + M(1 + R)} \tag{10.84}$$

with the mean stress sensitivity ($0 \le M \le 0.4$) for spot welds in steel (see Fig. 9.34).

The influence of load ratio on the fatigue strength of spot welds is mainly a consequence of plasticity-induced crack closure (Henrysson,[962] see Section 11.3.4).

Integration of Forman's crack propagation equation with neglect of the threshold effect (see eq. (11.18)) results in a change of the endurable load cycles by the following factor:

$$f_{NR} = \frac{1}{1 - R} \qquad (R \ge 0) \tag{10.85}$$

10.3.2 Equivalent stress intensity factors under mixed-mode conditions

Mixed-mode loading conditions at crack or slit tips pose the question of how the stress intensity factors of the different modes should be superimposed to give an equivalent stress intensity factor (also termed 'resultant stress intensity factor'), equivalent in respect of fatigue failure by crack initiation and propagation. This includes the question of what critical value of K_{II} or K_{III} is equivalent to the critical value of K_I. The answer to these questions is complicated by the fact that the crack under mixed-mode loading conditions usually propagates in a non-coplanar manner, i.e. the crack changes its direction of propagation ('branch crack'). The crack propaga-

tion angle must be found first. Additional assumptions are necessary to do this. Several hypotheses and related criteria have been proposed to describe crack initiation and propagation under mixed-mode conditions. They are not generally verified by testing. It is therefore necessary to check the applicability of the criterion selected in each individual case.

The critical conditions for crack initiation and propagation under mixed mode I and II, specified according to different failure criteria, are plotted in Fig. 10.20. The tensile K_I part of the diagram is mainly taken from Sih.[923] The compressive part is supplemented as far as the criteria are defined in this region. The curves of maximum tangential stress ($\sigma_{t\,max}$, Erdogan and Sih[866]), minimum strain energy density (S_{min}, Sih[609,923]), maximum dilatational strain energy density (S_V^*, Radaj and Heib[905]), resultant energy release rate (G_{res}, Irwin[874]) and maximum energy release rate (G_{max}, Hussain *et al.*[873]) are compared with those of the process zone criteria proposed by Radaj and Zhang[914,919] (brittle initiation of fracture marked σ_{1b}, 'ductile' initiation of fracture marked τ_{1d} and σ_{1d} with critical shear stress and critical tensile stress, respectively, in the process zone).

There are major differences in curve shape and curve position both in the tensile and the compressive range of K_I which are caused by the

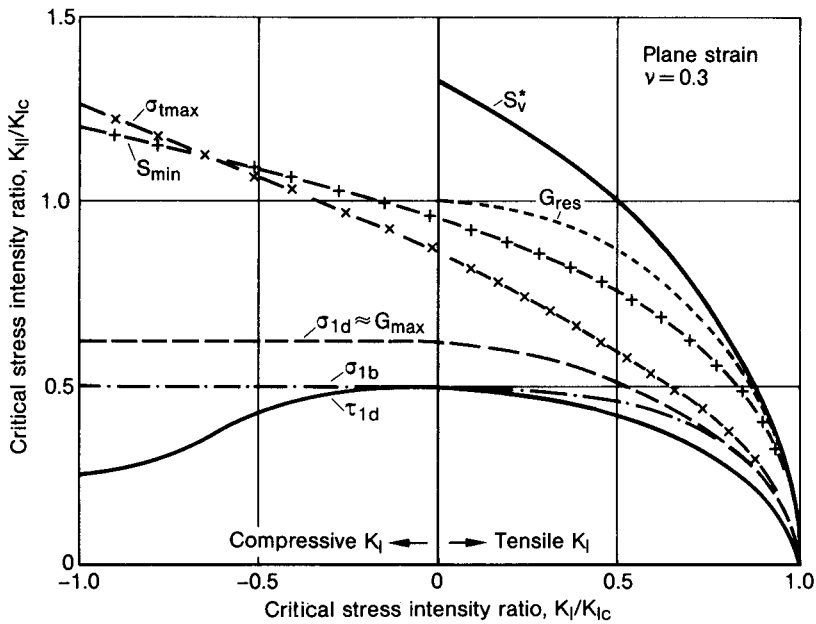


Fig. 10.20. Critical stress intensity curves characterising crack initiation under mixed mode I and II loading conditions; various fracture criteria; designation of the curves specified in the text; after Radaj and Zhang.[914]

different formal and physical contents of the criteria. The process zone criteria differ from one another to a minor extent only. They are conservative compared with the conventional criteria. The curve for the well-known and usually preferred Erdogan–Sih criterion of maximum tangential stress, for example, runs considerably higher, especially in the compressive K_I range. The reason for this is the fact that the criterion takes only the tangential stresses around the crack tip into account and incorrectly neglects the radial stresses which are especially high under mode II conditions.

The consideration above refers to constant-amplitude loading of an ideal crack or slit tip with neglectible mean stress effects. In reality further important influencing parameters have to be considered such as mean stress intensity, residual stress intensity, non-singular stresses, non-proportional loading, crack or slit tip microstructural conditions and crack closure effects among others. Whether or not a definite criterion is applicable in the special case under consideration should finally be decided on the basis of mixed mode fatigue testing results. Such data are not readily available from the literature. The simplified procedure of defect assessment based on fracture mechanics which considers the projected areas of the crack in the principal stress directions under mode I loading instead of solving the mixed mode loading problem may result in an unconservative design (Radaj and Heib[903]).

The preferred criterion in the case of spot-welded or seam-welded lap joints is the maximum tangential stress criterion proposed by Erdogan and Sih.[866] It states that the crack or slit tip subjected to mixed mode I and II loading will propagate in the direction in which the tangential tensile stress at a small distance from the crack tip reaches its maximum. This results in the crack propagation angle φ_0 as a function of the stress intensity factor ratio K_{II}/K_I, Fig. 10.21. The equivalent stress intensity factor K_{eq} then follows from a critical value of this stress:

$$K_{eq} = \left(K_I \cos^2 \frac{\varphi_0}{2} - \frac{3}{2} K_{II} \sin \varphi_0 \right) \cos \frac{\varphi_0}{2} \tag{10.86}$$

$$\tan \frac{\varphi_0}{2} = \frac{1}{4} \left(\frac{K_I}{K_{II}} \right) \pm \frac{1}{4} \sqrt{\left(\frac{K_I}{K_{II}} \right)^2 + 8} \tag{10.87}$$

where the positive root corresponds to a negative K_{II}, the negative root to a positive K_{II} (with positive K_I). Pure mode I loading results in $\varphi_0 = 0°$ and $K_{eq} = K_I$, whereas pure mode II loading is associated with $\varphi_0 = 70.5°$ and $K_{eq} = 1.15 K_{II}$.

The strain energy density criterion proposed by Sih[609,923] which comprises not only K_I and K_{II} but also K_{III}, is open to more varied physical interpretations and adaptable to more complex test data. The criterion states that the crack propagates in the direction of the minimum total strain energy

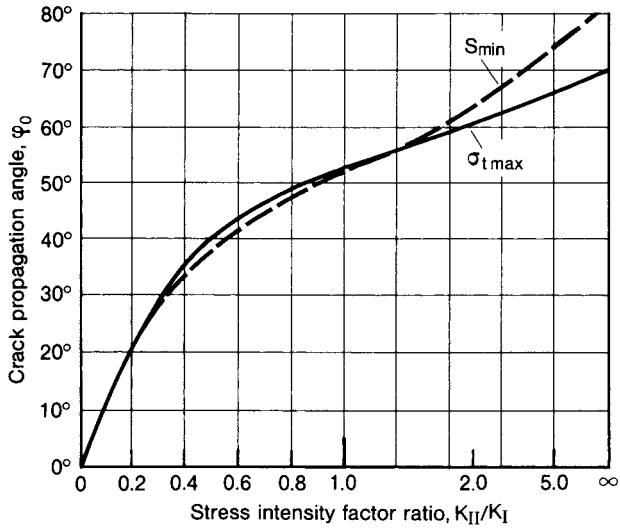


Fig. 10.21. Crack propagation angle relative to ligament direction dependent on stress intensity factor ratio; maximum tangential stress criterion ($\sigma_{t\,max}$) compared with strain energy density criterion (S_{min}); after Yuuki *et al.*[934–937]

density (approximately equivalent to the maximum dilatational strain energy density[905]), and that a critical value of the energy densities mentioned must be reached. The equivalent stress intensity factor K_{eq} follows from:

$$K_{eq} = \sqrt{A_{11}K_I^2 + A_{12}K_IK_{II} + A_{22}K_{II}^2 + A_{33}K_{III}^2} \tag{10.88}$$

The coefficients A_{11} to A_{33} are mainly dependent on the crack propagation angle (besides Poisson's ratio) which in turn is defined by the stress intensity factor ratios K_{II}/K_I and K_{III}/K_I, respectively. The coefficients are often introduced as constant in order to simplify the procedure. The following simplified version of eq. (10.88) follows from the application of the strain energy density criterion to the single-mode loading states at a central crack in the infinite plate. With Poisson's ratio $\nu = 0.28$, the ratios of critical stress intensity factors according to Sih[609] (*ibid*. eqs. (18) and (19)) are $K_{IIc}/K_{Ic} = 0.985$ and $K_{IIIc}/K_{Ic} = 0.663$ thus yielding the following formula:

$$K_{eq} = \sqrt{K_I^2 + 1.03K_{II}^2 + 2.27K_{III}^3} \tag{10.89}$$

A similar equation is obtained proceeding from the maximum strain energy release rate criterion proposed by Irwin[874] which likewise assumes coplanar crack propagation and ignores the influence of the crack propagation angle (K_{eq}, K_I and K_{II} in plane strain, $\nu = 0.28$, see eqs. (10.97) and (10.98)):

$$K_{eq} = \sqrt{K_I^2 + K_{II}^2 + 1.39K_{III}^2} \tag{10.90}$$

This relationship has been applied to spot-welded lap joints by Linder *et al.*[878]

The process zone criteria proposed by Radaj and Zhang[914,919] also yield the general form of eq. (10.88) partly extended by the addition of linear K_I and K_{II} terms. The corresponding curves in Fig. 10.20 (σ_{1d} and τ_{1d} for 'ductile' behaviour, σ_{1b} for brittle behaviour) result from evaluating the crack propagation angle in the different mixed-mode (inclusive of single-mode) loading states. The following more conservative form, eq. (10.91), is proposed on the basis of the lower plotted curves in Fig. 10.20 substituting the older, less conservative form, eq. (10.92), chosen in the comparative evaluations by Radaj *et al.*:[816,900,901,917]

$$K_{eq} = \sqrt{K_I^2 + 3K_{II}^2 + K_{III}^2} \tag{10.91}$$

$$K_{eq} = \sqrt{K_I^2 + K_{II}^2 + K_{III}^2} \tag{10.92}$$

Kurath[785] found that K_{II}^2 combined with factor 3 was valid in the case of spot welds in low-carbon steels and combined with factor 2 in the case of spot welds in high strength steels. The factor 4.3 is derived by Lee and Kim[877] from fatigue test results gained from single-spot specimens with various ratios K_I/K_{II}.

A diagram derived by Pook[890] from the branching condition under mixed-mode loading of the crack tip in non-welded steels is presented in Fig. 10.22. The reference quantity ΔK_0^* is the cyclic threshold stress intensity factor for branching crack propagation which is about twice the threshold value for coplanar crack propagation in modus I. This matter is further discussed by Radaj,[6] *ibid*. pp. 308–310.

Swellam *et al.*[929] defined a 'stress index' K_i comprising the equivalent stress intensity factor $K_{eq\,\infty}$ (derived for the half-space configuration, eqs. (10.46–10.49)), the load ratio R and a geometry correction factor G empirically derived from fatigue test results with varying specimen geometry and loading conditions (remarks at the end of Section 10.2.6):

$$K_i = (1-R)^{0.85}\,\frac{K_{eq\,\infty}}{G} \tag{10.93}$$

$$K_{eq\,\infty} = \sqrt{K_{I\,\infty}^2 + \beta K_{II\,\infty}^2} \tag{10.94}$$

$$G = \sqrt{\frac{8t^2 w}{d^3}\left(\frac{36t^2}{d^2} + 1\right)} \tag{10.95}$$

with plate thickness t, plate width w, spot diameter d and material factor β. Contrary to Kurath's original assignment,[785] Swellam *et al.*[988] use $\beta = 2$ with low-carbon steels and $\beta = 3$ with high strength steels.

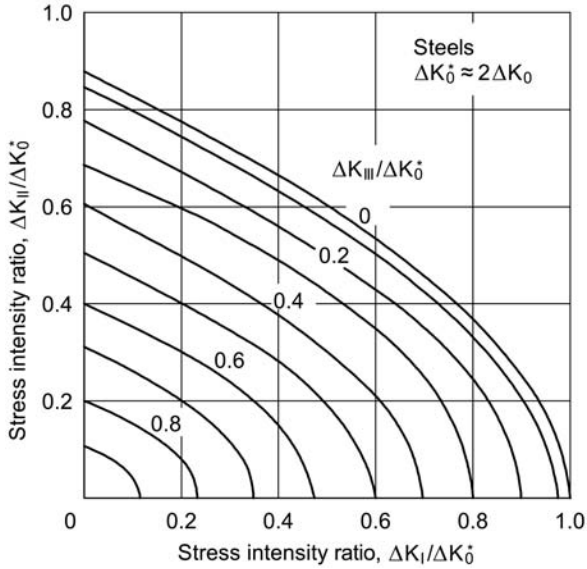


Fig. 10.22. Lower limit curves of the cyclic stress intensity factors for branching crack propagation under mixed mode loading conditions (modi I, II and III superimposed), based on test results for various steels; after Pook.[890]

The application of eqs. (10.93–10.95) with $R = 0$ to the tensile-shear specimen yields:

$$K_i = \frac{F\sqrt{36t^2 + \beta d^2}}{2t\sqrt{\pi w(36t^2 + d^2)}} \tag{10.96}$$

with tensile-shear force F. There is no explanation where the first term under the square-root in the numerator, corresponding to $K_{I\infty}$ (i.e. the cross-tension term) comes from. The evaluation of eq. (10.96) for the tensile-shear specimen considered in Table 10.1 (with w = 40 mm) results in K_I = 34.4 N/mm$^{3/2}$ and K_{II} = 28.6 N/mm$^{3/2}$, i.e. values which are too small by a factor of 2–5. Swellam *et al.*[929] were obviously aware of this deficiency and have therefore termed K_i a 'stress index'.

The equivalent stress intensity factors according to eqs. (10.86–10.92) applied to cyclic loading do not include the further influencing variables mentioned at the end of Section 10.3.1. A fundamental shortcoming is the absence of non-singular stress terms whose influence on fatigue crack initiation and propagation cannot be neglected (see the notch stresses in Fig. 11.6 and the basic theoretical derivations by Haefele and Lee[870]).

10.3.3 *J*-integral and nugget rotation variants

The stress intensity factors may be substituted by other more or less equivalent parameters. The parameter most often used is the *J*-integral derived by Rice[921] (substituting for K_I and K_{II}) or the *J**-integral derived by Radaj and Zhang[908] (substituting for K_{III}). These integrals describe the specific energy release rate in coplanar crack propagation (an irrelevant assumption for most loading modes and material responses). But an essential point is that the *J*- and *J**-integrals comprise elastic-plastic crack tip behaviour. The following equations give the relationship between the *J*-integral (with plane strain condition) or *J**-integral and the stress intensity factors:

$$J = \frac{1 - \nu^2}{E}\left(K_I^2 + K_{II}^2\right) \tag{10.97}$$

$$J^* = \frac{1}{2G} K_{III}^2 = \frac{1 + \nu}{E} K_{III}^2 \tag{10.98}$$

where E is the elastic modulus, G is the shear modulus and ν is the Poisson's ratio.

The equivalent stress intensity factor K_{eq} according to Irwin,[874] eq. (10.90), can be determined by the following relationship:

$$K_{eq}^2\left(1-\nu^2\right) = (J + J^*)E \tag{10.99}$$

The ΔJ-related approximation for the number of cycles N up to failure has the following form:

$$N = A_J(\Delta J)^{-k} \tag{10.100}$$

with the inverse slope k and the coefficient A_J assumed to be material parameters.

A variant of the stress intensity approach has been used in fatigue tests with the tensile shear specimen (Davidson *et al.*[852,862–864]). It is based on the relationship between the stress intensity factor K_I and the crack or slit opening displacement δ at the crack tip with local plastic zone:

$$\delta = \frac{(1 - \nu^2)K_I^2}{\kappa\sigma_Y E} \tag{10.101}$$

where σ_Y is the yield limit and κ is a constraint factor ($\kappa = 0.8$–2.2 according to measurements).

The slit opening displacement δ is proportional to the slit opening angle θ which describes the rotation of the overlapping plates against each other. Both quantities are difficult to determine. Therefore, the nugget rotation θ_n is measured and set equal to θ (actually $\theta_n > \theta$), Fig. 10.23. It follows

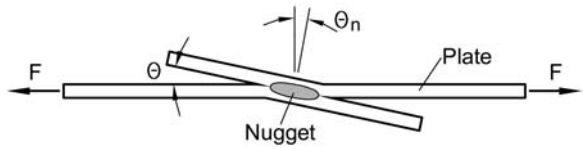


Fig. 10.23. Slit opening angle θ and nugget rotation θ_n (easier to measure) in tensile-shear specimen; simplified cross-sectional view with straight plate edges in alignment and $\theta_n = \theta$ (actually $\theta_n > \theta$); after Barsom *et al.*[852]

$K_I \propto \sqrt{\theta}$, so that $\sqrt{\theta}$ can be used instead of K_I (or θ instead of J) to characterise the fatigue strength or life of spot-welded or seam-welded lap joints presupposing pure mode I loading (which is not really the case in the tensile-shear specimen). The tendency towards joint face shear fractures instead of plate fractures increases with the ratio τ/θ (with joint face shear stress τ).

The approach was further elaborated by the authors mentioned above. Originally, they considered the structure-related rotational stiffness of the spot weld, $\Delta F/\theta_n$, as the essential parameter controlling the fatigue strength and life. But they found empirically that the parameter $\Delta F\sqrt{\theta_n}/t$ collapses the plate fracture data from tensile-shear fatigue tests into one narrow scatter band. The number of cycles N up to failure is approximated by:

$$N = A_\theta \left(\frac{\Delta F \sqrt{\theta_n}}{t} \right)^{-3} \tag{10.102}$$

with the tensile-shear force F, the plate thickness t and the coefficient A_θ assumed to be a material parameter. This holds for constant-amplitude loading. Barsom *et al.*[852] and El-Sayed *et al.*[865] extended the approach to variable-amplitude loading histories on the basis of rainflow cycle counting and Miner's rule applied to the mean stress corrected amplitudes.

10.4 Comparative evaluation of spot-welded and similar specimens

10.4.1 General survey

The stress intensity approach has been applied extensively by Radaj *et al.*[4,816,900–902,917] to assess the fatigue strength of common spot-welded specimens mainly relative to one another and to detect the decisive geometric parameters which have an influence on the strength. Fatigue strength here means mainly crack initiation strength based on the threshold stress

intensity factor or, derived therefrom, the endurance limit of the specimen. In the following, this relative assessment is reviewed for the common single- and multi-spot specimens. Additionally, the spot-welded double-hat section specimen, the H-shaped specimen and the double-cup specimen are dealt with in more detail. Only the multi-spot 'double-hat specimen' used by Di Fant-Jaeckels *et al.*[759] is not included. The stress and deformation patterns are discussed in respect of specimen performance.

Attempts have also been made to use the stress intensity approach to predict the fatigue life of laser beam welded tensile-shear and peel-tension specimens (Section 10.4.7).

The comparative investigation of spot-welded specimens by Radaj *et al.*[816] performed on the basis of finite element analysis in connection with eqs. (10.2–10.4) comprises the specimen types and loading modes summarised in Fig. 10.24. The plate thickness is $t = 1$ mm (or $t = 0.8$ mm in one case), the

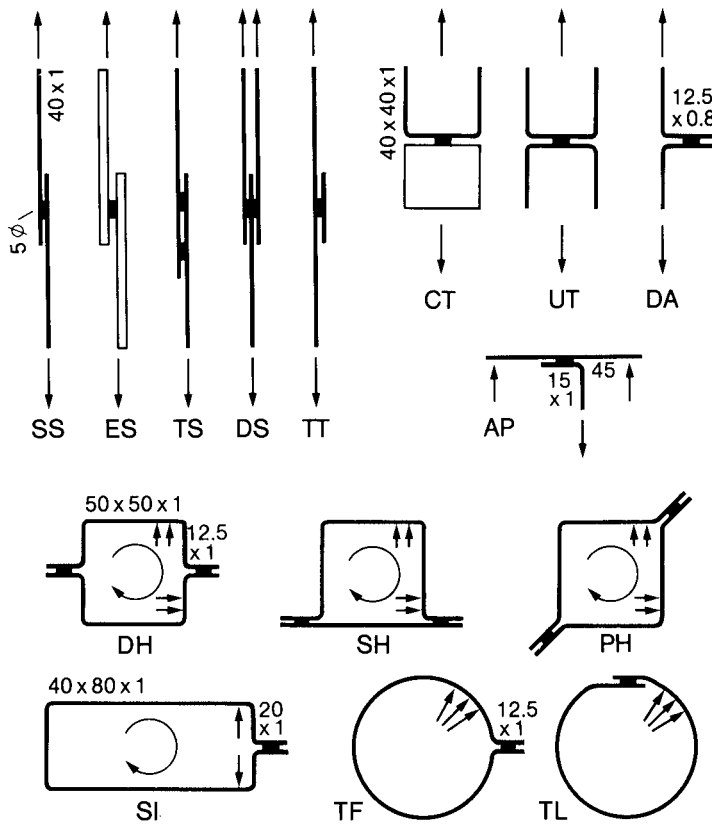


Fig. 10.24. Spot-welded specimen types and loading modes, scope of the investigation performed on the basis of finite element analysis; after Radaj *et al.*[816]

weld spot diameter $d = 5\,\text{mm}$. Thereafter, these two parameters are varied. The grammalogues stated in parentheses are used in the diagrams representing the results.

The group of simple plate specimens mainly used for production control purposes comprises the following types:

- single-face tensile-shear specimen (SS) conforming to standards and variant with edge stiffening (ES);
- two-spot tensile-shear specimen (TS);
- double-face tensile shear specimen (DS);
- through-tension specimen (TT);
- cross-tension specimen in cross shape (CT) conforming to standards and in U-shape (UT);
- peel-tension specimen as double-angle specimen (DA) and as angle-to-plate variant (AP).

The group of design-related structural component specimens comprises the following types:

- double-hat section specimen (DH) subjected to torsional moment and internal pressure;
- single-hat section specimen (SH) subjected to torsional moment and internal pressure;
- peaked-hat section specimen (PH) subjected to torsional moment and internal pressure;
- single-sided hat section specimen (SI) subjected to torsional moment and straddling force;
- tubular flange joint specimen or tubular peel-tension specimen (TF) and tubular lap joint specimen or tubular tensile-shear specimen (TL) subjected to internal pressure.

The review below additionally comprises the analysis results of special investigations related to the double-hat section specimen,[917] the H-shaped specimen,[900,902] and the double-cup specimen.[901,902]

It is only possible to summarise the results of the calculations here. This summary is restricted to the stress intensity factors, the resulting equivalent value of which, K_{eq} according to equation (10.92), is used to assess the relative load-carrying capacity of the particular weld spot. The equivalent structural stress and notch stress not shown here (but contained in the original publication[816]) behave in a similar manner as the equivalent stress intensity factor does. The larger deviations occurring in some cases are caused particularly by the fact that the transverse shear stress does not have any effect on the equivalent structural stress in the plate surface but does affect the stress intensity. On the other hand, the eigenforces manifest themselves primarily in the equivalent structural stress and scarcely in the stress

intensity. With regard to K_{eq}, the failure criteria in mixed-mode slit tip loading on which it is based is open to discussion and a modification on the basis of future experimental results will probably be necessary.

The stress intensity factors reviewed in the following are calculated on the basis of the structural stresses in the centre of the plate elements adjacent to the weld spot edge. The evaluated stress intensity factors may thus be slightly too low (see Table 10.1) whereas their mutual relations remain more or less unchanged. A non-linear extrapolation onto the weld spot edge is recommended for future analysis projects.

Nominal stress intensity factors were used in some cases as reference quantities, but more general comparisons were not made. Such nominal quantities approximating the real ones can be calculated to the extent that the weld spot forces (joint face forces and eigenforces) are available. But the corresponding formulae for stress intensity factors in common spot-welded specimens and components proposed by Zhang[938–942] may be misleading. The effect of the eigenforces is not taken into account by these formulae, the effect of plate width is not captured and some further shortcomings can be traced (Radaj[898,899]). These formulae are appropriate only under special conditions.

10.4.2 Spot-welded tensile-shear specimens

The distribution of the stress intensity factors, K_I, K_{II}, K_{III} and K_{eq} at the weld spot edge of tensile-shear specimens subjected to the same tensile-shear force, $F = 1$ kN, is presented in Fig. 10.25 (including the tubular tensile-shear specimen). The stress intensity factor K_{II} is dominant. Its maximum value $K_{II\,max}$ appears at the front face, mostly in combination with $K_{I\,max}$ (markedly smaller in general), while $K_{III\,max}$ can be found at the side face. Stiffening the edges of the specimen by folding reduces $K_{I\,max}$ to approximately two thirds.

The two-spot specimen displays a reduced K_{II} as a consequence of the distribution of the load onto two spots. In the case of the double-face tensile-shear specimen, K_{II} is reduced to one third (with the same weld spot resultant force as in the single-face specimen) as a consequence of completely suppressed weld spot rotation, whereas K_{III} at the side-face remains unchanged and now limits the load-carrying capacity. The stress intensity factor K_{II} in the through-tension specimen is, as is to be expected, very small. The stress intensity factors in the tubular tensile-shear specimen are partly enlarged, because of the particularly short lap length and the slightly asymmetrical stressing of the joint. A striking element in the comparative evaluation of weld spot load-carrying capacity according to K_{eq}, Table 10.6, is the high load-carrying capacity of the double-face tensile-shear specimen (factor $2 \times 2.09 = 4.18$). Considering the greatly differing load-carrying

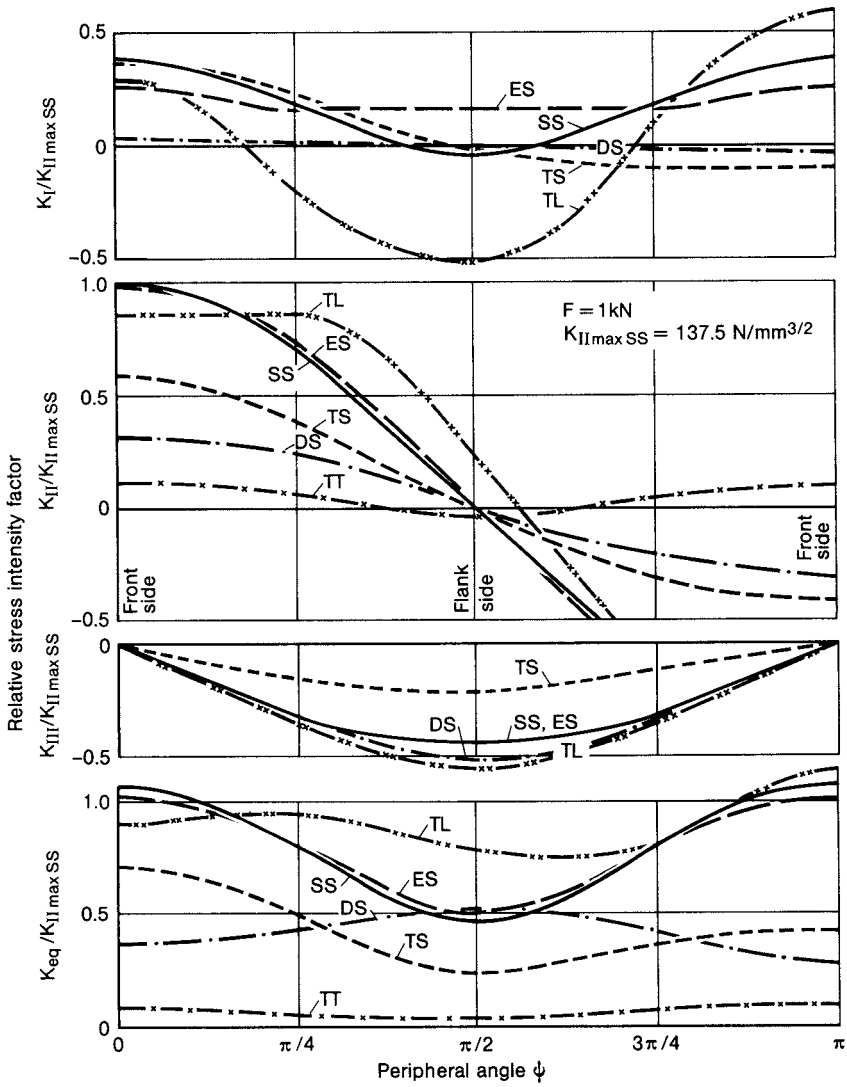


Fig. 10.25. Relative stress intensity factors at weld spot edge of various tensile-shear specimens subjected to the same tensile-shear force; grammalogues according to Fig. 10.24; after Radaj *et al.*[816]

Table 10.6. Load-carrying capacity of weld spot ($t = 1$ mm, $d = 5$ mm); relation according to K_{eq} of various tensile-shear specimens; tubular lap-joint specimen included; after Radaj *et al.*[816]

Specimen type	SS	ES	TS	DS	TT	TL
Load-carrying capacity	1.0	1.06	1.54	2.09	10.4	0.93

capacity of the weld spot in the different specimens it follows that there cannot be a uniform endurable value of the tensile-shear force transferable from the specimen to the structural component.

On the basis of $\Delta K_I = 54.0\,N/mm^{3/2}$, $\Delta K_{II} = 137.5\,N/mm^{3/2}$ and thus $\Delta K_{eq} = 147.7\,N/mm^{3/2}$ for the standardised tensile-shear specimen with $t = 1\,mm$, $d = 5\,mm$, $\Delta F = 1\,kN$ and on the basis of $\Delta K_{en} = 180\,N/mm^{3/2}$ at $N = 5 \times 10^6$ cycles, the endurable cyclic tensile shear force $\Delta F_{en} = 1.22\,kN$ is calculated. When using the slightly higher ΔK-values from Table 10.1, the result is $\Delta F_{en} = 1.13\,kN$. These values of ΔF_{en} correspond well to lower limit values actually measured.

Within the framework of the analysis[816] summarised above, an answer is also given to the question of what effect a variation of plate thickness, t, or of weld spot diameter, d, has on the structural stress parameters at the weld spot edge. This is done, proceeding from $t = 1\,mm$ and $d = 5\,mm$, by halving and doubling t, on the one hand (with constant d), and by halving and doubling d (with constant t), on the other hand. In addition, consideration is given to the parameter coupling $d = 5\sqrt{t}$ often used in practice.

A first approximation of the parameter dependence is obtained on the basis of the nominal structural stress formula. Hence, for the tensile-shear specimen, it follows from eq. (9.3):

$$\sigma_{sn} \propto 1/t \text{ with } d = \text{const},$$
$$\sigma_{sn} \propto 1/d \text{ with t} = \text{const},$$
$$\sigma_{sn} \propto 1/t^{3/2} \text{ with } d = 5\sqrt{t}.$$

The inverse values of the proportional relations presented above directly state the load-carrying capacity dependence of the weld spot if σ_{sn} is regarded as being decisive for local strength. If, on the other hand, the stress intensity factor is considered to be the decisive strength parameter, the proportional relations stated have to be multiplied by $\sqrt{t}$ and their inverse values divided by $\sqrt{t}$. This weakens the influence of plate thickness on load-carrying capacity.

The parameter dependencies presented above are approximations, which, however, are confirmed with a deviation of less than nine per cent in terms of load-carrying capacity by the more precise numerical results from finite element analysis, Table 10.7. On the other hand, the details of stress distribution may be different. For example, the ratio K_I/K_{II} depends on plate thickness and weld spot diameter (Radaj *et al.*[816]).

Cooper and Smith[859,927] have calculated the stress intensity factor, K_{eq}, for the tensile-shear specimen (K_{eq} in accordance with the tangential stress criterion, eqs (10.86) and (10.87)), using finite solid element models and thus achieved more accurate results compared with those of Pook[886,887] and Yuuki *et al.*,[934–937] Fig. 10.26 and Table 10.1. The parameter range of d and t

Table 10.7. Load-carrying capacity of weld spot in tensile-shear specimen on the basis of nominal structural stress formulae (subscript sn) and more precisely on the basis of finite element analysis (subscript fe); relation for variable plate thickness t and weld spot diameter d, according to strength criterion K_{eq} (subscript 1/5 means $t = 1$ mm, $d = 5$ mm); after Radaj *et al.*[816]

Load ratio	Plate thickness, t [mm]			Spot diameter, d [mm]		
	0.5	1.0	2.0	2.5	5.0	10.0
$(F/F_{1/5})_{sn}$	0.71	1.0	1.41	0.5	1.0	2.0
$(F/F_{1/5})_{fe}$	0.74	1.0	1.29	0.55	1.0	1.87

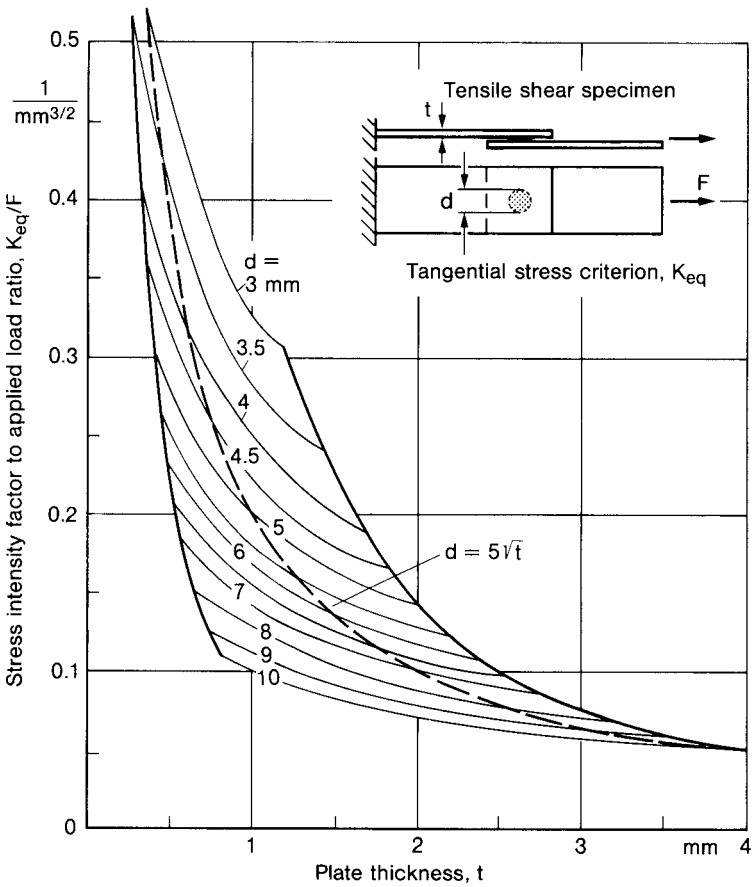


Fig. 10.26. Stress intensity factor to applied load ratio at weld spot of tensile-shear specimen dependent on plate thickness for different weld spot diameters; after Cooper and Smith.[859,927]

covers the cases of particular importance in practice. The broken curve identifies dimensioning commonly used based on $d = 5\sqrt{t}$. The curve patterns in this diagram approximately agree with the proportional relations substantiated above, $K_{eq} \propto \sigma_s\sqrt{t}$ and $\sigma_s \propto F/td$, from which follows the relation $K_{eq}/F \propto 1/d\sqrt{t}$.

The finite element results of Yuuki *et al.*[934–937] for the stress intensity factors, K_I and K_{II}, of the single-face tensile-shear, double-face tensile-shear and cross-tension specimens are compiled by Murakami[543] (*ibid.* pp. 1202–1205) including variation of plate thickness and plate width. A new efficient boundary element procedure for determining the stress intensity factors at spot welds has been published by Yuuki and Ohira.[935]

The contributions of Fujimoto *et al.,*[867] Hahn and Wender[871] and Kuang and Liu[784] are worth mentioning as historically early finite element solutions (based on solid elements) providing the structural stress distribution in the tensile-shear specimen. These stress analyses included the notch effect of the weld spot edge to some extent but stress intensity factors were not evaluated.

10.4.3 Spot-welded cross-tension and peel-tension specimens

The stress intensity factors, K_I and K_{II}, for the cross-tension and peel-tension specimens subjected to the same cross-tension or peel-tension force, $T = 0.1\,\text{kN}$, are presented in Fig. 10.27. The stress intensity factor K_I is dominant. It is constant over the circumference of the weld spot in the case of the standardised cross-tension specimen, and it is slightly increased or decreased in the vertices in the case of the U-shaped cross-tension specimen. In the case of the peel-tension specimens, a sharp increase occurs, as is to be expected, in the vertex facing the peel force. The weld spot load-carrying capacities according to K_{eq} are compared in Table 10.8. The peel-tension specimens resist to less than half the load of the pure cross-tension specimens. The load-carrying capacity in cross-tension is significantly less than the capacity in tensile-shear. The relations stated vary greatly with plate thickness and support spacing. The difference between load-carrying capacities in cross-tension and peel-tension can be considerably reduced but not totally eliminated by including the resulting bending moment of the weld spot joint face in the characteristic parameter of the load-carrying capacity. It is, therefore, not possible to state a uniform endurable value of the cross-tension or peel-tension force transferable from the specimen to the structural component.

On the basis of $\Delta K_I = 91.0\,\text{N/mm}^{3/2}$, $\Delta K_{II} = 20.0\,\text{N/mm}^{3/2}$ and thus $\Delta K_{eq} = 93.2\,\text{N/mm}^{3/2}$ for the standardised cross-tension specimen with $\Delta T = 0.1\,\text{kN}$

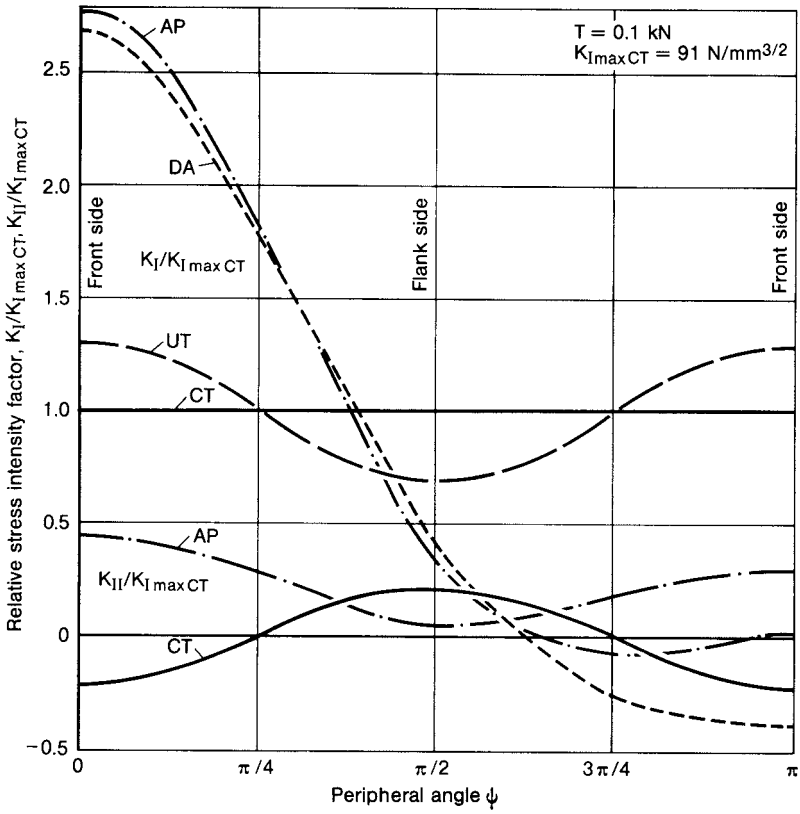


Fig. 10.27. Relative stress intensity factors at weld spot edge of various cross-tension specimens subjected to the same cross-tension force; grammalogues according to Fig. 10.24; after Radaj *et al.*[816]

Table 10.8. Load-carrying capacity of weld spot ($t = 1$ or 0.8 mm, $d = 5$ mm); relation according to K_{eq} of various cross-tension specimens; relation to the tensile-shear specimen; after Radaj *et al.*[816]

Specimen type	CT	UT	DA	AP	CT/SS
Load-carrying capacity	1.0	0.79	0.38	0.37	0.16

and on the basis of $\Delta K_{en} = 180\,\text{N/mm}^{3/2}$ at $N = 5 \times 10^6$ cycles, the endurable cyclic cross-tension force $\Delta T_{en} = 0.193\,\text{kN}$ is calculated. This value of ΔT_{en} corresponds well with the lower limit values actually measured.

A first approximation for the dependency of the structural stress parameters at the weld spot edge on a variation of plate thickness, t, or of weld spot diameter, d, is obtained on the basis of the nominal structural stress

formulae. Hence, for the cross-tension specimen, it follows from eqs. (9.4–9.8) with D/d constant:

$$\sigma_{sn} \propto 1/t^2 \text{ with } d = \text{const},$$
$$\sigma_{sn} \text{ independent of } d \text{ with } t = \text{const},$$
$$\sigma_{sn} \propto 1/t^2 \text{ with } d = 5\sqrt{t}.$$

The inverse values of the proportional relations presented above directly state the load-carrying capacity dependency of the weld spot if σ_{sn} is regarded as being decisive for local strength. If, on the other hand, the stress intensity factor is considered to be the decisive strength parameter, the proportional relations stated have to be multiplied by $\sqrt{t}$ and their inverse values divided by $\sqrt{t}$. This weakens the influence of the plate thickness compared with the above expressions. The conclusion, which can be additionally drawn from the different exponents of thickness is that the cross-tension strength increases relative to the tensile-shear strength as plate thickness increases.

The parameter dependencies presented are approximations, which, however, are confirmed with a deviation of less than six per cent in terms of load-carrying capacity by the more precise numerical results from finite element analysis, Table 10.9. The finite element results of Yuuki *et al.*[934–937] for the stress intensity factors, K_I and K_{II}, of the cross-tension specimen (see Murakami,[543] *ibid*. p. 1204) agree well with these data of Radaj *et al.*[816]

The peel-tension specimen has also been analysed in comparison to the tensile-shear specimen by Wang and Ewing.[932,933] These authors evaluated the *J*-integral at the weld spot edge on the basis of finite element modelling and virtual crack extension (into the joint face). They used *J*–*N* curves determined from fatigue tests to predict the welded joint life to failure, but the deviations in the strength values in the two specimen types were disturbingly large (see Table 10.5).

Table 10.9. Load-carrying capacity of weld spot in cross-tension specimen on the basis of nominal structural stress formulae (subscript sn) and more precisely on the basis of finite element analysis (subscript fe), relation for variable plate thickness t and weld spot diameter d, according to strength criterion K_{eq} (the subscript 1/5 means $t = 1$ mm, $d = 5$ mm); after Radaj *et al.*[816]

Load ratio	Plate thickness, t [mm]			Spot diameter, d [mm]		
	0.5	1.0	2.0	2.5	5.0	10.0
$(T/T_{1/5})_{sn}$	0.35	1.0	2.83	0.75	1.0	1.50
$(T/T_{1/5})_{fe}$	0.35	1.0	2.79	0.80	1.0	1.52

10.4.4 Spot-welded hat section specimens

The stress intensity factors, K_I, K_{II} and K_{III}, for the hat section specimens subjected to a torsional moment producing the same shear force at the weld spots (according to Bredt's formula) are shown in Fig. 10.28. The stress intensity factor K_{II} dominates. Its maximum value $K_{II\,max}$ appears approximately 30° in the direction of the web near to the front face vertex of the weld spot, while $K_{III\,max}$ can be found at the side face on the inside of the flange. A stress intensity K_I appears only with the single-hat section specimen. The ratios of the weld spot load-carrying capacities (weld spot shear force according to Bredt's formula) according to K_{eq} indicate only slight differences, both relative to each other and also compared with the tensile-shear specimen, Table 10.10.

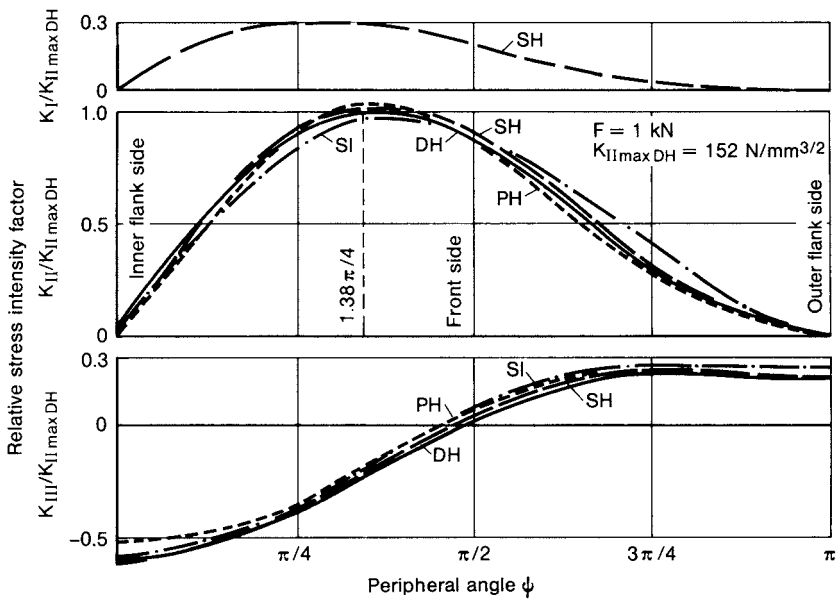


Fig. 10.28. Relative stress intensity factors at weld spot edge of various hat section specimens subjected to torsional loading with the same shear force at the weld spot; grammalogues according to Fig. 10.24; after Radaj *et al.*[816]

Table 10.10. Load-carrying capacity of weld spot ($t = 1$ mm, $d = 5$ mm); relation according to K_{eq} of various hat section specimens subjected to torsional moment; relation to the tensile-shear specimen; after Radaj *et al.*[816]

Specimen type	DH	SH	PH	SI	DH/SS
Load-carrying capacity	1.0	0.95	0.99	1.04	0.95

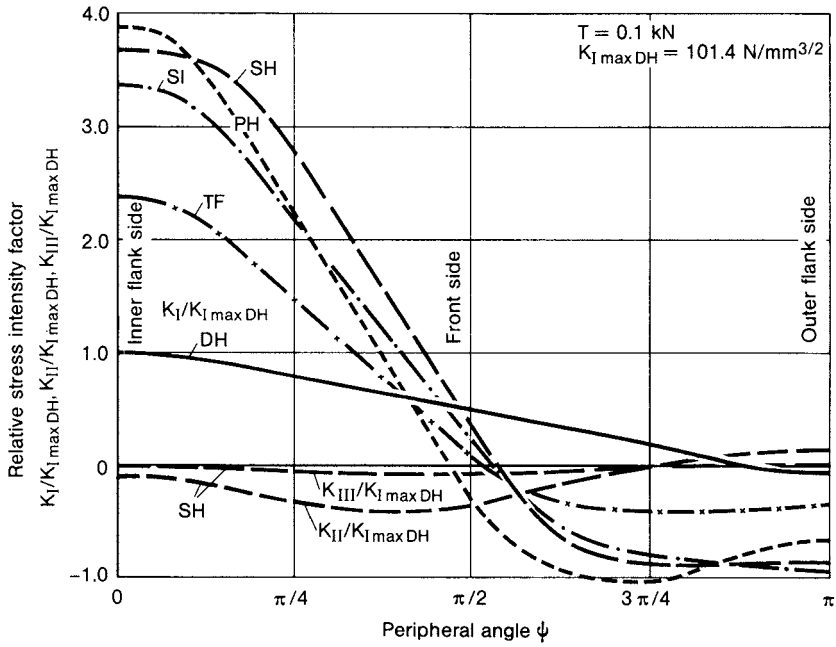


Fig. 10.29. Relative stress intensity factors at weld spot edge of various hat section specimens subjected to internal pressure with the same cross-tension force at the weld spot; flank and front sides related to flange direction; grammalogues according to Fig. 10.24; after Radaj *et al.*[816]

Table 10.11. Load-carrying capacity of weld spot (t = 1 mm, d = 5 mm); relation according to K_{eq} of various hat section specimens subjected to internal pressure; tubular flange-joint specimen included; relation to the cross-tension specimen; after Radaj *et al.*[816]

Specimen type	DH	SH	PH	SI	TF	DH/CT
Load-carrying capacity	1.0	0.27	0.26	0.30	0.42	0.92

For the hat section specimens and the tubular flange-joint specimen subjected to internal pressure, the stress intensity factors, K_I, K_{II} and K_{III}, with the same cross-tension force at the weld spot, show the single-sided curve rise known from the peel-tension specimens, Fig. 10.29. The ratios of the weld spot load-carrying capacities according to K_{eq} reveal particularly favourable conditions for the double-hat section specimen, Table 10.11, as a result of the favourable location of the flanges relative to the bending moment distribution along the section contour. The load-carrying capacity

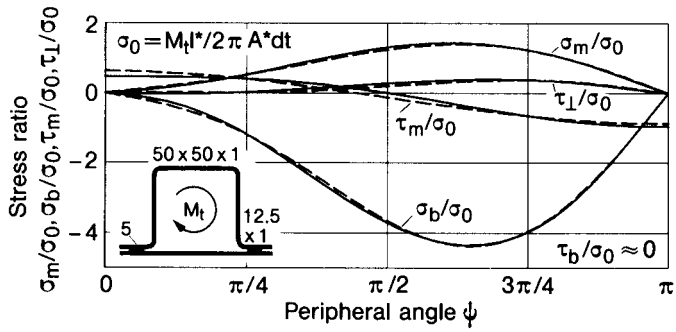


Fig. 10.30. Structural stress ratios at weld spot edge (flange side) of single-hat section specimen subjected to torsional loading; precise distribution according to finite element analysis (solid lines), and approximation based on vertex point stresses (dashed lines), reference system chosen in the principal loading direction ($\psi = 45°$), with nominal structural membrane stress σ_0 according to the Bredt formula, with σ_m and τ_m membrane structural stresses, σ_b bending structural stress and $\tau_\perp$ transverse shear structural stress; after Radaj.[808]

Table 10.12. Resultant weld spot forces gained from vertex point stresses in the hat section flange (finite element results, non-linear extrapolation to weld spot edge) and referred to 'nominal' forces explained in the text; after Radaj[808]

Specimen type	F_y/F_0	M_{bx}/M_0	M_{tz}/M_0^*
Double-hat section	1.001	0.0	–0.178
Single-hat section	1.007	0.229	–0.154

of the double-hat section specimen is for this reason (and as a result of a smaller peel force moment) close to that of the cross-tension specimen.

The hat section specimens subjected to torsional moments have been analysed by Radaj and Zhang[808,813] in respect of the weld spot resultant forces used to determine the structural stresses around the weld spot on the basis of the vertex point stresses and the nominal structural stress distributions, Fig. 10.30 (i.e. without extensive finite element analysis, despite this method being used as a substitute for measurement in the case considered). The reference stress σ_0 is the nominal structural stress from the weld spot shear force according to the Bredt formula (i.e. membrane stress portion according to eq. (9.1)). The relative weld spot resultant forces determined from the vertex point stresses are shown in Table 10.12: relative shear force F_y/F_0 with $F_0 = M_t l^*/2A^*$ (first Bredt formula according to eq. (10.58)

with M_t torsional moment, l^* weld spot pitch and A^* contour-enclosed area), relative bending-moment M_{bx}/M_0 with $M_0 = F_0 t/2$, relative torsional moment M_{tz}/M_0^* with $M_0^* = F_0 d/2$. No other weld spot forces occur with the exception of a very small relative eigenforce F_z/F_0.

Both types of specimen predominantly produce a shear force in flange direction, F_y. This force acts slightly eccentrically at the weld spot thus producing the torsional moment, M_{tz}. The bending moment, M_{bx}, in the joint face is typical for the single-hat section with its reduced symmetry.

Nominal structural stresses can be calculated on the basis of the weld spot forces. This is the result for $F_0 = 1000\,\text{N}$, $d = 5\,\text{mm}$ and $t = 1\,\text{mm}$: $\sigma_{sn} = 254.7\,\text{N/mm}^2$ from F_y and eq. (9.3), $\sigma_{sn} = 43.7\,\text{N/mm}^2$ from M_{bx} and eq. (9.2), and finally $\tau_{sn} = 11.3$ or $9.8\,\text{N/mm}^2$ from M_{tz} and eq. (9.9), i.e. in the ratio of 100 : 17 : 4. These nominal structural stresses do not give sufficient information in respect of load-carrying capacity. Superposition of stress curves is necessary yielding the maximum stress between the vertex points. A suitable failure criterion must be selected characterising the actual failure condition. The evaluation of the load-carrying capacity according to K_{eq} (see Table 10.10) is straightforward. It can be seen from Fig. 10.28 that the stress intensity factors are nearly the same in the two specimens with the exception of K_I produced in the single-hat section specimen by the weld spot bending moment.

In addition to the above, the hat section specimens subjected to internal pressure loading and also the single-spot specimens subjected to different loading conditions have been analysed in respect of the weld spot resultant forces proceeding from the vertex point stresses gained from finite element analysis as a substitute for stress measurements (Radaj[808]).

The double-hat section specimen subjected to torsional loading, Fig. 10.31, has been further analysed by Radaj and Zhang[917] in respect of the local stress parameters at the weld spot edge (structural stress, notch stress and stress intensity factors) under variation of the characteristic geometric parameters (compare Niisawa *et al.*[880] and Tomioka *et al.*[930]). The specimen dimensions are not standardised so that different choices are possible for fatigue testing, and the question arises how to compare the test results gained with different specimens. On the other hand, it may be the aim of testing to determine the influence on strength of definite geometric parameters such as plate thickness, weld spot diameter or weld spot pitch. Finally, geometric imperfections occur due to the fabrication process which may distort the test results or at least cause their scatter. In all three cases mentioned above, relative strength predictions are possible on the basis of the calculated stress intensity factors using the K_{eq} criterion according to eq. (10.92).

The following geometric variants with starting values indexed by 0 are numerically analysed, Fig. 10.32: specimen height $h = 25, 50, 100\,\text{mm}$ with

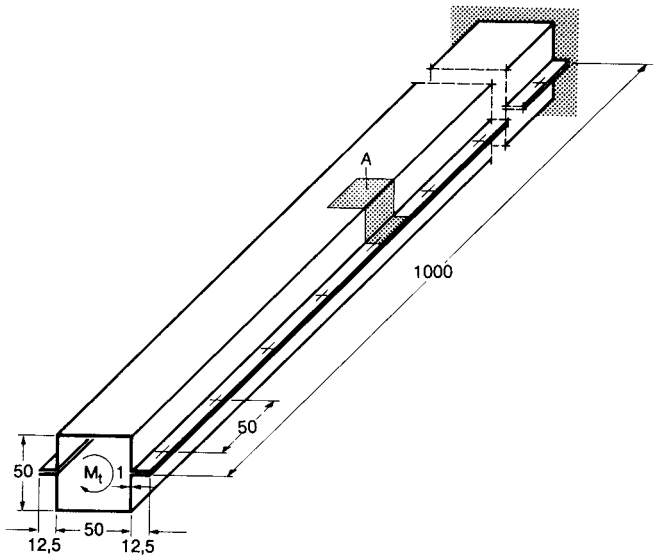


Fig. 10.31. Spot-welded double-hat section specimen subjected to torsional loading, with section A modelled by finite elements; after Radaj and Zhang.[917]

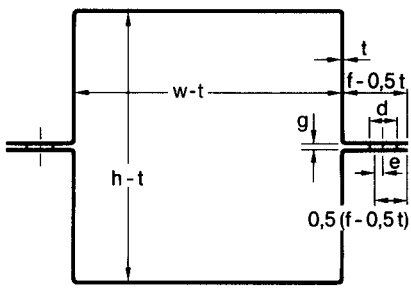


Fig. 10.32. Dimensional parameters of cross-section of spot-welded double-hat section specimen; after Radaj and Zhang.[917]

$h_0 = 50\,\text{mm}$, specimen width $w = 25, 50, 100\,\text{mm}$ with $w_0 = 50\,\text{mm}$, weld spot pitch $l^* = 25, 50, 100\,\text{mm}$ with $l_0^* = 50\,\text{mm}$, flange width $f = f_0 = 12.5\,\text{mm}$ (not varied), plate thickness $t = 0.5, 1, 2\,\text{mm}$ with $t_0 = 1\,\text{mm}$, weld spot diameter $d = 3.33, 5, 7.5\,\text{mm}$ with $d_0 = 5\,\text{mm}$, weld spot eccentricity $e = -3.5, 0, +3.5$ mm with $e_0 = 0\,\text{mm}$ and gap width $g = 0, 0.1, 0.2\,\text{mm}$ with $g_0 = 0\,\text{mm}$.

The finite element model for determining the structural stresses can be reduced to a section model, the boundary conditions of which in terms of prescribed displacements are derived from the symmetry and anti-symmetry conditions of the deformed structure, Fig. 10.33. A deformation plot with the isolines of deflection normal to the respective plate plane is shown in Fig. 10.34.

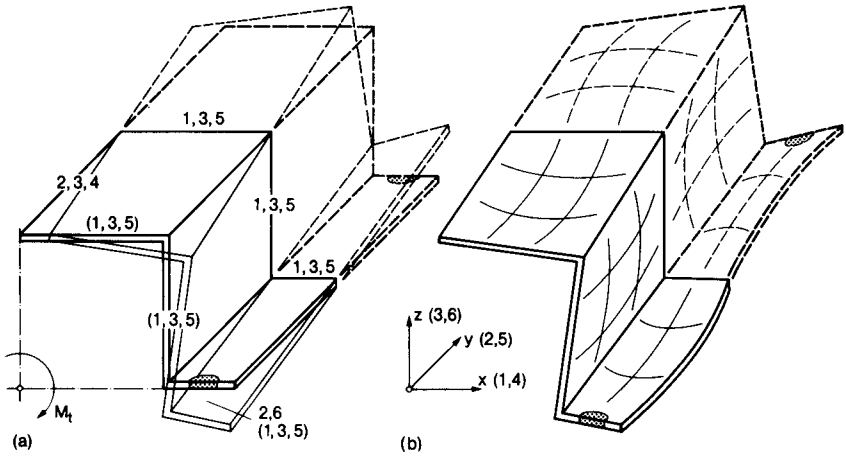


Fig. 10.33. Section model of the double-hat section specimen subjected to torsional loading, with dashed line continuation for easier visualisation, torsional displacements (a) and related bending deformations (b), suppressed and prescribed boundary degrees of freedom designated by numbers (2, 6 referring to the weld spot cross-section only); after Radaj.[805]

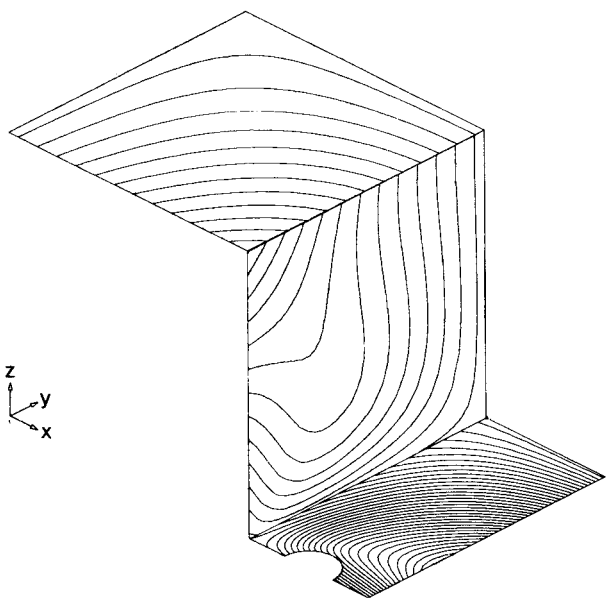


Fig. 10.34. Deformation of the double-hat section specimen subjected to torsional loading (section model); isolines of deflections normal to the respective plate plane; after Radaj and Zheng (unpublished).

The stress intensity factors derived from eqs. (10.2–10.4) and (10.92) on the basis of the finite element stress results are plotted over the peripheral angle of the weld spot for different plate thicknesses and weld spot diameters, Fig. 10.35 and Fig. 10.36. The stress intensity factors are referred to their nominal values, $K_n = K_{IIn}$, according to eqs. (9.3) and (10.61) proceeding from the first Bredt formula, eq. (10.58). The maximum stress intensity factor ratios occurring between the vertex points are only slightly dependent on plate thickness or weld spot diameter. They are about 20%

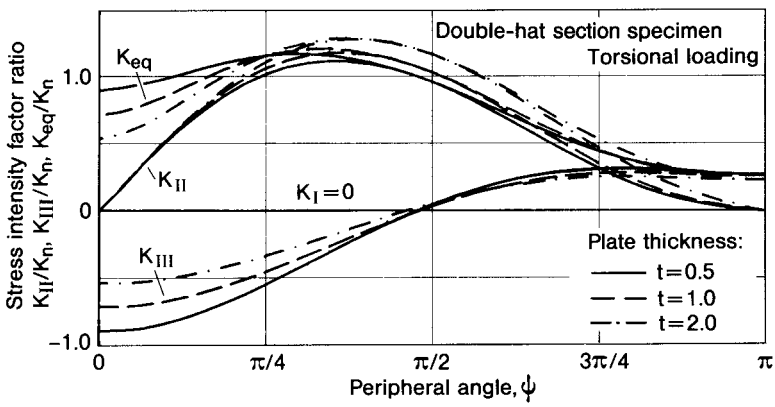


Fig. 10.35. Stress intensity factor ratios at weld spot edge for different plate thicknesses; double-hat section specimen subjected to torsional loading; after Radaj and Zhang.[917]

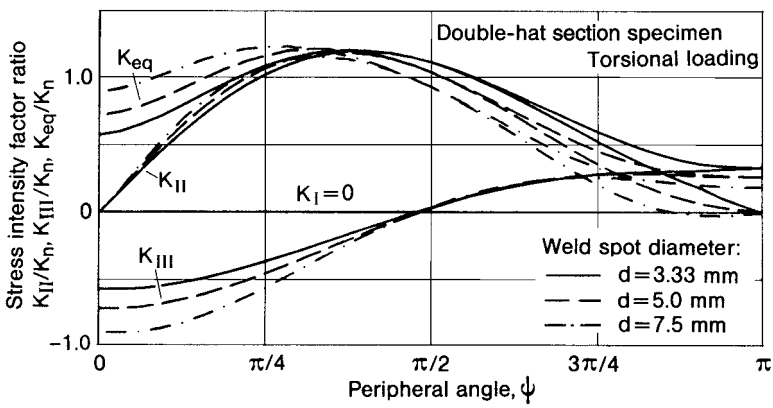


Fig. 10.36. Stress intensity factor ratios at weld spot edge for different weld spot diameters; double-hat section specimen subjected to torsional loading; after Radaj and Zhang.[917]

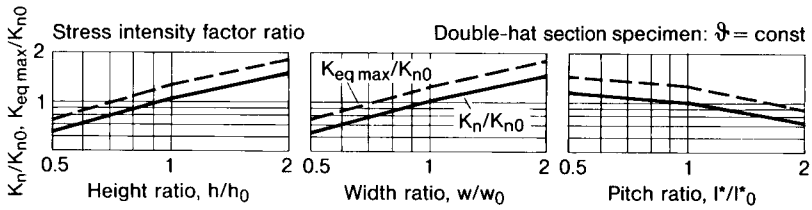


Fig. 10.37. Maximum stress intensity factor ratio at weld spot edge of double-hat section specimen subjected to the same angle of twist ϑ dependent on height, width and pitch ratio, nominal values (solid lines) and finite element results (dashed lines); after Radaj and Zhang.[917]

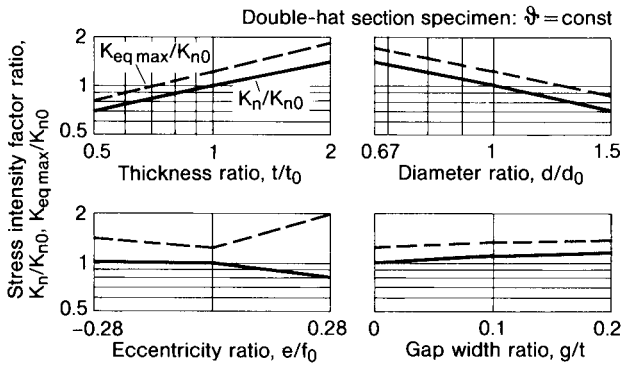


Fig. 10.38. Maximum stress intensity factor ratio at weld spot edge of double-hat section specimen subjected to the same angle of twist ϑ dependent on thickness, diameter, eccentricity and gap width ratio, nominal values (solid lines) and finite element results (dashed lines); after Radaj and Zhang.[917]

above the nominal values. A much stronger effect is detected for weld spots with large (positive) eccentricity e (see Fig. 10.32). The weld spot touching the outer edge of the flange increases the stress intensity factor up to 2.5 times its original value.

The maximum stress intensity factor ratios dependent on specimen height, specimen width, weld spot pitch, plate thickness, weld spot diameter, weld spot eccentricity and gap width are summarised in Figs. 10.37 and 10.38. The reference value is the nominal stress intensity factor for the starting values of the geometric parameters being considered (marked by index 0). The stress intensity factor ratios from finite element analysis, K_{eq}/K_{n0},

are set against the nominal ratios, K_n/K_{n0}, under the assumption of the same angle of twist ϑ. The latter condition is not made clear in the original publication which additionally contains printing errors at the ordinates of some of the diagrams (see emendation[917]). The angle of twist can be calculated basically according to the second Bredt formula, eq. (10.59), but this angle is enlarged by the effect of discontinuous spot joining. Note that $K_{eq}/K_{n0} = (K_{eq}/K_n)(K_n/K_{n0})$ when comparing the different figures.

As can be seen from Fig. 10.37 and Fig. 10.38, the actual maximum values correlate rather well with the nominal values enlarged by the factor 1.2 (with the exception of the extreme-eccentricity case). This factor results from the maximum stress intensity factor occurring between the vertex points where the nominal values are calculated. The relationship $K_n = 1.2 \times 0.5\sigma_{tbn}\sqrt{t} = 0.6\sigma_{tbn}\sqrt{t}$ is an excellent approximation to the exact maximum values. This includes the validity of the first Bredt formula according to eq. (10.58). Also the influence of non-zero gap width g is correctly simulated by eq. (10.62) yielding a factor of 1.075 for $g/t = 0.1$ and of 1.15 for $g/t = 0.2$ (the nominal stress intensity factors K_n modified by these factors are used in Fig. 10.38 in the case of $g \neq 0$).

The conclusion is that the nominal stress intensity factor derived on the basis of the Bredt formula and enlarged by the first-mentioned factor 1.2 is well suited to the prediction of relative strength values of the spot-welded double-hat section specimen subjected to torsional loading.

10.4.5 Spot-welded H-shaped specimens

A specimen with H-shaped cross-section consisting of a channel-section bar joined by spot-welding to overlapping plate strips or angle-section bars, Fig. 10.39, has been proposed by Singh[926] for standardisation and has actually been used in several research projects. The first design version produces tensile-shear loading of the weld spots and the second design version produces cross-tension (or peel-tension) loading of the weld spots.

The specimen has been analysed in respect of the local stress parameters by Radaj and Giering[900,902] on request of the IIW Commission III 'Resistance Welding' which had to decide on the standardisation proposal (it was rejected). Practical problems with the specimen are excessive welding distortion and uneven screw bearing, resulting in major scattering of the test results. The results of the investigation in respect of the stress intensity factor dependencies are summarised below.

The stress intensity factors are determined on the basis of the structural stresses derived from a finite element model and transferred into eqs. (10.2–10.4) and (10.92). The nominal structural stress in the tensile-shear loading case is introduced according to eq. (9.3). The nominal structural stress in the cross-tension loading case is derived according to eq. (9.7) and

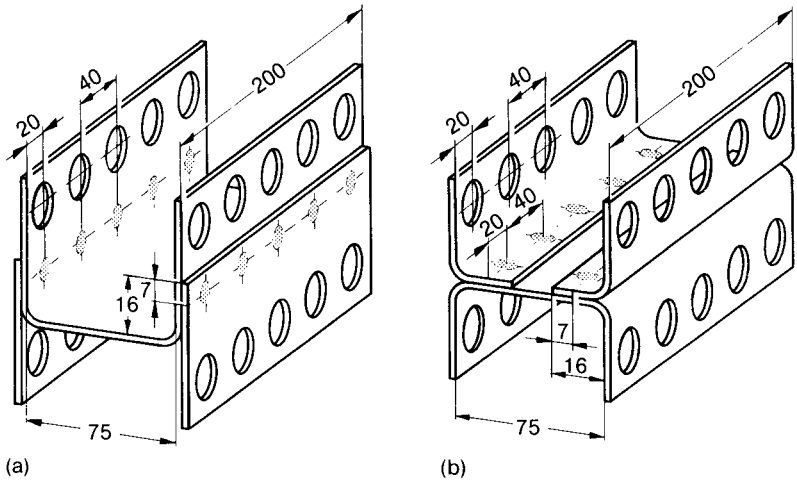


Fig. 10.39. H-shaped multi-spot specimens used for tensile-shear loading (a) and cross-tension (or peel-tension) loading (b) of the weld spots; after Radaj and Giering.[900]

multiplied by the factor two in order to take the single-sided peel-tension loading into account. The cross-tension force is designated by T. The support diameter D is set equal to $2d^*$ with a distance d^* between weld spot centre and clamping plane (substituting the stress increase by the bending moment). The resulting equation is: $\sigma_{sn} = 1.38(T/t^2)\ln(2d^*/d)$. The stress intensity factors are referred to a nominal value $K_n = 0.5\sigma_{sn}\sqrt{t}$ in both loading cases (eq. (10.60) would be more appropriate in the case of cross-tension loading).

The local stress parameters of the H-shaped specimen subjected to tensile-shear or cross-tension loading are similar in value and distribution to those of the relevant single-spot tensile-shear and cross-tension (or peel-tension) specimens, provided the corresponding geometric data are identical. The peripheral distribution of the stress intensity factors in tensile-shear loading is shown in Fig. 10.40. There is almost no deviation from the results for the standardised tensile-shear specimen. The distribution in cross-tension loading of the H-shaped specimen, Fig. 10.41, is set in comparison with that of the standardised cross-tension specimen. The curves are not similar because of the difference between single-sided and double-sided peel-tension loading. Also the distance between weld spot edge and clamping plane is not the same. The double-angle peel-tension specimen is better suited for comparisons, but it is deficient in not being standardised.

The maximum stress intensity factor ratios (occurring at the vertex points of the weld spot) dependent on plate thickness with weld spot diameter

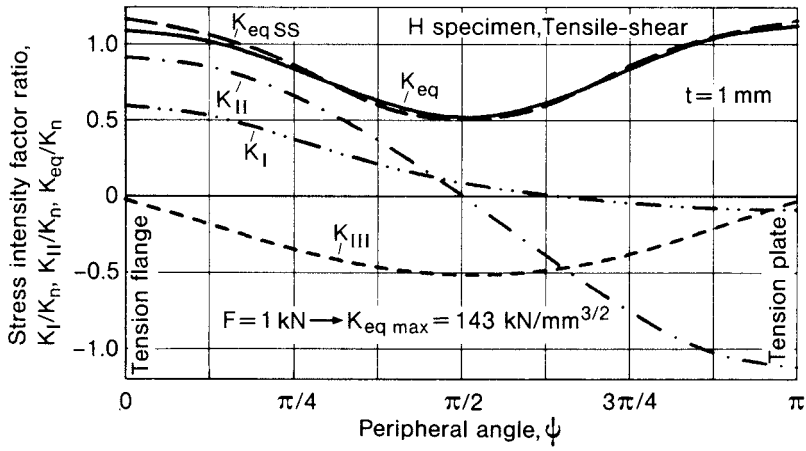


Fig. 10.40. Stress intensity factor ratio at weld spot edge of H-shaped specimen (plate thickness $t = 1$ mm) subjected to tensile-shear loading in comparison with standardised tensile-shear specimen (SS); with the nominal stress intensity factor as reference quantity; after Radaj and Giering.[900]

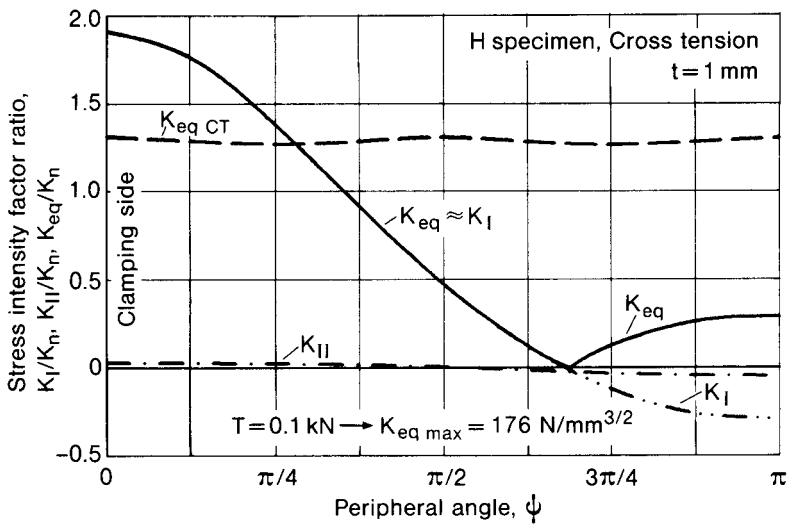


Fig. 10.41. Stress intensity factor ratio at weld spot edge of H-shaped specimen (plate thickness $t = 1$ mm) subjected to cross-tension (or peel-tension) loading in comparison to standardised cross-tension specimen (CT); with the nominal stress intensity factor as reference quantity; after Radaj and Giering.[900]

$d = 5\sqrt{t}$ (i.e. the weld spot diameter is varied together with the plate thickness) are plotted in logarithmic scales, Fig. 10.42. The spot-welded parts of the specimen have equal plate thickness. Some cases of unequal plate thickness are dealt with in the original publication.[900] The reference value is the nominal stress intensity factor K_{n0} for $t = 1$ mm. It can be seen from the plots that the nominal values K_n/K_{n0} (solid lines) reflect the finite element results K_{eq}/K_{n0} (dashed lines) sufficiently well, at least in trend. The deviations in value in the case of cross-tension loading can be explained from the effect of transverse shear stresses on the stress intensity factor which is not included in the nominal parameters. The stress intensity factor ratios with K_n instead of K_{n0} as the reference value are shown in Table 10.13.

An unintended shear force occurs at the weld spots of the cross-tension loaded H-shaped specimen resulting in mixed-mode loading of the slit tip at the weld spot edge. This shear force is almost as large as the cross-tension

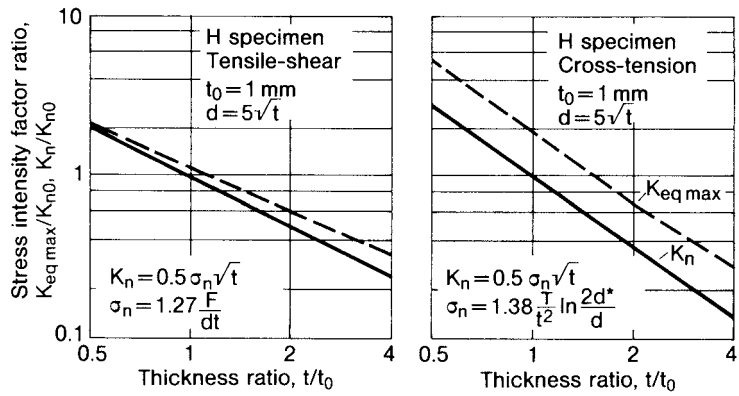


Fig. 10.42. Maximum stress intensity factor ratio at weld spot edge of H-shaped specimen subjected to tensile-shear and cross-tension loading dependent on thickness ratio; nominal values (solid lines) and finite element results (dashed lines); after Radaj and Giering.[900]

Table 10.13. Maximum stress intensity factors from finite element analysis referred to nominal values dependent on plate thickness; spot-welded H-shaped specimen subjected to tensile-shear and cross-tension loading; after Radaj and Giering[900]

Loading case	$K_{eq\,max}/K_n$ for thickness t			
	0.5 mm	1.0 mm	2.0 mm	4.0 mm
Tensile-shear	1.07	1.13	1.22	1.36
Cross-tension	2.02	1.91	1.90	2.03

force, but the effect on the structural stresses is small because of the dominant plate bending moments at the weld spot edge. The intended pure mode I loading of the weld spot edge could be achieved by using an H-shaped specimen consisting of two channel-section bars joined back to back.

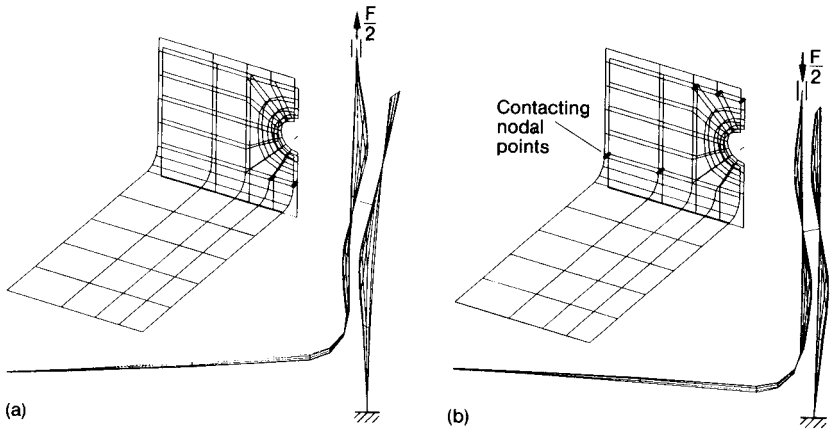


Fig. 10.43. Deformation plots of the H-shaped specimen subjected to tensile-shear (a) and compressive-shear (b) loading (weld spot shear force $F = 1.5\,\text{kN}$); large displacements and gap closure taken into account; contacting mesh nodes marked by thick-line connecting rods; after Radaj and Giering.[900]

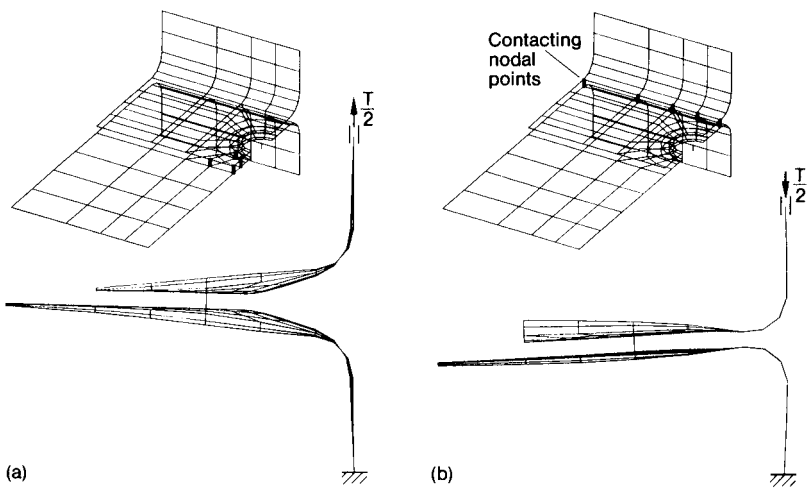


Fig. 10.44. Deformation plots of the H-shaped specimen subjected to cross-tension (a) and cross-compression (b) loading (weld spot normal force $T = 0.2\,\text{kN}$); large displacements and gap closure taken into account; contacting mesh nodes marked by thick-line connecting rods; after Radaj and Giering.[900]

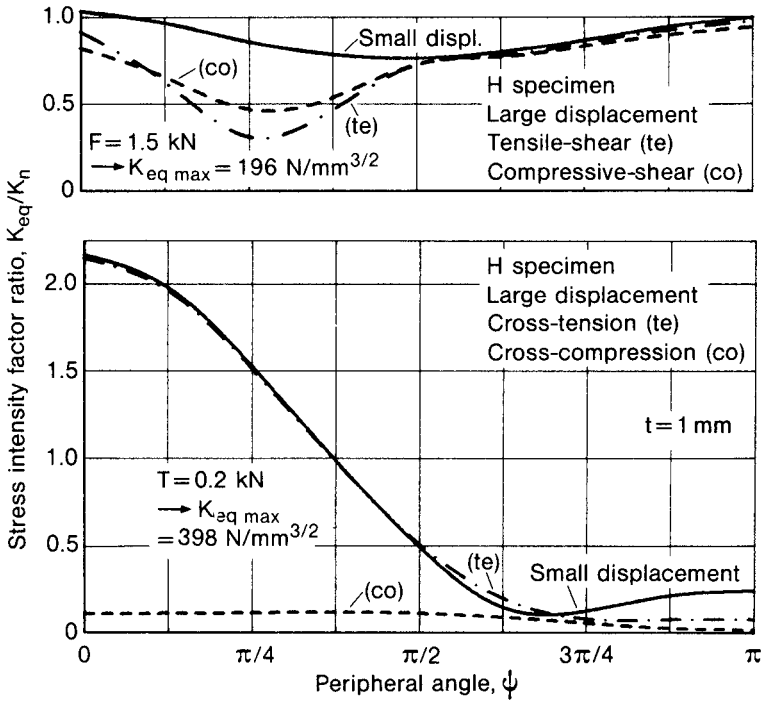


Fig. 10.45. Stress intensity factor ratio at weld spot edge of H-shaped specimen subjected to tensile or compressive shear loading (upper diagram) and cross-tension or cross-compression loading (lower diagram); small displacement analysis compared with large displacement analysis (inclusive of gap closure); after Radaj and Giering.[900]

The effect of large displacements including slit or gap closure (see Sections 9.3.2 and 9.3.3 for the fundamentals) was also investigated for the plate thickness $t = 1$ mm. Large displacements without gap closure only have a minor effect (definitely less than 1%). Gap closure may result in major changes in the local stress parameters. This is shown in the following using a coarse finite element mesh with sufficient relative but not absolute accuracy of local stress results.

The contacting mesh nodes of the specimen model in tensile and compressive shear loading, Fig. 10.43, and in cross-tension and cross-compression loading, Fig. 10.44, are marked by thick-line connecting rods. The structural stresses and stress intensity factors at the weld spot edge are changed to some extent (i.e. mostly reduced), mainly on that side of the weld spot where the contact takes place. The reduction in stress intensity factor is shown in Fig. 10.45.

10.4.6 Spot-welded double-cup specimens

The double-cup single-spot specimen (DC specimen), Fig. 10.46, has been proposed by Gieske and Hahn[868] as a design-related specimen with the capability of fatigue-testing different spot-like joints in comparison (e.g. spot-welded, clinched and riveted). The specimen is subjected to a combined shear and cross-tension loading including the pure (i.e. non-combined) loading states. The pure loading states, shear and cross-tension loading, have been analysed by Radaj and Giering[901,902] in respect of the local stress parameters. The results are reviewed in the following.

The stress intensity factors are determined on the basis of the structural stresses derived from a finite element model and transferred into eqs. (10.2–10.4) and (10.92). The nominal structural stresses in shear and cross-tension loading of the specimen are introduced according to eqs. (9.3) and (9.7). The diameter of the bottom plate of the cup is used as diameter D in the latter equation, whereas clamping occurs a little further outside and upside after a curved rim (with substantially increased stiffness because of the curvature). The nominal stress intensity factor is determined from $K_n = 0.5\sigma_{sn}\sqrt{t}$ in both loading cases (eq. (10.60) would be more appropriate in the case of cross-tension loading).

The stress intensity factor ratios at the weld spot edge for tensile-shear and cross-tension loading, respectively, are plotted versus the peripheral angle in Figs. 10.47 and 10.48. The relevant curves for the conventional standardised tensile-shear and cross-tension specimens (designated by the indices SS and CT) are included for comparison. The peripheral distribution of the stress intensity factors is similar but more homogeneous and of higher symmetry in the case of the double-cup specimen. A remarkable feature of the double-cup specimen is the mixed K_{II}–K_{III} loading mode without a K_I component in the shear loading case as well as the pure K_I loading mode in the cross-tension case.

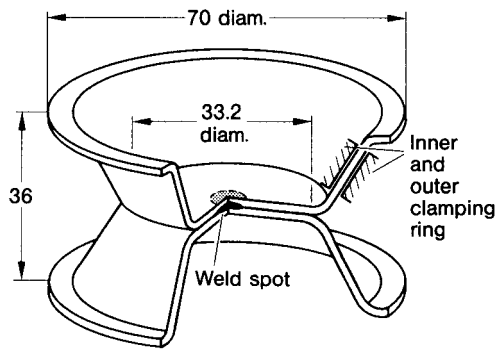


Fig. 10.46. Double-cup singe-spot specimen (DC specimen) with typical dimensions; according to Gieske and Hahn.[868]

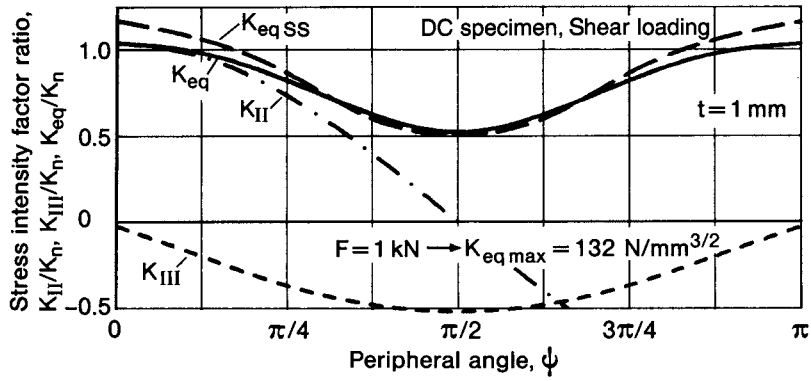


Fig. 10.47. Stress intensity factor ratio at weld spot edge of double-cup specimen (plate thickness $t = 1$ mm) subjected to shear loading in comparison with standardised tensile-shear specimen (SS), with the nominal stress intensity factor as reference quantity; after Radaj and Giering.[901]

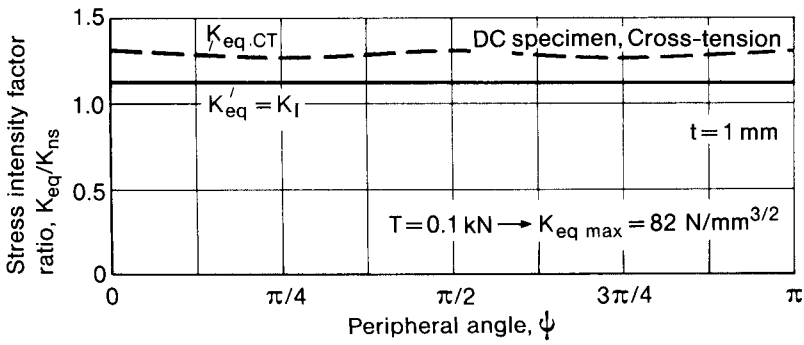


Fig. 10.48. Stress intensity factor ratio at weld spot edge of double-cup specimen (plate thickness $t = 1$ mm) subjected to cross-tension loading in comparison with standardised cross-tension specimen (CT), with the nominal stress intensity factor as reference quantity; after Radaj and Giering.[901]

The maximum stress intensity factor at the front face of the weld spot is plotted versus the plate thickness ratio and weld spot diameter ratio in logarithmic scales, Fig. 10.49 for shear and cross-tension loading of the double-cup specimen. The varied thickness is t = 0.5, 1.0 and 2.0 mm with diameters $d = 5\sqrt{t}$ and $D = 33.2$ mm. The varied outside diameters are D = 16.6, 33.2 and 66.4 mm with thickness $t = 1$ mm and diameter $d = 5\sqrt{t}$. The reference value K_{n0} of the stress intensity factor is related to $t/t_0 = 1$ and $D/D_0 = 1$ with $t_0 = 1$ mm and $D_0 = 32.2$ mm. It can be seen from the plots that the nominal stress intensity factors reflect the finite element results

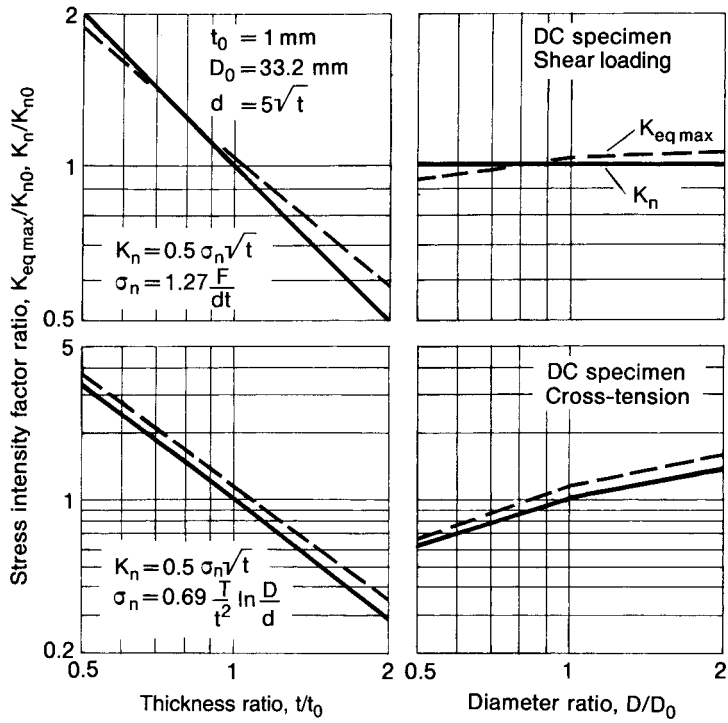


Fig. 10.49. Maximum stress intensity factor ratio at weld spot edge of double-cup specimen subjected to shear loading (upper plots) and cross-tension loading (lower plots) dependent on plate thickness and plate diameter ratio, nominal values (solid lines) and finite element results (dashed lines); after Radaj and Giering.[901]

Table 10.14. Maximum stress intensity factors from finite element analysis referred to nominal values dependent on plate thickness and base plate diameter; spot-welded double-cup specimen subjected to shear and cross-tension loading; after Radaj and Giering[901]

Loading case	$K_{eq\,max}/K_n$ for thickness t			$K_{eq\,max}/K_n$ for diameter D		
	0.5 mm	1.0 mm	2.0 mm	16.6 mm	33.2 mm	66.4 mm
Shear loading	0.96	1.04	1.19	0.94	1.04	1.07
Cross-tension	1.11	1.12	1.19	1.04	1.12	1.17

very well. The correspondence in the cross-tension case is further enhanced if the more accurate nominal stress intensity factor $K_n = (1/\sqrt{3})\sigma_{sn}\sqrt{t}$ is introduced instead of $K_n = 0.5\sigma_{sn}\sqrt{t}$ which yields a factor of 1.15 on the nominal values. On the other hand, complete correspondence cannot be expected

because the effect of transverse shear stress on the stress intensity factor is neglected in its nominal value. Also, non-linear extrapolation of the finite element structural stresses to the weld spot edge would result in slightly higher stress intensity factors with minor changes in the stress intensity factor ratios considered.

A survey of the stress intensity factor ratios with K_n instead of K_{n0} as the reference value is given in Table 10.14.

10.4.7 Laser beam welded tensile-shear and peel-tension specimens

The tensile-shear specimen with a transverse laser beam weld (substituting the weld spot) has been analysed in respect of its fatigue life by Wang[931] on the basis of the stress intensity approach, using the variant with the *J*-integral. The dimensions of the weld and the specimen in sheet steel of type SAE1005 were the following: sheet thickness 0.76 and 1.78 mm, weld length 25.4 mm, weld width in joint face 1.2 and 1.4 mm, specimen width 38.1 mm, overlap length 38.1 mm, gap width 0, 0.12 and 2.0 mm.

The cyclic *J*-integral at the interface edge of the weld seam was calculated by the finite element method applied to virtual crack extension (into the ligament as usual, well suited to joint face shear fractures but not to the observed plate fractures in or near the heat-affected zone). A uniform *J*–*N* curve was evaluated with mean values according to Table 10.15. The number of crack initiation cycles was considered to be negligibly small.

The endurable ΔJ-values of laser-beam-welded joints and of spot-welded joints are not expected to be identical because of the different geometric and metallurgical conditions at the interface edge of the weld seam and at the weld spot edge, respectively. Contrary to this expectation, the values for laser beam welds are rather close to those of spot welds in tensile-shear loading (compare values by Wang–Ewing in Table 10.5).

Table 10.15. Endurable cyclic *J*-integral ΔJ_{en} ($P_f = 50\%$, $R = 0$) and corresponding endurable cyclic stress intensity factor $\Delta K_{J\,en}$ at the interface edge of laser beam welds in tensile-shear loaded lap joints made of low-alloy sheet steel; after Wang[931]

	Number of cycles *N*		
	10^5	10^6	10^7
J-integral ΔJ_{en} [kJ/m^2]	0.637	0.237	0.088[a]
Stress intensity factor $\Delta K_{J\,en}$ [N/mm$^{3/2}$][b]	383	234	143

[a] Linear extrapolation in logarithmic scales.
[b] $\Delta K_J^2 = E\Delta J/(1 - \nu^2)$, 1 kJ/m^2 = 1 N/mm.

Another tentative investigation by Radaj *et al.*[907] into the fatigue strength of laser beam welds in mild steel of type St14 (sheet thickness $t = 0.9$ and 2.0 mm, seam width $w_s = 1.0$ mm) subjected to tensile-shear and peel-tension loading, Fig. 10.50, resulted in the following mean values of endurable equivalent stress intensity factors (maximum tangential stress criterion) at $N = 2 \times 10^6$ cycles (technical endurance limit):

$$\Delta K_{\text{eq en}} = 144\ \text{N/mm}^{3/2} \text{ in tensile-shear loading,}$$
$$\Delta K_{\text{eq en}} = 212\ \text{N/mm}^{3/2} \text{ in peel-tension loading.}$$

The investigation included joints with a gap between the slit faces. Such gaps in combination with a small joint face width result in excessive bending stresses in the joint face as far as bending moments are acting. The statistical basis of these mean values is poor (Eibl and Sonsino[953,954]).

The following statements on the structure of the stress intensity parameters that are suitable for describing the fatigue strength or life of laser-beam-welded lap joints may be made. Parameters of type $\Delta\sigma_{s\,pl}\sqrt{t}$ are appropriate for $w_s/t \geq 1.0$ whereas parameters of type $\Delta\sigma_{s\,jf}\sqrt{w_s}$ or $\Delta\tau_{s\,jf}\sqrt{w_s}$ are preferable for $w_s/t \leq 1.0$ (with structural stresses in the plate, $\sigma_{s\,pl}$, or in the joint face, $\sigma_{s\,jf}$ or $\tau_{s\,jf}$). The w_s/t condition may be substituted by a fracture type demarcation separating plate fractures from joint face fractures.

Zhang *et al.*[944] proposed use of the fatigue parameter $p_a = \sigma_{sa} f_1(w_s/t)\sqrt{w_s} = \sigma_{sa} f_2(w_s/t)\sqrt{t}$ (with structural stress amplitude σ_{sa}, plate thickness t and joint face or seam width w_s) to characterise the fatigue strength of laser-beam-welded lap joints by a uniform fatigue parameter p–N curve. The procedure is similar to that with spot-welded joints, see Section 9.4.1, but in contrast to the derivations there, the method here is explicitly based on stress intensity factors. Laser-beam-welded joints come off worse than spot-welded joints in terms of the endurable cyclic stress intensity factor. This may be surprising but can be explained, in principle, by a 'softer' material

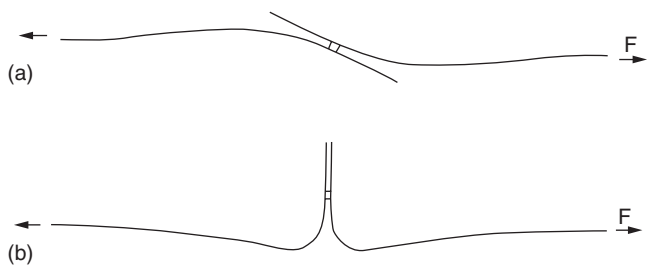


Fig. 10.50. Deformation plots of the thin-shell element models of the laser-beam-welded tensile-shear specimen (a) and of the peel-tension specimen (b), plotted deflections greatly enlarged; after Radaj *et al.*[907]

treatment, more favourable residual stresses and different crack path behaviour in spot-welded joints. Further investigations of the fatigue strength of laser-beam-welded lap joints are reviewed in Sections 9.4.4, 11.2.4 and 11.3.5.

The fatigue strength of a GMA fillet-welded lap joint in aluminium alloy of type AlMg4MnCr of sheet thickness $t = 2.5$ mm, subjected to tensile-shear loading (weld root failures), has been investigated by Beretta and Sala[856] based on the stress intensity approach. The stress intensity factors K_{I} and K_{II} at the weld root are superimposed by the partial factors in three basic load cases: pure bending moment, axial tension force and transverse bending force. It is shown that defects at the weld root, especially flaws originating from shrinkage cavity formation, may substantially enlarge the stress intensity factor, thus resulting in different positions of the corresponding S–N curves. A statistical evaluation gave most probable defect depths of 0.15–0.55 mm with aspect ratios $a/c = 0.1$–0.2. The threshold stress intensity factor introduced for predicting the endurance limit was $\Delta K_{\mathrm{th}} = 70$ N/mm$^{3/2}$ ($R = 0.1$). The predicted endurance limit was $\Delta\sigma_{\mathrm{nE}} = 13$–$19$ N/mm^2.

11

Notch- and crack-based approaches for spot-welded and similar lap joints

11.1 Basic procedures

11.1.1 Principles of the notch stress, notch strain and crack propagation approaches

The principles of the notch stress, notch strain and crack propagation approaches have been described in the previous Chapters 4, 5 and 6 with regard to seam-welded joints. These principles are now considered with regard to spot-welded and similar lap joints.

A survey of the different approaches relating to crack initiation and propagation under fatigue loading is given in Fig. 11.1. The different approaches are positioned in the upper part. The crack size and load cycle scales are drawn in the lower part. The introduced scale values only designate the tendency. The actual values and their correlation depend on the configuration considered. A common feature is that the through-thickness propagation of the semi-ovaloid crack at the front side of the weld spot in tensile-shear loading is most important, whereas macrocrack initiation (i.e. microcrack formation growth and coalescence) may be neglected in certain cases and crack propagation over the plate width may be neglected in others. Different mechanisms of crack growth are connected to the three stages of crack behaviour just mentioned.

The notch stress approach shown in Fig. 11.1 in the first bar designates the procedure developed for seam-welded joints on the basis of an elastic model which takes the microstructural support effect at sharp notches into account (see Section 4.1.3). This effect is introduced by fictitious notch rounding. The approach is transferred to spot-welded joints with minor modifications: thickness correction is mandatory in thin-sheet material and the material parameters should conform to the rolled or wrought material instead of the cast material. The endurance limit of the spot-welded joint or its substitute value at $N \approx 5 \times 10^6$ cycles, the technical endurance limit, is the target parameter of the analysis. With the endurance limit being

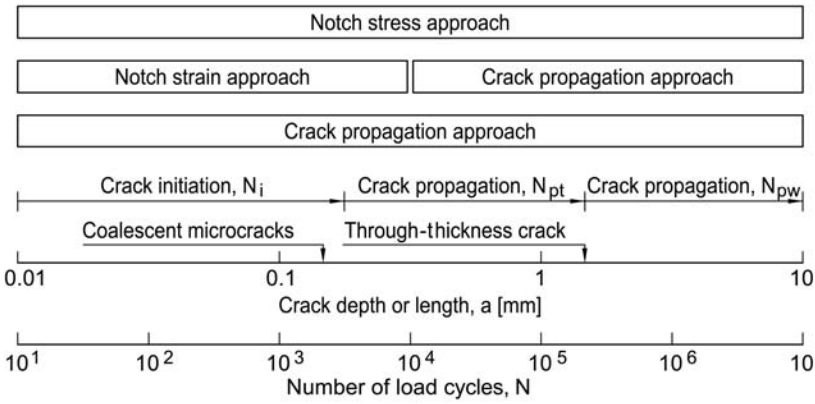


Fig. 11.1. Notch stress, notch strain and crack propagation approaches for determining the fatigue life of spot-welded joints in relation to crack size; schematic representation: crack size and load cycles depend on the configuration considered; with numbers of cycles: N_i related to crack initiation, N_{pt} related to crack propagation over plate thickness and N_{pw} related to crack propagation over specimen width.

determined, the *S–N* curve can be drawn with an assumed inverse slope exponent. The failure criterion in this context is the final fracture of the specimen or, as an alternative, the through-crack at the weld-spot, the difference in corresponding load cycles being small in single-spot specimens. The assessment procedure is described in Section 4.2.6. An application example of this approach related to spot welds is recorded in Section 11.2.1. A more recently proposed variant of the notch stress approach is based on a small-size substitute notch (see Section 11.2.4).

The notch strain approach shown in Fig. 11.1 in the second bar is related to the initiation of a macrocrack ($a_i \approx 0.25$ mm) at the notch root caused by cyclic elastic-plastic deformation. Further growth of the initiated crack is described by the crack propagation approach entered on the right-hand side of the bar (Dowling[950]). The conventional form of the notch strain approach (see Section 5.1.3) applied to spot-welded joints is described first below. A version of the approach more adapted to spot welds is presented thereafter. The description is graphically supported by Fig. 11.2. An assessment procedure for more general use is not yet available.

The slit tip at the weld spot edge is considered as a sharp notch where the elastic-plastic strains (and stresses) are determined either by elastic-plastic finite element analysis or by an approximation (e.g. Neuber's micro-support formula) based on the initial elastic notch stresses (upper bars in Fig. 11.2). The usual procedure is to determine the fatigue-effective notch stresses at the endurance limit where crack initiation is just prevented and elastic material behaviour can be presumed. These fatigue-effective elastic

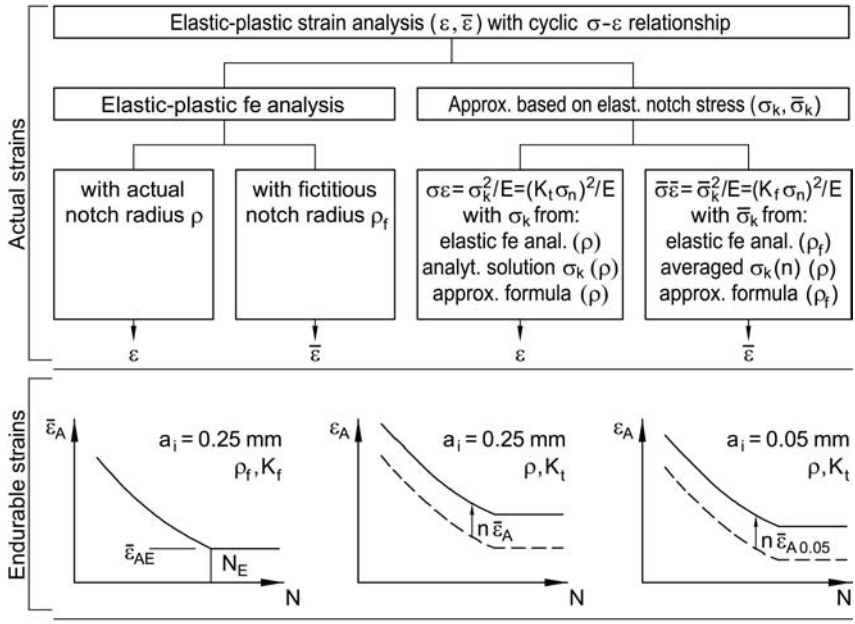


Fig. 11.2. Variants of the notch strain approach for spot-welded joints; with explanation of the symbols in Table 11.1; after Seeger *et al.*[981] (extended slightly).

Table 11.1. Explanation of the symbols in Fig. 11.2

Symbol	Meaning of the symbol
σ, ε	Elastic-plastic notch stress and strain with ρ
$\bar{\sigma}$, $\bar{\varepsilon}$	Elastic-plastic notch stress and strain with ρ_f (fatigue-effective)
σ_k	Elastic notch stress with ρ
$\bar{\sigma}_k$	Elastic notch stress with ρ_f
ρ, ρ_f	Real and fictitious notch radius
σ_n	Nominal stress
E	Elastic modulus
K_t	Stress concentration factor
K_f	Fatigue notch factor
a_i	Depth of initiated crack
ε_A, $\varepsilon_{A\,0.05}$	Endurable strain amplitude with ρ (a_i = 0.25 and 0.05 mm)
$\bar{\varepsilon}_A$, $\bar{\varepsilon}_{A\,0.05}$	Endurable strain amplitude with ρ_f (a_i = 0.25 and 0.05 mm)
$\bar{\varepsilon}_{AE}$	Endurance limit of strain amplitude with ρ_f (a_i = 0.25 mm)
N_E	Number of cycles at the endurance limit
n	Notch support factor, $n = K_t/K_f$

notch stresses can be determined, e.g. by averaging the actual notch stresses over the material-characteristic microstructural length in the assumed crack initiation line normal to the notch contour or – more easily, but also less accurately – by fictitious notch rounding (as proposed by Neuber). The fatigue notch factor K_f and the notch support factor $n = K_t/K_f$ which include the size effect of the notch fatigue problem are thus established. Relevant elastic calculation methods are the finite element method, analytical solutions and approximation formulae. The result of the elastic-plastic analysis or of the elastic analysis introduced into Neuber's macrosupport formula give the fatigue-effective strains which have to be compared with the relevant endurable values. The endurable values are related to the parent metal. They are modified as far as hardening or softening in the heat-affected zone is taken into account.

In the conventional variant, the endurable fatigue-effective strains are related to the formation of a macrocrack with a crack depth (or length) of 0.25 mm (bottom left-hand diagram in Fig. 11.2). Identical results are achieved by performing the analysis with the real instead of the fatigue-effective (i.e. averaged) notch strains (bottom middle diagram in Fig. 11.2). The endurable strains are shifted upwards by the relevant notch support factor.

There is a serious objection to apply the above conventional procedure without modification to spot-welded joints (e.g. as performed by Lawrence *et al.*,[967] see Section 11.3.2). The available strain *S–N* curves are based on a relatively large, easy to detect surface crack. In spot-welded thin-sheet structures, this crack size compromises a major portion of through-thickness crack propagation which occurs under extremely inhomogeneous stress and strain conditions here, in contrast to the homogeneous conditions in smooth specimens. The notch dimensions at the weld spot edge are so small and the related notch stress variations so localised that essential features of the crack initiation and propagation process are substantially altered. Key issues are short crack behaviour, notch-controlled versus crack-controlled plastic zone and crack initiation without further crack propagation.

It is possible in principle, but has not yet been worked out in detail, to use strain *S–N* curves related to an initiated crack size of e.g. 0.05 mm instead of 0.25 mm. These curves can be derived by tracking the detected larger crack size back to the smaller crack size based on crack propagation analysis. Once more, two formal variants are possible in comparing actual and endurable notch strains (second variant: bottom right-hand diagram in Fig. 11.2). Further propagation of the very small initial crack can realistically be simulated in the notch strain field under consideration or can be approximated based on empirical findings on initial crack propagation at weld spots.

Defining the crack initiation length by $a_i = 0.25$ or 0.05 mm is more or less arbitrary. Socie *et al.*[986] have proposed to derive the crack initiation length

using the following consideration. The crack initiation life is determined according to the (elastic-plastic) notch strain approach, not only at the notch root, but also for the material elements on the potential crack path normal to the notch contour. The number of cycles to failure, N_f, increases with the distance normal to the notch root, n^*, resulting in a decreasing gradient dn^*/dN_f along the potential crack path. The propagation of a crack starting at the notch root, on the other hand, shows an increasing propagation rate, da/dN, described by the Paris equation (presuming elastic conditions). The point of intersection of the two curves defines the crack initiation length a^*. The crack initiation life is determined by integrating dn^*/dN_f between zero and a^* resulting in N_f at this point. The crack propagation life follows on the basis of this initiated crack length. The value of a^* was found to be dependent on notch acuity, stress level, stress ratio and relevant material parameters, but is approximately $a^* = 0.025$ mm for low strength steels, high strength steels and aluminium alloys. As expected, the relative portion of fatigue life spent in crack initiation decreases with increasing notch acuity. Some analysis results were verified experimentally, but only with regard to the total life. Not all results are consistent with expectation.

The crack propagation approach entered in Fig. 11.1 in the third bar is characterised by describing the whole fatigue range by a macrocrack propagation model (compare Section 6.1.1). Crack propagation is assumed to start with the first loading cycle at the crack-like slit tip. The slit tip stress singularity is characterised by the initial stress intensity factor. The Paris equation can immediately be applied to describe the formation and growth of the actual crack which shows a kink relative to the slit direction, in general (Newman and Dowling[970]). Crack propagation over plate thickness may be subdivided in a first stage where the initial slit tip stress intensity is the dominant factor and in a second stage where the crack tip stress intensity of the initiated macrocrack is decisive (Zhang and Taylor[992]). The analysis of crack propagation may be limited by the through-crack or further extended to final fracture. The latter stage of crack propagation over the width of the specimen can be neglected in single-spot specimens, but may be important in multi-spot configurations or in situations with crack-induced load-shedding effects.

11.1.2 Weak points and potential of the notch stress approach

The conventional notch stress approach which is characterised by fictitious notch rounding that simulates the notch support effect is a well-proven procedure for assessing the fatigue strength of seam-welded joints at the endurance limit (see Chapter 4). It has also been proposed for application to spot-welded lap joints (Radaj[4,816]), but was not actually used in the context of industrial product development. The fictitious notch radius is not

small in relation to the thickness of the thin-sheet material so that the resulting fatigue-effective notch stresses must be corrected with regard to cross-sectional weakening. The fatigue strength in the medium-cycle range is estimated on the basis of an assumed inverse slope of the *S–N* curve proceeding from its value at the technical endurance limit. The failure criterion is defined by the final fracture of the specimen. Therefore, the conventional notch stress approach allows only rough estimates without resolution of the details of the fatigue process and its influencing parameters. There is a tendency to substitute the conventional approach by an improved approach.

The improved notch stress approach combined with a small-size notch (real or substitute) proceeds without fictitious notch rounding related to the notch support effect. There is no problem with small plate thicknesses. The notch support effect is taken into account by averaging the notch stresses over a small distance on the expected crack path normal to the notch contour. The approach can also be applied with the endurable non-averaged notch stresses derived experimentally for the assumed notch radius. The complications and the potential of the improved notch stress approach are included in the discussion below of the notch strain approach.

11.1.3 Weak points and potential of the notch strain approach

The notch strain approach described in Section 11.1.1 involves the following weak points when applied to spot-welded lap joints. Uncertainties exist with regard to the shape and size of the notch at the weld spot edge, crack initiation is possibly displaced from the notch at the weld spot edge and individual-grain effects take place at the notch root. These points are further elaborated in the following.

The shape and size of the notch at the weld spot edge depends on the welding conditions, Fig. 11.3. Any gap formation vanishes and the crack-like slit tip is located in the solid-phase pressure-welded part of the heat-effected zone (see Fig. 11.25), if welding current and electrode force remain near the lower limit of the weldability condition. The problem with such welding is that sticking spots may be produced instead of welded spots (stick limit). The former are difficult to detect by non-destructive inspection techniques. Therefore, higher welding currents and electrode forces are advisable under industrial production conditions. This operational setting is associated with a deeper electrode indentation and with increasing gap formation (gap width up to 0.2 mm, also intentionally enforced to make evaporation of zinc coatings easier). A roll-shaped expulsion penetrates into the gap as soon as the expulsion limit is exceeded. The expulsion is coupled with excessive electrode indentation. Therefore, the latter welding condition should also be avoided.

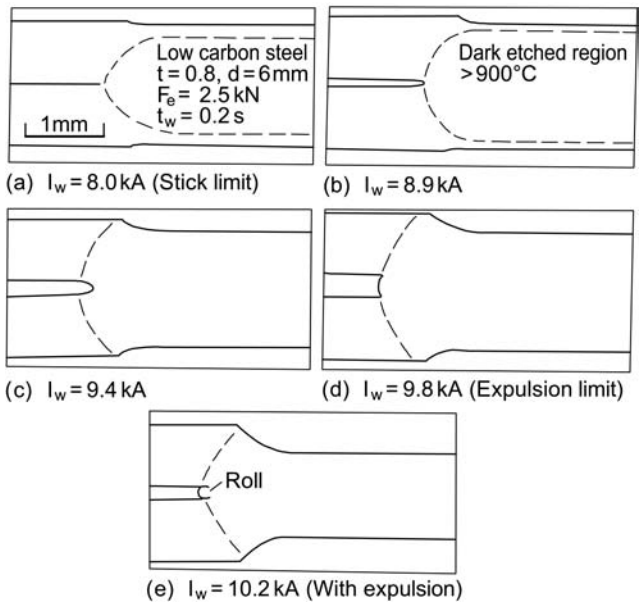


Fig. 11.3. Geometric contour lines of radially arranged macrosections of weld spots produced with different welding currents I_w (welding time t_w and electrode force F_e being constant); dark-etched high-temperature regions indicated by dashed border lines; drawn according to etched macrosections published by Anastassiou *et al.*[947]

An unexpected result of fatigue testing is that the fatigue resistance of weld spots with expulsion is relatively high, whereas welding close to the stick limit, establishing an 'ideal' sectional shape, results in poorer performance, Fig. 11.4. Only in the high-cycle fatigue range ($N \geq \approx 2 \times 10^6$ cycles), the joint with an ideal shape comes off better than the other expulsion-free joints. This unexpected behaviour may be explained from different notch geometries (the notch shape produced by 9.4 kA seems to be most favourable) and from different radial tensile residual stresses at the weld spot edge (these stresses being lowest for 8.0 kA close to the stick limit, highest for 9.8 kA close to the expulsion limit and substantially reduced by an expulsion).

Similar macrogeometrical conditions in the cross-section occur with laser-beam-welded lap joints (keyhole lap welds), but the microgeometrical conditions and the metallurgical processes are different. Therefore substantial deviations in fatigue strength may occur.

There are two ways of defining the shape and size of the notch at the weld spot edge, Fig. 11.5, either close to the real cross-sectional microshape of the slit tip, avoiding any unrealistic undercut (i.e. an U-shaped, semi-elliptical or parabolic notch), or as a substitute notch with pronounced

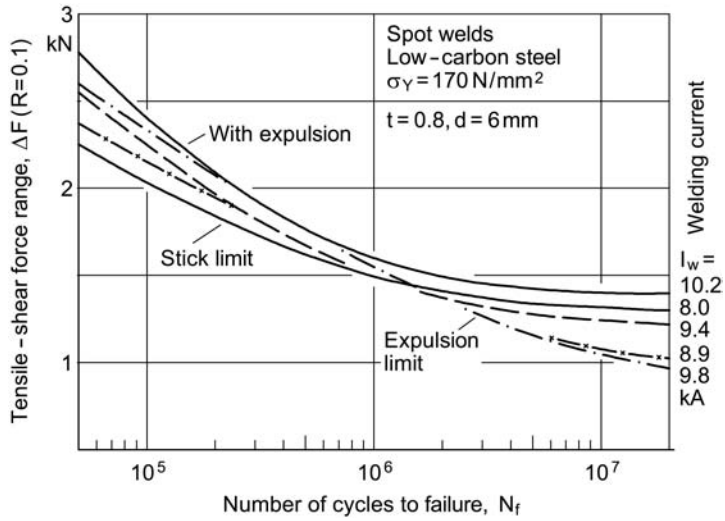


Fig. 11.4. F–N curves of spot welds in tensile-shear specimen dependent on production conditions (welding current I_w varied, all other operational settings constant); after Anastassiou *et al.*[947]

undercut (i.e. keyhole or double-keyhole notch). The U-shaped notch proposed by Pan and Sheppard[973] and also by Zhang and Richter[846] or the semi-elliptical notch applied for comparison by Seeger *et al.*[981] enforces an extremely small notch radius in gapless joints (radius equal to surface roughness). The parabolic notch proposed by Lawrence *et al.*[967] greatly underestimates the notch effect in mode II loading. The keyhole notch in gapless joints proposed by Radaj *et al.*[978] and the corresponding double-keyhole notch in gaping joints proposed by Eibl[952] in a not quite satisfactory form (i.e. the C-shaped notch: two semicircles connected by a straight line positioned at the slit tip instead of two three-quarter circles with their centre above and below the slit tip) may represent worst case conditions with the restriction that the undercut (or notch depth) is more effective in mode II than in mode I loading. A necessary condition for the notch shape to be suitable is that the notch curvature and the fictitious notch depth at the crack initiation points is the same within the series of cases to be considered. This is the reason why the keyhole notch (inclusive of its derivative, the U-shaped notch) is superior to other substitute notch designs.

The size of the keyhole notch should be as small as possible in order to keep the cross-sectional weakening effect low. A notch radius of $\rho = 0.05$ mm is recommended in low-carbon steels, based on consideration of the grain size at the slit tip (details discussed below). Zuniga and Sheppard[993,994] as well as Pan[972] use $\rho = 0.0762$ mm for modelling spot welds in high-strength low-alloy (HSLA) steels. The depth of electrode indentation and the gap half-width are considered to be equal (see Fig. 11.26). An even smaller

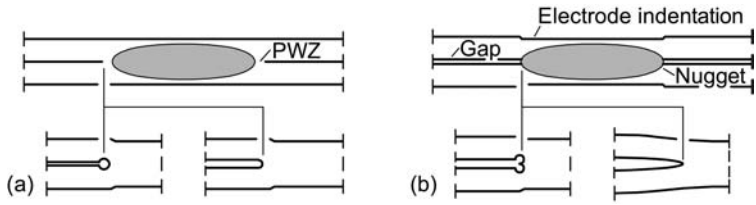


Fig. 11.5. Cross-sectional views of spot-welded joints with enlarged substitute notches at the weld spot edge: gapless joint with slit tip in pressure-welded zone (PWZ) leading to a keyhole or U-shaped notch (a) and gaping joint with slit tip at the nugget edge leading to a double-keyhole or parabolic notch (b).

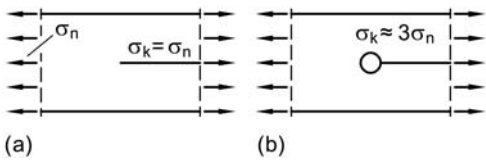


Fig. 11.6. Crack-like slit (a) subjected to tension load without stress concentration and substitute keyhole notch (b) with stress concentration; nominal stress σ_n and maximum notch stress σ_k.

radius may be justified under special conditions, e.g. $\rho = 0.005$ mm for small-size laser beam welds (Schlemmer[979]). The small-size notch has primarily the function of initiating elastic-plastic deformation and cracking without having a major influence on subsequent larger-scale deformation and crack propagation. Only a notch with finite radius catches the effect of the non-singular stresses at the slit tip. For example, the crack-like slit subjected to tensile loading in the slit direction shows no stress concentration, whereas a small keyhole notch substituting the slit tip produces a pronounced stress concentration, Fig. 11.6. The stress concentration is less pronounced when using the U-shaped notch.

Crack initiation outside the notch at the weld spot edge (displaced crack initiation) occurs in two different forms. Displaced crack initiation in high-cycle fatigue very near to the weld spot edge (or slit tip) may take place as a consequence of microstructural effects such as unsteady local stresses caused by the grain structure, residual stresses between grains and grain constituents, weakened grain boundaries and others. The notch stress concentration in the homogeneous material remains a guide value especially when using the fatigue-effective notch stress related to a crack size of 0.25 mm. Displaced crack initiation in low-cycle fatigue further away from the weld spot edge where the heat-affected zone merges into the parent material is of quite another origin. Here, cyclic yielding under the structural stresses (without notch effect) may be so severe that cracks may be initiated earlier than at the slit tip. This complication can be easily overcome

by applying the conventional notch strain approach at the suspected point of displaced crack initiation.

The individual-grain effects at the weld spot edge notch are severe because of the small notch radii being considered. One positive influence is the elastic microstructural support effect leading to reduced fatigue-effective notch stresses. On the other hand, the notch stresses in neighbouring grains may well be enlarged, leading to slightly displaced crack initiation. Data on the grain size in spot-welded joints are not readily available. An average grain size of about 20 μm is recorded by Sheppard and Strange[985] for the heat-affected zone of low-carbon steel, type SAE 960X. Grain sizes of about 10 μm in the grain-refined heat-affected zone, in contrast to about 30 μm in the parent material, were found by Henrysson *et al.*[966] This means that the notch radius in the weld spot model should not fall below about 50 μm for low-carbon steels. Even then, microstructural effects may cause large deviations from predictions.

The notch strain approach for spot-welded joints provides the capability to take crack initiation in addition to crack propagation into account. There are special cases where the crack initiation cycles can be neglected, but there are other more general cases where the crack initiation cycles contribute essentially to the total fatigue life. A convincing argument should be that the crack initiation life must converge towards the total life near the actual endurance limit. It is a characteristic of the approach when applied to welded joints that two parameters influencing fatigue strength are emphasised more than in other approaches: the influence of hardening or softening in the heat-affected zone and the residual stress condition at the crack initiation point (positive effect with compressive stresses, negative effect with tensile stresses). The above potential is clearly indicated by the investigation of Lawrence *et al.*[967] (see Section 11.3.2).

11.1.4 Weak points and potential of the crack propagation approach

The crack propagation approach introduced in Section 11.1.1 is associated with the following weak points when applied to spot-welded lap joints: deviations from simplified plate fracture behaviour, inadequate neglect of non-singular stress portions, uncertainties about the initial crack size, inconsistencies with regard to the material parameters controlling crack propagation and uncertainties about the branching crack situation. These points are further elaborated in the following.

The subdivision of the fatigue fracture process at spot welds into the stages of crack initiation, crack propagation traversing the plate thickness and crack propagation traversing the plate width is a simplification which is realistic only in the case of tensile-shear-loaded weld spots in the high-cycle

fatigue range (see Section 10.1.2). With higher cyclic loads or other loading states such as cross-tension or peel-tension, other crack paths are observed, e.g. cracks separating the joint faces or cracks propagating around the weld spot, thus causing its buttoning out of the plate (plug-type fractures). Also, in the low-cycle fatigue range, the crack initiation point may be shifted from the slit tip area to the outer boundary of the heat-affected zone.

The conventional crack propagation approach is based on the singular stress portions at the crack tip expressed by stress intensity factors. The influence of the non-singular stress portions is neglected in the short crack stage described by the slit tip stress intensity factor, but possibly taken into account in subsequent crack propagation stages. The aforementioned neglect may be a severe deficiency, as can be seen from the example of slit-parallel loading shown in Fig. 11.6.

Another weak point of the crack propagation approach is the more or less arbitrary choice of the initial crack size. Neglecting the short crack stage in the fatigue life analysis is too conservative in general. Starting the analysis with a grain size microcrack (e.g. $a_i = 20\,\mu m$) and applying the Paris equation is non-conservative: the short-crack propagation rate is substantially larger despite crack arrest stages at grain boundaries, the crack opening mode II is initially decisive for short-crack initiation and propagation, and short-crack coalescence is an important phenomenon increasing the growth rate. Short-crack models could be used, but are complicated and uncertain. The notch strain approach is the only acceptable alternative analysis method for crack initiation.

There are inconsistencies in the crack propagation approach with regard to the material parameters controlling crack propagation. The exponent m is taken from test results with spot welds in low-carbon and high-strength low-alloy steels (structure-related inverse slope, $m = 3.5–7.0$), but used as if it was the material-related parameter, $m = 2.5–3.5$. The enlarged inverse slope may be explained by various support effects in the medium- to low-cycle fatigue range (large deflections, plastic deformation, extended crack paths, concurrent crack formation, often in combination with special failure criteria) and by a substantial crack initiation phase in the high-cycle fatigue range. A structure-related threshold stress intensity factor ΔK_{th} may be used to describe the endurance limit, and a structure-related static strength value may serve as a limit in the low-cycle fatigue range (Newman and Dowling[970]). The aforementioned restrictions stand against the claimed generality of the crack propagation approach.

Branching crack initiation prevailing in spot-weld fatigue is inadequately described by the crack propagation approach. The slit tip stress intensity factor is generally used as the initial value causing crack propagation. This does not conform to available material-related concepts (e.g. Pook[889,890]). Also, the possible influence of the non-singular stress portion is not taken into account.

The weak points described above mean that the crack propagation approach in the available form lacks sufficient generality. Related investigations are restricted to tensile-shear specimens. Further, more general developments with the inclusion of the crack initiation stage are mandatory. Nevertheless, the crack propagation approach for spot-welded lap joints provides the capability to take crack propagation, in addition to crack initiation, into account. Crack propagation inclusive of crack closure effects may adequately be described based on crack-size-dependent and structure-related stress intensity factors combined with material-related propagation rate parameters. Therefore, combination with the notch strain approach for crack initiation offers a realistic view for future development.

11.2 Analysis tools

11.2.1 Fatigue assessment through conventional notch stress approach

The fatigue strength of spot-welded or similarly seam-welded lap joints can be assessed based on the conventional notch stress approach provided that elastic conditions are prevailing at the notch root thus resulting in the technical endurance limit (see Chapter 4). The application of the approach to spot-welded lap joints is demonstrated by the example of the standardised tensile-shear and cross tension specimens (see Radaj[4,892,893] for further useful data). The assessment below in absolute values of strength extends the relative assessment[4,816] of spot-welded specimens. The ratio of the endurable values of tensile-shear force F and cross-tension force T is determined as $F/T = 4.76$ based on the notch stress approach which correlates with experimental findings.

The two specimens (designated SS and CT) are depicted among other specimens in Fig. 10.24. The sheet thickness is $t = 1$ mm, the spot diameter $d = 5$ mm and the specimen width $w = 40$ mm. The structural stresses around the weld spot were determined on the basis of the finite element model shown in Fig. 9.11 for the tensile-shear specimen. The principal internal force method was applied to obtain the fatigue-effective notch stresses. The slit end at the nugget edge was fictitiously rounded for that purpose. The fictitious notch radius $\rho_f = 0.25$ mm was chosen according to a basic consideration (substitute microstructural length $\rho^* = 0.1$ mm for rolled steel in respect of the solid state pressure-welded annular zone around the nugget where crack initiation is expected). The result of the boundary element analysis of the cross-sectional model of the nugget edge in the vertex points of the weld spot with the maximum stresses is plotted in Fig. 11.7 for the tensile-shear specimen and in Fig. 11.8 for the cross-tension specimen. The

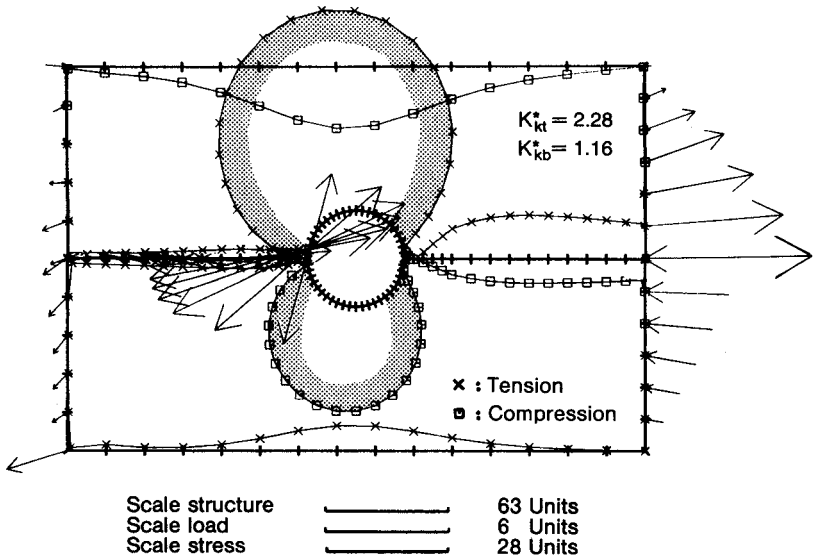


Fig. 11.7. Notch stress pattern at fictitiously rounded slit tip ($\rho_f = 0.25t$) of cross-sectional model in vertex point of weld spot of tensile-shear specimen; reduced stress concentration factors K^*_{kt} and K^*_{kb} of top and bottom plate identical to fatigue notch factors (referring to $\sigma_{sn} = 4F/\pi dt$), load on right edge and support reaction on left edge represented by arrows; two-sided arrows on left of rounding designating forces between the two substructures; after Radaj *et al.*[4,816]

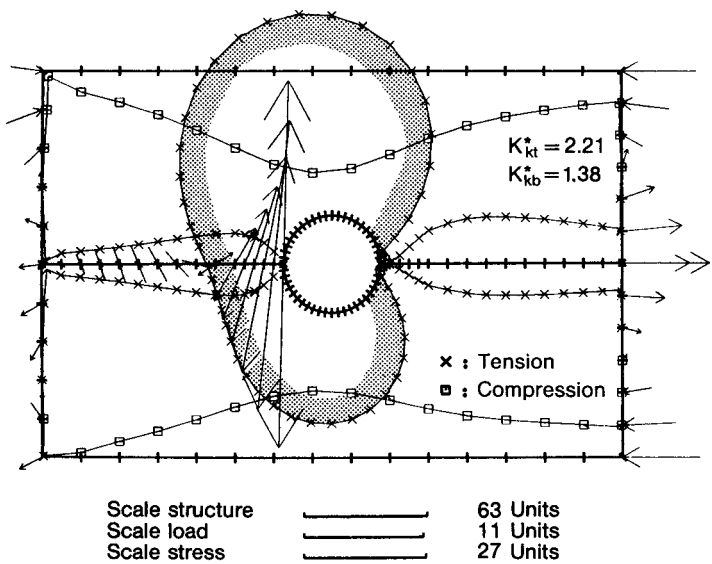


Fig. 11.8. Details as Fig. 11.7, but weld spot of cross tension specimen, $\sigma_{sn} = 0.6(T/t^2)\ln(w/d)$; after Radaj *et al.*[4,816]

notch stress concentration factors, K^*_{kt} and K^*_{kb}, of the top and bottom plate, respectively, are contained in the figures. They are corrected in respect of the weakening of the cross-section by fictitious notch rounding, eq. (4.32). They refer to the nominal structural stresses, $\sigma_{sn} = 4F/\pi dt$ in tensile-shear loading and $\sigma_{sn} = 0.69(T/t^2)\ln(w/d)$ in cross-tension loading according to eqs. (9.3) and (9.7).

The technical endurance limit of the fatigue-effective maximum notch stress range $\Delta\bar{\sigma}_k$ is introduced as $\Delta\bar{\sigma}_{kE} \approx 300\,\text{N/mm}^2$ ($N = 10^7$ cycles, $R = 0$, $P_f = 10\%$; interpolation from values in Tables 4.4 and 4.5). Evaluating the relation $\bar{\sigma}_k = \sigma_{sn}K^*_{kt}$ with the above data, gives $\Delta F = 517.2\,\text{N}$ and $\Delta T = 108.6\,\text{N}$. Actually, $\Delta F \approx 800\,\text{N}$ and $\Delta T \approx 160\,\text{N}$ are observed with $P_f = 10\%$ in conventional fatigue tests. This means that $\rho_f = 0.25\,\text{mm}$ turns out to be too small and that $\rho_f \approx 0.6\,\text{mm}$ (i.e. $\rho^* \approx 0.24\,\text{mm}$) seems to be more appropriate and justifiable with $R = 0$ instead of $R = -1$. The conversion of the stress concentration or fatigue notch factors from $\rho_f = 0.25\,\text{mm}$ to $\rho_f = 0.6\,\text{mm}$ is based on the relation $K_t \propto 1/\sqrt{\rho_f}$ according to eq. (11.1).

The technical endurance limit of a seam-welded lap joint in tensile-shear loading is also assessed on the basis of the notch stress approach. The sheet thickness $t = 1\,\text{mm}$, the specimen width $w = 40\,\text{mm}$ and the seam width $w_s = 5\,\text{mm}$ were originally chosen for spot-welded joints.[4,816] The unconventionally large seam width can be produced by diffusion welding or by two correspondingly spaced keyhole welds. The cross-sectional model is evaluated with pure shear loading in the joint face, Fig. 11.9. A slightly smaller fictitious notch radius is introduced than that with the spot-welded joints discussed above, $\rho_f = 0.2\,\text{mm}$ (of no general account). The structural stress at the inner surface of the plate is four times the nominal stress, $\sigma_s = 4\sigma_n$ (with $\sigma_n = F/wt$). The notch stress concentration factor referring to the structural stress, $K_k = 3.15$, results in $K^*_k = 1.83$ after reduction for cross-

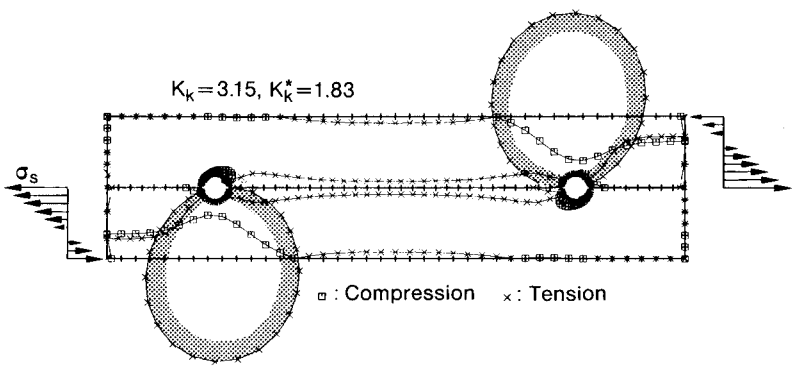


Fig. 11.9. Notch stress pattern at fictitiously rounded slit tips of seam-welded lap joint under tensile-shear loading; reduced stress concentration factor K^*_k referring to structural stress σ_s; after Radaj.[4]

sectional weakening. The relevant factor for $\rho_f = 0.25\,\text{mm}$ chosen for the spot-welded joints above is approximated by $K_k^* = 1.83\sqrt{0.2/0.25} = 1.64$. Introducing the endurance limit of the fatigue-effective notch stress range, $\Delta\bar{\sigma}_{kE} \approx 300\,\text{N/mm}^2$, the endurable force range is $\Delta F = 1.832\,\text{kN}$, i.e. substantially larger than for the comparable spot-welded joint (0.517 kN), but naturally smaller than for the non-overlapping parent material (12 kN). Relevant test data are not available.

Lawrence *et al.*[967] have derived the stress concentration factor of tensile-shear loaded spot welds on the basis of Pook's stress intensity factor approximation[886,887] (basically correct but of poor accuracy, see Table 10.1), Creager's blunt crack solution,[860] and the maximum tangential stress criterion according to Erdogan and Sih[866] (with nominal stress, $\sigma_n = F/wt$):

$$K_t = \frac{w}{d}\sqrt{\frac{t}{\rho}}\, f\left(\frac{d}{t}\right) \tag{11.1}$$

where K_t is the stress concentration factor at the nugget edge, w is the specimen width, t is the plate thickness, d is the weld spot diameter, ρ is the notch radius at the nugget edge and f is a function of d/t ($f \approx 1.2$ for $d/t = 3.0$–5.0). The resulting K_t value may be too large (factor 1.3 in a spot check).

11.2.2 Fatigue assessment through improved notch stress approach

The fatigue strength assessment for spot-welded or similarly seam-welded lap joints based on the notch stress approach has been substantially improved (Radaj *et al.*[978]). This development comprises accurate simple formulae for the notch stresses at the real small-size keyhole (i.e. not fictitiously rounded) subjected to the basic 'singular' (i.e. mode I, II and III loading) and 'non-singular' (i.e. tension, bending and shear loading) loading states. The loading modes result from the structural stresses at the weld spot edge after decomposition into singular and non-singular as well as symmetric and anti-symmetric portions. The fatigue-effective notch stress is calculated as the averaged value over the substitute microstructural length ρ^* normal to the keyhole edge which is much more accurate and reliable than using fictitious notch rounding. These fatigue-effective notch stresses may provide the basis for the notch strain approach to be applied in the finite-life fatigue range.

The analysis refers to the spot weld configuration depicted in Fig. 11.10: an in-plane loaded cross-sectional model subsequently supplemented by an out-of-plane (shear) loaded cross-sectional model. A keyhole notch with small diameter constitutes the slit tip in the model based on the arguments presented in Section 11.1.3. A gapless slit is presumed. Analytical notch stress solutions were derived for the basic in-plane loading states simulated

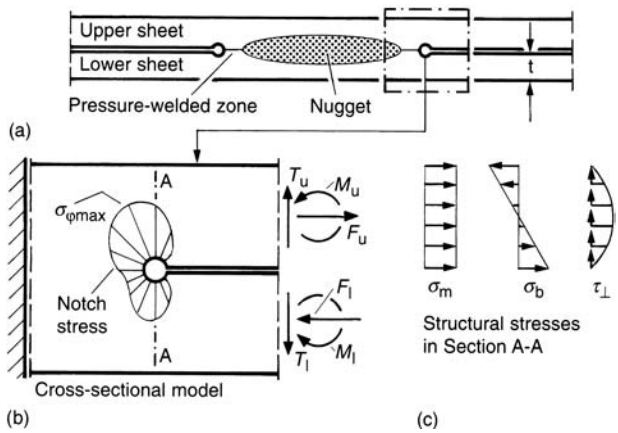


Fig. 11.10. Weld configurations: weld spot cross-section with rounded slit tips (a), cross-sectional model of the weld spot edge area with keyhole notch and internal resultant forces (b), as well as structural stresses in section A–A (c); after Radaj *et al.*[978]

for the infinite plate, Fig. 11.11, proceeding from Airy's stress functions. The same was done for the basic out-of-plane loading states proceeding from harmonic complex stress functions. The Neuber mean stress or microstructural support hypothesis (see Section 4.2.6) was used to determine the reduction of the elastic notch stresses to the fatigue-effective notch stresses. Numerical results are plotted in Fig. 11.12.

In the following, the equations for the notch stresses at the keyhole and their relation to the decomposed structural stress state are summarised. The solutions for the keyhole notch are transferable to the U-shaped notch as far as the notch stresses at $\varphi < \pi/2$ are considered where the maximum generally occurs.

The notations in the case of cross-sectional in-plane loading are indicated in Fig. 11.13. The notch stress results from:

$$\begin{aligned}\sigma_\varphi &= \sigma_{\varphi\infty}(\varphi, \rho)\kappa(\varphi, \rho/t) \\ &= \left[\frac{K_\mathrm{I}}{\sqrt{2\pi\rho}}\left(2\cos\frac{\varphi}{2} + \cos\frac{3\varphi}{2}\right) + \frac{K_\mathrm{II}}{\sqrt{2\pi\rho}}\left(2\sin\frac{\varphi}{2} + 3\sin\frac{3\varphi}{2}\right)\right. \\ &\quad \left. + 1.02\sigma_\mathrm{t}(1-\cos 2\varphi) + 1.12\sigma_\mathrm{b}^*(\sin\varphi - \sin 3\varphi)\right]\kappa(\varphi, \rho/t) \qquad (11.2)\end{aligned}$$

with $\sigma_{\varphi\ \max}(\varphi = \varphi_0, \rho) = \sigma_\mathrm{k}$ to be determined from $\mathrm{d}\sigma_\varphi/\mathrm{d}\varphi = 0$ or numerically from $\sigma_{\varphi\infty}(\varphi, \rho)$. The term $\sigma_{\varphi\infty}(\varphi, \rho)$ denotes the analytical solution for the infinite plate with the factors 1.02 and 1.12 on the right side of the equation being inserted in order to improve the accuracy of the solution.

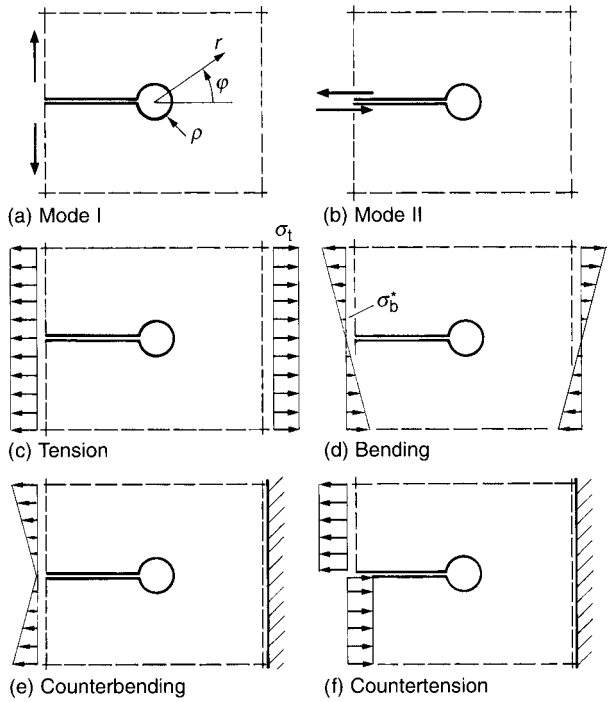


Fig. 11.11. Basic in-plane loading modes of the keyhole notch: 'singular' modes (a, b), 'non-singular' modes (c, d, e, f), symmetric modes (a, c, e) and anti-symmetric modes (b, d, f); after Radaj *et al.*[978]

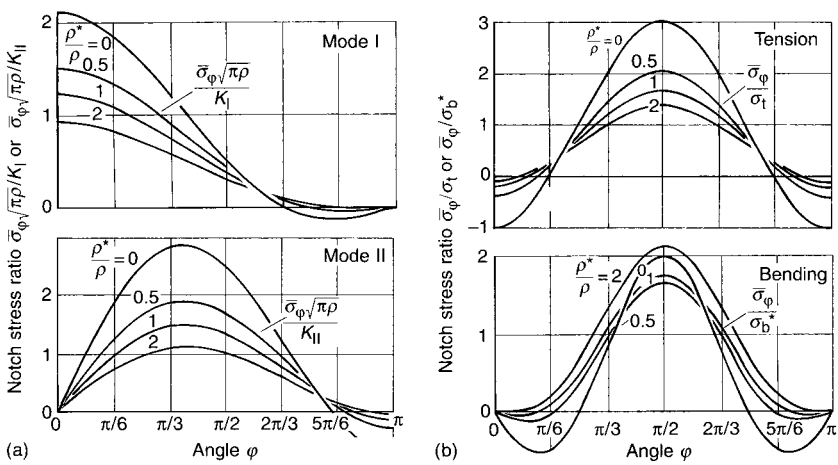


Fig. 11.12. Theoretical fatigue-effective notch stresses at the keyhole (with radius ρ) under mode I and mode II loading (a) and tension and bending loading (b) with notch stress $\bar{\sigma}_\varphi$ averaged over the substitute microstructural length ρ^*; after Radaj *et al.*[978]

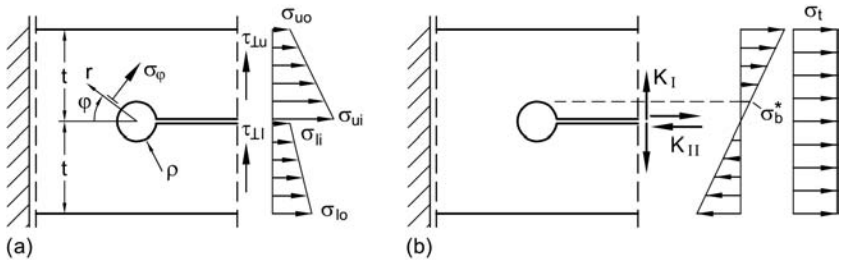


Fig. 11.13. Notations for original (a) and decomposed (b) in-plane loading of overlapping plates at weld spot edge with keyhole (cross-sectional model).

The decomposed cross-sectional in-plane loading state of the (upper) plate is characterised by the following quantities (eqs. (11.3) and (11.4) derived by Seeger *et al.*[981] proceeding from Radaj *et al.*[978]):

$$K_{\mathrm{I}} = \left[\frac{1}{4\sqrt{3}}(\sigma_{\mathrm{ui}} - \sigma_{\mathrm{uo}} + \sigma_{\mathrm{li}} - \sigma_{\mathrm{lo}}) + \frac{2.23}{2}(\tau_{\perp\mathrm{u}} - \tau_{\perp\mathrm{l}})\right]\sqrt{t} \tag{11.3}$$

$$K_{\mathrm{II}} = \left[\frac{1}{4}(\sigma_{\mathrm{ui}} - \sigma_{\mathrm{li}}) + \frac{0.55}{2}(\tau_{\perp\mathrm{u}} + \tau_{\perp\mathrm{l}})\right]\sqrt{t} \tag{11.4}$$

$$\sigma_{\mathrm{t}} = \frac{1}{8}[\sigma_{\mathrm{uo}} + 5\sigma_{\mathrm{ui}} + \sigma_{\mathrm{li}} + \sigma_{\mathrm{lo}} - (\sigma_{\mathrm{ui}} - \sigma_{\mathrm{li}})]\sqrt{\frac{t}{2\pi\rho}} \tag{11.5}$$

$$\sigma^{*}_{\mathrm{b}} = \frac{1}{8}(6\sigma_{\mathrm{uo}} - 3\sigma_{\mathrm{ui}} - \sigma_{\mathrm{li}} - 2\sigma_{\mathrm{lo}})\frac{\rho}{t} \tag{11.6}$$

The correction factor for finite plate thickness reads:

$$\kappa(\varphi, \rho/t) = \frac{2 - \dfrac{\rho}{t}\sin\varphi\left(1 + \dfrac{\sigma_{\mathrm{uo}}}{\sigma_{\mathrm{ui}}}\right)}{2\left(1 - \dfrac{\rho}{t}\sin\varphi\right)^{2}} \qquad (\sigma_{\mathrm{uo}} < \sigma_{\mathrm{ui}}) \tag{11.7}$$

The notations in the case of cross-sectional out-of-plane (shear) loading are indicated in Fig. 11.14. The shear notch stress results from:

$$\begin{aligned}\tau_{z\varphi} &= \tau_{z\varphi\infty}(\varphi, \rho)\kappa^{*}(\varphi, \rho/t) \\ &= \left[\frac{K_{\mathrm{III}}}{\sqrt{2\pi\rho}}2\cos\frac{\varphi}{2} + 2\tau_{\parallel}^{++}\sin\varphi\right]\kappa^{*}(\varphi, \rho/t)\end{aligned} \tag{11.8}$$

with $\tau_{z\varphi\ \max}(\varphi = \varphi_0, \rho)$ to be determined from $\mathrm{d}\tau_{z\varphi}/\mathrm{d}\varphi = 0$ or numerically from $\tau_{z\varphi}(\varphi, \rho)$. The term $\tau_{z\varphi\infty}(\varphi, \rho)$ denotes the analytical solution for the infinite plate.

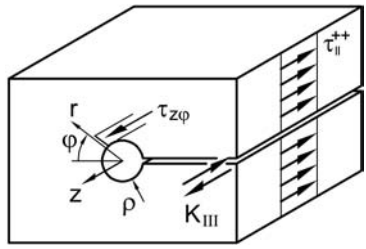


Fig. 11.14. Notations for decomposed out-of-plane (shear) loading of overlapping plates at weld spot edge with keyhole.

The decomposed cross-sectional out-of-plane loading state of the upper plate is characterised by:

$$K_{\mathrm{III}} = \frac{1}{\sqrt{2}}(\tau_{\mathrm{II u}} - \tau_{\mathrm{II l}})\sqrt{t} \tag{11.9}$$

$$\tau_{\mathrm{II}}^{++} = \frac{1}{2}(\tau_{\mathrm{II u}} + \tau_{\mathrm{II l}}) \tag{11.10}$$

with $\tau_{\mathrm{II u}}$ and $\tau_{\mathrm{II l}}$ depicted in Fig. 10.8.

The correction factor for finite plate thickness reads:

$$\kappa^*(\varphi, \rho/t) = \frac{1}{1 - \dfrac{\rho}{t}\sin\varphi} \tag{11.11}$$

The notch stress formulae derived by Zhang[938–942] for a parabolic notch at the weld spot edge on the basis of stress intensity factors which imply shortcomings (see Sections 10.2.7 and 10.4.1) are additionally distorted by neglecting the notch effect caused by the non-singular stress portions and by missing the correct local notch curvature in the case of mode II loading (Radaj[898,899]).

11.2.3 Fatigue assessment through notch strain approach

The fatigue strength assessment for spot-welded or similarly seam-welded joints can be performed based on the notch strain approach (as far as crack initiation is concerned) in two formal variants with identical results. In the first variant, the fatigue-effective cyclic stresses and strains occurring at the elastic-plastic notch root are compared with the endurable stresses and strains in unnotched specimens. In the second variant, the real cyclic stresses and strains occurring at the elastic-plastic notch root are compared with endurable stresses and strains in unnotched specimens increased by the (elastic) notch support factor.

The elastic notch support factor n related to the microstructural support effect is defined as follows:

$$n = \frac{\sigma_k}{\overline{\sigma}_k} = \frac{K_t}{K_f} \tag{11.12}$$

with the theoretical (maximum) notch stress σ_k, the fatigue-effective (maximum) notch stress $\overline{\sigma}_k$, the stress concentration factor K_t and the fatigue notch factor K_f. The quantities n, $\overline{\sigma}_k$ and K_f depend primarily on the material, the notch radius and the notch loading mode (Radaj[6]).

The two versions above of the notch strain approach reduced to the (elastic) endurance limit can then be formulated as follows:

$$\overline{\sigma}_k \le \overline{\sigma}_{kE} \qquad (\overline{\sigma}_k = K_f \sigma_n,\ \overline{\sigma}_{kE} = \sigma_E) \tag{11.13}$$

$$\sigma_k \le \sigma_{kE} \qquad (\sigma_k = K_t \sigma_n,\ \sigma_{kE} = n\sigma_E) \tag{11.14}$$

with the nominal stress σ_n, the endurable notch stresses σ_{kE} and $\overline{\sigma}_{kE}$, the endurance limit σ_E and the notch support factor n.

The basic formulae and material data of the notch strain approach are listed in Section 5.2.2. They comprise among others:

- the stress–strain relationship proposed by Ramberg and Osgood,
- the strain S–N relationship proposed by Manson, Coffin and Morrow,
- the stress–strain hysteresis loop relationship after Masing,
- the elastic-plastic notch stresses and strains approximated by Neuber's macrostructural support formula, by other approximation formulae or by nonlinear finite element analysis,
- the initial residual stresses taken into account by a variant of Neuber's formula, see eqs. (5.43–5.45), or by finite element analysis,
- the damage parameter relationship taking the effects of mean stress and of stress multiaxiality into account,
- the cyclic material parameters estimated on the basis of the uniform material law (initiated crack length: $a_i = 0.25\,\text{mm}$).

The notch strain approach (second variant) was applied by Seeger *et al.*[981] to a spot-welded tensile-shear specimen. The geometrical and material data correspond to the investigation of McMahon *et al.*[968] in order to compare the calculation results with the published experimental data referring to a spot diameter $d = 6.1\,\text{mm}$, a sheet thickness $t = 1.4\,\text{mm}$, a specimen width $w = 38\,\text{mm}$ and a high-strength low-alloy steel.

The elastic structural stresses in the specimen which are the basis for the elastic-plastic notch stresses and strains, resulted from a fine-meshed finite element model. The elastic notch stresses at the front side of the weld spot considered as the crack initiation site, were determined for the relevant cross-sectional model (keyhole radius $\rho = 0.05\,\text{mm}$) according to the for-

mulae of Radaj *et al.*[978] proceeding from the structural stresses (reference value σ_{s0} at the inner side of the tensile-loaded plate). The (elastic) notch support factor n was derived as the ratio of theoretical and fatigue-effective (maximum) notch stresses, eq. (11.12), the latter being calculated as mean value over the microstructural length ρ^* normal to the keyhole edge.

Different S–N curves result from the above-mentioned formulae of the notch strain approach, depending on the choice of the material parameter ρ^*, Fig. 11.15. Referring to Neuber's diagram, Fig. 4.29, $\rho^* = 0.07$ mm has to be chosen with the considered yield limit of ferritic steels. Another evaluation by Kuhn (see Radaj,[6] *ibid.* Fig. 4.33) results in $\rho^* = 0.1$ mm with the ultimate tensile strength of wrought steel being considered. The available fatigue strength data for spot-welded joints suggest a fictitious notch radius $\rho_f \approx 0.6$ mm (see Section 11.2.1) leading to $\rho^* = 0.22$ mm when introducing a real radius $\rho = 0.05$ mm. A slight increase in the value of ρ^* is justifiable from the load ratio $R = 0$ instead of $R = -1$ (the strength being lower, but the notch support being larger). The values of the inverse slope k entered into the diagram are approximations for the calculated curves.

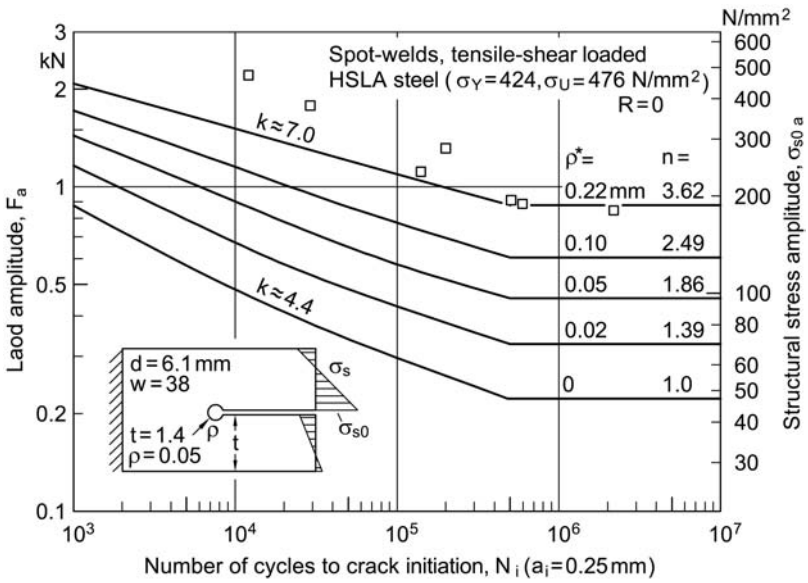


Fig. 11.15. S–N curves characterising crack initiation ($a_i = 0.25$ mm) in spot-welded tensile-shear specimen; calculation results based on the notch strain approach (solid line curves) in comparison to test results (square points) by McMahon *et al.*;[968] structural stresses σ_s in finite element model transferred to cross-sectional model with keyhole; notch support factor n determined with microstructural length ρ^*; after Seeger *et al.*[981]

The comparison of the theoretical with the experimental results confirms that $\rho^* = 0.22$ mm should be used instead of $\rho^* = 0.07$ mm. The theoretical endurance limit occurs at $N_E = 5 \times 10^5$ cycles (corresponding to the base material) whereas the test results indicate a slightly higher value of N_E. The slope in the medium-cycle fatigue range seems to be insufficiently reproduced by the theoretical results corresponding to $\rho^* = 0.22$ mm, but the number of experimental results is too small for a definite statement. Additionally, deviations have to be expected because an initiated crack length of $a_i = 0.25$ mm is not adequate for a keyhole notch with a radius of $\rho = 0.05$ mm (see Section 11.1.3).

The assessment procedure based on notch strains described above was used to investigate the effect of further influencing parameters (Seeger *et al.*[981]). Introducing the material parameters of the heat-affected zone (hardness increased by factor 1.5) reduces ρ^* and n with the consequence that the increase in fatigue strength is compensated by the reduction in notch support. Reducing the notch radius from $\rho = 0.05$ mm to $\rho = 0.01$ mm increases the high-cycle fatigue strength, an effect which is well known from small holes in homogeneous stress fields.

An essentially different notch strain or stress approach has been applied to spot-welded joints by Adib *et al.*[945] The approach was originally proposed by Weixing[991] as a volume-type method relating to the damaging zone in fatigue, and was later on modified by Adib and Pluvinage[946,976] to a line-type version. The fatigue-effective 'stress field intensity' at the notch root under elastic-plastic behaviour is the basic quantity. The notch stresses normal to the prospective crack path, weighted by the relative stress gradient times the distance from the notch root is averaged over a distance from the notch root extending to the point of minimum gradient, thus emphasising the influence of the stress on the borderline of the elastic-plastic zone. These conditions are demonstrated here by the example of front-side radial stresses in the tensile-shear specimen, Fig. 11.16. There are three zones to be distinguished. In the elastic-plastic zone I, the radial stress σ_r is slightly increasing to a maximum, leading via the transition zone II to the elastic zone III where the drop from the original elastic stress singularity is maintained. The distance z_{eff} results from the minimum in relative stress gradient χ. The fatigue-effective 'stress field intensity' σ_{fi} (not to be confused with σ_{eff} at z_{eff}) is given by the following relationships:

$$\sigma_{fi} = \frac{1}{z_{eff}} \int_0^{z_{eff}} \sigma_r(z)(1 - \chi z)\mathrm{d}z \tag{11.15}$$

$$\chi = \frac{1}{\sigma_r(z)} \frac{\mathrm{d}\sigma_r(z)}{\mathrm{d}z} \tag{11.16}$$

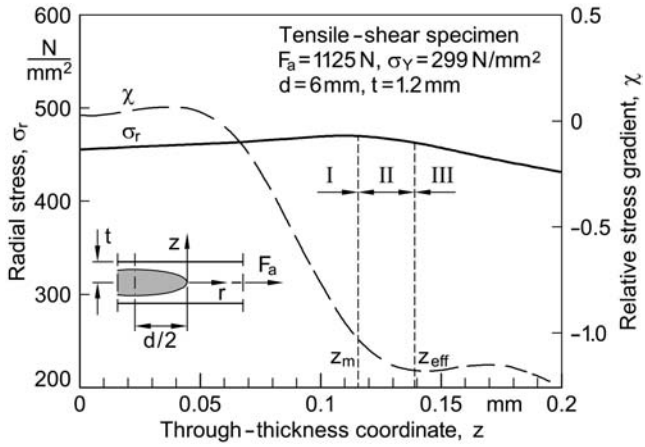


Fig. 11.16. Radial stress over plate thickness at weld spot edge in tensile-shear specimen; locally elastic-plastic conditions; solid element size $0.1 \times 0.4 \times 0.4\,\text{mm}^3$; position of z_{eff} at $\chi_{\min}$; after Adib *et al.*[945]

with the radial stress σ_r normal to the crack path assumed in the direction of the coordinate z. In the example above, the value $z_{\text{eff}} \approx 0.14\,\text{mm}$ is related to $F_a = 1125\,\text{N}$ corresponding to $N \approx 5 \times 10^5$ endurable load cycles. It is doubtful whether the details of stress distribution mentioned are sufficiently caught with the applied size of the solid elements ($\Delta z = 0.1\,\text{mm}$).

11.2.4 Fatigue assessment through simplified small-size notch approach

A simplified variant of the notch stress and notch strain approaches for spot-welded thin-sheet material or laser-beam-welded small-size parts proceeds, as in Sections 11.2.2 and 11.2.3 above, from rounding the slit tip with a small radius which corresponds to the half-width of the gap in the case of joints with a gap or which defines a substitute keyhole notch in the case of gapless joints. A typical choice for low-carbon steels is $\rho = 0.05\,\text{mm}$ (see Section 11.1.3). Larger values occur with larger gap widths. Smaller values should be avoided in order to exclude dominating grain size effects.

The resulting notch stresses (elastic finite element analysis) or notch damage parameters derived from notch stresses and notch strains (elastic-plastic finite element analysis) are compared with endurable values expressed by the relevant *S–N* curve (termed 'master curve' by Eibl[952]). This curve is determined by evaluation of the available fatigue test results with the structural parts or specimens under consideration. It thus includes an empirical notch support factor related to the selected notch radius which

has a decisive influence on the notch stresses or notch damage parameters. The notch support factor is not explicitly defined, but it is obviously considered as sufficiently uniform so that the scatter band of test results is not unduly widened. This uniformity can only be expected within narrow geometrical and other relevant parameter ranges.

The endurable radial notch stress amplitude at the technical endurance limit ($N = 10^6$ cycles) in spot-welded low-carbon steel specimens amounts to σ_{kaE} = 600–700 N/mm^2 for ρ = 0.05 mm in comparison to laser-beam-welded specimens with σ_{kaE} = 400–500 N/mm^2, but the notch stresses are higher in spot welds than in comparable laser beam welds (Zhang *et al.*[944]).

The *S–N* curves of equivalent notch stresses (ρ = 0.05 mm) derived by Eibl *et al.*[952–954] for various laser-beam-welded specimens (tensile-shear, peel-tension, H-shaped, hat section and tube specimens), loading modes (tension, shear and mixed-mode loading), geometrical parameters (sheet thicknesses 1.0–2.0 mm, seam widths 0.7–1.8 mm) and sheet materials (various steels and aluminium alloys) are presented in Fig. 11.17. The von Mises equivalent stress criterion is applied. Failure is defined as the total fracture of the specimen. Large deflections and elastic-plastic deformations are taken into account in the structural stress analysis. The *S–N* curves show a further slight drop in the high-cycle fatigue range beyond the endurance limit. The investigation was extended to out-of-phase loading using the 'effective equivalent stress hypothesis' by Sonsino *et al.*[987] It was carried on

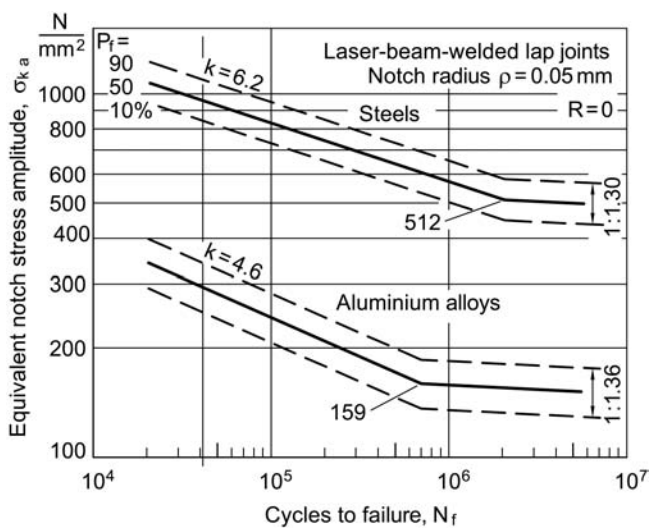


Fig. 11.17. Notch stress *S–N* curves (various specimens, tensile-shear and peel-tension loading) related to a notch radius of ρ = 0.05 mm (elastic analysis) for various steels and aluminium alloys; after Eibl.[952]

by Wallmichrath and Eibl[843] with emphasis on comparisons with the structural stress and stress intensity approaches.

Another investigation by Schlemmer[979] based on similar methods was related to laser beam welds in small-size circular components of engine injection systems loaded by internal pressure (various steels, geometries and weld types, wall thickness $t = 0.5$–1.5 mm). The failure criterion in the fatigue tests was a through-thickness crack detected by leaking oil. The internal pressure S–N curves were evaluated with regard to their endurance limit. The pressure amplitude at the technical endurance limit was used to perform an elastic notch stress analysis for $\rho = 0.05$ mm and compared with an elastic-plastic notch stress analysis for $\rho = 0.005$ mm (U-shaped notches in both cases). The analysis revealed that the different variants of material and geometry result in endurable notch stress amplitudes within a wide scatter range, from which the permissible values are derived. The elastic analysis with a notch radius of $\rho = 0.05$ mm is recommended for further industrial application.

The notch strain approach in connection with small-size notches at the crack initiation site has also been applied to GTA fillet-welded lap joints (plate thickness $t = 3$ mm) in aluminium alloy of type AlMgSi1 (AA6082-T6), Fig. 11.18. The crack initiated in the heat-affected zone and propagated thereafter in the parent metal. Failure criterion in the displacement-controlled tests was a 10% drop in load. As-welded specimens were

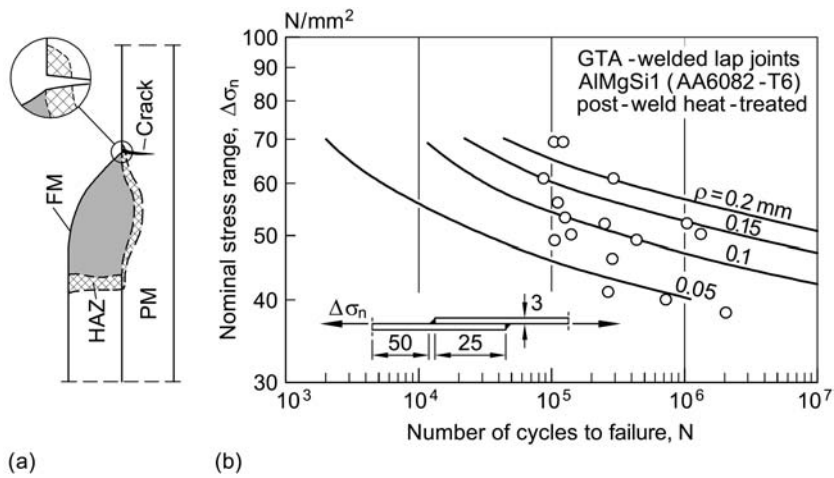


Fig. 11.18. Macrograph (a) of GTA fillet weld in lap joint made of AlMgSi1 aluminium alloy (PM: parent metal, HAZ: heat-affected zone, FM filler metal) and S–N curves (b), calculated according to the notch strain approach and compared with test results (circle points) for the post-weld heat-treated condition; after da Cruz *et al.*[949]

compared with postweld heat-treated specimens that provided the original T6 condition. The averaged measured toe radius was $\rho = 0.7$ mm with worst case values near $\rho = 0.1$ mm. The elastic-plastic notch stress and strain conditions were derived based on Neuber's and Glinka's formulae and compared with more accurate finite element results. The life predictions were found to be sensitive to the weld toe radius. A toe radius $\rho = 0.1$ mm seems to fit the experimental results best. The postweld heat treatment for recovering the T6 condition improved the fatigue strength significantly (by 50% at $N = 10^6$ cycles).

11.2.5 Fatigue assessment through crack propagation approach

Using the crack propagation approach, the life spent in propagating the crack is determined by integration of the Paris equation (occasionally extended by a stress ratio term) between the initial crack size a_i and the final crack size a_f (see Sections 6.2.3 and 6.2.4). The endurance limit is expressed by the structure-related threshold stress intensity factor. This approach is applied to spot-welded joints in the following simplified form. The total fatigue life N_t is the sum of three phases, the phase N_i in which the crack is initiated, the phase N_{pt} in which the crack traverses the plate thickness and the phase N_{pw} in which the crack propagates over the plate width (Wang *et al.*[990]):

$$N_t = N_i + N_{pt} + N_{pw} \tag{11.17}$$

The crack initiation phase is either described by the notch strain approach (see Section 11.2.3, procedures to be found in Section 5.2.2) or by the crack propagation approach in the following form. Crack initiation and early crack growth are controlled by the equivalent stress intensity factor range, ΔK_{eq}, at the slit tip at the weld spot edge, starting with zero crack depth, $a_i = 0$, and limited by the transition crack depth, a_{tr}. The assumption of a constant da/dN presumes a constant ΔK_{eq}. Integration of the Paris crack propagation equation in an R-dependent extended form, either as Forman's variant with the threshold effect neglected, or as corrected by an R-dependent factor f_R (see Section 10.3.1) or as modified by introduction of the effective stress intensity factor range, ΔK_{eff}, characterising the opened crack, gives the following crack initiation lives N_i:

$$N_i = \frac{a_{tr}(1-R)}{C(\Delta K_{eq})^m} \tag{11.18}$$

$$N_i = \frac{a_{tr} f_R^m}{C(\Delta K_{eq})^m} \tag{11.19}$$

$$N_{\mathrm{i}} = \frac{a_{\mathrm{tr}}}{C(\Delta K_{\mathrm{eff}})^{m}} \tag{11.20}$$

$$\Delta K_{\mathrm{eff}} = K_{\mathrm{max}} - K_{\mathrm{op}} \tag{11.21}$$

The equivalent stress intensity factor at the slit tip depends on loading type and load F, as well as on the dimensional parameters of the spot-welded specimen, mainly weld spot diameter d and plate thickness t, $\Delta K_{\mathrm{eq}} = f(\Delta F, d, t)$. The material constants of crack propagation are C (for $R = 0$) and $m \approx 3$ (for steel). The stress intensity factor describing crack opening, K_{op}, depends on R and K_{max} (e.g. according to eqs. (11.25) and (11.26)). The residual stresses are neglected despite their influence on crack initiation. The transition crack depth, a_{tr}, defining the point on the crack path where the slit tip stress intensity factor has lost its influence, is introduced differently depending on the respective author (if considered at all): a definite value of a_{tr}/t (Zhang and Taylor[992]), the value a_{tr} determined from the threshold stress intensity K_{th} (Fischer *et al.*[956]) or a fixed small value $a_{\mathrm{tr}} =$ 0.1, 0.2 or 0.25 mm (Lawrence *et al.*,[967] Wang *et al.*,[990] Swellam *et al.*[929]).

The phase of further crack propagation across the plate thickness provides the following life in terms of load cycles (only the first variant of eqs. (11.18–11.20) is specified):

$$N_{\mathrm{pt}} = \frac{(t - a_{\mathrm{tr}})(1 - R)}{C(\Delta K_{\mathrm{I}})^{m}} \tag{11.22}$$

The integration assumes a semi-elliptical crack with constant depth-to-length ratio, a/c, and crack propagation controlled by the mode I stress intensity factor, ΔK_{I}, derived for the membrane and bending stresses in the plate, $\Delta K_{\mathrm{I}} = f(\Delta F, t, a/c)$, and assumed to be constant. The residual stresses are neglected.

Occasionally, the first mentioned relationships for crack initiation, eqs. (11.18–11.20), are extended to the through-thickness crack propagation (only the first variant is specified):

$$N_{\mathrm{i}} + N_{\mathrm{pt}} = \frac{t(1 - R)}{C(\Delta K_{\mathrm{eq}})^{m}} \tag{11.23}$$

The phase of crack propagation across the plate width (in single-spot specimens often negligible) results in the following number of cycles, found by integration starting with the through-thickness crack length, $2a \approx d$, and ending with the plate width $2a \approx w$ (again, only the first variant is specified):

$$N_{\mathrm{wt}} = \frac{(w - d)(1 - R)}{2C(\Delta K_{\mathrm{I}})^{m}} \tag{11.24}$$

The stress intensity factor $\Delta K_I = f(\Delta F, w/d)$ is assumed to be constant in order to simplify the integration. Again, the residual stresses are neglected.

The effect of the load ratio R in the crack propagation approach applied to spot welds is correctly described by Henrysson[962] mainly as a consequence of elastic-plastic crack closure. Crack propagation takes place only to the extent the crack is open. The stress intensity factor at the moment of crack opening, K_{op}, depends on the load ratio R and the maximum stress intensity factor, K_{max}. Using the conventional load ratio correction proposed by Rupp[821] (see Section 9.4.2) in combination with the well-proven assumption that the crack remains completely open for $R \geq 0.5$, the following relationships are derived for tensile-shear (TS) and peel-tension (PT) specimens, respectively:

$$K_{op} = (0.15 + 0.69R)K_{max} \qquad \text{(TS)} \tag{11.25}$$

$$K_{op} = (0.07 + 0.86R)K_{max} \qquad \text{(PT)} \tag{11.26}$$

The above relationships are applied to the equivalent stress intensity factors K_{eq}. With K_{max} and K_{op} being known, the effective stress intensity factor range can be determined from eq. (11.21).

Newman and Dowling[970] apply a relationship proposed by Walker[989] on spot welds subjected to tensile-shear loading:

$$\Delta K_{eff} = K_{max}(1 - R)^{\gamma} \tag{11.27}$$

with the material-dependent exponent γ.

The simplified form of the crack propagation approach described above may be transfered to crack initiation shifted to the outer edge of the heat-affected zone, but is not transferable to the joint face shear fractures or buttoning weld spots occurring in the medium-cycle fatigue range of tensile-shear loading or to other loading types in the whole fatigue range. These other cracking modes and crack paths can also be described by crack propagation relationships, but such variants are not yet developed. Promising new software tools for this purpose are finite element programs which allow crack paths to be simulated.[497]

The simplified crack propagation approach proceeding from Pook's weld spot stress intensity factors combined with the maximum tangential stress criterion proposed by Erdogan and Sih[866] for mixed mode loading was applied by Newman and Dowling[970] to simulate the fatigue strength and life of spot-welded tensile-shear specimens, Fig. 11.19. The material parameters of crack propagation which are related to the parent metal were introduced: $C = 1.42 \times 10^{-13}$ [N, mm] (mean value supplemented by upper and lower bound values), $m = 3.0$ and $\gamma = 0.75$. The static failure stress (ultimate tensile strength σ_U) serves as the upper limit of the F–N curve. The fatigue threshold stress intensity factor provides the lower limit. A uniform F–N curve is

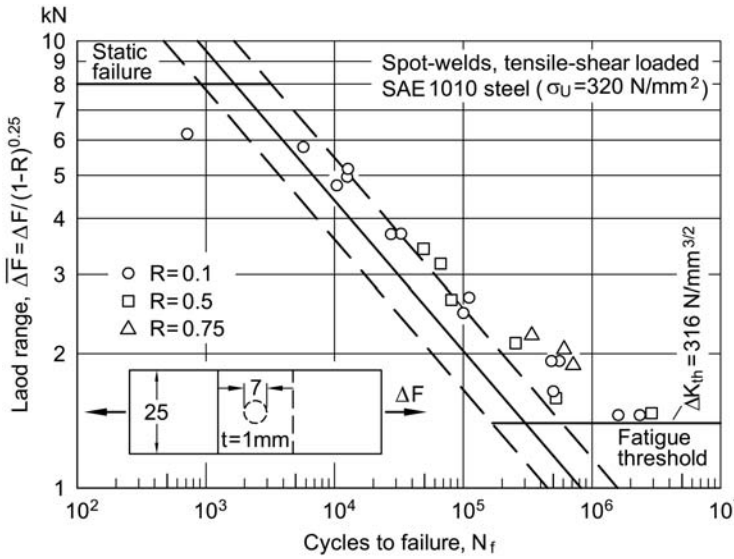


Fig. 11.19. *F–N* curves of spot-welded tensile-shear specimens (upper, lower and mean values of material constants) calculated according to simplified crack propagation approach and compared with test results; after Newman and Dowling.[970]

produced for various R ratios ($R > 0$) by plotting the load range modified according to Walker's proposal, eq. (11.26). The calculated *F–N* curves describe the experimental results sufficiently well, but the applied stress intensity factors according to Pook's formulae, eqs. (10.42) and (10.43), are too large, see Fig. 10.4 and Table 10.1, so that the calculated numbers of cycles to failure above have to be reduced by a factor of approximately 5 (Seeger *et al.*[981]) and the threshold load by a factor of approximately 1.7 (moreover, the threshold stress intensity factor is derived from spot weld testing; it is by a factor of two larger than the corresponding material constant). Also, the inverse slope of the theoretical curve ($k = 3.0$) is smaller than the corresponding value characterising the experimental results ($k \approx 4.5$). The latter discrepancy can be explained from support effects in the low-cycle fatigue range and from crack initiation cycles in the high-cycle fatigue range. Both effects are neglected in the simplified crack propagation approach.

A similar, more convincing calculation of the fatigue strength and life of spot-welded tensile-shear specimens was performed by Seeger *et al.*[981] The stress intensity factors are determined with high accuracy on the basis of the structural stresses at the weld spot edge gained from a finite element model. The material parameters of crack propagation inclusive of the threshold stress intensity factor are taken from the German FKM

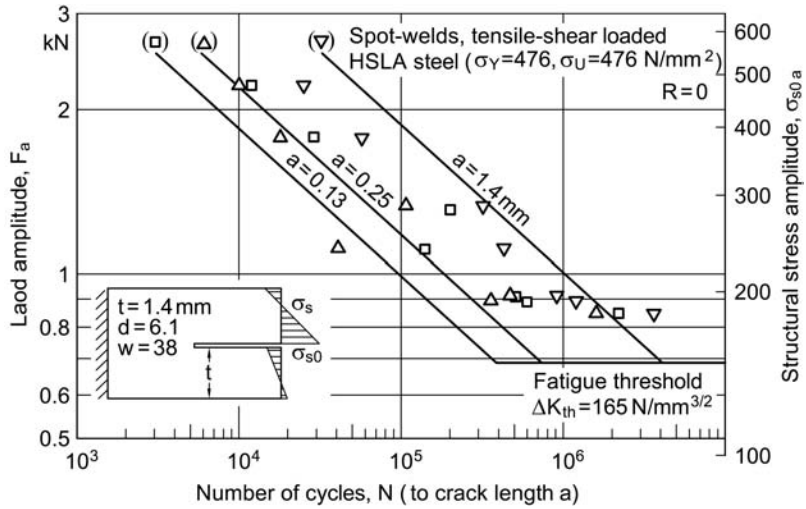


Fig. 11.20. F–N curves of spot-welded tensile-shear specimens (curves designating different initiated crack lengths) calculated according to simplified crack propagation approach and compared with test results published by McMahon *et al.*;[968] after Seeger *et al.*[981]

guideline for strength assessments based on fracture mechanics. *S–N* curves for different initiated crack lengths are established, Fig. 11.20. Results of calculation are compared with experimental results obtained by McMahon *et al.*[968] The degree of correspondence is acceptable despite obvious deviations in the slope of the (not yet drawn) fitting curves of the experimental data.

11.2.6 Residual stress distribution in spot-welded joints

Residual stresses are an important influencing factor when assessing the fatigue strength of spot-welded lap joints on the basis of the notch stress, notch strain or crack propagation approach. Available knowledge on the residual stress state at weld spots is small and, at this stage, not sufficient for generalisations. Formation of welding residual stresses is a complex nonlinear and transient phenomenon influenced by a multitude of parameters related to material, design and welding process. Attempts to model it numerically for the purpose of obtaining generally valid statements encounter many difficulties. Residual stress measurements, on the other hand, are expensive and the results cannot be generalised. Moreover, the welding residual stresses are subject to change as a consequence of operational loading. Especially the set-up loading cycle may produce a change

in the residual stress distribution which is accompanied by permanent deformations, e.g. slit opening displacements.

The residual stress fields can principally be subdivided into internal forces acting between neighbouring weld spots (welding sequence effect) or boundary supports and internal forces around a single weld spot without the aforementioned interaction. Experimental investigations into weld spot interaction have been performed by Le Duff *et al.*[786] with the result that no major influence was found on fatigue life. The opposite position is held by Dong *et al.*[760] who refer to larger sheet separation and smaller contact areas (possibly expulsions) within a sequence of weld spots. Examples for the single-spot behaviour are presented below.

In the finite element analysis by Schröder and Macherauch[980] (reviewed by Radaj[7] together with further references supplemented by Bolton[948]) with solid ring elements for spot welding of 2 and 10 mm thick plates made of type X4CrNiMo1913 austenitic stainless steel, the temperature field modelled close to reality, including the strong heat conduction into the water-cooled electrodes, but setting the electrode pressure unrealistically at zero, has been taken as the basis. No microstructural transformations of relevance to the residual stresses take place. Particularly steep temperature gradients occur at the electrode contact surface on the outside of the plates and at the nugget edge on the inside of the plates. The thermomechanical state on the inside of the plates at the end of heating is characterised by a high temperature in the weld spot centre, a sharp temperature drop at the weld spot edge, a temperature-related yield stress reduction in the weld spot, and a surface stress maximum somewhat outside the weld spot edge. Temperatures and stresses vary widely in the axial direction. After complete cooling, the stress curves for the inside and outside of the plate, shown in Fig. 11.21, are relatively less variable in the axial direction. The basic pattern of the stresses known from the corresponding membrane ring models is confirmed. Biaxial tension exists in the weld spot. The radial tensile stresses, σ_r, decrease slowly to zero outside the weld spot. The tangential tensile stresses, σ_t, decrease at a faster rate, reach into the compressive range and only then approach zero level. These membrane and bending stresses are structural stresses without the more local notch effect.

The local effects resulting from the three-dimensionality of the model, however, should be emphasised. A triaxial tensile stress state occurs at the nugget edge. The axial stress σ_z on the inside of the plates occurs under the condition that slit opening is suppressed. On account of the triaxial nature of the tensile stresses, the tangential stress σ_t at the weld spot edge is raised considerably above the uniaxial yield limit, $\sigma_Y = 440\,\mathrm{N/mm^2}$ (with yield criterion according to von Mises resulting in the equivalent stress σ_{eq}).

Popkovskii and Berezienko[977] report on residual stress calculations according to the finite element method for spot-welded joints made of mild

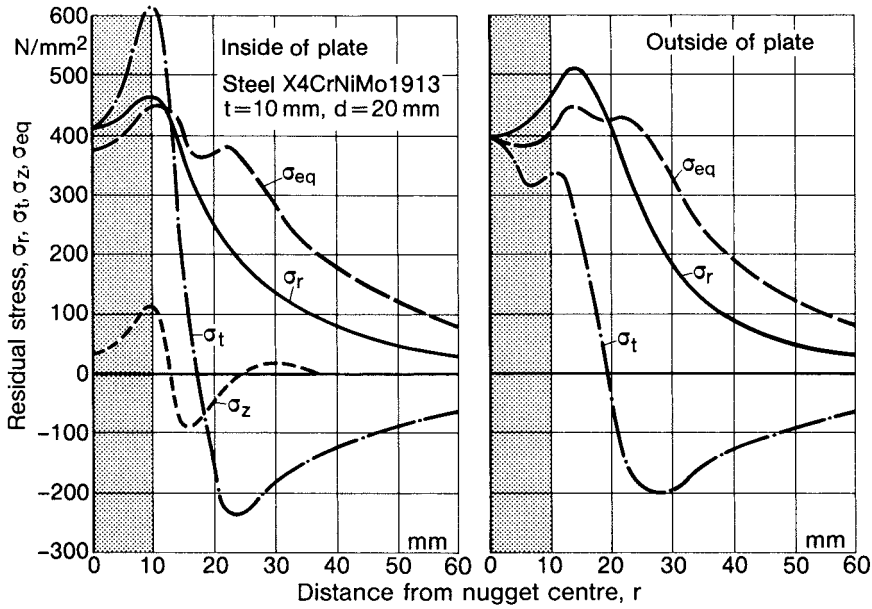


Fig. 11.21. Residual stress distribution at spot-welded joint at inside (a) and outside (b) of plate surface; stresses σ_r, σ_t, σ_z and σ_{eq} explained in the text; finite element results confirmed by measurement; after Schröder and Macherauch.[980]

and low-alloy steel with plate thicknesses between 3 and 8 mm. The investigation concentrates on the influence of welding time, welding current, postweld upset force and postweld upset time. The calculation result for plates made of mild low-carbon steel with variation of welding current and welding time ('hard' to 'soft' settings) but without postweld upsetting is shown in Fig. 11.22. The axial compressive residual stresses at the weld nugget edge at the inner plate surface are attributed to the temperature difference between the centre and the periphery of the weld nugget during cooling. Simultaneously, they exert a reducing effect on the radial and tangential residual stresses at the edge of the weld nugget. Obviously, the 'hard' process setting is particularly favourable with regard to this region which is at risk of fatigue cracking. Based on further calculations, favourable setting conditions for the post-weld upsetting process (especially the start and the end of the upsetting period) were determined. Since more detailed information on the applied finite element model is not provided in the evaluated publication, it is difficult to assess the quality of simulation and the accuracy of the results.

A well-conceived experimental (X-ray) residual stress investigation on spot welds in low-carbon steel was performed by Anastassiou *et al.*[947] The

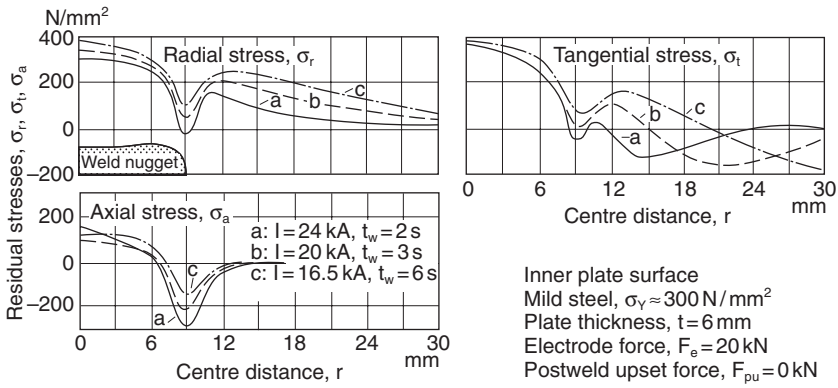


Fig. 11.22. Radial, axial and tangential residual stresses on inner plate surface of spot-welded joint between overlapping plates ($t = 6$ mm) made of mild steel ($\sigma_Y \approx 300$ N/mm^2); electrode force $F_e = 20$ kN; stress state after complete cooling down; results of finite element analysis; after Popkovskii and Berezienko.[977]

focus was on the influence of welding conditions on the fatigue resistance. Welding current, welding time, electrode force and post-heating were varied. Etched macrosections were evaluated with regard to the notch shape and notch size (see Fig. 11.3). The radial tensile residual stresses in the midplane of the sheets close to the weld spot edge were measured after electrochemical removal of corresponding layers. The stress redistribution induced by layer removal was not taken into account in a corrective manner, so that only relative statements are possible. The residual stresses were smallest after welding close to the stick limit and largest after welding close to the expulsion limit. They were substantially reduced after the expulsion occurred. Post-heating of the weld spot is another means of significantly reducing the residual stresses.

The residual stress analysis after Henrysson *et al.*[965] for a spot-welded specimen using a finite element model is emphasised because it is directed to the future needs of operational life assessment in automotive engineering (integrated calculation of welding residual stresses). The subject of the investigation is a resistance-spot-welded tensile-shear specimen.

The welding residual stress state is initially considered as axisymmetric and calculated in a circular plate with a diameter of 50 mm according to a ring element model. The basis of the temperature field calculation is the electrical potential field in the plates between the electrode faces. The formation of the contact surfaces is modelled using gap elements. Uncertain assumptions were introduced with regard to the contact resistances. The simulation results comprise the shape and dimensions of the weld nugget (identical with the fusion zone, diameter 5 mm) as well as of the

surrounding solid-phase pressure-welded zone (diameter 6 mm) at the edge of which the plates start to gape. The temperature field is also the basis of the microstructural changes in the heat-affected zone and of the yield limit increase (hardening) connected with the microstructural changes. All these data together form the basis of the residual stress calculation in which the pressing force between the electrodes, the transformation strain and the transformation plasticity are taken into account. The calculated residual stress values reach several hundred Newton per square millimetre. Stress maxima can be found on the outer plate surface in the weld spot centre, in the midplane of the plate at the outer edge of the heat-affected zone, at the edge of the electrode indentation (a notch effect) and at the edge of the joint face (also a notch effect). The radial residual stresses outside the weld spot do not drop steeply, unlike in calculations according to simpler models.

The calculated axisymmetric residual stress field was transferred to the solid element model of the spot-welded tensile-shear specimen, Fig. 11.23. This is performed in such a way that the Gauss points or mesh nodal points of the ring element model nearest to the corresponding points of the solid element model are picked up (the maximum distance is 0.05 mm) in order to transfer their state variables (stresses and displacements). As a result of

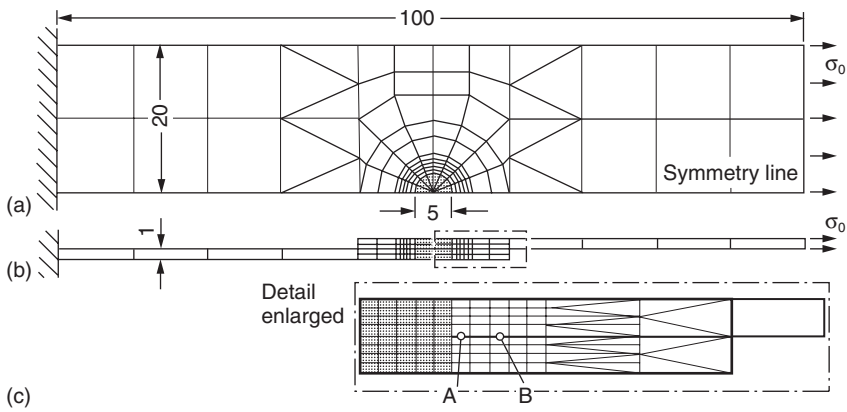


Fig. 11.23. Solid element model of resistance-spot-welded tensile-shear specimen subjected to a constant remote loading stress σ_0 (symmetry half) with transfer of the axisymmetric residual stress state established based on a ring element model; top view (a), longitudinal section (b) in the symmetry line and enlarged detail (c) with the reference point A in the heat-affected zone and the reference point B in the parent material; after Henrysson *et al.*[965]

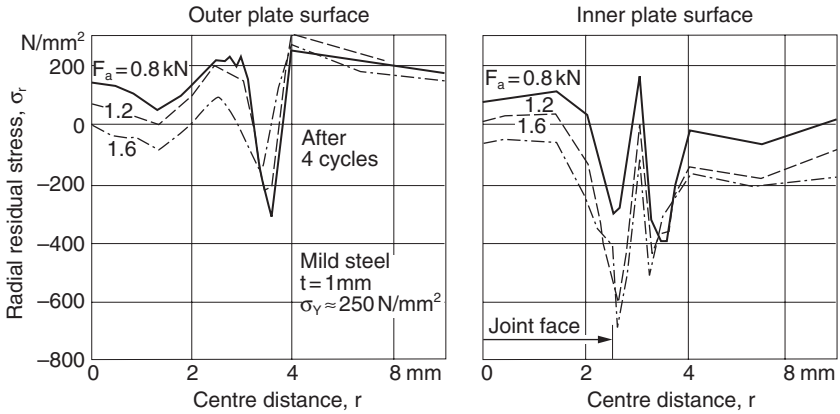


Fig. 11.24. Calculated radial residual stresses in the longitudinal centre section of a resistance-spot-welded tensile shear specimen (joint face diameter 5 mm) on the outer and inner plate surface after four loading cycles with load amplitudes F_a; after Henrysson *et al.*[965]

residual stress measurements at the weld spot in the tensile-shear specimen, it has been confirmed that rotational symmetry actually exists close to the weld spot. The axisymmetric residual stress and displacement states transferred from the circular plate model, particularly those at a greater distance from the weld spot, are nevertheless not completely compatible. However, compatibility is established by performing a calculation step with a zero loading increment, thus somewhat modifying the residual stress state at a greater distance from the weld spot. The calculated radial residual stresses in the longitudinal middle section of the specimen after four tensile-shear loading cycles with the load amplitude F_a are plotted in Fig. 11.24. Following the higher load amplitudes, the tensile residual stresses are reduced and the compressive residual stresses increased. The stress distribution following the lowest load amplitude F_a = 0.8 kN comes closest to the original residual stress.

11.2.7 Hardness distribution in spot-welded joints

The local fatigue strength expressed by endurable fatigue-effective notch stresses or strains is dependent on the local hardness of the material. Increased hardness correlates with higher resistance against crack initiation. It is recommended that the local hardness change at the crack initiation site be taken into account in the context of the notch stress or notch strain approaches. Hardness changes relative to the parent metal occur in the heat-affected zone and fusion zone dependent on the material

composition and the thermal cycles produced by welding. Typical examples are the local hardening of carbon steels and the local softening of hardened aluminium alloys.

The microstructural zones and the microhardness profile in spot-welded low-carbon deep-drawing sheet steel are presented in Fig. 11.25 (ideal geometrical conditions of gapless joints). The weld nugget (diameter d_N) with cast grain structure is surrounded by the heat-affected zone (diameter d_{HAZ}) which may extend up or down to the electrode indentation area (diameter d_E). The free slit faces end at an annular zone (outer diameter d_A) of solid phase pressure welding (Granjon[957]). The notch at the weld spot edge is located at the outer rim of this zone. The hardness profile is characterised by relatively high hardness in the weld nugget, a steep decrease in hardness in the heat-affected zone and a hardness peak at the edge of the weld nugget. This rough assessment already reveals three possible locations of failure: crack initiation outside the heat-affected zone in the unnotched plate with relatively low hardness and fatigue strength, crack initiation in the heat-affected zone at the point of the edge notch with increased (widely scattering) hardness levels and crack initiation at the edge of the weld nugget under strongly increased hardness and fatigue strength after the annular bonding face has torn open. The above considerations reveal that a notch stress, notch strain or stress intensity factor approach with the

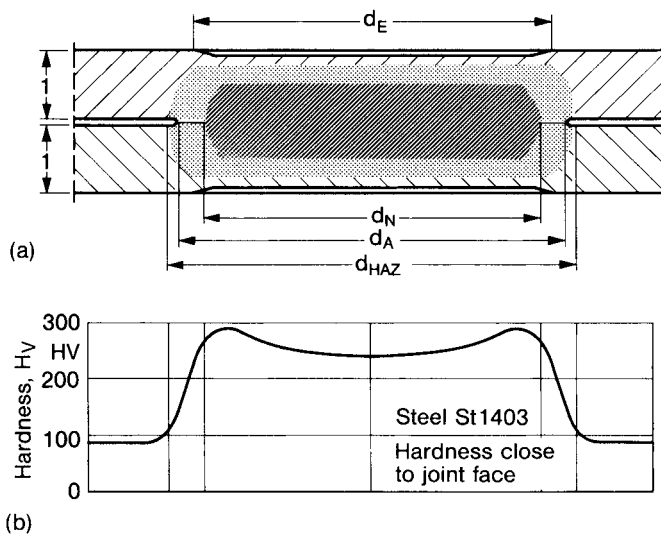


Fig. 11.25. Microstructural zones (a) and microhardness profile (b) after spot-welding of type St1403 low strength deep-drawing sheet steel ($\sigma_Y \approx 160\,N/mm^2$, $\sigma_U \approx 320\,N/mm^2$); diameters d_E, d_N, d_A and d_{HAZ} explained in the text; after Radaj.[4,284]

fatigue strength values of the non-hardened parent metal is likely to be conservative.

A typical distribution of hardness and yield limit in a spot-welded joint made of high-strength low-alloy steel, the former used for the purpose of nonlinear finite element modelling, is shown in Fig. 11.26.

The microstructural zones and the measured microhardness profile in a spot-welded aluminium alloy are shown in Fig. 11.27. The work-hardened alloy of type AlMgCu for deep-drawing sheet metal was under discussion in the Japanese automotive industry. Obviously, rather complex hardening and softening effects are observed both within the nugget and outside it in the heat-affected zone. The region HAZ 1 is characterised by softening, the region HAZ 2 by hardening, whereas the parent metal has a hardness of about 80 HV outside the diagram.

The hardness distribution in laser-beam-welded lap joints in steels or aluminium alloys can be estimated on the basis of Fig. 4.22 and Fig. 4.23 which refer to butt-welded joints.

Fatigue crack initiation in spot-welded joints made of steel may be shifted from the nugget edge to the outer boundary of the heat-affected zone especially in the low-cycle fatigue range, Fig. 11.28. The shift of the crack location can be explained on the basis of the hardness distribution at the weld spot. The increased hardness in the heat-affected zone reduces the plastic deformation at the nugget edge so that the maximum plastic strain occurs further outside. This has been demonstrated by Satoh *et al.*[834] by finite element modelling of the tensile-shear specimen with and without the hardening effect (i.e. with and without increased yield limit in the heat-affected zone). A coarse mesh of solid elements was used. It has also been shown experimentally by Satoh *et al.*[836] that the shifting effect is more pronounced in the case of spot-welded joints between coated steel sheets because of a wider heat-affected zone.

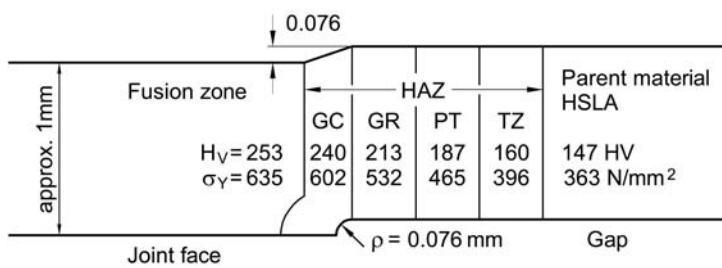


Fig. 11.26. Distribution of hardness H_V and yield limit σ_Y in spot-welded high-strength low-alloy (HSLA) steel for the purpose of finite element modelling; subzones of the heat-affected zone (HAZ): grain-coarsened zone (GC), grain-refined or recrystallised zone (GR), partially transformed zone (PT) and tempered zone (TZ); after Zuniga and Sheppard[994] and Pan.[972]

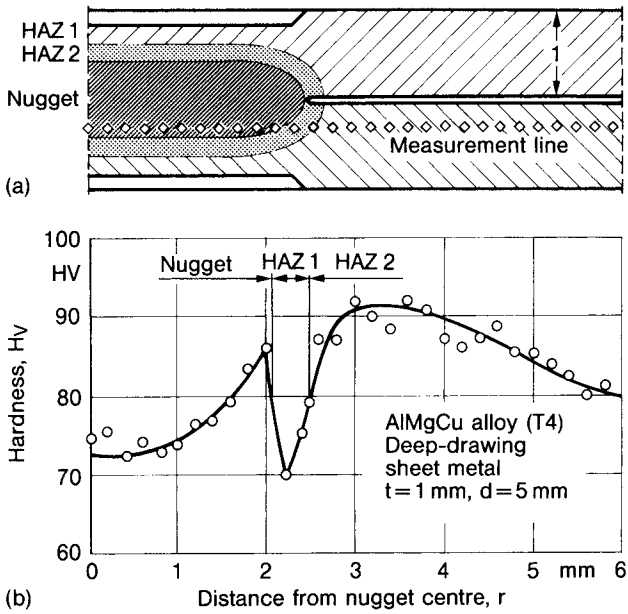


Fig. 11.27. Microstructural zones (a) with heat-affected zones HAZ1 and HAZ2 together with weld spot nugget, and measured microhardness profile (b) after spot-welding of AlMgCu alloy deep-drawing sheet metal presumably in the naturally aged condition (T4); after Nakaho *et al.*[969]

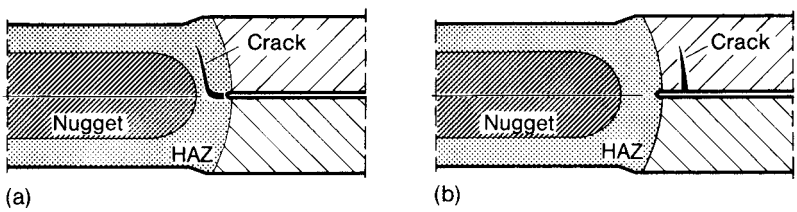


Fig. 11.28. Fatigue crack propagation in the heat-affected zone (HAZ) starting from the slit tip typical of high-cycle fatigue (a) and fatigue crack propagation outside the heat-affected zone (HAZ) starting from plain parent metal typical of low-cycle fatigue (b); after Satoh *et al.*[834]

11.3 Comprehensive modelling examples

11.3.1 General survey

In the following, further modelling examples related to the fatigue strength and life of spot-welded joints are presented based on Lawrence *et al.*,[967,990] Sheppard *et al.*[973–975,982–985] and Henrysson.[959–966] Other pioneering develop-

ments have already been reviewed in the preceding chapters. Attempts by Oh[801] and Kan[779] (spot-welded joints) as well as by Hsu and Albright[777] (laser-beam-welded joints) to use local stress-strain concepts are not yet convincing (see commentary by Radaj,[4] *ibid*. p. 332). The modelling examples described below can be characterised as being more comprehensive than other attempts. The notch stress and strain approaches describing crack initiation are originally or expressively combined with the crack propagation approach in order to determine the total life. The publications include noteworthy experimental work. The influence of a larger number of parameters (geometry, material, loading) is investigated. The section concludes with a noteworthy modelling example related to laser-beam-welded lap joints based on the crack propagation approach.

11.3.2 Modelling examples presented by Lawrence

The notch strain approach, early version according to Lawrence (see Sections 5.1.2 and 5.2.1), has successfully been applied to spot-welded joints in the form of the tensile-shear specimen, Fig. 11.29. The first investigation by Lawrence *et al.*[967] is directed to the crack initiation strength and life (a_i = 0.25 mm) neglecting further crack propagation through the thickness and across the width of the specimen. A parametric study has been performed covering the effects of geometry, mean stress, residual stress and material properties. The second investigation by Wang *et al.*[990] additionally takes crack propagation through the sheet thickness and across the specimen width into account. A parametric study of another, less general type concludes this analysis.

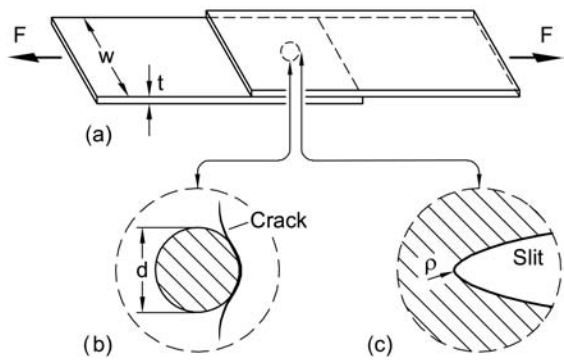


Fig. 11.29. Model of the tensile-shear specimen (a) with geometrical parameters and enlarged details: top view of sectioned weld spot nugget with crack (b) and side view of parabolic slit tip notch at weld spot edge (c); after Lawrence *et al.*[967]

The investigation first mentioned,[967] which is related to the high-cycle fatigue behaviour ($N = 10^7$ cycles), uses the simplified version of the notch strain approach based on the elastic portion of the strain S–N curve. The fatigue notch factor K_f is determined from the maximum tangential stress along the contour of the blunt crack (evaluating Creager's solution[860] with stress intensity factors K_I and K_{II} according to Pook's formulae). The worst-case notch radius at the blunt crack tip is assumed to be $\rho = a^*$ (with Peterson's constant a^* which depends on the ultimate tensile strength σ_U). The factor K_f is found dependent on ultimate tensile strength σ_U, specimen width w, nugget diameter d and sheet thickness t (based on eq. (11.1)). The value of σ_U is determined from microhardness measurements in the heat-affected zone. With K_f introduced into the formula for the elastic portion of the strain S–N curve (eq. (5.3)), the endurable load range ΔF is expressed dependent on the essential parameters, $\Delta F = f(w, t, d, \sigma_U, \sigma_{kr}, R, N_i)$.

The predicted effect of sheet thickness t, nugget diameter d, local residual stress σ_{kr}, load ratio R and ultimate tensile strength σ_U (in the heat-affected zone) on the endurable load range ΔF (at $N_i = 10^7$ cycles) for spot welds in type SAE 1006 low-carbon steel ($\sigma_Y \approx 225\,N/mm^2$) and type SAE 960X high-strength low-alloy (HSLA) steel ($\sigma_Y = 400\,N/mm^2$) are shown in Fig. 11.30. The endurable load increases both with sheet thickness, Fig. 11.30(a), and nugget diameter, Fig. 11.30(b), but the effect of diameter is stronger than that of thickness. The endurable load is highly dependent on the stress ratio R, Fig. 11.30(d). The influence of material strength is small in all three cases, Fig. 11.30(a, b, d), whereas local residual stresses exert a great influence, Fig. 11.30(c). The dark points designate the two steels being considered with the local residual stress either at zero (stress-relieved) or at the tensile or compressive yield limit of the parent metal. The arrow-marked gradients designate the transition from the low-carbon to the high strength steel. Note that the high strength steel in the as-welded condition exhibits a lower load-carrying capacity than the low-carbon steel (with $\sigma_{kr} = \sigma_Y$ in both cases).

The spot-welded tensile-shear specimen has been further investigated in respect of crack propagation in the investigation mentioned second.[990] Other high-strength low-alloy steels (B60XK G-90 and SAE 960X) and another low-carbon steel (DQSK G-90) are used in this investigation. The fatigue properties of the materials are approximated on the basis of hardness measurements in the heat-affected zone. The residual stress at the notch root, σ_{kr}, is assumed to be equal to the parent metal yield strength ($\sigma_{kr} = +\sigma_Y$ in the as-welded condition and $\sigma_{kr} = -\sigma_Y$ with prior overloading or in the coined condition).

The total fatigue life is subdivided into the stages of crack initiation, crack propagation through the sheet thickness and crack propagation across the specimen width (see eq. (11.17)). The crack initiation life is determined

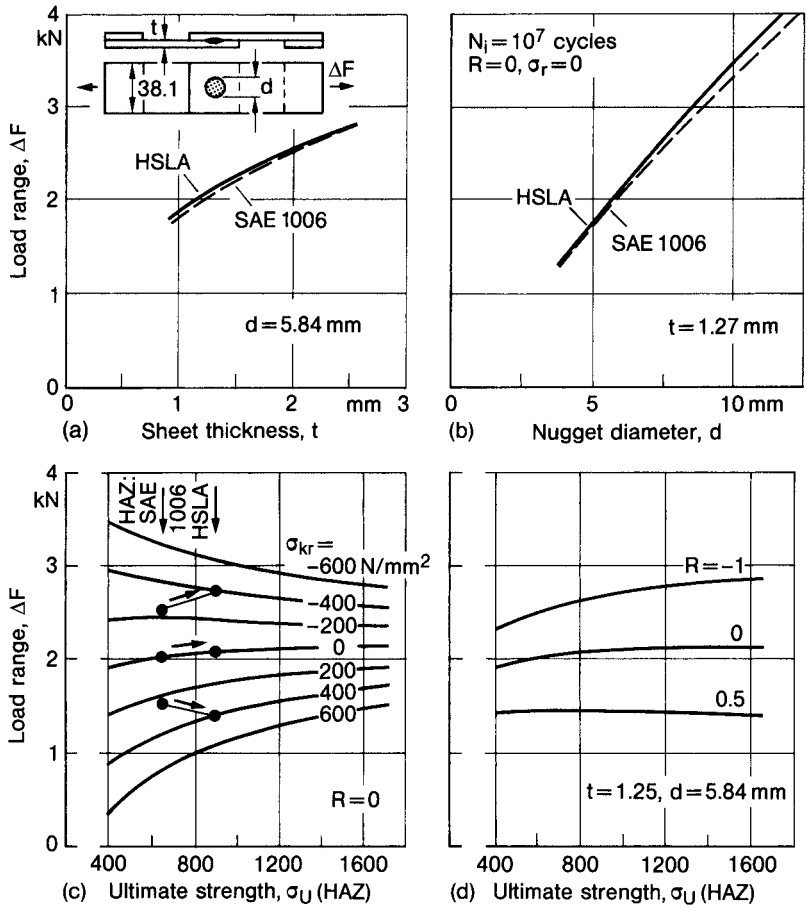


Fig. 11.30. Predicted fatigue strength (crack initiation, $a_i = 0.25$ mm, $N_i = 10^7$ cycles) of a tensile-shear specimen made of low-carbon steel (SAE1006, $\sigma_Y = 225\,N/mm^2$) or high-strength low-alloy (HSLA) steel (SAE960X, $\sigma_Y = 400\,N/mm^2$) dependent on sheet thicknesst t, nugget diameter d, notch root residual stress σ_{kr}, load ratio R and ultimate tensile strength σ_U in the heat-affected zone (HAZ); after Lawrence *et al.*[976]

according to the procedure described above (elastic notch strain approach) supplemented by Neuber's macrostructural support formula covering elastic-plastic deformation at the notch root in the set-up loading cycle.

Crack propagation through the thickness starts with the initial crack depth $a_i = 0.25$ mm covered by the crack initiation analysis and ends with a through-thickness crack of about nugget diameter size. The initial crack is assumed to be semi-elliptical with a length-to-depth ratio, $2c/a = 5.0$. The

geometric correction factors which define the relevant stress intensity factor comprise evaluations of fatigue crack growth in the specimens (substituting a more extensive finite element analysis) and factors from the literature describing the effect of the front and back surfaces as well as of the specimen width.

Crack propagation across the specimen width starts with an initial crack length equal to the nugget diameter covered by the through-thickness propagation analysis and ends with a crack length equal to the specimen width. The stress intensity factor is derived from a comparable plate model of a crack emanating from a small hole which is loaded by a concentrated force normal to the crack at the hole edge, equilibrated by a distributed force at the remote plate edge. This 'rivet hole crack problem' is comparable because the force flow concentrates similarly at the rivet hole and at the weld spot. The hole diameter is assumed to be small relative to the crack length. The stress intensity factor is derived dependent on crack length using linear superposition of two simple load cases for which theoretical solutions are available, Fig. 11.31. The bending stresses are superimposed to the membrane stresses when calculating the stress intensity factors. This approximation is open to objection because the crack propagation behaviour under membrane and bending stresses, respectively, is different.

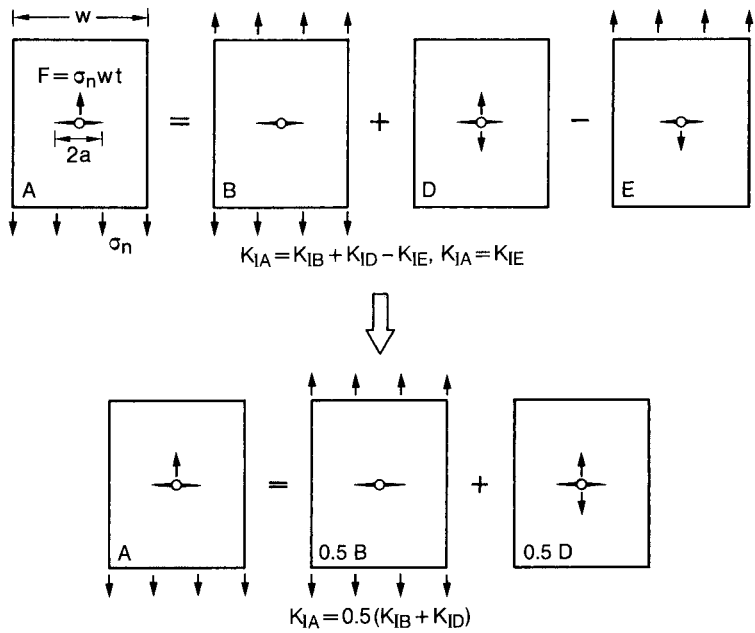


Fig. 11.31. Stress intensity factor of a rivet hole crack derived by linear superposition of simple load cases for which theoretical solutions are available; after Broek.[429]

Parametric studies have been performed predicting the effect on fatigue life of the ratios of specimen width to nugget diameter (w/d), Fig. 11.32, sheet thickness to specimen width (t/w) and nugget diameter to sheet thickness (d/t). It is shown that the ultimate tensile strength in the heat-affected zone has only a minor influence on the results. The predicted fatigue lives have been cross-checked by the results of fatigue testing.

The conclusion from the investigation is that the crack initiation portion of the fatigue life is predominant in the case of a small specimen width, whereas crack propagation through the thickness and across the width prevails for larger design-typical widths.

The investigations by Lawrence *et al.*[967] were carried on by McMahon *et al.*[968] with focus on crack propagation measurements in comparison with several analytical model variants for predicting the fatigue life of spot-welded tensile-shear specimens. The model variants are defined within the framework of the notch strain and crack propagation approach described above.

Fatigue crack initiation and propagation in spot-welded tensile-shear specimens made of galvanised high-strength low-alloy steel of type SAE 960X (sheet thickness 1.4 mm) were studied by sectioning companion specimens, as well as by replicating the exposed site of crack initiation in a pre-sectioned weld spot, Fig. 11.33. Constant-amplitude tests ($R = 0$ and $R = -1$),

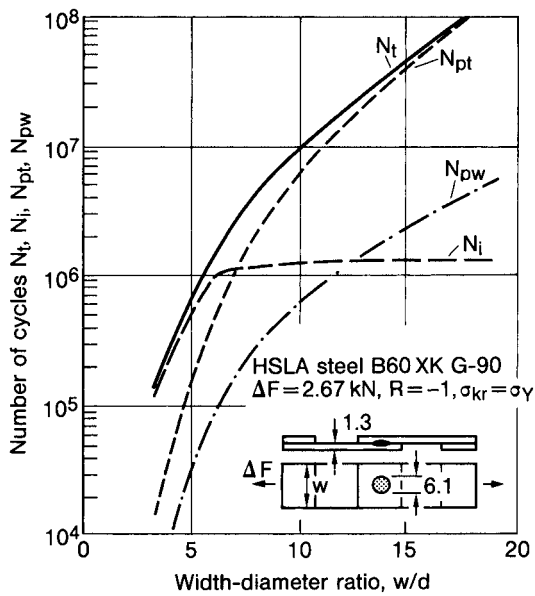


Fig. 11.32. Fatigue life of spot-welded specimen in as-welded condition dependent on specimen width w: total life N_t, crack initiation life N_i with $a_i = 0.25$ mm, through-thickness propagation life N_{pt} and across-width propagation life N_{pw}; after Yung and Lawrence.[407]

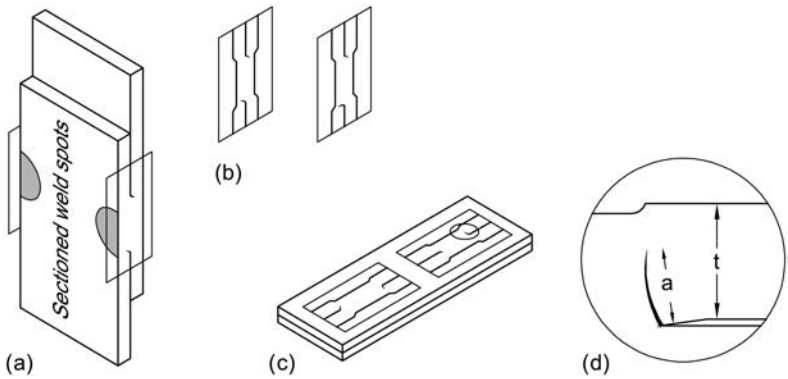


Fig. 11.33. Presectioning method for monitoring fatigue crack growth: replicas made of exposed surfaces with the specimen under load (a); replicas stripped (b); replicas mounted between glass slides (c); observation of crack length using transmitted light microscopy (d); after McMahon *et al.*[968]

as well as variable-amplitude tests were performed on weld spots in the as-welded condition and on weld spots treated by post-weld coining.

Approximately 50% of the total fatigue life was devoted to developing a crack of 0.25 mm depth under constant-amplitude loading in the life range 10^4–10^6 cycles. At lives greater than 10^6 cycles, this percentage appeared to increase. Similar results were found under variable-amplitude loading, although in this case only 40% of the life was devoted to developing a crack of 0.25 mm depth. Post-weld coining increased the fatigue life by over an order of magnitude.

The investigations were resumed by Swellam *et al.*[988] using the electric potential drop technique for sensing the depth of the fatigue cracks. The resistivity measurement probe was located at the electrode indentation edge opposite to the crack initiation site. Calibration on crack depth was possible for $a_i \geq 0.18$ mm with plate thicknesses $0.89 \leq t \leq 2.72$ mm.

The strength of the models proposed by Lawrence *et al.*[967] and Wang *et al.*[990] is that the initiation and propagation phases of the fatigue crack are separated, that the local stress condition inclusive of residual stresses is taken into account and that the actual local material constants are used as the basis. Shortcomings are a too large crack initiation depth (relative to the notch radius), the inaccuracy of Pook's stress intensity factor solution and an exponent $m = 5$ applied in the Paris equation instead of $m = 3$.

11.3.3 Modelling examples presented by Sheppard

The models proposed by Sheppard and Pan[972–975,982–985] comprise various approaches, applied not only to tensile-shear specimens, but also to cross-

tension and peel-tension specimens with the aim of providing a method applicable to spot-welded structural parts in general. In all the approaches, the structural stress analysis performed using the finite element method is basic. The procedural steps remain within the framework of the approach proposed by Lawrence *et al.*,[967] but the details are further developed.

The notch strain approach of Pan and Sheppard[972,973] for determining the crack initiation life ($a_i = 0.25$ mm) combines the maximum structural stress range, $\Delta\sigma_s$, with a uniform fatigue notch factor K_f, estimated on the basis of Neuber's notch stress theory and Neuber's macrostructural support formula. The hardness increase in the heat-affected zone and the estimated local residual stresses are taken into account. The crack initiation phase turned out to be only a minor part of the estimated total life (6–26%) at $N = 10^6$ cycles in high-strength low-alloy steel. The progress achieved by the above contribution is the derivation of the maximum structural stress at the weld spot edge on the basis of the nodal point forces in coarse finite element mesh designs where the weld spot is represented by a single bar between the overlapping plates (see Section 9.2.2).

The crack propagation approach of Sheppard and Strange[982,985] for the determination of the through-thickness crack propagation life combines the maximum structural stress range, $\Delta\sigma_s$, with linear-elastic fracture mechanics. The following assumptions are introduced:

- The crack propagation described by using the Paris or Forman equation, respectively, provides the basis for the relationship between structural stress and propagation life, i.e. the notch stress at the slit tip is not considered explicitly.
- Crack propagation is controlled by the mode I loading component.
- The crack propagates through the plate thickness, i.e. not through the joint face.
- The semi-elliptical crack propagates normal to the inner plate surface with an aspect ratio $0.33 \le a/c \le 1.0$.
- The crack length, a_i, at which crack initiation ends and crack propagation begins, is equal to the grain size in the heat-affected zone, i.e. about 20 μm that is much less than the plate thickness, t.
- No crack closure effects are considered in welds in the as-welded, stress-relieved or prestressed condition.
- The fracture toughness, K_c, is much higher than the applied stress intensity factor range, ΔK_I.
- Crack initiation and early growth (up to 20 μm) represent a small fraction of the life up to a through-thickness crack (considered as total life) and can therefore be neglected.

The result of the above crack propagation approach is a linear relationship on the logarithmic scale between the structural stress range and the

crack propagation life. The analysis results show acceptable correspondence with several experimental results.

A more comprehensive evaluation by Sheppard[983] for various specimens introduces structure-related 'material constants' of crack propagation which deviate from the parent material values, e.g. $m = 2.42$ or 3.56 instead of $m = 3.0$. The deviations can be put down to the fact that the notch effect of the slit tip is not considered and the peculiarities of short-crack behaviour are not taken into account. The structural-stress-related crack propagation approach described above was further extended and validated by Pan:[972]

- The structural stress analysis by the finite element method for various specimens takes large deflections into account (geometrically nonlinear model).
- Unequal thickness joints ($t = 0.91$–1.5 mm) are included.
- Dissimilar material joints are included (low strength steel sheets spot-welded to high-strength low-alloy sheets).
- Non-zero load ratios are included ($R = -1, 0, 0.5$).
- Variable-amplitude loading is included in order to test the applicability of Miner's rule combined with rainflow cycle counting and mean-stress-corrected structural stress amplitudes.
- The heat-affected zone is subdivided in subzones with material constants related to the hardness increase.
- The elastic-plastic notch strain analysis is applied using a small-size notch at the slit tip ($\rho = 0.076$ mm).
- The stress intensity factors for semi-elliptical curved surface cracks at the weld spot edge are determined by the finite element method and, in comparison, by the Newman–Raju relationship (for crack depth $a \geq 0.25$ mm).
- The validation of the analysis results from the structural stress approach is based on fatigue test results with various specimens made of low-carbon steel and high-strength low-alloy steel.

These investigations consolidate and generalise the structural-stress-related crack propagation approach, but the shortcomings mentioned above are not removed. There is no progress with regard to the initial short-crack behaviour in the narrow notch stress zone at the slit tip. But there is the innovative suggestion to use the principal strain range, $\Delta\varepsilon_{k1}$, at the small-size notch representing the slit tip for characterising the fatigue strength and life of various specimens with equal and unequal sheet thicknesses, Fig. 11.34. The notch strain ranges are determined by elastic-plastic finite element analysis. In contrast to this, the corresponding structural stress ranges do not collapse to a uniform S–N curve.

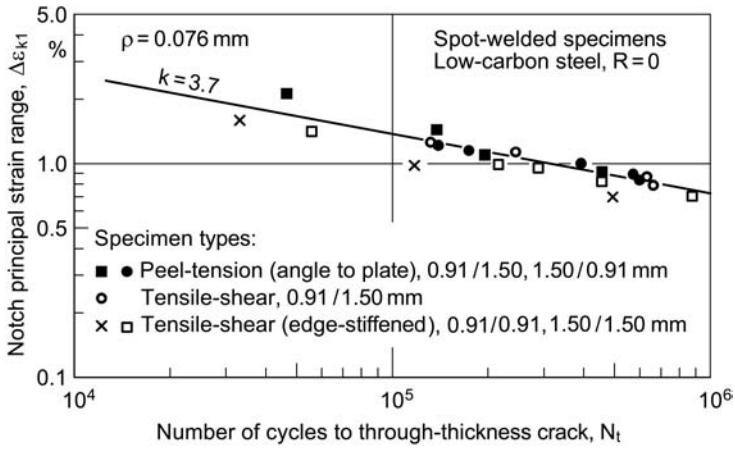


Fig. 11.34. Fatigue test results forming a uniform notch strain *S–N* curve; various spot-welded specimens in low-carbon steel; combinations of equal and unequal plate thicknesses; after Pan and Sheppard.[973]

Another remarkable result of Pan's investigation are curves of K_{eq} versus crack depth which remain related to tensile K_I values in the case of tensile-shear specimens, whereas a change to compressive K_I values occurs at large crack depths in the case of peel-tension specimens. This may explain part of the higher fatigue strength of the peel-tension specimens (in terms of the initial ΔK_{eq} value) by crack retardation, but the main reason is that different initial crack paths are followed in tensile-shear and peel-tension loading (Henrysson[959]).

11.3.4 Modelling examples presented by Henrysson

The models proposed by Henrysson[959–966] comprise the (elastic-plastic) notch strain approach and the (elastic) crack propagation approach, but these are considered as concurrent methods in the case of crack initiation ($a_i = 0.1$ mm) or restricted to only the second method in the case of through-thickness cracks. Typically, one of Henrysson's publications[966] is subtitled 'Fracture mechanics or strain life approach?' Important aspects of the problem are separately addressed, such as residual stresses, crack propagation paths, influence of mean stress or crack closure on fatigue and procedures for determining damage accumulation under variable-amplitude loading. The aforementioned contributions are reviewed in the following.

First, the elastic-plastic notch strain approach is applied by Henrysson *et al.*[965] to the tensile-shear specimen, taking its residual stresses (see

Figs. 11.23 and 11.24) into account. The stress–strain cycles at reference point A (heat-affected zone, joint face edge) and at reference point B (parent material, edge of the heat-affected zone) determined for the solid element model of the tensile-shear specimen (joint face diameters of 5 and 6 mm, respectively) subjected to tensile-shear loading with residual stresses are plotted in Fig. 11.35. Based on the stress–strain cycles above, the values of the damage parameter P_{SWT} proposed by Smith–Watson–Topper are derived. The specimen life up to crack initiation follows from two damage parameter *S–N* curves derived from published data for parent material and heat-affected zone. The use of the radial stresses and strains in the equation of the damage parameter is justified by the dominance of these quantities in the crack initiation process at the edge of the weld spot. Crack initiation is possible at both reference points. According to experience, crack initiation at the notch of the joint face edge is dominant in the high-cycle fatigue range. In contrast, the incipient cracks originate from the outer edge of the heat-affected zone in the parent material in the low-cycle fatigue range. This is qualitatively confirmed by the above analysis, but the quantitative correspondence between calculated life related to crack initiation ($a_i = 0.1$ mm) and measured total life related to a through-thickness crack is unsatisfactory.

The subsequent application of the notch strain approach by Henrysson *et al.*[966] is further substantiated with regard to several details, which are partly depicted in Fig. 11.36:

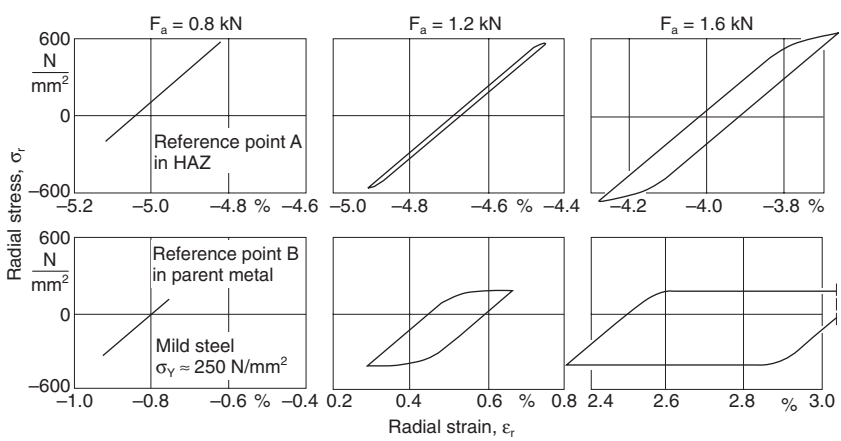


Fig. 11.35. Calculated stress–strain cycles resulting from load amplitudes F_a at reference points A (heat-affected zone) and B (parent metal) in the longitudinal centre section of a resistance-spot-welded tensile-shear specimen (joint face diameter 5 mm) with welding residual stresses; after Henrysson *et al.*[965] (redrawn from a partially unclear copy).

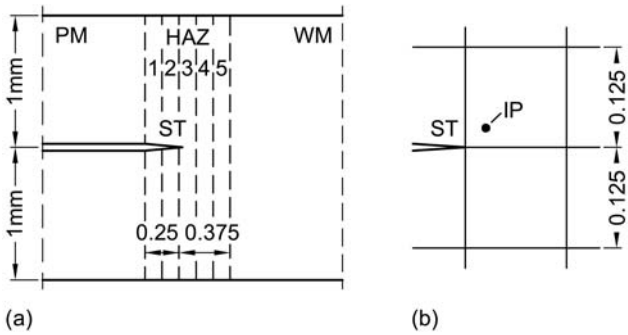


Fig. 11.36. Cross-sectional model (a) of the weld spot edge area with five element groups in the heat-affected zone (HAZ) between parent metal (PM) and weld metal (WM) as well as finite element mesh (b) at the slit tip (ST) with Gaussian integration point (IP); after Henrysson *et al.*[966]

– finer subdivision of the mesh,
– advanced nonlinear kinematic hardening model,
– cyclic material properties derived from measured microhardness,
– heat-affected zone subdivided into five element groups with different hardness-related material properties,
– reference strain range $\Delta\varepsilon_1$ (first principal strain) taken from the Gaussian integration point closest to the slit tip (distance approx. 0.03 mm).

Mean stress effects and residual stresses, on the other hand, are neglected. The relative correspondence between calculated life related to crack initiation ($a_i = 0.1$ mm) and measured total life related to a through-thickness crack is once more unsatisfactory. This is not surprising, as $\Delta\varepsilon_1$ depends on the applied mesh size and does not reflect the crack initiation angle.

The crack propagation approach based on structural stresses from thin-shell element models with coarse meshes (element size at the weld spot approximately twice the weld spot diameter) and stiff beam elements simulating the weld spot joint is applied by Henrysson[960] with the following peculiarities:

– The nodal point forces (inclusive of moments) of the shell elements at the weld spot beam are used as the basis for structural stress calculation instead of the nodal point forces of the beam element. The 'eigenforces' are thus included.
– The radial structural stresses at the crack initiation site of the weld spot edge are determined from the aforementioned forces using the model of a circular rigid core (simple formulae, see Section 9.2.6). The factor $\lambda = 2.5$ is applied to the membrane stress in tensile-shear loading in

order to collapse the *S–N* curve data for tensile-shear and peel-tension loading.

– The stress intensity factor ranges, ΔK_I and ΔK_{II}, are determined from the aforementioned structural stresses using Radaj's simple formulae (see Section 10.2.2). Eigenforce effects are included to the extent of the separated nodal point forces above. The equivalent stress intensity factor K_{eq} is derived in accordance with Erdogan and Sih's maximum tangential stress criterion.
– The endurable values of ΔK_{eq} are derived from fatigue testing of tensile-shear and peel-tension specimens resulting in a linear relationship of ΔK_{eq} versus N/t on the logarithmic scale. Alternatively the Paris equation is integrated with insertion of ΔK_{eq} (substituting ΔK_I) together with the material-related crack propagation constants. The assumption of a constant value ΔK_{eq} causing a constant crack propagation rate, da/dN, is introduced. The resulting relationship has the form $t/N = C(\Delta K_{eq})^m$ (see eq. (11.22) with $R = 0$).

Again, the effects of mean stress and residual stress are neglected. The difference in level of the *K–N* curves for tensile-shear and peel-tension loading is explained by different crack paths and rates of crack propagation in the two loading cases considered. The crack path follows the joint face initially in peel-tension loading, exhibiting an approximately constant propagation rate. It traverses the plate thickness from the beginning in tensile-shear loading with a rising stress intensity factor and propagation rate (in contrast to the findings of Cooper and Smith[859]). The different crack paths are depicted in Fig. 10.19. The slight differences in the slope of the *K–N* curves are reduced by using strain intensity factors, $\Delta K_{\varepsilon eq}$, instead of stress intensity factors, ΔK_{eq}, the former derived from the principal strain $\Delta\varepsilon_1$ in the Gaussian integration point close to the slit tip.

The described crack propagation approach based on coarse meshes has been applied to various specimens and load cases, Fig. 11.37, in order to validate the method. The solid curve ($k = 4.19$) in Fig. 11.38 represents the result of the calculation fitted to the experimental data for low-carbon steel. These data appear as point symbols in the diagram. The dashed curves limit the scatter in fatigue life by $T_N = 1/9$ or in endurable stress by $T_\sigma = 1/1.7$. The scatter band achieved by the above method is substantially smaller in comparison to evaluations by Rupp (Fig. 9.31) or Maddox (Fig. 9.36) on the basis of the structural stress approach.

The crack propagation approach has also been used by Henrysson *et al.*[966] to determine the crack initiation life ($a_i = 0.1$ mm) in order to compare the results with those from the notch strain approach. Higher accuracy is achieved by substituting the coarse-mesh beam-to-shell model by a fine-

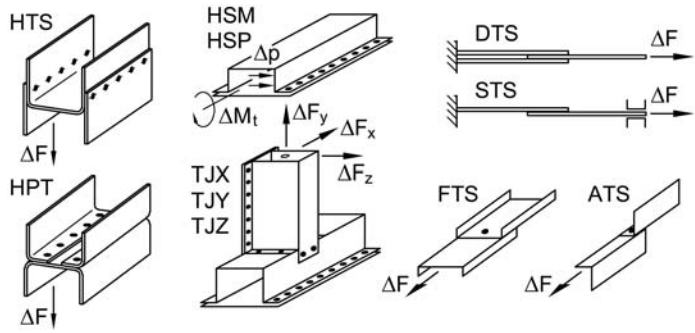


Fig. 11.37. Spot-welded specimens and loading conditions analysed by Henrysson:[960] H-shaped specimen under tensile-shear and peel-tension force (HTS, HPT), hat section under torsional moment and internal pressure (HSM, HSP), T-joint under forces in *x*, *y*, *z* directions (TJX, TJY, TJZ), double-face and single-face tensile-shear specimens (DTS, STS), flanged and angled tensile-shear specimens (FTS, ATS).

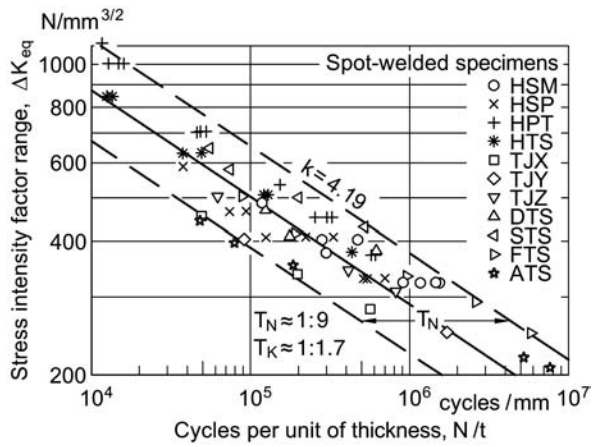


Fig. 11.38. Fatigue life of various spot-welded specimens (depicted in Fig. 11.37); evaluation based on calculated stress intensity factors merged into the formalism of the crack propagation approach (solid line) and scatter band (dashed lines); after Henrysson.[960]

mesh solid element model with the stress intensity factor determined from quarter-point singular elements.

Another modification of the described crack propagation approach has been applied by Henrysson[962] when determining the effect of mean stress and crack closure on fatigue strength. The weld spot is modelled by a rigid core within a fine mesh of shell elements. The stress intensity factors were derived from the (linearised) structural stresses at the crack initiation site using Radaj's simple formulae together with the corrections mentioned

above related to the membrane stresses and eigenforces. A comparison of the predicted and measured fatigue life of spot welds is shown in Fig. 11.39. The prediction based on the crack propagation approach uses material constants given by Verreman *et al*.[651] The predicted curve constitutes a lower limit to the experimental results which might be too large by an estimated factor of 1.2 on endurable cycles. This has to be taken into account when comparing the results with Yuuki's too small values (see Fig. 10.18). The relatively large differences are thus explained.

The investigations by Henrysson[964] cumulate in a new method for determining the fatigue life of spot-welded specimens and structural parts subjected to variable-amplitude loading. The idea behind the method is that stresses for which the fatigue crack remains closed, do not cause damage or crack growth. The method based on the concept of crack closure (see Section 11.2.5) is carried out as follows:

- calculation of the K_{eq} history at the crack initiation site of the weld spot edge using the finite element method (coarse beam-to-shell element model or finer rigid-core-in-shell model) in combination with Radaj's simple stress intensity factor formulae,
- determination of K_{op} from K_{max} and K_{min} in the K history based on a proven mean stress correction,
- calculation of the closure-free K history suppressing $K < K_{op}$ in the original K history,

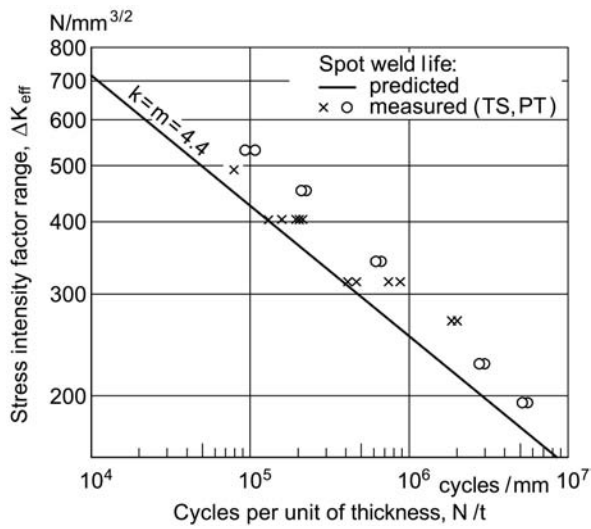


Fig. 11.39. Predicted and measured life of spot welds under tensile-shear (TS) and peel-tension (PT) loading with crack closure taken into account; after Henrysson.[963]

- rainflow count of the closure-free K history, i.e. the (effective) K_{eff} history,
- calculation of damage using Miner's damage accumulation rule (D = 1.0) together with the ΔK_{eff}–N curve for the considered spot welds (linearly extended to the below threshold range).

A comparison of the fatigue life of tensile-shear and peel-tension specimens under various load histories, determined experimentally and by the above calculation procedure showed acceptable correspondence. The experimental results were up to a factor of three larger than the calculated life as demanded in practice.

The prediction of life in the low cycle fatigue range of spot welds under constant- and variable-amplitude loading was addressed by Henrysson in cooperation with other authors (Fermér *et al.*[955]). Three different procedural variants for calculating damage according to Miner's damage accumulation rule on the basis of the F–N curves for displacement-controlled tensile-shear and peel-tension-loaded H-shaped multi-spot specimens, respectively, were applied to a Gaussian distribution of load signals with and without occasional overloads simulating misuse events:

- Damage calculation using directly measured 'elastic-plastic' force signals (originating from elastic-plastic structural behaviour) and the 'elastic-plastic' F–N curve of the specimen. This corresponds to using suitable stresses, strains or stress intensity factors from a nonlinear finite element analysis together with an 'elastic-plastic' S–N curve. This method yields non-conservative results.
- Damage calculation using indirectly measured 'elastic' force signals (taken as component stiffness multiplied by the measured component deformation) and the 'elastic-plastic' F–N curve of the specimen. This corresponds to using stresses or stress intensity factors from a linear finite element analysis together with an 'elastic-plastic' S–N curve. This method which is commonly used in the automotive industry yields too conservative results.
- Damage calculation using the measured 'elastic' force signals (described above) and the 'elastic' F–N curve of the specimen (established using specimen stiffness multiplied by the measured specimen deformation). This corresponds to using linear finite element analysis together with an elastic S–N curve. This method yields the most accurate results.

The investigations reviewed by Henrysson into the notch strain approach on the one hand and the crack propagation approach on the other show a broad spectrum of application-relevant results, well suited to a more accurate prediction of the fatigue life of spot welds. A shortcoming is the lack of a combination of the two methods in order to determine the total life.

Neglect of the crack initiation phase may often be justifiable, but not always. Important influence parameters may be lost in the crack propagation approach described above, e.g. the residual stresses. Short crack initiation and early growth is still a field where further effort is needed in method development.

11.3.5 Modelling example presented by Nykänen

The investigation by Nykänen[971] into the fatigue strength of laser-beam-welded lap joints subjected to tensile-shear loading uses the crack propagation approach. It is mainly based on theoretical derivations, but the results are checked against experimental data available at that time. A plane strain finite element model was used to determine the stress intensity factors K_I and K_{II} by the virtual crack extension method combined with quarter-point crack tip elements, starting with the crack-like slit tip under mixed-mode loading and proceeding with increasing crack lengths under pure mode I loading. The crack path was determined according to the maximum tangential stress criterion.

The variables were as follows: crack length, a, plate thicknesses, t and T, and weld width at the slit face, w_s. These are expressed in terms of a/T, t/T and w_s/T. Integrating the Paris equation following the crack path up to approximately the thickness of the thinner plate (note that the upper limit of the crack propagation integral evaluated by Nykänen,[971] *ibid*. eq. (13), is

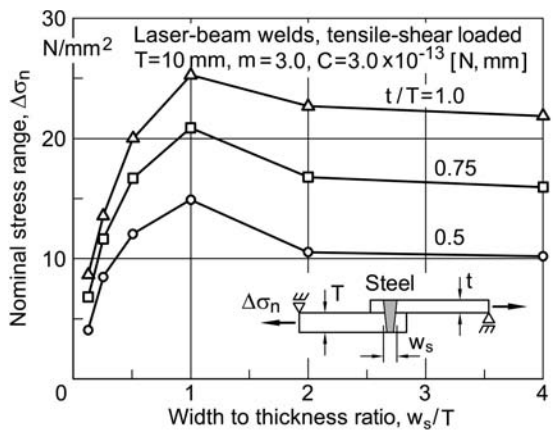


Fig. 11.40. Permissible nominal stress range $\Delta\sigma_n$ (97.7% survival limit) dependent on seam width to plate thickness ratio w_s/T, for laser-beam-welded tensile-shear loaded lap joints in steel; results of numerical analysis according to the crack propagation approach; after Nykänen.[971]

t/T instead of 1) results in endurable and permissible nominal stress ranges in the thinner or thicker plate, respectively, with material constants $m = 3.0$ and $C = 1.7 \times 10^{-13}$ [N, mm] (endurable mean value) or $C = 3.0 \times 10^{-13}$ [N, mm] (permissible value, 97.7% survival limit). Analysis results for $\Delta\sigma_n$ relating to $T = 10$ mm are plotted in Fig. 11.40. The corresponding permissible nominal stress range in the thinner plate, $\Delta\sigma_n T/t$, is only slightly influenced by the thickness ratio. The highest fatigue strength corresponds to approximately $w_s/T = 1.0$. The w_s/T value should be greater than 0.5 in order to avoid a strength reduction below the constant value for larger weld widths.

12

Significance, limitations and potential of local approaches

12.1 Significance of local approaches

The prediction of fatigue strength and service life of welded joints is an ambitious task for which global and local approaches are available. The global approaches which comprise resultant force and nominal stress approaches have found their way into the national and international design codes. They are generally recognised and under permanent further discussion and amendment. The local approaches which comprise structural stress, notch stress and strain, crack propagation and stress intensity approaches are less suited to standardisation as will be shown further below. However, they are all the more important for the design development in industry in respect of satisfactory reliability, higher strength and longer life.

Local versus global approaches

Some authors consider the global approach, especially the widespread nominal stress approach to be superior to local approaches in respect of 'robustness' achieved by formal simplicity and statistical validation (e.g. Graf and Zenner[995]). But formal simplicity and statistical validation are bound to the condition that the fatigue-loaded structural member and the relevant test specimens correspond in respect of all essential influencing parameters, the nominal stress definition and the stress concentration factor among them. Considering the multitude of parameters which have an influence on the fatigue strength or service life of structural components such a correspondence is rather the exception than the rule. Any deviation between structural member and test specimen, including loading and environmental conditions, must be assessed without statistical proof. The local approach is the most important means of doing this in a well-founded manner (e.g. by the notch or detail class assignment based on the local approach). Therefore, the local approach is indispensable at least as a supplement to the global approach if structural member and test

specimen differ in respect of individual parameters which is generally the case.

Additionally, the local approach is important as a means of assessing strength and life without reference to the global approach. This must take place if global approach data are not available (e.g. in cases of unconventional design and service conditions, or in cases of new materials and welding processes) or if nominal stresses cannot be meaningfully defined. It is noteworthy that the design engineer primarily needs relative statements. The question is put forward very often what fatigue strength or service life can be expected with a definite new design variant in relation to a well-proven former design. The local approach offers an essential aid for answering such questions. The tendency or sensitivity of the resulting parameters to variations of the input parameters is often a sufficient basis for decisions thus avoiding more problematic absolute statements.

The discussion above is a little bit unrealistic with regard to the statistical validation of the design *S–N* curves. There are indeed statistically evaluated fatigue test results behind these curves, but the results from the test series of different investigators and laboratories do not coincide. And, most important, the commissions responsible for the standardisation of design *S–N* curves decide to the best of their scientific knowledge, but non-scientific arguments are also taken into account, e.g. utmost simplification, foolproof specification, adjustment to earlier and other standards. Therefore, the global approach based on design *S–N* curves is often no more than a first guideline for dimensioning, from which further design improvement based on local approaches may originate.

Degree of local concern

Different views exist between experts as to the degree of detail to which the local situation has to be taken into account within the assessment procedure, either based on structural stresses alone or additionally on notch stresses and strains or even comprising crack propagation. No general answer is possible because the circumstances of the individual case determine which approach is chosen. A structural stress analysis is generally required because most local parameters such as notch stresses and stress intensity factors are based on structural stresses. But this does not mean that the structural stress approach can be brought to a conclusion because endurable stress values may be missing. Taking the step from the structural stress analysis to the notch stress and notch strain approach and possibly further to the stress intensity and crack propagation approach is justified especially if the local geometric notch parameters are well defined or if the scatter of these parameters can be passed over by a worst case consideration.

12.2 Limitations of local approaches

There are many problems connected with the application of the local approaches, both cursory ones which can be overcome in due time and more profound ones which need long-term research to be solved and must be passed by intelligently at present. The typical problems are reviewed below together with proposed measures to overcome the problems.

Definition of influencing parameters

A realistic assessment of fatigue strength and service life is bound to the condition that the decisive influencing parameters are well defined. At least part of this information is generally uncertain, especially the information referring to environmental effects (e.g. variable-amplitude loading, changing temperatures, corrosive agents). This problem is not specific to local approaches. A probabilistic description of these effects has been developed in connection with the global approach (e.g. the concept of load spectra[2,6] and the statistics of extremes[996]). It can be transferred to the local situation but this necessitates transfer functions and may result in more complicated local conditions. Also, the engineer is better acquainted with the global service conditions of a structure than with its more complex local effects. Attention must be directed more to the local situation if local approaches are applied. Better control must be gained over the local influencing parameters which means greater effort and expenditure.

Structural fatigue damage is a typical multiparameter problem: the damaging process results from the combined effect of a large number of influencing parameters attributable to loading, geometry, material, manufacture and environment. The number of influencing parameters increases drastically when switching from the global to the local approach (escalation of details). For example, the single material of the global approach is substituted by at least three material states in the local approach (i.e. parent material, heat-affected zone and weld metal). One macroshape (e.g. cruciform joint with fillet welds) is broken down into a large number of geometric details (e.g. weld toe notch radii, weld toe angles, weld end shape parameters). The single failure criterion (total fracture) is subdivided into several damage stages (e.g. definite plastic deformation, crack initiation, through-thickness crack and final fracture). This enhanced multiparameter situation makes excessive detail modelling necessary and is connected with the possibility of innumerable procedural variants. But it is completely unfeasible to simulate reality in all details without concentrating on the decisive influencing parameters.

Concentration on those parameters which have a decisive influence is the most important basis for the successful application of local approaches. Which parameters are decisive depends on the type of strength and life problem and the aim of the relevant assessment procedure. That means that each individual case has its own set of parameters with decisive influence.

Decisive parameters for determining the location and load level of crack initiation, for example, are particular geometric quantities that describe the macroshape (e.g. the attachment length) or microshape (e.g. weld toe radius and toe angle). Differentiation between the microstructural material states is less important as far as manufacturing measures are taken to equalise the mechanical properties (especially the hardness). Technical crack initiation is for the most part a suitable criterion for design decisions, whereas crack propagation up to the through-thickness crack is more important for safety considerations. The influence of residual stresses on the fatigue process is often unduly neglected in the local approaches. Decisive additional parameters in the crack propagation approach are the initial crack depth, the crack shape and the crack path.

Completeness of the set of parameters with decisive influence is a prerequisite for successful application of the local approaches. It is a shortcoming of many published assessment cases that one or the other important parameter is not defined in correspondence to observations in reality and is only introduced as a rough post-analysis correction of the final analysis results (e.g. the local residual stress state).

Which parameters are decisive must be defined mainly on the basis of existing knowledge of the fatigue-loaded structure and the aim of simulation. If this knowledge is missing or uncertain, a sensitivity analysis should be performed on the basis of a provisional model in order to find out what input parameters are most influential on the final result (e.g. major differences occur for different actual or assumed residual stress states and minor differences are often met when using different damage parameters and multiaxial strength criteria).

Diversity of local approach versions

There are several local approaches available for the fatigue assessment of welded structural members which can be applied in a partly supplementary, partly alternative manner, e.g. the structural stress, notch stress, notch strain, stress intensity and crack propagation approaches. Each approach is available in at least as many versions as there are main scientific contributors and industrial users.

This is not only a matter of different traditions and schools or a matter of progress in methods development and analysis tools but a characteristic

feature pointing to the fact that individual fatigue assessment problems generate individual solutions on the basis of local approaches. For example, the versions for seam-welded and spot-welded joints are for the most part markedly different. Some versions have resulted from research projects sponsored by industrial groups (e.g. automotive or offshore), others are more industry-internal supporting design decisions by relative assessments. Some versions are intended as code-conforming procedures, whereas others are applied to explain definite testing results.

Standardisation of the local approaches is not possible to the extent that has been achieved for global approaches. It is impossible to develop a national or international standard which takes into account the many variants, data and applications which are typical of the local approaches. But this does not mean that related standardisation on a smaller scale is impossible. At least guidelines are highly desirable within restricted areas of application. They should mainly be related to the fundamental procedures, the available data and the parameters with a decisive influence. But such guidelines cannot regulate to the extent that standards based on global approaches do, and they cannot be legally binding. The FKM guideline[1] is a remarkable step in the indicated direction.

Objectionable non-scientific procedures

A procedure or assumption within the local approach is termed 'non-scientific' if it does not correspond to the physical phenomena which it pretends to simulate mathematically. It is unacceptable within local approaches – unlike within global approaches – to achieve the desired results on the basis of inadequate modelling combined with scaling factors. Both the final and the intermediate analysis results should remain comparable with experimental checks. Falsification of calculation results should thus be possible. It is better to remain with the global approach than to rely on a local approach which is only formally adapted without experimental validation.

The physical basis is also questioned if 'laws' or 'rules' are introduced as absolutely valid instead of considering them as being bound to definite presuppositions. It is well known that Miner's 'rule' must be adjusted to the special application under consideration by substantial modifications in order to arrive at acceptable results. Neuber's 'rule' of local elastic-plastic deformation is strictly valid only for sharp notches in anti-plane shear loading in the case of steadily work-hardening materials. The Paris 'law' of crack propagation is bound to not too small and not too large stress intensity factors, to a non-varying microstructural cracking mechanisms and to non-corrosive environments.

Another deficiency occasionally met in the application of local approaches is the unreflected combination of material parameters of different microstructural states within a single assessment, for example, microstructural support parameters of the weld metal combined with fatigue strength values of the parent material.

Indispensable experimental verification

Experimental verification of theoretical analysis results within definite test examples is indispensable. This is a common principle of mathematical sciences applied to real-world phenomena. Verification is necessary not only in respect of the final result in terms of strength or life but also in respect of intermediate states, for example, local stresses and strains, local microstructural states, location of crack initiation, size and shape of initiated cracks and the crack path geometry up to fracture. This is also necessary in respect of the input parameters of the local approach, especially the material parameters which must be checked if taken from available sources or determined experimentally for the first time. Hardness measurements on structural members and on specimens by comparison are an effective control measure in this connection.

The relevant local approach should be subdivided into self-contained procedural steps which can be subject to experimental control. Modern measuring techniques allow reliable detection of the different damage stages (i.e. first plastic deformation, initiation of microcracks, occurrence of a technical crack, a through-thickness crack and final fracture) to the extent that the critical region is accessible. At least, these stages can be traced back on the basis of striation markings on the fracture surface (if available) combined with crack propagation analysis.

Validation impeded by scatter

Validation of local approaches means that the reliability and accuracy of the approaches in respect of definite applications is investigated. The main problem of validation is the scatter of the input and output parameters both in the theoretical analysis and the testing results.

Scatter in connection with fatigue testing is taken into account by appropriate statistical evaluation methods. Also, transfer of the test results to scattering service conditions can be based on a statistical analysis. Predictions of failure probability under real-world conditions are thus possible. The experts are well aware of these probabilistic aspects of the fatigue problem.

What is less generally known is the significance of scatter associated with calculation procedures. All the input parameters of the numerical

assessment are scattering to some extent. The scatter of some parameters is extremely large, e.g. the geometric conditions at the weld toe, especially with unmechanised welding processes, or the hardness peaks in the heat-affected zone. The scatter of other parameters is better controlled by quality standards and acceptance conditions, e.g. plate thickness, misalignment of parts, welding distortion, or some strength parameters and the chemical composition of the parent material.

To introduce worst case conditions into the calculation is not a general solution of the problem of scatter. It has been successful in connection with the weld toe notch radius because this radius is without major influence if it is very small. It is also common practice to handle the residual stress problem by assuming the worst case of local tensile residual stresses close to the yield limit. But if all the input parameters of the local approaches were introduced with the intention of producing the worst case, an unacceptably conservative design would result with no advantage compared with the global approach. Additionally, it is not always clear in what direction and to what extent a parameter must be varied in connection with other parameters to produce a worst case result.

The sensitivity analysis mentioned in connection with the search for the decisive influencing parameters can be used for numerical tests revealing the scatter ranges of output parameters dependent on realistically assumed scatter ranges of input parameters.

The mean relative errors of numerical analysis and of testing added up in quadratic form give the mean relative error of verification also in quadratic form if Gaussian normal distributions of scatter are assumed for simplification. The analysis error results from superposition of partial errors connected with the modelling assumptions, the numerical solution and the geometric and material parameters. Such a probabilistic error estimate has not yet been performed with respect to the local approaches but it is well established in respect of other areas of numerical analysis, e.g. in respect of computational welding process simulation (Sudnik *et al.*[997]).

Documentation of the assessment procedure

The application of local approaches is generally connected with so many assumptions, tentative calculations and intermediate results (i.e. an escalation of details takes place) that the analyst himself is permanently at risk of losing control of the assessment procedure. Even after successfully finishing the assessment, it is difficult to document the different procedural steps and variants in such a way that readers of the documentation have no difficulties in obtaining all the essential information necessary to understand and check the results.

These shortcomings can be eliminated by defining a sequence of indispensable procedural steps supplemented by optional variants, by providing this calculation and assessment scheme with the available material parameters, by enforcing the definition of scatter ranges by the user for all input parameters and by incorporating the procedures and data into an interactive program system, giving support to expert users.

The fact that non-interactive black box program systems based on local approaches are offered in some cases is not a contradiction. These systems can only be used under severe restrictions in applicability and accuracy.

The problem of consistent and better readable documentation of all the assessment steps can be solved in connection with the proposed development of the above support system for experts. Further progress in the application of the local approaches in industry will depend to some extent on the availability of such a system.

Required expertise in application

Local approaches cannot be applied in a black box manner as it is the case with the global approach, especially with the nominal stress approach of the design codes. Local approaches require a high degree of expertise on the side of the analyst together with adequate computer and testing facilities, whereas the global approach addresses design and calculation engineers without special knowledge on fatigue strength and service life. The expert's knowledge and experience is indispensable for successful application of the local approaches.

The expert who applies local approaches should be acquainted with and should have access to theoretical and experimental analysis methods which are specific to local approaches: finite element and boundary element methods, stress measuring methods, testing methods directed to cyclic material parameters, methods of service life evaluation under variable-amplitude loading, analysis and detection methods for crack initiation and propagation among others. Cooperation with a research and development institute specialising in the area of fatigue strength and service life evaluations can generally be recommended. Dependency on expertise will remain even with the availability of the support system mentioned above.

Specific problems with welded joints

The application of local approaches to welded joints is connected with specific problems resulting from the pecularities of welded joints which have been addressed in Section 1.2.3 and repeatedly mentioned in the

subsequent chapters. These problems refer to inhomogeneous material, welding defects and imperfections, welding residual stresses and distortions, and undefined geometric parameters of the weld.

There are cases of application where the peculiarities of welded joints are of minor relevance and others where a successful application is extremely difficult. An example for the latter case is the explanation of the unsatisfactorily low fatigue strength of welded joints in high strength steel in the as-welded condition compared to the same joints in low strength steels. On the one hand, only the local approach has the potential to clarify the situation, on the other hand, decisive influencing parameters tend to neutralise one another so that the local approach has an accuracy problem. High strength steels provide higher fatigue strength, but they are more 'notch-sensitive' especially in the fine-grained condition, so that sharp notches are more detrimental. Additionally, high strength steels compared to low strength steels produce higher residual stresses which (in the case of tensile stresses) reduce the fatigue strength even in mildly notched welded joints.

Further research and development is necessary to make the local approaches applicable to fatigue strength problems of the more complex type just described. On the other hand, the conclusion from the 'neutralising situation' above should be to recommend a reduction in both the notch sharpness and the tensile residual stresses (or even to convert them into compressive stresses) if benefit is to be drawn from high strength steels in welded structures subjected to cyclic loading. The local approach is easier to apply after this has been done. It can generally be recommended that sophisticated local approaches should not be applied before the obvious possibilities for design and quality improvement have been put into effect.

12.3 Potential of local approaches

The potential of the local approaches lies in the support they can give to the development of structural designs. Only local approaches trace the parameters which have a decisive influence on the fatigue strength and service life of welded joints, whereas global approaches do not separate these parameters. Testing procedures without local approaches are too expensive and time-consuming to achieve the aim of an appropriate design. The following tasks may be advantageously solved on the basis of local approaches.

Relative fatigue assessments

The first task where special benefits can be derived from local approaches is the assessment of new design and loading variants relative to a well-

proven existing design. The new design may consist of modified shape parameters, changed dimensions or varied parent material. Loading variants may result from customer demands or environmental conditions. It is typical of many automotive designs that newly designed members have to fit into an existing vehicle or engine design. Bridges, aeroplanes or processing equipment may be expected to sustain more severe service loading than originally planned or longer service life than the nominal design life. The admissibility of such demands can be advantageously checked on the basis of local approaches.

Effectiveness of design measures

The second task where special benefits can be derived from local approaches is the assessment of the effectiveness of design options and related manufacturing measures. Typical related questions are the following. To what extent can the loading capacity or service life be increased by modifying shape, dimensional or material parameters? What is the benefit of a full penetration weld relative to the same weld with lack of penetration? What life extensions can be achieved by postweld treatments?

Optimisation of designs

The third task where special benefits can be derived from local approaches is the optimisation of the design and its manufacture in respect of fatigue strength and service life. The basis of such an optimisation is knowledge of the effects of the decisive (local and non-local) influencing parameters and their adjustment under a situation of partly counteracting effects. At least the trends of the effects of certain influencing parameters can be predicted on the basis of local approaches even at a more rudimentary stage of their development and application.

Fitness-for-purpose evaluations

The fourth task where special benefits can be derived from local approaches is the fitness-for-purpose assessment of welded members containing crack-like imperfections exceeding the tolerable size detected after fabrication or in service. The actual residual fatigue life can be approximately determined.

Backtracing of fatigue failures

The fifth task where special benefits can be derived from local approaches is the backtracing of fatigue failures which occurred in testing or in

service. Crack initiation being a local phenomenon, the local approach, especially the combined crack initiation and propagation approach, is decisive in determining the cause of failure and in defining preventive measures.

Bibliography

Chapter 1 Introduction

1 FKM Guideline, *Analytical Strength Assessment of Components in Mechanical Engineering*, Frankfurt/M, VDMA Verlag, 2003 (5th edn).
2 Haibach E, *Betriebsfestigkeit – Verfahren und Daten zur Bauteilbemessung (Service Fatigue Strength – Methods and Data for Structural Analysis)*, Berlin, Springer-Verlag, 2002 (2nd edn).
3 Hobbacher A (Ed), *Fatigue Design of Welded Joints and Components – Recommendations of IIW Joint Working Group XIII-XV*, IIW Doc XIII-1539-96/XV-845-96, Cambridge, Abington Publ, 1996; IIW Doc XIII-1965-03/XV-1127-03 (updated edn 2005, see reference 133).
4 Radaj D, *Design and Analysis of Fatigue Resistant Welded Structures*, Cambridge, Abington Publ, 1990; German edn by DVS-Verlag 1985.
5 Radaj D, 'Review of fatigue-strength assessment of non-welded and welded structures based on local parameters', *Int J Fatigue*, 1996, **18** (3), 153–170.
6 Radaj D, *Ermüdungsfestigkeit – Grundlagen für Leichtbau, Maschinen- und Stahlbau (Fatigue Strength – Fundamentals for Light-Weight Design, Mechanical and Structural Engineering)*, Berlin, Springer-Verlag, 2003 (2nd edn).
7 Radaj D, *Welding Residual Stresses and Distortion – Calculation and Measurement*, Düsseldorf, DVS-Verlag, 2003; German edn 2002.
8 Seeger T, 'Grundlagen für Betriebsfestigkeitsnachweise (Fundamentals for service fatigue strength assessments)', *Stahlbau Handbuch (Handbook of Structural Engineering)*, Köln, Stahlbau-Verlagsges, 1996, Vol 1B, pp 5–123.

Chapter 2 Nominal stress approach for welded joints

9 AD-S2, Arbeitsgemeinschaft Druckbehälter – Berechnung auf Schwingbeanspruchung (Working group for pressure vessels – dimensioning for cyclic loading), Berlin, Beuth-Verlag, 1998.
10 ASME, Boiler and pressure vessel code, Section III, Rule for construction of nuclear power plant components, Division 1, Subsection NB, Class 1 components, New York, American Society of Mechanical Engineers, 1989.
11 Bäckström M, Multiaxial fatigue life assessment of welds based on nominal and hot spot stresses, VTT Publ No 502, Espoo, Finland, 2003.

12 Bäckström M and Marquis G, 'Interaction equations for multiaxial fatigue assessment of welded structures', *Fatigue Fract Engng Mater Struct*, 2004, **27** (11), 991–1003.
13 BS5400 Pt10, Specification for steel, concrete and composite bridges – code of practice for fatigue, London, British Standards Institution, 1980.
14 BS5500, Specification for unfired fusion-welded pressure vessels, London, British Standards Institution, 1988.
15 BS7608, Fatigue design and assessment of steel structures – code of practice, London, British Standards Institution, 1993.
16 BS8118, The structural use of aluminium, London, British Standards Institution, 1991.
17 BS7910, Guide on methods for assessing the acceptability of flaws in metallic structures, London, British Standards Institution, 1999 and 2004, replacement for BSPD6493, 1991.
18 Byggnevi M, Life prediction of a complex welded structure using different methods, IIW Doc XIII-1949-02.
19 DIN15018, Krane, Grundsätze für Stahltragwerke, Berechnung (Cranes, principles for steel structures, dimensioning), Berlin, Beuth-Verlag, 1984.
20 DS804, Vorschrift für Eisenbahnbrücken und sonstige Ingenieurbauwerke (Specification for railway bridges and other engineering structures), Munich, Deutsche Bundesbahn, 1984.
21 ECCS/CECM/EKS, Recommendations for the fatigue design of steel structures, Brussels, ECCS, 1985.
22 ECCS/CECM/EKS, Recommendations for aluminium alloy structures: fatigue design, Brussels, ECCS, 1992.
23 Eurocode 3, Design of steel structures, Part 1–9, Fatigue, EN 1993-1-9, Brussels, CEN, 2005.
24 Eurocode 9, Design of aluminium structures, Part 2, Structures susceptible to fatigue, ENV 1999-2, Brussels, CEN, 2000.
25 Gimperlein D, '*S–N* curve slope for welded structures', *Welding in the World*, 1998, **41**, 399–406.
26 Gurney T R, *Fatigue of Welded Structures*, Cambridge, University Press, 1979 (2nd edn).
27 Gurney T R, *Cumulative Damage of Welded Joints,* Cambridge, Abington Publ, 2006.
28 Haagensen P J and Maddox S J (Eds), IIW recommendations on post-weld improvement of steel and aluminium structures, Doc. XIII-1815-00, Rev July 2004.
29 Haibach E and Atzori B, 'Ein statistisches Verfahren für das erneute Auswerten von Ergebnissen aus Schwingfestigkeitsversuchen und für das Ableiten von Bemessungsunterlagen, angewandt auf Schweißverbindungen aus AlMg5', *Aluminium*, 1975, **51** (4), 267–272.
30 IIW, 'Design recommendations for cyclic loaded welded steel structures', *Welding in the World*, 1982, **20** (7/8), 153–165.
31 IIW, Guidance on assessment of the fitness for purpose of welded structures, IIW/IIS-SST-1157-90.
32 Jaccard R, Kosteas D and Ondra R, Data re-evaluation and finalization of ERAAS fatigue, Report, Technical University of Munich and Alusuisse-Lonza Neuhausen, 1990/1991.

33 Jaccard R, Kosteas D and Ondra R, Background document to fatigue design Curves for Welded Aluminium Components, IIW Doc XIII-1588-95.
34 JSSC, Fatigue design recommendations for steel structures (English version), JSSC Technical Report 32, Tokyo, Japan Soc Steel Construction, 1995.
35 Jung T and Gudehus H, 'Vergleich von Programmsystemen zur Lebensdauervorhersage', *Stahl u Eisen*, 1998, **118** (2), 89–92.
36 Jung T, Gudehus H and Zenner H, Vergleich von Programmsystemen zur Lebensdauervorhersage, Bericht ABF, Düsseldorf, Verlag Stahleisen, 1997.
37 Katajamäki K, Lehtonen M, Marquis H and Mikkola T, Fatigue stress FEA round robin – soft toe gusset on I-beam flange, IIW Doc XIII-1918-02.
38 Kloos K H, Adelmann J, Bieker G and Oppermann T, 'Oberflächen und Randschichteinflüsse auf die Schwingfestigkeitseigenschaften', *Dauerfestigkeit und Zeitfestigkeit*, VDI-Berichte 661, Düsseldorf, VDI-Verlag, 1988, pp 215–245.
39 Kosteas D and Gietl B, 'A comparative analysis of existing test data on welded aluminium tubular joints', *Fatigue Fract Engng Mater Struct*, 1996, **19** (6), 731–738.
40 Krebs J, Hübner P and Kaßner M, *Eigenspannungseinfluss auf Schwingfestigkeit und Bewertung in geschweißten Bauteilen*, DVS-Bericht 234, Düsseldorf, DVS-Verlag, 2004.
41 Kueppers M and Sonsino C M, 'Critical plane approach for the assessment of the fatigue behaviour of welded aluminium under multiaxial loading', *Fatigue Fract Engng Mater Struct*, 2003, **26** (6), 507–513.
42 Küppers M and Sonsino C M, 'Critical plane approach for the assessment of the fatigue behaviour of welded aluminium under multiaxial spectrum loading', *Proceedings International Conference on Biaxial/Multiaxial Fatigue and Fracture*, Berlin, DVM, 2004, pp 361–368.
43 Maddox S J, *Fatigue Strength of Welded Structures*, Cambridge, Abington Publ, 1991 (2nd edn).
44 Maddox S J, 'Treatment of low stresses when applying Miner's rule in the fatigue design of welded aluminium alloys', *Fatigue – Core Research from TWI*, Cambridge, Abington Publ, 2002, pp 101–119.
45 Maddox S J, 'Review of fatigue assessment procedures for welded aluminium structures', *Int J Fatigue*, 2003, **25** (12), 1359–1378.
46 Maddox S J and Razmjoo G R, 'Interim fatigue design recommendations for fillet welded joints under complex loading', *Fatigue Fract Engng Mater Struct*, 2001, **24** (5), 329–338, and IIW-Doc XIII-1787-99/XV-1030-99.
47 Martinsson J and Samuelsson J, Fatigue assessment of a welded component in a construction machinery based on different methods, IIW Doc XIII-1905-01.
48 Neumann A, *Schweißtechnisches Handbuch für Konstrukteure, Teil 1, Grundlagen, Tragfähigkeit, Gestaltung (Handbook of Welding Technology for Designers, Part 1, Fundamentals, Load Carrying Capacity, Design)*, Düsseldorf, DVS-Verlag, 1996 (7th edn).
49 Neumann A, *Kompendium der Schweißtechnik, Bd 4, Berechnung und Gestaltung von Schweißkonstruktionen (Compendium of Welding Technology, Vol 4, Analysis and Design of Welded Structures)*, Düsseldorf, DVS-Verlag, 1997.
50 Neumann A and Hobbacher A, *Schweißtechnisches Handbuch für Konstrukteure, Teil 4, geschweißte Aluminium-Konstruktionen (Handbook of Welding Technology for Designers, Part 4, Welded Aluminium Structures)*, Düsseldorf, DVS-Verlag, 1993.

51 Niemi E, 'Random loading behaviour of welded components', *Proceedings International Conference on Performance of Dynamically Loaded Welded Structures*, New York, WRC, 1997, pp 339–353.
52 Olivier R and Ritter W, Wöhlerlinienkatalog für Schweißverbindungen aus Baustählen (Catalogue of *S–N* curves of welded joints in structural steels), DVS-Bericht 56, Düsseldorf, DVS-Verlag, 1979–1985.
53 Petterson G, 'Fatigue analysis of a welded component based on different methods', *Welding in the World*, 2002, **46** (9/10), 41–51.
54 Radaj D, 'Abminderungsfaktor der Schwingfestigkeit bei Schweißverbindungen', *Konstruktion*, 1998, **50** (11/12), 55–62.
55 Razmjoo G R, 'Fatigue of load-carrying fillet welded joints under multiaxial loading', *Fatigue – Core Research from TWI*, Cambridge, Abington Publ, 2000, pp 63–99.
56 Razmjoo G R, 'An investigation into fillet welded plate joints under varying principal stress direction', *Fatigue – Core Research from TWI*, Cambridge, Abington Publ, 2000, pp 145–172.
57 Ritter W, Kenngrößen der Wöhlerlinien für Schweißverbindungen aus Stählen (Characteristic parameters of *S–N* curves of welded joints in structural steels), Heft 53, Inst f Stahlbau u Werkstoffmech, Darmstadt, Techn Univ, 1994.
58 Siljander A, Kurath P and Lawrence F V, 'Non-proportional fatigue of welded structures', *Advances in Fatigue Lifetime Predictive Techniques*, ASTM STP 1122, Philadelphia Pa, ASTM, 1992, pp 319–338.
59 Sonsino C M, 'Festigkeitsverhalten von Schweißverbindungen unter kombinierten und phasenverschobenen mehrachsigen Beanspruchungen', *Materialwiss u Werkstofftechn*, 1994, **25** (9), 353–368.
60 Sonsino C M, 'Multiaxial fatigue of welded joints under in-phase and out-of-phase local strains and stresses', *Int J Fatigue*, 1995, **17** (1), 55–70.
61 Sonsino C M, 'Overview on the state of the art on multiaxial fatigue of welds', *Multiaxial Fatigue and Fracture*, Amsterdam, Elsevier Science, 1999, pp 195–218.
62 Sonsino C M, Berg-Pollack A and Grubisic V, Betriebsfestigkeitsnachweis von Aluminium-Sicherheitsbauteilen – zum Stand der Technik (Structural durability proof of aluminium safety components – state of the art), LBF Bericht FB-225, Darmstadt, Fraunhofer Inst f Betriebsfest, 2004.
63 Sonsino C M and Küppers M, 'Lebensdauer von Schweißverbindungen unter mehrachsigen Belastungen mit variablen Amplituden – Schadensakkumulation und Hypothese der wirksamen Vergleichsspannung', *Materialwiss und Werkstofftechn*, 2000, **31** (1), 81–95.
64 Sonsino C M and Küppers M, 'Multiaxial fatigue of welded joints under constant and variable loadings', *Fatigue Fract Engng Mater Struct*, 2001, **24** (5), 309–328.
65 Sonsino C M, Lagoda T and Demofonti G, 'Damage accumulation under variable amplitude loading of welded medium- and high-strength steels', *Int J Fatigue*, 2004, **26** (6), 487–495.
66 Sonsino C M and Maddox S J, 'Multiaxial fatigue of welded structures – problems and present solutions', *Proc International Conference on Biaxial/Multiaxial Fatigue and Fracture*, Lisboa, IST 2001, Vol I, pp 3–15.
67 Sonsino C M, Maddox S J and Hobbacher A, 'Fatigue life assessment of welded joints and variable amplitude loading – state of present knowledge and rec-

ommendations for fatigue design regulations', *Proceedings International Conference on Trends and Future Perspectives of Welding Technology for Transportation*, Osaka, Kuroki Publ, 2004, pp 87–102.
68 Sonsino C M, Maddox S J and Haagensen P, A Short study about the course of the *S–N* curve in the high-cycle fatigue regime, IIW-Doc. XIII-2045-05.
69 Sonsino C M, Wallmichrath M and Küppers M, Assessment of multiaxial fatigue test results on welded joints by application of the IIW-formula and modifications, IIW-Doc. XIII-2046-05.
70 Stüssi F, 'Zur Dauerfestigkeit von Schweißverbindungen', *Schweizerische Bauzeitung*, 1957, **75** (52), 805–808.
71 Susmel L and Tovo R, 'On the use of nominal stresses to predict the fatigue strength of welded joints under biaxial cyclic loading', *Fatigue Fract Engng Mater Struct*, 2004, **27** (11), 1005–1024.
72 TRD301, Technische Regeln für Dampfkessel – Zylinderschalen unter innerem Überdruck, Berechnung (Technical rules for boilers – cylindrical shells subjected to internal pressure, dimensioning), Berlin, Beuth-Verlag, 1979.

Chapter 3 Structural stress or strain approach for seam-welded joints

73 Alessandri E, Labesse-Jied F and Huther I, Comparison between different methods to calculate geometrical stress for welded cruciform joint, IIW Doc XIII-1850-00.
74 Anami K and Miki C, 'The role of full-size and large-size fatigue tests on structural fatigue problem', *International Conference on Fatigue of Welded Components and Structures*, Les Ulis, Soc Française de Métallurgie et de Matériaux, 1996.
75 Andrews R M, 'The effect of misalignment on the fatigue strength of welded cruciform joints.' *Fatigue Fract Engng Mater Struct*, 1996, **19** (6), 755–768, and IIW-Doc. XIII-1180-85.
76 Andrews R M, 'The stress magnification effect of angular misalignment at butt welds', *Fatigue – Core Research from TWI*, Cambridge, Abington Publ, 2000, pp 145–172.
77 API, Recommended practice for planning, designing and constructing fixed offshore platforms – API recommended practice 2A (RP2A4), 19th edn, Washington D C, American Petroleum Institute, 1991.
78 Atzori B, Blasi G and Pappalettere C, 'Evaluation of fatigue strength of welded structures by local strain measurements', *Exp Mech*, 1995, **25** (2), 129–139; translation from *Rivista Italiana della Saldatura*, 1998, **50** (2), 153–158.
79 Atzori B, Crivellaro A and Meneghetti G, 'Interpretation of the hot spot approach to fatigue of welded structures', *Welding Int*, 1999, **13** (4), 276–281.
80 Atzori B and Meneghetti G, 'Fatigue strength of fillet welded structural steels – finite elements, strain gauges and reality', *Int J Fatigue*, 2001, **23**, 713–721.
81 Atzori B, Meneghetti G and Susmel L, 'Estimation of the fatigue strength of light alloy welds by an equivalent notch stress analysis', *Int J Fatigue*, 2002, **24**, 591–599.
82 AWS, Structural welding code – steel, ANSI/AWS D1.1-94, Miami Fla, American Welding Society, 1994 (14th edn).

83 Bäckström M and Marquis G, 'A review of multiaxial fatigue of weldments: experimental results, design code and critical plane approaches', *Fatigue Fract Engng Mater Struct*, 2001, **24**, 279–291.
84 Bathe K J, *Finite Element Procedures*, Englewood Cliffs N J, Prentice Hall, 1995.
85 Bauer H and Saal H, 'Nozzles in the knuckle region of pressure vessel heads – strength and stiffness under various loading conditions', *Proceedings International Conference on Load Carrying Capacity of Steel Shell Structures*, Brussels, ECCS, 1997, pp 138–144.
86 Berge S and Myhre H, 'Fatigue strength of misaligned cruciform and butt joints', *Norwegian Maritime Res*, 1977, **5** (1), 29–39.
87 Chang E and Dover W D, 'Prediction of degree of bending in tubular X and DT joints', *Int J Fatigue*, 1999, **21** (2), 147–161.
88 Chang E and Dover W D, 'Prediction of stress distributions along the intersection of tubular Y and T joints', *Int J Fatigue*, 1999, **21**, 361–381.
89 Chang E and Dover W D, 'Parametric equations to predict stress distributions along the intersection of tubular X and DT joints,' *Int J Fatigue*, 1999, **21** (6), 619–635.
90 Chiew S P, Soh C K and Wu N W, 'General SCF design equations for steel multiplanar tubular XX joints', *Int J Fatigue*, 2000, **22** (4), 283–293.
91 DEn, Offshore installation: guidance on design and construction, London, Department of Energy, 1990.
92 Dijkstra O D and de Back J, 'Fatigue strength of welded tubular T- and X-joints', *Proceedings Offshore Technical Conference* (OTC 3639), Houston Tex, 1980.
93 Doerk O, Fricke W and Weissenborn C, 'Comparison of different calculation methods for structural stresses at welded joints', *Int J Fatigue,* 2003, **25**, 359–369.
94 Dong P, 'A structural stress definition and numerical implementation for fatigue analysis of welded joints', *Int J Fatigue*, 2001, **23**, 865–876.
95 Dong P, 'The mesh-insensitive structural stress and master *S–N* curve method for ship structures', *Proceedings OMAE Specialty Conference on FPSO Systems*, OMAE-FPSO'04-0021, Houston Tex, ASME International Technical Institute, 2004.
96 Dong P, 'Recommended structural stress procedure for fatigue assessment', *Proc OMAE Specialty Conf on FPSO Systems*, OMAE-FPSO'04-0029, Houston Tex, ASME International Technical Institute, 2004.
97 Dong P and Hong J K, 'The master *S–N* curve approach to fatigue of piping and vessel welds', *Welding in the World*, 2004, **48** (1/2), 28–36.
98 Dong P and Hong J K, An effective structural stress parameter for evaluation of multiaxial fatigue, IIW Doc XIII-2036-04/XV-1173-04.
99 Dong P and Hong J K, 'A robust structural stress parameter for evaluation of multiaxial fatigue data of welds', *J ASTM Int*, 2006, **3** (7), 1–17.
100 Dong P, Hong J K and Cao Z, Structural stress based master *S–N* curve for welded joints, IIW Doc XIII-1930-02/XV-1119-02.
101 Dong P, Hong J K and Cao Z, 'Stresses and stress intensities at notches – anomalous crack growth revisited', *Int J Fatigue*, 2003, **25** (9–11), 811–825.
102 Dong P, Hong J K and de Jesus A M, 'Analysis of recent data using the structural stress procedure in ASME Div 2 rewrite', *Proceedings ASME Pressure Vessel and Piping Conference*, PVP2005-71511, New York, ASME, 2005.

103 Dong P, Hong J K, Osage D and Prager M, 'Master *S–N* curve method for fatigue evaluation of welded components', *WRC Bulletin*, No. 474, New York, WRC, 2002.
104 Dong P, Hong J K, Osage D and Prager M, 'Assessment of ASME's FSRF rules for vessel and piping welds using a new structural stress method', *Welding in the World*, 2003, **47** (1/2), 31–43.
105 Dong P, Hong J K, Potukutchi R and Agrawal H, Master *S–N* curve development and validations for aluminium MIG and laser welds, IIW Doc XIII-2035-04/XV-1172-04.
106 Efthymiou M, 'Development of SCF formulae and generalised influence functions for use in fatigue analysis', *Offshore Tubular Joints Conference (OTJ '88)*, UEG Offshore Research, Englefield Green near Egham UK, 1988.
107 Eichelseder W and Unger B, 'Prediction of the fatigue life with the finite element method', *SAE Technical Paper* 940245, Warrendale Pa, SAE, 1994.
108 Eichelseder W and Unger B, 'Assessment of welded seams with the finite element method', *SAE Technical Paper* 950712, Warrendale Pa, SAE 1995.
109 Findley W N, 'A theory for the effect of mean stress on fatigue of metals under combined torsion and axial load or bending', *Trans ASME, J Eng Ind*, 1959, **81**, 301–306.
110 Fricke W, 'Recommended hot spot analysis procedure for structural details of ships and FPSOs based on round-robin FE analyses', *Int J Offshore Polar Engng*, 2002, **12** (1), 40–47.
111 Fricke W, 'Fatigue design and structural hot-spot stress determination for welded joints', *Proceedings 9th Portuguese Conference on Fracture*, Sétubal, Portugal, Society of Materials, 2004.
112 Fricke W and Bogdan R, Determination of hot spot stress in structural members with in-plane notches using a coarse mesh, IIW Doc XIII-1870-01.
113 Fricke W, Borchardt H, Gritl D and Pohl S, 'Bewertung der Betriebsfestigkeit schiffbaulicher Strukturdetails mit Hilfe von Formzahlen', *Jahrbuch Schiffbautechn Ges*, Vol 85, Berlin, Springer-Verlag, 1991.
114 Fricke W, Cui W, Kierkegaard H, Kihl D, Koval M, Mikkola T, Parmentier G, Toyosada M and Yoon J H, 'Comparative fatigue assessment of a structural detail in a containership using various approaches of classification societies', *Marine Structures*, 2002, **15**, 1–13.
115 Fricke W and Doerk O, Simplified approach to fatigue strength assessment of fillet-welded attachment ends, *Int J Fatigue*, 2006, **28**, 141–150.
116 Fricke W, Doerk O and Grünitz L, 'Fatigue strength investigation and assessment of fillet-welds around stiffener and bracket toes', *Proceedings OMAE Specialty Conference on FPSO Systems*, OMAE-FPSO'04-0010, Houston Tex, ASME International Technical Institute, 2004.
117 Fricke W, Kahl A and Paetzold H, Application of the structural stress approach to root failure of fillet welds subject to throat bending, IIW-Doc XIII-2072-05/XV-1198-05.
118 Fricke W and Paetzold H, 'Fatigue strength assessment of scallops – an example for the application of nominal and local stress approaches', *Marine Struct*, 1995, **8**, 423–447.
119 Fricke W and Petershagen H, 'Anwendung örtlicher Konzepte auf die Betriebsfestigkeit schiffbaulicher Schweißkonstruktionen', *Berechnung, Gestaltung*

und Fertigung von Schweißkonstruktionen im Zeitalter der Expertensysteme, DVS-Bericht 133, Düsseldorf, DVS-Verlag, 1991, pp 89–93.
120 Fricke W and Petershagen H, 'Detail design of welded ship structures based on hot spot stresses', *Practical Design of Ships and Mobile Units*, London, Elsevier Applied Science, 1992, Vol 2, pp 1087–1100.
121 Fricke W and von Selle H, 'Formzahlermittlung für komplexe schiffbauliche Strukturdetails und Einbindung in Betriebsfestigkeitsanalysen', *Fortschritte bei der Konstruktion und Berechnung geschweißter Bauteile*, DVS-Bericht 187, Düsseldorf, DVS-Verlag, 1997, pp 59–64.
122 Fricke W and Weißenborn C, 'Vereinfachte Formzahlen für ermüdungskritische Strukturdetails in der Schiffskonstruktion', *Schiffbauforschung*, 2004, **43** (2), 39–50.
123 Gaßner E and Haibach E, 'Die Schwingfestigkeit von Schweißverbindungen aus der Sicht einer örtlichen Beanspruchungsmessung', *Tragfähigkeitsermittlung bei Schweißverbindungen (Determination of Load-Carrying Capacity of Welded Joints)*, Düsseldorf, DVS-Verlag, 1968, Vol 1, pp 47–73.
124 Gho W M, Fung T C and Soh C K, 'Stress and strain concentration factors of completely overlapped tubular K(N) joints', *J Struct Engng*, 2003, **29** (1), 21–29.
125 Glinsner K, 'Fatigue calculation of complex welded structures based on finite element results', *Proceedings of 5th INALCO'92*, München, 1992.
126 Glinsner K, Sridharan N and Unterleutner K, 'Design of fatigue-resistant complex welded structures with CAE tools', *Engineering Design in Welded Constructions*, Oxford, Pergamon Press, 1992, pp 93–101.
127 Gurney T R, 'The influence of thickness on fatigue of welded joints – 10 years on (a review of British work)', *Proceedings International Conference on Offshore Mechanics and Arctic Engng (OMAE'89)*, New York, ASME, 1989, Vol 3, pp 1–8.
128 Gurney T R, *The Fatigue Strength of Transverse Fillet Welded Joints*, Cambridge, Abington Publ, 1991.
129 Haibach E, Die Schwingfestigkeit von Schweißverbindungen aus der Sicht einer örtlichen Beanspruchungsmessung (The fatigue strength of welded joints considered on the basis of a local stress measurement), LBF-Bericht FB-77, Darmstadt, Fraunhofer-Inst f Betriebsfest, 1968.
130 Haibach E and Köbler H G, 'Beurteilung der Schwingfestigkeit von Schweißverbindungen aus AlZnMg1 auf dem Weg einer örtlichen Dehnungsmessung', *Aluminium*, 1971, **47** (12), 725–730.
131 Hannah R L and Reed S E (Eds), *Strain Gauge Users' Handbook*, London, Elsevier Applied Science, 1992.
132 Healy B E, 'Hot spot stress analysis of a side shell connection using surface extrapolation and the Battelle structural stress method', *Proceedings OMAE Specialty Conference on FPSO Systems*, OMAE-FPSO'04-0022, Houston Tex, ASME International Technical Institute, 2004.
133 Hobbacher A (Ed), Recommendations for fatigue design of welded joints and components, IIW Doc XIII-1965-03/XV-1127-03, final form 2006.
134 Hong J K and Dong P, 'Hot spot and structural stress analysis of FPSO fatigue details', *Proceedings OMAE Specialty Conference on FPSO Systems*, OMAE-FPSO'04-0023, Houston Tex, ASME International Technical Institute, 2004.

135 Huther I, Gorski S, Lieurade H P, Laborde S and Recho N, 'Longitudinal non loaded welded joints geometrical stress approach', *Welding in the World*, 1999, **43** (3), 20–26.
136 Huther M and Henry J, Recommendations for the hot spot stress definition in welded joints, IIW Doc XIII-1416-91 and IIW Doc XIII-1416a-92.
137 Huther M and Lieurade H P, 'Application of the hot spot stress method', *Proceedings International Conference on Performance of Dynamically Loaded Welded Structures*, New York, WRC, 1997, pp 332–338.
138 Huther I, Lieurade H P, Sayhi N and Buisson R, 'Fatigue strength of longitudinal non-load-carrying welded joints – use of the hot spot stress approach', *International Conference on Fatigue of Welded Components and Structures*, Les Ulis, Soc Française de Métallurgie et de Matériaux, 1996, pp 57–64.
139 Huther M, Parmentier G and Henry J, Hot spot stress in cyclic fatigue for linear welded joints, IIW Doc XIII-1466-92.
140 Iida K, Application of hot spot strain concept to fatigue life prediction, IIW Doc XIII-1103-83.
141 Iida K and Iino N, Effect of angular distortion on fatigue strength of transverse butt welds in high-strength steels, IIW Doc XIII-827-77.
142 Iida K and Matoba M, Evaluation of fatigue strength of hull frame ends in shiphulls, IIW Doc XIII-950-80.
143 Iida K, Ochiai O, Kawai T, Hirakawa K, Fujisawa K and Okazawa T, Effect of misalignment in welded joints on low-cycle fatigue strength of a hemispherical pressure vessel made of high tensile strength steel, IIW Doc XIII-815-77.
144 Kim W S, Kim D H, Lee S G and Lee Y K, 'Fatigue strength of load-carrying box fillet weldment in ship structure', *Practical Design of Ships and Other Floating Structures*, Amsterdam, Elsevier, 2001, Vol 2, pp 1161–1167.
145 Kim W S and Lotsberg I, 'Fatigue test data for welded connections in ship-shaped structures', *Proceedings OMAE Specialty Conference on FPSO Systems*, OMAE-FPSO'04-0018, Houston Tex, ASME International Technical Institute, 2004.
146 Koskimäki M and Niemi E, Fatigue strength of welded joints in three types of stainless steel, IIW Doc XIII-1603-95.
147 Kyuba H and Dong P, 'Equilibrium-equivalent structural stress approach to fatigue analysis of a rectangular hollow section joint', *Int J Fatigue*, 2005, **27**, 85–94.
148 Labesse F and Recho N, 'Geometrical stress level at the weld toe and associated local effects', *Welding in the World*, 1999, **43** (1), 23–32.
149 Lee M M, 'Estimation of stress concentrations in single-sided welds in offshore tubular joints', *Int J Fatigue*, 1999, **21**, 895–908.
150 Longobardi V, Natale U and Tizzano G, 'An evaluation procedure for hot-spot tensions in welded plates', *Welding Int*, 2002, **16** (8), 532–643; translation from *Rivista Italiana della Saldadura*, 2001, **2**, 155–167.
151 Lotsberg I, 'Stress concentration factors at circumferential welds in tubulars', *Marine Struct*, 1998, **11**, 207–230.
152 Lotsberg I, Fatigue capacity of fillet welded connections subjected to axial and shear loading, IIW Doc XIII-2000-03/XV-1146-03.

153 Lotsberg I, 'Recommended methodology for analysis of structural stress for fatigue analysis of plated structures', *Proceedings OMAE Specialty Conference on FPSO Systems*, OMAE-FPSO'04-0013, Houston Tex, ASME International Technical Institute, 2004.
154 Lotsberg I and Sigurdsson G, 'Hot spot *S–N* curve for fatigue analysis of plated structures', *Proceedings OMAE Specialty Conference on FPSO Systems*, OMAE-FPSO'04-0014, Houston Tex, ASME International Technical Institute, 2004.
155 Machida S, Matoba M, Yoshinari H and Nishimura R, Definition of hot spot stress in welded plate-type structure for fatigue assessment, IIW Doc XIII-1448-92.
156 Maddox S J, 'Hot-spot fatigue data for welded steel and aluminium as a basis for design', *Int J Offshore Polar Engng*, 2002, **12**, 134–141; similar in IIW Doc XIII-1900a-01.
157 Manson S S, 'Fatigue: A complex subject – some simple approximations', *Exp Mech*, 1965, **5** (7).
158 Marquis G, Bäckström M and Siljander A, 'Multiaxial fatigue damage parameters for welded joints – design code and critical plane approaches', *Welded High-Strength Steel Structures*, Warley UK, Engineering Materials Advisory Service, 1997, pp 127–141.
159 Marshall P W, *Design of Welded Tubular Connections – Basis and Use of AWS Code Provisions*, Amsterdam, Elsevier Science, 1992.
160 Marshall P W and Wardenier J, 'Tubular versus non-tubular hot spot stress methods', *Proc Int Symp Offshore and Polar Engng (ISOPE'05)*, Golden Colo, International Society of Offshore and Polar Engineers, 2005.
161 Matoba M, Kawasaki T, Fuji T and Yamauchi T, Evaluation of fatigue strength of welded steel structures, hull's members, hollow section joints, piping and vessel joints, IIW Doc XIII-1081-83.
162 Miki C and Tateishi K, Fatigue design of cope hole details in steel bridges, IIW Doc XIII-1633-96, and *Int J Fatigue*, 1997, **19** (6), 445–455 (abridged version).
163 Niemi E, On the determination of hot spot stresses in the vicinity of edge gussets, IIW Doc XIII-1555-94.
164 Niemi E (Ed), *Stress Determination for Fatigue Analysis of Welded Components*, IIW Doc XIII-1221-93, Cambridge, Abington Publ, 1995.
165 Niemi E, Fricke W and Maddox S J, *Fatigue Analysis of Welded Components – Designer's Guide to the Structural Hot Spot Stress Approach*, Cambridge, Woodhead Publ, 2006.
166 Niemi E and Tanskanen P, 'Hot spot stress determination for welded edge gussets', *Welding in the World*, 2000, **44** (5), 31–37.
167 Örjasäter O, Effect of plate thickness on fatigue of welded components, IIW Doc XIII-1582-95.
168 Packer J A and Henderson J E, *Design Guide for Hollow Structural Section Connections*, Willowdale, Ontario, Canadian Institute of Steel Construction, 1996.
169 Paetzold H, Doerk O and Kierkegaard H, 'Fatigue behaviour of different bracket connections', *Practical Design of Ships and Other Floating Structures*, Amsterdam, Elsevier Science, 2001, Vol 2, pp 1137–1143.
170 Partanen T and Niemi E, Collection of hot spot *S–N* curves based on tests of small arc-welded steel specimens, IIW Doc XIII-1602-95.

171 Partanen T and Niemi E, 'Hot spot stress approach to fatigue-strength analysis of welded components – fatigue test data for steel plate thicknesses up to 10 mm', *Fatigue Fract Engng Mater Struct*, 1996, **19** (6), 709–722.
172 Partanen T and Niemi E, 'Hot spot *S–N* curves based on fatigue tests of small MIG-welded aluminium specimens', *Welding in the World*, 1999, **43** (1), 16–22.
173 Partanen T, Tarjavuori P and Niemi E, Definition of the hot spot stress gradient in stiffened plate structures based on the beam on elastic foundation theory, IIW Doc XIII-1478-92.
174 Petershagen H, Fricke W and Massel T, Application of the local approach to the fatigue stress assessment of welded structures in ships, IIW Doc XIII-1409-91.
175 Petershagen H and Paetzold H, Untersuchungen zur Bewertung schweißtechnischer Gestaltungsformen im Schiffbau (Investigations into the assessment of welded designs in shipbuilding), Bericht 142, Inst f Schiffbau, Hamburg Univ, 1983.
176 Peterson R E, 'Fatigue of metals in engineering and design', *ASTM Marburg Lecture*, Philadelphia Pa, ASTM, 1962.
177 Poutiainen I and Marquis G, A single-point structural stress assessment procedure for load-carrying fillet joints, IIW Doc XIII-2012-04/XV-1174-04.
178 Poutiainen I and Niemi E, The determination of hot spot stress in gusset structures using a coarse mesh, IIW Doc XIII-1820-2000.
179 Poutiainen I, Tanskanen P and Marquis G, 'Finite element methods for structural hot spot determination – a comparison of procedures', *Int J Fatigue*, 2004, **26**, 1147–1157.
180 Roark R J and Young W C, *Formulas for Stress and Strain*, New York, McGraw-Hill, 1975 (5th edn).
181 Rohrbach C, *Handbuch für experimentelle Spannungsanalyse (Handbook of Experimental Stress Analysis)*, Düsseldorf, VDI-Verlag, 1989.
182 SAE, *Fatigue Design Handbook*, Warrendale Pa, Society of Automotive Engineers, 1968.
183 Savaidis G and Vormwald M, 'Hot-spot stress evaluation of fatigue in welded structural connections supported by finite element analysis', *Int J Fatigue*, 2000, **22**, 85–91.
184 Sørensen J D, Tychsen J, Andersen J U and Brandstrup R D, 'Fatigue analysis of load-carrying fillet welds', *J Offshore Mech Arctic Engng*, 2006, **128**, 65–74.
185 Soh A K, 'Improved procedure for the determination of hot spot stresses in tubular joints', *Fatigue Fract Engng Mater Struct*, 1997, **20** (12), 1709–1718.
186 Storsul R, Landet E and Lotsberg I, 'Calculated and measured stress at welded connections between side shell longitudinals and web frames in ship shaped structures', *Proceedings OMAE Specialty Conference on FPSO Systems*, OMAE-FPSO'04-0017, Houston Tex, ASME International Technical Institute, 2004.
187 Sunamoto D, Yamauchi T and Matoba M, 'A new evaluation method on the fatigue strength of welded joints', *Mitsubishi Heavy Ind Techn Review*, 1979 (Oct), 211–226.
188 Tveiten B W and Moan T, 'Determination of structural stress for fatigue assessment of welded aluminium ship details', *Mar Struct*, 2000, **13**, 189–212.
189 Ulleland T, Svensson M and Landet E, 'Stress concentration factors in side shell longitudinals connected to transverse webframes', *Proceedings International*

Offshore and Polar Engineering Conference, Vol 4, pp. 81–88, Cupertino, International Society for Offshore Polar Engineering, 2001.

190 van Wingerde A M, Packer J A and Wardenier J, 'Criteria for the fatigue assesment of hollow structural section connections', *J Construct Steel Res*, 1995, **35**, 71–115.

191 van Wingerde A M, Packer J A and Wardenier J, 'New guidelines for fatigue design of HSS connections', *J Struct Engng*, 1996, **122** (2), 125–132.

192 van Wingerde A M, Packer J A, Wardenier J and Dutta D, The fatigue behaviour of K-joints made of square hollow sections, CIDECT Rep 7P-19/96, and IIW Doc XIII-1626-96.

193 van Wingerde A M, Packer J A and Wardenier J, Beyond the IIW design recommendations – simplified design charts for in-plane loading, IIW Doc XIII-1854-00/XV-1063-00.

194 van Wingerde A M, Packer J A and Wardenier J, 'Simplified SCF formulae and graphs for CHS and RHS K and KK connections', *J Construct Steel Res*, 2001, **57**, 221–252.

195 Wagner M, Fatigue strength of structural members with in-plane notches, IIW Doc XIII-1730-98.

196 Wagner M, 'Schwingfestigkeit geschweißter Konstruktionsdetails – das Strukturspannungskonzept bei ebenen Blechen mit seitlich angeschweißten Blechen', *Konstruktion*, 1999, **51** (7/8), 40–44.

197 Wardenier J, *Hollow Section Joints*, Delft, Delft University Press, 1982.

198 Window A L (Ed), *Strain Gauge Technology*, London, Elsevier Applied Science, 1992.

199 Xiao Z G and Yamada K, 'A method of determining geometric stress for fatigue strength evaluation of steel welded joints', *Int J Fatigue*, 2004, **26**, 1277–1293, and IIW Doc XIII-2022-04/XV-1175-04.

200 Yagi J, Machida S, Tomita Y, Matoba M and Kawasaki T, Definition of hot spot stress in welded plate-type structure for fatigue assessment, IIW Doc XIII-1414-91.

201 Youn J G and Kim H S, 'Geometric effect on the fatigue properties of a side frame in a hull structure', *Welding in the World*, 1998, **41**, 288–297.

202 Zenner H and Grzesiuk J, 'Einfluss der Nahtvorbereitung und Nahtausführung auf die Schwingfestigkeit hochwertiger Aluminiumkonstruktionen', *Schweißen u Schneiden*, 2004, **56** (2), 58–62.

203 Zhao X L, Herion S, Packer J A and Wardenier J, *Design Guide for Circular and Rectangular Hollow Section Welded Joints under Fatigue Loading*, Köln, CIDECT u TÜV Verlag, 2000.

204 Zhao X L and Packer J A (Eds), *Recommended Fatigue Design Procedure for Welded Hollow Section Joints; Part 1 – Recommendations; Part 2 – Commentary*, IIW Doc XIII-1804-99/XV-1035-99, Cambridge, Abington Publ, 2000.

Chapter 4 Notch stress approach for seam-welded joints

205 Anthes R J, Köttgen V B and Seeger T, 'Kerbformzahlen von Stumpfstößen und Doppel-T-Stößen', *Schweißen u Schneiden*, 1993, **45** (12), 685–688.

206 Anthes R J, Köttgen V B and Seeger T, 'Einfluß der Nahtgeometrie auf die Dauerfestigkeit von Stumpf- und Doppel-T-Stößen', *Schweißen u Schneiden*, 1994, **46** (9), 433–436.

207 Argyris J H and Radaj D, 'Parametrische Untersuchung der Kerbspannungen in Kreuzknoten nach Finite-Element-Verfahren', *Konstruktion*, 1971, **23** (5), 179–181.
208 Argyris J H and Radaj D, 'Parametrische Kerbspannungsuntersuchung am elastischen Kern', *Acta Mechanica*, 1972, **13**, 303–314.
209 Barro G, Labesse-Jied F, Lieurade H P and Recho N, Lack of penetration effect on the stress profile at the weld toe of fillet welds, IIW Doc XIII-1790-99.
210 Bausinger R and Kuhn G, *Die Boundary-Element-Methode (The Boundary Element Method)*, Ehningen, Expert-Verlag, 1987.
211 Bell R, Vosikovsky O and Bain S A, 'The significance of weld toe undercuts in the fatigue of steel plate T-joints', *Int J Fatigue*, 1989, **11** (1), 3–11.
212 Bellett D, Taylor D, Marco S, Mazzeo G, Guillois J and Pircher T, 'The fatigue behaviour of three-dimensional stress concentrations', *Int J Fatigue*, 2005, **27**, 207–221.
213 Brandt U, Lehrke H P and Sonsino C M, Anwendung des Kerbgrundkonzeptes für die schwingfeste Bemessung von Schweißverbindungen aus Aluminiumknetlegierungen (Application of the notch stress approach to the fatigue resistant dimensioning of welded joints in aluminium wrought alloys*)*, LBF-Bericht 7195, Darmstadt, Fraunhofer-Inst f Betriebsfest, 1998.
214 Brebbia C A, Telles J C and Wrobel L C, *Boundary Element Techniques*, Berlin, Springer-Verlag, 1984.
215 Brennan F P, Peleties P and Hellier A K, 'Predicting weld toe stress concentration factors for T and skewed T-joint plate connections', *Int J Fatigue*, 2000, **22** (7), 573–584.
216 Cherry W R, 'Stress concentration factors in main members due to welded stiffeners', *Welding J, Res Suppl*, 1941, **20** (12), 603s ff.
217 Coker E G and Filon L N, *A Treatise on Photoelasticity*, Cambridge, Cambridge University Press, 1931.
218 Coker E G and Levi R, 'The stress distributions in fusion joints', *Proc Inst Mech Eng*, 1931, (**5**), 569ff.
219 Crupi G, Crupi V, Guglielmino E and Taylor D, 'Fatigue assessment of welded joints using critical distance and other methods', *Engng Failure Anal*, 2005, **12**, 129–142.
220 Dahl W and Reinhold P, Experimentelle Ermittlung und rechnerische Überprüfung der Dauerfestigkeit praxisnah hergestellter Laserstrahlschweißverbindungen verschiedener Geometrien (Experimental determination and numerical checks of the fatigue strength of laser beam welded joints of different geometries), Forschungsbericht P 262, Düsseldorf, Studienges Stahlanwendung, 1996.
221 Dally J W and Riley W F, *Experimental Stress Analysis*, New York, McGraw-Hill, 1991.
222 Dang Van K, 'Macro-micro approach in high-cycle multiaxial fatigue', *Advances in Multiaxial Fatigue*, ASTM STP 1191, Philadelphia Pa, ASTM, 1993, pp 120–130.
223 El Haddad M H, Smith K N and Topper T H, 'Fatigue crack propagation of short cracks', *J Engng Mater Technol*, 1979, **101** (1), 42–46.
224 Frocht M M, *Photoelasticity*, New York, John Wiley, 1941 and 1948.
225 Gimperlein D, 'Tragverhalten von Rahmenecken mit geknickten Gurten', *Schweißen u Schneiden*, 1990, **42** (5), 234–240, with English version.

226 Gosch T and Petershagen H, 'Einfluß von Einbrandkerben auf die Schwingfestigkeit von Stumpfnähten', *Schweißen u Schneiden*, 1997, **49** (3), 158–163, with English version.
227 Guan D, 'A method of predicting the fatigue life curve for misaligned joints', *Int J Fatigue*, 1996, **18** (4), 221–226.
228 Hentschel K, Berger P, Rossler K and Schmidt M, 'Weld geometry as a factor controlling the fatigue strength of butt-welded joints', *Welding Int* 1990, **4** (6), 494–499.
229 Heywood R B, *Designing by Photoelasticity*, London, Chapman & Hall, 1952.
230 Iida K and Uemura T, 'Stress concentration factor formulas widely used in Japan', *Fatigue Fract Engng Mater Struct*, 1995, **19** (6), 779–786, and IIW Doc XIII-1530-94.
231 Jakubovskii V V and Valteris I I, Geometrical parameters of butt and fillet welds and their influence on the welded joint fatigue life, IIW Doc XIII-1326-89.
232 Janosch J J and Debiez S, 'Optimisation de la tenue en fatigue des assemblages d'angle par l'approche mechanique locale', *Soud Techn Conn*, 1998, **52** (3/4), 3–9.
233 Janosch J J and Debiez S, Evaluation of the fatigue strength of longitudinal welded assemblies as a function of the industrial welding practice – application of the local approach, IIW Doc XIII-1719-98.
234 Janosch J J and Debiez S, 'Influence of the shape of undercut on the fatigue strength of fillet welded assemblies – application of the local approach', *Welding in the World*, 1998, **41**, 350–360.
235 Janosch J J, Debiez S, Clerge M and Dang Van K, 'Application of the local mechanical approach for optimising the fatigue strength of fillet weld assemblies', *Proceedings International Conference on Performance of Dynamically Loaded Welded Structures*, New York, WRC, 1997, pp 265–272.
236 Kalla G U, Einflußgrößen auf die Nahteigenschaften CO_2-laserstrahlgeschweißter Stahlbleche in Dicken von 10 bis 20 mm (Influencing parameters on weld properties of CO_2 laser beam welded sheet steel in thicknesses of 10 to 20 mm), Dr-Ing thesis, Aachen, Techn Univ, 1994, and DVS-Bericht 167, Düsseldorf, DVS-Verlag, 1994.
237 Karkhin V A, 'Effects of weld shape on the distribution of stresses, in tension, in butt joints in thick metal', *Automatic Welding*, 1985, (9), 24–27.
238 Karkhin V A, 'Influence of weld shape on stress distribution in tension-loaded butt joints of large thickness' (in Russian), *Avt Svarka*, 1985, (9), 25–28.
239 Karkhin V A, 'Influence of loading configuration and weld shape on stress distribution in T joints' (in Russian), *Avt Svarka*, 1987, (11), 14–18.
240 Karkhin V A, Kostylev V I and Stakanov V I, 'The influence of geometric parameters of butt joints, T joints and cruciform joints on the stress concentration factor' (in Russian), *Avt Svarka*, 1988, (3), 6–11.
241 Kaufmann H, Sonsino C M, Demofonti G, Budano S, Hannus F, Wegmann H, Sedlacek G and Müller C, Fatigue behaviour of welded medium and high strength steels – evaluation on basis of notch factors and local stresses, IIW-Doc. XIII-1767-99.
242 Kobayashi A S (Ed), *Handbook on Experimental Mechanics*, Bethel Conn, Society Experimental Mechanics, 1999 (2nd edn).
243 Köttgen V B, Olivier R and Seeger T, 'The influence of plate thickness on fatigue strength of welded joints, a comparison of experiments with prediction

by fatigue notch factors', *Steel in Marine Structures*, Amsterdam, Elsevier Science, 1987, pp 303–313.
244 Köttgen R, Olivier R and Seeger T, 'Schwingfestigkeitsanalyse für Schweißverbindungen auf die Grundlage örtlicher Beanspruchungen (Fatigue analysis of welded connections based on local stresses)', *Expert'91 – Berechnung, Gestaltung und Fertigung von Schweißkonstruktionen im Zeitalter der Expertensysteme,* DVS-Bericht 133, Düsseldorf, DVS-Verlag, 1991, pp 75–85, and IIW Doc XIII-1408-91.
245 Köttgen V B, Olivier R and Seeger T, 'Der Schaden an der großen Windkraftanlage GROWIAN, Schwingfestigkeitsanalyse der versagenkritischen Schweißverbindungen', *Konstruktion*, 1993, **45**, 1–9.
246 Kuguel R, 'A relation between theoretical stress concentration factor and fatigue notch factor deduced from the concept of highly stressed volume', *ASTM Proc 61*, 1961, 732–744.
247 Lang O, 'Dimensionierung komplizierter Bauteile aus Stahl im Bereich der Zeit- und Dauerfestigkeit', *Z Werkstofftech*, 1979, **10** (1), 24–29.
248 Lehrke H P, 'Berechnung von Formzahlen bei Schweißverbindungen', *Konstruktion*, 1999, **51** (1/2), 47–52, and LBF-Bericht 7195/2, Darmstadt, Fraunhofer-Inst f Betriebsfest, 1995.
249 Morgenstern C, Sonsino C M, Hobbacher A and Sorbo F, 'Fatigue design of aluminium welded joints by the local stress concept with the fictitious notch radius of r_f = 1 mm', *Welding and Cutting*, 2005, **4** (6), 318–322.
250 Morgenstern C, Sonsino C M, Kotowski J, Dilger K and Sorbo F, 'Anwendung des Konzepts der Mikrostützwirkung zur Schwingfestigkeitsbewertung geschweißter Aluminiumverbindungen aus AlMg4.5Mn and AlMgSi1-T6', *Schweißen u Schneiden*, 2004, **56** (10), 538–544, and *Welding and Cutting*, 2005, **4** (6), 318–322 (English version).
251 Muskhelishvili N I, *Some Basic Problems of the Mathematical Theory of Elasticity*, Groningen, Noordhoff, 1953 and 1963.
252 Neuber H, *Kerbspannungslehre*, Berlin, Springer-Verlag, 1937, 1958, and 1985.
253 Neuber H, *Theory of Notch Stresses*, Ann Arbor Mich, Edwards, 1946.
254 Neuber H, 'Über die Berücksichtigung der Spannungskonzentration bei Festigkeitsberechnungen', *Konstruktion*, 1968, **20** (7), 245–251.
255 Nishida M, *Stress Concentration* (in Japanese), Morikita Shuppan, 1967 and 1973.
256 Nitschke-Pagel T and Wohlfahrt H, 'Einfluss von Eigenspannungen auf die Schwingfestigkeit geschweißter Feinkornbaustähle', *Eigenspannungen und Verzug durch Wärmeeinwirkung*, Weinheim, Wiley-VHC, 1999, pp 231–308.
257 Norris C H, 'Photoelastic investigation of stress distribution in transverse fillet welds', *Welding J, Res Suppl*, 1945, **24** (10), 557s ff.
258 Ohta S, Asai K and Ohja S, 'Root failure resulting from fillet toe dressing', *Trans Japan Welding Soc*, 1992, **23** (1), 24–32, and IIW Doc XIII-1465-92.
259 Olivier R, Köttgen V B and Seeger T, Schweißverbindung I – Schwingfestigkeitsnachweise für Schweißverbindungen auf der Grundlage örtlicher Beanspruchungen (Welded Joints I – Fatigue strength assessment method for welded joints based on local stresses), FKM-Forschungsheft 143, Frankfurt/M, FKM, 1989.
260 Olivier R, Köttgen V B and Seeger T, Schweißverbindung II – Untersuchung zur Einbindung eines neuartigen Zeit- und Dauerfestigkeitsnachweises von

Schweißverbindungen aus Stahl in Regelwerke (Welded joints II – investigation of inclusion into codes of a novel fatigue strength assessment method for welded joints in steel), FKM-Forschungsheft 180, Frankfurt/M, FKM, 1994.
261 Petershagen H, A comparison of different approaches to the fatigue strength assessment of welded components, IIW Doc XII-1208-86.
262 Petershagen H, 'Erfahrungen mit dem Kerbspannungskonzept nach Radaj', *Kerben und Betriebsfestigkeit*, DVM-Bericht 115, Berlin, DVM, 1989, pp 89–102.
263 Petershagen H, A comparison of two different approaches to the fatigue-strength assessment of cruciform joints, IIW Doc XIII-1410-91.
264 Petershagen H, Fatigue tests with hyperbaric dry butt welded specimens, Bericht 522, Inst f Schiffbau, Hamburg Univ, 1992, and IIW Doc XIII-1445–92.
265 Peterson R E, *Stress Concentration Factors*, New York, John Wiley, 1953 and 1974.
266 Peterson R E, 'Relation between stress analysis and fatigue of metals', *Proc SESA*, 1950, **11** (2), 199–206.
267 Peterson R E, 'Notch sensitivity', *Metal Fatigue*, New York, McGraw Hill, 1959, pp 293–306.
268 Prowatke G, Fischer L and Weydling C, 'Zur Abschätzung der Wöhler-Linien von Schweißverbindungen nach dem Kerbgrundkonzept', *Jahrbuch Schiffbautechn Ges*, 1993, **87**, 415–424.
269 Radaj D, Unendlich ausgedehnte Scheibe mit stirnseitig angeschlossenen, beidseitigen Rechteckplastern unter Zugbelastung, ein Beitrag zur Spannungsermittlung, Dr-Ing thesis, Braunschweig, Techn Univ, 1964, and *Grundlagen d Landtechnik*, 1964, **19**, 37–65.
270 Radaj D, 'Formzahlen geschlitzter und ungeschlitzter Kreuzknoten bei Zug und Biegung', *Konstruktion*, 1965, **17** (7), 257–260.
271 Radaj D, 'Beitrag zur Frage der Tragfähigkeit geschweißter I-Träger bei Dauerschwingbelastung', *Schweißen u Schneiden*, 1966, **18** (2), 57–60.
272 Radaj D, 'Grundzüge eines neuen Verfahrens zum Bestimmen der Tragfähigkeit von Schweißverbindungen', *Forschung im Ingenieurwesen*, 1967, **33** (1), 26–31, and **33** (2), 43–58.
273 Radaj D, 'Vergleich errechneter und gemessener Spannungen für einen Zugstab mit aufgeschweißten Kreislaschen', *Schweißen u Schneiden,* 1967, **19** (3), 107–110.
274 Radaj D, 'Zur Frage der Formzahlen von Kreuzknoten', *Konstruktion*, 1967, **19** (8), 328–330.
275 Radaj D, 'Beitrag zum Berechnen der Spannungskonzentration bei Schweißverbindungen', *Tragfähigkeitsermittlung bei Schweißverbindungen*, Düsseldorf, DVS-Verlag, 1968, Vol 1, pp 132–172 and Vol 2, pp 168–172.
276 Radaj D, 'Näherungsweise Berechnung der Formzahl von Schweißnähten', *Schweißen u Schneiden*, 1969, **21** (3), 97–103, and **21** (4), 151–158.
277 Radaj D, *Kerbspannungen an Öffnungen und starren Kernen (Notch Stresses at Openings and Rigid Cores)*, DVS-Bericht 9, Düsseldorf, DVS-Verlag, 1970.
278 Radaj D, 'Untersuchungen zur geometrischen Form von Stumpf- und Kehlnähten', *Schweißen u Schneiden*, 1970, **22** (5), 206–209.
279 Radaj D, *Kerbspannungen an Öffnungen und starren Kernen*, habilitation thesis, Braunschweig Techn Univ, 1971, and Stuttgart, published by the author, 1971.

280 Radaj D, 'Kerbspannungsanalyse nach der Finite-Element-Methode an Kehlnähten', *Schweißen u Schneiden*, 1975, **27** (3), 86–89.
281 Radaj D, 'Kerbwirkung zweiachsig schräg beanspruchter Schweißstöße', *Schweißen u Schneiden*, 1984, **36** (6), 254–259, and E86–E88 (English version).
282 Radaj D, 'Kerbwirkung von Schweißstößen hinsichtlich Ermüdung', *Konstruktion*, 1984, **36** (8), 285–292.
283 Radaj D, 'Kerbspannungsnachweis für die dauerschwingfeste geschweißte Konstruktion', *Konstruktion*, 1985, **37** (2), 53–59.
284 Radaj D, *Gestaltung und Berechnung von Schweißkonstruktionen – Ermüdungsfestigkeit*, Düsseldorf, DVS-Verlag, 1985; English edition given in reference 4.
285 Radaj D, 'Schwingfestigkeit von Biegeträgern mit Quersteife nach dem Kerbgrundkonzept', *Stahlbau*, 1985, **54** (8), 243–249, and **54** (12), 384.
286 Radaj D, 'Evaluation of finite element stresses at corners, welded structures as an example', *Finite Element News*, 1986, (1), 12–13.
287 Radaj D, 'Zur vereinfachten Darstellung der mehrparametrigen Fromzahlabhängigkeit', *Konstruktion*, 1986, **38** (5), 193–197.
288 Radaj D, 'Wirksamkeit der Entlastungsnut im geschweißten Behälterboden', *Konstruktion*, 1986, **38** (6), 237–242.
289 Radaj D, 'Berechnung der Dauerfestigkeit von Schweißverbindungen ausgehend von den Kerbspannungen', *Dauerfestigkeit und Zeitfestigkeit,* VDI-Berichte 661, Düsseldorf, VDI-Verlag, 1988, pp 67–98.
290 Radaj D, 'Rechnerische Ermittlung der Kerb- und Rißbeanspruchung', *Konstruktion*, 1990, **42**, 143–148.
291 Radaj D, 'Fatigue notch factor of gaps in welded joints reconsidered', *Engng Fract Mech*, 1997, **57** (4), 405–407.
292 Radaj D, Gerlach H D and Gorsitzke B, 'Experimentell-rechnerischer Kerbspannungsnachweis für eine geschweißte Kesselkonstruktion', *Konstruktion*, 1988, **40**, 447–452.
293 Radaj D and Helmers K, 'Bewertung von Schweißverbindungen hinsichtlich Schwingfestigkeit nach dem Kerbspannungskonzept', *Konstruktion*, 1997, **49**, 41–27.
294 Radaj D and Kandel W, 'Kerbspannungen am Last tragenden elastischen Kern', *Forschung im Ingenieurwesen*, 1973, **39** (1), 1–12.
295 Radaj D and Möhrmann W, 'Kerbwirkung querbeanspruchter Schweißstöße', *Schweißen u Scheiden*, 1984, **36** (2), 57–63, and E20–E23 (English version).
296 Radaj D and Möhrmann W, 'Kerbwirkung an Schulterstäben unter Querschub', *Konstruktion*, 1984, **36** (10), 399–402.
297 Radaj D and Schilberth G, *Kerbspannungen an Ausschnitten und Einschlüssen (Notch Stresses at Cut-outs and Inclusions)*, Düsseldorf, DVS-Verlag, 1977.
298 Radaj D and Schilberth G, 'Kerbspannungen an Ausschnitten begurteter Biegeträger', *Schweißen u Schneiden*, 1978, **38** (8), 294–296.
299 Radaj D and Schilberth G, 'Kerbspannungsberechnungen für eine Schwerlasttraverse im Vergleich', *Schweißen u Schneiden*, 1981, **33** (5), 220–223, and E74–E75 (English version).
300 Radaj D and Zafirakopoulos N, 'Kräfte und Formänderungen an der Quersteife dünnwandiger U-Stäbe', *Forschung im Ingenieurwesen*, 1973, **39** (3), 69–80.
301 Radaj D and Zhang S, 'Mehrparametrige Strukturoptimierung hinsichtlich Spannungserhöhungen', *Konstruktion*, 1990, **42**, 289–292.

302 Radaj D and Zhang S, 'Multiparameter design optimisation in respect of stress concentrations', *Engineering Optimisation in Design Processes*, Berlin, Springer-Verlag, 1991, pp 181–189.
303 Radaj D and Zhang S, 'Notch effect of welded joints subjected to antiplane shear loading', *Engng Fract Mech*, 1992, **43** (4), 663–669.
304 Rainer G, Errechnen von Spannungen in Schweißverbindungen mit der Methode der Finiten Elemente, FKM-Forschungsheft No 74, Frankfurt/M, FKM, 1979.
305 Rainer G, 'Parameterstudien mit finiten Elementen, Berechnung der Bauteilfestigkeit von Schweißverbindungen unter äußeren Beanspruchungen', *Konstruktion*, 1983, **37** (2), 45–52.
306 Rapp J, Laserschweißeignung von Aluminiumwerkstoffen für Anwendungen im Leichtbau (Welding suitability of aluminium alloys for application in lightweight design), Dr-Ing thesis, Stuttgart Univ, 1996, and Stuttgart, Teubner, 1996.
307 Ring M, Schwingfestigkeit von Laserstrahlschweißverbindungen hochfester Baustähle, Dr-Ing thesis, Aachen, Techn Univ, 1994.
308 Rodriguez J E, Brennan F P and Dover W D, 'Minimization of stress concentration factors in fatigue crack repairs', *Int J Fatigue*, 1998, **20** (10), 719–725.
309 Rudolph J, Weiß E and Forster M, Konzeptkonforme Modellierung ermüdungsgefährdeter Druckbehälterschweißnähte als Modul einer modernen rechnerischen Lebensdauerabschätzung, Report, Aachen, Shaker Verlag, 2001.
310 Ruge J and Drescher G, 'Der Kreuzstoß spezieller Sondergüte mit der Dauerfestigkeit der Stumpfstoß-Sondergüte', *Schweißen u Schneiden*, 1985, **37** (4), 149–157, with English version.
311 Savin O N, Stress distribution around holes (translated from Russian), NASA Rep TTF-607, 1970; German in-part translation by VEB Technik, Berlin, 1956.
312 Schijve J, 'Stress gradients around notches', *Fatigue Engng Mater Struct*, 1980, **3** (4), 325–338.
313 Seeger T and Amstutz H, 'Betriebsfestigkeitsnachweise für Schweißverbindungen auf der Grundlage örtlicher Konzepte', *Fortschritte bei der Konstruktion und Berechnung geschweißter Bauteile*, DVS-Bericht 187, Düsseldorf, DVS-Verlag, 1997, pp 190–208.
314 Siebel E and Stieler M, 'Ungleichförmige Spannungsverteilung bei schwingender Beanspruchung', *VDI-Zeitschrift*, 1955, **97** (5), 121–126.
315 Solakian A G, 'Stresses in transverse fillet welds by photoelastic methods', *Welding J*, 1934, **13** (2), 22ff.
316 Sonsino C M, 'Zur Bewertung des Schwingfestigkeitsverhaltens von Bauteilen mit Hilfe örtlicher Beanspruchungen', *Konstruktion*, 1993, **45**, 25–33.
317 Sonsino C M, 'Über den Einfluß von Eigenspannungen, Nahtgeometrie und mehrachsigen Spannungszuständen auf die Betriebsfestigkeit geschweißter Konstruktionen aus Baustählen', *Materialwiss u Werkstofftechn*, 1994, **25** (3), 97–109.
318 Sonsino C M, 'Multiaxial and random loading of welded structures', *Proceedings International Conference on Performance of Dynamically Loaded Welded Structures*, New York, WRC, 1997, pp 317–331.
319 Sonsino C M, 'Influence of load and deformation controlled multiaxial tests on fatigue life to crack initiation', *Int J Fatigue*, 2001, **23**, 159–167.

320 Sonsino C M and Brandt U, Influence of the weld-geometry on the fatigue behaviour of 15 mm thick aluminium weldments of AlMg4.5Mn (AA 5083), IIW Doc XIII-1821-00.
321 Sonsino C M and Küppers M, 'Spannungskonzentration und Schadensakkumulation bei mehrachsig belasteten Schweißverbindungen', *Bauteillebensdauer – Rechnung oder Versuch?* DVM-Bericht 126, Berlin, DVM, 1999, pp 85–98.
322 Sonsino C M and Lagoda T, 'Assessment of multiaxial fatigue behaviour of welded joints under combined bending and torsion by application of a fictitious notch radius', *Int J Fatigue*, 2004, **26** (5), 265–279.
323 Sonsino C M and Pfohl R, 'Multiaxial fatigue of welded shaft-flange connections of stirrers under random non-proportional torsion and bending', *Int J Fatigue*, 1990, **12** (5), 425–431.
324 Sonsino C M, Radaj D, Brandt U and Lehrke H P, 'Fatigue assessment of welded joints in AlMg4.5Mn (5083) aluminium alloy by local approaches', *Int J Fatigue*, 1999, **21** (9), 985–999, and IIW Doc XIII-1717-98.
325 Sonsino C M and Werner S, Die Ersatzstrukturlänge nach Peterson und Neuber–Radaj und das Konzept des höchstbeanspruchten Werkstoffvolumens am Beispiel des Baustahls St52-3, LBF-Bericht 8137, Darmstadt, Fraunhofer-Inst f Betriebsfest, 1996.
326 Soya I, Fatigue strength evaluation of welded joint based on local and structural stress concentration factors at weld toe, IIW-Doc. XIII-1672-97.
327 Soya I, Seto A and Tanaka Y, Fatigue-strength and its thickness effect of steel joints with improved weld, IIW Doc XIII-1447-92.
328 Stötzel J and Sedlacek G, Material Woehler curves of welded aluminium connections, *Proceedings 10th Nordic Steel Construction Conference*, Copenhagen, Danish Steel Inst, 2004, pp 211–220.
329 Takahashi I, Yoshii T, Iidaka H, Fujii E and Matsuoka K, 'Fatigue-strength of non-load-carrying fillet welded joints, effects of weld residual stresses and stress concentration', *Fatigue Fract Engng Mater Struct*, 1993, **16** (1), 37–51.
330 Taylor D, Barrett N and Lucano G, 'Some new methods for predicting fatigue in welded joints', *Int J Fatigue*, 2002, **24**, 509–518.
331 Taylor D and Wang G, 'A critical distance theory which unifies the prediction of fatigue limits for large and small cracks and notches', *Proceedings Fatigue '99*, Higher Education Press, Beijing, China, Vol 1, pp 579–584.
332 Taylor D and Wang G, 'The validation of some methods of notch fatigue analysis', *Fatigue Fract Engng Mater Struct*, 2000, **23** (3), 387–395.
333 Thouvenel L and Lieurade H P, The fatigue strength of friction welded joints, IIW Doc XIII-1849-00.
334 Topper T H and El Haddad M H, 'Fracture mechanics analysis for short fatigue cracks', *Canadian Metall Quart*, 1979, **18**, 207–213.
335 Tsuji I, 'Estimation of stress concentration factor at weld toe of non-load-carrying fillet welded joints' (in Japanese), *West Japan Soc Naval Architects*, 1990, **80**, 241–251.
336 Ushirokawa O and Nakayama E, Stress concentration factor at welded joints (in Japanese), Ishikawajima-Harima Gihou (Techn Rep), 1983, **23** (4).
337 Watanabe O, Matsumoto S, Nakano Y and Saito Y, 'Fatigue Strength of welded joints in high strength steel – effects of stress concentration factor and welding residual stress', *Welding Int*, 1996, **10** (3), 201–206.

338 Weibull W, A Statistical Theory of Strength of Materials, *Proceedings Royal Swedish Institute Engineering Research*, no 151, Stockholm, Generalstabens Litografiska Anstalts Förlag, 1939.
339 Weichel F and Petershagen H, Fatigue-strength of laser-welded structural steels with thicknesses between 8 and 20 mm, IIW Doc XIII-1590-95.
340 Wellinger K and Dietmann H, *Festigkeitsberechnung (Strength Calculation)*, Stuttgart, Kröner-Verlag, 1976.
341 Werner S, Radaj D and Sonsino C M, 'Schwingfestigkeit von Schweiß verbindungen aus der Aluminiumlegierung AlMg4,5Mn (AA5083) nach dem Konzept der Mikrostützwirkung', *Materialwiss u Werkstofftechn*, 1999, **30**, 125–135.
342 Witt M, Yousefi F and Zenner H, 'Fatigue strength of welded joints under multiaxial loading: comparisons between experiments and calculations', *Multiaxial Fatigue and Deformation: Testing and Prediction*, ASTM STP 1387, Philadelphia Pa, ASTM, 2000, pp 191–210.
343 Wu B, Dekoopmann X, Zakrzewski D, Robin C, Mesmacque G and Lieurade H P, Multiaxial fatigue life assessment for aluminium welded structures, IIW Doc XIII-2037-04.
344 Zienkiewicz O C and Taylor R L, *The Finite Element Method, Vol 1: The Basis*, Oxford, Butterworth-Heinemann, 2000.

Chapter 5 Notch strain approach for seam-welded joints

345 Bäumel A and Seeger T, 'Thick surface layer model – life calculations for specimens with residual stress distribution and different material zones', *Proceedings International Conference on Residual Stresses (ICRS2)*, London, Elsevier Science, 1989, pp 809–914.
346 Bäumel A and Seeger T, *Materials Data for Cyclic Loading, Suppl 1*, Amsterdam, Elsevier Science, 1990.
347 Basquin O H, 'The exponential law of endurance tests', *Proc ASTM*, 1910, **10**, 625–630.
348 Bauschinger J, 'Über die Veränderung der Elastizitätsgrenze und der Festigkeit des Eisens und Stahls durch Strecken, Quetschen, Erwärmen und Abkühlen und durch oftmals wiederholte Belastung', *Mitt Mech-Tech Lab*, 1886, **13**, Munich.
349 Bertini L, Fontanari V and Straffelini G, 'Influence of postweld treatment on the fatigue behaviour of Al-alloy welded joints', *Int J Fatigue*, 1998, **20** (10), 749–755.
350 Bhuyan G and Vosikovski O, 'Prediction of fatigue crack initiation lives for welded plate T-joints based on the local stress-strain approach', *Int J Fatigue*, 1989, **11**, 153–159.
351 Bohlmann B, Zur Schwingfestigkeit von Schweißverbindungen – das örtliche Konzept am Beispiel einer Rohrverzweigung (Fatigue strength of welded joints – the local concept applied to a pipe branching), Bericht 549, Inst f Schiffbau, Hamburg Univ, 1995.
352 Bohlmann B, Applications of local approaches to the fatigue assessment of welded tubular joints (actually a welded pipe branching), IIW Doc XIII-1591-95.

353 Boller C and Seeger T, *Materials Data for Cyclic Loading, Part A-E*, Amsterdam, Elsevier Science, 1987.
354 Brandt U, Lawrence F V and Sonsino C M, 'Fatigue crack initiation and growth in AlMg4,5Mn butt weldments', *Fatigue Fract Engng Mater Struct*, 2001, **24**, 117–126.
355 Clormann U H, Örtliche Beanspruchungen von Schweißverbindungen als Grundlage des Schwingfestigkeitsnachweises (Local stresses and strains in welded joints as basis of fatigue strength assessment), Heft 45, Inst f Stahlbau u Werkstoffmech, Darmstadt, Techn Univ, 1986.
356 Clormann U H and Seeger T, 'Örtliche Beanspruchungssingularitäten in Schweißverbindungen ohne Riß', DVM-Bericht, AK Bruchvorgänge, Berlin, DVM, 1987, pp 95–104.
357 Coffin L F, 'A study of the effects of cyclic thermal stresses on a ductile metal', *Trans ASME*, 1954, **76** (6), 931–950.
358 Coffin L F, 'Fatigue in machines and structures – power generation', *Fatigue and Microstructure*, Materials Park, ASM, 1979, pp 1–27.
359 Fricke W and Paetzold H, 'Application of the cyclic strain approach to the fatigue failure of ship structural details', *J Ship Res*, 1987, **31** (9), 177–185.
360 Glinka G, 'Energy density approach to calculation of inelastic strain-stress near notches and cracks', *Engng Fract Mech*, 1985, **22** (3), 485–508.
361 Glinka G, 'Calculation of inelastic notch tip strain-stress histories under cyclic loading', *Engng Fract Mech*, 1985, **22** (5), 839–854.
362 Gonyea D C, 'Method for low-cycle fatigue design including biaxial stress and notch effects', ASTM STP 520, Philadelphia Pa, ASTM, 1973, pp 678–687.
363 Goodman J, *Mechanics Applied to Engineering*, London, Longmans & Green, 1899.
364 Heuler P and Seeger T, 'Rechnerische und experimentelle Lebensdauervorhersage am Beispiel eines geschweißten Bauteils', *Konstruktion*, 1983, **35** (1), 21–26.
365 Higashida Y, Burk J D and Lawrence F V, 'Strain-controlled fatigue behaviour of ASTM A36 and A515, grade F steels and 5083-O aluminium weld materials', *Welding J, Res Suppl*, 1978, **57**, 334s–344s.
366 Ho N H and Lawrence F V, 'Constant-amplitude and variable load history fatigue test results and predictions for cruciform and lap welds', *Theor Appl Fract Mech*, 1984, **1**, 3–21.
367 Hou C Y and Charng J J, 'Models for the estimation of weldment fatigue crack initiation life', *Int J Fatigue*, 1997, **19** (7), 537–541.
368 Hou C Y and Lawrence F V, 'A crack closure model for the fatigue behaviour of notched components', *Advances in Fatigue Lifetime Predictive Techniques*, ASTM STP 1292, Philadelphia Pa, ASTM, 1996, Vol 3, pp 116–135.
369 Iida K, Shimamoto H and Itoh N, 'Surface micro-cracks in block and random fatigue cycling of 500 MPa strength steel and weld material', *Fatigue Fract Engng Mater Struct*, 1996, **19** (6), 635–646.
370 Jakubczak H and Glinka G, 'Fatigue analysis of manufacturing defects in weldments', *Int J Fatigue*, 1986, **8** (2), 51–57.
371 Jhansale H R and Topper T H, 'Engineering analysis of the inelastic stress response of a structural metal under variable cyclic strains', *Cyclic Stress-Strain Behaviour – Analysis, Experimentation and Fatigue Prediction*, ASTM STP 519, Philadelphia Pa, ASTM, 1973, pp 246–270.

372 Kandil F A, Brown M W and Miller K J, 'Biaxial low-cycle fatigue failure of 315 stainless steel at elevated temperatures', *International Conference on Mechanical Behaviour and Nuclear Applications of Stainless Steel at Elevated Temperatures*, London, The Metals Soc, 1982, pp 203–209.
373 Klee S, Das zyklische Spannungs-Dehnungs- und Bruchverhalten verschiedener Stähle (The cyclic stress–strain and fracture behaviour of different steels), Heft 22, Inst f Stahlbau u Werkstoffmech, Darmstadt, Techn Univ, 1973.
374 Kloos K H, 'Kerbwirkung und Schwingfestigkeitseigenschaften', *Kerben und Betriebsfestigkeit*, DVM-Berichte 115, Berlin, DVM, 1989, pp 7–40.
375 Lawrence F V, Burk J D and Yung J Y, 'Influence of residual stress on the predicted fatigue life of weldments', *Residual Stress Effects in Fatigue*, ASTM STP 776, Philadelphia Pa, ASTM, 1982, pp 33–43.
376 Lawrence F V, Dimitrakis S D and Chen N, 'The fatigue resistance of automotive weldments', *Proceedings International Conference on Performance of Dynamically Loaded Welded Structures*, New York, WRC, 1997, pp 254–264.
377 Lawrence F V, Ho N J and Mazumdar P K, 'Predicting the fatigue resistance of welds', *Ann Rev Mater Sci*, 1981, **11**, 401–425.
378 Lawrence F V, Mattos R J, Higashida Y and Burk J D, 'Estimating the fatigue crack initiation life of welds', *Fatigue Testing of Weldments*, ASTM STP 648, Philadelphia Pa, ASTM, 1978, pp 134–158.
379 Lawrence F V and Mazumdar P K, 'Application of strain-controlled fatigue concepts to the prediction of weldment fatigue life', *Kurzzeitschwingfestigkeit und elastoplastisches Werkstoffverhalten*, DVM-Bericht 105, Berlin, DVM, 1979, pp 469–478.
380 Manson S S, 'Behaviour of materials under conditions of thermal stress', *Heat Transfer Symposium*, University of Michigan, Engineering Research Institute, 1953, pp 9–75, and NACA TN 2933, 1954.
381 Manson S S, 'Fatigue – a complex subject – some simple approximations', *Exp Mech*, 1965, **5** (7), 193–226.
382 Masing G, 'Eigenspannungen und Verfestigung beim Messing', *Proceedings International Congress of Applied Mechanics,* Zürich, 1926, pp 332–335.
383 Matsuishi M and Endo T, *Fatigue of Metals Subjected to Varying Stress* (in Japanese), Fukuoka, Japan Society of Mechanical Engineers, 1968.
384 Mattos R J and Lawrence F V, 'Estimation of the fatigue crack initiation life in welds using low cycle fatigue concepts', *SAE SP-424*, Warrendale Pa, SAE, 1977.
385 Miner M A, 'Cumulative damage in fatigue', *Trans ASME, J Appl Mech*, 1945, **12** (3), A159–A164.
386 Molski K and Glinka G, 'A method of elastic-plastic stress and strain calculation at a notch root', *Mater Sci Engng*, 1981, **50**, 93–100.
387 Morrow J D, 'Cylic plastic strain energy and fatigue of metals', ASTM STP 378, Philadelphia Pa, ASTM, 1965, pp 45–87.
388 Petitpas E, Bebrun B, de Meerleer S, Fournier P, Charrier A and Pollet F, Use of the local approach for the calculation of the fatigue strength of welds, IIW Doc XIII-1850-00.
389 Ramberg W and Osgood W R, Description of stress–strain curves by three parameters, Techn Rep 902, NACA, 1943.

390 Reemsnyder H S, 'Evaluating the effect of residual stresses on notched fatigue resistance', *Materials, Experimentation and Design in Fatigue*, Society Environmental Engineers, 1981, pp 273–295.
391 Rudolph J and Weiß E, Ein Modernes Konzept für den Ermüdungsnachweis von Druckbehälterschweißverbindungen unter spezieller Berücksichtigung von Beanspruchungen im niedrigzyklischen Bereich und Schadensakkumulationseffekten, Report, Aachen, Shaker-Verlag, 2000.
392 Seeger T and Heuler P, 'Generalized application of Neuber's rule', *J Testing Evaluation*, 1980, **8** (4), 199–204.
393 Seeger T and Zacher P, 'Lebensdauervorhersage zwischen Traglast und Dauerfestigkeit am Beispiel ausgeklinkter Träger,' *Bauingenieur*, 1994, **69**, 13–23.
394 Siljander A, Kurath P and Lawrence F V, 'Multiaxial nonproportional fatigue of weldments', *International Conference Offshore Mechanics and Arctic Engineering (OMAE 1990)*, New York, ASME, 1990, Vol 3A, pp 229–237.
395 Singh P J, Achar D R, Guha B and Nordberg H, 'Fatigue life prediction of gas tungsten arc welded AISI 304L cruciform joints with different LOP sizes', *Int J Fatigue*, 2003, **25** (1), 1–7.
396 Skopura M, 'Fatigue crack initiation life prediction for welded joints by low cycle fatigue approach', *Fatigue Fract Engng Mater Struct*, 1990, **13**, 597–613.
397 Smith K N, Watson R and Topper T H, 'A stress-strain function for the fatigue of metals', *J Mater, JMLSA*, 1970, **5** (4), 767–778.
398 Socie D F and Marquis G B, *Multiaxial Fatigue*, Warrendale Pa, SAE, 2000.
399 Socie D F, Waill L A and Dittmer D F, 'Biaxial fatigue of Inconel 718 including mean stress effects', *Multiaxial Fatigue*, ASTM STP 853, Philadelphia Pa, ASTM, 1985, pp 463–481.
400 Sonsino C M, Einfluß von Kaltverformungen bis 5% auf das Kurzzeitschwingfestigkeitsverhalten metallischer Werkstoffe (Influence of cold forming up to 5% on the low-cycle fatigue behaviour of metallic materials), LBF-Bericht FB-161, Darmstadt, Fraunhofer-Inst f Betriebsfest, 1982.
401 Sonsino C M, Schwingfestigkeit von geschweißten Komponenten unter komplexen elasto-plastischen, mehrachsigen Verformungen (Fatigue strength of welded components under complex elastic-plastic multiaxial deformations), EU Rep 16024DE, Brussels, ECCS, 1997.
402 Tateishi K and Hanji T, 'Low cycle fatigue strength of butt-welded steel joints by means of new testing system with image technique', *Int J Fatigue*, 2004, **26** (12), 1349–1356.
403 Testin R A, Yung J Y, Lawrence F V and Rice R C, 'Predicting the fatigue resistance of steel weldments', *Welding J, Res Suppl*, 1987, **66** (4), 93s–98s.
404 Tricoteaux A, Fardoun F, Degallaix S and Sauvage F, 'Fatigue crack initiation life prediction in high strength structural steel welded joints', *Fatigue Fract Engng Mater Struct*, 1995, **18** (2), 189–200.
405 Vormwald M and Seeger T, 'Crack initiation life estimations for notched specimens with residual stresses based on local strains', *Residual Stresses in Science and Technology*, Oberursel, DGM-Informationsges, 1987, pp 743–750.
406 Vormwald M and Seeger T, 'The consequences of short crack closure on fatigue crack growth under variable-amplitude loading', *Fatigue Fract Engng Mater Struct*, 1991, **14** (2/3), 205–225.
407 Yung J Y and Lawrence F V, 'Analytical and graphical aids for the fatigue design of weldments', *Fatigue Fract Engng Mater Struct*, 1985, **8** (3), 223–241.

Chapter 6 Crack propagation approach for seam-welded joints

408 Aaghaakouchak A, Glinka G and Dharmavasan S, 'A load shedding model for fracture mechanics analysis of fatigue cracks in tubular joints', *Proceedings International Conference on Offshore Mechanics and Arctic Engng (OMAE'89)*, New York, ASME, 1989, pp 159–165.

409 Albrecht P and Yamada K, 'Rapid calculation of stress intensity factors', *J Struct Div ASCE*, 1977, **103** (ST2), 377–389.

410 Amstutz H, Störzel K and Seeger T, 'Fatigue crack growth of a welded tube-flange connection under bending and torsional loading', *Fatigue Fract Engng Mater Struct*, 2001, **24** (5), 357–368.

411 Anderson T L, *Fracture Mechanics – Fundamentals and Applications*, Boca Raton Fla, CRC Press, 1995 (2nd ed).

412 Bayley C, Glinka G and Porter J, 'Fatigue crack initiation and growth in A517 submerged arc welds under variable amplitude loading', *Int J Fatigue*, 2000, **22** (9), 799–808.

413 Beghini M and Bertini L, 'Fatigue crack propagation through residual stress fields with closure phenomena', *Engng Fract Mech*, 1990, **36** (3), 379–387.

414 Bell R, Stress intensity factors for weld toe cracks in welded T plate joints, Rep CANMET Project 708803, Faculty to Engineering, Carleton University, Ottawa Ont, Canada, 1987.

415 Bell R and Vosikovsky O, 'A fatigue life prediction model for multiple cracks in welded joints for offshore structures', *Proceedings 11th International Conference OMAE*, Houston Tex, ASME International Technical Institute, 1992, pp 501–507.

416 Bell R, Vosikovsky O, Burns D and Mohaupt U, 'A fracture mechanics model for life prediction of welded plate joints', *Steel in Marine Structures*, *Proceedings 3rd International ECSC Offshore Conference*, Amsterdam, Elsevier, 1987, pp 901–910.

417 Beretta S and Boniardi M, 'Microstructure and fatigue properties of a welded duplex stainless steel', *Fatigue Fract Engng Mater Struct*, 1996, **19** (6), 647–654.

418 Beretta S and Murakami Y, 'Statistical analysis of defects for fatigue strength prediction and quality control of materials', *Fatigue Fract Engng Mater Struct*, 1998, **21**, 1049–1065.

419 Berkovitis A, Kelly D W and Di S, 'Consideration of the effect of residual stresses on fatigue of welded aluminium alloy structures', *Fatigue Fract Engng Mater Struct*, 1998, **21** (2), 159–170.

420 Blom A F, 'Spectrum fatigue behaviour of welded joints', *Int J Fatigue*, 1995, **17** (7), 485–491.

421 Bowness D and Lee M M, 'The development of an accurate model for the fatigue assessment of doubly curved cracks in tubular joints', *Int J Fatigue*, 1995, **73**, 129–147.

422 Bowness D and Lee M M, 'Stress intensity factor solutions for semi-elliptical weld-toe cracks in T-butt geometries', *Fatigue Fract Engng Mater Struct*, 1996, **19** (6), 787–798.

423 Bowness D and Lee M M, 'Fatigue crack curvature under the weld toe in an offshore tubular joint', *Int J Fatigue*, 1998, **20** (6), 481–490.

424 Bowness D and Lee M M, 'Weld toe magnification factors for semi-elliptical cracks in T-butt joints', *Int J Fatigue*, 2000, **22** (5), 369–387.
425 Bowness D and Lee M M, 'Weld toe magnification factors for semi-elliptical cracks in T-butt joints – comparison with existing solutions', *Int J Fatigue*, 2000, **22** (5), 389–396.
426 Branco C M, Maddox S J, Infante V and Gomes E C, 'Fatigue performance of tungsten inert gas (TIG) and plasma welds in thin sections', *Int J Fatigue*, 1999, **21**, 587–601.
427 Brejev V K and Karkhin V A, 'Investigation of the influence of geometric shape of welded joints on the crack path and on the parameters of fracture mechanics by application of the finite element method' (in Russian), *Avt Svarka*, 1989, (1), 12–18.
428 Brennan F P, Dover W D, Karé R F and Hellier A K, 'Parametric equations for T-butt weld toe stress intensity factors', *Int J Fatigue*, 1999, **21**, 1051–1062.
429 Broek D, *Elementary Engineering Fracture* Mechanics, Amsterdam, Martinus Nijhoff Publ, 1988 (4th edn).
430 Bueckner H F, 'Ein neues Verfahren zur Berechnung von Spannungsintensitätsfaktoren', *Z Angew Math u Mech*, 1970, **50**, 529–546.
431 Bueckner H F, 'Weight functions and fundamental fields for the penny-shaped and the half plane crack in three-space', *Int J Solids Struct*, 1987, **23** (1), 57–93.
432 Buirette C, Degallaix G, Dauphin J Y and Ménigault J, Microstructural effects on short fatigue crack initiation and propagation in high-strength steel butt-welded joints, IIW Doc XIII-1693-97.
433 Burk J D and Lawrence F V, 'Influence of bending stresses on fatigue crack propagation life in butt joint welds', *Welding J, Res Suppl*, 1977, **56** (2), 61s–66s.
434 Burk J D and Lawrence F V, 'Effects of lack of penetration and lack of fusion on the fatigue properties of 5083 aluminium alloy welds', *WRC Bulletin 234*, **4** (4), New York, WRC, 1979, pp 1–14.
435 Bussu G and Irving P E, 'The role of residual stress and heat affected zone properties on fatigue crack propagation in friction stir welded 2024-T351 aluminium joints', *Int J Fatigue*, 2003, **25** (1), 77–88.
436 Carpinteri A (Ed), *Handbook of Fatigue Crack Propagation in Metallic Structures*, Amsterdam, Elsevier Science, 1994, Vols 1 and 2.
437 Carpinteri A, Brighenti R, Huth H J and Vantadori S, 'Fatigue growth of a surface crack in a welded joint', *Int J Fatigue*, 2005, **27** (1), 59–69.
438 Castiglioni C A and Gianola P, 'Parametric analysis of weld toe stress concentration in longitudinal attachments', *Welding Int*, 1192, **6** (4), 278–286.
439 Chapetti M D and Otegui J L, 'Importance of toe irregularity for fatigue resistance of automatic welds', *Int J Fatigue*, 1995, **17** (8), 531–538.
440 Chapetti M D and Otegui J L, 'Controlled waviness as means to increase fatigue resistance of automatic welds in transverse loading', *Int J Fatigue*, 1997, **19** (10), 667–675.
441 Chapetti M D, Otegui J L and Motylicki J, 'Fatigue assessment of an electrical resistance welded oil pipeline', *Int J Fatigue*, 2002, **24** (1), 21–28.
442 Cheng X, Fisher J W, Prask H J, Gnäupel-Herold T, Yen B T and Roy S, 'Residual stress modification by post-weld treatment and its beneficial effect on fatigue strength of welded structures', *Int J Fatigue*, 2003, **25** (9–11), 1259–1269.
443 Clark W G, 'How fatigue crack initiation and growth properties affect material selection and design criteria', *Metals Engng Quart*, 1974, **16**.

444 Cotterell B, 'Notes on the paths and stability of cracks', *Int J Fract Mech*, 1966, **2**, (3), 526–533.
445 Cremona C, 'Reliability updating of welded joints damaged by fatigue', *Int J Fatigue*, 1996, **18** (8), 567–575.
446 Cruse T A, *Boundary Element Analysis in Computational Fracture Mechanics*, Dordrecht, Kluwer Academic Publ, 1988.
447 de Jesus A M, Ribiero A S, Portela A, de Castro P M and Fernandes A A, Software development for the fatigue life prediction of structural components, IIW Doc XIII-1801-99.
448 Dijkstra O D, Snijder H H, Overbeeke J L and Wildschut H, 'Prediction of fatigue crack growth for welded joints using stress intensity factors determined by fem calculations', *Proceedings International Conference on Steel in Marine Structures (SIMS'87)*, Amsterdam, Elsevier Science, 1987, pp 885–899.
449 Dijkstra O D, Snijder H H and van Straalen I J, 'Fatigue crack growth calculations using stress intensity factors for weld toe geometries', *Proceedings International Conference on Offshore Mechanics and Arctic Engng (OMAE'89)*, New York, ASME, 1989, Vol 3, pp 137–143.
450 Dijkstra O D and van Straalen I J, 'Fracture mechanics and fatigue of welded structures', *Proceedings International Conference on Performance of Dynamically Loaded Welded Structures*, New York, WRC, 1997, pp 225–239.
451 Dong P, *Treatment of Residual Stresses in Fracture and Fatigue Assessment*, Battelle Lecture Notes, Columbus, Ohio, Battelle, 2005.
452 Dong P and Hong J K, 'Consistent treatment of weld residual stresses in fracture assessment', PVP-Vol 434, *Computational Weld Mechanics, Constraint and Weld Fracture*, New York, ASME, 2002, pp 89–99.
453 Dong P, Hong J K and Cao Z, A robust *K* estimation scheme using mesh-insensitive structural stresses, IIW Doc X-1548-2003.
454 Dover W D, Dharmavasan S, Brennan F P and Marsh K J (Eds), *Fatigue Crack Growth in Offshore Structures*, Cradley Heath, Warley, UK, Engineering Materials Advisory Services, 1995.
455 Ellyin F, *Fatigue Damage, Crack Growth and Life Prediction*, London, Chapman & Hall, 1997.
456 Emery A F, 'Stress intensity factors for thermal stresses in thick hollow cylinders', *Trans ASME, J Basic Engng,* 1965, **88** (1), 45–52.
457 Etube L S, Brennan F P and Dover W D, 'Review of empirical and semi-empirical *Y* factor solutions for cracked welded tubular joints', *Marine Struct*, 1999, **12**, 565–583.
458 Etube L S, Brennan F P and Dover W D, 'A new method for predicting stress intensity factors in cracked welded tubular joints', *Int J Fatigue*, 2000, **22**, 447–456.
459 Ferreira J A and Branco C M, 'Fatigue analysis and prediction in fillet welded joints in the low thickness range', *Fatigue Fract Engng Mater Struct*, 1990, **13**, 201–212.
460 Fisher J W, *Fatigue and Fracture in Steel Bridges*, New York, John Wiley, 1984.
461 Fisher J W, 'Improved performance through large scale dynamic testing of structures', *Proceedings International Conference on Performance of Dynamically Loaded Welded Structures*, New York, WRC, 1997, pp 1–21.
462 Folias E S, 'Axial crack in pressurized cylindrical shell', *Int J Fract Mech*, 1965, **1** (2), 104–113.

463 Forbes J W, Desjardin J L, Glinka G and Burns D J, 'Stress intensity factors for semi-elliptical surface cracks in weldments', *Proceedings International Conference OMAE*, New York, ASME, 1991, Vol 3B, pp 529–536.
464 Forman R G, Kearney V E and Engle R M, 'Numerical analysis of crack propagation in cyclic loaded structures', *Trans ASME, J Basic Engng*, 1967, **89**, 459–464.
465 Frank K H and Fisher J W, 'Fatigue-strength of fillet-welded cruciform joints', *J Struct Div, ASCE*, 1979, **105** (ST9), 1727–1740.
466 Fricke W, Rißfortschrittsuntersuchungen an versteiften Plattenfeldern (Crack propagation investigations at stiffened plate areas), Bericht 469, Inst f Schiffbau, Hamburg Univ, 1986.
467 Fu B, Haswell J V and Bettess P, 'Weld magnification factors for semi-elliptical surface cracks in fillet-welded T-butt joint models', *Int J Fracture*, 1993, **63**, 155–171.
468 Galatolo R and Lanciotti A, 'Fatigue crack propagation in residual stress fields of welded plates', *Int J Fatigue*, 1997, **19** (1), 43–49.
469 Garwood S J and Maddox S J, 'Fatigue crack growth retardation in welded steel', *International Conference on Fatigue of Welded Components and Structures*, Les Ulis, Societé Française de Métallurgie et de Matériaux, 1996, pp 217–224.
470 Glinka G, 'Effect of residual stresses on fatigue crack growth in steel weldments under constant and variable-amplitude loads', *Fracture Mechanics,* ASTM STP 677, Philadelphia Pa, ASTM, 1979, pp 198–214.
471 Graville B A and Watkinson F, Research programme to investigate the fatigue of high-strength steels – investigation in fillet welds, BWRA Rep C215/3/67, British Welding Research Association, 1967.
472 Greasley A and Naylor S G, 'Influence of residual welding stresses on fatigue crack growth under compressive loading', *Engng Fract Mech*, 1986, **24** (5), 717–726.
473 Gross D and Seelig T, *Bruchmechanik (Fracture Mechanics)*, Berlin, Springer-Verlag, 2001.
474 Gurney T R, 'Finite element analyses of some joints with the welds transverse to the direction of stress', *Welding Res Int*, 1976, **6** (4), 40–72.
475 Hahn H G, *Bruchmechanik – Einführung in die theoretischen Grundlagen (Fracture Mechanics – Introduction to the Theoretical Fundamentals)*, Stuttgart, Teubner, 1976.
476 Harrison J D, The analysis of fatigue test results for butt welds with lack of penetration defects using a fracture mechanics approach, BWRA Rep E/13/67, British Welding Research Association, 1967.
477 Harrison J D, 'An analysis of the fatigue behaviour of cruciform joints', *Metal Constr Brit Welding J*, 1969, 1 (7), 333–339, and *Welding Res Int*, 1971, **1** (1), 1–7.
478 Harrison J D, 'The basis for an acceptance standard for weld defects, Part 2: Slag inclusions', *Metal Constr*, 1972, **4** (7), 262–268.
479 Harrison J D, 'The effect of residual stresses on fatigue behaviour', *Proc Welding Inst (Abington)*, 1981, **47**, 9–16.
480 Harrison J D, 'Damage-tolerant design', *Fatigue Crack Growth – 30 Years of Progress*, Oxford, Pergamon Press, 1986, pp 117–131.
481 Harrison J D and Doherty J, 'A re-analysis of fatigue data from butt-welded specimens containing slag inclusions', *Welding Res Int*, 1978, **8** (2).

482 Hartt W H, 'The interactive nature of fatigue and cathodic protection with application to offshore structures', *Proceedings International Conference on Performance of Dynamically Loaded Welded Structures*, New York, WRC, 1997, pp 354–374.
483 Hirt M A, 'Anwendung der Bruchmechanik auf die Ermittlung des Ermüdungsverhaltens geschweißter Konstruktionen', *Bauingenieur*, 1982, **57**, 95–101.
484 Hirt M A and Fisher J W, 'Fatigue crack growth in welded beams', *Engng Fract Mech*, 1973, **5** (5), 415–429.
485 Hirt M A and Kummer E, 'Einfluß der Spannungskonzentration auf die Ermüdungsfestigkeit geschweißter Konstruktionen', *Experimentelle Spannungsanalyse*, VDI-Berichte 313, Düsseldorf, VDI-Ver, 1978, pp 539–545.
486 Hobbacher A, 'Zur Betriebsfestigkeit der Schweißverbindungen auf bruchmechanischer Grundlage', *Archiv Eisenhüttenw*, 1977, **48** (2), 109–114.
487 Hobbacher A, 'Cumulative fatigue by fracture mechanics', *Trans ASME, J Appl Mech*, 1977, **44** (12), 769–771.
488 Hobbacher A (Ed), Recommendations for assessment of weld imperfections in respect to fatigue, IIW Doc XIII-1266-88/XV-659-88.
489 Hobbacher A, 'Stress intensity factors of plates under tensile load with welded-on flat side gussets', *Engng Fract Mech*, 1992, **41** (6), 897–905.
490 Hobbacher A, 'Stress intensity factors of welded joints', *Engng Fract Mech*, 1993, **46** (29), 173–182.
491 Hou C Y and Lawrence F V, 'Crack closure in weldments', *Fatigue Fract Engng Mater Struct*, 1996, **19** (6), 683–694.
492 Huang X and Hanock J W, 'The stress intensity factors of semi-elliptical cracks in a tubular welded T-joint under axial loading', *Engng Fract Mech*, 1988, **30** (1), 25–35.
493 Itoh Y Z, Saruga S and Kashiwaya H, 'Prediction of fatigue crack growth rate in welding residual stress field', *Engng Fract Mech*, 1989, **33** (3), 397–407.
494 Jaccard R, Fatigue crack propagation in aluminium, IIW Doc XIII-1377-90.
495 Jaccard R and Ogle M H, 'Aluminium Eurocode – design for fatigue', *Proceedings International Conference on Performance of Dynamically Loaded Welded Structures*, New York, WRC, 1997, pp 205–224.
496 James L A, 'Fatigue crack propagation behavior of several pressure vessel steels and weldments', *Welding J, Res Suppl*, 1977, **56** (12), 386s–391s.
497 James M and Swenson D, FRANC2D/L – a crack propagation simulator for plane layered structures, available from http://www.mne.ksu.edu/~franc2d/, and Carter B J, Wawrzynek P A and Ingraffea A R, 'Automated 3-D crack growth simulation', *Int J Numerical Methods Engng*, 2000, **47** (1–3), 229–253.
498 Janosch J J, Lipinski P and Lebienvenu M, Investigation into the fatigue-strength of fillet-welded assemblies in E-364 steel as a function of the penetration of the weld subjected to tensile and bending loads', IIW Doc XIII-1430-91.
499 John R, Jata K V and Sadananda K, 'Residual stress effects on near-threshold fatigue crack growth in friction stir welds in aerospace alloys', *Int J Fatigue*, 2003, **25** (9–11), 939–948.
500 Kanazawa T and Kobayashi A S (Eds), *Significance of Defects in Welded Structures*, Tokyo, Tokyo Univ Press, 1974.
501 Karlsen A and Tenge P, 'Alexander L Kielland', estimation of fatigue cracks in hydrophone region on brace D-6, Det Norske Veritas Rep 80-0410, 1980.

502 Karzov G P, Karkhin V A, Leonov V P and Margolin B Z, 'Effect of residual stresses on the trajectory and rate of crack propagation in cyclic loading of welded joints', *Automatic Welding*, 1986, (3), 3–8.
503 Kim I T, 'Weld root crack propagation under mixed mode I and III cyclic loading', *Engng Fract Mech*, 2005, **73** (2005).
504 King R N, Stacey A and Maddox S J, 'Background to the new fatigue crack growth rate recommendations used in the revision of PD6493:1991', *Proceedings Conference on Recent Advances in Corrosion Fatigue*, Institute of Materials, Sheffield 1997, and IIW Doc XIII-1731-98.
505 Labesse F, Recho N, Lieurade H P and Mervaux P, *S–N* fatigue curves of welded joints submitted to variable amplitude loading, IIW Doc XIII-1736-98.
506 Lawrence F V, 'Estimation of fatigue crack propagation life in butt welds', *Welding J, Res Suppl*, 1973, **53** (5), 212s–220s.
507 Lawrence F V and Munse W H, 'Fatigue crack propagation in butt welds containing joint penetration defects', *Welding J, Res Suppl*, 1973, **52** (5), 221s–225s and 232s.
508 Lecsek R L, Yee R, Lambert S B and Burns D J, 'A probabilistic model for initiation and propagation of surface cracks in welded joints', *Fatigue Fract Engng Mater Struct*, 1995, **18** (7/8), 821–831.
509 Lee M M and Bowness D, 'Fatigue life prediction of offshore tubular joints using fracture mechanics', *Fatigue Fract Engng Mater Struct*, 2002, **25**, 1025–1032.
510 Lee M M and Bowness D, 'Estimation of stress intensity factor solutions for weld toe cracks in offshore tubular joints', *Int J Fatigue*, 2002, **24** (8), 861–875.
511 Lee Y B, Chung C S, Park Y K and Kim H K, 'Effects of redistributing residual stress on the fatigue behavior of SS330 weldment', *Int J Fatigue*, 1998, **20** (8), 565–573.
512 Lee H K, Kim K S and Kim C K, 'Fracture resistance of a steel weld joint under fatigue loading', *Engng Fract Mech*, 2000, **66**, 403–419.
513 Lehrke H P, Brandt U and Sonsino C M, 'Bruchmechanische Beschreibung der Wöhlerlinien geometrisch ähnlicher Schweißproben aus Aluminium', *Schweißen u Schneiden*, 1998, **50** (8), 492–497, and LBF-Bericht 7195/4, Darmstadt, Fraunhofer-Inst f Betriebsfest, 1996.
514 Li X Y, Partanen T, Nykänen T and Björk T, The effect of weld geometry and loading conditions on the fatigue strength of welded cover plate details, IIW Doc XIII-1878-01.
515 Li X, Zhu H and Tian X, A study of fatigue crack growth and crack closure in mechanical heterogeneous welded joints of model SHS, IIW Doc XIII-1538-94.
516 Lie S T and Bian C, 'Load-carrying fillet welds using dual boundary element method', *J Struct Engng*, 1997, **123** (12), 1603–1613.
517 Lie S T and Lan S, 'A boundary element analysis of misaligned load-carrying cruciform welded joints', *Int J Fatigue* 1998, **20** (6), 433–439.
518 Lie S T, Zhao Z and Yan S H, 'Two-dimenional and three-dimensional magnification factors, M_k, for non-load-carrying fillet welds cruciform joints', *Engng Fract Mech*, 2000, **65**, 435–453.
519 Lieurade H P, 'Application of fracture mechanics to the fatigue of welded structures', *Welding in the World*, 1983, **21** (11/12), 272–294.

520 Lieurade H P (Ed), *Fatigue and Stress of Engineering Materials and Structures*, Gournay-sur-Marne, IITT-Int, 1989.
521 Maddox S J, 'Calculating the fatigue-strength of a welded joint using fracture mechanics', *Metal Constr Brit Welding J*, 1970, **2** (8), 327–331.
522 Maddox S J, 'Fatigue crack propagation in weld metal and HAZ', *Metal Constr*, 1970, **2** (7), 285–289.
523 Maddox S J, 'Some further crack propagation results relevant to welded joints in steel', *Welding Res Int*, 1973, **3** (1), 72ff.
524 Maddox S J, 'Assessing the significance of flaws in welds subject to fatigue', *Welding J, Res Suppl*, 1974, **53** (9), 401s–409s.
525 Maddox S J, 'An analysis of fatigue cracks in fillet welded joints', *Int J Fract*, 1975, **11** (2), 221–243.
526 Maddox S J, 'The effect of mean stress on fatigue crack propagation, a literature review', *Int J Fract*, 1975, **11** (3), 389–408.
527 Maddox S J, 'Scale effect in fatigue of fillet-welded aluminium alloys', *International Conference on Aluminium Weldments*, Cleveland, Ohio, 1995.
528 Maddox S J, 'Fatigue crack growth in tubular T-joints under in-plane bending', *Proc Int Symp on Tubular Structures*, Rotterdam, Balkema, 1996, pp 285–292.
529 Maddox S J and Andrews R M, 'Stress intensity factors for weld toe cracks', *Computer Aided Assessment and Control of Localized Damage*, Portsmouth, Computational Mechanics Publications, 1990, Vol 2, pp 329–342.
530 Maddox S J, Lechocki J P and Andrews R M, Fatigue analysis for the revision of BS PD 6493:1980, TWI Rep 3873/1/86, Abington, TWI, 1986.
531 Maddox S J and Webber D, 'Fatigue crack propagation in aluminium-zinc-magnesium alloy fillet welded joints', *Fatigue Testing of Weldments*, ASTM STP 648, Philadelphia Pa, ASTM, 1978, pp 139–184.
532 Masuda C, Sumiyoshi H, Kosuge A, Ohta A and Nishijima S, 'Variation of fractographic appearance for different microstructures in welded joints having the same fatigue crack propagation properties', *Int J Fatigue*, 1987, **9** (4), 233–237.
533 Matoba M and Inoue K, Some stress intensity factors for hull members in relation to fatigue crack propagation, IIW Doc XIII-1081-83.
534 McClung R C, 'Finite element analysis of fatigue crack closure: a historical and critical review', *Proceedings Fatigue '99*, Beijing, Higher Education Press, 1999, Vol 1, pp 495–502.
535 Miki C and Sakano M, A survey of fatigue cracking experience in steel bridges, Techn Rep 39, Department Civil Engineering, Tokyo Institute of Technology, 1988, and IIW-Doc XIII-1383-90.
536 Miki C, Sakano M, Toyoda Y and Yoshizawa T, 'Early stage propagation behaviour of fatigue cracks in fillet welded joints', *Struct Engng Earthquake Engng*, 1990, **7** (1), 123s–131s.
537 Mochizuki M, Miyazaki K and Toyoda M, Surface crack propagation analysis under residual stress field, IIW-Doc X-1526-2003.
538 Monahan C C, 'Early fatigue crack growth at welds', *Topics in Engineering*, Southampton, Computational Mechanics Publications, 1995, vol 26.
539 Mori T and Kainuma S, A study on fatigue strength evaluation method for load-carrying fillet welded cruciform joints, IIW Doc XIII-1884-01.
540 Mori T, Kainuma S and Ichimiya M, A study on the fatigue crack initiation point in load-carrying type of fillet welded joints, IIW Doc XIII-1832-2000.

541 Motarjemi A K, Kokabi A H and Burdekin F M, 'Comparison of fatigue life for T and cruciform welded joints with different combinations of geometrical parameters', *Engng Fract Mech*, 2000, **67**, 313–328.
542 Motarjemi A K, Kokabi A H, Ziaie A A, Manteghi S and Burdekin F M, 'Comparison of the stress intensity factor of T and cruciform welded joints with different main and attachment plate thickness', *Engng Fract Mech*, 2000, **65**, 55–66.
543 Murakami Y (Ed), *Stress Intensity Factors Handbook*, Oxford, Pergamon Press, 1987.
544 Mutoh Y and Sahamoto I, 'Fatigue crack propagation in the weld bond region of a type 304 stainless steel weldment', *Advances in Fracture Research*, Oxford, Pergamon Press, 1984, pp 1695–1702.
545 Neumann P and Schott G, 'Charakterisierung von Schweißverbindungen aus unlegierten und niedriglegierten Vergütungsstählen durch bruchmechanische Kennwerte', *Schweißen u Schneiden*, 1991, **43** (2), 102–105.
546 Newman J C and Raju I S, 'An empirical stress intensity factor equation for the surface crack', *Engng Fract Mech*, 1981, **15** (1/2), 185–192.
547 Newman J C and Raju I S, Stress intensity factor equations for cracks in three-dimensional finite bodies subjected to tension and bending loads, NASA TM85793, Langley Research Center, NASA, 1984.
548 Nguyen N T and Wahab M A, 'The effect of residual stresses and weld geometry on the improvement of fatigue life', *J Mater Processing Technol*, 1995, **48**, 581–588.
549 Nguyen N T and Wahab M A, 'A theoretical study of the effect of weld geometry parameters on fatigue crack propagation life', *Engng Fract Mech*, 1995, **51** (1), 1–18.
550 Nguyen N T and Wahab M A, 'The effect of undercut, misalignment and residual stresses on fatigue behaviour of butt welded joints', *Fatigue Fract Engng Mater Struct*, 1996, **19** (6), 769–778.
551 Nguyen N T and Wahab M A, 'The effect of undercut and residual stresses on fatigue behaviour of misaligned butt joints', *Engng Fract Mech*, 1996, **55** (3), 453–469.
552 Niu X and Glinka G, 'The weld profile effect on stress intensity factors in weldments', *Int J Fracture*, 1987, **35**, 3–20.
553 Niu X and Glinka G, 'Stress intensity factors for semi-elliptical surface cracks in welded joints', *Int J Fracture*, 1989, **40**, 255–270.
554 Niu X and Glinka G, 'Weight functions for edge and surface semi-elliptical cracks in flat plates and plates with corners', *Engng Fract Mech*, 1990, **36**, 459–475.
555 Niu X and Glinka G, 'Theoretical and experimental analyses of surface fatigue cracks in weldments', *Surface-Crack Growth – Models, Experiments and Structures*, ASTM STP 1060, Philadelphia Pa, ASTM, 1990, pp 390–413.
556 Noblett J E and Andrews R M, 'A stress intensity factor solution for root defects in fillet and partial penetration welds', *Fatigue – Core Research from TWI*, Cambridge, Abington Publ, 2000, pp 124–144.
557 Nykänen T, On fatigue crack growth simulation in a transverse double lap joint, IIW Doc XIII-1583-95.
558 Nykänen T, Fatigue crack growth simulations in transverse butt welds made on permanent backing bars, IIW Doc XIII-1624-96.

559 Nykänen T, Geometric dependency of fatigue strength in transverse load-carrying cruciform joint with partial penetration K-welds, IIW Doc XIII-1709-98.
560 Nykänen T, 'Geometric dependency of fatigue strength in a transverse load-carrying cruciform joint with partially-penetrating K-welds', *Welding in the World*, 1999, **43** (5), 47–53.
561 Nykänen T and Lihavainen V M, Geometric dependency of fatigue strength in a transverse load-carrying cruciform joint with partially penetrating V-welds, IIW Doc XIII-1838-2000.
562 Nykänen T, Partanen T and Björk T, A parametric fracture mechanics analysis of fatigue of a single fillet welded T-joint, IIW Doc XIII-1874-01.
563 Nykänen T, Partanen T and Björk T, A parametric fracture mechanics analysis of fatigue of a fillet welded corner joint, IIW Doc XIII-1875-01.
564 Ohta A, Kosuge M, Mawari T and Nishijima S, 'Fatigue crack propagation properties of HT80 steel welded joints, heat-treated for relieving residual stresses', *Trans Nat Res Inst Metals*, 1988, **30** (1), 8–14.
565 Ohta A, Kosuge M, Mawari T and Nishijima S, 'Fatigue crack propagation in tensile residual stress fields of welded joints under fully compressive cycling', *Int J Fatigue*, 1988, **10** (4), 237–242.
566 Ohta A, Maeda Y, Kosuge M, Machida S and Yoshinari H, 'Fatigue crack propagation curve for design of welded structures', *Trans Japan Welding Soc*, 1989, **20** (1), 17–23.
567 Ohta A, Maeda Y, Machida S and Yoshinari H, 'Near-threshold fatigue crack propagation in welded joints under random loadings', *Trans Japan Welding Soc*, 1988, **19** (2), 69–73.
568 Ohta A, Maeda Y, Machida S and Yoshinari H, 'Fatigue crack propagation in welded joints under variable-amplitude loading in synthetic seawater', *Int J Fatigue*, 1990, **12** (6), 475–480.
569 Ohta A, Soya I, Nishijima S and Kosuge M, 'Statistical evaluation of fatigue crack propagation properties including threshold stress intensity factor', *Engng Fract Mech*, 1986, **24** (6), 789–802.
570 Ohta A and Suzuki N, Statistical evaluation of fatigue crack propagation including fatigue threshold, IIW-Doc XIII-1883-01.
571 Ohta A, Suzuki N and Maeda Y, 'Effect of residual stresses on fatigue of weldment', *Proceedings International Conference on Performance of Dynamically Loaded Welded Structures*, New York, WRC, 1997, pp 108–122.
572 Ohta A, Suzuki N and Mawari T, 'Effect of Young's modulus on basic crack propagation properties near the fatigue threshold', *Int J Fatigue*, 1992, **14** (4), 224–226.
573 Otegui J L, Kerr W, Burns D J and Mohaupt U H, 'Fatigue crack initiation from defects at weld toes in steel T joints', *Int J Pressure Vessels Piping*, 1989, **38**, 385–417.
574 Otegui J L, Mohaupt U H and Burns D J, 'Effect of weld process on early growth of fatigue cracks in steel T joints', *Int J Fatigue*, 1991, **13**, 45–58.
575 Otegui J L, Mohaupt U H and Burns D J, 'A strain gauge technique for monitoring small fatigue cracks in welds', *Engng Fract Mech*, 1991, **40** (3), 549–569.
576 Otsuka A, Tohgo K and Matsuyama H, 'Fatigue crack initiation and growth under mixed mode loading in aluminium alloys 2017-T3 and 7075-T6', *Engng Fract Mech*, 1987, **28** (5/6), 721–732.

577 Otsuka A, Tohgo K and Skjolstrup E, 'Fatigue crack growth in high-strength aluminium alloy weldments under mode II loading', *International Conference on Fatigue, Corrosion Cracking, Fracture Mechanics and Failure Analysis – The Mechanism of Fracture*, Materials Park, Ohio, ASM, 1986, pp 265–275.
578 Pang H L, A review of stress intensity factors for a semi-elliptical surface crack in a plate and fillet-welded joint, TWI Res Rep 428/1990, Abington, TWI, 1990.
579 Pang H L and Gray T G, 'Fatigue analysis of surface cracks and fillet-welded toes', *Fatigue Fract Engng Mater Struct*, 1993, **16** (2), 151–164.
580 Paris P C and Erdogan F, 'A critical analysis of crack propagation law', *Trans ASME, J Basic Eng*, 1963, **85**, 528–539.
581 Paris P C, McMecking R M and Tada H, 'The weight function method for determining stress intensity factors', *ASTM STP 601*, Philadelphia Pa, ASTM, 1976, pp 471–489.
582 Parker A P, 'Stress intensity factors, crack profiles and fatigue crack growth rates in residual stress fields', *Residual Stress Effects in Fatigue*, ASTM STP 776, Philadelphia Pa, ASTM, 1982, pp 13–31.
583 Parry M, Nordberg H and Hetzberg R, 'Fatigue crack propagation in A514 base plate and welded joints', *Welding J, Res Suppl*, 1972, **51** (10), 485s–490s.
584 Pellini W S, *Guidelines for Fracture-Safe and Fatigue-Reliable Design of Steel Structures*, Abington, TWI, 1983.
585 Petroski H J and Achenbach J D, 'Computation of the weight function for a stress intensity factor', *Engng Fract Mech*, 1978, **10**, 257–266.
586 Pook L P, 'On fatigue crack paths', *Int J Fatigue*, 1995, **17**, 5–13.
587 Pook L P, *Linear Elastic Fracture Mechanics for Engineers – Theory and Applications*, Southampton, WIT Press, 2000.
588 Pook L P, *Crack Paths*, Southampton, WIT Press, 2002.
589 Pook L P, Kam J C and Mshana Y, 'On mixed mode fatigue crack growth in tubular welded joints', *Proceedings 11th International Conference OMAE*, New York, ASME, 1992, Vol 3B, pp 251–258.
590 Quian J and Fatemi A, 'Mixed-mode fatigue crack growth – a literature survey', *Engng Fract Mech*, 1996, **55** (69) 969–990.
591 Radaj D, 'Besonderheiten der bruchmechanischen Analyse von Schweißkonstruktionen', *Schweißen u Schneiden*, 1975, **27** (6), 211–214.
592 Radaj D, 'Integrated finite element analysis of welding residual stress and distortion', *Mathematical Modelling of Weld Phenomena 6*, London, Maney Publ, 2002, pp 469–487.
593 Rading G O, 'The effect of welding on the fatigue crack growth rate in structural steel', *Welding J, Res Suppl*, 1993, **72**, 307s–312s.
594 Rajasankar J, Iyer N R and Rao A T, 'Structural integrity assessment of offshore tubular joints based on reliability analysis', *Int J Fatigue*, 2003, **25** (7), 609–619.
595 Raju I S and Newman J C, 'Stress intensity factors for a wide range of semi-elliptical surface cracks in finite-thickness plates', *Engng Fract Mech*, 1979, **11** (4), 817–829.
596 Rhee H C, Han S and Gipson G S, 'Reliability of solution method and empirical formulas of stress intensity factors for weld toe cracks of tubular joints', *Proceedings International Conference OMAE*, New York, ASME, 1991, Vol 3B, pp 441–452.

597 Rice J R, 'Some remarks on elastic crack tip stress fields', *Int J Solids Struct*, 1972, **8** (5), 751–758.
598 Rice J R and Levy N, 'The part-through surface crack in an elastic plate', *Trans ASME, J Appl Mech*, 1972, **39**, 185–194.
599 Righiniotis T D, 'Influence of management actions on fatigue reliability of a welded joint', *Int J Fatigue*, 2004, **26** (3), 231–239.
600 Rodriguez-Sanchez J E, Dover W D and Brennan F P, 'Application of short repairs for fatigue life extension', *Int J Fatigue*, 2004, **26** (4), 413–420.
601 Rooke D P and Cartwright D J, *Compendium of Stress Intensity Factors*, London, Her Majesty's Stationary Office, 1976.
602 Rörup J, 'Mean compressive stresses – experimental and theoretical investigations into the influence on fatigue strength of welded structures', *J Strain Anal*, 2005, **40** (7), 631–642, and *Materialprüfung*, 2004, **46**, 220–230 (German version).
603 Schiebel C, *Schweißen unter Betriebsbeanspruchung – Eigenspannungen und bruchmechanische Betrachtungen*, Dr thesis, *Fortschrittsber 18/235*, VDI, 1998.
604 Schütz W and Oberparleiter W, 'Rißfortschritts- und Restfestigkeitseigenschaften neuer hochfester Aluminiumlegierungen, *Aluminium*, 1972, **48** (11), 734–738.
605 Seto A, Yoshida Y and Galtier A, 'Fatigue properties of arc-welded lap joints with weld start and end points', *Fatigue Fract Engng Mater Struct*, 2004, **27** (12), 1147–1155.
606 Shen G and Glinka G, 'Weight function for a surface semi-elliptical crack in a finite thickness plate', *Theor Appl Fract Mech*, 1991, **15**, 247–255.
607 Shi Y W, Chen B Y and Zhang J X, 'Effects of welding residual stresses on fatigue crack growth behaviour in butt welds of pipeline steel', *Engng Fract Mech*, 1990, **36** (6), 893–902.
608 Signes E G, Baker R G, Harrison J D and Burdekin F M, 'Factors affecting the fatigue-strength of welded high-strength steels', BWRA Rep M/11/66, *British Welding J,* 1967, **14** (3), 108–116.
609 Sih G C, *Handbook of Stress Intensity Factors*, Bethlehem Pa, Lehigh University, 1973.
610 Skopura M, 'Fatigue life prediction of cruciform joints failing at the weld toe', *Welding J, Res Suppl*, 1992, **71**, 269s–275s.
611 Smith E, 'The stress intensity factor for a crack perpendicular to a longitudinal weld in a large plate', *Int J Fracture*, 1985, **27**, 75–79.
612 Smith I J, Stress intensity factors for toe defects in single-sided transverse attachments of varying thickness made with fully penetrating welds, IIW Doc XIII-1177-85.
613 Smith I F and Gurney T R, 'Changes in the fatigue life of plates with attachments due to geometrical effects', *Welding J, Res Suppl*, 1986, **65**, 244s–250s.
614 Smith I J and Hurworth S J, The effect of geometry upon the predicted fatigue strength of welded joints, TWI Rep 7819.01/84/394.3, Abington, TWI, 1984.
615 Smith I F and Smith R A, 'Defects and crack shape development in fillet weld joints', *Fatigue Fract Engng Mater Struct*, 1982, **5** (2), 151–165.
616 Smith I F and Smith R A, 'Fatigue crack growth in a fillet welded joint', *Engng Fract Mech*, 1983, **18** (4), 861–869.
617 Socie D F and Antolovich S D, 'Subcritical crack growth characteristics in welded ASTM A537 steel', *Welding J, Res Suppl*, 1974, **53** (6), 267s–271s.

618 Spies H J, Pusch G, Henkel C and Roßler K, 'Fatigue crack propagation in high strength low alloy steels', *Theor Appl Fracture Mech*, 1989, **11**, 121–125.
619 Sprung I and Zilberstein V A, 'Analysis of a backing bar notch effect', *Engng Fract Mech*, 1986, **24** (1), 145–152.
620 Stanley P (Ed), *Fracture Mechanics in Engineering Practice*, London, Appl Science, 1977.
621 Sumi Y, 'Fatigue crack propagation and computational remaining life assessment of ship structures', *J Marine Sci Techn*, 1998, **3**, 102–112.
622 Sumi Y, 'Analysis of three-dimensional cracks in ship structures subjected to an arbitrary loading by numerical weight function method', *Practical Design of Ships and Other Floating Structures*, Amsterdam, Elsevier Science, 2001, pp 1105–1111.
623 Sumi Y, Chen Y and Hayashi S, 'Morphological aspects of fatigue crack propagation. Part I. Computational procedure', *Int J Fracture*, 1996, **82**, 205–220.
624 Sumi Y, Chen Y and Wang Z N, 'Morphological aspects of fatigue crack propagation. Part II. Effects of stress biaxiality and welding residual stress', *Int J Fracture*, 1996, **82**, 221–235.
625 Sumi Y, Nemat-Nasser S and Keer L M, 'On crack path stability in a finite body', *Engng Fract Mech*, 1985, **22** (5), 759–771.
626 Suzuki N, Takeda H, Ohta A and Ohuchida H, 'Evaluation of fatigue crack propagation properties under random loading avoiding crack closure', *Fatigue Fract Engng Mater Struct*, 1991, **14**, 815–821.
627 Tada H and Paris P C, 'The stress intensity factor for a crack perpendicular to the welding bead', *Int J Fracture*, 1983, **11**, 279–284.
628 Tada H, Paris P C and Irwin G R, *The Stress Analysis of Cracks Handbook*, Hellertown Pa, DES Research Corp, 2000 (3rd edn).
629 Taylor D, *A Compendium of Fatigue Thresholds and Growth Rates*, Cradley Heath, Warley, UK, Engineering Materials Advisory Services, 1985.
630 Taylor D and Jianchun I, *Sourcebook on Fatigue Crack Propagation: Thresholds and Crack Closure*, Cradley Heath, Warley, UK, Engineering Materials Advisory Services, 1993.
631 Terada H, 'An analysis of the stress intensity factor of a crack perpendicular to the welding bead', *Engng Fract Mech*, 1976, **8**, 441–444.
632 Terada H and Nakajima T, 'Analysis of stress intensity factor of a crack approaching welding bead', *Int J Fracture*, 1985, **27**, 83–90.
633 Terai K, Tomita Y, Hashimoto K and Osawa N, Fatigue design method of ship structural members based on fatigue crack growth analysis, IIW-Doc XIII-1908-01 / XV-1091-01.
634 Thurlbeck S D and Burdekin F M, Effects of geometry and loading variables on the fatigue design curve for tubular joints, IIW Doc XIII-1428-91.
635 To S H, Lambert S B and Burns D J, 'A multiple crack model for fatigue in welded joints', *Int J Fatigue*, 1993, **15** (4), 333–340.
636 Tobe Y and Lawrence F V, 'Effect of inadequate joint penetration on fatigue resistance of high-strength structural steel welds', *Welding J, Res Suppl*, 1977, **56** (9), 259s–266s.
637 Toyosada M, Gotoh K and Niwa T, 'Fatigue crack propagation for a through thickness crack: a crack propagation law considering cyclic plasticity near a crack tip', *Int J Fatigue*, 2004, **26**, 983–992.

638 Toyosada M, Gotoh K and Niwa T, 'Fatigue life assessment for welded structures without initial defects: an algorithm for predicting fatigue crack growth from a sound site', *Int J Fatigue*, 2004, **26**, 993–1002.
639 Toyosada M and Niwa T, 'The significance of RPG load for fatigue crack propagation and the development of a compliance measuring system', *Int J Fracture*, 1994, **67**, 217–230.
640 Toyosada M and Niwa T, 'Simulation model of fatigue crack opening/closing phenomena for predicting RPG load under arbitrary stress distribution field', *Proceedings 5th International Conference on Offshore and Polar Engineering*, The Hague, ISOPE, 1995, Vol 4, pp 169–176.
641 Toyosada M, Niwa T and Sakai J, 'Physical meaning of ΔK_{RP} and fatigue crack propagation in the residual stress distribution field', *Int J Fatigue*, 1997, **19**, Suppl. 1, S161–S166.
642 Trufiakov V I, Mikheev P P, Knyshi V V and Kovalenko I S, 'Cyclic crack resistance of welded joints with non-uniform fields of residual welding stresses', *Fatigue Fract Engng Mater Struct*, 1996, **19** (6), 695–701.
643 Tsai C L and Kim D S, 'Analysis of fatigue crack propagation behaviour in fillet-welded T-joint', *Engng Fract Mech*, 1990, **36** (4), 653–660.
644 Tsai C L, Liaw M L and Teng J I, 'Effect of residual stresses on design assessment of partial penetration laser welds in a pressure valve component', *Welding J, Res Suppl*, 1998, **77** (10), 403s–410s.
645 Tsay L W, Chung C S and Chen, C, 'Fatigue crack propagation of D6AC laser welds', *Int J Fatigue*, 1997, **19** (1), 25–31.
646 Tsay L W and Tsay C Y, 'The effect of microstructures on the fatigue crack growth in Ti-6Al-4V laser welds', *Int J Fatigue*, 1997, **19** (10), 713–720.
647 Tubby P J, 'Fatigue crack growth in tubular joints in seawater – a sensitivity analysis', *Proceedings International Conference on Offshore Mechanics and Arctic Engineering* (OMAE'95), New York, ASME, 1995, Vol 3, pp 135–140.
648 Unger D J, '*Analytical Fracture Mechanics*, New York, Academic Press, 1995.
649 Usami S and Kusumoto S, 'Fatigue-strength at root of cruciform, tee and lap joints', *Trans Japan Welding Soc*, 1978, **9-1**, 1–10, and IIW Doc XIII-833-77.
650 van Straalen I J, Dijkstra O D and Snijder H H, 'Stress intensity factors and fatigue crack growth of semi-elliptical surface cracks at weld toes', *Proceedings International Conference on Weld Failures*, Abington, TWI, 1988, pp 367–376.
651 Verreman Y, Bailon J P and Masounave J, 'Fatigue short crack propagation and plasticity-induced crack closure at the toe of a fillet-welded joint', *The Behaviour of Short Fatigue Cracks*, London, Mechanical Engineering Publ, 1986, pp 387–404.
652 Verreman Y and Nie B, 'Early development of fatigue cracking at manual fillet welds', *Fatigue Fract Engng Mater Struct*, 1996, **19** (6), 669–681.
653 Verreman Y and Nie B, 'Short crack fatigue propagation at fillet welds', *Proceedings International Conference on Performance of Dynamically Loaded Welded Structures*, New York, WRC, 1997, pp 240–253.
654 Vormwald M, Anrißlebensdauervorhersage auf der Basis der Schwingbruchmechanik für kurze Risse (Prediction of crack initiation life on the basis of short crack fracture mechanics), Heft 47, Inst f Stahlbau u Werkstoffmech, Darmstadt, Techn Univ, 1989.
655 Vormwald M and Seeger T, Vorhersage der Ausbreitung von Rissen in zyklisch elastisch-plastisch beanspruchten Kerbbereichen (Prediction of crack

propagation at notches under cyclic elastic-plastic loading*)*, Report FD-4/1989, Inst f Stahlbau u Werkstoffmech, Darmstadt, Techn Univ, 1989.

656 Vormwald M and Seeger T, 'The consequences of short crack closure on fatigue crack growth under variable amplitude loading', *Fatigue Fract Engng Mater Struct*, 1991, **14** (2/3), 205–225.

657 Wais E A, Dodabaugh E C and Carter R, 'Investigation of torsional stress intensity factors and stress indices for girth butt welds in straight pipe', *Design and Analysis of Piping, Vessel and Components*, ASME PVP, New York, ASME, 2002, Vol 440, pp 83–89.

658 Wang X and Lambert S B, 'Local weight functions for semi-elliptical surface cracks in finite thickness plates', *Theor Appl Fract Mech*, 1995, **23**, 199–208.

659 Wang X and Lambert S B, 'Stress intensity factors for low aspect ratio semi-elliptical surface cracks in finite thickness plates subjected to non uniform stresses', *Engng Fract Mech*, 1995, **51**, 517–532.

660 Wang X and Lambert S B, 'Stress intensity factors and weight functions for longitudinal semi-elliptical surface cracks in thin pipes', *Int J Pressure Vessels Piping*, 1996, **65**, 75–87.

661 Wang X and Lambert S B, 'Weight functions and stress intensity factor for semi-elliptical cracks in T-plate welded joints', *Fatigue Fract Engng Mater Struct*, 1998, **21**, 99–117.

662 Wang X and Lambert S B, 'On the calculation of stress intensity factors for surface cracks in welded pipe-plate and tubular joints', *Int J Fatigue*, 2003, **25** (1), 89–96.

663 Wang Y, Tomita Y, Hashimoto K, Osawa N and Balakrishnan B, Simulation of fatigue crack propagation in weld joints considering coalescence of multiple surface cracks, IIW Doc XIII-2016-04.

664 Watkinson F, Bodger P H and Harrision H D, 'The fatigue-strength of welded joints in high-strength steels and methods for its improvement', *Proceedings Conference on Fatigue of Welded Structures*, Abington, TWI, 1971, pp 97–113.

665 Wernicke R, Fatigue strength assessment of cruciform joints with misalignment, IIW-Doc. XIII-1872-01.

666 Wildschut H, Kuijpers T B, Snijder H H and Dijkstra O D, 'Fatigue crack development and stress intensity factors in specimens with the shape of weldments', *Proceedings International Conference on Steel in Marine Structures (SIMS'87)*, Amsterdam, Elsevier Science, 1987, pp 871–883.

667 Williams S and Mudge P J, 'Fatigue crack growth monitoring – Fracture mechanics and non-destructive testing requirements', *Conference on Periodic Inspection of Pressurised Components*, London, Institute of Mechanical Engineering, 1982.

668 Woollin P, 'Fatigue crack propagation in CMn steel HAZ microstructure tested in air and seawater', *Proceedings International Conference on Offshore Mechanics and Arctic Engineering (OMAE'98)*, Lisbon, 1998, and IIW-Doc XIII-1713-98.

669 Wu X R and Carlsson J, 'Welding residual stress intensity factors for half-elliptical surface cracks in thin and thick plates', *Engng Fract Mech*, 1984, **19** (3), 407–426.

670 Xu T and Bea R, 'Load shedding of fatigue fracture in ship structures', *Marine Struct*, 1997, **10**, 49–80.

671 Zettelmoyer N and Fisher J W, 'Stress gradient correction factor for stress intensity at welded stiffeners and cover plates', *Welding J, Res Suppl*, 1977, **56** (12), 393s–398s.
672 Zhang Y H and Wang L J, 'Statistical analysis of the surface fatigue crack growth in welded joints', *Engng Fract Mech*, 1993, **46** (6), 1031–1035.
673 Zheng X J and Glinka G, 'Weight functions and stress intensity factors for longitudinal semi-elliptical cracks in thick-wall cylinders', *J Pressure Vessel Techn*, 1995, **117**, 383–389.
674 Zheng X and Tienxi C, 'Life prediction of butt welds containing welding defect', *Engng Fract Mech*, 1989, **34** (5/6), 1005–1011.
675 Zwerneman F J and Frank K H, 'Stress intensity factor for a T-shaped weldment', *Engng Fract Mech*, 1989, **32** (4), 561–572.

Chapter 7 Notch stress intensity approach for seam-welded joints

676 Atzori B and Lazzarin P, 'A three-dimensional graphical aid to analyse fatigue crack nucleation and propagation phases under fatigue limit conditions', *Int J Fract*, 2002, **118**, 271–284.
677 Atzori B and Lazzarin P, 'Notch sensitivity and defect sensitivity under fatigue loading: two sides of the same medal', *Int J Fract*, 2000, **107**, L3–L8.
678 Atzori B, Lazzarin P and Filippi S, 'Crack and notches: analogies and differences of the relevant stress distributions and practical consequences in fatigue limit predictions', *Int J Fatigue*, 2001, **23**, 355–362.
679 Atzori B, Lazzarin P and Meneghetti G, 'Fracture mechanics and notch sensitivity', *Fatigue Fract Engng Mater Struct*, 2003, **26**, 257–267.
680 Atzori B, Lazzarin P and Tovo R, 'Stress distributions for V-shaped notches under tensile and bending loads', *Fatigue Fract Engng Mater Struct*, 1997, **20** (8), 1083–1092.
681 Atzori B, Lazzarin P and Tovo R, 'From a local stress approach to fracture mechanics: a comprehensive evaluation of the fatigue strength of welded joints', *Fatigue Fract Engng Mater Struct*, 1999, **22**, 369–381.
682 Atzori B, Lazzarin P and Tovo R, 'Stress field parameters to predict the fatigue strength of notched components', *J Strain Anal*, 1999, **34** (6), 437–453.
683 Atzori B, Meneghetti G and Susmel L, 'Estimation of the fatigue strength of light alloy welds by an equivalent notch stress analysis', *Int J Fatigue*, 2002, **24**, 591–599.
684 Boukharouba T, Tamine T, Nui L, Chehimi C and Pluvinage G, 'The use of notch intensity factor as a fatigue crack initiation parameter', *Engng Fract Mech*, 1995, **52**, 503–512.
685 Carpenter W C, 'Calculation of fracture mechanics parameters for a general corner', *Int J Fract*, 1984, **24**, 45–58.
686 Chen D H, 'Stress intensity factors for V-notched strip under tension or in-plane bending', *Int J Fract*, 1995, **70**, 81–97.
687 Dini D and Hills D A, 'Asymptotic characterisation of nearly-sharp notch root stress fields', *Int J Fatigue*, 2004, **130**, 651–666.
688 Dunn M L, Suwito W and Cunningham S, 'Stress intensities at notch singularities', *Engng Fract Mech*, 1997, **57** (4), 417–430.

689 El Haddad M H, Topper T H and Smith K N, 'Prediction of non-propagating cracks', *Engng Fract Mech*, 1979, **11**, 573–584.
690 Engesvik K and Lassen T, 'The effect of weld geometry on fatigue life', *Proceedings 3rd International Conference OMAE*, New York, ASME, 1988, pp 440–446.
691 Filippi S, Ciavarella M and Lazzarin P, 'An approximate analytical approach to the HRR-solution for sharp notches', *Int J Fract*, 2002, **117**, 269–286.
692 Filippi S and Lazzarin P, 'Distributions of the elastic principal stress due to notches in finite size plates and rounded bars uniaxially loaded', *Int J Fatigue*, 2004, **26**, 377–391.
693 Filippi S, Lazzarin P and Tovo R, 'Developments of some explicit formulas useful to describe elastic stress fields ahead of notches in plates', *Int J Solids Struct*, 2002, **39**, 4543–4565.
694 Glinka G and Newport A, 'Universal features of elastic notch-tip stress fields', *Int J Fatigue*, 1987, **9**, 143–150.
695 Gross R and Mendelson A, 'Plane elastostatic analysis of V-notched plates', *Int J Fract Mech*, 1972, **8**, 267–276.
696 Gurney T R, *The Fatigue Strength of Transverse Fillet Welded Joints*, Cambridge, Abington Publ, 1991.
697 Hasebe N, Nakamura T and Iida J, 'Notch mechanics for plane and thin-plate bending problems', *Engng Fract Mech*, 1990, **37** (1), 87–99.
698 Hutchinson J W, 'Singular behavior at the end of a tensile crack in a hardening material', *J Mech Phys Solids*, 1968, **16**, 13–31.
699 Hutchinson J W, 'Plastic stress and strain fields at a crack tip', *J Mech Phys Solids*, 1968, **16**, 337–347.
700 Koibuchi K, To K, Iida M and Hosomi T, 'Fatigue strength assessment of welded toes and defects of structures based on cyclic plastic zone size', *Engineering Against Fatigue*, Rotterdam, Balkema, 1999, pp 373–380.
701 Lassen T, 'The effect of welding process on the fatigue crack growth', *Welding J, Res Suppl*, 1990, **69**, 75s–81s.
702 Lazzarin P, 'The influence of bending on stress fields and fatigue strength of cruciform welds', *Welding Int*, 2000, **14** (2), 115–119, translation from *Rivista Italiana della Saldatura*, 1999, **51** (2), 137–143.
703 Lazzarin P, Berto F and Radaj D, 'Uniform fatigue strength of butt and fillet welded joints in terms of the local strain energy density', *Fatigue'06, Proc 9th Int Fatigue Congress*, FT 179, pp 1–10, Oxford, Elsevier Science 2006.
704 Lazzarin P, Lassen T and Livieri P, 'A notch stress intensity approach applied to fatigue life predictions of welded joints with different local toe geometry', *Fatigue Fract Engng Mater Struct*, 2003, **26**, 49–58.
705 Lazzarin P and Livieri P, 'Dimensione della zona plastica al piede dei cordoni in giunti saldati in acciaio e lega leggera (Plasitic zone size at the weld toe in welded joints made of steel and light alloys)', *Rivista Italiana Della Saldatura*, 2000, **52** (7/8), 421–437.
706 Lazzarin P and Livieri P, 'Notch stress intensity factors and fatigue strength of aluminium and steel welded joints', *Int J Fatigue*, 2001, **23**, 225–232.
707 Lazzarin P, Livieri P and Zambardi R, 'A *J*-integral-based approach to predict the fatigue strength of components weakened by sharp V-shaped notches', *Int J Comp Appl Techn*, 2002, **15** (4/5), 202–210.
708 Lazzarin P, Sonsino C M and Zambardi R, 'A notch stress intensity approach to assess the multiaxial fatigue strength of welded tube-to-flange joints

subjected to combined loadings', *Fatigue Fract Engng Mater Struct*, 2004, **27**, 127–140.
709 Lazzarin P and Tovo R, 'A unified approach to the evaluation of linear elastic stress fields in the neighborhood of cracks and notches', *Int J Fract*, 1996, **78**, 3–19.
710 Lazzarin P and Tovo R, 'A notch stress intensity factor approach to the stress analysis of welds', *Fatigue Fract Engng Mater Struct*, 1998, **21**, 1089–1103.
711 Lazzarin P, Tovo R and Filippi S, 'Elastic stress distributions in finite size plates with edge notches', *Int J Fract*, 1998, **91**, 269–282.
712 Lazzarin P, Tovo R and Meneghetti G, 'Fatigue crack initiation and propagation phases near notches in metals with low notch sensivity', *Int J Fatigue*, 1997, **19** (8/9), 647–657.
713 Lazzarin P and Zambardi R, 'A finite volume energy based approach to predict the static and fatigue behavior of components with sharp V-shaped notches', *Int J Fract*, 2001, **112**, 275–298.
714 Lazzarin P and Zambardi R, 'The equivalent strain energy density approach reformulated and applied to sharp V-shaped notches under localized and generalized plasticity', *Fatigue Fract Engng Mater Struct*, 2002, **25**, 917–928.
715 Lazzarin P, Zambardi R and Livieri P, 'Plastic notch stress intensity factors for large V-shaped notches under mixed load conditions', *Int J Fract*, 2001, **107**, 361–377.
716 Livieri P and Lazzarin P, 'Fatigue strength of steel and aluminium welded joints based on generalised stress intensity factors and local strain energy values', *Int J Fract*, 2005, **133**, 247–276.
717 Maddox S J, *The Effect of Plate Thickness on the Fatigue Strength of Fillet Welded Joints*, Cambridge, Abington Publ, 1987.
718 Maddox S J, 'Scale effect in fatigue of fillet welded aluminium alloys', *Proceedings 6th International Conference on Aluminium Weldments*, Cleveland, Ohio, 1995, pp 77–93.
719 Noda, N A, Nisitani H, Harada S and Takase Y, 'Fatigue strength of notched specimens having nearly equal sizes of ferrite', *Int J Fatigue*, 1995, **17**, 237–244.
720 Nui L S, Chehimi C and Pluvinage G, 'Stress field near a large blunted tip V-notch and application of the concept of the critical notch stress intensity factor (nsif) to the fracture toughness of very brittle materials', *Engng Fract Mech*, 1994, **49** (3), 325–335.
721 Quian J and Hasebe N, 'Property of eigenvalues and eigenfunctions for an interface V-notch in antiplane elasticity', *Engng Fract Mech*, 1997, **56** (6), 729–734.
722 Rice J R and Rosengren G F, 'Plane strain deformation near a crack tip in a power-law hardening material', *J Mech Phys Solids*, 1968, **16**, 1–12.
723 Susmel L and Tovo R, 'Multiaxial fatigue life prediction of two welded details subjected to local complex stress states', *Proceedings 7th International Conference on Biaxial/Mulitaxial Fatigue and Fracture*, Berlin, DVM, 2004, pp 447–452.
724 Tanaka K, Okajima H and Koibuchi K, 'Fatigue strength CAE system for three-dimensional welded structures', *Fatigue Fract Engng Mater Struct*, 2002, **25**, 275–282.
725 Tovo R and Lazzarin P, 'Relationships between local and structural stress in the evaluation of the weld toe stress distribution', *Int J Fatigue*, 1999, **21**, 1063–1078.

726 Williams M L, 'Stress singularity resulting from various boundary conditions in angular corners of plates in tension', *J Appl Mech*, 1952, **19**, 526–528.
727 Xu R X, Thompson J C and Topper T H, 'Practical stress expressions for stress concentration regions', *Fatigue Fract Engng Mater Struct*, 1995, **18**, 885–895.
728 Yao W, Xia K and Gu Y, 'On the fatigue notch factor K_f', *Int J Fatigue*, 1995, **17**, 245–251.

Chapter 8 Local approaches applied to a seam-welded tubular joint

729 Hück M and Heuler P, The common load sequence for fatigue evaluation of offshore structures – background and generation, IABG-Bericht TF1892, Ottobrunn, 1988.
730 Lachmann E, Schütz W and Sonsino C M, 'Corrosion fatigue of V-shaped welded and cast specimens in seawater under variable-amplitude loading', *Proceedings International Conference on Steel in Marine Structures* (*SIMS'87*), Amsterdam, Elsevier Science, 1987, pp 551–564.
731 Morgan M R and Lee M M, 'Prediction of stress concentration factors in K-joints under balanced axial loading', *Proceedings International Symposium on Tubular Structures*, Rotterdam, Balkema, 1996, pp 301–308.
732 Morgan M R and Lee M M, 'New parametric equations for stress concentration factors in tubular K-joints under balanced axial loading', *Int J Fatigue*, 1997, **19** (4), 309–317.
733 Morgan M R and Lee M M, 'Parametric equations for distributions of stress concentration factors in tubular K-joints under out-of-plane moment loading', *Int J Fatigue* 1998, **20** (6), 449–461.
734 Payne J G and Porter-Gof R F, 'Experimental residual stress distributions in welded tubular T-nodes', *Proceedings International Conference Fatigue Crack Growth in Offshore Structures*, London, Institute of Mechanical Engineers, 1986, pp 109–116.
735 Potvin A B, Kuang J G, Leick R D and Kahlich J L, 'Stress concentration in tubular joints', *Soc Petroleum Engng J*, 1977, **8**, 287–299.
736 Radaj D, Sonsino C M and Flade D, 'Prediction of service fatigue strength of a welded tubular joint on the basis of local approaches', *Int J Fatigue*, 1998, **20** (6), 471–480, and DVS-Bericht 187, *Fortschritte bei der Konstruktion und Berechnung geschweißter Bauteile*, Düsseldorf, DVS-Verlag, 1997, pp 114–120, (German version).
737 Seyffarth P, *Atlas Schweiß-ZTU-Schaubilder*, Düsseldorf, DVS-Verlag, 1982.
738 Sonsino C M and Lipp K, Übertragbarkeit des an Winkelproben ermittelten Betriebsfestigkeitsverhaltens auf große Rohrknoten für die Offshoretechnik, LBF-Bericht TB-180, Darmstadt, Fraunhofer-Inst f Betriebsfest, 1988, pp 243–272.
739 Sonsino C M and Umbach R, 'Corrosion fatigue of welded and cast-steel hybrid nodes under constant and variable-amplitude loading', *Proceedings International Conference on Offshore Mechanics and Artic Engineering (OMAE'93)*, New York, ASME, 1993, Vol 3B, pp 667–674.
740 Umbach R, Sonsino C M *et al,* Korrosionsschwingfestigkeit von geschweißten Rohrknoten und Stahlguß-Verbundkonstruktionen in bauteilähnlichem, Maß-

stab (Corrosion fatigue of welded tubular joints and cast-steel compound tubular joints in large size scale), EU Rep 14316DE, Brussels, ECCS, 1993.
741 Vormwald M, 'A fracture-mechanics-based fatigue life prediction for offshore tubular joints', *Proc Int Symp Offshore and Polar Engng (ISOPE'91)*, Golden Colo, International Society of Offshore and Polar Engineers, 1991, Vol 4, pp 451–457.
742 Wordsworth A C, 'Stress concentration factors at K and KT-joints', *Proceedings Conference on Fatigue in Offshore Structural Steels*, London, Thomas Telford, 1981.
743 Zheng X and Wang R, 'On the corrosion fatigue crack initiation model and expression of metallic notched elements', *Engng Fract Mech*, 1997, **57** (6), 617–624.

Chapter 9 Structural stress or strain approach for spot-welded and similar lap joints

744 Abe H and Satoh T, 'Method for non-destructive detection of fatigue cracks in spot-welded joints' (in Japanese), *Quart J Japan Welding Soc*, 1986, **4** (4), 12–19.
745 Abe H and Satoh T, 'Development and investigation of a strain gauge for estimation of fatigue life of multi-spot-welded joints – confirmation of validity using single-spot-welded joint specimens', *Welding Int*, 1993, **7** (1), 35–41.
746 Abe H, Yokomine T, Nakaoka T and Satoh T, 'Fatigue life of single-spot-welded joints under cyclic load – comparison of mild steel and high-strength steel', *Welding Int*, 1994, **8** (1), 16–22.
747 Aristotile R, Comportamento a fatica di particolari per autoveicoli in lamierini saldati a punti, influenza sulla salda del tipo di materiale (Fatigue behaviour of motor vehicle parts of spot welded sheets – influence of type of material on the results), EU Rep 10157IT, Brussels, Commission of the European Community, 1985.
748 Atzori B, Lazzarin P and Stacco E, 'Effect of spot welded distribution characteristics on the fatigue strength of resistance welded joints', *Welding Int*, 1988, **8**, 707–712, translation from *Rivista Italiana della Saldatura*, 1987, **39** (4), 317–324.
749 Blarasin A, Atzori B, Filippa P and Gastaldi G, 'Design fatigue data for joining steel sheets in the automotive industry', *SAE Techn Paper 900742*, Warrendale Pa, SAE, 1990.
750 Brenner C E, Unger B, Gaier C, Steinwender G and Eichlseder W, 'Fatigue assessment of welding seams and spot joints based on FEA', *SAE Techn Paper 2000-01-0780*, Warrendale Pa, SAE, 2000.
751 Chen W and Deng X, 'Performance of shell elements in modeling spot-welded joints', *Finite Element Analysis and Design*, 2000, **35**, 41–57.
752 Chu C C, 'Multiaxial fatigue life prediction method in the ground vehicle industry', *Int J Fatigue*, 1997, **19** (Suppl 1), S325–S330.
753 Conle F A and Chu C C, 'Fatigue analysis and the local stress-strain approach in complex vehicular structures', *Int J Fatigue*, 1977, **19** (Suppl 1), S317–S323.
754 Dang Van K, Bignonnet A, Fayard J L and Janosch J, 'Assessment of welded structures by a local multiaxial fatigue approach', *Fatigue Fract Engng Mater Struct*, 2001, **24**, 369–376.

755 Dattoma V and Lazzarin P, 'Fatigue bahaviour of laser-welded lap joints in AISI 304', *Proceedings 4th International Conference on Fatigue and Fatigue Thresholds*, 1990, pp 2317–2322.
756 Davidson J A, 'A review of the fatigue properties of spot-welded sheet steels', *SAE Techn Paper 830033*, Warrendale Pa, SAE, 1983.
757 Davidson J A and Imhof E J, 'The effect of tensile strength on the fatigue life of spot-welded sheet steels', *SAE Techn Paper 840110*, Warrendale Pa, SAE, 1984.
758 Deng X, Chen W and Shi G, 'Three-dimensional finite element analysis of the mechanical behaviour of spot welds', *Finite Element Anal Design*, 2000, **35**, 17–39.
759 Di Fant-Jaeckels H, Galtier A and Barthelemy J Y, Towards a numerical model for lifetime prediction of spot welded structures under multiaxial loading, IIW Doc XIII-1647-96.
760 Dong P, Sun X, Lu F and Zhang J, 'A framework for modeling spot welds in finite element analysis of auto-body structures', *SAE Techn Paper 1999-01-3191*, Warrendale Pa, SAE, 1999.
761 Dunst A, Automatisierte FEM-Modellgenerierung von Konzeptmodellen von Fahrzeugkarrosserien unter korrekter Steifigkeitsabbildung der Fügestelle, diploma thesis, Graz University of Technology, and Steyr-Daimler-Puch Fahrzeugtechnik AG, Graz, 2000.
762 Fayard J L, Bignonnet A and Dang Van K, 'Fatigue design of welded thin-sheet structures', *Proceedings Fatigue Design 95*, London, Mechanical Engineering Publ, 1995, pp 723–729.
763 Fayard J L, Bignonnet A and Dang Van K, 'Fatigue design criterion for welded structures', *Fatigue Fract Engng Mater Struct*, 1996, **19** (6), 723–729.
764 Fayard J L, Bignonnet A and Dang Van K, 'Fatigue assessment of automobile welded structures', *International Conference on Fatigue of Welded Components and Structures*, pp 65–72, Les Ulis, Soc Française de Métallurgie et de Matériaux, 1996, and IIW Doc XIII-1643-96.
765 Fayard J L, Bignonnet A and Dang Van K, 'Fatigue design of welded thin sheet structures', *Fatigue Design of Components*, Amsterdam, Elsevier Science, 1997, pp 145–152.
766 Fermér M, Andréasson M and Frodin B, 'Fatigue life prediction of MAG-welded thin-sheet structures', *SAE Techn Paper 982311*, Warrendale Pa, SAE, 1998.
767 Fermér M, Klingberg J, Weinert M, Fels D, Devlukia J and Blows A, 'Statistical correlation of measured and predicted fatigue life of car bodies tested under constant and variable amplitude loading', *Numerical Analysis and Simulation in Vehicle Engng*, VDI-Berichte 1846, Düsseldorf, VDI-Verlag, 2004, pp 479–491.
768 Fermér M and Svensson H, 'Industrial experiences of FE-based fatigue life predictions of welded automotive structures', *Fatigue Fract Engng Mater Struct*, 2001, **24**, 489–500.
769 Fischer G and Grubisic V, 'Data for the design of welded aluminum sheet suspension components', *SAE Techn Paper 1999-01-0662*, Warrendale Pa, SAE, 1999.
770 Flavenot J F, Deville J P, Diboine A, Cantello M and Gobbi S L, 'Fatigue resistance of laser-welded lap joints of steel sheets', *Welding in the World*, 1993, **31** (5), 358–361.

771 Gao Y, Chucas D, Lewis C and McGregor I J, 'Review of CAE fatigue analysis techniques for spot-welded high strength steel automotive structures' *SAE Techn Paper 2001-01-0835*, Warrendale Pa, SAE, 2001.
772 Grubisic V *et al.*, 'Verbesserung der Bauteilfestigkeit durch höherfeste Feinblechwerkstoffe und optimierte Fügeverfahren', *Fügen im Leichtbau*, DVM-Bericht 120, Berlin, DVM, 1994, pp 47–61.
773 Gurney T R, *Fatigue of Thin-Walled Joints under Complex Loading*, Cambridge, Abington Publ, 1997.
774 Hahn O, Gieske D, Klasfauseweh U and Rohde A, *Fatigue Resistance of Spot Welds under Multiaxial Loads*, IIW Doc XIII-1544-94.
775 Heiserer D, Sielaff J and Chargin M, 'High-performance process-oriented weld spot approach', *Proceedings 1st MSC Worldwide Automotive Users' Conference*, Munich 1999, P25, Costa Mesa Cal, MSC Software Corp, 1999.
776 Heyes P and Fermér M, 'A spot-weld fatigue analysis module in the MSC/FATIGUE environment', *Proceedings 1996 MSC World Users' Conference*, Costa Mesa Cal, MSC Software Corp, 1996, pp 1–13.
777 Hsu C and Albright C E, 'Fatigue analysis of laser-welded lap joints', *Engng Fract Mech*, 1991, **39** (3), 575–580.
778 Jonscher A, Lewerenz M and Lührs G, 'The new spot weld element in the CAE process', *Proceedings 1st MSC Worldwide Automotive Users' Conference*, Munich 1999, P26, Costa Mesa Cal, MSC Software Corp, 1999.
779 Kan Y R, 'Fatigue resistance of spot welds – an analytical study', *Metals Engng Quart*, 1976, **11**, 26–36.
780 Kang H, Barkey M E and Lee Y, 'Evaluation of multiaxial spot weld fatigue parameters for proportional loading', *Int J Fatigue*, 2000, **22**, 691–702.
781 Kasahara T, Maruo Y, Nakamaru T, Magara S and Koibuchi K, 'Method of fatigue life estimation for arc-welded structures', *SAE Techn Paper 2000-01-0781*, Warrendale Pa, SAE, 2000.
782 Kitagawa H, Satoh T and Fujimoto M, 'Fatigue strength of single spot-welded joints of rephosphorised high-strength and low-carbon steel sheets', *SAE Techn Paper 850371*, Warrendale Pa, SAE, 1985.
783 Koenigsberger F, *Design for Welding in Mechanical Engineering*, London, Longmans & Green, 1948.
784 Kuang J H and Liu A H, 'Study of the stress concentration factor on spot welds', *Welding J, Res Suppl*, 1990, **69**, 469s–474s.
785 Kurath P, 'Multiaxial fatigue criteria for spot welds', *SAE Techn Paper 920668*, Warrendale Pa, SAE, 1992.
786 Le Duff J A, Masalski D and Duchanois G, Évaluation de la résistance en fatigue des assemblages soudés par points en tenant compte de l'influence des contraintes résiduelles, IIW Doc XIII-1348–89.
787 Lee Y L, Fatigue reliability analysis of resistance spot welds, *SAE Techn Paper 94RM-040*, Warrendale Pa, SAE, 1994.
788 Lee Y L, Raymont M N and Villaire M A, 'Durability design process of a vehicle suspension component', *J Testing Evaluation*, 1995, **23**(5), 354–363.
789 Linder J and Melander A, 'Fatigue strength of spot-welded stainless sheet steels exposed to 3% NaCl solution', *Int J Fatigue*, 1998, **20** (5), 383–388.
790 Lindgren C, Sperle J O and Jonsson M, Fatigue strength of spot-welded beams in high-strength steels, IIW Doc XIII-1553-94.

791 Mabuchi A, Niisawa J and Tomioka N, 'Fatigue life prediction of box-section beams under repeated torsion', *SAE Techn Paper 860603*, Warrendale Pa, SAE, 1986.
792 Maddox S J, 'Fatigue design of welded structures', *Engineering Design in Welded Constructions*, Oxford, Pergamon Press, 1992, pp 31–56.
793 Maddox S J, 'Developments in fatigue design codes and fitness-for-service assessment methods', *International Conference on Performance of Dynamically Loaded Welded Structures*, New York, WRC, 1997, pp 22–42.
794 Mayer A, Haidann J and Kepplinger G, 'Automatisierte Schweißpunktgenerierung in FEM-Karosseriemodellen: optimierte Anordnung, Bewertung von Steifigkeit und Lebensdauerabschätzung', *Berechnung und Simulation im Fahrzeugbau*, VDI-Berichte 1559, Düsseldorf, VDI-Verlag, 2000.
795 Mayer A, Haidann J, Meinhart H and Kepplinger G, 'Theoretical fatigue life estimation as a tool for vehicle body development', *SAE Techn Paper 1999-01-3151*, Warrendale Pa, SAE, 1999.
796 Mayer A and Preis N, 'Berechnungsverfahren zur Spannungsbeurteilung von Punktschweißverbindungen', *Konstruktion*, 1994, **46**, 287–291.
797 Mizui M, Sekine T, Tsujimura A, Takishima T and Shimazaki Y, 'An evaluation of fatigue strength for various kinds of spot-welded specimens', *SAE Techn Paper 880375*, Warrendale Pa, SAE, 1988.
798 Mori N, Amago T, Ono M, Sasanabe M and Hiraide T, 'Fatigue life prediction methods for spot welds in T-shaped members under bending', *SAE Techn Paper 860604*, Warrendale Pa, SAE, 1986.
799 Nakahara Y, Takahashi M, Kawamoto A, Fujimoto M and Tomioka N, 'Method of fatigue life estimation for spot-welded structures', *SAE Techn Paper 2000-01-0779*, Warrendale Pa, SAE, 2000.
800 Ni K and Mahadevan S, 'Strain based probabilistic fatigue life prediction of spot-welded joints', *Int J Fatigue*, 2004, **26**, 763–772.
801 Oh H L, 'Fatigue life prediction for spot welds using Neuber's rule', *Design of Fatigue and Fracture Resistant Structures*, ASTM STP 761, Philadelphia Pa, ASTM, 1982, pp 296–309.
802 Oshima M and Kitagawa H, 'Buckling-assisted fatigue of spot-welded box beam under bending', *SAE Techn Paper 860605*, Warrendale Pa, SAE, 1986.
803 Radaj D, 'Strukturspannungserhöhung an Punktschweißverbindungen', *Konstruktion*, 1986, **38**, 41–47 (Part 1), 1986, **38**, 397–404 (Part 2), 1987, **39**, 51–63 (Part 3) and 1988, **40**, 159–164, with emendation, 1989, **41**, 101.
804 Radaj D, 'Hot spot stress concept for spot-welded joints', *Structural Design and Crash Worthiness of Automobiles*, Berlin, Springer, 1987, pp 149–170.
805 Radaj D, 'Hot-Spot-Strukturspannungsberechnung für die punktgeschweißte Scherzug- und Hutprofilprobe, *Schweißen u Schneiden*, 1987, **39**, 7–12, and E2-E4 (English version).
806 Radaj D, 'Nennstrukturspannungen für gängige Schweißpunktproben', *Konstruktion*, 1989, **41**, 255–259.
807 Radaj D, 'Vollständige Bestimmung der Kräfte am Schweißpunkt', *Ing-Archiv*, 1990, **60**, 389–398.
808 Radaj D, 'Theory of forces and stresses in spot-welded overlap joints', *Archive Appl Mech*, 1996, **67**, 2–34.

809 Radaj D, Glatzel G and Kizler W, 'Spannungsoptische Beanspruchungstypbilder an Punktschweißverbindungen', *Schweißen u Schneiden*, 1988, **40** (1), 7–13, and E2-E3 (English version).
810 Radaj D and Stoppler W, 'Loading state in spot-like overlap joints determined by correlation of deformation patterns', *Materialwiss u Wertstofftechn*, 2004, **35** (1), 5–12.
811 Radaj D and Zhang S, 'Geometrically nonlinear behaviour of spot-welded joints in cross tension loading', *Stahlbau*, 1994, **63** (5), 147–154.
812 Radaj D and Zhang S, 'Geometrically nonlinear behaviour of spot-welded joints in tensile and compressive shear loading', *Engng Fract Mech*, 1995, **51** (2), 281–294.
813 Radaj D and Zhang S, 'Anschauliche Grundlagen für Kräfte und Spannungen in punktgeschweißten Überlappverbindungen', *Konstruktion*, 1996, **48**, 65–71.
814 Radaj D and Zhang S, 'Strukturspannungen am starren Kern in endlich berandeter Platte', *Konstruktion*, 1996, **48**, 195–199.
815 Radaj D and Zhang S, 'Weld spot force evaluation with dented sheet material', *Engng Fract Mech*, 1998, **61**, 673–678.
816 Radaj D, Zheng Z and Möhrmann W, 'Local stress parameters at the weld spot of various specimens', *Engng Fract Mech*, 1990, **37** (5), 933–951, and *Konstruktion*, 1990, **42** (5/6), 181–188 and 201–206 (German version).
817 Rathbun R W, Matlock D K and Speer J G, 'Fatigue behaviour of spot-welded high-strength sheet steels', *Welding J, Res Suppl*, 2003, **82** (8), 207s–218s.
818 Reemsnyder H S, Modelling of the fatigue resistance of single-lap spot-welded steel sheet, IIW Doc XIII-1469–92.
819 Rossetto E, Rossi F, Vaschetto L and Atzori B, 'The fatigue limit of spot-welded lap joints', *SAE Techn Paper 870640*, Warrendale Pa, SAE, 1987.
820 Rui Y, Borsos R S, Gopalakrishnan R, Agrawal H N and Rivard C, 'The fatigue life prediction method for multi-spot-welded structures', *SAE Techn Paper 930571*, Warrendale Pa, SAE, 1987.
821 Rupp A, Beanspruchung und Beanspruchbarkeit von Punktschweißverbindungen unter Schwingbelastung – ein Auslegungsverfahren (Stresses and strains and their limit values in spot welded joints subjected to cyclic loads – a procedure for design), Dr-Ing thesis, Braunschweig Techn Univ, 1992.
822 Rupp A, Ermittlung ertragbarer Beanspruchungen an Aluminium-Punktschweißverbindungen auf Basis der Schnittkräfte (Determination of endurable stresses in aluminium spot welded joints on the basis of the joint face forces), FAT-Schriftenreihe 138, Frankfurt/M, FAT, 1997.
823 Rupp A, 'Fatigue life prediction of thin sheet structures – theoretical and experimental results', *Proceedings International Body Engineering Conference*, Stuttgart, 1997.
824 Rupp A and Grubisic V, Ermittlung ertragbarer Beanspruchungen am Schweißpunkt auf Basis der übertragenen Schnittgrößen (Determination of endurable stresses at weld spots on the basis of joint face forces), FAT-Schriftenreihe 111, Frankfurt/M, FAT, 1994.
825 Rupp A, Grubisic V and Radaj D, 'Betriebsfestigkeit von Punktschweißverbindungen', *Materialprüfung*, 1990, **32** (6), 175–179.
826 Rupp A, Grubisic V and Radaj D, 'Rechnergestützte Auslegung punktgeschweißter Bauteile', *Fügen im Leichtbau*, DVM-Bericht 120, Berlin, DVM, 1994, pp 159–175.

827 Rupp A, Grubisic V, Störzel K and Steinhilber H, Ermittlung von ertragbaren Schnittkräften für die betriebsfeste Bemessung von Punktschweißverbindungen im Automobilbau (Determination of endurable joint face forces for the fatigue-resistant dimensioning of spot-welded joints in automotive engineering), FAT-Schriftenreihe 78, Frankfurt/M, FAT, 1989.
828 Rupp A, Störzel K and Grubisic V, 'Computer-aided dimensioning of spot-welded automotive structures', *SAE Techn Paper 950711*, Warrendale Pa, SAE, 1995.
829 Salvini P, Scardecchia E and Demofonti G, 'A procedure for fatigue life prediction of spot-welded joints', *Fatigue Fract Engng Mater Struct*, 1997, **20** (8), 1117–1128.
830 Salvini P, Scardecchia E and Vivio F, 'Fatigue life prediction on complex spot welded joints', *Trans J Mater Manufact*, 1997, **106**, 967–975.
831 Salvini P, Vivio F and Vullo V, 'A spot weld finite element for structural modelling', *Int J Fatigue*, 2000, **22**, 645–656.
832 Satoh T and Abe H, 'Non-destructive detection method of fatigue crack in spot-welded joint specimens', *SAE Techn Paper 860601*, Warrendale Pa, SAE, 1986.
833 Satoh T and Abe H, 'Development and availability of SA-gauge for prediction method of fatigue strength of spot welds', *Proceedings International Symposium Japan Welding Society*, Tokyo, JWC, 1990, pp 1007–1012.
834 Satoh T, Abe H, Nishikawa K and Morita M, 'On three-dimensional elastic-plastic stress analysis of spot-welded joint under tensile shear load', *Trans Japan Welding Soc*, 1991, **22** (2), 1–6, and IIW Doc XIII-967-91.
835 Satoh T, Abe H, Yokomine T and Nakaoka T, 'On the fatigue life of the single spot-welded joint under the 2-steps repeating loads', *Trans Japan Welding Soc*, 1993, **24** (1), and IIW Doc XIII-1009-93.
836 Satoh T, Katayama J and Ueda M, On fatigue strength of spot-welded joint in coated steels, IIW Doc XIII-926-89.
837 Sonsino C M, Müller F and Radaj D, 'Ertragbare Strukturspannungen von lasergeschweißten Stahlblechen', *Fügen im Leichtbau*, DVM-Bericht 120, Berlin, DVM, 1994, pp 63–86.
838 Sperle J O, 'Fatigue strength of non-load-carrying spot welds', *Metal Constr*, 1984, **16** (11), 678–679.
839 Stoppler W and de Boer A, Meßverfahren für Kräfte und Momente an strich- und punktgeschweißten Überlappverbindungen (Measuring method for forces and moments in seam-welded and spot-welded lap joints), FAT-Schriftenreihe 134, Frankfurt/M, FAT, 1997.
840 Störzel K and Rupp A, Software-Entwicklung für betriebsfeste Bemessung von Punktschweißverbindungen im Automobilbau (Software development for fatigue-resistant dimensioning of spot-welded joints in automobile components), Bericht 6866, Darmstadt, Fraunhofer-Inst f Betriebsfest, 1993.
841 Vopel H G and Glas E, Rechnerische Erfassung von Eigenschaften der Schweißpunkte in Karosseriemodellen, *ATZ*, 1997, **99** (6), 1–6.
842 Vopel H G and Hillmann J, 'Berücksichtigung der Schweißpunkte bei der FEM-Modellierung von Karosserien', *Berechnung und Simulation im Fahrzeugbau*, VDI-Berichte 1283, Düsseldorf, VDI-Verlag, 1992, pp 171–182.
843 Wallmichrath M and Eibl M, Ingenieurmäßige Berechnungsverfahren zur Lebensdauerabschätzung von geschweißten Dünnblechverbindungen – Teil 1:

Punktschweißen, Teil 2: Laserstrahlschweißen, FAT-Schriftenreihe 179, Frankfurt/M, FAT, 2003.
844 Wang P C and Ewing K M, 'A comparison of fatigue strengths: laser beam versus resistance spot welds', *Welding J*, 1991, **70** (10), 43–47.
845 Wang P C and Ewing K M, 'Effect of weld design on the fatigue-strength of laser and resistance spot-welded tubular T-joints for automotive applications', *Welding J, Res Suppl*, 1994, **73** (9), 209s–217s.
846 Zhang G and Richter B, 'A new approach to the numerical fatigue-life prediction of spot-welded structures', *Fatigue Fract Engng Mater Struct*, 2000, **23**, 499–508.
847 Zhang G, Singh S, Hahn O and Kurzok J P, 'Ein neuer Parameter zur Lebensdauervorhersage von Schweißpunkten basierend auf der Nennstrukturspannung, unter Berücksichtigung des Blechdickeneffekts', *Schweißen u Schneiden*, 2000, **52** (9), 530–542.
848 Zhang S and Radaj D, 'Forces and stresses in seam-welded overlap joints derived from outer surface deformation', *Engng Fract Mech*, 1996, **54** (6), 743–750.

Chapter 10 Stress intensity approach for spot-welded and similar lap joints

849 Banks-Sills L, 'Application of the finite element method to linear elastic fracture mechanics', *Appl Mech Rev*, 1991, **44**, 447–461.
850 Banks-Sills L and Bortman Y, 'Re-appraisal of the quarter-point quadrilateral element in linear elastic fracture mechanics', *Int J Fract*, 1984, **25**, 169–180.
851 Barkey M E, Kang H and Lee Y, 'Failure modes of single resistance spot welded joints subjected to combined fatigue loading', *Int J Mater Prod Techn*, 2001, **16** (6/7), 510–527.
852 Barsom J M, Davidson J A and Imhoff E J, 'Fatigue behavior of spot welds under variable-amplitude loading', *SAE Techn Paper 850369*, Warrendale Pa, SAE, 1985.
853 Barsoum R S, 'On the use of isoparametric finite elements in linear fracture mechanics', *Int J Numerical Methods Engng*, 1976, **10**, 25–32, and 1977, **11**, 85–98.
854 Barsoum R S, 'Triangular quarter-point elements as elastic and perfectly-plastic crack tip elements', *Int J Numerical Methods Engng*, 1977, **11**, 85–98.
855 Benthem J P and Koiter W T, 'Asymptotic approximations to crack problems', *Methods of Analysis and Solutions of Crack Problems*, Leyden, Noordhoff, 1973, pp 131–178.
856 Beretta S and Sala G, 'A model for fatigue strength of welded lap joints', *Fatigue Fract Engng Mater Struct*, 2005, **28**, 257–364.
857 Chang D J and Muki R, 'Stress distribution in a lap joint under tension-shear', *Int J Solids Struct*, 1974, **10**, 503–517.
858 Cooper A P and Sawyer J W, A critical examination of stress in an elastic single lap joint, NASA Techn Paper 1507, 1979.
859 Cooper J F and Smith R A, 'Initial fatigue crack growth at spot welds', *Proceedings Conference on Fatigue of Engng Materials and Structures*, London, Institute of Mechanical Engineering, 1986, Vol 2, pp 283–288.

860 Creager M and Paris P C, 'Elastic field equations for blunt cracks with reference to stress corrosion cracking', *Int J Fract Mech*, 1967, **3**, 247–252.
861 Cruse T A, 'An improved boundary integral equation for three-dimensional elastic stress analysis', *Computers and Structures*, 1974, **4**, 741–754.
862 Davidson J A, 'Design related methodology to determine the fatigue life and related failure mode of spot-welded sheet steels', *HSLA Steels, Technology and Application*, Materials Park, Ohio, ASM, 1984.
863 Davidson J A and Imhof E J, 'A fracture mechanics and system stiffness approach to fatigue performance of spot-welded steel sheets', *SAE Techn Paper 830034*, Warrendale Pa, SAE, 1983.
864 Davidson J A and Imhof E J, 'The effect of tensile strength on the fatigue life of spot-welded sheet steels', *SAE Techn Paper 840110*, Warrendale Pa, SAE, 1984.
865 El-Sayed M E, Stawiarski T and Frutiger R, 'Fatigue analysis of spot-welded joints under variable-amplitude load history', *Engng Fract Mech*, 1996, **55** (3), 363–369.
866 Erdogan F and Sih G C, 'On the crack extension in plates under plane loading and transverse shear', *Trans ASME, J Basic Engng*, 1963, **85**, 519–527.
867 Fujimoto M, Mori N and Sakuma S, Stress distribution analysis of spot-welded joints under tension-shear load, IIW Doc III-721-82.
868 Gieske D and Hahn O, 'Neue Einelementproben zum Prüfen von Punktschweißverbindungen unter kombinierten Belastungen', *Schweißen u Schneiden*, 1994, **46** (1), 9–12.
869 Goland M and Reissner E, 'The stresses in cemented joints', *J Appl Mech*, 1944, **11**, A-17.
870 Haefele P M and Lee J D, 'The constant stress term', *Engng Fract Mech*, 1995, **50** (5/6), 869–882.
871 Hahn O and Wender B, 'Finite-Element-Analyse einer auf Zug beanspruchten einschnittig überlappten Widerstandspunktschweißverbindung mit Hilfe unterschiedlicher Strukturmodelle', *Schweißen u Schneiden*, 1983, **35** (4), 174–178.
872 Henshell R D and Shaw K G, 'Crack tip elements are unnecessary', *Int J Numerical Methods Engng*, 1975, **9**, 495–507.
873 Hussain M A, Pu S L and Underwood J, 'Strain energy release rate for a crack under combined mode I and mode II', *Fracture Analysis*, ASTM STP 560, Philadelphia Pa, ASTM, 1974, pp 2–28.
874 Irwin G R, 'Analysis of stresses and strains near the end of a crack traversing a plate', *Trans ASME, J Appl Mech*, 1957, **24**, 361–364.
875 Kassir M K and Sih G C, 'External elliptical crack in elastic solid', *Int J Fract Mech*, 1968, **4**, 347–356.
876 Lai Y H, Rakestraw M D and Dillard D, 'The cracked lap-shear specimen revisited – a closed form solution', *Int J Solids Struct*, 1996, **33**, 1725–1743.
877 Lee H and Kim N, 'Fatigue life prediction of multi-spot-welded panel structures using an equivalent stress intensity factor', *Int J Fatigue*, 2004, **26**, 403–412.
878 Linder J, Melander A, Larsson M and Bergengren Y, 'Fatigue design of spot-welded austenitic and duplex stainless sheet steels', *Fatigue Fract Engng Mater Struct*, 1998, **21**, 673–686.
879 Makhnenko V I, Ryabchuk T G and Pochinok V E, 'Improvement of strength calculation procedure for welded joints with spot welds' (in Russian), *Automatcheska Svarka*, 1990, **442** (1), 9–14.

880 Niisawa J, Tomioka N and Yi W, 'Analytical method of rigidities of thin-walled beams with spot welding joints and its application to torsion problems', *JSAE Review*, 1984, **13**, 76–83.
881 Overbeeke J L and Draisma J, The *F–N* curve of heavy-duty spot-welded lap joints at $R = 0$, Rep WH 72–3, Department of Mechanical Engineering, Eindhoven, Techn Univ, 1972.
882 Overbeeke J L and Draisma J, 'Fatigue characteristics of heavy duty spot welded lap joints', *Metal Constr*, 1974, **6** (7), 213–219.
883 Paris P C and Sih G C, 'Stress analysis of cracks', *Fracture Toughness Testing*, ASTM STP 381, Philadelphia Pa, ASTM, 1965.
884 Partanen T, Lindberg I and Niemi E, On fatigue behaviour of transverse fillet welds in lap joints, IIW Doc XIII-1505-93.
885 Pollard P, 'Fatigue-strength of spot welds in titanium-bearing HSLA steels', *SAE Techn Paper 820284*, Warrendale Pa, SAE, 1982.
886 Pook L P, Approximate stress intensity factors for spot and similar welds, NEL Rep 588, Glasgow, National Engineering Laboratory, 1975.
887 Pook L P, 'Fracture mechanics analysis of the fatigue behaviour of spot welds', *Int J Fract*, 1975, **11** (2), 173–176.
888 Pook L P, 'Approximate stress intensity factors obtained from simple plate bending theory', *Engng Fract Mech*, 1979, **12**, 505–522.
889 Pook L P, 'Mixed mode threshold behaviour of mild steel', *Fatigue Thresholds, Fundamentals and Engineering Applications*, Cradley Heath, Warley UK, Engineering Materials Advisory Services, 1982, Vol 2, pp 1007–1032.
890 Pook L P, 'The significance of mode I branch cracks for mixed mode fatigue crack growth threshold behaviour', *Biaxial and Multiaxial Fatigue*, London, Mechanical Engineering Publ, 1989, pp 247–263.
891 Pu S L, Hussain M A and Lorensen W E, 'The collapsed cubic isoparametric element as a singular element for crack problems', *Int J Numerical Methods Engng*, 1987, **12**, 1727–1742.
892 Radaj D, 'Stress singularity, notch stress and structural stress at spot-welded joints', *Engng Fract Mech*, 1989, **34** (2), 495–506, and *Schweißen u Schneiden*, 1989, **41** (3), 117–119 (German version).
893 Radaj D, 'Festigkeitsbeurteilung von Punktschweißverbindungen auf der Grundlage der örtlichen Beanspruchung', *Schweißen u Schneiden*, 1989, **41** (1), 26–31, and E10–E13 (English version).
894 Radaj D, 'Local fatigue-strength characteristic values for spot-welded joints', *Engng Fract Mech*, 1990, **37** (1), 245–250, and *Schweißen u Schneiden*, 1990, **42** (1), 30–34 (German version).
895 Radaj D, 'Structural stress, notch stress and stress intensity factor approach for assessment of fatigue-strength of spot-welded joints', *Welding in the World*, 1990, **28**, 29–39.
896 Radaj D, 'Nachweis der Ermüdungsfestigkeit von Punktschweißverbindungen auf Basis örtlicher Beanspruchungsgrößen', *Stahlbau*, 1990, **59** (7), 201–208.
897 Radaj D, 'Lokale Konzepte des Betriebsfestigkeitsnachweises für Schweißkonstruktionen', *Konstruktion*, 1995, **47**, 168–176.
898 Radaj D, 'Fatigue assessment of spot welds based on local stress parameters – critical annotations to formulas proposed by S Zhang', *Welding J, Res Suppl*, 2000, **79** (2), 51s–53s.

899 Radaj D, 'Fatigue assessment of spot welds by approximated local stress parameters', *Int J Fract*, 2000, **102**, L3–L8.
900 Radaj D and Giering A, 'Spot-welded H-specimen – the local stress parameters', *Materialprüf*, 1994, **36**, 275–281.
901 Radaj D and Giering A, 'Spot-welded double-cup specimen – the local stress parameters, *Materialprüf*, 1995, **37**, 458–462, with emendation 1997, **39** (10), 430.
902 Radaj D and Giering A, 'Local stress parameters of the spot-welded specimen. Part A: H-specimen, Part B: Double-cup specimen', *Welding in the World*, 1995, **35** (1), 12–22.
903 Radaj D and Heib M, 'Numerische Untersuchungen zum Rißbruchkriterium bei überlagerter Zug-, Druck- und Schubbeanspruchung', *Schweißen u Schneiden*, 1977, **29** (4), 135–139.
904 Radaj D and Heib M, 'Spannungsintensitätsdiagramme für die Praxis', *Konstruktion*, 1978, **30** (7), 268–270.
905 Radaj D and Heib M, 'Energy density fracture criteria for cracks under mixed-mode loading', *Materialprüf*, 1978, **20** (7), 256–262.
906 Radaj D, Schlüter A and Baur A, 'Schälzugschwingfestigkeitsversuch für Punktschweißnähte und Bruchflächenanalyse', *Schweißen u Schneiden*, 1986, **38** (3), 113–118, and E36–E38 (English version).
907 Radaj D, Sonsino C M and Zhang S, 'Schwingfestigkeit laserstrahlgeschweißter Dünnblechproben aus Stahl nach lokalen Konzepten', *Materialwiss u Werkstofftechn*, 1999, **30**, 249–256.
908 Radaj D and Zhang S, 'Stress intensity factors for spot welds between plates of unequal thickness', *Engng Fract Mech*, 1991, **39** (2), 391–413.
909 Radaj D and Zhang S, 'Simplified formulae for stress intensity factors of spot welds', *Engng Fract Mech*, 1991, **40** (1), 233–236.
910 Radaj D and Zhang S, 'Stress intensity factors for spot welds between plates of dissimilar materials', *Engng Fract Mech*, 1992, **42** (3), 407–426.
911 Radaj D and Zhang S, 'On the relations between notch stress and crack stress intensity in plane shear and mixed-mode loading', *Engng Fract Mech*, 1993, **44** (5), 691–704.
912 Radaj D and Zhang S, 'Analogies between crack tip and rigid line tip stresses and displacements', *Engng Fract Mech*, 1993, **44** (6), 913–919.
913 Radaj D and Zhang S, 'Loading modes and stress intensity factors at rigid layer edges', *Engng Fract Mech*, 1993, **46** (2), 199–208.
914 Radaj D and Zhang S, 'Simplified process zone fracture criteria at crack tips', *Structural Integrity – Experiments, Models and Applications*, Cradley Heath, Warley, UK, Engineering Materials Advisory Services, 1994, pp 363–368.
915 Radaj D and Zhang S, 'Stress distribution at bimaterial crack tips', *Engng Fract Mech*, 1994, **47** (4), 613–617.
916 Radaj D and Zhang S, 'Thermal stress singularity and fracture strength at bimaterial crack tips', *Mismatching of Welds*, London, Mechanical Engineering Publ, 1994, pp 177–194.
917 Radaj D and Zhang S, 'Punktgeschweißte Doppelhutprofilprobe unter Torsionsbelastung – lokale Beanspruchungsparameter und Schwingfestigkeit', *Materialprüf*, 1995, **37**, 458–462, with emendation 1997, **39** (10), 426.
918 Radaj D and Zhang S, 'Fracture initiation outside the slit tip', *Engng Fract Mech*, 1995, **50** (2), 309–310.

919 Radaj D and Zhang S, 'Process zone fracture criteria for crack tips', *Engng Fract Mech*, 1995, **50** (1), 111–120.
920 Radaj D and Zhang S, 'Stress concentration at fictitiously rounded sharp notches in shear loading', *Engng Fract Mech*, 1996, **55** (4), 675–676.
921 Rice J R, 'A path-independent integral and the approximate analysis of strain concentration by notches and cracks', *Trans ASME, J Appl Mech*, 1968, **35** (6), 379–386.
922 Shih C F, DeLorenzi H G and Germart M D, 'Crack extension modelling with singular quadratic isoparametric elements', *Int J Fract*, 1976, **12**, 647–651.
923 Sih G C, 'A three-dimensional strain energy density factor theory of crack propagation', *Three-dimensional Crack Problems*, Leyden, Noordhoff, 1975, pp 15–80.
924 Sih G C, 'External cracks under longitudinal shear', *J Franklin Inst*, 1965, **280** (2), 139–149.
925 Sih G C and Chen E P, 'Moving cracks in a finite strip under tearing action', *J Franklin Inst*, 1979, **290** (1), 25–35.
926 Singh S, Fatigue testing of jointed sheet material specimens, IIW Doc III-998-92.
927 Smith R A and Cooper J F, 'Theoretical predictions of the fatigue life of shear spot welds', *Fatigue of Welded Constructions*, Abington, TWI, 1988, pp 287–295.
928 Swellam M H, Ahmad M F, Dodds R H and Lawrence F V, 'The stress intensity factors of tensile-shear spot welds', *Computing Systems Engng*, 1992, **3** (1–4), 487–500.
929 Swellam M H, Banas G and Lawrence F V, 'A fatigue design parameter for spot welds', *Fatigue Fract Engng Mater Struct*, 1994, **17** (10), 1197–1204.
930 Tomioka N, Niisawa J and Mabuchi A, 'On theoretical analysis of stress at welding flange of spot-welded box section member under torsion', *SAE Techn Paper 860602*, Warrendale Pa, SAE, 1986.
931 Wang P C, 'Fracture mechanics parameter for the fatigue resistance of laser welds', *Int J Fatigue*, 1995, **17** (1), 25–34.
932 Wang P C and Ewing K, 'A *J*-integral approach to fatigue resistance of a tensile-shear spot weld', *SAE Techn Paper 880373*, Warrendale Pa, SAE, 1988.
933 Wang P C and Ewing K W, 'Fracture mechanics analysis of fatigue resistance of spot-welded coach-peel joints', *Fatigue Fract Engng Mater Struct*, 1991, **14** (9), 915–930.
934 Yuuki R and Ohira T, 'Fracture mechanics analysis of the fatigue strength of various spot-welded joints', *Seisan Kenyu*, 1986, **38** (10), 475–478.
935 Yuuki R and Ohira T, Development of the method to evaluate the fatigue life of spot-welded structures by fracture mechanics, IIW Doc III-928-89/XIII-1358-89.
936 Yuuki R, Ohira T, Kishi N and Mori N, 'Fracture mechanics evaluating of the fatigue strength of spot-welded joints and structures', *JSAE Paper 852096*, JSAE, 1985, pp 501–506.
937 Yuuki R, Ohira T, Nakatsukasa H and Li W, 'Fracture mechanics analysis and evaluation of the fatigue-strength of spot-welded joints' (in Japanese), *Trans JSME*, 1985, **51** (467), 1772–1779.
938 Zhang S, 'Stress intensities at spot welds', *Int J Fract*, 1997, **88**, 167–185.

939 Zhang S, 'Approximate stress intensity factors and notch stresses for common spot-welded specimens', *Welding J, Res Suppl*, 1999, **78** (5), 173s–179s.
940 Zhang S, 'Recovery of notch stress and stress intensity factors', *NAFEMS World Congress '99 on Effective Engineering Analysis*, NAFEMS, Glasgow, 1999, Vol 2, pp 1103–1114.
941 Zhang S, 'Recent developments in analysis and testing of spot welds', *SAE Techn Paper 2001-01-0432*, Warrendale Pa, SAE, 2001.
942 Zhang S, 'Approximate stress formulas for a multiaxial spot welded specimen', *Welding J, Res Suppl*, 2001, **80** (8), 201s–203s.
943 Zhang J, Dong P and Gao Y, 'Evaluation of stress intensity factor based predictive technique for fatigue life of resistance spot welds', *SAE Techn Paper 2001-01-0830*, Warrendale Pa, SAE, 2001.
944 Zhang G, Eibl M, Singh S, Hahn O and Kurzok J R, 'Methods of predicting the fatigue lives of laser-beam-welded lap welds under shear stresses', *Welding and Cutting,* 2002, **54** (3), 96–103, and *Schweißen u Schneiden*, 2002, **54** (3), 132–141 (German version).

Chapter 11 Notch- and crack-based approaches for spot-welded and similar lap joints

945 Adib H, Gilgert J and Pluvinage G, 'Fatigue life prediciton for welded spots by volumetric method', *Int J Fatigue*, 2004, **26**, 81–94.
946 Adib H and Pluvinage G, 'Theoretical and numerical aspects of the volumetric approach for fatigue life prediction in notched components', *Int J Fatigue*, 2003, **25**, 67–76.
947 Anastassiou M, Babbit M and Lebrun J L, 'Residual stresses and microstructure distribution in spot-welded steel sheets – relation with fatigue behaviour', *Mater Sci Engng,* 1990, **A125**, 141–156.
948 Bolton W, 'Residual stress distribution in and around spot welds', *Brit Welding J*, 1961, **8** (2), 57–60.
949 da Cruz P, Costa J D, Borrego L F and Ferreira J A, 'Fatigue life prediction in AlMgSi1 lap joint weldments', *Int J Fatigue*, 2000, **22** (7), 601–610.
950 Dowling N E, 'Notched member fatigue life predictions combining crack initiation and propagation', *Fatigue Fract Engng Mater Struct*, 1979, **2**, 129–138.
951 Dowling N E, *Mechanical Behaviour of Materials – Engineering Methods for Deformation, Fracture and Fatigue*, Englewood Cliffs, NJ, Prentice Hall, 1993.
952 Eibl M, Berechnung der Schwingfestigkeit laserstrahlgeschweißter Feinbleche mit lokalen Konzepten, Bericht FB-224, Darmstadt, Fraunhofer-Inst f Betriebsfest, 2004.
953 Eibl M and Sonsino C M, 'Stand der Technik zur Schwingfestigkeitsberechnung von laserstrahlgeschweißten Dünnblechen aus Stahl', *Fügetechnik im Automobilbau*, DVM-Bericht 668, Berlin, DVM, 2001, pp 155–171.
954 Eibl M, Sonsino C M, Kaufmann H and Zhang G, 'Fatigue assessment of laser-welded thin sheet aluminium', *Int J Fatigue*, 2003, **25**, 719–731.
955 Fermér M, Henrysson H F, Wallmichrath M and Rupp A, 'Low cycle fatigue of spot welds under constant and variable amplitude loading', *SAE Techn Paper 2003-01-0913*, Warrendale Pa, SAE, 2003.

956 Fischer K F, Gruhle M, Günther W, Preß H and Simon G, 'Simulation des Rißwachstums in zyklisch belasteten Widerstandspunktschweißverbindungen', *Schweißen u Schneiden*, 1994, **46** (1), 12–16.
957 Granjon H, *Fundamentals of Welding Metallurgy* (translated from French), Cambridge, Abington Publ, 1991.
958 Gruhle M, Günther W, Fischer K F, Berndt A, Preß H and Simon G, 'Bestimmung von Rißwachstumskurven punktgeschweißter Proben', *Schweißen u Schneiden*, 1998, **50** (1), 18–27.
959 Henrysson H F, 'Short fatigue crack propagation at spot welds – experiments and simulations', *Small fatigue cracks: mechanics, mechanisms and applications*, Amsterdam, Elsevier Science, 1999, pp 483–490.
960 Henrysson H F, 'Fatigue life prediction of spot welds using coarse FE meshes', *Fatigue Fract Engng Mater Struct*, 2000, **23**, 737–746.
961 Henrysson H F, Fatigue of spot-welded joints – experiments and life predictions, Ph D thesis, Chalmers University of Technology, Göteborg, 2001.
962 Henrysson H F, 'Effects of mean stress and crack closure on fatigue life of spot welds', *Fatigue Fract Engng Mater Struct*, 2002, **25**, 1175–1185.
963 Henrysson H F, 'Variable amplitude fatigue of spot welds', *Fatigue Fract Engng Mater Struct*, 2002, **25**, 1187–1197.
964 Henrysson H F, 'A comparison of variable amplitude fatigue life predictions for spot welds', *Fatigue 2002, Proceedings 8th International Fatigue Congress*, Cradley Heath, Warley UK, Engineering Materials Advisory Services, 2002, Vol 1, pp 397–404.
965 Henrysson H F, Abdulwahab F, Josefson B L and Fermér M, 'Residual stresses in resistance spot welds: finite element simulations, X-ray measurements and influence on fatigue behaviour', *Welding in the World*, 1999, **43** (1), 55–63.
966 Henrysson H F, Josefson B L and Sotkovszki P, Fatigue crack initiation at spot welds: fracture mechanics or strain life approach, Report F 233, Dep Solid Mech, Göteborg, Univ of Technol, 2001.
967 Lawrence F V, Wang P C and Corten H T, 'An empirical method for estimating the fatigue resistance of tensile-shear spot welds', *SAE Techn Paper 830035*, Warrendale Pa, SAE, 1983.
968 McMahon J C, Smith G A and Lawrence F V, 'Fatigue crack initiation and growth in tensile-shear spot weldments', *Fatigue and Fracture Testing of Weldments*, ASTM STP 1058, Philadelphia Pa, ASTM, 1990, pp 47–77.
969 Nakaho T, Tsunekawa Y and Suzuki T, Strength of spot welding joints in thin aluminium plates, report on resistance welding and related welding processes studies in Japan 1991, IIW Doc XIII-989-92, pp 13–14.
970 Newman J A and Dowling N E, 'A crack growth approach to life prediction of spot-welded lap joints', *Fatigue Fract Engng Mater Struct*, 1998, **21**, 1123–1132.
971 Nykänen T, 'Fatigue crack growth simulations in laser-welded lap joints', *Welding in the World*, 1999, **43** (5), 42–46.
972 Pan N, Fatigue life study of spot welds, Ph D thesis, Stanford University, 2000.
973 Pan N and Sheppard S D, 'Spot welds fatigue life prediction with cyclic strain range', *Int J Fatigue*, 2002, **24**, 519–528.
974 Pan N and Sheppard S D, 'Stress intensity factors in spot welds', *Engng Fract Mech*, 2002, **70**, 671–684.

975 Pan N, Sheppard S D and Widmann J M, 'Fatigue life prediction of resistance spot welds under variable amplitude loads', *Fatigue Fract Mech*, ASTM STP 1332, Philadelphia Pa, ASTM, 1999, pp 802–814.
976 Pluvinage G, 'Application of notch effect in high cycle fatigue', *Proceedings 9th International Conference on Fracture*, *ICF 9*, *Advances in Fracture Research*, Oxford, Pergamon Press, 1997, Vol 3, pp 1239–1250.
977 Popkovskii V A and Berezienko V P, 'Effect of resistance spot welding conditions on the distribution of residual stresses', *Welding Int*, 1998, **2** (12), 1058–1061.
978 Radaj D, Lehrke H P and Greuling S, 'Theoretical fatigue-effective notch stresses at spot welds', *Fatigue Fract Engng Mater Struct*, 2001, **24**, 293–308.
979 Schlemmer J, Berechnung der Schwingfestigkeit von laserstrahlgeschweißten mesoskopischen Bauteilen der Benzin- und Dieseleinspritzung, Bericht FB-222, Darmstadt, Fraunhofer-Inst f Betriebsfest, 2002.
980 Schröder R and Macherauch E, 'Berechnung der Wärme- und Eigenspannungen bei Widerstandspunktschweißverbindungen unter Zugrundelegung unterschiedlicher mechanisch-thermischer Werkstoffdaten', *Schweißen u Schneiden*, 1983, **35** (6), 270–276, and E2–E4 (English version).
981 Seeger T, Greuling S, Brüning J, Leis P, Radaj D and Sonsino C M, Bewertung lokaler Berechnungskonzepte zur Ermüdungsfestigkeit von Punktschweißverbindungen (Assessment of local concepts predicting the fatigue strength of spot-welded joints), FAT-Schriftenreihe 196, Frankfurt/M, FAT, 2005.
982 Sheppard S D, 'Estimation of fatigue propagation life in resistance spot welds', *Advances in Fatigue Lifetime Predictive Techniques*, Vol 2, ASTM STP 1211, Philadelphia Pa, ASTM, 1993, pp 169–185.
983 Sheppard S D, 'Further refinement of a methodology for fatigue life estimation in resistance spot weld connections', *Advances in Fatigue Lifetime Predictive Techniques*, Vol 3, ASTM STP 1292, Philadelphia Pa, ASTM, 1996.
984 Sheppard S D and Pan N, 'A look at fatigue resistance spot welds – notch or crack?', *SAE Techn Paper 2001-01-0433*, Warrendale Pa, SAE, 2001.
985 Sheppard S D and Strange M, 'Fatigue life estimation in resistance spot welds: initiation and early growth phase', *Fatigue Fract Engng Mater Struct*, 1992, **15** (6), 531–549.
986 Socie D F, Morrow J and Chen W C, 'A procedure for estimating the total fatigue life of notched and cracked members', *Engng Fract Mech*, 1979, **11**, 851–859.
987 Sonsino C M, Kueppers M, Eibl M and Zhang G, 'Multiaxial fatigue behaviour of laser beam welded thin steel sheets for automotive applications', *Proceedings International Conference on Biaxial/Multiaxial Fatigue and Fracture*, Berlin, DVM, 2004, pp 619–627.
988 Swellam M H, Kurath P and Lawrence F V, 'Electric-potential-drop studies of fatigue crack development in tensile-shear spot welds', *Advances in Fatigue Lifetime Predictive Techniques*, ASTM STP 1122, Philadelphia Pa, ASTM, 1992, pp 383–401.
989 Walker K, 'The effect of stress ratio during crack propagation and fatigue for 2024-T3 and 7075-T6 aluminium', *Effects of Environment and Complex Load History on Fatigue Life*, ASTM STP 462, Philadelphia Pa, ASTM, 1970, pp 1–14.

990 Wang P C, Corten H T and Lawrence F V, 'A fatigue life prediction method for tensile-shear spot welds', *SAE Techn Paper 850370*, Warrendale Pa, SAE, 1985.
991 Weixing Y, 'Stress field intensity approach for predicting fatigue life', *Int J Fatigue*, 1993, **15** (3), 243–245.
992 Zhang Y and Taylor D, 'Sheet thickness effect of spot welds based on crack propagation', *Engng Fract Mech*, 2000, **67**, 55–63.
993 Zuniga S M, Predicting overload pull-out failures in resistance spot welded joints, Ph D thesis, Stanford University, 1994.
994 Zuniga S M and Sheppard S D, 'Determining the constitutive properties of the heat-affected zone in a resistance spot weld', *Modeling Simul Mater Sci Engng*, 1995.

Chapter 12 Significance, limitations and potential of local approaches

995 Graf T and Zenner H, 'Lebensdauervorhersagen – Vorhersagefehler aufgrund ungenauer Kenntnis der erforderlichen Kenngrößen', *Materialprüfung*, 1994, **36** (3), 71–76.
996 Gumbel E J, *Statistics of Extremes*, New York, Columbia Univ Press, 1958.
997 Sudnik W, Radaj D and Erofeew W, 'Validation of computerised simulation of welding processes', *Mathematical Modelling of Weld Phenomena*, London, IOM Communications, 1998, pp 477–493.

Notes concerning the bibliography

The references are arranged in groups corresponding to the chapters in the book. The assignment to a group may be arbitrary in those cases where the publication refers to the topics of more than one chapter. Also, supplementary references of a more general character are included in that group from where they are mainly quoted.

The IIW documents in the bibliography are not available from public libraries. They can be ordered from any national welding society forming the IIW (International Institute of Welding) or from the IIW itself (www.iiw-iis.org). The Roman numerals in the document's designation refer to the commission responsible. The last two arabic numerals designate the year of the document's presentation.

Index

acrylic model, 340
aircraft engineering, 266
aluminium alloy, 16, 21, 23, 26, 29, 62, 69, 72, 80, 124, 127, 129, 130, 145–148, 197, 207, 214, 216, 218, 220, 263–267, 270, 280, 282, 290–292, 321, 322, 416, 425, 512, 536, 537
angular joint specimen, 343–345, 357
API guideline, 34, 37, 41, 45, 47, 63
ASME code 16, 20, 25, 40, 70, 72, 271
austenitic stainless steel, 127, 324, 412, 413, 417, 474, 543, 544
automotive engineering, 150–152, 366, 367, 372, 426–432, 443
AWS guideline, 34, 37, 41, 45, 63, 81, 82, 185

backing bar, 74
back-tracing of failures, 241, 577, 578
Basquin relationship, 94, 194, 197, 203, 247
Bauschinger effect, 208
bead-on-plate weld, 31
beam-to-shell element model of weld spot, 373–376, 387
bending loading mode, 178–180
biaxial fatigue, 135, 136, 176–178, 201, 206, 212, 213, 423
blunt corner notch, 301–304
blunt crack, 303, 468–470
boiler, welded joint, 157, 158
boundary element modelling, 36, 97, 107, 162, 168–189, 244, 454, 455, 458
Bredt formula, 465, 495, 498, 501
bridge construction, 61, 84, 283
British standards, 16, 20, 22, 155, 241, 250, 252, 254, 255, 263–265, 267, 362
buckling fatigue at spot weld, 400–404
butt-welded joints, 21, 50, 74, 104, 109–123, 167–169, 178, 181, 182, 214–221, 258, 283, 287–292

calibration of assessment procedure, 267, 364, 365
car loading standard, 426
CIDECT recommendation, 47
clam shell markings, 8
comparison specimen, 192, 197, 225
containment, welded joint, 224–227
cope hole, 84, 224
corner joint, 31, 85, 172, 173
corner notch stress intensity, 239, 240, 297–304
corrosive environment, 27, 263–266, 410
cover plate joint, 78, 86, 110–121, 132, 133, 171, 172, 258, 286, 316
crack branching, 234, 436, 476, 481, 523
crack closure, 198, 246, 250, 410, 540, 564
crack coalescence, 148, 260, 261, 277, 293
crack growth retardation, 249, 250
crack initiation, 3, 191, 196, 202, 207, 217, 277, 289, 324, 343–345, 437, 514, 515, 550, 555
crack loading mode definition, 445
crack opening displacement, 435, 482
crack path, 248, 262, 276, 293, 437, 475, 550
crack propagation angle, 479
crack propagation approach, 214, 233–295, 323–326, 355–363, 513–517, 522–524, 538–542, 566, 567, 602–616, 631–634
crack propagation life, 3, 197, 203, 217, 247–250, 360, 361, 514, 538–542, 555
crack shape, 252–254, 259–262, 293
crane construction, 102
Creager formula, 468–470
critical distance approach, 93–96, 125, 126
critical plane criterion, 195, 370, 428
critical stress intensity factor, 245, 246, 267
cross-sectional model, 97, 98, 109, 140, 151, 156, 159, 161, 166–190, 222, 346, 520, 525, 526, 528
cross-tension specimen, 398–400, 407, 474, 484, 485, 490–492, 524–527
cruciform joint, 21, 31, 35, 50, 66, 89, 90, 101, 104, 110–121, 169, 170, 178, 181, 183, 186–190, 221–224, 256, 257, 281–286, 316, 317, 327, 330

damage parameter, 193, 200, 210, 230, 428, 560
damage parameter, endurable value, 226, 229
damage parameter *P–N* curve, 200, 201, 209, 210, 226, 229
damage sum limit, 19, 22, 25, 200, 211, 240, 275, 276, 343, 416, 426
damage zone approach, 276–278, 534, 535
Dang Van criterion, 103, 137, 423
degree of bending, 68, 77, 285, 355
DEn guideline, 45, 47, 63, 344, 345
design optimisation, 365, 427–432, 577
design *S–N* curve, 19–23
detail class, 1, 15, 22
displacement-controlled fatigue, 69, 232, 258, 271, 537, 565
displacement loading, 173, 174
distortional strain energy criterion, 25, 72, 93, 105, 128, 137, 198, 201, 206, 212, 386
documentation of assessment procedure, 574, 575
Dong's crack propagation approach, 271–275
Dong's structural stress approach, 41–43, 55–57
double-cup specimen, 507–510,
Dugdale–Newman model, 240, 277

ECCS or ECSC recommendation, 22, 23, 47, 64, 335, 336, 344
edge attachment joint, 21, 40, 42, 49, 54, 56, 86–88
eigenforce at weld spot, 369–371, 377, 378, 466, 561
elevated temperature, 27
energy release rate criterion, 246, 453, 477, 479, 480
equivalent stress intensity factor, 440, 476–480
Eurocode, 16, 22, 23, 25, 45, 63–65, 82, 155, 163

failure probability, 17
fatigue class (FAT), 1, 15, 21
fatigue-effective notch stress, 36, 96, 106, 127, 326, 347, 348, 470, 529
fatigue notch factor of welds, 95, 106, 121–138, 143, 145, 151, 152, 156, 158, 167–180, 471
fatigue strength reduction factor, 29–32, 98–101, 152–155
fictitious notch radius, 96, 100, 127–130, 166, 185–190, 524–527, 533
fictitious notch rounding approach, 36, 96–101, 126–143, 150–163, 166–190, 517, 518
fictitious undercut, 131, 132
fillet weld sector model, 327, 328
final crack size, 247, 268, 358

Findley criterion, 71, 126, 137, 206
finite element modelling, 8, 51–55, 78, 107, 244, 329, 337, 420–422, 452, 453, 545–547, 561
fitness for purpose, 22, 183, 241, 266, 577
FKM guideline, 2, 23, 428, 541
flange attachment joint, 86–89
force *F–N* curve, 231, 352–355, 410, 483, 520, 533, 541, 542, 553, 565
forcing function, 259
Forman equation, 246, 538
frame corner joint, 150–155, 158–160
friction-welded joint, 109, 270
functional analysis method, 107, 109, 110, 243
fusion zone, 123–125, 130, 196, 226–228, 349, 351, 352, 547–550

geometric stress, 33, 39, 331
German standards, 16, 20, 155
girder, welded joint, 61, 62, 84–89, 102, 152–155
girth butt weld, 160, 161, 258
Glinka formula, 209, 538
global approach, 1, 7, 568, 569
Goodman relationship, 206
grain size, 522
gusset plate joint, 31, 85, 163–165

Haigh diagram, 144, 369, 415
hardness distribution, 123–125, 290, 547–550
hardness effect, 123, 203, 224, 349
hat section specimen, 392, 400–404, 411, 484, 485, 493–501, 563
heat affected zone, 123–125, 196, 201, 207, 218, 229, 230, 266, 349, 352, 355, 548–550, 560, 561
high strength steel, 82, 104, 144, 161, 197, 198, 214, 216, 218, 224–227, 232, 238, 266, 279, 281, 289, 408–413, 553
highly stressed volume approach, 93, 105, 145–150, 202
hot spot location, 39, 47, 49
hot spot structural stress, 38, 39–41, 46–55, 85, 87, 329, 330, 340
hot spot structural stress, endurable value, 62–73, 165, 344, 345, 412, 415, 420–425
H-shaped specimen, 417, 501–506, 563, 565

IIW recommendations, 2, 16, 20, 21, 24, 27, 45, 63, 70, 74, 90, 101, 128, 145, 155, 183, 264, 265, 284, 286, 343, 417, 501
imperfection, 9, 108, 241
inhomogeneous material, 9, 123–125, 196, 201, 236, 355
initial crack size, 105, 214, 236, 237, 240, 267, 289, 355, 358, 523
inspection interval, 241
intermittent weld, 140

internal displacement method, 139, 346
internal force splitting method, 139, 140–143
Irwin criterion, 246, 453, 477, 479
I-section girder, 61, 62, 84–89, 152–155

Japanese standards, 16, 70, 84
J-integral, 210, 234, 307, 308, 450, 454, 482
J-integral, endurable value, 321, 322, 473, 482, 510
J-integral damage parameter, 210, 235
J–*N* curve, 482, 492, 510
joint face fracture, 437, 438

Kandil–Brown–Miller damage parameter, 210

lap joint, 31, 104, 110–121, 171, 172, 256, 258, 286, 317, 327, 433–512, 536, 537
lap joint in dissimilar materials, 457–459
lap joint with large deflections, 395–400, 459–461, 536
lap joint with unequal plate thickness, 453–456
laser beam welded joint, 165, 166, 168–173, 417–420, 432, 510–512, 536, 551, 566, 567
layered material model, 236
leak-before-break criterion, 82, 268
limit load factor, 209
load-carrying fillet weld, 24, 50, 66, 167, 256, 276, 283, 324
load shedding, 258, 259
load spectrum, 250, 335, 358, 426
load–strain curve, 200, 230, 351
local approach, 1–12, 568–578, 634
longitudinal attachment joint, 7, 21, 31, 44, 49, 66, 161–163, 256, 279–281, 292–295
longitudinal section model, 140, 152, 379, 394, 395, 396, 399, 511
low-cycle fatigue, 17, 39, 46, 72, 73, 93, 195, 202, 212, 213, 394, 437

macrostructural support formula, 8, 200, 202, 208, 211, 515
Manson–Coffin–Morrow relationship, 200, 207, 232
Masing relationship, 200, 205, 208
material parameters, 199, 207, 215, 222, 226, 230, 263–267, 288, 290, 349, 357, 358, 440
mean stress effect, 23, 24, 136, 137, 144, 206, 263, 415
mean stress sensitivity, 24, 415, 476
microcrack, 3, 263, 237, 277
microstructural support hypothesis, 92, 122, 126, 127, 240
microstructural zones, 123–125, 198, 266, 548–550
Miner's rule, 19, 64, 82, 106, 197, 206, 211, 225, 236, 249, 370, 410, 416, 426, 565
misalignment, 50, 69, 168, 221–224, 283
mixed-mode crack loading, 234, 246, 476–481
modified notch rounding approach, 101–104, 143–145
multiaxial fatigue, 24–27, 70–73, 135, 136, 147–150, 201, 202, 212, 313, 405

Neuber formula, 8, 200, 202, 208, 211, 232, 538
Neuber hyperbola, 218, 350
nominal stress approach, 13–32, 579–583
nominal stress, endurable value, 19–23, 101, 165, 184, 419
nominal stress intensity factor, 465, 466
nominal stress *S*–*N* curve, 13–16, 19–23, 216, 219–221, 223, 234
nominal structural stress, 383–388, 466
nominal weld stress, 14, 74, 75, 80
nominal weld stress, endurable value, 75, 79
non-fused weld root face, 74
non-load-carrying fillet weld, 50, 66, 123, 167, 276, 316, 324
non-proportional loading, 24–27, 137, 149, 194
normal strain criterion, 230, 558, 559, 561, 562
normal stress criterion, 25, 137, 370, 388
normalised *S*–*N* curve, 15, 28, 29, 125
notch class, 1, 14, 15, 21–23
notch effect, 38, 91
notch loading mode, 298–300
notch sensitivity, 122
notch shielding, 33
notch strain approach (elastic-plastic), 191–232, 348–355, 513–522, 531–538, 551–566, 598–601, 631–634
notch strain, endurable value, 207, 215, 226, 229, 515, 559
notch strain energy density, 308–310
notch strain energy density, endurable value, 322, 323, 520
notch stress approach (elastic), 91–190, 345–348, 467–471, 513–518, 524–531, 535–537, 590–598, 631–634
notch stress concentration factor of welds, 95, 107–121, 182, 183, 188, 235, 356, 527
notch stress, endurable value, 106, 128, 143–150, 165, 536
notch stress evaluation methods, 107
notch stress gradient, 92, 105, 145, 146
notch stress intensity approach, 41, 239, 240, 296–333, 616–619
notch stress intensity factor, endurable value, 310–313, 319–321
notch stress intensity factor of fillet welds, 8, 297–304, 313–317
notch stress on structural stress superposition, 39, 141, 142, 331, 332
notch stress *S*–*N* curve, 147, 150, 536

notch support factor, 194, 515, 516, 532
nuclear engineering, 224–227
nugget fracture, 368, 369, 370, 388, 414, 438
nugget rotation, 483

oblique notch, 135, 136, 176, 177
occurance probability, 20
octahedral shear strain criterion, 73, 212, 213, 230
offshore engineering, 334–365
one-millimetre-stress approach, 43, 44, 69, 70
optimised weld contour, 185, 186–190
out-of-phase loading, 26, 72, 93, 149, 213, 536
overload effect, 250

Paris equation, 8–23, 194, 245
partial penetration butt weld, 71, 120, 216, 219–221, 287–292
partial penetration fillet weld, 74, 110–120, 284, 285, 470
peel tension specimen, 484, 485, 490–492, 510, 511, 564
permissible stress, 18–23, 165
photoelastic model, 8, 107, 108, 109, 390
pipe branch, 227
plastic hinge at weld spot, 394
plastic notch stress intensity, 304–307
plate fracture, 189, 282, 368, 369, 412, 414, 437, 438
plate-type joint, 40, 48–51, 61
postweld treatment, 27, 108, 198, 220, 545, 556
pressure vessel, welded joint, 155–157
principal internal force method, 138, 139, 141–143, 153
process zone criterion, 477

quality class, 14, 22, 74

rainflow cycle counting, 211, 368, 426, 428, 483
Ramberg–Osgood relationship, 205, 207, 348
refined crack propagation approach, 275–279, 292–295
residual fatigue life, 241, 262
residual stress effect, 23, 24, 104, 137, 138, 144, 198, 201, 217–221, 268–271, 283, 354, 359, 361, 542–547
rigid core model of weld spot, 369, 384–386, 561, 564
rivet hole crack model, 554
RPG load, 276–279, 294

SAE recommendation, 37
safety factor, 18–20
scatter range index of *S–N* curve, 17, 20
seam-welded joints, 13–365
seam-welded thin-sheet lap joints, 417–426, 510–512, 566, 567
seawater corrosion, 266, 336, 344, 352, 357, 358, 359
service life *S–N* curve, 5, 18, 227, 344
set-up loading cycle, 197, 205, 218
shear stress criterion, 25, 72, 137
shear-loaded weld, 26, 31, 134, 150, 174, 175
shipbuilding, 84–90, 158–163
short crack, 8, 237, 238, 275, 471
short slit correction factor, 133, 134
shoulder-notched bar, 115, 315
size effect, 300, 301, 306, 307, 320, 428
slit closure, 397, 505, 543
slope exponent of *S–N* curve, 15, 17, 231, 232, 416
small size notch approach, 94, 520–522, 527–531, 535–538
Smith–Watson–Topper damage parameter, 200, 210, 230, 428, 560
S–N curve, 15–16, 19–23, 216, 219–221, 223, 234
software tools for fatigue evaluation, 19, 107, 242, 372, 374, 426, 427
solid-to-shell element model of weld spot, 382, 383
spot-welded joints, 28, 31, 172, 366–578
steel, 16, 21, 22, 26, 28, 29, 62–70, 73, 79, 82, 95, 104, 124, 127, 128, 143, 144, 147, 150, 161, 184, 189, 197, 198, 214, 216, 218, 224–232, 238, 263–267, 320–324, 334, 344, 405–426, 473, 474, 510, 511, 536, 541–550, 553
storm load spectrum, 250
strain energy density criteria, 322, 323, 477
strain gauge measurement, 8, 34–36, 38, 45, 47, 63, 107, 158, 338, 389–393
strain *S–N* curve, 191, 200, 207, 215, 226, 229, 352, 426, 428, 515, 516, 559
stress averaging approach, 92, 470, 529
stress gradient approach, 92
stress index, 480, 481
stress intensity approach, 433–512, 626–631
stress intensity factor determination, 243–245, 443, 452, 467–469
stress intensity factor, endurable value, 471–476, 563, 564
stress intensity factor of fillet weld, 250–259
stress intensity factor of lap joint, 447–466
stress intensity geometry factor, 246, 250–255
stress intensity *K–N* curve, 472–475, 538, 539, 562–564
stress intensity magnification factor, 50, 246, 250–255, 325, 375
stress ratio effect, 23, 24, 101, 128, 144, 246, 247, 352, 354, 415, 475, 476, 540
stress relaxation, 197, 200, 205
stress relief groove, 155–157
stress rise at weld toe, 35, 36, 181, 317–319, 330, 331
stress singularity, 297–300, 443–447, 457

stress–strain curve, 205, 207, 213, 225, 228, 349
stress–strain cycle, 218, 560
stress–strain path, 200
striations on fracture surface, 263
structural strain approach, 33–37, 336–340, 392, 393, 411
structural strain at weld spot, 389–393
structural strain, endurable value, 34, 62, 81, 82, 405–407
structural strain *S–N* curve, 407
structural stress approach, 33–90, 326–332, 336–340, 366–432, 583–590, 620–626
structural stress at weld spot, 380–388, 495
structural stress concentration factor, 57–62, 235, 340–343
structural stress definition, 7, 38–45, 371, 380–388
structural stress, endurable value, 62–73, 165, 344, 345, 412, 415, 420–425
structural stress *S–N* curve, 62–73, 344, 345, 408, 411, 417, 422, 423, 533
structural weld stress, 73–80, 90
substitute microstructural length, 127, 524, 533
survival probability, 20

tangential stress criterion, 286, 440, 477, 478, 540
T butt joint, 252–254
technical crack, 3, 197, 233
technical endurance limit, 15, 17
tensile-shear specimen, 379–383, 394–398, 407, 412, 417, 441, 464, 474, 484–490, 510–512, 524–527, 533, 534, 551, 563–567
thickness effect, 27, 36, 64, 65, 67, 180, 300, 306, 307, 320, 372, 408, 488, 489, 492, 553, 563, 566
threshold stress intensity factor, 245, 265–267, 542
through-tension specimen, 484, 485
titanium alloy, 266, 270
T-joint, 52, 110–121, 179, 224, 256, 258, 285
transition fatigue life, 203, 215
transverse attachment joint, 21, 31, 44, 49, 51, 66, 101, 104, 110–121, 170, 171, 178, 256, 258, 279–281, 317, 320–325
tube-to-plate joint, 26, 149, 150, 317
tubular flange or lap joint specimen, 484, 485
tubular joint, 37–39, 46–48, 59–65, 81–84, 227–231, 255, 259, 261, 334–365, 426

uniform material law, 199, 207

validation of assessment procedures, 86–89, 121, 573, 574
variable-amplitude loading, 19, 22, 25, 197, 206, 249, 250, 344, 358, 361, 415, 416, 556
verification by experiment, 573
von Mises criterion, 25, 72, 105, 128, 137, 198, 201, 206, 212, 350, 369, 386, 536

wave load standard spectrum, 335, 358
web stiffener joint, 152–155
weight function method, 243, 254
weld defect, 9, 168
weld reinforcement, 161
weld root fatigue, 44, 73–80
weld root fracture, 100, 189, 223, 248, 282, 286, 287, 324
weld root radius, 108
weld seam end, 140, 141, 424
weld seam modelling, 51–55, 329, 422, 424
weld spot contour, 519
weld spot failure type, 437, 438, 523
weld spot force decomposition, 376–378, 466
weld spot force, endurable value, 410, 414, 487, 489, 491, 492, 494–496, 524, 526, 553
weld spot modelling, 373–376, 382–387, 427, 428
weld spot resultant force, 369, 373–381, 392, 393
weld spot rotation, 394, 395–397
weld spot stress decomposition, 447–459
weld toe angle, 108, 161, 180–183, 255, 288, 289, 297, 363
weld toe dressing, 27, 108, 198, 220
weld toe fracture, 100, 189, 223, 282, 283, 323, 324
weld toe radius, 35, 108, 161, 185, 255, 297, 363
weld toe undercut, 161, 183–185, 283
welded joint pecularities, 8–10, 575, 576
welding distortion, 9
welding imperfection, 9, 108
welding residual stress, 9, 24, 218, 284, 542–547
wind energy converter, 163–165
worst case assessment, 96, 97, 128, 129, 574

yield curve, load–strain, 200, 230, 351